

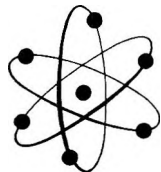
THE JOURNAL OF  
**PHYSICAL CHEMISTRY**

---

*Volume 69, Number 11 November 1965*

The Radiolysis of Methanol and Methanolic Solutions. IV. The Effect of Water on Peroxide Yields . . . . . Norman N. Lichtin and Judith W. Wilson	3673
Measurement of the Diffusion of Oxygen in Polymers by Phosphorescent Quenching . . . . . Ellis I. Hormats and Fred C. Unterleitner	3677
Gas-Liquid Partition Chromatography in Benzene-Polyphenyl Systems and Polymer Statistical Thermodynamics . . . . . Ronald K. Clark and Hartland H. Schmidt	3682
Single-Ion Activity Coefficients of Gegenions in Sodium Polyacrylate . . . . . Tsuneo Okubo, Yasuko Nishizaki, and Norio Ise	3690
A Kinetic Study of the Lipoamide Dehydrogenase-NADH-Dye Reaction . . . . . George G. Guilbault, David N. Kramer, and P. Goldberg	3696
The Kinetics of the Tetrafluorohydrazine-Fluorine Reaction . . . . . Joseph B. Levy and B. K. Wesley Copeland	3700
Samarium Borides. The Tetraboride-Hexaboride Conversion . . . . . George D. Sturgeon and Harry A. Eick	3705
Optical Rotatory Dispersion of <i>d</i> -Camphor . . . . . Ajit Singh and Leonard I. Katzin	3708
Electron Spin Resonance Spectroscopy of Irradiated Acrylamide . . . . . G. Adler and J. H. Petropoulos	3712
On the Ionic Strength Dependence of Micelle Number . . . . . M. F. Emerson and A. Holtzer	3718
A Near-Infrared Study of Hydrogen Bonding in Water and Deuterium Oxide . . . . . Mary R. Thomas, Harold A. Scheraga, and Eugene E. Schrier	3722
An Electron Diffraction Study of Trifluoronitrosomethane . . . . . M. I. Davis, J. E. Boggs, D. Coffey, Jr., and H. P. Hanson	3727
Appearance Potentials and Mass Spectra of Fluorinated Ethylenes. II. Heats of Formation of Fluorinated Species and Their Positive Ions . . . . . Chava Lifshitz and F. A. Long	3731
Appearance Potentials and Mass Spectra of Fluorinated Ethylenes. III. Calculations Based on the Statistical Theory of Mass Spectra . . . . . Chava Lifshitz and F. A. Long	3737
Appearance Potentials and Mass Spectra of C <sub>2</sub> F <sub>6</sub> , C <sub>3</sub> F <sub>5</sub> Cl, and <i>c</i> -C <sub>3</sub> F <sub>6</sub> . . . . . Chava Lifshitz and F. A. Long	3741
Some Observations Concerning the Positive Ion Decomposition of C <sub>2</sub> F <sub>6</sub> and C <sub>3</sub> F <sub>6</sub> in the Mass Spectrometer . . . . . Chava Lifshitz and F. A. Long	3746
Diffusion of Methane, Ethane, Propane, and <i>n</i> -Butane in Water from 25 to 43° . . . . . P. A. Witherspoon and D. N. Saraf	3752
Relative Determination of Soret Coefficients of Electrolytes. II . . . . . Toshio Ikeda and Mitsuhiro Matsumoto	3755
Thermochemical Studies. XV. Thermodynamics of Protonation of Triethylenediamine, Triethylamine, Trimethylamine, and Ammonia in Aqueous Solution at 25° . . . . . Piero Paoletti, John H. Stern, and Alberto Vacca	3759
Formation Constants of Silver(I) Cyanide Complexes in Equimolar Sodium-Potassium Nitrate Melts . . . . . H. Ti Tien	3763
Gas-Solid Partition Chromatography with Real Carrier Gases . . . . . David C. Locke	3768
Absorption Isotherms of Hydrogen in the $\alpha$ -Phase of the Hydrogen-Palladium System . . . . . J. W. Simons and Ted B. Flanagan	3773
Viscosity of NaK 78 at Low Temperature . . . . . George Macur, E. L. Grove, Allan J. Gaynor, and Charles K. Hersh	3782
Sedimentation and Electrophoresis of Interacting Substances. IV. Theory of the Analysis of Interacting Systems by Differential Boundary Experiments . . . . . R. C. L. Jenkins	3785
Charge-Transfer Absorption and Luminescence Spectra of Alkyl Halide Salts of Pyridine . . . . . J. S. Brinen, J. G. Koren, H. D. Olmstead, and R. C. Hirt	3791

Reference Books for Physical Chemists



from  
**SAUNDERS**

**Stevenson—MULTIPLY STRUCTURE  
of ATOMS and MOLECULES New!**

By **RICHARD STEVENSON,**

**McGill University, Montreal**

This book offers practical assistance in undertaking calculations of various properties of atoms and molecules. Key features include concise calculations for use in group theory, the use of symmetry consideration, the calculation of parameters in terms of the radial part of the wave function, and the use of projection operator techniques and tensor operator methods. Previously unpublished tables and information on Ligand field theory are included. Topics covered include The Virial Theorem, Schrödinger's Equation, The Exclusion Principle, Coupling of Angular Momentum, Molecular Orbital Calculations, and Rumer's Method.

190 pages \* illustrated \* \$5.75 \* Just Published!

**Smart—EFFECTIVE FIELD THEORIES  
of MAGNETISM New!**

By **J. SAMUEL SMART,**

**IBM Watson Research Center**

This new monograph probes more deeply into magnetically ordered phenomena than the usual solid state text. It is readily comprehensible to those with grounding in elementary quantum theory. The author builds his discussions around insulating materials rather than metals and alloys. He uses the Heisenberg model of magnetic interactions in solids to develop the descriptions of effective field theories. Material moves logically from discussion of the simple paramagnet to such specific subjects as the application of the Néel theory to ferrites and garnets. Throughout the book, the author maintains a close contact between the theoretical development, its physical interpretation, and its relation to actual physical properties. Physicists, metallurgists, and those working in the physical sciences can gain a new appreciation of the complex phenomena of magnetism.

188 pages \* illustrated \* about \$5.50 \* Just Ready!

*These are but the first of many titles to come in  
STUDIES in PHYSICS and CHEMISTRY*

Look for future books in this new series of short books on advanced topics. Coming in the Summer of 1966 are: Kyrala—VECTORIAL METHODS OF THEORETICAL PHYSICS, and Spencer—THE CHEMISTRY AND PHYSICS OF DNA AND RNA. Four more titles are due in the Fall of 1966.

**W. B. SAUNDERS COMPANY**

**West Washington Square, Philadelphia, Pa. 19105**

Please send and bill me:

Stevenson: MULTIPLY STRUCTURE . . . . . \$5.75

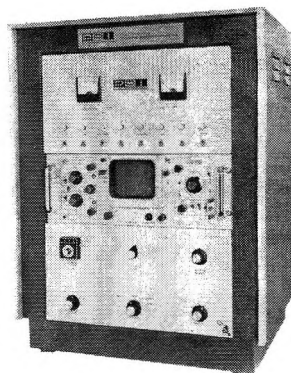
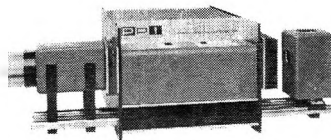
Smart: EFFECTIVE FIELD THEORIES. About \$5.50

Gladly sent to college instructors on approval JPC 11-65

Name \_\_\_\_\_

Address \_\_\_\_\_ Zip \_\_\_\_\_

. . . carries on  
where other  
**SPECTROPHOTOMETERS**  
leave off.



**THE NEW PHOENIX SCANNING  
DUAL WAVELENGTH  
SPECTROPHOTOMETER**

**WANT TO MEASURE ABSORPTION CHANGES OF  $3 \times 10^{-3}$  O.D. UNITS IN TURBID MEDIA?** Conventional spectrophotometers are not satisfactory under these stringent conditions, so we've provided an unconventional spectrophotometer for this purpose. It is a single instrument capable of operation both in a dual wavelength mode and as a high sensitivity scanning double beam spectrophotometer. Although it is primarily intended for studies in enzyme kinetics, oxidative phosphorylation and photosynthesis, it is expected to have application in other areas where small O.D. differences have to be measured in optically dense media. For complete technical details write for Bulletin PMD-1000.



**PHOENIX PRECISION INSTRUMENT CO.**

A Subsidiary of CENCO INSTRUMENTS CORP.  
3803-05 N. 5th Street, Phila., Penna. 19140, U.S.A.  
World Wide Sales and Service

**CONTACT ANGLE, WETTABILITY,  
AND ADHESION**

ADVANCES IN CHEMISTRY SERIES 43

contains twenty-six papers given at the 1963 Kendall Award Symposium.

This is the largest and best collection of up-to-date papers giving both theoretical and practical approaches to wettability and adhesion—a subject important to many areas of science and technology.

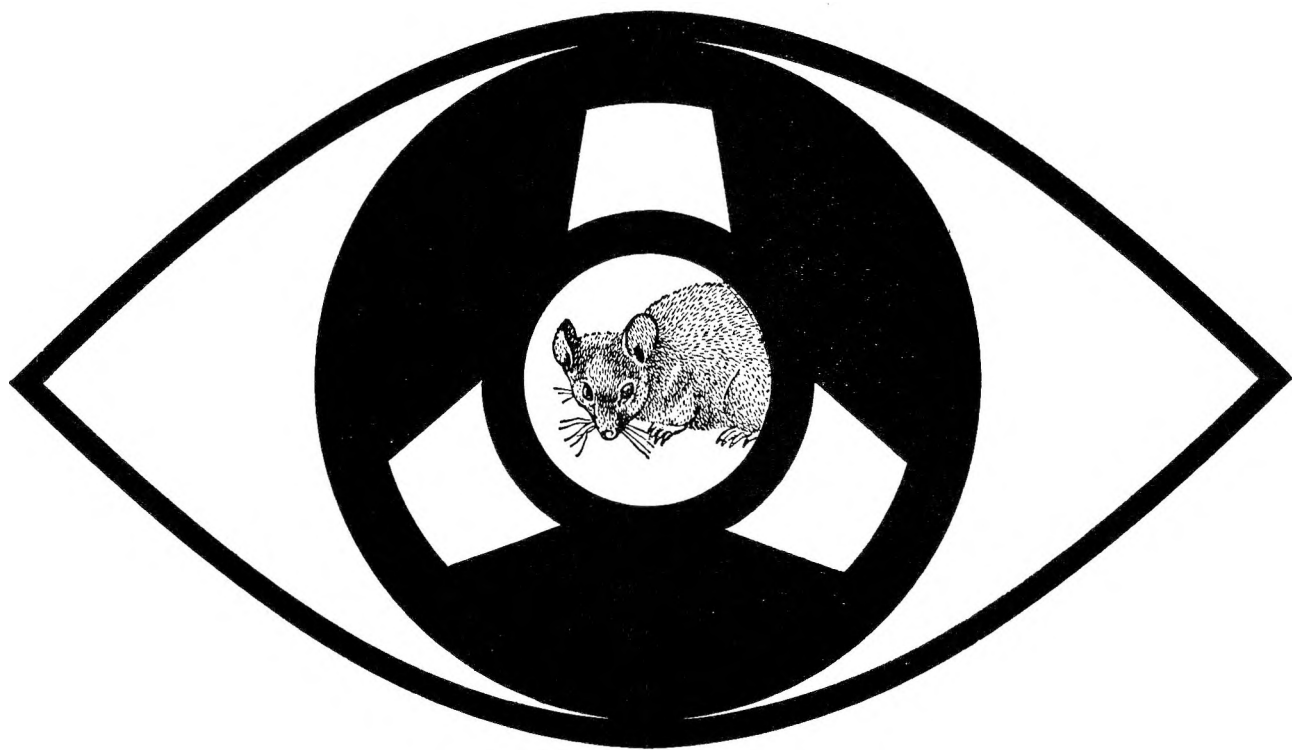
In a sense this book is a tribute to the fundamental work of W. A. Zisman, 1963 recipient of the Kendall Award, who opens the symposium with a 48-page article which includes 107 references to other work.

Some papers deal with the chemical structure of solid surfaces, solid-fluid interfacial tensions, and flow in capillaries as related to contact angle discussed in other papers. Still others explore adhesion theories, thermodynamics of wettability, chemisorption, coadsorption on metals, spreading of oils on surfaces and its prevention, a computer study of wettability, and other areas.

**Order from: Special Issues Sales  
American Chemical Society  
1155 Sixteenth St., N. W.  
Washington, D. C. 20036**



Volume Changes in Hydrocarbon-Water Systems. Partial Molal Volumes of Alcohol-Water Solutions Michael E. Friedman and Harold A. Scheraga	3795
The Degree of Coupling and Efficiency of Fuel Cells and Membrane Desalination Processes S. R. Caplan	3801
An Electron Paramagnetic Resonance Study of Alcohol Oxidation by Fenton's Reagent Takeshi Shiga	3805
The Diffusion Coefficient of Atomic Mercury in Isooctane Maurice M. Kreevoy and Herbert B. Scher	3814
Interfacial Tension of Indium Amalgams in 0.1 M Perchloric Acid at 25° James N. Butler	3817
Thermodynamic Stabilities as a Function of Composition for Indium Sulfide Phases from Mass Spectrometer Intensity vs. Time Data Alan R. Miller and Alan W. Searcy	3826
A Radiotracer Study of Competitive Adsorption at the Gold-Oil Interface Morris L. Smith, Benjamin E. Gordon, and Richard C. Nelson	3833
The Thermodynamic Properties and Allotropy of Beryllium Chloride between 13 and 715°K. R. A. McDonald and F. L. Oetting	3839
The Structure of Sodium Silicate Glasses and Their Far-Infrared Absorption Spectra Rinoud Hanna	3846
A Small Angle X-Ray Scattering Study of Colloidal Thorium Oxide Paul W. Schmidt	3849
Catalysis over Supported Metals. IV. Ethane Hydrogenolysis over Dilute Nickel Catalysts W. F. Taylor, J. H. Sinfelt, and D. J. C. Yates	3857
The Heat of Formation of Nitric Oxide(g) Margaret A. Frisch and John L. Margrave	3863
The Barium-Sodium Equilibrium System F. A. Kanda, R. M. Stevens, and D. V. Keller	3867
The Dimer Spectrum of Acridine Orange Hydrochloride Michael E. Lamm and David M. Neville, Jr.	3872
The Conductance of the Symmetrical Tetraalkylammonium Halides and Picrates in Acetonitrile at 25° D. Fennell Evans, C. Zawoyski, and Robert L. Kay	3878
Raman Studies of Iodic Acid and Sodium Iodates James R. Durig, O. D. Bonner, and W. H. Breazeale	3886
Ionization and Dissociation of Ruthenium and Osmium Tetroxides John G. Dillard and Robert W. Kiser	3893
The Elimination of HF from "Hot" Fluorinated Ethanes. An Estimation of the Activation Energies and Rate Parameters Sidney W. Benson and Gilbert Haugen	3898
The Activity Coefficients of Solutes in Acid Solutions. II. The Relative Activity Coefficients of the Chloride and Silver Ions in Aqueous Sulfuric Acid Richard H. Boyd and Chin-hsien Wang	3906
The Thermodynamics of Vaporization of Thallous Fluoride and Its Gaseous Dimerization F. J. Keneshea and Daniel Cubicciotti	3910
The Vapor Pressure and Enthalpy of Vaporization of Molten Bismuth Chloride to the Critical Point J. W. Johnson, W. J. Silva, and Daniel Cubicciotti	3916
Carbon-13 Magnetic Resonance Study of Alkyl Cyanides, Isocyanides, Isocyanates, and Isothiocyanates Gary E. Maciel and David A. Beatty	3920
Carbon-13 Magnetic Resonance Study of Some Saturated Heterocyclic Compounds Gary E. Maciel and George B. Savitsky	3925
Adsorption of Polar Molecules on Metal Oxide Single Crystals Yung-Fang Yu Yao	3930
Diffusion in the Three-Component Liquid System Acetone-Benzene-Carbon Tetrachloride H. T. Cullinan, Jr., and H. L. Toor	3941
The Adsorption of Hexachloroacetone on Alumina-Containing Surfaces M. L. Hair and I. D. Chapman	3949
Conformation of Polystyrene Adsorbed at the $\theta$ -Temperature Robert R. Stromberg, Daniel J. Tutas, and Elio Passaglia	3955
The Bromine Ultraviolet Lamp. Studies of the Oxygen-Ozone and Carbon Dioxide Equilibria B. A. Thompson, R. R. Reeves, Jr., and P. Harteck	3964
Properties of Organic-Water Mixtures. V. Self-Diffusion Coefficients of Na <sup>+</sup> in Alcohol-Water Mixtures at 25° Arthur E. Marcinkowsky, Harold O. Phillips, and Kurt A. Kraus	3968
The Scandium-Yttrium-Hydrogen System M. L. Lieberman and P. G. Wahlbeck	3973
Studies of Membrane Phenomena. I. Membrane Potential Yonosuke Kobatake, Noriaki Takeguchi, Yoshinori Toyoshima, and Hiroshi Fujita	3981



**Now  
you can search  
Chemical Titles  
magnetic tapes  
by computers**

Update your information dissemination program through the use of CHEMICAL TITLES Tapes or Custom Searches! These services are being offered for the first time by the Chemical Abstracts Service.

The list of uses to which you can put the tapes, compiled during the production of the printed CT, is almost endless. Indexes for the chemical journals in your company or institutional library which are covered by CT can be generated on an author, selected keyword, or title basis (or any combination of the three). Bibliographies on particular subjects that pertain to your work (reactivity of the phenanthrolines, crystal structure of ternary silicides, metabolism of porphyrins, etc.) can be compiled. Keyword indexes for any number of terms which you may suggest can be generated. Correlative machine searches can be conducted (mice that eat cheese, mice that eat cheddar cheese and Swiss cheese, white mice that eat cheddar cheese but not Swiss cheese, white mice that eat cheddar cheese or Swiss cheese, etc.) to any degree of specificity.

Answers can be in the form of bibliographies, author indexes, keyword indexes or any combination

of the three. AND, all of these indexes, bibliographies, etc., can easily be duplicated and distributed to members of your staff at very low cost. No matter how you choose to use the tapes, you are screening a vast amount of unnecessary material from information which is of specific interest to you.

This tape searching service is offered in two forms—CAS will send you tapes on a biweekly basis, along with a user's manual and a searching program for an IBM 1401/1410 system, or CAS will perform the biweekly search of the tapes for you in Columbus.

The subscription price includes a \$1,500-per-year base rate plus a use charge of \$5 for each scientist at the subscriber's address who will use the service or who will benefit from its use. For searches performed by CAS, the rate is based on one search per set of terms per issue of CT, and an additional charge of \$100 per hour for computer use time is made.

*Direct inquiries to Mr. E. H. Heilman at CAS, Ohio State Univ., Columbus, Ohio 43210. and direct orders to the ACS, 1155 16th St., N.W., Washington, D. C. 20036.*

The Activation Energy of Viscous Flow of Pure Water and Sea Water in the Temperature Region of Maximum Density . . . . .	<b>R. A. Horne, R. A. Courant, D. S. Johnson, and F. F. Margosian</b>	3988
Activity Coefficients of Sodium Chloride in Aqueous Three-Component Solutions by Cation-Sensitive Glass Electrodes . . . . .	<b>R. D. Lanier</b>	3992
Infrared Spectra and Bonding of Nitric Oxide Adsorbed on Nickel and Iron . . . . .	<b>George Blyholder and Marvin C. Allen</b>	3998
Potentiometric Titration of Stereoregular Polyelectrolytes . . . . .	<b>Mitsuru Nagasawa, Takashi Murase, and Kotaro Kondo</b>	4005
Tracer Diffusion in Binary Solutions Subject to a Dimerization Equilibrium . . . . .	<b>R. H. Stokes</b>	4012
Electrokinetic Flow in a Narrow Cylindrical Capillary . . . . .	<b>C. L. Rice and R. Whitehead</b>	4017
Application of a High Intensity, Multislit Rayleigh Interferometer to Sedimentation Studies . . . . .	<b>Irwin H. Billick and Robert J. Bowen</b>	4024

#### NOTES

The Enthalpy of Formation and the Dissociation Energy of Thallium Monofluoride . . . . .	<b>Daniel Cubicciotti and Gettis L. Withers</b>	4030
The Temperature Coefficient of Conductance of Aqueous Sodium Sulfate around 32.4° . . . . .	<b>Robert L. Kay, George W. Vidulich, and Thomas Vituccio</b>	4033
$\gamma$ -Radiolysis of Ethylene Sensitized by "Inert" Gases . . . . .	<b>A. Delle Site and A. Mele</b>	4033
The Thermodynamic and Physical Properties of Beryllium Compounds. VIII. Heat of Fusion and High-Temperature Heat Capacity of Beryllium Oxide . . . . .	<b>Michael A. Greenbaum, Justine Weiher, and Milton Farber</b>	4035
Salt Effects on Nonionic Association Colloids . . . . .	<b>Pasupati Mukerjee</b>	4038
Transitions in Gelatin and Vitrified Gelatin-Water Systems . . . . .	<b>Joseph V. Koleske and Joseph A. Faucher</b>	4040
A Rotating-Disk Thermocell. I. Theory . . . . .	<b>Benson R. Sundheim and Werner Sauerwein</b>	4042
The Vapor Pressure and Heat of Sublimation of Chromium . . . . .	<b>D. S. Dickson, J. R. Myers, and R. K. Saxer</b>	4044

#### COMMUNICATIONS TO THE EDITOR

Photosensitization of Carbon Dioxide with Hg 6 <sup>31</sup> P <sub>i</sub> Atoms . . . . .	<b>C. M. Wolff and Richard Pertel</b>	4047
Effects of Oxygen Adsorbed in the Skin of a Platinum Electrode on the Determination of Carbon Monoxide Adsorption . . . . .	<b>Theodore B. Warner and Sigmund Schuldiner</b>	4048
The Correction for Electrode Oxidation in the Estimation of Adsorbed CO on Smooth Platinum by Anodic Stripping . . . . .	<b>S. B. Brummer</b>	4049
On the Number of Hydroxyl Groups at the Exterior Surfaces of Faujasite Crystals . . . . .	<b>G. T. Kerr, E. Dempsey, and R. J. Mikovsky</b>	4050
A Direct Measurement of Surface Charge in the Presence of an Electrode Reaction . . . . .	<b>James N. Butler and Mary L. Meehan</b>	4051

# So you're taking another degree

If that's news to you, stop and think about it for a minute. Haven't you learned enough on the job to add up to another degree or two?

And don't you agree that you have to keep learning—or find yourself working with outdated methods, on old materials, with theories no longer accepted? Things happen fast in modern science. One way for you to maintain your technical competence is by getting new information from the following:

**The Journal of Organic Chemistry**  
**The Journal of Physical Chemistry**  
**Journal of the American Chemical Society**  
**Biochemistry**  
**Journal of Agricultural and Food Chemistry**  
**Journal of Medicinal Chemistry**  
**Journal of Chemical and Engineering Data**  
**I&EC**  
**I&EC Process Design and Development**  
**I&EC Fundamentals**  
**I&EC Product Research and Development**  
**Journal of Chemical Documentation**  
**Inorganic Chemistry**  
**Chemical Reviews**  
**Analytical Chemistry**

Select from these research journals the ones which cover your own professional interests. Subscribe to them . . . and read them regularly. It's the best way to keep educated . . . and keep your performance at the optimum level.

Order from:

**American  
Chemical  
Society**

1155 Sixteenth Street, N. W.  
Washington, D. C. 20036

## AUTHOR INDEX

- Adler, G., 3712  
 Allen, M. C., 3998
- Beatty, D. A., 3920  
 Benson, S. W., 3898  
 Billick, I. H., 4024  
 Blyholder, G., 3998  
 Boggs, J. E., 3727  
 Bonner, O. D., 3886  
 Bowen, R. J., 4024  
 Boyd, R. H., 3906  
 Breazeale, W. H., 3886  
 Brinen, J. S., 3791  
 Brummer, S. B., 4049  
 Butler, J. N., 3817, 4051
- Caplan, S. R., 3801  
 Chapman, I. D., 3949  
 Clark, R. K., 3682  
 Coffey, D., Jr., 3727  
 Copeland, B. K. W., 3700  
 Courant, R. A., 3988  
 Cubicciotti, D., 3910, 3916, 4030  
 Cullinan, H. T., Jr., 3941
- Davis, M. I., 3727  
 Delle Site, A., 4033  
 Dempsey, E., 4050  
 Dickson, D. S., 4044  
 Dillard, J. G., 3893  
 Durig, J. R., 3886
- Eick, H. A., 3705  
 Emerson, M. F., 3718  
 Evans, D. F., 3878
- Farber, M., 4035  
 Faucher, J. A., 4040  
 Flanagan, T. B., 3773  
 Friedman, M. E., 3795  
 Frisch, M. A., 3863  
 Fujita, H., 3981
- Gaynor, A. J., 3782  
 Goldberg, P., 3696  
 Gordon, B. E., 3833  
 Greenbaum, M. A., 4035  
 Grove, E. L., 3782  
 Guilbault, G. G., 3696
- Hair, M. L., 3949  
 Hanna, R., 3846  
 Hanson, H. P., 3727  
 Harteck, P., 3964  
 Haugen, G., 3898  
 Hersh, C. K., 3782  
 Hirt, R. C., 3791  
 Holtzer, A., 3718  
 Hormats, E. I., 3677  
 Horne, R. A., 3988
- Ikeda, T., 3755  
 Ise, N., 3690
- Jenkins, R. C. L., 3785  
 Johnson, D. S., 3988  
 Johnson, J. W., 3916
- Kanda, F. A., 3867  
 Katzin, L. I., 3708  
 Kay, R. L., 3878, 4033  
 Keller, D. V., 3867
- Keneshea, F. J., 3910  
 Kerr, G. T., 4050  
 Kiser, R. W., 3893  
 Kobatake, Y., 3981  
 Koleske, J. V., 4040  
 Kondo, K., 4005  
 Koren, J. G., 3791  
 Kramer, D. N., 3696  
 Kraus, K. A., 3968  
 Kreevoy, M. M., 3814
- Lamm, M. E., 3872  
 Lanier, R. D., 3992  
 Levy, J. B., 3700  
 Lichtin, N. N., 3673  
 Lieberman, M. L., 3973  
 Lifshitz, C., 3731, 3737, 3741, 3746  
 Locke, D. C., 3768  
 Long, F. A., 3731, 3737, 3741, 3746
- Maciel, G. E., 3920, 3925  
 Macur, G., 3782  
 Marcinkowsky, A. E., 3968  
 Margosian, F. F., 3988  
 Margrave, J. L., 3863  
 Matsumoto, M., 3755  
 McDonald, R. A., 3839  
 Meehan, M. L., 4051  
 Mele, A., 4033  
 Mikovsky, R. J., 4050  
 Miller, A. R., 3826  
 Mukerjee, P., 4038  
 Murase, T., 4005  
 Myers, J. R., 4044
- Nagasawa, M., 4005  
 Nelson, R. C., 3833  
 Neville, D. M., Jr., 3872  
 Nishizaki, Y., 3690
- Oetting, F. L., 3839  
 Okubo, T., 3690  
 Olmstead, H. D., 3791
- Paoletti, P., 3759  
 Passaglia, E., 3955  
 Pertel, R., 4047  
 Petropoulos, J. H., 3712  
 Phillips, H. O., 3968
- Reeves, R. R., Jr., 3964  
 Rice, C. L., 4017
- Saraf, D. N., 3752  
 Sauerwein, W., 4042  
 Savitsky, G. B., 3925  
 Saxer, R. K., 4044  
 Scher, H. B., 3814  
 Scheraga, H. A., 3722, 3795  
 Schmidt, H. H., 3682  
 Schmidt, P. W., 3849  
 Schrier, E. E., 3722  
 Schuldiner, S., 4048  
 Searcy, A. W., 3826  
 Shiga, T., 3805  
 Silva, W. J., 3916  
 Simons, J. W., 3773  
 Sinfelt, J. H., 3857  
 Singh, A., 3708  
 Smith, M. L., 3833  
 Stern, J. H., 3759
- Stevens, R. M., 3867  
 Stokes, R. H., 4012  
 Stromberg, R. R., 3955  
 Sturgeon, G. D., 3705  
 Sundheim, B. R., 4042
- Takeguchi, N., 3981  
 Taylor, W. F., 3857  
 Thomas, M. R., 3722  
 Thompson, B. A., 3964  
 Tien, H. T., 3763  
 Toor, H. L., 3941  
 Toyoshima, Y., 3981  
 Tutas, D. J., 3955
- Unterleitner, F. C., 3677
- Vacca, A., 3759  
 Vidulich, G. A., 4033  
 Vituccio, T., 4033
- Wahlbeck, P. G., 3973  
 Wang, C., 3906  
 Warner, T. B., 4048  
 Weiher, J., 4035  
 Whitehead, R., 4017  
 Wilson, J. W., 3673  
 Withers, G. L., 4030  
 Witherspoon, P. A., 3752  
 Wolff, C. M., 4047
- Yao, Y.-F. Y., 3930  
 Yates, D. J. C., 3857
- Zawoyski, C., 3878

# The Naming and Indexing of Chemical Compounds from **CHEMICAL ABSTRACTS**

This succinct volume represents the first major revision of the CHEMICAL ABSTRACTS' Nomenclature Manual since 1945. With its description of up-to-date nomenclature and indexing practices, it is an indispensable tool for gaining maximum use of the Subject and Formula Indexes to CHEMICAL ABSTRACTS. It is invaluable to anyone concerned with chemical information since it provides a basic guide to good systematic nomenclature.

Here CA's broad indexing policies for General, Biological, Inorganic and Organic fields of chemistry are set forth. Detailed rules are given in 433 sections for the naming and indexing of inorganic and organic compounds by classes; numerous examples are shown with easy-to-comprehend structural formulas. Useful appendices list anions, inorganic and organic groups and radicals, and organic suffixes by both name and formula. Other features include a list of miscellaneous chemical prefixes, a classified bibliography and a subject index.

Every chemist who wants to search the literature with top efficiency can use this book to advantage.

**Paper bound.**

**98 pages.**

**Price: \$5.00**

---

*Order from:* **Chemical Abstracts Service**

**The Ohio State University, Columbus 10, Ohio**

*and make checks payable to:* **AMERICAN CHEMICAL SOCIETY**

# THE JOURNAL OF PHYSICAL CHEMISTRY

Registered in U. S. Patent Office © Copyright, 1965, by the American Chemical Society

VOLUME 69, NUMBER 11 NOVEMBER 15, 1965

## The Radiolysis of Methanol and Methanolic Solutions. IV.

### The Effect of Water on Peroxide Yields<sup>1,2</sup>

by Norman N. Lichtin and Judith W. Wilson

Department of Chemistry, Boston University, Boston, Massachusetts (Received July 7, 1965)

---

Radiolytically generated or added approximately  $10^{-4}$  to  $10^{-3}$  M  $H_2O_2$  is unstable in dry, aerated methanolic solution and decays by a first-order process. As little as 0.1 wt. % of  $H_2O$  inhibits the decay significantly. The nature of the protective action of water is obscure.  $G(CH_3OOH)$  appears to be approximately 0.2, in agreement with a previously assigned value of  $G_{CH_3}$ .

---

#### Introduction

It was reported<sup>3</sup> a few years ago that  $G(H_2O_2)$  from the  $Co^{60}$   $\gamma$ -radiolysis of aerated methanol is sharply dependent on water concentration. Thus, it was found that peroxide production is not detectable in dry methanol but that  $G(H_2O_2)$  increases abruptly upon addition of water and reaches a value of about 2.8 with a water concentration somewhat less than 1 wt. %. Higher water concentrations up to 6.5 wt. % were found to have no further effect on  $G(H_2O_2)$ . Subsequent investigation of this phenomenon, reported herein, has established that the effect of water is on the postradiolytic decay of  $H_2O_2$  and that  $G(H_2O_2)$  is not significantly affected by modest concentrations of water.

#### Experimental Section

**Materials.** Eastman Spectrograde methanol was refluxed with 0.5 wt. % of  $NaBH_4$  for approximately 3 hr. and then rectified on a Todd column at a 10:1 reflux ratio. The middle third of the distillate was dried by refluxing with 2 wt. % of magnesium turnings

for approximately 10 hr. while protected from atmospheric moisture and  $CO_2$  by Drierite and Ascarite. It was then distilled under similar protection from the same  $\text{T-joint}$  equipped apparatus through an attached Vigreux column into a collection flask. The flask was transferred as quickly as possible to a drybox (which was kept under slight positive pressure of Matheson prepurified nitrogen) where the methanol was aerated with air which had been passed through cotton, Drierite, and Ascarite. Aliquots were then transferred in the drybox to irradiation cells. Solutions of stock  $H_2O_2$  were prepared in methanol which had been purified in the same way.

Other reagents, used without purification, were Baker

---

(1) Research carried out under the auspices of the U. S. Atomic Energy Commission under Contract AT(30-1) 2383. This report is based on a thesis which was submitted to the Graduate School of Boston University in partial fulfillment of the requirements for the A.M. degree, granted in June 1964.

(2) For paper III in this series, cf. S. U. Choi and N. N. Lichtin, *J. Am. Chem. Soc.*, **86**, 3948 (1964).

(3) N. N. Lichtin, L. A. Rosenberg, and M. Imamura, *ibid.*, **84**, 3587 (1962).



Analyzed or Fisher Certified grade except that chromotropic acid was Eastman Practical grade and methyl borate was obtained from Matheson Coleman and Bell. Water was redistilled in Pyrex.

**Irradiation.** A Schwarz-Allen type source<sup>4</sup> provided dose rates<sup>5</sup> to methanol of  $1.5$  to  $2.1 \times 10^{17}$  e.v. ml.<sup>-1</sup> min.<sup>-1</sup>. Total doses fell in the range  $8$ – $26 \times 10^{17}$  e.v. ml.<sup>-1</sup>. Irradiations were carried out in glass-stoppered 30-ml. test tubes with no more than 1 ml. of free air space. Under these conditions variations in consumption of O<sub>2</sub> do not affect  $G(\text{peroxide})$ .<sup>2</sup> Aliquots for analysis were removed in the drybox under a positive pressure of Matheson prepurified nitrogen.

**Analyses.** Hydrogen peroxide was determined by the method of Hochanadel<sup>6</sup> with the aid of a Bausch and Lomb Spectronic 505 spectrophotometer. A calibration curve, determined with 1-ml. aliquots of aqueous solutions of known concentration, provided the value: molecules of H<sub>2</sub>O<sub>2</sub> ml.<sup>-1</sup> =  $1.176 \times 10^{18} \times \text{O.D.}$  Radiolytic H<sub>2</sub>O<sub>2</sub> was distinguished from (presumed) CH<sub>3</sub>OOH by the procedure of Johnson, *et al.*<sup>7</sup> This procedure was verified by following the change in absorbance at 350 m $\mu$  of radiolyzed methanol as a function of time after it was subjected to the Hochanadel procedure.<sup>6</sup> Maximum and constant absorbance was reached in about 2 hr. Accordingly, H<sub>2</sub>O<sub>2</sub> and the sum of H<sub>2</sub>O<sub>2</sub> plus CH<sub>3</sub>OOH were determined from the absorbance measured within a few minutes of mixing the reagents and after several hours, respectively.

The decay of nonradiolytic methanolic H<sub>2</sub>O<sub>2</sub> was followed by removing aliquots from a closed 200-ml. bulb through a rubber syringe cap with a hypodermic syringe.

Formaldehyde was determined by the chromotropic acid method<sup>8</sup> with the aid of a Bausch and Lomb Spectronic 505 spectrophotometer. A calibration curve determined with 1-ml. aliquots of methanolic solutions of known concentration provided the value: molecules of CH<sub>2</sub>O ml.<sup>-1</sup> =  $1.944 \times 10^{18} \times \text{O.D.}$

## Results

The postradiolytic decay of H<sub>2</sub>O<sub>2</sub> in "dry" methanol is illustrated in Figure 1 by data from three typical samples. The decay process is apparently first order in H<sub>2</sub>O<sub>2</sub> but the specific rate is poorly reproducible under the conditions employed. The fact that these experiments did not employ a thermostat can be responsible for only a minor part of the scatter. On the basis of data presented below, the poor reproducibility can be ascribed, at least in part, to variation in the water content of the "dry" methanol. Ten experiments, including those summarized in Figure 1,

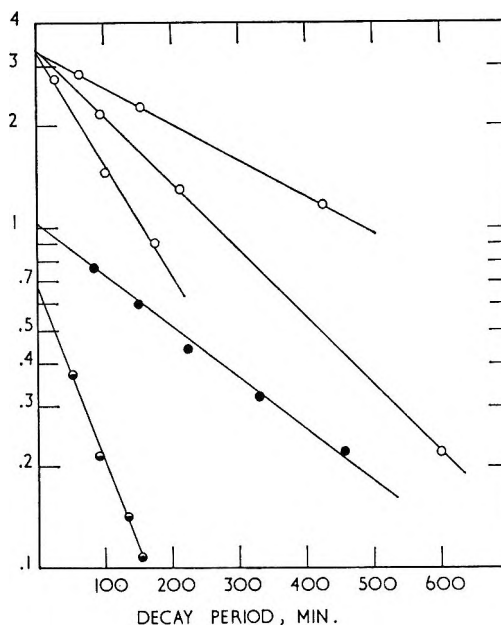


Figure 1. Decay of methanolic H<sub>2</sub>O<sub>2</sub>. Radiolytic H<sub>2</sub>O<sub>2</sub> at room temperature: O (ordinate in units of molecules/100 e.v. absorbed). Made up from 3% aqueous H<sub>2</sub>O<sub>2</sub>: ● (ordinate in units of  $10^{-3} M$ ). Made up from 30% aqueous H<sub>2</sub>O<sub>2</sub>: ◐ (ordinate in units of  $10^{-3} M$ ).

yielded a mean half-life of 190 min. with a standard deviation of 85 min. This wide spread was not, however, reflected in the  $G(\text{H}_2\text{O}_2)$  values extrapolated to "zero time", *i.e.*, the instant of completion of irradiation<sup>9</sup> which averaged to 3.28 with a standard deviation of 0.12.

The effect of water added prior to radiolysis is illustrated in Table I which lists representative data obtained with two radiolysis samples. The effect of water added after radiolysis is illustrated in Figure 2.

The fact that other products of radiolysis are not essential to the decay process was demonstrated by experiments employing methanolic solutions prepared by serial dilution in the drybox of 3 or 30% aqueous hydrogen peroxide to concentrations of  $0.7$ – $2 \times 10^{-3} M$  in H<sub>2</sub>O<sub>2</sub>. Data of two typical experiments are included in Figure 1. Although these solutions were maintained at constant temperature, the half-lives

(4) H. A. Schwarz and A. O. Allen, *Nucleonics*, **12**, 58 (1954).

(5) M. Imamura, S. U. Choi, and N. N. Lichtin, *J. Am. Chem. Soc.*, **85**, 3565 (1963).

(6) C. J. Hochanadel, *J. Phys. Chem.*, **56**, 587 (1952).

(7) G. R. A. Johnson and G. A. Salmon, *ibid.*, **65**, 177 (1961); G. R. A. Johnson and J. Weiss, *Chem. Ind. (London)*, 358 (1955).

(8) C. E. Briker and H. R. Johnson, *Ind. Eng. Chem., Anal. Ed.*, **17**, 400 (1945).

(9) It should be noted that irradiation times were of the order of 10 min., *i.e.*, short compared with the half-life of decay.

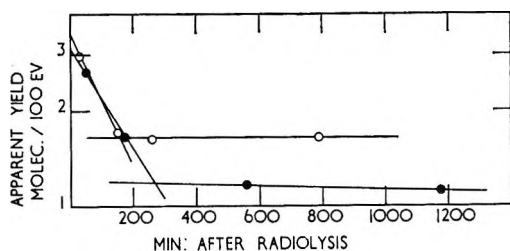


Figure 2. Inhibition of decay of radiolytic  $\text{H}_2\text{O}$  by water; 1.1 wt. % water added 180 min. after radiolysis, O; 0.55 wt. % water added 219 min. after radiolysis, ●.

Table I: Effect of Water, Added before Radiolysis, on the Postradiolytic Decomposition of Methanolic  $\text{H}_2\text{O}_2$

Wt. % added $\text{H}_2\text{O}$	Apparent $G(\text{H}_2\text{O}_2)$ , <sup>a</sup> molecules/100 e.v.		
	Initial	24 hr.	72 hr.
None	3.23 <sup>b</sup>	0	0
0.27	3.34 <sup>b</sup>	0	0
1.58	3.29 <sup>b</sup>	2.87	...
None	3.04 <sup>c</sup>	0	0
0.53	3.04 <sup>c</sup>	2.49	1.89

<sup>a</sup> Determined at the indicated time after completion of irradiation. <sup>b</sup> Two minutes. <sup>c</sup> One hour.

for their (first-order) decay were not reproducible. Four solutions prepared from 3%  $\text{H}_2\text{O}_2$  which contained 0.1 to 0.2 wt. % water inescapably added along with peroxide as well as approximately  $10^{-5}$  M acetophenetidine decayed with an average half-life of  $232 \pm 108$  min. at  $25.0^\circ$ . The fact that a solution prepared from 30%  $\text{H}_2\text{O}_2$ , and which therefore contained only 0.01% added water, decayed with a half-life of only 58 min. at  $25.0^\circ$  again suggests that adventitious water is responsible for the variation in rate of decay. Rigorous vacuum line techniques would apparently have to be employed to limit the presence of adventitious water sufficiently to permit evaluation of true decay rates and of the kinetic order of water in the inhibitory process.

The effect of other products of radiolysis on the rate of decay was evaluated semiquantitatively by comparing the half-times for decay of pairs of methanolic solutions of  $\text{H}_2\text{O}_2$  of identical history except that one member of a pair was irradiated immediately after its preparation. Similar results were obtained with solutions prepared from 3 and 30%  $\text{H}_2\text{O}_2$ . In every one of seven cases irradiation produced a net increase in  $\text{H}_2\text{O}_2$  concentration and the specific rate of decay of the  $\text{H}_2\text{O}_2$  in the irradiated solution was greater than in its unirradiated analog even though water is a product of the radiolysis of methanol.<sup>10</sup> The mean ratio of the

first-order rates was 1.8 but the usual scatter of the data did not permit any correlation to be made with magnitude of dose.

No systematic study of products arising from the decay of hydrogen peroxide was undertaken. It was found, however, that a small amount of formaldehyde was formed, of the order of one molecule for every ten molecules of peroxide decomposed. This relationship also maintained when added formaldehyde (approximately  $10^{-3}$  M) was present initially even though this solute seemed to accelerate the decay somewhat.

The effect of methyl borate on the decay of methanolic  $\text{H}_2\text{O}_2$  was inspected because of its relevance to studies<sup>3,5</sup> of the radiolysis of oxygenated methanol by  $^{10}\text{B}(n,\alpha)^7\text{Li}$  recoils in which methyl borate was used as the source of boron. It was found that as little as 0.15 wt. %, added before irradiation, rendered the rate of decay of radiolytic  $\text{H}_2\text{O}_2$  at room temperature negligible. Thus methyl borate appears to be even more effective than water in inhibiting the decay of  $\text{H}_2\text{O}_2$  in methanolic solution.

Several experiments established that sulfuric acid also stabilizes methanolic  $\text{H}_2\text{O}_2$ . Thus no postradiolytic decay was observed for as long as 72 hr. at room temperature in solutions to which 0.1 to 0.3 wt. % of concentrated sulfuric acid had been added prior to irradiation.

If the increase in optical density observed with aliquots of irradiated aerated methanol during the first 2 hr. after treatment with Hockadel's reagent<sup>6</sup> is ascribed to the slow reaction of iodide with  $\text{CH}_3\text{OOH}$ ,<sup>7</sup> then a value of  $G(\text{CH}_3\text{OOH})$  can be estimated from the data. A number of such measurements were in good agreement that  $G(\text{CH}_3\text{OOH})$  is 0.2. This value is consistent with the reported<sup>2</sup> value of  $G_{\text{CH}_3}$  derived from the limiting reduction of  $G(\text{CH}_4)$  by oxygen. That  $\text{CH}_3\text{OOH}$  decays at a slower rate in dry methanol than does  $\text{H}_2\text{O}_2$  was indicated by the fact that even after decay of radiolytic  $\text{H}_2\text{O}_2$  was complete, more than half the initial concentration of  $\text{CH}_3\text{OOH}$  still remained. Typical data for aliquots of the same sample taken at different times after radiolysis are presented in Table II.

## Discussion

Lack of information concerning the nature of the products renders any attempt at explanation of the data highly speculative. Formaldehyde, the only potential product investigated, appears to be at most a minor one. It is not known whether methanol is attacked to any significant degree in the decay process.

(10) N. N. Lichtin, *J. Phys. Chem.*, **63**, 1444 (1959).

The role of photolysis in the decay process is also obscure. Samples were exposed to illumination by fluorescent room lights through the window of the drybox during storage. No attempt was made to exclude or to test the effect of light. Nevertheless, whether water interferes with a thermal process or a photolytic one or a combination of the two, its inhibitory action appears to be highly unusual.

**Table II:** Change in Absorbance at 350  $m\mu$  with Time after Mixing of Radiolyzed Methanol with Hochanadel's Reagent<sup>a</sup>

Decay time before analysis, min.	Time after mixing, <sup>b</sup> min.	O.D.	G(peroxide), molecules/100 e.v.
95	9	0.225	2.18
	55	0.243	2.36
	92	0.243	2.36
	152	0.253	2.46
	191	0.251	2.44
1215	5	0.000	0
	35	0.000	0
	60	0.008	0.08
	100	0.016	0.16
	135	0.019	0.18
	167	0.016	0.16

<sup>a</sup> Dose =  $2.42 \times 10^{18}$  e.v./ml. <sup>b</sup> Five-milliliter aliquots of radiolyzed solution.

It is conceivable that this action is due to the interaction of water with trace impurities which catalyze the decay process or processes, but we can offer no specific suggestion as to what these may be. Suspect oxidizable or reducible inorganic ions are active in aqueous solution.

An alternative type of explanation is based on the selective interaction of water with  $H_2O_2$ . There is considerable evidence supporting the possibility of such

an interaction but it must be recognized at the outset that it is not at all apparent why association with water should stabilize  $H_2O_2$ . Thus, the value of the dielectric constant of aqueous  $H_2O_2$  is maximum in the vicinity of 0.35 mole fraction of  $H_2O_2$ ,<sup>11</sup> at about the same composition as that of the crystalline hydrate,<sup>12,13</sup>  $H_2O_2 \cdot 2H_2O$ . Since, in the present work, the molar ratio of water to  $H_2O_2$  in "wet" solutions was at least 100, the formation of this species is at least possible. That water might complex with  $H_2O_2$  in the presence of a molar excess of methanol over water which was also of the order of 100-fold is supported by the facts that  $H_2O_2$  is relatively acidic and methanol is a weaker base than water.<sup>14</sup> (This is not meant to imply that complete proton transfer occurs. Selective hydrogen bonding is more reasonable.) It is particularly relevant that the limiting conductance of HCl falls half the distance from its value in dry methanol, characteristic of proton jump conduction,<sup>15</sup> to the value observed in solutions containing small amounts of water, characteristic of the conductance of  $H_3O^+Cl^-$ , when the concentration of water is approximately 0.25  $M$ ,<sup>16</sup> that is, the same as its concentration when inhibition of decay of  $H_2O_2$  becomes important.

The available data do not indicate whether the stabilizing action of  $H_2SO_4$  is due to its acidity or to  $HSO_4^-$  or  $SO_4^{2-}$  or to the formation of persulfate ion. Further comment on the action of sulfuric acid or of methyl borate is not warranted.

(11) P. M. Gross, Jr., and R. C. Taylor, *J. Am. Chem. Soc.*, **72**, 2075 (1950).

(12) P. A. Giguere and O. Maass, *Can. J. Res.*, **188**, 66 (1940).

(13) I. Olovsson and D. H. Templeton, *Acta Chem. Scand.*, **14**, 1325 (1960).

(14) Cf. R. P. Bell, "The Proton in Chemistry," Cornell University Press, Ithaca, N. Y., 1959, pp. 43-45.

(15) E. Grunwald, C. F. Jumper, and S. Meiboom, *J. Am. Chem. Soc.*, **84**, 4664 (1962).

(16) Cf. R. W. Gurney, "Ionic Processes in Solution," McGraw-Hill Book Co., Inc., New York, N. Y., 1953, pp. 74-76.

# Measurement of the Diffusion of Oxygen in Polymers by Phosphorescent Quenching<sup>1</sup>

by Ellis I. Hormats and Fred C. Unterleitner

Quantum Physics Laboratory, General Dynamics, Electronics Division, Rochester, New York 14601  
(Received December 28, 1964)

The rate of diffusion of oxygen into bulk polymers may be measured through use of the quenching of phosphorescence of aromatic organic compounds dissolved in the polymer. The diffusivity of oxygen from the pure gas into polymethyl methacrylate was found to be  $3.3 \times 10^{-9}$  cm.<sup>2</sup>/sec. at 22° while from air it was found to be  $2.3 \times 10^{-9}$  cm.<sup>2</sup>/sec. The measured diffusivity is independent of the phosphor concentration used for the measurements.

## Introduction

The usual method for measuring the diffusion of gases through plastic materials is based on the technique of measuring the quantity of gas that permeates a thin film of the material,<sup>2</sup> thus limiting measurements to those plastics that may be obtained as thin films. Other methods based on measurements of the rate of gas sorption<sup>3a</sup> and the oxygen bleaching of radiation-induced color centers<sup>3b</sup> have been developed. Comprehensive reviews have been recently published.<sup>4</sup> This paper presents a method of measuring the rate of diffusion of oxygen in transparent bulk polymers based on the quenching by oxygen of phosphorescence of organic materials dissolved in the polymer.

It has been observed in this laboratory and independently by others<sup>5</sup> that plastic rods in which certain organic phosphors have been dissolved to show, over a period of time, a phosphorescent core surrounded by a dark region when illuminated by ultraviolet light. With time this core becomes smaller until it eventually disappears. This effect depends on the concentration of oxygen in the plastic and so may be used to measure the rate of diffusion of oxygen into the polymer. The line of demarcation, the terminator, is assumed to occur at the minimum concentration of oxygen required to quench the phosphorescence of the activator. The quenching is due to a nonradiative energy-transfer process and is completely reversible. This has been demonstrated by restoration of the phosphorescence

when oxygen is removed by diffusion outward into a vacuum.

Polymethyl methacrylate was chosen as the polymer for study as it is being used extensively as a glassy matrix for triplet state studies. The organic phosphor should be one that shows oxygen quenching, that phosphoresces in the blue or green region so it may be easily photographed, that has well-separated phosphorescent and fluorescent bands so fluorescent light may be easily removed by an optical filter, and that has a high quantum efficiency at room temperature so the phosphorescent emission will be much brighter than the background. Triphenylene meets these requirements so it was used as the phosphor.

## Experimental Section

**Materials.** Monomeric methyl methacrylate (Rohm

(1) Presented at the 147th National Meeting of the American Chemical Society, Philadelphia, Pa., April 1964, before the Division of Polymer Chemistry.

(2) (a) ASTM Procedure D1434; *ASTM Std.*, **9**, 460 (1958); (b) P. Meares, *J. Am. Chem. Soc.*, **76**, 3415 (1954); (c) V. Stannett, M. Szwarc, R. Bhargava, J. Meyer, A. Myers, and C. Rogers, "Permeability of Plastic Films and Coated Papers to Gases and Vapors," TAPPI Monograph Series No. 23, TAPPI, New York, N. Y.

(3) (a) A. S. Michaels, W. R. Veith, and H. J. Bixler, *J. Polymer Sci.*, **B1**, 19 (1963); (b) R. E. Barker, *ibid.*, **58**, 533 (1962).

(4) (a) N. N. Li, R. B. Long, and E. J. Henley, *Ind. Eng. Chem.*, **57**, 19 (1965); (b) C. E. Rogers, "Physics and Chemistry of the Organic Solid State," Vol. II, Interscience Publishers, Inc., 1965, Chapter 6.

(5) (a) M. A. El-Sayed, *J. Opt. Soc. Am.*, **53**, 797 (1963); (b) M. Windsor, *Chem. Eng. News*, **41**, 53 (1963); (c) G. Oster, N. Geacintov, and A. U. Khan, *Nature*, **196**, 1089 (1962).

& Haas) inhibited with 25 p.p.m. of hydroquinone was thoroughly purified.<sup>6</sup> Triphenylene (Rutgerswerke-Aktiengesellschaft) was recrystallized once from alcohol.  $\alpha,\alpha$ -Azodiisobutyronitrile (Borden Chemical Co.), the polymerization catalyst, was used as received. The polymerized samples were prepared by dissolving the requisite amount of triphenylene and catalyst in the monomer. The catalyst concentration in all cases was 0.033% by weight; the phosphor concentration is presented later. The solution was then transferred to Pyrex polymerization tubes, 1.0-cm. i.d. and 30 cm. long, with a bulb of 2.5-cm o.d. and 6 cm. long at one end and an 18/9 ball joint at the other, for connecting to a vacuum system. Set A was sealed off with no further treatment. Sets B and C were thoroughly degassed by repeated freezing and evacuation and then filled to 1 atm. with dry nitrogen, before being sealed, except as indicated. The polymerization was carried out with the monomer in the 1.0-cm. diameter section at 42° for 5 days, at 65 and 75° each for 1 day in a water bath, and at 115° for 1 day in an oven, followed by slow cooling to room temperature. Samples were removed, cut to length, and their ends squared and polished using a series of five grades of emery paper and a buffing wheel. Care was taken to prevent contamination of the cylindrical surface during these operations. The rods for sets A and C were placed into 25-mm. o.d.  $\times$  20-cm. Pyrex tubes with a flat Pyrex window at one end cemented in place by epoxy cement. The rods were supported at each end by a copper wire ring. These tubes were then sealed to the vacuum system, evacuated, filled with the requisite atmosphere, and sealed off. Not more than 2 hr. elapsed between opening the polymerization tube and the final seal-off. The rods for set B were kept in 50-ml. beakers in an aluminum desiccator over silica gel. The elevated temperature tubes for set A were placed in a water bath at the requisite temperature; the tubes at room temperature were stored in a cupboard. The diameters and lengths of all rods were measured with a micrometer before sealing.

The extensive purification of the monomeric methyl methacrylate was necessary to minimize phosphorescence of the polymer. Material, cleaned with sodium hydroxide only, had a strong, slowly decaying, yellow phosphorescence after polymerization. On the other hand, the extensively purified material had a barely detectable phosphorescence even at 77°K. The yellow phosphorescence is due to small traces of residual hydroquinone as indicated by the phosphorescent spectra. Also, some blue-green phosphorescence possibly due to peroxides was noted. This was particularly strong when benzoyl peroxide was used as the

polymerization catalyst. When *t*-butyl hydroperoxide was used as the polymerization catalyst, it quenched the phosphorescence of triphenylene. Thus  $\alpha,\alpha$ -azodiisobutyronitrile, which had no deleterious effect, is the polymerization catalyst most suited for this application.

*Measurements.* A photographic method was used for the measurement of the ratio of the diameter of the phosphorescent core to the sample diameter. This was necessary to minimize exposure of the sample to ultraviolet light as would be experienced if direct measurements were made with a filar eyepiece since it was observed that exposures to ultraviolet light caused the phosphorescent core to grow back into the quenched region at an initial rate of about 0.7%/min. The rod or the Pyrex tube, with the sample against the flat window, was supported horizontally in a frame about 5 cm. below and parallel to a Long Wave Mineralight (Ultraviolet Products, Inc.). The sample was photographed through a Wild M5 stereomicroscope at 3 $\times$  on Polaroid 3000 film using a Corning sharp cutoff CS3-70 filter (15% at 500 m $\mu$ , 75% at 520 m $\mu$ ) to filter out scattered ultraviolet light and fluorescence of both phosphor and polymer. With proper exposure, about 30 sec., both the core and the outer edge were clearly visible and separated by a dark area (Figure 1). The illumination of the edge is a light pipe effect from the central core. The measurements of the diameters were carried out using the Wild microscope at 3 $\times$  with a mechanical stage equipped with a micrometer reading to 0.001 in., the next place being estimated. Since the limit of the micrometer was 1.0 in., a 0.5000-in. gauge block was used to extent the range to cover the photograph.

*Restoration by Vacuum.* A partially quenched sample (A1) was placed in a 50-mm. diameter Pyrex tube, on one end of which was sealed a flat Pyrex

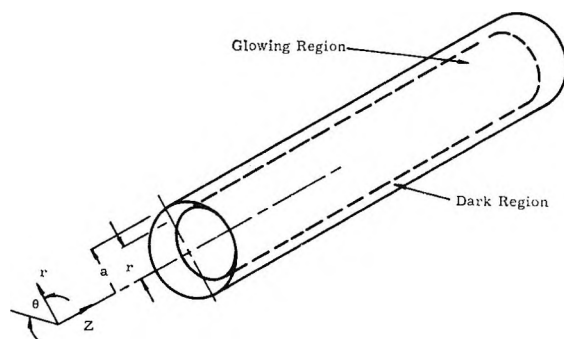


Figure 1. Coordinate system of partly quenched plastic rod.

(6) A. R. Schultz, *J. Phys. Chem.*, **65**, 967 (1961).

window. In a 15-mm. diameter side arm, a few grams of Wood's metal was placed to act as an oxygen getter. The assembly was evacuated on a high vacuum system to  $5 \times 10^{-5}$  torr and sealed off. The Wood's metal was melted by immersing the side arm in boiling water, to getter any oxygen present. The sample was observed at regular intervals as described above. After each observation the Wood's metal was again melted to getter released oxygen. After the sample had been kept under vacuum for about 2 weeks it was observed when the sample was viewed endwise under ultraviolet illumination that there was a glowing ring enclosing a dark ring and a glowing core. Within a few days more the glowing ring moved inward to merge with the glowing core. This indicates that the quenching oxygen in the outer layer diffuses outward dropping below the level for quenching near the outer surface, thus restoring the glow. The hump in oxygen concentration between these two regions drops as oxygen diffuses outward until its inhibiting effect on the triphenylene phosphorescence is removed and the two glowing regions coalesce. The spectrum of restored phosphorescence and the unquenched phosphorescence are identical, thus showing the complete reversibility of the process.

### Diffusion Equation

The reversible diffusion and solution of low molecular weight gases in polymers obey Henry's and Fick's laws with the diffusion coefficient independent of concentration.<sup>2b,c</sup> Expressed in cylindrical coordinates

$$\frac{\partial v}{\partial t} = D \left[ \frac{\partial^2 v}{\partial r^2} + \frac{1}{r} \frac{\partial v}{\partial r} + \frac{1}{r^2} \frac{\partial^2 v}{\partial \theta^2} + \frac{\partial^2 v}{\partial Z^2} \right] \quad (1)$$

where  $r$ ,  $\theta$ , and  $Z$  are the radial, angular, and axial coordinates, respectively,  $v$  is the concentration of the diffusing substance,  $t$  is the time, and  $D$  is the diffusion coefficient. Since the cylinder is completely surrounded by gas, diffusion is independent of  $\theta$ . Since the sample is long compared to its diameter and it is viewed from the end so the maximum diameter of the core is seen, diffusion may be considered to be independent of  $Z$ . At the start ( $t = 0$ ) the concentration of oxygen in the polymer is 0 ( $v = 0$ ). The concentration of oxygen in the surface of the polymer ( $r = a$ ) is constant ( $v = V$ ). This concentration  $V$  is proportional to the concentration of oxygen in the surrounding gas by Henry's law. Solving the equation by standard methods<sup>7</sup> under these restrictions gives

$$\frac{v}{V} = 1 - 2 \sum_{m=1}^{\infty} \frac{J_0(\beta_m R)}{\beta_m J_1(\beta_m)} \exp(-\beta_m^2 T) \quad (2)$$

where  $T = Dt/a^2$ ,  $R = r/a$ , and the  $\beta_m$  terms are the roots of the equation  $J_0(\beta_m) = 0$ . For large values of

$T$  the terms of eq. 2 with  $m \geq 2$  may be neglected to a first approximation. For example, at a  $T$  of 0.083, the term with  $m = 2$  is about 4.6%, and  $m = 3$ , about 0.05% of the first term. Thus eq. 2 may be put into the form

$$\ln J_0(\beta_1 R) = \ln Q + \beta_1^2 Dt/a^2 \quad (3)$$

where

$$Q = \frac{1}{2} [\beta_1 J_1(\beta_1)] (1 - v/V) = 0.624(1 - v/V) \quad (4)$$

Since the terminator corresponds to a certain concentration of oxygen, required to quench the phosphorescence in a given sample, it thus corresponds to a certain  $v/V$ . Thus  $Q$  is fixed for a given sample, and a semilog plot of  $J_0(\beta_1 R)$  vs.  $t$  will give a straight line for large  $t$ , the slope,  $S$ , being related to the diffusion coefficient by

$$D = Sa^2/\beta_1^2 \quad (5)$$

and the intercept at  $t = 0$  giving  $v/V$  through eq. 4. This is a consequence of the one-term approximation since the boundary condition that  $v = 0$  at  $t = 0$  for all  $r$  except  $r = a$  was used in solving the differential equation.

### Results and Discussion

The determinations of the diffusion coefficients and quenching concentrations were carried out using semilog plots. The resultant graphs for the different conditions are given in Figures 2 to 4 and summarized in Tables I to III. These semilog plots of  $J_0(\beta_1 R)$  vs. time were fitted to the experimental data by least-square calculations; the diffusion coefficient was obtained from the slope, and the quenching coefficient from the intercept. It was noted that the points representing long times (over 40 days) generally fell onto a straight line with the earlier points below. The earlier points deviate owing to contributions from the  $m = 2$  and greater terms. Calculation of these terms to  $m = 6$  for run B-1 at  $t = 10$ , using the  $D$  obtained from the least-square fit and applying this as a correction, lifted the value of  $J_0$  to the indicated point on Figure 3.

The results obtained from the one-term solution as presented in Tables I to III form the basis for the following conclusions.

**Diffusion Coefficient.** The small concentrations of activating molecules that must be dissolved in the polymer in this procedure did not affect the diffusivity, as shown by the constancy of  $D$  for a 100-fold change in triphenylene concentration (e.g., B-1, B-2, B-3).

(7) J. Crank, "Mathematics of Diffusion," Oxford University Press, London, 1956, p. 66, eq. 5.22, 5.24.

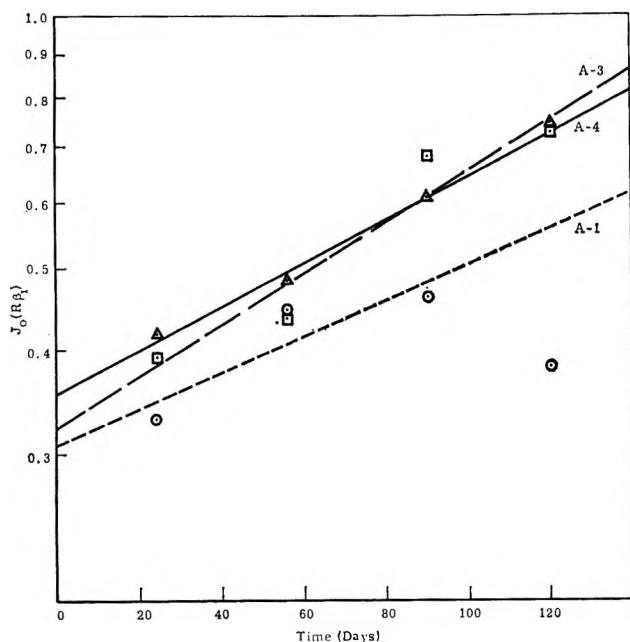


Figure 2. Time dependence of diffusion at various temperatures:  $\circ$ , ———, air, 22°, A-1;  $\square$ , - - - -,  $O_2$ , 22°, A-3;  $\triangle$ , ———, air, 72°, A-4.

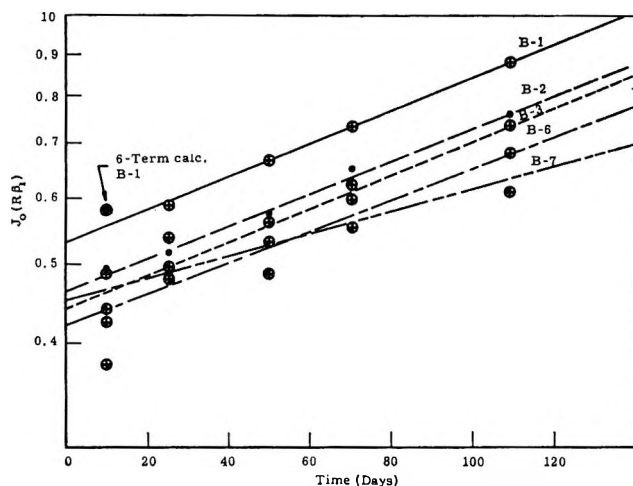


Figure 3. Time dependence of diffusion of oxygen from air at various triphenylene concentrations at 22°:  $\oplus$ , ———,  $437 \times 10^{-6}$  mole/g. of polymer, degassed monomer;  $\bullet$ , - - - -,  $43.7 \times 10^{-6}$  mole/g. of polymer, degassed monomer;  $\ominus$ , - - - -,  $4.37 \times 10^{-6}$  mole/g. of polymer, degassed monomer;  $\oplus$ , - - - -,  $437 \times 10^{-6}$  mole/g. of polymer,  $O_2$ -saturated monomer;  $\bullet$ , - - - -,  $4.37 \times 10^{-6}$  mole/g. of polymer,  $O_2$ -saturated monomer.

That the quenching is due to oxygen diffusion into the sample is clearly established since in the sample sealed in dry nitrogen (A-2) a nonphosphorescent layer did not appear, whereas those sealed in pure oxygen or air did show quenching.

Table I: Diffusion Coefficients and Quenching Ratio for Oxygen in Polymethyl Methacrylate

Run	$10^6 \times$ moles of triphenylene/g. of polymer	Temp., °C.	Gas	O.d., cm.	Diffusivity, $cm.^2 \text{ sec.}^{-1} \times 10^9$	Quenching ratio
A-1	43.9	22	Air	0.970	$2.3 \pm 0.7^a$	$0.51 \pm 0.05^a$
A-2	43.9	22	$N_2$	0.970	0.0	...
A-3	43.9	22	$O_2$	0.970	$3.3 \pm 0.5$	$0.48 \pm 0.04$
A-4	43.9	72	Air	0.970	$2.8 \pm 0.1$	$0.43 \pm 0.04$

<sup>a</sup> Precision based on least-square-curve-fitting statistics.

Table II: Effect of Concentration of Triphenylene on Diffusion Coefficient and Quenching Ratio<sup>a</sup>

Run	$10^6 \times$ moles of phosphor/g. of polymer	O.d., cm.	Diffusivity, $cm.^2 \text{ sec.}^{-1} \times 10^9$	Quenching ratio
B-1	437.0	0.993	$2.31 \pm 0.02^b$	$0.149 \pm 0.004^b$
B-2	44.0	0.980	$2.2 \pm 0.1$	$0.26 \pm 0.02$
B-3	4.26	0.985	$2.3 \pm 0.2$	$0.29 \pm 0.03$
B-4	0.426	0.983	Too faint for photography	
B-5	0.0426	1.003	Too faint for photography	
B-6 <sup>c</sup>	437.0	1.062	$2.4 \pm 0.3$	$0.32 \pm 0.03$
B-7 <sup>c</sup>	4.26	1.054	$1.7 \pm 1.0$	$0.3 \pm 0.1$

<sup>a</sup> All samples stored in air at 22°. <sup>b</sup> Precision based on least-square-curve-fitting statistics. <sup>c</sup> Monomer saturated with oxygen before cure.

Table III: Effect of Gas Composition on Diffusion Coefficient and Quenching Ratio<sup>a</sup>

Run	Gas	Compn., mole fraction of $O_2$	Press., torr	O.d., cm.	Diffusivity, $cm.^2 \text{ sec.}^{-1} \times 10^9$	Quenching ratio
C-1	$O_2$	1.0	190	0.9553	$3.6 \pm 0.6^b$	$0.53 \pm 0.04^b$
C-2	$O_2-N_2$	0.5	750	0.9377	$2.31 \pm 0.06$	$0.24 \pm 0.01$
C-3	$O_2-N_2$	0.2	750	0.9338	$2.2 \pm 0.1$	$0.13 \pm 0.01$
C-4	$O_2$	1.0	750	0.9453	$3.34 \pm 0.01$	$0.463 \pm 0.001$

<sup>a</sup> Temperature 22°;  $4.30 \times 10^{-6}$  mole of triphenylene/g. of polymer. <sup>b</sup> Precision based on least-square-curve-fitting statistics.

The activation energy for diffusion is quite small, +740 cal./mole. This low activation energy is probably due to diffusion freely occurring through tunnels slightly larger than the diameter of the oxygen molecule rather than by a site-to-site movement. Meares<sup>2b</sup> postulates that in the glass region the polymer consists of densely packed chains with no freedom of rotation separated by regions where the chains are disordered



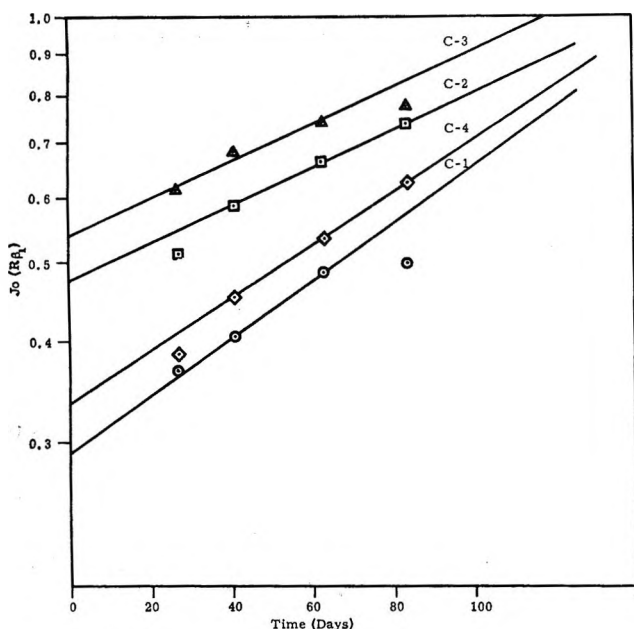


Figure 4. Time dependence of diffusion at various gas concentrations:  $\diamond$ , 100% O<sub>2</sub>, 1 atm.;  $\circ$ , 100% O<sub>2</sub>, 0.25 atm.;  $\square$ , 50% O<sub>2</sub>-50% N<sub>2</sub>, 1 atm.;  $\Delta$ , 20% O<sub>2</sub>-80% N<sub>2</sub>, 1 atm.

in which are the "holes" through which the molecules move. Diffusing molecules must pass through the densely packed regions to go from disordered region to disordered region. It may well be that in polymethyl methacrylate the disordered regions actually are interconnected, forming continuous "tunnels." Thus, little energy is expended in pushing through ordered regions, resulting in a low activation energy.

An interesting and unexpected effect is the change in diffusivity in the presence of another gas, namely, nitrogen. The diffusivity at 22° in an atmosphere of pure oxygen was found to be  $3.3 \times 10^{-9}$  cm.<sup>2</sup> sec.<sup>-1</sup>, while with 0.2 mole fraction oxygen in nitrogen the rate was found to be  $2.3 \times 10^{-9}$  cm.<sup>2</sup> sec.<sup>-1</sup> as measured by triphenylene quenching.

Stannett, *et al.*,<sup>2c</sup> found no interaction between the components in a mixture in their permeation studies on polymers above the glass transition. In our experiments below the glass transition, it was observed that the diffusivity of oxygen from a mixture is about 67% of the diffusivity from pure oxygen. Diffusivity of gases through polymethyl methacrylate seems to involve movement through cracks and holes of molecular size; thus, there would be competition between nitrogen and oxygen molecules for these holes, and so the presence of nitrogen molecules could interfere with the diffusion of oxygen molecules.

**Quenching Ratio.** The quenching ratio, the ratio of oxygen concentration at the terminator ( $v$ ) to the con-

centration of oxygen in the surface layers, *i.e.*, solubility ( $V$ ), is obtained through eq. 4 from the intercept at  $t = 0$ . This is equivalent to the value of  $v/V$  obtained using the first terms of eq. 2 only. The relationships between runs are rather erratic. Comparing run B-3 with C-3 and A-1 with B-2, which are identical in conditions but from different batches of polymer, it is noted that the quenching coefficients differ by approximately a factor of 2 in each case. On the other hand, the diffusion coefficient is quite consistent for these four runs. Since it is apparent that the quenching coefficient depends partly on polymer properties, no attempt will be made to draw conclusions from this data.

**Comparison with Other Data.** Diffusion of oxygen in polymethyl methacrylate has been measured by bleaching of color centers produced by high energy irradiation.<sup>3b</sup> The diffusion coefficient at 22° was found to be about  $6.2 \times 10^{-10}$  cm.<sup>2</sup> sec.<sup>-1</sup> which is about 0.185 of the value of  $3.3 \times 10^{-10}$  cm.<sup>2</sup> sec.<sup>-1</sup> of this paper. Considering the simplifications in the mathematics in both cases the agreement is quite reasonable. Barker's activation energy includes the activation energy of trapping as well as the activation energy of diffusion, hence the wide discrepancy between these figures.

## Conclusions

The measurement of oxygen diffusion through phosphorescent quenching provides methods for study of gas diffusion in bulk polymers. Other transparent polymers may be investigated by this same technique. Opaque materials may be studied by removing slices from the end of the sample and immediately photographing the phosphorescent ring while illuminating the end. The primary requirement on the material to be studied is that a quenchable phosphor be soluble in it.

If a rectangular rather than a circular cross section is used, a cosine function or error function of the distance replaces the Bessel function with a resultant simplification in calculation. Since the terminator will be a straight line in this case, measurements of its location should also be easier.

The major limitation on this method is that the diffusing gas or vapor must quench phosphorescence. This limits the gas to oxygen and possibly to nitric oxide.

It may be possible to study diffusion of other gases by measuring their interference with oxygen diffusion as was noted for the slower diffusion rate of oxygen from air compared to that from pure oxygen.

**Acknowledgments.** The authors wish to acknowledge the many helpful discussions with Dr. Ernest Brock and Dr. Jack Taylor and the valuable assistance of Mr. Kermit Mercer with the experimental work.

# Gas-Liquid Partition Chromatography in Benzene-Polyphenyl Systems and Polymer Statistical Thermodynamics<sup>1</sup>

by Ronald K. Clark<sup>2</sup> and Hartland H. Schmidt

Department of Chemistry, University of California, Riverside, California (Received December 29, 1964)

Gas-liquid partition chromatography (g.l.p.c.) was used to measure activity coefficients and heats of solution at infinite dilution for benzene in biphenyl, *m*-terphenyl, and *o*-terphenyl over a range from the melting point of the solvent to about 125°. The infinite dilution mole fraction activity coefficients at 90° and the heats of solution (cal./mole) are, respectively: in biphenyl, 1.110, 150; in *m*-terphenyl, 1.020, 180; in *o*-terphenyl, 0.939, 76. The results for biphenyl compare very well with available bulk thermodynamic data. The thermodynamic quantities are used in conjunction with a corresponding states theory of polymer mixtures of Prigogine, *et al.*, to show the contributions to the measured properties, according to this model, of solvent structure, configurational heat capacity, and intermolecular potential parameters. The results give intermolecular segment interaction energies within 2% of the geometric mean rule. Activity coefficients are also predicted from modified regular solutions types of theories, the solubility parameter treatment being fairly good for the biphenyl and *m*-terphenyl systems but not for the *o*-terphenyl system. The Prigogine model indicates in detail the important structural and thermal contributions to the thermodynamic properties in a manner consistent with all available g.l.p.c. and bulk thermodynamic data.

## Introduction

In several recent publications relating to g.l.p.c. and the use of polymer solution theory to interpret chromatographic data,<sup>3-6</sup> the thermodynamic properties are separated into two contributions, one energetic and the other due to mixing molecules of different sizes. The latter so-called "athermal" contribution arises from the effect of the combinatorial factor in the partition function of the mixture. The excess of the "athermal" contribution over that of an ideal mixture is estimated by the use of a rigid lattice model such as that of the Guggenheim-Miller<sup>7</sup> or Flory-Huggins<sup>8</sup> polymer theories. In the more recent polymer solution models of Prigogine, *et al.*,<sup>9-11</sup> and of Flory<sup>12</sup> other contributions, which are of obvious importance in g.l.p.c., are considered. The additional effects included are an energetic effect due to volume changes on mixing, effects due to the nonzero configurational heat capacity in the liquid arising from the fact that the lattice is not rigid and is not at 0°K., and allowance for the effect of polymer structural rigidity in lowering the

number of external degrees of freedom of the polymer segment.

We will use infinite dilution activity coefficients of

(1) This work was supported in part by an equipment grant under Contract AT(11-1)-34, Project No. 79, from the U.S.A.E.C. Division of Reactor Development and by Petroleum Research Fund Grant No. 2183-A5.

(2) A National Defense Education Act Fellow, 1964-1965.

(3) D. E. Martire, "4th International Symposium on Gas Chromatography," Academic Press Inc., New York, N. Y., 1963, pp. 33-53.

(4) S. H. Langer and J. H. Purnell, *J. Phys. Chem.*, **67**, 263 (1963).

(5) J. H. Purnell, "Gas Chromatography," John Wiley and Sons, Inc., New York, N. Y., 1962, Chapter 2.

(6) A. J. Ashworth and D. H. Everett, *Trans. Faraday Soc.*, **56**, 1609 (1960).

(7) E. A. Guggenheim, "Mixtures," Oxford at the Clarendon Press, London, 1952, Chapter X.

(8) P. Flory, *J. Chem. Phys.*, **10**, 51 (1942).

(9) I. Prigogine, N. Trappeniers, and V. Mathot, *ibid.*, **21**, 559 (1953); I. Prigogine, N. Trappeniers, and V. Mathot, *Discussions Faraday Soc.*, **15**, 93 (1953).

(10) I. Prigogine, "The Molecular Theory of Solutions," Interscience Publishers, Inc., New York, N. Y., 1957, Chapters XVI and XVII.

benzene in various polyphenyl solvents measured by g.l.p.c. techniques in conjunction with molecular parameters previously derived by us, in evaluating the significance of the additional contributions. The benzene-polyphenyl systems are especially appropriate for this test of solution models since there is a considerable amount of statistical thermodynamic data available on the pure components and since, unlike the alkane examples previously most commonly used, the polyphenyls possess considerable internal rigidity so as to exaggerate these effects while also fitting very well the specification that the polymer segments should have intermolecular energy and distance parameters close to those of the monomer. The experimental activity coefficients will also be compared with those predicted by modified regular solution theory and solubility parameters.

### Experimental Procedure and Results

Columns were made from 0.25-in. copper tubing 210 cm. in length. The column material consisted of approximately 26.7 g. of Johns-Manville acid-washed, dimethyldichlorosilane-treated Chromosorb G, 100-120 mesh, coated with various weights of stationary phase. Stationary phase weights were 0.5, 0.8, and 1.3 g. for *o*-terphenyl columns, 0.45, 0.55, and 0.65 g. for *m*-terphenyl columns, and 0.77 and 0.99 g. for the two biphenyl columns. Sources and purities of the polyphenyls are given elsewhere.<sup>13</sup> The stationary phases were deposited on the support by first dissolving them in *n*-pentane and then evaporating the pentane after addition of the support. An Aerograph A-90P chromatograph was modified by including a mercury manometer attached to the column head for accurate measurement of the pressure drop across the column, an intermittent heater and thermistor probe fitted in the column oven for temperature control to better than 0.1°, and a calibrated soap film flow rate meter. The latter had an especially long exit tube, so that the helium carrier gas swept out the air above the soap bubble since it was found that otherwise there was considerable diffusion of helium through the bubble. Chromatograms were recorded on a Leeds and Northrup Speedomax H operating at a chart speed of 0.5 in./min.

Column temperatures were measured by means of two iron-constantan thermocouples attached to the column. Injector temperatures were generally within 3° of the column temperature, and the detector temperature was maintained at 150° at all times. Each column was run at four or five different temperatures between the solvent melting point and about 125°, except in the case of biphenyl where the maximum was 112°. Higher

temperatures were not feasible owing to uncertainties in solvent vapor pressure used to correct for volatility. Two or three 0.1-ml. samples of benzene vapor and air were injected at each temperature.

Retention times were measured from the air peak (found to coincide in tests with an argon peak) and the specific retention volume calculated from the equation of Littlewood<sup>14</sup> after correction for solvent evaporation. The solvent volatility correction was found to be relatively small for the terphenyl columns at these temperatures; for biphenyl the correction was quite large owing to the high vapor pressure. Vapor pressures used for the correction were taken from Yanko and Ellard,<sup>15</sup> except that for biphenyl a corrected vapor pressure had to be used in order to account for slower column losses than predicted. (Considerable discrepancy exists in the literature among biphenyl vapor pressure measurements, and these have been extrapolated from higher temperatures than used here.) A threefold variation in the flow rate and a tenfold increase in the sample size did not affect the retention volume beyond experimental error. The total estimated error in the measured specific retention volume was less than 0.5%.

The mole fraction activity coefficient at infinite dilution is then simply related to the specific retention volume ( $V_g^0$ ) of solute by<sup>3</sup>

$$\gamma_A^0 = 273R / (M_B f_A^0 V_g^0) \quad (1)$$

where  $R$  is the gas constant,  $M_B$  the molecular weight of solvent, and  $f_A^0$  the fugacity of the pure liquid solute, which enters the equation as the standard state fugacity of the solute. The fugacity of benzene was calculated by means of the usual thermodynamic relation<sup>16</sup> using vapor pressure data of Bender, Furukawa, and Hyndman<sup>17</sup> and second virial coefficient data of Andon, Cox, Herrington, and Martin.<sup>18</sup> Equation 1 contains the assumption of Dalton's law for the benzene partial pressure at infinite dilution in 1.0 to

(11) A. Bellemans and C. Colin-Naar, *J. Polymer Sci.*, **15**, 121 (1955).

(12) P. J. Flory, R. A. Orwoll, and A. Vrig, *J. Am. Chem. Soc.*, **86**, 3507, 3515 (1964).

(13) J. Opdycke, J. P. Dawson, R. K. Clark, M. Dutton, J. J. Ewing, and H. H. Schmidt, *J. Phys. Chem.*, **68**, 2385 (1964).

(14) A. B. Littlewood, C. S. G. Phillips, and D. T. Price, *J. Chem. Soc.*, 1480 (1955).

(15) W. H. Yanko and J. A. Ellard, Monsanto Research Corp., Dayton, Final Report IDO-1,008, 1963, U.S.A.E.C.

(16) G. N. Lewis and M. Randall, "Thermodynamics," 2nd Ed., McGraw-Hill Book Co., Inc., New York, N. Y., 1961, p. 185.

(17) P. Bender, G. Furukawa, and J. Hyndman, *Ind. Eng. Chem.*, **44**, 387 (1952).

(18) R. J. L. Andon, J. D. Cox, E. F. G. Herrington, and J. F. Martin, *Trans. Faraday Soc.*, **53**, 1074 (1957).

1.4 atm. of helium for the gas phase. An additional term in the fugacity correction containing the cross second virial coefficient for the benzene-helium mixture has been neglected. An estimate of the cross virial coefficient was made by corresponding states arguments of Guggenheim and McGlashan<sup>19</sup> and found to give a correction less than experimental error. From measurements of the retention volume as a function of temperature, the partial molar heat of solution of benzene at infinite dilution can be calculated by means of the Gibbs-Helmholtz relation. This fitting was done by a least-squares analysis.

The results of the activity coefficient measurements are summarized in Table I. Only the values at 90° are given, since it is these which we will use to compare with theory. At this temperature the necessary thermodynamic quantities for benzene are available with only slight extrapolation, and all g.l.p.c. runs spanned this temperature. The values for the molar heat of solution of benzene at infinite dilution, in Table I, can be used to reproduce the temperature dependence of the activity coefficient. The standard deviation among the various sets of runs is listed and is somewhat larger than the estimated  $\pm 0.005$  in each activity coefficient determination which in turn is about equal to the standard deviation of the least-squares fit of data to the Gibbs-Helmholtz plot of a single set of runs for a single day.

**Table I:** Properties of Benzene at Infinite Dilution (with Standard Deviations) from G.l.p.c. Runs

Solvent	$\gamma_A$ (90°)	$\bar{H}^{\circ}_{soln}$ , cal./mole	No. of columns	No. of runs
Biphenyl	1.110 $\pm$ 0.003	150 $\pm$ 16	2	22
<i>m</i> -Terphenyl	1.020 $\pm$ 0.008	180 $\pm$ 50	3	75
<i>o</i> -Terphenyl	0.939 $\pm$ 0.006	76 $\pm$ 18	3	31
Biphenyl <sup>a</sup>	1.105	153		
Biphenyl <sup>b</sup>		136		

<sup>a</sup> From Baxendale, Enüstün, and Stern<sup>20</sup> and Everett and Penney<sup>21</sup> by extrapolation (vapor pressure measurements).

<sup>b</sup> From Kortüm, Dreesen, and Freier<sup>22</sup> by extrapolation (calorimetric measurements).

Activity coefficients of benzene in biphenyl have been calculated from vapor pressure measurements over a series of concentrations and temperatures from 30 to 80° by Baxendale, Enüstün, and Stern<sup>20</sup> and Everett and Penney.<sup>21</sup> The reported values have been recalculated by Guggenheim.<sup>7</sup> We have extrapolated these to 90° and infinite dilution to find values for the activity coefficient and heat of solution which are

included in Table I. The heats of solution measured calorimetrically by Kortüm, Dreesen, and Freier<sup>22</sup> extrapolated to 90° and infinite dilution give the calorimetric value in Table I. Our g.l.p.c. values compare favorably with all of these. Some activity coefficient data in the dilute polymer region at lower temperature are also available on the *o*-terphenyl-benzene and *m*-terphenyl-benzene systems.<sup>23</sup>

### Theory

The solution theory of Prigogine, Trappeniers, Mathot, and Bellemans<sup>9-11</sup> utilizes the rigid lattice treatment for the entropy of mixing but makes an estimate of the energetic and structural terms by using a modified cell partition function method for the liquid state and evaluating the parameters in the model empirically using a corresponding states theorem.

The major assumptions necessary to establish the corresponding states theorem and to apply it to pure polymer liquids and their mixtures are as follows.

(a) The rigid lattice approximation is valid for calculation of the combinatorial entropy of mixing.

(b) The cell partition function of a polymer segment in the pure *r*-mer liquid is a product of two parts, a temperature-dependent part and a volume-dependent part.

(c) The cell partition function can be applied to all "external" degrees of freedom of the polymer segment allowed by free rotations and translations of the molecule and its parts. Bond vibrational force constants are large compared to force constants for these external motions.

(d) All intermolecular interactions between segments are described by a spherically symmetric Lennard-Jones potential of the same form regardless of the nature of the interacting segments.

(e) The average pair potential of a segment in the mixture has the Lennard-Jones form with energy and spacing parameters given by segment fraction averages of the energy and spacing parameters of each species involved.

The recent Flory<sup>12</sup> treatment results in a similar corresponding states equation of state but is more detailed in evaluating the absolute potential function

(19) E. A. Guggenheim and M. L. McGlashan, *Proc. Roy. Soc. (London)*, **A206**, 448 (1951).

(20) J. H. Baxendale, B. V. Enüstün, and J. Stern, *Phil. Trans. Roy. Soc. (London)*, **A243**, 169 (1951).

(21) D. H. Everett and M. F. Penney, *Proc. Roy. Soc. (London)*, **A212**, 164 (1952).

(22) G. Kortüm, G. Dreesen, and H. J. Freier, *Z. Naturforsch.*, **8a**, 546 (1953).

(23) R. G. Satterfield, Dissertation, University of California at Los Angeles, Los Angeles, Calif., 1964.

parameters rather than just their ratios to those of the monomer.

For further details of other assumptions and the evaluation of thermodynamic quantities see ref. 9-12. This type of model has been used for the normal aliphatic hydrocarbons and for short polyphenyls as well as for mixtures of benzene with diphenyl and some other pseudo-dimers. The treatments have been quite successful in fitting density and compressibility data for pure compounds<sup>24</sup> and heats of mixing for mixtures.<sup>10</sup>

In order to relate the quantities measured by g.l.p.c. to this theory, we first need an expression for the excess free energy of mixing for mixtures of  $r_A$ -mer of mole fraction  $x_A$  and  $r_B$ -mer of mole fraction  $x_B$  with  $3c_A$  and  $3c_B$  external degrees of freedom, respectively. For a rigid linear polymer  $3c$  would be 5 while for a nonlinear rigid polymer the value would be 6. For molecules which do not fold back upon themselves, the average number of intermolecular contacts per molecule is  $zq = zr + 2 - 2r$ , where  $z$  is the number of intra- plus intermolecular nearest-neighbor segments per segment and  $r$  is the number of segments per molecule. For molecules which do fold back upon themselves,  $zq$  must be modified for exclusions of nearest neighbors other than those due to segment-segment bonds. This additional number of exclusions can be estimated by fixing the total number of segment neighbors in the ring plane at 6. Define the parameters

$$\delta = (\epsilon^*_{BB} - \epsilon^*_{AA})/\epsilon^*_{AA} \quad \rho = (r^*_{BB} - r^*_{AA})/r^*_{AA}$$

$$\alpha = c_B/q_B \quad \theta = [\epsilon^*_{AB} - (\epsilon^*_{AA} + \epsilon^*_{BB})/2]\epsilon^*_{AA}^{-1} \quad (2)$$

In terms of the above parameters, the logarithm of the infinite dilution activity coefficient,  $\ln \gamma^0_A$ , with the solute as reference component can be written as (see Appendix for derivation)

$$\ln \gamma^0_I = (h_A/RT)(2\theta - 9\rho^2) + (c_{PA}/R) \times$$

$$[2\theta(\alpha - \delta\alpha - 1) + (1 - \alpha)(9\rho^2 + \delta - 1) -$$

$$1/2\delta^2(1 - 2\alpha) - \ln \alpha] + (\partial c_{PA}/\partial T)_P(T/R)[\theta(1 - \alpha) \times$$

$$(1 - \alpha + 2\delta\alpha) + (1 - \alpha)(1/2\delta^2 - 3/2\delta^2\alpha + 1) +$$

$$(1 - \alpha)^2(1/2 - \delta - 9/2\rho^2) + \ln \alpha] -$$

$$3/2\rho[\rho(\alpha - 1/4) + (1 - \alpha) - \alpha(\theta - 1/2\delta - 17/4\rho)] \quad (3a)$$

$$\ln \gamma^0_{II} = -\ln r_B - 1 + 1/r_B \quad \text{Flory-Huggins} \quad (3b)$$

$$\ln \gamma^0_{II} = -\ln r_B - (z/2) \ln [1 - 2/z + 2/(zr_B)]$$

$$\text{Guggenheim-Miller} \quad (3c)$$

$$\ln \gamma^0_A = \ln \gamma^0_I + \ln \gamma^0_{II} \quad (3d)$$

the solute being considered monomer with  $c_A = q_A = 1$

and the experimental quantities  $h_A$  and  $c_{PA}$  being the molar configurational enthalpy and heat capacity of the solute. The effects of structural variations and molecular parameters appear in this equation through the structural parameters  $c_B$  and  $q_B$  and the potential function parameters  $\rho$ ,  $\delta$ , and  $\theta$ . The effects of the volume changes on mixing are included implicitly by a free energy minimization process during the derivation (see pp. 191-195 and p. 350, ref. 10). The second term,  $\ln \gamma^0_{II}$ , is the infinite monomer dilution Flory-Huggins or Guggenheim-Miller<sup>3</sup> approximation for the excess entropy of athermal mixing common to all g.l.p.c. polymer solution treatments, the justification of which will be given later.

The parameters  $\delta$  and  $\rho$  can be obtained from *PVT* data on the pure components and  $\theta$  from *PVT* or g.l.p.c. data on the mixture. For simple dispersion forces, the geometric mean rule for combining energy parameters is valid and

$$\epsilon^*_{AB} = (\epsilon^*_{AA}\epsilon^*_{BB})^{1/2} \quad \theta = -\delta^2/8 \quad (4)$$

while for the arithmetic mean rule  $\theta = 0$ .

The appropriate temperature derivative of the activity coefficient yields the infinite dilution heat of solution

$$\bar{H}^0_A = R(\partial(\ln \gamma^0_A)/\partial(1/T))_P = (2\theta - 9\rho^2)(h_A -$$

$$Tc_{PA}) - T^2(\partial c_{PA}/\partial T)_P[\theta(\alpha^2 - 1 - 2\delta\alpha^2) +$$

$$\delta\alpha(1 - \alpha) + \delta^2\alpha(3/2\alpha - 1) + 1/2(1 - \alpha)^2 +$$

$$(9\rho^2/2)(1 - \alpha^2)] \quad (5)$$

Two equations are now available for calculation of  $\theta$ . By using both we can check for consistency between eq. 3 and 5.

The form of regular solution theory which relates the solubility parameters of the mixture components to the excess free energy of mixing will be used to predict activity coefficients which will be compared to the experimental values. In this theory the energetic term is given by<sup>3,25</sup>

$$\ln \gamma^0_I = (v_A/RT)(\delta_A - \delta_B)^2 \quad (6)$$

where  $v_A$  is the partial molar volume of the solute, set equal to the liquid molar volume of the solute, and  $\delta_i$  is the solubility parameter of component  $i$ . (The symbol  $\delta_i$  should not be confused with  $\delta$  of eq. 2.) This term is then combined with  $\ln \gamma^0_{II}$  as given in eq. 3 to give the activity coefficient.

(24) H. H. Schmidt, J. Opdycke, and R. K. Clark, *J. Phys. Chem.*, **68**, 2393 (1964).

(25) J. H. Hildebrand and R. L. Scott, "The Solubility of Nonelectrolytes," 3rd Ed., Dover Publications, Inc., New York, N. Y., 1964, Chapter VII.

## Discussion

Table II lists the necessary molecular parameters derived from previous measurements,<sup>24</sup> along with the thermodynamic properties of benzene which are needed in the Prigogine treatment. The configurational heat capacity has been calculated from two separate sources with the added uncertainty that the liquid heat capacity was extrapolated from measurements up to 80°. The probable error in the heat capacity derivative is correspondingly quite large but affects other calculated quantities almost negligibly.

**Table II:** Molecular Parameters and Thermodynamic Properties

	External deg. of freedom, $3c_i$	Nearest neighbors, $zq_i$	$\rho$	$\delta$
Benzene <sup>a</sup>	3	10	0	0
Biphenyl <sup>a</sup>	5	18	-0.029	0.259
<i>m</i> -Terphenyl <sup>c</sup>	6	25	-0.041	0.226
<i>o</i> -Terphenyl <sup>a</sup>	6	24	-0.038	0.231

	$T, ^\circ\text{K.}$	$h_A, ^b$ cal./mole	$c_{PA}, ^{b-d}$ cal. mole <sup>-1</sup> deg. <sup>-1</sup>	$T(\partial P_A/\partial T)_P, ^{c,d}$ cal. mole <sup>-1</sup> deg. <sup>-1</sup>
Benzene	363	-7300	12	-5.5 ± 6

<sup>a</sup> Molecular parameters from ref. 24; the value of  $\delta$  has been carried out to one more significant figure as justified by the data.

<sup>b</sup> P. W. Allen, D. H. Everett, and M. F. Penney, *Proc. Roy. Soc. (London)*, **A212**, 149 (1952). <sup>c</sup> D. W. Scott, G. Waddington, J. C. Smith, and H. M. Huffman, *J. Chem. Phys.*, **15**, 565 (1947).

<sup>d</sup> J. S. Burlew, *J. Am. Chem. Soc.*, **62**, 696 (1940).

Substituting the quantities in Tables I and II into eq. 3 and 5 yields two different values of  $\theta$  which are listed in Table III along with the sizes of the two terms which make up eq. 3. Both values are nearly within experimental error of being the same for each of the three systems. In all three systems  $\theta$  is positive; however, a lowering of the value of  $\epsilon^*_{AB}$  by less than 2% would change the sign and give a value corresponding to eq. 4 and the geometric mean rule ( $\theta \cong -0.007$ ) as one would predict for spherically symmetric dispersion forces. Positive values have no theoretical justification, but according to Rowlinson<sup>26</sup> agreement with experiment to within a few per cent is all one can expect of the geometric mean rule even in the most ideal cases. Thus, the internal consistency of the theory is as much as one could hope for as evidenced by the value of  $\theta$  it requires. It should also be mentioned that the values calculated for  $\theta$  are quite insensitive to the benzene heat capacity derivative in our range and to varia-

tions of  $z$  between 8 and 12 except in  $\ln \gamma^{0_{II}}$ . Only one literature value for  $\theta$  of the benzene-biphenyl system is available—that from Bellemans and Colin-Naar,<sup>11</sup> who give -0.0123. Some of the discrepancy between this and our value of  $\theta$  is due to small differences in  $\rho$  and  $\delta$  values used. Bellemans and Colin-Naar used older and less complete data to calculate these parameters.

In order to show the effect of structure on the activity coefficient we have listed in Table IV the values of  $\ln \gamma^0_I$  and  $\ln \gamma^{0_{II}}$  for various values of  $r_B$  and  $c_B$  with  $\rho = \delta = \theta = 0$ . In all cases  $q_B$  was calculated from the relation for an open-chain molecule,  $q_B = r_B - 2(r_B - 1)/z$ . The magnitudes of  $\ln \gamma^0_I$  for a rigid linear or nonlinear molecule ( $c_B = 5/3$  or 2) are close to those of  $\ln \gamma^{0_{II}}$  for chains of about five segments but become much larger for longer chains where the model of a polymer as being strictly rigid to within the free volume of a segment cell would probably be unrealistic. At these longer chain lengths  $\ln \gamma^0_I$  calculated assuming a more flexible nonlinear chain ( $c_B = 1 + (r_B/3)$ ) is comparable to  $\ln \gamma^{0_{II}}$  up to about 40 segments; for higher chain lengths the combinatorial entropy effect is by far the most important. All the molecular parameters, the structural parameters, and one cross term between structural and energetic parameters contribute significantly to eq. 3 for the mixtures treated here.

In Table V the solubility parameters of the pure components are listed along with the predicted activity coefficients calculated from eq. 6 and  $\ln \gamma^{0_{II}}$  of eq. 3. The solubility parameters were calculated from *PVT* data on the pure compounds by means of the equation<sup>25</sup>

$$\delta_i \cong [(\partial E/\partial V)_T]^{1/2} = [T(\partial P/\partial T)_V - P]^{1/2} \quad (7)$$

The data for benzene were taken from Staveley, Tupman, and Hart,<sup>27</sup> and those for biphenyl and the terphenyls from ref. 13. The agreement between calculated and observed activity coefficients in the biphenyl and *m*-terphenyl systems is fairly good; however, the predicted activity coefficient in the *o*-terphenyl system is much too high. The discrepancy is probably due to the lack of consideration of structural contributions in the regular solution treatment.

Another method for applying a regular solution type of model (similar to Guggenheim's zeroth-order approximation with interchange energy independent of

(26) J. S. Rowlinson, "Liquids and Liquid Mixtures," Butterworths Scientific Publications, London, 1959, p. 257.

(27) L. A. K. Staveley, W. I. Tupman, and K. R. Hart, *Trans. Faraday Soc.*, **51**, 323 (1955).

**Table III:** Calculated Parameters for Eq. 3 and 5 from G.l.p.c. Data ( $T = 363^\circ\text{K}$ .)

Solvent	$\text{Ln } \gamma_{II}^0{}^a$	$\text{Ln } \gamma_{II}^0{}^a$	$\theta, {}^c$ eq. 3	$\theta, \text{ eq. 5}$
Biphenyl	-0.193 (-0.168)	+0.298 (0.273)	+0.004 $\pm$ 0.001 (0.005)	+0.001 $\pm$ 0.002
<i>m</i> -Terphenyl	-0.432 (-0.379)	+0.452 (0.399)	+0.011 $\pm$ 0.001 (0.013)	+0.006 $\pm$ 0.003
<i>o</i> -Terphenyl	-0.432 (-0.379)	+0.369 (0.316)	+0.010 $\pm$ 0.001 (0.013)	+0.008 $\pm$ 0.002

<sup>a</sup> Calculated using the Flory-Huggins approximation for  $\text{Ln } \gamma_{II}^0$ , eq. 3b, and the Guggenheim-Miller approximation, eq. 3c, in parentheses.

**Table IV:** Contributions to  $\text{Ln } \gamma_A^0$  at  $x_A \rightarrow 0$  at  $T = 363^\circ\text{K}$ .<sup>a</sup>

$r_B$	$\text{Ln } \gamma_{II}^0$ Eq. 3b	$\text{Ln } \gamma_{II}^0$		
		$c_B = 1/2$	$c_B = 2$	$c_B = 1 + (r_B/3)^b$
2	-0.193	0.018	...	0.018
3	-0.432	0.594	0.203	0.203
4	-0.636	1.418	0.792	0.412
7	-1.089	3.977	2.794	0.877
10	-1.403	6.096	4.944	1.149
40	-2.714	16.371	14.900	1.804
100	-3.615	24.002	22.474	1.970
$\infty$	$-\text{Ln } r_B + 1$	$8.75 \text{ Ln } r_B - 16.5$	$8.75 \text{ Ln } r_B - 18.1$	2.089

<sup>a</sup>  $z = 10$ ;  $q_B z = r_B z - 2r_B + 2$ ;  $\rho = \delta = \theta = 0$ . <sup>b</sup> The value of  $c_B$  appropriate for idealized  $n$ -alkane type of chains.

temperature for infinitely dilute solutions<sup>7</sup>) to g.l.p.c. data is the treatment which assumes separability of "thermal" and "athermal" terms contributing to the excess free energy of solution but sets

$$\bar{H}^0_{\text{calcd}} = RT \text{Ln } \gamma_A^0 - RT \text{Ln } \gamma_{II}^0 \quad (8)$$

This calculated heat of solution is compared with that derived from the experiment.<sup>4-6</sup> Our comparison is presented in Table V, and it is obvious that the discrepancy is considerable.

The Flory-Huggins (F-H), Guggenheim-Miller (G-M), and several higher approximations to the excess athermal entropy, while rigorous at the low polymer concentration limit, represent series truncations or configuration counting approximations of uncertain validity at  $x_A \rightarrow 0$ . The monomer-dimer problem has been most discussed,<sup>7,28</sup> and most of the higher approximations fall between the F-H and G-M (with  $z = 10$ ) approximations but tend nearer to the former at the  $x_A \rightarrow 0$  limit as the approximations improve. Less work has been done on the rigid nonlinear trimer-monomer case, but the triangles with monomers one approximation available<sup>7</sup> would place the  $x_A \rightarrow 0$  limiting partial molar excess entropy of A outside the span of the F-H and G-M approximations but near the latter. The dimer case would suggest the possibility of higher approximations entering the span. Thus,

the span of values in Tables III and V based upon the F-H and G-M approximations probably includes or nearly includes the actual solution to the combinatorial problem. We have chosen to use these two simple formulas, eq. 3b and c, to illustrate the range of results and are presently investigating better approximations in this concentration range for particular polymer shapes. At any rate, all present g.l.p.c. theories depend upon these approximations, and our conclusions are roughly the same over the range of values of  $\text{Ln } \gamma_{II}^0$  used here.

We have shown that for the particular systems under consideration, which appear to be ideal from the standpoint of amount of data available and appropriateness of the model, the validity of the F-M or G-M approximations in the  $x_A \rightarrow 0$  limit would also indicate that the detailed contributions envisioned by the Prigogine model would be significant within the precision of the g.l.p.c. measurements and that the model is fairly self-consistent. The model indicates why deviations from ideal mixing in these cases are small, as  $\text{Ln } \gamma_A^0$  is a small difference in large quantities (Table III), in a manner which gives insight into the various contributions. However, we would not claim that the consistency displayed by the model is in any sense "proof" of the validity of its assumptions at this point, especially in light of the uncertainty concerning the proper entropy of mixing contribution.

We are continuing the gathering of data on the higher polyphenyls to attempt further tests of polymer statistical thermodynamic models. The g.l.p.c. methods used to supplement compressibility data on the pure compounds appear to give data which compare very well in precision with the bulk thermodynamic data available, and the g.l.p.c. methods have a great advantage in speed and experimental simplicity. We hope to be able to improve the g.l.p.c. precision considerably over that obtained in these initial experiments by custom building a chromatograph for these purposes.

(28) D. H. Trevena, *Proc. Phys. Soc. (London)*, **84**, 969 (1964).



Table V: Predicted Activity Coefficients and Heats of Solution from Regular Solution Theories ( $T = 363^\circ\text{K}$ .)

	$\delta_1^a$	$\text{Ln } \gamma_{\text{A}}^{\text{calcd.},b}$ eq. 6	$\text{Ln } \gamma_{\text{A}}^{\text{obsd.}}$	$\bar{H}_{\text{calcd.},b}$ cal./mole	$\bar{H}_{\text{obsd.}}$ cal./mole
Benzene	8.6				
Biphenyl	10.1	+0.084 (0.109)	+0.105 $\pm$ 0.003	215 (198)	150 $\pm$ 16
<i>m</i> -Terphenyl	10.5	+0.025 (0.078)	+0.020 $\pm$ 0.008	328 (290)	180 $\pm$ 50
<i>o</i> -Terphenyl	10.6	+0.092 (0.145)	-0.063 $\pm$ 0.006	267 (230)	76 $\pm$ 18

<sup>a</sup> Solubility parameter treatment, eq. 6 and 7. <sup>b</sup>  $\bar{H}_{\text{calcd.}}$  calculated by eq. 8. Approximation for  $\text{Ln } \gamma_{\text{II}}$ : Flory-Huggins, eq. 3b, and the Guggenheim-Miller approximation, eq. 3c, in parentheses.

## Appendix

In this section the general expression for the excess free energy of mixing of  $r$ -mers will be derived from the Prigogine theory. The derivation of Chapter 17, ref. 10, represents an expansion only to first order in structural parameters and omits complete expansion of cross terms between structural and segment potential function parameters. Since neither of these approximations were completely justified in our cases and since the previous derivation has never been put in a convenient form for g.l.p.c., with monomer concentration approaching zero, we have sketched the additional steps here.

It is useful to define the following average quantities

$$\begin{aligned} \bar{q} &= x_{\text{A}q_{\text{A}}} + x_{\text{B}q_{\text{B}}} & \bar{c} &= x_{\text{A}c_{\text{A}}} + x_{\text{B}c_{\text{B}}} \\ X_{\text{A}} &= x_{\text{A}q_{\text{A}}}/\bar{q} & \bar{r} &= x_{\text{A}r_{\text{A}}} + x_{\text{B}r_{\text{B}}} \\ \bar{c}/\bar{q} &= X_{\text{A}c_{\text{A}}}/q_{\text{A}} + X_{\text{B}c_{\text{B}}}/q_{\text{B}} \end{aligned} \quad (\text{A1})$$

Define an average potential energy parameter and an average reduced temperature for the mixture as

$$\langle \epsilon^* \rangle = X_{\text{A}} \langle \epsilon^*_{\text{A}} \rangle + X_{\text{B}} \langle \epsilon^*_{\text{B}} \rangle \quad \langle \bar{T} \rangle = kT\bar{c}/(\langle \epsilon^* \rangle \bar{q}) \quad (\text{A2})$$

where  $\langle \epsilon^* \rangle$  is an average potential energy constant, the mole fraction average of the average potential energy parameters of the separate components in the mixture. Also

$$\chi(\bar{T}) = F(\bar{T})/(ckT) + (\ln r^*)/c + \text{constant} \quad (\text{A3})$$

where  $F(\bar{T})$  is the configurational free energy of the component at the reduced temperature denoted by  $\bar{T}$ .

Using the above definitions, the excess free energy of mixing is written as (see eq. 17.4.1 of ref. 10)

$$\begin{aligned} F^{\text{e}} &= \bar{q}[\langle \epsilon^* \rangle \langle \bar{T} \rangle \chi(\langle \bar{T} \rangle)] - X_{\text{A}} \epsilon^*_{\text{AA}} \bar{T}_{\text{AA}} \chi(\bar{T}_{\text{AA}}) - \\ &X_{\text{B}} \epsilon^*_{\text{BB}} \bar{T}_{\text{BB}} \chi(\bar{T}_{\text{BB}})] - 3RT[x_{\text{A}c_{\text{A}}} \ln \langle (r^*_{\text{A}})/r^*_{\text{AA}} \rangle + \\ &x_{\text{B}c_{\text{B}}} \ln \langle (r^*_{\text{B}})/r^*_{\text{BB}} \rangle] - TS^{\text{e}} = W + Y - TS^{\text{e}} \end{aligned} \quad (\text{A4})$$

As in the case of the potential energy parameter,  $\langle r^*_{\text{A}} \rangle$  is the average minimum energy distance of com-

ponent A in the mixture and  $r^*_{\text{AA}}$  is the same quantity in pure A. The excess combinatorial entropy of mixing, the "athermal contribution," is denoted by  $S^{\text{e}}$ . For further discussion see Chapter 17 of ref. 10.

In order to relate  $F^{\text{e}}$  to molecular quantities, we will start with  $W$  of eq. A4 and expand  $\chi(\bar{T})$  in terms of  $\chi(\bar{T}_{\text{AA}})$  around  $(\bar{T} - \bar{T}_{\text{AA}})$ .

$$\chi(\bar{T}) = \chi(\bar{T}_{\text{AA}}) + \sum_{n=1}^{\infty} (\partial^n \chi / \partial \bar{T}^n)_{\bar{T}=\bar{T}_{\text{AA}}} (\bar{T} - \bar{T}_{\text{AA}})^n / n! \quad (\text{A5})$$

Taking the necessary derivatives of  $\chi(\bar{T}_{\text{AA}})$ , assuming we can neglect terms in higher derivatives of the heat capacity than the first, we have

$$\begin{aligned} \chi(\bar{T}) &= \chi(\bar{T}_{\text{AA}}) + (h_{\text{A}}/c_{\text{A}}kT) \sum_{n=1}^{\infty} (-1)^n (\bar{T}/\bar{T}_{\text{AA}} - 1)^n - \\ &(Tc_{\text{PA}}/c_{\text{A}}k) \sum_{n=2}^{\infty} (-1)^n (n-1)n^{-1} (\bar{T}/\bar{T}_{\text{AA}} - 1)^n + \\ &(T^2/c_{\text{A}}k) (\partial c_{\text{PA}}/\partial T)_P \sum_{n=3}^{\infty} (-1)^n (n-2)(2n)^{-1} \times \\ &(\bar{T}/\bar{T}_{\text{AA}} - 1)^n \end{aligned} \quad (\text{A6})$$

All thermodynamic quantities are molar configurational quantities. Substituting the expansions for  $\chi(\langle \bar{T} \rangle)$  and  $\chi(\bar{T}_{\text{BB}})$  in  $W$  of eq. A4 gives

$$\begin{aligned} W &= (\bar{q}h_{\text{A}}/q_{\text{A}}) \left[ \sum_{n=1}^{\infty} (-1)^n (\langle \bar{T} \rangle / \bar{T}_{\text{AA}} - 1)^n - \right. \\ &\left. X_{\text{B}} \sum_{n=1}^{\infty} (-1)^n (\bar{T}_{\text{BB}} / \bar{T}_{\text{AA}} - 1)^n \right] - \\ &(\bar{q}Tc_{\text{PA}}/q_{\text{A}}) \left[ \sum_{n=2}^{\infty} (-1)^n (n-1)n^{-1} (\langle \bar{T} \rangle / \bar{T}_{\text{AA}} - 1)^n - \right. \\ &\left. X_{\text{B}} \sum_{n=2}^{\infty} (-1)^n (n-1)n^{-1} (\bar{T}_{\text{BB}} / \bar{T}_{\text{AA}} - 1)^n \right] + \\ &[\bar{q}T^2(\partial c_{\text{PA}}/\partial T)_P/q_{\text{A}}] \left[ \sum_{n=3}^{\infty} (-1)^n (n-2)(2n)^{-1} \times \right. \\ &\left. (\langle \bar{T} \rangle / \bar{T}_{\text{AA}} - 1)^n - X_{\text{B}} \sum_{n=3}^{\infty} (-1)^n (n-2)(2n)^{-1} \times \right. \\ &\left. (\bar{T}_{\text{BB}} / \bar{T}_{\text{AA}} - 1)^n \right] = f(h_{\text{A}}) + g(c_{\text{PA}}) + j((\partial c_{\text{PA}}/\partial T)_P) \end{aligned} \quad (\text{A7})$$

Looking first at  $f(h_A)$  and noting that the summations are given by

$$\sum_{n=1}^{\infty} (-1)^n (\tilde{T}/\tilde{T}_{AA} - 1)^n = (\tilde{T}_{AA}/\tilde{T} - 1) \quad (\text{A8})$$

we have

$$f(h_A) = (\bar{q}h_A/q_A)[\langle\epsilon^*\rangle/\epsilon^*_{AA} - X_B(\epsilon^*_{BB}/\epsilon^*_{AA}) - X_A]$$

where the relation  $\tilde{T} = kTc/\epsilon^*q$  has been used. In order to put  $f(h_A)$  in terms of the parameters  $\rho$ ,  $\delta$ , and  $\theta$ , we use the expressions for the energy parameter ratios evaluated in ref. 10

$$\langle\epsilon^*\rangle/\epsilon^*_{AA} = 1 + \delta X_B + (2\theta - 9\rho^2)X_A X_B \epsilon^*_{BB}/\epsilon^*_{AA} = 1 + \delta$$

neglecting from here on all terms in  $\rho$ ,  $\delta$ , and  $\theta$  of order  $\geq 3$ . Substituting these ratios into eq. A8 gives

$$f(h_A) = \bar{q}X_A X_B h_A (2\theta - 9\rho^2)/q_A \quad (\text{A9})$$

In the same way we expand the summations in  $g(c_{PA})$  to find

$$g(c_{PA}) = -(\bar{q}Tc_{PA}/q_A)[\langle\epsilon^*\rangle/\epsilon^*_{AA} - X_B(\epsilon^*_{BB}/\epsilon^*_{AA}) - X_A + \bar{\alpha} \ln(\bar{\alpha}\epsilon^*_{AA}/\langle\epsilon^*\rangle) - \alpha X_B \ln(\alpha\epsilon^*_{AA}/\epsilon^*_{BB})] \quad (\text{A10})$$

where  $\bar{\alpha} = \bar{c}q_A(c_A\bar{q})^{-1}$  and  $\alpha = c_Bq_A(c_Aq_B)^{-1}$ . Substituting the energy parameter ratios and expanding the logarithm to terms up to second order in  $\rho$ ,  $\delta$ , and  $\theta$ , we find

$$g(c_{PA}) = -\bar{q}Tc_{PA}q_A^{-1}X_A X_B \{ (2\theta - 9\rho^2)(1 - \bar{\alpha}) - \delta(1 - \alpha) + 1/2\delta^2[X_B - \alpha(X_B + 1)] + 2\bar{\alpha}(\theta^2 X_A X_B + \delta\theta X_B) + \sum_{n=1}^{\infty} (-1)^{n+1} (\alpha - 1)^n n^{-1} \times [X_B^{n-1} - \alpha(X_B^{n-1} + X_B^{n-2} \dots + 1)] \} \quad (\text{A11})$$

In the same way, we find

$$j((\partial c_{PA}/\partial T)_P) = 1/2\bar{q}T^2(\partial c_{PA}/\partial T)_P q_A^{-1} \{ (2\theta - 9\rho^2)(1 - \alpha)^2 X_B^2 - \delta(1 - \alpha)^2 (X_B + 1) + \delta^2(1 - \alpha)[X_B^2(1 - \alpha) - X_B\alpha - \alpha] + 4X_B\bar{\alpha}(1 - \bar{\alpha})(\theta^2 X_A + \delta\theta) + (1 - \alpha)^2 + 2\sum_{n=1}^{\infty} (-1)^{n+1} n^{-1} (\alpha - 1)^n [X_B^{n-1} - \alpha(X_B^{n-1} + X_B^{n-2} + \dots + X_B + 1)] \} X_A X_B \quad (\text{A12})$$

The second term of  $F^e$  (designated by  $Y$ ) can be treated in the same manner by expanding the logarithms and substituting the following expressions for the distance ratios in terms of  $\rho$ ,  $\delta$ , and  $\theta$

$$\langle r^*_A \rangle / r^*_{AA} = 1 + 1/2\rho X_B [1 + (\theta + 1/2\delta + 17/4\rho)X_A] \\ \langle r^*_B \rangle / r^*_{BB} = 1 - 1/2\rho X_A [1 - \rho + (\theta - 1/2\delta - 17/4\rho)X_B]$$

Then

$$Y = -3/2RT\bar{q}c_Aq_A^{-1}X_A X_B \{ \rho[1 + (\theta + 1/2\delta + 17/4\rho)X_A] - \rho\alpha[1 - \rho + (\theta - 1/2\delta - 17/4\rho)X_B] - 1/4\rho^2(X_B + \alpha X_A) \} \quad (\text{A13})$$

The third term will be approximated by the Guggenheim-Miller formula for the excess entropy of mixing of two  $r$ -mers

$$-TS^e = -RT[(z/2 - 1)(\bar{r} \ln \bar{r} - x_A r_A \ln r_A - x_B r_B \ln r_B) - (z/2)(\bar{q} \ln \bar{q} - x_A q_A \ln q_A - x_B q_B \ln q_B)] \quad (\text{A14})$$

or the limit of this expression for  $z \rightarrow \infty$  (Flory-Huggins approximation).

For the case of most frequent interest in gas chromatography where the solute is infinitely diluted monomer and the solvent is  $r$ -mer, we can set  $r_A = q_A = c_A = 1$  with  $x_A \rightarrow 0$ . The result, setting

$$RT \ln \gamma^3_A = \lim_{x_A \rightarrow 0} (F^e/x_A)$$

is given as eq. 3 of the text.

# Single-Ion Activity Coefficients of Gegenions in Sodium Polyacrylate

by Tsuneo Okubo, Yasuko Nishizaki, and Norio Ise

Department of Polymer Chemistry, Kyoto University, Kyoto, Japan (Received February 2, 1965)

Using a glass electrode sensitive to sodium ions, single-ion activity coefficients of gegenions were determined with aqueous sodium polyacrylate solutions. The stoichiometric activity coefficient was found to be almost independent of concentration except at low concentrations. Experimental results were successfully compared with a previously published theory from this laboratory. This theory also explained the experimental data obtained with extremely low molecular weight analogs of polyethylenimine.

## I. Introduction

In another paper,<sup>1</sup> the determination of mean activity coefficients of polyelectrolytes will be reported. This quantity has been poorly treated in studies of polyelectrolyte solutions; in other words, many theoretical works do not meet the basic requirement concerning electrolyte activities alleged by Guggenheim.<sup>2</sup> On the basis of agreement with experiment, some of these theories have been claimed to describe successfully the complicated phenomena of polyelectrolyte solutions. If one accepts and follows the strictest interpretation of Guggenheim, however, these successes cannot easily be accepted, and the theories should be re-examined in terms of mean activity coefficients.

Recently, Frank<sup>3</sup> has proposed a return to the ascription of physical significance to single-ion activities. At first sight, this proposal justifies, at least qualitatively, the determination of single-ion activity coefficients of gegenions in polyelectrolyte solutions. It should not be overlooked, however, that Frank's reinstatement of single-ion activities (or single-ion activity coefficients) as working quantities has never been based on the denial of mean activities (or mean activity coefficients) as thermodynamic quantities. It would thus be acceptable to consider both mean and single-ion activities (or activity coefficients) of polyelectrolytes. While it is expected that the concurrent determinations and comparative studies of these two kinds of activity coefficients can eventually lead to a better understanding of polyelectrolyte solutions, attention will be focused on single-ion activity coefficients in this paper.

The measurements were carried out with the same

Na-glass electrodes and sodium polyacrylate as used for mean activity coefficient measurements in another paper.<sup>1</sup>

The determinations of Na<sup>+</sup> activity in polyelectrolyte solutions have been performed by many authors, and various methods have been used.<sup>4</sup> The Na-glass electrode method used in this paper has the advantage of simplicity, and the reversibility of the electrode with respect to Na<sup>+</sup> in a wide range of activity is also a merit.<sup>5</sup>

## II. Experimental Section

*A. Materials.* The polyelectrolyte sample was sodium polyacrylate (NaPAA), a gift from Professor M. Nagasawa, Nagoya University. The weight-average degree of polymerization was 1640. The sample was originally an aqueous solution containing about 5% polymer. This solution was diluted and passed through a column containing cation- and anion-exchange resins. The polyacid thus obtained was neutralized with sodium hydroxide by potentiometric titration, using a Horiba Model P pH meter. This pH meter has an accuracy comparable to that of a Beckman Model G pH meter. Final polymer concentration was calculated from the data of this potentiometry. Reagent grade sodium chloride and sodium

(1) N. Ise and T. Okubo, *J. Phys. Chem.*, in press.

(2) E. A. Guggenheim, *ibid.*, **33**, 842 (1929).

(3) H. S. Frank, *ibid.*, **67**, 1554 (1963).

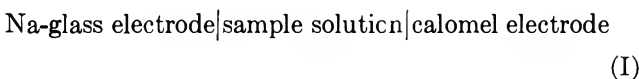
(4) S. A. Rice and M. Nagasawa, "Polyelectrolyte Solutions," Academic Press Inc., New York, N. Y., 1961.

(5) For a discussion of the properties of Na-glass electrodes, see G. Eisenman, D. O. Rudin, and J. U. Casby, *Science*, **126**, 831 (1957).

hydroxide were used without further purification. Sodium chloride solutions were prepared by diluting a 0.1 *M* stock solution. The densities of polymer and simple electrolyte solutions were determined to obtain molalities. Reagent grade uranyl acetate and zinc acetate were used without further purification for the preparation of zinc uranyl acetate solution. Conductivity water was used for the preparation of all the solutions for all measurements. The specific conductance of the water was  $10^{-7}$  ohm $^{-1}$  cm. $^{-1}$  as collected from the delivery tip of columns of ion-exchange resins.

*B. E.m.f. Measurements. Electrodes.* The Na-glass electrodes (Horiba Manufacturing Co., Kyoto) will be described in another paper.<sup>1</sup> Saturated potassium chloride calomel electrodes of the same manufacturer were used as reference electrodes. The glass electrodes were conditioned in 0.1 *M* NaCl aqueous solution for 2 months before a series of experiments were started and were stored in the same solution while not in use.

*Cell.* The cell used to obtain the Na<sup>+</sup> activity was



Assuming that the liquid junction potential between KCl solution in the calomel electrode and sample solution does not vary with the concentration of the sample, the electromotive force (e.m.f.), *E*, can be expressed as

$$E = E_0 - \frac{RT}{F} \ln a_{\text{Na}^+} \quad (1)$$

where *E*<sub>0</sub> is the standard e.m.f. of the above cell, *a*<sub>Na<sup>+</sup></sub> the single-ion activity of Na<sup>+</sup>, *R* the gas constant, *T* the temperature, and *F* the Faraday charge. Although the above assumption cannot rigorously be established, we assume that it is not very far from reality, as in the cases of pH measurements, or gegenion activity measurements in general reported to date.<sup>4</sup>

Medium-size weighing bottles were used as cell vessels. The Na-glass electrode and calomel electrode were supported in a rubber stopper tightly fitting into the top of the cell vessel. Since the absolute value of the e.m.f. of the above cell increased appreciably at first after immersion of the electrodes into the solutions and reached exponentially a limiting value which was constant within 0.1 mv. over a 30-min. period, this limiting value was recorded as a reliable e.m.f. Usually, it took 60 to 90 min. to accomplish one determination though the reason is not completely clear.<sup>6</sup>

The effect of K<sup>+</sup> from the saturated potassium chlo-

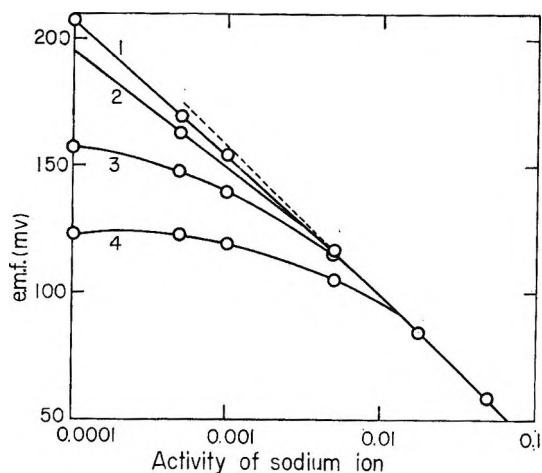


Figure 1. Sodium response at four different constant background levels of potassium. Potassium ion concentration (*m*) is 0 for curve 1, 0.001 for curve 2, 0.01 for curve 3, and 0.1 for curve 4; temperature 25°. The broken line represents the Nernstian slope.

ride calomel electrode may be ignored because of the following two reasons. First, diffusion of K<sup>+</sup> through the orifice of our fiber-type calomel electrode should increase the concentration of K<sup>+</sup> in the bulk of sample solutions with time, and this increase should result in a decrease of the absolute value of the e.m.f. This is contrary to our above-mentioned observation. Secondly, it is to be noted that the glass electrode displays the theoretical response to Na<sup>+</sup> activity in solution containing both sodium and potassium ions, until the potassium ion activity exceeds that of the sodium ion. This conclusion was drawn from Figure 1, which shows the data on the performance of the glass electrode in solutions containing mixtures of K<sup>+</sup> and Na<sup>+</sup>. Under our experimental conditions, it is highly improbable that the activity of potassium ions becomes larger than that of sodium ions.

The pH values of the solutions have also been determined. In all cases the hydrogen ion concentrations were so small (see, for example, Table I) that the glass electrodes may be assumed to respond to sodium ions exclusively.

Before and after e.m.f. measurement, calibration of the glass electrode was undertaken at 0.1 *M* NaCl using cell II.

(6) Some preliminary experiments were carried out at low degrees of neutralization. The tight-fitting stopper was not necessary in these cases supposedly since carbon dioxide did not interfere with accurate determinations of Na<sup>+</sup> activity. These experiments took also about 90 min. for one measurement. Therefore, the equilibration time mentioned in the text does not appear to be due to a pressure effect produced by the tight-fitting stopper.

Na-glass electrode|NaCl solution|calomel electrode  
(II)

The precision of e.m.f. measurements was  $\pm 0.5$  mv., and the reproducibility was  $\pm 2\%$ .

*Apparatus.* The measuring circuit consists of a precision potentiometer, Type K-2, of the Shimadzu Manufacturing Co., Kyoto, and a vibrating-reed electrometer, modified TR-85, manufactured by the Takeda Riken Industry Co., Tokyo, as a null detector. The input impedance of the electrometer was more than  $10^{14}$  ohms, and the maximum sensitivity was 0.1 mv. All e.m.f. measurements were carried out in a liquid paraffin bath ( $25 \pm 0.02^\circ$ ) in a large grounded-metal box. The high impedance side of the circuit was carefully shielded.

*C. Transference Experiments.* The principles and details of the experiments have been described by Huizenga, Grieger, and Wall.<sup>7</sup> An H-type glass tube divided into two compartments by a sintered-glass frit sealed at the center was used as the cell. Two kinds of cells having different dimensions were used for measurements in high and low concentration ranges. The electrodes were bright platinum wire. Gas evolved during electrolysis was allowed to escape to the outside of the cell through a filling tube above the electrode. The range of the current provided by a regulated power supply of the Kikusui Electronics Corp., Tokyo, (Model 722C) was  $2 \times 10^{-3}$  to  $4 \times 10^{-3}$  amp., and the field strength was between 1 and 4 v./cm. At most, 10% of the sodium polyacrylate originally present was transferred from one compartment to the other.

The experiments were carried out in a liquid paraffin thermostat at  $25 \pm 0.1^\circ$ . The change in weight of total solute was determined by evaporation of 20-ml. aliquots from each compartment. To determine the change in weight of sodium in solution, a 10-ml. aliquot was taken from the anode compartment, and concentrated  $H_2SO_4$  was added. Then the solution was ashed in a crucible. Upon dissolving the ash in water, the sodium was precipitated as sodium uranyl zinc acetate. The accuracy of this sodium content determination is  $\pm 0.5\%$ .<sup>8</sup>

The electric conductivity of the solution was measured at 1000 c.p.s., using a Wheatstone-type bridge.

The weight changes of total solute and sodium were used to calculate the polymer charge fraction.<sup>9</sup> This fraction for each solution was determined in duplicate transference runs. The two measurements were always in excellent agreement.

### III. Results

*Calibration of Na-Glass Electrode.* Using a cell shown by (II), calibration of our Na-glass electrodes

was carried out. In the activity range of 0.1–0.01, the relation between  $E$  and  $\log a_{Na^+}$  was linear having the Nernstian slope,<sup>10</sup> whereas in the low activity range (0.001–0.0001) the slope was 54.0 mv., as is shown in Figure 1. Although this slope deviates from its theoretical value by 8.6%, we regarded these calibration lines as reliable and used them to determine  $a_{Na^+}$ .

*Activity Coefficient Data.* The results obtained in e.m.f. measurements are shown in Table I. In Table I, the single-ion activity coefficients ( $\gamma_{Na^+}^*$ ) of  $Na^+$  at a degree of neutralization of 1.00 are given as functions of concentration.  $\gamma_{Na^+}^*$  is found to be about 0.3 and is independent of concentration to the first approximation, except at very low concentrations. It should be noted that this value is in rough agreement with those found by Kern<sup>11</sup> with sodium polyacrylate at a degree

**Table I:** Molal Activity Coefficients of Sodium Ions in Solutions of Sodium Polyacrylates (Degree of Neutralization, 1.00; Degree of Polymerization, 1640)

Polymer concn., monomolal	e.m.f., mv.	$\gamma_{Na^+}^*$	pH
0.253	48.3	$0.29 \pm 0.01$	8.60
0.202	53.6	0.29	8.68
0.167	60.0	0.28	...
0.0995	73.0	0.28	8.89
0.0663	83.4	0.28	...
0.0166	117.4	0.28	...
0.0116	125.6	0.29	9.57
0.00829	134.4	0.28	...
0.00331	158.1	0.25	...
0.00167	175.7	0.24	...

of neutralization of 0.8. We conclude that  $\gamma_{Na^+}^*$  is almost independent of concentration above 0.008  $m$ , whereas Kern found that it increased. Nagasawa and Kagawa also obtained similar results to Kern's, using sodium polyvinyl sulfate, sodium cellulose sulfate, sodium polystyrene sulfonate, and sodium carboxymethylcellulose.<sup>12</sup> On the other hand, Hardisty

(7) J. R. Huizenga, P. F. Grieger, and F. T. Wall, *J. Am. Chem. Soc.*, **72**, 2636 (1950).

(8) F. P. Treadwell and W. T. Hall, "Analytical Chemistry," John Wiley and Sons, Inc., New York, N. Y., 1942, Chapter 5.

(9) The transference experiments were originally carried out to determine the transference number of macroions, which was needed to measure mean activities of polyelectrolytes.<sup>1</sup> In this paper, only the value of the polymer charge fraction is required.

(10)  $a_{Na^+}$  was calculated with the assumption of  $\gamma_{Na^+} = (\gamma_{NaCl})^{1/2} / \gamma_{\pm KCl}$ , where  $\gamma_{Na^+}$  is the single-ion activity coefficient of  $Na^+$  and  $\gamma_{\pm}$  is the mean activity coefficient of the component specified by the suffix.

(11) W. Kern, *Makromol. Chem.*, **2**, 279 (1948).

**Table II:** Transference and Related Measurements on Sodium Polyacrylate Solutions (Degree of Polymerization, 1640; Degree of Neutralization, 0.98)

$c$ , $N$	pH	$10^4\kappa$ , mho cm. <sup>-1</sup>	$10^3g$ , g.	$10^3q_1$ , equiv.	$10^3q_2$ , equiv.	$10^3N_e$ , equiv.	$\Lambda_{Na}$	$f$	$t_{2p}$	$i/s$
0.2	8.08	70.3	1.02	-21.8	+2.25	1.68	38.2	0.419	0.554	0.413
0.15	8.18	52.9	1.35	-4.27	+2.03	1.68	39.6	0.437	0.519	0.429
0.07	8.51	25.4	2.19	-2.35	+3.15	2.98	42.9	0.438	0.484	0.429
0.05	8.64	18.3	2.18	-11.5	+3.38	2.98	44.0	0.436	0.483	0.427
0.0378 <sup>a</sup>	8.78	11.4	2.66	+9.70	+3.43	3.00	45.9	0.383	0.427	0.375
0.0151 <sup>a</sup>	8.96	5.344	1.00	+4.35	+1.27	0.93	47.3	0.377	0.503	0.369
0.01	9.22	4.16	0.53	-0.63	+0.770	0.75	47.3	0.463	0.482	0.467
0.008	9.29	3.17	0.55	-1.25	+0.811	0.75	47.8	0.440	0.480	0.442

<sup>a</sup> From ref. 7.

and Neale<sup>13</sup> reported that the single-ion activity coefficients of Na<sup>+</sup> in sodium alginate and sodium carboxymethylcellulose decreased with increasing concentration. A research group of Chicago<sup>14</sup> has also published similar results with polyethylenimine, the gegenion being Cl<sup>-</sup>. As was mentioned earlier,<sup>15</sup> the concentration dependence of the activity coefficient is closely related to the dimension of macroions in solution. If this factor is properly considered, the discrepancy between the above-mentioned various experimental results is not so serious as it appears.

**Transference Data.** Table II shows the experimental results for six stoichiometric polyacrylate concentrations,  $c$ , at a degree of neutralization of 0.98.<sup>16</sup> The symbols are defined as follows:  $\kappa$ , total specific conductivity minus solvent specific conductivity;  $g$ , increase in weight of solute in anode compartment;  $q_1$ , increase in equivalents of sodium in anode compartment;  $q_2$ , increase in equivalents of polymer anion in anode compartment;  $N_e$ , total equivalents of electricity;  $\Lambda_{Na}$ , ion conductance of sodium ion;  $f$ , fraction of sodium ions not associated with polyion;  $t_{2p}$ , transference number of polyion;  $i/s$ , polymer charge fraction;  $i$ , number of charges on polymer chain;  $s$ , degree of polymerization.

Transference data, transference number, and polymer charge fraction should be discussed in this section. For comparison, the experimental data and relevant quantities at a degree of neutralization of 0.979 reported by Huizenga, Grieger, and Wall<sup>7</sup> are shown in the seventh and eighth lines of Table II. It is clear that  $f$  and  $i/s$  reported by these authors are smaller than ours, and their  $t_{2p}$  is not far from ours. Since they have carried out radioactive counting measurements and we have used a gravimetric method to determine  $q_1$ , the difference in the accuracies of these two methods may explain the discrepancy. However, as mentioned already in ref. 7,  $q_1$  is greatly uncertain

so that, to calculate  $f$ , we have used the "recommended" procedure,<sup>7</sup> in which  $f$  is "only weakly dependent" on  $q_1$ . Thus, this accuracy problem can be excluded from the present consideration. The next factor to be considered is the difference in the degrees of polymerizations ( $s$ ). Huizenga, *et al.*, have chosen 250 for  $s$ , whereas our  $s$  was estimated to be 1640 by viscometry. We suspect that the larger the degree of polymerization, the lower the charge density in a macroion sphere, and accordingly a smaller fraction of the sodium ions is associated with the polymer. Therefore, our  $f$  is larger than that of Huizenga, *et al.* This is a very rough estimate, and a correct answer will be given in our forthcoming experiments involving polyelectrolytes of various degrees of polymerization. In the present paper, we will continue our discussion on the basis of our own experimental results.

Huizenga, *et al.*,<sup>7</sup> reported that  $f$  and  $i/s$  increase very slightly and  $t_{2p}$  decreases with increase in polymer concentration. This finding disagrees with our results, which show that  $f$  and  $i/s$  decrease and  $t_{2p}$  increases with increasing concentration. (The concentration dependence in the low concentration range (0.008 to 0.01  $N$ ), which is the reverse of what was observed at high concentrations, is omitted from the present considerations. It will be discussed after more experimental data have been accumulated.) Though the reason for this disagreement is not yet clear, our interpretation is that the macroion shrinks with increasing concentration; *i.e.*, the charge density in a

(12) M. Nagasawa and I. Kagawa, *J. Polymer Sci.*, **24**, 61 (1957).(13) D. R. Hardisty and S. M. Neale, *ibid.*, **46**, 195 (1960).(14) S. Lapanje, J. Haevig, H. T. Davis, and S. A. Rice, *J. Am. Chem. Soc.*, **83**, 1590 (1961).(15) N. Ise and M. Hosono, *J. Polymer Sci.*, **39**, 389 (1959).(16) For the assumptions and equations relevant to the calculation of polymer charge fraction,  $i/s$ , from the data of transference experiment, see ref. 7.

macroion sphere becomes large, so that the fraction of free sodium ions decreases with increasing concentration. The same interpretation applies to  $i/s$ . The tendency for  $t_{2p}$  to increase with increasing concentration is also understandable if one assumes that shrinking of the macroion increases the mobility.<sup>17</sup>

#### IV. Discussion

Before comparing theory with experiment, single-ion activity coefficients of gegenions should be defined in two ways. The first definition refers to the total stoichiometric concentration of gegenions, whereas the second refers to the concentration of free gegenions. In other words, the first definition is based on the assumption that the electrolyte is fully dissociated, and the second, on the assumption that the electrolyte is partially dissociated. The single-ion activity coefficient according to the first definition is usually called the "stoichiometric activity coefficient"<sup>18</sup> and is denoted by  $\gamma_{2g}^*$  in this paper. The difference between these two definitions was previously discussed by one of the present authors.<sup>15</sup> This author has calculated single-ion activity coefficients in solution containing  $\alpha$ -valent macroions assuming partially dissociated polyelectrolytes.<sup>19</sup> It should be noted that the electrostatic interaction between dissociated free ions ( $n_2$  macroions and  $\alpha n_2$  gegenions per unit volume of solution) was considered in this calculation. The single-ion activity coefficient thus determined follows the second definition and will be denoted by  $\gamma_{2g}$  in the present paper. In the previous paper,<sup>15</sup> for foreign salt-containing solutions,  $\gamma_{2g}$  was formulated as

$$kT \ln \gamma_{2g} = -\frac{\kappa e_0^2}{3\epsilon} \left\{ \tau(\kappa\delta_2) + \frac{1}{2} [\alpha n_2(\alpha\sigma(\kappa r) + \sigma(\kappa\delta_2)) + 2n_3\sigma(\kappa\delta_3)] \left( \frac{1 - 2\alpha n_2 v_{2g}}{\alpha^2 n_2 \mathfrak{M}_{2p} + \alpha n_2 \mathfrak{M}_{2g} + 2n_3 \mathfrak{M}_2} \right) \right\} \quad (2)$$

with

$$\kappa^2 = (4\pi e_0^2 / \epsilon kT) [\alpha n_2(\alpha \mathfrak{M}_{2p} + \mathfrak{M}_{2g}) + 2n_3 \mathfrak{M}_3]$$

where  $e_0$  is the absolute value of the elementary charge,  $k$  the Boltzmann constant,  $\epsilon$  the dielectric constant of solvent,  $\delta_2$  the mean radius of an ionized group and a gegenion,  $\delta_3$  the mean radius of positive and negative ions of foreign salt,  $n_2$  the number of macroions per unit volume of solution,  $n_3$  the number of foreign salt molecules per unit volume of solution,  $r$  the radius of macroion,  $\mathfrak{M}_i$  the exclusion volume parameter of ion  $i$  ( $\mathfrak{M}_i = 1 - n_2 v_i$ , e.g., for macroion), and  $v_i$  the exclusion volume of ion  $i$  ( $v_i = 4\pi r^3/3$  for macroion). The subscripts 2 and 3 refer to polyelectrolyte and foreign salt, respectively, and  $p$  and  $g$  to macroion

and gegenion, respectively.<sup>20</sup>  $\sigma$  and  $\tau$  are familiar functions which appeared in the Debye-Hückel theory.<sup>21</sup>

By extending the treatment of mean activity coefficient for low molecular weight weak electrolytes<sup>22</sup> to the single-ion activity coefficients of polyelectrolytes, we find the following relationship between  $\gamma_{2g}^*$  and  $\gamma_{2g}$

$$\gamma_{2g}^* = \beta \gamma_{2g} \quad (3)$$

where  $\beta$  denotes the stoichiometric fraction of free gegenions. Using the results of transference experiments, we have determined the polymer charge fraction,  $i/s$ . In the following, we will assume that  $i/s$  is equal to  $\beta$  in eq. 3. Preliminary calculation has shown that the  $\gamma_{2g}^*$  is weakly dependent on  $i/s$ , so that an average of 0.44 obtained from Table II will be used for  $i/s$  and will be used for the calculation of  $\gamma_{2g}^*$ , irrespective of the concentration, without sacrificing the generality of our conclusion. Thus, it is possible to compare the observed and the theoretical values for  $\gamma_{2g}^*$ .

In Figure 2, the observed values of  $\gamma_{2g}^*$  are shown by circles. The solid curve in this figure shows the theoretical values, which were obtained using eq. 2 and 3, and numerical values of  $T = 298^\circ\text{K}$ ,  $\epsilon = 80$ ,  $Z = 1640$ ,  $\beta = 0.44$ ,  $\alpha = \beta Z = 720$ ,  $\delta_2 = 4 \text{ \AA}$ ., and  $r = 100, 200, \text{ and } 400 \text{ \AA}$ .

From Figure 2, the radius of the macroion sphere is seen to be between 100 and 400  $\text{\AA}$ . if the concentration is higher than 0.08 monomolal and is seen to decrease with increasing concentration. This tendency is in accord with the usual expectation. Below 0.03 monomolal, a much smaller value should be assigned to the radius. However, it should be pointed out that e.m.f. measurements in the dilute region could not be carried out as accurately as those in the concentrated region.<sup>23,24</sup>

(17) This interpretation is consistent with the concentration dependence of mobility which can be estimated from conductivity and  $i/s$ .

(18) R. A. Robinson and R. H. Stokes, "Electrolyte Solutions," Butterworth Scientific Publications, London, 1959, Chapter 2.

(19)  $\alpha$  is the net valency of a macroion. The macroion was assumed to have  $Z$  ionized groups and  $\lambda$  bound gegenions, and  $\alpha = Z - \lambda$  was approximately assumed.

(20) Note that the notations adopted in the present paper are different from the ones in the previous paper.<sup>15</sup>

(21) See, for example, R. H. Fowler and E. A. Guggenheim, "Statistical Thermodynamics," 1st Ed., Cambridge University Press, London, 1939, Chapter 9.

(22) See ref. 18, Chapters 2 and 12.

(23) It is possible that eq. 2 or the theory connected with it does not hold at low concentrations or for large macroions and gives an inconceivably small closest distance of approach. This situation has also been encountered by applying the Debye-Hückel theory to large ions.<sup>24</sup>

(24) J. N. Brønsted and V. K. La Mer, *J. Am. Chem. Soc.*, **46**, 555 (1924).



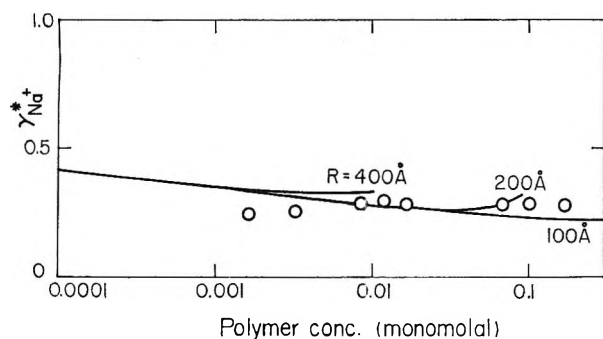


Figure 2. Polymer concentration dependence of the stoichiometric activity coefficient of sodium ion in sodium polyacrylate: O, observed; —, calculated with  $r = 400, 200, \text{ and } 100 \text{ \AA}$ .

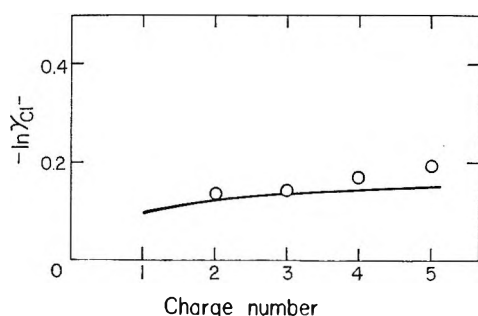


Figure 3. Activity coefficient of chlorine ion in low molecular weight analogs of polyethylenimine salt; concentration  $0.01 \text{ m}$ : O, observed; —, calculated by eq. 2.

Thus, the agreement between theory and experiment demonstrated in Figure 2 is satisfactory.

As mentioned in the preceding paragraph, the dimension of macroions generally varies with concentration. Owing to this variation, a conclusive discussion of the validity of eq. 2 is difficult. Therefore, it is interesting to apply eq. 2 to solutions containing ions, the dimension of which can be assumed to be independent of concentration. We think that polyelectrolytes of extremely low molecular weights can meet our requirement. Use is made here of the measurements<sup>14</sup> of gegenion activity of very low molecular weight analogs of polyethylenimine. Figure 3 is a comparison of theory and experimental data showing  $-\ln \gamma_{\text{Cl}^-}$  as a function of charge number at  $0.010 \text{ m}$ .<sup>25</sup> The theoretical values have been obtained using eq. 2 and  $\delta_2 = 4 \text{ \AA}$ ,  $T = 298^\circ \text{K}$ .,  $\epsilon = 80$ , and appropriate  $r$  values.  $r = 5, 7.05, 8.65, 10, \text{ and } 11.20 \text{ \AA}$ . were used for ethylamine (EA), ethylenediamine (ED), diethylenetriamine (DT), triethylenetetramine (TT), and tetraethylenepentamine (TP), respectively.  $\beta$  was assumed

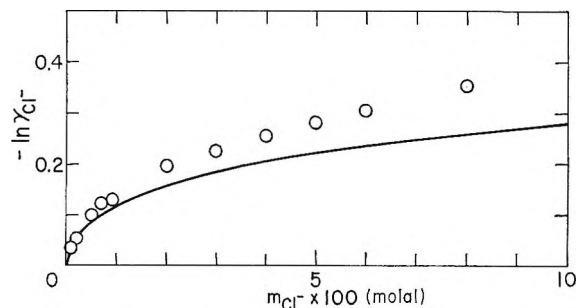


Figure 4. Concentration dependence of the activity coefficient of chlorine ion in ethylenediamine salt: O, observed; —, calculated by eq. 2.

to be unity on the basis of the diffusion experiments of Lapanje, *et al.*<sup>14</sup> It was found that the calculated value of  $\gamma_{\text{Cl}^-}$  varied only slightly with large changes in the assumed value for  $\delta_2$  and  $r$ . For example, a 100% decrease or increase in  $r$  resulted in a 10% change in  $-\ln \delta_{\text{Cl}^-}$  with a  $0.10 \text{ m}$  TP solution, which is the most sensitive case to the change. The effect of  $\delta_2$  was also negligible. Although reliable data of ionic radii of these amines are not available, we believe that the above-mentioned  $r$  values are correct estimates. Thus, the agreement between theory and experiment shown in Figure 3 is physically significant. Figure 4 gives the experimental data<sup>26</sup> of a bolaform electrolyte, ED, as a function of electrolyte concentration and the corresponding theoretical curve constructed with eq. 2. The agreement between theory and experiment is excellent for low concentrations and satisfactory for a wide range of high concentrations. The calculations for other amines also show very satisfactory results though the agreement was found to become increasingly less satisfactory with increasing charge number.<sup>27</sup>

From this discussion, we conclude that arguments against the usefulness and validity of eq. 2 have been weakened and the reliability of eq. 2 in the study of polyelectrolytes is greatly enhanced.

*Acknowledgments.* The authors appreciate Professor Ichiro Sakurada's encouragement and useful comments. This work would have been extremely difficult to perform without the experience of N. I. in the laboratory of Professor U. P. Strauss.

(25) See Figure 7 in ref. 14.

(26) Compare with Figure 5 in ref. 14.

(27) It should be added that a similar comparison was carried out with the  $\text{Na}^+$  activity coefficient data of sodium  $\alpha$ -methylglutarate and sodium  $\gamma$ -carboxypimelate (low molecular weight analogs of sodium polyacrylate) reported by Kern,<sup>11</sup> and a satisfactory agreement was also obtained.

## A Kinetic Study of the Lipoamide Dehydrogenase-NADH-Dye Reaction

by George G. Guilbault, David N. Kramer, and P. Goldberg

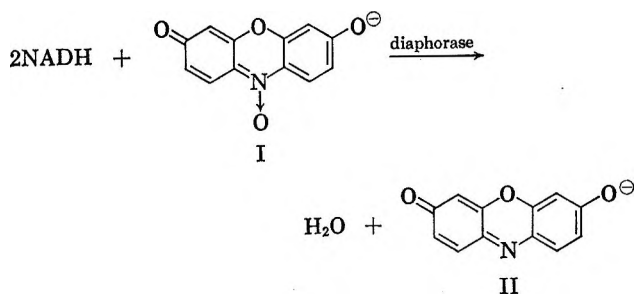
Defensive Research Division, U. S. Army Chemical Research and Development Laboratories, Edgewood Arsenal, Maryland (Received February 12, 1965)

Fluorometric and spectrophotometric techniques have been used to study the kinetics of the diaphorase-NADH-dye reaction. Differences are observed in the kinetic relationships depending on the synthetic substrate: resazurin or dichloroindophenol. For resazurin, initial reaction velocities ( $v_0$ ) are independent of NADH (nicotinamide adenine dinucleotide, reduced form) concentration, but in the case of the indophenols, a dependence on NADH was found. These results have been interpreted on the basis of a particular reaction scheme:  $e/V_0 = \phi_1/[S_1] + \phi_2/[S_2]$ , where  $e$  represents the diaphorase total concentration,  $[S_1]$  the NADH concentration,  $[S_2]$  the concentration of the dye, resazurin or dichloroindophenol, and  $\phi_1$  and  $\phi_2$  are constants. Experimental evidence is consistent with the idea that the substrate is reduced by the reduced form of the enzyme, rather than by an enzyme-NADH complex.

### Introduction

Because of the inhibition of the enzyme lipoamide dehydrogenase, diaphorase, by sulfhydryl binding chemical agents, interest developed in the mechanism by which this enzyme acts on various substrates. In this report the application of a fluorescence method for following reactions of the reduced form of nicotinamide adenine dinucleotide, NADH, with the enzyme diaphorase is shown. Fluorescence methods are generally preferred over absorption methods because of greater sensitivity.<sup>1</sup> Similar techniques have been applied in the past to follow enzymatic reactions. Dalziel monitored the fluorescence of NADH itself during reactions catalyzed by lactic acid dehydrogenase.<sup>2</sup> Massey<sup>3</sup> and Searls and Sanadi<sup>4</sup> have studied the diaphorase-catalyzed oxidation of NADH using various lipoamide and lipoate substrates. In this study, the kinetics of reaction of two synthetic substrates, resazurin (I) and dichloroindophenol (DIP) have been followed, and kinetic formulas have been applied as a test of the mechanism for these synthetic substrate reactions. When resazurin (I) is reduced in the presence of diaphorase, resorufin (II) is produced, which is strongly fluorescent ( $\lambda_{\text{ex}}$  560 m $\mu$ ;  $\lambda_{\text{em}}$  580 m $\mu$ ). Dichloroindophenol, on the other hand, is reduced in the enzymatic reaction to the dihydro compound, which is nonfluorescent.

In the course of this study, it became clear that the enzyme kinetics showed some uncommon properties.



The initial reaction velocities of resazurin reduction were found to be independent of NADH concentration. Calculations showed (see Discussion) that in such a case a complex between diaphorase and NADH was probably not responsible for the reduction of the resazurin. To clarify this result, additional studies were made in which dichloroindophenol was substituted for resazurin, and the kinetics were followed by absorption spectrophotometry. A mechanism and a single kinetic expression will be given below that satisfactorily summarize the results with both resazurin and DIP. The mechanism is distinguishable from other possible enzymatic mechanisms when the data for initial velocities

(1) S. Udenfriend, "Fluorescence Assay in Biology and Medicine," Academic Press, New York, N. Y., 1962, p. 312.

(2) K. Dalziel, *Biochem. J.*, **80**, 440 (1961).

(3) V. Massey, *Biochim. Biophys. Acta*, **37**, 314 (1960).

(4) R. L. Searls and D. R. Sanadi, *J. Biol. Chem.*, **236**, 580 (1961).

are analyzed according to the method of Dalziel.<sup>5</sup> The mechanism states that there is a direct reduction of the enzyme by the coenzyme NADH, and this reduced enzyme, in turn, reduces the resazurin to the fluorescent resorufin or the colored DIP to its leuco form. This is consistent with the mechanism of the diaphorase-NADH reaction offered by Massey<sup>3</sup> and by Searls and Sanadi.<sup>6</sup>

### Experimental Section

**A. Reagents.** All reagents were prepared in triply distilled water or specially purified solvents. Enzyme and coenzyme solutions were freshly prepared each day before use. (1) Enzymes, diaphorase (Worthington Biochemical Co.), activity 10.4 units/mg. One unit equals a decrease in absorbance of 1.00/min. at 600  $m\mu$  using the dye 2,6-dichloroindophenol and the coenzyme NADH.<sup>7</sup> (2) Substrates, (a) resazurin (Eastman Organics Co.). A stock  $10^{-3}$  *M* solution was prepared in Methyl Cellosolve. (b) NADH (Calbiochem. Co., 83.2% pure). A stock 0.006 *M* solution was prepared, and the purity was analyzed by standard procedures.<sup>7</sup> (c) 2,6-Dichloroindophenol (DIP), sodium salt (Eastman Organics). A stock 0.0012 *M* solution was prepared in triply distilled water.

**B. Apparatus.** All fluorescence measurements were made with an Aminco-Bowman spectrophotofluorometer, as described in a previous publication.<sup>8</sup>

**C. Procedures. Fluorometric Determination of Enzyme Kinetics.** Appropriate dilutions of resazurin and NADH in Tris buffer, pH 7.5, are placed into a 3.0-ml. fluorescence cell thermostated at 25° in an Aminco-Bowman spectrofluorometer, and the instrument is adjusted to read zero fluorescence at 560 and 580  $m\mu$ . At zero time, a 0.1-ml. solution of diaphorase is added, and the change in the fluorescence with time,  $\Delta F/\Delta t$ , is automatically recorded. The initial slopes are taken from these curves and the rate of formation of resorufin,  $v_0$ , is calculated as

$$v_0 \text{ (moles l.}^{-1} \text{ min.}^{-1}) = \frac{\Delta F \text{ (fluorescence units)/min.}}{1.56 \times 10^7}$$

where  $1.56 \times 10^7$  represents the fluorescence units/moles per liter of resorufin.

**D. Colorimetric Procedure.** The rate of the diaphorase-NADH-DIP reaction was measured colorimetrically at 600  $m\mu$ . The absorbance on the Beckman Model DB spectrophotometer was set at zero with DIP and NADH in Tris buffer, pH 7.5, in both cells. At zero time the diaphorase is added to the left cell, and the change in the optical density is recorded *vs.* time ( $\Delta A/\text{min.}$ ). The reaction velocities were then cal-

culated by dividing  $\Delta A/\text{min.}$  by the molar absorptivity of DIP,  $1.25 \times 10^4$ .

### Results

The dependence of the initial velocity of the diaphorase-NADH-dye reaction on diaphorase concentration is given in Table I. A first-order dependence is observed with both resazurin (A) and DIP (B). Figure 1 gives the Lineweaver-Burk plot<sup>9</sup> of initial velocity *vs.* resazurin concentrations at fixed enzyme and NADH concentrations. This curve passes through the origin. In Figure 2 data are presented to show that  $v_0$  is independent of NADH concentration using resazurin as the synthetic substrate.

**Table I:** Dependence of the Initial Velocity of the Diaphorase-NADH-Resazurin (A) and the Diaphorase-NADH-Indophenol (B) Reactions on Diaphorase Concentration. (NADH and Resazurin in (A) are held constant at  $2 \times 10^{-4}$  and  $6.6 \times 10^{-6}$  *M*, respectively; in (B) NADH and DIP are held constant at  $2 \times 10^{-4}$  and  $4 \times 10^{-6}$  *M*, respectively.)

[Diaphorase], unit/ml. of soln.	$v_0$ , mole l. <sup>-1</sup> min. <sup>-1</sup>	
	(A)	(B)
0.0040	$3.3 \times 10^{-8}$	$1.3 \times 10^{-6}$
0.0080	$6.6 \times 10^{-8}$	$2.6 \times 10^{-6}$
0.0120	$1.0 \times 10^{-7}$	$4.0 \times 10^{-6}$
0.020	$1.67 \times 10^{-7}$	$6.6 \times 10^{-6}$
0.028	$2.33 \times 10^{-7}$	$9.5 \times 10^{-6}$
0.040	$3.3 \times 10^{-7}$	$1.35 \times 10^{-5}$
0.080	$6.6 \times 10^{-7}$	$2.7 \times 10^{-5}$

Interesting comparisons can be made of the kinetic data for DIP and resazurin. Both reactions are first order in diaphorase concentration (Table I). Figure 3 shows a linear Lineweaver-Burk plot with a nonzero intercept in which DIP is varied and NADH is held constant. Also, Figure 4, a plot of  $1/V_0$  *vs.*  $1/[\text{NADH}]$  at constant  $[\text{DIP}]$ , in sharp contrast to Figure 2, exhibits a linear Lineweaver-Burk plot with a nonzero slope. It is this difference that underlies the choice of reaction mechanisms given below.

### Discussion

These results can be summarized by a single reaction scheme, *i.e.*, type IVii in Dalziel's paper<sup>5</sup>

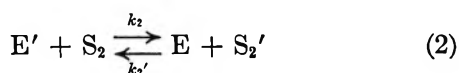
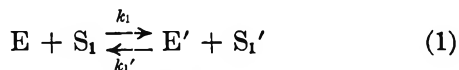
(5) K. Dalziel, *Acta Chem. Scand.*, **11**, 1706 (1957).

(6) R. L. Searls and D. R. Sanadi, *J. Biol. Chem.*, **236**, 2371 (1961).

(7) O. H. Lowry, N. R. Roberts, and J. I. Kapphahn, *ibid.*, **224**, 1047 (1957).

(8) D. N. Kramer and G. G. Guilbault, *Anal. Chem.*, **36**, 1662 (1964).

(9) H. Lineweaver and D. Burk, *J. Am. Chem. Soc.*, **56**, 658 (1934).



where E is the enzyme, diaphorase,  $S_1$  is NADH, and  $S_2$  is either resazurin or DIP.  $E'$  and  $S_2'$  are the reduced forms of the enzyme and substrate, respectively, and  $S_1'$  is  $NAD^+$ , the oxidized form of NADH. A reduced form of the enzyme is formed *via* (1). In reaction 2 the reduced enzyme reduces the substrate and is thereby regenerated in its original form. This mechanism leads to the following expression for the initial reaction velocities,  $v_0$ , for the disappearance of substrate<sup>6</sup>

$$\frac{e}{v_0} = \frac{k_1'}{k_1 k_2 [S_1]} + \frac{1}{k_2 [S_2]} \quad (3)$$

where  $e$  is the total enzyme concentration.

Equation 3 is in good agreement with the data in Figure 3 and 4 and Table I for DIP. Equation 3 also

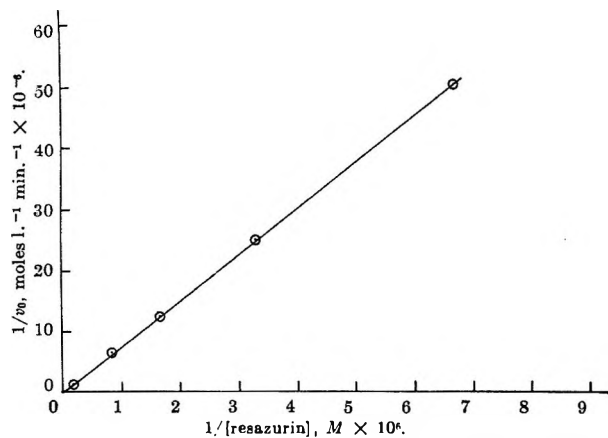


Figure 1. Lineweaver-Burk plot of reciprocal initial velocity vs. reciprocal resazurin concentration:  $[NADH] = 2 \times 10^{-4} M$ ; [diaphorase] = 0.08 unit/ml.

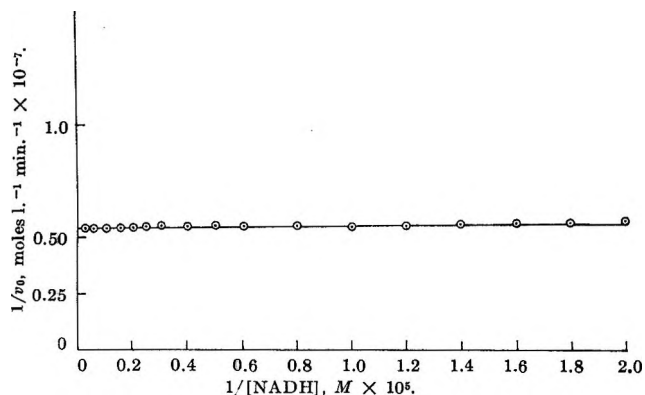


Figure 2. Lineweaver-Burk plot of  $1/v_0$  vs.  $1/[NADH]$ : resazurin =  $6.6 \times 10^{-6}$ , [diaphorase] = 0.04 unit/ml.

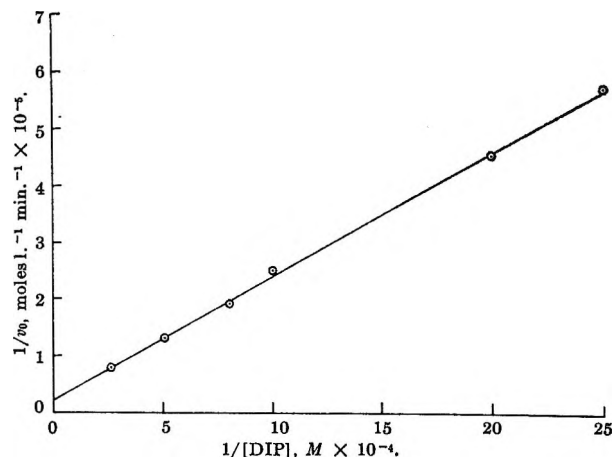


Figure 3. Lineweaver-Burk plot of  $1/v_0$  vs.  $1/[DIP]$ :  $[NADH] = 2 \times 10^{-4} M$ ; [diaphorase] = 0.16 unit/ml.

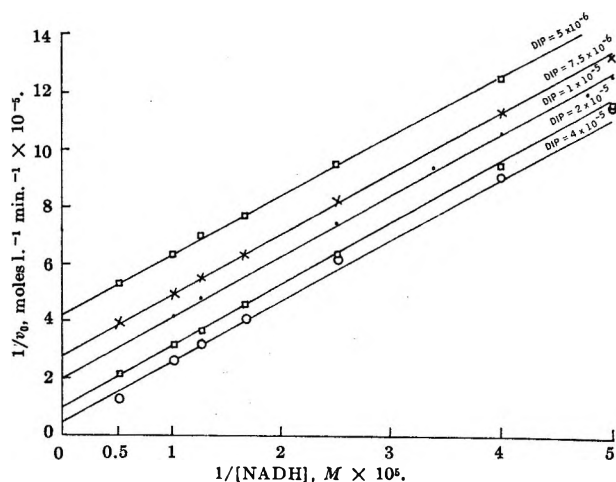


Figure 4. Family of Lineweaver-Burk plots of  $1/v_0$  vs.  $1/[NADH]$  with [DIP] as a parameter; [diaphorase] = 0.08 unit/ml.

satisfies the data of Table I and Figures 1 and 2 for resazurin, provided  $k_1[S_1] \gg k_2[S_2]$ . Assuming this, the second reaction (2) becomes rate determining, and  $V_0$  should become independent of NADH concentration. This is experimentally observed (see Figure 2). According to eq. 3, for various DIP concentrations, a secondary plot of the intercept of a family of Lineweaver-Burk plots should vary linearly with the corresponding DIP concentration. In addition, this line should pass through the origin. A family of such Lineweaver-Burk plots is shown in Figure 4. Figure 5 illustrates this secondary plot of the intercepts of Figure 4 and shows good agreement with eq. 3. Furthermore, the lines of Figure 4 are parallel, which is again in agreement with eq. 3. Thus the experimental data strongly suggest the correctness of eq. 1, 2, and 3.

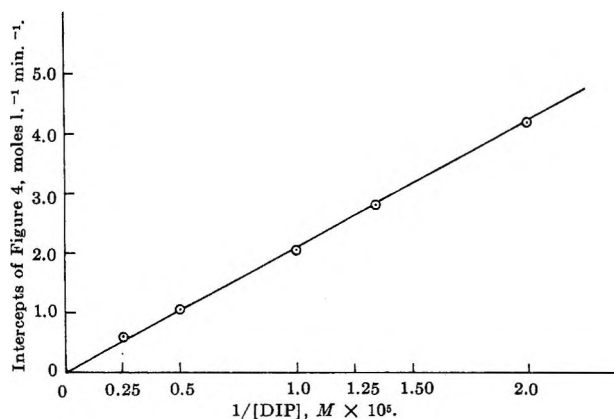
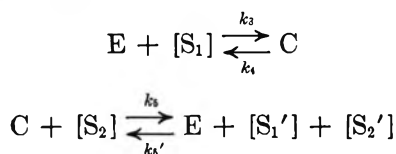


Figure 5. Intercepts on the ordinate of Figure 4 vs. the reciprocals of the corresponding [DIP] concentrations.

In the derivation of the above kinetics, it has been assumed that the dye is reduced by a reduced form of the enzyme, rather than by the complex [diaphorase-NADH]. We can show that a complex does not contribute to the substrate reduction as follows. Let us assume that (i) enzyme and NADH form a complex, and (ii) that it is this complex that serves to reduce the substrate, as in the mechanism proposed by Theorell and Chance<sup>10</sup> and reviewed by Dalziel<sup>5</sup>



where  $C = [ES_1]$ .

Since only initial velocities are considered, we may write as the result of the steady-state treatment

$$\frac{e}{v_0} = \frac{1}{k_3[S_1]} + \frac{1}{k_5[S_2]} + \frac{k_4}{k_3k_5[S_1][S_2]} \quad (4)$$

where again  $e$  is the total enzyme concentration.

This expression is eq. 1a of ref. 5, simplified in accordance with the restriction that only initial velocities are considered.

Equation 4 may be rearranged to

$$\frac{e}{v_0} = \left[ 1 + \frac{k_4}{k_5[S_2]} \right] \frac{1}{k_3[S_1]} + \frac{1}{k_5[S_2]} \quad (5)$$

Equation 5 predicts that, in a plot of  $1/v_0$  vs.  $1/[S_1]$ , the slope will vary as  $1/[S_2]$ . The data of Figure 4 show clearly that this is not the case (NADH =  $S_1$ ; DIP =  $S_2$ ), the slopes being independent of  $[S_2]$ . This mechanism cannot explain the data of Figure 2. We cannot, however, exclude the possibility of enzyme complexes forming which decompose to give the products of (1) and (2). All that can be said is that, if the complexes form, they decompose rapidly and they do not themselves reduce the substrate.

It is not possible to proceed further by the methods suggested by Alberty<sup>10</sup> and by Dalziel<sup>5</sup> to make the mechanism unequivocal. This would require evaluation of the kinetic constants for the reverse of eq. 1 and 2, as well as independent verification that the equilibrium constant,  $K_{eq} = k_1k_2/k_1'k_2'$ . This experimental test is not possible, since eq. 1 and 2 are not reversible for resazurin. We are able to estimate, however, the ratio  $k_1'/k_1$  for DIP substrates. From eq. 3 at  $1/v_0 = 0$ ,  $k_1[S_1]_0 = -k_1'[S_2]$ , where  $[S_1]_0$  is the intercept on the ordinate of the Lineweaver-Burk plot of  $1/v_0$  vs.  $1/[S_1]$ . Now from Figure 4, we find that  $k_1'/k_1 = 1.15$ .

Finally, it should be mentioned that these kinetic expressions may apply only to reactions involving synthetic substrates. The absence of enzyme complexes precludes the possibility of evaluating a true constant for the dissociation of an enzyme-substrate complex.

(10) R. A. Alberty, *J. Am. Chem. Soc.*, **75**, 1928 (1953).

## The Kinetics of the Tetrafluorohydrazine-Fluorine Reaction<sup>1</sup>

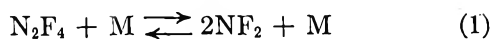
by Joseph B. Levy and B. K. Wesley Copeland

Atlantic Research Corporation, Alexandria, Virginia (Received February 23, 1965)

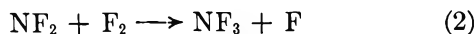
The reaction between fluorine and tetrafluorohydrazine has been investigated from 35 to 86°. Nitrogen trifluoride has been shown to be the only product. The kinetics have been measured by a colorimetric technique and have been shown to be homogeneous. It has been found that the kinetic data obey the expression  $-d(F_2)/dt = k(F_2)(N_2F_4)^{1/2}$  and  $k = 1.0 \times 10^{11.0 \pm 0.2} \exp(-20,400 \pm 400/RT) M^{-1/2} \text{ sec.}^{-1}$ . It is proposed that  $k = K^{1/2}k_2$  where  $K$  is the equilibrium constant for the dissociation of tetrafluorohydrazine and  $k_2$  is the rate constant for the reaction  $NF_2 + F_2 \rightarrow NF_3 + F$ .

### Introduction

In the course of our studies of the hydrogen-fluorine reaction<sup>2</sup> we have become interested in finding species that would react with molecular fluorine to yield fluorine atoms at a known rate. Among the possibilities considered was tetrafluorohydrazine. It seemed reasonable that this would react with fluorine in a manner analogous to that observed for nitrogen dioxide.<sup>3</sup> The equilibrium



has been studied<sup>4</sup> and the constants have been established. The reactions



would complete the analogy to the nitrogen dioxide-fluorine reaction. We have investigated the reaction kinetics for this system and report the results here.

### Experimental Part

**Chemicals.** The fluorine used in this work was General Chemical Co. fluorine that was freed of hydrogen fluoride by passage through a potassium fluoride trap. It has been found<sup>5</sup> that this treatment yields fluorine containing approximately 0.2 mole % oxygen as the only impurity. The nitrogen was Southern Oxygen Co. prepurified grade specified as 99.998 mole % nitrogen with the remainder oxygen. The tetrafluorohydrazine was Air Products Co. technical grade. Mass spectrographic analysis showed it to be 99.2 mole % pure, containing 0.6 mole % nitric oxide and 0.2 mole

% carbon dioxide as impurities. It was used without further treatment. The nitric oxide and carbon dioxide were taken directly from the cylinders without further treatment. The former was Matheson Co. product rated as 98.5 mole % pure while the latter was Southern Oxygen Co. product with a minimum purity of 99.9 mole %.

**Apparatus and Procedure.** The reaction rate measurements have been made by determining the fluorine concentration optically by means of its absorption at 2849 Å. The reaction vessel was a magnesium block designed to fit into the cell compartment of a Beckman DK spectrophotometer. Two cells path, 1.8 and 0.90 cm. in diameter, and 10 cm. long, machined through the block, constituted the reaction chambers. Sapphire windows were compression-sealed through Teflon gaskets to the block. The block was electrically heated and could be maintained at  $\pm 0.5^\circ$  manually. Both cell paths were thoroughly passivated before use. The apparatus is described in more detail elsewhere.<sup>2</sup>

Nitrogen trifluoride was found to be completely transparent at 2849 Å., but tetrafluorohydrazine was found to have a small absorption, presumably due to a tail of the difluoramino peak at 2650 Å.<sup>4</sup> A correction

(1) This work was supported by the Air Force Office of Scientific Research of the Office of Aerospace Research under Contract No. AF 49(638)-1131.

(2) J. B. Levy and B. K. Wesley Copeland, *J. Phys. Chem.*, **69**, 408 (1965).

(3) R. L. Perrine and H. S. Johnston, *J. Chem. Phys.*, **21**, 2202 (1953).

(4) F. A. Johnson and C. B. Colburn, *J. Am. Chem. Soc.*, **83**, 3043 (1961).

(5) J. B. Levy and B. K. W. Copeland, *J. Phys. Chem.*, **67**, 2156 (1963).

was applied for this absorption. Nitrosyl fluoride also showed absorption at this wave length, and, in experiments where nitric oxide was added, a correction was applied for this absorption. Our procedure was to add the reagents consecutively to the cell in the order fluorine, nitrogen, and tetrafluorohydrazine (or tetrafluorohydrazine-additive mixture). Where mixtures were used, they were prepared in a reservoir bulb and mixed by agitating a number of pieces of Teflon tubing by means of a Teflon-covered stirring bar and magnetic stirrer. The reaction began on the introduction of the tetrafluorohydrazine. Only a few seconds were required for this introduction. The fluorine concentration was recorded continuously on the recorder chart.

Auxiliary experiments were performed with a magnesium cup fabricated from a cylindrical block of magnesium, 13 cm. in diameter. The inner diameter and depth of the cup were 7 and 5.75 cm., respectively. The cup was closed by a magnesium cover which was bolted to the cup through a Teflon gasket. Entry to the cup was through a 0.635-cm. magnesium tube welded to the top. A Teflon valve was attached to the tube by means of a Swagelok fitting.

## Results

*The Nature of the Reaction.* Preliminary experiments were carried out in the 221-cc. magnesium cup described in the Experimental Part. We first sought to establish that tetrafluorohydrazine did not decompose by itself in the temperature range of our studies. This did not seem probable since equilibrium constants for the dissociation of this species have been measured between 100 and 150° without difficulty.<sup>4</sup> The possibilities of catalysis by the container walls or reaction with the container still existed however.

Two experiments were performed by admitting measured amounts of reagents to the cup at room temperature, immersing the cup in a bath of boiling water for a period of 45 min., cooling it to room temperature, and examining the contents. It was found that: (a) for 50 mm. of tetrafluorohydrazine alone, no pressure change occurred, and the infrared spectrum of the contents at the end of the experiment was that of pure tetrafluorohydrazine; (b) when equal amounts of tetrafluorohydrazine and fluorine were admitted to the cell ( $P_{N_2F_4} = P_{F_2} = 50$  mm. at 25°), the pressure at the end of the experiment was unchanged, and the infrared spectrum of the product was that of pure nitrogen trifluoride. Comparison of the intensity of the 1940-cm.<sup>-1</sup> peak of this product with that of a sample of pure nitrogen trifluoride at almost the same pressure showed the product to be only nitrogen trifluoride.

The above results were taken as evidence that the stoichiometry of the reaction was that shown by steps 1 and 3. This conclusion was confirmed by examination of the infrared spectrum of the products obtained in kinetic runs where the initial fluorine and tetrafluorohydrazine pressures were equal and where the experiment had been allowed to go to completion. The infrared spectrum of the products was that of nitrogen trifluoride and the amount found corresponded to that calculated from the amount of tetrafluorohydrazine (or fluorine) present. Finally, in an experiment, see Table I, no. 9, in which the initial fluorine pressure was four times the tetrafluorohydrazine pressure, the decrease in fluorine absorbance for complete reaction agreed well with that calculated for the stoichiometry written above.

**Table I:** Rate Constants for the Fluorine-Tetrafluorohydrazine Reaction

Table no.	Expt. no.	Temp., °C.	Pressures, mm. <sup>a</sup>			<i>k</i> , M <sup>-1/2</sup> sec. <sup>-1</sup>
			F <sub>2</sub>	N <sub>2</sub> F <sub>4</sub>	Diluent gas	
1	597	75	50	50	660 (N <sub>2</sub> )	0.0170
2	598	75	50	50	...	0.0155
3	643-A	75	50	50	...	0.0169
4 <sup>b</sup>	606	75	50	300	410 (N <sub>2</sub> )	0.0166
5 <sup>b</sup>	607	75	50	300	410 (N <sub>2</sub> )	0.0158
6	599	75	50	500	210 (N <sub>2</sub> )	0.0159
7	619-A	75	50	500	210 (N <sub>2</sub> )	0.0173
8 <sup>c</sup>	619-B	75	50	500	210 (N <sub>2</sub> )	0.0167
9	604	75	200	50	510 (N <sub>2</sub> )	0.0172
10	730	75	50	50	659 (N <sub>2</sub> ), 1 (NO)	0.0165
11	643-C	75	50	50	660 (O <sub>2</sub> )	0.0155
12	739	75	50	50	657 (O <sub>2</sub> ), 3 (CO <sub>2</sub> )	0.0173
13	603	52	50	500	210 (N <sub>2</sub> )	0.00204
14	601	61	50	500	210 (N <sub>2</sub> )	0.00483
15	600	86	50	500	210 (N <sub>2</sub> )	0.0394
16	600	86	50	500	...	0.0394
17	736	35	50	500	210 (N <sub>2</sub> )	0.000328

<sup>a</sup> Measured at the temperature of the experiment. <sup>b</sup> These runs were made in the 0.9-cm. i.d. cell path. All the others were made in the 1.8-cm. i.d. cell path. <sup>c</sup> In this run the cell was shut off from the light beam at all times except for the brief period needed for a reading.

*The Kinetics of the Reaction.* A series of experiments was performed at 75° to determine the order of the reaction in the two reagents, the effects of the impurities on the rate, the effect of total pressure, of surface area-to-volume ratio, and of the light of the spectrophotometer beam. The temperature dependence of the rate was determined from experiments at 35, 52, 61, 75, and 86°.

*The Order of the Reaction.* In view of the chemical similarity of the tetrafluorohydrazine-fluorine system

to the nitrogen tetroxide-fluorine system, it seemed quite likely that the kinetics of the former would be expressible by  $-d(F_2)/dt = k(F_2)(N_2F_4)^{1/2}$ . A series of kinetic experiments with varying reagent concentrations was performed at 75°, and the results were plotted according to the appropriate integrated form of the above expression. Good straight lines were obtained in all cases, and the rate constants found were in good agreement. The results are shown in Table I, no. 1-12, and confirm the validity of the above expression.

In the experiments containing comparatively small amounts of tetrafluorohydrazine—entries where the initial pressure was 50 mm.—calculations were made to see if the extent of dissociation of tetrafluorohydrazine was large enough to require a correction for the fraction dissociated. To do this the following expression for the equilibrium constant was calculated from available thermodynamic data<sup>6</sup>

$$K = 3.2 \times 10^8 \exp(-21,500 \pm 1000/RT) M$$

The value at 75° is  $K = 1.0 \times 10^{-5} M$ . For a pressure of tetrafluorohydrazine of 50 mm. ( $2.3 \times 10^{-3} M$ ), the fraction of tetrafluorohydrazine undissociated at 75° is 0.97; for pressures of 25 and 12.5 mm. at 75° the corresponding fractions are 0.95 and 0.94. Since the tetrafluorohydrazine concentration appears as the square root function in the kinetic expression, the correction for the smallest of the above pressures, corresponding to 75% reaction, is only 3%. We have therefore not corrected our data for dissociation of tetrafluorohydrazine. In Figure 1 the data for entry 1 of Table I are plotted for the above rate expression. The data are linear to about 85% reaction.

*The Effects of Impurities.* The mass spectrographic analysis indicated the presence of 0.6 mole % nitric oxide and 0.2 mole % carbon dioxide in the tetrafluorohydrazine. The fluorine contained about 0.2 mole % oxygen. Since removal of these small amounts of impurities, although desirable, would present very great difficulties, it was decided to test the belief that they were not affecting the rate by performing experiments where they were added deliberately in amounts substantially greater than were present in the other experiments. The results of such experiments at 75° are shown in Table I in no. 10-12. In entry 10 the nitric oxide-to-tetrafluorohydrazine ratio was 0.02 while in entry 12 the carbon dioxide-to-tetrafluorohydrazine ratio was 0.06. These figures compare to the corresponding figures of 0.006 and 0.002 for tetrafluorohydrazine with nothing added. In entry 11 oxygen replaced nitrogen as the diluent gas. The results support the belief that these compounds do not affect the reaction. It may be pointed out that, al-

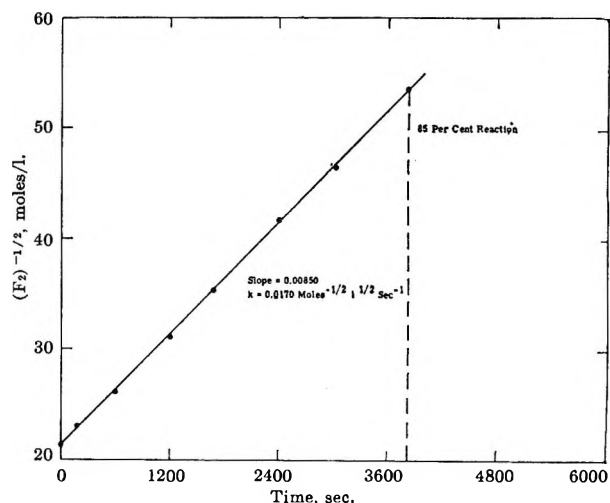


Figure 1. Test of integrated rate expression for  $(F_2)_0 = (N_2F_4)_0$ ;  $t = 75^\circ$ ;  $(F_2) = 2.21 \times 10^{-3} M$ ;  $P_{F_2} = 44.5$  mm.

though nitric oxide is known to react with difluoramino radicals to yield nitrosodifluoramine,  $NF_2NO$ ,<sup>7</sup> this compound would be completely dissociated at the temperatures of our experiments. On the other hand, nitric oxide would react very rapidly with fluorine<sup>8</sup> to yield nitrosyl fluoride so that the effect of adding nitric oxide is really to add nitrosyl fluoride.

*The Effects of Total Pressure, Surface Area-to-Volume Ratio, the Light of the Spectrophotometer Beam.* A comparison of the results of runs 2 and 3 with those of 1 and 4-9 shows that the rate is independent of total pressure in this pressure region. Runs 2 and 3 were at a total pressure of 100 mm. while the others were at a total pressure of 1 atm. Runs 12 and 13 illustrate a smaller variation of total pressure, 550 and 760 mm., respectively, at a higher temperature. The data at the different pressures are in satisfactory agreement.

Comparison of runs 4 and 5 with the other runs at 75° shows that surface effects in this reaction are negligible. The cell used in runs 4 and 5 had a surface area-to-volume ratio twice that of the other runs. This is not a large variation, but the agreement of the pertinent data is so good that it seems safe to rule out surface effects.

Run 8 differed from the other runs at 75° in that the cell was shut off from the spectrophotometer beam by a shutter at all times except for the few seconds required for a reading. The agreement of the rate obtained in

(6) "JANAF Thermochemical Tables," prepared under the auspices of the Joint Army-Navy-Air Force Thermochemical Panel, Air Force Contract No. AF 33 (616)-6149, Dow Chemical Co., Midland, Mich., 1963.

(7) C. B. Colburn, *Advan. Fluorine Chem.*, **3**, 88 (1962).

(8) D. Rapp and H. S. Johnson, *J. Chem. Phys.*, **33**, 695 (1960).



this way with the other runs at the same temperature rules out any photochemical effects resulting from the light beam.

*The Treatment of the Rate Data and the Precision of the Rate Constants.* We have extracted the rate constants from our data by drawing a straight line visually through the points, as we have done in Figure 1. When all the experiments at 75° were completed, it was clear that the uncertainty as to the slope of any particular line was much less than the variation in the results of the different experiments. It seemed that the most likely source of this variation was the uncertainty in the temperature. The activation energy found for this reaction (see below) is 20.4 kcal./mole. It is easy to show that the fractional error in the rate constant arising from a given fractional temperature error  $dT/T$  is<sup>9</sup>

$$dk/k = \frac{E_{\text{act}}}{RT} \frac{dT}{T}$$

For  $T = 348^\circ\text{K}$ ,  $dT = 0.5$ , and  $R = 20,000$ ,  $dk/k = 0.04$ ; *i.e.*, the error in  $k$  is  $\pm 4\%$ . The 12 values of  $k$  determined at 75° yield an average value of  $k = 0.0165 \pm 0.006 M^{-1/2} \text{sec}^{-1}$ , where the uncertainty indicated is the average deviation and is 4% of the value of  $k$ . We therefore conclude that the errors in our measurements arise solely from the temperature error, and we report our rate constants as being accurate to  $\pm 4\%$ .

*The Temperature Dependence of the Rate.* The data of Table I are plotted as the Arrhenius function in Figure 2. In view of the temperature uncertainty discussed above, the points are represented by horizontal lines whose length is a measure of the uncertainty in the  $1/T$  parameters. The average value of the 75° data is plotted instead of putting all 12 data points on the curve. The points are linear enough so that a line can be drawn through them visually. The resultant expression for the rate constant is  $k = 1.0 \times 10^{11} \exp(-20,400/kT) M^{-1/2} \text{sec}^{-1}$ . The error in  $E_{\text{act}}$  arising from the  $\pm 0.5$  temperature uncertainty may be shown<sup>7</sup> to be

$$\frac{dE_{\text{act}}}{E_{\text{act}}} = \frac{dT_2 - dT_1}{T_2 - T_1}$$

If we take  $T_2$  and  $T_1$  as the extreme temperatures and assume  $dT_2$  and  $dT_1$  are additive (the worst case), the resultant fractional error in  $E$  is 0.02. We therefore report the activation energy as  $20,400 \pm 400$  cal./mole. A similar treatment shows the frequency factor uncertainty to be  $10^0$ ,<sup>2</sup> so that the general rate expression is

$$k = 1.0 \times 10^{11.0 \pm 0.2} \exp(-20,400 \pm 400/RT) M^{-1/2} \text{sec}^{-1}$$

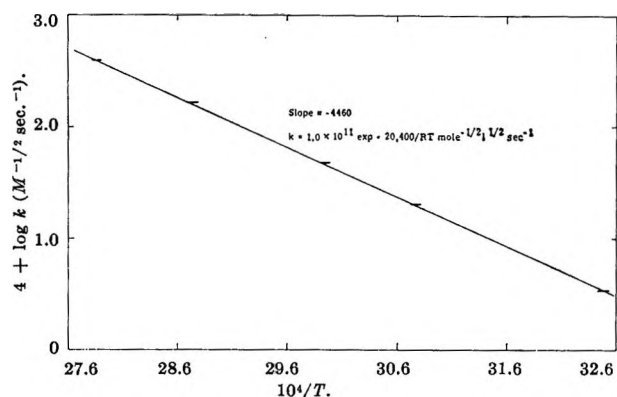
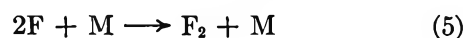
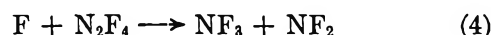


Figure 2. Temperature dependence of the tetrafluorohydrazine-fluorine reaction.

### Discussion

*The Mechanism of the Reaction.* In addition to the steps 1 to 3, we may consider the steps



The kinetics expression found is consistent with an equilibrium first step (1), followed by the slower rate-determining step (2). Support for the belief that step 1 (the dissociation step will be referred to as step 1 and the recombination as step -1) is fast compared to the over-all reaction rate can be found in the results of Modica and Hornig,<sup>10</sup> who studied the rate of dissociation of tetrafluorohydrazine in a shock tube between 350 and 450°K. at pressures of 0.58 to 2.7 atm. In the presence of argon diluent, the rate of dissociation could be expressed by

$$k_A = 3.0 \times 10^8 T^{1/2} \left( \frac{18,400}{RT} \right)^4 \exp \left( \frac{-18,400}{RT} \right) M^{-1} \text{sec}^{-1}$$

The results for helium, sulfur hexafluoride, and tetrafluorohydrazine as the third body differed from the above by less than a factor of two so that we feel the above expression is approximately valid for nitrogen as the third body.

At 348°K., the above expression yields  $k_A = 5.6 \times 10^3 M^{-1} \text{sec}^{-1}$ . For a pressure of tetrafluorohydrazine of 50 mm. and a total pressure of 1 atm. the rate of dissociation of tetrafluorohydrazine is  $0.45 M \text{sec}^{-1}$ . At the same temperature for 50 mm. each of tetrafluorohydrazine and fluorine our data yield  $1.6 \times 10^{-6}$

(9) B. K. Morse in "Techniques of Organic Chemistry," Vol. VIII, Part I, S. L. Friess, E. S. Lewis, and A. Weissberger, Ed., Interscience Publishers, Inc., New York, N. Y., 1961, p. 505.

(10) A. P. Modica and D. F. Hornig, Technical Report No. 4, ONR Contract No. Nonr 1858(26), Princeton University, Princeton, N. J., Oct. 31, 1963.

$M \text{ sec.}^{-1}$  as the rate of reaction. The rate of dissociation is thus much faster than the reaction rate, and the assumption of step 1 as an equilibrium seems justified.

The above discussion has not considered step 5. It seems evident that the concentration of fluorine atoms will be so much smaller than that of difluoramino radicals that step 5 can be neglected in comparison with step 3. Thus, at  $348^\circ\text{K.}$ , for 50 mm. pressure of tetrafluorohydrazine, the equilibrium pressure of difluoramino radicals is calculated as 2.7 mm. while for the same pressure of fluorine, the equilibrium fluorine atom pressure would be about  $2.7 \times 10^{-7}$  mm.<sup>6</sup> The factor of  $10^7$  should suffice to rule out step 5.

The reaction mechanism therefore consists of steps 1, 2, and 3 or of steps 1, 2, and 4. From a kinetics point of view the two sequences are indistinguishable. In either case

$$-d(\text{F}_2)/dt = 2k_2K^{1/2}(\text{N}_2\text{F}_4)^{1/2}(\text{F}_2)$$

where  $K$  is the equilibrium constant in moles per liter for the dissociation of tetrafluorohydrazine, *i.e.*,  $k_1/k_{-1}$ .

We may compare steps 3 and 4. Step 3 is a termolecular reaction, and we may assume that reaction occurs on each collision. At 1 atm. the ratio of termolecular to bimolecular collisions is about 0.001. If we take the  $\text{NF}_2:\text{N}_2\text{F}_4$  ratio as 2.7:48.6, *i.e.*, 0.056, as computed above for 50 mm. and  $348^\circ\text{K.}$ , we may write

$$\frac{\text{extent of reaction via (3)}}{\text{extent of reaction via (4)}} = \frac{k_3(\text{NF}_2)(\text{F})(\text{M})}{k_4(\text{N}_2\text{F}_4)(\text{F})} = 0.001 \times 0.056 \exp(E_4/kt)$$

where  $E_4$  is the activation energy for step 4. In order for the above ratio to be 0.01, *i.e.*, for reaction 4 to predominate,  $E_4$  would have to be about 1.5 kcal./mole. For the ratio to be 100, *i.e.*, for reaction 3 to predominate,  $E_4$  would have to be about 4.5 kcal./mole. We have no way of deciding between these possibilities.

*The Kinetics of Step 2.* Returning to the kinetics, the rate expression derived from the temperature dependence of the rate may be written

$$2k_2K^{1/2} = 1.0 \times 10^{11.0 \pm 0.2} \exp(-20,400 \pm 400/RT) M^{-1/2} \text{ sec.}^{-1}$$

Inserting the value of  $K$  calculated earlier yields

$$k_2 = 1.8 \times 10^7 \exp(-9650 \pm 700/RT) M^{-1} \text{ sec.}^{-1}$$

The frequency factor of  $1.8 \times 10^{-7} M^{-1} \text{ sec.}^{-1}$  corresponds to a steric factor<sup>11</sup> of about  $10^{-3}$  which is of the order expected for a reaction between species of the type involved here.

It is of some interest to compare activation energies and exothermicities for this and related reactions since it is widely felt that a simple linear relationship exists between these quantities.<sup>12</sup>

Table II

Reaction	Exothermicity, <sup>a</sup> kcal./mole	Activation energy, kcal./mole
$\text{NO} + \text{F}_2 \rightarrow \text{NOF} + \text{F}$	24.8	1.5 <sup>b</sup>
$\text{NO}_2 + \text{F}_2 \rightarrow \text{NO}_2\text{F} + \text{F}$	$8.1 \pm 2$	10.5 <sup>b</sup>
$\text{NF}_2 + \text{F}_2 \rightarrow \text{NF}_3 + \text{F}$	$21.1 \pm 2$	$9.7 \pm 0.7$

<sup>a</sup> Calculated from heats of formation taken from ref. 6.

The three reactions listed in the Table II all involve reaction of a free radical with fluorine to form an N-F bond and a fluorine atom. It is clear that no simple relationship between exothermicity and activation energy can fit the data of the Table II. It is likewise notable that nitrogen dioxide and the difluoramino radical, which are structurally very similar even to the extent that the N-F bonds in the latter like the N-O bonds in the former exhibit a degree of double-bond character,<sup>13</sup> show very similar activation energies despite the large difference in exothermicity. This indicates that structural factors may play a more important role than thermochemical factors in determining reactivity in some cases.

(11) S. W. Benson, "The Foundations of Chemical Kinetics," McGraw-Hill Book Co., Inc., New York, N. Y., 1960, Chapter XII.

(12) N. M. Semenov, "Some Problems in Chemical Kinetics and Reactivity," Princeton University Press, Princeton, N. J., 1958, pp. 29-33.

(13) J. J. Kaufman, L. A. Burnelle, and J. R. Hamann, Abstracts, 149th National Meeting of the American Chemical Society, Detroit, Mich., 1965, p. 1J.

## Samarium Borides. The Tetraboride-Hexaboride Conversion<sup>1</sup>

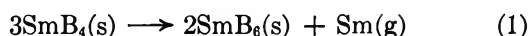
by George D. Sturgeon and Harry A. Eick

Department of Chemistry, Michigan State University, East Lansing, Michigan (Received February 25, 1965)

The high-temperature conversion of solid samarium tetraboride into solid hexaboride and elemental samarium vapor was studied by the Knudsen effusion technique. The partial pressure of samarium was determined by neutron activation assays of the effusate which was condensed onto silica collectors. From the pressure *vs.* temperature data, values for the standard enthalpy and entropy of the reaction were obtained. The heat of formation of the hexaboride is calculated to be  $-50$  kcal./mole.

### Introduction

Rare earth metal borides exhibit a number of stoichiometries ranging from diborides through tetraborides, hexaborides, and dodecaborides, to compounds having a very high boron to metal ratio.<sup>2,3</sup> It has been observed that the rare earth metal involved dictates which boride stoichiometry is congruently vaporizing.<sup>4,5</sup> Whatever the theoretical reasons for the differing stabilities of the various boride structures for different rare earth metals, it is necessary that quantitative thermodynamic data for transitions from one type of boride to another be collected. For the reaction



the relationship

$$\Delta G^\circ_T = -RT \ln P_{\text{Sm}(\text{g})} = -RT \ln K_{\text{eq}} \quad (2)$$

holds.

If the change in heat capacity accompanying the reaction is assumed to be negligible, the high-temperature enthalpy and entropy changes become equal to the same changes at 298.17°K. Thus, from the slope and intercept of the experimental curve relating pressure and reciprocal temperature, values for  $\Delta H^\circ_{298}$  and  $\Delta S^\circ_{298}$ , respectively, may be calculated.

### Experimental Section

**Materials.** The molybdenum from which the effusion cell was fashioned was of 99.5% purity. The primary container, a zirconium diboride cup (obtained from the Borolite Corp., Pittsburgh, Pa.), was heavily contaminated with binder material. It was purified by outgassing under vacuum at high temperatures (up to 2200°) until no more binder material transport from

the zirconium diboride was observed. Pure samarium tetraboride was prepared from samarium metal (99%, Michigan Chemical Corp., St. Louis, Mich.) and elemental boron (99.15%, U. S. Borax and Chemical Corp., Pacific Coast Borax Co. Division, Los Angeles, Calif.) by allowing the elements to react in a closed molybdenum bomb with excess samarium present. The finely ground tetraboride product was freed from excess samarium by treatment with cold hydrochloric acid solution (6 *N*). Samarium hexaboride was prepared by volatilizing samarium from a tetraboride-hexaboride mixture prepared from the elements. The hexaboride and tetraboride were identified by their characteristic X-ray powder diffraction patterns obtained using a 114.59 mm. Debye-Scherrer powder camera and either Cu or Cr K $\alpha$  radiation.

**Apparatus and Technique.** The vacuum-line assembly employed was similar in design to that reported by Ackermann, Gilles, and Thorn.<sup>6</sup> The collection device, which was cooled with liquid nitrogen, held a series of aluminum planchets which, in turn, held thin fused-silica disks (Supracil II, Englehard In-

(1) Based, in part, on the Ph.D. Thesis of G. D. S., Michigan State University, 1964.

(2) B. Post, "Refractory Binary Borides," Technical Report No. 6, Nonr 839 (12), NF 032-414, Polytechnic Institute of Brooklyn, 1963.

(3) P. K. Smith and P. W. Gilles, *J. Inorg. Nucl. Chem.*, **26**, 1465 (1964).

(4) G. D. Sturgeon and H. A. Eick, Proceedings of the 3rd Conference on Rare Earth Research, Clearwater, Fla., 1963.

(5) P. K. Smith, Ph.D. Thesis, University of Kansas, 1964.

(6) R. J. Ackermann, P. W. Gilles, and R. J. Thorn, *J. Chem. Phys.*, **25**, 1089 (1956).

dustries, Inc., Hillside 5, N. J.) on which effusate was collected.

The effusion cell was designed to meet the requirements of inertness to the hot boride mixtures and practicality of fashioning a suitable cell for effusion experiments.

Zirconium diboride was chosen as the primary container for the mixed samarium borides since preliminary experiments and the results of other workers<sup>5,7</sup> had shown it to be effectively inert to rare earth borides up to temperatures of 2000°. The base of the cell was fashioned with a male taper from presintered molybdenum stock. Inside the molybdenum base, a zirconium diboride cup (inside diameter  $\sim 1.5$  cm.) was positioned on tungsten pins so that there was no molybdenum-zirconium diboride contact. Tungsten had been shown in preliminary experiments to have no interaction with zirconium diboride at temperatures as high as 2200°. The lid with female taper was penetrated by the knife-edged orifice and the two sections were sealed irreversibly to each other at the first heating to form a cell 38 mm. tall. Two different knife-edged orifices were used. The first was  $7.460 \times 10^{-3}$  cm.<sup>2</sup> in area; the second, produced by machining carefully a few mils from the top of the cell, was  $1.142 \times 10^{-2}$  cm.<sup>2</sup> in area.

With precaution that the boride sample fall directly into the zirconium diboride cup, the effusion cell was loaded through the orifice with a 1-g. charge of samarium tetraboride-hexaboride mixture (approximate surface area of  $1 \times 10^4$  cm.<sup>2</sup>), and was positioned on the pedestal in the vacuum system. After evacuation to a pressure less than  $10^{-5}$  torr, the cell was heated by induction. When stable temperatures were attained, disks were exposed to the effusing beam of samarium vapor for varying periods of time at different cell temperatures. Fresh samples of samarium tetraboride were introduced into the cell before each run, and, at the end of the series of runs, the cell was cut open so that the boride charge could be examined.

The temperatures were determined with a Leeds and Northrup disappearing-filament type optical pyrometer (calibrated by the National Bureau of Standards), sighted *via* an optical window and a prism into the black-body hole in the cell base. The observed temperatures were corrected for window and prism absorption and for a slight (10° or less) temperature difference between the effusion cell interior and the black-body hole. Exposure time was measured by a frequency-dependent laboratory timer accurate to the nearest hundredth of a minute.

The linear dimensions required for calculation of the equilibrium samarium vapor pressure, the orifice-to-

collimator distance, the collimator area, and the effusion orifice area were determined using a cathetometer, vernier caliper, and a microscope with calibrated field, respectively.

After completion of a series of exposures, the silica disks were removed from the storage chamber, separated from the aluminum plachets and, together with blank disks and with standards prepared by evaporation of a measured amount of diluted standard solution of samarium nitrate on clean disks, wrapped in aluminum foil and subjected to neutron irradiation. By means of a  $\gamma$ -ray spectrometer, the activity of the resulting <sup>152</sup>Sm (102 kev., 47.1 hr.) in both standard and unknown samples was determined, and from the comparison of the activities corrected for counting time, the deposits of samarium on the disks were determined quantitatively.

The complete  $\gamma$ -ray spectrum of a neutron-activated disk with deposit was recorded and compared to the reported spectrum<sup>8</sup> of <sup>152</sup>Sm. The deposits on the silica disks were also examined by X-ray spectroscopy for the presence of zirconium, molybdenum, and tungsten.

The molecular weight of the effusing samarium species, critical to the calculations based on the Knudsen equation, was monitored in a Bendix time-of-flight mass spectrometer.

## Results and Discussion

Lattice parameters of the hexaboride and tetraboride (hexaboride: simple cubic,  $a_0 = 4.13$  Å.; tetraboride: tetragonal,  $a_0 = 7.16$  Å.,  $c_0 = 4.07$  Å.) were in good agreement with the accepted literature values.<sup>9</sup> At the end of the series of experiments, the effusion cell charge consisted of both.

The  $\gamma$ -ray spectrum of the neutron-activated disks with samarium deposit matched the known spectrum with no other species observed. X-Ray spectroscopy on the disks (before neutron activation) also showed the absence of elements other than samarium.

Within the limits of detection (sensitivity  $4 \times 10^{-6}$  atm.) and the temperature limit for the heating source of the mass spectrometer (1500°), only monatomic samarium metal species were observed in the effusate escaping from a molybdenum cell containing metallic samarium. This observation is consistent with the previously reported results of pressure measurement on pure samarium metal using a Knudsen cell coupled to a mass spectrometer.<sup>10</sup>

(7) G. L. Galloway, Ph.D. Thesis, Michigan State University, 1961.

(8) "Applied Gamma-Ray Spectrometry," C. E. Crouthamel, Ed., Pergamon Press, Inc., New York, N. Y., 1960.

(9) H. A. Eick and P. W. Gilles, *J. Am. Chem. Soc.*, **81**, 5030 (1959).

The samarium pressures were computed from the Knudsen equation with a cosine law correction for the fraction of effusate collected on the targets

$$P(\text{atm}) = \frac{A}{S_0 t} (2\pi MRT) \left( \frac{r^2 + d^2}{r^2} \right) \quad (3)$$

where  $A$  is the number of moles of effusate striking the target,  $S_0$  is the orifice area,  $t$  is the time of exposure,  $T$  is the absolute temperature,  $r$  is the radius of the target disk, and  $d$  is the distance from orifice to target. With the geometry actually employed, approximately  $1/100$  of the effusate from the cell was collected on the target disks.

The method of least squares was applied to the logarithm of pressure *vs.* reciprocal temperature data to obtain the following equation for the partial pressure of samarium in equilibrium with the two solid boride phases

$$\log P_{\text{Sm}}(\text{atm}) = - \frac{(2.00 \pm 0.07) \times 10^4}{T} + 5.38 \pm 0.43 \quad (4)$$

A few (4 out of 81) initial points in different series of data indicated excessively high samarium pressures, perhaps due to residual oxygen in the vacuum system or to reaction of small amounts of samarium boride with the molybdenum of the cell. With these exceptions, no accepted points lay a distance further than twice the standard deviation from the straight line of eq. 4 so that any finite heat-capacity change for the reaction was not detected.

From the slope and intercept of the experimental linear equation given above (4) describing data gathered between the temperatures of 1300 and 2300°K., the values of  $91.5 \pm 3.3$  kcal. and  $24.6 \pm 2.0$  cal./deg. are calculated for the standard enthalpy and entropy, respectively, for reaction 1.

A knowledge of the value of the heat capacity change for reaction 1 is of importance. It must be approximately equal to that accompanying the sublimation of samarium,  $\sim 2$  e.u./g. atom.<sup>11</sup> One method of estimation<sup>12</sup> first assumes that, for each atom in a solid compound at high temperatures,  $C_v$  (which is further assumed to approximate  $C_p$ ) equals  $3R$  ( $R$  is the gas constant). In reaction 1, the transport of 1 g.-atom of samarium from a solid to a gas phase would have a heat capacity change of  $5/2R - 3R$ , or  $-0.5R$ . A constant  $\Delta C_p$  of 1 cal./deg. would cause a maximum deviation of 2 kcal. in the enthalpy change and 2 cal. in the entropy calculated from the experimental data for this reaction. Because the estimated correction is quite small, we have assumed the heat capacity change to be negligible.

Approximately one-fourth of the data used to calculate the slope and intercept for eq. 4 was collected with the larger orifice. Values of 90.8 kcal. and 24.4 cal./deg. for the standard enthalpy and entropy, respectively, calculated from these data, compare favorably with the values obtained from all the points and indicate the absence of an orifice effect.

Making use of tabulated free-energy functions<sup>11</sup> (f.e.f.) and estimating the free energy functions for the solid borides to be the sum of the free energy functions of the components, and employing the relationship

$$\Delta f.e.f. = R \ln P_{\text{Sm}(g)} - \Delta H^\circ_{298}/T \quad (5)$$

a value for the standard enthalpy for the reaction was calculated for each experimental pressure-temperature point. The average of such calculated values led to a third-law heat of  $93.9 \pm 2.0$  kcal. for the standard enthalpy of reaction 1, in satisfactory agreement with the second-law value.

The heats of formation are not known for either the tetraboride or the hexaboride of samarium. Estimates of the heat of formation of the tetraboride are more likely to be reliable, however, in light of the relative insensitivity of heat of formation of ionic lanthanides to lanthanon;  $-48$  kcal./g.f.w. is a reasonable value.<sup>5</sup> Employing the value 49.9 kcal./g.f.w.<sup>11</sup> for the standard heat of formation of samarium vapor at 298°K. allows the calculation of the heat of formation of samarium hexaboride to be  $-50$  kcal./g.f.w.

The entropy of lanthanum hexaboride at 298°K. equals 19.88 e.u./g.f.w.<sup>13</sup> The standard entropies for 1 g.-atom of lanthanum and 6 g.-atoms of boron<sup>11</sup> sum to 21.98 e.u. The entropy of formation of lanthanum hexaboride is therefore  $-2.10$  e.u./g.f.w. By assuming this entropy of formation to be the same for samarium except for a positive 0.24 e.u. correction for the larger atomic weight of samarium,<sup>14</sup> and employing the enthalpy of formation from above, the free energy of formation of samarium hexaboride is calculated to be  $-49$  kcal./g.f.w.

(10) W. R. Savage, D. E. Hudson, and F. H. Spedding, *J. Chem. Phys.*, **30**, 221 (1959).

(11) D. R. Stull and G. C. Sinke, *Advances in Chemistry Series*, No. 18, American Chemical Society, Washington, D. C., 1956.

(12) G. N. Lewis and M. Randall, "Thermodynamics," 2nd Ed., revised by K. S. Pitzer and L. Brewer, McGraw-Hill Book Co., Inc., New York, N. Y., 1961, p. 57.

(13) E. F. Westrum, Jr., H. L. Cleaveland, and J. T. S. Andrews, *Proceedings of the 4th Conference on Rare Earth Research*, Phoenix, Ariz., April 1964.

(14) W. M. Latimer, "Oxidation Potentials," 2nd Ed., Prentice-Hall, Inc., New York, N. Y., 1942.

*Error Analysis.* An analysis of the sources of error in this work indicates that the greatest deviations arise in the determination of the amounts of samarium deposits on the target disks—one of the factors in the Knudsen equation (3). The difficulties in samarium assays arose from three sources: first, the preparation of very accurate standards with very small, but accurately known, amounts of samarium (as little as  $10^{-9}$  g.-atom of samarium) proved troublesome. Secondly, the wide range of samarium activity on the several disks precluded the assay of all disks in a single series of countings. The most active disks first overloaded the scintillation counter and the activity of the least active disks had died to background before the highly active samples could be accommodated. (To

have accumulated significantly larger amounts of samarium at the lowest temperatures and pressures would have required prohibitively long periods of time per exposure, but to reduce the amount of samarium collected at the highest temperatures and pressures would have required exposures of less than 1 min. resulting in inflation of the time-measurement error.) Finally, the activity of the samples and the associated amount of samarium present were not related linearly over the range of amounts of samarium deposited (a range of  $10^6$ ), making interpolation much less reliable.

*Acknowledgment.* The support of the U. S. Atomic Energy Commission, under Contract AT(11-1)-716, is gratefully acknowledged.

## Optical Rotatory Dispersion of *d*-Camphor<sup>1,2</sup>

by Ajit Singh and Leonard I. Katzin

Chemistry Division, Argonne National Laboratory, Argonne, Illinois 60440 (Received March 12, 1965)

Optical rotatory dispersion of the solutions of *d*-camphor has been studied. The solvents used were acetone, acetonitrile, benzene, 2-butanol, *n*-butyl acetate, carbon tetrachloride, chloroform, 1,4-dioxane, ethanol, methylcyclohexane, and tetrahydrofuran. The rotation data for 6400–3800 Å. can be reproduced by two-term, four-parameter Drude equations. The first characteristic absorption wave length of the Drude equation falls within the carbonyl absorption band, while the second falls in the far-ultraviolet region. Refractive index corrections are shown to affect primarily the intensity of the first Drude term, leaving its wave length parameters unmodified.

### Introduction

The relationship between absorption spectrum and rotatory dispersion of an optically active substance has been given by Drude<sup>3</sup> as

$$[\alpha] = \sum \frac{A}{\lambda^2 - \lambda_a^2} \quad (1)$$

where the *A*'s are the rotation or intensity constants and the  $\lambda_a$ 's are the characteristic absorption wave lengths controlling the dispersion.

The determination of the parameters of the Drude equation from experimental data has been rather unsatisfactory, in the earlier literature. The situation is exemplified by the literature on *d*-camphor. Owen<sup>4</sup>

(1) Based on work performed under the auspices of the U. S. Atomic Energy Commission.

(2) Presented, in part, at the 148th National Meeting of the American Chemical Society, Chicago, Ill., Aug.-Sept. 1964.

(3) P. Drude, "Theory of Optics," Longmans, Green and Co., London, 1920; Dover Publications, Inc., New York, N. Y., 1959.

(4) G. Owen, *Trans. Faraday Soc.*, 26, 423 (1930).

considered his data for 38% *d*-camphor in ethanol to be adequately represented by the equation<sup>5</sup>

$$[\alpha] = \frac{17.030}{\lambda^2 - 0.0939} - \frac{7.418}{\lambda^2} \quad (2)$$

while Singh and Mahanti<sup>6</sup> represented similar data, for 34% *d*-camphor in ethanol, by the equation

$$[\alpha] = \frac{11.030}{\lambda^2 - 0.1484} - \frac{0.093}{\lambda^2 - 0.2253} \quad (3)$$

Lowry and Cutter<sup>7</sup> fitted their data for camphor in benzene to the equation

$$[\alpha] = \frac{29.384}{\lambda^2 - 0.08720} - \frac{20.138}{\lambda^2 - 0.05428} \quad (4)$$

Using the same data but electronic computation, with a least-squares fitting criterion, Katzin and Gulyas<sup>8</sup> showed that eq. 5 gave a better fit.

$$[\alpha] = \frac{19.0834}{\lambda^2 - 0.092746} - \frac{10.14135}{\lambda^2 - 0.017626} \quad (5)$$

Heller<sup>9</sup> has discussed the usefulness of the Drude equation and also elaborated upon some graphical methods of calculation for the parameters of the same. There has been a revival of interest<sup>8,10-13</sup> in the Drude equation, of late, and electronic computers have been employed profitably for its fitting.

Work by Katzin and Gulyas<sup>8,10</sup> has shown that the Drude equation represents rotatory dispersion data most satisfactorily if the data are precise, taken over a wide range of wave lengths, and the parameter fitting is done by statistical least-squares fitting criteria.

With systems whose absorption bands lie far in the ultraviolet, it has not been possible to make direct comparison between the calculated Drude parameters and the absorption spectral features. We have therefore undertaken a reinvestigation of the rotatory dispersion of *d*-camphor and the influence of various solvents on the same, with the techniques evolved in this laboratory. The near-ultraviolet absorption and Cotton effect wave lengths of *d*-camphor lie in the 2500-3300 Å. region and are, therefore, open to direct observation and comparison with deductions from data at longer wave lengths.

### Experimental Section

**Materials.** A sample of *d*-camphor (~99.7%; estimated by gas chromatographic analysis on a polyphenyl ether column) was recrystallized from petroleum ether (b.p. 30-60°) before use. The concentration of the solutions was 4 g. of *d*-camphor/100 ml. of the solution at room temperature (20-25°), unless otherwise stated.

1,4-Dioxane was purified according to the PbO<sub>2</sub> method of Fisher and Baxter.<sup>14</sup> *n*-Butyl acetate was shaken with a solution of sodium bicarbonate, washed with water, and distilled before use. All other solvents (Spectro-quality, wherever possible) were used as supplied.

**Polarimetry.** The rotatory dispersion measurements were made at room temperature (21-28°) with a Rudolph photoelectric spectropolarimeter, Model 260/659/810-609, using a 150-w. xenon compact arc lamp. The temperature variation on any particular day was  $\lesssim 3^\circ$ . Measurements in the region 6400 to 3400 Å. were made in a 100-mm. polarimeter cell with quartz end plates. The rotations were measured at 50-Å. intervals between 6400 and 4000 Å. and at 100-Å. intervals between 4000 and 3400 Å. At each wave length setting a minimum of four readings was taken and averaged to give the recorded rotation. The average deviation of the observed rotations was about  $\pm 0.002^\circ$ . For most of the solutions studied (4 g. of *d*-camphor in 100 ml. of solution) a measured rotation of  $0.002^\circ$  corresponds to  $0.050^\circ$  in specific rotation.

It was found necessary to monitor frequently the wave length settings of the monochromator of the polarimeter. Both the 5461-Å. line from a mercury lamp and the rotatory dispersion of a plate of quartz were used.<sup>11,15,16</sup> The latter was also used to calibrate the wave length cam. The values of the wave lengths of light used were reliable to better than  $\pm 3$  Å. at the red end of the spectrum and to better than  $\pm 2$  Å. at 3600 Å. We are indebted to Dr. Elsie Gulyas for making her calibration data available to us.

**Spectrophotometry and Refractometry.** The ultraviolet absorption of the solutions was recorded by a Cary spectrophotometer, Model 14 M.

Refractive indices of the solvents and solutions, at sodium yellow lines, were measured with a Bausch and Lomb Abbé refractometer.

(5) Wave lengths are in microns, unless otherwise stated.

(6) B. K. Singh and I. Mahanti, *Proc. Indian Acad. Sci.*, **A2**, 378 (1935).

(7) T. M. Lowry and J. O. Cutter, *J. Chem. Soc.*, 604 (1925).

(8) L. I. Katzin and E. Gulyas, *J. Phys. Chem.*, **66**, 494 (1962).

(9) W. Heller, *ibid.*, **62**, 1569 (1958).

(10) L. I. Katzin and E. Gulyas, *J. Am. Chem. Soc.*, **86**, 1655 (1964).

(11) L. I. Katzin, *J. Phys. Chem.*, **68**, 2367 (1964).

(12) Y. Tsuzuki, K. Tanabe, M. Akagi, and S. Tejima, *Bull. Chem. Soc. Japan*, **37**, 162 (1964).

(13) J. T. Yang, *Proc. Natl. Acad. Sci. U. S.*, **53**, 438 (1965).

(14) F. R. Fisher and R. A. Baxter, *Mines, Mag.* (Denver), **30**, 447 (1940); see *Chem. Abstr.*, **34**, 8111 (1940).

(15) T. M. Lowry and W. R. C. Coode-Adams, *Phil. Trans. Roy. Soc., London*, **A226**, 391 (1927).

(16) T. M. Lowry and C. P. Snow, *Proc. Roy. Soc. (London)*, **A127**, 271 (1930).



**Data Fitting.** The experimental data were fitted to a two-term Drude equation (containing either three or four parameters, as required) with the aid of an IBM 1620-II computer working with ten significant digits. The program used previously<sup>8,10</sup> on the IBM-704 was rewritten for this machine with the cooperation of Mr. L. Douglas and modified by Dr. T. Bürer.

## Results

**Rotatory Dispersion outside the Carbonyl Absorption Region.** The rotatory dispersion data could not be fitted to a one-term, two-parameter Drude equation. Fit was obtained to a two-term Drude equation though the minimum number of parameters necessary depended upon the range of the data over which the fit was attempted.

In the region 6400 to 4350 Å. (42 points), the value of  $\lambda_b^2$  in the equation

$$[\alpha] = \frac{A}{\lambda^2 - \lambda_a^2} - \frac{B}{\lambda^2 - \lambda_b^2} \quad (6)$$

became so large that the second Drude term effectively reduced to a constant, giving a three-parameter equation of the type

$$[\alpha] = \frac{A}{\lambda^2 - \lambda_a^2} - B' \quad (7)$$

A better fit was found for three parameters in the form

$$[\alpha] = \frac{A}{\lambda^2 - \lambda_a^2} - \frac{B'}{\lambda^2} \quad (8)$$

However, any increase beyond this wave length range required eq. 6 with four parameters. Values of the parameters of eq. 6 for solutions of *d*-camphor in various solvents studied, for the range 6400 to 3800 Å. (51 points), are given in Table I. The root-mean-square error (r.m.s.) for this fitting was always smaller than that for computation with eq. 8 or even than for the shorter span (to 4350 Å.) with eq. 8.

The parameters obtained from a given set of data were found to be reproducible to better than 0.1%. The first critical wave length,  $\lambda_a$ , was found to agree within ca. 50 Å. when data from two solutions, made to the same target concentration in the same solvent, were used. The second critical wave length,  $\lambda_b$ , varied rather more, and in the opposite sense to the variations in  $\lambda_a$ . This is a special case of the general question of computing Drude parameters from dispersion data, which is discussed in detail elsewhere.<sup>17</sup> The values of  $\lambda_a$  tabulated in Table I all fall within 31 Å., a comparable range of variations. It must be emphasized, however, that to give fit to the data, a change of such a mag-

**Table I:** Rotatory Dispersion Parameters of *d*-Camphor in Various Solvents<sup>a,b</sup>

Solvent	$n_D^c$	A	B	$\lambda_a$ , Å.	$\lambda_b$ , Å.	Optical absorption maxima, Å.	A - B
Benzene	1.4987	20.112	12.268	3032	1503	2917	7.844
Chloroform	1.4451	20.032	11.227	3016	1653	2924	8.805
Ethanol	1.3597	18.514	9.159	3024	1404	2905	9.355
2-Butanol	1.3942	20.339	10.804	3001	1325	2900	9.535
Carbon tetrachloride	1.4589	23.284	13.600	3015	1839	2926	9.684
Acetonitrile	1.3419	19.719	9.742	3005	1665	2900	9.977
1,4-Dioxane	1.4212	21.399	10.878	3013	1679	2908	10.521
Acetone	1.3582	20.008	8.961	3025	1346	...	11.047
Tetrahydrofuran	1.4051	22.219	10.196	3017	1650	2912	12.023
<i>n</i> -Butyl acetate	1.3940	22.445	10.376	3004	1760	2924	12.069
Methylcyclo- hexane	1.4217	22.329	9.139	3031	1199	2925	13.190

<sup>a</sup>  $[\alpha] = A/(\lambda^2 - \lambda_a^2) - B/(\lambda^2 - \lambda_b^2)$ ; units of  $\lambda$ : microns.

<sup>b</sup> Range of wave lengths used: 6400 to 3800 Å.; concentration of *d*-camphor in solutions, 4 g./100 ml. Average root-mean-square deviation between calculated and experimental values of the specific rotations, for this set, is  $\pm 0.083^\circ$ . <sup>c</sup> Refractive index at 20–25°.

nitude in this parameter must be accompanied by compensating alterations of the other parameters. In this sense, the limits placed on these parameters may be different in meaning than for other types of data and equations.

**Refractive Index Correction and the Wave Length Parameters of the Drude Equation.** In derivation of theoretical equations for optical rotation or optical absorption, a multiplicative term always appears which is a function of the refractive index. This factor is given different forms by different authors, e.g.,  $(n^2 + 2)/3$ ,<sup>18</sup>  $(n^2 - 1)/(2n^2 + 1)$ ,<sup>19</sup> and  $(n^2 + 2)^2/9n$ .<sup>20</sup> The refractive indices of the different solvents used in our study were quite different and had different dispersions. To see whether the differences in rotatory behavior of *d*-camphor in the solvents might be an expression of this factor, the following test was made.

Literature data on the refractive dispersion of 1,4-dioxane<sup>21</sup> and of benzene<sup>22</sup> were computer-fitted by the dispersion equations

(17) L. I. Katzin and T. Bürer, to be published.

(18) W. J. Kauzmann, J. E. Walter, and H. Eyring, *Chem. Rev.*, **26**, 339 (1940).

(19) N. S. Bayliss, *J. Chem. Phys.*, **18**, 292 (1950).

(20) N. Q. Chako, *ibid.*, **2**, 644 (1934); L. W. Pickett, E. Paddock, and E. Sackter, *J. Am. Chem. Soc.*, **63**, 1073 (1941).

(21) C. B. Allsopp and H. F. Willis, *Proc. Roy. Soc. (London)*, **A153**, 379 (1936).

(22) T. M. Lowry and C. B. Allsopp, *ibid.*, **A133**, 26 (1931).



$$n_{\text{diox}} = 1.20754 + \frac{0.20486\lambda^2}{\lambda^2 - 0.01603} \quad (9)$$

$$n_{\text{benz}} = 1.27909 + \frac{0.20121\lambda^2}{\lambda^2 - 0.03283} \quad (10)$$

Each  $[\alpha]$  value was then divided by the refractive index function for the wave length, and the revised data were refitted to the Drude equation. Even for benzene, with the highest refractive index and sharpest dispersion change of all the solvents tested, none of the refractive index functions changed the value of  $\lambda_a$  by more than 2 Å. 1,4-Dioxane showed smaller effects. It, therefore, seems clear that medium refractive index, in the transparency region, primarily affects apparent intensity values and does not give any significant wave length shifts.

### Discussion

The specific optical rotation of camphor in the traditional sodium D-line region varies by a factor of about 1.5 between the solvents in which it is extreme. The numbers in Table I and the r.m.s. values of  $\pm 0.05$ – $0.1^\circ$  between computed and experimental values over a wave length span from 6400 to 3800 Å. show (a) that the two-term Drude equation is an appropriate one for reproducing the rotatory dispersion data and (b) that the rotational differences observed in the long-wavelength region are less a mark of alterations in the critical wave lengths, which are alike within the fitting uncertainty mentioned earlier, than of the intensity characteristic  $A - B$ , whose variation they follow closely. (The significance of  $A - B$  has been discussed elsewhere,<sup>8,10</sup> and that discussion will not be repeated here.) The wave length parameters computed (eq. 5) from the data of Lowry and Cutter<sup>7</sup> for camphor in benzene are essentially the same as we have derived from our own data. There is a difference in the  $A - B$  value, ours being somewhat lower. Similarly, our  $A - B$  value for the ethanol solution is slightly lower than Owen's value.<sup>4</sup> The differences in both these cases are most likely due to the differences in the concentrations of the solutions used.<sup>4</sup>

The fitting with three parameters in the abbreviated wave length span, 6400–4350 Å., could conceivably reflect a contribution from the infrared, analogous to a much smaller contribution seen in the quartz dispersion.<sup>11</sup> It is much more probable, however, that the major portion of this effect, if not all of it, is an artifact from the combination of abbreviated wave length span, intensity of the rotation in the 3000-Å. region, and the remoteness of the second rotatory absorption (below 2000 Å.).<sup>17</sup>

The values of  $\lambda_a$  lie, consistently, at longer wave

lengths than the maxima of the absorption spectra, as has also been observed by others.<sup>4,6,7,23–25</sup> Possible reasons for such behavior have been given in the past,<sup>24,26</sup> but model studies on Drude fitting of dispersion data suggest this is a characteristic artifact of the fitting<sup>17</sup> in addition to asymmetry of the circular dichroism with respect to the absorption spectrum.<sup>27–29</sup>

As was indicated above, the solvent effects which have most often been studied as intensity changes at one or a few wave lengths<sup>30,31</sup> are most understandably summarized in the variation of the Drude parameters that fit the dispersion curves, and of these, the  $A - B$  value seems most clearly related to the effects. Two physical factors which are most often proposed to explain solvent effects are refractive index and dipole moment.<sup>24,30–32</sup> As has been seen above, the refractive index effect does not significantly alter the Drude wave lengths. As the refractive index term occurs in the form of a multiplier, it conceivably might account for the relationship of  $A - B$  and the solvent effect. It is true that benzene, at the top of the array (Table I), has the highest refractive index of the group, but the refractive index of methylcyclohexane, at the foot of the array, is exceeded only by those of chloroform and carbon tetrachloride, in addition to benzene. The refractive index of ethanol, third in the array, is significantly higher only than that of acetonitrile and less than 0.002 higher than that of acetone. The solvent effect cannot, therefore, be correlated with refractive index alone. Similarly, a comparison of the dipole moments of the solvents<sup>33</sup> listed in Table I shows that the array does not correlate with the dipole moments either: the dipole moments of benzene, carbon tetrachloride, and methylcyclohexane are all zero, and acetonitrile has the highest dipole moment.

(23) J. O. Cutter, H. Burgess, and T. M. Lowry, *J. Chem. Soc.*, 1262 (1925).

(24) T. M. Lowry, "Optical Rotatory Power," Longmans, Green and Co., London, 1935; Dover Publications, Inc., New York, N. Y., 1964.

(25) J. P. Mathieu and J. Perrichet, *J. phys. radium*, 7, 138 (1936).

(26) W. Kuhn and E. Braun, *Z. physik. Chem. (Leipzig)*, B8, 293 (1930).

(27) T. Burer, L. I. Katzin, and A. Singh, to be published.

(28) W. Moffit and A. Moscovitz, *J. Chem. Phys.*, 30, 648 (1959).

(29) A. Moscovitz, K. M. Wellman, and C. Djerassi, *Proc. Natl. Acad. Sci. U. S.*, 50, 799 (1963).

(30) H. G. Rule, et al., *J. Chem. Soc.*, 674, 2652 (1931); 1400, 1409, 2332 (1932); 376, 1217 (1933).

(31) A. J. Mukhedkar, *J. Univ. Poona, Sci. Technol.*, 18, 41 (1960); *Z. physik. Chem. (Frankfurt)*, 25, 56 (1960); *J. Chem. Phys.*, 35, 2133 (1961).

(32) J. R. Partington, "An Advanced Treatise on Physical Chemistry. Vol. IV, Physico-Chemical Optics," Longmans, Green and Co., London, 1953.

(33) A. L. McClellan, "Tables of Experimental Dipole Moments," W. H. Freeman and Co., San Francisco, Calif., 1963.

Recently, Moscovitz, *et al.*,<sup>29</sup> have ascribed their results on the temperature dependence of the circular dichroism of camphor to solvation of camphor in the solutions studied. They correlate this with the finding by Pariaud<sup>34</sup> that at very low temperatures solid phases containing both camphor and solvent separate from certain solutions, with phase characteristics of compounds. With the high temperature coefficients usual to the implied intermolecular complex formation, however, one might question whether such stoichiometric complexes would survive to any significant concentration at room temperature. Any related sort of solute-solvent interaction would obviously be consistent with the regularities in the solvent effects we have pointed

out. It would also seem reasonable to take the view that the solvent effects in this system, and very possibly in other optically active systems, are a more or less quantitative measure of the cumulative effect of various intermolecular interactions in the system. The exact nature or number of such interactions cannot be completely predicted at this time, nor can the point at which they become specific "complexes." Hydrogen-bond formation in the solutions in alcohols and in chloroform is one obvious factor, interaction with the  $\pi$ -electron system of the benzene molecule is another, and other influences also exist.

(34) J. C. Pariaud, *Bull. soc. chim. France*, 103 (1950); *Ann. Chim. (Paris)*, 6, 880 (1951).

## Electron Spin Resonance Spectroscopy of Irradiated Acrylamide<sup>1</sup>

by G. Adler and J. H. Petropoulos

*Nuclear Engineering Department, Brookhaven National Laboratory, Upton, New York*  
(Received March 15, 1965)

It is shown by means of e.s.r. spectroscopy that acrylamide scavenges hydrogen atoms formed during radiolysis. The free radical thus obtained is identical with the one seen in the radiolysis of propionamide. At low temperature the radical is well oriented. Between  $-125$  and  $-30^\circ$  the spectra change in a manner which indicates that the radical reacts with its next nearest neighbor in the direction of the screw axis. Between  $-30$  and  $-20^\circ$  the e.s.r. spectrum loses all orientation dependence and becomes that of the propagating radical. This suggests that although the first step of the reaction may be constrained to a given crystallographic direction, polymerization takes place only at those temperatures where the propagating radical can react with near neighbors at random and the polymer becomes amorphous.

### Introduction

The radical-induced solid-state polymerization of acrylamide has been known since 1954.<sup>2</sup> Subsequently, it was shown that there was a considerable postirradiation reaction; that is, the reaction can proceed for long periods of time after the removal of the material from the radiation source.<sup>3-5</sup> It was also demonstrated that the resulting polymer is amorphous,<sup>3,6</sup> that the polymer nucleated as a second phase early in the reac-

tion,<sup>3,6,7</sup> and that defects were favored as nucleation sites. Further reaction then occurred at the interface

(1) Work done under the auspices of the U. S. Atomic Energy Commission.

(2) R. B. Mesrobian, P. Ander, D. S. Ballantine, and G. J. Dienes, *J. Chem. Phys.*, 22, 565 (1954).

(3) G. Adler, *ibid.*, 31, 848 (1959).

(4) (a) T. A. Fadner, I. Rubin, and H. Morawetz, *J. Polymer Sci.*, 37, 549 (1959); (b) B. Baysal, G. Adler, D. S. Ballantine, and P. Colombo, *ibid.*, 44, 117 (1960).

between monomer and polymer. The kinetics of this reaction were shown to be unusual and different from those of normal polymerizations.<sup>4b,5</sup>

The irradiated crystals showed an electron spin resonance spectrum at room temperature which was relatively stable with respect to time in a manner consistent with the reaction kinetics.<sup>8</sup> In solid solutions of acrylamide in propionamide the electron spin resonance spectrum is quenched to a large extent by oxygen. Furthermore, the polymerization is also suppressed to a large extent by oxygen in these solid solutions.<sup>9</sup> For these and other reasons, it was believed that the reaction was free-radical initiated.

It was shown, however, that the e.s.r. spectrum seen at room temperature in irradiated acrylamide showed little change of shape with time, was very similar to that seen in other solid state vinyl polymerization,<sup>8</sup> and showed no orientation dependence in single crystals, as was consistent with formation of amorphous polymer. These facts indicated that the free radical observed was the propagating radical and not the initiating radical. In order to understand the reaction more completely, it therefore became important to determine the nature and orientation of the initiating radical, how the first addition steps take place, and the influence of the crystal lattice on this. It is with this end in view that the investigation reported here was undertaken.

### Experimental Section

The acrylamide and propionamide used was recrystallized twice from acetone and then ground. The solid solutions of acrylamide in propionamide were made by shock cooling in the manner described by Fadner and Morawetz, who first demonstrated that these two substances form solid solutions in all proportions.<sup>5</sup> The powdered material was then sealed under vacuum ( $10^{-6}$  torr) in the sample tubes previously described.<sup>8</sup> They were irradiated to the required dose at  $-196^\circ$  in a  $\text{Co}^{60}$  source. The dose rate was 0.75 Mrad/hr. as determined by the Fricke dosimetry method.<sup>10</sup> In most cases a total dose of about 20 Mrads was used since this gave an e.s.r. spectrum of good amplitude and it was shown that there was no qualitative difference between the spectra at these doses and the lowest ones at which they could be detected. After irradiation, the tip of the specimen tube was annealed while the sample was still kept at  $-196^\circ$ . The samples were then placed in a Varian Model V4500 e.s.r. spectrometer with 100-kc. modulation. The microwave power was sufficiently low so that no pronounced saturation effects were observed. Between readings the samples were stored in a thermostat at the required temperature and for the re-

quired length of time. All e.s.r. spectra were measured at  $-196^\circ$ . To determine the anisotropy of the spectra, large acrylamide crystals were grown from acetone solution. These were irradiated and observed under the same conditions as the powdered specimens.

### Results

*Acrylamide and Propionamide.* Propionamide differs from acrylamide in that the latter contains an  $\alpha$ , $\beta$  double bond. Therefore, if acrylamide were to scavenge the hydrogen atoms liberated during radiolysis, the resulting radicals would be equivalent to those produced from propionamide by a loss of a hydrogen atom. The e.s.r. spectra obtained from either powdered material when irradiated and measured at  $-196^\circ$  are essentially the same as is shown in Figure 1. Both spectra are very similar to that obtained from propionamide at room temperature and quite different from that of acrylamide at  $25^\circ$  where polymerization complicates the picture.<sup>5</sup> These low-temperature spectra show five rather broad main peaks. These peaks and their intensity distribution can be attributed to a system of two overlapping quartets, each with a 1:3:3:1 peak-

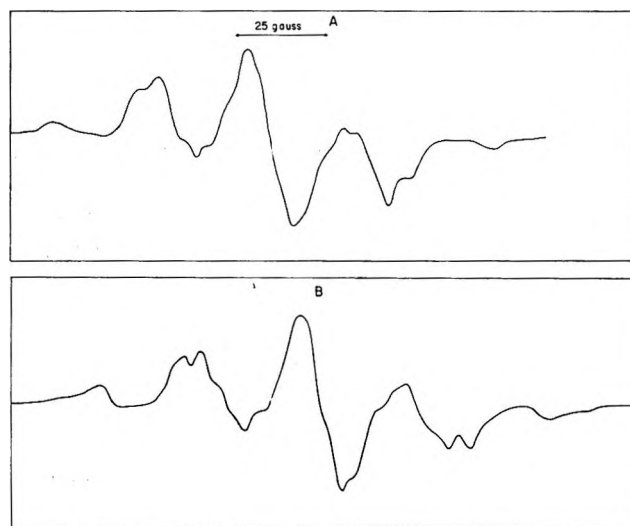


Figure 1. E.s.r. spectra of acrylamide (A) and propionamide (B) irradiated and stored at  $-196^\circ$ : radiation dose 20 Mrads.

- (5) T. A. Fadner and H. Morawetz *J. Polymer Sci.*, **45**, 475 (1960).
- (6) G. Adler and W. Reams *J. Chem. Phys.*, **32**, 1698 (1960).
- (7) C. Sella and J. J. Trillat, *Compt. rend.*, **253**, 1511 (1961).
- (8) G. Adler, D. S. Ballantine, and B. Baysal, *J. Polymer Sci.*, **48**, 195 (1960).
- (9) G. Adler, Proceedings of the International Symposium on Radiation Induced Polymerization and Graft Copolymerization, Battelle Memorial Institute, Columbus, Ohio, Nov. 1962, TID 7643.
- (10) A.S.T.M. Method D-1671-59T.

height ratio. This is the spectrum that would be expected from a radical having the structure  $\text{CH}_3\text{-}\dot{\text{C}}\text{H-CONH}_2$ . We shall hereafter refer to this as the P radical. The double quartet nature of the spectrum and the structural assignment of the radical have been confirmed by single crystal data. The latter data also show that the radical is well oriented in the lattice. The details of the single crystal experiments will be reported in full in a subsequent publication.

Deuteration of the amide group in propionamide showed no observable change in the e.s.r. spectrum thus indicating that the amide group is not significantly involved. There seems to be evidence of very small amounts of some component other than the P radical but this spectrum was too weak to get any clear-cut indication of its nature.

Thus it appears that the P radical, the principal one seen in acrylamide irradiated at  $-196^\circ$ , is produced by hydrogen scavenging. This scavenging is consistent with the low temperature ( $-78^\circ$ ) hydrogen yields reported by Adler, *et al.*<sup>11</sup>

The changes in the e.s.r. spectra of acrylamide and propionamide were followed by warming the samples to various temperatures, usually for 16 hr., and then recooling to  $-196^\circ$ .

Upon warming to  $145^\circ$  both spectra show similar but minor changes which can be explained most easily by assuming the decay of a minor radical other than the P radical (Figure 2). On further heating the spectrum of propionamide remains the same, except for intensity, until it decays completely upon being kept for protracted periods. In contrast to this, the acrylamide spectrum shows very marked differences in behavior. Thus, after warming above  $-125^\circ$ , the spectrum slowly changes to a broad triplet, very similar to that seen in acrylamide and other vinyl polymerizations at room temperature. [This change becomes most clear-cut and easily seen at about  $-80^\circ$  (Figure 2).] The most important difference between this and the room temperature spectra is that the former shows pronounced orientation effects in single crystals though the orientation does not appear to be as precisely defined as that of the P radical. We believe the radical responsible for this spectrum to be A. It is the species obtained

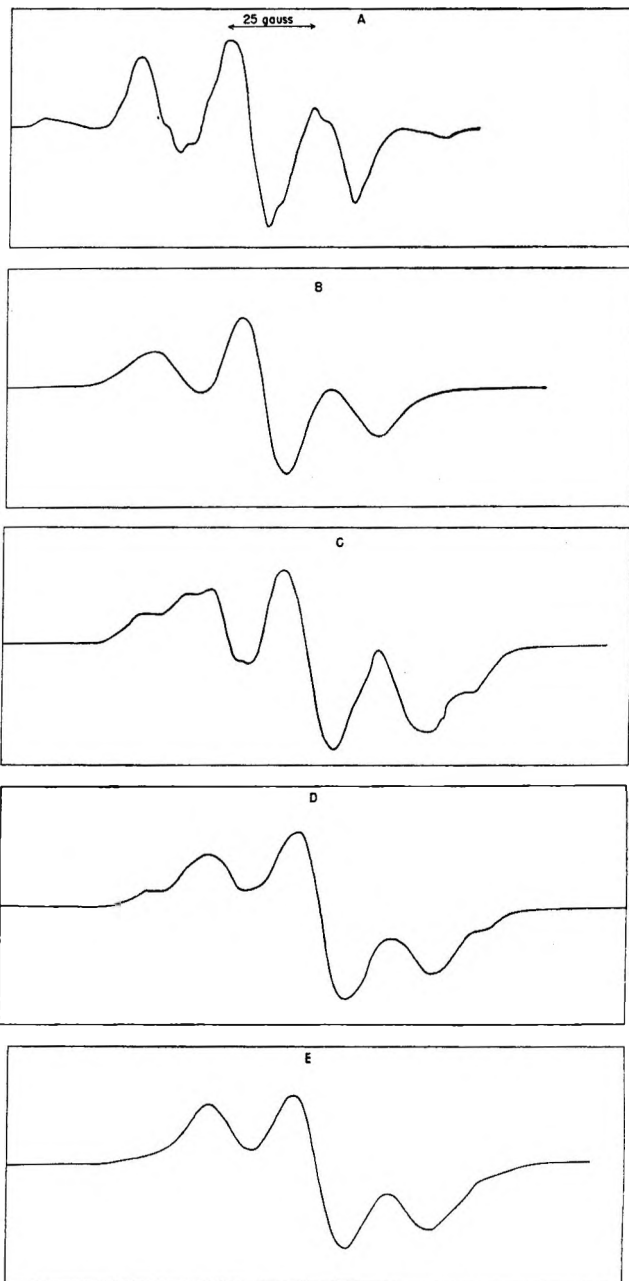
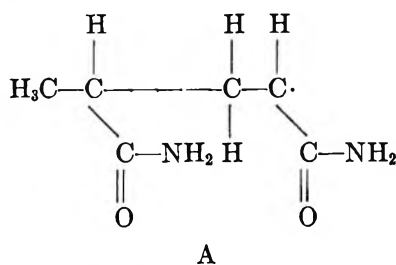


Figure 2. E.s.r. spectra of acrylamide irradiated at  $-196^\circ$  and stored for 16 hr. at (A)  $-145^\circ$ , (B)  $-80^\circ$ , (C)  $-40^\circ$ , (D)  $-30^\circ$ , and (E)  $-20^\circ$ : radiation dose 20 Mrads. The e.s.r. spectra of propionamide at  $-145^\circ$  and above are essentially similar to that of acrylamide at  $-145^\circ$ .

by adding an acrylamide molecule to the P radical. The disappearance of the two outermost peaks of the P radical spectrum, the general broadening, and the directional dependency of the A radical spectrum indicate

(11) G. Adler, D. S. Ballantine, T. Davis, and R. Ranganathan, *J. Phys. Chem.*, **68**, 2184 (1964).

that at least dimerization can occur above  $-125^{\circ}$ . The crystal is monoclinic space group  $P2_{1/c}$ . The monomer addition seems to be most probable with its neighbor in the direction of the screw axis. Addition across the center of symmetry seems to have a lower probability. Crystallographic considerations similar to those of Adler and Reams<sup>12</sup> and the fact that no polymer formation has ever been reported at these temperatures indicate this cannot proceed much beyond dimerization at this stage.

One would normally expect a free radical such as A to have a more complex spectrum than is shown in Figure 2 and the single crystal spectrum bears this out. Figure 3 shows the spectrum of the A radical in three different orientations  $15^{\circ}$  apart. This also shows that the spectra has a marked dependence on direction. It is only because the spectra seen in powdered samples are averaged over all orientations that the spectrum seems as simple as in Figure 2. The data in Figure 3 were taken at  $-100^{\circ}$  but the spectra are essentially the same at  $-80^{\circ}$ .

The A radical exhibits only a decrease in intensity until  $-60^{\circ}$ . Between  $-60$  and  $-40^{\circ}$  some small new peaks become apparent. These are probably due to small amounts of another minor radical which we shall call B. At present we can say little about the B radical since its spectrum cannot be separated from that of the A radical in a clear-cut fashion. It could have arisen from the conversion of a small amount of A to B or it could have been present initially but masked by the much more intense P and A spectra. We feel the latter is more probable since the B radical appears to be very precisely oriented whereas a small amount of disorientation has already taken place in the A radical.

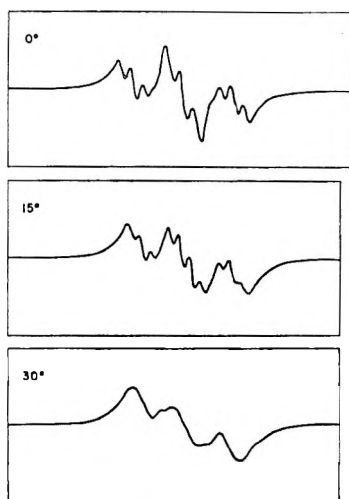


Figure 3. E.s.r. spectrum of a single crystal of acrylamide showing the A spectrum. Three orientations  $15^{\circ}$  apart are shown: temperature  $-100^{\circ}$ .

Between  $-30$  and  $-20^{\circ}$  the e.s.r. spectrum changes somewhat and, more importantly, loses all orientation dependence. It becomes essentially the same radical spectrum as that observed after room temperature irradiation (Figure 2). The upper part of this temperature range corresponds to that at which polymer yields can first be measured.<sup>13</sup> We shall call this new spectrum  $A_1$  and attribute it to the propagating polymer radical. The loss in directional dependence may be taken as an indication that the radical can now react with near neighbors in directions other than that of the screw axis.

One would expect the  $A_1$  radical to have the same e.s.r. spectrum as the A radical. However, the loss of directional dependency should make the single crystal and powder spectrum at  $-20^{\circ}$  almost identical and very similar to the powder spectra of the A radical at, say,  $-80^{\circ}$ . We have indeed found this to be true. Figure 2 shows the powder spectra.

Above room temperature the e.s.r. data we obtained are similar to that of Ueda and Kuri<sup>14</sup> and need not be described here.

#### Solid Solutions

E.s.r. studies of solid solutions of acrylamide and propionamide provide interesting confirmation of most of the above points. Two solid solutions, containing 65 and 92% acrylamide, were studied over a wide range of temperatures. Their spectra were compared to a physical mixture of the two components used as a control.

The e.s.r. spectra of the solid solutions at  $-196^{\circ}$  are indistinguishable from that of the P radical as obtained from the individual components. As the temperature is increased, the distinction between A and P radicals can most easily be seen by observation of the outermost peaks of the solid-solution spectra. The relevant portions of the spectra are shown in Figure 4.

The behavior of the 92% solid solution closely resembles that of pure acrylamide and that of the physical mixture. This is not unexpected since there was not enough propionamide present to produce easily observable effects.

The 65% acrylamide solid solution presents a different story, as shown in Figure 4. The following points should be noted. Firstly, at  $-50^{\circ}$  the P radical peak is more prominent relative to the A radical in solid solutions than in the physical mixture. The P radical

(12) G. Adler and W. Reams, *J. Polymer Sci.*, **A2**, 2617 (1964).

(13) P. Ander, Thesis, Polytechnic Institute of Brooklyn, 1954.

(14) H. Ueda and Z. Kuri, *J. Polymer Sci.*, **61**, 333 (1962).

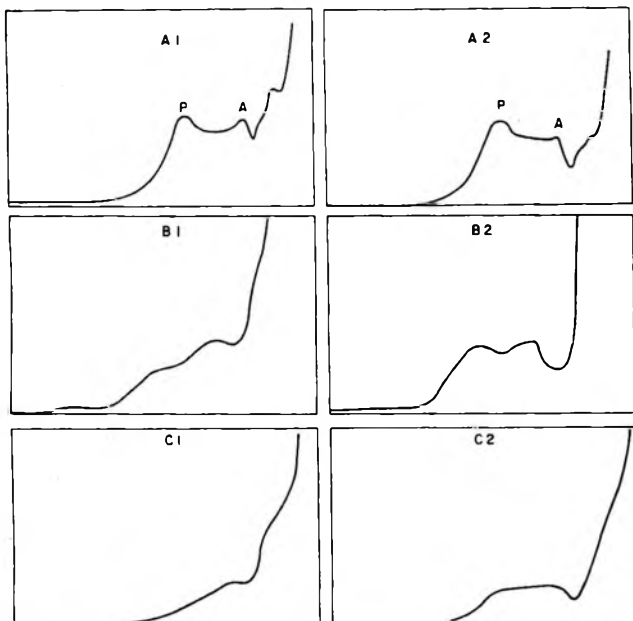


Figure 4. Outer, low-field side of the spectrum of solid solutions (subscript 1) and physical mixtures (subscript 2) of acrylamide and propionamide: acrylamide content 65%; storage temperature (A)  $-50^{\circ}$ , (B)  $-30^{\circ}$ , (C)  $-20^{\circ}$ ; radiation dose 20 Mrads.

therefore persists to a greater extent than is explainable simply by the ratio of the two components of the solid solution, and this persistence occurs at temperatures above that at which the P radical disappears in pure acrylamide. Secondly, the P peak disappears from the solid solution between  $-30$  and  $-20^{\circ}$ . The first observation apparently indicates that if the P radical does not find an acrylamide molecule in the *b*-axis direction at low temperature, it will not react. The second observation shows that at the temperatures at which the unoriented A radical appears in pure acrylamide, the restriction implied by the first observation is no longer important. The spectrum now corresponds to that obtained at room temperature where no P radical is observed until the acrylamide content of the solid solution is less than 10%. This indicates that the radicals now have sufficient mobility to allow reaction with near neighbors in directions other than the screw axis. Similar arguments accounted for the previously noted change of A to  $A_1$  radicals in the same temperature region. The solid solution data are therefore consistent with and amplify that obtained from the pure materials.

Relative radical populations were estimated for the solid solutions at various temperatures. Below  $-60^{\circ}$ , the results are not sufficiently satisfactory from a quantitative viewpoint to permit definitive conclusions to be drawn. However, above  $-60^{\circ}$  the data are reason-

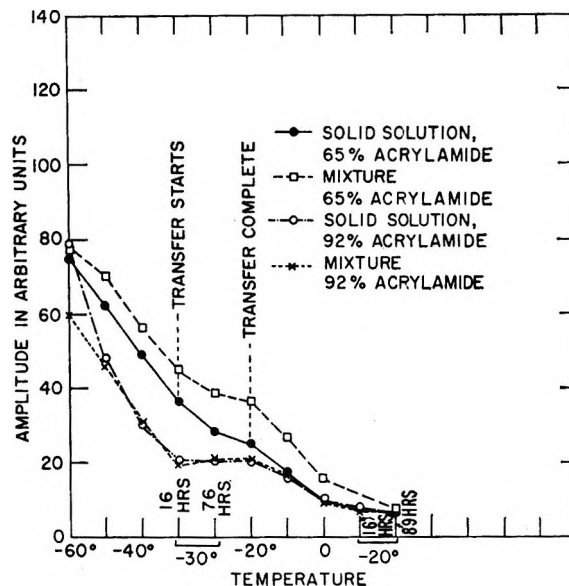


Figure 5. Decay of the e.s.r. spectrum of solid solutions and physical mixtures of acrylamide and propionamide as a function of temperature: time of storage at a given temperature, 16 hr. except where noted.

ably consistent and reproducible and are plotted in Figure 5. Considerable radical decay occurs in the 65% acrylamide solution up to  $-30^{\circ}$ , the temperature at which the P radicals disappear. The corresponding physical mixture shows somewhat less decay. During prolonged storage at the  $-30$  to  $-20^{\circ}$  temperature range the 65% solid solutions and mixture show appreciable radical decay. The 92% acrylamide solution, however, shows very little. Furthermore, the observable difference in behavior between the solid solution and the physical mixture is very small at this composition.

The over-all radical yield upon irradiation at  $-196^{\circ}$  is greater in the solid solution than in pure acrylamide. However, the radical decay in the solid solutions is greater so that after prolonged storage at room temperature pure acrylamide exhibits a more intense spectrum. The mechanism for the decay of the radical spectrum is not known, but it is probably similar to that of pure propionamide at room temperature which apparently decays by a second-order process.

### Discussion

The foregoing results in which P-type radicals are formed in the radiolysis of acrylamide clearly indicate the ability of acrylamide to scavenge hydrogen. It has recently been demonstrated that acrylic acid<sup>15</sup> and

(15) Y. Shioji, S. Ohnishi, and I. Nitta, *J. Polymer Sci.*, A1, 3373 (1963).

barium methacrylate<sup>16</sup> can also scavenge hydrogen atoms in the solid state. Similarly, Klein and Scheer have shown that frozen terminal olefins exhibit this same scavenging ability.<sup>17</sup> The phenomenon, therefore, appears to be fairly common and not too surprising in view of the high diffusive capability of the small hydrogen atom. An analogous diffusion capability has been previously reported in acrylamide-propionamide solid solutions where the much larger oxygen molecule was shown to be an effective polymerization inhibitor.<sup>9</sup> This efficient scavenging process helps explain the depressed hydrogen yield in the radiolysis of propionamide-acrylamide solid solutions at low temperature.<sup>11</sup>

The P radical which results from the scavenging process is relatively stable since it can be stored indefinitely at  $-196^\circ$ . It is also very precisely oriented within the lattice. The stability of the P radical below  $-125^\circ$  strongly suggests that the mobility in this temperature range is severely restricted.

Above approximately  $-125^\circ$  the P radical begins to change to an A-type radical. This transition requires the onset of sufficient mobility so that the P radical can approach the nearest double bond on a neighboring molecule with sufficient energy so that dimerization can take place. This A radical still exhibits a pronounced orientation dependence which requires this first addition step to be nonrandom in direction. It is not unreasonable to assume, and indeed the evidence indicates, that the first addition is in the direction of the twofold screw (*b*) axis of the crystal. The addition of another molecule to form a trimer radical is not excluded. However, it has a much lower probability than dimerization.

The net shrinkage which accompanies the monomer addition process (about one-third of a unit cell in the *b*-axis direction for every two monomer units added) quickly puts the radical out of phase with the original crystal lattice.<sup>12</sup> At this point, the nearest neighbors are no longer in the *b*-axis direction and further additions must take place in other directions and this would lead to a loss of orientation dependence of the observed radical signal.

It should be noted that this P  $\rightarrow$  A transition takes place over a broad temperature range. This is not too surprising since the transition requires mobility and the mobility will be affected by the immediate crystallographic environment of the radical. The achievement of the required mobility will occur more readily at defects such as edge dislocations or mosaic boundaries. One should also consider that the shrinkage consequent upon monomer addition necessarily introduces strain within the crystal lattice. Further reaction can be enhanced by an annealing process and again annealing

will occur preferentially near those defects and at those temperatures where greater mobility is possible. In a crystal there is likely to be a range of different defects which, in turn, imply a limited range of localized environments and energies, all within the possibilities allowed by the crystal structure. The broad temperature range of the P  $\rightarrow$  A transition becomes easily explainable in these terms.

These latter comments regarding a spectrum of defects and their possible effect on solid-state reactions point to considerations that are sometimes overlooked and indicate that activation energies for solid-state processes should be treated with caution. Furthermore, collisional factors should be considered more carefully than is usual in kinetic studies.

It has been pointed out that after the first addition the nearest neighbors to the radical are no longer in the screw-axis direction. The second transition from A to A<sub>1</sub> radicals reflects again the attainment of sufficient thermal motion for further reaction. There are three pronounced characteristics associated with this temperature region. Firstly, it is the temperature range where measurable polymerization first occurs. Secondly, it marks the loss of all orientation dependence of the free-radical spectrum. Thirdly, it is the range where the P spectrum finally disappears in the solid solution.

The loss of orientation dependence and P radical in the solid solution is the consequence of further addition in directions other than the *b* axis. It is at this point that as we have previously suggested the polymer "nucleates as a second phase." The random directional addition also accounts for the acrylamide polymer being completely amorphous. The fact that this temperature range appears to be the threshold for observable polymerization is also explainable in these terms. At least a limited amount of mobility is required for the addition reaction. It is only when the thermal motion reaches a stage where it allows the radical and monomer molecules to approach within reaction distances that polymer will be formed. It would seem, therefore, that one of the important roles of the crystal lattice in influencing a chemical reaction, aside from controlling the pure geometry, is determining the type and extent of mobility possible in a given situation.

We also wish to call attention again to the possible contributions of annealing processes to the reaction. Increasing the temperature will promote anneal-

(16) H. Morawetz, 148th National Meeting of the American Chemical Society, Chicago, Ill., Sept. 1964.

(17) R. Klein and M. D. Scheer, *J. Am. Chem. Soc.*, **80**, 1007 (1958); *J. Phys. Chem.*, **62**, 1011 (1958).



ing and the annealing temperature will have a range of values. It has been noted that in some solid-state polymerizations the polymer yield reaches a limiting value which is temperature dependent. It is possible that in many cases this is due to the reaction being carried out in a temperature range which is insufficient for annealing out most of the lattice strain induced by the reaction and/or sufficient to provide adequate mobility over only a limited range of sites.

In a recently published paper<sup>18</sup> the powder spectra

from irradiated propionamide were determined and the radical was taken to be  $\text{CH}_3\text{-}\dot{\text{C}}\text{H-CONH}_2$ , the same as our P radical.

*Acknowledgment.* The authors wish to thank Dr. D. S. Ballantine for his help in writing the manuscript and Mr. W. Reams for preparing the samples used in these experiments.

(18) M. T. Rogers, S. Bolte, and P. S. Rao, *J. Am. Chem. Soc.*, **87**, 1875 (1965).

## On the Ionic Strength Dependence of Micelle Number<sup>1,2</sup>

by M. F. Emerson and A. Holtzer

*Department of Chemistry, Washington University, St. Louis, Missouri (Received March 22, 1965)*

Examination of the thermodynamics of micelle formation reveals that the quantity  $RT \ln$  (c.m.c.) is equal to the standard free energy change of addition of one more detergent molecule to a micelle that already contains the number of molecules most probable at the c.m.c. This result is independent of the usual assumption about phase separation. This standard free energy can be conceptually divided into a hydrocarbon part and an electrical part. The magnitude of the electrical part can be estimated from numerical (computer) solutions to the nonlinearized Poisson-Boltzmann equation assuming that the micelle is a sphere with smeared charge and using published values of the radius (determined by low angle X-ray scattering) and of the micelle number (determined by light scattering). Subtraction of the electrostatic contribution from the total provides the hydrocarbon part of the standard free energy. Applying this method to published data for sodium dodecyl sulfate and dodecyltrimethylammonium bromide, we find that the hydrocarbon contribution is roughly independent of detergent and ionic strength, having an approximate value of 8000 cal./reaction unit (infinitely dilute reference state, molality basis).

### Introduction

In a germinal paper by Debye<sup>3</sup> the model of a micelle adopted is that of a platelet-shaped aggregate of detergent ions limited in size (*i.e.*, in the number of detergent molecules per micelle or "micelle number,"  $N$ ) by the electrostatic repulsion of the charged head groups and stabilized by the hydrophobic adhesion of the hydrocarbon tails. Debye further assumed that in the ab-

sence of added electrolyte the electrical (repulsive) part of the free energy of formation of the platelike

(1) This investigation was supported by Research Grant RG-5488 from the Division of General Medical Sciences, Public Health Service.

(2) Support for some of the computation was provided by National Science Foundation Grant G 22296 to the Washington University Computer Center.

(3) P. Debye, *Ann. N. Y. Acad. Sci.*, **51**, 575 (1949).



micelle from the individual detergent ions is proportional to  $N^{3/2}$  and that the hydrophobic (attractive) part is proportional to  $N$ .

Reich<sup>4</sup> and Ooshika,<sup>5</sup> however, have pointed out that the minimization of free energy is incorrectly performed in Debye's work, and they have also marshalled convincing arguments against the assumption that the hydrocarbon part of the interaction is directly proportional to  $N$  for all  $N$ .

Three factors have led us to re-examine the question of the stability of ionic micelles. First, there now is direct evidence from low angle scattering of X-rays that micelles are spherical rather than platelike, at least in the vicinity of the critical micelle concentration (c.m.c.).<sup>6</sup> Since most physical measurements on detergent solutions are meaningful only when extrapolated to the c.m.c. anyway, this does not restrict the discussion unduly.

Second, given that the micelle is spherical, it is possible to estimate the electrostatic contribution to the free energy in aqueous solutions containing added salt, in spite of the existence of a high potential at the micellar surface which renders the Debye-Hückel approximation invalid; this estimate can be made using numerical (computer) solutions to the nonlinearized Poisson-Boltzmann equation.

Third, we believe there is a core of truth to Debye's analysis that criticism, because of its cogency, has tended to obscure. Micelles of ionic detergents are considerably stabilized by addition of neutral salt and are ordinarily considerably smaller than nonionic micelles. This clearly argues in favor of the existence of an electrostatic size-limiting mechanism that becomes important at micelle sizes sufficiently small so that forces which limit the size of nonionic micelles have not as yet come into play. Simple geometrical considerations confirm this: using experimental values of  $N$  and of the micelle radius, it is easy to show that there is plenty of room on the surface of the micelle for the charged head groups—steric factors cannot be important except for values of  $N$  far larger than those found in ionic micelles.

Furthermore, although arguments showing that the hydrocarbon part of the free energy of micelle formation cannot be strictly proportional to  $N$  for all  $N$  are undeniably correct, they tend to prevent consideration of the possibility that this relationship may be approximately correct in precisely the range of values of  $N$  of interest. That is, while the addition of one detergent molecule to another to form a dimer undoubtedly produces a different change in the hydrocarbon part of the free energy than the addition of 1 more detergent molecule to an aggregate of 50, it is not unlikely that the latter free energy is not very different from that ob-

tained on addition of 1 to an aggregate of 100. In fact the text below presents some evidence in favor of this.

### The Model

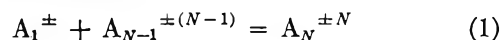
We limit our discussion, then, to concentrations near the c.m.c. We assume that micelles in this region occupy a constant volume and remain spherical in shape even though  $N$  may change with added salt.

The assumption of constant micellar volume requires some comment and justification since the micelle number increases considerably as the amount of added salt goes from zero to 0.5  $M$ . The radius of sodium dodecyl sulfate (SDS) micelles in pure water at the c.m.c., as measured by low angle X-ray scattering, is 19.7 Å,<sup>6</sup> approximately the same as the extended length of an SDS chain ( $\sim 17$  Å). It seems to us unreasonable that a spherical micelle could have a radius appreciably larger than the extended length of its constituent molecules and still exclude water from its interior. Consequently, we have assumed that the radius remains at 19.7 Å, even as the micelle number increases with added salt. As pointed out above, there is no steric difficulty in forming even the largest micelles with this radius.

We further assume that the electrostatic repulsion of the ionic heads of the detergent molecules is the factor which limits the micelle number.

### Theory and Results

Consider the reaction



i.e., the addition of 1 more detergent ion to an aggregate of  $N - 1$  detergent ions. Using the infinitely dilute solution of each detergent species in the aqueous salt solution as the reference state and using molality concentration units, we can write the standard free energy change for this reaction as

$$\Delta G_N^{\circ} = -RT \ln [m_{A_N}/(m_{A_{N-1}})(m_{A_1})] \quad (2)$$

Equilibrium concentrations are used instead of activities since the c.m.c. is normally sufficiently low so that detergent-detergent interaction may be neglected.

If we apply eq. 2 to the most probable micelle size  $\hat{N}$  (where  $m_{A_N} \cong m_{A_{N-1}}$ ) we obtain

$$RT \ln m_{A_1} = \Delta G_{\hat{N}}^{\circ} \quad (2a)$$

and using this result in the vicinity of the c.m.c. gives

$$RT \ln (\text{c.m.c.}) = \Delta G_{\hat{N}}^{\circ} \quad (3)$$

(4) I. Reich, *J. Phys. Chem.*, **60**, 257 (1956).

(5) Y. Ooshika, *J. Colloid Sci.*, **9**, 254 (1954).

(6) F. Reiss-Husson and V. Luzzati, *J. Phys. Chem.*, **68**, 3504 (1964).

Equation 3 deserves some comment since ordinarily this system is treated in a different manner.<sup>7</sup> In the more usual approach, the chemical reaction is written for the complete assembly of micelle from individual detergent ions, *i.e.*

$$NA_1^\pm = A_N^{\pm N} \quad (4)$$

for which reaction we write  $\Delta G^\circ$  as the standard free energy change (on the same basis as before); of course, the obvious and exact relation  $\Delta G^\circ = \sum_{N=1}^N \Delta G^\circ_N$  holds.

In the subsequent development, the assumption is usually made that the micelle may be considered as a separate phase; this leads directly to the result

$$RT \ln (\text{c.m.c.}) = (\Delta G^\circ/N) \quad (5)$$

and it is from this relation that most experimental "free energies of micelle formation" have been obtained.

The derivation of eq. 3 makes clear that the quantity  $RT \ln (\text{c.m.c.})$  has a definite physical significance that is independent of the assumption of phase separation: it is the standard free energy change accompanying addition of a single detergent molecule to an aggregate having the size most probable at the c.m.c. Consequently, eq. 3 may always be used to interpret measurements of the c.m.c., even when the validity of (5) is questionable.

Conceptually, it is possible to divide the free energy change of eq. 3 into a hydrocarbon part ( $\Delta G^\circ_{\text{HC}}$ ) and an electrical part ( $\Delta G^\circ_{\text{el}}$ ). The electrostatic free energy is identical with that used in the theory of protein titration curves and may be replaced by  $N_0 \epsilon \psi_b$ , where  $\epsilon$  is the magnitude of the electronic charge,  $N_0$  is Avogadro's number, and  $\psi_b$  is the magnitude of the electrostatic potential at the micellar surface.<sup>8-10</sup> Thus, we have

$$RT \ln (\text{c.m.c.}) = \Delta G^\circ_{\text{HC}} + N_0 \epsilon \psi_{b,\hat{N}} \quad (6)$$

The left-hand side of eq. 6 is readily determined by experiment. The quantity  $\psi_{b,\hat{N}}$  depends, of course, on the electric charge on the micelle (which is given by  $\hat{N}$ ) and on the ionic atmosphere, and it may be calculated by solving the Poisson-Boltzmann equation. Since the Debye-Hückel approximation is not valid for the cases treated here ( $\epsilon \psi_b \sim 5kT$ ) we have used, instead, numerical solutions obtained with a high speed electronic computer (IBM 7072). The computer solutions actually provide  $\psi_{a,\hat{N}}$ , the potential at the distance of closest approach of small ions and the micelle, but this can readily be converted to  $\psi_{b,\hat{N}}$ . The method of computation has been described previously.<sup>11</sup>

In the present case, values of  $\hat{N}$  as determined by

light scattering on sodium dodecyl sulfate (SDS)<sup>12</sup> and dodecyltrimethylammonium bromide (DTAB)<sup>13</sup> solutions at various ionic strengths were used in the computations along with an assumed micelle radius of 19.7 Å. Again, this radius is an experimental result for SDS micelles in pure water,<sup>6</sup> and we have assumed that the same value is valid for DTAB and SDS under all conditions considered. The distance of closest approach,  $a$ , was then calculated as  $19.7 + r_{\text{Na}^+}$  ( $=21.8$  Å) for SDS and  $19.7 + r_{\text{Br}^-}$  ( $=21.7$  Å) for DTAB. These two quantities,  $\hat{N}$  and  $a$ , along with the ionic strength of the solution, were then used to calculate the boundary conditions (*i.e.*, the electric field at the micelle surface) that apply, and the computer solution for the appropriate boundary value was obtained from the computer tables by interpolation. Insertion of  $\psi_{b,\hat{N}}$  and the experimental c.m.c. into eq. 6 allows computation of  $\Delta G^\circ_{\text{HC}}$ . Results of this computation for the two detergents at several ionic strengths are presented in Tables I and II.

## Discussion

The magnitude of  $\Delta G^\circ_{\text{HC}}$  obtained may be compared with two other indirect measurements of the same

Table I: Computation of  $-\Delta G^\circ_{\text{HC}}$  for SDS

Concn. of added NaCl, $M$	C.m.c., $M$	$N$	$\epsilon \psi_a/kT$	$-\Delta G^\circ_{\text{HC}}$
0.00 <sup>a</sup>	0.00813 <sup>b</sup>	62 <sup>b</sup>	6.96	8,300
0.03	0.00312	72	5.85	8,420
0.10	0.00133	85	4.97	8,650
0.20	0.00090	101	4.78	9,140
0.40	0.00055	130	4.63	9,960
0.50	0.00052	142	4.68	10,300

<sup>a</sup> The micelles in these solutions exist in the presence of monomeric detergent ions of concentration equal to the c.m.c. Thus, the ionic strength used was the added electrolyte concentration plus the c.m.c. This only has an appreciable effect on the results for the solution containing no added salt. <sup>b</sup> All values of c.m.c. and  $N$  are from data in ref. 12.

(7) J. M. Corkill, J. F. Goodman, and S. P. Harrold, *Trans. Faraday Soc.*, **60**, 202 (1964).

(8) M. Nagasawa and A. Holtzer, *J. Am. Chem. Soc.*, **86**, 531 (1964).

(9) J. Edsell and J. Wyman, "Biophysical Chemistry," Academic Press Inc., New York, N. Y., 1958, pp. 477-549, Chapter 9.

(10) Inconsistencies that may be encountered in substituting the mean electrostatic potential for the potential of mean force are assumed to be small. See L. Onsager, *Chem. Rev.*, **13**, 73 (1933), for discussion of this point.

(11) See ref. 8, eq. 9 and 10.

(12) K. Mysels and L. Princen, *J. Phys. Chem.*, **63**, 1696 (1959).

(13) E. W. Anacker, R. M. Rush, and S. S. Johnson, *ibid.*, **68**, 81 (1964).

quantity. Wishnia estimates the hydrocarbon contribution to the free energy (from his measurements of solubilities of gaseous hydrocarbons in detergent solutions) as between  $-4730$  and  $-8430$  cal. for a 12-carbon chain.<sup>14</sup> We find from the experiments of Corkill and co-workers on nonionic detergents for the same length hydrocarbon chain about  $-6200$  cal.<sup>15</sup> Both values are in fair agreement with those found here.

**Table II:** Computation of  $-\Delta G_{\text{HC}}^{\circ}$  for DTAB

Concn. of added NaBr, $M$	C.m.c., $M$	$N$	$e\psi_a/kT$	$-\Delta G_{\text{HC}}^{\circ}$
0.00 <sup>a</sup>	0.0146 <sup>b</sup>	61 <sup>b</sup>	6.32	7490
0.1001	0.00436	74	4.63	7460
0.250	0.00254	83	4.18	7700
0.5016	0.00167	90	3.65	7760

<sup>a</sup> See footnote *a* of Table I. <sup>b</sup> All values of c.m.c. and  $N$  are from data in ref. 13.

The results of table I and perhaps II show a slight increase of  $-\Delta G_{\text{HC}}^{\circ}$  with increasing ionic strength. Since the hydrocarbon part of the free energy would be expected to be insensitive to salt concentration, this change may be a result of a real residual dependence of  $\Delta G_{\text{HC}}^{\circ}$  on  $N$  as discussed by Reich<sup>4</sup> and by Ooshika<sup>5</sup>; however, the variation is small in any case and may, as well, be an artifact of our assumption that the micellar radius is approximately independent of  $N$ . In fact, an

adjustment in  $a - b$  over a range of only  $1 \text{ \AA}$ . applied to the data of the tables would allow the same value of  $\Delta G_{\text{HC}}^{\circ}$  to be used in all cases.

The small apparent difference in  $\Delta G_{\text{HC}}^{\circ}$  for SDS and DTAB may also be a result of small differences in radius of the micelles of the two detergents, or it may reflect small specific differences in the supporting electrolyte (NaCl as opposed to NaBr) in the two cases.

In spite of these small discrepancies, we think it fair to proceed on the assumption that the simple approach adopted here may very well be adequate to explain the ionic strength dependence of the micelle number, that is, that the micelle number is limited by electrostatic factors that may be estimated through numerical solution of the Poisson-Boltzmann equation. Obviously, the crucial experiments that remain consist of measurements of micelle radii (by low angle X-ray scattering) for solutions containing added salt and comparison of measurements of  $N$  (by, say, light scattering) for SDS and DTAB in solutions containing various salts. Such measurements should allow an unambiguous decision to be made on whether  $\Delta G_{\text{HC}}^{\circ}$  is, in fact, not quite independent of detergent and of  $N$ , as indicated in the tables, or whether the micelle radius is changing, with attendant changes in  $\Delta G_{\text{el}}^{\circ}$ , and whether specific salts have a residual, specific effect.

(14) A. Wishnia, *J. Phys. Chem.*, **67**, 2079 (1963). We have converted Wishnia's results to a molality basis.

(15) See ref. 7. To eliminate the effect of the polar head groups, we have extrapolated the data in this paper to zero head group (zero  $E$ ); values have been corrected to a molality basis.

# A Near-Infrared Study of Hydrogen Bonding in Water and Deuterium Oxide<sup>1</sup>

by Mary R. Thomas, Harold A. Scheraga,

*Department of Chemistry, Cornell University, Ithaca, New York*

and Eugene E. Schrier

*Department of Chemistry, State University of New York at Binghamton, Binghamton, New York*  
(Received March 26, 1965)

The spectra of liquid H<sub>2</sub>O, liquid D<sub>2</sub>O, H<sub>2</sub>O ice, and D<sub>2</sub>O ice have been obtained in the 1.16–1.25- $\mu$  region for H<sub>2</sub>O and the 1.56–1.69- $\mu$  region for D<sub>2</sub>O. The temperature dependence of the liquid spectra and the extinction coefficients for the solids have been utilized to calculate the concentrations of the unbonded, singly hydrogen-bonded, and doubly hydrogen-bonded water molecules as a function of temperature for liquid H<sub>2</sub>O and for liquid D<sub>2</sub>O. The fraction of possible hydrogen bonds remaining intact at various temperatures for H<sub>2</sub>O compares well with previous experimental and theoretical results. The results for D<sub>2</sub>O are consistent with the calculations of Némethy and Scheraga.<sup>2</sup>

## Introduction

The structure of liquid water continues to receive considerable attention. Recently, Némethy and Scheraga<sup>2</sup> have shown that their theoretical treatment of liquid water<sup>3</sup> is applicable to deuterium oxide. Their calculations indicate that more structural order exists in D<sub>2</sub>O than in H<sub>2</sub>O at a given temperature. However, the breakdown of the structural order with increasing temperature was shown to be more rapid for D<sub>2</sub>O than for H<sub>2</sub>O.

Buijs and Choppin<sup>4</sup> have investigated the absorption spectrum of water in the 1.16–1.25- $\mu$  region. They suggested that these bands were due to the presence of three types of water molecules, those having zero, one, and two hydrogen bonds, respectively, to neighboring molecules. By assigning extinction coefficients to each of the species, based on the H<sub>2</sub>O liquid spectrum at different temperatures and additional data given by the spectra of ice and of water in aqueous salt solutions, they computed the fraction of each type of water molecule at a series of temperatures. Goldstein and Penner<sup>5</sup> applied a somewhat different treatment to the 1.45- and 1.93- $\mu$  absorption bands of H<sub>2</sub>O. They assigned values to the extinction coefficient of the doubly bonded species using absorbance data for ice as did Buijs and Choppin,<sup>4</sup> but, instead of attempting to evaluate the extinction coefficients for the other species

from various experimental data, they left them as unknown parameters to be determined along with the unknown concentrations at each of four temperatures by a least-squares computer method. Since we have employed the same calculation scheme,<sup>5</sup> further details will be given below. The fractions of hydrogen bonds unbroken in liquid water at various temperatures, obtained in these investigations,<sup>4,5</sup> were in fair agreement with those calculated by Némethy and Scheraga.<sup>3</sup>

Luck<sup>6</sup> has also investigated several of the near-infrared bands of H<sub>2</sub>O. His calculations are not as extensive as those of the workers already mentioned. He gives the concentrations of the doubly bonded and free water molecules as a function of temperature in the range 0–90°. He suggests<sup>6b</sup> that there is a considerable fraction of hydrogen bonding in water up to the vicinity of the critical point, basing this conclusion on experiments with water under high pressure.

(1) This work was supported by a research grant (AI-01473) from the National Institute of Allergy and Infectious Diseases of the National Institutes of Health, U. S. Public Health Service, and by a research grant (GB-2238) from the National Science Foundation.

(2) G. Némethy and H. A. Scheraga, *J. Chem. Phys.*, **41**, 680 (1964).

(3) G. Némethy and H. A. Scheraga, *ibid.*, **36**, 3382 (1962).

(4) K. Buijs and G. R. Choppin, *ibid.*, **39**, 2035 (1963).

(5) R. Goldstein and S. S. Penner, *J. Quant. Spectry. Radiative Transfer*, **4**, 441 (1964).

(6) (a) W. Luck, *Z. Elektrochem.*, **67**, 186 (1963); (b) W. Luck, *ibid.*, **68**, 895 (1964).

These methods of treating the data suffer from distinct uncertainties. The temperature dependence of the various extinction coefficients used in the calculations is assumed to be negligible. Experimental verification of this assumption is a very difficult undertaking. Another problem is the large base-line corrections which must be made for the contributions from the absorbance of neighboring peaks. On the theoretical side, the assignment of the bands in Buijs and Choppin's<sup>4</sup> treatment has been challenged.<sup>7</sup> These criticisms have been answered by Buijs and Choppin,<sup>8</sup> but the definitive assignment must await further investigation. Even with these difficulties, it seemed useful to obtain spectral data for liquid D<sub>2</sub>O and also some measure of the structural order in D<sub>2</sub>O as a function of temperature, using a procedure similar to those mentioned above.<sup>4,5</sup> Comparison of these data for D<sub>2</sub>O with the calculations of Némethy and Scheraga<sup>2</sup> for D<sub>2</sub>O and the previous results<sup>3-5</sup> for H<sub>2</sub>O was then the main objective of this work. In addition, the experiments of Buijs and Choppin on liquid H<sub>2</sub>O were repeated with more precise temperature control.

#### Apparatus and Procedures

A Cary Model 14 spectrophotometer equipped with thermostated cell holders was used to obtain the spectra of solid and liquid H<sub>2</sub>O and D<sub>2</sub>O. Most of the data were obtained using matched 1-cm. infrared quartz cells. Investigation of the shape of the much more intense OH (and OD) stretching overtone bands, which was necessary to obtain background contributions, was done using matched 1-mm. quartz cells. A calibrated thermistor and resistance bridge was used to monitor the temperature of the cells. The temperatures reported are precise to  $\pm 0.1^\circ$ .

Water was purified by distillation. Analysis for ionic impurities was carried out using conductivity measurements. Deuterium oxide was obtained from the Atomic Energy Commission, Oak Ridge, Tenn. The reported isotopic purity of 99.7% was verified by density and spectrophotometric measurements.

The D<sub>2</sub>O and H<sub>2</sub>O solid samples were prepared by freezing the liquid in suitable plastic tubes contained in an evacuated vessel. The resulting billets of ice were then shaped with a razor blade to fit a copper tube which had been cut on a lathe to the length desired, usually 1 or 2 cm. The ends of the ice billet were polished down to the ends of the tube by rubbing on manila paper towels covering a flat surface. Polishing of the faces of the billets just before they were inserted into the cell holder (maintained at  $-8^\circ$ ) eliminated light scattering from condensation. With careful handling, reproducible spectra with low background

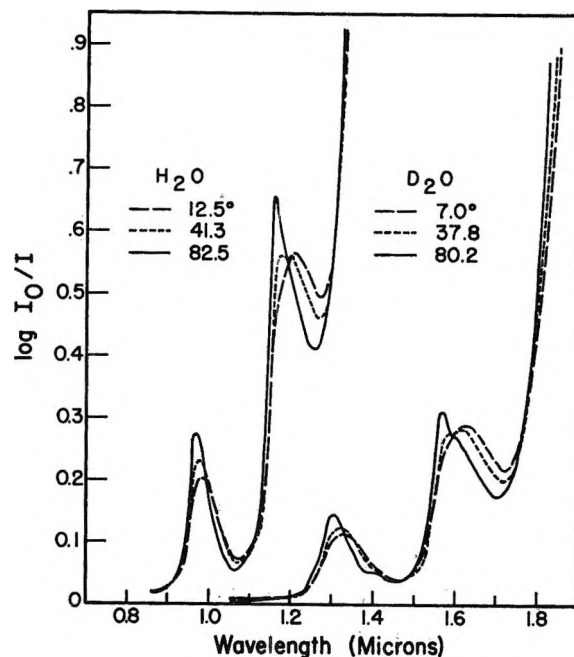


Figure 1. Near-infrared spectra of liquid H<sub>2</sub>O and of liquid D<sub>2</sub>O at various temperatures.

due to light scattering were observed for both solid H<sub>2</sub>O and D<sub>2</sub>O.

The cell compartment of the spectrophotometer was purged with nitrogen.

#### Results

The spectra of liquid H<sub>2</sub>O and D<sub>2</sub>O at three different temperatures are shown in Figure 1 while Figure 2 shows the D<sub>2</sub>O and H<sub>2</sub>O ice spectra. Carbon tetrachloride was the reference for the liquid samples and air for the solids.

The procedure employed to analyze the spectra was that suggested by Buijs and Choppin.<sup>4</sup> Absorbances were read from the H<sub>2</sub>O liquid spectrum at 1.16, 1.20, and 1.25  $\mu$ , these wave lengths representing the assumed absorption peaks<sup>4</sup> of the unbonded water molecules, the species having one hydrogen bond, and those with two hydrogen bonds, respectively. There are, of course, smaller contributions to the absorbance at each of these wave lengths from overlap of the bands of the other species. The corresponding peak absorbances in D<sub>2</sub>O were at 1.562, 1.62, and 1.69  $\mu$ . The temperature dependence of the band shapes, particularly the sharpening of the peaks at 1.16  $\mu$  for H<sub>2</sub>O and at 1.562  $\mu$  for D<sub>2</sub>O with increasing temperature, leading to their assignment as the peak absorbances for the unbonded species, are shown in Figure 1. The peaks at 1.25 and

(7) D. F. Hornig, *J. Chem. Phys.*, **40**, 3119 (1964).

(8) K. Buijs and G. R. Choppin, *ibid.*, **40**, 3120 (1964).

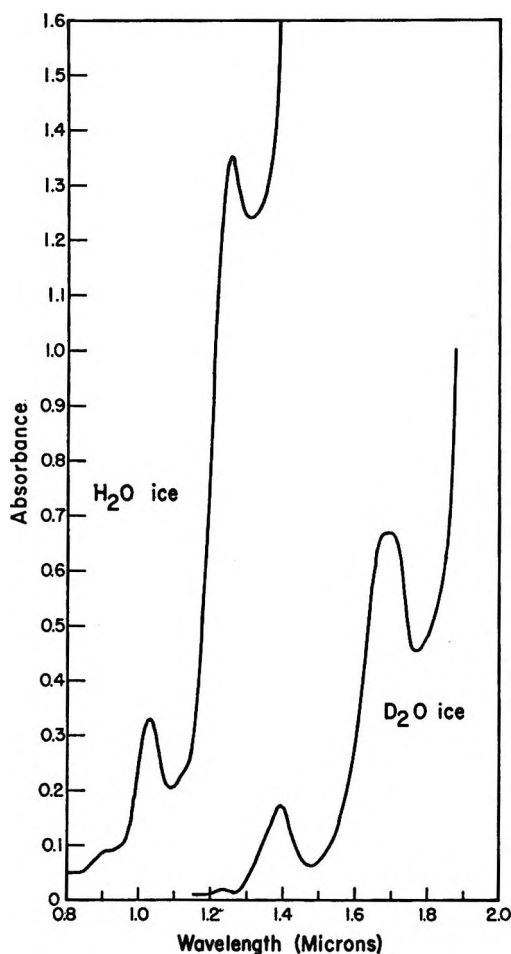


Figure 2. Spectra of H<sub>2</sub>O ice and D<sub>2</sub>O ice at  $-8^{\circ}$ ; path length, 2 cm.

1.69  $\mu$ , for H<sub>2</sub>O and D<sub>2</sub>O, respectively, are most readily seen in the ice spectra in Figure 2. Absorbances were obtained for the wave lengths of interest at seven different temperatures for H<sub>2</sub>O and nine temperatures for D<sub>2</sub>O in the range 7.0–82.5 $^{\circ}$ .

Corrections to these raw data are necessary because of the large contribution of the overtone band at 1.45  $\mu$  for H<sub>2</sub>O and at 1.93  $\mu$  for D<sub>2</sub>O to the long wave length side of the respective bands under investigation. Our studies of this overtone band for H<sub>2</sub>O supported the conclusion of Buijs and Choppin<sup>4</sup> that the lower portion of the short wave length side of the overtone band may be expressed as the sum of exponentials. A similar conclusion could be drawn from experiments on D<sub>2</sub>O. For H<sub>2</sub>O, the contribution of the background to the total absorption at 1.25  $\mu$  in pure water in the mid-temperature range is approximately 50%; at 1.16  $\mu$  the contribution drops to 20%. For D<sub>2</sub>O the corresponding contribution is less since the overtone band is more separated from the band under consideration than for

H<sub>2</sub>O. In the middle temperature region the contribution of the 1.93- $\mu$  band to the absorption at 1.69  $\mu$  is about 36% and at 1.56  $\mu$ , about 14%. The over-all uncertainty in the background corrections was estimated to be  $\pm 5\%$ .

These data were treated by the method of Goldstein and Penner.<sup>5</sup> The following equations may be used to calculate the concentrations of each species from the spectrum of H<sub>2</sub>O (or D<sub>2</sub>O) at the various temperatures

$$\begin{aligned} \epsilon_1^0 C_0 + \epsilon_1^1 C_1 + \epsilon_1^2 C_2 &= E_1 \\ \epsilon_2^0 C_0 + \epsilon_2^1 C_1 + \epsilon_2^2 C_2 &= E_2 \\ \epsilon_3^0 C_0 + \epsilon_3^1 C_1 + \epsilon_3^2 C_2 &= E_3 \\ C_0 + C_1 + C_2 &= 1 \end{aligned} \quad (1)$$

Here,  $E_1$ ,  $E_2$ , and  $E_3$  are the gross molar extinction coefficients (corrected for background absorption) measured at the wave lengths mentioned above, where the unbonded, one-bonded, and two-bonded species are presumed to have their peak absorbance. The  $\epsilon_j^i$  terms are extinction coefficients for the individual species,  $i = 0, 1, 2$ , signifying the number of intact hydrogen bonds, and  $j = 1, 2, 3$ , designating the wave length region where the absorbance of zero-, one-, or two-bonded species is assumed to be maximal. The  $C$  terms are the mole fractions of the various species.

To use these equations in the calculation of the concentrations of the various species at the different temperatures, the following hypotheses are employed. The extinction coefficients  $\epsilon_1^2$ ,  $\epsilon_2^2$ , and  $\epsilon_3^2$  are calculated, in each case, from the spectra of H<sub>2</sub>O and D<sub>2</sub>O ice. It is assumed<sup>4</sup> that  $\epsilon_1^1$  and  $\epsilon_3^1$  are of equal magnitude since the band for the singly bonded species may be symmetrical. The sharpness of the band for the unbonded species permits the assumption that  $\epsilon_3^0$  is negligible. The extinction coefficients  $\epsilon_1^0$ ,  $\epsilon_2^0$ ,  $\epsilon_1^1$ , and  $\epsilon_2^1$  and the three concentrations thus remain unknown at each temperature. A least-squares procedure for fitting the four unknown extinction coefficients and  $3n$  unknown concentrations of the hydrogen-bonded species at  $n$  different temperatures was used in conjunction with the CDC-1604 computer at the Cornell Computing Center. Since it is assumed in this treatment that the extinction coefficients of the various species do not vary with temperature, the selection of a sufficiently large number of temperatures serves to determine all the variables. The estimated over-all uncertainty in the final concentrations of the various species, taking into account errors of fit and the uncertainties in the background corrections, is  $\pm 7\%$ .

Tables I and II show the extinction coefficients obtained from the data for H<sub>2</sub>O and D<sub>2</sub>O ice (*i.e.*,  $\epsilon_1^2$ ,  $\epsilon_2^2$ ,

<sup>3</sup>) and also those calculated in the fitting procedure for the various H<sub>2</sub>O and D<sub>2</sub>O species.

**Table I:** Molar Extinction Coefficients<sup>a</sup> for H<sub>2</sub>O Species

$\epsilon_1^0$ 19.06	$\epsilon_1^1$ 4.45	$\epsilon_1^2$ 1.33
$\epsilon_2^0$ 1.25	$\epsilon_2^1$ 14.03	$\epsilon_2^2$ 5.78
$\epsilon_3^0$ 0	$\epsilon_3^1$ 4.45	$\epsilon_3^2$ 8.97

<sup>a</sup> All  $\times 10^{-3} M^{-1} \text{ cm.}^{-1}$ .

**Table II:** Molar Extinction Coefficients<sup>a</sup> for D<sub>2</sub>O Species

$\epsilon_1^0$ 9.27	$\epsilon_1^1$ 1.85	$\epsilon_1^2$ 0.91
$\epsilon_2^0$ 1.10	$\epsilon_2^1$ 7.00	$\epsilon_2^2$ 3.50
$\epsilon_3^0$ 0	$\epsilon_3^1$ 1.85	$\epsilon_3^2$ 4.88

<sup>a</sup> All  $\times 10^{-3} M^{-1} \text{ cm.}^{-1}$ .

The mole fractions of the various species, calculated by the fitting procedure from eq. 1, are given for H<sub>2</sub>O in Table III and for D<sub>2</sub>O in Table IV. The last column in each table gives the fraction of hydrogen bonds remaining unbroken at each temperature. This number is equal to  $C_2 + (1/2)C_1$ .

**Table III:** Mole Fractions of Hydrogen-Bonded Species for H<sub>2</sub>O at Various Temperatures

<i>t</i> , °C.	<i>C</i> <sub>0</sub>	<i>C</i> <sub>1</sub>	<i>C</i> <sub>2</sub>	<i>C</i> <sub>H</sub> bonds unbroken
12.5	0.243	0.360	0.397	0.577
32.0	0.296	0.374	0.330	0.517
41.3	0.320	0.379	0.301	0.491
54.8	0.357	0.384	0.259	0.451
68.2	0.391	0.386	0.223	0.416
73.4	0.406	0.384	0.210	0.402
82.5	0.430	0.381	0.189	0.380

**Table IV:** Mole Fractions of Hydrogen-Bonded Species for D<sub>2</sub>O at Various Temperatures

<i>t</i> , °C.	<i>C</i> <sub>0</sub>	<i>C</i> <sub>1</sub>	<i>C</i> <sub>2</sub>	<i>C</i> <sub>H</sub> bonds unbroken
7.0	0.232	0.396	0.372	0.570
13.8	0.241	0.398	0.361	0.560
21.0	0.262	0.402	0.336	0.537
28.1	0.282	0.410	0.308	0.513
37.8	0.312	0.411	0.276	0.482
51.3	0.357	0.401	0.241	0.442
60.5	0.385	0.405	0.210	0.413
70.7	0.417	0.399	0.183	0.383
80.2	0.444	0.390	0.162	0.357

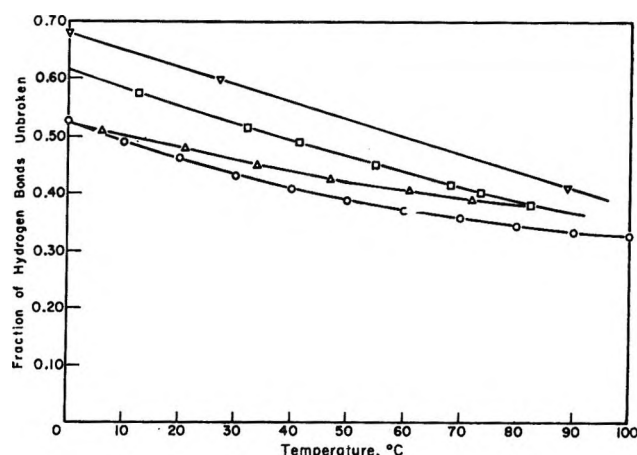


Figure 3. Fraction of hydrogen bonds unbroken as a function of temperature for H<sub>2</sub>O:  $\nabla$ , Goldstein and Penner<sup>5</sup>;  $\Delta$ , Buijs and Choppin<sup>4</sup>;  $\circ$ , Némethy and Scheraga<sup>3</sup>;  $\square$ , this work.

## Discussion

The fraction of hydrogen bonds unbroken for H<sub>2</sub>O as a function of temperature is plotted in Figure 3, along with the experimental results of Buijs and Choppin<sup>4</sup> and of Goldstein and Penner<sup>5</sup> and the values obtained in the theoretical treatment of Némethy and Scheraga.<sup>3</sup> The results of this investigation fall midway between those of Buijs and Choppin<sup>4</sup> and Goldstein and Penner.<sup>5</sup> If it is assumed that the limits of error on their calculated values are the same as those given here ( $\pm 7\%$ ), the sets of data are in agreement.

In comparing the results, further discussion of the assumptions may be useful. In all the investigations, it was assumed that the extinction coefficients for the various species were independent of temperature (in one investigation,<sup>5</sup> over a 200° range). This may be only a crude approximation, but the variation of intermolecular potentials and hydrogen-bond lengths and configurations with temperature is generally unknown. The method of assigning the unknown extinction coefficients to the different water species differed in the various studies. Goldstein and Penner<sup>5</sup> and the present investigators used sets of optical densities at various temperatures to obtain both the unknown extinction coefficients and the mole fraction of the various species at each temperature. Buijs and Choppin<sup>4</sup> obtained the unknown extinction coefficients by using absorbances of aqueous salt solutions at high salt concentrations together with data obtained at various temperatures for pure water. While it is not clear from their paper exactly how they combined this information to obtain the unknown extinction coefficients, the neglect of possible ion-dipole interactions in the use of data from concentrated salt solutions may be a serious drawback

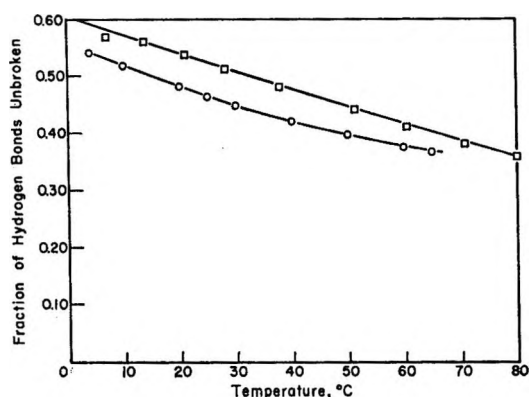


Figure 4. Fraction of hydrogen bonds unbroken as a function of temperature for  $D_2O$ : O, Némethy and Scheraga<sup>2</sup>; □, this work.

to their method of calculation. Acknowledging these limitations, the agreement between our results and those of Buijs and Choppin<sup>4</sup> for the over-all set of extinction coefficients and the agreement of all investigators as to the fraction of hydrogen bonds unbroken at a given temperature for  $H_2O$  is satisfactory and may indicate that the above-mentioned approximations are of secondary importance in the over-all procedure. It should also be recalled that Goldstein and Penner<sup>5</sup> analyzed a different set of spectral bands than the other investigators.

These results may be compared with the theoretical values of Némethy and Scheraga.<sup>3</sup> Although their model dealt with five water species, the fraction of hydrogen bonds unbroken has the same meaning as in the experimental studies since the total number of possible hydrogen bonds is the same in each case. The general agreement of the data within the limits of error may be noted, as well as the comparable trends with increasing temperature in the experimental and theoretical results.

The dependence of the fraction of hydrogen bonds unbroken on temperature for  $D_2O$  is given in Figure 4. In this figure, the results of the present study are compared with those calculated by Némethy and Scheraga.<sup>2</sup> The good agreement for both the values and the trend with temperature is again noteworthy. The differences between the experimental and theoretical values are about the same for  $D_2O$  as for  $H_2O$  and are approximately within the limit of error of the spectroscopic method. This is significant in view of the fact that the band shapes, background corrections, and the assigned extinction coefficients for  $D_2O$  differed considerably from those for  $H_2O$ .

*Acknowledgment.* We wish to thank Mrs. Marcia Pottle for her help in setting up the computer program for the numerical computations.



## An Electron Diffraction Study of Trifluoronitrosomethane

by M. I. Davis, J. E. Boggs, D. Coffey, Jr.,

*Department of Chemistry, University of Texas, Austin, Texas 78712*

and H. P. Hanson

*Department of Physics, University of Texas, Austin, Texas 78712 (Received April 7, 1965)*

The molecular structure of trifluoronitrosomethane has been determined by gas phase electron diffraction. The predominant conformation was found to be eclipsed. The principal structure parameters are found to be:  $r(\text{C-F}) = 1.321 \pm 0.004 \text{ \AA.}$ ,  $\angle \text{FCF} = 111.9 \pm 0.4^\circ$ ,  $r(\text{C-N}) = 1.555 \pm 0.015 \text{ \AA.}$ ,  $r(\text{N-O}) = 1.171 \pm 0.008 \text{ \AA.}$ ,  $\angle \text{CNO} = 121.0 \pm 1.6^\circ$ . The fact that the C-N bond is appreciably longer than the value observed in amines is consistent with the results of investigations of certain other nitro and nitroso compounds. It would appear that many of the structural features of this compound are consistent with an appreciable shift of charge in the direction of the fluorine atoms. The C-N bond direction differs from the  $\text{CF}_3$  axis by about  $1^\circ$ .

### Introduction

Fluorine n.m.r. chemical shifts have been reported for a wide range of compounds containing the trifluoromethyl group.<sup>1</sup> Of the reported values, the most positive is the one for  $\text{CF}_3\text{NO}$ . This fact, together with an unexpectedly low value for the dipole moment, led to the prediction of marked ionic character.<sup>1</sup> Specifically, it was suggested that there exists an appreciable contribution of the resonance structure  $(\text{CF}_3)^-(\text{NO})^+$ .

This situation is analogous to that found in certain nitrosyl halides.<sup>2,3</sup> In those instances, studies of N-Hal bond lengths, N=O bond-order considerations, and bond-moment calculations all lead to the prediction of an appreciable  $\text{Hal}^-(\text{NO})^+$  contribution.

A gas phase electron diffraction study was initiated to ascertain whether or not the N-C bond in  $\text{CF}_3\text{NO}$  is significantly different from the usual single-bond values. A study of the nitro analog  $\text{CF}_3\text{NO}_2$  reveals that the C-N bond in that compound is considerably longer than the normally encountered values.<sup>4</sup>

### Experimental Section

Intensity data were collected using the University of Texas diffraction unit. In order to keep the vapor pressure of this highly volatile substance down at a reasonable value ( $\sim 30 \text{ mm.}$ ) the bulk of the sample was maintained at  $-120^\circ$ . The nozzle temperature

would be expected to be fairly low itself because of radiation losses to the cold trap which contained liquid nitrogen.

The data were collected photographically at nozzle-to-camera distances of 100, 50, and 25 cm. A reproducible interference pattern could be discerned out to about  $s = 40 \text{ \AA.}^{-1}$ . The handling of the experimental data was carried out along lines similar to those described elsewhere.<sup>5</sup>

### Theory

The molecular scattering intensities were analyzed on the basis of the following expression

$$M_B(s) = \sum_{ij} n_{ij} [Z_i - F_i(s)] [Z_j - F_j(s)] \cos [\eta_i(s) - \eta_j(s)] \exp(-l_{ij}^2 s^2) (sr_{ij})^{-1} \sin(sr_{ij}) \quad (1)$$

where  $M_B(s) = M_X(s)s^{-4}$ ,  $M_X(s)$  being the observed molecular intensities and  $s$  (the scattering parameter)

(1) J. E. Boggs, D. Coffey, Jr., and J. C. Davis, Jr., *J. Phys. Chem.*, **68**, 2383 (1964).

(2) D. W. Magnusson, *J. Chem. Phys.*, **19**, 1071 (1951).

(3) D. J. Millen and J. Pannel, *J. Chem. Soc.*, 1322 (1961).

(4) I. L. Karle and J. Karle, *J. Chem. Phys.*, **36**, 1969 (1962); R. E. Knudsen, C. F. George, and J. Karle, Abstracts, Winter Meeting of the American Crystallographic Association, Suffern, N. Y., Feb. 1965.

(5) M. I. Davis and H. P. Hanson, to be published.

$= 4\pi\lambda^{-1} \sin \theta$ ,  $\theta$  being one-half the scattering angle, and  $\lambda$  the de Broglie wave length.

$F_i(s)$  and  $\eta_i(s)$  are, respectively, the atomic scattering factors and atomic phase shifts for the element with atomic number  $Z_i$ . The parameters  $r_{ij}$  and  $l_{ij}$  are, respectively, the internuclear distance and mean vibrational amplitude of the atom pair type ( $ij$ ). There are  $\eta_{ij}$  symmetrically equivalent pairs of this type in the molecule.

### Refinement of Data

From a model set of atomic coordinates, it is possible to calculate all of the internuclear distances of the molecule. It is unfortunate that the majority of these distances belong to one or the other of two sets of very similar values. For this reason the data analysis could not be expected to lead to highly precise values of all of the dimensional parameters, particularly if one were attempting to obtain the complete set of internuclear distances without introducing any geometric constraint.

A radial distribution curve was calculated from the molecular-scattering intensities, according to eq. 2.

$$\sigma(r)/r = \sum_s M_X(s) s Z_F^2 / [Z_F - F_F(s)]^2 e^{-ks^2} \sin(sr) \Delta s \quad (2)$$

The damping factor  $k$  was introduced to compensate for the finite upper limit of  $s$ , beyond which useful data could not be obtained. For the smaller values of  $s$ , where intensity values were either unobtainable or unreliable, theoretical values were adopted.

There exists for this compound the possibility of either eclipsed or staggered conformations. In this respect the radial distribution curve is of great value (see Figure 1). Approximate values for the two O-F distances can be calculated for both models. In the eclipsed model, the two predicted distances are of the order of 2.5 and 3.1 Å., respectively. The staggered model has distances of 2.8 and 3.4 Å. The shape of the radial distribution curve can only be explained satisfactorily by the acceptance of the eclipsed model, *i.e.*, one in which the NO bond is *cis* with respect to one of the three CF bonds. There is a significant radial distribution peak at 3.15 Å., but none at either 2.8 or 3.4 Å. The symmetry of a peak at 2.2 Å. is such that it can only be explained by a contribution in the general region of 2.5 Å. This evidence does not preclude a small amount of the staggered conformation, but there was no indication that any contribution to the radial distribution curve existed to an extent larger than the experimental error. One further feature of the molecular structure became evident from the initial radial distribution curve, namely that the C-N bond length

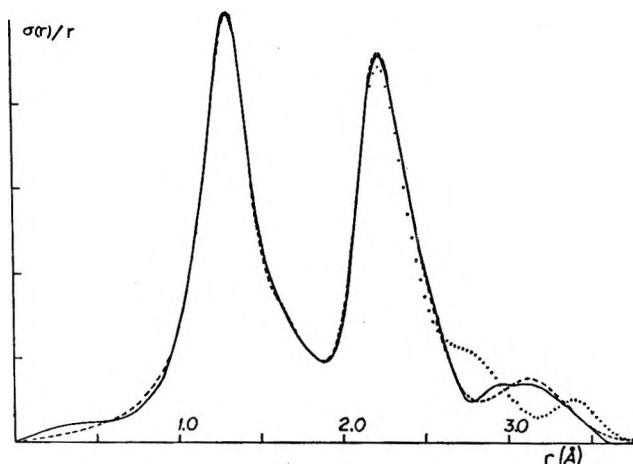


Figure 1. The radial distribution curve of trifluoronitrosomethane ( $k = 0.0025$ ). The broken line is the theoretical version for the eclipsed conformation; the dotted line is that for the staggered.

must be significantly longer than the value of 1.47 Å., which has been found for amines.

In addition to the radial distribution method, three other approaches were used for the structure refinement. These methods all involved the comparison of theoretical and experimental molecular-scattering curves. The methods differ in the manner in which the structure parameters are adjusted. One of these is the least-squares matrix method of Hedberg.<sup>6</sup> The other methods involve continuous adjustment of the dimensional parameters and vibrational amplitudes in the direction of improving compatibility between the theoretical and experimental molecular intensities. The latter two methods differ in that one involves simultaneous adjustment of all parameters, while the other uses cyclic adjustment of the individual parameters in turn.

It was found to be feasible to consider the C-N bond direction to be different from the axis of the  $CF_3$  group. It was not possible, however, to make any meaningful distinction between the two types of C-F bond lengths or of the symmetrically nonequivalent FCF bond angles.

### Results

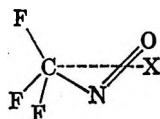
The results of the four methods that were used to evaluate the structural parameters are shown in Table I. The intensity curve analyses were conducted on the basis of a geometric model described by six variable coordinates. No such constraint was used in the radial distribution curve analysis which was performed essentially as a check to ensure that the computational

(6) K. Hedberg and M. Iwasaki, *Acta Cryst.*, 17, 529 (1964).

**Table I:** Molecular Structure Parameters for Trifluoronitrosomethane as Obtained from Various Analytical Procedures<sup>a</sup>

Method	Bond distances, Å.			Bond angles, deg.			<i>l</i> (C-F), Å.	<i>l</i> (F-F), Å.
	<i>r</i> (C-F) (mean)	<i>r</i> (C-N)	<i>r</i> (N=O)	FCF (mean)	CNO	XCN		
R.d.	1.324	1.54	1.175	111.4	117	3		
A	1.322	1.555	1.170	111.8	121.6	1.8	0.044	0.073
B	1.320	1.55	1.169	112.0	122.6	1.4	0.045	0.073
C	1.321	1.56	1.174	111.8	120.5	0.7	0.050	0.070

<sup>a</sup> The point X is taken to be on the symmetry axis of the CF<sub>3</sub> group, the angle XCN is taken to be positive when the N atom lies on the opposite side of X to the planar CF bond. R.d., radial distribution; A, intensity curve analysis using individual parameter ad-



justment; B, intensity curve analysis using simultaneous parameter adjustment; C, intensity curve analysis using Hedberg's method.

intensity curve analyses had not inadvertently led us to a false result.

The experimental radial distribution curve is shown in Figure 1. The broken-line curve is a theoretical version obtained by Fourier inversion of the "best" theoretical molecular-scattering curve. The dotted curve is the theoretical version for the staggered conformation. The experimental and theoretical molecular-scattering curves are shown in Figure 2.

The molecular structure parameters for trifluoronitrosomethane, as determined by this investigation, are given in Table II. The values are based upon the intensity curve refinement procedures. In Bartell's notation, the bond lengths cited are the  $r_g(1)$  values.<sup>7</sup> However the distinction would only be realistic in the case of the C-F bond, in view of the rather large uncertainties.

**Table II:** Trifluoronitrosomethane Molecular Structure

<i>r</i> (C-F)	$1.321 \pm 0.004$ Å.
∠FCF	$111.9 \pm 0.4^\circ$
<i>r</i> (C-N)	$1.555 \pm 0.015$ Å.
<i>r</i> (N=O)	$1.171 \pm 0.008$ Å.
∠CNO	$121 \pm 1.6^\circ$
∠XCN	$1.3 \pm 0.8^\circ$

The limits of tolerance are those obtained from the results of an error matrix calculation of the type described by Hedberg.<sup>6</sup> The computed values have been increased to take into account the systematic errors involved in measuring the electron wave length and the nozzle-to-camera distances.

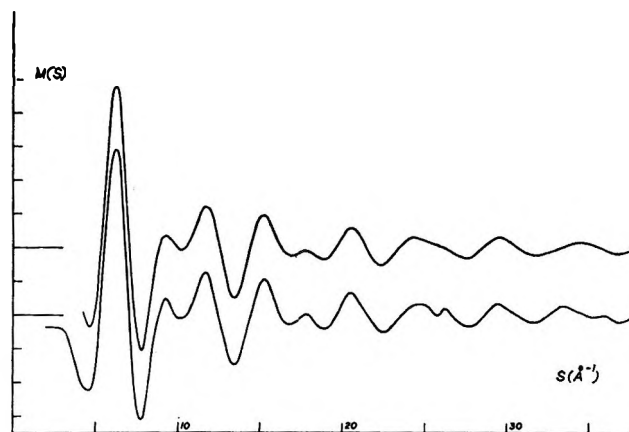


Figure 2. Experimental and theoretical molecular-scattering curves for trifluoronitrosomethane. The lower curve is the experimental version.

## Discussion

Prior to this investigation it had been argued that CF<sub>3</sub>NO should be markedly ionic in character.<sup>1</sup> In valence-bond terminology this implies a significant contribution of the resonance form (CF<sub>3</sub>)<sup>-</sup>(NO)<sup>+</sup>. It appears that the results of this investigation are consistent with that model.

It has been noted by Lindqvist<sup>8</sup> that a chemical bond will be weakened and consequently lengthened when the introduction of a suitable substituent produces a marked increase in its polarity. In CF<sub>3</sub>NO, the C-N bond is presumed to be far more polar than in the amines. The observed bond length of 1.555 Å.

(7) L. S. Bartell, *J. Chem. Phys.*, **23**, 1219 (1955).

(8) I. Lindqvist, *Nova Acta Regiae Soc. Sci. Upsalensis*, [4] **17g**, No. 11 (1960).

is certainly appreciably longer than the typical amine values of 1.474 (methylamine)<sup>9</sup> and 1.471 Å. (piperazine).<sup>10</sup> It is interesting to note that for the series of compounds CF<sub>3</sub>NO<sub>2</sub>, CCl<sub>3</sub>NO<sub>2</sub>, and CBr<sub>3</sub>NO<sub>2</sub>, the C-N bond lengths are all found to be in the range 1.56–1.59 Å.<sup>4</sup>

N=O bond lengths have been obtained for a large number of compounds; some typical values are shown in Table III. The CF<sub>3</sub>NO value lies between those for the nitrosyl halides, on the low side, and CH<sub>3</sub>·O·NO. This variation can be correlated with the electronegativities of the groups bonded to the nitrogen. Values of  $\sigma_I$  (the inductive electron-withdrawing power) are given in Table IV. It appears that the greater the electron-withdrawing power of the group, the shorter and presumably stronger is the N=O bond. The N=O bond length in CF<sub>3</sub>NO also lies between those of NO<sub>2</sub><sup>+</sup> and NO<sub>2</sub>, where the bond orders are taken to be 2.0 and 1.5, respectively.

Table III: N=O Bond Lengths<sup>a</sup>

Compd.	r(N=O), Å.
NO	1.151
N <sub>2</sub> O	1.186
NO <sub>2</sub>	1.197 <sup>b</sup>
NO <sup>+</sup>	1.062
NO <sub>2</sub> <sup>+</sup>	1.154
ClNO	1.139 <sup>c</sup>
FNO	1.13
CH <sub>3</sub> ONO''	1.22 <sup>d</sup>
CH <sub>3</sub> NO <sub>2</sub>	1.22
CF <sub>3</sub> NO	1.171 <sup>e</sup>

<sup>a</sup> All values taken from ref. 11 except where indicated. <sup>b</sup> G. R. Bird, *J. Chem. Phys.*, **25**, 1040 (1956). <sup>c</sup> See ref. 3. <sup>d</sup> This value refers to the N-O'' bond. <sup>e</sup> Present investigation.

C-F bond lengths in compounds of the type CF<sub>3</sub>X appear to be quite insensitive to the nature of the group X, all of the reported values falling within the range 1.32–1.33 Å.<sup>11</sup> The flattening of the CF<sub>3</sub> group in this compound is consistent with the long C-N bond and the appreciable ionic character of the molecule.

Table IV: Electron-Withdrawing Powers (Inductive)<sup>a</sup>

Group	$\sigma_I$
F	+0.46
Cl	+0.44
CF <sub>3</sub>	+0.380
OCH <sub>3</sub>	+0.230

<sup>a</sup> Calculated from the Hammett substituent constants, compiled by D. H. McDaniel and H. C. Brown [*J. Org. Chem.*, **23**, 420 (1958)].

The available evidence<sup>12,13</sup> indicates that in compounds of the type CX<sub>3</sub>-Y=Z, the more stable configuration is that in which the double bond is eclipsed by one of the C-X bonds. This is found to be the case for CF<sub>3</sub>N=O.

The distance between the oxygen atom and its nearest fluorine (2.51 Å.) is somewhat less than the van der Waals distance. The repulsion that must exist between these two atoms may be taken to account for two further features of the structure. Pauling<sup>12</sup> has tabulated a number of XNO bond angles for nitroso compounds, all of which lie in the range 110–118°. The observed value of 121° for the CNO angle in this compound is somewhat larger than those cited. It is found that the C-N bond direction does not coincide exactly with the axis of the CF<sub>3</sub> group. The direction of the deviation is that which increases the oxygen-to-fluorine distance.

*Acknowledgments.* We wish to thank Mr. Stanley Speed for assistance in collecting the data and Mr. Charles Preiss for his help in the preliminary stages of the data handling. This investigation was supported by the Robert A. Welch Foundation of Houston, Texas.

(9) D. R. Lide, *J. Chem. Phys.*, **27**, 1181 (1963).

(10) M. Davis and O. Hassel, *Acta Chem. Scand.*, **17**, 1181 (1963).

(11) L. E. Sutton, Ed., "Tables of Interatomic Distances," Special Publication No. 11, The Chemical Society, London, 1958.

(12) L. Pauling, "Nature of the Chemical Bond," 3rd Ed., Cornell University Press, Ithaca, N. Y., 1960, p. 140.

(13) R. Curl, *J. Chem. Phys.*, **41**, 2562 (1964).

## Appearance Potentials and Mass Spectra of Fluorinated Ethylenes. II. Heats of Formation of Fluorinated Species and Their Positive Ions<sup>1</sup>

by Chava Lifshitz and F. A. Long

Department of Chemistry, Cornell University, Ithaca, New York (Received April 7, 1965)

Mass spectrally determined appearance potentials of fragment ions from several fluorinated ethylenes have been used to calculate heats of formation of a series of hydrofluorocarbon radicals and ions. Supplementary determinations were carried out on fragments from fluorinated methanes and ethanes. The data lead to maximum values of 9.6, 11.7, and 9.45 for the ionization potentials of CF, CF<sub>2</sub>, and CH<sub>2</sub>F, respectively. Some derived heats of formation are:  $\Delta H_f(\text{CF}_2) \leq -1.6$  e.v.;  $\Delta H_f(\text{CH}_2\text{F}) = -0.95 \pm 0.1$  e.v.;  $\Delta H_f(\text{C}_2\text{F}_3) = -1.1 \pm 0.3$  e.v. Different ionization potentials are calculated for both CF<sub>2</sub>H and CF<sub>3</sub> depending on whether the calculations are from appearance potentials of CF<sub>3</sub><sup>+</sup> and CF<sub>2</sub>H<sup>+</sup> from the paraffin series or from appearance potentials of the olefin series. These and further disagreements in calculations based upon the paraffin and olefin series are discussed.

### Introduction

The mass spectra and appearance potentials for a group of fluorinated ethylenes were presented in a previous paper.<sup>2</sup> A few thermochemical calculations were carried out in developing the probable decomposition mechanisms for the parent ions. The number of possible direct calculations is however small since thermochemical data on fluorocarbons and their radicals and ions are quite scarce. Heats of formation of some of the low molecular weight saturated fluoroparaffins are known,<sup>3</sup> but attempts to obtain thermochemical data for fluorocarbon radical ions, especially CF<sub>3</sub><sup>+</sup>, from appearance potential measurements on fluoroparaffins have not been very successful.<sup>4,5</sup> The main difficulty appears to be the occurrence of ions with considerable amounts of kinetic energy. The fluorinated ethylenes, however, offer another route since they show yields of ions which are of great thermochemical interest (CF<sup>+</sup>, CX<sub>2</sub><sup>+</sup>, and CX<sub>3</sub><sup>+</sup>, where X is either F or H). The present paper gives further thermochemical calculations using the available appearance potentials and other available thermochemical data and some newly determined appearance potential values.

### Experimental Section

The mass spectrometer and the techniques used were described in part I which also gives appearance poten-

tials of fragments from fluorinated ethylenes. Table I<sup>6-10</sup> presents results of appearance potential measurements on some paraffins and C<sub>3</sub>F<sub>6</sub>.

Perfluoromethane was purchased from Matheson; CHF<sub>3</sub>, C<sub>2</sub>F<sub>6</sub>, and C<sub>3</sub>F<sub>6</sub> were kindly furnished by the Jackson Laboratory of the Du Pont Co. CH<sub>3</sub>CHF<sub>2</sub> was from the Allied Chemical Co. while CH<sub>2</sub>F<sub>2</sub> was from the Columbia Chemicals Co. These were all of high purity (>99%) and were used without further purification.

Several appearance potentials of fragments from these

(1) Work supported by the Advanced Research Projects Agency through the Cornell Materials Science Center.

(2) C. Lifshitz and F. A. Long, *J. Phys. Chem.*, **67**, 2463 (1963); hereafter called part I.

(3) C. R. Patrick, *Advan. Fluorine Chem.*, **2**, 1 (1961).

(4) V. H. Dibeler, R. M. Reese, and F. L. Mohler, *J. Res. Natl. Bur. Std.*, **57**, 113 (1956).

(5) J. B. Farmer, I. H. S. Herderson, F. P. Lossing, and D. G. H. Marsden, *J. Chem. Phys.*, **24**, 348 (1956).

(6) S. Stokes and A. B. F. Duncan, *J. Am. Chem. Soc.*, **80**, 6177 (1958).

(7) D. L. Hobrock and R. W. Kiser, *J. Phys. Chem.*, **68**, 575 (1964).

(8) J. W. Warren and J. D. Craggs, *Mass Spectrometry, Rept. Conf. Manchester, Engl.*, 1950, 36 (1952).

(9) F. M. Matsunaga and K. Watanabe, private communication.

(10) V. H. Dibeler, R. M. Reese, and F. L. Mohler, *J. Chem. Phys.*, **20**, 761 (1951).

**Table I:** Appearance Potentials (e.v.)<sup>a</sup>

Species	CH <sub>2</sub> F <sub>2</sub>	CHF <sub>3</sub>	CF <sub>4</sub>	CH <sub>3</sub> CHF <sub>2</sub>	C <sub>2</sub> F <sub>4</sub>	C <sub>2</sub> F <sub>6</sub>
CH <sub>3</sub> <sup>+</sup>				18.6		
CF <sup>+</sup>	18.8	20.75 20.2 <sup>c</sup>				
CFH <sup>+</sup>	17.7					
CFH <sub>2</sub> <sup>+</sup>	15.28					
C <sub>2</sub> FH <sub>3</sub> <sup>+</sup>				14.8		
C <sub>2</sub> FH <sub>4</sub> <sup>+</sup>				14.9		
CF <sub>2</sub> <sup>+</sup>	20.7	20.2 17.5 <sup>c</sup> 22.4 <sup>f</sup>	22.2 20.3 <sup>e</sup>			
CF <sub>2</sub> H <sup>+</sup>	13.11	15.75 16.4 <sup>c</sup>		13.21		
CF <sub>2</sub> H <sub>2</sub> <sup>+</sup>	12.6 12.56 <sup>b,i</sup>					
C <sub>2</sub> F <sub>2</sub> H <sub>2</sub> <sup>+</sup>				16.5		
C <sub>2</sub> F <sub>2</sub> H <sub>3</sub> <sup>+</sup>				12.33		
C <sub>2</sub> F <sub>2</sub> H <sub>4</sub> <sup>+</sup>				12.68 12.59 <sup>g,i</sup>		
CF <sub>2</sub> <sup>+</sup>		14.42 14.40 <sup>g</sup> 14.53 <sup>d</sup> 14.67 <sup>c</sup>	16.2 15.44 <sup>d</sup> 16.0 <sup>f</sup>		14.2 14.3 <sup>h</sup>	
CF <sub>3</sub> H <sup>+</sup>		13.84 <sup>b,i</sup>				
C <sub>2</sub> F <sub>4</sub> <sup>+</sup>						13.15

<sup>a</sup> Values without superscript are from the present electron impact study. <sup>b</sup> Spectroscopic values from ref. 6. <sup>c</sup> Electron impact values from ref. 7. <sup>d</sup> Electron impact values from ref. 5. <sup>e</sup> Electron impact values from ref. 4. <sup>f</sup> Electron impact values from ref. 8. <sup>g</sup> Photoionization from ref. 9. <sup>h</sup> Electron impact value from ref. 10. <sup>i</sup> Parent molecule ion.

gases have been reported previously, and the earlier results are given in Table I for comparison. Mass spectra of molecules CH<sub>3</sub>CHF<sub>2</sub>, CF<sub>3</sub>H, CF<sub>2</sub>H<sub>2</sub>, C<sub>2</sub>F<sub>6</sub>, and CF<sub>4</sub> show little or no parent peak intensity, and measurement of their ionization potentials by electron impact is either impossible or subject to large error. The listed ionization potentials for these species, except the value for CF<sub>4</sub>, were measured by photoionization by Mr. F. M. Matsunaga and Professor K. Watanabe using samples forwarded by us. If no parent ion is observable in the mass spectrum of a molecule, it is probable that the lowest observed photoionization potential is the appearance potential of the first appearing fragment ion since no mass analysis was employed in the photoionization experiments. In CF<sub>3</sub>H the lowest photoionization potential agrees very well with the electron impact appearance potential for CF<sub>3</sub><sup>+</sup> but is distinctly higher than the spectroscopic ionization potential for CF<sub>3</sub>H (see Table I).

### Thermochemical Calculations

The appearance potential of an ion may be combined

with other thermochemical data for calculations of a heat of formation subject to the assumption that none of the products of the mass spectral reaction is produced either in an excited state or with excess kinetic energy. The present calculations utilize the appearance potentials of part I and those of Table I of this paper. Various other thermochemical data, available in the literature, are employed in the calculations. The heats of formation of C<sub>2</sub>F<sub>4</sub> and CH<sub>2</sub>CF<sub>2</sub> have been determined experimentally.<sup>11</sup> The heats of formation of CH<sub>2</sub>CHF and CHF<sub>2</sub>CF<sub>2</sub> are known from estimations which are good to within 5 to 10%.<sup>12</sup> These values are given in Table II.<sup>13-18</sup>

**Table II:**  $\Delta H_f(g)$  Values at 298°K. Used in the Thermochemical Calculations

Species	$\Delta H_f$ , e.v.	Quality <sup>a</sup>	Ref.
CH <sub>2</sub> CHF	-1.22	2	12
CH <sub>2</sub> CF <sub>2</sub>	-3.36	1	11
CHF <sub>2</sub> CF <sub>2</sub>	-4.82	2	12
CF <sub>2</sub> CF <sub>2</sub>	-6.59	1	11
CH <sub>2</sub> F <sub>2</sub>	-4.60	1	13
CHF <sub>3</sub>	-7.05	1	13
CF <sub>4</sub>	-9.45	1	11, 14
CH <sub>3</sub> CHF <sub>2</sub>	-5.10	1	15
CF <sub>3</sub> CF=CF <sub>2</sub>	-11.22	1	16
CF	+3.23	1	17

<sup>a</sup> The symbols in this column mean (1) direct measurements or data of good precision and (2) data based on estimations.

Additional heats of formation listed in Table II and used in the calculations are those for some of the parent molecules of Table I and for the CF radical; these are reliable values which are obtained by methods other than electron impact. Heats of formation of hydrocarbons, their radicals, or ions are from ref. 19; any other heats of formation used are from ref. 20 and 21.

(11) C. A. Neugebauer and J. L. Margrave, *J. Phys. Chem.*, **60**, 1318 (1956).

(12) P. G. Maslov and Y. P. Maslov, *Khim. i Tekhnol. Toplivo i Masel*, **3**, 50 (1958); *Chem. Abstr.*, **53**, 1910 (1959).

(13) C. A. Neugebauer and J. L. Margrave, *J. Phys. Chem.*, **62**, 1043 (1958).

(14) D. W. Scott, W. D. Good, and G. Waddington, *J. Am. Chem. Soc.*, **77**, 245 (1955).

(15) K. R. Lacher, A. Kianpour, F. Oetting, and J. D. Park, *Trans. Faraday Soc.*, **52**, 1500 (1956).

(16) H. C. Duus, *Ind. Eng. Chem.*, **47**, 1445 (1955).

(17) E. B. Andrews and R. F. Barrow, *Nature*, **165**, 890 (1950).

(18) E. B. Andrews and R. F. Barrow, *Proc. Roy. Soc. (London)*, **A64**, 681 (1951).

(19) R. R. Bernecker and F. A. Long, *J. Phys. Chem.*, **65**, 1565 (1961).

**Table III:** Calculated  $\Delta H_f(g)$  Values at 298°K. from Appearance Potentials

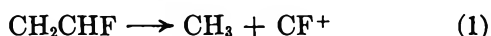
Species	Reaction	$\Delta H_f$ , e.v.
CF <sup>+</sup>	CH <sub>2</sub> CHF → CH <sub>3</sub> + CF <sup>+</sup>	+12.82
CF <sub>2</sub>	CH <sub>2</sub> F <sub>2</sub> <sup>a</sup> → CF <sup>+</sup> + H <sub>2</sub> + F	+13.4
	C <sub>2</sub> F <sub>6</sub> <sup>b</sup> → C <sub>2</sub> F <sub>4</sub> <sup>+</sup> + CF <sub>2</sub>	-1.60
	CH <sub>2</sub> CF <sub>2</sub> → CH <sub>2</sub> <sup>+</sup> + CF <sub>2</sub>	+0.04
CFH <sup>+</sup>	CH <sub>3</sub> CHF <sub>2</sub> → CH <sub>3</sub> <sup>+</sup> + H + CF <sub>2</sub>	+0.01
	CFHCF <sub>2</sub> <sup>c</sup> → CFH <sup>+</sup> + CF <sub>2</sub>	+12.16
	CH <sub>2</sub> F <sub>2</sub> → CFH <sup>+</sup> + F + H	+10.0
CF <sub>2</sub> <sup>+</sup>	or CH <sub>2</sub> F <sub>2</sub> → CFH <sup>+</sup> + HF	+15.9
	C <sub>2</sub> F <sub>6</sub> <sup>c</sup> → CF <sub>2</sub> <sup>+</sup> + CF <sub>2</sub>	+10.14
	CH <sub>2</sub> F <sub>2</sub> → CF <sub>2</sub> <sup>+</sup> + 2H	+11.6
	CHF <sub>3</sub> → CF <sub>2</sub> <sup>+</sup> + H + F	+10.1
	CF <sub>4</sub> → CF <sub>2</sub> <sup>+</sup> + 2F	+11.1
CH <sub>2</sub> F	CH <sub>2</sub> CF <sub>2</sub> <sup>d</sup> → CH <sub>2</sub> F + CF <sup>+</sup>	-0.95
CF <sub>2</sub> H	CHF <sub>2</sub> CF <sub>2</sub> <sup>d</sup> → CF <sub>2</sub> H + CF <sup>+</sup>	-2.67
CF <sub>3</sub>	CF <sub>2</sub> CF <sub>2</sub> <sup>d</sup> → CF <sub>3</sub> + CF <sup>+</sup>	-5.35
CH <sub>2</sub> F <sup>+</sup>	CH <sub>2</sub> CF <sub>2</sub> → CH <sub>2</sub> F <sup>+</sup> + CF	+8.49
CF <sub>2</sub> H <sup>+</sup>	CH <sub>2</sub> F <sub>2</sub> → CH <sub>2</sub> F <sup>+</sup> + F	+9.86
	CHF <sub>2</sub> CF <sub>2</sub> → CF <sub>2</sub> H <sup>+</sup> + CF	+6.17
	CH <sub>2</sub> F <sub>2</sub> → CF <sub>2</sub> H <sup>+</sup> + H	+6.25
	CHF <sub>3</sub> → CF <sub>2</sub> H <sup>+</sup> + F	+7.88
CF <sub>3</sub> <sup>+</sup>	CH <sub>2</sub> CHF <sub>2</sub> → CH <sub>3</sub> + CHF <sub>2</sub> <sup>+</sup>	+6.72
	CF <sub>2</sub> CF <sub>2</sub> → CF <sub>3</sub> <sup>+</sup> + CF	+3.72
	CHF <sub>3</sub> → CF <sub>3</sub> <sup>+</sup> + H	+5.11
	CF <sub>4</sub> → CF <sub>3</sub> <sup>+</sup> + F	+5.93
C <sub>2</sub> H <sub>2</sub> <sup>+</sup>	C <sub>2</sub> H <sub>4</sub> → C <sub>2</sub> H <sub>2</sub> <sup>+</sup> + H <sub>2</sub>	+13.7
(C <sub>2</sub> H <sub>3</sub> <sup>+</sup> or CH <sub>2</sub> =C <sup>+</sup> )	CH <sub>2</sub> CF <sub>2</sub> → C <sub>2</sub> H <sub>2</sub> <sup>+</sup> + 2F	+14.8
C <sub>2</sub> HF <sup>+</sup>	CH <sub>2</sub> CHF → C <sub>2</sub> HF <sup>+</sup> + H <sub>2</sub>	+12.8
	CHF <sub>2</sub> CF <sub>2</sub> → C <sub>2</sub> HF <sup>+</sup> + 2F	+13.0
C <sub>2</sub> H <sub>3</sub> <sup>+</sup>	C <sub>2</sub> H <sub>4</sub> → C <sub>2</sub> H <sub>3</sub> <sup>+</sup> + H	+12.34
	CH <sub>2</sub> CHF → C <sub>2</sub> H <sub>3</sub> <sup>+</sup> + F	+12.34
C <sub>2</sub> H <sub>2</sub> F <sup>+</sup> (CH <sub>2</sub> =CF <sup>+</sup> or CHF=CH <sup>+</sup> )	CH <sub>2</sub> CHF → C <sub>2</sub> H <sub>2</sub> F <sup>+</sup> + H	+10.54
(probably CH <sub>2</sub> =CF <sup>+</sup> )	CH <sub>2</sub> CF <sub>2</sub> → C <sub>2</sub> H <sub>2</sub> F <sup>+</sup> + F	+10.64
C <sub>2</sub> F <sub>2</sub> H <sup>+</sup>	(probably CF <sub>2</sub> =CH <sup>+</sup> )	
(CF <sub>2</sub> CH <sup>+</sup> or CFHCF <sup>+</sup> )	CH <sub>2</sub> CF <sub>2</sub> → C <sub>2</sub> F <sub>2</sub> H <sup>+</sup> + H	+11.05
C <sub>2</sub> F <sub>3</sub> <sup>+</sup>	CFHCF <sub>2</sub> → C <sub>2</sub> F <sub>2</sub> H <sup>+</sup> + F	+10.44
	C <sub>2</sub> F <sub>4</sub> → C <sub>2</sub> F <sub>3</sub> <sup>+</sup> + F	+8.59

<sup>a</sup> This cycle is chosen because the metastable transition CH<sub>2</sub>F<sup>+</sup> → CF<sup>+</sup> + H<sub>2</sub> is observed. <sup>b</sup> The appearance potential of C<sub>2</sub>F<sub>4</sub><sup>+</sup> from C<sub>2</sub>F<sub>6</sub> is lower than that of any other fragment from C<sub>2</sub>F<sub>6</sub> (unpublished results) so that it has to be the product of a direct rearrangement in which CF<sub>2</sub> is also formed; for I.P. (C<sub>2</sub>F<sub>4</sub>), see part I. <sup>c</sup>  $\Delta H_f(\text{CF}_2) = -1.6$  e.v. was used in this calculation. <sup>d</sup>  $\Delta H_f(\text{CF}^+) = +12.82$  was used in this calculation.

Table III summarizes the calculations. The occasional marked discrepancies in calculated heats of formation for a given species are discussed in the next section.

### Discussion

$\Delta H_f(\text{CF}^+)$  and I.P.(CF). The formation of CF<sup>+</sup> from CH<sub>2</sub>CHF involves a direct rearrangement



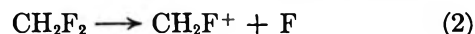
and one computes  $\Delta H_f(\text{CF}^+) \leq 12.82$  e.v. Since  $\Delta H_f(\text{CF}) = 3.23$  e.v. (Table II), this implies I.P. (CF)  $\leq 9.6$  e.v.

The heat of formation computed from process 1 is

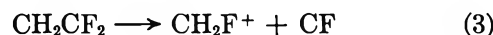
an upper limit since a rearrangement process of this type may involve excess energy.

An alternative way of computing  $\Delta H_f(\text{CF}^+)$  is from the CF<sup>+</sup> appearance potential from CH<sub>2</sub>F<sub>2</sub>. This, however, leads to 13.4 e.v., *i.e.*, considerably higher than the above value (Table III). CF<sup>+</sup> is formed in two stages from CH<sub>2</sub>F<sub>2</sub>. The formation of CH<sub>2</sub>F<sup>+</sup> in the first stage involves excess energy as may be seen by comparison of  $\Delta H_f(\text{CH}_2\text{F}^+)$  calculated from CH<sub>2</sub>F<sup>+</sup> appearance potentials in CH<sub>2</sub>CF<sub>2</sub> and CH<sub>2</sub>F<sub>2</sub> (Table III). Furthermore, all the C-F bond breakages in the methane series appear to involve excess energy as compared to the C-H breakages. (Compare the computed heats of formation for CF<sub>2</sub>H<sup>+</sup> from CF<sub>2</sub>H<sub>2</sub> and from CHF<sub>3</sub> or those for CF<sub>3</sub><sup>+</sup> from CF<sub>3</sub>H and CF<sub>4</sub>, Table III.) This is also the reason for the discrepancy between our computed value for  $\Delta H_f(\text{CF}^+)$  and the one based upon the appearance potential of CF<sup>+</sup> from CHF<sub>3</sub>.<sup>7</sup>

One can estimate the excess energy in the process



If one assumes the rearrangement energy in the process



to be negligible, then the excess energy involved in (2) is  $9.86 - 8.49 = 1.37$  e.v. Using this, one calculates the heat of formation of CF<sup>+</sup> from its appearance potential in CH<sub>2</sub>F<sub>2</sub> as  $\Delta H_f(\text{CF}^+) = 13.4 - 1.4 = 12.0$  e.v. and I.P.(CF) = 8.8 e.v. These are lower by 0.8 e.v. than the values computed from process 1. Even so, in view of the uncertainties involved in this second calculation, we shall tentatively adopt the higher values, as given above, for both  $\Delta H_f(\text{CF}^+)$  and I.P.(CF).

There are several conflicting values for the ionization potential of CF, namely, 13.81 e.v.<sup>22</sup> (by direct electron impact on the CF radical), 11 e.v.<sup>23</sup> (based on spectroscopic evaluations of the dissociation energies of CF and CF<sup>+</sup> in their ground states), and 8.9 e.v.<sup>24</sup> (by a similar spectroscopic evaluation). The values from spectroscopy are based on linear extrapolations and are not highly reliable. The present value of 9.6 e.v. agrees best with the latest spectroscopic value of 8.9 e.v.,<sup>24</sup> especially in view of the previously discussed

(20) F. D. Rossini, D. D. Wagman, W. H. Evans, W. H. Levine, and I. Jaffe, National Bureau of Standards Circular No. 500, U. S. Government Printing Office, Washington, D. C., 1952.

(21) "Janaf Interim Thermochemical Tables," The Dow Chemical Co., Midland, Mich., Dec. 31, 1960-June 30, 1961.

(22) R. I. Reed and W. Snedden, *Trans. Faraday Soc.*, **54**, 301 (1958).

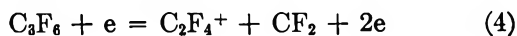
(23) G. Herzberg, private communication.

(24) J. W. C. Johns and R. F. Barrow, *Proc. Roy. Soc. (London)*, **A71**, 476 (1958).

possibility of excess rearrangement energy in process 1. The relatively low ionization potential of CF, compared to 11.1 e.v. for CH,<sup>25</sup> is explained by Price and co-workers<sup>26</sup> as being due to an increased sharing of the nonbonding  $p\pi$  electrons of fluorine with carbon in the ion relative to the radical. No explanation has been given for why direct electron impact leads to an ionization potential of CF which is higher by several electron volts.<sup>22</sup>

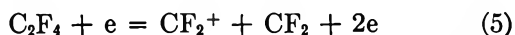
$\Delta H_f(\text{CF}_2)$ . Two recent groups of workers give  $\Delta H_f(\text{CF}_2)$  from appearance potential calculations as close to  $-1.6$  e.v.,<sup>27,28</sup> similar to the estimation from onset bands from  $\text{CF}_4 + \text{C}$  of  $-1.5 \pm 0.5$  e.v.<sup>29</sup>

Our data permit a similar calculation from the appearance potential of  $\text{C}_2\text{F}_4^+$  from  $\text{C}_3\text{F}_6$  for which the process is



(A conceivable alternative is production of  $\text{CF}_2^-$ , but direct search for this species in the negative ion spectrum of  $\text{C}_3\text{F}_6$  was unsuccessful which is consistent with the presumed small electron affinity of  $\text{CF}_2$ .<sup>30</sup>) From process 4 and the observed appearance potential of  $\text{C}_2\text{F}_4^+$  from  $\text{C}_3\text{F}_6$  of 13.15 e.v., one computes  $\Delta H_f(\text{CF}_2) = -1.60$ .<sup>31</sup> This is in excellent agreement with the results of the Majer and Lossing groups.

$\Delta H_f(\text{CF}_2^+)$  and  $I.P.(\text{CF}_2)$ . Fisher, Homer, and Lossing give the ionization potential of  $\text{CF}_2$  as 11.7 by direct measurement.<sup>28</sup> Our calculation from the appearance potential of  $\text{CF}_2^+$  from  $\text{C}_2\text{F}_4$  fully confirms this. Assuming the process



the appearance potential of  $15.13 \pm 0.1$  e.v. leads to  $\Delta H_f(\text{CF}_2^+) = 10.1$  e.v. and  $I.P.(\text{CF}_2) = 11.7$  e.v. This excellent agreement between direct measurement and indirect calculation from olefin mass spectral data contrasts favorably with the situation for fluoro paraffins and aromatics where agreement is much poorer.<sup>32</sup>

*Heats of Formation of the  $\text{CX}_3$  ( $X = \text{H}, \text{F}$ ) Radicals.* The heats of formation of  $\text{CH}_2\text{F}$ ,  $\text{CF}_2\text{H}$ , and  $\text{CF}_3$  are obtained from rearrangement processes of fluorinated olefins as listed in Table III. The assumption made in the calculations for  $\text{CF}_2\text{H}$  and  $\text{CF}_3$  is that  $\text{CF}^+$  from the olefins is produced at its threshold by a rearrangement process rather than by an ion-pair process. In view of the experiments of part I this seems justified. Previous values, from methods other than electron impact, are available only for  $\Delta H_f(\text{CF}_3)$ . The best value is the one calculated from an analysis of kinetic data by Rabinovitch and Reed,<sup>33</sup>  $\Delta H_f(\text{CF}_3) = -5.2$  e.v., which agrees very well with our electron impact value of  $-5.35$ . The Table III values for the other two radi-

cals are  $\Delta H_f(\text{CF}_2\text{H}) = -2.67$  and  $\Delta H_f(\text{CFH}_2) = -0.95$  e.v. For comparison  $\Delta H_f(\text{CH}_3) = +1.39$  e.v.

$\Delta H_f(\text{CH}_2\text{F}^+)$  and  $I.P.(\text{CH}_2\text{F})$ .  $\Delta H_f(\text{CH}_2\text{F}^+) = 8.5$  e.v. if excess rearrangement energy in process 3 is negligible.  $I.P.(\text{CH}_2\text{F}) = \Delta H_f(\text{CH}_2\text{F}^+) - \Delta H_f(\text{CH}_2\text{F}) = 8.49 - (-0.95) = 9.4$  e.v. Actually the preferred procedure in calculating  $I.P.(\text{CH}_2\text{F})$  from our results does not involve the heat of formation of the radicals but goes as follows:  $\text{CH}_2\text{F}^+$  and  $\text{CF}^+$  are both formed from  $\text{CH}_2\text{CF}_2$ , and the difference in their appearance potentials is

$$\begin{aligned} A.P.(\text{CF}^+) - A.P.(\text{CH}_2\text{F}^+) &= \Delta H_f(\text{CF}^+) + \\ &\Delta H_f(\text{CH}_2\text{F}) - \Delta H_f(\text{CH}_2\text{F}^+) - \Delta H_f(\text{CF}) \\ &= \Delta H_f(\text{CF}) + I.P.(\text{CF}) + \Delta H_f(\text{CH}_2\text{F}) - \\ &\Delta H_f(\text{CH}_2\text{F}) - I.P.(\text{CH}_2\text{F}) - \Delta H_f(\text{CF}) \\ &= I.P.(\text{CF}) - I.P.(\text{CH}_2\text{F}) \end{aligned}$$

Using for  $I.P.(\text{CF})$  its appearance potential in  $\text{CH}_2\text{-CHF}$ , we calculate  $I.P.(\text{CH}_2\text{F}) = 9.4 \pm 0.1$  e.v.

The value of  $I.P.(\text{CH}_2\text{F})$  determined by direct electron impact is 9.35 e.v.<sup>34</sup> The agreement between our result and this direct electron impact value leads to a greater degree of confidence in our value of  $I.P.(\text{CF})$ . Furthermore, it suggests that the rearrangement energy in reactions such as (1) and (3) is small (perhaps not more than 0.1 e.v.).

$\Delta H_f(\text{CF}_2\text{H}^+)$  and  $I.P.(\text{CF}_2\text{H})$ . The appearance potentials of  $\text{CF}_2\text{H}^+$  from  $\text{CHFCF}_2$  and  $\text{CH}_2\text{F}_2$  lead to the same value for  $\Delta H_f(\text{CF}_2\text{H}^+)$ , namely, 6.2 e.v. The appearance potentials of  $\text{CF}_2\text{H}^+$  from  $\text{CF}_3\text{H}$  and  $\text{CF}_2\text{-HCH}_3$  lead to  $\Delta H_f(\text{CF}_2\text{H}^+)$  values higher by 1.6 and 0.5 e.v., respectively. We shall assume that the lowest value (6.2 e.v.) is the correct one.

From the relationship

- (25) A. E. Douglas and G. Herzberg, *Can. J. Res.*, **A20**, 71 (1942).  
 (26) R. Bralsford, P. V. Harris, and W. C. Price, *Proc. Roy. Soc. (London)*, **A258**, 459 (1960).  
 (27) J. R. Majer and C. R. Patrick, *Nature*, **201**, 1022 (1964).  
 (28) I. P. Fisher, J. B. Homer, and F. P. Lossing, *J. Am. Chem. Soc.*, **87**, 957 (1965).  
 (29) L. Brewer, J. L. Margrave, R. F. Porter, and J. Wieland, *J. Phys. Chem.*, **65**, 1913 (1961).  
 (30) J. L. Margrave, *J. Chem. Phys.*, **31**, 1432 (1959).  
 (31) This was earlier reported in a paper by C. Lifshitz and F. A. Long to the 10th ASTM Conference on Mass Spectrometry, New Orleans, La., June 1962.  
 (32) See Table II of ref. 28.  
 (33) B. S. Rabinovitch and J. F. Reed, *J. Chem. Phys.*, **22**, 2092 (1954).  
 (34) F. P. Lossing, P. Kebarle, and J. B. Desousa, "Advances in Mass Spectrometry," J. O. Waldron, Ed., Pergamon Press Ltd London, 1958, p. 439.



$$\text{A.P.}(\text{CF}_2\text{H}^+)_{\text{C}_2\text{F}_4\text{H}} - \text{A.P.}(\text{CF}^+)_{\text{C}_2\text{F}_4\text{H}} = \text{I.P.}(\text{CF}_2\text{H}) - \text{I.P.}(\text{CF})$$

one calculates  $\text{I.P.}(\text{CF}_2\text{H}) = 8.9 \pm 0.2$  e.v. Owing to the unusual shape of the  $\text{CF}^+$  ionization efficiency curve from  $\text{CF}_2\text{CFH}^2$  there is some uncertainty in the value of  $\text{I.P.}(\text{CF}_2\text{H})$ .

A direct electron impact measurement of  $\text{I.P.}(\text{CF}_2\text{H})$  gave 9.45 e.v.,<sup>34</sup> in good agreement with the value of  $\text{I.P.}(\text{CF}_2\text{H}) = 9.4$  e.v. calculated from  $\Delta H_f(\text{CF}_2\text{H}) = -2.67$  e.v. (Table III) and  $\Delta H_f(\text{CF}_2\text{H}^+) = 6.72$  e.v. (Table III based on  $\text{CF}_2\text{H}^+$  appearance potential from  $\text{CF}_2\text{HCH}_3$ ).

$\Delta H_f(\text{CH}_3^+)$  and  $\text{I.P.}(\text{CF}_3)$ .  $\Delta H_f(\text{CF}_3^+) = 3.72$  e.v. if the  $\text{CF}$  radical is formed with  $\text{CF}_3^+$  from  $\text{C}_2\text{F}_4$  and if the excess rearrangement energy involved in the process is negligible. Curiously enough, neither the H loss nor the F loss from the methanes gives a similar value for  $\Delta H_f(\text{CF}_3^+)$ . The formation of  $\text{CF}_3^+$  from  $\text{CF}_4$  involves approximately 0.8 e.v. excess kinetic energy,<sup>4,5</sup> and if this is taken into account, then the appearance potentials of  $\text{CF}_3^+$  from  $\text{CF}_3\text{H}$  and  $\text{CF}_4$  give the same value for  $\Delta H_f(\text{CH}_3^+)$ , namely, 5.1 e.v.

From the relationship

$$\text{A.P.}(\text{CF}_3^+)_{\text{C}_2\text{F}_4} - \text{A.P.}(\text{CF}^+)_{\text{C}_2\text{F}_4} = \text{I.P.}(\text{CF}_3) - \text{I.P.}(\text{CF})$$

one calculates  $\text{I.P.}(\text{CF}_3) = 9.1 \pm 0.2$  e.v. if neither  $\text{CF}_3^+$  nor  $\text{CF}^+$  is formed by an ion-pair process. A direct calculation of  $\text{I.P.}(\text{CF}_3)$  based on the appearance potential of  $\text{CF}_3^+$  from  $\text{C}_2\text{F}_4$  and on the heat of formation of  $\text{CF}_3^+$ <sup>33</sup> (-5.2 e.v.) gives  $\text{I.P.}(\text{CF}_3) = 8.9 \pm 0.2$  e.v. Similar calculations based on the  $\text{CF}_3^+$  appearance potentials from  $\text{CF}_3\text{Cl}$ ,  $\text{CF}_3\text{Br}$ , and  $\text{CF}_3\text{I}$  lead to a value of  $9.3 \pm 0.2$  e.v.<sup>4</sup> for the ionization potential of the  $\text{CF}_3$  radical. Direct electron impact by Lossing and co-workers<sup>34</sup> gave  $\text{I.P.}(\text{CF}_3) = 10.1$  e.v. in good agreement with the  $\text{CF}_3^+$  appearance potentials from the paraffins  $\text{CF}_3\text{H}$ ,  $\text{CF}_4$ ,  $\text{CF}_3\text{CH}_3$ , and  $\text{C}_2\text{F}_6$  (see also ref. 5). However, Fisher, Homer, and Lossing<sup>28</sup> recently re-estimated the value of  $\text{I.P.}(\text{CF}_3)$  to be 9.5-9.6 e.v.

Price<sup>26</sup> has pointed out that the decrease in the ionization potential of ethylene upon fluorination can be attributed to the large resonance stabilization of the planar fluoroethylene ions which more than compensates for the inductive effect of the fluorine atoms. Price also points out that, since the fluoromethyl radical ions are planar in the ground state, a similar lowering of the ionization potential of the methyl radical should result upon fluorination. The present results do show an over-all decrease in ionization potential upon fluorination ( $\text{CH}_3$ , 9.85 e.v.;  $\text{CH}_2\text{F}$ , 9.45 e.v.;

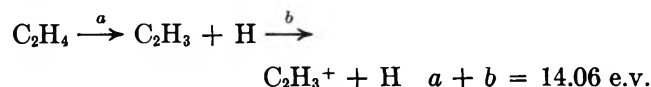
$\text{CHF}_2$ , 8.85 e.v.;  $\text{CF}_3$ , 9.1 e.v.) although there is an increase from  $\text{CHF}_2$  to  $\text{CF}_3$ . Lossing's direct electron impact values<sup>34</sup> show a decrease from  $\text{CH}_3$  to  $\text{CH}_2\text{F}$ , but then an increase:  $\text{CF}_2\text{H}$ , 9.45 e.v.; and  $\text{CF}_3$ , 10.1 e.v. On the other hand,  $\text{I.P.}(\text{CH}_3) = 9.85$ ,  $\text{I.P.}(\text{CH}_2\text{Cl}) = 9.32$ ,  $\text{I.P.}(\text{CHCl}_2) = 9.30$ ,  $\text{I.P.}(\text{CCl}_3) = 8.78$ .<sup>34</sup>

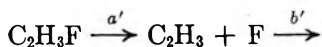
In all of the above cases the ionization potentials for fluorinated methyl radicals as calculated from mass spectral results from the paraffin series are much larger than the values which result from the data for the olefin series. Direct measurements on ionization of the radicals lead to the larger values. There is, however, good reason to believe that both the direct results<sup>28</sup> and the indirect results for the methyl ion paraffins involve formation of  $\text{CX}_3^+$  ions in excited states. Lossing, *et al.*, suggest<sup>28</sup> that one plausible explanation for the discrepant direct results is that  $\text{CF}_3^+$  is planar in the ground state and  $\text{CF}_3$  nonplanar so that direct ionization of the latter leads to an excited  $\text{CF}_3^+$ . The  $\text{CX}_3^+$  ions from the olefins result from decomposition of an olefin molecule ion, a relatively slow process which should permit formation of the  $\text{CX}_3^+$  in its ground state. With the fluoroparaffins, however, no parent molecule ions are observed, and there is a good possibility that the electron impact leads directly to a dissociative state and rapid formation of a  $\text{CX}_3^+$  ion which thus has a greater likelihood of retaining its tetrahedral structure, *i.e.*, of being formed in an excited state.

$\Delta H_f(\text{C}_2\text{X}_2^+)$  ( $X = \text{H}, \text{F}$ ). The heat of formation of  $\text{C}_2\text{H}_2^+$  calculated from the  $\text{H}_2$  loss from ethylene is equal to values found by direct measurements on  $\text{C}_2\text{H}_2^{+19}$  whereas the value based on HF loss from  $\text{CH}_2\text{CHF}$  is much higher.<sup>2</sup> A similar effect is observed for  $\text{C}_2\text{FH}^+$ .<sup>2</sup> If  $\text{H}_2$  abstraction from any ethylene involves no excess energy (by analogy with  $\text{C}_2\text{H}_4$ ), then  $\Delta H_f(\text{C}_2\text{HF}^+) = 12.8$  e.v. is a reliable value.

Excess energy was encountered in the HF losses from the ethylene series. A similar behavior is found for  $\text{CH}_3\text{CHF}_2$ . The  $\text{CH}_2\text{CHF}^+$  appearance potential from this molecule (see Table I) is 14.8 e.v., in comparison with the value calculated from the  $\text{CH}_2\text{CFH}$  heat of formation and ionization potential, namely, 11.6 e.v.

$\Delta H_f(\text{C}_2\text{X}_3^+)$  ( $X = \text{H}, \text{F}$ ). These ions are formed by a single bond rupture from the parent molecules so that their calculated heats of formation should be reliable. There is some uncertainty with the heats of formation of the more highly fluorinated members of the series because of the possible entrance of excess activation energies.<sup>2</sup> From part I one calculates for the processes



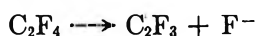


$$\text{C}_2\text{H}_3^+ + \text{F} \quad a' + b' = 14.38 \text{ e.v.}$$

Since  $b$  equals  $b'$ ,  $a' - a = 0.32$  e.v.; *i.e.*, the carbon-fluorine bond energy in  $\text{C}_2\text{H}_3\text{F}$  is 0.32 e.v. higher than the carbon-hydrogen bond energy in  $\text{C}_2\text{H}_4$ .

In the series  $\text{C}_2\text{H}_3^+$ ,  $\text{C}_2\text{H}_2\text{F}^+$ , and  $\text{C}_2\text{F}_2\text{H}^+$ , formed by an H atom loss from the parent, the appearance potentials are 14.06, 14.02, and 16.6, respectively (Table II, part I).<sup>2</sup> Each appearance potential is equal to the C-H bond energy in the parent plus the ionization potential of  $\text{C}_2\text{X}_3$ . Thus, in this series either the bond energy or the ionization potential or both of these quantities increase. A similar behavior is encountered for the series  $\text{C}_2\text{X}_3^+$  formed by an F atom loss.

From the first resonance capture process forming  $\text{F}^-$  in  $\text{C}_2\text{F}_4$  at 2.7 e.v. (observed by J. D. Morrison and F. H. Dorman, see part I<sup>2</sup>) and assuming the following capture process for it



one computes the  $\text{C}_2\text{F}_3\text{-F}$  bond energy to be 6.3 e.v. and  $\Delta H_f(\text{C}_2\text{F}_3) = -1.1$  e.v. From  $\Delta H_f(\text{C}_2\text{F}_3^+) = 8.6$  e.v. (Table III) one computes  $\text{I.P.}(\text{C}_2\text{F}_3) = 9.7$  e.v. The ionization potential of  $\text{C}_2\text{H}_3$  is 9.45 e.v.<sup>19</sup> This increase in ionization potential upon fluorination is contrary to the trend in the ethylene molecules and may be due to a relatively small resonance stabilization of the ion radical  $\text{C}_2\text{F}_3^+$ . On the other hand, the possibility of excess activation energy in the process forming  $\text{C}_2\text{F}_3^+$  cannot be excluded.

Table IV summarizes the heats of formation of some simple fluorocarbon molecules, radicals, and ions. It contains those values from the present study which are

considered reliable, as well as selected literature values for comparison. This table is of the same format and is based on the same fundamental constants as the similar table of Bernecker and Long.<sup>19</sup>

**Table IV:**  $\Delta H_f(\text{g})$  Values for Neutral Species and Their Positive Ions

Species	Un-ionized			Ionized		
	$\Delta H_f$ , e.v.	Qual. <sup>a</sup>	Ref. <sup>b</sup>	$\Delta H_f$ , e.v.	Qual. <sup>a</sup>	Ref. <sup>b</sup>
CF	+3.23	S	17, 18	+12.8	2	P
	X			X + 8.9	S	24
CH <sub>2</sub>	+4.0	3, S	19, c	+14.4	3	19
CHF	+0.36	3	P	+12.16	3	P
CF <sub>2</sub>	-1.60	2	P, 28	+10.10	2	P, 28
CH <sub>3</sub>	+1.39	1	20	+11.23	S	d
CH <sub>2</sub> F	-0.95	2	P	+8.49	2	P
	X			X + 9.45	2	P
CF <sub>2</sub> H	-2.67	2	P	+6.17 (olefin)	2	P
				+6.72 (paraffin)	2	P
	X			X + 8.85 (olefin)	2	P
CF <sub>3</sub>	-5.35	2	P	+3.72 (olefin)	2	P
				+5.11 (paraffin)	2	P
	X			X + 9.1 (olefin)	2	P
C <sub>2</sub> H <sub>2</sub>	+2.350	1	19	+13.75	S	19
C <sub>2</sub> FH				+12.8	2	P
C <sub>2</sub> H <sub>3</sub>	+2.83	2	19	+12.28	2	19
C <sub>2</sub> H <sub>2</sub> F	+1.15	3	e	+10.65	2	P
C <sub>2</sub> F <sub>2</sub> H				+10.8	2	P
C <sub>2</sub> F <sub>3</sub>	-1.1	2	P	+8.59	2	P

<sup>a</sup> Quality standards as in ref. 19. <sup>b</sup> P refers to present data. <sup>c</sup> G. Herzberg, *Can. J. Phys.*, **39**, 1511 (1961). <sup>d</sup> G. Herzberg and J. Shoosmith, *ibid.*, **34**, 523 (1956). <sup>e</sup> W. M. D. Bryant, *J. Polymer Sci.*, **56**, 277 (1962).

*Acknowledgments.* We thank Dr. J. D. Morrison and Dr. F. H. Dorman for their measurements of appearance potentials of negative ions from  $\text{C}_2\text{F}_4$ , as well as for very helpful discussions.

## Appearance Potentials and Mass Spectra of Fluorinated Ethylenes. III.

### Calculations Based on the Statistical Theory of Mass Spectra<sup>1</sup>

by Chava Lifshitz and F. A. Long

*Department of Chemistry, Cornell University, Ithaca, New York (Received April 7, 1965)*

Calculations based upon the statistical theory of mass spectra have been carried out for three parallel primary reactions in the spectrum of difluoroethylene. Theoretical expressions derived by Marcus are utilized for computation of the unimolecular rate constants for the processes at near threshold energies. These are compared with the reciprocal of the parent ion residence time in the ion source of the mass spectrometer. The dependence of relative rates of the three processes upon the internal energy of the active molecule ion is also computed. The much faster increase with energy of the rate constant for a reaction possessing a "loose" activated complex relative to that for one which has a "rigid" complex is demonstrated. It is further shown that for a high activation energy process to compete effectively enough with a low activation energy one to be detected in the mass spectrometer, it is not enough for the rate constant of the former to be comparable to the reciprocal of the residence time; rather, it has to be a certain fraction of the rate constant of the faster process. In all of these calculations exact sums of states were computed for the activated complexes, while the approximation formula due to Whitten and Rabinovitch was used for the active molecule. For some processes, qualitative agreement between theory and experiment can be obtained by plausible assignment of molecular parameters. In other cases there are various difficulties, in particular for the relative yields of carbon-fluorine and carbon-hydrogen bond breakages.

#### Introduction

The statistical theory of mass spectra assumes that the mass spectrum of a polyatomic molecule is due to parallel and successive unimolecular decompositions of vibrationally excited ions. It was first developed by Rosenstock, *et al.*,<sup>2</sup> and has been used to compare computed and experimental mass spectra of hydrocarbons, in particular those of propane and butane.<sup>3</sup> One of the reasons for undertaking a study of the mass spectra of fluorocarbons<sup>4,5</sup> was that these compounds permit different sorts of comparisons to be made with the theory. In this paper attention is focused on the application of theory to the spectra of fluorinated ethylenes.

The major ion yields in the spectra of the fluorinated ethylenes result from primary decomposition processes of the parent molecule ion. The processes have quite differing energy requirements; some involve simple bond breakages while others are rearrangement proc-

esses or four-centered reactions. In spite of these differences, the ion yields are roughly comparable. It is thus of interest to see whether calculations from theory can reproduce the relative rates of these competing processes as a function of the internal excitation energy of the parent molecule ion. Such calculations are similar in character to those suggested by Wolfsberg<sup>6</sup>; however, results will be presented up to higher excitation energies.

*The Computing Procedure.* The formulas developed

(1) Work supported by the Advanced Research Projects Agency through the Materials Science Center.

(2) H. M. Rosenstock, M. B. Wallenstein, A. L. Wahrhaftig, and H. Eyring, *Proc. Natl. Acad. Sci. U. S.*, **38**, 667 (1952).

(3) M. Vestal, A. L. Wahrhaftig, and W. H. Johnston, Aeronautical Research Laboratories, Report ARL 62-426, Sept. 1962.

(4) C. Lifshitz and F. A. Long, *J. Phys. Chem.*, **67**, 2463 (1963).

(5) C. Lifshitz and F. A. Long, *ibid.*, **69**, 3731 (1965).

(6) M. Wolfsberg, *J. Chem. Phys.*, **36**, 1072 (1962).

in the unimolecular reaction rate theory of Marcus<sup>7</sup> were used for computing reaction rates for decomposition reactions of the polyatomic molecule ion. The general expression for the rate constant for reaction of an excited molecule is<sup>8</sup>

$$k_a = \frac{\sum_{E_v \leq E^+} P(E_v)(E^+ - E_v)^{r/2} \left(\frac{8\pi^2}{h^2}\right)^{r/2} \prod_i (I_i)^{1/2} \Gamma(1/2)}{\Gamma(r/2 + 1) h N^*(E)} \quad (\text{I})$$

where  $E_a$  is the activation energy,  $E$  is the internal energy of active molecule,  $E^+$  is the internal energy of activated complex, such that  $E = E_a + E^+$ ,  $P(E_v)$  is the number of vibrational states of an activated complex whose nonfixed vibrational energy is  $E_v$ ,  $N^*(E)$  is the number of quantum states per unit energy of active molecule,  $r$  is the number of active internal rotations in activated complex, and  $I_i$  is the moment of inertia of  $i$ th rotation.

A Fortran program was set up for the CDC 1604 computer to obtain  $\sum_{E_v \leq E^+} P(E_v)$  by exact summation at low energies. This is virtually the same procedure as that of Whitten and Rabinovitch,<sup>9</sup> *i.e.*, counting all lattice points in an energy phase space for vibrational energy levels (assumed harmonic). It has been shown recently that anharmonicities play only a minor role in changing the sum of states for molecules of the size that we are dealing with.<sup>10</sup> We have verified this for even smaller molecules, specifically methane and acetylene for which anharmonicity constants are known and the summations may thus be carried out rigorously. In particular, for methane even at 4.5 e.v. internal energy, the number of states considering anharmonicity is only twice as large as the number obtained when assuming harmonic vibrations.<sup>11</sup>

At high nonfixed energies and, in particular, in the case of the active molecule, the approximation for  $\sum_{E_v \leq E^+} P(E_v)$  due to Whitten and Rabinovitch<sup>9</sup> was used.

Comparisons with exact counting have shown this approximation to be very good for the fluorocarbons studied.

The rate at threshold is never assumed to be zero<sup>6</sup> and is computed according to

$$k_a = \frac{1}{h N^*(E)} \quad (E = E_a) \quad (\text{II})$$

The ratio of the yields of two competing processes at energy  $E$  is given by the ratio of the sum of states for activated complex 1 at energy  $E_1^+ = E - E_{a1}$  to the similar sum of states for activated complex 2 at energy  $E_2^+ = E - E_{a2}$ .<sup>6</sup>

*The Reactions and the Models Chosen for Their Activated Complexes.* Calculations were carried out for the  $\text{CH}_2\text{CF}_2$  molecule, the spectrum of which is not complicated by the occurrence of negative ions.<sup>12</sup> The observed spectrum indicates the occurrence of six competing primary decomposition processes for the parent molecule ion  $\text{CH}_2\text{CF}_2^+$  (Figure 6 of ref. 4). From the appearance potential differences, all the processes appear to require additional energy of from 4 to 7 e.v. Calculations were made for three of the processes, chosen to illustrate some of the different characteristics noted earlier. The processes are given in Figure 1 together with their activation energies, per cent yields, and observed appearance potential differences  $\Delta\text{A.P.}$  Because of the high  $\Delta\text{A.P.}$  values, one expects from statistical theory the rate of reaction to be very small at energies close to the threshold. Hence, the minimum energy requirement, *i.e.*, the activation energy  $E_a$ , should be somewhat smaller than the observed  $\Delta\text{A.P.}$  value. This is apparent for process 3 (Figure 1) where the  $E_a$  value can be calculated from the known thermochemistry and is over 1.5 v. smaller than  $\Delta\text{A.P.}$  This, however, reflects a special situation, as will be shown later, and for processes 1 and 2, where  $E_a$  cannot be calculated *a priori*, there should be a much smaller but not negligible difference between  $E_a$  and  $\Delta\text{A.P.}$  The listed  $E_a$  values for these two processes have been chosen so as to make the specific rate constants for decomposition equal to approximately  $10^6$  to  $10^6 \text{ sec.}^{-1}$  at the experimentally observed appearance potentials. This particular selection is consistent with the observation characteristics of the mass spectrometer, and it is of interest that the requisite  $E_a$  values are only slightly lower than the  $\Delta\text{A.P.}$  values.

Since all three processes involve high activation energies to make them at all observable near threshold, we necessarily have had to assume that the active molecule ion was rigid in all cases. This implies no free internal rotations and no very "soft" vibrations.

For a given appearance potential difference, the value of the activation energy needed to produce a rate

(7) R. A. Marcus, *J. Chem. Phys.*, **20**, 355, 359, 364 (1952).

(8) The partition function ratio for the adiabatic rotations of activated complex and active molecule, which should enter expression I, can be approximated by the number of equivalent ways of obtaining this reaction.

(9) G. Z. Whitten and B. S. Rabinovitch, *J. Chem. Phys.*, **38**, 2466 (1963).

(10) F. W. Schneider and B. S. Rabinovitch, *J. Am. Chem. Soc.*, **84**, 4215 (1962); E. W. Schlag, R. A. Samdmarck, and W. G. Valance, *J. Chem. Phys.*, **40**, 1461 (1964).

(11) C. Lifshitz and M. Wolfsberg, unpublished results.

(12) R. M. Reese, V. H. Dibeler, and F. L. Mohler, *J. Res. Natl. Bur. Std.*, **51**, 367 (1956).

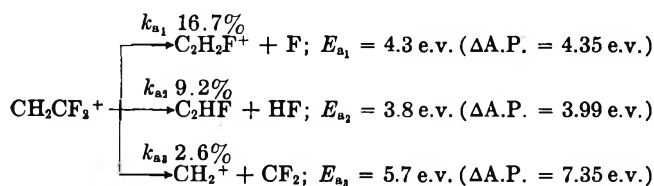


Figure 1. Three processes in the mass spectrum of  $\text{CH}_2\text{CF}_2$ . The numbers above the fragment ion formulas are the observed yields in per cent of total ionization for 70-e.v. ionizing electrons;  $E_{a1}$ ,  $E_{a2}$ , and  $E_{a3}$  are the assumed activation energies, and the  $\Delta\text{A.P.}$  figures in parentheses are the observed appearance potential differences.

constant of  $10^6 \text{ sec.}^{-1}$  or slightly greater depends upon whether a rigid or loose activated complex is assumed. For the four-centered HF loss it seemed inescapable to assume that the activated complex is rigid. For the other two reactions, in which a bond is broken in the activated complex but no intermediate cyclic structure has to be formed, loose activated complexes were assumed. In the latter two activated complexes the twisting vibration was changed into a free internal rotation, and a plausible moment of inertia was computed, *i.e.*, assuming linear methylene groups with a C-F distance of 1.35 Å. and a C-H distance of 1.07 Å. The calculations are not very sensitive to the actual value assigned to the moment of inertia; however, changing a vibration into a free rotation increases the sum of states by several orders of magnitude. The frequencies of the parent molecule ion were taken to be those of neutral  $\text{CH}_2=\text{CF}_2$ .<sup>13</sup> In the HF loss a C-H stretching frequency was transformed into the reaction coordinate, a C-F frequency was reduced, and the C-C frequency increased. In the C-F and C-C breakages, the respective stretching frequencies were transformed into reaction coordinates, and some bending frequencies were reduced. The models for the activated complexes are thus as follows: A. Carbon-fluorine and also carbon-carbon bond breakage: 10 vibrational degrees of freedom; 1 internal rotation; frequencies (e.v.): 0.3819 (2), 0.1736 (3), 0.1085 (2), 0.0651 (3);  $8\pi^2 I/h^2 = 34238 \text{ e.v.}^{-1}$  ( $I$  is the internal moment of inertia). B. Hydrogen fluoride loss: 11 vibrational degrees of freedom; frequencies (e.v.): 0.3819 (2), 0.1736 (3), 0.1085 (2), 0.0670 (4).

For the parent-ion density of states, 12 vibrational degrees of freedom were taken. Using the Whitten and Rabinovitch<sup>9</sup> notation:  $-\langle \nu^2 \rangle = 2.442 \times 10^6 \text{ cm.}^{-2}$ ;  $\langle \nu \rangle^2 = 1.664 \times 10^6 \text{ cm.}^{-2}$ ;  $V = 1.4675$ ;  $\beta = 1.3452$ ; and  $E_0 = 7740.0 \text{ cm.}^{-1}$ .

## Results and Discussion

The results of the calculations are given in Tables I and II. All values for  $k_{a1}$  and  $k_{a2}$  should for complete-

ness be multiplied by a factor of 2 to take into account the two equivalent ways of forming the activated complexes for reactions 1 and 2.

Table I: Computed Reaction Rates for Processes 1 and 2

$E$ , e.v.	$k_{a1}$ , sec. <sup>-1</sup>	$k_{a2}$ , sec. <sup>-1</sup>	$k_{a2}/k_{a1}$
3.8		$9 \times 10^3$	
4.0		$1.6 \times 10^6$	
4.3	$3 \times 10^8$	$4.3 \times 10^6$	1400
4.4	$7.8 \times 10^8$	$9.4 \times 10^6$	12
4.6	$1.35 \times 10^7$	$3.3 \times 10^7$	2.5
4.8	$8.7 \times 10^7$	$8.5 \times 10^7$	1.0
5.1	$6.3 \times 10^8$	$3.0 \times 10^8$	0.48

Table II: Computed Reaction Rates for Processes 1 and 3

$E$ , e.v.	$k_{a1}$ , sec. <sup>-1</sup>	$k_{a3}$ , sec. <sup>-1</sup>	$10^3 k_{a3}/k_{a1}$
5.7	$9.9 \times 10^9$	$2.4 \times 10^2$	$2.45 \times 10^{-5}$
6.0	$2.3 \times 10^{10}$	$1.3 \times 10^6$	$5.74 \times 10^{-2}$
6.3	$5.0 \times 10^{10}$	$2.2 \times 10^7$	0.43
6.6	$9.6 \times 10^{10}$	$1.3 \times 10^8$	1.4
6.9	$1.7 \times 10^{11}$	$6.0 \times 10^8$	3.5
7.3	$3.4 \times 10^{11}$	$2.7 \times 10^9$	8

As Table I shows, by using our assumptions concerning the activated complexes, it is possible to produce the result that the HF loss is the faster reaction at low energies, while the C-F bond breakage is the more important one at higher energies. This is what is observed experimentally. However, even though the active molecule was assumed to be rigid, the rate constant for the HF loss at threshold is so small that a sizable metastable peak should result. This, however, is not observed experimentally.

For the C-C bond breakage the activation energy is assumed to be given by the thermochemical demand for reaction to give unexcited products. This is 1.6 e.v. lower than the experimentally observed appearance potential. This may be rationalized in terms of the theory in the following way. Although  $k_{a3}$  (Table II) becomes of the order of  $10^6 \text{ sec.}^{-1}$  at energies of only a few tenths of a volt above threshold, the decomposition process only starts to compete effectively with the other two, *i.e.*, to be  $\sim 1\%$  in yield, at  $\sim 1.6 \text{ e.v.}$  above the threshold. The point is that, for a high-energy process to compete effectively with one of lower

(13) D. C. Smith, J. R. Nielsen, and H. H. Claassen, *J. Chem. Phys.*, **18**, 326 (1950).

activation energy, the former must have a rate constant which leads to a detectable *yield* in the presence of the more rapid process.

Although, as Tables I and II show, one can get plausible results from the statistically based calculations when comparing them with experiment, this holds only for a selected number of reactions. It does not appear to be possible for  $\text{CH}_2\text{CF}_2$  to compute the whole spectrum and get a result which compares well with experiment. The difficulty is particularly great with the C-H bond breakage. If this has as its activation energy 6.3 e.v., the observed appearance potential difference,<sup>4</sup> its yield is much too high. Unfortunately, independent thermochemical data for this process are unavailable.

This same difficulty is qualitatively apparent in the mass spectra for other partly fluorinated olefins.<sup>4</sup> For  $\text{CH}_2\text{CHF}$ , the yield from C-H bond break relative to C-F bond break is about as expected if the relative appearance potential differences are treated as activation energies. For  $\text{CHF}\text{CF}_2$  the yield from C-H bond break is relatively much too small although the argument here is somewhat weakened by the fact that the  $\Delta A.P.$  of 5.3 for C-H bond break (*vs.* 5.8 for C-F break) is only known from thermochemical calculations.

Some difficulties with statistical theory are to be expected for a small molecule, such as a substituted ethylene. In particular, one might expect not to have enough closely spaced electronic states for the molecule ion to cross each other, and the existence of many such crossings is one of the basic assumptions of the theory.<sup>2</sup>

The alternative, nonstatistical approach to mass

spectra assumes direct decompositions from excited states. For example, differences in appearance potentials and ion abundances in *cis* and *trans*  $\text{CHCl}=\text{CHCl}$  and  $\text{CHBr}=\text{CHBr}$  were explained by predissociation of the molecular ions to give  $\text{C}_2\text{H}_2\text{Cl}^+$  and  $\text{C}_2\text{H}_2\text{Br}^+$ , respectively.<sup>14</sup> In our case, the possibility cannot therefore be excluded that  $\text{C}_2\text{H}_2\text{F}^+$  is similarly formed by predissociation from  $\text{CH}_2=\text{CF}_2^+$ . Furthermore, the large excess energy observed in process 3 for this molecule (Figure 1) may be due to the un-ionized  $\text{CF}_2$  being formed in an excited electronic state. It was, in fact, recently suggested that the analogous reaction in  $\text{C}_2\text{H}_4$  leads to electronically excited  $\text{CH}_2$ .<sup>15</sup> Finally, excited states which autoionize were observed for neutral  $\text{CH}_2=\text{CF}_2$  above its ionization potential.<sup>16</sup> For this to occur appears to violate one of the basic assumptions of the statistical theory, that the ionization is a fast Franck-Condon type process. We conclude that the relatively satisfactory results of Tables I and II, even though consistent with statistical theory, do not constitute proof of its validity.

For large nonsymmetric molecule ions the assumption that many closely spaced electronic state occur and cross each other should hold. Calculations concerning some larger fluorinated molecules are reported in the paper which follows.

*Acknowledgment.* We thank Dr. Max Wolfsberg for valuable discussions and help with the calculations.

(14) J. Momigny, *Bull. soc. chim. Belges*, **70**, 241 (1961).

(15) H. Prophet, *J. Chem. Phys.*, **38**, 2345 (1963).

(16) J. Momigny, *Nature*, **199**, 805 (1963).

# Appearance Potentials and Mass Spectra of $C_3F_6$ , $C_3F_5Cl$ , and $c-C_3F_6$ <sup>1</sup>

by Chava Lifshitz and F. A. Long

Department of Chemistry, Cornell University, Ithaca, New York (Received April 19, 1965)

Appearance potentials and mass spectra have been determined for  $C_3F_6$ ,  $C_3F_5Cl$ , and  $c-C_3F_6$ . As with the decomposition of the fluorinated ethylenes, rearrangement processes play prominent roles, notably in the formation of  $CF_3^+$  and  $C_2F_4^+$ . The appearance potential values permit assignment of most of the primary decomposition processes; they also give further information on the thermochemistry of the fluorinated ions and radicals. Ionization efficiency curves for the parent  $C_3F_6$  and  $C_3F_5Cl$  ions, as well as for some of the fragments from  $C_3F_6$  and  $c-C_3F_6$ , have been determined for several volts above the thresholds. The parent  $C_3F_6$  ionization curve shows a pronounced break, similar to the one which has previously been observed for  $C_2F_4$ , indicating again the influence of a competitive process. Appearance potential differences of several volts are found for some of the prominent decomposition processes and are discussed qualitatively in terms of the statistical theory of mass spectra.

## Introduction

Previous papers in this series have dealt with the mass spectral decomposition mechanisms and thermochemistry of fluorinated ethylenes and their positive ions.<sup>2,3</sup> The present study extends these considerations to  $CF_3CF=CF_2$ ,  $CF_2ClCF=CF_2$ , and  $c-C_3F_6$ . These compounds were chosen to study further the thermochemistry of the radicals and ions involved. The mass spectra and appearance potentials are presented for these three species, and breakdown patterns are proposed. Ionization efficiency curves are discussed qualitatively in terms of competing processes<sup>4</sup> and the statistical theory of mass spectra. The validity of utilizing observed energy differences as activation energies for processes of the type, parent molecule ion  $\rightarrow$  product ion, is also considered in terms of the statistical theory.

A general review of the mass spectra of fluorinated hydrocarbons has recently been published,<sup>5</sup> and recent information is also available on the mass spectra of partly fluorinated propanes and propylenes,<sup>6</sup> on the mass spectra of cyclic perfluoroalkanes and their hydrogen analogs,<sup>7</sup> and on appearance potentials for fully fluorinated ethane, propane, and cyclobutane.<sup>8</sup>

## Experimental Procedures and Results

The experimental procedure for recording the spectra and obtaining appearance potentials is the same as previously described.<sup>2,3</sup>

$CF_3CF=CF_2$  was kindly furnished by the Du Pont Jackson Laboratory.  $c-C_3F_6$  was prepared by Dr. D. C. England of Du Pont by photolysis of hexafluorocyclobutanone and was purified by preparative gas chromatography by Dr. A. Fainberg, Pennsalt Chemicals Corp.  $CF_2ClCF=CF_2$  was synthesized by Dr. R. Becker, Cornell University, by pyrolysis of  $CF_2ClCFClCF_2COONa$ .<sup>9</sup> Table I gives the spectra (in percentage yields of the various ions) of the three compounds studied. These were taken at an accelerating voltage of 105 v. compared to the normal operating voltage of 210 v. for the Consolidated 21-401 mass spectrometer. The low voltage permitted this machine to be used for  $m/e$  values larger than 100. Use of the lower voltage slightly reduces the focusing power of the machine but appears to have no other effect; e.g., spectra of standard compounds taken at 105 and 210 v. were found to be

(1) Work supported by the Advanced Research Projects Agency through the Materials Science Center.

(2) C. Lifshitz and F. A. Long, *J. Phys. Chem.*, **67**, 2463 (1963).

(3) C. Lifshitz and F. A. Long, *ibid.*, **69**, 3731, 3737 (1965).

(4) C. Lifshitz and F. A. Long, *J. Chem. Phys.*, **41**, 2468 (1964).

(5) J. R. Majer, *Advan. Fluorine Chem.*, **2**, 55 (1961).

(6) W. C. Steele and F. G. A. Stone, *J. Am. Chem. Soc.*, **84**, 3450 (1962).

(7) P. Natalis, *Bull. Soc. Roy. Sci. Liege*, **29**, 94 (1960).

(8) M. M. Bibby and G. Carter, *Trans. Faraday Soc.*, **59**, 2455 (1963).

(9) P. Resnick, Ph.D. Thesis, Cornell University, 1961.

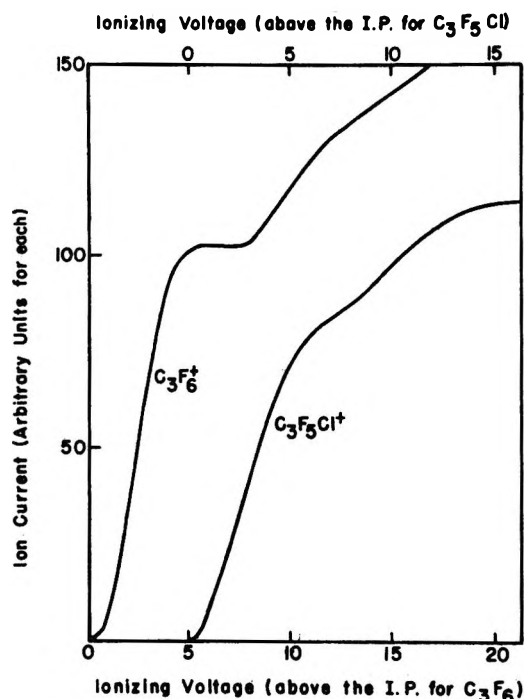


Figure 1. Ionization efficiency curves for the parent ions from  $\text{CF}_3\text{CF}=\text{CF}_2$  and  $\text{CF}_2\text{ClCF}=\text{CF}_2$ .

very similar. In the case of  $\text{CF}_2\text{ClCF}=\text{CF}_2$  the yields of isotopic ions containing  $\text{Cl}^{35}$  and  $\text{Cl}^{37}$  were added to calculate the total yield of a given ionic species.

The observed spectrum of  $\text{CF}_3\text{CF}=\text{CF}_2$  differs slightly from that reported by Mohler and co-workers,<sup>10</sup> small fragments showing relatively lower yields in our machine.

Table I: Mass Spectra (at 75 v.)

Species	$\text{CF}_3\text{CF}=\text{CF}_2$	$\text{CF}_2\text{ClCF}=\text{CF}_2$	<i>c</i> - $\text{C}_3\text{F}_6$
$\text{CF}^+$	11.9	10.5	16.4
$\text{CCl}^+$		1.2	
$\text{CF}_2^+$	1.0	0.9	5.5
$\text{CFCl}^+$		1.0	
$\text{CF}_3^+$	25.0	23.2	33.2
$\text{CF}_2\text{Cl}^+$		4.1	
$\text{C}_2\text{F}_2^+$	0.2	0.9	0.4
$\text{C}_2\text{FCl}^+$		0.3	
$\text{C}_2\text{F}_3^+$	3.2	2.5	3.3
$\text{C}_2\text{F}_2\text{Cl}^+$		1.2	
$\text{C}_2\text{F}_4^+$	15.2	0.2	34.6
$\text{C}_2\text{F}_3\text{Cl}^+$		1.9	
$\text{C}_2\text{F}_5^+$	0.6	2.5	0.6
$\text{C}_2\text{F}_6^+$	23.8	33.5	4.4
$\text{C}_2\text{F}_4\text{Cl}^+$		6.1	
$\text{C}_2\text{F}_5^+$	19.2 P		0.4 P
$\text{C}_2\text{F}_5\text{Cl}^+$		5.9 P	

Table II summarizes the appearance potentials for the principal ions from the three compounds. Since the main interest in the present paper is in the per-fluorocarbon radical ions and since  $\text{CF}_2\text{ClCF}=\text{CF}_2$  was run only for comparison, appearance potentials from this compound were measured only for the fully fluorinated fragment ions.

Table II: Appearance Potentials in Volts

Species	$\text{CF}_3\text{CF}=\text{CF}_2$	$\text{CF}_2\text{ClCF}=\text{CF}_2$	<i>c</i> - $\text{C}_3\text{F}_6$
$\text{CF}^+$	18.1	17.8	17.3
$\text{CF}_2^+$	19.8		17.4
$\text{CF}_3^+$	15.96	15.63	15.38
$\text{C}_2\text{F}_3^+$	19.32		18.3
$\text{C}_2\text{F}_4^+$	13.15		11.85
$\text{C}_2\text{F}_5^+$	15.18	11.22; 11.8 <sup>a</sup>	14.14
$\text{C}_2\text{F}_6^+$	11.11 P		11.3 P <sup>b</sup>
$\text{C}_2\text{F}_5\text{Cl}^+$		10.79 P	

<sup>a</sup> J. D. Morrison, private communication. <sup>b</sup> This ionization potential is less certain than the others because of the low intensity of the parent ion in the spectrum.

Figure 1 gives ionization efficiency curves for the parent ions from  $\text{CF}_3\text{CF}=\text{CF}_2$  and  $\text{CF}_2\text{ClCF}=\text{CF}_2$ . Figures 2 and 3 show ionization efficiency curves for the main fragments from  $\text{CF}_3\text{CF}=\text{CF}_2$  and *c*- $\text{C}_3\text{F}_6$ . Each fragment ion curve is drawn together with an  $\text{Ar}^+$  curve, so that the two curves are parallel at high voltages. In this way it is easy to demonstrate the occurrence of curves with unusually slow onset of ionization. Thus, the  $\text{C}_3\text{F}_5^+$  curves from  $\text{CF}_3\text{CF}=\text{CF}_2$  and *c*- $\text{C}_3\text{F}_6$  demonstrate long "tails," while the similar one from  $\text{CF}_2\text{ClCF}=\text{CF}_2$  does not. Similarly, the tailing on the  $\text{CF}_3^+$  and  $\text{CF}^+$  curves is much more pronounced for the  $\text{C}_3\text{F}_6$  isomers than for  $\text{C}_3\text{F}_5\text{Cl}$ . For the fragments which have long tails one would obtain a quite different result for the appearance potential if the semilog matching technique<sup>11</sup> were used instead of the vanishing current method which has been used in this study.

## Discussion

*Ionization Potentials.* There is a marked increase in ionization potential upon changing the three hydrogen atoms in the  $\text{CH}_3$  group of propylene to fluorines and a similar effect on going from *c*- $\text{C}_3\text{H}_6$  to *c*- $\text{C}_3\text{F}_6$ .<sup>8,12-14</sup>

(10) F. L. Mohler, V. H. Dibeler, and R. M. Reese, *J. Res. Natl. Bur. Std.*, **49**, 343 (1952).

(11) R. E. Honig, *J. Chem. Phys.*, **16**, 105 (1948).

(12) F. H. Field and J. L. Franklin, "Electron Impact Phenomena," Academic Press Inc., New York, N. Y., 1957.

(13) K. Watanabe, T. Nakayama, and J. Mottl, "Final Report on Ionization of Molecules by a Photoionization Method," University of Hawaii, Dec. 1959.



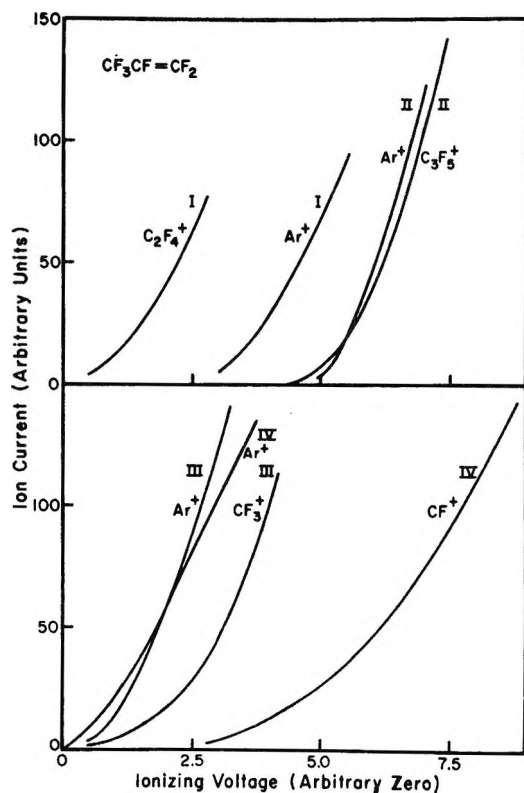


Figure 2. Ionization efficiency curves for the main fragment ions from  $CF_3CF=CF_2$ . (Each curve is drawn together with its calibrating  $Ar^+$  curve, so that the two curves are parallel at high voltages.)

These increases are in keeping with similar observations on other fluorine compounds where the inductive effect of the fluorine is the dominant factor.<sup>14</sup> On the other hand, upon changing the three other hydrogen atoms of  $CF_3CH=CH_2$  to fluorines, there is a slight decrease in ionization potential. This is similar to the result from fluorination of ethylene<sup>2</sup> and is explained by resonance stabilization due to the fluorines.<sup>14</sup> Upon replacing the fluorine of monofluorethylene with  $CF_3$  there is an increase of 0.54 e.v. in ionization potential, and a similar change from  $C_2F_4$  to  $C_3F_6$  increases the ionization potential by 0.49 e.v. A similar increase of 0.52 e.v. was also observed in the ionization potentials for the change from  $C_2F_5$  to  $i-C_3F_7$  and was ascribed to the electrophilic nature of the  $CF_3$  group.<sup>16</sup>

The electron impact ionization potential of  $C_2F_4$  is the same as the photoionization value<sup>2</sup>; on the other hand, the electron impact value for  $CF_3CF=CF_2$  is 0.5 e.v. higher than the photoionization value.<sup>16</sup> This different behavior suggests that the nuclear structure of the ionized propylene is considerably different from that of the neutral molecule at the minima of their potential curves, whereas the analogous structures are

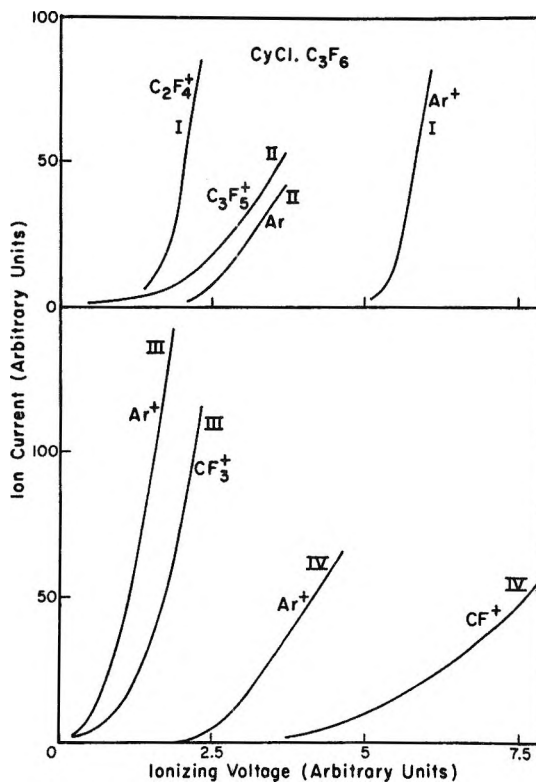


Figure 3. Ionization efficiency curves for the main fragment ions from  $c-C_3F_6$ . (The curves are drawn as in Figure 2.)

quite similar for the ethylenes. In fact, a useful way to look at the ion  $CF_3CF=CF_2^+$  is to assume a structure which permits a rapid reversible shift of a fluorine atom from the left-hand carbon to the right-hand one. This is consistent with the occurrence of high yields of certain rearrangement ions, e.g.,  $CF_3^+$  from  $CF_2ClCF=CF_2^+$ . It is also in keeping with previous suggestions about the structure of propylene ions.<sup>17</sup>

*75-E.v. Spectra.* Of the three compounds studied,  $c-C_3F_6$  shows the greatest amount of parent ion decomposition, in agreement with the behavior of other perfluorocyclics in the mass spectrometer.<sup>10</sup>  $CF_2ClCF=CF_2$  shows a greater degree of decomposition than  $CF_3CF=CF_2$ . There is a considerably larger degree of decomposition of the C-Cl bond than of the C-F bonds, and perfluorinated fragment ions are more common than the ion fragments containing Cl. The ions  $CF^+$  and  $CF_3^+$  are abundant in all three spectra.  $C_2F_4^+$  is

(14) R. Bralsford, P. V. Harris, and W. C. Price, *Proc. Roy. Soc. (London)*, **A258**, 459 (1960).

(15) I. P. Fisher, J. B. Homer, and F. P. Lossing, *J. Am. Chem. Soc.*, **87**, 957 (1965).

(16) F. M. Matsunaga and K. Watanabe, private communication, 1962.

(17) W. M. McFadden, *J. Phys. Chem.*, **67**, 1074 (1963).

abundant in the spectra of the two  $C_3F_6$  isomers while  $C_3F_5^+$  is abundant for the two olefins. One of the interesting features in the  $CF_2ClCF=CF_2$  spectrum is the occurrence of  $CF_3^+$  at a high yield, higher than that of the  $CF_2Cl^+$  ion, even though the  $CF_3$  group does not appear in the molecule itself. Similar rearrangement ions have been found in other propylenes; *e.g.*,  $CF_3^+$  and  $CF_2H^+$  are of approximately equal yield from  $CF_3CH=CH_2$ .<sup>6</sup>  $CF_3^+$  from *c*- $C_3F_6$  must be also a rearrangement ion;  $C_2F_4^+$  from  $CF_3CF=CF_2$  is probably a rearrangement ion in view of the relatively high yield of  $C_2H_3F^+$  from  $CF_3CH=CH_2$ .<sup>6</sup>  $C_2F_3^+$  from  $CF_3CF=CF_2$  is a low yield ion in comparison with  $CF_3CH=CH_2$ , where  $C_2H_3^+$  shows the largest yield in the spectrum.

**Breakdown Patterns.** The decomposition mechanisms are mainly established from appearance potentials, but, since very little is known about the thermochemistry of many of the radicals and ions involved, there is some uncertainty, particularly about secondary processes.  $C_3F_5^+$  is surely formed directly from the parent ion by a loss of halogen atom (F or Cl from  $C_3F_6$  and  $C_3F_5Cl$ , respectively). Ion-pair forming processes for  $C_3F_5Cl$  were searched for but not detected.<sup>18</sup> The energy needed to form  $C_3F_5^+$  from the parent ions, as measured by the appearance potential differences  $\Delta A.P.$ , is only 0.4 e.v. for  $CF_2ClCF=CF_2$ , but is 4.1 e.v. for  $CF_3CF=CF_2$ , and this presumably reports the difference between a C-Cl bond break and a C-F break.

For both isomers of  $C_3F_6$  the ion formed at lowest energy is  $C_2F_4^+$ . Hence, this must be formed in a single-step decomposition along with  $CF_2$ . For *c*- $C_3F_6$  this involves breaking two C-C bonds. For  $CF_3CF=CF_2$  it involves a C-C bond break and a simultaneous fluorine transfer.

The high-yield ions  $CF_3^+$  and  $CF^+$  may be formed by single-bond breaks. For example,  $CF_3CF=CF_2^+$  may alternatively decompose to give  $CF_3^+ + C_2F_3$  and  $CF^+ + C_2F_5$ . However, decompositions in which two C-C bonds are simultaneously broken have been suggested for the propylenes<sup>19</sup> and in other cases also.<sup>20</sup> Thus,  $CF_3^+$  from  $C_3F_6^+$  may be formed along with  $CF$  and  $CF_2$ . It is conceivable but not plausible that  $CF_3^+$  arises from secondary decomposition of  $C_3F_5^+$  since, if this were so, its appearance potential for each of the three parent compounds should differ by a constant value from that for the species  $C_3F_5^+$ , and this is not observed. It is also known<sup>2</sup> that  $CF_4^+$  is not formed in significant yield from  $C_2F_4^+$ . It is notable that the appearance potential differences for  $CF^+$  and  $CF_3^+$  are virtually the same for the three parent molecules, implying that similar bond breaks are involved. The strong implication of these results is that  $CF_3^+$  is

formed by a primary decomposition. This is possible although less sure for the formation of  $CF^+$  since in this case also several of the conceivable secondary processes to form it, as for example formation of  $CF^+$  from  $CF_3^+$ ,<sup>21</sup> turn out to be quite implausible.

Secondary processes may be involved in the production of  $C_2F_3^+$  and of  $CF_2^+$ , but the yields of both are small. In fact, a significant comment for all three of the parent molecules is that primary decomposition processes of the molecule ions appear to be the source of the high yield products even for bombardment by 75-e.v. electrons.

**Thermochemical Calculations.** The thermochemical calculations were carried out in a similar way to those for radicals and ions from the fluorinated ethylenes.<sup>2,3</sup> Table III summarizes some thermochemical calculations<sup>22-24</sup> for the processes which can lead to the observed ions and compares the calculated appearance potentials with the experimental values.

Table III

Process	Calcd. A.P., e.v.	Obsd. A.P., e.v.
(1) $CF_3CF=CF_2 \rightarrow CF_3^+ + C_2F_3^a$	15.2	15.96
(1') $CF_3CF=CF_2 \rightarrow CF_3^+ + CF + CF_2^b$	17.96	15.96
(2) $CF_3CF=CF_2 \rightarrow CF^+ + C_2F_5^c$	15.0	18.1
(2') $CF_3CF=CF_2 \rightarrow CF^+ + CF_2 + CF_3$	17.4	18.1
(2'') $CF_3CF=CF_2 \rightarrow CF^+ + C_2F_4 + F$	18.2	18.1
(2''') $CF_3CF=CF_2 \rightarrow CF^+ + 2CF_2 + F$	21.6	18.1
(3) $CF_3CF=CF_2 \rightarrow C_2F_3^+ + CF_2 + F^d$	19.03	19.32
(4) $CF_3CF=CF_2 \rightarrow CF_2^+ + 2CF_2^e$	18.12	19.8
(4') $CF_3CF=CF_2 \rightarrow CF_2^+ + CF + CF_3$	19.6	19.8
(10) $c-C_3F_8 \rightarrow C_2F_4^+ + C_2F_4^f$	12.3	12.3

<sup>a</sup>  $\Delta H_f(CF_3^+)$  used in this calculation is based upon the appearance potential of  $CF_3^+$  in  $CF_3H^3$  and is about 0.4 e.v. lower than the value based on the appearance potential in  $CF_3C_2H_3$ .<sup>6</sup> The heat of formation of  $C_2F_3$  is estimated to be  $-1.1$  e.v.<sup>3</sup> <sup>b</sup>  $\Delta H_f(CF_3^+)$  as in *a*;  $\Delta H_f(CF)$  and  $\Delta H_f(CF_2)$  as reported previously.<sup>3</sup> <sup>c</sup>  $\Delta H_f(CF^+)$  as reported previously;<sup>3</sup>  $\Delta H_f(C_2F_5)$  is based upon an estimated  $C_2F_5-F$  bond energy<sup>22</sup> and is  $-9$  e.v. <sup>d</sup> Using the appearance potential of  $C_2F_3^+$  in  $C_2F_4$ .<sup>2</sup> <sup>e</sup> Using the appearance potential of  $CF_2^+$  in  $C_2F_4$ .<sup>2</sup> <sup>f</sup> Based upon the heat of reaction:  $c-C_3F_8 \rightarrow 2C_2F_4$ .<sup>23,24</sup> and I. P. ( $C_2F_4$ ).

(18) See footnote *a*, Table II.

(19) H. R. Harless, ASTM E-14 Mass Spectrometry Conference, Chicago, Ill., 1961.

(20) R. R. Bernecker and F. A. Long, *J. Chem. Phys.*, **39**, 253 (1963).

(21) V. H. Dibeler, R. M. Reese, and F. L. Mohler, *J. Res. Natl. Bur. Std.*, **57**, 113 (1956).

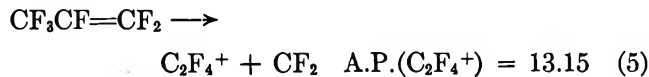
(22) W. M. D. Bryant, *J. Polymer Sci.*, **56**, 277 (1962).

(23) J. N. Butler, *J. Am. Chem. Soc.*, **84**, 1393 (1962).

(24) H. C. Duus, *Ind. Eng. Chem.*, **47**, 1445 (1955).

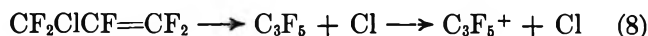
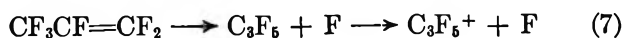
The heat of formation of CF<sub>3</sub>CF=CF<sub>2</sub> is known to be -11.22 e.v.,<sup>24</sup> and from the appearance potential of C<sub>2</sub>F<sub>4</sub><sup>+</sup> from this compound the heat of formation of CF<sub>2</sub> was previously calculated to be -1.6 e.v.<sup>3</sup> Useful calculations can also be made for production of CF<sub>3</sub><sup>+</sup>, CF<sup>+</sup>, C<sub>2</sub>F<sub>3</sub><sup>+</sup>, and CF<sub>2</sub><sup>+</sup>. If only two fragments (one positive and one neutral) are formed in a process (*e.g.*, process 1) and there is agreement between the computed and observed values for the appearance potential of the positive fragment, then this is probably the process which takes place at the threshold energy. The species CF<sub>3</sub><sup>+</sup> is probably formed by a simple primary bond split which additionally gives C<sub>2</sub>F<sub>3</sub>. If three fragments are formed in a process (*e.g.*, process 3), then, even if there is agreement between the computed and observed appearance potentials, it is still not certain whether the process takes place the way it is written, *i.e.*, in a single step. Production of CF<sup>+</sup> appears to come from process 2'' of Table III. On the basis of the calculations of Table III the most likely process for formation of C<sub>2</sub>F<sub>3</sub><sup>+</sup> is (3) and that for formation of CF<sub>2</sub><sup>+</sup> is (4').

Not enough information is available on heats of formation of *c*-C<sub>3</sub>F<sub>6</sub> and C<sub>3</sub>F<sub>5</sub>Cl to permit detailed calculations for reactions of these species. However, comparison of their behavior with that of C<sub>3</sub>F<sub>6</sub> permits a few useful points to be made. Since the following two processes take place



one calculates  $\Delta H_f(c\text{-C}_3\text{F}_6) - \Delta H_f(\text{CF}_3\text{CF}=\text{CF}_2) = 1.30$  e.v. Since  $\Delta H_f(\text{CF}_3\text{CF}=\text{CF}_2) = -11.22$  e.v., this implies  $\Delta H_f(c\text{-C}_3\text{F}_6) = -9.9$  e.v. If the C<sub>3</sub>F<sub>5</sub><sup>+</sup> ion has the same structure whether formed from CF<sub>3</sub>-CF=CF<sub>2</sub> or *c*-C<sub>3</sub>F<sub>6</sub>, then a slightly smaller value of 1.0 e.v. is calculated for the difference in heats of formation of these two compounds. On the other hand, the possibility cannot be excluded that at threshold energies C<sub>3</sub>F<sub>5</sub><sup>+</sup> from *c*-C<sub>3</sub>F<sub>6</sub> is the cyclopropyl radical ion and not the allyl ion. The similar difficulty with the C<sub>3</sub>H<sub>5</sub><sup>+</sup> ion from *c*-C<sub>3</sub>H<sub>6</sub> has been noted before.<sup>25</sup>

A further anomaly concerning the C<sub>3</sub>F<sub>5</sub><sup>+</sup> ion is observed. If the C<sub>3</sub>F<sub>5</sub><sup>+</sup> ions formed from CF<sub>3</sub>CF=CF<sub>2</sub> and CF<sub>2</sub>ClCF=CF<sub>2</sub> are the same and if no excess energy is involved in either process, then the difference in appearance potentials of C<sub>3</sub>F<sub>5</sub><sup>+</sup> from these two compounds should be equal to the difference in the C<sub>3</sub>F<sub>5</sub>-F and C<sub>3</sub>F<sub>5</sub>-Cl bond energies.



Thus

$$\text{A.P.}[\text{C}_3\text{F}_5^+(\text{CF}_3\text{CF}=\text{CF}_2)] -$$

$$\text{A.P.}[\text{C}_3\text{F}_5^+(\text{CF}_2\text{ClCF}=\text{CF}_2)] = D(\text{C}_3\text{F}_5\text{-F}) -$$

$$D(\text{C}_3\text{F}_5\text{-Cl}) = 3.96 \text{ e.v.}$$

If the value  $\text{A.P.}[\text{C}_3\text{F}_5^+(\text{CF}_2\text{ClCF}=\text{CF}_2)] = 11.8^{18}$  is used, the calculated bond energy difference is 3.4 e.v.

A computed difference of 3.5 to 4 e.v. in the C-F and C-Cl bond energies is quite out of line with the normally observed differences of 1 to 2 e.v. When the C<sub>2</sub>F<sub>3</sub><sup>+</sup> appearance potentials from C<sub>2</sub>F<sub>4</sub> and C<sub>2</sub>F<sub>3</sub>Cl were compared, the difference between the values agreed with the difference in bond energies (1.2 e.v.).<sup>4</sup>

The appearance potential of C<sub>3</sub>F<sub>5</sub><sup>+</sup> from *c*-C<sub>4</sub>F<sub>8</sub> was measured in order to get some further information concerning the heat of formation of this ion. The appearance potential of the other major ion in the *c*-C<sub>4</sub>F<sub>8</sub> spectrum, namely, C<sub>2</sub>F<sub>4</sub><sup>+</sup>, was measured as well. The value obtained in either case was  $12.3 \pm 0.1$  e.v. in excellent agreement with other recent measurements.<sup>8</sup> These values correspond, presumably, to the reactions



The appearance potential for process 10 is calculated in Table III and agrees very well with the observed value. If no excess energy is involved in process 9, one computes  $\Delta H_f(\text{C}_3\text{F}_5^+) = +2.2$  e.v. If this value is used to recalculate an appearance potential for reaction 7, one arrives at an observed excess energy for reaction 7 of  $\sim 1$  e.v. This question will be discussed further in the next section on ionization efficiency curves.

*Ionization Efficiency Curves.* The ionization efficiency curve of C<sub>3</sub>F<sub>5</sub><sup>+</sup> (Figure 1) resembles closely the C<sub>2</sub>F<sub>4</sub><sup>+</sup> curve from C<sub>2</sub>F<sub>4</sub> which has been discussed in a previous paper.<sup>4</sup> The sharp break in the C<sub>3</sub>F<sub>5</sub><sup>+</sup> curve occurs about 4 e.v. above the threshold, at the energy at which C<sub>3</sub>F<sub>5</sub><sup>+</sup> starts to appear; the analogous break in the C<sub>2</sub>F<sub>4</sub><sup>+</sup> curve occurred about 6 e.v. above threshold, a value which corresponded to the energy at which C<sub>2</sub>F<sub>3</sub><sup>+</sup> started to appear. C<sub>2</sub>F<sub>4</sub><sup>+</sup> from CF<sub>3</sub>CF=CF<sub>2</sub> appears at an energy lower than the energy at which the break in the C<sub>3</sub>F<sub>5</sub><sup>+</sup> curve occurs and exhibits normal behavior at the threshold of its appearance; *i.e.*, it is parallel to the Ar<sup>+</sup> curve (Figure 2). On the other hand, all the other curves (C<sub>3</sub>F<sub>5</sub><sup>+</sup>, CF<sub>3</sub><sup>+</sup>, and CF<sup>+</sup>) exhibit long tails since in the energy region where they appear the parent ion concentration remains practically

(25) R. F. Pottie, A. G. Harrison, and F. P. Lossing, *J. Am. Chem. Soc.*, **83**, 3204 (1961).

constant. The most obvious explanation for these results is that there is competition from decomposition into fragments<sup>4</sup> and that this affects the ionization efficiency curves of both parent and fragment ions.

In the absence of more complete thermochemical data it is not possible to determine whether statistical theory will account for the observed mass spectra. There is considerable uncertainty whether the  $\Delta A.P.$  values represent true thermochemical differences and hence are truly activation energies for the decompositions. In several cases the  $\Delta A.P.$  values for parent ion and primary product are large enough to indicate activation

energies well over 3 e.v. In such cases decomposition rates should be very small for energies close to threshold.<sup>3</sup> This would invalidate the use of  $\Delta A.P.$  as the activation energy and might also be the source of the long "tails" of the ionization efficiency curves. However, these and other uncertainties must await for resolution the development of more extensive thermochemical data.

*Acknowledgments.* We wish to thank Dr. J. D. Morrison and Dr. F. H. Dorman for parallel appearance potential measurements of ions from  $C_3F_8Cl$ .

## Some Observations Concerning the Positive Ion Decomposition of $C_2F_6$ and $C_3F_8$ in the Mass Spectrometer<sup>1</sup>

by Chava Lifshitz and F. A. Long

Department of Chemistry, Cornell University, Ithaca, New York (Received April 19, 1965)

Appearance potentials were measured for the positive ions formed by carbon-carbon and carbon-fluorine bond ruptures in  $C_2F_6^+$  and  $C_3F_8^+$ . For these ions the carbon-fluorine bond breakage occurs at an energy higher by 2.0 and 2.7 e.v., respectively, than the carbon-carbon breakage. In terms of the statistical theory of mass spectra, these values represent differences in activation energies for the unimolecular decomposition reactions. Relative rates of the two processes have been computed for the two compounds, for various internal excitation energies. In order to fit theory to experiment, one has to make extreme assumptions about the structures for the activated complexes of the two processes. Since the assumptions are not reasonable, we conclude that the statistical theory is not applicable to fluorocarbon decomposition. Most probably, these reactions involve direct decompositions from repulsive electronic states.

### Introduction

The statistical theory for the production of positive ion mass spectra<sup>2</sup> assumes: (a) there is a large number of densely spaced electronic states for a polyatomic molecule ion; (b) if the Franck-Condon ionization of a molecule leads to an excited electronic state, the electronic energy is transformed into vibrational energy of the lowest electronic state before the molecule ion under-

goes any chemical reaction; (c) there is complete equilibration of the excitation energy among the various internal degrees of freedom of the molecule ion before decomposition occurs. A consistent theory, based on

(1) Work supported by the Advanced Research Projects Agency through the Materials Science Center.

(2) H. M. Rosenstock, M. B. Wallenstein, A. L. Wahrhaftig, and H. Eyring, *Proc. Natl. Acad. Sci. U. S.*, **38**, 667 (1952).

these assumptions, has been developed and applied to paraffinic hydrocarbons with moderate success.<sup>2,3</sup> The present study is an attempt to find out whether the theory holds equally well for saturated fluorocarbons.

In working with hydrocarbons it has frequently been noted that, in comparison to the breaking of a skeletal C-C bond, the breaking of a C-H bond is a low yield process.<sup>2,4</sup> This was explained in the early development of the theory<sup>2</sup> as well as in later stages<sup>3,5</sup> by assuming a rather rigid activated complex for the C-H bond breakage and assuming a relatively nonrigid activated complex for the carbon-carbon breakage, by either reducing some of the vibrational frequencies or assuming free internal rotations.

The present study compares the C-F breakage with the C-C breakage in a group of fluoroparaffins. Appearance potentials and relative yields of the processes are presented. Theoretical calculations, based upon statistical theory, are carried out to compute the relative yields of the processes. It will be shown that some unacceptably extreme assumptions concerning the activated complexes have to be made in order to fit theory to experiment.

### Experimental Section and Results

The data were taken on a Consolidated Engineering Corp. mass spectrometer, Model 21-401, which has been modified as described previously.<sup>6</sup>

The percentage yields of the principal positive ions in the spectra of C<sub>2</sub>F<sub>6</sub> and C<sub>3</sub>F<sub>8</sub> are given in Table I. Listed are also the appearance potentials for the ions resulting from simple carbon-carbon and carbon-fluorine bond breakages in the two molecules. The ap-

pearance potentials for the two processes (*i.e.*, C-C and C-F breakage) precisely. Semilogarithmic plots of the ion current *vs.* the ionizing voltage were drawn for CF<sub>3</sub><sup>+</sup> and C<sub>2</sub>F<sub>5</sub><sup>+</sup> from C<sub>2</sub>F<sub>6</sub> and for CF<sub>3</sub><sup>+</sup> and C<sub>3</sub>F<sub>7</sub><sup>+</sup> from C<sub>3</sub>F<sub>8</sub>. The curves for each pair of ions were parallel over a twofold change in ion current. The difference in appearance potentials in the case of C<sub>2</sub>F<sub>6</sub> was found to be 1.96 v., and in the case of C<sub>3</sub>F<sub>8</sub> it was 2.72 v.

The present results show a different behavior than the one encountered for hydrocarbons. The C-F bond breakage needs an energy higher by 2.0-2.7 e.v. than the C-C breakage, and yet its yield is fairly high (about 0.4 of the C-C breakage yield in C<sub>2</sub>F<sub>6</sub> and about 0.2 of that yield in C<sub>3</sub>F<sub>8</sub>; Table I).

Figures 1 and 2 give the directly recorded dependence of the ionic currents upon ionizing energy. Relatively high yields are observed for the C-F breakages at the threshold, and no "tailing" is observed at the foot of the ionization efficiency curve for this process. These curves were obtained using an electron beam nonhomogeneous in energy, so that the thermal spread in energies "smears out" any sharp breaks in the ionization efficiency. However, the upward curvature in the CF<sub>3</sub><sup>+</sup> curves from both compounds, which holds over a fairly wide energy range (much wider than the spread in the ionizing electron energy, as shown from a calibrating He<sup>+</sup> curve), before the curves get to be linear, is believed to be due to onsets of excited electronic states for the parent ion. (The parent ions are missing in the spectra of both molecules.) This curvature is also believed to be the reason for the higher appearance potentials measured by Bibby and Carter<sup>9</sup> as compared to ours, since they used the method of "extrapolated linear intercepts," while we used the "vanishing current method."

The results for a mixed fluorohydrocarbon are given for comparison in Table II.<sup>10</sup> One observes again the relatively low yield, when considering the low appearance potential, for the C-H breakage and the relatively

**Table I:** Appearance Potentials and Percentage Yields at 70 E.v.

Product species	C <sub>2</sub> F <sub>6</sub>		C <sub>3</sub> F <sub>8</sub>	
	% at 70 e.v.	A.P., e.v.	% at 70 e.v.	A.P., e.v.
CF <sup>+</sup>	5.2		4.0	
CF <sub>2</sub> <sup>+</sup>	3.2		0.8	
CF <sub>3</sub> <sup>+</sup>	66.5	14.3	71.2	14.4
C <sub>2</sub> F <sub>4</sub> <sup>+</sup>	0.25		3.2	
C <sub>2</sub> F <sub>5</sub> <sup>+</sup>	24.9	16.3	7.5	15.3
C <sub>3</sub> F <sub>7</sub> <sup>+</sup>			13.3	17.1

pearance potentials were measured to  $\pm 0.1$  e.v. There is agreement in the values of the appearance potentials for the CF<sub>3</sub><sup>+</sup> ion from both compounds with those obtained by Mohler, Dibeler, and Reese.<sup>7,8</sup> There is, however, considerable disagreement with more recent measurements by Bibby and Carter.<sup>9</sup>

(3) M. Vestal, A. L. Wahrhaftig, and W. H. Johnston, Aeronautical Research Laboratories Report ARL 62-426, Sept. 1962.

(4) L. Friedman, F. A. Long, and M. Wolfsberg, *J. Chem. Phys.*, **30**, 1605 (1959).

(5) M. Wolfsberg, *ibid.*, **36**, 1072 (1962).

(6) A. B. King and F. A. Long, *ibid.*, **29**, 374 (1958).

(7) F. L. Mohler, V. H. Dibeler, and R. M. Reese, *J. Res. Natl. Bur. Std.*, **49**, 343 (1952).

(8) V. H. Dibeler, R. M. Reese, and F. L. Mohler, *Phys. Rev.*, **87**, 213 (1952), abstract.

(9) M. M. Bibby and G. Carter, *Trans. Faraday Soc.*, **59**, 2455 (1963).

(10) C. Lifshitz and F. A. Long, *J. Phys. Chem.*, **67**, 3731 (1965).

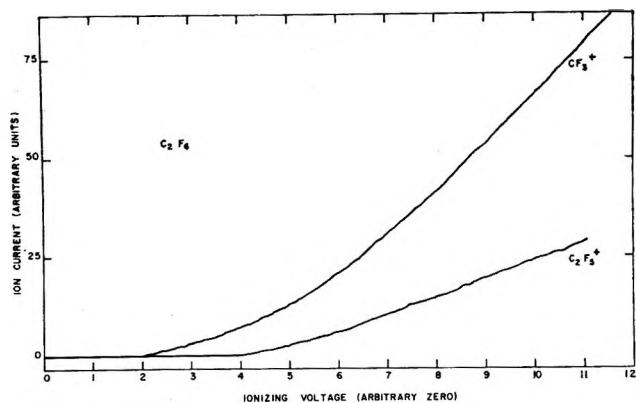


Figure 1. Directly recorded ionization efficiency curves for  $\text{CF}_3^+$  and  $\text{C}_2\text{F}_5^+$  from  $\text{C}_2\text{F}_6$ .

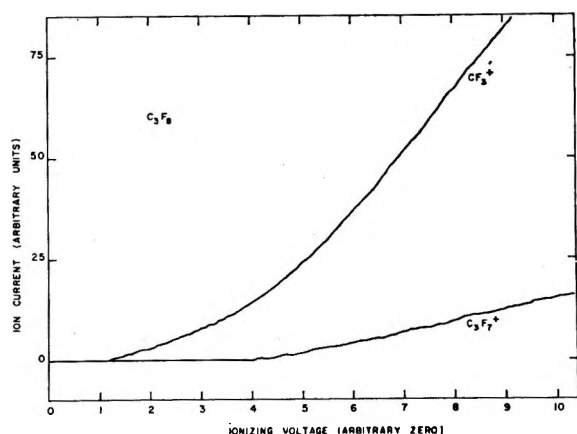


Figure 2. Directly recorded ionization efficiency curves for  $\text{CF}_3^+$  and  $\text{C}_3\text{F}_7^+$  from  $\text{C}_3\text{F}_8$ .

high yield for the C-F breakage, when considering its relatively high A.P.

Table II

Dissociation process	Appearance potential, <sup>10</sup> e.v.	Percentage yield
$\text{CH}_3\text{CHF}_2 \rightarrow \text{CH}_3\text{CF}_2^+ + \text{H}$	12.3	23.0
$\text{CH}_3\text{CHF}_2 \rightarrow \text{CF}_2\text{H}^+ + \text{CH}_3$	13.2	48.4
$\text{CH}_3\text{CHF}_2 \rightarrow \text{CH}_3\text{CHF}^+ + \text{F}$	14.9	5.9

In order to get some information concerning the thermochemistry of the  $\text{C}_2\text{F}_5^+$  and  $\text{C}_3\text{F}_7^+$  radical ions we have measured their appearance potentials from  $n\text{-C}_4\text{F}_{10}$ . The results are presented in Table III.

*Some Observations Concerning Thermochemistry.*  $\text{C}_2\text{F}_5^+$  and  $\text{C}_3\text{F}_7^+$  are involved in the processes studied in  $\text{C}_2\text{F}_6$  and  $\text{C}_3\text{F}_8$ , which will form the basis for our calcula-

Table III: Appearance Potential of Selected Ions from  $n\text{-C}_4\text{F}_{10}$

Ion	Appearance potential, e.v.
$\text{CF}_3^+$	14.3
$\text{C}_2\text{F}_5^+$	14.6
$\text{C}_3\text{F}_7^+$	15.0

tions. It is, therefore, important to know the energies involved in the transitions from the parent molecule to these two fragment ions.

If it is assumed that  $\text{CF}_3^+$ ,  $\text{C}_2\text{F}_5^+$ , and  $\text{C}_3\text{F}_7^+$  are formed by simple carbon-carbon breakages from  $n\text{-C}_4\text{F}_{10}$  and if it is further assumed that the two types of C-C bonds in  $n\text{-C}_4\text{F}_{10}$  are of similar strength, then the observed differences in appearance potentials of the three ions from this molecule (Table III) reflect differences in the ionization potentials of the radicals. The results of Table III would predict, under these assumptions, that

$$\text{I.P.}(\text{C}_2\text{F}_5) = \text{I.P.}(\text{CF}_3) + 0.3 \text{ e.v.}$$

$$\text{I.P.}(\text{C}_3\text{F}_7) = \text{I.P.}(\text{CF}_3) + 0.7 \text{ e.v.}$$

The ionization potential of  $\text{CF}_3$  is itself still an unsettled matter. Recent results gave  $\text{I.P.}(\text{CF}_3) = 9.1$ <sup>10</sup> and showed that excess energy was involved in the formation of  $\text{CF}_3^+$  from fluoroparaffins. Fisher and Lossing estimated recently that  $\text{I.P.}(\text{CF}_3) = 9.5$ ,<sup>11</sup> and their direct electron impact measurements on  $\text{C}_2\text{F}_5$  and  $\text{C}_3\text{F}_7$  gave<sup>11</sup>  $\text{I.P.}(\text{C}_2\text{F}_5) = 10.0$ ;  $\text{I.P.}(n\text{-C}_3\text{F}_7) = 10.0$ , and  $\text{I.P.}(i\text{-C}_3\text{F}_7) = 10.5$ . Therefore

$$\text{I.P.}(\text{C}_2\text{F}_5) = \text{I.P.}(\text{CF}_3) + 0.5 \text{ e.v.}$$

$$\text{I.P.}(i\text{-C}_3\text{F}_7) = \text{I.P.}(\text{CF}_3) + 1.0 \text{ e.v.}$$

Both sets of results (direct electron impact and appearance potentials from  $n\text{-C}_4\text{F}_{10}$ ) show that the following relationship surely exists, namely:  $\text{I.P.}(\text{CF}_3) < \text{I.P.}(\text{C}_2\text{F}_5) \leq \text{I.P.}(\text{C}_3\text{F}_7)$ .

From the above considerations, concerning the ionization potentials of  $\text{C}_2\text{F}_5$  and  $\text{C}_3\text{F}_7$ , one can draw a conclusion about the thermochemistry of the processes leading to  $\text{C}_2\text{F}_5^+$  and  $\text{C}_3\text{F}_7^+$  in  $\text{C}_2\text{F}_6$  and  $\text{C}_3\text{F}_8$ , respectively. From self-consistent estimated heats of formation of the fluorocarbon radicals  $\text{CF}_3$ ,  $\text{C}_2\text{F}_5$ , and  $\text{C}_3\text{F}_7$ ,<sup>12</sup> one computes that the C-C bond is weaker than the C-F bond in both  $\text{C}_2\text{F}_6$  and  $\text{C}_3\text{F}_8$  by approximately 1.8 e.v. If the ionization potential of  $\text{CF}_3$  were equal

(11) I. P. Fisher, J. B. Homer, and F. P. Lossing, *J. Am. Chem. Soc.*, **87**, 957 (1965).

(12) W. M. D. Bryant, *J. Polymer Sci.*, **56**, 277 (1962).

to those of C<sub>2</sub>F<sub>5</sub> and C<sub>3</sub>F<sub>7</sub>, this would lead to an observed difference of  $\sim 1.8$  e.v. for the C–C breakage and C–F breakage in either C<sub>2</sub>F<sub>6</sub> or C<sub>3</sub>F<sub>8</sub>, to give the respective radical ions. The observed differences are higher than 1.8 e.v. in both compounds, since the ionization potentials of C<sub>2</sub>F<sub>5</sub> and C<sub>3</sub>F<sub>7</sub> are higher than that of CF<sub>3</sub>. On the basis of the above given differences in ionization potentials of CF<sub>3</sub>, C<sub>2</sub>F<sub>5</sub>, *n*-C<sub>3</sub>F<sub>7</sub>, and *i*-C<sub>3</sub>F<sub>7</sub>, one can compute the thermochemical differences. The observed difference of 2.0 e.v. coincides within 0.2 e.v. with the expected thermochemical difference for C<sub>2</sub>F<sub>6</sub>. It is hard to decide whether the C<sub>3</sub>F<sub>7</sub><sup>+</sup> radical ion formed from C<sub>3</sub>F<sub>8</sub> is *n*-C<sub>3</sub>F<sub>7</sub><sup>+</sup> at threshold energies. However,  $\Delta H_f(\text{C}_3\text{F}_7^+)$  and  $\Delta H_f(\textit{i}\text{-C}_3\text{F}_7^+)$  are approximately the same since *i*-C<sub>3</sub>F<sub>7</sub> is more stable than *n*-C<sub>3</sub>F<sub>7</sub>,<sup>12</sup> but its ionization potential is higher.<sup>11</sup> Thus, again the observed difference of 2.7 e.v. in the case of C<sub>3</sub>F<sub>8</sub> coincides within 0.2 e.v. with the expected thermochemical difference.

In conclusion, no appreciable kinetic shift is observed in the appearance potentials of C<sub>2</sub>F<sub>5</sub><sup>+</sup> from C<sub>2</sub>F<sub>6</sub> and of C<sub>3</sub>F<sub>7</sub><sup>+</sup> from C<sub>3</sub>F<sub>8</sub>. The experimentally observed appearance potentials are considered to coincide with the expected values from thermochemistry.

*Some Observations Concerning Negative Ions.* In the present study neutral fragments are assumed to be formed along with the positive ions; *i.e.*, ion-pair forming processes are excluded. Since the parent molecule ions are absent in the spectra of C<sub>2</sub>F<sub>6</sub> and C<sub>3</sub>F<sub>8</sub>, even at low ionizing voltages one might have expected ion-pair forming processes. Negative ions were observed in both spectra.<sup>9</sup> These were, however, found to be due to electron-capture processes rather than ion-pair forming processes.

*Theoretical Calculations.* Calculations were carried out for the relative yields of carbon–carbon and carbon–fluorine breakages in C<sub>2</sub>F<sub>6</sub> and C<sub>3</sub>F<sub>8</sub>. The differences in appearance potentials (2.0 and 2.7 e.v., respectively) were taken as differences in activation energies of the processes involved. Since no parent ion is observed in either molecule, the plausible assumption to make, in terms of the theory, is that the activation energy for CF<sub>3</sub><sup>+</sup> formation (the lowest appearing and most abundant ion in either case) is, in fact, zero. The activation energies for the C–F breakage are then 2.0 and 2.7 e.v. in C<sub>2</sub>F<sub>6</sub> and C<sub>3</sub>F<sub>8</sub>, respectively. [The unimolecular rate constant at the threshold energy is given by<sup>5,13</sup>  $k = 1/hN^*(E)$ , where  $h$  is Planck's constant and  $N^*(E)$  is the density of states of the active molecule at internal energy  $E$ . This expression forms the basis for our assumptions that, if the activation energy for a process in the mass spectrometer is zero, no parent ion will be observed. If the activation energy is zero,  $k =$

$1/hN^*(0)$ ; now from known dependences of sums of vibrational states upon internal energy, one can estimate a maximum value for  $N^*(0)$  of approximately 100 e.v.<sup>-1</sup>. Thus, the minimum value of  $k$  at threshold is  $2.4 \times 10^{12}$  sec.<sup>-1</sup>;  $k$  at any higher energy  $E$  will certainly be higher. The fraction of parent ions remaining at the end of 10<sup>-5</sup> sec. is then less than 10<sup>-10</sup>, *i.e.*, negligibly small.]

The basis for the calculations is the unimolecular reaction rate theory as developed by Marcus.<sup>13</sup> The relative yields of the C–C and C–F breakages are computed as a function of the internal energy  $E$  of the active molecule.<sup>5,13</sup>

Let  $E_a(\text{C–C})$  and  $E_a(\text{C–F})$  be the activation energies for the C–C and C–F breakages, respectively, and  $E^+(\text{C–C}) = E - E_a(\text{C–C})$  and  $E^+(\text{C–F}) = E - E_a(\text{C–F})$  be the internal energies of the two activated complexes. Let  $Y(\text{C–C})$  and  $Y(\text{C–F})$  be the yields of carbon–carbon and carbon–fluorine breakages, respectively. Then  $(Y(\text{C–C})/Y(\text{C–F}))_E$  equals the sum of states for the C–C activated complex at  $E^+(\text{C–C})$  over the sum of states for the C–F complex at  $E^+(\text{C–F})$ .

The sum of vibrational–rotational states for energy  $E^+$  is given by the formula<sup>13</sup>

$$\sum_{E_v \leq E^+} P(E_v) [(\Gamma r/2 + 1)]^{-1} \times (8\pi^2/h^2)^{r/2} \times (E - E_v)^{r/2} \prod_{i=1}^r [I_i^{-1/2} \Gamma(1/2)]$$

where  $P(E_v)$  is the number of vibrational states at energy  $E_v$ ,  $r$  is the number of singly degenerate rotations participating in the internal energy transfer, and  $I_i$  is the moment of inertia of  $i$ th rotation.

A Fortran program was set up to compute these sums of states. The vibrational part was obtained by frequency grouping (up to five groups), where the representative frequency of each group is the geometric mean of the frequencies used.

*Calculations for C<sub>2</sub>F<sub>6</sub>. C–C Complex.* The frequencies are those of the neutral C<sub>2</sub>F<sub>6</sub> molecule<sup>14</sup> except for the C–C stretching frequency, which is the reaction coordinate. Three groups were used: six frequencies of 1400 cm.<sup>-1</sup>, six of 600 cm.<sup>-1</sup>, and five of 300 cm.<sup>-1</sup>. The torsional frequency is assumed to be 300 cm.<sup>-1</sup>. The torsional frequency is not assumed to be a free internal rotation in this case, in order to minimize the computed rate constant for this reaction as much as possible.

*C–F Complex.* A C–F stretching frequency is trans-

(13) R. A. Marcus, *J. Chem. Phys.*, **20**, 355, 359, 364 (1952).

(14) J. R. Nielsen, C. M. Richards, and H. L. McMurry, *ibid.*, **16**, 67 (1948).



formed into the reaction coordinate. Several other frequencies are lowered. The frequencies are those of the  $C_2F_5$  radical (inferred from those of  $C_2F_6$ ), the torsional vibration is transformed into a free internal rotation, and two further inactive rotations of the  $C_2F_5$  radical ion are assumed. The definition of an inactive degree of freedom as given by Marcus<sup>13</sup> is a degree of freedom which contributes its energy freely only when the active molecule has been transformed into its activated complex. Since what we assume here is a freely rotating  $C_2F_5^+$  radical in the  $F \cdots C_2F_5^+$  activated complex, this is essentially a "loose" complex, again in the sense in which a "loose" complex has been defined by Marcus.<sup>13</sup>

The frequencies used are: 1400 (3), 600 (5), and 300 (6)  $cm^{-1}$ . The moments of inertia used are, in terms of  $8\pi^2 I/h^2$ , 64,270 (2) and 99,370 e.v.<sup>-1</sup>.

The results of the calculations are presented in Table IV.

**Table IV:** Computed Relative Yields in  $C_2F_6$

$E$	$E^+(C-C)$	$E^+(C-F)$	Sum of states		$\frac{Y(C-F)^a}{Y(C-C)}$
			C-C complex	C-F complex	
2.0	2.0	0	$3.1 \times 10^{11}$	1	$3.2 \times 10^{-12}$
2.1	2.1	0.1	$5.7 \times 10^{11}$	$1.8 \times 10^7$	$3.2 \times 10^{-6}$
2.2	2.2	0.2	$1.0 \times 10^{12}$	$5.9 \times 10^8$	$5.9 \times 10^{-4}$
2.3	2.3	0.3	$1.8 \times 10^{12}$	$8.1 \times 10^9$	$4.5 \times 10^{-3}$
2.4	2.4	0.4	$3.1 \times 10^{12}$	$7.1 \times 10^{10}$	$2.3 \times 10^{-2}$
2.5	2.5	0.5	$5.3 \times 10^{12}$	$4.5 \times 10^{11}$	$8.5 \times 10^{-2}$

<sup>a</sup> These numbers should still be multiplied by 3, in order to take into account the various possibilities of obtaining the C-F reaction (6) vs. the C-C reaction (2).

**Calculations for  $C_3F_8$ . C-C Complex.** The frequencies are those of the neutral  $C_3F_8$  molecule<sup>16</sup> except for the C-C stretching frequency, which is the reaction coordinate. Plausible guesses were made of a few missing frequencies, by comparing the known frequencies of  $C_3F_8$  with those of  $C_3H_8$ . Calculations were carried out using the approximation of Whitten and Rabinovitch.<sup>16</sup> (This approximation was tested by us for some fluorocarbon molecules by comparing it with exact sums of states at lower internal energies and found to agree very well.) The equation for this approximation follows; symbols are as defined in the original paper

$$\log \Sigma P(E_v) = S \log (E' + 1 - \beta W) + S \log E_z - \log S' - \Sigma \log h\nu_i$$

taking  $S = 26$ ,  $\beta = 1.2154$ ,  $E_z = 10,087 \text{ cm}^{-1}$ , and

using the formula<sup>16</sup>  $\log W = -1.0506(E')^{0.25}$  to compute  $W$  as a function of  $E' = E^+/E_z$ .

**C-F Complex.** A C-F stretching frequency is transformed into the reaction coordinate. Four rotations are assumed: two internal and two inactive ones of the  $C_3F_7^+$  radical ion. The frequencies are thus essentially those of the  $C_3F_7$  radical (inferred from  $C_3F_8$ ) except for the two torsional frequencies which are absent and for a few other frequencies which are lowered. The frequencies used are 1400 (5), 530 (16), and 100 (1)  $cm^{-1}$ . The moments of inertia used are, in terms of  $8\pi^2 I/h^2$ , 191,077 (2) and 116,000 (2) e.v.<sup>-1</sup>.

The results of the calculations are presented in Table V.

**Table V:** Computed Relative Yields in  $C_3F_8$

$E$	$E^+(C-C)$	$E^+(C-F)$	Sum of states		$\frac{Y(C-F)^a}{Y(C-C)}$
			C-C complex	C-F complex	
2.7	2.7	0	$3.0 \times 10^{16}$	1	$3.3 \times 10^{-17}$
2.8	2.8	0.1	$5.9 \times 10^{16}$	$6.6 \times 10^9$	$1.1 \times 10^{-7}$
2.9	2.9	0.2	$1.1 \times 10^{17}$	$3.2 \times 10^{11}$	$2.9 \times 10^{-6}$
3.0	3.0	0.3	$2.2 \times 10^{17}$	$7.0 \times 10^{12}$	$3.2 \times 10^{-6}$
3.1	3.1	0.4	$4.0 \times 10^{17}$	$9.1 \times 10^{13}$	$2.3 \times 10^{-4}$
3.2	3.2	0.5	$7.4 \times 10^{17}$	$8.6 \times 10^{14}$	$1.2 \times 10^{-3}$
3.3	3.3	0.6	$1.3 \times 10^{18}$	$3.9 \times 10^{16}$	$3.0 \times 10^{-2}$

<sup>a</sup> These numbers (like those in Table IV) should for the sake of completeness be multiplied by a factor of 4.

## Discussion

Very low relative yields were computed for the carbon-fluorine bond breakages (Tables IV and V) in comparison with the observed ones in Figures 1 and 2. The discrepancy is even more pronounced if one takes into account the fact that the energy in Figures 1 and 2 is the ionizing electron energy rather than the internal energy of the molecule ion. The internal energies of most of the molecule ions will be lower, the maximum internal energy of any molecule being equal to the electron energy above the ionization potential. "Rigid" complexes have been assumed for the C-C breakages in  $C_2F_6$  and  $C_3F_8$ , while "loose" ones were adopted for the C-F breakages. This attitude was taken in order to get comparable computed yields for the carbon-carbon and carbon-fluorine breakages, at high internal energies  $E$ , in agreement with observation. However, even under these extreme assumptions,

(15) W. F. Edgell, H. D. Mallory, and D. G. Weiblen, *J. Am. Chem. Soc.*, **72**, 4856 (1950).

(16) G. Z. Whitten and B. S. Rabinovitch, *J. Chem. Phys.*, **38**, 2466 (1963).



the C-F yields are by several orders of magnitude smaller than the C-C yields at threshold energies and a few tenths of a volt above threshold. "Tailing" at the foot of the ionization efficiency curves for the C-F breakages is, furthermore, not observed. The assumptions made about the activated complexes are the most extreme ones. It is not plausible to reduce further vibrational frequencies in the C-F complexes; furthermore, the greatest effect on increasing the number of vibrational-rotational states is achieved by introducing the four rotational degrees of freedom. The statistical theory of mass spectra is thus inadequate for explaining the  $C_2F_6$  and  $C_3F_8$  spectra.

Let us consider next mixed hydrofluorocarbons such as  $CH_3CHF_2$  (Table II). A rigid complex was assumed for the carbon-carbon breakage in the perfluoro compounds. It is impossible to make the complex for the carbon-hydrogen breakage in  $CH_3CHF_2$  even more rigid. This is necessary in order to account for the low yield of the C-H breakage in this molecule.

Great difficulties are thus encountered when one is trying to fit the statistical theory to the experimental observations for these compounds. The reason might be the violation of some of the basic assumptions of the theory. Direct decomposition from an excited electronic state of the ion, without prior transformation of electronic into vibrational energy, may very well occur. Indeed, since no parent ion is observed, one would expect the occurrence of repulsive electronic states. One of the basic preconditions of the theory is that the low-lying excited electronic states are in general not repulsive.<sup>17</sup> Our conclusion for the time being is that the statistical theory gives an adequate description for the mass spectra of hydrocarbon paraffins, but not for their fluorinated analogs.

*Acknowledgments.* We wish to thank Dr. Max Wolfsberg for very helpful discussions and comments concerning the manuscript.

(17) A. L. Wahrhaftig in "Advances in Mass Spectrometry," J. D. Waldron, Ed., Pergamon Press Ltd., London, 1959, p. 274.

## Diffusion of Methane, Ethane, Propane, and *n*-Butane

### in Water from 25 to 43°

by P. A. Witherspoon and D. N. Saraf

*Department of Mineral Technology, University of California, Berkeley, California (Received April 12, 1965)*

Diffusion coefficients for methane, ethane, propane, and *n*-butane in water were measured at temperatures ranging from 24.8 to 42.6° using the capillary-cell method.  $D\sqrt{M}$ , where  $D$  is the diffusion coefficient and  $M$  is the molecular weight, was not found to be a constant, as reported by others. Instead,  $D$  for each hydrocarbon investigated is 1.235 times that of its next heavier homolog. Activation energies were found to be the same for all four hydrocarbons, *viz.*, 2900 cal./mole. The results are consistent with the concept that diffusion is controlled by molecular size.

#### Introduction

The diffusion of hydrocarbons in water is a basic consideration in many processes, but very few data on diffusion coefficients are available in the literature. Soviet workers<sup>1</sup> have reported results credited to Antonov for the diffusion of methane, ethane, propane, and *n*-hexane in water. Diffusion coefficients have recently been reported for ethane, propane, and *n*-butane in water at 29.9°.<sup>2</sup> With regard to other hydrocarbons, diffusion data have been reported for propylene at 25°<sup>3</sup> and acetylene at 18°.<sup>4</sup> Diffusion coefficients have also been obtained for ethylene, propylene, and butylene in water at temperatures ranging from 6 to 65°.<sup>5</sup> Aside from these meager data, nothing else has been found in the literature.

A project has therefore been undertaken in this laboratory to study the general problem of the diffusion through water of the hydrocarbons found in petroleum. The following results on methane, ethane, propane, and *n*-butane constitute the first progress report from this investigation.

#### Experimental Section

The capillary-cell method of measuring diffusion coefficients perfected by Wang<sup>6</sup> has been modified for this work. The details have been reported elsewhere<sup>2,7</sup> and will only be reviewed here.

We used a specially designed capillary of variable length having an internal diameter of about 0.1 cm. The capillary was made from a 50- $\mu$ l. syringe manu-

factured by the Hamilton Co., Inc., Whittier, Calif., and was ground flat on one end. The close-fitting stainless steel plunger makes it possible to use any desired length of capillary up to about 7 cm. By filling a known length of the capillary with an aqueous solution of a given hydrocarbon, the system is then ready for immersion in a constant-temperature bath of unstirred pure water. This bath was kept in a larger water bath whose temperature was controlled to  $\pm 0.01^\circ$ .

The aqueous solutions were prepared by bubbling the hydrocarbon gas<sup>8</sup> through distilled water for about 0.5 hr. and allowing the solutions to equilibrate for 1 or more days in a constant-temperature air bath. The temperature of the air bath was kept equal to that of the water bath. The saturated solutions had con-

(1) A. A. Kartsev, *et al.*, "Geochemical Prospecting for Petroleum," University of California Press, 1959, p. 69.

(2) D. N. Saraf, P. A. Witherspoon, and L. H. Cohen, *Science*, **142**, 955 (1963).

(3) J. E. Vivian and C. J. King, *A.I.Ch.E. J.*, **10**, 220 (1964).

(4) G. Tammann and V. Z. Jensen, *Z. anorg. allgem. Chem.*, **179**, 125 (1929).

(5) A. A. Unver and D. M. Himmelblau, *J. Chem. Eng. Data*, **9**, 428 (1964).

(6) J. H. Wang, *J. Am. Chem. Soc.*, **73**, 510 (1951); **74**, 1182 (1952); **76**, 4763 (1954).

(7) D. N. Saraf, M.S. Thesis, University of California, Berkeley, Calif., 1963.

(8) All hydrocarbons used were research grade, 99.9% pure or better, and were obtained from Phillips Petroleum Co., Bartlesville, Okla.

centrations of 20 to 60 p.p.m. depending on the gas used.

After an appropriate diffusion time had elapsed, the hydrocarbon concentrations remaining in the capillary were measured in a gas chromatograph equipped with a hydrogen-flame ionization detector. A mixture of nitrogen and steam was used as the carrier gas. The sample size was usually about 20  $\mu$ l., and this amount could be analyzed in less than 1 min. with a precision of about 0.5%. Details of the analytical procedure have been published elsewhere.<sup>2,7</sup>

Diffusion takes place past the open end of the capillary while it is immersed in pure solvent, and the coefficient ( $D$ ) may be calculated from

$$\frac{C_a}{C_0} = \frac{8}{\pi^2} \sum_{n=0}^{\infty} \frac{1}{(2n+1)^2} \exp\left[-(2n+1)^2 \pi^2 \frac{Dt}{4L^2}\right] \quad (1)$$

where  $C_a$  is the average concentration of hydrocarbons in the capillary at the end of the diffusion time, any units;  $C_0$  is the original concentration, same units as  $C_a$ ;  $t$  is the time of diffusion, seconds;  $L$  is the length of the capillary, centimeters.

The infinite series in eq. 1 converges rapidly, and, when the value of the parameter  $Dt/L^2$  is greater than 0.23, all but the first term can be neglected without introducing a mathematical error greater than 0.2%. In this case, eq. 1 reduces to

$$D = \frac{4L^2}{\pi^2 t} \ln \frac{8C_0}{\pi^2 C_a} \quad (2)$$

In this work, 75% of the values of  $Dt/L^2$  was 0.23 or higher, and therefore eq. 2 was generally used. In those instances where this parameter was less than 0.23, it was necessary to use the first two terms in eq. 1 to avoid an appreciable error in  $D$ .

Another error that can occur is the so-called "Δl effect," which arises because the actual length of the diffusion path may differ from the geometric length owing to the effects of convection currents that sweep past the capillary mouth.<sup>6,9</sup> Two factors must be considered: (a) loss of material during immersion of the capillary in the bath and (b) loss of material after immersion. By allowing a slight excess of the initial solution to cover the mouth of the capillary prior to placing it in the water bath, we found that the excess solution was completely removed during immersion without disturbing the contents of the capillary to any measurable degree.

To evaluate the second factor, we performed experiments with the same solution in capillaries of different length and with various rates of stirring in the inner bath containing the capillary. The results suggested

that, as the rate of stirring was reduced to zero, the Δl effect decreased to the point where it was negligible by comparison with other experimental errors. We therefore used no stirring in the inner bath.

The results of the diffusion measurements are summarized in Table I. The data represent the averages of four to six repetitive runs, except for ethane and propane at 35.1° where nine runs were made with each gas.

Table I: Results of Diffusion Measurements<sup>a</sup>

Hydrocarbon	24.8°	29.9°	35.1°	42.6°
Methane	1.88 ± 0.01 <sup>b</sup>	...	2.12 ± 0.03	2.41 ± 0.02
Ethane	1.52 ± 0.03	1.59 ± 0.025	1.72 ± 0.02	1.95 ± 0.03
Propane	1.21 ± 0.04	1.27 ± 0.02	1.39 ± 0.01	1.59 ± 0.02
<i>n</i> -Butane	0.96 ± 0.04	1.03 ± 0.025	1.12 ± 0.03	1.28 ± 0.01

<sup>a</sup> Diffusion coefficient,  $D \times 10^5$  cm.<sup>2</sup>/sec. <sup>b</sup> The precision shown is the standard deviation of the arithmetic mean.

## Discussion

According to Antonov,<sup>1</sup> diffusion coefficients for the paraffin gases in water are inversely proportional to the square root of their molecular weights. He has published data on the steady-state diffusion of CH<sub>4</sub>, C<sub>2</sub>H<sub>6</sub>, C<sub>3</sub>H<sub>8</sub>, C<sub>4</sub>H<sub>10</sub>, and C<sub>6</sub>H<sub>14</sub> through clays containing 25% water by weight.<sup>10</sup> The diffusion coefficients are, of course, lower than those for pure water because of the presence of the clay, but these results are used by him to support the interpretation that  $D\sqrt{M} = \text{constant}$ . In analyzing our data, we found  $D\sqrt{M} \neq \text{constant}$ , and, after reviewing Antonov's results,<sup>10</sup> we concluded that the same interpretation could be given to his data. This is shown by the convex upward curves in Figure 1. We also found that  $D$  is not proportional to  $(1/V)^{1/3}$ , where  $V$  is the molecular volume. However, by plotting  $\log D$  vs. carbon number as shown on Figure 1, our results can be correlated at all temperatures by one simple exponential relationship. From the single slope of these parallel lines, we obtained

$$D_n = 1.235D_{n+1} \quad (3)$$

where  $D_n$  is the diffusion coefficient of a given paraffin hydrocarbon at a fixed temperature and  $D_{n+1}$  is the diffusion coefficient of its homolog of next higher molecular weight at the same temperature.

(9) L. Nanis, S. R. Richards, and J. O'M. Bockris, *Rev. Sci. Instr.*, **36**, 673 (1965).

(10) P. L. Antonov, *Geokhim. Metody Poiskov Nefi i Gaz. Mestorozhd. Akad. Nauk SSSR, Tr. Soveshch., Moscow, 1958* (1959).

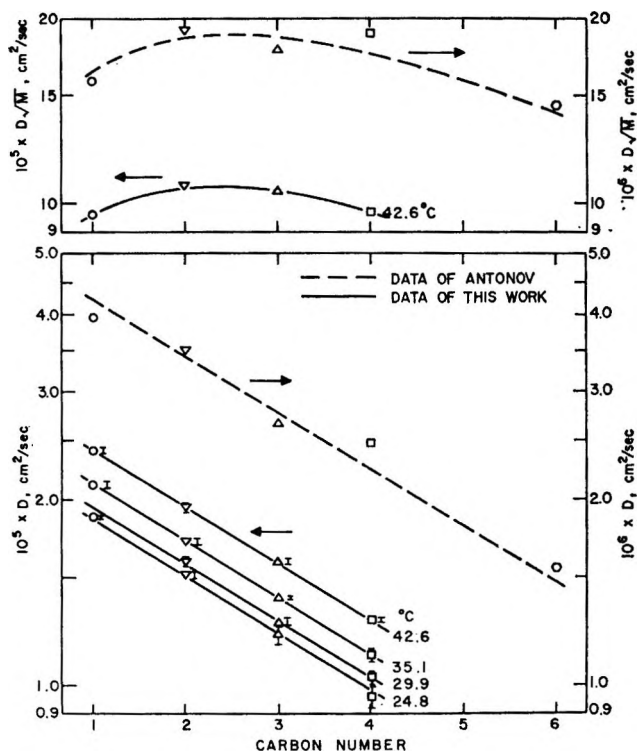


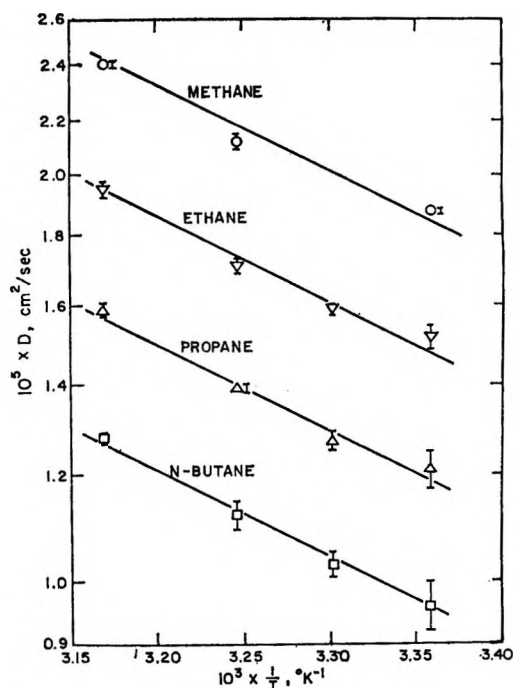
Figure 1. Diffusion data vs. carbon number.

The diffusion coefficients of Antonov are also included on Figure 1, and the same correlation fits his data within  $\pm 6\%$  at all points, except for  $C_4H_{10}$ .

To obtain energies of activation for diffusion, an Arrhenius plot of the data of Table I was made as shown in Figure 2. While there is some indication on this figure that the energy of activation for each hydrocarbon may be changing with temperature, the range in our data ( $18^\circ$ ) is such that a constant value is all that is presently justified.

It is important to note, however, that within the limits of our precision, the activation energies for the diffusion of  $CH_4$ ,  $C_2H_6$ ,  $C_3H_8$ , and  $C_4H_{10}$  all appear to be the same, *viz.*, 2900 cal./mole. Ross and Hildebrand<sup>11</sup> have reported data on the diffusion of  $N_2$ , Ar,  $CH_4$ , and  $CF_4$  gases in  $CCl_4$ , and they also found that the activation energies for all four gases were the same. In two earlier investigations on the self-diffusion of  $CCl_4$ <sup>12</sup> and the diffusion of  $I_2$  in  $CCl_4$ ,<sup>13</sup> the same result was obtained.

In considering the mechanism of diffusion, Hildebrand and co-workers<sup>12-14</sup> have supported the concept that movement by diffusion is a "random-walk" process, wherein the molecules undergo a series of displacements that are small compared to the interatomic spacing. Ross and Hildebrand<sup>11</sup> have recently proposed that, if diffusion is such a process, the relative

Figure 2. Arrhenius plot of  $D$  vs.  $1/T$ .

diffusion of a group of gases in a given liquid should be controlled mainly by molecular cross section. They reported data for  $N_2$ , Ar,  $CH_4$ , and  $CF_4$  gases in  $CCl_4$  and show that the product of the diffusion coefficient and the square of the molecular diameter,  $D\sigma^2$ , is essentially a constant.

To investigate this, collision diameters that were calculated from viscosity data by Flynn and Thodos<sup>15</sup>

**Table II:** Correlation of Diffusion Coefficients with Molecular Diameters

Hydrocarbon	$\sigma, \text{\AA}$	$\sigma, \text{\AA}$	$T = 24.8^\circ$		$T = 42.6^\circ$	
			$D\sigma \times 10^{11}, \text{cm.}^2/\text{sec.}$	$D\sigma^2 \times 10^{21}, \text{cm.}^4/\text{sec.}$	$D\sigma \times 10^{11}, \text{cm.}^2/\text{sec.}$	$D\sigma^2 \times 10^{21}, \text{cm.}^4/\text{sec.}$
Methane	3.808	3.81	7.16	27.2	9.18	35.0
Ethane	4.384	4.52	6.87	30.8	8.81	39.8
Propane	5.240	5.15	6.23	32.0	8.19	42.1
<i>n</i> -Butane	5.869	5.70	5.47	31.7	7.30	41.6

<sup>a</sup> From ref. 15. <sup>b</sup> Smoothed values.

(11) M. Ross and J. H. Hildebrand, *J. Chem. Phys.*, **40**, 2397 (1964).

(12) H. Watts, B. J. Alder, and J. H. Hildebrand, *ibid.*, **23**, 659 (1955).

(13) E. W. Haycock, B. J. Alder, and J. H. Hildebrand, *ibid.*, **21**, 1601 (1953).

(14) J. H. Hildebrand and R. L. Scott, "Regular Solutions," Prentice-Hall, Inc., New York, N. Y., 1962.

(15) L. W. Flynn and G. Thodos, *A.I.Ch.E. J.*, **8**, 362 (1962).

were used to obtain  $D\sigma^2$  as shown in Table II. Since these literature values of  $\sigma$  are not entirely consistent, the data were smoothed so as to agree more closely with the basic relation given by Flynn and Thodos that the collision diameter depends directly on the cube root of the critical volume. The smoothed values were used in obtaining  $D\sigma^2$ , and, for comparison,  $D\sigma$  was also calculated.

The results for  $D\sigma^2$ , while nearer to a constant value than  $D\sigma$ , are not so good as those obtained by Ross and Hildebrand in their work. Apparently, collision diameters that are calculated from viscosity data for a

group of hydrocarbons of increasing chain length are not an adequate measure of the effective cross-sectional area in the diffusion process. Despite these shortcomings, the data of Table II are at least consistent with the findings of Ross and Hildebrand.

*Acknowledgment.* We wish to thank Dr. J. H. Hildebrand for many helpful discussions at various points in this work. Acknowledgment is also made to the donors of the Petroleum Research Fund, administered by the American Chemical Society, for support of this research.

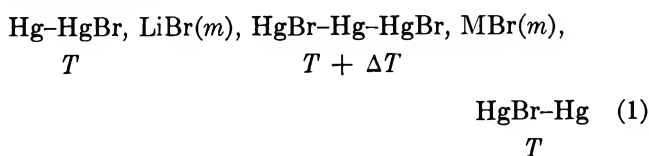
## Relative Determination of Soret Coefficients of Electrolytes. II<sup>1</sup>

by Toshio Ikeda and Mitsuhiro Matsumoto

Department of Chemistry, Shizuoka University, Shizuoka, Japan (Received April 15, 1965)

From the thermoelectric power of a combined thermocell with a common electrode system, the Soret coefficient,  $\sigma$ , was determined for seven uni-univalent electrolytes at 25° and 0.01 *M* upon using lithium bromide as a reference. The results were in fair agreement with the best values reported so far. A very high value resulted for tetraalkylammonium bromides, particularly for *n*-Bu<sub>4</sub>NBr. The results obtained for  $-\sigma \times 10^3 \text{ deg.}^{-1}$  are: 8.39, (0.05), 2.22, 1.64, 0.003, 6.39, 8.34, and 22.94 for HBr, LiBr, NaBr, KBr, NH<sub>4</sub>Br, Me<sub>4</sub>NBr, Et<sub>4</sub>NBr, and *n*-Bu<sub>4</sub>NBr, respectively, taking 0.05 for LiBr.

In the previous paper<sup>1</sup> it was shown that for a number of chlorides, in spite of its simple construction, a combined thermocell is very useful for determining the Soret coefficient of electrolytes to a considerable degree of accuracy. In the present work, the same method as previously used was applied to the bromide series by using the system



where MBr represents a univalent bromide of the same concentration as that of lithium bromide, which was

chosen as a reference substance because it shows a very slight Soret effect. Once the initial thermoelectric power,  $(dE/dT)_0$ , of the cell system (1) is measured, the Soret coefficient of the unknown MBr can be calculated<sup>1</sup> by the equation

$$\sigma^{\text{MBr}} = \frac{t_{\text{Li}^+}^{\text{LiBr}} B^{\text{LiBr}}}{t_{\text{M}^+}^{\text{MBr}} B^{\text{MBr}}} \sigma^{\text{LiBr}} - \frac{F(dE/dT)_0}{2RT t_{\text{M}^+}^{\text{MBr}} B^{\text{MBr}}} - \frac{(\bar{S}_{\text{Br}^-}^{\text{MBr}} - \bar{S}_{\text{Br}^-}^{\text{LiBr}})}{2RT t_{\text{M}^+}^{\text{MBr}} B^{\text{MBr}}} \quad (2)$$

where  $\sigma$  is the Soret coefficient,  $t$  is the ionic transport number for the ion indicated by the subscript corre-

(1) T. Ikeda and H. Kimura, *J. Phys. Chem.*, **69**, 41 (1965).

sponding to the solution phase indicated by the superscript,  $F$  is the Faraday constant,  $T$  is the absolute temperature, and  $B$  is defined by

$$B^{\text{LiBr}} = (1 + d \ln \gamma_{\pm}^{\text{LiBr}} / d \ln m)_{T,P}$$

$$B^{\text{MBr}} = (1 + d \ln \gamma_{\pm}^{\text{MBr}} / d \ln m)_{T,P}$$

where  $\gamma_{\pm}$  is the mean activity coefficient on the molality scale in an  $m$  molal solution.  $\bar{S}_{\text{Br}^-}$  represents the transported molar entropy of the bromide ion in the solution phase. If the solutions are so dilute that the ideal condition is satisfied to a sufficient extent,  $\bar{S}_{\text{Br}^-}^{\text{LiBr}} = \bar{S}_{\text{Br}^-}^{\text{MBr}}$  and the third term on the right-hand side of (2) vanishes. This condition may be fulfilled in the present work.

### Experimental Section

**Materials.** Hydrogen bromide, which was liberated from concentrated hydrobromic acid (Kosô Guaranteed Reagent grade) by the addition of concentrated sulfuric acid drop by drop, was passed through wet red phosphorus to eliminate free bromine and was then led into pure water to make hydrobromic acid.

Ammonium bromide was prepared by neutralizing Kosô Analyzed ammonia water with hydrobromic acid prepared above, followed by several recrystallizations from water.

Lithium, sodium, and potassium bromides and three symmetrical tetraalkylammonium bromides (including methyl, ethyl, and *n*-butyl) were Kosô Guaranteed Reagent grade and were used without further purification.

The water used for the preparation of solutions was distilled from a glass still in the presence of a trace of potassium permanganate acidified with sulfuric acid. The concentration of bromide in solutions was checked and adjusted by titration to 0.01  $M$  within 0.5%. In the case of tetrabutylammonium bromide, the concentration was determined by weighing because titration with silver nitrate was impossible.

Mercury used for electrodes was purified by the usual chemical refinements, followed by distillation *in vacuo*.

Mercurous bromide was prepared by mixing and stirring 200 ml. of a 25% aqueous solution of Kosô Guaranteed potassium bromide with 25 g. of Kosô Guaranteed mercurous nitrate, which was dissolved in 172 g. of water containing 3 g. of pure nitric acid. All of the processes were carried out in a dark room. The mercurous bromide thus precipitated in the mixture was stored as such in the dark and was taken out as needed, filtered, washed well with water, and was used for the preparation of electrodes. Mercurous bromide should not be allowed to dry because, once dry, it will

not exhibit a stable potential when used for the electrodes.

**Preparation of Cell.** Mercurous bromide, which was washed several times with the same electrolyte as that used for measurements, was brought into equilibrium with electrolyte for about 24 hr. in the dark under nitrogen. A portion of the mercurous bromide so treated was taken out and shaken together with a little pure mercury to yield a greenish gray paste. In this case, however, the paste-forming condition is somewhat sensitive compared with the mercury-calomel system: namely, in the presence of too much electrolyte (with the exception of tetra-*n*-butylammonium bromide), the mercurous bromide does not turn into paste but separates into mercury and a colloidal dispersion of mercurous bromide. The tetra-*n*-butylammonium bromide is peculiar since in this solution mercurous bromide can easily form a very stable paste with mercury. The paste was carefully flowed into the H-cell<sup>1</sup> together with the electrolyte to form a layer about 5 to 10 mm. thick on the surface of the electrode mercury, and the cell was then filled with electrolyte. The cell so prepared stood for 2 or 3 days to bring it to a steady state, prior to use for the measurements.

**Temperature and Potentiometry.** Two thermocells, which were filled, respectively, with aqueous solutions of lithium bromide and MBr of the same concentration, 0.01  $M$ , were connected by the legs of two H-cells. These were placed in water thermostated at different temperatures,  $T$  and  $T + \Delta T$ , in two dewar vessels. The terminals of these two thermocells were joined electrically to each other on the side of  $T + \Delta T$ , and the remaining terminals on the side of  $T$  were utilized for measuring e.m.f. Two ways of imposing temperature difference were tried: (i) the temperature was fixed constant at 25° on one side of the two dewar vessels, while it was changed on the other side from about 17 to 33° so as to yield the over-all mean 25°, or, alternatively, (ii) a temperature difference was imposed upon the cell system so as to yield the mean of the higher and lower temperatures of two dewar vessels to be 25°. However, in practice, no appreciable difference could be found between the results found in these two cases. Therefore, either of these two methods could be used. Under moderate agitation of the thermostat water *via* air bubbling, the system attained a thermal equilibrium in about 10 min. The temperature difference between the two dewar vessels was read with calibrated mercury thermometers to an accuracy of 0.05° at the moment at which the e.m.f. of cell system 1 was measured. The e.m.f. was measured with a precision potentiometer (Type P-7, Yokogawa Electric Works, Ltd., for low voltage use with an index of pre-

cision down to  $0.1 \mu\text{v.}$ ) by the aid of a sensitive Yokogawa galvanometer as a zero indicator. Here, the sign convention of e.m.f. of the system (1) refers to the sign of the terminal electrode of MBr on the side of  $T$ .

It is important to take care to minimize any thermal convection occurring in the cell because any convection would give rise to a fluctuation or a gradual change of e.m.f. owing to the production of an extra diffusion potential or an extra thermocell effect which would make it impossible to determine the true e.m.f. It was found that such an unfavorable phenomenon could be reduced effectively by keeping the room temperature at about  $25^\circ$ , near the medium temperature of the cell system. Other detailed factors to be taken into consideration in the experiments were described in a previous paper.<sup>1</sup>

## Results

Measurements were repeated on every possible combination of four or five well-conditioned MBr thermocells with four or five well-conditioned reference Li-

Br thermocells. Some of the typical results are represented in Figure 1. The plots of e.m.f.,  $E$ , against the applied temperature difference,  $\Delta T$ , fell on a straight line with a slope characteristic of the electrolyte, MBr, that was coupled with LiBr. The values of  $(dE/dT)_0$ , determined by the method of least squares, are listed in Table I. The data are reproducible in most cases within a fluctuation of 1 to 3%, except for  $\text{NH}_4\text{Br}$ . In the case of  $\text{NH}_4\text{Br}$ , however, the absolute deviation is rather small.

**Table I:** Soret Coefficients of Bromides in Water at  $25^\circ$  and  $0.01 M$

Bromide	$t_+$	$B^c$	$(dE/dT)_0$ , $\mu\text{v./deg.}$	$-\sigma \times 10^{-3} \text{ deg.}^{-1}$ This work	Obad.
HBr	0.828 <sup>a</sup>	0.959 <sup>d</sup>	$341.4 \pm 4.3$	8.39	...
LiBr	0.3226 <sup>b</sup>	0.962 <sup>e</sup>	...	(0.05)	$0.05^h$
NaBr	0.3853 <sup>b</sup>	0.963 <sup>e</sup>	$41.42 \pm 0.94$	2.22	$2.12^h$
KBr	0.4833 <sup>b</sup>	0.957 <sup>e</sup>	$38.05 \pm 0.86$	1.64	$1.46^h$
$\text{NH}_4\text{Br}$	0.4833 <sup>b</sup>	0.944 <sup>f</sup>	$-0.75 \pm 0.88$	0.003	...
$\text{Me}_4\text{NBr}$	0.3505 <sup>b</sup>	0.949 <sup>g</sup>	$108.3 \pm 2.76$	6.39	...
$\text{Et}_4\text{NBr}$	0.2671 <sup>b</sup>	0.945 <sup>g</sup>	$107.3 \pm 3.07$	8.34	$6.15^i$
$n\text{-Bu}_4\text{NBr}$	0.1617 <sup>b</sup>	0.949 <sup>g</sup>	$180.0 \pm 5.23$	22.94	...

<sup>a</sup> Calculated from the data on ion conductivity: B. E. Conway, "Electrochemical Data," Elsevier Publishing Co., Amsterdam, The Netherlands, 1952. <sup>b</sup> J. C. Goodrich, F. M. Goyan, E. E. Morse, R. G. Preston, and M. B. Young, *J. Am. Chem. Soc.*, **72**, 4411 (1950). <sup>c</sup> Graphical determination. <sup>d</sup> H. B. Haltzer, R. A. Robinson, and R. G. Bates, *J. Phys. Chem.*, **66**, 1423 (1962). <sup>e</sup> "Physikalischen Chemischen Tabellen," Landolt-Börnstein, Erg. Bd. II, 1931, and III, 1936. <sup>f</sup> G. Scatchard and S. S. Prentis, *J. Am. Chem. Soc.*, **54**, 2696 (1932). Original values at  $0^\circ$  were adjusted to  $25^\circ$  values by the aid of the Debye-Hückel equation. <sup>g</sup> S. Lindenbaum and G. E. Boyd, *J. Phys. Chem.*, **68**, 911 (1964). Values for the concentration below  $0.1 M$  were estimated by extrapolation. <sup>h</sup> Values of ref. 2 were corrected to  $25^\circ$ . <sup>i</sup> J. Chapman and H. J. V. Tyrrell, *J. Chem. Soc.*, 2142 (1957).

The Soret coefficient of LiBr, which was used as a reference in the present work, was assumed to be  $-0.05 \times 10^{-3} \text{ deg.}^{-1}$ , which was obtained by adjusting the Snowdon and Turner value<sup>2</sup> of  $-0.08 \times 10^{-3} \text{ deg.}^{-1}$  at  $25.3^\circ$  and  $0.01 M$  to the  $25^\circ$  value. Using this value and our data on  $(dE/dT)_0$ , the relative values of the Soret coefficient,  $\sigma^{\text{MBr}}$ , at  $25^\circ$  and  $0.01 M$  were determined by the aid of (2) taking  $\bar{S}_{\text{Br}^-}^{\text{MBr}} = \bar{S}_{\text{Br}^-}^{\text{LiBr}}$ . The results are compared with Snowdon and Turner's values<sup>2</sup> in Table I and are found to be in fair agreement with each other.

(2) P. N. Snowdon and J. C. R. Turner, *Trans. Faraday Soc.*, **56**, 1409 (1960).

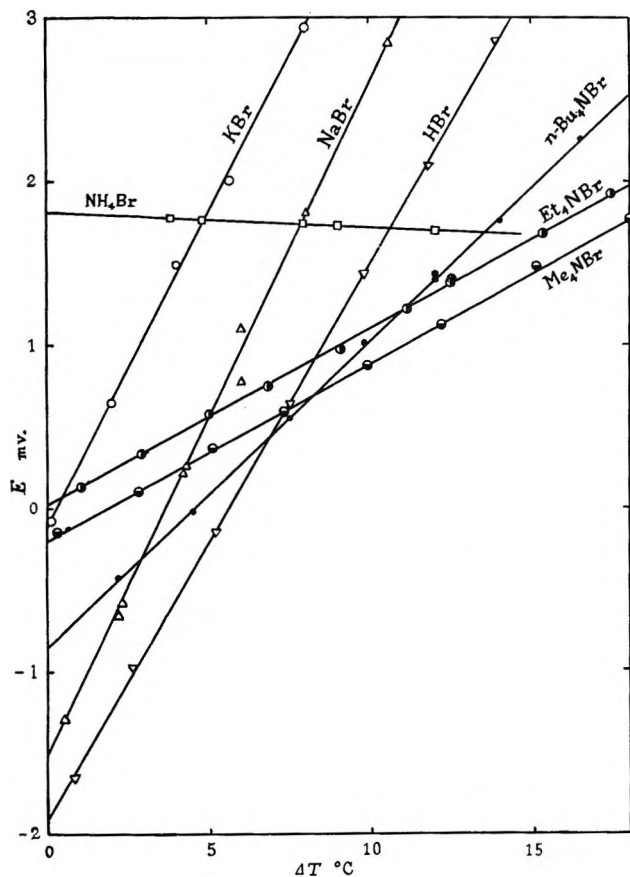


Figure 1. Plot of e.m.f. of combined thermocells of type 1 at  $m = 0.01 M$  and around the mean temperature  $25^\circ$ ,  $\Delta T$ , the temperature difference; e.m.f. scale for NaBr, KBr, and  $\text{NH}_4\text{Br}$  is one-tenth of the  $E$  scale indicated.

## Discussion

The Soret coefficients of tetraalkylammonium bromides, except for tetraethylammonium bromide, had not yet been determined by the direct method. By using the similar principle on thermocell data, Chapman and Tyrrell<sup>3</sup> estimated the Soret coefficients for tetramethyl-, tetraethyl-, and tetra-*n*-butylammonium bromides to be approximately  $-6 \times 10^{-3}$ ,  $-10 \times 10^{-3}$ , and  $-17 \times 10^{-3} \text{ deg.}^{-1}$ , respectively, at 25° and 0.01 *M*. One of the present writers<sup>4</sup> has predicted from the transported entropy of the bromide ion the following values:  $-5.78 \times 10^{-3}$ ,  $-9.65 \times 10^{-3}$ , and  $-16.3 \times 10^{-3} \text{ deg.}^{-1}$  for  $\text{Me}_4\text{NBr}$ ,  $\text{Et}_4\text{NBr}$ , and *n*- $\text{Bu}_4\text{NBr}$ , respectively, at 25° and 0.01 *M*. In the present work, also, a very high Soret coefficient was found for tetraalkylammonium bromides, particularly for tetrabutylammonium bromide. This is in contrast to ammonium bromide, which exhibited a near-zero Soret coefficient. This might be related to the anomalous property of the partial molar heat capacity of the tetrabutylammonium bromide in aqueous solution.<sup>5</sup>

According to the Helfand and Kirkwood theory<sup>6</sup> on the ionic heat of transfer, the transported entropy,  $\bar{S}_k$ , of an ion species *k* cannot be independent of its counterion; hence, in general, it should be  $\bar{S}_{\text{Br}^-}^{\text{MBr}} \neq \bar{S}_{\text{Br}^-}^{\text{LiBr}}$ . However, in the case where solutions are so dilute that ideal conditions are nearly satisfied and also in the case where the bromide ion and its counterion in a solution are similar in valence type and size, one may be allowed approximately to take  $\bar{S}_{\text{Br}^-}^{\text{MBr}} - \bar{S}_{\text{Br}^-}^{\text{LiBr}} = 0$ . This allowance seems not to be applicable to the tetraalkylammonium bromides. These are different from other simple salts in that they are characterized by a large difference in ionic size<sup>7</sup> and by a dissimilarity in the single-ion activity coefficients between conjugate ions, as judged from the analogous properties of  $\text{R}_4\text{NI}$ .<sup>8</sup> Such an anomalous property of tetraalkylammonium bromides should introduce a considerable difference between  $\bar{S}_{\text{Br}^-}^{\text{R}_4\text{NBr}}$  and  $\bar{S}_{\text{Br}^-}^{\text{LiBr}}$ , at least in the ion entropy term by a factor of  $\{R\partial[T \ln(\gamma_{\text{Br}^-}^{\text{R}_4\text{NBr}}/\gamma_{\text{Br}^-}^{\text{LiBr}})]/\partial T\}$ , where  $\gamma_{\text{Br}^-}^{\text{R}_4\text{NBr}}$  and  $\gamma_{\text{Br}^-}^{\text{LiBr}}$  represent the single-ion activity coefficients of the bromide ion in the solution phases of  $\text{R}_4\text{NBr}$  and  $\text{LiBr}$ , respectively. This contribution should be considerable, affecting largely the  $\sigma$  value calculable from (2), whereas the

Soret coefficient of tetraethylammonium bromide, calculated from (2) by taking  $\bar{S}_{\text{Br}^-}^{\text{Et}_4\text{NBr}} = \bar{S}_{\text{Br}^-}^{\text{LiBr}}$ , was found to be  $-8.34 \times 10^{-3} \text{ deg.}^{-1}$  at 25° and 0.01 *M*, which is somewhat lower than the value of  $-6.15 \times 10^{-3} \text{ deg.}^{-1}$  determined by Agar<sup>3</sup> by the direct method. The difference between these two values corresponds to  $\bar{S}_{\text{Br}^-}^{\text{Et}_4\text{NBr}} - \bar{S}_{\text{Br}^-}^{\text{LiBr}} = -0.66 \text{ cal./deg. mole}$ ; in other words,  $\bar{S}_{\text{Br}^-}^{\text{LiBr}}$  is higher than  $\bar{S}_{\text{Br}^-}^{\text{Et}_4\text{NBr}}$  by 0.66 e.u. On the other hand, Snowdon and Turner<sup>2</sup> have found the Soret coefficient of tetraethylammonium chloride to be  $-8.41 \times 10^{-3} \text{ deg.}^{-1}$  at 25.3° and 0.01 *M*, which may be reduced to  $-8.38 \times 10^{-3} \text{ deg.}^{-1}$  at 25°. Now we have evidence that<sup>2</sup> the chlorides and bromides, when they have a common cation, will display very close Soret coefficients, being a bit higher for the chloride than for the bromide by about  $0.05 \times 10^{-3} \text{ deg.}^{-1}$ . Hence, it may be reasonable to assume that tetraethylammonium bromide has a Soret coefficient nearly as large as that of tetraethylammonium chloride, say *ca.*  $-8.4 \times 10^{-3} \text{ deg.}^{-1}$ , at 25° and 0.01 *M*. The value of  $-6.15 \times 10^{-3} \text{ deg.}^{-1}$  observed by Agar<sup>3</sup> at 25° and 0.01 *M* seems to be rather low (in the absolute value). If tetraethylammonium bromide had the Soret coefficient of  $-8.4 \times 10^{-3} \text{ deg.}^{-1}$ , we see that our value of  $-8.34 \times 10^{-3} \text{ deg.}^{-1}$  agrees with this estimation. This consequence should lead directly to the conclusion that  $\bar{S}_{\text{Br}^-}^{\text{Et}_4\text{NBr}} = \bar{S}_{\text{Br}^-}^{\text{LiBr}}$ . This conclusion, if it were true, proves in the reverse sense that the condition  $\bar{S}_{\text{Br}^-}^{\text{Et}_4\text{NBr}} = \bar{S}_{\text{Br}^-}^{\text{LiBr}}$  holds practically in the case of tetraethylammonium bromide. This is a surprising fact when one reflects upon the argument made above. However, for lack of the necessary data, nothing can be said at present whether such an approximation,  $\bar{S}_{\text{Br}^-}^{\text{R}_4\text{NBr}} = \bar{S}_{\text{Br}^-}^{\text{LiBr}}$ , is allowable or not for other higher members of  $\text{R}_4\text{NBr}$  beyond  $\text{Et}_4\text{NBr}$ . More accurate data on the Soret coefficient of  $\text{R}_4\text{NBr}$  are being determined by the direct method.

(3) J. Chapman and H. J. V. Tyrrell, *J. Chem. Soc.*, 2142 (1957).

(4) T. Ikeda, *Rep. Liberal Arts Sci. Fac. Shizuoka Univ., Nat. Sci.*, 2, 153 (1959); *cf.* T. Ikeda, *J. Chem. Phys.*, 30, 345 (1959).

(5) H. S. Frank and W. Y. Wen, *Discussions Faraday Soc.*, 24, 133 (1957).

(6) E. Helfand and J. G. Kirkwood, *J. Chem. Phys.*, 32, 857 (1960).

(7) W. Y. Wen and S. Saito, *J. Phys. Chem.*, 68, 2639 (1964).

(8) H. S. Frank, *ibid.*, 67, 1554 (1963).



# Thermochemical Studies. XV.<sup>1</sup> Thermodynamics of Protonation of Triethylenediamine, Triethylamine, Trimethylamine, and Ammonia in Aqueous Solution at 25°

by Piero Paoletti, John H. Stern,<sup>2</sup> and Alberto Vacca

*Istituto di Chimica Generale, Università, Florence, Italy (Received April 19, 1965)*

Thermodynamic functions of protonation  $\Delta F$ ,  $\Delta H$ , and  $\Delta S$  were determined *via* e.m.f. and calorimetric methods for triethylenediamine, triethylamine, trimethylamine, and ammonia. Correlations for the above series, as well as for other related amines in terms of ion-solvent interactions and amine type, were also made.

## Introduction

Previous communications in this series<sup>3,4</sup> have dealt with the thermodynamics of stepwise protonation of several amines (B):  $B + xH^+ = BH_x^{x+}$  ( $x = 1, 2, 3, \dots$ ). Direct reaction calorimetry and e.m.f. measurements have yielded  $\Delta H$  and  $\Delta F$ , respectively. The entropy of protonation  $\Delta S$  was calculated from the above properties. This contribution describes an analogous determination of thermodynamic functions of protonation for a series of related amine bases in aqueous solution at 25°. The series consists of triethylenediamine,  $N(CH_2-CH_2)_3N$ , triethylamine, trimethylamine, and ammonia. Very few thermodynamic data are available for triethylenediamine. Studies on this globular molecule include determination of the heat capacity, heats of fusion, and transition of the pure solid,<sup>5</sup> and the basicity constants<sup>6</sup> in aqueous solution.

Triethylamine and trimethylamine were studied to provide a basis for thermodynamic comparison, particularly for the first protonation step of the diamine. The values of  $\Delta H$  are believed to be the first obtained calorimetrically. Calculated values of  $\Delta H$ <sup>7,8</sup> have been reported by others from e.m.f. measurements, but this method has in many cases led to heats of much lower accuracy than those determined directly. Finally, the thermodynamics of protonation of ammonia were included in this study since a direct calorimetric determination of this important reaction seemed advisable.<sup>9</sup> The observed differences in these thermo-

dynamic properties provide an interesting insight on weak base-strong acid behavior, particularly from the standpoint of solute-solvent interactions, type of amine, molecular structure, and their effects on protonation. Analogous studies have been reported by others on weak acid-strong base behavior.<sup>10</sup>

## Experimental Section

**Materials.** Pure triethylenediamine was obtained as a gift from the Houdry Co. and repurified by vacuum sublimation. Solutions were prepared by weight, with carbon dioxide free water. The concentration was further checked by titrating the amine with standard hydrochloric acid. Triethylamine, trimethyl-

- (1) Part XIV: P. Paoletti, *Trans. Faraday Soc.*, **61**, 219 (1965).
- (2) International Faculty Fellow (1964-1965), American Chemical Society Petroleum Research Fund.
- (3) (a) L. Sacconi, P. Paoletti, and M. Ciampolini, *J. Am. Chem. Soc.*, **82**, 3831 (1960); (b) M. Ciampolini and P. Paoletti, *J. Phys. Chem.*, **65**, 1224 (1961); (c) P. Paoletti, M. Ciampolini, and A. Vacca, *ibid.*, **67**, 1065 (1963).
- (4) (a) P. Paoletti and M. Ciampolini, *Ric. Sci.*, **33** (II-A), 405 (1963); (b) P. Paoletti and A. Vacca, *J. Chem. Soc.*, 5051 (1964).
- (5) J. C. Trowbridge and E. F. Westrum, Jr., *J. Phys. Chem.*, **67**, 2381 (1963).
- (6) G. Schwarzenbach, B. Maissen, and H. Ackermann, *Helv. Chim. Acta*, **35**, 2333 (1952).
- (7) D. H. Everett and W. F. K. Wynne-Jones, *Trans. Faraday Soc.*, **35**, 1380 (1939).
- (8) W. S. Fyfe, *J. Chem. Soc.*, 1347 (1955).
- (9) E. J. King, "Acid-Base Equilibria," Pergamon Press, Ltd., London, 1965, p. 197.
- (10) (a) L. P. Fernandez and L. G. Hepler, *J. Am. Chem. Soc.*, **81**, 1783 (1959); (b) L. G. Hepler, *ibid.*, **85**, 3089 (1963).

amine, and ammonia were all prepared from A.R. grade stock solutions and their concentrations determined *via* titration with standard acid. The purity of all solutions of the three organic amines was examined by vapor-liquid chromatography. Hydrochloric acid was standardized gravimetrically as silver chloride. Carbon dioxide free solutions of potassium hydroxide, used in e.m.f. measurements, were kept in Jena-glass flasks.

**Calorimetric Measurements.** The calorimeter<sup>11</sup> and details of experimental measurements<sup>3</sup> at 25° have been described elsewhere. The estimated over-all experimental accuracy was  $\pm 0.6\%$ . The ionic medium was 0.1 *N* KCl and the concentration of protonated amines ranged from approximately 1.5 to  $3 \times 10^{-2}$  *M*.

**E.m.f. Measurements.** The potentiometric experiments were performed with a Radiometer PHM 4 potentiometer using a glass electrode (Radiometer G 2025/B), a 0.1 *M* calomel electrode, and a bridge filled with 0.1 *M* KCl solution. All titrations were carried out in a 150-ml. seven-necked flask while the solution was stirred continuously by a magnetic stirrer. Argon was bubbled through the solution which contained 0.1 *N* KCl, and the cell assembly was thermostated at  $25.0 \pm 0.1^\circ$ . In each determination 100 ml. of a solution of 0.002 *M* amine hydrochloride was titrated with varying volumes of 0.1 *M* KOH added by a piston buret graduated to 0.01 ml. The titer of the KOH solution was checked daily against standard HCl. The hydrogen ion concentrations were calculated from the experimental e.m.f. values, using the formula

$$[\text{H}^+] = \text{antilog} [(E - E_0)/59.154]$$

The standard potential of the electrode system,  $E_0$ , was determined from the experimental e.m.f. values. These were obtained during the titration of a solution of 0.001 *M* HCl (in 0.1 *M* KCl), with 0.1 *M* KOH, either in the acidic or basic region. This determination was carried out before and after each basicity constant experiment, and the observed variation in  $E_0$  was found to be negligible (less than 0.3 mv.) in all measurements.

Each neutralization curve was drawn from at least 20 experimental points. A minimum of 12 points and three curves was used to calculate the basicity constant. The agreement between the observed e.m.f. values and those calculated on the basis of the computed equilibrium constants was excellent. A representative sample of the data for triethylamine follows:  $[\text{Et}_3\text{N}\cdot\text{HCl}]_{\text{initial}} = 1.868 \times 10^{-3}$  *M*;  $V_{\text{initial}} = 100.3$  ml.; volume of 0.1456 *M* KOH added: 0.40, 0.60, 0.80, 1.00 ml.; e.m.f. (calcd.) =  $-311.4, -324.2,$

$-333.1, -340.4$  mv.; e.m.f. (obsd.) =  $-311.9, -324.2, -332.9, -340.2$  mv.;  $E_0 = 287.5$  mv.

## Results

The two-step heats of protonation of triethylenediamine were determined by measuring the heats evolved for different amine-HCl ratios and by calculating the exact amounts of mono- and diprotonated forms of the polyamines before and after the reaction. The calorimetric measurements for triethylamine, trimethylamine, and ammonia were carried out with a slight excess of amine in the dewar. All heats were corrected for the side reaction  $\text{H}^+ + \text{OH}^- = \text{H}_2\text{O}$ , where  $\text{OH}^-$  results from the hydrolysis of the amine in aqueous solution. The heat of formation of water chosen for the correction was 13.34 kcal./mole, which is the consensus of the most reliable recent determinations.<sup>12</sup> In all cases the net correction applied to the calorimetric results was very small. The concentrations of all species present in the calorimeter before and after the HCl addition were calculated by solving the following system of equations *via* successive approximation

$$[\text{acid}]_{\text{total}} = [\text{H}^+] - [\text{OH}^-] + \sum_{j=1}^m j k_j [\text{H}^+]^j [\text{L}]$$

$$[\text{amine}]_{\text{total}} = [\text{L}] + \sum_{j=1}^m k_j [\text{H}^+]^j [\text{L}]$$

$$[\text{OH}^-] = k_w [\text{H}^+]^{-1}$$

$$[\text{H}_j\text{L}^{j+}] = k_j [\text{H}^+]^j [\text{L}]$$

[L] is the free amine concentration,  $j$  is the number of protons with a maximum of  $m$  in the protonated amine  $\text{H}_j\text{L}^{j+}$  with a formation constant  $k_j$ .  $k_w$  is the dissociation constant of water in 0.1 *M* KCl ( $1.62 \times 10^{-14}$ ).<sup>13</sup> This procedure follows the method of Schwarzenbach<sup>14</sup> and others.<sup>15</sup>

Appropriate programs were written for the IBM 1620 computer to perform the following calculations: (a) least-square determination of basicity constants from the e.m.f. data, (b) equilibrium distribution of all species before and after the reaction in the calorim-

(11) P. Paoletti, R. Usenza, and A. Vacca, *Ric. Sci.*, **35** (II-A), 201 (1965).

(12) (a) J. D. Hale, R. M. Izatt, and J. J. Christensen, *J. Phys. Chem.*, **67**, 2605 (1963); (b) C. E. Vanderzee and J. A. Swanson, *ibid.*, **67**, 2608 (1963); (c) L. Sacconi, P. Paoletti, and M. Ciampolini, *Ric. Sci.*, **29**, 2412 (1959).

(13) H. S. Harned and B. B. Owen, "The Physical Chemistry of Electrolytic Solutions," 3rd Ed., Reinhold Publishing Corp., New York, N. Y., 1958, p. 762.

(14) G. Schwarzenbach, *Helv. Chim. Acta*, **33**, 947 (1950).

(15) M. J. L. Tillotson and L. A. K. Staveley, *J. Chem. Soc.*, 3613 (1958).

eter, (3) least-square determination of the heats of protonation together with appropriate standard deviations. Table I shows a summary of all calorimetric measurements. The third column shows the heat evolved in each run,  $Q$ , corrected for the heat of dilution of HCl. The last column reports the calculated hydrolysis corrections,  $Q_c$ .

Table II shows the values of the thermodynamic functions  $\Delta F$ ,  $\Delta H$ , and  $\Delta S$  for all protonations. Values of basicity constants for triethylenediamine reported in ref. 6, measured at 20° and in a different ionic medium, are in poor agreement with present results. The values of ref. 8 for the indirectly determined  $\Delta H$  and  $\Delta S$  of triethylamine are also in disagreement with this work. All three thermodynamic variables previously determined for trimethylamine<sup>7</sup> and ammonia,<sup>9</sup> however, are in excellent agreement with the data of Table II.

**Table I:** Calorimetric Data for the Systems Amine + HCl

Base	Base, mmoles	HCl, mmoles	$Q$ , cal.	$Q_c$ , <sup>a</sup> cal.
Triethylenediamine (165 ml.)	4.974	4.822	35.75	1.33
	4.980	4.825	35.75	1.34
	4.995	4.833	35.83	1.34
	4.985	4.824	35.95	1.34
	2.412	4.827	23.55	0.93
	2.412	4.824	23.55	0.93
	2.422	4.855	23.70	0.93
Triethylamine (165 ml.)	5.22	4.697	51.23	10.65
	5.22	4.687	50.95	10.68
	5.22	4.605	50.00	10.64
	5.22	4.645	50.75	10.66
Trimethylamine (165 ml.)	4.35	3.969	36.32	3.45
	4.35	3.968	36.21	3.45
	4.35	3.918	35.95	3.45
Ammonia (165 ml.)	4.22	3.554	44.01	1.99
	4.22	3.557	44.63	1.99
	4.22	3.551	43.80	1.99
	3.99	3.583	44.74	1.89
	3.99	3.623	45.34	1.89
	3.99	3.564	44.90	1.89

<sup>a</sup> This term is subtracted from the corresponding  $Q$  value to yield the net heat of protonation.

## Discussion

We shall discuss the heat of protonation of triethylenediamine in relation to other similar amines whose thermodynamic properties have been reported previously.

It may be observed that  $-\Delta H_1$  of this compound is lower than that of any other similar diamine. For example, one may consider the related series ethylenediamine,<sup>16</sup>  $H_2N-CH_2-CH_2-NH_2$ , piperazine,<sup>3c</sup>  $HN-(CH_2-CH_2)_2NH$ , and triethylenediamine, where each of the molecules contains the basic chain  $N-CH_2-CH_2-N$ . The values of  $\Delta H_1$  are  $-11.91$ ,  $-10.17$ , and  $-7.30$  kcal./mole, respectively. Triethylenediamine is a tertiary amine, and heats of protonation of these are generally lower than those of primary and secondary amines; thus, this result is not unexpected. One may compare in this context the series methylamine,<sup>7</sup> dimethylamine,<sup>7</sup> and trimethylamine, whose heats of protonation are  $-13.09$ ,  $-11.88$ , and  $-8.86$  kcal./mole, respectively.

In the tertiary amine series triethylamine, trimethylamine, and triethylenediamine, the inductive effect and  $-\Delta H_1$  decrease in the given order. The value of  $\Delta S_1$  is approximately equal in all three cases, and it is likely to be due mainly to solvent-ion and solvent-molecule interactions, *i.e.*, external effects,<sup>10b</sup> which do not change appreciably during the protonations of the above amines. Thus, the diminution of enthalpy corresponds to a decrease in the strength of the N-H bond formed.

The differences in the enthalpy of protonation between methylamine<sup>7</sup> and trimethylamine and between ethylenediamine<sup>16</sup> and triethylenediamine are 4.3 and 4.9 kcal./mole, respectively; *i.e.*, the differences are approximately equal in both pairs of amines. If internal strain changed significantly during the protonation of triethylenediamine, the differences should certainly be larger than those observed. We may thus conclude that changes in internal strain are not likely to be among the major contributing factors in the observed enthalpy lowering of triethylenediamine.

The decrease in  $-\Delta H_2$  with respect to  $-\Delta H_1$  for triethylenediamine is in part a consequence of the electrostatic repulsion between the two charged ammonium groups. Repulsion also explains the diminution of  $-\Delta H_{1-2}$  for the series ethylenediamine  $\cdot H_2^{2+}$ , piperazine  $\cdot H_2^{2+}$ , and triethylenediamine  $\cdot H_2^{2+}$  as the distance between the two nitrogens decreases from 3.9 through 2.9 to 2.5 Å. in the above order of amines.<sup>17</sup> It is clear that the two charges of the diprotonated diamines are not sufficiently separated from each other to behave as single charges. These charge fields overlap in accord with the observed lowering of  $-\Delta H_{1-2}$ .

(16) T. Davies, S. S. Singer, and L. A. K. Staveley, *J. Chem. Soc.*, 2304 (1954).

(17) Calculated from standard crystallographic distances and angles.

**Table II:** Thermodynamic Functions of Protonation in 0.1 M KCl at 25°: Triethylenediamine (Dabco), Triethylamine, Trimethylamine, and Ammonia<sup>a</sup>

	$pK_b$	$-\Delta F$ , kcal./mole	$-\Delta H$ , kcal./mole	$\Delta S$ , e.u.
$\text{Dabco} + \text{H}^+ \rightleftharpoons \text{DabcoH}^+$	$8.82 \pm 0.01$	12.03	$7.30 \pm 0.01$	$15.9 \pm 0.05$
$\text{Dabco} + 2\text{H}^+ \rightleftharpoons \text{DabcoH}_2^{2+}$	$11.79 \pm 0.02$	16.09	$10.31 \pm 0.03$	$19.4 \pm 0.2$
$\text{Et}_3\text{N} + \text{H}^+ \rightleftharpoons \text{Et}_3\text{NH}^+$	$10.75 \pm 0.01$	14.66	$10.38 \pm 0.03$	$14.4 \pm 0.2$
$\text{Me}_3\text{N} + \text{H}^+ \rightleftharpoons \text{Me}_3\text{NH}^+$	$9.79 \pm 0.01$	13.36	$8.86 \pm 0.02$	$15.1 \pm 0.2$
$\text{NH}_3 + \text{H}^+ \rightleftharpoons \text{NH}_4^+$	$9.29 \pm 0.02$	12.67	$12.43 \pm 0.10$	$0.8 \pm 0.4$

<sup>a</sup> Uncertainty intervals associated with all values are standard deviations.

The total entropies of protonation are positive for all amines under discussion. This may be attributed to a net release of water molecules during the protonation. Certain trends as a function of amine order may also be observed. For example, the series ammonia, methylamine,<sup>7</sup> dimethylamine,<sup>7</sup> and trimethylamine has entropies of protonation which increase regularly by approximately 5 e.u. in the above order. The values of  $\Delta S_1$  as well as their differences are similar in the diamine series ethylenediamine, piperazine, and triethylenediamine.

The second-step protonation entropy  $\Delta S_2$  in the series ethylenediamine, piperazine, and triethylenediamine is lower than  $\Delta S_1$ . This is in accord with the interpretation of Everett and Pinsent<sup>18</sup> that the extent of hydration of a short-chain diammonium ion is more than twice that of a singly charged monoammonium ion.

The observed trends of  $\Delta S_2$  in the above series may be explained by the following argument: the diprotonated forms of the amines become more rigid as a

result of the repulsion between the two like charges. The structure stiffening<sup>18</sup> relative to the unprotonated forms decreases from the chainlike ethylenediamine, through the cyclic piperazine, to the globular triethylenediamine. The last compound is already constrained to a rigid form prior to protonation. Low-lying vibrational states which normally contribute significantly to the free amine energy are raised as a consequence of the stiffening, to such an extent that their contribution to the entropy diminishes. This relative effect also decreases in the above order of amines.

*Acknowledgments.* The authors wish to thank Professor L. Sacconi for encouragement of this work and the Italian Consiglio Nazionale delle Ricerche and the American Chemical Society Petroleum Research Fund for financial assistance.

(18) D. H. Everett and B. R. W. Pinsent, *Proc. Roy. Soc. (London)*, **A215**, 416 (1952).

# Formation Constants of Silver(I) Cyanide Complexes in Equimolar Sodium-Potassium Nitrate Melts<sup>1</sup>

by H. Ti Tien

Department of Chemistry, Northeastern University, Boston 15, Massachusetts (Received April 19, 1965)

Using a gallium-filled silica glass reference electrode in conjunction with a silver electrode, the behavior of silver(I) in fused equimolar sodium-potassium nitrate in the presence of cyanide ions was studied potentiometrically. The change of e.m.f. of the cell before precipitation of silver cyanide is ascribed to the formation of complex ions in the melt. The species formed were assumed to be  $\text{Ag}^+\text{-CN}^-$  and  $\text{Ag}(\text{CN})_2^-$ . The formation constants thus obtained for  $\text{Ag}^+\text{-CN}^-$  and  $\text{Ag}(\text{CN})_2^-$  are, respectively,  $1.1 \times 10^4$  and  $1.1 \times 10^8$  in molarity units at 521°K. The discrepancy of formation constants for  $\text{Ag}(\text{CN})_2^-$  between those previously reported and the one given here is pointed out. The use of gallium-filled glass reference electrodes in fused salt systems at high temperatures is briefly mentioned.

## Introduction

Formation constants of Ag(I) and cyanide ions in fused equimolar sodium nitrate-potassium nitrate mixtures were reported recently by Manning and Blander.<sup>2</sup> They evaluated the formation constants for  $\text{AgCN}$ ,  $\text{Ag}(\text{CN})_2^-$ , and  $\text{Ag}_2\text{CN}^+$  from the analysis of e.m.f. changes in concentration cells. Manning and Blander were apparently the first to report the formation constant of  $\text{AgCN}$  in any medium. The formation constant for  $\text{Ag}(\text{CN})_2^-$  given by Manning and Blander is  $3.1 \times 10^{10}$  in mole fraction units at 246° which is in excellent agreement with the value given by Jordan and Pendergrast.<sup>3</sup> Previously, Flengas and Rideal<sup>4</sup> using a similar type of concentration cell (and under essentially identical conditions) carried out electro-metric titration of Ag(I) with potassium cyanide. The formation constant for  $\text{Ag}(\text{CN})_2^-$  reported by Flengas and Rideal is  $8.5 \times 10^{12}$  in mole fraction units at 250°. In view of the large discrepancy between the reported values for  $\text{Ag}(\text{CN})_2^-$ , the present study was initiated. The purpose of this study, in addition to re-evaluating the formation constants of silver(I) cyanide complexes, was to demonstrate the applicability of the glass reference electrode to studies of this nature.<sup>5-7</sup>

## Experimental Section

All reagent grade chemicals were used without further purification other than oven drying at 150° when-

ever feasible. The electrolytic cell assembly, furnace, and general procedure were essentially the same as described previously<sup>6</sup> with minor changes noted below. A larger crucible furnace (Type M-506, Hevi-Duty Electric Co., Milwaukee, Wis.) was used. The temperature of the furnace was controlled by a Wheelco temperature regulator. Instead of using a Hg-filled Pyrex glass reference electrode, the reference electrode was constructed with Vycor glass and filled with gallium. The advantage of a Ga-filled Vycor glass electrode permits measurements at much higher temperatures. The construction of the gallium-filled glass reference electrode was essentially the same as previously reported.<sup>5</sup> Instead of using platinum or tungsten wire to establish electrical contact, carbon rods had to be used since metal wires were rapidly attacked at elevated temperatures. Additions of  $\text{AgNO}_3$  and  $\text{NaCN}$  to the melts were made using a slightly modi-

(1) Presented at the 149th National Meeting of the American Chemical Society, Detroit, Mich., April 4-9, 1965.

(2) D. L. Manning and M. Blander, *Inorg. Chem.*, **1**, 594 (1962).

(3) J. Jordan and J. Pendergrast, Proceedings of the 7th International Conference on Coordination Chemistry, Stockholm, 1962, p. 102.

(4) S. N. Flengas and E. Rideal, *Proc. Roy. Soc. (London)*, **A233**, 443 (1956).

(5) G. W. Harrington and H. T. Tien, *J. Phys. Chem.*, **66**, 173 (1962).

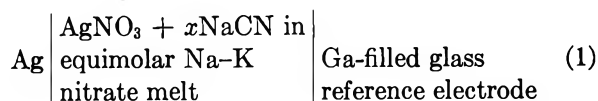
(6) H. T. Tien and G. W. Harrington, *Inorg. Chem.*, **2**, 369 (1963).

(7) H. T. Tien, *Anal. Chem.*, **36**, 929 (1964).

fied technique<sup>1</sup> since very small amounts of  $\text{AgNO}_3$  and  $\text{NaCN}$  introduced to the melt made direct weighing difficult. Fused solutions of equimolar  $\text{NaNO}_3$ - $\text{KNO}_3$  mixture containing known quantities of either reagent grade  $\text{AgNO}_3$  or  $\text{NaCN}$  were first prepared. Small portions of these fused solutions in the form of beads were allowed to solidify on watch glasses. These beads, containing a known amount of the solute, were stored in a desiccator until used.

### Results and Discussion

The cell used in the present study differs from those used in previous work in that the glass reference electrode replaced half of the concentration cell, which may be represented as



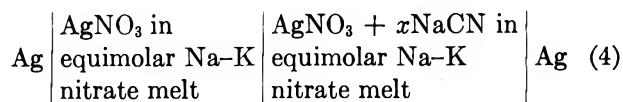
The e.m.f. of the cell is given by a modified Nernst equation

$$E_1 = E' - \frac{RT}{F} \ln C_{\text{Ag}} \quad (2)$$

in the absence of cyanide ions (*i.e.*,  $x = 0$ ) and

$$E_2 = E' - \frac{RT}{F} \ln [\text{Ag}^+] \quad (3)$$

in the presence of cyanide ions. Hence,  $\Delta E$  is the e.m.f. change of the following hypothetical cell



The e.m.f. change for the hypothetical cell is therefore given by

$$\Delta E = -\frac{RT}{F} \ln \frac{C_{\text{Ag}}}{[\text{Ag}^+]} \quad (5)$$

The results of the measurements for typical runs at  $248^\circ$  with initial silver(I) ion concentrations at  $2.76 \times 10^{-5}$  (circles),  $3.52 \times 10^{-5}$  (crossed circles), and  $4.23 \times 10^{-5}$  in molarity units are shown in Figure 1. The use of molarity is a matter of convenience since the present data will be discussed in terms of Bjerrum's ion association theory.<sup>8</sup> Assuming that the change of e.m.f. of the cell (4) as a function of the added cyanide ions is due to complex ion formation, the over-all formation constants are calculated according to a modification of the mathematical treatment developed by Bjerrum and Leden.<sup>9</sup>

The results of these calculations and the graphical

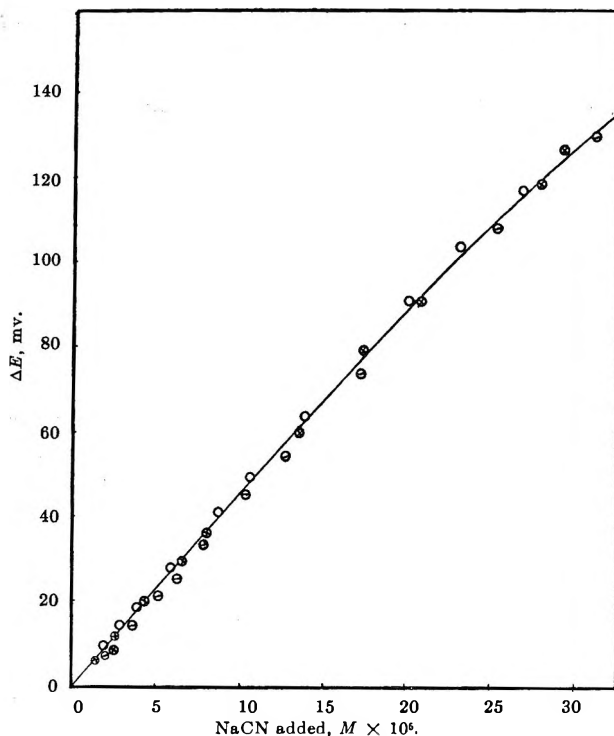


Figure 1. Variation of cell potential with concentration of  $\text{NaCN}$ .

extrapolations are presented, respectively, in Table I and Figure 2. The extrapolated formation constants for  $\text{AgCN}$  ( $\beta_1$ ) and  $\text{Ag}(\text{CN})_2^-$  ( $\beta_2$ ) are, respectively,  $1.1 \pm 0.1 \times 10^4$  and  $1.1 \pm 0.3 \times 10^8$  in molarity units. The values obtained in this study are in good agreement with the formation constants reported by Manning and Blander and by Jordan and Pendergrast. The formation constant  $\beta_2$  appears to be inconsistent with the result obtained earlier by Flengas and Rideal. A summary of these values is given in Table II. It is interesting to note that Jordan and Pendergrast used a nonelectrochemical method (thermometric enthalpy titration) for obtaining their formation constants.

Two significant points should be made in regard to this study. First, the cell as represented by (1), in which silver ion concentration was changed, was shown to be quite stable in the absence of added cyanide ions. For a typical run, the experimental slope is  $105 \pm 1$  m.v. at  $248^\circ$  as compared with the theoretical slope 104.5 calculated according to eq. 2. The data for the run, together with a schematic diagram of the glass reference electrode, are shown in Figure 3. The use of

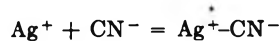
(8) H. T. Tien, Abstracts, 149th National Meeting of the American Chemical Society, Detroit, Mich., April 1965, p. 7M; details to be published.

(9) H. T. Tien and G. W. Harrington, *Inorg. Chem.*, **3**, 215 (1964).

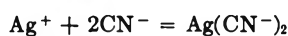
**Table I:** Electromotive Force Data Used to Determine the Formation Constants for Species in Equimolar NaNO<sub>3</sub>-KNO<sub>3</sub> Melt<sup>a</sup>

$\Delta E$ , mv. <sup>b</sup>	-Log C <sub>CN<sup>-</sup></sub>	$\bar{n}$	[CN <sup>-</sup> ] × 10 <sup>3</sup>	[Ag <sup>+</sup> ] × 10 <sup>3</sup>	$\phi$ ([CN <sup>-</sup> ]/ [CN <sup>-</sup> ] × 10 <sup>-4</sup> )	([CN <sup>-</sup> ] [CN <sup>-</sup> ] × 10 <sup>-3</sup> )
0	0	...		3.50		
0.8	5.70	0.0134	0.153	3.42	1.53	28.1
1.6	5.40	0.0268	0.306	3.38	1.16	1.96
2.3	5.22	0.0514	0.420	3.33	1.21	2.62
3.2	5.10	0.0603	0.589	3.26	1.25	2.55
4.0	5.00	0.0760	1.34	3.20	0.70	...
5.7	4.82	0.109	1.12	3.08	1.22	1.07
7.5	4.70	0.155	1.46	2.95	1.27	1.17
9.5	4.60	0.201	1.80	2.83	1.31	1.17
11.2	4.52	0.245	2.14	2.72	1.35	1.17
14.8	4.40	0.345	2.79	2.51	1.41	1.11
18.5	4.30	0.442	3.45	2.31	1.49	1.13
22.2	4.22	0.550	4.07	2.13	1.58	1.18
30.0	4.10	0.760	5.34	1.79	1.79	1.29
38.2	4.00	0.990	6.53	1.49	2.07	1.53
46.7	3.92	1.21	7.77	1.23	2.90	2.32
60.0	3.82	1.56	9.54	0.914	2.97	1.96
68.5	3.77	1.78	10.76	0.757	3.37	2.11

<sup>a</sup> Data taken from the smoothed curve (see Figure 1). <sup>b</sup> Initial silver ion concentration:  $3.50 \times 10^{-5}$  (molarity units).

**Table II:** Values of Formation Constants (in molarity units)<sup>a</sup> in Equimolar Sodium Nitrate-Potassium Nitrate Melt


$$\beta_1 = \frac{[\text{Ag}^+\text{-CN}^-]}{[\text{Ag}^+][\text{CN}^-]}$$

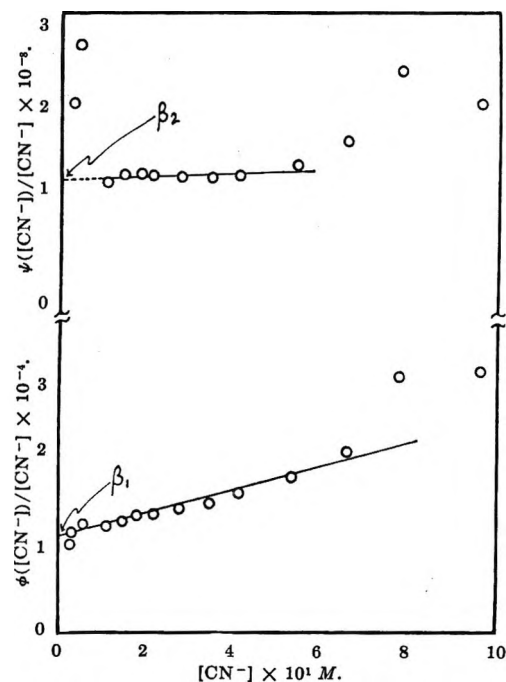
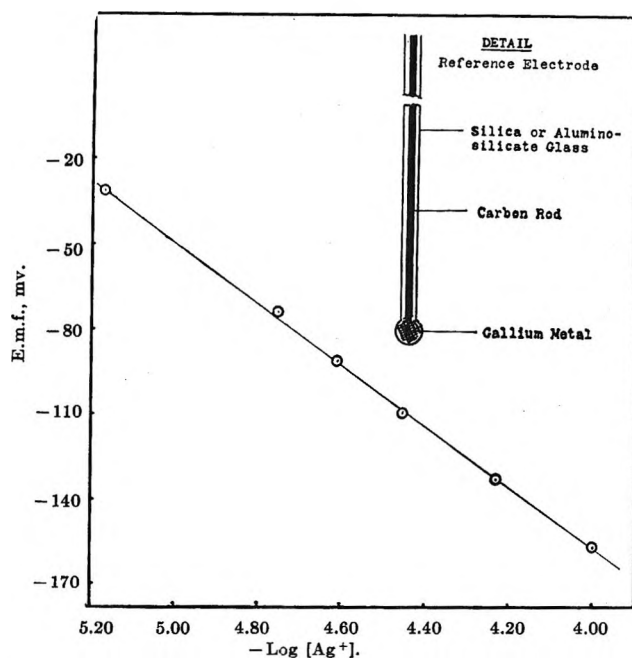


$$\beta_2 = \frac{[\text{Ag}(\text{CN}^-)_2]}{[\text{Ag}^+][\text{CN}^-]^2}$$

	$\beta_1$	$\beta_2$
Flengas and Rideal (ref. 4) <sup>b</sup>	...	$2.1 \times 10^{10}$ (250°)
Jordan and Pendergrast (ref. 3) <sup>b</sup>	...	$8.0 \times 10^7$ (250°)
Manning and Blander (ref. 2) <sup>c</sup>	$1.1 \times 10^4$	$7.8 \times 10^7$ (248°)
This study <sup>d</sup>	$(1.1 \pm 0.1) \times 10^4$	$(1.1 \pm 0.3) \times 10^8$ (248°)

<sup>a</sup> The density of the melt is estimated to be 1.9 g./cc. based on the data given by Smithells, which are used to convert all formation constants: C. J. Smithells, "Metal Reference Book," Butterworth and Co. Ltd., London, 1955, p. 620. <sup>b</sup> Original values of formation constants given in molality units. <sup>c</sup> Original values of formation constants given in mole fraction units. <sup>d</sup> Solutions were prepared by weight.

gallium in place of mercury greatly extended the usefulness of such reference electrodes in fused-salt solutions. To date, gallium-filled glass reference electrodes


**Figure 2.** Extrapolation of over-all formation constants.

**Figure 3.** Nernst plot of potential between equilibrated glass reference electrode and silver electrode vs. silver ion concentration. Theoretical slope, 104.5; experimental,  $105 \pm 1$ ; temperature 521°K.

have been successfully tested well above 360°. It is anticipated that, if suitable ion-sensitive material can be found in place of glass, the suitability of this

type of reference electrode would be practicable up to the boiling point of gallium (2070° at 1 atm.).<sup>10</sup>

A relevant comment should be made in regard to the mechanism of the operation of the glass reference electrodes. As discussed previously,<sup>5</sup> the equilibration of reference electrodes in fused salts is of paramount importance. Equilibration seems to follow an exponential rate suggesting an exchange process is taking place between the glass and the melt. That the superficial washing with water and drying in the air have no apparent deleterious effect on stability strongly suggests that more than the surface layer is involved during the equilibration. Some of these facts are reminiscent of the glass electrode used in pH determinations. It is a well-known fact that the glass electrode has a so-called salt "error" at high pH values, which implies that the glass membrane is sensitive to other ions in the solution. This fact has been amply demonstrated by the work of Lengyel and Sammt,<sup>11</sup> who used a sodium glass electrode to measure the sodium ion concentration in molten PbCl<sub>2</sub>. Prior to this work, Horovitz<sup>12</sup> has suggested that the glass membrane behaved like a solid electrolyte, and the operation of the glass electrode depended on the exchange reactions of cations, which were limited to those ions able to migrate into the glass. These ideas were fully justified and supported by Sollner<sup>13</sup> (ion-exchange membrane electrodes), Delimarskii<sup>14</sup> (sodium glass electrode in fused salts), and Rudin, *et al.*<sup>15</sup> (sodium glass electrode in aqueous solutions). The suitability of a glass reference electrode in various fused salt solutions containing either Li, Na, K, or Na-K ions has been tested. In the cases studied, the cell reactions obeyed the Nernst equation. Thus, it is clear that the glass electrode must act like a cation electrode reversible to alkali ions of the fused salts used. That the reason for equilibration is important may be explained on the basis of ion-exchange reaction between the glass and the melt. Considering the glass as a solid electrolyte as first suggested by Horovitz, in a way not unlike synthetic ion-exchange resins, the residual charge of the silicon-oxygen lattice is balanced by cations (usually Na or K). Upon immersion in the melt, it is highly likely an exchange process takes place between the cations present in the glass and those in the melt. However, it seems that not all of the cations can participate in this exchange reaction, presumably on account of charge and ionic radius of the cation involved. Once equilibrated, the glass electrode behaves like a specific cation electrode for Li, Na, or K. In the melt containing Na-K, as in the present case, a mixed-electrode function must have developed. The operation of the glass electrode as a reference

electrode in different fused-salt solutions is thus apparent since the potentiometric measurements were carried out in the melt in which the glass electrode had been equilibrated. The constancy of the reference electrode potential is, therefore, believed to be the result of the exchange reaction of cations between the glass and the melt, whose composition was practically invariant during the course of a run.<sup>16</sup>

Secondly, in the case studied the mathematical manipulation of data for the evaluation of formation constants according to the procedure previously described<sup>9</sup> appears to be valid and sensitive as evidenced by the results, which are in good agreement with the published values obtained by two different methods<sup>2,3</sup> (see Table II). The internal consistency and the accuracy of the formation constants thus obtained can be checked readily by substituting the results in the fundamental equation relating the formation constants and the equilibrium concentrations of the ligand and the metal ion (eq. 7 of ref. 9). For the present case the equation may be written as

$$\frac{C_{Ag} - [Ag]}{[Ag]} = \beta_1[CN^-] + \beta_2[CN^-]^2 \quad (6)$$

The results of calculations are given in Table III using the data presented in Table I and the extrapolated  $\beta$  values.

Table III

$[CN^-] \times 10^6$	$(C_{Ag} - [Ag])/[Ag]$	$\beta_1[CN^-] + \beta_2[CN^-]^2$
0.306	0.0355	0.0347
0.420	0.0510	0.0481
0.589	0.0736	0.0686
1.12	0.136	0.137
1.46	0.186	0.184
1.80	0.237	0.234
2.14	0.287	0.287
2.79	0.395	0.393
3.45	0.515	0.511
4.07	0.644	0.629

(10) For detailed discussions, see (a) R. W. Laity in "Reference Electrodes," D. J. G. Ives and G. J. Janz, Ed., Academic Press Inc., New York, N. Y., 1961, Chapter 12; (b) J. D. Corbett and F. R. Duke in "Technique of Inorganic Chemistry," Vol. 1, H. B. Jonassen and A. Weissberger, Ed., John Wiley and Sons, Inc., New York, N. Y., 1963, Chapter 3.

(11) B. Lengyel and A. Sammt, *Z. physik. Chem. (Leipzig)*, **181**, 55 (1937).

(12) K. Horovitz, *Nature*, **127**, 440 (1931).

(13) K. Sollner, *J. Phys. Chem.*, **49**, 171, 265 (1945).

(14) Yu. K. Delimarskii, *Ukr. Khim. Zh.*, **21**, 449 (1956).

(15) G. Eisenman, D. O. Rudin, and J. U. Casby, *Science*, **126**, 831 (1957).

(16) H. T. Tien, Ph.D. Thesis, Temple University, 1962.



The physical significance of Table III is that the data obtained in this study can be adequately described by a two-parameter equation (eq. 6), thereby substantiating the postulated species in the melt for the concentration range investigated. It can be seen however that, at low cyanide concentrations, eq. 6 is only approximately correct in describing the experimental data. This fact can be traced in part to the failure to take into consideration the possibility of  $\text{Ag}_2\text{CN}^+$  formation at very low cyanide concentrations. The existence of  $\text{Ag}_2\text{CN}^+$  and its formation constant have been reported by Manning and Blander.<sup>2</sup> It is interesting to note that, if data were independent of  $\text{Ag}^+$  concentration or were extrapolated to zero  $\text{Ag}^+$  concentration, the formation constant  $\beta_1$  can be readily estimated from Figure 1, according to the methods developed by Braunstein, Blander, and Lindgren<sup>17</sup> and by Braunstein, *et al.*<sup>18</sup> Thus, it can be readily shown that from the limiting slope of the curve in Figure 1, a value  $1.0 \times 10^4$  for  $\beta_1$  is obtained as compared with the extrapolated value  $1.1 \times 10^4$  in Figure 2. Braunstein, *et al.*, state that their methods of calculat-

ing formation constants lead to a more reliable extrapolation with equal weights to all experimental points. It should be mentioned however that the method proposed by Bjerrum, which was not discussed in the paper of Braunstein, *et al.*, and on which the present calculation is based, is also fairly simple and does not require more than one successive approximation. For interested readers, an excellent analysis of Bjerrum's mathematical formulation, together with those suggested by Leden and by Fronaeus, may be found in a paper by Sullivan and Hindman.<sup>19</sup>

*Acknowledgments.* The author wishes to acknowledge the assistance given by Lawrence Gray in obtaining some of the preliminary data. The author is also grateful to Dr. George W. Harrington for many helpful discussions.

(17) J. Braunstein, M. Blander, and R. M. Lindgren, *J. Am. Chem. Soc.*, **84**, 1529 (1962).

(18) J. Braunstein, H. Braunstein, and A. S. Minano, *Inorg. Chem.*, **3**, 1334 (1964).

(19) J. C. Sullivan and J. C. Hindman, *J. Am. Chem. Soc.*, **74**, 6091 (1952).

## Gas-Solid Partition Chromatography with Real Carrier Gases<sup>1a,b</sup>

by David C. Locke<sup>2</sup>

*Department of Chemistry, Stevens Institute of Technology, Hoboken, New Jersey 07030*  
(Received April 21, 1965)

The effects of gas phase nonideality and mean column pressure on sample retention have been considered in several gas-solid partition chromatographic systems defined in terms of the observed sample and carrier gas isotherms. As in gas-liquid partition chromatography, the distribution coefficient is dependent upon the mean column pressure, decreasing slightly with increasing pressure of thermodynamically imperfect carrier gases. In the limiting case of gas phase ideality, the distribution coefficient is proportional to the sample adsorption constant. Considerable potential is seen for the extraction of second virial coefficients, adsorption constants, and quantities calculable from these parameters from gas-solid partition chromatographic data.

### Introduction

Gas-solid partition chromatography (g.s.p.c.) has been used for the separation of gaseous mixtures somewhat longer than gas-liquid partition chromatography (g.l.p.c.). However, being restricted mainly to the analysis of the fixed gases and simple organic compounds, the study of g.s.p.c. became submerged in the deluge of theory and application following the introduction of g.l.p.c. in 1952. More recently, renewed interest has arisen in the theory and practice of linear elution g.s.p.c.

In this paper, several systems defined in terms of the observed sample and carrier gas adsorption isotherms are considered. Quantitative predictions are made as to the effect of mean column pressure and gas phase nonideality on the retention behavior of adsorbates in g.s.p.c. As in g.l.p.c.,<sup>3</sup> for a given carrier gas in the simpler adsorption systems, absolute sample retention is linearly related to the mean column pressure; at constant pressure, the distribution coefficient decreases slightly with increasing gas phase nonideality. It is anticipated that g.s.p.c. will provide a simple, reasonably accurate method for the determination of the second virial coefficients which characterize these gas phase imperfections. Furthermore, the utilization of small changes in partition ratio with mean column pressure or carrier gas nonideality may have important analytical consequences for the resolution of difficultly separable mixtures. Since the distribution coefficient is proportional to the adsorption constant of the sample,

it is apparent that g.s.p.c. offers a means for obtaining information about gas-solid interactions.

### Theory

We define the fundamental adsorption distribution coefficient,  $K_a$ , by

$$K_a = \frac{\left( \begin{array}{l} \text{number of moles of component adsorbed} \\ \text{per unit weight of adsorbent} \end{array} \right)}{\left( \begin{array}{l} \text{number of moles of component in the gas} \\ \text{phase per unit volume of gas phase} \end{array} \right)} \quad (1)$$

The distribution coefficient is related to the partition ratio,  $k_a$ , defined as the amount of component in the adsorbed phase divided by the amount of component in the gas phase, according to

$$K_a = k_a(V^g/w_a) \quad (2)$$

where  $V^g$  is the interstitial volume of the column, the retention volume of an unadsorbed component, and  $w_a$  is the weight of adsorbent in the column. Note that  $K_a$  has units of cubic centimeters per gram of adsorbent, while  $k_a$  is dimensionless. We could have as

(1) (a) Work supported by the National Aeronautics and Space Administration under Contract No. NSG-494; (b) presented at the Pittsburgh Conference on Analytical Chemistry and Applied Spectroscopy, Pittsburgh, Pa., March 1-5, 1965.

(2) Analytical Research Division, Esso Research and Engineering Co., Linden, N. J. 07036.

(3) D. H. Desty, A. Goldup, G. R. Luckhurst, and W. T. Swanton, "Gas Chromatography," M. van Swaay, Ed., Butterworth and Co. Ltd., London, 1963, p. 67.

easily defined  $K_a$  in terms of the number of moles of component adsorbed per unit area of adsorbent, in which case  $K_a$  would have units of centimeters. However, the weight of adsorbent is more readily measured than its surface area. In any case the final numerical values will differ only a constant. Often we need to know both quantities anyway.

$k_a$  can be determined experimentally from the sample retention time,  $t_r$ , since  $t_r = (L/u)(1 + k_a)$ , where  $L$  is the column length and  $u$  is the carrier gas velocity.  $K_a$  can be obtained from eq. 2 and is related to the corrected retention volume,  $V_R^0$ , by  $V_R^0 = V^g + K_a w_a$ , and to the heat of adsorption,  $\Delta H_a$ , by  $K_a = c \exp(-\Delta H_a/RT)$ .

In this paper we shall be mainly concerned with the effect of gas phase nonideality on retention ( $K_a$  or  $k_a$ ). The development used here relies heavily on the similar treatment of g.l.p.c. by Luckhurst, who with Desty, *et al.*,<sup>3</sup> considered this effect in gas-liquid partition chromatographic systems. The case of g.s.p.c., however, is slightly more complicated: both the component of interest and the carrier gas may be adsorbed, and each may follow a different adsorption isotherm. Furthermore, the carrier gas may behave ideally for all practical purposes, as is effectively the case with helium at high temperatures, but the adsorbate vapors may deviate appreciably from ideal behavior. It is apparent that several distinct situations need to be considered.

It will be assumed in most cases that the adsorbate obeys Henry's adsorption law, *i.e.*, that the amount of component present is so small that its adsorption isotherm is linear. Experimentally, this qualification is easily met since very small samples can be used in conjunction with sensitive ionization detectors or micro-volume thermal conductivity cells. The carrier gas may not be adsorbed, or it may follow a linear or a Langmuir-type adsorption isotherm, depending upon the experimental conditions, the characteristics of the adsorbent, and the nature of the carrier gas.

Situations involving multimolecular adsorption will not be considered in this paper. Although mean column pressures may be as large as several atmospheres, normal operating temperatures are considerably higher than the critical temperatures of the usual carrier gases. Thus, carrier gas adsorption usually will occur only to an extent which can be described by a linear or a Langmuir-type isotherm.

It will be necessary in all cases to consider that second-order adsorbed phase interactions are negligible. This assumption will be valid if we restrict our attention to situations where only very small quantities of sample are present. In such cases, lateral interactions

between adsorbed molecules and interactions between the bulk gas and the adsorbed species will be negligible.<sup>4,5</sup> This is an important point if the deviations of our measurements from ideality are to reflect gas phase interactions only.

The first case to be considered (case I) is the simplest: the carrier gas is not adsorbed, the adsorbate follows a linear isotherm, and the gas phase is considered ideal. In practice, such a situation could be approximated with very small samples of simple adsorbates, He carrier gas, and moderately high column temperatures. Letting  $n_2^a$  and  $n_2^g$  be the number of moles of component adsorbed and the number in the gas phase, respectively

$$K_a = \frac{n_2^a/w_a}{n_2^g/V^g} \quad (3)$$

Following Barker and Everett's derivation,<sup>4</sup> we find an expression for Henry's adsorption law

$$n_2^a = k_H A p_2^g \quad (4)$$

where  $k_H$  (in mole atm.<sup>-1</sup> cm.<sup>-2</sup>) is the adsorption constant, a function of the gas-solid interaction potential energy;  $A$  is the surface area of the adsorbent present; and  $p_2^g$  is the partial pressure of sample component above the adsorbent. Adsorption is linear with the quantity of sample. For ideal gases

$$n_2^g/V^g = p_2^g/RT \quad (5)$$

Thus

$$K_a = k_H A p_2^g RT/w_a p_2^g = k_H A RT/w_a \quad (6)$$

In terms of the adsorption partition ratio,  $k_a = k_H A RT/V^g$ .  $k_a$  is dimensionless, as it should be.

The next situation to consider (case II) is the same as case I except that the gas phase behaves nonideally. These conditions may be experienced with, for example, H<sub>2</sub> carrier gas and a low activity adsorbent (such as graphitized carbon black<sup>6</sup>) at moderate column temperatures. The adsorbate of interest follows a linear isotherm, but the carrier gas is not adsorbed. For real gases, we have in place of eq. 4.

$$n_2^a = k_H A f_2^g \text{ or } \ln n_2^a = \ln k_H A + \ln f_2^g \quad (7)$$

where  $f_2^g$  is the fugacity of the adsorbate above the adsorbent, related<sup>7</sup> to the partial pressure according to

(4) J. A. Barker and D. H. Everett, *Trans. Faraday Soc.*, **58**, 1608 (1962).

(5) J. F. Hanlan and M. P. Freeman, *Can. J. Chem.*, **37**, 1575 (1959).

(6) A. A. Isivikyan and A. V. Kiselev, *J. Phys. Chem.*, **65**, 601 (1961).

(7) E. A. Guggenheim, "Thermodynamics," North-Holland Publishing Co., Amsterdam, 1950, p. 179.

$$\ln f_2^g = \ln p_2^g + (\bar{P}/RT)[B_{22} - (1 - y)^2(B_{11} - 2B_{12} + B_{22})] \quad (8)$$

In this equation,  $y$  is the mole fraction of adsorbate vapor in the gas phase,  $\bar{P}$  is the mean column pressure (see Discussion), and  $B_{11}$  and  $B_{22}$  are the second virial coefficients of the pure carrier gas and adsorbate vapors, respectively.  $B_{12}$  is the interaction second virial coefficient, characterizing the interactions between unlike molecules, in this case, those of the carrier gas and sample vapor.  $B_{12}$  is given by the expression<sup>8</sup> relating  $B_{11}$  and  $B_{22}$  to the second virial coefficient of a gaseous mixture,  $B_m$

$$B_m = y^2 B_{22} + 2y(1 - y)B_{12} + (1 - y)^2 B_{11} \quad (9)$$

Since

$$y = n_2^g / (n_2^g + n_1^g) = p_2^g / (p_2^g + p_1^g) = p_2^g / \bar{P} \quad (10)$$

where  $n_1^g$  is the number of moles of carrier gas present in the column and  $p_1^g$  is the carrier gas partial pressure and since

$$\bar{P}V^g = (n_2^g + n_1^g)(RT + B_m \bar{P}) \quad (11)$$

eq. 3 becomes

$$K_a = (n_2^g/w_a)(\bar{P}/p_2^g)[RT/\bar{P} + y^2 B_{22} + 2y(1 - y)B_{12} + (1 - y)^2 B_{11}] \quad (12)$$

Combining eq. 7, 8, 10, and 12, we have

$$\ln K_a = \ln (k_H A \bar{P} / w_a) + \ln [RT/\bar{P} + y^2 B_{22} + 2y(1 - y)B_{12} + (1 - y)^2 B_{11}] + (\bar{P}/RT)[B_{22} - (1 - y)^2(B_{11} - 2B_{12} + B_{22})] \quad (13)$$

For very small samples,  $y \rightarrow 0$ . Then after rearranging eq. 13, expanding the resulting term in  $\ln(1 + B_{11} \bar{P}/RT)$ , and neglecting all but first-order terms in the expansion

$$\ln K_a = \ln (k_H A RT / w_a) + 2B_{12} \bar{P} / RT \quad (14)$$

A plot of  $\ln K_a$  vs.  $\bar{P}$  should be linear, with a slope of  $2B_{12}/RT$  and an intercept identical with eq. 6.

Another case of lesser importance might also be considered. In case III, the carrier gas closely approximates ideal behavior while the adsorbate vapors are thermodynamically imperfect. Such a circumstance might effectively arise if He were used as a carrier gas at high temperatures. Equation 11 now becomes  $\bar{P}V^g = (n_2^g + n_1^g)RT$ . Assuming,<sup>7</sup> furthermore, that  $\ln f_2^g = \ln p_2^g + B_{22} \bar{P}/RT$ , substitution into eq. 3 gives

$$\ln K_a = \ln (k_H A RT / w_a) + B_{22} \bar{P} / RT \quad (15)$$

At ordinary operating temperatures, it is expected

that most common carrier gases other than  $H_2$  and He will be adsorbed on the active solid. One of the simpler nonlinear isotherms that a carrier gas might obey is that of Langmuir. This treatment, a kinetic approach, assumes monolayer adsorption on a uniform, homogeneous surface. Lateral interactions between the adsorbed species are negligible. In g.s.p.c., where the carrier gas and sample components may both be adsorbed, this requires that the only effect one adsorbate can have on the adsorption of another is to reduce the available surface area.<sup>9</sup> It is readily shown that the Langmuir isotherm for mixed adsorption is given by

$$n_1^a = n_m^1 b_1 p_1^g / (1 + b_1 p_1^g + b_2 p_2^g) \\ n_2^a = n_m^2 b_2 p_2^g / (1 + b_1 p_1^g + b_2 p_2^g) \quad (16)$$

where  $n_m^i$  is the number of moles of the  $i$ th component required to produce a monolayer on the surface of the adsorbent, and  $b_i$  is its over-all adsorption constant, the ratio of the adsorption/desorption rate constants. Each gas or vapor decreases the amount of adsorption of the other according to the relative magnitudes of the  $b_i p_i^g$  products.

In g.s.p.c., component 2, the adsorbate of interest, will in general obey a linear isotherm ( $b_2 p_2^g \ll 1$ ). This situation produces limiting cases of eq. 16

$$n_1^a = n_m^1 b_1 p_1^g / (1 + b_1 p_1^g) \\ n_2^a = n_m^2 b_2 p_2^g / (1 + b_1 p_1^g) \quad (17)$$

The adsorption of carrier gas (component 1) is not appreciably affected by the presence of component 2, but the linear adsorption of 2 is strongly influenced by the adsorption of carrier gas.

Solving eq. 17 for  $(1 + b_1 p_1^g)$  and equating

$$n_2^a = c_1 n_1^a p_2^g / p_1^g \quad (18)$$

where  $c_1 = n_m^2 b_2 / n_m^1 b_1$ .

We can now consider case IV, where the adsorbate obeys Henry's law, the carrier gas follows the Langmuir isotherm, and the gas phase behaves ideally. We can then identify  $p_1^g$ , the partial pressure of carrier gas, with the mean column pressure,  $\bar{P}$ . From eq. 3, 5, 17, and 18

$$K_a = c_1 n_1^a RT / \bar{P} w_a = c_2 RT / w_a (1 + b_1 \bar{P}) \quad (19)$$

where  $c_2 = c_1 n_m^1 b_1 = n_m^2 b_2$ . Thus for these systems, the distribution coefficient should decrease with both increasing column pressure, as could be anticipated with a nonlinear isotherm, and with increasing strength

(8) J. E. Lennard-Jones and W. R. Cook, *Proc. Roy. Soc. (London)*, **A115**, 334 (1927).

(9) S. Brunauer, "The Adsorption of Gases and Vapors," Vol. 1, Princeton University Press, Princeton, N. J., 1945, p. 476.

Table I: Summary of Expressions for  $K_a$  in Gas-Solid Partition Chromatography

Case	Adsorbate isotherm	Carrier gas isotherm	Adsorbate vapor	Carrier gas	$K_a$
I	Linear	NA <sup>a</sup>	I <sup>b</sup>	I	$K_a = k_H ART/w_a$
II	Linear	NA	R <sup>c</sup>	R	$\ln K_a = \ln (k_H ART/w_a) + 2B_{12}\bar{P}/RT$
III	Linear	NA	R	I	$\ln K_a = \ln (k_H ART/w_a) + B_{22}\bar{P}/RT$
IV	Linear	Langmuir	I	I	$K_a = c_2 RT/w_a(1 + b_1\bar{P})$
V	Linear	Langmuir	R	R	$\ln K_a = \ln [c_2 RT/w_a(1 + b_1\bar{P})] + (\bar{P}/RT)(2B_{12} - B_{11})$
VI	Linear	Linear	I	I	$K_a = c_2 RT/w_a$
VII	Linear	Linear	R	R	$\ln K_a = \ln (c_2 RT/w_a) + (\bar{P}/RT)(2B_{12} - B_{11})$
VIII	Langmuir	NA	I	I	$K_a = c_2 RT/w_a(1 + b_2 p_2^g)$
IX	Langmuir	Linear	I	I	$K_a = c_2 RT/w_a(1 + b_2 p_2^g)$
X	Langmuir	Langmuir	I	I	$K_a = c_2 RT/w_a(1 + b_1 p_1^g + b_2 p_2^g)$

<sup>a</sup> NA = not adsorbed. <sup>b</sup> I = ideal gas phase. <sup>c</sup> R = real, nonideal gas phase.

of carrier gas adsorption (increasing  $b_1$ ). This is in agreement with the experimental results of Greene and Roy.<sup>10</sup>

In case V, the system under consideration is the same as case IV except that all components in the gas phase behave imperfectly. Replacing partial pressures in eq. 18 with fugacities, recalling the definition of  $y$ , the mole fraction of sample vapor in the gas phase, and proceeding as above, we arrive at the desired result, given in Table I.

Under the proper circumstances, the adsorption of both the carrier gas and the sample may best be described by a linear isotherm. It will be noted that eq. 16 is applicable to both linear and Langmuir adsorption, it being implicit in this equation that the only effect adsorption of one has on the other is to reduce the available surface area.

For the present case of linear adsorption of both sample and carrier gas,  $b_1 p_1^g$  and  $b_2 p_2^g$  are both much less than 1, and the number of moles of carrier gas adsorbed is given by  $n_1^a = n_m^1 b_1 p_1^g = n_m^1 b_1 \bar{P}$  for very small samples. We thus arrive at the expressions given in Table I for cases VI and VII. Descriptions of the features of these systems are given in the table.

Several more special cases might also be mentioned. The first of these, case VIII, would apply if the sample component followed the Langmuir isotherm. In this case the carrier gas is not adsorbed, and the gas phase is ideal. From eq. 16, since now  $b_1 = 0$ , we have  $n_2^a = n_m^2 b_2 p_2^g / (1 + b_2 p_2^g)$ . The distribution coefficient is

$$K_a = n_m^2 b_2 RT/w_a(1 + b_2 p_2^g) \quad (20)$$

Now retention is dependent upon sample size ( $p_2^g$ ), decreasing with increasing  $p_2^g$ . This is also in agreement with experimental observations.<sup>11</sup> If the amount

of sample is allowed to become very small, eq. 20 becomes equivalent to eq. 6.

Langmuir-type adsorption of the sample in conjunction with linear or Langmuir adsorption of the carrier gas leads to systems described by cases IX and X, respectively. These results are also given in Table I.

Considerations similar to those employed above will allow assessment of the effect of gas phase nonideality on retention in these cases. A summary of the final results for  $K_a$  for the various cases considered is presented in Table I.

## Discussion

The equations in Table I are of interest from both a chromatographic and a thermodynamic point of view. Chromatographically, a prediction of the g.s.p.c. behavior of several systems is presented. The equilibrium distribution coefficient per unit weight of adsorbent is proportional to the adsorption constant of the system if the gas phase can be considered ideal or proportional to this constant plus correction factors accounting for the nonideality of the gas phase. It should be pointed out that the *apparent* ideality or nonideality of such systems is to a large extent dependent on the accuracy of the measurements made. Analytically, most chromatographic systems behave ideally (in the thermodynamic sense) for all practical purposes. Those equations derived for the ideal gas phases are limiting cases for the real systems. For the cases with linear isotherms, but nonideal gas phases,  $\ln K_a$  should show a slight but linear dependence on the mean column pressure for a given carrier gas; at constant pressure,  $\ln K_a$  should de-

(10) S. A. Greene and H. E. Roy, *Anal. Chem.*, **29**, 569 (1957).

(11) A. V. Kiselev, Yu. S. Nikitin, R. S. Petrova, K. D. Shcherbakova, and Ya. I. Yashin, *ibid.*, **36**, 1526 (1964); cf. Figure 7.

crease with increasing gas phase nonideality. For those systems with nonlinear carrier gas isotherms, this pressure dependence arising from gas phase nonideality will be superimposed upon, and obscured by, the more direct, stronger pressure dependence exerted through the factor of  $(1 + b_1 \bar{P})^{-1}$ . The actual contribution of the correction terms to  $\ln K_a$  is quite small, amounting to only a few per cent at most.

The reliability of the results obtained with the aid of the equations developed above depends on the extent to which the various cases studied here faithfully describe the physical systems under consideration. From the slopes of plots of  $\ln K_a$  (or  $\ln k_a$ ) vs.  $\bar{P}$ , the mean column pressure, we can extract second virial coefficients for several of the real systems described. There are definite limitations on the generality of the method.

Obviously, in case V, the major pressure dependence of  $K_a$  lies in the "constant" term, in the factor of  $(1 + b_1 \bar{P})^{-1}$ . This will make measurements on the nonideality of the gas phase virtually impossible. Thus, for these purposes, we must avoid conditions which lead to nonlinear adsorption of the carrier gas; certain carrier gases are eliminated from useful consideration. This is an immediate limitation.

Case III, where the carrier gas is considered ideal, will only hold, and then only approximately, for He carrier gas, which is not ordinarily adsorbed. In this case, we can extract from the retention data values of  $B_{22}$ , the second virial coefficient of the pure sample adsorbate vapors. Other information can be obtained from systems described in cases II and VII. Recall that here the carrier gas is either not adsorbed, or is adsorbed linearly, respectively. Case II will be most applicable at ordinary chromatographic temperatures with  $H_2$  carrier gas; other carrier gases may be used at higher temperatures. Systems involving heavier carrier gases at lower temperatures can best be treated as examples of case VII. The slope of the  $\ln K_a$  vs.  $\bar{P}$  plot provides values of  $B_{12}$  for case II and  $2B_{12} - B_{11}$  for case VII. Used conjunctively, we have a potential method for the determination of both quantities. Two different adsorbents of different activities are required. If case II describes sample retention for the lower activity solid phase, and case VII that for the more active adsorbent, we can determine both  $B_{12}$  and  $B_{11}$ . Alternatively, we can obtain  $B_{12}$  from g.l.p.c. measurements<sup>2</sup> and then apply case VII to g.s.p.c. experiments. Thus, two columns are required, either two adsorbent columns of different activity, or one with an adsorbent and one with an adsorbent fixed phase. Since we are measuring gas phase interactions, the nature of the column materials in either case should not be critical for all practical purposes. This is a major advantage

of the chromatographic method, in addition to its speed and simplicity.

Adsorption constants can be recovered from the intercept of the  $\ln K_a$  vs.  $\bar{P}$  plot, or directly from the measured  $K_a$ , depending on the system. As in the measurement of activity coefficients in g.l.p.c., extrapolation to zero mean column pressure will be necessary if carrier gases exhibiting nonideal behavior are used.

It might be noted that experimental adsorption isotherms are readily obtained by the frontal analysis technique of James and Phillips.<sup>12,13</sup> In addition to being experimentally simpler and faster than conventional methods, this procedure is especially suited to the measurement of very low adsorptions (surface areas 0.25 m.<sup>2</sup>/g. or less).

Since deviations from adsorption linearity are largely due, even at low sample pressures, to adsorbent non-homogeneities, it is anticipated that graphitized carbon black will be a valuable adsorbent for experimental studies in g.s.p.c. These active solids are prepared by heating carbon blacks to about 3000°, which causes a crystallization to small graphite polyhedra with a very homogeneous surface of 6–30 m.<sup>2</sup>/g.<sup>6,11</sup> Specially modified adsorbents, such as NaOH-treated  $Al_2O_3$ ,<sup>14</sup> also possess apparently homogeneous surfaces and produce linear isotherms.

A finite pressure gradient must exist across the column to produce carrier gas flow. Because of this, it has been common in gas chromatographic studies to employ the mean column pressure,  $\bar{P}$ , and to correct all pressure-dependent quantities to this value.  $\bar{P}$  can be calculated from the inlet/outlet pressure ratio using the Martin and James compressibility factor, or if high column pressures and decidedly nonideal carrier gases are used, from the nonideal carrier gas compressibility factor.<sup>16</sup> It is necessary to recognize these nonisobaric conditions as a possible limitation on the general validity of parameters calculated from gas chromatographic data. Experimentally, it may be necessary at each  $\bar{P}$  to vary systematically the inlet/outlet pressure ratio while maintaining that  $\bar{P}$  constant. Extrapolation to a unit pressure ratio would provide retention values effectively obtained under isobaric ( $P = \bar{P}$ ) conditions. Some studies in this direction have been made by Everett and Stoddart,<sup>16</sup> but more information is needed to resolve the question completely.

(12) D. H. James and C. S. G. Phillips, *J. Chem. Soc.*, 1066 (1954).

(13) R. H. Perrett and J. H. Purnell, *J. Chromatog.*, 7, 455 (1962).

(14) C. G. Scott, *Nature*, 193, 159 (1962).

(15) D. E. Martire and D. C. Locke, *Anal. Chem.*, 37, 144 (1965).

(16) D. H. Everett and C. T. H. Stoddart, *Trans. Faraday Soc.*, 57, 746 (1961).

Unfortunately, sufficient data appropriate for testing the theory presented here have not been given in the

literature. Experimental studies to this end are therefore being undertaken in this laboratory.

## Absorption Isotherms of Hydrogen in the $\alpha$ -Phase of the Hydrogen-Palladium System

by J. W. Simons and Ted B. Flanagan

*Department of Chemistry, University of Vermont, Burlington, Vermont (Received April 22, 1965)*

Isotherms for the absorption of hydrogen in the  $\alpha$ -phase of the H<sub>2</sub>-Pd system between 0 and 90° have been determined from variations in the electrode potential and electrical resistivity of palladium wires during slow absorption of hydrogen from dilute HCl solutions. Evidence is presented which shows that the absorption isotherms obtained represent equilibrium data. The average isosteric heat of absorption is  $4780 \pm 100$  cal./mole of H<sub>2</sub> from H-Pd = 0.002 to 0.014. The isotherms are analyzed in terms of a general statistical model based upon interacting absorbed protons.

### Introduction

Thermodynamic data in the  $\alpha$ -phase of the hydrogen-palladium system offer particularly relevant quantitative tests of statistical models for hydrogen absorption by palladium,<sup>1-5</sup> since complications, such as hysteresis, arising from the formation of the high content  $\beta$ -phase are absent and yet the postulated H-H interaction which leads to the  $\beta$ -phase formation must still be present.

Below  $\sim 120^\circ$  equilibrium isotherm data utilizing conventional gas phase absorption techniques have been difficult to obtain because of slow equilibration. The early gas phase absorption isotherms (0, 30, and 80°) of Gillespie and Hall<sup>6</sup> were the only available  $\alpha$ -phase data at low temperatures until the recent, and quite different, results between 0 and 75° obtained by Wicke and Nernst,<sup>7</sup> using a novel gas phase technique in which a catalyst, more active for H<sub>2</sub> dissociation than a palladium surface, was placed in intimate contact with a palladium sample, thus allowing a relatively rapid attainment of equilibrium.

In view of the difficulties encountered with conven-

tional gas phase techniques at lower temperatures ( $<120^\circ$ ), the present study of the  $\alpha$ -phase, which was undertaken prior to the publication of Wicke and Nernst's results, utilized the technique of absorption from dilute HCl solutions. The technique of direct absorption from hydrogen-stirred dilute HCl solutions has been shown to be a valid method of obtaining thermodynamic data in the two-phase region of the hydrogen-palladium system.<sup>8-11</sup> While it has been known for some time that the electrode potentials and resistiv-

(1) J. R. Lacher, *Proc. Roy. Soc. (London)*, **A161**, 525 (1937).

(2) A. Harasima, T. Tanaka, and K. Sakaoku, *J. Phys. Soc. Japan*, **3**, 208 (1948).

(3) R. Fowler and E. A. Guggenheim, "Statistical Thermodynamics," Cambridge University Press, London, 1939, pp. 558-563.

(4) D. H. Everett and P. Nordon, *Proc. Roy. Soc. (London)*, **A259**, 341 (1960).

(5) J. W. Simons and T. B. Flanagan, *Can. J. Chem.*, **43**, 1665 (1965).

(6) L. J. Gillespie and F. P. Hall, *J. Am. Chem. Soc.*, **48**, 1207 (1926).

(7) E. Wicke and G. H. Nernst, *Z. Elektrochem. Ber. Bunsenges. physik. Chem.*, **68**, 224 (1964).

(8) P. Nylen, *Z. Elektrochem.*, **43**, 915 (1937).



ity changes occurring at contents below the two-phase region represent absorption into the  $\alpha$ -phase,<sup>10-12</sup> the question of whether such data are of thermodynamic significance has not been considered in detail. It has been shown that the slow step in the absorption process is the diffusion of dissolved hydrogen molecules through the solution up to the surface of the specimen.<sup>13,14</sup> This does not imply that an equilibrium distribution of hydrogen atoms exists within the specimen at all times but only that the adsorption  $\rightarrow$  absorption transition at the surface is rapid compared to diffusion of hydrogen molecules up to the surface. (For convenience, the absorbed species will be referred to as hydrogen atoms with the realization that the absorbed species probably exist as protons screened by a "pile-up" of electrons from the d band of palladium.<sup>15</sup>) The rate of internal equilibration of absorbed hydrogen atoms was necessarily investigated independently in the present work.

Statistical models of hydrogen absorption by palladium, based on protons occupying interstitial sites and electrons being donated to the partially empty d-band states of the palladium metal, postulate an attractive interaction between absorbed protons.<sup>1-5</sup> According to this model the interaction energy should be reflected in a linear increase in the heat of absorption with hydrogen content, H/Pd, in the  $\alpha$ -phase. A recent modification of the model,<sup>5</sup> in which consideration is given to the effect of the variation of the density of states with energy using an approximate d-band shape, has shown that gradual filling of the d band leads to a decreasing heat of absorption; however, this decrease becomes important relative to the H-H interaction energy only at contents in considerable excess of the maximum  $\alpha$ -phase content at the highest temperature of the present study. Thus all of the "proton" absorption models predict an approximately linear increase of the heat of absorption with H/Pd in the  $\alpha$ -phase (0-90°). Earlier values of the calorimetric<sup>16</sup> and isosteric heats of absorption<sup>6</sup> in the  $\alpha$ -phase are less than the values obtained for the two-phase region. Until the recent work of Wicke and Nernst,<sup>7</sup> there was no serious attempt to determine systematic variations of the heat of absorption with content in the  $\alpha$ -phase.

In view of the importance of quantitative  $\alpha$ -phase data as tests of theory and the discrepancies between the results of Wicke and Nernst and those of earlier workers,<sup>6</sup> the present results are reported and discussed in terms of a statistical mechanical model.

### Experimental Section

The apparatus and procedure employed in this study are similar to previous descriptions.<sup>11</sup> The absorption

was followed by the increase of the relative electrical resistivity,  $R/R_0$ , of palladium wire and the electrode potential,  $E$ , of the specimen was measured against a Ag-AgCl reference electrode in the same solution. The electrode potentials were converted to values against a H<sub>2</sub> electrode by subtracting them from experimentally determined values of the Ag-AgCl reference electrode *vs.* a Pt-H<sub>2</sub>(1 atm.) electrode. The concentration of HCl in the solution (0.001-0.002 *N*) was sufficiently small so as to minimize any coconduction effects on the resistivity measurements.<sup>17</sup> The rate of absorption was reduced, thus helping to ensure internal equilibration, by reducing the hydrogen partial pressure using helium-hydrogen mixtures. Both gases passed through platinized asbestos at 300° and a liquid nitrogen trap before entering the absorption vessel. The partial pressure of hydrogen could be conveniently determined from the potential of the Ag-AgCl *vs.* a Pt-H<sub>2</sub>(P) electrode. Most of the data were obtained with a 0.032-cm. diameter specimen; however some data were obtained with a 0.062-cm. diameter specimen; results were closely similar in each case.

In order to convert the  $E$  *vs.*  $R/R_0$  data into absorption isotherms, calibration relationships between the relative resistivity,  $R/R_0$ , and the hydrogen content, H/Pd, were carefully determined between 0 and 90°. Although these relationships differ somewhat from previous determinations,<sup>18-20</sup> their use here as an analytical tool only does not require further discussion. A discussion of these resistivity results will be reported elsewhere.<sup>21</sup>

- (9) A. L. Fedorova and A. N. Frumkin, *Zh. Fiz. Khim.*, **27**, 247 (1953).
- (10) R. J. Ratchford and G. W. Castellan, *J. Phys. Chem.*, **62**, 1123 (1958).
- (11) T. B. Flanagan and F. A. Lewis, *Trans. Faraday Soc.*, **55**, 1409 (1959).
- (12) P. C. Aben and W. G. Burgers, *ibid.*, **58**, 1989 (1962).
- (13) R. J. Fallon and G. W. Castellan, *J. Phys. Chem.*, **64**, 4 (1960).
- (14) A. W. Carson, T. B. Flanagan, and F. A. Lewis, *Trans. Faraday Soc.*, **56**, 371 (1960).
- (15) N. F. Mott, *Advan. Phys.*, **13**, 325 (1964).
- (16) D. M. Nace and J. G. Aston, *J. Am. Chem. Soc.*, **79**, 3619 (1957).
- (17) C. A. Knorr and E. Schwartz, *Z. Elektrochem.*, **39**, 281 (1933); A. W. Carson, T. B. Flanagan, and F. A. Lewis, *Naturwiss.*, **46**, 374 (1959); A. W. Carson, T. B. Flanagan, and F. A. Lewis, *Trans. Faraday Soc.*, **56**, 1311, 1324 (1960).
- (18) D. P. Smith, "Hydrogen in Metals," Chicago University Press, Chicago, Ill., 1948.
- (19) T. B. Flanagan and F. A. Lewis, *Z. physik. Chem.*, **27**, 104 (1961).
- (20) W. T. Lindsay and F. W. Pement, *J. Chem. Phys.*, **36**, 1229 (1962).
- (21) J. W. Simons and T. B. Flanagan, to be published.



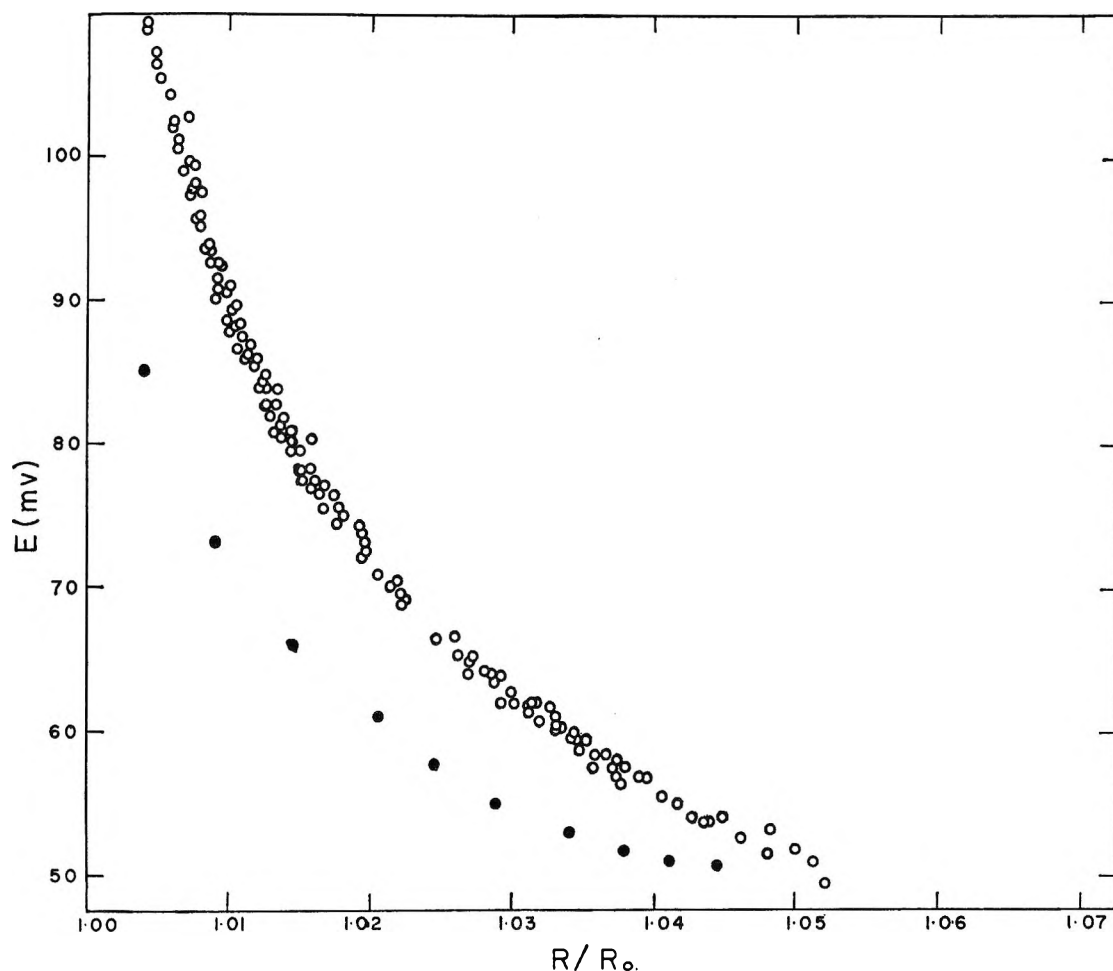


Figure 1.  $E$  vs.  $R/R_0$  ( $25^\circ$ ): O, data from slow absorption runs ( $P_{H_2} = 0.10$  to  $<0.05$ ); ●, data from a fast absorption run ( $P_{H_2} = 1$  atm.).

## Results and Discussion

*Equilibrium  $E$  vs.  $R/R_0$  Relationships and Absorption Isotherms.* Figure 1 shows typical  $E$  vs.  $R/R_0$  data ( $25^\circ$ ) obtained under slow absorption conditions as compared to data obtained from rapid absorption conditions, *i.e.*, with 1 atm. of hydrogen ( $25^\circ$ ). The lower electrode potentials for the rapid absorption data are attributed to a nonequilibrium internal distribution of H atoms within the specimen; the potential being a measure of the absorbed H-atom activity adjacent to the surface. It is seen that the extent of the deviation progressively decreases as the plateau potential is approached. The data shown for the composite slow absorption run consists of runs at partial pressures of hydrogen between  $\sim 0.1$  to less than 0.05 atm. This is believed to represent data corresponding closely to internal equilibration. Evidence for this conclusion is as follows: (a) limiting behavior in the  $E$  vs.  $R/R_0$  relationship was obtained, since further reduction of

the hydrogen pressure and thus the rate of absorption resulted in insignificant changes in the relationships obtained; (b) several isolated  $E$  vs.  $R/R_0$  points on the curve were found to be invariant after being allowed to equilibrate for as long as 12 hr.; (c) calculations based on approximate diffusion constants in the  $\alpha$ -phase show that deviations from equilibrium are at most quite small under the experimental conditions. This diffusion problem is well represented by radial diffusion with constant diffusion coefficient,  $D$ , into an infinitely long cylinder with zero initial concentration and a constant flux of diffusing material crossing the surface. The diffusion equation for this problem has been solved.<sup>22</sup> Using this solution, the ratio of the surface concentration to the flux,  $C_s/F_0$ , can be expressed in terms of the radius of the cylinder, the diffusion

(22) J. Crank, "Mathematics of Diffusion," Oxford University Press, London, 1956, p. 74.

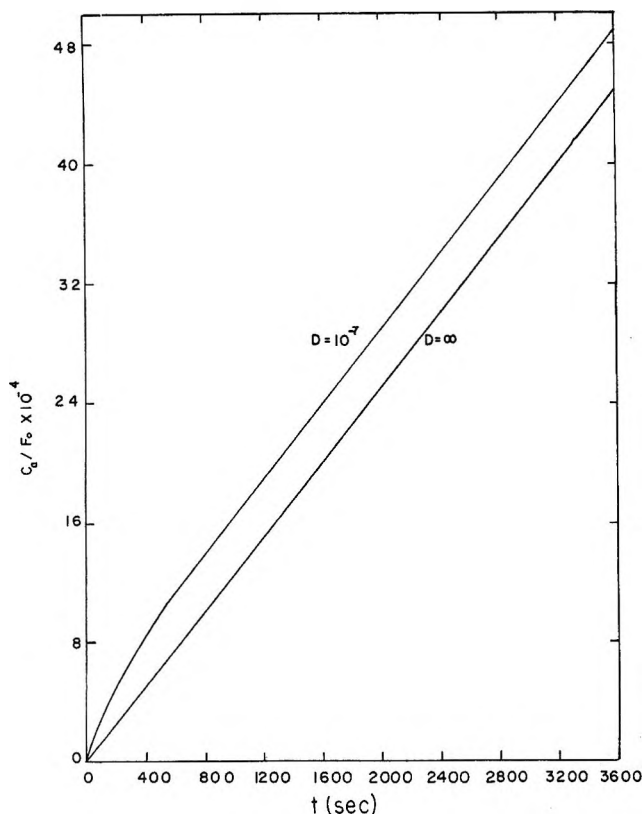


Figure 2. Plots of the ratio of surface concentration to flux ( $C_s/F_0$ ) as a function of time as calculated from the solution of the diffusion equation.

constant, and time. In Figure 2, plots of  $C_s/F_0$  vs. time are given for a cylinder having the radius of the smaller wire used in this study and values of  $D = 10^{-7}$   $\text{cm}^2 \text{sec}^{-1}$  and  $\infty$ . Clearly when  $D = \infty$  internal equilibration is established at all times. The value of  $D = 10^{-7}$   $\text{cm}^2 \text{sec}^{-1}$  is approximately the value for the diffusion constant of hydrogen in  $\alpha$ -phase Pd-H at  $0^\circ$ <sup>23</sup> and should represent the smallest value of  $D$  and therefore the largest deviation from equilibrium encountered in this study. It is seen from Figure 2 that the per cent deviation between the two curves decreases as time increases and is  $\sim 10\%$  after 1 hr. In all of the experiments in this study the rate of absorption was sufficiently reduced such that meaningful measurements of  $E$  vs.  $R/R_0$  were not taken until at least 1 hr. had elapsed. It is concluded from these arguments that the data from the slow absorption results obtained here represent, for all practical purposes, equilibrium data.

The equilibrium pressure of hydrogen at various contents was obtained from best fit curves through data similar to those in Figure 1 for several temperatures. Standard thermodynamic formulas were used to

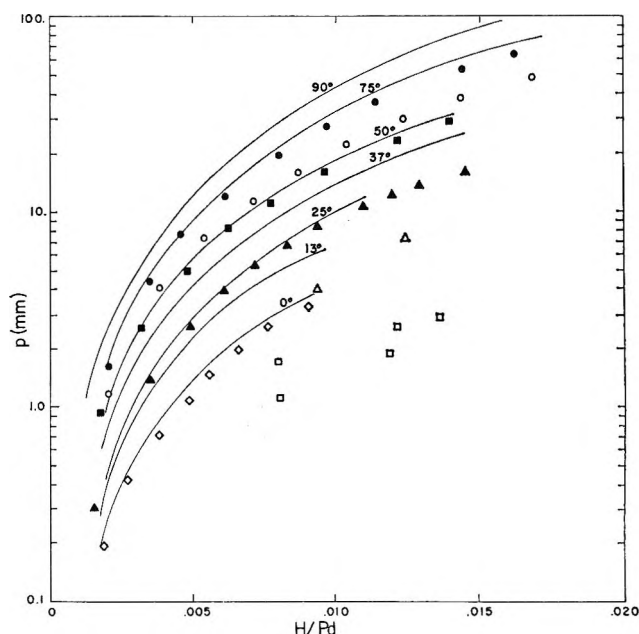


Figure 3. Absorption isotherms: —, our data; ●, ○, ■, ▲, ◇, data of Wicke and Nernst<sup>7</sup> at 75, 60, 50, 30, and  $0^\circ$ , respectively; □,  $0^\circ$  data of Gillespie and Hall<sup>6</sup>; △,  $30^\circ$  data of Gillespie and Hall.<sup>6</sup>

convert  $E$  to its equivalent pressure, e.g., ref. 10 and 24;  $R/R_0$  was converted to  $H/Pd$  from calibration curves determined for this research. The results of the present study are given in Table I and compared in Figure 3 with the recent data of Wicke and Nernst<sup>7</sup> and the data of Gillespie and Hall.<sup>6</sup> In view of the quite different experimental methods used in the present research and in that of Wicke and Nernst, the good agreement between these results is gratifying. Both sets of data seriously disagree with the often quoted  $\alpha$ -phase data of Gillespie and Hall.<sup>6</sup>

**$\alpha$ -Phase Boundaries.** The values of the upper limit of the  $\alpha$ -phase composition,  $\alpha_{\text{max}}$ , may be evaluated from the shape of the absorption isotherms. These limiting values for absorption are shown in Figure 4, where they are compared to earlier results. Again it is seen that the data of the present study and those of Wicke and Nernst<sup>7</sup> are in good agreement and these data extrapolate smoothly to the critical composition. It should also be noted that the value of  $\alpha_{\text{max}} = 0.015$  at  $25^\circ$  is smaller than that previously estimated from, for example, the change in slope of the  $R/R_0$  vs.  $H/Pd$  relationship (e.g., ref. 25); however, the redetermination of the  $\alpha$ -phase  $R/R_0$  vs.  $H/Pd$  relationships for

(23) J. W. Simons and T. B. Flanagan, to be published.

(24) J. C. Barton and F. A. Lewis, *Talanta*, **10**, 237 (1963).

(25) T. B. Flanagan and F. A. Lewis, *Trans. Faraday Soc.*, **55** 1400 (1959).

Table I: α-Phase Absorption Isotherm Data

H/Pd	P, mm.	H/Pd	P, mm.	H/Pd	P, mm.	H/Pd	P, mm.
0.0°		0.0037	1.62	0.0025	1.66	0.0120	44.48
0.00110	0.085	0.0044	2.21	0.0032	2.52	0.0127	47.65
0.00170	0.19	0.0050	2.84	0.0038	3.58	0.0134	51.75
0.00230	0.33	0.0056	3.51	0.0045	4.97	0.0140	56.10
0.00285	0.50	0.0062	4.28	0.0051	6.39	0.0147	59.90
0.00343	0.68	0.0068	5.04	0.0058	7.87	0.0154	64.23
0.00400	0.91	0.0074	5.86	0.0064	9.14	0.0161	67.90
0.00460	1.19	0.0080	6.78	0.0071	10.73	0.0168	75.55
0.00520	1.42	0.0087	7.75	0.0077	12.59	0.0203	88.86
0.00575	1.75	0.0093	8.79	0.0084	14.63	0.0224	103.50
0.00635	2.05	0.0099	9.81	0.0090	16.20	90°	
0.00690	2.42	0.0105	10.95	0.0096	18.23	0.0013	1.53
0.00750	2.78	37.0°		0.0103	20.37	0.0022	2.94
0.00805	3.17	0.0019	0.684	0.0109	22.50	0.0030	4.78
0.00865	3.48	0.0026	1.26	0.0115	24.40	0.0036	6.92
0.00920	3.72	0.0032	2.08	0.0121	26.93	0.0044	9.49
13.0°		0.0038	2.67	0.0128	29.00	0.0051	12.35
0.0018	0.32	0.0045	3.48	0.0134	31.30	0.0058	15.70
0.0024	0.57	0.0051	4.41	0.0140	33.60	0.0066	19.55
0.0030	0.87	0.0058	5.44	0.0147	35.96	0.0073	23.80
0.0036	1.20	0.0064	6.51	0.0153	38.47	0.0080	28.40
0.0042	1.63	0.0071	7.57	75°		0.0088	33.22
0.0048	2.08	0.0077	8.96	0.0028	3.38	0.0095	38.07
0.0054	2.59	0.0083	10.20	0.0035	4.94	0.0102	42.90
0.0060	3.19	0.0090	11.51	0.0043	6.71	0.0109	52.21
0.0066	3.72	0.0096	12.97	0.0050	8.61	0.0116	55.84
0.0072	4.28	0.0103	14.56	0.0057	11.11	0.0124	62.40
0.0078	4.77	0.0109	16.09	0.0064	13.92	0.0131	68.64
0.0084	5.44	0.0115	17.70	0.0071	17.00	0.0138	74.84
0.0090	5.89	0.0122	19.38	0.0078	20.37	0.0146	80.97
0.0096	6.38	0.0128	20.86	0.0085	23.64	0.0153	87.40
25.0°		0.0135	22.50	0.0092	27.82	0.0160	94.93
0.0014	0.41	0.0141	24.02	0.0099	31.80	0.0168	100.80
0.0019	0.73	50.0°		0.0106	35.35	0.0175	108.20
0.0025	1.13	0.0019	0.973	0.0113	40.27	0.0189	119.00

this research under conditions of extremely slow absorption confirm the low result.

*Sieverts' Law and Isothermic Heats.* Dissociating diatomic gases when dissolved in metals obey Sieverts' law at sufficiently small concentrations; *i.e.*, hydrogen content is proportional to  $P_{H_2}^{1/2}$ . It is seen from Figure 5 that there is a linear region at low H/Pd. The deviation from linearity at higher contents has been attributed by Lacher<sup>1</sup> as due to an attractive interaction between absorbed H atoms. This interaction was postulated to explain the formation of the β-phase although explanations based on vacancy interactions have also been proposed.<sup>26</sup> An explanation of the origin of the H-H interaction has been suggested in which the presence of strain leads to the aggregation of interstitial atoms in order to relieve the strain.<sup>27</sup>

On the other hand, Makrides has recently suggested that the interaction arises from relatively

long-rang forces characteristic of impurity centers in metals.<sup>28</sup> Whatever the origin of this interaction, according to the statistical models it should result in a linearly increasing heat of absorption with content in the α-phase.

Direct analysis of the isotherms using the Clausius-Clapeyron equation gives isothermic heats which within experimental error seem to be fairly constant with H/Pd. An average value of  $4780 \pm 100$  cal./mole of H<sub>2</sub> (1 atm.) between H/Pd = 0.002 and 0.014 was found. Although the predicted increase was not found in the direct isothermic heats, it is believed that the expected increase at such low contents is so small that it is masked

(26) A. L. G. Rees, *Trans. Faraday Soc.*, **50**, 335, 343 (1954), and G. G. Libowitz, *J. Appl. Phys.*, **33**, 399 (1962).

(27) M. von Stackelberg and P. Ludwig, *Z. Naturforsch.*, **19a**, 93 (1964).

(28) A. C. Makrides, *J. Phys. Chem.*, **68**, 2160 (1964).

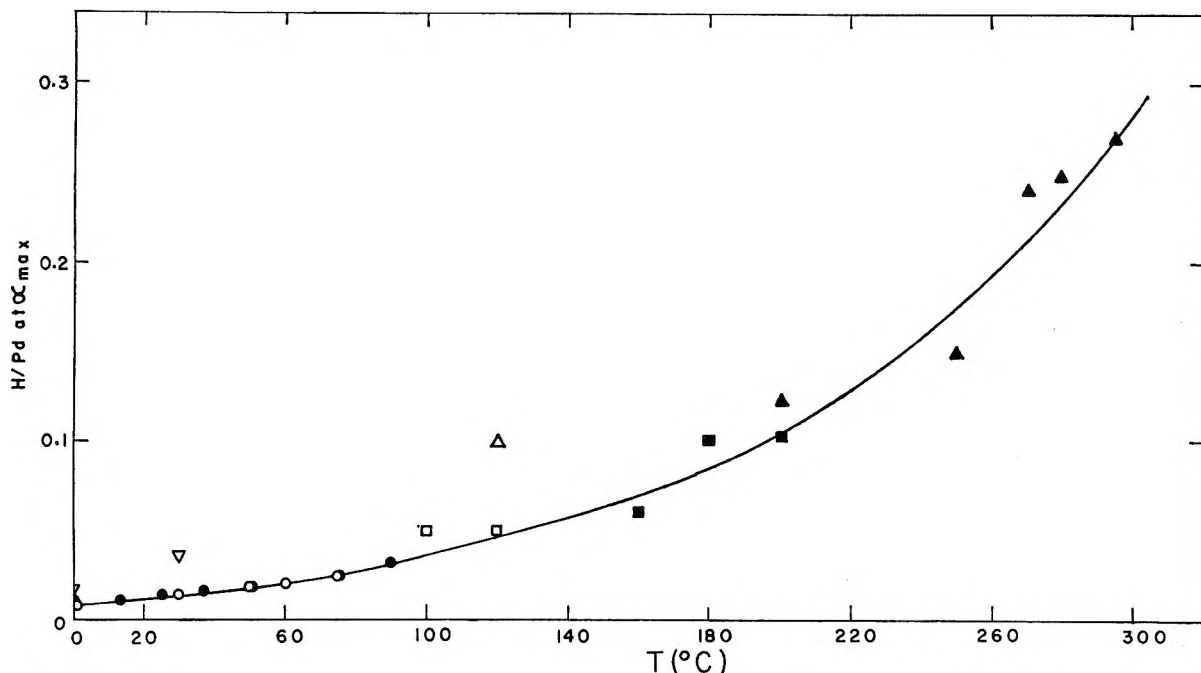


Figure 4. Composition of  $\alpha_{\max}$  (absorption data) as a function of temperature: ●, data of the present study; ○, data of Wicke and Nernst<sup>7</sup>; △, data of Everett and Nordon<sup>4</sup>; ▽, data of Gillespie and Hall<sup>6</sup>; ▲, data of Gillespie and Galstaun (*J. Am. Chem. Soc.*, **58**, 2565 (1936)); □, data of Bruning and Sieverts (*Z. physik. Chem.*, **A163**, 409 (1933)); ■, data of Sieverts and Danz (*ibid.*, **B34**, 158 (1936)).

by experimental error (see below). It should be noted that this  $\alpha$ -phase heat is considerably less than measured heats for the  $\alpha \rightarrow \beta$  phase transition, 9500 cal./mole of  $H_2$  (see ref. 10 for a review).<sup>29</sup>

*Analysis in Terms of Statistical Models.* The usefulness of the analysis of  $\alpha$ -phase data in terms of a rearranged form of Lacher's original statistical eq. 1 was first pointed out by Everett and Nordon.<sup>4</sup> Wicke and Nernst analyzed their results in terms of a variation of the same equation. All of the subsequent modifications, as well as Lacher's original model, give rise to equations which can be written in the general form

$$\ln p^{1/2}(1 - n/n_s)/(n/n_s) = C_1 + C_2/RT + C_3n/RTn_s \quad (1)$$

where  $p$  is the equilibrium pressure of hydrogen,  $n$  is the H-atom content, H/Pd,  $n_s$  is the total number of available sites per Pd for H atoms whose value depends upon the particular model in question. The constants  $C_1$  and  $C_2$  are in most cases identified with the entropy and enthalpy per gram atom of H, respectively, of interaction with the palladium lattice of isolated non-interacting hydrogen atoms. This equation can be simplified to

$$\ln p^{1/2}/n = C_1 + C_2/RT - \ln n_s + C_3n/RTn_s \quad (2)$$

for the small values of  $n$  encountered in this research.

Analysis of  $\alpha$ -phase isotherms in terms of eq. 2 was accomplished by plotting the left-hand side of eq. 2 vs.  $n$  at each temperature giving the expected linear relationships, e.g., Figure 6. The slopes of these plots gave  $C_3/RTn_s$  with intercepts  $(C_1 + (C_2/RT) - \ln n_s)$ . Values of  $C_1$  and  $C_2$  for  $n_s = 1$  were determined from the plot of  $(2C_1 + 2(C_2)/RT)$  vs.  $1/T$  shown in Figure 7. Clearly, the magnitudes of  $C_1$  and  $C_3$  obtained depend upon the value of  $n_s$  selected. Values of  $n_s$  from 0.59<sup>1</sup> to 1<sup>7</sup> have been employed in the past depending upon the particular statistical model in question and the interpretation of  $n_s$ . The authors have supported the value of  $n_s = 1$  in a previous publication.<sup>5</sup> Although in that work a value of  $n_s = 0.72$  was derived from an experimentally determined electronic band shape for palladium and the critical temperature isothermal data,<sup>5</sup> the authors believe that this value is not to be taken literally in view of the approximate nature of the band shape employed. A not unreasonable change in the band shape would yield a value of  $n_s \sim 1$ . In the present research  $n_s = 1$  has been employed.

The values obtained for  $C_1$ ,  $C_2$ , and  $C_3$  with  $n_s = 1$  lead to

(29) A. Maeland and T. B. Flanagan, *J. Phys. Chem.*, **68**, 1419 (1964).

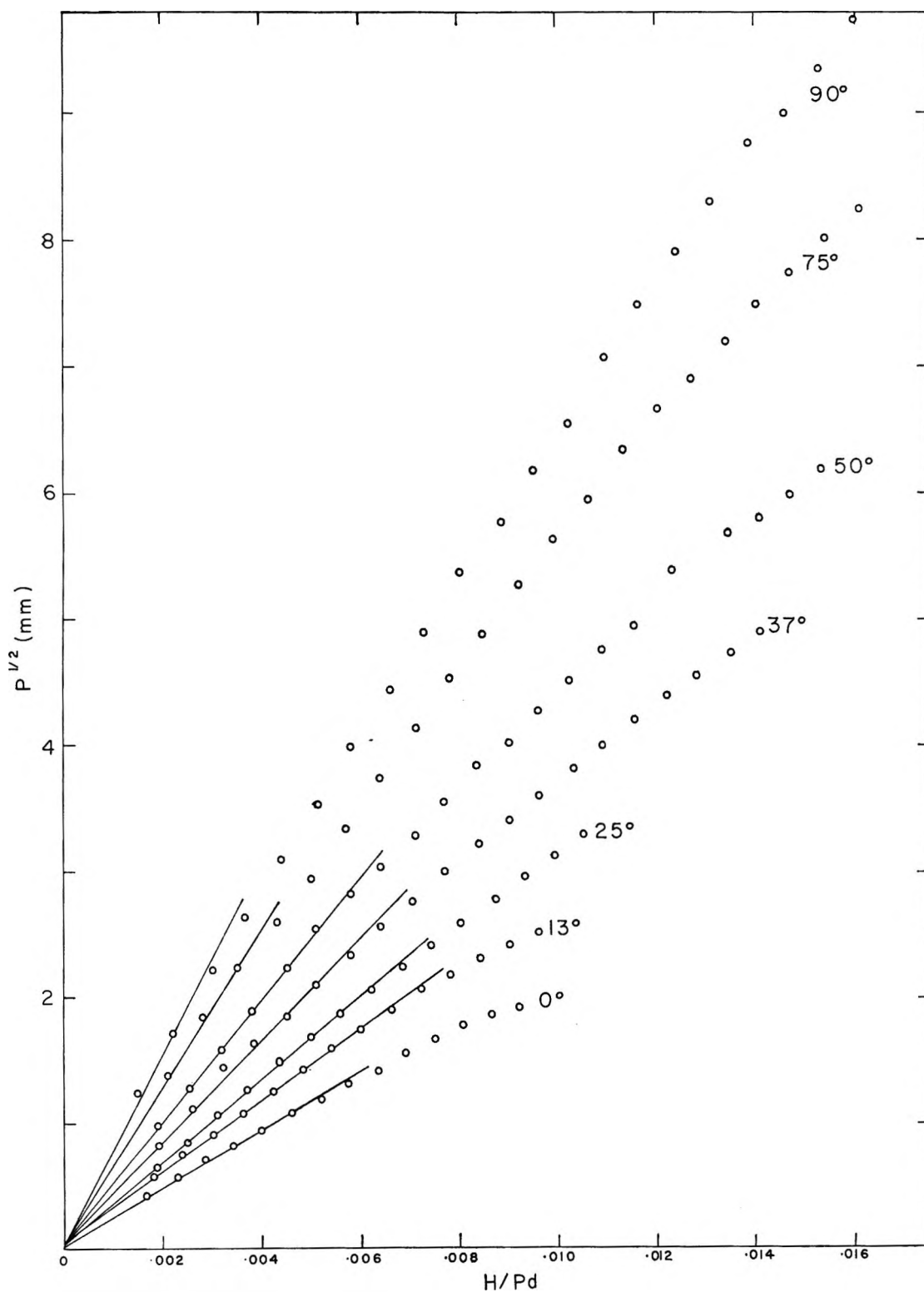


Figure 5. Sieverts' law plots of the α-phase data of the present study.

$$\ln p(\text{atm.}) = 13.04 - 2327/T - 11110n/T + 2 \ln n/(1 - n) \quad (3)$$

This equation predicts the observed isothermal data

quite well. This is similar to the equation given by Wicke and Nernst<sup>7</sup> except that they assign a temperature dependence to  $C_3$  which, however, is not necessary to fit either their data or the present data and it is

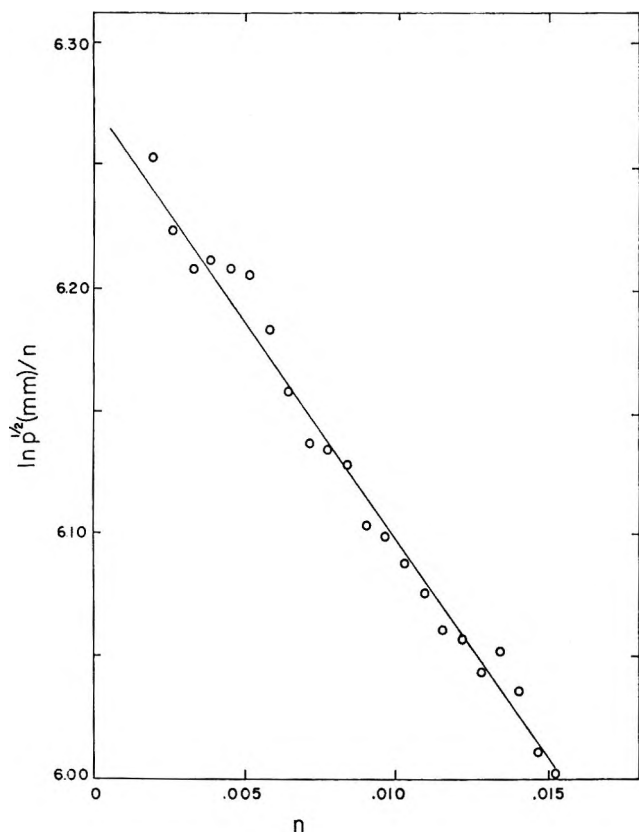


Figure 6. Typical plot of  $\ln p^{1/2}/n$  vs.  $n$  ( $50^\circ$ ).

believed that a magnitude for the temperature dependence of  $C_3$  has not been sufficiently well established experimentally to be given explicitly.

Applying the relationship  $\Delta\bar{H} = -R[(\partial \ln p)/(\partial 1/T)]$  to eq. 3 gives the expression in eq. 4 for the differential molar enthalpy of absorption.

$$\Delta\bar{H} = -2C_2 - 2C_3n = -4623 - 22,075n \quad (4)$$

The bar over the thermodynamic parameter signifies a differential quantity of absorption, *i. e.*, the change occurring at a given value of  $n$ , per mole, when an infinitesimal quantity of gas (1 atm.) is transferred from the gas to the solid phase. This equation predicts a change in  $\Delta\bar{H}$  of 309 cal./mole between  $n = 0$  and 0.014; it is not surprising that this small change could not be detected in the isosteric heats of absorption as determined from direct application of the Clausius-Clapeyron equation to the isotherms, since  $2C_2$  is much greater than  $2C_3n$  (eq. 4) and random experimental errors would mask the small dependence of  $\Delta\bar{H}$  on  $n$ . By contrast, the indirect approach, utilizing eq. 2, gives  $C_3/RT$  directly, so that the interaction constant,  $C_3$ , can be evaluated without influence from random errors in  $C_2$ . It is reassuring but not surprising that the observed isosteric heat falls within the range

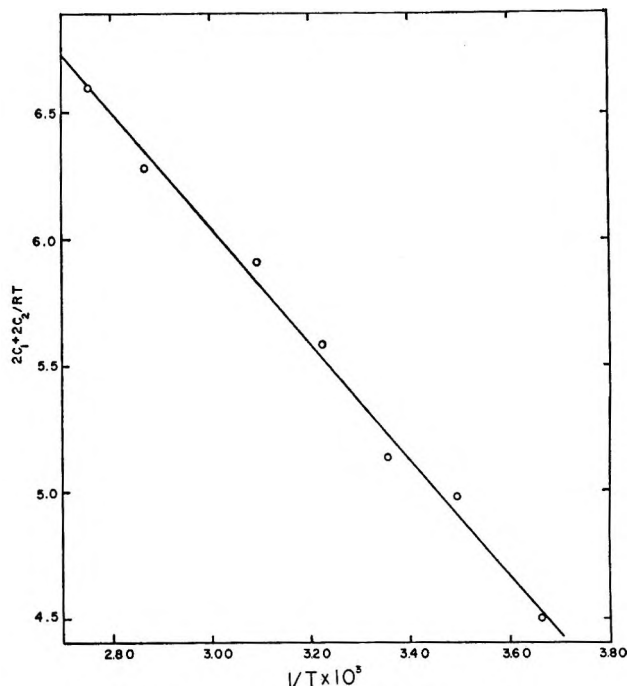


Figure 7. Plot of  $2C_1 + 2C_2/RT$  vs.  $1/T$  ( $0$  to  $90^\circ$ ).

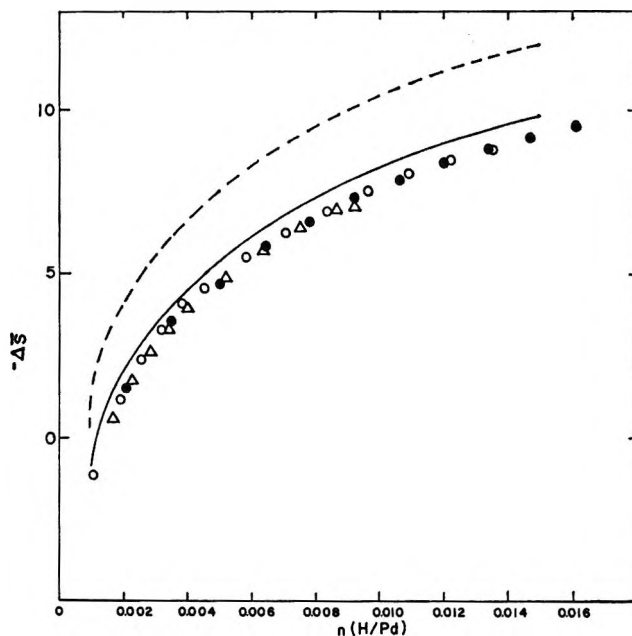


Figure 8. Plots of  $\Delta S$  vs.  $n$ : ———, calculated values for  $n_s = 1$  ( $25^\circ$ ); ———, calculated values for  $n_s = 0.6$  ( $25^\circ$ ); experimental values:  $\Delta$ ,  $0^\circ$ ;  $\circ$ ,  $37^\circ$ ;  $\bullet$ ,  $75^\circ$ .

predicted by eq. 4. The "final" equations of Lacher<sup>1</sup> and Everett and Nordon<sup>4</sup> in which all of the constants have been numerically evaluated using the data available at that time, yield values of  $\Delta\bar{H}$  considerably different from those observed here.

It is unfortunate that the increase in the absolute value of the enthalpy of absorption with content in the  $\alpha$ -phase should depend upon the use of eq. 2 and was not directly observable. However, it is difficult to question the applicability of eq. 2 to this problem since the general form, in a thermodynamic sense, simply implies the existence of nonideal solution behavior.<sup>30</sup> In addition, some preliminary results obtained in this laboratory on gold-palladium alloys, which have a much greater  $\alpha$ -phase solubility, show an easily observable change in the isosteric enthalpy of absorption with content.

At the critical point,  $n_c = 0.27$ , the enthalpy of absorption should correspond closely to the value for the two-phase region. From eq. 4 we predict  $\Delta\bar{H} = -10,583$  as compared to the two-phase value of approximately  $-9500$  cal./mole. The agreement is not bad considering the 20-fold extrapolation of the value of  $n$ .

It is instructive to consider the entropy change upon absorption separately because it allows the configurational and thermal entropy terms due to isolated absorbed hydrogen atoms to be separated from the less-clearly delineated H-H interaction term. Experimental values of  $\Delta\bar{S}$  were determined from the measured values of  $\Delta\bar{G}$  at a given  $n$  and the corresponding values of  $\Delta\bar{H}$  from eq. 4. These values of  $\Delta\bar{S}$  vs.  $n$  at 0, 37, and 75° are shown in Figure 8. In view of our use of eq. 4 to evaluate  $\Delta\bar{H}$ , it should be emphasized that its values and consequently the experimental values  $\Delta\bar{S}$  are nonetheless independent of  $n_s$  provided that  $n_s \gg n$  (a necessary condition in

going from eq. 1 to 2). Variations in  $n_s$  alter the values of  $C_1$  and  $C_3$  but not the fit of eq. 2 to the data or the numerical coefficients of the terms in eq. 3 or 4. Alternatively, the average value of the direct isosteric heat has been used; this gave insignificant changes from the experiment  $\Delta\bar{S}$  values in Figure 8. Theoretical values of  $\Delta\bar{S}$  were estimated by considering the absorbed hydrogen atoms as three-dimensional localized oscillators. Bergsma and Goedkoop<sup>31</sup> have found  $\nu_H = 13.54 \times 10^{12}$  sec.<sup>-1</sup> for  $\alpha$ -phase palladium hydride from neutron scattering experiments; we will assume that the same value is valid for the  $\alpha$ -phase, since  $\Delta\bar{S}$  is relatively insensitive to the precise value of  $\nu_H$ .

$$\Delta\bar{S}_{298} = 2S_a - S_{H_2} \quad (5)$$

where  $S_a = -R \ln (n/n_s)/(1 - n/n_s) - 3R \ln (1 - e^{-x}) + 3Rx/(e^x - 1)$ ,  $x = h\nu/kT$ , and  $S_{H_2} = 31.21$  e.u. (1 atm.). Values of  $\Delta\bar{S}_{298}$  with  $n_s = 1$  and 0.6 are also shown in Figure 8. It is seen from Figure 8 that the agreement of the experimental data with the curve for  $n_s = 1$  is good and lends support to this value.

*Acknowledgments.* The authors wish to thank Roger Kendall for assistance in obtaining the data. We gratefully acknowledge the financial support for this work by U. S. Atomic Energy Commission Contract AT(30-1)-3000. We wish to thank Professor E. Wicke for supplying us with his detailed  $\alpha$ -phase data.

(30) K. A. Moon, *J. Phys. Chem.*, **60**, 502 (1956).

(31) J. Bergsma and J. A. Goedkoop, *Physica*, **26**, 744 (1960).

## Viscosity of NaK 78 at Low Temperatures

by George Macur, E. L. Grove, Allan J. Gaynor, and Charles K. Hersh

*IIT Research Institute, Technology Center, Chicago, Illinois (Received May 3, 1965)*

The viscosities of sodium-potassium alloys containing 79.2 to 77.3 wt. % potassium were determined in the temperature range from  $-10$  to  $148.9^\circ$ . The oxygen content of the alloys ranged from 32.3 to 238 p.p.m. The viscosities of the alloys increase rapidly at low temperatures but are not abnormally high even at temperatures a few degrees above the point when the alloy begins to solidify. A plot of the data according to the second equation of Andrade is reasonably linear.

The use of NaK 78 as a working fluid in a high-temperature nuclear electric-generating system (SNAP) has created the need for data on its liquid viscosity at low temperatures. (NaK 78 is an alloy corresponding to the eutectic composition of 78.5 wt. % potassium and 21.5 wt. % sodium and is the lowest melting ( $-11.1^\circ$ ) alloy of the system.) During the 25-hr. lapse between launch and startup in orbit, the fluid temperature drops to about  $-6.67^\circ$ . The fluid is circulated through the system during this time interval, and pumping requirements change quite drastically with temperature. This study was undertaken to determine the effects of temperature ( $-3.9$  to  $148.9^\circ$ ) on the viscosity of NaK 78.

A review of the literature revealed that many investigators<sup>1-3</sup> have studied the viscosity of the NaK system but not in the temperature range of interest. A modified glass Ostwald viscometer was selected as the most useful for viscosity measurements.

### Experimental Work

*Analytical Apparatus and Handling Procedure.* The apparatus (Figure 1) used for the NaK analyses was a modification of the design first proposed by Williams and Miller<sup>4</sup> and by Lee and Walter.<sup>5,6</sup>

The amalgamation chamber of the apparatus was constructed of Vycor; the other components were constructed of Pyrex since NaK does not react with glass below  $149^\circ$ .<sup>7</sup> In order to have a sealed system, an inlet tube, which was connected to a NaK 78 reservoir with a 4-mm. bore stopcock, was inserted into the amalgamation chamber at a  $30^\circ$  angle. A modified Ostwald viscometer, which would be used with various amounts of liquid sample, was attached to the chamber

at the lower outlet by a ball joint. The stopcocks and ball joints were lubricated very sparingly with Apiezon N, a low-vapor-pressure stopcock grease.

Before assembly and after each run, all components were carefully cleaned. After assembly and before each run, the apparatus was flushed with purified argon, and the parts that were to receive the NaK alloy were flamed vigorously with a Bunsen burner to desorb moisture and any other gases. To scavenge oxygen from the argon gas stream, argon was passed through a heated tube packed with fine copper turnings and then through a large chamber containing molecular sieves (No. 4A).

*Analysis for Sample Size and Composition.* The NaK alloy was alloyed with mercury in the amalgamation chamber of the apparatus to separate the alloy from the oxides. This method of oxide-alloy separation by amalgamation and flotation was developed by Pepkowitz and Judd.<sup>8</sup> The oxide portions were analyzed for Na and K by flame spectrophotometry.

(1) C. T. Ewing, J. A. Grand, and R. R. Miller, *J. Am. Chem. Soc.*, **73**, 1168 (1951).

(2) C. T. Ewing, A. Grand, and R. R. Miller, *J. Phys. Chem.*, **58**, 1086 (1954).

(3) S. S. Kutateladze, V. M. Borishanskii, I. I. Novikov, and O. S. Fedynskii, *Az. Energ. Prilozhenie*, No. 2 (1958).

(4) D. D. Williams and R. R. Miller, *Anal. Chem.*, **23**, 1865 (1951).

(5) R. E. Lee and S. L. Walters, Mine Safety Appliances Co., Report No. TR-4, May 1940.

(6) R. N. Lyon, Ed., "Liquid Metals Handbook, Sodium and NaK Supplement," TID 5277, Atomic Energy Commission, Department of the Navy, Washington, D. C., 1955, p. 99.

(7) R. N. Lyon, Ed., "Liquid Metals Handbook," 2nd Ed., Atomic Energy Commission, Department of the Navy, Washington, D. C., 1952.

(8) L. P. Pepkowitz and W. C. Judd, *Anal. Chem.*, **22**, 1283 (1950).



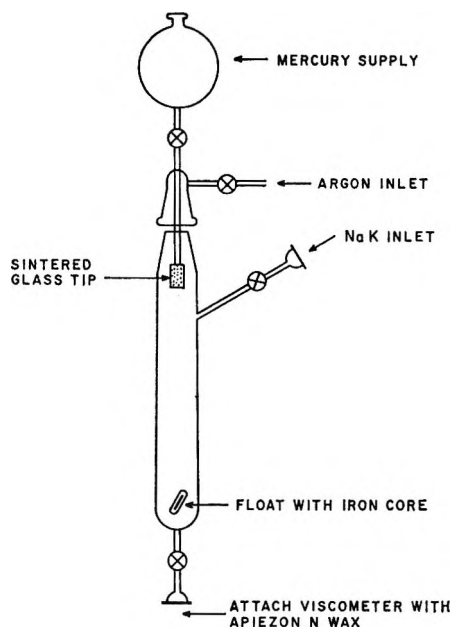


Figure 1. Apparatus used for NaK analyses.

The sample weight was determined by extracting the NaK with standardized hydrochloric acid and water. The process consisted of passing the amalgam through a capillary into a column of standard acid and then through a column containing water. The resultant solution was diluted volumetrically, and then appropriate aliquots were analyzed for Na and K by flame spectrophotometry. The total amount (milliequivalents) was determined by adding excess standard acid to the total sample and back-titrating with standard base. The standards for the flame analysis contained 78% K and 22% Na by weight to compensate for mutual radiation interference.

**Viscosity Measurements.** The modified Ostwald viscometer (Figure 2) used in this study was made from precision-bore tubing (4 mm.) with a capillary section 0.203 mm. in diameter and 12 cm. in length.

Liquid NaK was forced to a convenient height above the capillary section by argon pressure. Then the stopcock isolating the two arms of the viscometer was opened, and the readings of the height,  $h$ , of the liquid as it fell through the capillary were taken as a function of time. The driving pressure was proportional to the difference between the liquid and the equilibrium levels,  $h - h_e$ , and in the uniform-bore tubing the rate of flow was proportional to  $dh/dt$ . Hence, for liquids following Poiseuille's law,  $\log(h - h_e)$  should be proportional to the time of flow. In every case, the linear relation between  $\log(h - h_e)$  and time showed that NaK alloys are Newtonian fluids.

For convenience, the half-time ( $t_{1/2}$ ), which is the

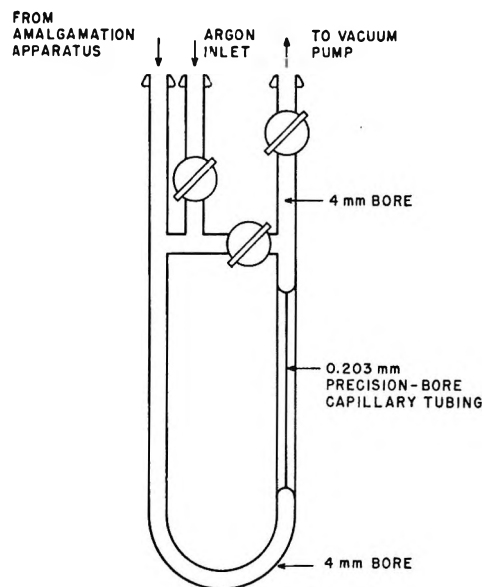


Figure 2. Modified Ostwald viscometer.

time for the liquid to fall half the distance from the initial level to the equilibrium level, was determined from the plot of  $h - h_e$  vs. time. The viscosity was calculated from the equation  $\mu = C t_{1/2} \rho$ , where  $\mu$  is viscosity,  $\rho$  is density, and  $C$  is an apparatus constant determined with liquids of known viscosity (0.008214 cp. ml./g. sec.).

In the majority of the measurements conducted, the viscometer was filled with NaK contained in small glass ampoules rather than with that in the NaK reservoir.

A new ampoule was used for each run. The ampoules were suspended in the apparatus and broken open under an argon atmosphere in the tube used for the amalgamation procedure. The NaK was then transferred to the viscometer.

After the viscosity determinations were completed, the NaK was transferred directly from the viscometer to the amalgamation vessel by argon pressure. Table I summarizes the viscosity data obtained from these measurements.

**Density.** The densities of the sodium-potassium alloys at the required temperatures were obtained by interpolation and extrapolation of the data given by Ewing, *et al.*<sup>1</sup> These workers report the densities of an alloy containing 78.6% K by weight in the temperature interval from 60 to 200°. They state that the accuracy of the reported densities is better than  $\pm 0.2\%$ . A reasonable estimate of the accuracy of the extrapolated and interpolated densities would be about  $\pm 1.0\%$ .

**Bath Temperature Uncertainties.** During the viscosity measurements the viscometer was immersed in

Table I: Viscosity of NaK Alloys at Various Temperatures

% composition—		Temp., °C.	Density, g./ml.	Viscosity, cp.	O <sub>2</sub> content, p.p.m.
Na	K				
22.7	77.3	0	0.872	1.19	40
		25.6	0.865	0.895	
		148.9	0.840	0.46	
20.8	79.2	0	0.872	1.18	238
		25.6	0.865	0.936	
		148.9	0.840	0.54	
21.5	78.5	0	0.872	1.18	34.2
		25.6	0.865	0.915	
		148.9	0.840	0.45	
20.7	79.3	0	0.872	1.16	423.5
		25.6	0.865	0.881	
		148.9	0.840	0.42	
21.5	78.5	-6.1	0.873	1.25	44.9
		0	0.872	1.08	
		25.6	0.865	0.866	
21.8	78.2	-6.1	0.873	1.25	106.4
		0	0.872	1.07	
		25.6	0.865	0.853	
21.3	78.7	-6.1	0.873	1.25	32.3
		0	0.872	1.12	
		25.6	0.865	0.880	

various constant-temperature baths: (1) Freon-C-318, b.p.  $-6.1^\circ$ , reported in technical data sheet; observed temperature (thermometer) ranged from  $-13.0$  to  $-5.0^\circ$ ; (2) crushed-ice bath  $0 \pm 0.1^\circ$  (estimated); (3) room temperature  $25.6 \pm 0.2^\circ$  (observed); (4) stirred, thermostated, paraffin oil bath  $93.3 \pm 1^\circ$  and  $148.9 \pm 1^\circ$ . (The range of temperature for the Freon-C-318 bath is similar to that observed by other workers with Freon-12 baths in our laboratories.)

*Over-all Accuracy of Viscosity Measurements.* The most accurate viscosity measurements ( $\pm 1\%$ ) are those made at room temperature ( $25.6^\circ$ ) since in this case there are no vessels to cut down the visibility of the NaK 78 meniscus inside the viscometer. Somewhat less accurate data are obtained at  $93.3$  and  $148.9^\circ$  owing to the fact that the flow times are shorter. The accuracy of the measurements with the crushed-ice bath is diminished because the cold stopcocks are more difficult to manipulate, the meniscus is harder to see, and also because the density of NaK 78 is extrapolated. It must also be remembered that NaK reacts explosively with water or ice.

Finally, the measurements in the Freon-C-318 bath were the most difficult to carry out and, consequently,

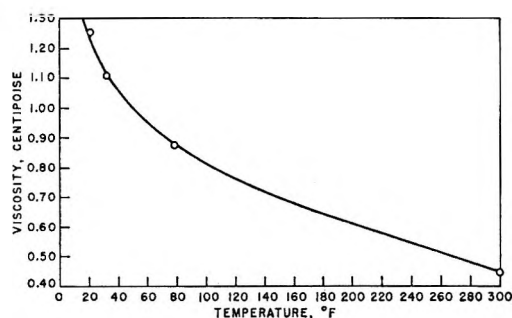
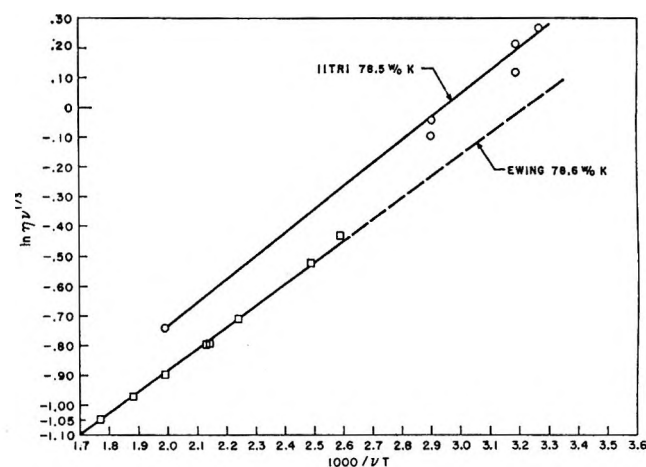


Figure 3. Plot of viscosity vs. temperature.

Figure 4. Plot of  $\ln \eta \nu^{1/2}$  vs.  $1000/\nu T$ .

are lowest in order of accuracy. Again, it is difficult to observe the meniscus level because of clouding of the Freon, bubbling due to boiling, and ice formation due to condensation of atmospheric moisture on the cold Freon surface and the glass dewar surface. Here the NaK 78 density must be extrapolated from  $60$  to  $-6.7^\circ$ . There is also the variation of the Freon-C-318 temperature already mentioned.

## Results and Discussions

The viscosity of NaK alloys of  $79.2$  to  $77.3\%$  K was determined in the temperature range  $-10$  to  $148.9^\circ$ . The oxygen content of the alloys ranged from  $32.3$  to  $238$  p.p.m. Most of the alloys contained  $78\%$  K and had oxygen contents below  $100$  p.p.m.

During measurements of the  $-6.1^\circ$  viscosities, lower temperatures were obtained for short periods. At  $-11.1^\circ$  NaK 78 did not flow and appeared to be solid, but at about  $-10^\circ$  the liquid alloy began to flow and behave normally. The viscosity values represent at least three independent measurements for each viscosity reported. A plot of viscosity vs. temperature is shown in Figure 3.

NaK alloys with compositions close to 78% K and with low oxygen contents behave normally with regard to flow and viscosity. Even at temperatures as low as  $-6.1^{\circ}$ , they flow readily and have viscosities that are only moderately higher than those at room temperature.

The effect of oxide content is not clear, and some investigation is required before a positive statement can be made. It does appear, however, that a small amount of oxide contaminant does reduce the viscosity.

A comparison of the data from this study with that of Ewing<sup>1</sup> is shown in the Andrade plot<sup>9</sup> given in Figure 4. On this plot  $\ln \eta \nu^{1/3}$  is plotted against  $1000/\nu T$ , where  $\eta$  is the viscosity,  $\nu$  is the specific volume, and  $T$  is the absolute temperature. Our viscosity data are in

agreement with the trend discussed by Ewing. He noted that the data below  $100^{\circ}$  showed significant deviations from the Andrade equation based on the data above  $100^{\circ}$ . Both our data and his show lower values than those predicted by the equation based on data above  $100^{\circ}$ . An Andrade plot of the data from this study is reasonably linear over a considerable range of temperature.

*Acknowledgment.* The authors wish to acknowledge the support of this work by Atomic International, Canoga Park, Calif., and Messrs. M. Perlow and R. Keene of that organization for their technical guidance.

(9) E. N. daC. Andrade, *Phil. Mag.*, 17, 698 (1934).

## Sedimentation and Electrophoresis of Interacting Substances. IV. Theory of the Analysis of Interacting Systems by Differential Boundary Experiments

by R. C. L. Jenkins

*Department of Mathematics, Portsmouth College of Technology, Portsmouth, Hants, England*  
(Received May 3, 1965)

The type of boundary formed in differential boundary sedimentation, electrophoresis, or chromatography experiments on reversibly interacting systems is investigated mathematically. With the simplifying assumption that the transport velocities of the components are independent of total concentration, it is shown that the boundary splits up into a number of separate parts, the velocities and "areas" of which are simply related to the free molar concentrations of the components and their transport velocities. This is in distinct contrast with conventional boundary experiments on reversibly interacting systems.

### Introduction

The detailed mathematical analysis of conventional sedimentation, electrophoresis, or chromatography experiments on reversibly interacting systems<sup>1</sup> is difficult with the exception of a few important but comparatively simple cases.<sup>2,3</sup> With the possible exception of these cases, differential boundary experiments,<sup>4,5</sup> in which a boundary is formed between two solutions of slightly differing constituent concentrations, seem to

offer distinct advantages.<sup>6</sup> It is shown in this paper that if the simplifying assumption is made that the

(1) L. W. Nichol, J. L. Bethune, G. Kegeles, and E. L. Hess in "The Proteins," 2nd Ed., H. Neurath, Ed., Academic Press, New York, N. Y., 1964, Chapter 9.

(2) G. A. Gilbert *Proc. Roy. Soc. (London)*, A250, 377 (1959).

(3) G. A. Gilbert and R. C. L. Jenkins, *ibid.*, A253, 420 (1959).

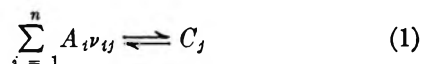
(4) L. G. Longworth in "Electrophoresis," M. Bier, Ed., Academic Press, New York, N. Y., 1959, Chapter 3.

transport velocities of the reacting species are independent of concentration, the initial boundary breaks up into several separate boundaries, each traveling with a characteristic velocity, and the mathematical analysis required to find reaction constants, etc., then consists of solving a set of linear (algebraic) equations. The case where the concentration dependence of the transport velocities cannot be neglected (as will usually be the case in practice) will be considered in a subsequent paper where it will be shown that the initial boundary again breaks up into several separate parts but the set of equations that have to be solved to determine reaction constants, etc., are no longer entirely linear.

In addition to the assumption of concentration independent transport velocities, it will be assumed that the transport of the reacting species occurs in a rectangular or cylindrical cell, their reactions are governed by the simple form of the law of mass action, and that they are subject to a uniform force field parallel to the axis of the cell. Finally, the effects of diffusion and finite time of reaction will be neglected. The neglect of such effects will not be as serious in the present context as it might appear as they will only tend to broaden the various separate parts of the boundary without altering their characteristic velocities or "areas."

### Theory

Consider a system in which  $n$  reactants  $A_1, A_2, \dots, A_n$  form  $m$  complexes  $C_1, C_2, \dots, C_m$  reversibly in solution according to the  $m$  linearly independent equations



where the  $\nu_{ij}$  are, of course, integral or fractional constants. These reactions are governed by the simple form of the law of mass action, *i.e.*

$$\prod_{i=1}^n a_i^{\nu_{ij}} = k_j c_j \quad (2)$$

where  $a_i$  and  $c_j$  are the free molar concentrations of  $A_i$  and  $C_j$ , respectively, and  $k_1, k_2, \dots, k_m$  are dissociation constants.

The constituent molar concentrations  $\bar{m}_1, \bar{m}_2, \dots, \bar{m}_n$  of the  $A_i$  are defined by

$$\bar{m}_i = a_i + \sum_{j=1}^m \nu_{ij} c_j \quad (3)$$

Let the velocities of  $A_i$  and  $C_j$  be  $v_i$  and  $u_j$ , respectively, which are by assumption independent of concentration. The constituent molar flux of  $A_i$  is  $v_i a_i + \sum_{j=1}^m \nu_{ij} u_j c_j$ . The net rate of accumulation of  $A_i$  in its free and combined states within a small region at a

distance  $x$  down the axis of the "cell" at a time  $t$  must equal the net rate at which it flows into this region. Since the effects of diffusion are being neglected this implies that

$$\frac{\partial}{\partial t} \left( a_i + \sum_{j=1}^m \nu_{ij} c_j \right) + \frac{\partial}{\partial x} \left( v_i a_i + \sum_{j=1}^m \nu_{ij} u_j c_j \right) = 0 \quad (4)$$

For a boundary that is sharp at a time  $t = 0$ , the molar concentrations  $a_i$  and  $c_j$  can be functions only of  $v = x/t$  where  $x$  is measured from the initial position of the boundary. This follows on dimensional grounds as only constants of the dimensions of molar concentration and velocity occur in the problem. Equation 4 therefore becomes<sup>7</sup>

$$(v_i - v) \frac{da_i}{dv} + \sum_{j=1}^m \nu_{ij} (u_j - v) \frac{dc_j}{dv} = 0 \quad (5)$$

As the assumption is being made that the reversible reactions 1 are so rapid that the components are always in chemical equilibrium, it follows from eq. 2 that

$$\frac{d}{dv} (\log c_j) = \sum_{i=1}^n \nu_{ij} \frac{d}{dv} (\log a_i) \quad (6)$$

If the

$$\frac{dc_j}{dv} = c_j \frac{d}{dv} (\log c_j)$$

are now eliminated from eq. 5 by means of eq. 6, it is found that

$$\sum_{j=1}^m (q_{ij} - v p_{ij}) \frac{d}{dv} (\log a_j) = 0 \quad (7)$$

where

$$p_{ij} = p_{ji} = a_i \delta_{ij} + \sum_{k=1}^m \nu_{ik} \nu_{jk} c_k \quad (8)$$

$$q_{ij} = q_{ji} = v_i a_i \delta_{ij} + \sum_{k=1}^m \nu_{ik} \nu_{jk} u_k c_k$$

and

$$\delta_{ij} = \begin{cases} 1 & \text{if } i = j \\ 0 & \text{if } i \neq j \end{cases}$$

Thus if all the  $d/dv(\log a_i)$  are not to be identically zero, the determinant of the coefficients of the set of  $n$  linear eq. 7 must vanish, *i.e.*

(5) R. T. Hersh and H. K. Schachman, *J. Am. Chem. Soc.*, **77**, 5528 (1955); *J. Phys. Chem.*, **62**, 170 (1958).

(6) G. A. Gilbert and R. C. L. Jenkins, *Nature*, **199**, 688 (1963).

(7) If  $f(v)$  is a function only of  $v$  where  $v = x/t$  then

$$\frac{\partial f}{\partial x} = \frac{\partial v}{\partial x} \frac{df}{dv} = \frac{1}{t} \frac{df}{dv}, \quad \frac{df}{\partial t} = \frac{\partial v}{\partial t} \frac{df}{dv} = -\frac{v}{t} \frac{df}{dv}$$

$$\begin{vmatrix} q_{11} - vp_{11} & q_{12} - vp_{12} & \dots & q_{1n} - vp_{1n} \\ q_{21} - vp_{21} & q_{22} - vp_{22} & \dots & q_{2n} - vp_{2n} \\ \dots & \dots & \dots & \dots \\ q_{n1} - vp_{n1} & q_{n2} - vp_{n2} & \dots & q_{nn} - vp_{nn} \end{vmatrix} = 0 \quad (9)$$

The determinant is a polynomial of degree  $n$  in  $v$ ,<sup>8</sup> and it can be shown that *all* the roots, say  $V_1, V_2, \dots, V_n$ , of this eq. 9 must be real (see Appendix). Hence all the  $d/dv(\log a_i)$  are zero unless  $v$  is equal to one of the  $V_k$ .

Now suppose a differential boundary experiment is carried out in which a solution of the  $A_i$  at constituent molar concentrations  $\bar{m}_i$  is layered over a similar solution with the  $A_i$  at slightly differing constituent molar concentrations  $\bar{m}_i + \Delta\bar{m}_i$  to form an initially sharp differential boundary. Let the corresponding free molar concentrations of the  $A_i$  and  $C_j$  in these solutions be  $a_i, c_j$ , and  $a_i + \Delta a_i, c_j + \Delta c_j$ , respectively. Since the over-all changes in the free molar concentrations across the boundary,  $\Delta a_i$  and  $\Delta c_j$ , are small, it follows that throughout the whole boundary region the free molar concentrations of the  $A_i$  and  $C_j$  differ little from the molar concentrations  $a_i$  and  $c_j$ . Therefore, eq. 7 with these values of the free molar concentrations are valid throughout the boundary region. Therefore, as the  $d/dv(\log a_i)$  are all zero unless  $v$  is equal to  $V_1, V_2, \dots$  or  $V_n$ , it follows that the boundary consists of  $n$  separate parts, the  $k$ th part traveling with a velocity  $V_k$ .

Let the changes in the free molar concentrations of the  $A_i$  and  $C_j$  across the  $k$ th part of the boundary by  $\Delta a_i^{(k)}$  and  $\Delta c_j^{(k)}$ . It then follows from eq. 7 that

$$\sum_{i=1}^n (q_{ij} - V_k p_{ij}) \Delta(\log a_j)^{(k)} = 0 \quad (10)$$

If the molecular weights of the  $A_i$  are  $M_i$ , the molecular weights of the  $C_j$  will be  $\sum_{i=1}^n M_i \nu_{ij}$ . Therefore, the total changes in concentration (w./v.) across the  $k$ th part of the boundary  $\Delta W_k$  will be given by

$$\begin{aligned} \Delta W_k &= \sum_{i=1}^n M_i \Delta a_i^{(k)} + \sum_{j=1}^m \left( \sum_{i=1}^n M_i \nu_{ij} \right) \Delta c_j^{(k)} \\ &= \sum_{i=1}^n M_i \left( \Delta a_i^{(k)} + \sum_{j=1}^m \nu_{ij} \Delta c_j^{(k)} \right) \end{aligned} \quad (11)$$

However, from eq. 2 or 6

$$\Delta(\log c_j)^{(k)} = \sum_{i=1}^n \nu_{ij} \Delta(\log a_i)^{(k)} \quad (12)$$

and if the  $\Delta c_j^{(k)} = c_j \Delta(\log c_j)^{(k)}$  are now eliminated from eq. 11 it is found that

$$\Delta W_k = \sum_{i=1}^n \sum_{j=1}^m M_i p_{ij} \Delta(\log a_j)^{(k)} \quad (13)$$

If the quantities  $\alpha_{ik}$  are now defined to be the solutions of the equations<sup>9</sup>

$$\sum_{j=1}^m (q_{ij} - V_k p_{ij}) \alpha_{jk} = 0 \quad (14)$$

and

$$\sum_{i=1}^n \sum_{j=1}^m M_i p_{ij} \alpha_{jk} = 1 \quad (15)$$

it follows from eq. 10 and 13 that the  $\Delta a_i^{(k)}$  are given by

$$\frac{\Delta a_i^{(k)}}{a_i} = \Delta(\log a_i)^{(k)} = \alpha_{ik} \Delta W_k \quad (16)$$

From the eq. 3 the changes in the constituent molar concentrations of the  $A_i$  across the  $k$ th part of the boundary  $\Delta \bar{m}_i^{(k)}$  are given by

$$\Delta \bar{m}_i^{(k)} = \Delta a_i^{(k)} + \sum_{j=1}^m \nu_{ij} \Delta c_j^{(k)} \quad (17)$$

By eq. 12, 16, and 8 these equations (17) reduce to

$$\Delta \bar{m}_i^{(k)} = \left( \sum_{j=1}^m p_{ij} \alpha_{jk} \right) \Delta W_k \quad (18)$$

However, the total changes in the constituent molar concentrations across the whole boundary region  $\Delta \bar{m}_1, \Delta \bar{m}_2, \dots, \Delta \bar{m}_n$  are just the sum of the changes across each part of the boundary and so by eq. 18

$$\Delta \bar{m}_i = \sum_{k=1}^n \Delta \bar{m}_i^{(k)} = \sum_{k=1}^n \sigma_{ik} \Delta W_k \quad (19)$$

where

$$\sigma_{ik} = \sum_{j=1}^m p_{ij} \alpha_{jk} \quad (20)$$

(8) It is clear that the determinant cannot be a polynomial in  $v$  of degree greater than  $n$ . The coefficient of  $v^n$  is the determinant  $|p_{ij}|$  but as the quadratic form

$$\begin{aligned} \sum_{i=1}^n \sum_{j=1}^m p_{ij} x_i x_j &= \sum_{i=1}^n \sum_{j=1}^m (a_i \delta_{ij} + \sum_{e=1}^m \nu_{ie} \nu_{je} c_e) x_i x_j \\ &= \sum_{i=1}^n a_i x_i^2 + \sum_{j=1}^m c_j \left( \sum_{i=1}^n \nu_{ij} x_i \right)^2 \end{aligned}$$

is evidently positive definite it follows from a well-known theorem that  $|p_{ij}|$  must be positive. Thus the determinant must be a polynomial degree  $n$  in  $v$ .

(9) It can be shown that if the constituent molar concentrations  $\bar{m}_i$  are chosen so that eq. 14 and 15 happen to be inconsistent for some value of  $k$ , then the corresponding total change in concentration (w./v.)  $\Delta W_k$  will be identically zero no matter how the  $\Delta \bar{m}_i$  are varied. Such an experiment is ill suited to the type of analysis proposed in this paper so the possibility of eq. 14 and 15 being inconsistent will be neglected.

As the  $\alpha_{jk}$  satisfy the eq. 15, it follows that the  $\sigma_{ik}$  are related to one another by the linear relations

$$\sum_{j=1}^n M_{ij} \sigma_{ik} = 1 \quad (21)$$

In an actual experiment, the  $\Delta \bar{m}_i$  will be known and the  $\Delta W_k$  measured. By repeating the experiment for different values of the  $\Delta \bar{m}_i$ , the values of the coefficients  $\sigma_{ik}$  can be determined using eq. 19 with the help of the eq. 21.<sup>10</sup> The  $V_k$  are just the velocities with which the various parts of the boundary are observed to travel. The velocities of the reactants  $v_i$  can be found by preliminary experiments.

The object of such a series of experiments is of course to determine the dissociation constants  $k_j$  together with the velocities of the complexes  $u_j$ . In order to derive equations that allow one to deduce these unknown quantities, consider the eq. A10 derived in the Appendix

$$\sum_{i=1}^n \sum_{j=1}^n p_{ij} \alpha_{ik} \alpha_{jl} = \frac{\delta_{kl}}{\lambda_k} \quad (22)$$

where it is shown that all the  $\lambda_k$  must be positive. These equations, with the help of eq. 20 (remembering that  $p_{ji} = p_{ij}$ ), can be written in the form

$$\sum_{j=1}^n \sigma_{jk} \lambda_k \alpha_{jl} = \delta_{kl} \quad (23)$$

If these equations (23) are multiplied in turn by the  $\sigma_{ik}$  and summed over  $k$  it is found that

$$\sum_{k=1}^n \sum_{j=1}^n \sigma_{ik} \sigma_{jk} \lambda_k \alpha_{jl} = \sigma_{il} = \sum_{j=1}^n p_{ij} \alpha_{jl} \quad (24)$$

with the help of eq. 20. These equations (24) can therefore be written in the form

$$\sum_{j=1}^n X_{ij} \alpha_{jl} = 0 \quad (25)$$

where the  $X_{ij}$  are given by

$$X_{ij} = p_{ij} - \sum_{k=1}^n \sigma_{ik} \sigma_{jk} \lambda_k \quad (26)$$

Again, if the eq. 23 are multiplied in turn by  $\sigma_{ik} V_k$  and summed over  $k$  it is found that

$$\sum_{k=1}^n \sum_{j=1}^n \sigma_{ik} \sigma_{jk} V_k \lambda_k \alpha_{jl} = \sigma_{il} V_l = \sum_{j=1}^n V_i p_{ij} \alpha_{jl} = \sum_{j=1}^n q_{ij} \alpha_{jl} \quad (27)$$

with the help of eq. 20 and 14. Equations 27 can therefore be written in the form

$$\sum_{j=1}^n Y_{ij} \alpha_{jl} = 0 \quad (28)$$

where the  $Y_{ij}$  are given by

$$Y_{ij} = q_{ij} - \sum_{k=1}^n \sigma_{ik} \sigma_{jk} V_k \lambda_k \quad (29)$$

Now the determinant  $|\alpha_{ik}| \neq 0$ <sup>11</sup> and so the eq. 25 and 28 imply that all the  $X_{ij}$  and  $Y_{ij}$  are zero. Hence by eq. 26 and 29

$$\begin{aligned} p_{ij} &= \sum_{k=1}^n \sigma_{ik} \sigma_{jk} \lambda_k \\ q_{ij} &= \sum_{k=1}^n \sigma_{ik} \sigma_{jk} V_k \lambda_k \end{aligned} \quad (30)$$

If eq. 30 are now written out in full, with the help of eq. 8, together with eq. 3 the following  $n(n+2)$  equations are obtained

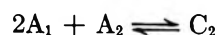
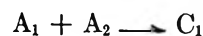
$$\begin{aligned} a_i + \sum_{k=1}^m \nu_{ik} c_k &= \bar{m}_i \\ a_i \delta_{ij} + \sum_{k=1}^m \nu_{ik} \nu_{jk} c_k &= \sum_{k=1}^n \sigma_{ik} \sigma_{jk} \lambda_k \quad (i \leq j) \end{aligned} \quad (31)$$

$$v_i a_i \delta_{ij} + \sum_{k=1}^m \nu_{ik} \nu_{jk} u_k c_k = \sum_{k=1}^n \sigma_{ik} \sigma_{jk} V_k \lambda_k \quad (i \leq j)$$

These  $n(n+2)$  equations are linear in the  $2(n+m)$  unknown quantities  $a_i$ ,  $c_j$ ,  $u_j c_j$ , and  $\lambda_k$ . Having determined the  $v_i$ ,  $\sigma_{ik}$ , and  $V_k$  experimentally, eq. 30 can be solved provided  $m \leq n^2/2$  and the free molar concentrations  $a_i$  and  $c_j$  together with  $u_j c_j$  and  $\lambda_k$  found. From these the dissociation constants  $k_j$  and the velocities of the complexes  $u_j$  can be immediately determined.

### Example

To provide a numerical example of the analysis of a differential boundary experiment, suppose reactants  $A_1$  and  $A_2$  form complexes  $C_1$  and  $C_2$  reversibly in solution according to the equations



Supposing an ultracentrifuge study is being made and that the reactants  $A_1$  and  $A_2$  roughly resemble pepsin and serum albumin, it will be assumed that  $M_1 = 35,000$ ,  $M_2 = 70,000$ , and, on the basis of the relative masses of the four components, that  $v_1 = 1$ ,  $v_2 = 2^{2/3} =$

(10) It should be noted that the linear relations between  $\Delta W_k$  and  $\Delta \bar{m}_i$  are valid only if the  $\Delta \bar{m}_i$  are sufficiently small.

(11) By a well-known theorem on products of determinants and eq. 22

$$|p_{ij}| \cdot |\alpha_{ij}|^2 = \left| \sum_{i=1}^n \sum_{j=1}^n p_{ij} \alpha_{ik} \alpha_{jl} \right| = \left| \frac{\delta_{kl}}{\lambda_k} \right| = \prod_{k=1}^n \frac{1}{\lambda_k} > 0$$

and as  $|p_{ij}| > 0$  and finite, it follows immediately that  $|\alpha_{ij}|$  must be nonzero.

1.587,  $u_1 = 3^{2/3} = 2.080$ ,  $u_2 = 4^{2/3} = 2.520$ , where the sedimentation velocity of  $A_1$  has been chosen as a convenient unit of velocity. To correspond to a study of the complexes between pepsin and serum albumin by Cann and Klapper,<sup>12</sup> it will be assumed that  $\bar{m}_1 = 0.849 \times 10^{-4}$  mole/l.,  $\bar{m}_2 = 2.190 \times 10^{-4}$  mole/l., and  $k_1 = 0.650 \times 10^{-4}$  mole/l. Finally, it will be assumed that  $k_2 = 4k_1^2$ . It is worth noting that from their study, Cann and Klapper had reason to believe that complexes containing more than one molecule of pepsin were being formed.

From the above data the free molar concentration of the components can be found and hence the  $p_{ij}$  and  $q_{ij}$ . From eq. 9 it is then found that  $V_1 = 1.540$  and  $V_2 = 1.948$ . The  $\alpha_{ij}$  can then be determined by eq. 14 and 15 and by eq. 20 it is found that  $\sigma_{11} = -0.421 \times 10^{-5}$ ,  $\sigma_{12} = 0.902 \times 10^{-5}$ ,  $\sigma_{21} = 1.639 \times 10^{-5}$ , and  $\sigma_{22} = 0.977 \times 10^{-5}$ .

Therefore, if a differential boundary experiment is performed on such a system, the velocities of the two parts of the boundary would be found to be 1.540 and 1.948 while the relations between the  $\Delta\bar{m}_1$ ,  $\Delta\bar{m}_2$  and the  $\Delta W_1$ ,  $\Delta W_2$  would be found, by such experiments, to be

$$\Delta\bar{m}_1 = -0.421 \times 10^{-5} \Delta W_1 + 0.902 \times 10^{-5} \Delta W_2$$

$$\Delta\bar{m}_2 = 1.639 \times 10^{-5} \Delta W_1 + 0.977 \times 10^{-5} \Delta W_2$$

Therefore, the set of equations that the experimenter would have to solve is

$$a_1 + c_1 + 2c_2 = 0.849 \times 10^{-4}$$

$$a_2 + c_1 + c_2 = 2.190 \times 10^{-4}$$

$$a_1 + c_1 + 4c_2 = 0.177 \times 10^{-10} \lambda_1 + 0.815 \times 10^{-10} \lambda_2$$

$$a_2 + c_1 + c_2 = 2.687 \times 10^{-10} \lambda_1 + 0.955 \times 10^{-10} \lambda_2$$

$$c_1 + 2c_2 = -0.690 \times 10^{-10} \lambda_1 + 0.882 \times 10^{-10} \lambda_2$$

$$a_1 + u_1 c_1 + 4u_2 c_2 = 0.273 \times 10^{-10} \lambda_1 + 1.586 \times 10^{-10} \lambda_2$$

$$1.587 a_2 + u_1 c_1 + u_2 c_2 = 4.137 \times 10^{-10} \lambda_1 + 1.860 \times 10^{-10} \lambda_2$$

$$u_1 c_1 + 2u_2 c_2 = -1.063 \times 10^{-10} \lambda_1 + 1.718 \times 10^{-10} \lambda_2$$

Actually, these equations when solved give  $a_1 = 0.219 \times 10^{-4}$  mole/l.,  $a_2 = 1.605 \times 10^{-4}$  mole/l.,  $c_1 = 0.540 \times 10^{-4}$  mole/l.,  $c_2 = 0.0454 \times 10^{-4}$  mole/l., and  $u_1 c_1 = 1.123 \times 10^{-4}$  mole/l.,  $u_2 c_2 = 0.114 \times 10^{-4}$  mole/l. (while  $\lambda_1 = 0.439 \times 10^6$  and  $\lambda_2 = 1.058 \times 10^6$ ). Hence, it follows that  $u_1 = 2.080$ ,  $u_2 = 2.518$ , and  $k_1 = a_1 a_2 / c_1 = 0.650 \times 10^{-4}$  mole/l.,  $k_2 = a_1^2 a_2 / c = 1.689 \times 10^{-2}$  mole<sup>2</sup>/l.<sup>2</sup>. These "unknown" parameters are of course in agreement (to sufficient accuracy) with their initially assumed values.

This example illustrates the relatively simple manner in which unique values for the unknown parameters of a reversibly interacting system can be determined from the results of differential boundary experiments provided of course that  $m \leq n^2/2$ . This should be compared with the problem of determining the unknown parameters in conventional boundary experiments where, with the exception of certain important cases,<sup>2</sup> the nonlinear ordinary differential equations that govern the form of the boundary at sufficiently large times must be solved numerically with some reasonable set of values for the unknown parameters involved and this procedure repeated until sufficiently good agreement is obtained with the observed experimental boundary. There is of course no guarantee in general that the answers obtained in this way are unique; *i.e.*, other values of the unknown parameters may happen to give equally good agreement with the experimental boundary.

*Acknowledgment.* The author is grateful to Dr. G. A. Gilbert for many helpful discussions during the preparation of this paper.

## Appendix

Consider the equations

$$\sum_{j=1}^n (q_{ij} - V_k p_{ij}) \alpha_{jk} = 0 \quad (A1)$$

where  $V_k$  is one of the roots of eq. 9. As the determinant of the coefficients of the eq. A1 therefore vanishes, one of these  $n$  equations at least is a linear combination of the others. Thus the  $\alpha_{ik}$  are not all identically zero but are defined (at most) to within a multiplicative constant (dependent on  $k$ ) by these equations. Note that until it has been proved that the roots  $V_k$  of eq. 9 are all real, it must not be assumed that the  $\alpha_{ik}$  are real.

Denoting the complex conjugate of  $\alpha_{il}$  by  $\alpha_{il}^*$  it is found on multiplying eq. A1 in turn by the  $\alpha_{il}^*$  and summing over  $i$  that

$$\sum_{i=1}^n \sum_{j=1}^n (q_{ij} - V_k p_{ij}) \alpha_{il}^* \alpha_{jk} = 0 \quad (A2)$$

On interchanging the  $i$  and  $j$  (and remembering that  $p_{ji} = p_{ij}$  and  $q_{ji} = q_{ij}$ ) these equations (A2) can be rewritten in the form

$$\sum_{i=1}^n \sum_{j=1}^n (q_{ij} - V_k p_{ij}) \alpha_{ik} \alpha_{jl}^* = 0 \quad (A3)$$

Taking the complex conjugate of eq. A2, it is found that

(12) J. R. Cann and J. A. Klapper, Jr., *J. Biol. Chem.*, **236**, 2446 (1961).

$$\sum_{i=1}^n \sum_{j=1}^n (q_{ij} - V_k^* p_{ij}) \alpha_{ik} \alpha_{jk}^* = 0 \quad (\text{A4})$$

Interchanging the  $k$  and  $l$ , eq. A4 become

$$\sum_{i=1}^n \sum_{j=1}^n (q_{ij} - V_l^* p_{ij}) \alpha_{il} \alpha_{jl}^* = 0 \quad (\text{A5})$$

and if eq. A5 are now subtracted from eq. A3, it is found that

$$(V_l^* - V_k) \sum_{i=1}^n \sum_{j=1}^n p_{ij} \alpha_{ik} \alpha_{jl}^* = 0 \quad (\text{A6})$$

Now consider eq. A6 in the case where  $l = k$ , *i.e.*

$$(V_k^* - V_k) \sum_{i=1}^n \sum_{j=1}^n p_{ij} \alpha_{ik} \alpha_{jk}^* = 0 \quad (\text{A7})$$

By eq. 8<sup>13</sup>

$$\begin{aligned} \sum_{i=1}^n \sum_{j=1}^n p_{ij} \alpha_{ik} \alpha_{jk}^* &= \sum_{i=1}^n \sum_{j=1}^n (a_i \delta_{ij} + \sum_{l=1}^m \nu_{il} \nu_{jl} c_l) \alpha_{ik} \alpha_{jk}^* \\ &= \sum_{i=1}^n a_i |\alpha_{ik}|^2 + \sum_{j=1}^m c_j \left| \sum_{i=1}^n \nu_{ij} \alpha_{ik} \right|^2 \\ &> 0 \end{aligned} \quad (\text{A8})$$

and so it follows from the eq. A7 that  $V_k^* = V_k$ , *i.e.*, the  $V_k$  must all be real. It then follows from the eq. A1 and 15 that all the  $\alpha_{ik}$  must be real also. Equations A6 can therefore be written in the form

$$(V_l - V_k) \sum_{i=1}^n \sum_{j=1}^n p_{ij} \alpha_{ik} \alpha_{jl} = 0 \quad (\text{A9})$$

Now in any experiment the constituent molar concentrations  $\bar{m}_i$  of the  $A_i$  would be chosen so that the various parts of the boundary are well separated; *i.e.*, no two of the  $V_k$  would be equal. Equations A9 then imply that

$$\sum_{i=1}^n \sum_{j=1}^n p_{ij} \alpha_{ik} \alpha_{jl} = \frac{\delta_{kl}}{\lambda_k} \quad (\text{A10})$$

where, by eq. A8, all the  $\lambda_k$  must be positive.

---

(13) The terms  $|\alpha_{ik}|$  and  $\left| \sum_{j=1}^m \nu_{ij} \alpha_{jk} \right|$  that occur in eq. A8 are intended to represent the modulus of  $\alpha_{ik}$  and  $\sum_{j=1}^m \nu_{ij} \alpha_{jk}$ , respectively, and not determinants.



# Charge-Transfer Absorption and Luminescence Spectra of Alkyl Halide Salts of Pyridine<sup>1a</sup>

by J. S. Brinen, J. G. Koren, H. D. Olmstead,<sup>1b</sup> and R. C. Hirt

American Cyanamid Company, Central Research Division, Stamford, Connecticut (Received May 4, 1965)

The long wave length absorption bands of alkyl halide salts of pyridine have been studied as a function of solvent and temperature. These systems luminesce brightly in the visible region at  $-196^\circ$ . The large separation between the absorption and luminescence bands is discussed in terms of solvent effects and the Franck-Condon principle.

## Introduction

The electronic absorption spectra of N-alkyl iodide<sup>2,3</sup> salts of nitrogen heterocyclic molecules exhibit long wave length absorption bands which are not present in the parent molecule. These bands are very sensitive to solvent and temperature changes and have been attributed, by Mason,<sup>3</sup> as being due to the transition of an electron from the anion to the cation within a solvated ion pair, *i.e.*, (N-methylpyridinium)<sup>+</sup> iodide<sup>-</sup> solvent. Further support for the assignment of these bands to charge-transfer transitions is that for pyridine methiodide in  $\text{CHCl}_3$ ; the maxima of the two long wave length bands are separated by  $7950 \text{ cm.}^{-1}$ . This agrees with the separation between the  $^2P_{1/2}$  and  $^2P_{3/2}$  states of the iodine atom ( $7600 \text{ cm.}^{-1}$ ).<sup>3</sup>

Mason<sup>3</sup> concentrated on varying the N-heterocyclic nucleus while using  $\text{CH}_3\text{I}$  for salt formation and  $\text{CHCl}_3$  as a solvent and concluded that the transition energy followed closely a delocalized model for the excited state. In the present investigation, the heterocycle is kept constant (pyridine) while the solvent and the alkyl halide are varied. Considerable attention is focused on the luminescence properties of these systems and on the behavior of the absorption spectrum as solvent and temperature are varied.

## Experimental Section

Absorption measurements were performed on a Cary Model 14 spectrophotometer using spectrograde alcohol,  $\text{CH}_2\text{Cl}_2$ , and distilled water as solvents. Variable temperature-absorption experiments were obtained using a variable temperature cell specifically designed for use with the instrument.<sup>4</sup>

Total luminescence spectra have been measured for the methiodide, methbromide, and ethiodide salts of pyridine at  $-196^\circ$  in various solvents. The samples were excited by ultraviolet radiation from an H-3 mercury arc (quartz envelope) through a 5-mm. thick Corning 9863 filter. A complementary filter, 10 mm. of dilute aqueous  $\text{NaNO}_2$  solution, was placed before the entrance slit of a modified Warren Electronics Spectracord used to record the luminescence spectra. The spectra are uncorrected for the response of the RCA 1P28 photomultiplier. Luminescence measurements were performed under higher resolution conditions for some of these systems, but no new features were observed in the spectra obtained.

The alkyl halide salts were prepared by standard methods described in the literature.<sup>5</sup>

## Spectroscopic Observations

The effect of solvent polarity on the absorption spectrum of pyridine methiodide may be seen in Figure 1. In  $\text{CH}_2\text{Cl}_2$  two low energy absorption bands are observed (as in  $\text{CHCl}_3$ ) with maxima at 27,100 and 34,400  $\text{cm.}^{-1}$ , a separation of  $\sim 7500 \text{ cm.}^{-1}$ .

(1) (a) Presented in part by J. S. Brinen at the 144th National Meeting of the American Chemical Society, Los Angeles, Calif., April 1963; (b) Summer Careers Program, 1964.

(2) (a) A. Hantzsch, *Ber.*, **44**, 1776, 1783 (1911); **52**, 1535, 1544 (1919); (b) E. M. Kosower, *J. Am. Chem. Soc.*, **80**, 3253, 3261, 3267 (1958).

(3) S. F. Mason, *J. Chem. Soc.*, 2437 (1960).

(4) J. G. Koren, J. S. Brinen and R. C. Hirt, *Appl. Opt.*, **3**, 1431 (1964).

(5) M. Smith and M. C. R. Symons, *Discussions Faraday Soc.*, **24**, 206 (1957).

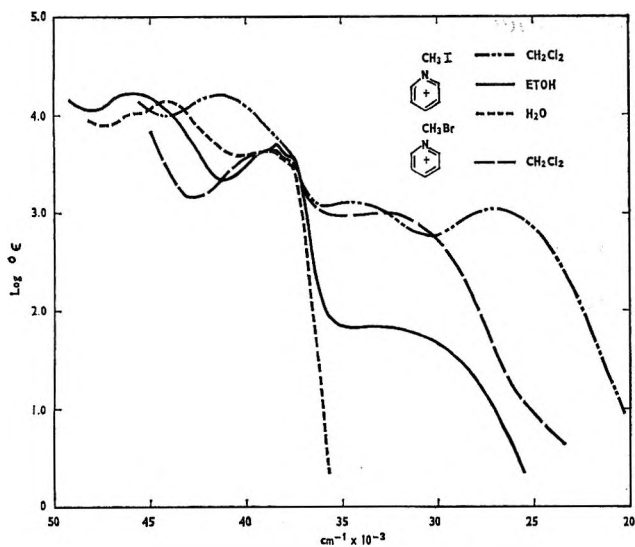


Figure 1. Absorption spectra of pyridine methiodide in: - - - -  $\text{CH}_2\text{Cl}_2$ , ——— alcohol, and - - - - water, and of pyridine methbromide in — — —  $\text{CH}_2\text{Cl}_2$ . The  $\epsilon$  values for the C.T. bands are only apparent because of deviations from Beer's law.

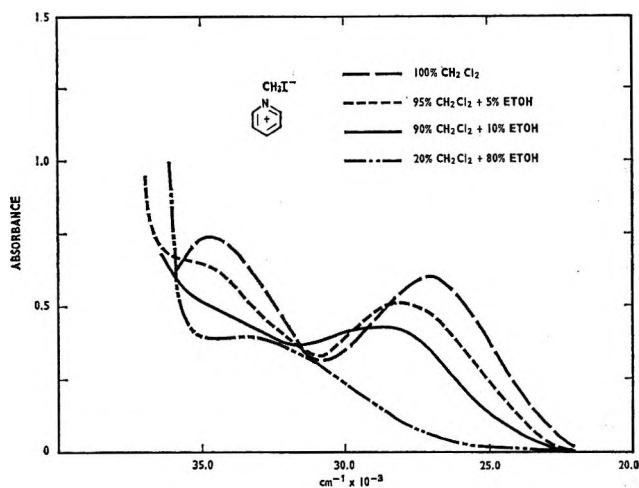


Figure 2. C.T. absorption spectrum of pyridine methiodide in  $\text{CH}_2\text{Cl}_2$  upon successive addition of alcohol.

In alcohol, there is only one low energy absorption band, and in water this band disappears entirely. These bands will be referred to as charge-transfer (C.T.) absorption bands.

Two additional absorption bands are observed in the region between 37,000 and 50,000  $\text{cm}^{-1}$  in alcohol and water solutions. The band centered at about 40,000  $\text{cm}^{-1}$  is due to absorption from the pyridinium ion and agrees well with an absorption spectrum of pyridinium perchlorate.<sup>3</sup> In  $\text{CH}_2\text{Cl}_2$  this absorption is partially hidden under a stronger absorption band due to the transition between the iodide ion and the sol-

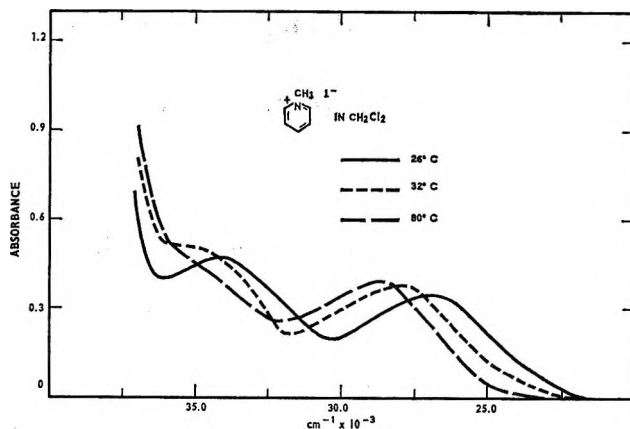


Figure 3. Temperature effects on the C.T. absorption bands of pyridine methiodide in  $\text{CH}_2\text{Cl}_2$ .

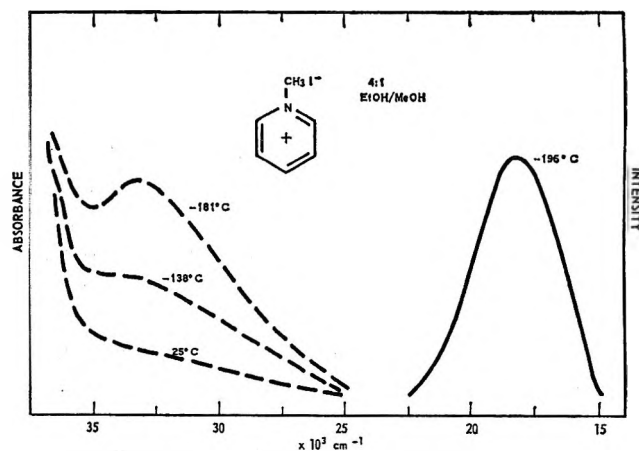


Figure 4. C.T. absorption spectrum of pyridine methiodide in alcohol as a function of temperature (left side). The right side shows the luminescence spectrum of a similar solution at  $-196^\circ$ .

vent<sup>2b,5</sup> and causes an apparent increase in the molar absorptivity,  $\epsilon$ , of the pyridinium absorption. The absorption band involving the iodide ion and the solvent is shifted to higher energy in alcohol and water (43,000  $\text{cm}^{-1}$ ), and the characteristic pyridinium absorption may be readily observed at 38,000  $\text{cm}^{-1}$ . For the  $\text{CH}_3\text{Br}$  salt in  $\text{CH}_2\text{Cl}_2$  the transition between  $\text{Br}^-$  and the solvent is shifted to higher energies, and the pyridinium absorption is readily observed.

The gradual shifting of the two low energy absorption bands with solvent polarity may be seen from Figure 2. Successive amounts of alcohol are added to a  $\text{CH}_2\text{Cl}_2$  solution of pyridine methiodide. The absorption is shifted to higher energies as the proportion of alcohol is increased, and the band originally at 34,400  $\text{cm}^{-1}$  gradually disappears under the higher energy pyridinium absorption band.

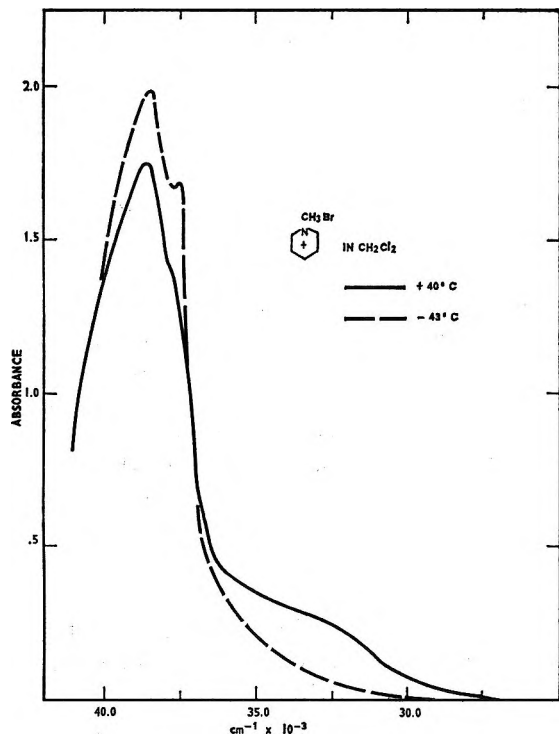


Figure 5. Absorption spectrum of pyridine methbromide in  $\text{CH}_2\text{Cl}_2$  as a function of temperature.

The effect of temperature on the absorption spectrum of pyridine methiodide in  $\text{CH}_2\text{Cl}_2$  and in alcohol is shown in Figure 3 and the left side of Figure 4. As the temperature is lower, the C.T. absorption bands in  $\text{CH}_2\text{Cl}_2$  are shifted to higher energies, a shift for both bands of  $\sim 975 \text{ cm}^{-1}$  at  $-32^\circ$ . Continued cooling results in a larger shift, and at  $-196^\circ$  (sample is opaque) the original yellow solution appears colorless. Cooling an alcohol solution of pyridine methiodide does not produce a large shift in the absorption energy but does result in considerable enhancement of C.T. absorption of the lower temperatures.

Pyridine ethiodide behaves in a similar manner with respect to solvent and temperature variations.

Pyridinium methbromide exhibits a similar low energy band only in  $\text{CH}_2\text{Cl}_2$  (or  $\text{CHCl}_3$ ) solution. This appears as a long wave length shoulder on the stronger pyridinium transition (at  $\sim 38,000 \text{ cm}^{-1}$ ). In the more polar solvents, this C.T. band is hidden under the pyridine transition. Figure 5 shows the spectrum of pyridinium methbromide in  $\text{CH}_2\text{Cl}_2$  as a function of temperature. As the temperature is decreased, the long wave length shoulder (C.T. band) disappears under the stronger pyridine band. At  $+40^\circ$ , the C.T. absorption is slightly more pronounced and is at lower energy than at room temperature.

The charge-transfer bands examined in this study do

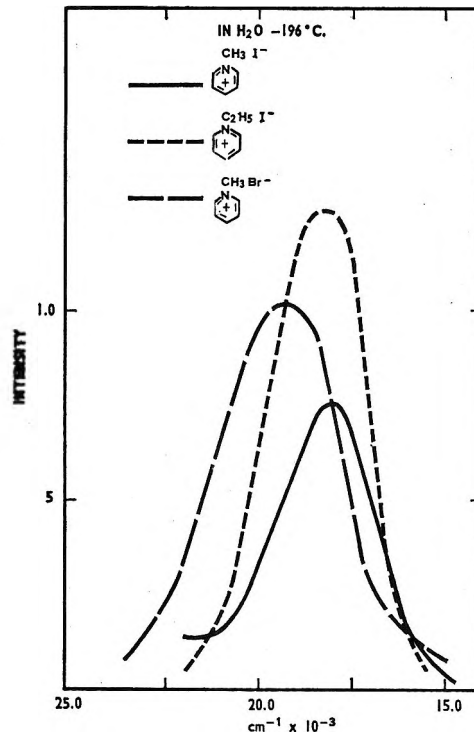


Figure 6. Luminescence spectra of some alkyl halide salts of pyridine in water at  $-196^\circ$ . The intensity scale is not the same for the three molecules.

not obey Beer's law in the concentration range studied (to  $10^{-4} M$ ).

When these solutions are frozen to  $-196^\circ$  and exposed to ultraviolet radiation, they were found to luminesce strongly; the iodide salts appear to be yellowish orange and the methbromide a greenish yellow. The emissions from these materials are broad and featureless. For alcohol solutions, the intensity maximum for the  $\text{CH}_3\text{I}$  salt luminescence is at  $\sim 18,200 \text{ cm}^{-1}$ ; for the  $\text{C}_2\text{H}_5\text{I}$  salt the maximum is  $\sim 18,000 \text{ cm}^{-1}$  while the  $\text{CH}_3\text{Br}$  salt is at somewhat higher energies of  $\sim 19,400 \text{ cm}^{-1}$ . Luminescence spectra in  $\text{CH}_2\text{Cl}_2$  are quite similar. Lifetime measurements using a mechanical phosphoroscope capable of fractional millisecond resolution indicate the lifetime of the luminescence is  $\leq 10^{-4} \text{ sec}$ .

Although for water solutions of these salts the C.T. absorption is hidden under the pyridine absorption and is not observed in the spectrum, these solutions when carefully frozen to  $-196^\circ$  luminesce when exposed to ultraviolet radiation. The luminescence of these salts in  $\text{H}_2\text{O}$  is shown in Figure 6 and is not shifted appreciably ( $\sim 100 \text{ cm}^{-1}$ ) from that in alcohol or  $\text{CH}_2\text{Cl}_2$  solution.

Figure 3 shows the absorption and luminescence spectrum of pyridinium methiodide in alcoholic solu-

tions at comparable temperatures. There is a large energy gap ( $\sim 2500 \text{ cm.}^{-1}$ ) between the onset of absorption and the onset of luminescence. The separation between absorption and emission is estimated as being somewhat smaller for  $\text{CH}_2\text{Cl}_2$  solutions and considerably larger for water solutions. The nature of the last two solvents prevents direct measurements at  $-196^\circ$ . A search for additional absorption bands below  $33,000 \text{ cm.}^{-1}$  which might correspond to the luminescence was made in a  $10 M$  aqueous solution of the  $\text{CH}_3\text{I}$  salt. No evidence of absorption was found.

### Discussion

Solvent and temperature variation studies on the absorption spectra of pyridine methiodide agree with Mason's<sup>3</sup> proposal that the species giving rise to the C.T. absorption is a solvated ion pair and that the transition involves a charged ground state and a neutral excited state. A charged ground state would be more stabilized by solvation in polar solvents than in solvents of lower polarity, and the charge-transfer absorption would be shifted to higher energies as the polarity increased. Increasing the alkyl chain by one carbon does not produce any appreciable difference in the absorption properties of the salt. Substituting  $\text{Br}^-$  for  $\text{I}^-$  shifts the charge-transfer absorption band to higher energies by about  $8500 \text{ cm.}^{-1}$  but does not seem to alter the behavior with respect to temperature and solvent variations. The shift agrees with the difference in absorption maxima of  $\text{CH}_3\text{Br}$  and  $\text{CH}_3\text{I}$  in the vapor phase of  $\sim 9500 \text{ cm.}^{-1}$ .<sup>6</sup>

Since neither of the components of the salt luminesces independently and since no evidence for multiplicity-forbidden absorption bands was observed, it is thought

that the emission observed in the experiments described here must be attributed to transitions between the same levels of the solvated ion pair which give rise to the C.T. absorption, that is, a charge-transfer fluorescence. Accepting this, the relative insensitivity of the luminescence with solvent and the large separation between the C.T. absorption and luminescence may be explained on the basis of solvent effects and the Franck-Condon principle.

As previously stated, the charged ground state of the solvated ion pair is very sensitive to solvent polarity. Energy differences in the transition from the ground state to the neutral excited state in different solvents primarily reflect changes in ground-state stabilization since, by the Franck-Condon principle, the solvent environment of the excited state during the transition must remain the same as that for the ground state. For the emission process, however, the molecule in the excited state has time to come to equilibrium with the solvent environment. The luminescence transition is now between states which have the solvent environment of the neutral excited state and thus might be expected to be fairly insensitive to solvent polarity. The observed energy gap reflects differences between the ground and excited states in a charged and neutral solvation environment. The role of the Franck-Condon principle in solvent effects as applied to luminescence phenomena has been examined by other authors.<sup>7</sup>

(6) G. Herzberg and G. Scheibe, *Z. physik. Chem. (Leipzig)*, **87**, 397 (1930).

(7) V. G. Krishna and L. Goodman, *J. Chem. Phys.*, **33**, 381 (1960), and references therein.

## Volume Changes in Hydrocarbon-Water Systems. Partial Molal

### Volumes of Alcohol-Water Solutions<sup>1</sup>

by Michael E. Friedman and Harold A. Scheraga

Department of Chemistry, Cornell University, Ithaca, New York (Received May 5, 1965)

Density data have been obtained for several alcohols over a range of concentrations and temperatures. From these data, calculations were made of the volume decreases accompanying the transfer of nonpolar groups from a nonpolar medium into an infinitely dilute aqueous solution. The experimental data for the aliphatic hydrocarbon groups appear to agree reasonably well with theoretical values, especially in the dependence of the volume decrease on hydrocarbon size.

#### Introduction

The calculation of the thermodynamic parameters for hydrophobic bond formation, carried out by Némethy and Scheraga,<sup>2</sup> was based on a statistical mechanical theory of water and of aqueous solutions of hydrocarbons.<sup>3</sup> In their studies, estimates were also made<sup>3</sup> of the decrease in volume when either aliphatic or aromatic hydrocarbons are transferred from a nonpolar medium into water. Specifically, the volume decrease,  $\Delta V^0$  in cm.<sup>3</sup>/mole, was computed from the equation

$$\Delta V^0 = -\frac{43}{24} Y^c x_4^c \quad (1)$$

where  $Y^c$  is the number of water molecules in the first layer around the hydrocarbon solute molecule, and  $x_4^c$  is the mole fraction of water in the first layer which is tetra-hydrogen-bonded; since  $Y^c$  has been estimated, and  $x_4^c$  is known for a given hydrocarbon in water,<sup>3</sup>  $\Delta V^0$  may be evaluated.

Since very few reliable data on volume changes exist,<sup>4</sup> because of the relative insolubility of hydrocarbons in water, it was decided to try to obtain these data from a study of the partial molal volumes of alcohol-water solutions. By studying a homologous series of alcohols, it should be possible to subtract the effect of the polar group of the alcohol, common to all members of the series, and obtain the contribution of the nonpolar group. This approach is based on the assumption that the contributions of the polar and nonpolar parts of the alcohol molecule are additive in both the pure

alcohol solution and in the infinitely dilute aqueous solution, an assumption the validity of which we cannot establish. However, this assumption might be expected to become more valid as the length of the nonpolar part increases.

Consequently, density measurements were made on pure alcohols and alcohol-water solutions for several linear and branched aliphatic alcohols and benzyl alcohol, and partial molal volumes were computed.

#### Theory

The apparent molal volume of the alcohol,  $\phi$ , is related to the densities<sup>5</sup> by the equation

$$\phi = \frac{M}{\rho} - \frac{1000(\rho - \rho_{H_2O})}{m\rho\rho_{H_2O}} \quad (2)$$

where  $m$  is the molality of the alcohol solute of molecular weight  $M$ , and  $\rho$  and  $\rho_{H_2O}$  are the densities of the solution (of molality  $m$ ) and of pure water, respectively. The partial molal volume of the alcohol,  $\bar{v}$ , is related to  $\phi$  by the equation

(1) This work was supported by a research grant (AI-01473) from the National Institute of Allergy and Infectious Diseases of the National Institutes of Health, U. S. Public Health Service, and by a research grant (GB-2238) from the National Science Foundation.

(2) G. Némethy and H. A. Scheraga, *J. Phys. Chem.*, **66**, 1773 (1962); **67**, 2888 (1963).

(3) G. Némethy and H. A. Scheraga, *J. Chem. Phys.*, **36**, 3382, 3401 (1962); **41**, 680 (1964).

(4) W. L. Masterton, *ibid.*, **22**, 1830 (1954).

(5) F. Daniels, J. H. Mathews, J. W. Williams, P. Bender, G. W. Murphy, and R. A. Alberty, "Experimental Physical Chemistry," 4th Ed., McGraw-Hill Book Co., Inc., New York, N. Y., 1949, p. 100.

$$\bar{v} = \phi + m \left( \frac{\partial \phi}{\partial m} \right)_{T,P,n} \quad (3)$$

where the number of moles of water,  $n$ , is kept constant. Experimentally, when  $\phi$  is plotted against  $m$  and extrapolated to zero concentration, the intercept is equal to  $\bar{v}$  at infinite dilution. Since such plots were found to be linear at very low concentration, the extrapolation was carried out using the method of least squares; for this purpose, the highest concentration of alcohol used was 2% by weight ( $\sim 0.01$  mole fraction).

Since the molar volume of pure alcohol,  $v^0$ , is

$$v^0 = \frac{M}{\rho_a} \quad (4)$$

where  $\rho_a$  is the density of the pure alcohol, the volume change  $\Delta\bar{v}$ , upon transfer of 1 mole of alcohol from the pure alcohol to the infinitely dilute aqueous solution, is given by

$$\Delta\bar{v} = \bar{v} - v^0 \quad (5)$$

If it is assumed that  $\Delta\bar{v}$  contains additive contributions from the polar and nonpolar parts of the alcohol, then a subtraction of two values of  $\Delta\bar{v}$  for two different alcohols should give the volume change for the transfer of the nonpolar part from a nonpolar medium into an infinitely dilute aqueous solution; *e.g.*, the contribution of a methylene group may be obtained by subtraction of data for *n*-propyl and ethyl alcohols.

$$\Delta\bar{v}_{\text{CH}_2} = \Delta\bar{v}_{\text{CH}_3\text{CH}_2\text{CH}_2\text{OH}} - \Delta\bar{v}_{\text{CH}_3\text{CH}_2\text{OH}} \quad (6)$$

A theoretical value, with which to compare this experimental value, may be obtained by a similar subtraction of data for the corresponding hydrocarbons, *i.e.*

$$\Delta\bar{v}_{\text{CH}_2} = \Delta\bar{v}_{\text{CH}_3\text{CH}_2\text{CH}_3} - \Delta\bar{v}_{\text{CH}_3\text{CH}_3} \quad (7)$$

The data for  $\Delta\bar{v}$  in eq. 7 were obtained from eq. 1, using appropriate values<sup>3</sup> for  $Y^c$  and  $x^c_4$ .

In eq. 6 and 7, we have assumed additivity and have assigned the resulting value of  $\Delta\bar{v}$  to the  $\text{CH}_2$  group. It should be pointed out that the values of  $Y^c$  for  $\text{CH}_2$  and  $\text{CH}_3$  groups differ,<sup>3</sup> being 2 and 8, respectively. For this reason, we should not expect the data obtained for the  $\text{CH}_2$  group (from eq. 6 or 7) to resemble one-half the value for ethane.

## Experimental Section

**Materials.** The alcohols were obtained from J. T. Baker, Eastman Organic, Matheson Coleman and Bell, and Fisher Scientific companies and were reported to be of the highest purity. They were fractionally distilled over magnesium,<sup>6</sup> only the middle third of the distillate being retained. The corrected boiling points

agreed with those in the literature<sup>7</sup> to within  $\pm 0.1^\circ$  (see Table I).

**Table I:** Comparison of Boiling Point Data at 1 Atm. Pressure

Alcohol	B.p., $^\circ\text{C}$ .	
	Range <sup>a</sup>	This work
MeOH	64.50–64.75	64.6–64.7
EtOH	78.2–78.41	78.3–78.4
<i>n</i> -PrOH	97.1–97.26	97.1–97.2
<i>i</i> -PrOH	82.2–82.44	82.2–82.3
<i>n</i> -BuOH	117.7–118.0	117.7–117.8
<i>i</i> -BuOH	107.89–108.80	108.1–108.2
<i>s</i> -BuOH	99.50–99.52	99.5–99.6
<i>n</i> -PeOH	137.95–138.25	138.0–138.1
BenzOH	205.25–205.45	205.2–205.3

<sup>a</sup> Data from ref. 7. The ranges quoted represent data from 4 to 31 different references, cited in ref. 7.

The water content of the alcohols was found to be less than 0.1% in all cases, by Karl Fischer titration<sup>8</sup>; nevertheless, a correction<sup>9</sup> for this small amount of water was applied in the calculations of the alcohol concentration. Organic acids and isomeric alcoholic impurities were found to be absent within the limits of gas chromatographic analyses on an F & M Model No. 500 instrument, which can detect impurities present to the extent of 0.1% by weight. The chromatographic column was 4.6 m. long and 0.32 cm. in diameter. It contained Chromasorb P, Johns-Manville, as the support, and dioctyl phthalate, J. T. Baker, as the absorbing phase.

Deionized water was further distilled, as described by Bauer,<sup>9</sup> from an alkaline potassium permanganate solution, and only the middle third of the distillate was retained.

**Solutions.** The solutions were prepared by adding a known weight of alcohol to a known weight of water. The weighings were made in a tightly sealed polyethylene bottle on a single-pan Mettler balance, Model No. M5. Introduction of the liquids into the bottle was made as rapidly as possible so that a possible error due to evaporation was kept to a minimum. The error

(6) H. Lund and J. Bjerrum, *Chem. Ber.*, **64B**, 210 (1931).

(7) J. Timmermans, "Physico-Chemical Constants of Pure Organic Compounds," Elsevier Publishing Co., New York, N. Y., 1950, pp. 304, 309, 314, 317, 319, 321, 323, 325, 457.

(8) J. Mitchell, Jr., and D. M. Smith, "Aquametry," Interscience Publishers, Inc., New York, N. Y., 1948, Chapters II–V.

(9) N. Bauer in "Physical Methods of Organic Chemistry," A. Weissberger, Ed., Interscience Publishers, Inc., New York, N. Y., 1949, Part I, Chapter 1.

**Table II:** Densities of the Normal Aliphatic Alcohols and of Their Aqueous Solutions from MeOH to PeOH at Several Temperatures

Alcohol	Wt. %	1°	20°	40°	50°
MeOH	0.4660	0.999065	0.997368	0.991383	0.987191
	0.9691	0.998133	0.996444	0.990431	0.986257
	1.4749	0.997209	0.995524	0.989493	0.985310
	1.9819	0.996312	0.994596	0.988561	0.984364
	100.0	0.809112	0.791228	0.772347	0.762761
		(0.80916) <sup>a</sup>	(0.7915-0.7914)	(0.7725-0.7723)	(0.7628-0.7627)
EtOH	0.5115	0.998964	0.997262	0.991275	0.987065
	0.9836	0.998091	0.986385	0.990379	0.986176
	1.4318	0.997264	0.995559	0.989541	0.985379
	1.9404	0.996332	0.994646	0.988590	0.984429
	100.0	0.805421	0.789461	0.772457	0.763373
		(0.80541)	(0.78945)	(0.77245-0.7722)	(0.7633-0.76314)
PrOH	0.6097	0.998919	0.997232	0.991234	0.987034
	1.0103	0.998265	0.996550	0.990575	0.986360
	1.3516	0.997718	0.995991	0.989990	0.985769
	1.7047	0.997138	0.995418	0.989443	0.985211
	2.0127	0.996658	0.994895	0.988922	0.984699
	100.0	0.818565	0.803551	0.787598	0.778630
	(0.81854)	(0.8035-0.80358)	(0.7875)	(0.7785)	
BuOH	0.5404	0.999091	0.997400	0.991417	0.987236
	0.9432	0.998485	0.996789	0.990799	0.986625
	1.3554	0.997864	0.996166	0.990165	0.986005
	1.6981	0.997365	0.995655	0.989656	0.985497
	1.9449	0.997018	0.995281	0.989283	0.985169
	100.0	0.823208	0.809704	0.795422	0.788199
	(0.82320)	(0.8099-0.8094)	(0.79543)	(0.78815)	
PeOH	0.4997	0.999194	0.997476	0.991476	0.987285
	0.7821	0.998791	0.997067	0.991048	0.986854
	0.9382	0.998580	0.996846	0.990818	0.986622
	1.1217	0.998331	0.996568	0.990548	0.986348
	1.4054	0.997949	0.996189	0.990133	0.985931
	100.0	0.828503	0.814687	0.799765	0.792071
	(0.8282-0.8289)	(0.8140-0.8149)	(0.7993-0.3003)	(0.7916-0.7924)	

<sup>a</sup> "International Critical Tables," Vol. III, McGraw-Hill Book Co., Inc., New York, N. Y., 1928, pp. 112, 115, 119, 121; National Bureau of Standards Circular 19, U. S. Government Printing Office, Washington, D. C., 1924; "Handbook of Physics and Chemistry," 44th Ed., Chemical Rubber Publishing Co., Cleveland, Ohio, 1964, pp. 864, 888, 988, 1056, 1064, 1098, 1144, 1182; J. Castell-Evans, "Physico-Chemical Tables," Vol. 2, Griffin and Co., London, 1911, pp. 690-692; J. Timmermans, "Physico-Chemical Constants of Pure Organic Compounds," Elsevier Publishing Co., New York, N. Y., 1950, pp. 315, 317, 319, 321, 457.

in the concentration of duplicate samples was less than 1 p.p.m.

The concentrations were expressed as weight per cent, taking into account the weight of air displaced from the weighing bottle (computed from the densities<sup>7</sup> of water, alcohol, and air).

*Density Measurements.* Densities were measured with pycnometers which were a modification of the "type F" form described by Bauer.<sup>9</sup> The total volume in each was approximately 300 ml., and the capillary extensions were made from precision-bore tubing having an inside diameter of 0.4 mm. The volumes were

computed at 1, 20, 40, and 50° from measurements on distilled deionized water, made at each of these temperatures, and density data from the literature.<sup>7</sup>

The temperature of the constant-temperature water bath was controlled to  $\pm 0.01^\circ$  or better with a Bayley Model No. 95 regulating unit which utilized a platinum resistance thermometer.

Liquids were forced through the capillary and into the pycnometer by the exertion of nitrogen pressure. The pycnometers were allowed to equilibrate in the water bath for 24 hr. at the highest temperature (50°) so that most of the dissolved air would be expelled.<sup>10</sup>

**Table III:** Densities of Isopropyl, Isobutyl, *sec*-Butyl, and Benzyl Alcohols and of Their Aqueous Solutions at Several Temperatures

Alcohol	Wt. %	1°	20°	40°	50°
<i>i</i> -PrOH	0.5435	0.998909	0.997206	0.991193	0.986985
	0.9335	0.998196	0.996483	0.990449	0.986225
	1.2469	0.997636	0.995927	0.989853	0.985622
	1.5968	0.997014	0.995307	0.989200	0.984954
	1.9406	0.996408	0.994704	0.988571	0.984319
	100.0	0.800704	0.785153	0.767781	0.758530
		(0.8007-0.8004 <sup>a</sup> )	(0.7854-0.7851)	(0.7677-0.7674)	(0.7586-0.7582)
<i>i</i> -BuOH	0.6027	0.998974	0.997247	0.991220	0.987026
	1.0217	0.998328	0.996579	0.990515	0.986321
	1.3134	0.997889	0.996123	0.990036	0.985845
	1.6269	0.997433	0.995637	0.989521	0.985346
	1.9386	0.996982	0.995162	0.989021	0.984858
	100.0	0.816242	0.801845	0.786000	0.777708
		(0.8164-0.8163)	(0.80196)		
<i>s</i> -BuOH	0.5394	0.999073	0.997357	0.991333	0.987120
	0.9760	0.998400	0.996657	0.990599	0.986366
	1.3148	0.997886	0.996125	0.990045	0.985719
	1.6028	0.997461	0.995688	0.989586	0.985315
	1.9092	0.997014	0.995225	0.989095	0.984810
	100.0	0.821692	0.806669	0.789618	0.780398
BenzOH	1.0386	1.000776	0.998955	0.992785	0.988470
	1.4359	1.001116	0.999238	0.992995	0.988622
	1.5189	1.001186	0.999298	0.993042	0.988657
	1.8659	1.001483	0.999547	0.993238	0.988815
	100.0	1.059860	1.045185	1.029740	1.021847
			(1.04535)		(1.0219)

<sup>a</sup> See footnote *a* of Table II.

After temperature equilibrium had been achieved, the liquid in the pycnometers was removed until the meniscus reached a mark near the top of the capillary tube. The pycnometers were then dried with a lint-free cloth and weighed on the Mettler balance. The total weight was between 400 and 500 g., and the precision of the weighing was approximately  $\pm 0.1$  mg. The precision in the determination of the volume of the pycnometers with water was  $\pm 10$  p.p.m.; that in the density of the alcohol-water solutions was also  $\pm 10$  p.p.m., while that in the density of the pure alcohols was  $\pm 15$  p.p.m. The greater error in the case of the pure alcohols was probably due to the high volatility of the pure alcohols, especially at the higher temperatures.

After weighing, the pycnometers were returned to the water bath for re-equilibration at the next lowest temperature.

The precision in the density measurements was computed from duplicate runs (in some cases only one run was made), while that in  $\bar{v}$  was evaluated from an

error analysis based on eq. 2. The precision in  $\Delta\bar{v}_R$  was taken as the sum of the errors in  $\Delta\bar{v}$  for each alcohol.

## Results

The density data for all the alcohols studied are given in Tables II and III; the values for the pure alcohols (in parentheses) were obtained from the literature and are in good agreement with our data. The range of concentrations of the alcohols, in these tables, was below that at which a minimum is normally observed in a plot of  $\Delta\bar{v}$  against alcohol concentration.<sup>12</sup>

The computed partial molal volumes and derived quantities are summarized in Tables IV and V.

(10) By equilibration at 50°, the formation of air bubbles in the density measurements was avoided. Even if *all* of the air had not been removed, the maximum error would have been only a few parts per 10 million,<sup>11</sup> which is small compared to the error (a few parts per million) in our density measurements.

(11) National Bureau of Standards Circular 19, U. S. Government Printing Office, Washington, D. C., 1924.

(12) See, for example, K. Nakanishi, *Bull. Chem. Soc. Japan*, **33**, 793 (1960).



The values of  $\bar{v}$  and  $\Delta\bar{v}$  may be compared with those of Alexander,<sup>13</sup> who made similar measurements on the unbranched aliphatic alcohols MeOH to PeOH between 0 and 60° (in a higher concentration range, up to

**Table IV:** Partial Molal Volumes for Alcohols at Infinite Dilution

Alcohol	$\bar{v}$ , ml./mole <sup>a</sup>	$\Delta\bar{v}$ , ml./mole <sup>a,b</sup>
1°		
MeOH	38.02	-1.58
EtOH	54.66	-2.54
<i>n</i> -PrOH	70.00	-3.42
<i>i</i> -PrOH	71.39	-3.76
<i>n</i> -BuOH	85.54	-4.50
<i>i</i> -BuOH	85.86	-4.35
<i>s</i> -BuOH	85.91	-4.86
<i>n</i> -PeOH	101.15	-5.25
BenzOH	99.37	-2.67
20°		
MeOH	38.05	-2.44
EtOH	54.97	-3.40
<i>n</i> -PrOH	70.20	-4.52
<i>i</i> -PrOH	71.73	-4.81
<i>n</i> -BuOH	85.77	-5.77
<i>i</i> -BuOH	86.42	-5.47
<i>s</i> -BuOH	86.63	-5.77
<i>n</i> -PeOH	101.92	-6.28
BenzOH	100.82	-2.64
40°		
MeOH	38.37	-3.12
EtOH	55.36	-4.28
<i>n</i> -PrOH	70.80	-5.51
<i>i</i> -PrOH	72.55	-5.71
<i>n</i> -BuOH	86.37	-6.82
<i>i</i> -BuOH	87.63	-6.24
<i>s</i> -BuOH	87.72	-6.54
<i>n</i> -PeOH	102.91	-7.31
BenzOH	103.44	-1.58
50°		
MeOH	38.58	-3.43
EtOH	55.71	-4.64
<i>n</i> -PrOH	71.29	-5.89
<i>i</i> -PrOH	73.18	-6.05
<i>n</i> -BuOH	86.72	-7.32
<i>i</i> -BuOH	88.44	-6.54
<i>s</i> -BuOH	88.38	-6.89
<i>n</i> -PeOH	103.52	-7.77
BenzOH	105.20	-0.63

<sup>a</sup> The error in  $\bar{v}$  and in  $\Delta\bar{v}$  is no greater than  $\pm 0.1$  ml. <sup>b</sup> Computed from eq. 5.

5% by weight). Except in a few cases, there is reasonable agreement between the two sets of data. For example, for PrOH, he obtained  $\bar{v} = 70.52$  and  $\Delta\bar{v} = -4.24$  at 20°, and  $\bar{v} = 70.95$  and  $\Delta\bar{v} = -5.32$  at 40.1°.

The data for BuOH and PeOH do not agree as well as do those for the other alcohols. For BuOH he obtained  $\bar{v} = 87.4$  and  $\Delta\bar{v} = -5.8$  at 39.8° while, for PeOH, he obtained  $\bar{v} = 103.55$  and  $\Delta\bar{v} = -6.60$  at 40°, his data for PeOH being based on measurement at only one concentration. The reason for the discrepancy may be that his data pertain to higher concentrations (up to 5%) than those employed here (up to 2%). Since there is a tendency for solute-solute interaction as the concentration increases, this effect may not have been completely eliminated in his extrapolation to infinite dilution. Despite these discrepancies, his average values of  $\Delta\bar{v}_R$  compare well with ours; *e.g.*, for  $\Delta\bar{v}_{CH_4}$  he obtained approximately -1.0 at 20 and 40°, respectively, while for  $\Delta\bar{v}_{C_2H_4}$  he obtained approximately -2.0 at these same two temperatures.

## Discussion

In examining the data for the average values in Table V, the following limitations should be kept in mind: (1) the assumption of additivity of the effects of the polar and nonpolar portions of the molecule may not be strictly valid; (2) that part of the theory<sup>3</sup> of aqueous hydrocarbon solutions, which pertains to volume changes (especially for a molecule as small as CH<sub>4</sub>), is not as rigorous as that for the other thermodynamic parameters. These limitations may account for the two discrepancies which are evident in Table V. The first is the difference between theoretical and experimental values for the aromatic phenyl group; while the uncertainty about the theoretical value for CH<sub>4</sub> might have been circumvented by using longer aliphatic side chains, the solubilities of the corresponding alcohols are too small for precise density measurements. The second discrepancy is that, while the experimental values of  $\Delta\bar{v}_R$  for a given nonpolar group are relatively insensitive to temperature, the theoretical values are temperature dependent.

On the other hand, the agreement between the theoretical and experimental values of  $\Delta\bar{v}_R$  is fairly good for aliphatic groups, especially at the higher temperatures. Further, the theory predicts a larger negative value for  $\Delta\bar{v}_R$  for the larger nonpolar groups; this is verified by experiment for the aliphatic hydrocarbons.

Considering the limitations and discrepancies mentioned above, the rough agreement between theoretical and experimental values in Table V provides a qualitative verification of the theory since the model<sup>3</sup> assumes that there will be a decrease in volume when hydrocarbon is transferred to water because the hydro-

(13) D. M. Alexander, *J. Chem. Eng. Data*, **4**, 252 (1959).

Table V: Partial Molal Volumes,  $\Delta\bar{v}$ , for Nonpolar Groups at Infinite Dilution

$\Delta\bar{v}_R,^{a,b}$ ml./mole											
R = CH <sub>3</sub>			R = C <sub>2</sub> H <sub>5</sub>			R = C <sub>3</sub> H <sub>7</sub>			R = C <sub>6</sub> H <sub>13</sub>		
Exptl.	Theor.	C <sub>x</sub> - C <sub>y</sub>	Exptl.	Theor.	C <sub>x</sub> - C <sub>y</sub>	Exptl.	Theor.	C <sub>x</sub> - C <sub>y</sub>	Exptl.	Theor.	C <sub>x</sub> - C <sub>y</sub>
1°											
-0.96	-2.8	C <sub>2</sub> - C <sub>1</sub>	-1.8	-4.7	C <sub>3</sub> - C <sub>1</sub>	-2.9	-6.5	C <sub>4</sub> - C <sub>1</sub>	-1.1	-7.0	C <sub>7</sub> - C <sub>1</sub>
-0.88	-1.8	C <sub>3</sub> - C <sub>2</sub>	-2.0	-3.7	C <sub>4</sub> - C <sub>2</sub>	-2.8	-5.6	C <sub>5</sub> - C <sub>2</sub>			
-1.1	-1.9	C <sub>4</sub> - C <sub>3</sub>	-1.9	-3.7	C <sub>5</sub> - C <sub>3</sub>						
-0.75	-1.9	C <sub>5</sub> - C <sub>4</sub>									
-1.2	-1.8	C <sub>3</sub> - C <sub>2</sub> *	-1.8	-3.7	C <sub>4</sub> - C <sub>2</sub> *						
-1.4	-1.9	C <sub>4</sub> - C <sub>3</sub> *									
Av.	-1.1 <sup>c</sup>		-1.9	-3.7		-2.9	-5.6				
20°											
-0.96	-2.3	C <sub>2</sub> - C <sub>1</sub>	-2.1	-3.9	C <sub>3</sub> - C <sub>1</sub>	-3.3	-5.4	C <sub>4</sub> - C <sub>1</sub>	-0.2	-0.57	C <sub>7</sub> - C <sub>1</sub>
-1.1	-1.5	C <sub>3</sub> - C <sub>2</sub>	-2.4	-3.1	C <sub>4</sub> - C <sub>2</sub>	-2.9	-4.6	C <sub>5</sub> - C <sub>2</sub>			
-1.3	-1.5	C <sub>4</sub> - C <sub>3</sub>	-1.8	-3.1	C <sub>5</sub> - C <sub>3</sub>						
-0.51	-1.5	C <sub>5</sub> - C <sub>4</sub>									
-1.4	-1.5	C <sub>3</sub> - C <sub>2</sub> *	-2.1	-3.1	C <sub>4</sub> - C <sub>2</sub> *						
-1.2	-1.5	C <sub>4</sub> - C <sub>3</sub> *									
Av.	-1.2		-2.1	-3.1		-3.1	-4.6				
40°											
-1.2	-1.9	C <sub>2</sub> - C <sub>1</sub>	-2.4	-3.1	C <sub>3</sub> - C <sub>1</sub>	-3.7	-4.4	C <sub>4</sub> - C <sub>1</sub>	1.5	-4.4	C <sub>7</sub> - C <sub>1</sub>
-1.2	-1.3	C <sub>3</sub> - C <sub>2</sub>	-2.5	-2.5	C <sub>4</sub> - C <sub>2</sub>	-2.9	-3.8	C <sub>5</sub> - C <sub>2</sub>			
-1.3	-1.3	C <sub>4</sub> - C <sub>3</sub>	-1.8	-2.5	C <sub>5</sub> - C <sub>3</sub>						
-0.49	-1.3	C <sub>5</sub> - C <sub>4</sub>									
-1.4	-1.3	C <sub>3</sub> - C <sub>2</sub> *	-2.0	-2.5	C <sub>4</sub> - C <sub>2</sub> *						
-1.0	-1.3	C <sub>4</sub> - C <sub>3</sub> *									
Av.	-1.2		-2.2	-2.5		-3.3	-3.8				
50°											
-1.2	-1.7	C <sub>2</sub> - C <sub>1</sub>	-2.5	-2.8	C <sub>3</sub> - C <sub>1</sub>	-3.9	-4.0	C <sub>4</sub> - C <sub>1</sub>	2.8	-4.0	C <sub>7</sub> - C <sub>1</sub>
-1.3	-1.1	C <sub>3</sub> - C <sub>2</sub>	-2.7	-2.3	C <sub>4</sub> - C <sub>2</sub>	-3.1	-3.4	C <sub>5</sub> - C <sub>2</sub>			
-1.4	-1.1	C <sub>4</sub> - C <sub>3</sub>	-1.9	-2.3	C <sub>5</sub> - C <sub>3</sub>						
-0.45	-1.1	C <sub>5</sub> - C <sub>4</sub>									
-1.4	-1.1	C <sub>3</sub> - C <sub>2</sub> *	-1.9	-2.3	C <sub>4</sub> - C <sub>2</sub> *						
-1.0	-1.1	C <sub>4</sub> - C <sub>3</sub>									
Av.	-1.3		-2.3	-2.3		-3.5	-3.4				

<sup>a</sup> The error in  $\Delta\bar{v}_R$  is  $\pm 0.1$  ml. <sup>b</sup> Experimental values computed from eq. 6, using data of Table IV, and theoretical ones from eq. 7. <sup>c</sup> The C<sub>x</sub> - C<sub>y</sub> values represent the difference in experimental values of  $\Delta\bar{v}$  (from eq. 6) for alcohols having *x* and *y* carbon atoms, respectively (similarly for the theoretical data). When the data were obtained from branched, rather than straight-chain alcohols, they are indicated by an asterisk. The theoretical data, when C<sub>1</sub> (*i.e.*, methane) is involved, differ from those for large-chain hydrocarbons because of a slightly smaller value<sup>3</sup> of *Y*<sup>c</sup> for methane. These values were omitted from the averages of the theoretical values.

carbon fills the icelike partial cages quite efficiently. The volume decrease is observed experimentally, and,

in fact, the values observed do not differ too much from theoretical predictions.

# The Degree of Coupling and Efficiency of Fuel Cells and Membrane Desalination Processes

by S. R. Caplan\*

*Polymer Department, Weizmann Institute of Science, Rehovoth, Israel (Received May 7, 1965)*

The efficiency of energy conversion in desalination processes and fuel cells depends on the degree of coupling of the flows concerned. Methods for determining the degree of coupling and hence the maximum efficiency of these systems are outlined.

The efficient operation of desalination processes and fuel cells is currently a matter of considerable importance, and consequently it seems worthwhile clarifying some of the considerations involved in assessing efficiency in these systems. Kedem and Caplan have recently shown that the phenomenological description of two coupled flows leads to a definition of their "degree of coupling."<sup>1</sup> This dimensionless parameter  $q$  is readily measurable and determines uniquely the maximum efficiency of energy conversion. In general the efficiency  $\eta$  (which is defined by means of the entropy production function) depends both on  $q$  and on the conditions of operation. The extension of these concepts to multiple-flow systems, such as biological membranes, has been discussed by Caplan.<sup>2</sup> The degree of coupling between any pair of flows is related to an over-all degree of coupling between sets of flows, which has a particularly simple form when *one* driving flow or energy input is present. In this case the maximum efficiency of energy conversion is again uniquely determined. An analysis, in these terms, of membrane desalination processes and fuel cells with side reactions and leaks will be outlined below.

For isothermal systems we may conveniently begin with the dissipation function  $\Phi$ . If  $n$  irreversible processes take place

$$\Phi = T(d_i S/dt) = \sum_1^n J_i X_i \geq 0 \quad (1)$$

where  $J_i$  and  $X_i$  refer to conjugate flows and forces and  $d_i S/dt$  is the rate of entropy production. It is assumed that the flows and forces are linearly related

$$J_i = \sum_{j=1}^n L_{ij} X_j \quad (2)$$

$$X_i = \sum_{j=1}^n R_{ij} J_j$$

and that the phenomenological coefficients obey Onsager symmetry. Two dimensionless coefficients are defined as

$$l_{ij} = L_{ij}/\sqrt{L_{ii}L_{jj}} \quad (3)$$

$$r_{ij} = -R_{ij}/\sqrt{R_{ii}R_{jj}}$$

As a consequence of symmetry,  $l_{ij} = l_{ji}$  and  $r_{ij} = r_{ji}$ . It has been shown that  $l_{ij}$  is a normalized force ratio, while  $r_{ij}$  is a normalized flow ratio.<sup>2</sup> The latter quantity can be envisaged as the extent to which the  $i$ th flow is "dragged" by the  $j$ th when all other flows are stopped and the force conjugate to the  $i$ th flow is zero, and is accordingly defined as the degree of coupling between the processes  $i$  and  $j$ . If there are only two terms in  $\Phi$

$$r_{12} = l_{12} = q \quad (4)$$

The summation in eq. 1 must always contain at least one positive term, which may be regarded as the energy input rate. If the  $n$ th term represents this spontaneous process, it is seen that

\* Biophysical Laboratory, Harvard Medical School, Boston 15, Mass.

(1) O. Kedem and S. R. Caplan, *Trans. Faraday Soc.*, **61**, 1897 (1965).

(2) S. R. Caplan, *J. Theoret. Biol.*, in press.

$$\eta = -\sum_{i=1}^{n-1} J_i X_i / J_n X_n \quad (5)$$

and the condition for energy conversion is  $0 \leq \eta \leq 1$ . When  $n = 2$ , one finds the relations<sup>1</sup>

$$q^2 = 1 - \left\{ (J_n)_{J_i=0} / (J_n)_{X_i=0} \right\} \quad (X_n \text{ constant}) \quad (6)$$

$$\eta_{\max} = q^2 / (1 + \sqrt{1 - q^2})^2 \quad (7)$$

Thus,  $q$  and  $\eta_{\max}$  may be determined, in the case of a linear two-flow system with constant driving force, by the ratio of fuel consumption rates in the two stationary states corresponding to  $\eta = 0$ . The first of these, when  $J_i = 0$ , was termed for convenience "static head" (it is sometimes known as the stationary state of first order); the second, when  $X_i = 0$ , was termed "level flow."

If  $n > 2$ , the over-all degree of coupling, although not in general independent of the forces or the flows, reaches a maximum value  $\bar{q}$  in a particular series of stationary states.<sup>2</sup> These "maximum coupling states" are states of minimal entropy production under conditions of energy conversion and include as limits the states of static head (all  $J_i = 0$ ) and level flow (all  $X_i = 0$ ). The latter two states may be used to measure  $\bar{q}$  and  $\eta_{\max}$  by eq. 6 and 7. In the case  $n = 3$

$$\bar{q}^2 = (r_{13}^2 + r_{23}^2 + 2r_{12}r_{13}r_{23}) / (1 - r_{12}^2) \quad (8)$$

Maximum coupling states are characterized by the following two mutually dependent conditions: the  $J_i$  are in the proportions (relative to one another) which they assume at level flow, and the  $X_i$  are in the proportions they assume at static head. There is no other series of stationary states in which the relative proportions of both the  $J_i$  and the  $X_i$  remain fixed.

In general phenomenological coefficients are functions of the parameters of state and are not constant. However, it is possible to determine  $\bar{q}$  over a narrow range of maximum coupling states by means of the relation<sup>2</sup>

$$\bar{q}^2 = \left\{ \frac{J_i/X_i}{(\partial J_i / \partial X_i)_{X_n}} - 1 \right\} / \left\{ \frac{J_n/X_i}{(\partial J_n / \partial X_i)_{X_n}} - 1 \right\} \quad (9)$$

where any flow  $i$  has been chosen among the "driven" flows, and the partial derivatives, forces, and flows refer to some maximum coupling state within the range. At static head this reduces to

$$\bar{q}^2 = 1 / \left\{ 1 - \frac{J_n^{\text{sh}}/X_i^{\text{sh}}}{(\partial J_n / \partial X_i)_{X_n}} \right\} \quad (10)$$

Any system in which the dissipation function has been reduced to two terms by maintaining all driven processes but the  $i$ th at static head or level flow (in any com-

ination) may also be evaluated by eq. 9 and 10. The degree of coupling in such circumstances is less than  $\bar{q}$ .

### Membrane Desalination Processes

It is useful to examine the over-all degree of coupling in a clear-cut physical system not unrelated to biology. For the system chosen we can express  $\bar{q}^2$  in terms of the practical phenomenological coefficients of Kedem and Katchalsky,<sup>3</sup> providing the membrane separates aqueous solutions of a single salt (and no other permeable solute is present). Electrodes reversible to one of the ions are immersed in the solutions. We shall use the practical coefficients without further explanation. The three flows involved are (1) volume flow, (2) salt flow, and (3) current flow. The dissipation function is

$$\Phi = J_v(\Delta p - \Delta\pi) + J_s \Delta\pi_s / c_s + IE \quad (11)$$

where  $\Delta p$  and  $\Delta\pi$  are mechanical and osmotic pressure differences, and  $c_s$  is the average concentration of the permeable salt. For the sake of simplicity, we define the following dimensionless parameters, all of which can be expressed in terms of  $l_{ij}$  or  $r_{ij}$  only

$$K = 1 - \kappa/\kappa' = \beta^2 \kappa / L_p = l_{13}^2$$

$$W = \omega'/\omega - 1 = c_s(1 - \sigma)^2 L_p / \omega \quad (12)$$

$$T = \tau_1'/\tau_1 - 1 = c_s(1 - \sigma)\beta v_1 z_1 F / \tau_1$$

where the coefficients involved are:  $\kappa$ ,  $\kappa'$ , electrical conductance under different restrictions;  $\omega$ ,  $\omega'$ , salt permeability under different restrictions;  $\tau_1$ ,  $\tau_1'$ , transport number under different restrictions (of ion not participating in electrode reaction);  $\beta$ , electroosmotic permeability;  $\sigma$ , reflection coefficient;  $L_p$ , filtration coefficient.

Three cases may now be considered

Driving process  $J_v(\Delta p - \Delta\pi)$

$$\bar{q}_1^2 = (K + W) / (1 + W) \quad (13)$$

Driving process  $J_s \Delta\pi_s / c_s$

$$\bar{q}_2^2 = \left\{ 1 + \frac{T^2(1 - K)}{W(T^2 + 2KT + K)} \right\}^{-1} \quad (14)$$

Driving process  $IE$   $\bar{q}_3^2 = K(T^2 + W) /$

$$(T^2 + KW) \quad (15)$$

However, it is not particularly useful to regard  $J_v(\Delta p - \Delta\pi)$  as an energy source. In practical salt filtration procedures (usually referred to as "hyperfiltration" or "reverse osmosis") the term  $J_s \Delta\pi_s / c_s$  remains positive in the dissipation function. One is really con-

(3) O. Kedem and A. Katchalsky, *Trans. Faraday Soc.*, **59**, 1918, 1931 (1963).

**Table I:** Over-all Degree of Coupling and Maximum Efficiency of Energy Conversion (%) for a Typical Synthetic Ion-Exchange Membrane<sup>3</sup> between Ag-AgCl Electrodes

Mean concn. of KCl, <i>M</i>	Hyperfiltration				Concentration cell				Electrodialysis			
	Either charge		Either charge		Cation exch.		Anion exch.		Cation exch.		Anion exch.	
	$\bar{q}_1^2$	$\eta_{\max}$	$\bar{q}_{1a}^2$	$\eta_{\max}$	$\bar{q}_2^2$	$\eta_{\max}$	$\bar{q}_2^2$	$\eta_{\max}$	$\bar{q}_2^2$	$\eta_{\max}$	$\bar{q}_2^2$	$\eta_{\max}$
$5.5 \times 10^{-3}$	3.68	0.94	6.35	1.64	99.6	88.1	0.05	0.01	99.6	88.1	3.64	0.93
$2.2 \times 10^{-2}$	4.02	1.03	4.43	1.13	95.5	65.1	5.12	1.31	95.5	65.1	8.13	2.12

cerned with the mechanical energy invested, in which case it is advantageous to transform eq. 11 into the form

$$\Phi = J_v \Delta p + J_D \Delta \pi_s + IE \quad (16)$$

which assumes that impermeable solutes do not contribute significantly to the total osmotic pressure difference. The diffusional flow  $J_D$  is given to a close approximation by

$$J_D \approx J_s/c_s - J_v \quad (17)$$

If we now define an additional parameter

$$W' = c_s \sigma^2 L_p / \omega \quad (18)$$

we may consider a further case based on eq. 16

$$\text{Driving process } J_v \Delta p \quad \bar{q}_{1a}^2 = (K + W') / (1 + W') \quad (19)$$

As a concrete example, the typical synthetic ion-exchange membrane described in detail by Kedem and Katchalsky<sup>3</sup> is evaluated in Table I. Two average salt concentrations within the range of their model have been chosen. The calculation of  $\bar{q}^2$  values offers a good check on the internal consistency of a set of assumed or measured coefficients, apart from setting an upper limit to  $\eta$  and providing a basis for comparison. The concentration cell (also referred to as "reverse electrodialysis") is included in Table I for comparison with the desalination processes. The asymmetry of coupling in both reverse and normal electrodialysis with respect to the membrane charge, for electrodes reversible to a given ion, disappears if one takes as the working unit a pair of membranes of opposite fixed charges.<sup>1</sup>

The efficiency of this particular membrane in converting mechanical energy to electrical and osmotic energy is extremely low. Note that in hyperfiltration the over-all degree of coupling, whichever way it is calculated, is independent of the transport number in the membrane. Actually, only the conversion of mechanical energy to osmotic energy is of importance, and the current is always zero, no electrodes being inserted. It is readily shown that under this restriction  $K$  vanishes in eq. 13 and 19, considerably reducing the figures

given in Table I. Since neither transport number nor conductivity are now involved explicitly in the degree of coupling, uncharged membranes may offer advantages. Loeb and Manjikian<sup>4</sup> have described the performance of a desalination cell incorporating cellulose acetate membranes. From their data, an efficiency  $\eta = -J_D \Delta \pi_s / J_v \Delta p$  of 7.8% is calculated for their conditions of operation. This is equivalent to a value of  $r_{12}^2$  not less than 25%.

### Fuel Cells

In a previous discussion<sup>1</sup> it was pointed out that the degree of coupling in a fuel cell operating without side reactions and leaks is unity. The appearance of side reactions (*i.e.*, incomplete oxidations) may partially decouple the system<sup>2</sup> and gives rise to additional terms in the dissipation function. The considerations set out above are then applicable.

Consider a working unit, in a stationary state, operating on a gaseous fuel. The unit includes the cell and any recycling arrangements and is provided with feed lines and exhaust lines. The dissipation function for this system, if we suppose that only one side reaction takes place, is

$$\Phi = IE + Av - A_s v_s + J_t \Delta \mu_t + J_0 \Delta \mu_0 \quad (20)$$

where  $A$ ,  $A_s$  and  $v$ ,  $v_s$  represent the affinities and velocities, respectively, of the main and side reactions, while  $J_t$ ,  $J_0$  and  $\Delta \mu_t$ ,  $\Delta \mu_0$  represent exhaust flows and chemical potential differences (across the unit) of fuel and oxygen. The affinities here are calculated by using the chemical potentials of the reactants on the feed side and the products on the exhaust side (if the feed lines contain products, this will simply contribute further flow terms to  $\Phi$ ). The last two terms arise owing to incomplete utilization of the fuel; this is characteristic of fuel cell technology since at high degrees of conversion appreciable polarization occurs. The reaction velocities are calculated on the basis of fuel actually consumed. Within the cell the vectorial flows  $J_t$  and  $J_0$

(4) S. Loeb and S. Manjikian, "Brackish Water Desalination by an Osmotic Membrane," University of California, Department of Engineering Report No. 63-37, 1963.

take place in isotropic spaces adjacent to the electrodes and, hence, cannot be coupled to the scalar chemical reactions. It is evident that they also cannot be coupled to the current, so that the sum of the last two terms is separately positively definite, and we can divide  $\Phi$  into two parts

$$\Phi' = IE + Av + A_s v_s \quad (21)$$

$$\Phi'' = J_t \Delta \mu_t + J_0 \Delta \mu_0 \quad (22)$$

$\Phi''$  represents an input of energy which is completely wasted and, hence, decreases the efficiency (although the fuel may subsequently be recovered by operating cells in cascade). However, the efficiency of the unit as an energy converter under given conditions of fuel utilization depends on  $\Phi'$ . Note that successive interactions in the cell, forming short-lived intermediates (such as hydrogen peroxide) which do not appear in the exhaust gases, contribute no terms to  $\Phi'$ . In order to evaluate the degree of coupling and the efficiency, we make the linear transformation

$$\Phi' = IE + Av_t + (A_s - A)v_s \quad (23)$$

where  $v_t = v + v_s$  denotes the total fuel actually consumed. The third term in eq. 23 now represents a back reaction; *i.e.*,  $v_s$  is the velocity and  $(A_s - A)$  the affinity of a hypothetical process in the exhaust gases whereby the products of the main reaction (usually carbon dioxide and water) are reduced to the products of the side reaction, releasing oxygen into the feed. This affinity is clearly negative if not zero, and it seems reasonable to assume that it is very small in comparison to  $A$  since otherwise in the presence of catalyst complete oxidation of the fuel would occur. If this is the case, the back reaction may be considered to be at level flow, and the efficiency is given by

$$\eta = -IE/Av_t \quad (24)$$

where the output is compared to the total input of chemical energy on the basis of complete oxidation of the fuel consumed.

For a variety of fuel cells operated at constant affinity, the linear region of the voltage-current curve is remarkably broad, frequently extending to open circuit.<sup>5</sup> For such cells eq. 10 may be used to evaluate the degree of coupling. For convenience it is rewritten below; static head in this case corresponds, of course, to open circuit

$$q^2 = \left[ 1 - \frac{v^{oc}/E^{oc}}{(\partial v/\partial E)_A} \right]^{-1} \quad (25)$$

Equation 25 requires the measurement of fuel consumption at several values of the load resistance. Once  $q^2$  has been determined, the efficiency is known<sup>1</sup> for any potential difference across the terminals

$$\eta = \frac{1 - (E/E^{oc})}{(E^{oc}/E q^2) - 1} \quad (26)$$

If the linear region of the voltage-current curve does not extend to open circuit, an extrapolated value for  $E^{oc}$  may be used in eq. 26,  $q^2$  having been determined either by using extrapolated values for both  $v^{oc}$  and  $E^{oc}$  in eq. 25 or by means of the following form of eq. 9

$$q^2 = \left\{ \frac{I/E}{(\partial I/\partial E)_A} - 1 \right\} / \left\{ \frac{v/E}{(\partial v/\partial E)_A} - 1 \right\} \quad (27)$$

Equation 27 also applies over any small region of a nonlinear characteristic. It will be observed that the degree of coupling  $q$  here is actually an  $l_{in}$ .

*Acknowledgments.* The author wishes to express his indebtedness to Drs. Ora Kedem and Donald C. Mikulecky for their stimulating criticism. This investigation was supported by P.H.S. Research Grants GM-09432-01 and GM-09432-02 from the National Institute of General Medical Sciences, Public Health Service.

(5) See, for examples, G. J. Young, Ed., "Fuel Cells," Reinhold Publishing Corp., New York, N. Y., 1960; W. Mitchell, Ed., "Fuel Cells," Academic Press Inc., New York, N. Y., 1963.

## An Electron Paramagnetic Resonance Study of Alcohol Oxidation

### by Fenton's Reagent

by Takeshi Shiga<sup>1</sup>

University of Oregon Medical School, Portland, Oregon (Received May 13, 1965)

Free radicals of alcohols produced by Fenton's reagent ( $\text{Fe}^{2+}$ -EDTA +  $\text{H}_2\text{O}_2$ ) were studied at room temperature in aqueous solutions (pH 7) using e.p.r. with a continuous-flow system. This system allowed any intermediate produced to be observed 5 msec. after mixing. The observed free radicals were characterized as  $\omega$ -oxidized products in which the farthest position from the alcoholic OH was the main point of attack. In contrast, it has been reported that the hydrogen abstraction took place at the carbon nearest to the alcoholic OH when oxidation by the  $\text{Ti}^{3+}$  +  $\text{H}_2\text{O}_2$  system or photooxidation in the presence of  $\text{H}_2\text{O}_2$  was employed. Therefore, a current hypothesis assuming the existence of OH radical as an active intermediate of Fenton's reagent becomes very doubtful. Presumably, the active species must be some sort of complex between the reactants rather than an OH radical. The hyperfine structure analysis showed that (1) the  $C_1$  coupling constant<sup>2</sup> (normally 20–22 gauss) decreased to 14–18 gauss upon  $C_1$  substitution by an OH group and also was dependent on the  $C_2$  substituent (OH, Cl, alkyl), and (2) the  $C_2$  coupling constant (normally 25–28 gauss) was also reduced to 19–22 gauss or to 9–11 gauss when the  $C_2$  position was substituted by OH, Cl, etc. The formation of the free radical was very fast; only the apparent decay of the alcohol radical could be observed.

### Introduction

Among the various chemical hydroxylating systems, Fenton's reagent has been extensively studied, but no direct evidence has been found concerning the reaction mechanism. The most valuable information would be the identification of the reactive intermediate, *i.e.*,  $\dot{\text{O}}\text{H}$ ,  $\dot{\text{O}}_2\text{H}$ , or even some sort of hydrogen peroxide-iron-EDTA complex. In order to detect this kind of short-lived intermediate, the electron paramagnetic resonance (e.p.r.) method combined with a suitable flow system should be a powerful method. Dixon and Norman,<sup>3</sup> for example, observed an e.p.r. signal ( $g = 2.01$ ,  $\Delta H = 1$  gauss) produced by the  $\text{Ti}^{3+}$  +  $\text{H}_2\text{O}_2$  system. This radical is said to be  $\dot{\text{O}}\text{H}$  because the signal is different from the  $\dot{\text{O}}_2\text{H}$  radical produced by the  $\text{Ce}^{4+}$  +  $\text{H}_2\text{O}_2$  system,<sup>4,5</sup> and, if substrate is added, the signal is replaced by that of a substrate radical.<sup>3b,6,7</sup> Recently, Piette, Bulow, and Loeffler studied these systems in detail<sup>8</sup> and disagreed with these identifications.

In Fenton's reagent such an intermediate species cannot be observed, but the free radicals formed from

the substrate can be detected. Norman, *et al.*, claimed that they observed the identical aromatic free-radical intermediate during oxidation in both systems, the  $\text{Ti}^{3+}$  +  $\text{H}_2\text{O}_2$  system and Fenton's reagent.<sup>9,10</sup> However, any identification of reactive species in the two

(1) On leave from the Faculty of Medicine, Osaka University, Osaka, Japan.

(2)  $C_1$ ,  $C_2$ , etc., are used to express the position relative to the carbon on which the unpaired electron locates and are commonly designated by  $\alpha$ ,  $\beta$ , etc., which are used to show the position of the group concerned relative to that of the carbon attached to the alcoholic OH group, following conventional notation.  $a_1$ ,  $a_2$ , etc., are used as hyperfine coupling constants for protons attached to  $C_1$ ,  $C_2$ , etc.  $Q$  and  $\rho$  are used in the conventional manner.

(3) (a) W. T. Dixon and R. O. C. Norman, *Nature*, **196**, 891 (1962); (b) *J. Chem. Soc.*, 3119 (1963).

(4) E. Saito and B. H. J. Bielski, *J. Am. Chem. Soc.*, **83**, 4467 (1961).

(5) B. H. J. Bielski and E. Saito, *J. Phys. Chem.*, **66**, 2266 (1962).

(6) W. T. Dixon, R. O. C. Norman, and A. L. Buley, *J. Chem. Soc.*, 3625 (1964).

(7) W. T. Dixon and R. O. C. Norman, *Proc. Chem. Soc.*, 97 (1963).

(8) L. H. Piette, G. A. Bulow, and K. O. Loeffler, Preprints, Symposium on the Use of E.s.r. in the Elucidation of Reaction Mechanisms, Vol. 9, No. 2-C, American Chemical Society, Washington, D. C., 1964, p. C-9.

systems which is based on the nature of aromatic free-radical products is ambiguous since the spin-density distribution of a free radical is determined mostly by resonance stabilization in the aromatic radicals formed. Thus the spin-density distribution of the free radical might be independent of the nature of the active oxidizing reagent. It appeared probable that more information concerning the character of the active reagent would be derived from a study of aliphatic radicals produced by Fenton's reagent and by  $Ti^{3+} + H_2O_2$  oxidation.

This study has revealed that the oxidized alcohol radicals produced by Fenton's reagent differ from the products of oxidation by the  $Ti^{3+} + H_2O_2$  system. In this paper certain aspects of the  $\omega$ -oxidation of alcohols by Fenton's reagent will be discussed in connection with the above problem, and, in addition, some general rules of the hyperfine coupling constants of OH-substituted alkyl radicals will be drawn.

### Experimental Section

**Material.** The following materials and their sources were used:  $H_2O_2$ , methyl, *n*-propyl, and *t*-butyl alcohols, and glycerol were obtained from Allied Chemical, General Chemical Division; ethanol from Commercial Solvent Corp.; isopropyl and *n*-butyl alcohols, ethylene glycol, propylene glycol, phosphate salts, ethylenediaminetetraacetic acid (EDTA), and  $TiCl_3$  from Matheson Coleman and Bell; isoamyl and *t*-amyl alcohols and sulfuric acid from J. T. Baker Chemical Co.; isobutyl alcohol and 2-chloroethanol from Eastman Organic Chemicals; *n*-amyl alcohol from Fisher Scientific Co.;  $FeSO_4 \cdot 7H_2O$  from Mallinckrodt Chemical Works.

**Method and Apparatus.** A Varian V-4500 e.p.r. spectrometer with a Fieldial magnetic field control unit and with a 100-kc. modulation unit was used. The first derivatives of e.p.r. absorption were recorded with a Varian F-80 XY recorder and with a Sanborn Model 320 recorder. The microwave circuit was modified in order to facilitate a low power experiment and to measure the incident microwave power<sup>11</sup>; a Hewlett-Packard 431B power meter was used.

**Flow System.** A flat cell with a four-jet mixer was made, modifying Borg's idea<sup>12</sup> and similar to Piette's cell.<sup>13</sup> Quartz glass was obtained from Engelhardt Co. The dimensions of the flat portion (observation chamber) are  $0.35 \times 8.0$  mm., 4 cm. height; a thickness of 0.35 mm. rather than the more common 0.1–0.2 mm. is chosen so that the hydrodynamic resistance is reduced. However, the sensitivity for an aqueous sample is decreased to about 70% of Varian's aqueous-solution sample cell. The mixing chamber, which is

just below the flat portion, has a capacity of 0.036 cm.<sup>3</sup>, and four holes of  $\phi = 0.5$  mm. through the wall (thickness *ca.* 1 mm.) are positioned along the bottom of the chamber. Four capillaries ( $\phi = 2$  mm.) are fixed one to each hole, and the opposing pairs are joined together.

**Driving System.** Two containers (capacity, 1 l.), having a liquid inlet, a bubbling tube, a pressure tube at the top, and a liquid outlet at the bottom, are placed on magnetic stirrers for mixing of the solutions. Deoxygenation is achieved by bubbling prepurified  $N_2$  gas ( $O_2$  content less than 10 p.p.m.) through the containers for at least 15 min. The outlet tubes lead to the e.p.r. cell through a pair of solenoid valves. Another valve is placed at the outlet of the flow cell for stopped-flow experiments. These three valves are normally closed, and they are opened simultaneously by a trigger. The driving pressure is supplied by an  $N_2$  bottle with a 20-l.  $N_2$  reservoir, acting as a ballast, connected to a mercury pressure gauge from which a direct reading of the applied pressure can be made.

**Characteristics of the Flow System.** At maximum pressure (90 cm. above atmospheric pressure), the flow rate is 13 ml./sec., *i.e.*, 465 cm./sec., for pure water at 20°. This speed ensures that the mixture of two solutions passes the entrance, the middle, and the exit of the e.p.r. cavity 3, 5, and 7 msec., respectively, after mixing. The efficiency of mixing was checked at various flow rates by observing a phenolphthalein color reaction. At a flow rate of 13–20 ml./sec., mixing seemed to be satisfactory, and no lamellar streaming was seen. However, a more rigorous method, flash photography, was not employed. The sensitivity of e.p.r. depends on the position of the sample in the cavity. Approximately 60% of the observed e.p.r. signal is contributed by the sample occupying the central third of the flat cell, while upper and lower thirds each contribute 20%.<sup>14</sup> The majority of the observed e.p.r. signals at maximal and minimal flow rate corresponds to the time of 4–6 msec. (mean 5 msec.) and 25–40 msec. (mean 32 msec.) after mixing, respectively. Therefore, in continuous-flow experiments there exists some uncertainty since the time

(9) L. Smith, W. T. Dixon, and R. O. C. Norman, *J. Chem. Soc.*, 2897 (1963).

(10) A. L. Buley, W. T. Dixon, and R. O. C. Norman, unpublished, quoted in ref. 6.

(11) H. Beinert and G. Palmer, *J. Biol. Chem.*, **239**, 1221 (1964).

(12) D. C. Borg, *Nature*, **201**, 1087 (1964).

(13) L. H. Piette in "Rapid Mixing and Sampling Techniques in Biochemistry," B. Chance, Q. H. Gibson, R. H. Eisenhardt, and K. K. Longberg-Holm, Ed., Academic Press Inc., New York, N. Y., 1964, pp. 131–134.

(14) B. T. Allen, Thesis, Southampton University, 1961.



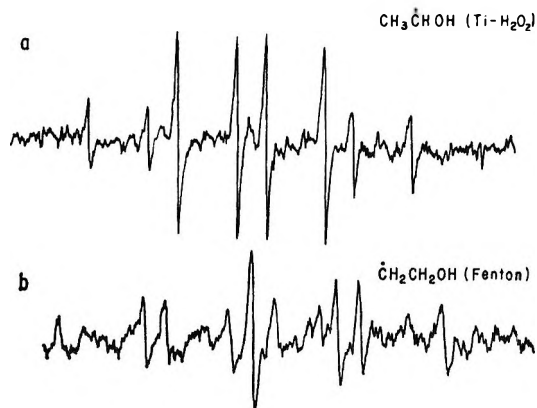


Figure 1. E.p.r. spectra of ethanol radicals: (a) produced by  $Ti^{3+} + H_2O_2$  system ( $10^{-2} M Ti^{3+}$  and 5% ethanol + 2 ml. of 30%  $H_2O_2/l.$  in 0.2  $N H_2SO_4$  solution) and (b) produced by Fenton's reagent ( $2.5 \times 10^{-3} M Fe^{2+}$ -EDTA and 5% ethanol + 2 ml. of 30%  $H_2O_2/l.$  in 0.67  $M$  phosphate buffer at pH 7). Microwave power, 25 mw. (a) and 80 mw. (b); modulation, 100 kc., 0.36 gauss (a) and 0.98 gauss (b); magnetic field scanning, 250 gauss/min. (a) and 250 gauss/5 min. (b).

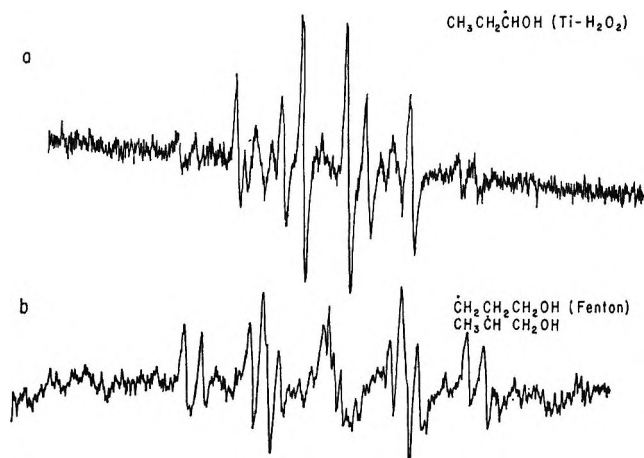


Figure 2. E.p.r. spectra of *n*-propyl alcohol radicals: (a) produced by the  $Ti^{3+} + H_2O_2$  system ( $10^{-2} M Ti^{3+}$  and 5% *n*-propyl alcohol + 2 ml. of 30%  $H_2O_2/l.$  in 0.2  $N H_2SO_4$  solution) and (b) produced by Fenton's reagent ( $2.5 \times 10^{-3} M Fe^{2+}$ -EDTA and 5% *n*-propyl alcohol + 2 ml. of 30%  $H_2O_2/l.$  in 0.67  $M$  phosphate buffer at pH 7). Microwave power, 25 mw. (a) and 80 mw. (b), modulation, 100 kc., 0.98 gauss (a, b); magnetic field scanning, 250 gauss/2.5 min. (a) and 250 gauss/5 min. (b).

scale varies with the flow rate and since a time corresponding to the mean time after mixing is used.

**Concentration Measurement.** The ethanol radical has a line width of 3.3 gauss, which is broadened by overmodulation and by an unresolved hyperfine structure (doublet) due to  $OH^{\cdot}$ .<sup>8</sup> For the kinetic study of the ethanol radical a quinhydrone solution<sup>15</sup>

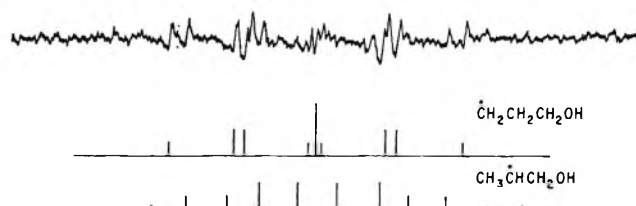


Figure 3. E.p.r. spectrum of the *n*-propyl alcohol radical produced by Fenton's reagent ( $2.5 \times 10^{-3} M Fe^{2+}$ -EDTA and 5% *n*-propyl alcohol + 2 ml. of 30%  $H_2O_2/l.$  in 0.67  $M$  phosphate buffer at pH 7). Microwave power, 80 mw.; modulation, 100 kc., 0.36 gauss; magnetic field scanning, 250 gauss/5 min.; recorder chart speed, 2 mm./sec. The assignments of the signals are shown; the central peak of  $\dot{C}H_2CH_2CH_2OH$  begins to split.

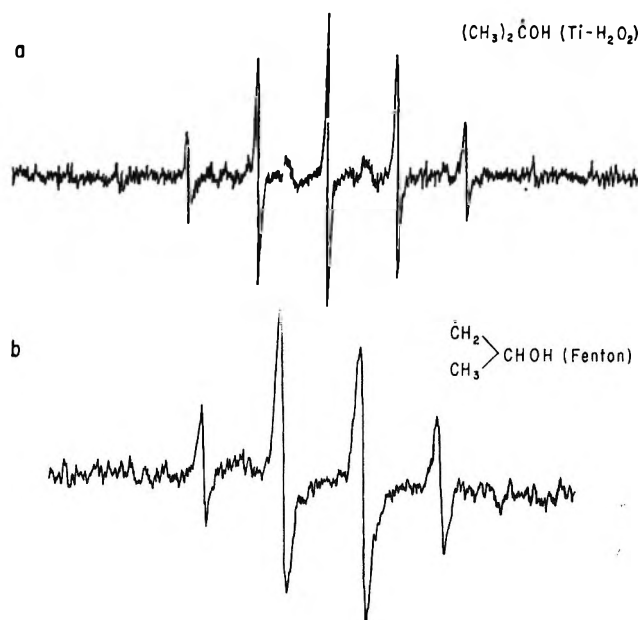


Figure 4. E.p.r. spectra of isopropyl alcohol radicals: (a) produced by the  $Ti^{3+} + H_2O_2$  system ( $10^{-2} M Ti^{3+}$  and 5% isopropyl alcohol + 2 ml. of 30%  $H_2O_2/l.$  in 0.2  $N H_2SO_4$  solution) and (b) produced by Fenton's reagent ( $2.5 \times 10^{-3} M Fe^{2+}$ -EDTA and 5% isopropyl alcohol + 2 ml. of 30%  $H_2O_2/l.$  in 0.67  $M$  phosphate buffer at pH 7). Microwave power, 25 mw. (a) and 80 mw. (b); modulation, 100 kc., 0.36 gauss (a) and 0.98 gauss (b); magnetic field scanning, 250 gauss/2.5 min. (a) and 250 gauss/5 min. (b).

was adopted as the standard for the spin-concentration measurement. The saturation phenomena were checked for both radicals. A *p*-semiquinone signal does not saturate below 34 mw. of incident microwave power at the cavity arm, and the methanol radical begins to saturate above 50 mw. (Figure 9). Therefore, an incident microwave power of 25 mw. was applied throughout the kinetic experiments.

(15) G. Narni, H. S. Mason, and I. Yamazaki, unpublished.

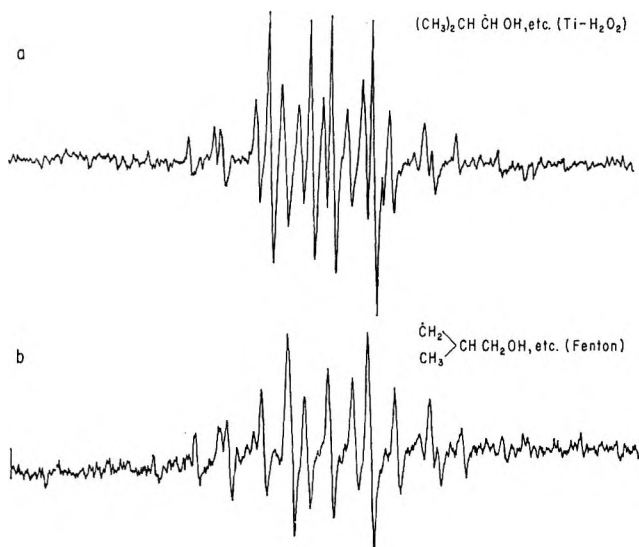


Figure 5. E.p.r. spectra of isobutyl alcohol radical: (a) produced by the  $\text{Ti}^{3+} + \text{H}_2\text{O}_2$  system ( $10^{-2} M \text{Ti}^{3+}$  and 5% isobutyl alcohol + 2 ml. of 30%  $\text{H}_2\text{O}_2/\text{l.}$  in 0.2  $N \text{H}_2\text{SO}_4$ ) and (b) Fenton's reagent ( $2.5 \times 10^{-3} M \text{Fe}^{2+}$ -EDTA and 5% isobutyl alcohol + 2 ml. of 30%  $\text{H}_2\text{O}_2/\text{l.}$  in 0.67  $M$  phosphate buffer at pH 7). Microwave power, 25 mw. (a) and 80 mw. (b); modulation, 100 kc., 0.98 gauss (a) and 0.61 gauss (b); magnetic field scanning, 250 gauss/2.5 min. (a) and 250 gauss/5 min. (b).

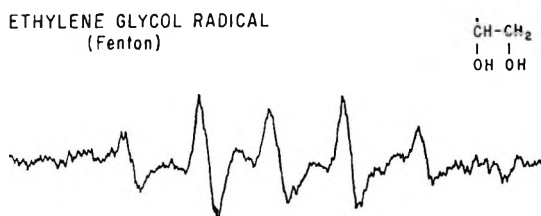


Figure 6. E.p.r. spectrum of the ethylene glycol radical produced by Fenton's reagent ( $2.5 \times 10^{-3} M \text{Fe}^{2+}$ -EDTA and 8% ethyleneglycol + 2 ml. of 30%  $\text{H}_2\text{O}_2/\text{l.}$  in 0.67  $M$  phosphate buffer at pH 7). Microwave power, 25 mw.; modulation, 100 kc., 0.98 gauss; magnetic field scanning, 100 gauss/2.5 min.

**Experimental Procedure.** The four-jet mixing flat cell and the driving system were used at  $22 \pm 1^\circ$ . To obtain reproducible quantitative results, deoxygenation was most important, for which prepurified  $\text{N}_2$  ( $\text{O}_2 < 10$  p.p.m.) was bubbled at least 15 min. The hyperfine coupling constants were measured from the spectra taken at a relatively slow magnetic field scanning speed; the error of the constants was within 3%.

## Results

**Formation of Alcohol Free Radicals.** Solutions of  $\text{Fe}^{2+}$ -EDTA (1:1) and of  $\text{H}_2\text{O}_2$ ,  $5 \times 10^{-3}$  and  $8.8 \times$

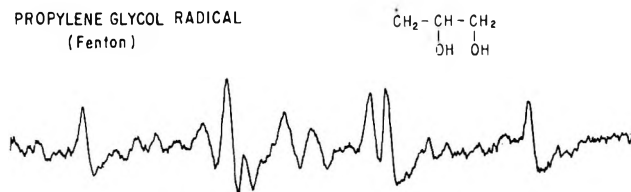


Figure 7. E.p.r. spectrum of the propylene glycol radical produced by Fenton's reagent ( $4.5 \times 10^{-3} M \text{Fe}^{2+}$ -EDTA and 5% propylene glycol + 2 ml. of 30%  $\text{H}_2\text{O}_2/\text{l.}$  in 0.67  $M$  phosphate buffer at pH 7). Microwave power, 25 mw.; modulation, 100 kc., 0.98 gauss; magnetic field scanning, 100 gauss/2.5 min.

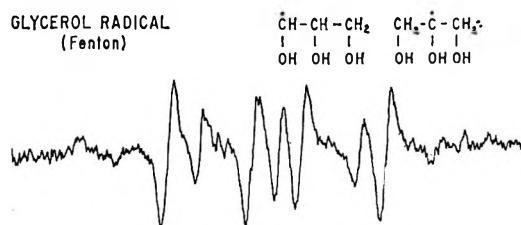


Figure 8. E.p.r. spectrum of the glycerol radical produced by Fenton's reagent ( $4.5 \times 10^{-3} M \text{Fe}^{2+}$ -EDTA and 5% glycerol + 2 ml. of 30%  $\text{H}_2\text{O}_2/\text{l.}$  in 0.67  $M$  phosphate buffer at pH 7). Microwave power, 25 mw.; modulation, 0.36 gauss; magnetic field scanning, 100 gauss/2.5 min.

$10^{-2} M$ , respectively, each buffered at pH 7 with 0.67  $M$  phosphate buffer, were mixed, and the region around  $g = 2.01$  to 2.00 was searched. However, no e.p.r. signal was observed.

When alcohol was added to  $\text{H}_2\text{O}_2$  solution (or both solutions), the alcohol radicals could be detected at  $g = 2.002$ . A comparison of the radicals produced by this system and the  $\text{Ti}^{3+} + \text{H}_2\text{O}_2$  system<sup>3b</sup> shows that the spectra are generally dissimilar (see Figures 1-8).

*Methanol* gives a triplet (1:2:1) radical identical with the  $\dot{\text{C}}\text{H}_2\text{OH}$  radical produced by the  $\text{Ti}^{3+} + \text{H}_2\text{O}_2$  system<sup>3b</sup>; further doublet splitting due to  $\text{OH}^\bullet$  could not be observed.

The *ethanol* radical has a nine-line spectrum (Figure 1b), a triplet (1:2:1) of a triplet (1:2:1), *i.e.*, two sets of  $\text{CH}_2$ . In contrast, the  $\text{Ti}^{3+} + \text{H}_2\text{O}_2$  system gave an eight-line spectrum, a quartet (1:3:3:1) of doublet (1:1) due to  $\text{CH}_2\dot{\text{C}}\text{HOH}$ <sup>3b</sup> (Figure 1a). Fenton's reagent gave  $\dot{\text{C}}\text{H}_2\text{CH}_2\text{OH}$ .

The radical of *n-propyl alcohol* shows a complicated spectrum which is the result of the superposition of two spectra (Figures 2b, 3). One of them is similar to the ethanol radical spectrum and therefore must be  $\dot{\text{C}}\text{H}_2\text{CH}_2\text{CH}_2\text{OH}$ , in which the central peak splits further by  $\text{C}_3$  protons ( $-\text{CH}_2\text{OH}$ ). The other signal

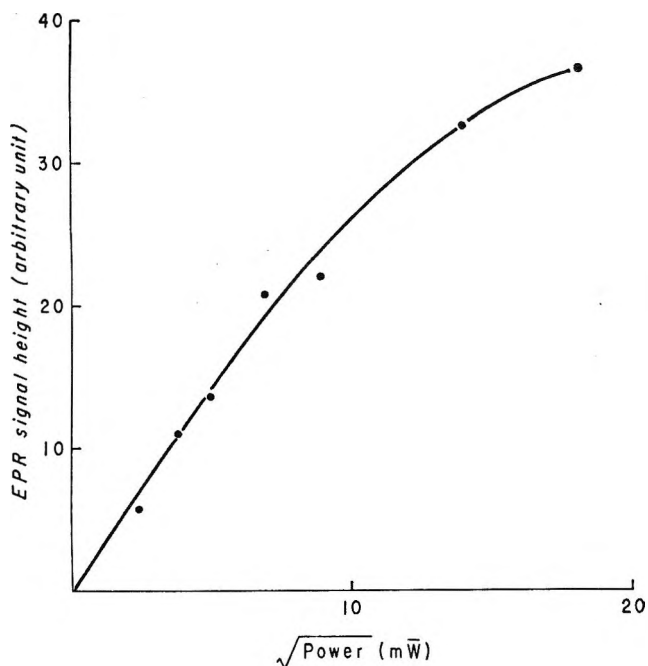


Figure 9. Saturation behavior of methanol radical produced by Fenton's reagent ( $10^{-3} M$   $Fe^{2+}$ -EDTA and 5% methanol + 2 ml. of 30%  $H_2O_2$ /l. in 0.67  $M$  phosphate buffer at pH 7) at  $22^\circ$ ; flow rate of reagents, 40 ml./5 sec. E.p.r. absorption is expressed by the signal height of the central peak of first-derivative curves since the line width is constant in this microwave power range. Microwave power is measured at the entrance of the cavity arm by a Hewlett-Packard 431B power meter; modulation, 100 kc., 0.98 gauss; response, 0.3 sec.; magnetic field scanning, 250 gauss/min.

is assumed to be due to  $CH_3\dot{C}HCH_2OH$ ; for a twelve-line spectrum, a doublet of a sextet (1:5:10:10:5:1), the number of lines fits this assumption, but their intensity does not, making this assignment an ambiguous one.

The  $Ti^{3+} + H_2O_2$  system definitely produced a triplet (1:2:1) of a doublet (1:1),  $CH_3CH_2\dot{C}HOH$ , and a weak signal corresponding to  $\dot{C}H_2CH_2CH_2OH$  could also be seen (Figure 2a).

The radical spectrum of *isopropyl alcohol* (Figure 4b) was accidentally a quartet (1:3:3:1), *i.e.*, a doublet (1:1) of a triplet (1:2:1), due to  $\dot{C}H_2CH(CH_3)OH$ .

On the other hand, the  $Ti^{3+} + H_2O_2$  system gave a typical septet from  $(CH_3)_2\dot{C}OH$ <sup>3a</sup> (Figure 4a).

The radicals of *n-butyl* and *n-amyl* alcohols showed very complicated spectra because (1) two or three kinds of radicals were produced, so that (2) yields of each species were relatively decreased, and (3) sufficient concentration of each free radical could not be obtained since the substrate concentration was limited by its solubility in water. However, if *n-propyl* alcohol radical spectra were superimposed on these

spectra, some typical peaks could be identified; hence, these spectra consist of  $\dot{C}H_2(CH_2)_nOH$ ,  $CH_3\dot{C}H(CH_2)_nOH$ , etc.

The spectra obtained from the  $Ti^{3+} + H_2O_2$  system also gave a complicated pattern and could not be analyzed.

The spectra of *isobutyl* and *isoamyl* alcohols were also complicated because of overlapping of the spectra of two or more kinds of radicals. For example, a spectrum of the isobutyl alcohol radical (Figure 5b), a doublet of a triplet (1:2:1), could be distinguished, owing to  $\dot{C}H_2CH(CH_3)CH_2OH$ . The  $Ti^{3+} + H_2O_2$  system gave a doublet of a doublet (Figure 5a) identified as  $(CH_3)_2CH\dot{C}HOH$ .<sup>3b</sup> In these two spectra, a widespread spectrum could be seen for each system. This second radical must be  $(CH_3)_2\dot{C}CH_2OH$  because nine lines are equally spaced and the central five lines could be reasonably distinguished from the ratio of these intensities (1:8:28:56:70:56:28:8:1).

The *t-butyl alcohol* radical gave an identical spectrum for both systems because each  $CH_3$  group has the same reactivity and is the only group to be oxidized. The spectrum was a triplet (1:2:1) of a septet (1:6:15:20:85:6:1), as shown by Dixon and Norman.<sup>3b</sup>

*t-Amyl alcohol* showed a quintet (1:4:6:4:1) due to  $\dot{C}H_2CH_2C(CH_3)_2OH$ , and each peak further split to a multiplet by the interaction of two methyl groups. Both systems gave the same spectra.

*Ethylene glycol* was oxidized to  $\dot{C}H(OH)CH_2OH$ , which showed a doublet (1:1) of a triplet (1:2:1), but two peaks were superimposed at the center of the spectrum. In Figure 6, a central peak has a broader line width than the others because of overlapping; the  $Ti^{3+} + H_2O_2$  system gave a  $\dot{C}H_2OH$  signal, a quickly decomposed product.<sup>3b</sup>

The *propylene glycol* radical (Figure 7) spectrum consists of a doublet (1:1) of a triplet (1:2:1) from  $\dot{C}H_2CH(OH)CH_2OH$ , and an unidentified small signal is also present. The  $Ti^{3+} + H_2O_2$  system gave an unidentified spectrum.

The *glycerol* radical also gave two kinds of spectra, a doublet (1:1) of a triplet (1:2:1) due to  $\dot{C}H(OH)-CH(OH)CH_2OH$ , and a quintet (1:4:6:4:1) due to  $CH_2(OH)\dot{C}(OH)CH_2OH$  (Figure 8). However, the  $Ti^{3+} + H_2O_2$  system produced an unidentified seven-line spectrum, which is probably due to an uncertain number of decomposed radicals.

The above assignments are summarized in Table I. In general, the action of the  $Ti^{3+} + H_2O_2$  system is characterized as  $\alpha$ -oxidation; in contrast, Fenton's reagent gave  $\omega$ -oxidized products. The hyperfine splitting constants will be discussed later.

Table I: Assignment of Alcohol Radicals

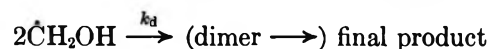
Substrate	Fenton's reagent	Ti <sup>3+</sup> + H <sub>2</sub> O <sub>2</sub> system
<i>n</i> -Alcohols		
CH <sub>3</sub> OH	$\dot{\text{C}}\text{H}_2\text{OH}$	$\dot{\text{C}}\text{H}_2\text{OH}$
CH <sub>3</sub> CH <sub>2</sub> OH	$\dot{\text{C}}\text{H}_2\text{CH}_2\text{OH}$	CH <sub>3</sub> $\dot{\text{C}}\text{HOH}$
CH <sub>2</sub> (Cl)CH <sub>2</sub> OH	...	CH <sub>2</sub> (Cl) $\dot{\text{C}}\text{HOH}$
CH <sub>3</sub> CH <sub>2</sub> CH <sub>2</sub> OH	$\dot{\text{C}}\text{H}_2\text{CH}_2\text{CH}_2\text{OH}$	CH <sub>3</sub> CH <sub>2</sub> $\dot{\text{C}}\text{HOH}$
CH <sub>3</sub> CH <sub>2</sub> CH <sub>2</sub> CH <sub>2</sub> OH	CH <sub>3</sub> $\dot{\text{C}}\text{HCH}_2\text{OH}$ $\dot{\text{C}}\text{H}_2\text{CH}_2\text{CH}_2\text{CH}_2\text{OH}$ and unidentified radical	Unidentified radicals
CH <sub>3</sub> (CH <sub>2</sub> ) <sub>4</sub> OH	Unidentified radicals	Unidentified radicals
<i>i</i> -Alcohols		
(CH <sub>3</sub> ) <sub>2</sub> CHOH	$\dot{\text{C}}\text{H}_2\text{CH}(\text{CH}_3)\text{OH}$	(CH <sub>3</sub> ) <sub>2</sub> $\dot{\text{C}}\text{OH}$
(CH <sub>3</sub> ) <sub>2</sub> CHCH <sub>2</sub> OH	$\dot{\text{C}}\text{H}_2\text{CH}(\text{CH}_3)\text{CH}_2\text{OH}$	(CH <sub>3</sub> ) <sub>2</sub> CH $\dot{\text{C}}\text{HOH}$
(CH <sub>3</sub> ) <sub>2</sub> CHCH <sub>2</sub> CH <sub>2</sub> OH	$\dot{\text{C}}\text{H}_2\text{CH}(\text{CH}_3)\text{CH}_2\text{CH}_2\text{OH}$ and unidentified radical	Unidentified radicals
<i>t</i> -Alcohols		
(CH <sub>3</sub> ) <sub>3</sub> COH	$\dot{\text{C}}\text{H}_2\text{C}(\text{CH}_3)_2\text{OH}$	$\dot{\text{C}}\text{H}_2\text{C}(\text{CH}_3)_2\text{OH}$
C <sub>2</sub> H <sub>5</sub> C(CH <sub>3</sub> ) <sub>2</sub> OH	$\dot{\text{C}}\text{H}_2\text{CH}_2\text{C}(\text{CH}_3)_2\text{OH}$	$\dot{\text{C}}\text{H}_2\text{CH}_2\text{C}(\text{CH}_3)_2\text{OH}$
Diols		
CH <sub>2</sub> (OH)CH <sub>2</sub> OH	$\dot{\text{C}}\text{H}(\text{OH})\text{CH}_2\text{OH}$	$\dot{\text{C}}\text{H}_2\text{OH}$
CH <sub>3</sub> CH(OH)CH <sub>2</sub> OH	$\dot{\text{C}}\text{H}_2\text{CH}(\text{OH})\text{CH}_2\text{OH}$ and unidentified radical	Unidentified radicals
Glycerol		
CH <sub>2</sub> (OH)CH(OH)CH <sub>2</sub> OH	$\dot{\text{C}}\text{H}(\text{OH})\text{CH}(\text{OH})\text{CH}_2\text{OH}$ $\dot{\text{C}}(\text{OH})(\text{CH}_2\text{OH})_2$	Unidentified radicals

*Saturation Behavior of the Methanol Radical.* The microwave power saturation of the methanol radical produced by Fenton's reagent was measured (Figure 9). Above 50 mw. of incident microwave power at the cavity arm, the signal starts to saturate. This phenomena would indicate, in a general sense, that the radical is liberated in the solution and that it would not be bound to the iron ion.

The onset of saturation was shifted to higher power, compared with the *p*-semiquinone radical. However, as mentioned by Sohma,<sup>16</sup> if the radical is short-lived, then the apparent observed  $T_1$  tends to shorten, especially when the measurement is carried out by means of a flow system. Therefore, one should not draw any definite conclusion from this data.

*Decay Kinetics of the Methanol Radical.* Some kinetic experiments were carried out in order to determine the radical formation rate. However, the appearance of the radical was too fast to be observed in any steady state. Only the apparent decay could be measured by several series of continuous-flow experiments, in which the flow rate was varied 13–20 ml./sec., *i.e.*, after mixing 5–30 msec. Although the concentration measurement was not accurate enough even to determine the type of the decay reaction, because of the poor signal-to-noise ratio (the error due to noise corresponds to  $\pm 1.5 \times 10^{-7} M$ , while the radical con-

centration range is  $6.5\text{--}1.2 \times 10^{-6} M$ ), but a second-order decay reaction fitted the decay curve most closely (Figure 10). Supposing the decay mechanism



$2k_d = 1.4 \times 10^7 \text{ mole}^{-1} \text{ sec.}^{-1}$  at 23° for  $5.0 \times 10^{-3} M$  Fe<sup>2+</sup>-EDTA (1:1), 5% methanol, and a wide range of H<sub>2</sub>O<sub>2</sub> concentrations.

## Discussion

*Hyperfine Structure Analysis of the Intermediate Radicals.* The identification of the radicals produced is described in the previous section (Table I). Such hyperfine coupling constants have been extensively studied, not only experimentally in polymers, crystals,<sup>17,18</sup> frozen solutions,<sup>19–20</sup> and the liquid

(16) J. Sohma, *J. Chem. Phys.*, **37**, 2151 (1962).

(17) J. R. Morton, *Chem. Rev.*, **64**, 453 (1964).

(18) D. Kivelson and C. Thomson, *Ann. Rev. Phys. Chem.*, **15**, 197 (1964).

(19) J. F. Gibson, D. J. E. Ingram, M. C. R. Symons, and M. G. Townsend, *Trans. Faraday Soc.*, **53**, 914 (1957).

(20) M. Fujimoto and D. J. E. Ingram, *ibid.*, **54**, 1304 (1958).

(21) D. J. E. Ingram, M. C. R. Symons, and M. G. Townsend, *ibid.*, **54**, 409 (1958).

(22) M. C. R. Symons and M. G. Townsend, *J. Chem. Soc.*, 263 (1959).

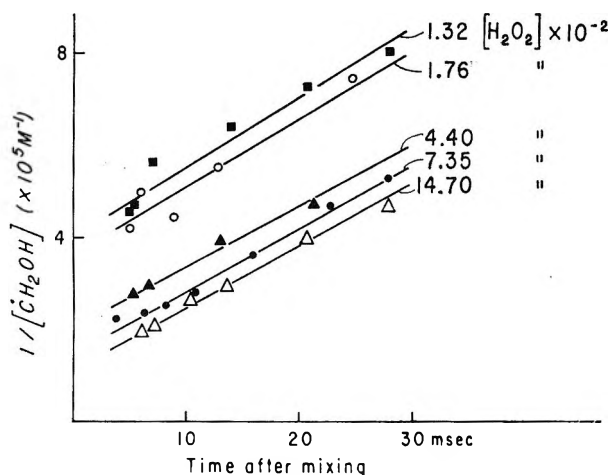


Figure 10. Second-order decay of methanol radical produced by Fenton's reagent ( $5 \times 10^{-3} M \text{Fe}^{2+}$ -EDTA and 5% methanol + various amounts of  $\text{H}_2\text{O}_2$ , in 0.67 M phosphate buffer at pH 7) at  $22^\circ$ . E.p.r. spectra were recorded at microwave power, 25 mw.; modulation, 100 kc., 0.98 gauss; response, 0.3 sec.; magnetic field scanning, 250 gauss/min. Flow rate of the reactants was varied. Time scale was expressed by mean time after mixing the two solutions.

phase,<sup>3,6,27</sup> but also theoretically.<sup>28-36</sup> The general rules can be summarized as follows.

(1)  $C_1$  Proton Coupling. The coupling constant ranges between 20 and 23 gauss. It is fairly constant for all molecules, and for each proton it is independent of temperature but is affected by substituents, for example, OH. This  $\sigma$ - $\pi$  interaction (or spin polarization) is generally expressed as  $a_1 = Q_1\rho_1$ ;  $Q \simeq -22.5$  or 25 gauss.

(2)  $C_2$  Proton Interaction. This coupling is due to the hyperconjugation. The coupling constants are neither uniform for each species nor equivalent for each proton; they are dependent on temperature because they are determined by rotational averaging. Heller and McConnell<sup>33</sup> proposed the equation  $a_2 = B + A \cos^2 \theta$ , where  $\theta$  is an angle between the H-C-C plane and the axis of the p orbital in which the odd electron exists and  $A$  and  $B$  are constants.  $B$  will be very small (less than a few gauss for the alkyl group), and  $A$  for the methyl group is 50 gauss (in the equation,  $a_2 = Q_2(\text{CH}_3)\rho_2$ ,  $Q_2(\text{CH}_3) \simeq 31.5$  gauss was proposed). If the  $C_2$  carbon is asymmetrically substituted, then certain configurations of the carbon skeleton predominate; therefore,  $Q_2$  changes with various substitutions. A series of values of  $a_2$  for  $\text{CH}_3$  was reported<sup>27</sup> for  $\text{CH}_3\text{-}\dot{\text{C}}\text{H}_2$ ,  $(\text{CH}_3)_2\dot{\text{C}}\text{H}$ , and  $(\text{CH}_3)_3\dot{\text{C}}$  as 26.87, 24.68, and 22.72 gauss, respectively.

(3)  $C_3$  Proton Coupling. The reported values of the  $C_3$  proton coupling of the alkyl group range from 0.6 to 1.3 gauss.

The results in this paper, based on the assignment described in the previous section, not only fit very well the above rules, but also give information for OH-substituted alkyl radicals.

$\dot{\text{C}}\text{H}_2\text{OH}$ . The coupling constant (17.2 gauss) is smaller than that of the methyl radical  $\dot{\text{C}}\text{H}_3$ , which was reported previously as 22 gauss ( $23^\circ$ )<sup>3b</sup> or 23.04 gauss ( $-176^\circ$ ).<sup>27</sup> This decrease has been explained as the reduction of the spin density on the carbon owing to the mesomeric effect of oxygen.<sup>3b</sup> This value was unchanged at pH 7 and 5, and in other acidic solutions.

$\dot{\text{C}}\text{H}_2(\text{CH}_2)_n\text{OH}$  (See Table II). The assignment of the ethanol radical presented no difficulties, but that of the  $n$ -alcohol radicals was somewhat uncertain. However, these assignments coincided with these kinds of radicals.<sup>6,27</sup> The values for  $a_1$  are 21-23 gauss. The lower values for  $a_2$ , as compared with alkyl radicals, can be explained by the higher asymmetry of the substituents.

Table II: Hyperfine Coupling Constants of  $\dot{\text{C}}\text{H}_2(\text{CH}_2)_n\text{OH}$  (in gauss)

Substrate	Radical	$a_1$	$a_2$	$a_3$
$\text{CH}_3\text{CH}_2\text{OH}$	$\dot{\text{C}}\text{H}_2\text{CH}_2\text{OH}$	22.2	27.6	
$\text{CH}_3(\text{CH}_2)_2\text{OH}$	$\dot{\text{C}}\text{H}_2(\text{CH}_2)_2\text{OH}$	21.6	26.6	1.8
$\text{CH}_3(\text{CH}_2)_3\text{OH}$	$\dot{\text{C}}\text{H}_2(\text{CH}_2)_3\text{OH}$	20.8	25.8	
$\text{CH}_3\text{CH}_2\text{C}(\text{CH}_3)_2\text{OH}$	$\dot{\text{C}}\text{H}_2\text{CH}_2\text{C}(\text{CH}_3)_2\text{OH}$	22.5	22.5	

$\dot{\text{C}}\text{H}_2\text{CH}(\text{CH}_3)(\text{CH}_2)_n\text{OH}$  (See Table III). The coupling constants of iso alcohols are shown in Table III. The  $a_1$  values remain constant (a small decrease due to methyl substitution can be seen; however, it is still within the range of experimental error).  $a_3$  values are not available.

(23) J. F. Gibson, M. C. R. Symons, and M. G. Townsend, *J. Chem. Soc.*, 269 (1959).

(24) C. F. Luck and W. Gordy, *J. Am. Chem. Soc.*, **78**, 3240 (1956).

(25) H. Zeldes and R. Livingston, *J. Chem. Phys.*, **30**, 40 (1959).

(26) R. S. Alger, T. H. Anderson, and L. A. Webb, *ibid.*, **30**, 695 (1959).

(27) R. W. Fessenden and R. H. Schuler, *ibid.*, **39**, 2147 (1963).

(28) R. Bersohn, *ibid.*, **24**, 1066 (1956).

(29) D. B. Chesnut, *ibid.*, **29**, 43 (1958).

(30) A. D. McLachlan, *Mol. Phys.*, **1**, 233 (1958).

(31) M. C. R. Symons, *J. Chem. Soc.*, 277 (1959).

(32) P. G. Lykos, *J. Chem. Phys.*, **32**, 625 (1960).

(33) C. Heller and H. M. McConnell, *ibid.*, **32**, 1535 (1960).

(34) E. W. Stone and A. H. Maki, *ibid.*, **37**, 1326 (1962).

(35) M. C. R. Symons, *Tetrahedron*, **18**, 333 (1962).

(36) K. Morokuma and K. Fukui, *Bull. Chem. Soc. Japan*, **36**, 534 (1963).

**Table III:** Hyperfine Coupling Constants of  $\dot{\text{C}}\text{H}_2\text{CH}(\text{CH}_3)(\text{CH}_2)_n\text{OH}$  (in gauss)

Substrate	Radical	$a_1$	$a_2$
$(\text{CH}_3)_2\text{CHCH}_2\text{OH}$	$\dot{\text{C}}\text{H}_2\text{CH}(\text{CH}_3)\text{CH}_2\text{OH}$	21.7	27.0
$(\text{CH}_3)_2\text{CH}(\text{CH}_2)_2\text{OH}$	$\dot{\text{C}}\text{H}_2\text{CH}(\text{CH}_3)(\text{CH}_2)_2\text{OH}$	20.4	26.2

$\dot{\text{C}}\text{H}_2\text{C}(\text{CH}_3)_2\text{OH}$  (See Table IV). The values of the *t*-butyl alcohol radical are a little higher than those of Dixon and Norman,<sup>3b</sup> but the differences are still within the range of experimental error. Table IV shows the effect of methyl substitution, which does not affect  $a_1$  but which decreases  $a_2$ .

**Table IV:** Hyperfine Coupling Constants of  $\dot{\text{C}}\text{H}_2\text{C}(\text{R})_2\text{OH}$  (in gauss)

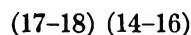
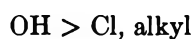
Substrate	Radical	$a_1$	$a_2$	$a_3$
$\text{CH}_3\text{CH}_2\text{OH}$	$\dot{\text{C}}\text{H}_2\text{CH}_2\text{OH}$	22.2	27.6	
$(\text{CH}_3)_2\text{CHOH}$	$\dot{\text{C}}\text{H}_2\text{CH}(\text{CH}_3)\text{OH}$	22.2	25.8	
$(\text{CH}_3)_3\text{COH}$	$\dot{\text{C}}\text{H}_2\text{C}(\text{CH}_3)_2\text{OH}$	21.7		1.37

$\dot{\text{C}}\text{H}_2\text{CH}(\text{OH})\text{R}$  (See Table V). In this case also,  $a_1$  is constant. The values of  $a_2$  vary with  $\text{C}_2$  substitutions in the order:  $\text{H} > \text{CH}_2\text{OH} > \text{CH}_3$ .

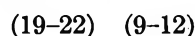
**Table V:** Hyperfine Coupling Constants of  $\dot{\text{C}}\text{H}_2\text{CH}(\text{OH})\text{R}$  (in gauss)

Substrate	Radical	$a_1$	$a_2$
$(\text{CH}_3)_2\text{CHOH}$	$\dot{\text{C}}\text{H}_2\text{CH}(\text{OH})\text{CH}_3$	22.2	22.2
$\text{CH}_3\text{CH}(\text{OH})\text{CH}_2\text{OH}$	$\dot{\text{C}}\text{H}_2\text{CH}(\text{OH})\text{CH}_2\text{OH}$	22.0	24.0
$\text{CH}_3\text{CH}_2\text{OH}$	$\dot{\text{C}}\text{H}_2\text{CH}(\text{OH})\text{H}$	22.2	27.6

$\dot{\text{C}}\text{H}(\text{OH})\text{R}$  (See Table VI).  $\alpha$ -Oxidation products by the  $\text{Ti}^{3+} + \text{H}_2\text{O}_2$  system gave this type of radical which has been studied by Dixon and Norman.<sup>3b,6</sup> Values of  $a_1$  are low and are affected by  $\text{C}_2$  substitution. The changes in  $a_1$  produced by  $\text{C}_2$  substituents are in the order



The changes in  $a_2$  values made by  $\text{C}_2$  substituents are



The latter order is similar to the effect of  $\text{C}_1$  substitution on  $a_1$ , in the case of the  $\dot{\text{C}}\text{H}_2\text{X}$ -type radical.<sup>6</sup>

**Table VI:** Hyperfine Coupling Constants of  $\dot{\text{C}}\text{H}(\text{OH})\text{R}$  (in gauss)

Substrate	Radical	$a_1$	$a_2$
$\text{CH}_2(\text{OH})\text{CH}_2\text{OH}$	$\dot{\text{C}}\text{H}(\text{OH})\text{CH}_2\text{OH}$	17.6	9.4
$\text{CH}_2(\text{OH})\text{CH}(\text{OH})\text{-CH}_2\text{OH}$	$\dot{\text{C}}\text{H}(\text{OH})\text{CH}(\text{OH})\text{-CH}_2\text{OH}$	17.3	10.9
$\text{CH}_3\text{CH}_2\text{OH}$	$\dot{\text{C}}\text{H}(\text{OH})\text{CH}_3^a$	15.0	22.2
$\text{C}_3\text{H}_7\text{OH}$	$\dot{\text{C}}\text{H}(\text{OH})\text{CH}_2\text{CH}_3^a$	14.7	21.1
$\text{C}_4\text{H}_9\text{OH}$	$\dot{\text{C}}\text{H}(\text{OH})(\text{CH}_2)_2\text{CH}_3^a$	14.9	19.5
$(\text{CH}_3)_2\text{CHCH}_2\text{OH}$	$\dot{\text{C}}\text{H}(\text{OH})\text{CH}(\text{CH}_3)_2^a$	14.0 <sup>b</sup>	21.4
$\text{CH}_2(\text{Cl})\text{CH}_2\text{OH}$	$\dot{\text{C}}\text{H}(\text{OH})\text{CH}_2\text{Cl}^a$	15.0	11.1

<sup>a</sup> Oxidized by  $\text{Ti}^{3+} + \text{H}_2\text{O}_2$  system in acidic solution. <sup>b</sup> The reported value<sup>3b</sup> is too small, compared with our value.

$\dot{\text{C}}(\text{OH})\text{R}_2$  (See Table VII). The available data are insufficient to warrant summarization. However, the effect of OH substitution on the  $\text{C}_2$  carbon is remarkable. The series of  $-\text{COOH}$  substitutions shows the same tendency<sup>8</sup> as the OH substitutions.

**Table VII:** Hyperfine Coupling Constants of  $\dot{\text{C}}(\text{OH})\text{R}_2$  (in gauss)

Substrate	Radical	$a_2$
$(\text{CH}_3)_2\text{CHOH}$	$\dot{\text{C}}(\text{OH})(\text{CH}_3)_2^a$	19.5
$\text{CH}_2(\text{OH})\text{CH}(\text{OH})\text{CH}_2\text{OH}$	$\dot{\text{C}}(\text{OH})(\text{CH}_2\text{OH})_2$	10.1

<sup>a</sup> Produced by  $\text{Ti}^{3+} + \text{H}_2\text{O}_2$  system in acidic solution.

As shown above, the hyperfine structural analysis of the radicals produced by Fenton's reagent is very consistent. This fact not only confirms the radical product analysis ( $\omega$ -oxidation) but also gives some general rules concerning coupling constants of OH-substituted, saturated, hydrocarbon free radicals.

*Reaction Mechanism of Fenton's Reagent.* Both  $\dot{\text{O}}\text{H}$  and  $\text{HO}_2$  have been proposed as the active species of Fenton's reagent. E.p.r. is one possible method for detecting this kind of active short-lived free radical. Saito and Bielski found an e.p.r. signal ( $g = 2.016$ ,  $\Delta H = 27$  gauss) with the  $\text{Ce}^{4+} + \text{H}_2\text{O}_2$  system.<sup>4,5</sup> This signal was thought to be due to the  $\text{HO}_2$  radical because (1) the  $g$  value and line width were similar to those of organic perhydroxy radicals and (2) the second-order decay rate of the radical was the same as that of the oxygen radical produced by an electron beam.<sup>37</sup> However, Piette, *et al.*,<sup>8</sup> recently repeated the experiments and suggested that the radical is complexed to

(37) G. Czapski and B. H. J. Bielski, *J. Phys. Chem.*, **67**, 2180 (1963).

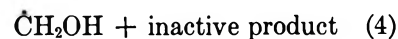
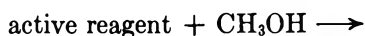
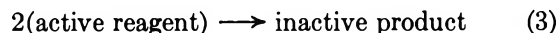
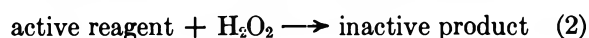
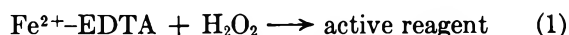
Ce<sup>4+</sup> since the shape and the  $g$  value of the e.p.r. signal were dependent on the particular ceric salts used. Dixon and Norman,<sup>3b</sup> on the other hand, observed an e.p.r. signal ( $g = 2.01$ ,  $\Delta H = 1$  gauss) produced by the  $Ti^{3+} + H_2O_2$  system, which was interpreted as an OH radical since, on the addition of substrate, the signal was replaced by substrate radicals. However, Piette, *et al.*,<sup>8</sup> detected two radicals in the same system. The one could be replaced by substrate radical, but the other could not. The former radical corresponded kinetically to OH, and the latter to HO<sub>2</sub>. However, they could not draw any definite conclusions as to whether or not OH and OH<sub>2</sub> are complexed.

With Fenton's reagent, such an intermediate radical was not observed using the present technique, but Norman, *et al.*,<sup>7,9</sup> claimed that they could produce an aromatic hydrocarbon radical with this reagent and that the intermediate aromatic free radicals were identical with those produced in the  $Ti^{3+} + H_2O_2$  system. These facts led them to conclude that the OH radical is the active species of Fenton's reagent. However, as is shown in this paper, when alcohols are used as substrates in these systems, the radicals produced by the two systems are dissimilar. Concerning alcohol radicals, Ingram's group showed<sup>19-23</sup> in their  $H_2O_2$  photolysis experiments that the OH radical formed from  $H_2O_2$  generally abstracts an  $\alpha$ -hydrogen from alcohols. If  $\alpha$ -oxidation of alcohols is a property of the OH radical, then the active species generated from  $Ti^{3+} + H_2O_2$  may be an OH radical, or at least it has a reactive character similar to the products of photolyzed  $H_2O_2$ . It is thus concluded that the active reagent of Fenton's system cannot be an OH radical but may be a kind of complex, such as Fe-EDTA- $H_2O_2$ . If the active agent of Fenton's reagent is a complex,  $\omega$ -oxidation may be explained by the different nature of the active reagent. It may also be explained by alcohols complexed to the iron ion, so that the hydrogens attached to the  $\alpha$ -carbon are protected from the attacking agent. However, the latter effect cannot be a critical factor since methanol was oxidized. On the other hand, two other possibilities must be considered, in which the same active agent (*i.e.*, OH-like reagent) might produce different radicals in the two systems: (1) the most reactive site of alcohols may change with pH, in which case the expected products would be different since the  $Ti^{3+} + H_2O_2$  system was studied at low pH, and (2) the initial oxidized product of the alcohol may be the same in the two systems, but it could decompose very quickly so that only secondary products could be observed. The first possibility can be excluded because, as we have seen, the  $Ti^{3+}$ -EDTA +  $H_2O_2$  system still attacks mainly

the  $\alpha$ -position of alcohol at pH 7. This fact also rules out the possibility that there is a drastic pH-dependent change in spin density of the radicals formed at least below pH 7 because no change in e.p.r. spectrum was seen. The second consideration is still valid since one cannot see any initial products with a low steady-state concentration and/or a high decay rate. However, if this were the case for Fenton's reagent, one should observe a quite high yield of secondary products, in addition to the  $\alpha$ -oxidized products in the  $Ti^{3+} + H_2O_2$  system. Thus, this mechanism is not very likely.

In the kinetic experiments, only the apparent decay of the radical could be observed by the present technique. In general, alkyl radicals disappear by bimolecular reaction.<sup>27,35,36</sup> The decay of  $\dot{C}H_2OH$ , produced by Fenton's reagent at pH 7.0, also apparently follows second-order kinetics, but the rate constant is much smaller than that of the alkyl radical<sup>27</sup> or of the ethanol radical.<sup>38,39</sup> There are two reasons for believing that this radical is not bound to Fe: (1) hyperfine splitting constants were not modified (a change of the constants was observed for *o*-semi-quinone-metal complex<sup>40</sup>), and (2) saturation behavior indicates that it is an ordinary free radical (observed apparent  $T_1$  might be even shorter than true  $T_1$ <sup>16</sup>). If the observed decay is due to the second-order decomposition of the methanol radical, this rather small value of the rate constants remains unexplained.

Therefore, some alternative explanations must be considered, for example



If reactions 1, 4, and 5 are much faster than the others, then the observed  $\dot{C}H_2OH$  concentration would be proportional to the concentration of the active reagent. Therefore, the observed decay rate represents the inactivation reaction of the active reagent. If this is the case, the apparent decay rate should be the same for various substrates. However, the apparent decay of the isopropyl alcohol radical, as well as that of

(38) I. A. Taub and L. M. Dorfman, *J. Am. Chem. Soc.*, **84**, 4053 (1962).

(39) L. M. Dorfman and I. A. Taub, *ibid.*, **85**, 2370 (1963).

(40) D. R. Eaton, *Inorg. Chem.*, **3**, 1268 (1964).



benzoic acid radical, was not the same as that of methanol radical, so all of the above reactions (1 to 5) must contribute to the apparent decay. In these experiments, the poor signal-to-noise ratio gives rise to an ambiguity in the decay pattern; therefore, no definite mechanism could be proposed using the present technique.

*Acknowledgment.* The author is grateful to Professor H. S. Mason for his encouragement and worthwhile discussions. Mr. Gunther Weiss' kindness in making the mixing cell and other apparatus is also appreciated. This study was supported by grants from the American Cancer Society and the United States Public Health Service.

## The Diffusion Coefficient of Atomic Mercury in Isooctane

by Maurice M. Kreevoy<sup>1a</sup> and Herbert B. Scher<sup>1b</sup>

*School of Chemistry, University of Minnesota, Minneapolis, Minnesota (Received May 14, 1965)*

The diffusion coefficient for atomic mercury in isooctane solution,  $1.6 \times 10^{-5}$  cm.<sup>2</sup> sec.<sup>-1</sup>, has been determined at 20° with an uncertainty of about 10% by experiments in which the mercury is removed from solution by a gold-plated rotating brass disk. When combined with other available information, this value strengthens the conclusion that the surface reaction of iodine with metallic mercury is impeded by nontransport (*i.e.*, chemical) factors.

In a previous paper,<sup>2</sup> it was suggested that the rate of reaction of molecular iodine in isooctane solution with metallic mercury is principally controlled by the rate of a chemical reaction, rather than by the rate of the transport process. A key factor in this conclusion was the observation that the rate constant for reprecipitation of dissolved atomic mercury was larger by a factor of about 3 than that for reaction of iodine. The validity of this argument rests on the assumption that the diffusion coefficient of iodine,  $D_{I_2}$ , in this solvent, is not much smaller than that of atomic mercury,  $D_{Hg^0}$ . The latter has now been measured and the former reliably estimated from closely related data. In fact,  $D_{I_2}/D_{Hg^0}$  would seem to be about 1.8, lending strong support to the original argument.

Levich<sup>3,4</sup> has solved the dynamic diffusion equation for the case of a circular disk rotating about a perpendicular axis under conditions of nonturbulent flow. The results is shown in eq. 1, where  $k$  is the apparent

$$k = \frac{D^{2/3} w^{1/2}}{1.612 \nu^{1/6}} \quad (1)$$

(transport-controlled) rate constant,  $D$  is the diffusion coefficient,  $w$  is the angular velocity of the disk (in rotations per unit time), and  $\nu$  is the kinematic viscosity of the solvent. If some substrate can be removed, irreversibly, at such a disk, at a rate substantially larger than the diffusion rate, then its diffusion coefficient can be evaluated if the rate constant for its disappearance from solution is measured.<sup>5</sup>

It has been known for some time that mercury is appreciably soluble in isooctane and that it exists as the free atoms in solution.<sup>6</sup> The present paper shows

(1) (a) Alfred P. Sloan Foundation Fellow, 1960-1964; (b) Esso Research and Engineering Fellow, 1963-1964.

(2) P. Warrick, Jr., E. M. Wewerka, and M. M. Kreevoy, *J. Am. Chem. Soc.*, **85**, 1909 (1963).

(3) V. G. Levich, *Acta Physicochim. URSS*, **17**, 257 (1942).

(4) V. G. Levich, *Russ. J. Phys. Chem.*, **18**, 335 (1944).

(5) A. C. Riddiford in "Advances in Electrochemistry and Electrochemical Engineering," Vol. 41, P. Delahay and C. W. Tobias, Ed., Interscience Publishers, Inc., New York, N. Y., forthcoming.

(6) H. H. Reichardt and K. F. Bonhoeffer, *Z. Elektrochem.*, **36**, 753 (1930).



that it reacts with gold-plated brass with the required speed and irreversibility.

### Experimental Section

A brass cylinder  $\sim 1.5$  cm. in diameter was machined so that the part projecting into the solution was trumpet-shaped and the upper part could be attached to a shaft. The entire surface of the piece, with the exception of the bottom, was coated with a thin layer of Kel-F polymer by dipping it into an appropriate dispersion (3M commercial product), wiping the bottom clean, air drying, and then baking in a vacuum oven for 2 hr. at  $240^\circ$ . The bottom surface was then electroplated with about  $3 \times 10^{-3}$  cm. of gold.<sup>7</sup> After electroplating, the gold surface was washed with distilled water, dried, and finally rinsed with isooctane.

To perform an experiment, the gold-plated brass piece was immersed up to an appropriate level in 150 ml. of isooctane, previously saturated with atomic mercury. The solution was contained in a 250-ml. round-bottom flask. The disk was coupled to a synchronous motor through a gear train and a rod and rotated at a known speed. Periodically, 15-ml. samples were withdrawn and analyzed spectrophotometrically for mercury (in a cell with a 5-cm. path length). After the analysis (requiring about 3 min.) the sample was returned to the reaction flask. During the period when the sample was out of the reaction flask, the motor and the timer (which were on the same circuit) were stopped. It was shown experimentally that almost no change in  $\text{Hg}^0$  concentration takes place, even over long time periods, when the motor is stopped.

After each experiment, the diameter of the gold-plated disk was measured with a micrometer caliper, and the mercury-contaminated gold plate was sanded off on a lathe. The brass was then polished and replated. (It was remeasured each time because its diameter changed with sanding and polishing.)

To verify the applicability of the Levich equation to the present mechanical and geometric situation, the apparatus was also used to measure the diffusion constant of triiodide ion. These experiments were carried out in exactly the same way except that the brass disk was not gold plated and an aqueous solution, 4.0 *M* in potassium iodide, 0.04 *M* in triiodide, and 0.005 *M* in sulfuric acid, was used in the place of the mercury in isooctane. A nitrogen atmosphere was maintained over the solution during the experiment by continuous purging. Samples (1-ml.) were withdrawn periodically and titrated for iodine with thiosulfate. These conditions are chemically identical with those used by Bircumshaw and Riddiford to verify the Levich equation.<sup>8</sup>

### Results

Good first-order kinetics were observed for the disappearance of triiodide ion, as previously reported by Bircumshaw and Riddiford. A rate law taking into account the minor diminution in volume during the course of the experiment was used.<sup>9</sup> At 2.00 rev. sec.<sup>-1</sup> it gave a rate constant of  $2.52 \times 10^{-3}$  cm. sec.<sup>-1</sup>. The uncertainty in this value, deduced from the deviation of points from the rate law, is  $\sim \pm 1\%$ , but other experience with rate constants measured in this way suggests that their usual reproducibility, in fact, is in the neighborhood of  $\pm 5$ – $10\%$ . The rate constant calculated from the Levich equation is  $2.77 \times 10^{-3}$  cm. sec.<sup>-1</sup>, taking  $1.27 \times 10^{-5}$  cm.<sup>2</sup> sec.<sup>-1</sup> as *D*,<sup>10</sup> and 0.581 centistokes as  $\nu$ .<sup>11</sup> The agreement with experiment is moderately satisfactory. If the diffusion coefficient had been calculated from the observed rate constant, it would have been 15% lower than the reported value.<sup>10</sup>

When the gold-plated disk was rotated in a saturated solution of mercury in isooctane (such a solution is  $4 \times 10^{-6}$  *M* in atomic mercury initially<sup>2</sup>), 70–90% of the mercury is removed over a period of time. If the disk is reused without cleaning, more mercury is removed, although not as much as that removed initially, and with repeated reuse the disk finally will take up no more mercury. The reaction is not reversible, for neither partially nor completely "saturated" disks will release mercury to fresh isooctane.

In each experiment with a freshly prepared disk, the disappearance of mercury followed a first-order rate law<sup>12</sup> for at least one half-life, and sometimes two. Figure 1 shows a typical plot of  $\log A$  (the absorbance at 257  $m\mu$ ) as a function of time. Such plots were used to evaluate *k* by means of eq. 2.

$$k = \frac{2.303}{t - t_0} \log \frac{A_0}{A_t} \quad (2)$$

Eight rate constants were obtained in this way, all at  $20.0^\circ$ , with stirring rates varying from 30 to 180 r.p.m. A plot of  $\log k$  against  $\log w$  is acceptably linear with a "best" slope of  $0.44 \pm 0.06$ ,<sup>13</sup> as determined by

(7) L. Weisberg and A. K. Graham, "Modern Electroplating," A. G. Gary, Ed., John Wiley and Sons, Inc., New York, N. Y., 1953, Chapter 9.

(8) L. L. Bircumshaw and A. C. Riddiford, *J. Chem. Soc.*, 698 (1952).

(9) R. S. Bradley, *Trans. Faraday Soc.*, **34**, 278 (1938).

(10) G. Edgar and S. H. Diggs, *J. Am. Chem. Soc.*, **38**, 253 (1916).

(11) L. L. Bircumshaw and A. A. Riddiford, *J. Chem. Soc.*, 1490 (1951).

(12) A. A. Frost and R. G. Pearson, "Kinetics and Mechanism," John Wiley and Sons, Inc., New York, N. Y., 1961, Chapter 3.

(13) The uncertainty is the 50% confidence limit.

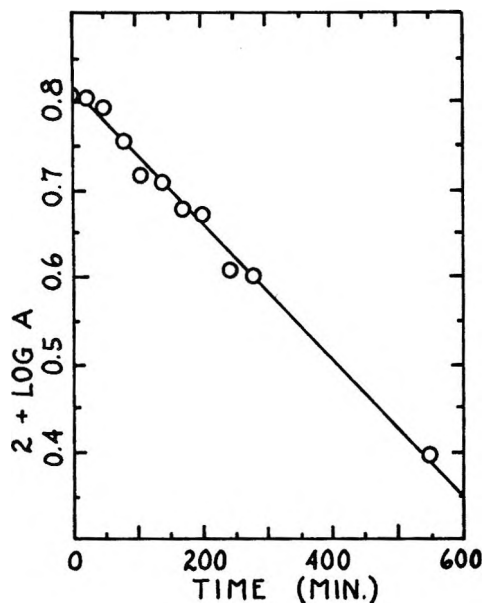


Figure 1. The log of the optical density at 257  $m\mu$ ,  $A$ , as a function of time in a typical rotated disk experiment.

the method of least squares. The average deviation of points from this line is the equivalent of about an 11% error in  $k$ , which is not inconsistent with the estimated experimental imprecision. This average deviation does not grow appreciably worse if the slope is arbitrarily given the theoretical<sup>3,4</sup> value of 0.5, and in that case  $D$  at 20° is  $1.62 \times 10^{-5}$  cm.<sup>2</sup> sec.<sup>-1</sup>. This value would seem to be uncertain by  $\sim 10\%$ , as judged either by the agreement in the triiodide case or by the deviation of points in the logarithmic plot of  $k$  vs.  $w$ .

### Discussion

It is well known that mercury vapor (atomic) readily amalgamates gold. It is not surprising that atomic mercury in solution should do the same. The obedience to the  $w^{1/2}$  law indicates that it does. If the mercury were not absorbed on every encounter,  $k$  would tend to become independent of  $w$  at higher  $w$ , and no such trend is observed.

The diffusion coefficient obtained for atomic mercury may be compared with that of carbon tetrachloride in isooctane at 25°,  $2.57 \times 10^{-5}$  cm.<sup>2</sup> sec.<sup>-1</sup>.<sup>14</sup> Presumably this would be a little lower at 20°, but still

larger than  $D_{\text{Hg}^0}$ . It is somewhat unexpected that  $\text{Hg}^0$  should have a smaller diffusion coefficient than  $\text{CCl}_4$ , as they are about the same size. The vapor phase radius of atomic mercury is 3 Å,<sup>15</sup> about the same as the hard-sphere radius for carbon tetrachloride estimated from its molecular volume. The difference may not be as large as it seems, since  $D_{\text{I}_2}$ —obtained in this apparatus was also somewhat low, but a value of  $D_{\text{Hg}^0}$  in excess of that for  $\text{CCl}_4$  seems very definitely excluded. For both  $\text{Hg}^0$  and  $\text{CCl}_4$  the Stokes-Einstein  $D$  is  $1.1 \times 10^{-5}$  cm.<sup>2</sup> sec.<sup>-1</sup> at 20° if one makes the usual assumption that the first layer of solvent “sticks” to the substrate and  $1.7 \times 10^{-5}$  cm.<sup>2</sup> sec.<sup>-1</sup> if it does not.<sup>16</sup>

The diffusion coefficient of iodine does not seem to be known in isooctane, but in a number of hydrocarbon solvents at temperatures around 20° it displays a Walden product around  $5 \times 10^{-10}$ .<sup>14,17</sup> Combining this with the viscosity of isooctane at 20° ( $0.502 \times 10^{-2}$  poise<sup>18</sup>) a value of  $2.9 \times 10^{-5}$  cm.<sup>2</sup> sec.<sup>-1</sup> is obtained. Thus the ratio  $D_{\text{I}_2}/D_{\text{Hg}^0}$  would seem to be about 1.8. It may be a little smaller than this but seems, surely, greater than 1.0, and approximately temperature independent.

If the  $D_{\text{I}_2}$  is equal to or larger than  $D_{\text{Hg}^0}$  it can be quite unambiguously concluded that a transport controlled reaction of  $\text{I}_2$  would have to be at least as fast as any reaction of  $\text{Hg}^0$  in the same mechanical system.<sup>19</sup> Since the rate of the heterogeneous conversion of  $\text{I}_2$  in isooctane solution is slower than the rate of  $\text{Hg}^0$  reprecipitation, the former reaction must be significantly impeded by nontransport (*i.e.*, “chemical”) factors.

(14) S. B. Tuwiler, “Diffusion and Membrane Technology,” Reinhold Publishing Corp., New York, N. Y., 1962, p. 372. The value actually given by Tuwiler is smaller than this by a power of ten but comparison of Tuwiler’s values with others’ reveals a typographical error.

(15) J. Jeans, “An Introduction to the Kinetic Theory of Gases,” Cambridge at the University Press, 1948, p. 183.

(16) (a) See ref. 15, p. 56; (b) H. Eyring, D. Henderson, B. J. Stover, and E. M. Eyring, “Statistical Mechanics and Dynamics,” John Wiley and Sons, Inc., New York, N. Y., 1964, p. 463.

(17) P. Chang and C. R. Wilke, *J. Phys. Chem.*, **59**, 592 (1955).

(18) R. R. Driesback, “Physical Properties of Chemical Compounds. II,” American Chemical Society, Washington, D. C., 1959, p. 47.

(19) L. L. Bircumshaw and A. C. Riddiford, *Quart. Rev. (London)*, **6**, 157 (1952).

## Interfacial Tension of Indium Amalgams in 0.1 M Perchloric Acid at 25°

by James N. Butler

*Tyco Laboratories, Inc., Waltham, Massachusetts 02154 (Received May 17, 1965)*

Absolute measurements were made of the interfacial tension of indium amalgams containing up to 64 mole % indium, in 0.1 M HClO<sub>4</sub> at 25°. The interfacial tension was obtained by fitting experimental measurements of the shape of a sessile drop to the theoretical curve calculated by an iterative computer program. The interfacial tension values were combined with previously measured values of zero-charge potential and differential capacity, to generate a family of electrocapillary curves from which the surface excess was calculated using the Gibbs equation. The surface excess is negative and passes through a maximum negative value at approximately 20 mole % indium. The parameters of the hydrogen evolution reaction on indium amalgams correlate with the bulk electronic properties of the amalgams but not with the surface composition.

### Introduction

One of the factors which may influence the rate of an electrocatalytic reaction at an alloy electrode is the chemical composition of the surface. Because of the different surface energies of the components of an alloy, the surface composition will, in general, be different from the bulk composition and will change in a way which minimizes the total surface energy. It is difficult to determine the surface composition of a solid electrode, but, for a liquid electrode, the measurement of interfacial tension as a function of bulk composition can give important information about the surface composition.

The interfacial tension is related to the surface composition by the Gibbs adsorption isotherm<sup>1,2</sup>

$$\Gamma_i = -\frac{\partial\gamma}{\partial\mu_i} \quad (1)$$

where  $\gamma$  is the interfacial tension,  $\mu_i$  is the chemical potential of a component in one phase, and  $\Gamma_i$  is the surface excess of that component with respect to a standard component (usually Hg in amalgams and H<sub>2</sub>O in aqueous electrolytes). The surface excess is not a true surface concentration but is the total difference in composition of the surface region from that of the bulk. The region of integration extends from the physical surface to where the composition equals that of the bulk. Although thermodynamic measurements cannot give the true surface composition, they can, with additional

assumptions, give a quantity which approximates the surface composition.

We have published calculations<sup>3</sup> of surface excess based on measurements of interfacial tension of thallium amalgams in aqueous solutions. These calculations showed that, at potentials where hydrogen evolution occurs (-0.8 to -1.2 v. vs. a reversible H<sub>2</sub> electrode), the surface is deficient in thallium by an amount which corresponds to approximately one monolayer. Of course, the profile of concentration vs. distance from the surface is not a step function, and so the true surface concentration of thallium is some fraction (probably one-half to three-fourths) of the bulk composition.

The most important method of obtaining absolute values for the interfacial tension between two liquid phases is to measure the shape of a drop. This method was first developed in 1883 by Bashforth and Adams,<sup>4</sup> who derived the theoretical form of a sessile or hanging drop and calculated tables of drop contours. These tables can, in principle, be used to determine surface tension by fitting the experimentally measured drop

(1) R. Parsons, "Modern Aspects of Electrochemistry, No. 1," J. O'M. Bockris, Ed., Butterworth and Co. Ltd., London, 1954, p. 103.

(2) R. Parsons and M. A. V. Devanathan, *Trans. Faraday Soc.*, **49**, 404 (1953).

(3) J. N. Butler, *J. Electroanal. Chem.*, **9**, 149 (1965).

(4) F. Bashforth and J. C. Adams, "An Attempt to Test the Theories of Capillary Action," Cambridge University Press, London, 1883.

contour to the theoretical curve, but such calculations are tedious. Consequently, most workers<sup>6,6</sup> have used a simplified method in which only the horizontal diameter of the drop and the distance from the equator of the drop to its apex are measured. This method suffers from difficulties in locating the equator accurately.

Recently Smolders and Duyvis<sup>7</sup> described a method for graphical interpolation of the Bashforth and Adams tables which enabled them to calculate the interfacial tension of mercury in aqueous solutions to within 0.1% by fitting points over the entire drop contour. However, their method of calculation is time consuming. It involves drawing an accurately scaled enlargement of the drop contour, comparing this with a number of theoretical curves, and interpolating to get the correct values for the drop shape parameters, from which surface tension can be calculated.

In our studies of the interfacial tension of amalgams in electrolyte solutions, we have used the sessile drop method, rather than other available methods, for two reasons. First, it gives an absolute measurement of surface tension which does not depend on calibrating the apparatus with a substance of known surface tension.

Second, unlike virtually all other methods, it does not require that the contact angle between the amalgam and the glass vessel be known. This last point is most important, for, if the contact angle is even slightly different from 180° and varies systematically with amalgam concentration, measurements made using a capillary electrometer or by the drop weight method might give misleading results. The results of Smolders and Duyvis have shown that the sessile drop method can be as precise as other methods. It is certainly the most accurate.

To make the calculations simple enough so that measurement of the shape of a sessile drop could be done routinely, we have prepared a computer program<sup>8</sup> which fits the experimentally measured drop contour to a theoretical drop contour and which, from the parameters associated with this theoretical curve, calculates the interfacial tension.

Although interfacial tension can be measured directly as a function of potential and composition, more precise results can be obtained by integrating measurements of double-layer capacity. If the composition of both the amalgam and the aqueous phase are held constant, the differential capacity is the second derivative of the interfacial tension with respect to potential<sup>1</sup>

$$C = 0.1 \frac{\partial^2 \gamma}{\partial \phi^2} \quad (2)$$

where  $C$  is the differential capacity in  $\mu\text{f./cm.}^2$ ,  $\gamma$  is the

interfacial tension in  $\text{erg/cm.}^2$ , and  $\phi$  is the potential with respect to a reference electrode.

We have published<sup>9</sup> measurements of zero-charge potential and double-layer capacity for indium amalgams in 0.1  $M$   $\text{HClO}_4$  solutions at 25°. With the additional experimental values of interfacial tension at the zero-charge potential, measured in the present work, we can obtain by integration the complete field of data required to calculate surface excess as a function of potential and electrode composition.

### Experimental Section

The shape of a sessile drop of amalgam was measured in a cell fitted with parallel, optically flat windows. A circular glass platform, 2.2 cm. in diameter, was supported on the top of a 2-mm. i.d. capillary through which the amalgam was admitted from an external reservoir. Contact was made to the drop through the column of amalgam in the capillary. To assure a cylindrically symmetric drop, the platform was ground with a concave surface, the radius of curvature being approximately 100 cm.

The potential of the drop was measured with respect to a reversible hydrogen (platinized platinum) electrode in a separate compartment of the cell. The electrolyte in all measurements was 0.100  $M$   $\text{HClO}_4$ , and the solution was saturated with hydrogen.

The electrolyte was prepared from reagent grade perchloric acid (J. T. Baker) and triple-distilled water. Further purification was accomplished by pre-electrolysis overnight prior to measurements. The amalgams were prepared by dissolving 99.999% indium (American Smelting and Refining Co.) in triple-distilled mercury (Doe and Ingalls) under an atmosphere of argon, to prevent surface oxidation. Organic impurities were rigorously excluded: the cell was constructed entirely of glass and Teflon and was cleaned with chromic-sulfuric acid and washed in triple-distilled water before use. Measurements made at 1 min. after drop formation agreed within experimental error with the more accurate measurements made approximately 15 min. after drop formation.

The shape of the drop was measured using a Gaertner  $x$ - $y$  traveling microscope, which was accurate to  $\pm 0.00005$  in. and could be read to  $\pm 0.00002$  in. A

(5) E. B. Dismukes, *J. Phys. Chem.*, **63**, 312 (1959).

(6) C. Kemball, *Trans. Faraday Soc.*, **42**, 526 (1946).

(7) C. A. Smolders and E. M. Duyvis, *Rec. trav. chim.*, **80**, 635 (1961).

(8) J. N. Butler and B. H. Bloom, *Surface Sci.*, in press.

(9) J. N. Butler, M. L. Meehan, and A. C. Makrides, *J. Electroanal. Chem.*, **9**, 237 (1965).

complete set of measurements consisted of approximately 20 readings of vertical coordinates, together with the 40 corresponding left and right horizontal coordinates. As a test for cylindrical symmetry of the drop, the sums of the left and right horizontal coordinates were examined for any systematic trend. If such a trend was discovered, the data were discarded. A complete set of measurements could be made in approximately 15 min. The drop was illuminated from behind with parallel light in the manner described by Smolders and Duyvis.<sup>7</sup> Instantaneous photographic measurements were made on the drop contour, but these proved to be less accurate than the direct measurements using the traveling microscope because of uncertainties in the magnification ratio and difficulties in maintaining the focal plane of the camera precisely vertical.

The density of the indium amalgams, required for the sessile drop calculations, was measured using a pycnometer calibrated with mercury. The values obtained agreed with those in the literature.<sup>10</sup>

### Calculations

The equilibrium shape of a cylindrically symmetric sessile drop (Figure 1) is governed by the equation<sup>4</sup>

$$\frac{b}{R} = \left(\frac{b}{x}\right) \sin \phi = 2 + \beta \left(\frac{z}{b}\right) \quad (3)$$

where

$$\beta = \frac{gb^2}{\gamma}(d_1 - d_2) \quad (4)$$

In these equations,  $R$  is the radius of curvature in the vertical plane at the point  $(x,z)$ ,  $b$  is the radius of curvature at the origin,  $\phi$  is the angle made by the radius of curvature with the  $z$  axis,  $g$  is the acceleration of gravity,  $d_1$  and  $d_2$  are the densities of the denser and lighter fluid, respectively, on each side of the interface, and  $\gamma$  is the interfacial tension.

This form of the equation is especially useful because the linear dimensions  $R$ ,  $x$ , and  $z$  appear as ratios to the maximum radius of curvature  $b$ . Thus, a given value for the constant  $\beta$  gives the same drop shape, regardless of drop size, and changing  $b$  influences only the size of the drop without altering its shape. Of course, changing the size of the drop while holding the surface tension and density constant causes both  $\beta$  and  $b$  to change simultaneously.

Both  $R$  and  $\phi$  can be expressed in terms of derivatives of  $z$  with respect to  $x$ , and eq. 3 can be transformed into the nonlinear differential equation

$$b \frac{d^2z}{dx^2} + \frac{b}{x} \left\{ 1 + \left(\frac{dz}{dx}\right)^2 \right\} \frac{dz}{dx} = \left( 2 + \frac{\beta z}{b} \right) \left\{ 1 + \left(\frac{dz}{dx}\right)^2 \right\}^{3/2} \quad (5)$$

This equation cannot be solved in terms of any conventional functions. Some solutions of this equation have been tabulated by Bashforth and Adams<sup>4</sup> and have been approximated in terms of analytic functions by Staicopolus.<sup>11</sup> Approximations which apply for very large values of  $\beta$  are sometimes used.<sup>12</sup>

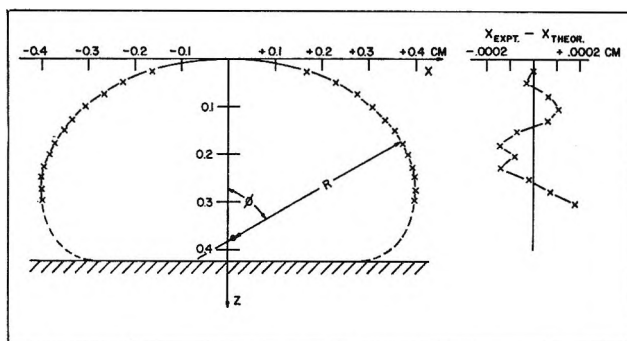


Figure 1. The shape of a typical sessile drop. The shaded area indicates the surface on which the drop rests. The curve was calculated from the equations in the text assuming  $\beta = 5.397$  and  $b = 0.5766$  cm. The crosses indicate the experimental measurements obtained for a 63.0% indium amalgam.

For our purposes, however, we want to fit a number of experimental measurements of  $x,z$  pairs to the theoretical drop contour and to obtain the best values of  $b$  and  $\beta$  consistent with these experimental values. Neither the tables of Bashforth and Adams nor the empirical approximations derived by Staicopolus are sufficiently accurate to assure that the best possible fit of the parameters is obtained.

We have, therefore, devised a method which generates the function  $z(x, b, \beta)$  defined by eq. 5 by an iterative solution of the differential equation. The parameters  $b$  and  $\beta$  are then adjusted so that the best fit is obtained for the experimental data. The interfacial tension is then calculated using eq. 4. The details of this method have been published elsewhere.<sup>8</sup>

If the composition of the amalgam and the electrolyte are held constant, the first derivative of interfacial

(10) D. A. Olsen and D. C. Johnson, *J. Phys. Chem.*, **67**, 2529 (1963).

(11) D. N. Staicopolus, *J. Colloid Sci.*, **17**, 439 (1962); **18**, 793 (1963).

(12) A. M. Worthington, *Phil. Mag.*, **20**, 51 (1885); A. W. Porter, *ibid.*, **15**, 163 (1933); **25**, 752 (1938).

tension with respect to potential gives the surface charge, and the second derivative gives the differential capacity (eq. 2). Thus, knowing two integration constants, curves of capacity as a function of potential, obtained using an a.c. bridge method,<sup>13</sup> can give the complete curve of interfacial tension *vs.* potential. We have used our previously published<sup>9</sup> values for differential capacity and zero-charge potential<sup>9,14</sup> of indium amalgams in 0.1 *M* HClO<sub>4</sub> together with the values of interfacial tension at the zero-charge potential measured in the present work.

The surface charge on the electrode is given by<sup>1</sup>

$$q = \int_{\phi_z}^{\phi} C d\phi \quad (6)$$

where *C* is the differential capacity in  $\mu\text{f./cm.}^2$ ,  $\phi$  is the potential with respect to a reference electrode, and  $\phi_z$  is the zero-charge potential with respect to the same electrode. A second integration gives the interfacial tension

$$\gamma = \gamma_z - 10 \int_{\phi_z}^{\phi} q d\phi \quad (7)$$

where  $\gamma_z$  is the interfacial tension at the zero-charge potential, or electrocapillary maximum. The factor 10 arises because the conventional units for the integral are  $\mu\text{coulomb-volts per square centimeter}$ , whereas the conventional units for interfacial tension are  $\text{ergs per square centimeter}$ .

The integration was performed numerically using a simple program for the IBM 7090 computer. Measurements of capacity<sup>9</sup> were made at closely spaced intervals (0.01 to 0.05 v.). Since the values sometimes scattered slightly about a smooth curve, a simple trapezoidal rule was used for the integration instead of a more sophisticated numerical integration algorithm.

## Results

A typical set of measurements of the shape of a sessile drop is shown in Figure 1, together with the theoretical curve calculated by the computer program described above. Because the deviation of the experimental points from the curve is too small to be visible on an ordinary plot, the difference between the experimental and theoretical values of  $x$  is plotted on the right-hand side of the figure, using an expanded scale. The mean-square deviation of the experimental points from the curve is approximately 0.0001 cm., which is close to the limit of error for the traveling microscope.

Our experimental value for the interfacial tension of mercury in 0.1 *M* HClO<sub>4</sub>, under the most stringent conditions of purity, was  $426 \pm 1 \text{ ergs/cm.}^2$ . This

agrees with the value of  $425.2 \text{ ergs/cm.}^2$  obtained by Hansen, Kelsh, and Grantham<sup>15</sup> using a capillary electrometer which was calibrated against 0.05 *M* Na<sub>2</sub>SO<sub>4</sub>. The calibration value of  $426.2 \pm 0.2 \text{ ergs/cm.}^2$  was obtained by Smolders and Duyvis,<sup>7</sup> using the sessile drop method.

In Table I are listed our best experimental values for the interfacial tension of the indium amalgams. The parameters determined for the particular sessile drop are also given, together with the standard deviation of the experimental points from the theoretical curve. The potential is in each case the zero-charge potential measured previously by the streaming-electrode method.<sup>9,14</sup> The density values are also listed.

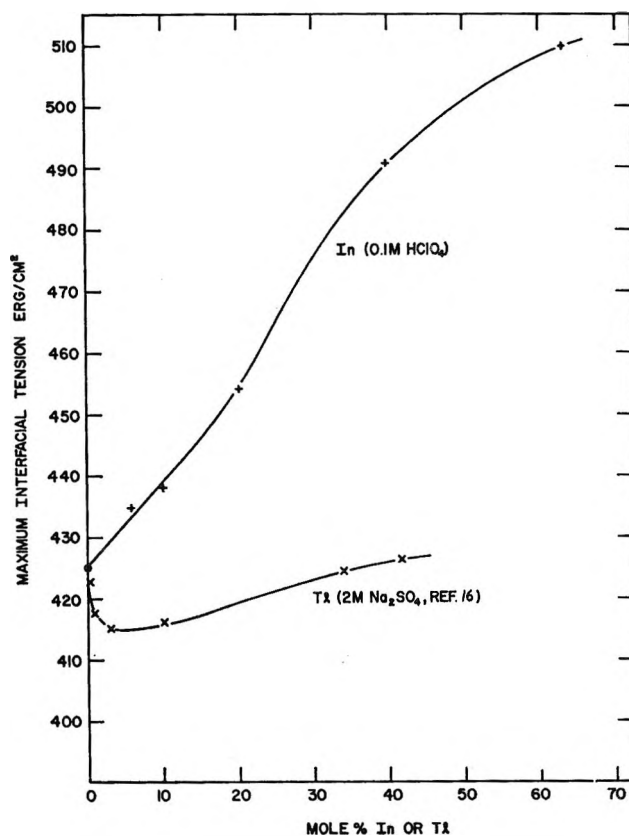


Figure 2. Variation of interfacial tension (measured at the zero-charge potential) with composition. The values for indium amalgam are those listed in Table I. The values for thallium amalgams were taken from ref. 16.

(13) D. C. Grahame, *Chem. Rev.*, **41**, 441 (1947).

(14) J. N. Butler and A. C. Makrides, *Trans. Faraday Soc.*, **60**, 1664 (1964).

(15) R. S. Hansen, D. J. Kelsh, and D. H. Grantham, *J. Phys. Chem.*, **67**, 2316 (1963).

(16) A. N. Frumkin and A. Gorodetskaya, *Z. physik. Chem.*, **136**, 451 (1928).

**Table I:** Interfacial Tension of Indium Amalgams in 0.1 M HClO<sub>4</sub> at 25°

Mole % In	Potential, <sup>a</sup> v.	Density, g./cm. <sup>3</sup>	Parameters of sessile drop shape			γ, ergs/cm. <sup>2</sup>
			β	b, cm.	Std. dev. <sup>b</sup>	
0.0	-0.165	12.534	9.88	0.586	1.21	426.0 <sup>c</sup>
5.97	-0.310	12.168	5.15	0.433	0.82	434.5
10.00	-0.333	11.92	6.68	0.500	0.86	437.9
20.00	-0.388	11.305	12.22	0.707	1.46	454.0
39.83	-0.480	10.03	3.75	0.432	0.85	491.0
63.02	-0.558	8.52	2.86	0.418	0.55	510.8

<sup>a</sup> Zero-charge potential, with respect to a reversible H<sub>2</sub> electrode in 0.1 M HClO<sub>4</sub>. See ref. 9 and 14. <sup>b</sup> Standard deviation of experimental points from theoretical curve, in microns. <sup>c</sup> Reference 15 gives a more accurate value of 425.2 ergs/cm.<sup>2</sup>.

Figure 2 shows the interfacial tension at the zero-charge potential as a function of amalgam composition. For comparison, we have also plotted the values for the interfacial tension of thallium amalgams at the zero-charge potential in 2 M Na<sub>2</sub>SO<sub>4</sub>, obtained by Frumkin and Gorodetskaya,<sup>16</sup> using a capillary electrometer standardized against mercury. Some uncertainty exists in these measurements because the contact angle of the amalgams with glass may not be the same as that of mercury, and no measurements have been made by an independent method.

The values of interfacial tension at the zero-charge potential in dilute aqueous solutions closely parallel the values of surface tension under vacuum. This is shown in Figure 3, where our results for indium amalgams in 0.1 M HClO<sub>4</sub> are compared with the measurements by Olsen and Johnson<sup>10</sup> of the surface tension under vacuum. A similar parallelism exists between the interfacial tension of thallium amalgams in aqueous solutions and their surface tension under vacuum.<sup>17</sup>

Figure 4 compares an integrated interfacial tension curve with experimental electrocapillary curves obtained by other workers. The curve shown was calculated, as described in the previous section, from our previously reported values<sup>9</sup> for the capacity of mercury in 0.1 M HClO<sub>4</sub>, which agreed with the capacity measurements of Hansen, Kelsh, and Grantham,<sup>15</sup> and of Grahame.<sup>13,18</sup> In Figure 4, we have also plotted two independent sets of experimental electrocapillary measurements. Those of Hansen, Kelsh, and Grantham<sup>15</sup> were made in 0.1 M HClO<sub>4</sub>, and those of Kovac<sup>19</sup> were made in 0.1 M NaClO<sub>4</sub>. Except at the most negative potentials, the agreement is within experimental error.

Figure 5 shows 6 of the 11 integrated interfacial

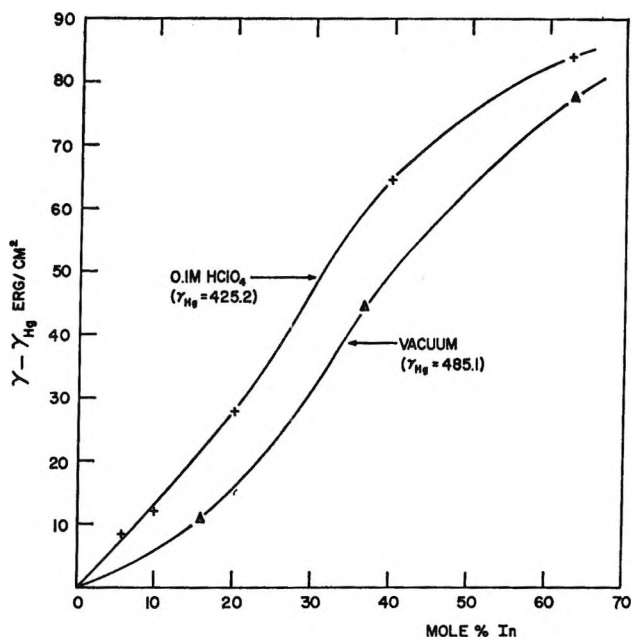


Figure 3. Comparison of interfacial tension at the zero-charge potential of 0.1 M HClO<sub>4</sub> with the surface tension under vacuum.<sup>10</sup>

tension curves which we obtained. The interfacial tension at the zero-charge potential,  $\gamma_z$ , required as an integration constant, was obtained by interpolation on the curve given in Figure 2. From these integrated interfacial tension curves, we also obtained curves of interfacial tension as a function of amalgam composition at constant potential. Using the activity coefficients of indium amalgams measured previously,<sup>20</sup> the curves of interfacial tension as a function of log activity, shown in Figure 6, were obtained.

The slopes of the curves in Figure 6 give the surface excess with respect to Hg, according to the Gibbs adsorption isotherm<sup>1</sup>

$$RT\Gamma_{\text{In}} = -\frac{\partial \gamma}{\partial \ln a_{\text{In}}} \quad (8)$$

where  $a_{\text{In}}$  is the activity of indium in the amalgam,  $R$  is the gas constant, and  $T$  is the absolute temperature. Using a Gerber Derivimeter slope reader, the required derivatives were obtained from several different enlarged plots like Figure 6. The values of surface excess so obtained are shown in Figure 7.

(17) V. A. Kuznetsov, V. V. Ashpur, and G. S. Poroshina, *Dokl. Akad. Nauk SSSR*, **101**, 301 (1955).

(18) D. C. Grahame, Proceedings of the Third Meeting of the International Committee on Electrochemical Thermodynamics and Kinetics, Manfredi, Milan, 1952, p. 330.

(19) Z. Kovac, Thesis, University of Pennsylvania, 1964.

(20) J. N. Butler, *J. Phys. Chem.*, **68**, 1828 (1964).



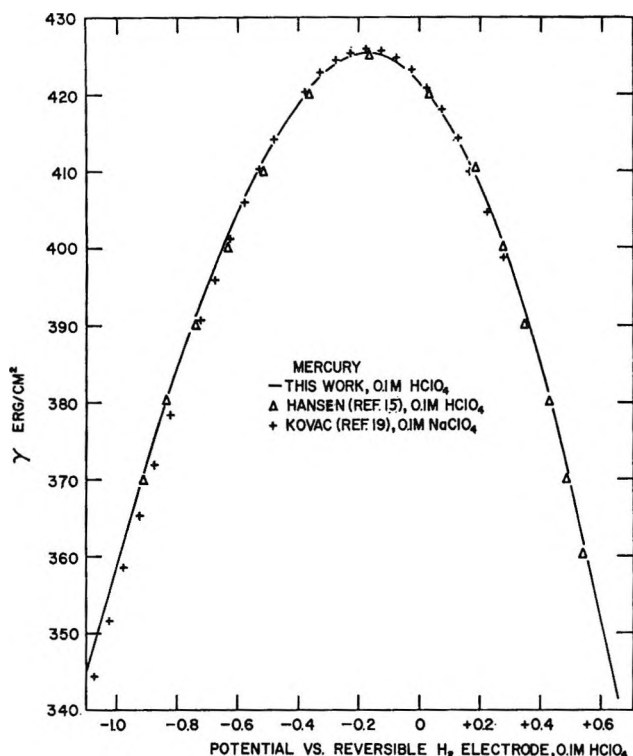


Figure 4. Comparison of experimental electrocapillary curves for mercury in 0.1  $M$   $HClO_4$  (ref. 15) and 0.1  $M$   $NaClO_4$  (ref. 19) with the curve obtained by integration of differential capacity measurements.

The points in Figure 7 do not correspond to experimental measurements, but to the most accurate slope values read. The curves were drawn smoothly through the points, and only the inflections and maxima which were beyond the errors in slope reading ( $\pm 0.1$  to  $0.5 \times 10^{-10}$  mole/cm.<sup>2</sup>) were included in the curves.

If the surface-excess curves for indium amalgams are compared with those for thallium amalgams,<sup>3</sup> a striking difference is noted. Whereas the surface deficiency ( $-Γ$ ) of thallium amalgams increases monotonically with increasing bulk concentration up to the solubility limit, the surface deficiency of indium amalgams passes through a maximum at approximately 20 mole % indium; and an increase in bulk composition beyond this point causes the surface deficiency to decrease in magnitude. As with the thallium amalgams, the surface excess of indium amalgams was found to be potential dependent. This phenomenon is discussed below.

### Discussion

One of the principal objects of this investigation was to relate the surface composition of indium amalgams to the observed electrocatalytic activity. As shown in Figure 8, the rate of the hydrogen evolution

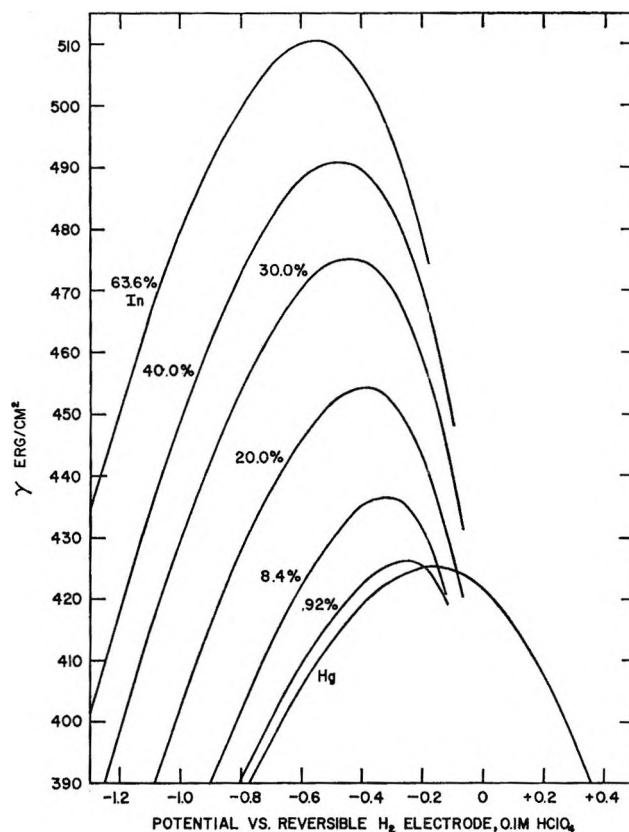


Figure 5. Interfacial tension of indium amalgams as a function of potential and composition, plotted as electrocapillary curves.

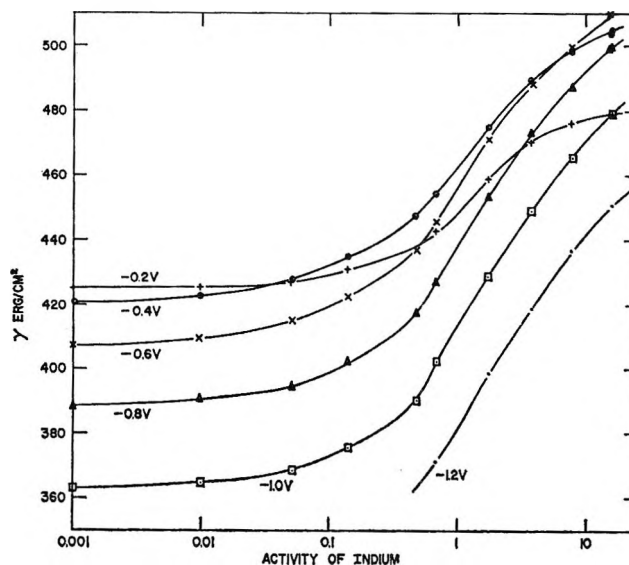


Figure 6. Interfacial tension of indium amalgams at constant potential plotted as a function of the activity of indium. The slope of these curves gives the surface excess.

reaction, as reflected by the exchange current  $i_0'$ , is a smooth monotonic function of composition.<sup>14,21</sup>



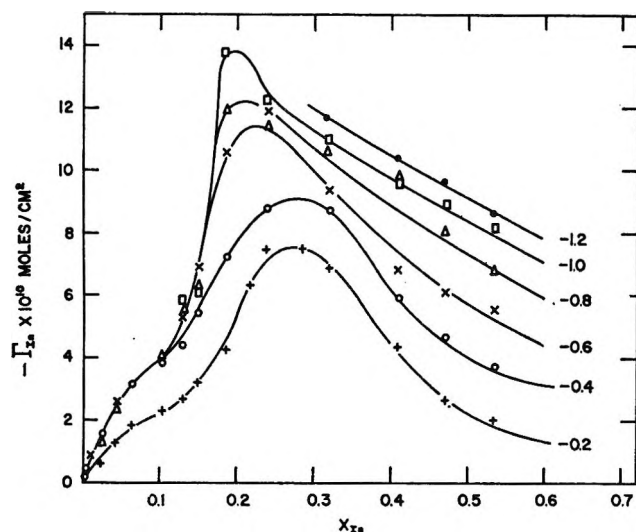


Figure 7. Surface excess calculated from the slopes of the curves in Figure 6. The scatter of the points gives some indication of the random errors involved.

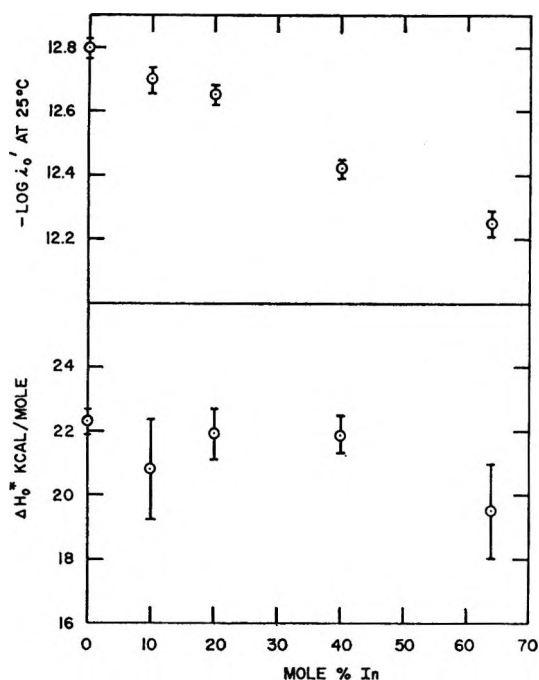


Figure 8. Exchange current  $i_0'$  and enthalpy of activation at the reversible potential  $\Delta H_0^*$ , for the hydrogen evolution reaction at an indium amalgam electrode (ref. 21).

In the region from 10 to 30% indium, no salient features appear which might be correlated with the maximum surface deficiency seen in Figure 7. On the other hand, the enthalpy of activation  $\Delta H_0^*$  may have a minimum value around 10% and a maximum value around 20 to 30%. This variation would correlate with the surface deficiency maximum of Figure 7,

but the variations in  $\Delta H_0^*$  mentioned are really within experimental error.<sup>21</sup>

Two alternative explanations may be made of this lack of correlation: the first, that the surface composition is essentially that of the bulk, and the second, that the electrocatalytic properties are more closely related to the bulk electronic properties of the alloy than to the surface composition.

If the composition profile in a direction perpendicular to the surface is so slowly varying that the observed surface deficiency is spread over more than 20 atomic layers, the surface composition would be essentially that of the bulk. Such a diffuse surface structure seems unlikely. No evidence for specific long-range ordering in liquid Hg-In amalgams has been found by X-ray diffraction<sup>22</sup> or thermodynamic<sup>20</sup> methods. The mean free path of electrons in mercury-indium alloys is only about 2.5 interatomic distances,<sup>23</sup> so that appreciable space charge is unlikely. The diffusion coefficients of metals in amalgams are comparable to the diffusion coefficients of solutes in non-associated solutions.<sup>24,25</sup> Thus a more reasonable estimate would be that the surface deficiency arises in the first four or five atomic layers.

A self-consistent method by which a surface composition can be calculated from the surface-excess values has been outlined by Guggenheim.<sup>26-28</sup> From the interfacial tension measurements, we obtain the surface excess (eq. 8), which can be expressed as a combination of surface concentration values

$$\Gamma_{\text{In}} = \Gamma'_{\text{In}} - \frac{X_{\text{In}}}{1 - X_{\text{In}}} \Gamma'_{\text{Hg}} \quad (9)$$

where  $\Gamma'_{\text{In}}$  and  $\Gamma'_{\text{Hg}}$  are the total concentrations in an interphase of arbitrary thickness, in moles per square centimeter. Absolute values can be obtained for  $\Gamma'_{\text{In}}$  and  $\Gamma'_{\text{Hg}}$  if values are assumed for the surface areas  $A_{\text{In}}$  and  $A_{\text{Hg}}$  per mole of each component in the interphase. These must satisfy the condition

$$A_{\text{In}}\Gamma'_{\text{In}} + A_{\text{Hg}}\Gamma'_{\text{Hg}} = 1 \quad (10)$$

(21) J. N. Butler and M. L. Meehan, *Trans. Faraday Soc.*, in press.

(22) Y. S. Kim, C. L. Standley, R. F. Kruh, and G. T. Clayton, *J. Chem. Phys.*, **34**, 1464 (1961).

(23) N. Cusack, P. Kendall, and M. Fielder, *Phil. Mag.*, **10**, 871 (1964).

(24) W. T. Foley and L. E. Reid, *Can. J. Chem.*, **41**, 1782 (1963).

(25) Y. Okinaka, I. M. Kolthoff, and T. Murayama, *J. Am. Chem. Soc.*, **87**, 423 (1965).

(26) E. A. Guggenheim, "Thermodynamics," 3d Ed., North-Holland Publishing Co., Amsterdam, 1957, pp. 265-268.

(27) E. A. Guggenheim, *Trans. Faraday Soc.*, **41**, 150 (1945).

(28) E. A. Guggenheim and N. K. Adam, *Proc. Roy. Soc. (London)*, **A139**, 218 (1933).

Between these two equations, the values of  $\Gamma'_{\text{In}}$  and  $\Gamma'_{\text{Hg}}$ , and hence the composition of the surface layer, are determined. The arbitrary assumptions come in the values used for  $A_{\text{In}}$  and  $A_{\text{Hg}}$ . In considering the adsorption of alcohol and water at the free surface of alcohol-water solutions, Guggenheim<sup>26,28</sup> assumed that the molecules at the surface had reasonable dimensions and that the interphase consisted only of the first atomic layer. From these assumptions he obtained reasonable values for the surface composition.

If one assumes diameters for mercury (3.00 Å) and indium (3.25 Å) corresponding to the interatomic distances in crystals of the pure materials and assumes that the interphase consists of only the first atomic layer, one obtains  $A_{\text{Hg}} = 0.0469 \times 10^{10}$  and  $A_{\text{In}} = 0.0551 \times 10^{10}$  cm.<sup>2</sup>/mole. When substituted into eq. 9 and 10, these values give negative values of  $\Gamma'_{\text{In}}$ , indicating that the model is unrealistic.

In order to obtain positive values of  $\Gamma'_{\text{In}}$  for the data obtained in this study, it is necessary to assume that the surface deficiency arises in an interphase at least three atomic diameters thick. This assumption gives  $A_{\text{Hg}} = 0.0156 \times 10^{10}$  and  $A_{\text{In}} = 0.0184 \times 10^{10}$  cm.<sup>2</sup>/mole. The composition of the surface is then given by

$$X_{\text{In}}^{(s)} = \frac{\Gamma'_{\text{In}}}{\Gamma'_{\text{In}} + \Gamma'_{\text{Hg}}} \quad (11)$$

Curves of surface composition as a function of bulk composition, calculated according to these assumptions from the data in Figure 7, at potentials of  $-0.2$  and  $-1.0$  v., are shown in Figure 9. Note that the surface composition at  $-1.0$  v. passes through a maximum and a minimum, corresponding to the shape of the surface-excess curve in Figure 7.

Since the liquid metal is a conductor, one might expect its surface composition to be independent of potential. Instead, we observe that it is strongly potential dependent. This effect most probably arises from the difference in electronegativity of indium and mercury. At  $-1.0$  v., the surface charge<sup>9</sup> is approximately  $-12.4$   $\mu\text{coulombs/cm.}^2$  for 63% In amalgam, and  $-14.6$   $\mu\text{coulombs/cm.}^2$  for pure mercury, nearly independent of composition. This negative surface charge is an electron excess on the surface of the metal, and, because mercury is more electronegative (1.9) than indium (1.7), the mercury is preferentially attracted to the surface, making the surface deficient in indium compared to the bulk. This surface deficiency would thus be expected to be higher at the more negative potentials, which can be seen from Figure 7 or 9. At  $-0.2$  v., the surface charge on mercury is nearly zero, and the surface charge on the concentrated

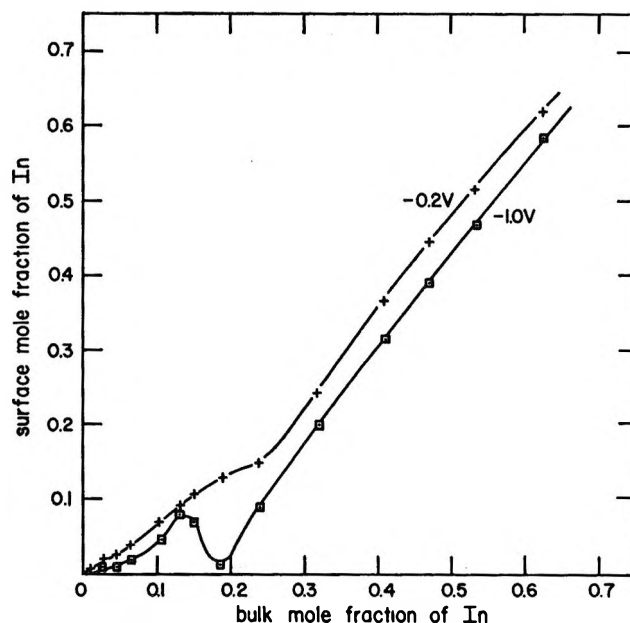


Figure 9. Surface composition at  $-1.0$  and  $-0.2$  v., calculated as described in the text. The interphase was assumed to extend over three atomic layers.

indium amalgams is quite positive, so that the preferential adsorption of mercury at the surface is much less.

In contrast to the complex way in which the surface composition (Figure 9) varies, the electronic properties of mercury-indium alloys show relatively simple behavior. The resistivity, temperature coefficient of resistivity, and Hall coefficient all decrease monotonically as the concentration of indium increases.<sup>23</sup> The optical reflectivity<sup>29</sup> increases monotonically with increasing indium concentration. None of these properties agrees precisely with the values calculated from a free-electron theory, even though pure mercury and pure indium both are well described by such a theory.<sup>23,29</sup> The only property which shows a complex behavior is the thermoelectric power, which goes through an unexplained maximum at approximately 3 atom % indium.<sup>23</sup> From Figure 8, we can see that the exchange current and probably the enthalpy of activation for the hydrogen evolution reaction decrease monotonically as the concentration of indium increases.

We have previously<sup>14,30</sup> made a dichotomy between the "atomic approach" and the "continuum approach" to electrocatalysis. The atomic approach assumes that the electrocatalytic properties of an alloy result

(29) L. G. Schulz, *J. Opt. Soc. Am.*, **47**, 70 (1957).

(30) J. N. Butler and A. C. Makrides, *Trans. Faraday Soc.*, **60**, 938 (1964).

from independently additive properties of the surface atoms; the continuum approach assumes that the electrocatalytic activity of an alloy is a cooperative property and may bear little relation to the properties calculated on the basis of the atomic approach. In our studies of hydrogen evolution at platinum and palladium amalgam electrodes,<sup>80</sup> we showed that the continuum approach was probably closer to the truth since the atomic approach gave an answer which was many orders of magnitude different from the experimental results.

The results of the present study on indium amalgams also indicate that the continuum approach is the fruitful one. We have seen that the electronic properties of these alloys are virtually all simple monotonic functions of the bulk composition, as are the electro-

catalytic properties. The surface composition, on the other hand, shows very complex behavior and does not correlate well with electrocatalytic activity. It would thus seem likely that electrocatalytic activity is more closely related to the cooperative electronic properties of an alloy rather than to its surface composition.

*Acknowledgments.* The author thanks Burton H. Bloom, who suggested the mathematical methods used to compute the shape of a sessile drop, Gloria G. Bloom, who coded and tested the computer program, Mary L. Meehan, who assisted very skillfully with the experiments, and Dr. A. C. Makrides, for his helpful criticism and advice. This work was supported by the U. S. Office of Naval Research, Materials Sciences Division.

# Thermodynamic Stabilities as a Function of Composition for Indium Sulfide Phases from Mass Spectrometer Intensity *vs.* Time Data<sup>1</sup>

by Alan R. Miller and Alan W. Searcy

*Inorganic Materials Research Division, Lawrence Radiation Laboratory, and Department of Mineral Technology, College of Engineering, University of California, Berkeley, California (Received May 17, 1965)*

The indium sesquisulfide phase is shown by X-ray diffraction and mass spectrometer measurements to have a wide solution range at 873 to 1073°K. The existence of InS and In<sub>5</sub>S<sub>6</sub> (here identified as InS<sub>1.12</sub>) is confirmed, and the existence of In<sub>3</sub>S<sub>4</sub> is disproved. Mass spectrometer intensities *vs.* time for In<sub>2</sub>S<sup>+</sup> and S<sub>2</sub><sup>+</sup> are used to obtain values of the partial pressures of In<sub>2</sub>S(g) and S<sub>2</sub>(g) as functions of composition in the range from InS(s) to InS<sub>1.5</sub>(s). At 873 to 1073°K. the heat of formation of the indium sesquisulfide phase for the composition range from 41 to 44 atomic % indium from liquid indium and S<sub>2</sub> gas is 0.37*y* - 44.3 kcal./mean g.-atom (where *y* is the atomic per cent In), and the corresponding heat of formation of InS<sub>1.12</sub> is -27.7 kcal./mean g.-atom (or -58.8 kcal./g.f.w. of InS<sub>1.12</sub>) and of InS is -26.5 kcal./mean g.-atom (-53.0 kcal./g.f.w. of InS).

For determination of the partial pressures of vapor species in multicomponent systems by a dynamic method (such as the Knudsen-effusion method), a choice of conditions that yield pressures which do not change with time at constant temperature is usually necessary. Time-independent pressures for a two-component system can be obtained by bringing two condensed phases to equilibrium with the vapor. Some, but not all, two-component systems have compositions of congruent vaporization that can also be studied by dynamic-pressure-measurement techniques. The pressures that characterize single-phase compositions of incongruent vaporization are not readily studied.

If, however, the variations in both composition and pressure can be determined as functions of time at constant temperature, a dynamic method for pressure measurement can be used to obtain pressure *vs.* composition data in single-phase regions of arbitrary compositions. The mass spectrometer should be especially suitable for obtaining such data because with a mass spectrometer continual records of the partial pressures of all species in a complex vapor can be obtained. However, apparently no experimental evaluation of this use of the mass spectrometer has been made. The principal purpose of this paper is to report the results of such an evaluation.

The indium sesquisulfide phase was chosen for study (a) because the partial pressures of the two major vapor species at the composition of congruent sublimation were accurately known as a function of temperature,<sup>2</sup> (b) because the vapor pressure range is a convenient one for study with a high-temperature mass spectrometer, and (c) because our preliminary investigations revealed the indium sesquisulfide phase to have a relatively wide solid solution range at high temperatures. As a preliminary to the mass spectrometer investigations, X-ray *vs.* composition studies were made to establish the stable phases to be expected at 900 to 1100°K.

## X-Ray Diffraction Pattern *vs.* Composition Studies

Previous investigators identified the phases In<sub>2</sub>S<sub>3</sub>, In<sub>5</sub>S<sub>6</sub>, and InS by X-ray diffraction examination of room-temperature samples.<sup>3</sup> A phase of approximate composition In<sub>3</sub>S<sub>4</sub> (InS<sub>1.33</sub>) was inferred from cooling

(1) This work was supported in part by a contract with the Office of Naval Research and the Advanced Research Projects Agency and in part by the U. S. Atomic Energy Commission.

(2) A. R. Miller and A. W. Searcy, *J. Phys. Chem.*, **67**, 2400 (1963).

(3) M. F. Stubbs, J. A. Schuffe, A. J. Thompson, and J. M. Duncan, *J. Am. Chem. Soc.*, **74**, 1441 (1952).

curves and differential thermal analysis to be stable above 643°K.

In the present study, room-temperature diffraction patterns of indium sesquisulfide which had been heated at about 873°K. with excess sulfur were found to be identical with the diffraction patterns of  $\beta$ -In<sub>2</sub>S<sub>3</sub>. Samples of composition between 42.0 and 42.5 atomic % indium, prepared by heating elemental indium with In<sub>2</sub>S<sub>3</sub>, showed a single phase with the 40% ( $\beta$ -In<sub>2</sub>S<sub>3</sub>) structure, but with contractions in the unit-cell volume. Samples whose compositions were 43 to 45% indium yielded X-ray patterns of the contracted In<sub>2</sub>S<sub>3</sub> phase and of a second phase. The second phase was obtained pure by quenching a sample in the mass spectrometer at a composition for which the ion intensities were rapidly changing with time.

The diffraction pattern of the second phase agreed in spacing and approximate intensities with the pattern of a phase previously reported to have the approximate formula In<sub>5</sub>S<sub>6</sub>,<sup>4</sup> but the present study indicates a composition somewhat richer in indium. We will call the phase InS<sub>1.12</sub> in this paper.

The X-ray diffraction pattern of the 50 atomic % In sample appeared to be that of a third single phase, identified thus as InS, and patterns of samples ranging from 47 to 50 atomic % In contained lines of both InS and InS<sub>1.12</sub>. The InS pattern,<sup>5</sup> however, differed from the one reported by Schuffle.<sup>6</sup> Perhaps there are two crystallographic modifications of InS. A sample of over-all composition In<sub>2</sub>S yielded the diffraction patterns of indium and of InS.

Since the mass spectrometer studies yielded further information on the composition of stable indium sulfide phases, a final evaluation of the X-ray data is deferred to the discussion section.

### Mass Spectrometer Studies

*Experimental Section.* Samples of over-all compositions 42 to 50 atomic % indium were prepared by heating indium sesquisulfide with excess indium in sealed, evacuated fused-silica tubes. Indium sesquisulfide samples, which were slightly enriched in sulfur, were prepared by adding sulfur to congruently subliming indium sesquisulfide and heating in a fused-silica tube *in vacuo*.

Samples were introduced into a cylindrical, fused-silica Knudsen cell 1.5 cm. high and 1.2 cm. in diameter. The fused-silica lids had cylindrical orifices that were 1.6 mm. long and had one of three different diameters: 0.86, 1.22, or 1.80 mm. The cell was placed inside a tantalum crucible fitted with a tantalum lid. The bottom of the cell was ground flat, and a 2-mil strip of tantalum was placed between the walls of the cell

and crucible in order to effect better heat transfer. The entire assembly was supported by three tungsten rods inside an Inghram-type mass spectrometer and was heated by radiation from two concentric tungsten filaments.

Temperatures were measured with a Pt—Pt—10% Rh thermocouple embedded in a cavity in the bottom of the tantalum crucible. The thermocouple was calibrated against another Pt—Pt—10% Rh thermocouple inserted through the orifice into the Knudsen cell and immersed in an indium sesquisulfide sample. Two independent calibration runs deviated by 8° at 873°K. and 3° at 1073°K. probably because of sensitivity of the temperatures to placement of the cell relative to the shields and heating elements.

Identification of In<sub>2</sub>S<sub>2.36</sub>(s) = In<sub>2</sub>S(g) + 0.98 S<sub>2</sub>(g) as the principal reaction at the composition of congruent sublimation was reported in our previous paper.<sup>2</sup> We can demonstrate from the thermodynamic data that other species remain unimportant over the composition range studied in this work. Recent analyses of our samples by Pankratz<sup>7</sup> indicate that the composition of congruent sublimation is In<sub>2</sub>S<sub>2.90</sub> or InS<sub>1.46</sub>. Our thermodynamic data are not significantly altered by this compositional change.

As a test of the reliability of our mass spectrometer studies, variations of ion intensities with temperature at the congruent composition were measured for comparison with our previous weight-loss measurements, which are inherently more precise. Second-law plots of  $-R \ln (I_{\text{In}_2\text{S}} I_{\text{S}_2} T^2)$  vs.  $1/T$  for indium sesquisulfide at the composition of congruent sublimation yielded for the heat of reaction 130, 136, 141, 142, 143, and 145 kcal./g.f.w. of In<sub>2</sub>S<sub>3</sub> at 1000°K. with an average of  $139.5 \pm 4.4$  kcal./g.f.w., compared to 141 kcal./g.f.w. calculated by the third-law method from the weight-loss experiments.<sup>2</sup> The variations in the temperature scale noted during the calibration runs are enough to cause 6-kcal. variations in the measured slopes.

Indium-rich samples were heated at 873, 923, 973, 1023, and 1073°K., and sulfur-rich samples were heated at 873, 923, 973, and 1023°K. During each run the intensities of the ions In<sub>2</sub>S<sup>+</sup> and S<sub>2</sub><sup>+</sup> were alternately recorded on a strip chart until the ion intensities became constant with time (Figure 1). The sample was then quickly cooled to room temperature. The samples were weighed before and after heating,

(4) American Society for Testing Materials X-Ray Card 5-0429.

(5) A. R. Miller, Ph.D. Thesis, UCRL-10857, Oct. 1963.

(6) American Society for Testing Materials X-Ray Card 5-0722.

(7) L. B. Pankratz, U. S. Department of the Interior, Bureau of Mines, Report of Investigations, No. 6592, Pittsburgh, Pa., 1965.

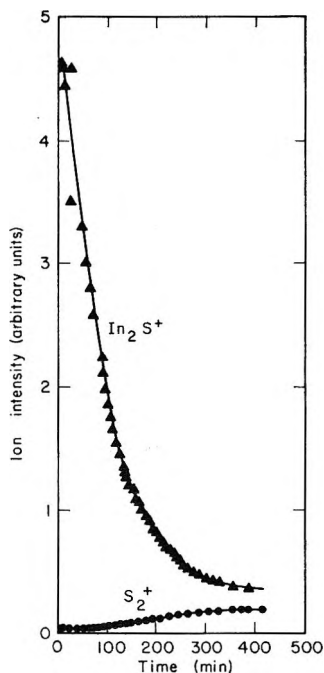


Figure 1. Ion ( $\text{In}_2\text{S}^+$  and  $\text{S}_2^+$ ) intensities vs. time in the indium sesquisulfide region.

and X-ray diffraction photographs of the powders were made before and after each run.

Several samples, initially about 50 atomic % indium, were heated in the temperature range 873 to 1023°K.; all showed constant ion intensities at first, then a rapid change in intensities in a very short time period (Figure 2). The rapid change indicated that a narrow, single-phase region was being traversed. The experiment was repeated, therefore, at 973°K., and the sample was quickly cooled when the middle of the composition of sharp intensity change was reached. An X-ray diffraction pattern was obtained for the product, which was calculated to have an over-all composition of 47.1 atomic % indium, corresponding to  $\text{InS}_{1.12}$ , with an uncertainty of about 0.5% in this composition.

The ion  $\text{In}_2\text{O}^+$  was observable during heating of indium sesquisulfide whenever an air leak developed in the vacuum system, even though the residual pressure was less than  $10^{-6}$  torr. The ion  $\text{InGaS}^+$  was seen when indium sesquisulfide was heated subsequent to several runs during which large amounts of GaN had been vaporized in the mass spectrometer. These ions were at negligible intensities during the studies reported in the remainder of this paper.

*Pressure vs. Composition Data from Ion Intensity vs. Time.* Provided that the intensity of an ion that is produced from each major vapor species can be followed as a function of time at constant temperature, a pressure vs. composition plot can be derived.

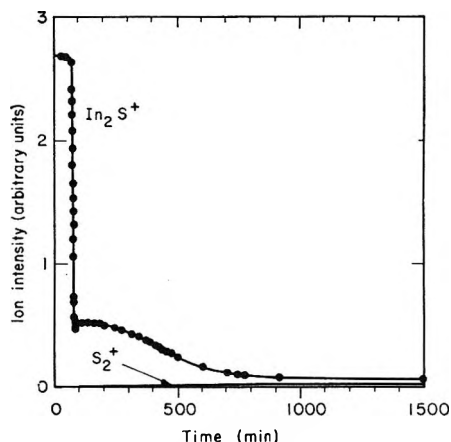


Figure 2. Ion ( $\text{In}_2\text{S}^+$  and  $\text{S}_2^+$ ) intensities as functions of time in the  $\text{InS}_{1.12}$  region.

The pressure  $P_i$  at any given time is related to the intensity  $I_i$  by the equation  $P_i = UI_iT$ , where  $T$  is the absolute temperature and  $U$  is a constant which is dependent on the ionization cross section of the vapor species and on the response of the electron multiplier to each particular kind of ion.

The constant can be evaluated for  $\text{In}_2\text{S}$  and  $\text{S}_2$  because the partial pressures of these species are known at the known composition of congruent sublimation. The composition for congruent sublimation is fixed at  $\text{InS}_{1.45 \pm 0.03}$  at 873 to 1098°K. by analytical studies of Pankratz<sup>7</sup> of samples heated at 1098°K. *in vacuo* and by the fact, demonstrated in experiments discussed later, that temperature changes in the 873 to 1098°K. range of a sample, which was known from its unchanging ratio  $\text{In}_2\text{S}^+/\text{S}_2^+$  to sublime congruently, produced only small, temporary variations in the ion ratio. From the Knudsen-effusion weight-loss experiments, the partial pressures of  $\text{In}_2\text{S}(\text{g})$  and  $\text{S}_2(\text{g})$  can be calculated with a probable absolute error of about 20%, compared to estimated errors of factors of 2 to 3 when usual calibration techniques that require estimation of ionization cross sections<sup>8</sup> are employed.

With pressures determined from the ion intensities, the remaining problem is to calculate the compositions that correspond to these pressures. The total weight loss  $\Sigma Y_j$  for each ion must first be related to the intensity vs. time data to obtain the relationship. For each ion  $\Sigma Y_j$  in milligrams was calculated from

$$\sum_0^t Y_j = \frac{\sum_0^t I_j P_i A k \Delta t}{I_t} \left( \frac{M_j}{T} \right)^{1/2} 2.66 \times 10^9 \quad (1)$$

(8) J. W. Otvos and D. P. Stevenson, *J. Am. Chem. Soc.*, **78**, 546 (1956).

where  $\Sigma I_j$  is the sum of the average intensities over time intervals  $\Delta t$  in minutes for ion  $j$ ,  $I_t$  is the final intensity of ion  $j$  (at the compositions for congruent sublimation),  $P_t$  is the partial pressure in atmospheres at the congruent sublimation point (*i.e.*, the pressure that produced the measured intensity  $I_t$ ),  $A$  is the orifice area in square centimeters,  $k$  is the Clausing correction,<sup>9</sup> and  $M$  is the molecular weight of the vapor species.

As a first approximation, the composition for congruent sublimation was assumed to correspond to stoichiometric indium sesquisulfide. The sums of the calculated losses by vaporization of  $\text{In}_2\text{S}$  and  $\text{S}_2$  are compared with directly measured losses in Table I. Most of the calculated weight losses agree with the directly measured weight losses to within a factor of 2. However, at 1031°K. the vaporization of the 46.1 atomic % indium sample produced a measured weight loss of six times the calculated value, and at 873°K. vaporization of the sulfur-rich sample produced a weight loss of five times the calculated value. These high losses are believed to be due, in part, to escape of vapor between the crucible and lid rather than through the orifice and, in part, to errors in temperature measurement.

**Table I:** Comparison of Observed and Calculated Weight Losses

Temp., °K.	Initial compn.	Obsd. wt. loss, mg.	Calcd. wt. loss, mg.	Calcd./ obsd.
871 ± 8	$\text{In}_{0.44}\text{S}_{0.56}$	0.2	0.500	2.5
923 ± 7	$\text{In}_{0.46}\text{S}_{0.56}$	0.8	0.602	0.75
976 ± 6	$\text{In}_{0.44}\text{S}_{0.56}$	7.2	2.98	0.41
973 ± 6	$\text{In}_{0.60}\text{S}_{0.50}$	15.1	12.8	0.85
1031 ± 5	$\text{In}_{0.461}\text{S}_{0.539}$	4.8	0.78	0.16
1082 ± 3	$\text{In}_{0.44}\text{S}_{0.56}$	16.5	30.7	1.8
873 ± 8	Sulfur-rich	0.2	0.04	0.2
923 ± 7	Sulfur-rich	0.7	0.57	0.81
974 ± 6	Sulfur-rich	2.2	1.00	0.45
1027 ± 5	Sulfur-rich	2.4	1.3	0.54

A constant factor,  $c$ , was applied to eq. 1 to correct both  $Y_{\text{In}_2\text{S}}$  and  $Y_{\text{S}_2}$ , so that the calculated weight loss would agree with the directly measured loss. The final composition was then calculated from the known initial weight and composition of the condensed phase, the weight of  $\text{In}_2\text{S}$  and  $\text{S}_2$  molecules vaporized, and the final weight of sample.

If this calculated composition for congruent sublimation differed from the stoichiometric composition, a second approximation was made in which the partial

pressures that characterize the composition for congruent sublimation, calculated in the first approximation, were assumed to be the final pressures. These pressures were calculated assuming that the free energy of vaporization per gram-atom for the indium sesquisulfide solid solution region is independent of composition. The final results of this study demonstrate this approximation to be valid to within a few tenths of a kilocalorie, except possibly at the lowest temperatures studied. This gives the relationships

$$[P^\circ_{\text{In}_2\text{S}}]^{0.2}[P^\circ_{\text{S}_2}]^{0.2} = [P_{\text{In}_2\text{S}}]^{(1-x)/2}[P_{\text{S}_2}]^{(3x-1)/4} \quad (2)$$

and

$$\frac{P_{\text{In}_2\text{S}}}{P_{\text{S}_2}} = \left(\frac{1-x}{2}\right)\left(\frac{4}{3x-1}\right)\left(\frac{M_{\text{In}_2\text{S}}}{M_{\text{S}_2}}\right)^{1/2} \quad (3)$$

where  $P^\circ$  is the partial pressure at stoichiometry and  $x$  is the mole fraction of sulfur in the solid phase. The simultaneous solution of (2) and (3) provides partial pressures closer to those at the congruent-subliming composition.

The end composition calculated in the second approximation usually agreed to within 0.1 atomic % with that of the first approximation, but this small correction is necessary to prevent anomalous reversal of calculated slopes of the partial pressure *vs.* composition curves.

The composition at any time  $t$  could be obtained by correcting the initial sample composition for the summation of the losses of  $\text{In}_2\text{S}$  and of  $\text{S}_2$  by effusion. For each gas species

$$\sum_0^t Y_i = \frac{\sum_0^t I_i}{I_t} P_t A k \Delta t \left(\frac{M}{T}\right)^{1/2} c 2.66 \times 10^6 \quad (4)$$

The compositions for congruent sublimation were calculated by the method described to be 40.5, 41.0, 41.2, 40.8, and 40.8 atomic % indium at 873, 923, 973, 1023, and 1073°K. Experiments described below lead us to believe that the composition for congruent sublimation varies by only about 0.1 atomic % in the temperature range studied, so the composition of 40.8 atomic % indium found by chemical analysis best identifies the composition of congruent sublimation over this temperature range. This composition of congruent sublimation must be considered uncertain by about 0.5 atomic %. From similar analysis of samples prepared with excess sulfur, initial compositions are found to have been 40.3, 40.7, 40.6, and 40.5 atomic % indium at 873, 923, 973, and 1023°K.;

(9) W. C. DeMarcus, Union Carbide Nuclear Co., Oak Ridge Gaseous Diffusion Plant, Report K-1502, Part III, AD 124579, 1957.

*i.e.*, all samples were sulfur deficient relative to the stoichiometric composition.

By the procedure just outlined, the composition of the phase designated  $\text{InS}_{1.12}$  was calculated to have compositions 47.9, 48.0, and 47.2 atomic % indium at 873, 923, and 973°K., compared to 47.1 found by quenching a single-phase sample in the mass spectrometer. The width of this phase was found to decrease with increasing temperature. The calculated phase widths are  $3.3 \pm 0.4$ ,  $2.8 \pm 0.2$ , and  $0.8 \pm 0.1$  atomic % at 873, 923, and 937°K., respectively.

The results of an experiment in a fused-silica crucible to determine the variation in composition of congruent sublimation with temperature are summarized in part A of Table II, which shows the temperatures, in the sequence followed, at which the sample was held, and the initial and final (*i.e.*, steady-state) intensity ratios of  $\text{S}_2^+$  to  $\text{In}_2\text{S}^+$  that resulted.

**Table II:** The  $\text{S}_2^+/\text{In}_2\text{S}^+$  Ratio above Indium Sesquisulfide Immediately after a Temperature Change (Initial) and after the Composition Has Attained That for Congruent Sublimation at the Same Temperature (Final)

Temp., °K.	Initial $\text{S}_2^+/\text{In}_2\text{S}^+$	Final $\text{S}_2^+/\text{In}_2\text{S}^+$
A		
1111	...	0.72
1041	1.2	0.67
999	0.5	0.7
1111	0.4	0.7
B		
1073	...	0.46
1023	4.1	0.59
973	0.36	0.56
1073	0.61	0.55

A value of 0.6 to 0.7 is characteristic of the  $\text{S}_2^+/\text{In}_2\text{S}^+$  ratio for congruent sublimation in our mass spectrometer. The high initial  $\text{S}_2^+/\text{In}_2\text{S}^+$  ratio obtained when the temperature was first dropped to 1041°K. presumably resulted because the composition for congruent sublimation at 1111°K. was richer in sulfur than the composition for congruent sublimation at 1041°K. Similarly, the composition for congruent sublimation at 999°K. presumably contains less sulfur than does the composition for congruent sublimation at either 1041 or 1111°K.

That the composition for congruent sublimation did not shift continuously in a single direction with temperature was surprising. The experiment was repeated, therefore, in a graphite crucible for which the

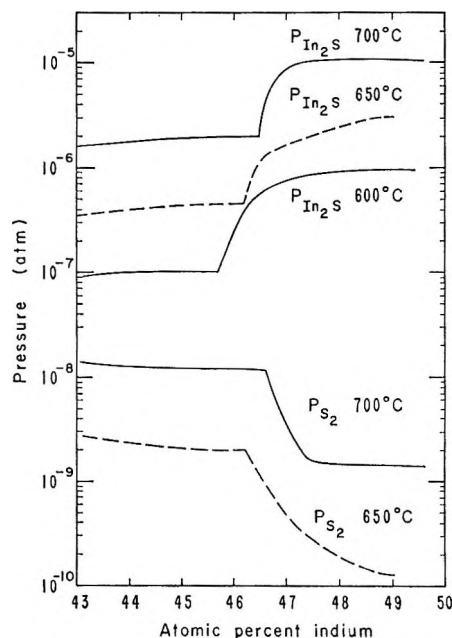


Figure 3. Vapor pressures of  $\text{In}_2\text{S}(\text{g})$  and  $\text{S}_2(\text{g})$  vs. composition in the  $\text{InS}_{1.12}$  region.

interior temperature had been carefully calibrated against the temperature on a thermocouple wedged against the bottom. The temperature sequence followed and the measured initial and final  $\text{S}_2^+/\text{In}_2\text{S}^+$  intensity ratios are summarized in part B of Table II. The results are similar to those found in silica.

From the time vs. temperature plots obtained during the second of these composition variation experiments, the maximum variation of the composition for congruent sublimation is calculated to be less than 0.1 atomic %. However, when samples that had been equilibrated in the mass spectrometer at a composition for congruent sublimation at temperatures below 1123°K. were raised to a temperature of 1153 to 1223°K., the  $\text{S}_2^+/\text{In}_2\text{S}^+$  intensity ratio initially rose from about 0.6 to 2.2. When a sample was held at these higher temperatures, the  $\text{S}_2^+/\text{In}_2\text{S}^+$  ratio decreased to a constant value of 0.5. Samples quenched after this treatment have the same X-ray diffraction pattern as samples of over-all composition 43 to 45 atomic % indium.

Presumably, at about 1123°K. the composition for congruent sublimation under the steady-state conditions of our experiments coincides with the indium-rich phase boundary of the indium sesquisulfide solid solution, and at higher temperatures the composition for congruent vaporization moves to about  $\text{InS}_{1.3}$  or  $\text{InS}_{1.2}$  in the liquid solution range.

Samples whose initial compositions corresponded to  $\text{InS}$  were heated to 873, 923, 973, and 1023°K. in the



mass spectrometer long enough to move their compositions into the two-phase region between the  $\text{InS}_{1.12}$  and indium sesquisulfide phases. The pressure *vs.* composition plots derived from these data are presented in Figure 3. At 1023°K. only the pressures in the two-phase region are known because the weight of the sample was not measured.

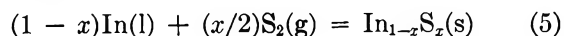
### Discussion

Our diffraction pattern *vs.* composition study indicates that a single-phase region extends from about  $\text{InS}_{1.5}$  on the sulfur-rich side (the limit depends on the sulfur pressure and the temperature) to about  $\text{InS}_{1.35}$  at the indium-rich phase boundary, and the pressure *vs.* composition studies indicate still lower sulfur contents for the indium-rich phase boundary,  $\text{InS}_{1.26}$  at 873°K. and  $\text{InS}_{1.17}$  at 973°K.

Quenching is often ineffective in preserving the compositions stable at annealing temperatures, and the limits of the partial pressure *vs.* composition studies should be accepted as providing the better measure of the high-temperature solid solution limits.

On the other hand, the pressure *vs.* composition curves show distinctly that no discrete phase of composition near  $\text{In}_3\text{S}_4$  is stable in the temperature range between 873 and 923°K., the approximate temperature at which the sesquisulfide phase boundary reaches this composition. Probably the thermal effect noted by Stubbs, *et al.*,<sup>3</sup> at 643°K. was the precipitation of  $\text{InS}_{1.12}$  from the supersaturated solution of indium in the indium sesquisulfide phase. Such precipitation reactions are necessarily exothermic.<sup>10</sup>

By means of the expression  $\Delta F^\circ = -RT \ln P_{\text{In}_2\text{S}}^{(1-x)/2} P_{\text{S}_2}^{(3x-1)/4}$ , the free energy of formation per gram-atom was calculated for the indium sesquisulfide solid solution region as a function of composition. These free energies can be combined with data that we have reported for the stability of  $\text{In}_2\text{S}$  gas<sup>2</sup> to yield the free energy of formation of the indium sesquisulfide phase as a function of composition, *i.e.*, for the reaction



The results are shown in Figure 4 as solid lines.

The slope of a  $\Delta F^\circ$  *vs.* composition plot for (5) should change smoothly with temperature and must always have a positive curvature<sup>11</sup> instead of the negative curvature indicated by the experimental data at 873 and 923°K. To obtain values of the proper curvature as a function of composition at 873, 923, 973, and 1023°K. from the experimental curve at 1073°K., the entropy of formation was assumed to be given by

$$S^\circ_{\text{In}_{1-x}\text{S}_x} - (1-x)S^\circ_{\text{In}(l)} - x/2S^\circ_{\text{S}_2} + \Delta S_m^\circ \quad (6)$$

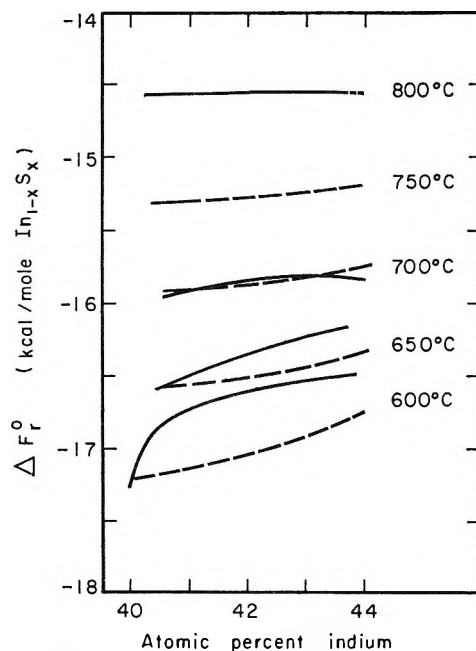


Figure 4. Free energy of formation of indium sesquisulfide as a function of composition and temperature: solid line, calculated from experimental data; dashed line, calculated from solid curve at 800° and the assumption of a model described in text.

where  $S^\circ_{\text{In}_{1-x}\text{S}_x}$  is the weighted average of the entropy of the sesquisulfide phase<sup>12</sup> and of solid indium<sup>13</sup> and where  $\Delta S_m$  is the difference between the entropy of mixing of the elements and vacant lattice sites<sup>14</sup> at the desired composition and at 40 atomic % indium.

The  $\Delta H^\circ$  of formation per mean gram-atom at each composition, which must be essentially temperature independent over the temperature region studied because  $\Delta C_p$  values for condensed-phase reactions are small, was calculated from the expression  $\Delta F^\circ_T = \Delta H^\circ - T\Delta S^\circ_T$  by use of the values of  $\Delta S^\circ$  and  $\Delta F^\circ$  at 1073°K. These values of  $\Delta H^\circ$  can be expressed as  $\Delta H^\circ = 0.37y - 44.3$  (where  $y$  is atomic % indium) for the range 41 to 44 atomic % indium. The heat of formation of stoichiometric  $\text{In}_2\text{S}_3(s)$  from liquid indium and  $\text{S}_2$  gas is then calculated to be  $-147.5 \pm 2$  kcal./g.f.w. The expression for the heat of formation was used with expression 6 to calculate the values of  $\Delta F^\circ$  at various compositions between 40 and 44 atomic % indium (shown as dashed lines in Figure 4). The

(10) A. W. Searcy, *Progr. Inorg. Chem.*, **3**, 46 (1962).

(11) L. S. Darkin and R. W. Gurry, "Physical Chemistry of Metals," McGraw-Hill Book Co., Inc., New York, N. Y., 1953, p. 328.

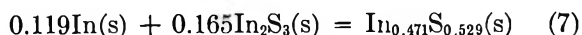
(12) E. G. King and W. W. Weller, U. S. Department of the Interior, Bureau of Mines, Report RI-6040, Pittsburgh, Pa., 1962.

(13) D. R. Stull and G. C. Sinke, *Advances in Chemistry Series*, No. 18, American Chemical Society, Washington, D. C., 1956.

(14) C. J. M. Rooymans, *J. Inorg. Nucl. Chem.*, **11**, 78 (1959).

resultant calculated curves agree with the solid curves to within the experimental error, but the calculated curves probably represent the true composition dependence of  $\Delta F^\circ$  for formation more correctly than do the curves of negative curvature.

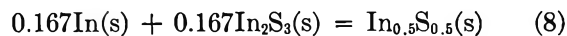
The free energy of formation of  $\text{InS}_{1.12}$  at the sulfur-rich boundary was determined at 873, 923, 973, and 1023°K. by the method used for indium sesquisulfide. The entropy of solid  $\text{InS}_{1.12}$  was estimated by means of the assumption that  $\Delta S$  for reaction 7 is zero. The



heat of formation per mean gram-atom from liquid indium and  $\text{S}_2$  gas was calculated from the free energy of formation and these entropies to be  $-27.5$  kcal. at 873 and 923°K.,  $-27.7$  at 973°K., and  $-28.0$  at 1023°K. A nearly constant value of  $\Delta H = -27.7 \pm 0.3$  kcal./mean g.-atom or  $-58.7 \pm 0.7$  kcal./g.f.w. of  $\text{InS}_{1.12}$  is an indication of internal consistency of the data. The free energy of formation per gram-atom can be expressed as  $\Delta F = -22.99 + 7.4 \times 10^{-3}T$  °K. kcal./g.f.w. Since the  $\text{InS}_{1.12}$  phase is only 1 to 3 atomic % wide,  $\Delta F$  and  $\Delta H$  for formation per gram-atom must be essentially constant with composition across the phase.

The heat and free energy of formation of  $\text{InS}$  from liquid indium and  $\text{S}_2$  gas were calculated at 873, 923, and 973°K. at the sulfur-rich boundary using the  $\text{In}_2\text{S}$  (g) and  $\text{S}_2$ (g) partial pressure in the two-phase region between  $\text{InS}_{1.12}$  and  $\text{InS}$ . The  $\text{S}_2$ (g) partial pressure was calculated from the measured  $\text{In}_2\text{S}$ (g) partial pressure and the free energy of formation of the  $\text{InS}_{1.12}$  phase. (The intensities of  $\text{S}_2^+$  were just measurable at 923 and 973°K. The measured  $\text{S}_2^+$  intensities gave free energy values 0.3 and 0.1 kcal./mean g.-atom less negative than values for calculated  $\text{S}_2$  pressures at 923 and 973°K., respectively.)

The free energy of formation, determined in the same manner as for the other phases, was found to be  $-15.9$ ,  $-15.7$ , and  $-15.4$  kcal./mean g.-atom at 873, 923, and 973°K., respectively. The entropy of solid  $\text{InS}$  was estimated by means of the assumption that  $\Delta S$  for reaction 8 is zero. The heat of formation was



calculated from the free energy of formation and these entropies. A nearly constant value of  $\Delta H = -26.5 \pm 0.3$  kcal./mean g.-atom or  $-53.0 \pm 0.6$  kcal./g.f.w. of  $\text{InS}$  was obtained.

# A Radiotracer Study of Competitive Adsorption at the Gold-Oil Interface<sup>1</sup>

by Morris L. Smith, Benjamin E. Gordon, and Richard C. Nelson

Shell Development Company, Emeryville, California (Received May 21, 1965)

The adsorption characteristics of an oleophilic detergent, calcium dinonylnaphthalenesulfonate tagged with radioactive sulfur-35, have been determined at the gold-white oil interface at room temperature. The adsorption increases with time, requiring 150 min. to reach a maximum value. The adsorption is completely reversible, and exchange with untagged sulfonate is observed. The force-area curve of the sulfonate at the air-water interface yields  $125 \text{ \AA}^2/\text{molecule}$  for a tightly packed film. Displacement of the adsorbed calcium dinonylnaphthalenesulfonate from the gold was achieved by using two nonionic polymeric detergents: (1) a polydisperse polyalcohol prepared by hydrolysis of a polyacetate made by copolymerizing vinyl acetate and  $C_8$ - $C_{18}$   $\alpha$ -olefins; and (2) a monodisperse polyester, poly(dodecyl methacrylate). The sulfonate-polymer competition is analyzed in terms of Langmuirian adsorption resulting in a close fit of the experimental data. A linear relation is obtained for a plot of the ratio of the surface coverage for each component *vs.* the ratio of their solution concentrations. The slopes of the lines are a measure of the relative "surface activity" of the two components. A comparison by weight shows that surface activity increases in the order: polyester < sulfonates < polyalcohol. However, the relative surface activity of the different polar groups (or adsorption sites for the polymers) increases in the order: ester < secondary alcohol < sulfonate.

## A. Introduction

Among the modern methods available for investigating interactions at surfaces, the use of radioactive tracer techniques has enjoyed considerable expansion in the last decade.<sup>2</sup> Since the adsorption of molecules on a metal surface is a subject of both practical and fundamental interest, studies of long-chain organic polar compounds tagged with  $C^{14}$  or  $H^3$  have received much attention.<sup>3-7</sup>

The current interest in detergency in the petroleum industry, particularly with respect to high molecular weight nonionic detergents, has led to several investigations of macromolecule adsorption at the solid-liquid interface.<sup>8-15</sup> Most of these works have dealt with single-solute systems in which the adsorbed film consisted of surfactant and solvent. However, of critical interest is the behavior of mixed films at the solid-liquid interface. Although the literature abounds with studies of mixed films at liquid-air and liquid-liquid interfaces, the data available for solid-liquid interfaces are meager. In any study of mixed films, the competition for a limited surface is of importance,

for by a detailed analysis the relative "strength of adsorption" of the components may be assessed.

The present study was initiated with this in mind and since the use of radiotracers is useful to this type of in-

(1) Presented in part at the 140th National Meeting of the American Chemical Society, Division of Colloid and Surface Chemistry, Chicago, Ill., Sept. 1961.

(2) J. T. Davies and E. K. Rideal, "Interfacial Phenomena," Academic Press Inc., New York, N. Y., 1963.

(3) (a) H. A. Smith and K. A. Allen, *J. Phys. Chem.*, **58**, 499 (1954); H. A. Smith and R. M. McGill, *ibid.*, **61**, 1025 (1957); H. A. Smith and T. Fort, Jr., *ibid.*, **62**, 519 (1958); (b) E. Rideal and J. Tadayon, *Proc. Roy. Soc. (London)*, **A225**, 346 (1954).

(4) J. W. Shepard and J. P. Ryan, *J. Phys. Chem.*, **60**, 127 (1956); **63**, 1729 (1959).

(5) H. E. Ries, Jr., and H. D. Cook, *J. Colloid Sci.*, **9**, 535 (1954); *J. Phys. Chem.*, **63**, 226 (1959).

(6) D. C. Walker and H. E. Ries, Jr., *J. Colloid Sci.*, **17**, 789 (1962).

(7) H. Schonhorn, *ibid.*, **18**, 445 (1963).

(8) J. Koral, R. Ullman, and F. R. Eirich, *J. Phys. Chem.*, **62**, 251 (1958).

(9) J. S. Binford, Jr., and A. M. Gessler, *ibid.*, **63**, 1376 (1959).

(10) H. L. Frisch, M. Y. Hellman, and J. L. Lundberg, *J. Polymer Sci.*, **38**, 441 (1959).

(11) F. M. Fowkes, M. J. Schick, and A. Bondi, *J. Colloid Sci.*, **15**, 531 (1960).

vestigation,<sup>16</sup> this sensitive, unambiguous technique was employed. Calcium dinonylnaphthalenesulfonate tagged with sulfur-35 was chosen as a reference since this compound approximates the present-day detergent petroleum sulfonates.<sup>17-18</sup> Two nonionic surface-active polymers were chosen for comparison: (1) a polydisperse polyalcohol prepared by hydrolysis of the product obtained from the copolymerization of vinyl acetate and C<sub>8</sub>-C<sub>18</sub>  $\alpha$ -olefins; and (2) a monodisperse polyester, poly(dodecyl methacrylate). Gold was chosen as the metallic substrate because of its low reactivity; *i.e.*, it uniquely does not chemisorb oxygen<sup>19</sup> although physical adsorption must certainly occur.

## B. Experimental Section

1. *Materials.* a. *Solvent.* The oil used as solvent was a highly refined naphthenic white oil which was freshly chromatographed through dry silica gel immediately prior to use.

b. *Calcium Dinonylnaphthalenesulfonate-S<sup>35</sup>.* Dinonylnaphthalene (b.p. 210-215 at 0.1 mm.) was obtained from a distillation of crude nonylated naphthalene (from R. T. Vanderbilt Co., Inc.) through a 900  $\times$  14 mm. Martin spinning-band column. Ultraviolet analysis showed the product to be greater than 95% disubstituted, with impurities consisting mainly of mono- and trinylated naphthalene. Although the structure of the dinonylnaphthalene is not precisely known, the two nonyl groups (from 1- $\alpha$ -nonenes derived from propylene trimerization) have been shown by infrared spectra to be substituted into the same ring, which is different from that containing the sulfonate group. The redistilled dinonylnaphthalene (0.1 mole) was then sulfonated with 0.065 mole of 101% sulfuric acid containing 110 mc. of S<sup>35</sup> as sulfuric acid. After neutralization of the reaction mixture with sodium hydroxide, the sodium sulfonates were separated from the unreacted starting material on a Florisil chromatographic column. The eluent for the sulfonate was a 50:50 mixture of dry benzene and methanol. The sodium sulfonates were converted to the calcium salt by treating a hot solution of 10% aqueous isopropyl alcohol with excess calcium chloride and washing the precipitate with water until the washings gave no evidence of reaction with silver nitrate.

The product was dried in a vacuum oven at 110° for 48 hr. and was a dry, light tan powder with specific activity of 3.69 mc./g. (determined by liquid scintillation counting techniques using standards). The infrared spectrum was identical with that of known calcium dinonylnaphthalenesulfonate whose preparation and characterization have been described.<sup>20</sup> The

yield based on sulfuric acid was 36.2% of the theoretical amount.

*Anal.* Calcd. for C<sub>56</sub>H<sub>86</sub>CaS<sub>2</sub>O<sub>6</sub>: C, 70.05; H, 8.99; Ca, 4.18; S, 6.69. Found: C, 69.69; H, 8.80; Ca, 4.10; S, 6.42.

c. *Stearic acid-1-C<sup>14</sup>* was purchased from Tracerlab, Inc., and was used without further purification (m.p. 69.5). The specific activity was found to be 4.42 mc./g.

d. *The polyalcohol* used in these studies was characterized and discussed in detail in a previous paper.<sup>11</sup> This polymer is the unfractionated product from the hydrolysis of the copolymerization of a C<sub>8</sub>-C<sub>18</sub>  $\alpha$ -olefin and vinyl acetate. The average molecular weight in chloroform is 20,000 as determined by the ultracentrifuge. The average distribution of monomers was determined as four hydroxyls per  $\alpha$ -olefin. The "equivalent weight" of the polymer is then assigned as 424, the equivalents per mole as 47, and the number of hydroxyls per molecule as 188.

e. *The poly(dodecyl methacrylate)* was prepared by radical polymerization of redistilled dodecyl methacrylate in benzene initiated by  $\alpha, \alpha'$ -azodiisobutylnitrile. The unreacted monomer was removed by dissolution of the crude product followed by methanol-induced precipitation of the polymer. This was repeated several times followed by drying the finished polymer in a vacuum oven at 60° for several hours. The weight-average molecular weight in chloroform is 50,000 as determined by the ultracentrifuge. The "equivalent weight" of the polymer was 254 (mole weight of dodecyl methacrylate), and each polymer has ca. 196 ester groups per molecule.

2. *Apparatus.* The detector for measuring the adsorption of the tagged sulfonate was a modification of that originally suggested by Cook.<sup>21</sup> It consisted of a conventional Tracerlab TGC-2 Geiger counter in which the mica window had been replaced by a thin

(12) B. J. Fontana and J. R. Thomas, *J. Phys. Chem.*, **65**, 480 (1961); B. J. Fontana, *ibid.*, **67**, 2360 (1963).

(13) C. Peterson and T. K. Kwei, *ibid.*, **65**, 1330 (1961).

(14) A. Silberberg, *ibid.*, **66**, 1872, 1884 (1962).

(15) R. R. Stromberg, E. Passaglia, and D. J. Tutas, *J. Res. Natl. Bur. Std.*, **A67**, 431 (1963); R. R. Stromberg and W. H. Grant, *ibid.*, **A67**, 601 (1963); R. R. Stromberg, W. H. Grant, and E. Passaglia, **A68**, 391 (1964).

(16) K. Shinoda and K. Kinoshita, *J. Colloid Sci.*, **18**, 174 (1963); K. Shinoda and J. Nakanishi, *J. Phys. Chem.*, **67**, 2547 (1963).

(17) F. M. Fowkes, *ibid.*, **67**, 1094 (1963).

(18) S. Kaufman and C. R. Singleterry, *J. Colloid Sci.*, **12**, 465 (1957).

(19) B. M. W. Trapnell, *Proc. Roy. Soc. (London)*, **A218**, 566 (1953).

(20) F. M. Fowkes, *J. Phys. Chem.*, **66**, 1843 (1962).

(21) H. D. Cook, *Rev. Sci. Instr.*, **27**, 1081 (1956).

(0.8 mg./cm.<sup>2</sup>) Mylar polyester film secured with EPON<sup>®</sup> resin glue. The gold was vacuum evaporated onto the Mylar and stored in a vacuum desiccator until use. While protected from gross contaminants in this way, the gold film presumably is covered with a physically adsorbed mixed layer of water and atmospheric gases. Nevertheless, the reproducibility of the isotherms was excellent at  $\pm 2\%$ . The entire tube was flushed with counting gas through two appropriately situated side arms. A constant rate of flow of gas was maintained through the tube at a pressure of 25 mm. of water above atmospheric. The geometric area of the gold film was 8 cm.<sup>2</sup>, and each surface was used only once.

The signal from the counter was measured by a Tracerlab SC-18A Superscaler driving a Tracerlab SC-5F Tracergraph printing interval timer. With these instruments, the time required to reach a preset number of counts was printed on a tape followed by automatic resetting to zero between each interval. This assembly was much more precise than a rate meter and allowed data to be collected automatically at short intervals over extended periods.

3. *Procedures.* a. *Adsorption studies* were carried out by inserting the counter into the solution of the radioactive sulfonate contained in a Teflon beaker. Concentrations from 0.001 to 0.300% weight were studied, and all gave the same saturation value. As the radioactive surfactant was deposited on the gold, the increase in counting rate with time was followed until the rate became constant. This increase could be observed because of the very short range of the S<sup>35</sup>  $\beta$  particles, *i.e.*, about 0.1 mm. in oil; the bulk of the activity in the solution did not contribute to the solution background. A solution concentration of 0.030% weight gave the most convenient counting rate and was used for most experiments. All experiments were at room temperature ( $22 \pm 1^\circ$ ).

b. *The thickness of the gold film* was measured by (1) directly weighing the amount deposited on a known area and (2) by  $\beta$ -ray adsorption of a standard C<sup>14</sup> source. Both of these methods gave gold-film thicknesses of 500–1000 Å. An electron micrograph showed the average size of the gold particles to be only 20–40 Å. in diameter, making it highly probable that the film was continuous and none of the Mylar backing was exposed. From these considerations, it was valid to assume that the gold film was sufficiently thick to serve as an infinitely thick layer of metal.

c. *Determination of the roughness factor* was achieved by depositing a monolayer of stearic acid-1-C<sup>14</sup> on the gold film from its melt at the melting point of the acid by the method of Zisman.<sup>22</sup> The method of the

molten drop ensured as nearly as possible the deposition of a condensed monolayer without concomitant problems arising from solvation of the carboxyl group or the "carry-out" difficulties noted by others.<sup>2,4,5</sup> A direct count yielded the amount of acid absorbed. As a check on the mechanical technique, the acid layer was then desorbed in 200 ml. of reagent toluene, and the total acid initially adsorbed in the monolayer was found by extrapolation of the desorption curve to zero time. These two numbers agreed to within 5%, but better precision was obtained with the extrapolated value for the monolayer. Consequently, the desorption curve value was used in the following roughness factor calculation. From the chosen value of 24 Å.<sup>2</sup> for the cross-sectional area of the carboxyl group, the true area of the gold film was calculated to be  $9.9 \times 10^{16}$  Å.<sup>2</sup> compared to the geometric area of  $8 \times 10^{16}$  Å.<sup>2</sup>. Thus, the roughness factor was 1.2 based on the stearic acid. This factor was used in the calculations on calcium dinonylnaphthalenesulfonate.

d. *The force-area curve* for calcium dinonylnaphthalenesulfonate spread from benzene solution on a 1 M aqueous solution of calcium chloride was carried out on a recording surface balance<sup>23</sup> thermostated at 25°. No significant hysteresis was noted with this sulfonate. The reproducibility of the curve in Figure 1 is about 90% at film pressures less than 10 dynes/cm. but rises to 97% at film pressures greater than 30 dynes/cm.

e. *The specific activity* of the sulfonates in terms of Geiger counter efficiency was determined by spreading 25 to 100  $\mu$ g. in benzene onto the slightly depressed gold-film tube followed by subsequent evaporation of the benzene. The specific activity was 972 c.p.m./ $\mu$ g. It was found that self-adsorption was not serious until a total deposit of at least 1000  $\mu$ g. was present.

f. *Competition Experiments.* The radioactive sulfonate was adsorbed on the gold film from white oil, and the counting rate was followed until equilibrium was reached. Known amounts of the inactive polymer were added from a concentrated stock solution in white oil, and the resulting decrease, if any, in counting rate attendant upon each increment of added polymer was recorded. There was a several thousandfold excess of both materials present at all concentration ratios above that required to cover the gold surface completely. The volume of the added solution was so small (the total of all additions in any one run was less than 1.5 ml.) that the concentration of the original

(22) R. L. Cottingham, E. G. Shafrin, and W. A. Zisman, *J. Phys. Chem.*, **62**, 513 (1958).

(23) M. J. Schick, *J. Polymer Sci.*, **25**, 465 (1957).

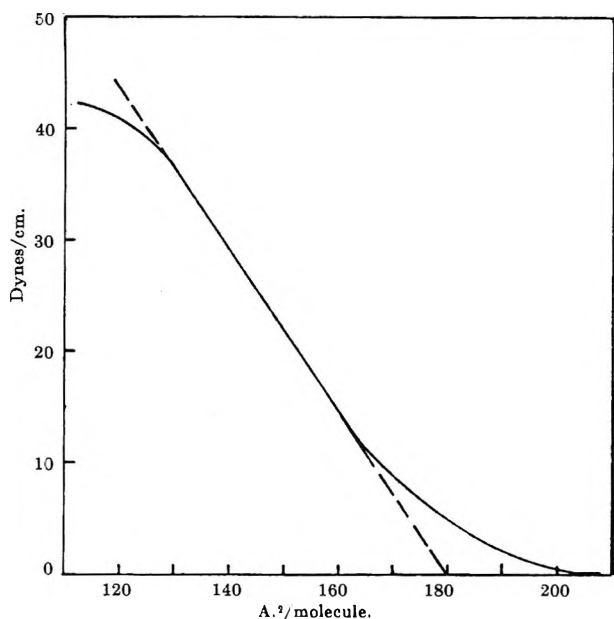


Figure 1. Force-area curve of calcium dinonylnaphthalenesulfonate at air-water interface ( $1 M \text{ CaCl}_2$ ).

test solution remained sensibly constant. Sufficient time elapsed (25–48 hr.) between each addition to ensure that all data represented the equilibrium state.

## Results and Discussions

1. *Force-Area Curve.* The force-area curve of calcium dinonylnaphthalenesulfonate at the water-air interface is shown in Figure 1. Sufficient similarity in the structure of adsorbed films is generally found between different interfaces to justify some extrapolation from one to the other. The shape of the curve indicates that the film is of the liquid-expanded type showing a maximum area per molecule of  $200 \text{ \AA}^2$ . The area per molecule when the film is tightly packed is about  $125 \text{ \AA}^2$  at 40 dynes/cm.

2. *Adsorption Curves.* A typical adsorption curve obtained with the calcium dinonylnaphthalenesulfonate- $\text{S}^{35}$  in white oil is shown in Figure 2. The time required to reach apparent maximum adsorption varied from ca. 4500 min. with no stirring to ca. 100 min. with rapid stirring. The reasons for these extremely slow adsorption times (compared to diffusion times) are not really understood, but have often been observed in solid-liquid solutions. Fowkes has noted this same phenomenon in rates determined by orientation potentials at the metal-ion interface.<sup>24</sup>

The adsorption was shown to be reversible by replacing the active solution with a new solution containing nonradioactive calcium dinonylnaphthalene-

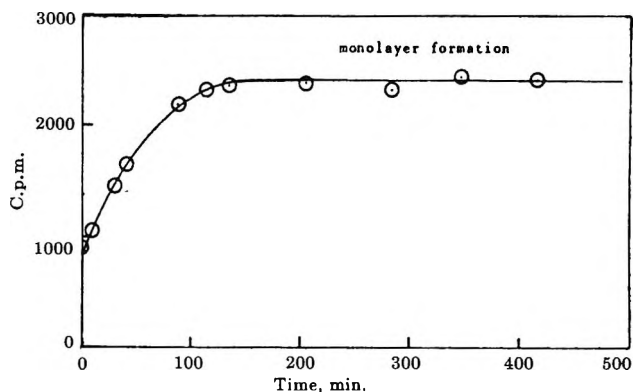


Figure 2. Adsorption of calcium dinonylnaphthalenesulfonate at gold-white oil interface: stirring in oil, at room temperature.

sulfonate and observing the drop in counting rate to near background. Upon exchange of the solution again, the counting rate increased once more to the value illustrated by the plateau in Figure 2.

3. *Monolayer Formation.* From the net increase in counting rate illustrated in Figure 2 (1440 c.p.m.), the specific activity ( $975 \text{ c.p.m./}\mu\text{g.}$ ), the area per molecule ( $125 \text{ \AA}^2$ ), and the roughness factor (1.2), the number of monolayers is 1.25. Values ranging from 1.20 to 1.35 were obtained many times on different tubes. In the monolayer calculation, there is some uncertainty in the choice of  $125 \text{ \AA}^2$  as the size of the molecule since the area is quite dependent on the film pressure. No information on film pressures at the gold-oil interface is available, so the point of film collapse was chosen for the calculation.

In light of these uncertainties and those inherent in the roughness factor evaluation, these values establish that the film is essentially a monolayer.

4. *Competition Studies.* Figure 3 illustrates the displacement of the preadsorbed sulfonates from gold by the polyalcohol and the polyester. Since only the sulfonates are radioactive, the activity observed at any time should be proportional to the area occupied by this compound; the amount covered by the polymer is determined by difference. The concentrations studied are listed in Table I.

If the Langmuir adsorption theory is applied to the "idealized" system represented by a gold surface, then for the  $i$ th component in a mixture of  $n$  components, all of which are simultaneously adsorbing, the rate of adsorption is

$$\text{adsorption rate} = k_i C_i (1 - \theta_1 + \theta_2 + \dots + \theta_n) \quad (1)$$

and for desorption, the rate is merely

(24) F. M. Fowkes, *J. Phys. Chem.*, **64**, 726 (1960).

$$\text{desorption rate} = k_{-i}\theta_i \quad (2)$$

Analogously after Langmuir, at equilibrium we have

$$k_i C_i (1 - \theta_1 + \theta_2 + \dots + \theta_n) = k_{-i} \theta_i \quad (3)$$

Now let  $K_i = k_i/k_{-i}$  be a measure of the "surface activity" of the  $i$ th component, and the general expression for the isotherm becomes

$$K_i C_i = \theta_i / (1 - \sum \theta_n) \quad (4)$$

which reduces simply to the classical Langmuir expression when  $n = 1$ . For two competing species, the relationship may be expressed as

$$\frac{\theta_i}{\theta_j} = \frac{K_i C_i}{K_j C_j} \quad (5)$$

with the slope of the line,  $K_i/K_j$ , being equal to the "relative surface activity" of  $i$  to  $j$ . If  $A_1$  is the radioactivity when only component 1 is adsorbed and  $A$  the observed activity when both 1 and 2 are adsorbed and only 1 is radioactive, then eq. 5 is expressed in experimental terms as

$$\frac{A_1 - A}{A} = \frac{K_2 C_2}{K_1 C_1} \quad (6)$$

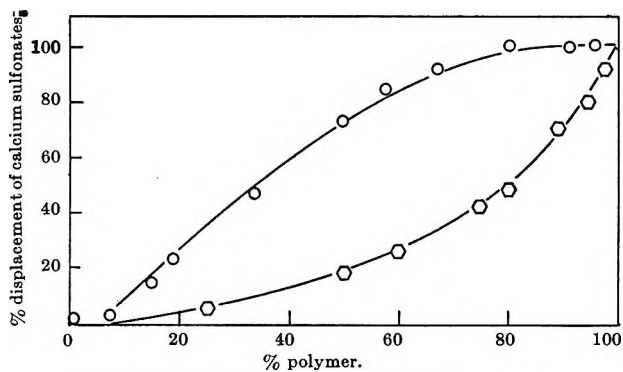


Figure 3. Gold-oil interface, at 21°, the effect of increasing polymer concentration to displace calcium dinonylnaphthalenesulfonates: O, polyalcohol; □, polyester.

Table I: Competitive Concentrations of Polymers<sup>a</sup>

Poyalcohol, g. × 10 <sup>-3</sup> in 100 ml.	Polyester, g. × 10 <sup>-3</sup> in 100 ml.
3.1	7.5
6.2	33.0
30.0	45.0
37.5	93.0
52.5	156.0
	282.0

<sup>a</sup> The concentration of calcium dinonylnaphthalenesulfonate was always 30.0 × 10<sup>-3</sup> g./100 ml.

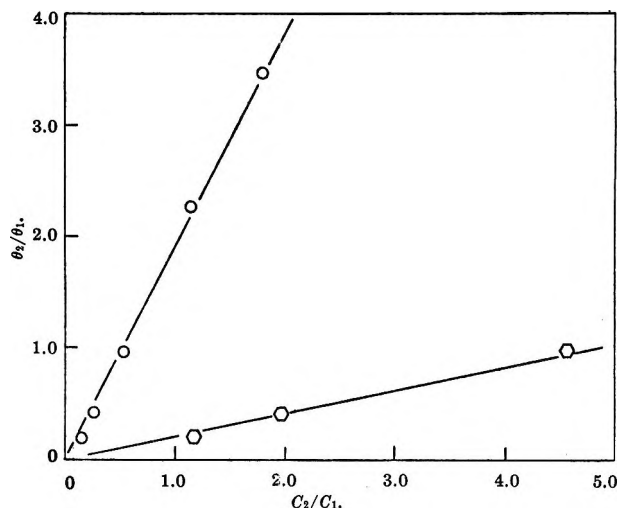


Figure 4. Langmuir plot of polyalcohol (2) vs. calcium dinonylnaphthalenesulfonate: O,  $C_2/C_1$  by weight; □,  $C_2/C_1$  by moles, moles of hydroxyl per moles of sulfonates.

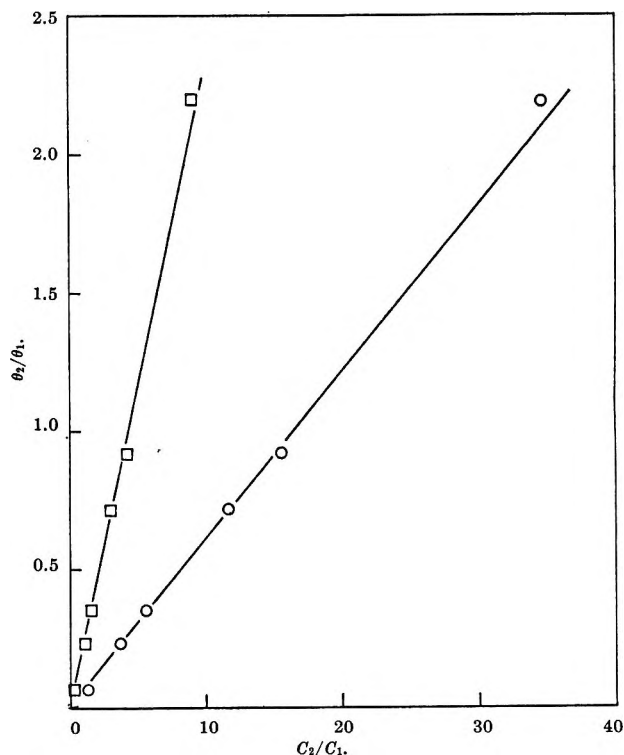


Figure 5. Langmuir plot of poly(dodecyl methacrylate) (2) vs. calcium dinonylnaphthalenesulfonate: O,  $C_2/C_1$  by weight; □,  $C_2/C_1$  by moles, moles of ester per moles of sulfonates.

The data for the polyalcohol vs. calcium dinonylnaphthalenesulfonate applied through eq. 6 are illustrated in Figure 4. These yield straight lines and exhibit no deviation from linearity even out to 75% displacement of the sulfonate.

When calcium dinonylnaphthalenesulfonate is displaced by poly(dodecyl methacrylate), the Langmuir plot results in Figure 5. Again, the curves are linear up to 70% displacement. The classical interpretation of adsorbed monolayers seems to explain this idealized system adequately even though the competing species are themselves complex.

5. *Surface Activity.* The slopes of the lines of Figures 4 and 5 are measures of the relative "surface activity" of the competing species. Once the values of  $K_2/K_1$  were determined from the experiments, another ratio, *i.e.*, polyester *vs.* polyalcohol, can be obtained indirectly. All of the values of  $K_2/K_1$  are listed in Table II. These values can be expressed in several ways depending on the concentration units chosen. The comparisons have been made by weight and by

theoretical value. The comparison of polar groups is significant, since a frequently cited mechanism of adsorption proposes that these are the sites of adsorption. Studies on the polyalcohol have shown<sup>11</sup> the polymer is uncoiled with most of the hydroxyls present at the interface. From the comparison given here, the relative strengths of adsorption are sulfonates > alcohol > polyester. It would indeed be helpful to be able to relate this order of surface activity to some other independent properties of the surfactants. However, such attempts in the past have resulted in little success.<sup>25,26</sup> It is apparent that numerous variables need be assessed before elucidation of the nature of solid-solution interfacial phenomena is forthcoming. However, the results presented here are gratifying in that relative surface activities have been quantitatively assigned to surfactants in a complex, heterogeneous system.

**Table II:** Relative Strengths of Adsorption,  $K_2/K_1$   
(Gold-Oil Interface, 21°)

Comparison	Weight	Polar group
Polyalcohol <i>vs.</i> Ca sulfonates	1.98	0.21
Polyester <i>vs.</i> Ca sulfonates	0.36	0.06
Polyalcohol <i>vs.</i> polyester	5.50	3.50

polar group. The former comparisons are of interest from an economic viewpoint while the latter possess

*Acknowledgments.* The authors thank F. W. Anderson for preparing the gold-filmed Geiger counters and examining this surface with the electron microscope. They also much appreciate the aid received from Dr. F. M. Fowkes during numerous discussions.

(25) See J. Arnold, *J. Am. Chem. Soc.*, **61**, 1911 (1939), for other leading references.

(26) B. Eric, E. V. Goode, and D. A. Ibbitson, *J. Chem. Soc.*, 55 (1960).



# The Thermodynamic Properties and Allotropy of Beryllium Chloride

between 13 and 715°K.<sup>1</sup>

by R. A. McDonald and F. L. Oetting

*Thermal Research Laboratory, The Dow Chemical Company, Midland, Michigan (Received May 21, 1965)*

The heat capacities of the  $\alpha'$  and  $\beta$  forms of beryllium chloride have been measured in an adiabatic calorimeter from 13 to 304°K. The absolute entropy at 298.15°K. is  $19.76 \pm 0.06$  cal./mole °K. for the  $\alpha'$  form and  $18.12 \pm 0.05$  cal./mole °K. for the  $\beta$  form. Using a copper block drop calorimeter, enthalpies were determined for the  $\beta$  form (relative to the  $\beta$  form) from 298 to 676°K., the  $\alpha$  form (relative to the  $\alpha'$  form) from 676 to 688°K., and the liquid (relative to the  $\alpha'$  form) from 688 to 713°K. The  $\alpha'$  form and the  $\alpha$  form are considered to be identical. The heat of the  $\alpha$ - $\beta$  transition at 676°K. was calculated to be  $1490 \pm 150$  cal./mole. The heat of fusion of the  $\alpha$  form at 688°K. was found to be  $2070 \pm 60$  cal./mole. The thermodynamic properties of beryllium chloride have been tabulated from 0 to 750°K.; the results of phase studies by thermal analysis are presented, and a schematic phase diagram is proposed.

## Introduction

Complete data for the compilation of the thermodynamic properties of beryllium chloride were not available in the literature, and this work was undertaken to measure the low-temperature heat capacity and the high-temperature heat content of beryllium chloride and to study further the allotropy of beryllium chloride.

Several different values have been published for the melting and transition temperatures of  $\text{BeCl}_2$ . Schmidt<sup>2</sup> found a melting point of 404° and a solid state transition on cooling at about 300°. His time vs. temperature cooling curve indicated the heat of transition to be greater than the heat of fusion. Klemm<sup>3</sup> reported a melting point equal to or less than  $416 \pm 2^\circ$ . Rahlfs and Fischer<sup>4</sup> determined  $405 \pm 1^\circ$  for the melting point and 3000 cal./g.f.w. for the heat of fusion. From melting point data covering a range from 395.5 to 403°, Furby and Wilkinson<sup>5</sup> chose a value of  $399 \pm 1^\circ$ . They also found a solid state transition at approximately 335° on cooling, but no relative comparison of the heats of fusion and transition was made.

Kuvyrkin, Breusov, Novoselova, and Semenenko<sup>6</sup> have reported the existence of at least three polymorphs of beryllium chloride. (This work is also mentioned in an earlier paper on the thermal analysis

of the  $\text{BeCl}_2$ - $\text{BeF}_2$  system by Kuvyrkin, Breusov, and Novoselova.<sup>7</sup>) According to these authors a metastable  $\alpha'$  form of  $\text{BeCl}_2$  is obtained by rapid cooling of the melt or by sublimation. The  $\alpha'$  modification has an orthorhombic, body-centered structure analogous to silicon sulfide<sup>8</sup> and, when heated, changes to the cubic  $\beta'$  form which is stable in the range of 250 to 340°. At 340° the  $\beta'$  form changes to the stable  $\beta$  form which is body-centered rhombic. The  $\beta$  form then changes, at 405°, to the  $\alpha$  form which melts at 425°. The stable  $\beta$  form is obtained by the slow cooling of the melt. The authors also suggested that the  $\alpha'$  form and the  $\alpha$  form might be identical. The transitions at 250 and 340° were observed to be exothermic on heating and

(1) This work was supported by the Advanced Research Projects Agency under U. S. Air Force Contract No. AF04(611)-7554(1).

(2) J. M. Schmidt, *Bull. soc. chim. France*, [4]39, 1686 (1926).

(3) W. Klemm, *Z. anorg. allgem. Chem.*, 152, 235 (1926).

(4) O. Rahlfs and W. Fischer, *ibid.*, 211, 349 (1933).

(5) E. Furby and K. L. Wilkinson, *J. Inorg. Nucl. Chem.*, 14, 123 (1960).

(6) O. N. Kuvyrkin, O. N. Breusov, A. V. Novoselova, and K. N. Semenenko, *Zh. Fiz. Khim.*, 34, 343 (1960).

(7) O. N. Kuvyrkin, O. N. Breusov, and A. V. Novoselova, *Nauchn. Dokl. Vysshei Shkoly, Khim. i Khim. Tekhnol.*, 660 (1958).

(8) R. E. Rundle and P. H. Lewis, *J. Chem. Phys.*, 20, 132 (1952).

were classed as monotropic; the transition at 405° was endothermic on heating and was classed as enantiotropic. Only one exothermic effect was noted on cooling the melt, corresponding to solidification, and on reheating only the enantiotropic transition at 405° and the fusion at 425° appeared. The accuracy of the temperature measurements is stated to be  $\pm 5^\circ$ .

### Experimental Section

**Materials.** Four samples of beryllium chloride were used as the investigation developed and the different samples became available. Sample 1 had been purified by sublimation from crude beryllium chloride purchased from The Beryllium Corp. X-Ray diffraction showed this sublimed product to be about 50%  $\alpha'$  and 50%  $\beta$  form. (The designations of Kuvyrkin, *et al.*,<sup>6</sup> for the various polymorphs of beryllium chloride will be used throughout this paper.) However, only the  $\alpha'$  form was found after this sample had been melted and cooled rapidly in the drop calorimeter.

Samples 2a and 2b were taken from the same shipment of beryllium chloride from the Nuclear Materials and Equipment Corp., although from different bottles and at different times. Sample 2a was all  $\alpha'$  form and was used for the low-temperature studies. Sample 2b, taken about 20 months later, was about 95%  $\alpha'$  and 5%  $\beta$  form when placed in the drop calorimeter sample capsule. Only the  $\alpha'$  form was found after "quenching" from the supercooled  $\alpha$  state in the drop calorimeter.

Sample 3, all  $\beta$  form, was again from The Beryllium Corp.

The samples were analyzed using several methods. Method 1 assayed beryllium by the volumetric sodium fluoride method and chloride by the potentiometric silver nitrate method; method 2 assayed beryllium gravimetrically as the oxide and chloride by the volumetric Volhard method; method 3 assayed beryllium gravimetrically as the oxide and chloride gravimetrically as silver chloride; method 4 assayed beryllium spectrophotometrically with 4-(*p*-nitrophenylazo)-ornicol (Zenia) and chloride by the Volhard method. The sample assays are given in Table I.

Table I: Assay of Beryllium Chloride

Method <sup>a</sup>	Theory	Sample 1			Sample 2a	Sample 2b	Sample 3
		1	2	3 <sup>b</sup>	4	2 <sup>b</sup>	2
% Be	11.28	11.26	11.48	11.42	11.18	11.59	11.54
% Cl	88.72	88.53	88.65	85.40	88.85	87.90	88.49
Total	100.00	99.79	100.13	96.82	100.03	99.49	100.03

<sup>a</sup> See text for description of methods. <sup>b</sup> Assayed after heat content measurements. A small amount of the sample was insoluble in water.

**Low-Temperature Heat Capacity.** The adiabatic low temperature calorimeter previously described<sup>9</sup> was used to measure the heat capacities of both the  $\alpha'$  form and the  $\beta$  form of beryllium chloride. Two series of measurements were made on a 33.613-g. portion of sample 2a ( $\alpha'$ ), and three series of measurements were made on a 54.494-g. portion of sample 3 ( $\beta$ ). A gram molecular weight of 79.927 was used for beryllium chloride. One calorie is defined to be equivalent to 4.1840 absolute joules, and the ice point is taken to be 273.15°K. One atmosphere of helium gas was admitted to the sample container before closing to serve as a heat-exchange medium, and all results were corrected for the helium present. Any change in weight of solder used to seal the container was accounted for in making the container correction. All weights were corrected to weight under vacuum.

The analysis of sample 3, 11.54  $\pm$  0.10% Be and 88.49  $\pm$  0.15% Cl, high in beryllium and low in chlorine, is consistent with a composition of 99.72 wt. %  $\beta$ -BeCl<sub>2</sub> and 0.28 wt. % Be metal. The observed heat capacities were corrected for the presence of beryllium metal using the data of Hill and Smith,<sup>10</sup> assuming the heat capacities to be additive. This is a correction of about 0.6% at 300°K.

**Heat Content.** The heat content,  $H_T - H_{298.15^\circ\text{K.}}$ , was measured from 279 to 713°K. using a copper block drop calorimeter described elsewhere.<sup>11</sup> Two series of measurements were made. For series I, a 3.264-g. portion of sample 1 was transferred to a platinum-10% rhodium alloy capsule (15.321 g.) in a drybox, and the loaded capsule with its close-fitting bottom was quickly moved to a welding chamber for sealing by arc welding under a helium pressure of about 8 cm. The sealed capsule was heated for 2 hr. at 450° in a hood as a safety check for leaks in the capsule weld. Thus, the sample was melted and frozen before any heat content measurements were made, and for this reason the first X-ray analysis of sample 1 showing a 50-50 mixture of  $\alpha'$  and  $\beta$  forms most probably does not pertain to any of the heat content measurements.

For the second series of measurements, a 2.354-g. portion of sample 2b was sealed in a similar manner in another platinum-10% rhodium alloy capsule weighing 13.886 g. However, this time the sample was not heated prior to use in the drop calorimeter in an attempt to obtain some heat content data on the  $\alpha'$  form in the lower drop calorimetry region.

(9) F. L. Oetting and R. A. McDonald, *J. Phys. Chem.*, **67**, 2737 (1963).

(10) R. W. Hill and P. L. Smith, *Phil. Mag.*, **44**, 636 (1953).

(11) R. A. McDonald and D. R. Stull, *J. Chem. Eng. Data*, **6**, 609 (1961).

Table II: Experimental Heat Capacity Data

<i>T</i> , °K.	<i>C<sub>p</sub></i> , cal./ (mole °K.)	<i>T</i> , °K.	<i>C<sub>p</sub></i> , cal./ (mole °K.)	<i>T</i> , °K.	<i>C<sub>p</sub></i> , cal./ (mole °K.)	<i>T</i> , °K.	<i>C<sub>p</sub></i> , cal./ (g. °K.)	<i>T</i> , °K.	<i>C<sub>p</sub></i> , cal./ (g. °K.)	<i>T</i> , °K.	<i>C<sub>p</sub></i> , cal./ (g. °K.)
α'-BeCl <sub>2</sub> <sup>a</sup>											
Series I						Sample 3 (99.72 wt. % β-BeCl <sub>2</sub> , 0.28 wt. % Be)					
12.93	0.473	174.69	11.85	83.98	7.095	12.70	0.0024	145.94	0.1267	140.83	0.1242
15.26	0.637	181.11	12.12	89.72	7.462	14.70	0.0037	151.11	0.1294	147.28	0.1276
17.21	0.849	199.84	12.79	95.14	7.784	17.00	0.0051	156.18	0.1325	153.59	0.1316
19.22	1.029	205.94	13.02	100.32	7.987	19.27	0.0068	161.17	0.1356	159.76	0.1345
21.15	1.238	211.97	13.22	105.30	8.339	21.24	0.0086	166.07	0.1384	165.81	0.1384
23.22	1.420	217.94	13.44	110.10	8.669	23.22	0.0105	171.48	0.1409	171.75	0.1412
25.70	1.651	224.93	14.20	114.74	8.944	25.28	0.0129	177.30	0.1440	177.61	0.1441
28.54	1.979	246.93	14.35	119.27	9.135	27.27	0.0149	188.68	0.1504	183.76	0.1478
31.50	2.281	252.61	14.48	123.69	9.372	29.57	0.0182	194.27	0.1528	190.22	0.1508
34.51	2.649	258.26	14.77	128.01	9.603	32.03	0.0214	199.78	0.1553	221.28	0.1638
37.81	3.029	269.42	14.96	132.23	9.898	34.52	0.0249	205.83	0.1579	227.28	0.1665
41.69	3.360	274.95	15.04	137.39	10.19	37.44	0.0292	212.39	0.1606	249.04	0.1732
50.84	4.211	280.45	15.20	143.45	10.48	40.96	0.0338	218.88	0.1633	256.42	0.1764
56.08	4.797	285.92	15.38	149.39	10.77	45.03	0.0387	225.30	0.1656	Series III	
61.62	5.322	291.75	15.53	155.20	11.06	49.51	0.0439	244.11	0.1718	122.18	0.1114
67.62	5.775	296.75	15.61	167.04	11.60	54.52	0.0501	250.28	0.1735	129.18	0.1167
74.18	6.257	302.12		173.60	11.84	59.63	0.0567	262.50	0.1778	135.93	0.1211
80.68	6.803		Series II	180.05	12.11	65.23	0.0631	268.53	0.1794	142.49	0.1252
86.71	7.213	15.79	0.707	192.65	12.52	76.56	0.0738	274.52	0.1813	148.88	0.1287
98.38	7.946	17.84	0.892	198.86	12.80	82.16	0.0802	286.38	0.1844	155.13	0.1330
104.69	8.290	19.96	1.116	204.98	12.98	87.99	0.0858	292.24	0.1862	161.25	0.1359
110.71	8.678	22.15	1.340	211.04	13.22	94.08	0.0904	298.06	0.1878	195.90	0.1536
116.51	8.973	24.53	1.577	217.03	13.39	99.85	0.0947	303.84	0.1894	201.41	0.1558
122.11	9.292	29.72	2.079	251.83	14.32	105.89	0.0991		Series II	246.74	0.1728
127.55	9.589	32.85	2.450	257.50	14.48	112.20	0.1044	103.70	0.0979	254.14	0.1754
132.86	9.897	36.18	2.812	268.71	14.81	118.25	0.1082	110.13	0.1029	261.48	0.1777
138.03	10.15	39.98	3.274	274.25	14.95	124.10	0.1137	116.30	0.1074	275.95	0.1820
143.11	10.37	44.43	3.651	279.78	15.04	135.29	0.1204	122.24	0.1115	283.10	0.1835
148.08	10.65	49.47	4.128	285.26	15.17	140.67	0.1233	128.31	0.1158	297.21	0.1880
152.97	10.85	54.92	4.693	290.72	15.30			134.51	0.1195	304.18	0.1898
157.79	11.09	60.62	5.280	296.13	15.45						
162.52	11.39	66.12	5.685	301.52	15.55						
168.16	11.55	71.65	6.084	306.88	15.68						
		77.81	6.554								

<sup>a</sup> Molecular weight, 79.927.

In each series, correction was made for the heat content of the capsule and for the heat loss during the drop, from previous empty capsule measurements. Correction was also made for heat of sublimation or heat of vaporization using the heat values given by Rahlfs and Fischer<sup>4</sup> and estimating the vapor space in the capsule. Greenbaum, Yates, and Farber<sup>12</sup> report considerably lower solid state vapor pressures and a higher heat of sublimation than do Rahlfs and Fischer, but they do not give any liquid state data. Neither paper mentions crystal form. Since the correction is small, insignificant below 650°K. and never greater than 0.2% in series I or 0.26% in series II, the data of Rahlfs and Fischer are used throughout for possibly better consistency between the solid and liquid state.

Measurements of the heat content of α-aluminum oxide (Calorimetry Conference synthetic sapphire) were also made, some before and some between the beryllium chloride measurements.

*Phase Studies.* At first, thermal analyses were made with the drop calorimeter sample sealed in the capsule by raising it above its normal position in the furnace and binding the platinum *vs.* platinum-10% rhodium furnace thermocouple junction to the side of the capsule with a fine platinum wire, the junction being located below the level of the melt.

Then observations were made with beryllium chlo-

(12) M. A. Greenbaum, R. E. Yates, and M. Farber, *J. Phys. Chem.*, **67**, 1802 (1963).

Table III: Thermodynamic Functions<sup>a</sup>

$T$ , °K.	$C_p$ , cal./ (mole °K.)	$S^\circ$ , cal./ (mole °K.)	$-(F_T - H_0)/T$ , cal./((mole °K.)	$H_T - H_0$ , cal./mole	$T$ , °K.	$C_p$ , cal./ (mole °K.)	$S^\circ$ , cal./ (mole °K.)	$-(F_T - H_0)/T$ , cal./((mole °K.)	$H_T - H_0$ , cal./mole
$\alpha'$ -BeCl <sub>2</sub> <sup>b</sup>					35	2.038	0.898	0.257	22.5
13	0.476	0.162	0.040	1.6	40	2.610	1.208	0.356	34.1
15	0.641	0.241	0.062	2.7	45	3.138	1.546	0.469	48.5
20	1.114	0.489	0.136	7.1	50	3.647	1.904	0.595	65.4
25	1.605	0.790	0.236	13.9	55	4.137	2.274	0.730	84.9
30	2.130	1.129	0.356	23.2	60	4.606	2.654	0.875	106.8
35	2.689	1.499	0.493	35.2	70	5.496	3.433	1.185	157.4
40	3.217	1.893	0.643	50.0	80	6.259	4.217	1.515	216.2
45	3.718	2.301	0.804	67.3	90	6.951	4.995	1.858	282.3
50	4.202	2.717	0.975	87.1	100	7.595	5.761	2.210	255.1
55	4.691	3.141	1.152	109.4	110	8.202	6.514	2.567	434.1
60	5.144	3.569	1.336	134.0	120	8.771	7.252	2.927	519.0
70	5.968	4.425	1.716	189.6	130	9.344	7.977	3.288	609.6
80	6.747	5.273	2.108	253.2	140	9.857	8.688	3.648	705.6
90	7.541	6.109	2.506	324.3	150	10.33	9.385	4.008	806.6
100	8.045	6.925	2.907	401.8	160	10.78	10.07	4.365	912.1
110	8.619	7.719	3.309	485.1	170	11.21	10.73	4.720	1,022
120	9.189	8.494	3.709	574.2	180	11.62	11.38	5.072	1,136
130	9.740	9.251	4.106	668.9	190	12.02	12.02	5.421	1,254
140	10.26	9.992	4.500	768.9	200	12.38	12.65	5.767	1,377
150	10.76	10.72	4.891	874.0	210	12.73	13.26	6.110	1,502
160	11.24	11.43	5.277	984.1	220	13.03	13.86	6.448	1,631
170	11.68	12.12	5.659	1,099	230	13.32	14.45	6.782	1,763
180	12.07	12.80	6.037	1,218	240	13.60	15.02	7.115	1,897
190	12.46	13.46	6.411	1,340	250	13.86	15.58	7.442	2,035
200	12.80	14.11	6.780	1,466	260	14.11	16.13	7.766	2,175
210	13.14	14.74	7.144	1,596	270	14.34	16.67	8.086	2,317
220	13.46	15.36	7.504	1,729	273.15	14.41	16.83	8.186	2,362
230	13.74	15.97	7.859	1,865	280	14.56	17.19	8.402	2,461
240	14.01	16.56	8.209	2,004	290	14.76	17.71	8.714	2,608
250	14.28	17.14	8.554	2,145	298.15	14.92	18.12	8.965	2,729
260	14.55	17.70	8.895	2,290	300	14.96	18.21	9.022	2,756
270	14.81	18.26	9.232	2,436	350	15.76	20.58	10.51	3,525
273.15	14.89	18.42	9.336	2,484	400	16.42	22.73	11.90	4,330
280	15.06	18.80	9.564	2,586	450	16.96	24.69	13.22	5,166
290	15.31	19.33	9.891	2,738	500	17.40	26.50	14.46	6,024
298.15	15.50	19.76	10.16	2,863	550	17.78	28.18	15.63	6,904
300	15.54	19.85	10.22	2,892	600	18.12	29.74	16.74	7,801
310	15.76	20.37	10.53	3,048	650	18.44	31.20	17.80	8,715
					676( $\beta$ )	18.60	31.93	18.33	9,197
					676( $\alpha$ )	19.39	34.13	18.53	10,687
13	0.209	0.064	0.011	0.7	680	19.41	34.25	18.42	10,764
15	0.300	0.101	0.020	1.2	684	19.42	34.36	18.51	10,842
20	0.600	0.226	0.055	3.4	688( $\alpha$ )	19.44	34.47	18.60	10,920
25	1.008	0.401	0.106	7.4	688(1)	29.02	37.48	18.60	12,990
30	1.499	0.627	0.173	13.6	700	29.02	37.99	18.94	13,338
					750	29.02	39.99	20.27	14,789
$\beta$ - $\alpha$ -BeCl <sub>4</sub> (l)									

<sup>a</sup> To retain internal consistency, some of the values in this table are given to more places than would be justified by experimental accuracy. <sup>b</sup> Molecular weight, 79.927.

ride sealed in quartz tubes with dry air over the sample. The 1.12-cm. o.d. tube was constricted about 3.8 cm. from the bottom and had a small re-entrant well sealed in the bottom to accommodate a thermocouple or a small platinum resistance thermometer. The over-all length of the tube was about 20 cm., a convenient length for sealing and handling. Heating or cooling was done in a special slotted aluminum block furnace in a clear-wall dewar vessel so that the sample could be seen at all times. The tube was positioned in the furnace so that the constriction was just out of the furnace, and beryllium chloride sublimate effectively blocked off the tube at this point and prevented loss of sample to colder parts of the tube.

Portions of both sample 1 and sample 2a were run in the quartz tubes.

### Results and Discussion

The observed low-temperature heat capacity values for  $\alpha'$ -beryllium chloride and the specific heat values for sample 3, 99.72 wt. %  $\beta$ -BeCl<sub>2</sub> and 0.28 wt. % Be, are listed in Table II. Smoothed values of heat capacity, entropy, free energy function, and enthalpy are given in Table III. The low-temperature heat capacities of the  $\alpha'$  form and the  $\beta$  form of beryllium chloride are conventional, and the low-temperature heat capacities of the  $\beta$  form join smoothly with the high-temperature results.

The entropy of  $\alpha'$ -beryllium chloride at 13°K. was calculated to be 0.16 cal./(mole °K.) from the Debye  $T^3$  law with  $\theta_D = 127.5^\circ$ . The integral of  $C_p dT/T$  from 13 to 298.15°K. is 19.60 cal./(mole °K.) which makes the absolute entropy  $19.76 \pm 0.06$  cal./(mole °K.) at 298.15°K.

The entropy of  $\beta$ -beryllium chloride at 13°K. was calculated to be 0.06 cal./(mole °K.) with  $\theta_D = 169.5^\circ$ ; the integral of  $C_p dT/T$  from 13 to 298.15°K. is 18.06 cal./(mole °K.). The absolute entropy at 298.15°K. is therefore  $18.12 \pm 0.05$  cal./(mole °K.).

The observed enthalpies of  $\alpha$ -aluminum oxide are compared with values calculated from the work of Furukawa, *et al.*,<sup>13</sup> in Table IV. The observed enthalpy data for beryllium chloride are given in Table V in chronological order since the results are affected by the thermal history of the sample. In the solid temperature range, both the initial and final states can be uncertain. X-Ray diffraction analyses have removed some of this uncertainty by showing that the  $\alpha'$  form was the final form obtained in the drop calorimeter when the initial state was liquid or was the supercooled  $\alpha$  form. When beryllium chloride is heated from near 25° to a drop temperature below 403° (676°K.), the normal smooth increase of heat content with tempera-

ture is followed. However, if the sample is first melted and then cooled to a drop temperature between 340 and 403° (613–676°K.), a small increase over the "normal" heat content is found. If the sample is first melted and then cooled to a drop temperature below 340°, this increase is not found, and the "normal" value is again obtained. This phenomenon correlates well with the thermal phase studies.

Table IV: Enthalpy of  $\alpha$ -Al<sub>2</sub>O<sub>3</sub><sup>a</sup>

$T, ^\circ\text{K.}^b$	$-H_T - H_{298.15}, \text{cal./mole}$		Dev.,	
	Obsd. <sup>b</sup>	N.B.S. eq. <sup>c</sup>	obsd. -	calcd. from N.B.S.
310.69	241.3	245.4	-4.1	-1.67
326.91	566.2	564.6	+1.6	+0.28
369.29	1,438.8	1,462.8	-24.0	-1.64
409.43	2,347.3	2,372.0	-24.7	-1.04
410.93	2,420.8	2,406.9	+13.9	+0.58
439.20	3,057.5	3,076.5	-19.0	-0.62
442.32	3,108.2	2,151.6	-43.4	-1.38
491.52	4,285.7	4,365.4	-79.7	-1.82
498.65	4,581.3	4,545.5	+35.8	+0.79
531.82	5,375.6	5,395.1	-19.5	-0.36
591.23	7,011.4	6,960.9	+50.5	+0.72
597.92	7,183.1	7,252.5	-69.4	-0.96
629.55	8,083.5	7,996.2	+87.3	+1.09
648.84	8,551.0	8,523.8	+27.2	+0.32
651.84	8,694.2	8,605.0	+89.2	+1.04
661.30	8,892.6	8,866.7	+25.9	+0.29
737.85	11,039.0	11,007.0	+32.0	+0.29

<sup>a</sup> Molecular weight, 101.96. <sup>b</sup> More significant figures than experimentally justified to minimize rounding error. <sup>c</sup> Furukawa, *et al.*, ref. 13.

The results of 60 time vs. temperature curves may be summarized as follows. Starting from room temperature and heating, a slight exothermic break is sometimes observed in the range of 310 to 370°. Localized dark spots become visible near this temperature. A sharp endothermic break occurs in the range of 402 to 405°, 403.4° on the average. Then a slight endothermic break occurs at 409–411°, and the sample takes on a darkened, wet appearance. The sample melts at 415–416° to form a black liquid containing small bubbles. This last break is not as sharp as the one at 403°.

On cooling the melt, one usually obtains only one break in the 400 to 415° range, ordinarily appearing to be near either 415 or 403–405°; supercooling prevents accurate interpretation. Occasionally, more than

(13) G. T. Furukawa, T. B. Douglas, R. E. McCoskey, and D. C. Ginnings, *J. Res. Natl. Bur. Std.*, **57**, 67 (1956).

Table V: Experimental Heat Content Data for BeCl<sub>2</sub><sup>a</sup>

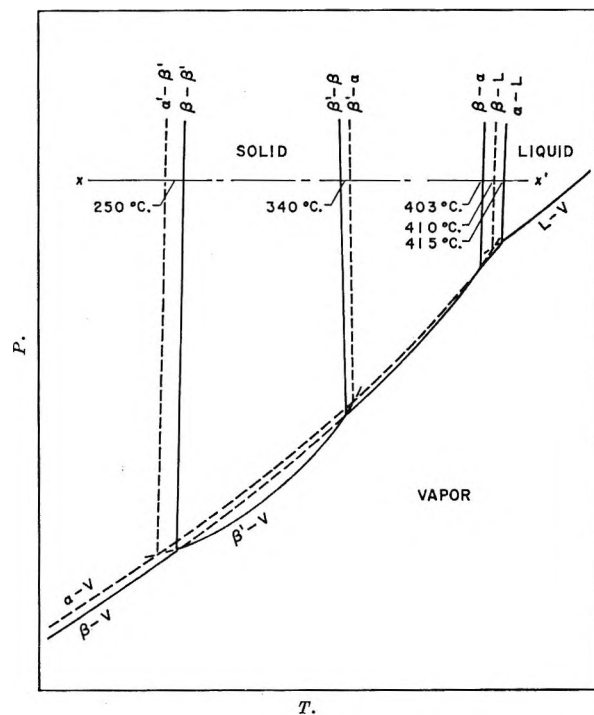
T, °K.	H <sub>T</sub> - H <sub>298.16</sub> , cal./mole	T, °K.	H <sub>T</sub> - H <sub>298.16</sub> , cal./mole	T, °K.	H <sub>T</sub> - H <sub>298.16</sub> , cal./mole
Series I					
279.3	-300.9 <sup>d</sup>	707.2	9447 <sup>b,c</sup>	472.3	2910 <sup>d</sup>
279.3	-266.7 <sup>d</sup>	667.3	6249 <sup>c,d</sup>	536.8	3990 <sup>d</sup>
324.7	404.4 <sup>d</sup>	687.5	8929 <sup>b,c</sup>	599.9	5137 <sup>d</sup>
340.7	641.8 <sup>d</sup>	713.0	9683 <sup>b,c</sup>	436.0	2226 <sup>d</sup>
364.7	1026 <sup>d</sup>	654.8	6069 <sup>c,d</sup>	665.2	6793 <sup>e</sup>
		678.9	7602 <sup>e</sup>	706.3	9560 <sup>b,c</sup>
389.7	1422 <sup>d</sup>	704.8	9416 <sup>b,c</sup>	391.6	1487 <sup>d</sup>
405.8	1689 <sup>d</sup>	630.8	5548 <sup>d</sup>	614.1	5336 <sup>d</sup>
424.8	2026 <sup>d</sup>	630.3	5611 <sup>d</sup>	654.1	6375 <sup>b,c,f</sup>
440.5	2248 <sup>d</sup>	651.6	5967 <sup>c,d</sup>	500.3	3344 <sup>d</sup>
482.4	2992 <sup>d</sup>	656.3	6308 <sup>b,c,f</sup>	535.5	3885 <sup>d</sup>
504.3	3386 <sup>d</sup>	662.3	6370 <sup>b,c,f</sup>	594.6	5014 <sup>d</sup>
518.8	3594 <sup>d</sup>	640.7	5952 <sup>b,f</sup>	653.5	6125 <sup>c,d</sup>
558.8	4323 <sup>d</sup>	593.3	4936 <sup>d,f</sup>	680.8	7814 <sup>e</sup>
582.4	4737 <sup>d</sup>	616.3	5532 <sup>b,f</sup>	696.8	9266 <sup>b,c</sup>
608.6	5188 <sup>d</sup>	597.1	4959 <sup>d,f</sup>	711.9	9712 <sup>b,c</sup>
622.6	5488 <sup>d</sup>	604.8	5167 <sup>d,f</sup>	652.7	6288 <sup>b,c,f</sup>
637.2	5763 <sup>d</sup>	Series II		621.0	5452 <sup>d</sup>
658.7	6132 <sup>c,d</sup>	422.2	1992 <sup>d</sup>	621.1	5623 <sup>b,f</sup>
686.2	8552 <sup>e</sup>	364.8	1057 <sup>d</sup>	545.9	4000 <sup>d,f</sup>
697.4	9238 <sup>b,c</sup>	467.6	2859 <sup>d</sup>	639.0	5979 <sup>b,f</sup>

<sup>a</sup> Molecular weight, 79.927. <sup>b</sup> Final state considered to be  $\alpha'$  form. <sup>c</sup> Corrected for heat of sublimation or vaporization. <sup>d</sup> Final state considered to be  $\beta$  form. <sup>e</sup> Premelting. <sup>f</sup> Sample melted and cooled to drop temperature.

one break appears in the 400–415° range. On further cooling, one may or may not pick up the 340° transition; sometimes it is definitely exothermic, contrary to what might be expected from the heating curve observations. Whether or not the 340° transition is observed, on reheating one always finds three breaks: at 403–405, 410, and 415°. If the sample is not cooled below about 360° before immediate reheating, then only one break at 415° is found. This is true even if more than one halt has been noted in the 400–415° range on cooling. Presumably, mainly  $\alpha$  form has crystallized even when more than one halt appears. In one instance the sample was melted and cooled to 390° and was held between 390 and 397° overnight. On heating again, the three breaks were found, but the 403 and the 410° breaks were much smaller than usual.

From this work, transition temperatures of 340 ± 30° and 403 ± 2° and melting points of 410 ± 2° and 415 ± 2° have been chosen.

The transition at 250° described by Kuvyrkin, *et al.*,<sup>6</sup> was not confirmed, possibly because this temperature range was passed through rapidly until after the samples had been melted at least once, or because

Figure 1. Proposed schematic phase diagram for BeCl<sub>2</sub>.

of a very small heat of transition and lack of sensitivity, or because of a slow rate of transition.

From the work presented here and that of Kuvyrkin, *et al.*, a schematic phase diagram, Figure 1, is proposed. The metastable  $\alpha'$  form and the  $\alpha$  form have been assumed to be the same. Near 250° two transitions are indicated: the metastable  $\alpha'$ - $\beta'$  transition and the  $\beta$ - $\beta'$  transition. At about 340° the  $\beta'$ - $\beta$  and the  $\beta'$ - $\alpha$  transitions are shown. While not common, the "intrusion" of the  $\beta'$  form within the  $\beta$  area is similar to regions in the iron and chromium phase diagrams.<sup>14</sup> The  $\beta$ - $\alpha$  transition occurs at 403°, and then the crystal melts at 415°. The slight endothermic halt on heating at 410° and the wet appearance of the sample have been interpreted as indications of the melting of the  $\beta$  crystal, not enough time being allowed during the experiment for all of the  $\beta$  form to transform to the  $\alpha$  form before the melting point of the  $\beta$  form was reached.

On cooling along the  $x$ - $x'$  isobar, the  $\alpha$  form crystallizes from the liquid and is easily supercooled as metastable  $\alpha$  form in the region between 340 and 403°. That the  $\alpha$  form will slowly change to the  $\beta$  form in this region was demonstrated when the sample was cooled from the melt to 390° and was held at about this tem-

(14) J. E. Ricci, "The Phase Rule and Heterogeneous Equilibrium," D. Van Nostrand Co., Inc., New York, N. Y., 1951, pp. 41, 42.

perature overnight; the  $\beta$ - $\alpha$  break was then observed on reheating. However, the  $\alpha$  form is not easily supercooled below  $340^\circ$  (except by quenching), and about here it changes to another form, conceivably either the  $\beta'$  form or the  $\beta$  form through the  $\beta'$  form in the region between the  $\beta'$ - $\alpha$  and the  $\beta'$ - $\beta$  transition lines.

Kuvyrkin's classification of the  $\beta'$ - $\beta$  transition at  $340^\circ$  as monotropic does not fit the interpretation presented in Figure 1. However, the exothermic break on cooling sometimes noted in the  $340^\circ$  region in this investigation and also reported by Schmidt<sup>2</sup> and Furby and Wilkinson<sup>5</sup> (not specified as exothermic by the latter but assumed to be) does support this picture. The exothermic effect on heating in the  $340^\circ$  area might be explained by some remaining metastable  $\alpha'$  form changing to  $\beta$  form at this temperature.

The thermal analytical phase investigations and the fact that rapid cooling of the liquid produces the  $\alpha'$  form certainly indicate that the drop calorimeter sample 1 which was originally 50%  $\alpha'$  and 50%  $\beta$  was converted by the leak-testing procedure to the  $\alpha'$  form or to the  $\beta$  form if the cooling was not rapid. Further heating in the drop calorimeter furnace would tend to produce the  $\beta$  form. Hildenbrand, *et al.*,<sup>15</sup> found that  $\alpha'$ - $\beta$  mixtures were predominantly  $\beta$  after heating at about  $500^\circ\text{K}$ . for approximately 4 hr.

Since the heat capacities derived from the heat content measurements, series I, join smoothly with the  $\beta$ -form low-temperature heat capacities and there are no observed discontinuities in heat content indicating a  $\beta'$  phase, the most reasonable interpretation is that the high-temperature data up to  $403^\circ$  (without special heating) pertain to the  $\beta$  form. The "reference state" at  $25^\circ$  would also be  $\beta$ , of course, since it is the most stable state at this temperature.

Sample 2b, known to be 95%  $\alpha'$  and 5%  $\beta$  before placing it in the drop calorimeter, did not yield results, series II, definitely different from series I. Therefore, the low-temperature heat capacities of the  $\alpha'$  form could not be extended to higher temperatures, and additional evidence for the identity of the  $\alpha'$  and  $\alpha$  forms was not obtained. The series II data up to  $403^\circ$  (without special heating) are also considered to represent the  $\beta$  form.

Smoothed enthalpy values obtained by the method of Shomate<sup>16</sup> and graphically smoothed average heat capacities are given in Table III.

Because of the different crystal forms of the "reference state" at  $298.15^\circ\text{K}$ . (the  $\alpha$  form always dropping to the  $\alpha'$  form and the  $\beta$  form always dropping to the  $\beta$  form), the heat of the  $\alpha$ - $\beta$  transition cannot be di-

rectly determined from the drop calorimeter measurements. However, considering the  $\alpha'$  and  $\alpha$  forms to be identical, one can calculate the entropies of the  $\alpha$  form and the  $\beta$  form at the transition temperature,  $676^\circ\text{K}$ ., by using the respective average of the heat capacities at  $298.15$  and  $676^\circ\text{K}$ . to approximate  $\int C_p dT/T$  and then by adding these to the respective entropies at  $298.15^\circ\text{K}$ . The difference between the two is, of course, the entropy of transition from which the heat of transition is easily computed. In this manner, the heat of the  $\alpha$ - $\beta$  transition was calculated to be  $1490 \pm 150$  cal./mole. The heat of fusion of the  $\alpha$  form at  $415^\circ$  ( $688^\circ\text{K}$ .) is approximately  $2070 \pm 60$  cal./mole. Over the short liquid range covered, the heat capacity is roughly  $29.02$  cal./mole  $^\circ\text{K}$ .

Three values for the heat of formation of beryllium chloride have been reported recently.<sup>17-19</sup> Johnson and Gilliland, and Gross, *et al.*, found  $-118.03 \pm 0.56$  and  $-117.1 \pm 0.4$  kcal./mole by direct reaction of beryllium and chlorine. These values just coincide at  $-117.5$  kcal./mole. Thompson, *et al.*, obtained  $-118.25 \pm 0.50$  kcal./mole from heat of solution data of sublimed beryllium chloride, later disclosed<sup>20</sup> to have been about 50%  $\alpha'$  and 50%  $\beta$  form. Gross, *et al.*, conclude that their figure refers to the  $\alpha'$  form. However, the product of a similar reaction was examined rather than the product of the actual reaction on which the heat measurements were made (experimentally not possible). It is evident from some of the work presented here, *viz.*, 50-50 mixtures in sublimates, and the work of others,<sup>15</sup> that sublimation of beryllium chloride cannot be depended upon to give a single-phase product. Uncertainty in the heat of formation remains.

*Acknowledgments.* This paper could not have been completed without the important help of many Dow Chemical Co. analytical chemists. Special thanks are extended to D. R. Stull for his encouragement and to H. Prophet for his critical review of an earlier manuscript.

(15) D. L. Hildenbrand, L. P. Theard, and F. Ju, Philco Research Laboratories, Publication No. U-2666, W. O. 2063, Contract AF 04(611)-8523, July 1964.

(16) C. H. Shomate, *J. Phys. Chem.*, **58**, 368 (1954).

(17) W. H. Johnson and A. A. Gilliland, *J. Res. Natl. Bur. Std.*, **A65**, 59 (1961).

(18) C. J. Thompson, G. C. Sinke, and D. R. Stull, *J. Chem. Eng. Data*, **7**, 380 (1962).

(19) P. Gross, C. Hayman, P. D. Greene, and J. T. Bingham, Fulmer Research Institute Limited, Report R. 163/SR. 1/Sept. 1964, Contract AF61(052)-447.

(20) G. C. Sinke, private communication, Feb. 1965.

# The Structure of Sodium Silicate Glasses and Their Far-Infrared Absorption Spectra<sup>1</sup>

by Rinoud Hanna

Chemical Engineering Department, University of Rochester, Rochester, New York (Received May 24, 1965)

The infrared absorption spectra of sodium silicate glasses were investigated in the 333–50-cm.<sup>-1</sup> spectral region. No absorption bands were observed. A mechanism is proposed for the transformation of vitreous silica into sodium silicate glass where the infrared spectrum is entirely due to the vibration of the point group T<sub>d</sub>. The force constants of the stretching and bending modes were calculated; the former decreased linearly with the increase of sodium oxide content.

## Introduction

The infrared absorption spectrum of sodium silicate glasses could be explained according to the fundamental frequencies of the SiO<sub>4</sub> group.<sup>2</sup> It was recently investigated in the 2500–333-cm.<sup>-1</sup> spectral region.<sup>3</sup> The lattice vibration frequencies of sodium silicate glasses consisted, in the case of Na<sub>2</sub>O·5SiO<sub>2</sub>, for example, of two strong bands at 1066 and 464 cm.<sup>-1</sup> and a weaker one at 786 cm.<sup>-1</sup>. The addition of Na<sub>2</sub>O to α-quartz has caused the shift of the stretching frequencies of the latter to lower values in the silicate glass. This was attributed to the decrease in the force constant owing to the formation of ionic bond between the sodium ion and the nonbridging oxygen.

Heaton and Moore<sup>2b</sup> explained the changes in frequencies and intensities of the absorption bands of silicate glasses according to the number of the SiO<sub>4</sub> groups having a single-bonded O<sup>-</sup> ion (nonbridging oxygen) at one or two corners and the forces exerted on this oxygen by the neighboring cations of the modifying oxide. It is thus possible to indicate, from the extent of the displacements of the stretching vibrations, whether the modifying oxide is taking part in the network formation or not.

In the present work the measurement of the absorption spectra of the sodium silicate glasses is extended to the wave number 50 cm.<sup>-1</sup>.

## Experimental Section

Blown films of sodium silicate glasses with molar composition Na<sub>2</sub>O·xSiO<sub>2</sub> (where x = 5, 4, and 3) were

prepared. The thickness of the films ranged from 1 to 4 μ as measured by means of a micrometer dial comparator in 0.001-mm. graduations. Room-temperature infrared transmission was measured with unpolarized radiation by means of a Perkin-Elmer double-beam spectrophotometer Model 301.

## Results

Figure 1 shows the absorption spectrum of the three glass compositions in the 333–50-cm.<sup>-1</sup> wave number region. While the absorption due to the attenuation of the electromagnetic waves by the glass structure is evident, there are no vibrational absorption bands. The increase in transmission at lower frequencies usually occurs whenever thin films are used irrespective of their structure. This could be attributed to the thinness of the film in comparison to the long wave length of the incident radiation. The structure appearing in the lower part of the wave number range (less than 100 cm.<sup>-1</sup>) is due to noise.

## Discussion

In order to interpret the absence of absorption bands in the spectra of sodium silicate glasses in the frequency region below 333 cm.<sup>-1</sup>, comparison should be made with the spectrum of vitreous silica. In Figure 2 the absorption spectra of the Na<sub>2</sub>O·5SiO<sub>2</sub> glass, vitreous

(1) This work was supported by the U. S. Office of Naval Research.

(2) (a) F. Matossi and O. Brönder, *Z. Physik*, **3**, 1 (1938); (b) H. M. Heaton and H. Moore, *J. Soc. Glass Technol.*, **41**, 28T (1957).

(3) R. Hanna and G.-J. Su, *J. Am. Ceram. Soc.*, **47**, 597 (1964).



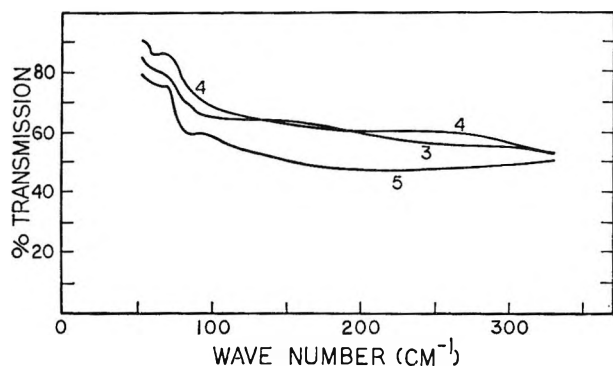


Figure 1. Per cent transmission of glass ( $\text{Na}_2\text{O} \cdot x\text{SiO}_2$ ) films in the wave number range 333 to 50  $\text{cm}^{-1}$ . Values of  $x$  are indicated on the curves.

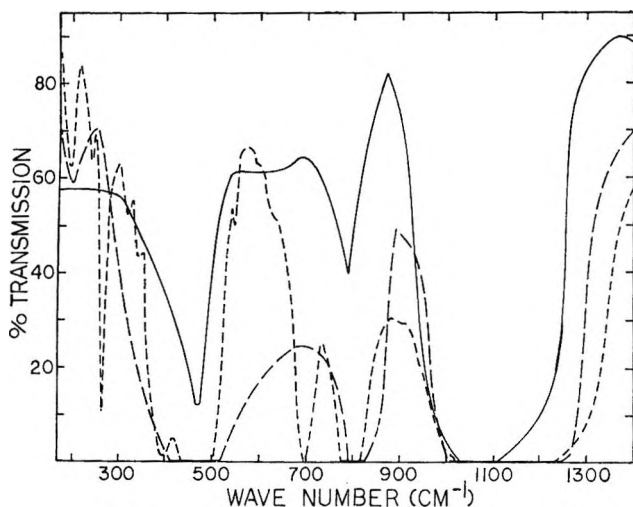


Figure 2. Per cent transmission in the wave number range 1400 to 170  $\text{cm}^{-1}$  of  $\text{Na}_2\text{O} \cdot 5\text{SiO}_2$  glass film (solid line), vitreous silica plate (long-dashed line), and  $\alpha$ -quartz plate (short-dashed line) (from ref. 3 and 4). The thickness of the vitreous silica and  $\alpha$ -quartz plates was  $22 \pm 2$  and  $32 \pm 2 \times 10^{-3}$  mm., respectively. The  $\alpha$ -quartz plate was an X-cut.

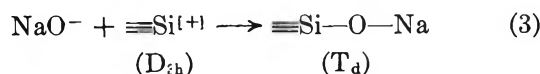
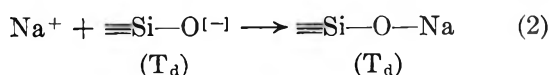
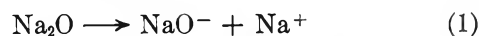
silica and crystalline quartz ( $\alpha$  form) in the 1400–170- $\text{cm}^{-1}$  wave number region are reproduced from ref. 3 and 4. The spectra of vitreous silica and  $\alpha$ -quartz were determined by using thin plates prepared by cutting and grinding the samples in the usual way. Table I gives the absorption frequency bands of sodium silicate glasses, vitreous silica, and the corresponding absorption bands of the  $\alpha$ -quartz in the 1400–50- $\text{cm}^{-1}$  region. The absorption spectrum of vitreous silica exhibits four absorption frequencies at 1126, 809, 452, and 200  $\text{cm}^{-1}$ . It was suggested<sup>4</sup> that, when crystalline quartz is fused at high temperatures, the ordered lattice is broken down to a random network characteristic of the vitreous state. Nonbridging

oxygen is formed in the vitreous silica to allow for the random orientation of the tetrahedral  $\text{SiO}_4$  groups (point group  $T_d$ ). This evidence is supported by the displacement of some of the absorption frequency bands of  $\alpha$ -quartz (at 1116 and 797  $\text{cm}^{-1}$ ) to higher wave numbers in vitreous silica due to the increase in the force constants of the stretching vibrations. For every nonbridging oxygen formed (with a negative charge), the silicon atom which was connected to it would become three-coordinated and be associated with a positive hole. Hence, the absorption frequencies of vitreous silica would result from two vibrating units of point groups  $T_d$  and  $D_{3h}$  simultaneously. The latter point group is due to the presence of the three-coordinated silicon atom. Thus, the frequency bands at 1126 and 452  $\text{cm}^{-1}$  in the vitreous silica were assigned, respectively, to the  $\nu_3$  and  $\nu_4$  of the type  $F_2$  vibration of the  $T_d$  point group. On the other hand, the frequency bands at 809, 200, 1126, and 452  $\text{cm}^{-1}$  were assigned to the symmetry species  $A'(\nu_1)$ ,  $A''(\nu_3)$ ,  $E'(\nu_3)$ , and  $E'(\nu_4)$  of the  $D_{3h}$  group, respectively. In other words, the  $\nu_3$  and  $\nu_4$  of both the  $T_d$  and the  $D_{3h}$  groups coincide. The assignment of the absorption frequencies of the vitreous silica is shown in Table I.

Table I: Comparison of the Absorption Frequency Bands of Sodium Silicate Glasses with Those of Vitreous Silica and  $\alpha$ -Quartz (from Ref. 3 and 4)

$\alpha$ -Quartz	Vitreous silica	Glass $\text{Na}_2\text{O} \cdot z\text{SiO}_2$		
		$z = 5$	$z = 4$	$z = 3$
1116	1126 $\nu_3(T_d)$ and $\nu_3(D_{3h})$	1066	1057	1038
797	809 $\nu_1(T_d)$ and $\nu_1(D_{3h})$	786	779	775
468	452 $\nu_4(T_d)$ and $\nu_4(D_{3h})$	464	464	464
192	200 $\nu_2(D_{3h})$	...	...	...

The following steps are proposed to occur in the formation of sodium silicate glasses



(4) R. Hanna, *J. Am. Ceram. Soc.*, in press.

In step 2 the sodium ion is connected to the nonbridging oxygen *via* an ionic bond. The  $\text{NaO}^-$  saturates the three-coordinated silicon (step 3) and thus transforms the point group  $D_{3h}$  to the  $T_d$  group of  $\text{SiO}_4$ . The frequencies which are due to the point group  $D_{3h}$  of the vitreous silica should disappear in the spectrum of sodium silicate glasses, and only the frequencies of the  $T_d$  group remain. The results show that the  $\nu_2$  of the  $D_{3h}$  at  $200\text{ cm.}^{-1}$  has vanished completely and the  $\nu_1$  at  $809\text{ cm.}^{-1}$  has decreased considerably in intensity in the sodium silicate glasses.

We may infer from the presence of the frequency band at  $809\text{ cm.}^{-1}$  of the vitreous silica in the sodium silicate glasses that it belongs to the point group  $T_d$  as well as  $D_{3h}$ ; otherwise, it should have disappeared completely. This point of view is supported by the fact that the  $809\text{-cm.}^{-1}$  band shifts to lower wave numbers in the sodium silicate glasses with the increase of  $\text{Na}_2\text{O}$  content in a fashion similar to the  $1126\text{-cm.}^{-1}$  band (the  $\nu_3$  of the  $T_d$  group).

The absorption spectrum of vitreous silica<sup>4</sup> exhibits an extremely weak band which appears as a shoulder at  $900\text{ cm.}^{-1}$  (Figure 2). This band was previously assigned to the symmetric  $A_1$  vibration of the  $\text{SiO}_4$  group. According to the selection rules, this vibration, in the case of tetrahedral gaseous molecules such as  $\text{CH}_4$ , is inactive in the infrared, and only the  $\nu_3$  and  $\nu_4$  are active.<sup>5</sup> Therefore, the appearance of the  $900\text{-cm.}^{-1}$  band was attributed to the deviation of the  $A_1$  vibration ( $\nu_1$ ) of the  $T_d$  point group from total symmetry since the stretching of the four Si-O bonds is not exactly the same. This results from the fact that part of the oxygen atoms in the  $\text{SiO}_4$  group are nonbridging in the vitreous silica.

If we assume that the selection rules are also approximate in the sodium silicate glasses, we may assign the  $809\text{-cm.}^{-1}$  band to the  $\nu_1$  vibration of the  $T_d$  point group. Its medium intensity indicates a considerable deviation from total symmetry. If this assignment is correct, it is reasonable to consider that this band in the vitreous silica is actually the  $\nu_1$  vibration rather than the  $900\text{-cm.}^{-1}$  band. This new assignment gives a value of  $6.18 \times 10^6$  dynes/cm. for the Si-O stretching mode in the vitreous silica. This value is lower than the  $7.65 \times 10^5$  dynes/cm. obtained when the  $900\text{-cm.}^{-1}$  band was originally assigned to the  $\nu_1$  vibration of the  $T_d$  point group.<sup>4</sup>

The force constant,  $f_d$ , of the Si-O stretching mode of each of the three sodium silicate glass compositions was calculated from its  $\nu_1$ . From  $\nu_3$  and  $\nu_4$ , the force constant,  $f_\alpha$ , of the O-Si-O bending mode was calculated using the secular equations obtained by Wilson's *F-G* matrix method.<sup>6</sup> Each  $f_\alpha$  has two values cor-

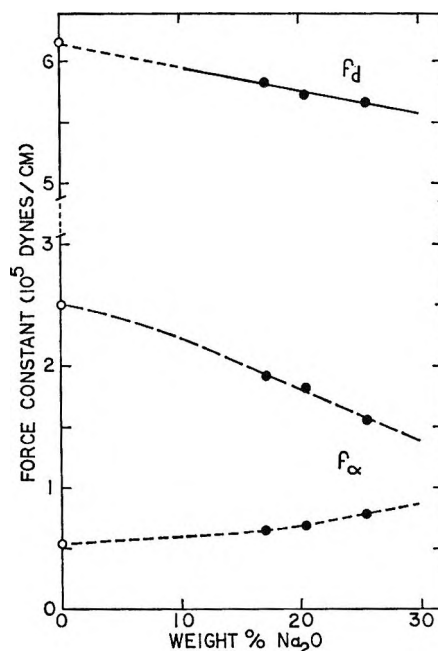


Figure 3. The force constants of sodium silicate glasses (closed circles) and vitreous silica (open circles) as a function of weight per cent sodium oxide. The long- and short-dashed lines are the higher and the lower values of  $f_\alpha$ , respectively.

responding to the two roots of the quadratic equation. Table II summarizes the values of the force constants,  $f_d$  and  $f_\alpha$ , thus calculated. It seems, that the lower values of  $f_\alpha$  are the correct ones since the  $0.53 \times 10^6$  dynes/cm. of the vitreous silica is comparable to the  $0.7 \times 10^5$  and  $0.38 \times 10^5$  dynes/cm. obtained for quartz by Saksena<sup>7</sup> and Matossi,<sup>8</sup> respectively.

Figure 3 shows  $f_d$  and  $f_\alpha$  plotted *vs.* the weight per cent of sodium oxide in the silicate glasses. It is evi-

Table II: The Force Constant,  $f_d$ , of Si-O Stretching Mode and the Two Values of the Force Constant,  $f_\alpha$ , of O-Si-O Bending Mode in the Glasses Assuming a Point Group  $T_d$

Glass	$f_d$	Force constant $\times 10^5$ dynes/cm.	
		Lower value	Higher value
Vitreous $\text{SiO}_2$	6.18	0.53	2.5
$\text{Na}_2\text{O} \cdot 5\text{SiO}_2$	5.83	0.66	1.92
$\text{Na}_2\text{O} \cdot 4\text{SiO}_2$	5.73	0.69	1.82
$\text{Na}_2\text{O} \cdot 3\text{SiO}_2$	5.67	0.79	1.57

(5) D. M. Dennison, *Astrophys. J.*, **62**, 84 (1925); *Rev. Mod. Phys.*, **12**, 175 (1940).

(6) A. G. Meister and F. F. Cleveland, *Am. J. Phys.*, **14**, 13 (1946).

(7) B. D. Saksena, *Trans. Faraday Soc.*, **57**, 242 (1961).

(8) F. Matossi, *J. Chem. Phys.*, **17**, 679 (1949).

dent that the force constant of the stretching mode decreased linearly as the Na<sub>2</sub>O content increased. When the straight line (obtained by the least-square method) was extrapolated to Na<sub>2</sub>O = 0, the value of  $f_a$  coincided with that calculated for vitreous silica. However, there was a slight deviation from linearity in the case of  $f_a$ . This may be due to some uncertainty concerning the exact value of the  $\nu_4$  owing to the broadness of this frequency band.

To summarize, the disappearing of the frequency band at 200 cm.<sup>-1</sup> in the sodium silicate glasses confirms step 3, above, where the point group D<sub>3h</sub> is transformed to T<sub>d</sub>. Although the 809-cm.<sup>-1</sup> band should vanish as well, yet from its presence, one could assign it to the  $\nu_1$  vibration of the T<sub>d</sub> point group. The force constants calculated accordingly changed in a quantitative manner along the glass series, thus confirming this assignment.

## A Small Angle X-Ray Scattering Study of Colloidal Thorium Oxide<sup>1</sup>

by Paul W. Schmidt

Physics Department, University of Missouri, Columbia, Missouri (Received May 24, 1965)

Small angle X-ray scattering data have been obtained from four dilute polydisperse colloidal thorium oxide sols and from two gels prepared by drying the sols. From the complete small angle X-ray scattering curve for a dilute polydisperse sol, one can obtain the quantities  $\bar{S}/\bar{V}$ ,  $\bar{V}^2/\bar{V}$ , and  $\bar{R}^2$ , where  $S$ ,  $V$ , and  $R$  represent, respectively, the surface area, volume, and radius of gyration of a single colloidal particle, and bars over a quantity indicate that the quantity is averaged over the polydisperse sample. For each value of  $\bar{S}/\bar{V}$ ,  $\bar{V}^2/\bar{V}$ , and  $\bar{R}^2$  which could be obtained for a sol an average particle dimension could be computed. By comparison of the different average particle dimensions for a sol with each other and with other workers' measurements by different techniques, qualitative information was obtained about the distribution of particle diameters in the sols. For dried gels, two different small angle X-ray scattering procedures can be used to find the specific surface  $\bar{S}/\bar{V}$ . To test the reliability of small angle X-ray scattering determinations of the specific surface in these gels, the two methods of measuring specific surface were used on a thoria gel with comparatively well-understood properties. The results obtained by the two methods agreed within the expected experimental error of  $\pm 15\%$ . The small angle X-ray scattering data for the specific surface of a second gel helped to explain the large discrepancy between the average particle dimensions obtained for this gel by B.E.T. nitrogen adsorption and X-ray diffraction line widths.

### Introduction

Interest in the use of colloidal thorium oxide in nuclear reactor fuel fabrication technology<sup>2</sup> suggested that a small angle X-ray scattering investigation of colloidal thoria could extend the information available from other studies<sup>3</sup> since, when X-ray data are com-

pared with results obtained by other methods, a more complete and detailed description of an inorganic colloidal system can be obtained than by use of a

(1) Work supported by the U. S. Atomic Energy Commission for the Oak Ridge National Laboratory Chemical Technology Division and by the National Science Foundation.

single technique.

Certain parameters, such as the specific surface and average particle weight, are often convenient for describing inorganic sols and gels which are composed of colloidal particles. By making some assumptions about the particles, these parameters can be used to compute average particle dimensions. Because of the complicated structures which are often present in these colloidal systems, a few average dimensions or other parameters can give only a limited description of the system. Nevertheless, when allowance is made for the nature and limitations of the average parameters and dimensions, these quantities can be valuable in describing and characterizing colloidal systems.

Average particle dimensions calculated from different experimental parameters will, in general, represent differently weighted averages and thus ordinarily will not be equal. By comparison of the average dimensions computed from several different experimental quantities, information can be obtained about the distribution of particle diameters in a colloidal system, and the system can often be described in more detail than would be possible if only one or two techniques were used.

When, as often happens, the parameters from X-ray scattering data are essentially equivalent to parameters obtained by other techniques, the average dimensions computed from X-ray measurements ordinarily agree with the average dimensions calculated from other determinations of the corresponding parameters. In some cases, however, agreement will not be obtained since, even though the same value of a parameter should, in principle, be obtained by two different techniques, the experimentally measured values will agree only for certain ranges of experimental conditions. For example, specific surfaces measured by small angle X-ray scattering and B.E.T. nitrogen adsorption often agree. However, because of the different physical assumptions involved in the application of these two methods, different specific surface values are obtained when the pores of a colloid are inaccessible to nitrogen but still are effective in determining the X-ray scattering. Because of the possibility of differences of this type, measurements of a parameter by two or more techniques are important and should not automatically be considered superfluous. In fact, the agreement or disagreement can often lead to important information about the structure of the colloidal sample.

The small angle X-ray scattering data which have been obtained for a group of colloidal thoria sols and gels, in addition to permitting a more complete characterization of these colloidal thorias, also illustrate small angle scattering methods for studying inorganic

colloids, showing what information can be obtained and how it is related to other methods of characterizing these colloids.

### Methods for Interpretation of Scattering Curves

For a dilute sol containing identical particles, the particle volume  $V$ , the specific surface area  $S/V$ , and the radius of gyration  $R$  can be determined if small angle X-ray scattering data are available over a sufficiently large range of scattering angles.<sup>4</sup> By averaging the equations for a single particle, one can show that for dilute polydisperse sols, the quantities  $V$ ,  $S$ , and  $R$  are replaced by average quantities, which are related to the intensity  $I(h)$  of the small angle X-ray scattering by the equations

$$\frac{\bar{V}^2}{\bar{V}} = \frac{2\pi^2 I(0)}{\int_0^\infty dh h^2 I(h)} \quad (1)$$

$$\frac{S}{\bar{V}} = \frac{\pi \lim_{h \rightarrow \infty} h^4 I(h)}{\int_0^\infty dh h^2 I(h)} \quad (2)$$

where a bar over a quantity indicates that the quantity is averaged over the polydisperse sample;  $h = 4\pi\lambda^{-1} \sin(\phi/2)$ ,  $\phi$  is the scattering angle, and  $\lambda$  is the X-ray wave length. When  $h^2 R^2$  is not large,  $I(h)$  can be approximated by the expression

$$I(h) = I(0) \exp(-1/3 h^2 \bar{R}^2) \quad (3)$$

where

$$\bar{R}^2 = (\overline{V^2 R^2}) / (\bar{V}^2) \quad (4)$$

The integral

$$\int_0^\infty dh h^2 I(h) \quad (5)$$

appearing in the denominator on the right side of (1) and (2) will be called the normalizing integral.

Average colloidal dimensions from X-ray data are directly comparable to dimensions obtained by other methods only when the dimensions represent similarly weighted averages. For example, (1) can be considered an X-ray analog of the determination of molecular weights by light scattering, and thus particle dimensions from light scattering would be expected to agree

(2) O. C. Dean, *et al.*, Proceedings of the Thorium Fuel Cycle Symposium, Gatlinburg, Tenn., Dec. 5-7, 1962, U.S.A.E.C. Report TID 7650, Paper No. 22.

(3) (a) A. Dobry, S. Guinand, and A. Mathieu-Sicaud, *J. Chim. Phys.*, **50**, 501 (1953); A. Dobry, *ibid.*, **50**, 507 (1953); (b) Y. Arai and W. O. Milligan, *J. Electronmicroscopy* (Tokyo), **12**, 92 (1963).

(4) A. Guinier, *et al.*, "Small Angle Scattering of X-Rays," John Wiley and Sons, Inc., New York, N. Y., 1955, pp. 16-19.

with dimensions from (1). Average particle sizes obtained from the ratio  $\bar{S}/\bar{V}$  from (2) should be equivalent to the dimensions computed from B.E.T. adsorption data.

The scattering data from colloidal samples such as dried gels, in which the particles cannot be considered independent, can be conveniently interpreted when the sample can be assumed to consist of colloidal regions in which the electron density has either one of two constant values. If  $\rho$  is the difference between these two values of electron densities and  $I_e$  is the intensity scattered by an electron, then the scattered intensity for a sample with total surface area  $\bar{S}$  is given by<sup>5</sup>

$$I(h) = 2\pi\rho^2 I_e \bar{S} h^{-4} \quad (6)$$

In this case the normalizing relation is<sup>6</sup>

$$\int_0^\infty dh h^2 I(h) = 2\pi\rho^2 \bar{V} c (1 - c) I_e \quad (7)$$

where  $\bar{V}$  is the total volume of the scattering sample and  $c$  is the fraction of the volume which is occupied by material with one of the two values of electron density. Equation 6 can be used to find the specific surface by comparing the scattering from a sample with the scattering from a sample with known surface area. Also, (6) and (7) can be combined to give a relation analogous to (2). The resulting equations will be modified to make them more convenient to apply.

In (6), no allowance is made for X-ray absorption in the sample. To account for this effect, the right side of (6) must be multiplied by the transmission  $T$ , where  $T = \exp(-\mu t)$  and where  $\mu$  is the mass absorption coefficient of the sample,  $t$  is the sample thickness in a direction perpendicular to the X-ray beam, and  $d$  is the mass density of the sample. If the sample is assumed to consist of thoria and water, with mass absorption coefficients and mass densities  $\mu_T$ ,  $d_T$ ,  $\mu_w$ , and  $d_w$ , respectively, and if  $k$  is the mass fraction of thoria in the sample, then

$$\mu = \mu_T k + (1 - k)\mu_w$$

If the sample volume is assumed to be the sum of the volumes that the masses of thoria and water contained in the sample would occupy if they were isolated and had densities  $d_T$  and  $d_w$

$$1/d = (k/d_T) + (1 - k)/d_w$$

Experiments showed that in the thoria samples this assumption was quite well satisfied and that it would not cause an appreciable error in the quantities calculated from the experimental data. Let  $I$  be the intensity scattered by a dried thoria gel at an angle in the region where the scattering is proportional to  $h^{-4}$ ,

and assume that, for a dilute thoria sol containing  $k_1$  g. of thoria/g. of sol, the scattered intensity in this angular region also is proportional to  $h^{-4}$  and has the value  $I_1$  at the angle where the gel intensity is  $I$ . The total surface area  $S$  of a sample can be written  $S = AtdkS^\circ$ , where  $A$  is the irradiated area of the sample in a direction perpendicular to the X-ray beam and  $S^\circ$  is the specific surface of the sample—that is, the surface area per gram of dry thoria. Then from (6) one obtains

$$S^\circ = \frac{T_1 \log(1/T_1)}{T \log(1/T)} \frac{k_1 \mu_T}{\mu_w} \frac{1 + \left(\frac{1}{k} - 1\right) \frac{\mu_w}{\mu_T}}{1 + k_1 \left(\frac{\mu_T}{\mu_w} - 1\right)} \frac{I}{I_1} S_1^\circ \quad (8)$$

where  $k$  is the mass fraction of thoria in the gel,  $S_1^\circ$  is the specific surface of the dilute sol, and  $T$  and  $T_1$  are the X-ray transmissions of the gel and sol, respectively. For a dried thoria gel

$$1 \gg \left(\frac{1}{k} - 1\right) \left(\frac{\mu_w}{\mu_T}\right)$$

since  $k \approx 1$  and  $\mu_T \gg \mu_w$ . (The mass absorption coefficients for thoria and water have the respective values 327 and 10.0 g.<sup>-1</sup> cm.<sup>2</sup> for copper K $\alpha$  radiation.) Thus, when (8) is used to find the specific surface of a thoria gel by comparing the scattering from the gel with the scattering from a dilute thoria sol for which the specific surface is known, the result is nearly independent of  $k$ , which thus needs not be determined. Also, when both samples have transmissions near the optimum value of 0.37, the measured specific surface will be relatively insensitive to errors in measurements of  $T$  and  $T_1$ .

When the volume fraction  $c$  of thoria in a gel with mass density  $d$  is expressed in terms of  $k$  by the relation  $cd_T = kd$ , (6) and (7) can be combined to give

$$S^\circ = \frac{S}{c\bar{V}d_T} = \frac{\tau}{d_T} \frac{d_T - d}{d_T - d_w} \frac{\lim_{h \rightarrow \infty} h^4 I(h)}{\int_0^\infty dh h^2 I(h)} \quad (9)$$

Equation 9, unlike (8), involves only relative values of the scattered intensity. It therefore avoids the experimental errors involved in comparing the scattered intensity from two different samples. However, to obtain the specific surface from (9), the gel density must be measured, while (8) is nearly independent of the gel density.

(5) See ref. 4, pp. 80, 81.

(6) See ref. 4, p. 81, eq. 111.

## Experimental Methods

The scattering data were obtained with a four-slit collimation system of the type developed by Beeman, *et al.*<sup>7</sup> A copper-anode X-ray tube operated at 24 kv. and 16 ma. was employed as the source of the X-rays, which were detected with a proportional counter. A Ni-foil  $\beta$  filter, a linear amplifier, and a pulse-height analyzer ensured that only counts in the wave length region about 1.54 Å. would be registered.

The slits of the collimating system were 1 cm. high. The slit width was adjusted to give as great a resolution as possible and still provide sufficient scattered intensity. For scattering angles from 2 to 20 mradians, the slit width was 0.011 in., while for angles from 7 to about 100 mradians, the slits were set at a width of 0.040 in. To measure the weak scattering at angles greater than about 50 mradians, wider slits were sometimes employed. The scattering curves for different slit widths were combined to form the composite scattering curve for a sample. All scattering curves shown were obtained in this way. The data obtained with different slit widths overlapped for an angular region wide enough to permit good matching of the scattering curves.<sup>7</sup> Collimation errors for slit widths were assumed to be negligible. The method of Schmidt and Hight<sup>8</sup> was employed to correct most of the scattering curves for distortion by the finite height of the collimating slits. The other curves were corrected by a modified technique,<sup>9</sup> which for these samples can be considered to give essentially the same results as the method of Schmidt and Hight.

During the time scattering data were being obtained, the intensity of the incident X-ray beam was checked by measuring the scattering at a single angle from a calibrated sample, either sodium lauryl sulfate or carbon black. The incident intensity was constant within at least a few per cent. To measure the transmission of the thoria sols and gels, the sodium lauryl sulfate sample was inserted in the collimating system, which was set at the scattering angle (about 35 mradians) for which sodium lauryl sulfate has a diffraction maximum. The transmission of the thoria samples was then measured by finding the counting rates from the sodium lauryl sulfate sample with the thoria sample inserted and removed from the X-ray beam.

Scattering data were obtained for four thoria sols, which were prepared by K. H. McCorkle and co-workers at Oak Ridge National Laboratory.

One sol, which will be called sol 850, was made by dispersing thoria in dilute nitric acid at 90°, followed by filtration and centrifugation. The thoria was obtained from thorium oxalate, calcined at 850°. A

second sol, called sol 500, was made in a similar manner, except that the thorium oxalate was calcined at 500°, and the filtration was omitted. The third sol, sol 450, was prepared like sol 500, except that sol 450 was not centrifuged, and the thoria was obtained by steam denitration of thorium nitrate at 450°. In the fourth sol, called the HTS sol, the thoria was derived by precipitation of hydrous thorium oxide with ammonia at 27° from a solution of thorium nitrate. The thoria was dispersed in nitric acid at room temperature, and the  $\text{NH}_3/\text{ThO}_2$  ratio was 0.011. In sols 850, 500, 450, and the HTS sol, the mole ratios of total nitrate to total thorium had the respective values of 0.031, 0.233, 0.270, and 0.90.

Sample cells were made from flat pieces of stainless steel with thickness approximately equal to the optimum sample thickness for a given thoria sol. This thickness ranged from 0.102 to 0.025 cm. A region about 0.48 × 3.17 cm. was cut from the stainless steel sheets to contain the sample. After epoxy resin was used to cement a 0.00064-cm. Mylar window on the sample holder, it was laid on a table and filled with the sol. After the holder had been filled, the second Mylar window was put on and held in place with stopcock grease.

The sols, which were supplied in concentrations of about 10% by weight, were diluted with distilled water to concentrations 2, 1, and 0.5% by weight. The effect of interparticle interference, which is appreciable only in the inner part of the scattering curve, was studied by measuring the scattering at a series of concentrations and was found to be negligible except in the inner part of the scattering curve.

Since the X-ray absorption in thoria is so great, uniform powdered samples of the dried gels could not be made. Instead, after one window was cemented on a sample holder, the holder was filled with a concentrated sol, which then was allowed to dry in a desiccator jar containing Ascarite and silica gel. Often the gel did not dry uniformly on the Mylar window, but in about half the samples, the gel layer appeared to be sufficiently uniform for scattering studies. After the gels were dried, a second Mylar window was applied and held in position with stopcock grease.

The measured X-ray transmission of a gel sample sometimes varied by as much as 25% after the sample had been removed from the beam and reinserted. The deviations are believed to be due to the nonuniformity of the gel layer since, when the sample was removed,

(7) See ref. 4, p. 95.

(8) P. Schmidt and R. Hight, Jr., *Acta Cryst.*, **13**, 480 (1960).

(9) P. W. Schmidt, *ibid.*, in press.

it could not be reinserted in exactly the same position, and as a result, the X-ray beam passed through an area with different thickness. When successive transmission measurements were made on a gel sample which was not moved between measurements, the results were reproducible within a few per cent. Also, for the sols, transmission values were reproducible within about 5%.

## Results

Table I shows the numerical values obtained from eq. 1-3 for the four thoria sols. For comparison, Table I also gives specific surface values obtained by B.E.T. nitrogen adsorption by K. H. McCorkle and co-workers at Oak Ridge National Laboratory.

**Table I:** Quantities Computed from the Small Angle X-Ray Scattering Data for the Thoria Sols, with B.E.T. Nitrogen Adsorption Specific Surface Values from Ref. 10

Sol	$\bar{S}/\bar{V}$ , m. <sup>2</sup> /g.		$\bar{V}^2/\bar{V}$ , Å. <sup>3</sup>	$(\bar{R}^2)^{1/2}$ , Å.
	X-Ray	B.E.T.		
500	97	85.2	$2.19 \times 10^6$	126
450	100	71.1		
850	14	13.1		
HTS		<1		
Large component	58		$2.2 \times 10^6$	78
Small component				8.6

Because of the surprisingly small specific surface values obtained for the HTS samples, the adsorption measurements on these samples were repeated a number of times, at various drying temperatures from room temperature up to 500°. The specific surface of a sample aged about 3 years was also determined. In all cases the specific surface was less than 1 m.<sup>2</sup>/g.

As has been mentioned, average particle dimensions for the sols can be computed by assuming a particle shape and then considering all the particles to be identical. Since thorium oxide forms fluorite-type cubic crystals, a cube seemed a natural shape to choose for expressing the average particle dimensions in thoria samples. If all particles are assumed to be identical cubes with cube edge  $D$ , values of  $D$  can be calculated from  $\bar{V}^2/\bar{V}$ ,  $\bar{S}/\bar{V}$ , and  $\bar{R}^2$ . The dimensions found from the small angle X-ray scattering data are shown in Table II, along with  $D$  values obtained by McCorkle and co-workers, using other techniques.<sup>10</sup>

For sol 500, the scattering curve could be measured or approximated for all angles in the small angle region, and therefore  $\bar{V}^2/\bar{V}$ ,  $\bar{S}/\bar{V}$ , and  $\bar{R}^2$  could all be determined or estimated. However, since the inner part of the scattering curve could not be obtained for sols 450

**Table II:** Average Particle Dimensions

Sol	Technique used to obtain average dimensions, Å.					
	$\bar{S}/\bar{V}$ X-Ray	B.E.T.	Line width	Light scattering	$\bar{V}^2/\bar{V}$	$\bar{R}^2$
500	62	68	74	154	130	252
450	60	84	54	272		
850	430	445	461	987		
HTS		>6000	<20	62	130	156
Large component	102					
Small component						17.2

and 850, the radius of gyration and zero-angle intensity could not be found. Thus, for these two sols, the X-ray scattering curves give only the specific surface. When  $\bar{V}^2/\bar{V}$  and  $\bar{R}^2$  could not be found, blanks were left in Table I, and the corresponding  $D$  values computed from these quantities could not be shown in Table II.

Although the radius of gyration plot for sol 500 was only approximately linear,  $\bar{R}^2$  and  $\bar{V}^2/\bar{V}$  could be estimated. These approximate values of the intensity in the inner portion of the scattering curve were sufficient for evaluation of the normalizing integral needed for finding  $\bar{S}/\bar{V}$  and  $\bar{V}^2/\bar{V}$ . The specific surface of 97 m.<sup>2</sup>/g. obtained from the scattering data is in good agreement with the B.E.T. specific surface of 85.2 m.<sup>2</sup>/g., and the average dimension of 130 Å. obtained from  $\bar{V}^2/\bar{V}$  agrees within experimental uncertainty with the value of 154 Å. computed from light scattering. The particle diameter computed from the average radius of gyration gives an average particle dimension of 252 Å. While there are no other measurements with which to compare this value, it is so much larger than the other average dimensions that possibly it may be in error because of an incorrect estimate of the radius of gyration. As  $\bar{R}^2$  values emphasize larger particles more strongly than do the average values of  $\bar{V}^2/\bar{V}$ , one would expect to obtain a larger average dimension from the former quantity than from the latter. However, since the distribution of particle diameters would have to contain a very great number of large particles if the particle dimension from  $\bar{R}^2$  is to be twice as large as the dimension computed from  $\bar{V}^2/\bar{V}$ , the large difference in these dimensions suggests that possibly the estimate of the radius of gyration may be in error.

As sols 450 and 850 contained so many large particles that the inner part of the scattering curve was located at angles too small to be accessible with the collimation system,  $\bar{R}^2$  and  $\bar{V}^2/\bar{V}$  could not be found, and only the

(10) K. H. McCorkle, private communication.



specific surface could be determined. For each of these sols,  $S/\bar{V}$  was found by comparing the scattered intensity from the sols with the intensity scattered by sol 500 at an angle in the region where the scattering from both sols was proportional to  $h^{-4}$ . In determining the specific surface of sols 450 and 850, the specific surface of sol 500 was taken to be 97 m.<sup>2</sup>/g. The X-ray scattering values of the specific surface of sols 450 and 850 agree quite well with the results from B.E.T. nitrogen adsorption.

Sols 450 and 500 have essentially the same specific surface, while a radius of gyration can be estimated for sol 500 but not for sol 450. Thus, one can expect a greater fraction of large particles in the latter sol than in the former. This conclusion is also suggested by the result that the ratio of the average particle diameter from light scattering to the average diameter from B.E.T. adsorption is greater in sol 450 than in sol 500. The average dimension computed from light scattering weights large particles more heavily than the dimension obtained from B.E.T. adsorption. Thus, when the ratio of these two dimensions is larger in one sol than in another, one can conclude that the former sol has a greater fraction of large particles. Because of the methods used in preparing the two sols, sol 500 can be expected to have a smaller fraction of large particles since only sol 500 was centrifuged.

As can be seen from Figure 1, the entire scattering curve for sol 850 is essentially proportional to  $h^{-4}$  since the particles are so large that only the outer portion of the scattering curve was accessible.

For the HTS sol, the radius of gyration plot was linear, and the slope of the plot corresponded to a radius of gyration of 78 Å. and to an average particle dimension of 156 Å. The HTS sol was the only sol for which the outer part of the scattering curve was not proportional to  $h^{-4}$ . This behavior in the outer part of the scattering curve and the linearity of the radius of gyration plot in the inner part of the scattering curve suggest that the HTS sol contains more relatively small particles than are found in the other three sols.

At intermediate angles of the scattering curve for the HTS sol, the scattering is nearly proportional to  $h^{-4}$ . A scattering curve of this type would be obtained from a sol consisting of a mixture of two groups of independent particles with one group, which will be called the large component, being composed of particles with an average dimension much larger than the average dimension of the particles in the other group, which will be referred to as the small component. The scattering from the large component will predominate in the inner part of the scattering curve, but, as it will decrease more rapidly than the scattering from

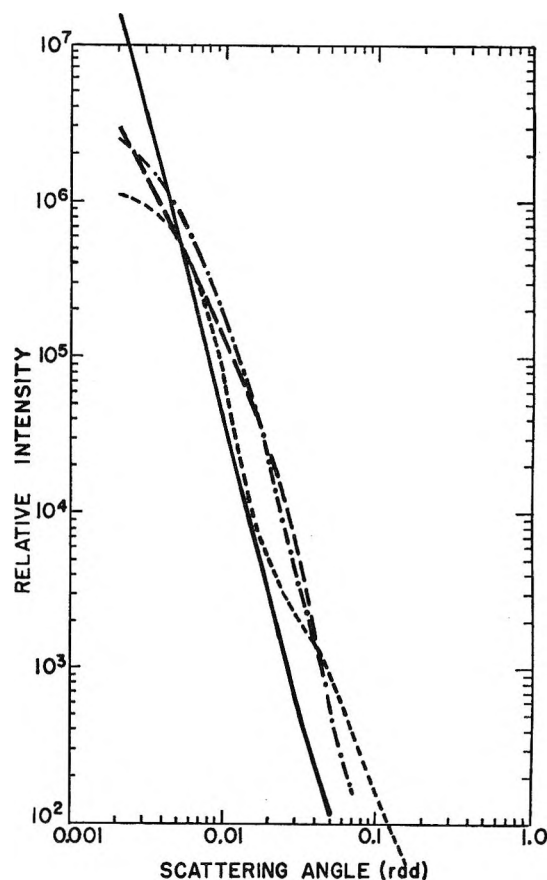


Figure 1. The scattering curve for the thoria sols, after correction for the effects of slit height. The curves are plotted on the same relative intensity scale, to permit comparison of the relative intensity of scattering from different sols. The solid line is the scattering curve for sol 850; the curve for sol 450 is indicated by large dashes; small dashes give the scattering curve for the HTS sol; and the line made up of dots and dashes is the scattering curve for sol 500.

the small component, in the outer portion of the scattering curve, the scattering from the small component will dominate. The particles of the small component will be considered to be so small that, even at the largest accessible scattering angles, the scattering is not proportional to  $h^{-4}$  since, for the scattering to have this angular dependence, the average particle dimension  $D$  must be large enough to satisfy the condition  $hD \gg 1$  in the outer part of the scattering curve.

There is independent evidence that this type of structure may be present in the HTS sol. Structure with dimensions of the order of those in the small component have been observed in high-resolution electron micrographs of thoria samples prepared by techniques similar to that used in making the HTS sol.<sup>3</sup> Dobry, Guinand, and Mathieu-Sicaud obtained elec-



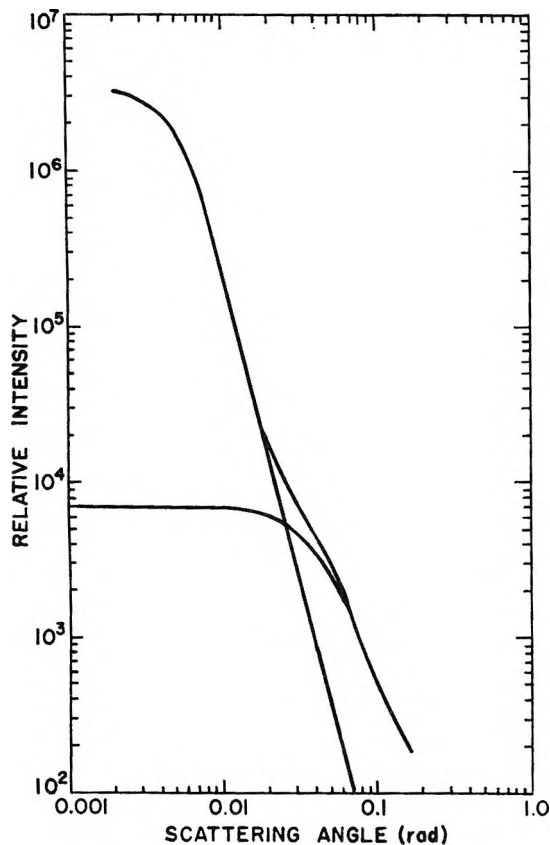


Figure 2. The scattering curve for the HTS sol, after collimation correction, showing the decomposition into the scattering curves assumed for the large and small components.

tron micrographs of a dried thoria sol showing filaments which appeared to be composed of particles no greater than 18 Å. in diameter. At times these filaments were observed to roll up into larger, more compact particles. In the electron micrographs of Arai and Milligan,<sup>3b</sup> a similar structure can be seen, and the primary particles with dimensions of the order of 8–20 Å. are clearly resolved.

With the above assumptions, from the scattering curve for the HTS sol, scattering curves can be constructed for the two components. This set of curves is shown in Figure 2.

At the angles at which the radius of gyration plot of the HTS sol is obtained, the scattering is essentially due entirely to the large component, and thus the average radius of gyration  $\bar{R}^2$  for the HTS sol is the value for the large component. Since the outer part of the scattering curve for the large component is proportional to  $h^{-4}$ , the normalizing integral can be evaluated, and  $S/\bar{V}$  and  $\bar{V}^2/\bar{V}$  can be determined. The corresponding average particle dimensions were calculated and are given in Table II.

If the mass fraction of thoria in the large component is known, the specific surface of this component could also be determined by comparing the intensity of the scattering from sol 500 with the intensity of the scattering from the large component of the HTS sol. This fraction cannot be found without further assumptions. However, if dimensions of the particles in both components are considered to follow the same type of distribution, the ratio of  $\bar{V}^2/\bar{V}$  for the two components would be expected to be equal to the ratio of the third powers of the average particle dimensions and thus to the cube of the ratio of the average radii of gyration. Under these assumptions, the two components are found to have essentially the same concentration—that is, about half the mass of the thoria in the HTS sol is in each of the two components. Comparison of the intensity of scattering from the large component and sol 500 then indicates that the specific surface of the large component is 41 m.<sup>2</sup>/g. Because of the possibility of errors resulting from the many assumptions that have been made, these values can be considered in essential agreement with the figure of 58 m.<sup>2</sup>/g. obtained from (2).

As is shown in Table II, for the HTS sol an average particle dimension of 62 Å. was obtained by light scattering. This value was computed from the weight-average molecular weight under the assumption that all particles in the sol contributed to the observed scattering. However, as there is essentially no light scattering from the small component, the effective concentration for light scattering will be the concentration of the large component, not the total thoria concentration. If the weight of thoria is equally divided between the large and small components, as has been assumed, then the effective concentration for light scattering is half the thoria concentration. Thus, the light scattering molecular weight should be doubled, and the average particle dimension should be increased by a factor of 2<sup>1/3</sup>. While the resulting value of 78 Å. is appreciably smaller than the average dimension of 130 Å. obtained from the small angle X-ray scattering determination of  $\bar{V}^2/\bar{V}$ , better agreement probably cannot be expected because of possible errors in the estimate of the relative concentration of the two components.

For the large component of the HTS sol, the average dimensions computed by different methods differ relatively little. Therefore, one would expect that in the large component there is less deviation about the average particle dimension than occurs in the other sols.

In the small component of the HTS sol, only the zero-angle scattering and average radius of gyration can be

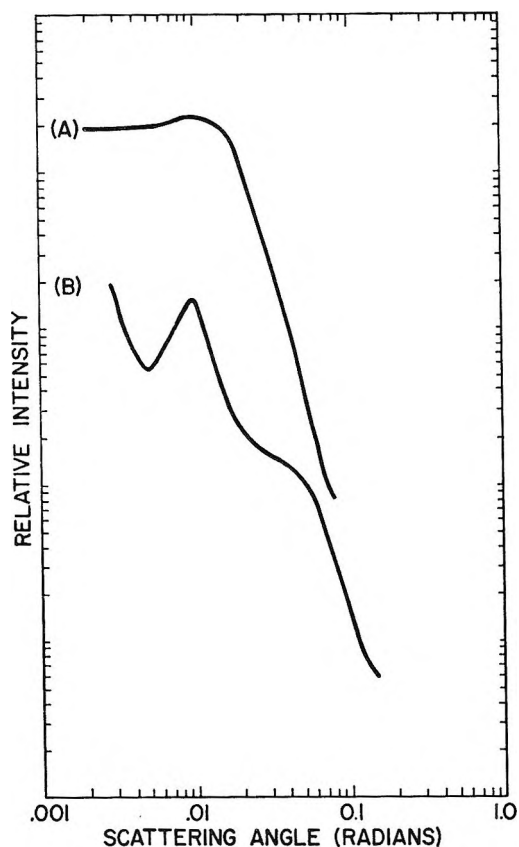


Figure 3. The scattering curves for the thoria gels from sol 500 (curve a) and the HTS sol (curve b) after collimation correction. The relative intensities of the two curves have been shifted and cannot be directly compared.

determined. The average radius of gyration of 8.6 Å corresponds to an average particle dimension of 17.2 Å.

Except for the HTS sol, the particle dimensions obtained by McCorkle, *et al.*, from X-ray diffraction line widths<sup>10</sup> are in quite good agreement with the dimensions computed from specific surface measurements, either from small angle X-ray scattering or B.E.T. nitrogen adsorption. This agreement may result from the line width method giving the average of a linear dimension.<sup>11</sup> This average value can be expected to agree more closely with dimensions computed from  $S/\bar{V}$  than with those calculated from quantities involving averages of higher powers of the particle dimensions.

To test the usefulness of eq. 8 and 9 in determining the specific surface of dried thoria gels, these equations were used to find the specific surface of a thoria gel prepared by drying sol 500. This sol was chosen for making a gel sample because the sol particles are well defined and stable, and thus the specific surfaces of the gel and sol would be expected to be nearly the same.

The scattering curve for this gel is shown in Figure

3. Use of (8) and (9) to compute the specific surface gave values of 58 and 72  $\text{m}^2/\text{g}$ ., respectively.

In (9), the gel density was taken to be 6.6  $\text{g}/\text{cm}^3$ . As density measurements could not be made on the gels used in the scattering studies, the density was found<sup>10</sup> for a gel dried under similar conditions. As the density of gels from sol 500 can vary with drying procedure,<sup>10</sup> the actual density of the gels used in the X-ray studies may have differed by 5 to 10% from a density of 6.6  $\text{g}/\text{cm}^3$ .

In the normalization integrals in the denominator of (9); the portion obtained by extrapolation was of the order of 15 to 25% of the total integral. Unless this extrapolated portion was in error by at least 50%, the extrapolation would not produce an error of more than about 10% in the specific surface of the gel. As such a large error in the extrapolated portion is unlikely, extrapolation errors probably are not responsible for the difference in specific surface computed from (8) and (9).

Without further study, there is no evidence to suggest which specific surface value is more reliable. When all factors which might contribute errors are considered, an error of about 10 or 15% can be expected. As the two values of specific surface differ by 11% from their average of 65  $\text{m}^2/\text{g}$ ., the X-ray values of specific surface can be considered in essential agreement.

In an attempt to resolve the great discrepancy shown in Table II for the particle dimensions computed for the HTS sample from B.E.T. nitrogen adsorption and from X-ray diffraction line broadening, a small angle X-ray scattering study was made from a gel prepared by drying the HTS sol. Figure 3 shows the scattering curve for this gel. The outer part of the scattering curve is more nearly proportional to  $h^{-3.5}$  than to  $h^{-4}$ . However, for an order of magnitude estimate of the specific surface, the scattering curve was assumed to be continuous and proportional to  $h^{-4}$  for angles greater than 100 mradians. Also, the scattering intensity for angles less than 2 mradians was assumed to make a negligible contribution to the normalizing integral. When the normalizing integral is evaluated under these assumptions, for a gel density of 4.5  $\text{g}/\text{cm}^3$  the specific surface found from (9) is 310  $\text{m}^2/\text{g}$ ., corresponding to an average particle dimension of 20 Å.

If the outer part of the scattering curve for this gel is assumed to be proportional to  $h^{-4}$ , (8) can be used to obtain the specific surface by comparing the intensity of the scattering from the gel and from sol 500.

(11) A. R. Stokes, "X-Ray Diffraction by Polycrystalline Materials," H. S. Peiser, H. P. Rooksby, and A. J. C. Wilson, Ed., Section 17.3.2, Institute of Physics, London, 1955, p. 415.

The resulting specific surface is  $100 \text{ m}^2/\text{g}$ , corresponding to an average particle dimension of  $60 \text{ \AA}$ .

Because of the many assumptions needed to apply (8) and (9) to the gels made from the HTS sol, these equations can be expected to give only the order of magnitude of the specific surface, and thus the difference between the results from (8) and (9) probably is not significant.

As the normalizing integral was probably underestimated, the specific surface computed from (9) may be too large, and a reasonable estimate of the order of magnitude of the specific surface would be  $200 \text{ m}^2/\text{g}$ , and the corresponding average particle dimension would be  $30 \text{ \AA}$ .

Since this average dimension is much nearer to the

value obtained by line broadening than to the dimension computed from nitrogen adsorption, one can conclude that in this gel most of the pores are inaccessible to nitrogen. This inaccessibility is responsible for the large difference between the average dimensions determined by adsorption and line broadening.

*Acknowledgments.* The author wishes to express his appreciation to K. H. McCorkle and co-workers for assistance in preparing the gels and for advice and guidance during the course of the investigation, to D. E. Andrews, James E. Thomas, and T. R. Taylor for aid in obtaining the scattering data, and to E. E. Pickett for assistance in preparing and handling the gel samples.

## Catalysis over Supported Metals. IV. Ethane Hydrogenolysis over Dilute Nickel Catalysts

by W. F. Taylor, J. H. Sinfelt, and D. J. C. Yates

*Process Research Division, Esso Research and Engineering Company, Linden, New Jersey  
(Received May 24, 1965)*

The kinetics of ethane hydrogenolysis have been studied over dilute nickel catalysts containing 1 and 5% nickel and compared with previous results on catalysts containing 10% nickel. Two different supports, silica and silica-alumina, were used for the nickel. The reaction rate measurements were made in the range  $175$  to  $335^\circ$ . The nickel surface areas of the catalysts were determined by hydrogen chemisorption. This made it possible to determine the specific catalytic activity of the nickel in terms of rate of hydrogenolysis per unit area of nickel surface. The specific catalytic activity and apparent activation energy vary significantly with the nickel concentration. The catalytic properties of the very dilute 1% nickel catalysts, in particular, are markedly different from those of higher nickel concentration and exhibit an especially large effect of the support used for the nickel.

### I. Introduction

The catalytic hydrogenolysis of ethane over supported nickel has previously been investigated by Taylor and co-workers,<sup>1,2</sup> using a catalyst containing 15% nickel deposited on kieselguhr. These studies

revealed some striking kinetic effects, particularly the strong inverse dependence of the reaction rate on

(1) K. Morikawa, W. S. Benedict, and H. S. Taylor, *J. Am. Chem. Soc.*, **58**, 1795 (1936).

(2) C. Kemball and H. S. Taylor, *ibid.*, **70**, 345 (1948).

hydrogen pressure. Published studies by the authors of the present paper have confirmed these results for catalysts containing 10% nickel and have demonstrated a marked effect of the support on the catalytic activity of nickel for this reaction.<sup>3,4</sup> Recently, we have extended the work to dilute nickel catalysts, *i.e.*, catalysts with nickel concentrations in the range of 1 to 5% nickel. The purpose of the work was to determine whether the catalytic properties of dilute nickel catalysts are significantly different from those of the more conventional nickel catalysts of higher concentration. Evidence of a critical nickel concentration has previously been reported by Hill and Selwood<sup>5</sup> in studies of benzene hydrogenation over a series of nickel on alumina catalysts of varying nickel concentration. These investigators found that catalysts containing less than 3% nickel were virtually inactive for the benzene hydrogenation reaction, while catalysts containing more than 10% nickel were highly active.

In the present paper, the results of kinetic studies on ethane hydrogenolysis over dilute nickel catalysts containing 1 and 5% nickel are discussed and compared with previously reported data on catalysts containing 10% nickel. The studies were made using both silica and silica-alumina as supports for the nickel. Hydrogen chemisorption measurements were made on all of the catalysts to determine the extent of dispersion of the nickel on the supports. Significant differences between the very dilute nickel catalysts and those of higher nickel concentration have been observed, both from the standpoint of the magnitude of catalytic activity and the kinetic relationships and parameters found for the different catalysts.

## II. Experimental Section

*A. Kinetic Measurements. Apparatus and Procedure.* The reaction rate measurements were carried out in a flow system at atmospheric pressure. Details of the reactor have been described previously.<sup>6</sup> The reaction gases were passed downflow through the catalyst bed, and the products were analyzed by a chromatographic unit coupled directly to the outlet of the reactor. The chromatographic column was 2 m. in length and 0.6 cm. in diameter. The column was packed with 100-mesh silica gel and was operated at 40°. Helium was used as a carrier gas, and a thermal conductivity detector was used with the column.

The reactant gases, ethane and hydrogen, were passed over the catalyst in the presence of helium diluent. Gas flow rates were measured using orifice-type flowmeters with manometers. A total gas flow rate of 1 l./min. was used throughout. The run procedure consisted of passing the reactant gases over

the catalyst for a period of 3 min., at which time a sample of the product was taken for chromatographic analysis. The ethane was then cut out, and hydrogen flow was continued for a period of 10 min. at the reaction temperature prior to another run. In this way, it was possible to minimize variation in catalyst activity from period to period. As an additional insurance against the complications due to varying catalyst activity, measurements at any given set of conditions were in most cases bracketed with periods at a standard set of conditions. In this way, the effect of changing a variable can be determined by comparison with the standard condition periods run immediately before and after the period in question. In each reaction study 0.2 g. of catalyst was diluted with 0.5 g. of ground Vycor. The catalysts were reduced in the reactor in flowing H<sub>2</sub> overnight at 370°.

*Materials.* The ethane was obtained from the Matheson Co. It is estimated that any hydrocarbon impurities amounted to less than 0.01% each. High purity hydrogen was obtained from the Linde Co. and was further purified by passing it through a Deoxo unit containing palladium catalyst to remove traces of oxygen as water, prior to passage through a molecular sieve dryer.

The nickel catalysts were prepared by impregnation of silica or silica-alumina with an aqueous solution of Ni(NO<sub>3</sub>)<sub>2</sub>·6H<sub>2</sub>O. The silica employed was Cabosil HS-5 (surface area 340 m.<sup>2</sup>/g., particle size less than 1 μ), obtained from the Cabot Corp., Boston, Mass. The silica-alumina used was DA-1 (nominally 13% Al<sub>2</sub>O<sub>3</sub>, 87% SiO<sub>2</sub>), obtained from the Davison Chemical Co., Baltimore, Md. The surface area of the silica-alumina was 450 m.<sup>2</sup>/g., and the particle size was less than 50 μ. In the case of the nickel on silica catalysts, the concentration of the impregnating solution ranged from 0.7 to 7.0 g. of Ni(NO<sub>3</sub>)<sub>2</sub>·6H<sub>2</sub>O/100 ml. of water, depending on the final nickel concentration desired. For the nickel on silica-alumina catalysts, the concentration ranged from 7.0 to 70 g./100 ml. of H<sub>2</sub>O. The lower concentrations in the case of the nickel on silica were necessary because much more solution was required to obtain satisfactory wetting of the Cabosil. After impregnation, the catalysts were dried overnight at 105°. The dried catalysts were then pressed into wafers at 8000 p.s.i., after which the wafers were

(3) D. J. C. Yates, W. F. Taylor, and J. H. Sinfelt, *J. Am. Chem. Soc.*, **86**, 2996 (1964).

(4) W. F. Taylor, D. J. C. Yates, and J. H. Sinfelt, *J. Phys. Chem.*, **68**, 2962 (1964).

(5) F. N. Hill and P. W. Selwood, *J. Am. Chem. Soc.*, **71**, 2522 (1949).

(6) J. H. Sinfelt, *J. Phys. Chem.*, **68**, 344 (1964).

crushed and screened. The 45–60-mesh fractions were used in the experiments.

*B. Chemisorption Measurements. Apparatus and Materials.* A conventional glass vacuum system was used, with a mechanical backing pump, an 80-l./sec. oil diffusion pump, and a trap cooled with either solid carbon dioxide or liquid nitrogen. The ultimate dynamic vacuum reached by the system was about  $10^{-7}$  torr and was measured by an Alpert-type ionization gauge. Details of the apparatus have been described previously.<sup>3</sup>

Hydrogen of 99.984% purity was purchased from the Linde Co., Linden, N. J. Traces of oxygen were removed from it by a Deoxo purifier, obtained from Englehard Industries, Inc., Newark, N. J. The water formed in the Deoxo unit was removed by a trap cooled with solid carbon dioxide. The helium, used in calibrating the cells, was obtained from the Bureau of Mines, Amarillo, Texas, and had a purity of 99.98% or better. It was dried by passage through a trap cooled by liquid nitrogen before use.

*Procedure.* The sample was glass-blown into the cell, no greased joint being used. The cell was weighed before and after putting in the sample so that corrections could be made for water driven off during the reduction and subsequent evacuation.

The sample was then heated and evacuated until  $100^\circ$  was reached. After evacuating at this temperature for 1 hr., the hydrogen was passed through the sample at a flow rate of 500 cm.<sup>3</sup>/min. The temperature was then slowly raised to  $370^\circ$ , while maintaining the above flow. The sample was then reduced overnight at  $370^\circ$  and 500 cm.<sup>3</sup>/min. The hydrogen was then cut off, and the sample was evacuated at  $370^\circ$  for 1 hr. At the end of this time, pressures in the region of  $10^{-6}$  torr were obtained. The sample cell was then isolated from the pumps and cooled to  $20^\circ$ . The hydrogen isotherm was then run, usually three or four points being obtained with the highest pressure used being about 30 cm.

### III. Results

The hydrogen chemisorption isotherms obtained on the nickel catalysts are plotted in Figure 1. The amount of hydrogen adsorbed at a pressure of 10 cm. was taken as a measure of the monolayer point. Nickel surface areas were calculated on the basis that each nickel atom in the surface adsorbs one hydrogen atom and that each nickel atom occupies  $6.5 \text{ \AA}^2$  of surface.<sup>7</sup> Nickel surface areas of the various catalysts are given in Table I. As the nickel content of the catalyst decreased, it can be seen that the amount of hydrogen adsorbed, and correspondingly the nickel surface area,

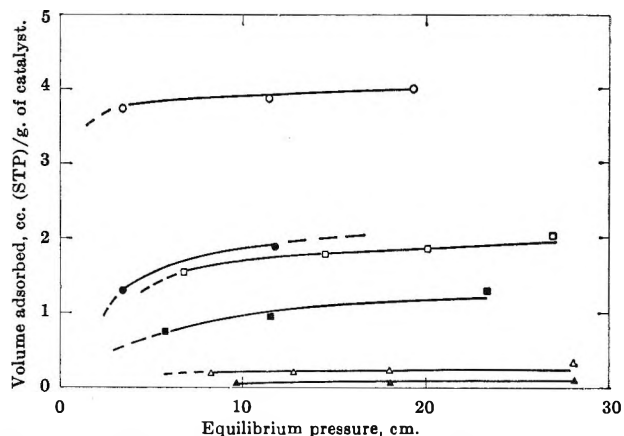


Figure 1. Adsorption isotherms for  $\text{H}_2$  on supported nickel catalysts at room temperature: O, 10% Ni on  $\text{SiO}_2$ ; □, 5% Ni on  $\text{SiO}_2$ ; △, 1% Ni on  $\text{SiO}_2$ ; ●, 10% Ni on  $\text{SiO}_2\text{-Al}_2\text{O}_3$ ; ■, 5% Ni on  $\text{SiO}_2\text{-Al}_2\text{O}_3$ ; ▲, 1% Ni on  $\text{SiO}_2\text{-Al}_2\text{O}_3$ .

decreased. Since the amounts of hydrogen adsorbed on the 1% nickel content catalysts are relatively low, it is probable that the nickel area measurements on these catalysts are less reliable than those on the higher nickel content catalysts. Adsorption of hydrogen on the supports was a negligible part of the total adsorption, except possibly for the 1% nickel on silica-alumina catalyst. In this case, the total volume of hydrogen adsorbed at 10 cm. approaches the limit of detectability of the adsorption apparatus, and, hence, it is difficult to make a reliable judgment about the contribution of the support to the total adsorption. However, it will become evident from subsequent results that a precise knowledge of the nickel surface area of this catalyst is not necessary for a comparison of its catalytic properties with those of the other catalysts.

Table I. Summary of Nickel Surface Areas Determined by  $\text{H}_2$  Chemisorption

Catalyst	Ni surface area, m. <sup>2</sup> /g. of catalyst
Ni on $\text{SiO}_2$	
1% Ni	0.7
5% Ni	5.9
10% Ni	13.6
Ni on $\text{SiO}_2\text{-Al}_2\text{O}_3$	
1% Ni	0.1
5% Ni	3.1
10% Ni	6.8

(7) D. F. Klemperer and F. S. Stone, *Proc. Roy. Soc. (London)*, **A243**, 375 (1958).

The hydrogenolysis of ethane to form methane was studied over the various catalysts at temperatures above about 180°. In studying the kinetics, the approach taken was to measure the rates of reaction at low conversion levels. The degree of conversion in the present work ranged from 0.02 to about 7%, most of the data having been obtained at conversion levels below 1.0%. Consequently, the partial pressures of the reactants (ethane and hydrogen) do not vary much through the reaction zone, and the system approaches that of a differential reactor. The reaction rates per gram of catalyst were determined from the relation

$$r = \frac{F}{W}x \quad (1)$$

where  $F$  represents the feed rate of ethane to the reactor in moles per hour,  $W$  represents the weight in grams of the catalyst charged to the reactor, and  $x$  represents the fraction of ethane converted to methane.

In an actual run to determine reaction rates, the catalyst was first prereduced with flowing hydrogen, after which the reactor was cooled in flowing hydrogen to a convenient reaction temperature. At a standard set of conditions of hydrogen and ethane partial pressures,  $p_H$  and  $p_E$ , respectively, the activity of the freshly reduced catalyst was determined. Following this, reaction rates were measured at a series of temperatures in a rising-temperature sequence. The data are shown in the Arrhenius plots in Figure 2. Data are not shown for the 1% nickel on silica-alumina catalyst since the rates were too low to measure even at 540°, which is close to the limit of the apparatus.

After determining the effect of temperature on rates over the freshly reduced catalyst, the temperature was lowered to an intermediate value in the range studied, and a series of measurements was made to determine the effects of the partial pressures of hydrogen and ethane on the rates. Since it had been observed from preliminary experiments that a series of such measurements over an extended period of time resulted in some loss of activity, it was decided to bracket all of the rate measurements with measurements at a standard set of conditions. In this way it was possible to detect variations in catalyst activity during the series of measurements. This procedure has been discussed in detail elsewhere.<sup>3,6</sup> The effect of a kinetic variable such as hydrogen or ethane partial pressure was then determined by comparing the rate at a given set of conditions with the average of the rates at the standard conditions immediately before and after the period in question. For each set of conditions the rate  $r$  relative to the rate  $r_0$  at the standard conditions can be expressed by the ratio  $r/r_0$ , which should be reasonably

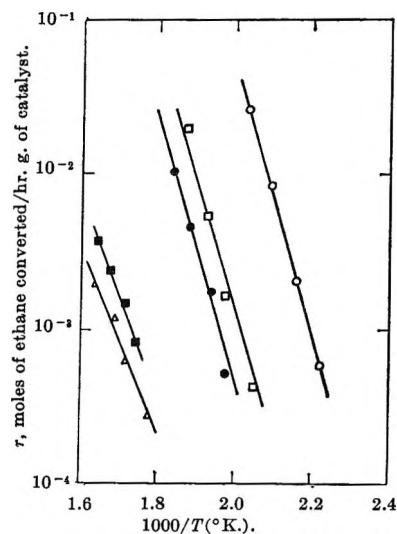


Figure 2. Effect of temperature on rate of ethane hydrogenolysis over supported nickel catalysts of varying nickel concentration;  $p_E = 0.030$  atm.;  $p_H = 0.20$  atm.: O, 10% Ni on  $\text{SiO}_2$ ;  $\square$ , 5% Ni on  $\text{SiO}_2$ ;  $\triangle$ , 1% Ni on  $\text{SiO}_2$ ;  $\bullet$ , 10% Ni on  $\text{SiO}_2\text{-Al}_2\text{O}_3$ ;  $\blacksquare$ , 5% Ni on  $\text{SiO}_2\text{-Al}_2\text{O}_3$ .

independent of moderate variations in catalyst activity. The value for  $r/r_0$  is unity by definition at the standard conditions ( $p_H = 0.20$  atm.,  $p_E = 0.030$  atm.). Values of the relative rates  $r/r_0$  as a function of ethane and hydrogen pressures are given in Table II.

Table II: Relative Rates of Ethane Hydrogenolysis as a Function of Ethane and Hydrogen Partial Pressures

$p_H$ , atm.	$p_E$ , atm.	$r/r_0^a$				
		Ni on $\text{SiO}_2$			Ni on $\text{SiO}_2\text{-Al}_2\text{O}_3$	
		1% Ni <sup>b</sup>	5% Ni <sup>c</sup>	10% Ni <sup>d</sup>	5% Ni <sup>e</sup>	10% Ni <sup>f</sup>
0.10	0.030	1.51	3.44	4.03	2.44	2.66
0.20	0.030	1.00	1.00	1.00	1.00	1.00
0.40	0.030	0.34	0.28	0.14	0.21	0.27
0.20	0.010	0.39	0.60	0.37	0.46	0.33
0.20	0.030	1.00	1.00	1.00	1.00	1.00
0.20	0.100	2.33	2.28	3.91	1.94	2.40

<sup>a</sup> Rate relative to the rate at the standard conditions ( $p_H = 0.20$  atm.,  $p_E = 0.030$  atm.) for the particular catalyst and temperature in question; the  $r/r_0$  values cannot be used by themselves to compare the activities of the catalysts. <sup>b</sup> Determined at 287°. <sup>c</sup> Determined at 218°. <sup>d</sup> Determined at 177–191°. <sup>e</sup> Determined at 304°. <sup>f</sup> Determined at 246°.

The data show that the rate of ethane hydrogenolysis increases with increasing ethane pressure but decreases markedly with increasing hydrogen partial pressure. The dependence of the rate on the partial pressures of ethane and hydrogen can be expressed in the form of a

imple power law,  $r = kp_E^n p_H^m$ . Approximate values of the exponents  $n$  and  $m$  as derived from experimental data are summarized in Table III. It can be seen that the effect of ethane and hydrogen pressure is directionally the same for all the catalysts.

**Table III:** Summary of Kinetic Parameters for Ethane Hydrogenolysis

Ni concn., wt. %	Catalyst				
	Ni on SiO <sub>2</sub>			Ni on SiO <sub>2</sub> -Al <sub>2</sub> O <sub>3</sub>	
Apparent activation energy, kcal./mole	28.7	38.2	40.6	32.1	39.2
Reaction orders <sup>a</sup>					
<i>n</i> , C <sub>2</sub> H <sub>6</sub>	0.8	0.6	1.0	0.6	1.0
<i>m</i> , H <sub>2</sub>	-1.1	-1.8	-2.2	-1.6	-1.8
Temp., °C. <sup>b</sup>	287	218	177	304	246

<sup>a</sup> Orders with respect to ethane and hydrogen in the power rate law,  $r = kp_E^n p_H^m$ . <sup>b</sup> Temperatures at which the reaction orders were determined.

Apparent activation energies derived from the slopes of the Arrhenius plots in Figure 2 are included in Table III. In Figure 3 the apparent activation energy is plotted as a function of the nickel concentration of the catalysts. The apparent activation energy for ethane hydrogenolysis is seen to increase with increasing nickel concentration.

A comparison of the specific catalytic activities of the various nickel catalysts at a given temperature can be made by dividing the observed reaction rate per gram of catalyst by the corresponding nickel area per gram of catalyst. A temperature of 205° has arbitrarily been chosen for such a comparison. For those catalysts on which reaction rates could not be measured at 205°, the rates were obtained by extrapolation of the Arrhenius plots in Figure 2. The specific catalytic activity,  $r_s$ , thus obtained is plotted as a function of the nickel content of the catalyst in Figure 4. It can be seen that the specific activity increases with increasing nickel concentration. Also, for a given nickel content, the specific activity of nickel on silica is higher than that of nickel on silica-alumina.

No quantitative data on specific catalytic activity and apparent activation energy could be obtained on the 1% nickel on silica-alumina catalyst because it was inactive at temperatures up to 537°. It is estimated that the specific activity of this catalyst at 537° is less than  $4 \times 10^{-4}$  mole/hr. m.<sup>2</sup> of nickel. Assuming an apparent activation energy of 20 kcal./mole, which is an extrapolation of the curve for the silica-alumina-

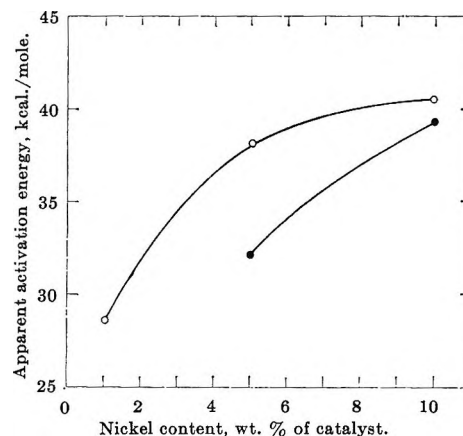


**Figure 3.** Effect of nickel concentration on apparent activation energy of ethane hydrogenolysis over supported nickel catalysts: O, Ni on SiO<sub>2</sub>; ●, Ni on SiO<sub>2</sub>-Al<sub>2</sub>O<sub>3</sub>.

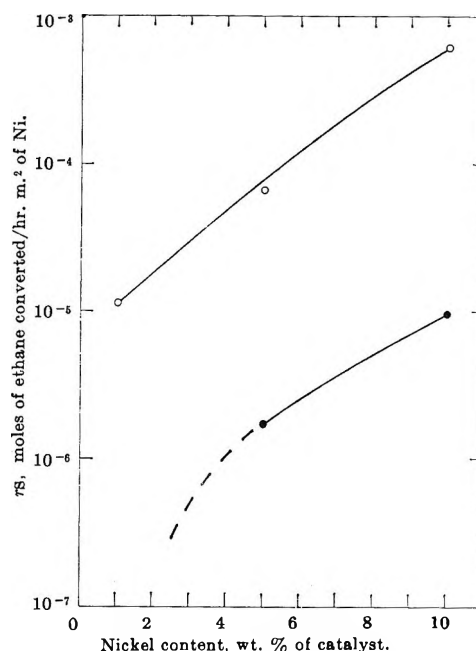


**Figure 4.** Specific catalytic activity of supported nickel as a function of nickel concentration: O, Ni on SiO<sub>2</sub>; ●, Ni on SiO<sub>2</sub>-Al<sub>2</sub>O<sub>3</sub>. Conditions: 205°;  $p_E = 0.030$  atm.;  $p_H = 0.20$  atm.

supported catalysts in Figure 3, the specific activity of the 1% nickel on silica-alumina catalyst at 205° would be less than  $8 \times 10^{-8}$  mole/hr. m.<sup>2</sup> of nickel. This indicates that the specific activity for the silica-alumina-supported catalyst also continues to decrease with decreasing nickel content in the range from 5 to 1% nickel.

#### IV. Discussion

The kinetics of ethane hydrogenolysis over the dilute nickel catalysts used in this work show some striking



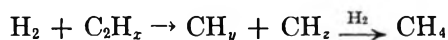
differences from the results observed with catalysts of higher nickel concentration. The apparent activation energies observed with the dilute nickel catalysts are significantly lower than the values observed for the 10% nickel catalysts. In addition, the specific catalytic activities are much lower. In the case of the very dilute 1% nickel on silica catalyst, the dependence of the reaction rate on hydrogen pressure is also quite different. These results demonstrate that dilute nickel catalysts are very different from more concentrated nickel systems with regard to their catalytic properties. The data show an interesting parallel with the earlier results of Hill and Selwood<sup>5</sup> on benzene hydrogenation over nickel on alumina catalysts. These investigators reported a critical nickel concentration (about 5%), below which the catalysts were inactive. They also found that the magnetic properties of the nickel in these catalysts varied markedly, the specific ferromagnetism increasing substantially with nickel concentration. They suggested that at low nickel concentrations few nickel particles are large enough to produce ferromagnetism and that the low catalytic activity results because the aggregates of nickel atoms are too small. In other words, they proposed that a geometric factor is involved such that a minimum-size aggregate of nickel atoms is required to catalyze the hydrogenation of benzene.

In the work reported in the present paper, the hydrogen chemisorption data do not indicate that the average crystallite size of the nickel decreases with decreasing nickel concentration. This is inferred from the values of the nickel surface areas, which do not show an increase in the surface area (per unit weight of nickel) at the low concentrations, as would have been expected if the nickel aggregates were smaller. To account for the large differences in the catalytic properties of dilute nickel catalysts from those of higher nickel concentration, it is suggested that the results are a consequence of an interaction of the metal with the support. Such an interaction could well be most pronounced at low nickel concentrations. The first increments of nickel impregnated on the surface of the support could selectively interact with the most energetic sites on the surface. This would lead to heterogeneity of the nickel sites. There is a close analogy between this suggestion and the extensive evidence for the heterogeneous nature of surfaces as derived from studies on chemisorption of gases.

The effect of the support on the catalytic properties of nickel is strongly demonstrated in comparisons of nickel supported on silica and on silica-alumina. The catalytic activity of nickel for ethane hydrogenolysis is markedly higher when the nickel is supported

on silica. The effect is evident over the whole range of nickel concentrations investigated but is particularly pronounced at the lowest nickel concentrations. The detailed nature of the interaction between the nickel and support is not known. However, it seems reasonable to expect that the metal would interact electronically with the support since electron transfer would, in general, occur at the junction between a metal and a semiconductor.

The general features of the kinetics of ethane hydrogenolysis have been reported previously by Taylor and co-workers<sup>8</sup> for a commercial nickel on kieselguhr catalyst. They proposed a mechanism involving a preliminary dehydrogenation of the ethane to an unsaturated radical on the surface, followed by attack of the surface radical by hydrogen



where  $a$  is equal to  $(6 - x)/2$ . Assuming that the dehydrogenation step is an equilibrated one and that the rupture of the carbon-carbon bond is the rate-limiting step, the following rate law results<sup>8</sup>

$$r = \frac{k p_{\text{H}} b (p_{\text{E}}/p_{\text{H}}^a)}{1 + b (p_{\text{E}}/p_{\text{H}}^a)}$$

where  $b$  is the equilibrium constant of the initial dehydrogenation step and  $k$  is the rate constant of the subsequent step leading to carbon-carbon bond rupture. It is conceivable that the differences in hydrogen pressure effects observed with the 1 and 10% nickel catalysts may, in part, be due to differences in the extent of dissociation of hydrogen from the ethane molecule in the initial dehydrogenation step. Thus, while  $a$  appears to have a value of 3 for catalysts containing 10-15% nickel,<sup>3,4,8</sup> it is possible that the value of  $a$  for a 1% nickel catalyst is lower, corresponding to a more saturated surface radical. This would account for the smaller inverse dependence of the rate on hydrogen pressure. This would imply that the properties of the nickel at low concentrations are quite different from the properties at high concentrations, probably because the first increments of nickel impregnated on the support interact strongly and selectively with certain sites on the support. Furthermore, if the initial dehydrogenation step is endothermic,<sup>9</sup> the lower

(8) A. Cimino, M. Boudart, and H. S. Taylor, *J. Phys. Chem.*, **58**, 796 (1954).

(9) J. H. Sinfelt, W. F. Taylor, and D. J. C. Yates, *ibid.*, **69**, 95 (1965).



apparent activation energy observed at the lower nickel concentrations can also be understood. The lower apparent activation energy could, in part, be a

consequence of a lower endothermicity of the initial dehydrogenation step, corresponding to less extensive dissociation of hydrogen from the molecule.

## The Heat of Formation of Nitric Oxide(g)

by Margaret A. Frisch and John L. Margrave<sup>1</sup>

*Department of Chemistry, University of Wisconsin, Madison, Wisconsin (Received May 28, 1965)*

The heat of the reaction  $\text{NO(g)} + \text{CO(g)} = \frac{1}{2}\text{N}_2\text{(g)} + \text{CO}_2\text{(g)}$  has been measured calorimetrically, and from these data the standard heat of formation of NO(g),  $\Delta H_f^\circ_{298}$ , has been established as  $21.556 \pm 0.060$  kcal./mole.

### Introduction

Thermochemical studies of NO had their beginning late in the nineteenth century when Berthelot<sup>2</sup> obtained 21.6 kcal./mole for the heat of formation of NO by treating cyanogen and ethylene with NO. Koerner and Daniels,<sup>3</sup> in 1952, studied the reaction of P and NO and their measurement gave  $21.8 \pm 0.3$  kcal./mole for  $\Delta H_f^\circ_{298}$  of NO(g).

The derivation of this quantity from spectroscopic and electron impact studies was not so straightforward. For nearly two decades, the preferred dissociation energies of  $\text{N}_2$  and NO varied because of uncertainties in the interpretation of the spectroscopic data. An early study of Schmid and Gero<sup>4</sup> listed 4.29 e.v. for  $D_0(\text{NO})$ . Glocker,<sup>5,6</sup> in 1948, chose  $D_0(\text{NO}) = 6.49$  e.v. and  $D_0(\text{N}_2) = 9.765$  e.v. At the same time, Hagstrum<sup>7</sup> concluded that the only values consistent with both electron impact and band spectroscopic results were  $D_0(\text{NO}) = 5.30$  e.v. and  $D_0(\text{N}_2) = 7.384$  e.v. Rosen,<sup>8</sup> upon examination of the problem, agreed with Herzberg<sup>9</sup> that the value for  $D_0(\text{NO})$  must be 5.29 e.v., while Gaydon<sup>10</sup> favored the higher value on the basis of temperature measurements on the cyanogen-oxygen flame.<sup>11</sup> In 1954, Brook and Kaplan<sup>12</sup> presented very strong arguments that the higher value was correct since they had observed the vibrational levels of NO up to  $v'' = 23$  which indicated that a sudden drop in

$\Delta G(v'')$  values would have to occur in order to agree with the 5.29-e.v. value. Their data led to  $D_0(\text{NO}) = 6.48$  e.v. and  $D_0(\text{N}_2) = 9.76$  e.v. Herzberg, *et al.*,<sup>13</sup> made a second measurement and obtained 6.50 e.v. for  $D_0(\text{NO})$ .

Brewer and Searcy<sup>14</sup> reviewed the existing data and recommended the following as the most probable

(1) Rice University, Houston, Texas, to whom correspondence should be addressed.

(2) (a) M. Berthelot, *Ann. chim. phys.*, (5)6, 178 (1875); (b) *ibid.*, (5)20, 255 (1880).

(3) W. E. Koerner and F. Daniels, *J. Chem. Phys.*, 20, 113 (1952).

(4) R. Schmid and L. Gero, *Math. naturw. Anz. ungar. Akad. Wiss.*, 62, 408 (1943).

(5) G. Glocker, *J. Chem. Phys.*, 16, 604 (1948).

(6) G. Glocker, *J. chim. phys.*, 46, 103 (1949).

(7) H. D. Hagstrum, *J. Chem. Phys.*, 16, 848 (1948).

(8) B. Rosen, *Mem. soc. roy. sci. Liege*, 12, 317 (1952).

(9) G. Herzberg, "Molecular Spectra and Molecular Structure. I. Spectra of Diatomic Molecules," D. Van Nostrand Co., Inc., New York, N. Y., 1950, p. 448.

(10) A. G. Gaydon, "Dissociation Energies and Spectra of Diatomic Molecules," 2nd Ed., Chapman and Hall, London, 1952.

(11) N. Thomas, A. G. Gaydon, and L. Brewer, *J. Chem. Phys.*, 20, 369 (1952).

(12) M. Brook and J. Kaplan, *Phys. Rev.*, 96, 1540 (1956).

(13) G. Herzberg, A. Lagerquist, and E. Miescher, *Can. J. Phys.*, 34, 622 (1956).

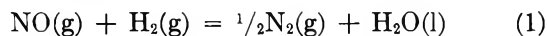
(14) L. Brewer and A. W. Searcy, *Ann. Rev. Phys. Chem.*, 1, 259 (1956).

values:  $D_0(\text{NO}) = 6.503 \pm 0.004$  e.v. =  $149.98 \pm 0.08$  kcal./mole and  $D_0(\text{N}_2) = 9.758 \pm 0.005$  e.v. =  $225.04 \pm 0.10$  kcal./mole. By using these data and the most recent value for  $D_0(\text{O}_2)$  of 5.115 e.v. = 117.96 kcal./mole,<sup>15</sup> one obtains  $21.52 \pm 0.15$  kcal./mole for  $\Delta H_f^\circ_{0^\circ\text{K.}}[\text{NO}(\text{g})]$ <sup>16</sup> and  $21.65 \pm 0.15$  kcal./mole for  $\Delta H_f^\circ_{298^\circ\text{K.}}[\text{NO}(\text{g})]$ .

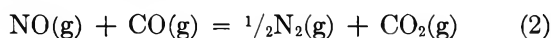
Since this quantity is the reference for nearly all of the enthalpies of formation of the nitrogen oxides, an additional calorimetric study was deemed necessary to reduce this large uncertainty.

### Experimental Approach

Two possible reactions were considered which could give a better  $\Delta H_f^\circ_{298}$  for NO(g) through measurements in a high-precision calorimeter.



Initial studies on this reaction indicated that with a NO:H<sub>2</sub> mole ratio of 1:1.2, the reaction went to completion, but subsequent problems with the quantitative analysis of the water were insurmountable. It was impossible in a reasonable period of time to remove all traces of water on the walls of the bomb before admitting the two gases and the identical difficulty arose during the flushing operation. For this reason the NO + H<sub>2</sub> reaction was abandoned and, instead, the NO + CO reaction was considered.



This reaction, although it presented no serious analytical problems, was nearly impossible to initiate. When the sample was ignited using a platinum wire, the reaction proceeded very slowly with a half-time of about 1 hr. Upon examination of the bomb, the platinum electrodes appeared to have catalyzed the reaction since they were quite warm to the touch. This premise was verified by observing the reaction in a glass bomb.<sup>17</sup> After the initial fusing of the platinum wire, the wire remnants continued to glow white hot at first with a gradual diminishing in the intensity.

The inability to start a chain reaction indicated that the melting point of platinum was too low to generate the threshold concentration of dissociated molecules. To test this assumption, 0.004-in. iridium wire (m.p. 2454°) was tried, and a continuous string of firing successes resulted. To check for a possible reaction of Ir with NO, a blank run was made in which only the iridium wire and 5.5 atm. of NO were present. The wire was fused in the center for about 2 mm. while in the reaction of NO with CO the wire was melted close to the electrodes. In neither case were any oxides of

iridium observed but only the fused Ir sputtered on the walls of the bomb.

### Experimental Section

*A. Materials.* The NO and CO gases were obtained in their highest commercial purity from the Matheson Co., Inc., and final purification was carried out while filling the bomb. Each gas was passed through a 30-cm. absorption tube containing equal amounts of Ascarite and Mg(ClO<sub>4</sub>)<sub>2</sub>, in that order. Important residual impurities were quantitatively assayed using a mass spectrometer which was previously calibrated with known pressures of N<sub>2</sub>O and H<sub>2</sub>, the only significant impurities. Both NO and CO gases had indications of trace amounts of water but this was deduced from a very small difference in a large H<sub>2</sub>O background, a usual problem with analytical mass spectrometers. The NO gas showed 0.025% H<sub>2</sub> and 0.85% N<sub>2</sub>O while the CO gas had only 0.030% H<sub>2</sub>.

*B. Calorimeter.* The experimental apparatus, which had been previously described by Neugebauer,<sup>18</sup> was modified<sup>19</sup> into a higher precision calorimeter capable of measuring a 6-kcal. heat release with a precision of  $\pm 0.01\%$ . The reaction was carried out in a Parr lithium bomb fitted with a double-needle valve system for flushing purposes. The electrodes and flushing tube were fabricated from platinum.

*C. Calibration.* The calorimeter was calibrated using National Bureau of Standards certified 39g benzoic acid under prescribed conditions. The energy equivalent  $\epsilon$  of the calorimeter during series A was  $80897.7 \pm 9.5$  cal. ohm<sup>-1</sup>, the average of six combustions. For series B, the energy equivalent was  $80885.1 \pm 29.7$  cal. ohm<sup>-1</sup> for eight determinations. The assigned uncertainty is the standard deviation of the mean. The second calibration series has an uncertainty about three times larger than a normal set because of a small undetected leak of water from the calorimeter. Since the energy equivalents of the two systems agree essentially within experimental uncertainty of the first, the results of the second series were given some consideration. The energy equivalents which are presented in Table I have been adjusted for heat capacity differences of the bomb contents between the calibration and reaction experiments.

(15) P. Brix and G. Herzberg, *Can. J. Phys.*, **32**, 110 (1954).

(16) "JANAF Thermochemical Tables," D. R. Stull, Ed., The Dow Chemical Co., Midland, Mich., Dec. 31, 1960, and June 30, 1963.

(17) R. L. Nutall, M. A. Frisch, and W. N. Hubbard, *Rev. Sci. Instr.*, **31**, 461 (1960).

(18) C. Neugebauer, Ph.D. Thesis, University of Wisconsin, 1957.

(19) M. A. Frisch, Ph.D. Thesis, University of Wisconsin, 1962.

**Table I:** Heat of Reaction,  $\text{NO(g)} + \text{CO(g)} = \frac{1}{2}\text{N}_2\text{(g)} + \text{CO}_2\text{(g)}$ 

Series	Run	Mass (CO <sub>2</sub> ), g. vac.	$\Delta R$ , ohm	$-\epsilon$ , cal./ohm	$-\Delta E_{\text{tot}}$ , cal.	$\Delta E_{\text{ign}}$ , cal.	$-\Delta E_{\text{react}}$ , cal./g.	Deviation, cal./g.
A	1	3.2794	0.0819834	80873.0	6630.24	1.00	2021.48	1.09
	2	3.3982	0.0849406	80869.2	6869.08	0.80	2021.15	0.76
	3	3.4198	0.0853920	80869.2	6905.58	0.90	2019.03	-1.36
	Average, series A							2020.55
B	1	3.32514	0.0829957	80858.6	6710.92	1.18	2017.88	
	2	3.36431	0.0841551	80858.6	6804.66	1.20	2022.25	
	3	3.35612	0.0837456	80858.6	6771.55	1.30	2017.28	
	4	3.39732	0.0849790	80858.6	6871.28	1.20	2022.21	
Average, series B							2019.90	-0.49
Combined average							2020.39	$\pm 0.57$

*D. Procedure.* The bomb was evacuated by a mechanical pump to a pressure lower than 1 mm. and the purified NO was introduced at a rate of 1 l./min. until a pressure of 5.5 atm. absolute was reached. CO was added in a similar manner up to a total pressure of 12.1 atm. The amount of NO added to the bomb and the CO in 20% excess would be equivalent to the heat release from the combustion of 1 g. of benzoic acid.

The number of moles of CO<sub>2</sub> formed was used as the measure of the extent of reaction. The product gases from the reaction were flushed through a series of absorption tubes following the method of Prosen and Rossini.<sup>20</sup> The first tube in the sequence was filled with Mg(ClO<sub>4</sub>)<sub>2</sub> to remove any traces of water in the bomb. This tube was followed by three Ascarite tubes, each of which had a small layer of Mg(ClO<sub>4</sub>)<sub>2</sub> to reabsorb any water released by the absorption of CO<sub>2</sub>. The ability to make this analysis had been previously verified by flushing the tubes with purified N<sub>2</sub> at 35 cc. min.<sup>-1</sup> for several hours and observing no significant change in the mass of each absorption tube. The bomb was discharged to atmospheric pressure at the flow rate of 35 cc. min.<sup>-1</sup>, requiring about 1 hr., and flushed with N<sub>2</sub> (H<sub>2</sub>O and CO<sub>2</sub> free) for another 2 hr. at the same rate. The transfer of water from the first to the second Ascarite tube, due to the heat released by the absorption of CO<sub>2</sub>, was reduced by immersing this tube in a beaker of cold water during the first 2 hr. of flushing. The tubes (approximately 100 g.) were weighed on an Ainsworth semimicro analytical balance to  $\pm 0.03$  mg. using a similar tube for a tare. Correction for variation in the mass of N<sub>2</sub> in the tubes due to a difference in the temperature and pressure between the two sets of weighings was made using the change in weight of the third Ascarite absorption tube. The second, which acted as a back-up tube, rarely picked up more than 1 mg. The first tube was always freshly charged with

Ascarite and Mg(ClO<sub>4</sub>)<sub>2</sub> to ensure maximum efficiency in the absorption of CO<sub>2</sub>. The buoyancy correction was made using the factor 1.00039 times the weight in air,<sup>20</sup> thereby adjusting for the volume increase of Ascarite in an atmosphere of N<sub>2</sub>.

*E. Fundamental Quantities.* The defined calorie equal to 4.1840 absolute joules was used in the evaluation of the energy equivalent of the calorimeter. The molecular weights for all materials used were based on the 1961 atomic weight scale: C = 12.01115, N = 14.0067, and O = 15.9994. Reduction from bomb conditions to standard states was made according to the method outlined by Hubbard, Scott, and Waddington.<sup>21</sup> To derive the heats of formation from the heat of reaction, the following standard heats of formation at 298.15°K. were employed, each having been adjusted to the 1961 atomic weight scale: CO(g),  $-26.4157 \pm 0.0308$  kcal./mole<sup>22</sup>; CO<sub>2</sub>(g),  $-94.0517 \pm 0.0108$  kcal./mole.<sup>23</sup>

## Results and Discussion

In Table I, the data for the two series of experiments are presented. Because of the large standard deviation of the energy equivalent during series B due to the water leak (29.7 cal./ohm for B vs. 9.5 cal./ohm for A), the experimental results of the B set could not be weighted equally with those of the first. Therefore, in consideration that the average of B differed by only 0.03% from A, the B series was given the weight of one experiment. The average experimental heat of reaction for the three acceptable runs of series A and the

(20) "Experimental Thermochemistry," F. D. Rossini, Ed., Interscience Publishers, Inc., New York, N. Y., 1956, Chapter 4, p. 59.

(21) See ref. 20, Chapter 5, p. 75.

(22) F. D. Rossini, *J. Res. Natl. Bur. Std.*, **22**, 407 (1939).

(23) E. J. Prosen, R. S. Jessup, and F. D. Rossini, *ibid.*, **33**, 447 (1944).

mean of series B is  $-2020.39 \pm 0.57$  cal./g. of  $\text{CO}_2$  or  $-88.917 \pm 0.025$  kcal./mole of  $\text{CO}_2$ . The uncertainty assigned to these numbers is the standard deviation of the mean. In converting  $\Delta E_r$  to the "per mole" basis, the 1961 atomic weight of  $\text{CO}_2$  (44.00995) was used. In Table II, the auxiliary data are listed for the reduction

Table II: Auxiliary Data

Compound	$\partial E/\partial P$ , cal./mole atm.
$\text{N}_2$	$-1.445^a$
$\text{CO}_2$	$-6.90^a$
NO	$-1.326^b$
CO	$-1.475^b$

<sup>a</sup> F. D. Rossini and M. Frandsen, *J. Res. Natl. Bur. Std.*, **9**, 733 (1932). <sup>b</sup> Estimated from  $-a/RT$ , where  $a$  is one of the constants from the van der Waals equation of state.

of the product and reactant gases to their standard states. Since the total pressure is moderately small (approximately 10 atm.), each gas was expanded from the total pressure to a negligibly small pressure (0 atm.). The net change in the internal energy of the gases amounted to 0.036 kcal./mole. To correct for the 0.85%  $\text{N}_2\text{O}$  ( $\Delta H_f^\circ_{298} = 19.49 \pm 0.3$  kcal./mole),<sup>24</sup> the difference of  $-1.78$  kcal./mole between the two  $\Delta E_r$  ( $-87.13$  kcal./mole for  $\text{N}_2\text{O}$  and  $-88.91$  kcal./mole for NO) was multiplied by 0.0085 and added to the experimental  $\Delta E_r$ . The possibility of a significant quantity of the  $\text{H}_2$  impurity reacting with NO was considered highly improbable since CO is a better reducing agent than  $\text{H}_2$  by 10 kcal./mole and, in addition, CO is in considerable excess. The  $\Delta H_f^\circ_{298.15}$  for NO(g) derived from this study is  $21.556 \pm 0.060$  kcal./mole. The un-

certainty intervals assigned to this and other thermodynamic functions are equal to twice the combined standard deviations arising from the calibration, reaction, impurity corrections, and the thermodynamic data for CO and  $\text{CO}_2$ , as recommended by Rossini.<sup>25</sup> These and other related thermodynamic functions can be found in Table III.

Table III: Derived Data<sup>a</sup> at 298.15°K.

NO(0.85% $\text{N}_2\text{O}$ ) + CO =		$\Delta E_r = -88.917 \pm 0.025$
$\frac{1}{2}\text{N}_2 + \text{CO}_2$		$\Delta E_r^\dagger = -88.932 \pm 0.025$
Correction for 0.85% $\text{N}_2\text{O}$	(-0.015)	$\Delta E_r^\circ = -88.896 \pm 0.050$
Reduction to standard states	(+0.036)	$\Delta H_f^\circ = -89.192 \pm 0.050$
Conversion to $\Delta H$	(-0.296)	$\Delta H_f^\circ = +21.556 \pm 0.060$
NO(g)		$\Delta S_f^\circ = +2.96 \pm 0.02$
		$\Delta G_f^\circ = +20.674 \pm 0.060$

<sup>a</sup> Values in kcal./mole except  $\Delta S_f^\circ$  in cal./deg. mole.

The result for  $\Delta H_f^\circ_{298}[\text{NO}(\text{g})]$  ( $21.556 \pm 0.060$  kcal./mole) obtained in this study is recommended as the best value based on the high precision of the data. The results of the previous investigators, listed above, agree with this value within their experimental uncertainty.

*Acknowledgments.* This work was supported financially by the Allied Chemical Corporation, the Wisconsin Alumni Research Foundation, and the Advanced Research Projects Agency through a contract administered by the U. S. Army Research Office, Durham, N. C.

(24) T. Carlton-Sutton, H. Ambler, and G. Williams, *Proc. Phys. Soc. (London)*, **48**, 189 (1936).

(25) See ref. 20, Chapter 14, p. 297.

## The Barium-Sodium Equilibrium System<sup>1</sup>

by F. A. Kanda, R. M. Stevens, and D. V. Keller

Chemistry Department, Syracuse University, Syracuse, New York (Received May 28, 1965)

The barium-sodium phase system has been investigated in the solid and liquid state over the entire range of compositions. The liquidus and solidus curves were determined by thermal analysis methods, whereas the solid-state equilibria were studied by X-ray diffraction methods. This system displays complete miscibility in the liquid state. The solid solubility of sodium in barium and barium in sodium is 3 and 0.5 atomic %, respectively, at room temperature. The system has two compounds: BaNa<sub>4</sub>, which is formed through a peritectoid solid-state reaction at 65°, and BaNa, which melts incongruently at 197°. Sodium is appreciably soluble in BaNa; barium is not. A eutectic, which melts at 82°, forms at 5.5 atomic % barium. X-Ray diffraction patterns have indicated BaNa<sub>4</sub> to be tetragonal with cell dimensions  $a_0 = b_0 = 9.19 \text{ \AA}$ . and  $c_0 = 17.20 \text{ \AA}$ . and BaNa to be orthorhombic with  $a_0 = 4.24 \text{ \AA}$ .,  $b_0 = 5.86 \text{ \AA}$ ., and  $c_0 = 9.65 \text{ \AA}$ ., all  $\pm 0.02 \text{ \AA}$ . The sodium metal used had a melting point of 97.5° and  $a_0 = 4.283 \pm 0.003 \text{ \AA}$ . at 22°. The barium melted at 729° and had  $a_0 = 5.026 \pm 0.003 \text{ \AA}$ . at 22°. A comparison of the results of this investigation with other data obtained for this system is presented.

### Introduction

The barium-sodium system was investigated in this laboratory as part of an over-all program to study the alloying behavior and characteristics of the alkaline earth metals. Several equilibrium systems involving the alkaline earth metals, e.g., Ba-Sr,<sup>2</sup> Ba-Li,<sup>3</sup> Ca-Sr,<sup>4</sup> Sr-Li,<sup>5</sup> and Sr-Na<sup>6</sup> studied previously or concurrently have led to techniques which allow for the accurate and reliable delineation of phase boundaries in these systems. At the onset of this present investigation, no complete study of the phase relationships within the barium-sodium system had been reported. Gould<sup>7</sup> and Miller<sup>8</sup> independently investigated the solubility of barium in sodium and reported conflicting results. During the course of this investigation Remy, *et al.*,<sup>9</sup> published the results of their investigations of the barium-sodium equilibrium system. However, it was decided to complete the study of the system in this laboratory since the results of the two independent investigations over the same composition ranges were considerably different. Also, the barium used by Remy, *et al.*, was obviously quite impure (m.p. 710°), and their differential thermal and time-temperature thermal results were inconsistent.

### Experimental Section

The sodium used in this study was obtained from the Baker and Adamson Chemical Co. This metal gave cooling curves which displayed ideal flat plateaus at the melting point. These isothermal arrests corresponded to a melting point of  $97.5 \pm 0.2^\circ$ . Barium was furnished by King Laboratories Inc., Syracuse, N. Y. It was purified before use by fractional distillation in a high-temperature stainless steel bomb

(1) Abstracted from the dissertation of R. M. Stevens submitted to the Chemistry Department of Syracuse University in partial fulfillment of the requirements for the Ph.D. Degree, June 1964.

(2) R. G. Hirst, A. J. King, and F. A. Kanda, *J. Phys. Chem.*, **60**, 302 (1956).

(3) D. V. Keller, F. A. Kanda, and A. J. King, *ibid.*, **62**, 732 (1958).

(4) J. C. Schottmiller, A. J. King, and F. A. Kanda, *ibid.*, **62**, 1446 (1958).

(5) F. E. Wang, F. A. Kanda, and A. J. King, *ibid.*, **66**, 2138, 2142 (1962).

(6) W. O. Roberts, Ph.D. Dissertation, Syracuse University, 1964.

(7) J. R. Gould, Knolls Atomic Power Laboratory, Schenectady, N. Y., KAPL 1398, 1955.

(8) R. R. Miller, private communication, reported in "Liquid Metals Handbook, Na-K Supplement," 3d Ed., U. S. Government Printing Office, Washington, D. C., 1955.

(9) H. Remy, G. Wolfrum, and H. W. Haase, *Schweiz. Arch. angew. Wiss. Techn.*, **26**, 5 (1960).

capable of holding pressures of  $10^{-6}$  mm. at  $900^{\circ}$ . After condensation of the distillate on the water-cooled cold finger in the distillation bomb, the porous condensate was melted off *in situ* in an argon atmosphere and collected as a cast ingot in a container below the cold finger. This technique avoided the exposure of the barium to the atmosphere until after it was cast, minimizing contamination by nitrogen, an effective depressant of the melting point.<sup>10</sup> As a consequence, only the top of the smooth surface of the ingot was subjected to atmospheric exposure and contamination during transfer of the charge from the bomb to the drybox. This proved important since noncast condensates are exceedingly porous and become extensively contaminated when exposed to the atmosphere, even for a short time interval. The latter porous material is also difficult or impossible to scrape clean of surface contaminants, such as barium nitride, when preparing alloys. Spectrographic analysis of the bright refined barium showed it to contain 0.07% Sr, 0.03% Ca, 0.01% Na, and traces of Mg, K, and Li. The melting point,  $729 \pm 1^{\circ}$ , was obtained as an essentially ideal flat plateau on a time-temperature cooling curve. This is in agreement with the highest melting point reported previously.<sup>11</sup> The authors also noted that barium purified in this manner displayed a softness approaching that of sodium.

Alloys were prepared by weighing the appropriate amounts of metals to within 0.001 g. in a drybox in which a purified argon atmosphere was maintained. The alloy samples, *ca.* 10 ml. in volume, were loaded and stoppered under argon in thin-walled, low-carbon steel tube crucibles approximately 2.54 cm. in diameter and 30.48 cm. long. These were ultimately transferred from the drybox to the thermal analysis unit and continually maintained under an argon atmosphere.

The basic equipment and techniques employed for the thermal analyses of the alloys have been described previously.<sup>2-4</sup> The thermal analysis furnace was provided with water and forced-air cooling features to allow for program-controlled linear cooling rates of  $0.8^{\circ}/\text{min.}$  in the lower thermal ranges of investigation, *e.g.*,  $50-125^{\circ}$ . Cooling rates between  $0.8$  and  $2.0^{\circ}/\text{min.}$  were used in the higher thermal ranges with the slower rates usually preferred.

The chromel-alumel thermocouples used in the thermal analysis were periodically checked against an N.B.S. certified standard thermocouple, and the temperatures reported in the phase diagram are considered reliable to within at least  $\pm 2^{\circ}$ . Both time-temperature and differential temperature-time curves were obtained simultaneously for all alloys.

Alloys were investigated in the solid state by X-ray

powder diffraction methods. Several alloys were also studied in the range  $25-200^{\circ}$  using either a high-temperature X-ray powder camera or a high-temperature atmosphere-controlled X-ray diffractometer. X-Ray specimens in the 0-20 atomic % barium range were prepared as fine slivers shaved from alloy slugs. Alloys above 20 atomic % barium content were sufficiently hard to be filed and, consequently, were prepared as fine filings. All X-ray samples were prepared in a drybox.

## Results

The results of the thermal and X-ray studies of the barium-sodium system are shown in Figures 1 and 2. A total of 47 different alloy compositions was ultimately investigated.

One eutectic is present, and this occurs at 5.5 atomic % barium. The eutectic temperature is  $82^{\circ}$ . Miller<sup>8</sup> reported two eutectics at barium contents of 2.9 atomic % ( $85^{\circ}$ ) and 8.3 atomic % ( $82^{\circ}$ ), while Remy, *et al.*,<sup>9</sup> reported four at 5.6 atomic % ( $85^{\circ}$ ), 12 atomic % ( $78^{\circ}$ ), 26 atomic % ( $57.2^{\circ}$ ), and 70 atomic % barium ( $180^{\circ}$ ).

No congruent-melting compounds were indicated by thermal analysis in this investigation. On the basis of thermal analysis, Miller's results indicate a congruent-melting compound of the approximate composition  $\text{BaNa}_{24}$ , and Remy, *et al.*, report  $\text{BaNa}_{12}$  and  $\text{BaNa}_6$  in the 0-20 atomic % barium range of the phase diagram. No reference is made to the use of X-ray techniques in order to validate the existence of these compounds in either investigation. X-Ray results of the present investigation prove that no compounds of such compositions exist. All diffraction patterns displayed a mixture of  $\alpha$ -sodium diffraction lines with the lines of  $\text{BaNa}_4$ . No other diffraction lines occur for specimens within the 0-20 atomic % barium composition range when the samples are properly equilibrated.

Cooling curves for alloys between 2.5 and 25 atomic % barium produced an additional isothermal pause following the eutectic solidification. This pause, which occurred at  $65 \pm 5^{\circ}$ , was due to the solid-state peritectoid reaction:  $\alpha + \gamma \rightarrow \text{BaNa}_4$ . This reaction was studied in the high-temperature X-ray diffractometer in both heating and cooling directions. Thus,  $\text{BaNa}_4$  was found to decompose readily into  $\alpha$  and  $\gamma$  solid solutions when heated at  $70^{\circ}$ . Specimens rapidly quenched from  $70^{\circ}$  displayed only  $\alpha$  and  $\gamma$

(10) V. A. Russell, M.S. Thesis, Syracuse University, 1949.

(11) D. T. Peterson and J. A. Hinkebein, *J. Phys. Chem.*, **63**, 1360 (1959).

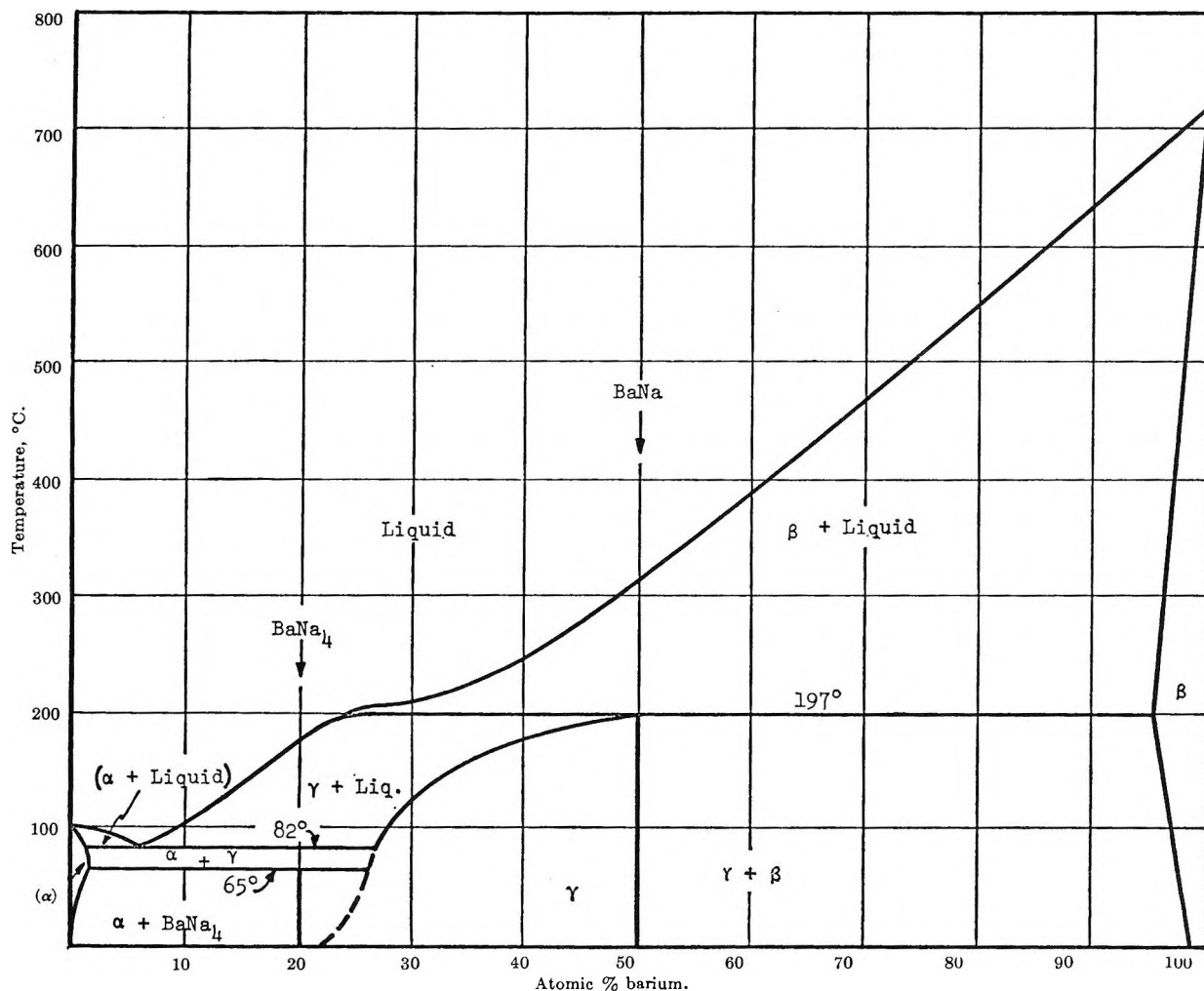


Figure 1. The barium-sodium equilibrium system.

diffraction patterns, but, in contrast, when these were slowly cooled through the peritectoid temperature, the lines of  $\text{BaNa}_4$  readily appeared.

During solidification of the  $\gamma$  intermediate phase from the melts of alloys in the range 5–23 atomic % barium, drastic cases of segregation occurred. The  $\gamma$  phase has a density approximately twice that of the melt from which it separates. As a consequence, it would readily settle to the bottom of the crucible resulting ultimately in an incomplete peritectoid reaction with the  $\alpha$  solid solution. Thus, X-ray specimens selected from the bottom portions of the crucibles displayed only  $\gamma$  diffraction lines whereas specimens from the top portions of the charge showed  $\alpha$  and  $\text{BaNa}_4$  lines. While these conditions pertained, the stoichiometry of the compound could not be ascertained. Small alloy specimens, *ca.* 1–2 ml. in volume, were prepared and cold-worked for 1–2 hr. in the jaws of a vise in the drybox. This continual

kneading physically homogenized the alloys. After annealing the alloys, X-ray patterns showed the  $\alpha$ -sodium lines to occur only in samples with less than 20 atomic % barium content at room temperature. The  $\gamma$  diffraction pattern only appeared in samples above 20 atomic % barium and existed exclusively in all samples between 21–50 atomic % barium when X-rayed at room temperature. As a consequence, it was deduced that the compound whose diffraction pattern appeared with both  $\alpha$  and  $\gamma$  had the composition  $\text{BaNa}_4$  which crystallized in a tetragonal cell (Table I).

This investigation found some alloys containing as high as 45 atomic % barium produced the eutectic pause at 82° owing to nonequilibrium of the peritectic reaction. This pause was readily eliminated by soaking the sample for a few hours below the peritectic temperature. Alloys of 28 and 30 atomic % barium content were soaked for as long as 6 weeks at 100° in order



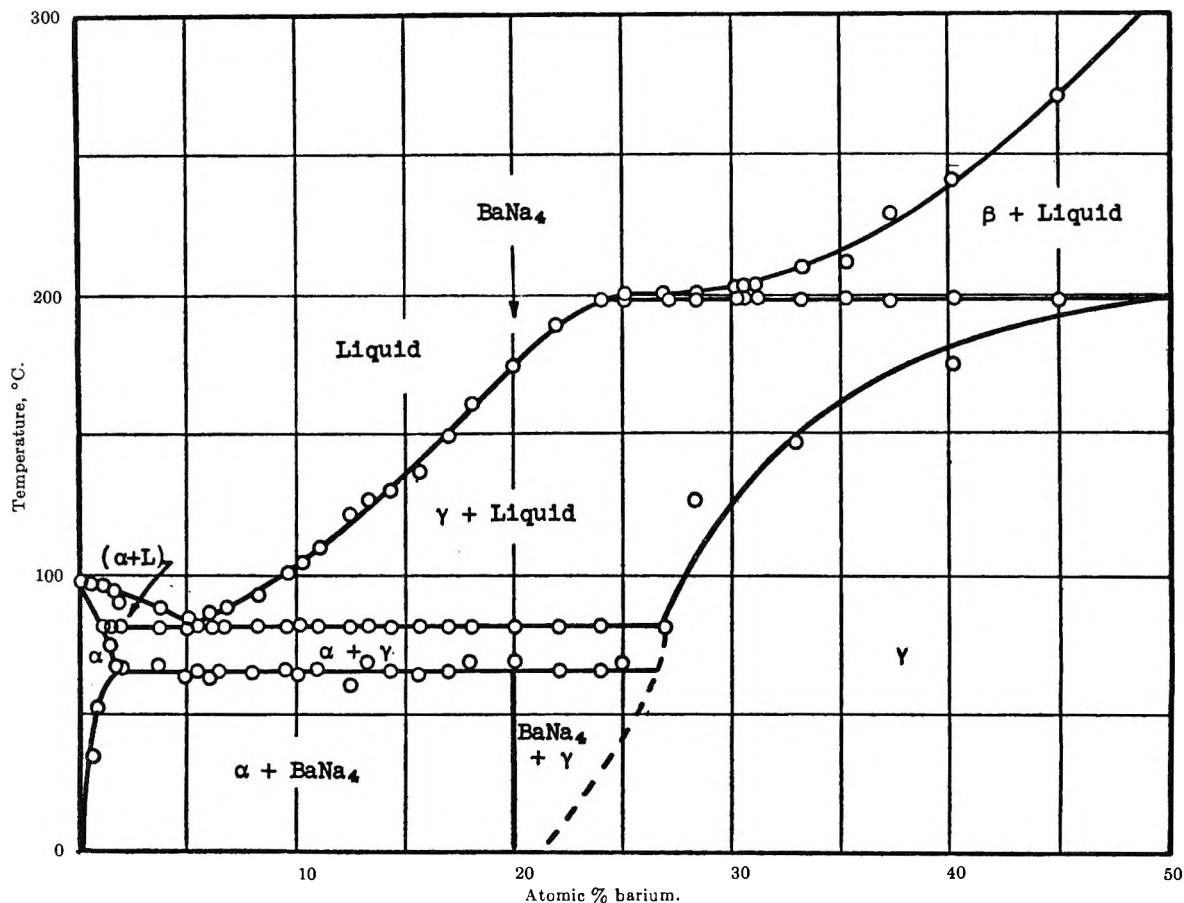


Figure 2. The sodium-rich end of the barium-sodium system.

to eliminate the eutectic pause. Thus, as a consequence of lengthy equilibration, it has been established that the eutectic horizontal does not extend beyond 28 atomic % barium. It is possible, in view of these findings, that equilibration over still longer time periods may prove this limit to be less than the 27 atomic % value shown in the diagram. The sloping boundary of the  $\gamma$  region between 27 atomic % at 82° and 21 atomic % barium at room temperature is dotted in order to indicate some uncertainty in both its composition limits and curvature due to the equilibration difficulties discussed above.

Miller's work<sup>8</sup> was concerned with the determination of the liquidus over a limited range of compositions. The results are substantially in accord with those of this investigation. In most cases, the variation of liquidus points is of the order of 3°.

The existence of BaNa has been previously reported<sup>9</sup>; however, it was reported as being a compound with a congruent melting point of 510°. On the basis of extensive thermal analysis investigations of several separate alloys of this composition, no solid

phase was found to form until the liquidus temperature of 315° was reached in conformity with Figures 1 and 2. Furthermore, reinvestigations of alloys covering the 40–60 atomic % barium range showed no evidence whatsoever of a congruent melting point dome but rather a continually rising liquidus boundary. Finally, a 40 atomic % barium alloy, when soaked at 210° and then rapidly quenched, clearly showed the presence of  $\beta$ -barium diffraction lines. The sluggish peritectic reaction was of aid here to allow the retention of the  $\beta$  phase. If there were a compound possessing a congruent melting point as postulated by Remy, *et al.*, the region in which the 40 atomic % barium alloy was soaked as described above, would have to be a phase region consisting of BaNa and liquid, and there would be no conceivable way for the  $\beta$ -barium to occur in the sample. A similar 40 atomic % barium alloy, when soaked and quenched from 175°, no longer showed the presence of  $\beta$ -barium but, instead, showed only the  $\gamma$  phase, indicating the peritectic reaction,  $\beta + \text{liquid} \rightarrow \gamma$  (197°), had occurred.

Room-temperature X-ray patterns indicated the



**Table I:** X-Ray Data for the Compound BaNa<sub>4</sub>;  
 $a_0 = b_0 = 9.16 \pm 0.03 \text{ \AA}$ ;  $c_0 = 17.28 \pm 0.03 \text{ \AA}$ .

Line no.	Sin $\theta$	$d$	$hkl$
1	0.083	9.23	100
2	0.092	8.43	002
3	0.118	6.51	110
4	0.125	6.13	102
5	0.134	5.73	003
6	0.173	4.44	201 (004)
7	0.205	3.75	104
8	0.229	3.36	123
9	0.241	3.19	105
10	0.251	3.06	300
11	0.305	2.53	304 (230)
12	0.313	2.46	232 (007)
13	0.325	2.37	206
14	0.339	2.27	305
15	0.357	2.16	008 (330)
16	0.368	2.09	108
17	0.379	2.03	333 (404)
18	0.388	1.98	235
19	0.398	1.93	334
20	0.414	1.86	119
21	0.421	1.83	500
22	0.437	1.76	245
23	0.449	1.72	250
24	0.471	1.63	505
25	0.506	1.52	601
26	0.536	1.44	450
27	0.565	1.36	361

**Table II:** X-Ray Data for the Compound BaNa;  
 $a_0 = 4.26 \text{ \AA}$ ;  $b_0 = 5.88 \text{ \AA}$ ;  $c_0 = 9.65 \text{ \AA}$ , all  $\pm 0.02 \text{ \AA}$ .

Line no.	Sin $\theta$	$d$	$hkl$
1	0.080	9.65	001
2	0.132	5.85	010
3	0.182	4.24	100
4	0.198	3.89	101
5	0.223	3.46	110
6	0.235	3.27	111 (003)
7	0.257	2.99	020
8	0.286	2.69	021
9	0.323	2.39	120 (004)
10	0.347	2.22	023
11	0.371	2.08	201
12	0.385	2.00	210
13	0.392	1.96	030
14	0.424	1.81	032
15	0.451	1.71	220
16	0.460	1.67	033
17	0.468	1.64	132
18	0.494	1.56	133
19	0.527	1.46	041
20	0.533	1.45	230
21	0.542	1.42	300
22	0.548	1.40	232
23	0.559	1.38	007
24	0.591	1.30	107
25	0.605	1.27	044

alloys ranging from 51 to 97 atomic % barium consisted of  $\gamma$  (BaNa) and  $\beta$ -barium with the  $\gamma$  diffraction lines becoming progressively weaker as alloys approached 97 atomic % barium. The powder pattern of BaNa has been indexed on the basis of an orthorhombic cell. The  $d$  values and indices are given in Table II.

The  $\gamma$ -solidus boundary, above  $82^\circ$ , could not be determined reliably by direct thermal analysis methods since this boundary represents completion of solidification accompanied by a changing composition of the solid phase. As pointed out above, equilibration in this region was very difficult to realize, necessitating prolonged soaking periods in order to allow for appropriate diffusion and consequent adjustment of the  $\gamma$  composition. For this reason, only a selected set of samples was prepared and cold-worked in the vise, homogenized, and soaked at  $100^\circ$  for several weeks for this part of the investigation. Diffractometer samples of these were then investigated at successively higher temperatures with a 2-hr. soak given at each temperature investigated. As the solidus was approached, the X-ray pattern became continuously more diffuse, but only showed the  $\gamma$  pattern. Simul-

taneously, while soaking, the sample could be observed in the camera furnace through a Mylar window. It was observed that, when the X-ray pattern displayed no evidence of crystallinity, beads of liquid appeared on the surface of the specimen. This temperature was plotted for each sample investigated to delineate the solidus boundary as shown in Figures 1 and 2. This boundary probably represents an upper limit for the initial melting of  $\gamma$ . It is conceivable that intermediate regions of the boundary between  $82$  and  $197^\circ$  may be as much as  $10^\circ$  lower than that shown.

The eutectic reported by Remy, *et al.*,<sup>9</sup> at  $180^\circ$ , with an erratic spread of temperature, is apparently the isothermal peritectic pause at  $197^\circ$ . It was found in the present investigation that this pause could be suppressed to as low as  $180^\circ$  by supercooling. However, if slow cooling rates and vigorous stirring were employed, this isothermal appeared consistently at  $197 \pm 2^\circ$ .

Thermal analysis and X-ray powder patterns proved the solidus and solvus of the terminal solid solutions  $\alpha$  and  $\beta$  to be as shown in Figures 1 and 2. Application of Vegard's law<sup>12</sup> to a series of room-temperature

(12) L. Vegard and H. Dale, *Z. Krist.*, **67**, 148 (1928).

films provided the room-temperature points on the solvus. The solubility of barium in sodium is of the order 0.5 atomic % barium at room temperature and a maximum solubility of 3 atomic % at 65°, the peritectoid temperature. The solubility of sodium in barium was found to be 3 atomic % sodium at room tempera-

ture and a maximum solubility of 5 atomic % at 197° the peritectic temperature.

*Acknowledgment.* The authors wish to express their gratitude to the Atomic Energy Commission for the financial support which made this study possible.

## The Dimer Spectrum of Acridine Orange Hydrochloride

by Michael E. Lamm\* and David M. Neville, Jr.

Laboratory of Neurochemistry, National Institute of Mental Health, Bethesda, Maryland  
(Received May 28, 1965)

The absorption spectra of the cationic dye acridine orange hydrochloride have been determined at eight different concentrations in water from  $10^{-6}$  to  $10^{-4}$  M. Over this range the spectra change continuously. An isosbestic point is observed at 470 m $\mu$ . The spectral data are interpreted in terms of monomer-dimer equilibria. Agreement of the data with two different equilibria has been checked by means of a computer program employing a reiterative procedure which varies the equilibrium association constant,  $K$ , as an arbitrary parameter until a value of  $K$  is found which gives the smallest root-mean-square deviation of the optical density data with the equilibrium model. The two models, (1) involving dye cations only,  $2D^+ = D_2^{2+}$ , and (2) anions as well,  $2D^+ + A^- = D_2A^+$ , fit the data equally well with  $K = 1.05 \times 10^4$  l. mole $^{-1}$  and  $K = 4.7 \times 10^8$  l. $^2$  mole $^{-2}$ , respectively. Dimer spectra obtained by extrapolating the data with the above models differ. Dimer spectrum 1 shows a symmetric splitting in relation to the monomer peak while dimer spectrum 2 exhibits a redistribution of intensity between the monomer peak band and shoulder band. The significance of the dimer spectrum in relation to current theories of metachromasy is discussed.

### Introduction

The pronounced effect of concentration on the color of aqueous cationic dye solutions has been known for over 50 years.<sup>1</sup> Various physical descriptions of this phenomenon have been proposed, yet to date the superiority of any one model remains to be demonstrated. The spectral changes are known to be associated with reversible polymerization of dye, and at low concentrations the predominant aggregate species is believed to be a dimer.<sup>2</sup> A knowledge of the absorption spectrum of the dimer is crucial to the understanding of the physical process involved in the spectral

changes. Unfortunately, the dimer never exists alone and its spectrum is obscured by contributions from monomers and higher aggregates.

To date, the dimer spectra of at least four different dyes have been derived utilizing certain critical assumptions.<sup>3-6</sup> In each case the reaction has followed the scheme

\*Department of Pathology, New York University School of Medicine, New York, N. Y.

(1) S. E. Sheppard, *Proc. Roy. Soc. (London)*, **A82**, 256 (1909).

(2) V. Zanker, *Z. physik. Chem.*, **199**, 225 (1952).



or



The ability of these models to fit the data has reduced interest in more complex models. Recently, however, Haugen and Hardwick<sup>7</sup> have presented evidence for a model which includes counterion participation in the equilibrium



In the present study we have investigated the nature of the dimer spectrum of acridine orange hydrochloride by employing a computer program to determine the best fit of a large quantity of spectral data to two different dimerization equilibria.

### Methods

**Purification of AO.** Twenty-five grams of commercial acridine orange (Chroma) was dissolved in 250 ml. of ice-cold water and titrated with 0.1 N NaOH to pH 10.5. The resulting suspension of free base was filtered in the cold, washed with water to remove residual salt, dried at 100°, and dissolved in methanol. The pH was lowered to 5.5 by the addition of an acid-methanol solution (1 vol. of concentrated HCl and 9 vol. of methanol), and the hydrochloride, AO·HCl, was precipitated by the addition of 10 vol. of diethyl ether. The dye was collected and dried, and the whole process was repeated once more.

One gram of AO·HCl was dissolved in absolute ethanol and passed through an 8 × 40-cm. acid-washed alumina column run in ethanol. Most of the dye emerged in the first peak leaving a pink trailing band and a pink band at the origin. The eluate comprising the main fraction was filtered to remove any alumina particles present. When rerun on both a small alumina column and on a thin layer of silica gel in CHCl<sub>3</sub>-CH<sub>3</sub>OH, 3:1, an aliquot of this solution moved as a single band. The AO·HCl was precipitated from the eluate by the addition of ether, collected by filtration, and dried at 100°.

To obtain a sample of dye for determination of the molar extinction coefficient, 200 mg. of the purified AO·HCl was converted to the free base as described above. The insoluble base was removed from the aqueous suspension and dried *in vacuo* overnight at 100°. The free base was dissolved in chloroform, which can be removed quantitatively.<sup>2</sup> The chloroform was evaporated off and the dye was dried *in vacuo* at 100° overnight (yield 120 mg.). Less than 0.25% total chlorine was found on analysis of this final sample.

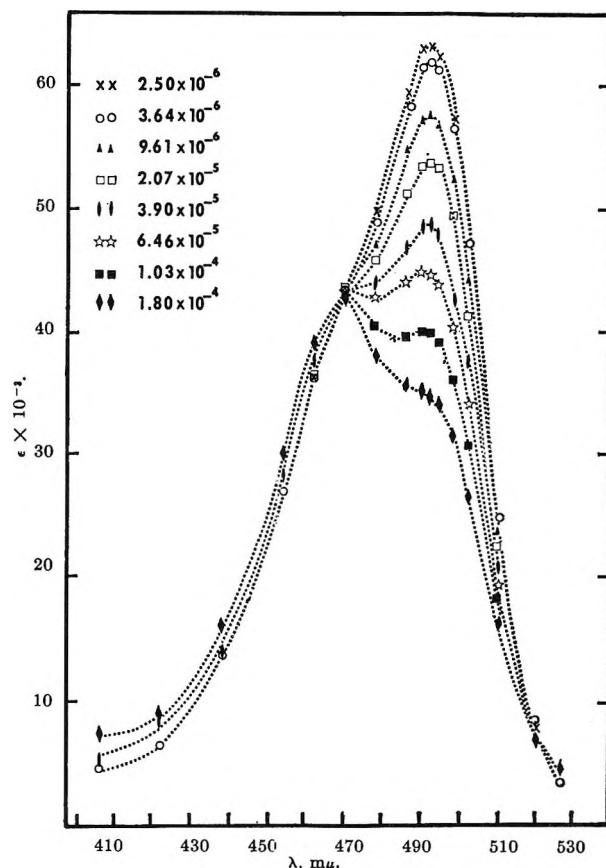


Figure 1. Absorption spectra of acridine orange hydrochloride in water are shown in units of molar extinction coefficients over a concentration range of  $2.5 \times 10^{-6}$  to  $1.8 \times 10^{-4} M$ .

**Determination of Molar Extinction Coefficients.** The main problem that had to be overcome in order to determine accurate and reproducible molar extinction coefficients was adsorption of dye from solution. The following surfaces were explored: Pyrex glass, siliconed glass, glass exposed to hydrofluoric acid, Teflon, polypropylene, and polyethylene. Polyethylene bottles (Nalge Corp., Rochester, N. Y.) were found to be most suitable. During the time required to take the absorption spectrum, adsorption could be held to about 1% of the dye content per dilution. No adsorption occurred during the first few minutes after addition of dye

(3) G. S. Levinson, W. T. Simpson, and W. Curtis, *J. Am. Chem. Soc.*, **79**, 4314 (1957).

(4) K. L. Arvan and N. E. Zaitseva, *Opt. Spectry.*, **11**, 38 (1961).

(5) K. Bergmann and C. T. O'Konski, *J. Phys. Chem.*, **67**, 2169 (1963).

(6) G. R. Haugen and W. H. Melhuish, *Trans. Faraday Soc.*, **60**, 386 (1964).

(7) G. R. Haugen and E. R. Hardwick, *J. Phys. Chem.*, **67**, 725 (1963).

solution to quartz cuvettes which had been rinsed with water, hydrochloric acid in ethanol, water, and ethanol, provided the dye solution was not stirred or mixed within the cuvette and providing the dye concentration was above  $10^{-5} M$ . As the dye concentration was reduced below  $10^{-5} M$ , optical density readings at a given dilution showed increased scatter, especially below  $470 m\mu$ . Only part of this error could be accounted for by the increase in dye adsorption at low concentrations.

Stock solutions of dye were prepared by placing a weighed sample of purified base in a dry polyethylene bottle and adding 1.05 equivalents of HCl converting all of the dye to the monovalent cation. Distilled water was added to make the dye concentration in the range  $2-7 \times 10^{-4} M$ . Stock solution pH ranged between 5.4 and 6.0. Aliquots of stock solutions were poured into dry polyethylene bottles, diluted with distilled water, mixed by swirling, and poured into 1- or 2.5-cm. path length cuvettes which had been cleaned as described above. Dye solutions were added to 0.1-cm. cuvettes by means of capillary pipets which had been rinsed in the dye solution. Optical densities were read on a Cary Model 14 spectrophotometer. For very dilute solutions an expanded-scale slide wire was used. All additions and dilutions were made by weight, and all determinations were done at  $25 \pm 0.5^\circ$ . Molarities were calculated by weights using a formula weight of 265 for AO base. The assumed identity of the formula weight and the molecular weight was based on the chromatography results and the demonstrated elimination of solvent of crystallization. All calculated molarities were corrected for dye adsorption by reducing the initially calculated value 1% per dilution. From the calculated molarity and the observed optical density at each dilution, the molar extinction coefficient was determined at that concentration. Multiple determinations were made from three separate weighed samples of solid AO base.

## Results

The visible absorption spectra in units of molar extinction of acridine orange hydrochloride over a 100-fold range in concentration are shown in Figure 1. The dye does not obey Beer's law. In dilute solutions the absorption maximum occurs at  $492 m\mu$  and a shoulder is present at  $\sim 470 m\mu$ . As the concentration is increased, the shoulder becomes more prominent as the main band decreases in intensity. This phenomenon is characteristic of the metachromatic dyes. At  $470 m\mu$  an isobestic point is present,  $\epsilon$  43,000, indicating that only two spectral species are present over the concentration range  $10^{-6}$  to  $10^{-4} M$ . The presence

of only two spectral species permits us to represent the total dye concentration  $C$  in units of moles per liter and the total molar extinction coefficient  $\epsilon$  as the sum of contributions from two species, monomer and dimer.

$$C = C_M + 2C_D \quad (3)$$

$$\epsilon = \alpha(\epsilon_M) + (1 - \alpha)\epsilon_D/2 \quad (4)$$

Where  $\alpha$  is the fraction of dyes present as monomers

$$\alpha = \frac{(D^+)}{C} \quad (5)$$

Assuming that  $\epsilon_M$  and  $\epsilon_D$  are independent of concentration, a plot of  $\epsilon$  vs.  $\alpha$  at any wave length should yield a straight line with intercepts at  $\epsilon_M$  for  $\alpha = 1$  and  $\epsilon_D/2$  for  $\alpha = 0$ . The value of  $\alpha$  can be computed from the relation between  $\alpha$  and the association constant. The association constant for equilibrium 1,  $K_1$ , is

$$K_1 = \frac{(1 - \alpha) \frac{C}{2}}{\alpha^2 C^2} \quad (6)$$

The association constant for equilibrium 2,  $K_2$ , is in the form of a cubic equation, the real roots of which were found by the usual methods

$$K_2 = \frac{(1 - \alpha)}{\alpha^2 C^2 + \alpha^3 C^2} \quad (7)$$

The value of  $K$  was determined by a reiteration procedure. In this study we used a computer program developed in this laboratory by Dr. H. DeVoe to perform the reiteration. An arbitrary  $K$  is chosen and the corresponding values of  $\alpha$  for each of several solutions with different concentrations are calculated using eq. 6 or 7. For each wave length the best straight-line fit of  $\epsilon$  vs.  $\alpha$  is found by weighted least squares. The procedure is repeated with different values of  $K$  until a minimum is reached in the root-mean-square deviation of the experimental O.D. values from the computed best straight-line values. The deviations in O.D. were weighted to be proportional to  $C$ .

When the data shown in Figure 1 were used as input (involving eight solutions and thirteen wave lengths), the computer found a single minimum for both equilibria. Figures 2 and 3 show a plot of root-mean-square deviation in units of O.D. vs.  $K$  for equilibria 6 and 7. For eq. 6 the minimum corresponds to  $K = 1.05 \times 10^4$  l. mole $^{-1}$  while for eq. 7 the best value is  $K = 4.7 \times 10^8$  l. $^2$  mole $^{-2}$ . At the minimum of each curve the root-mean-square deviations are essentially equal. Consequently, the data fit both equilibria

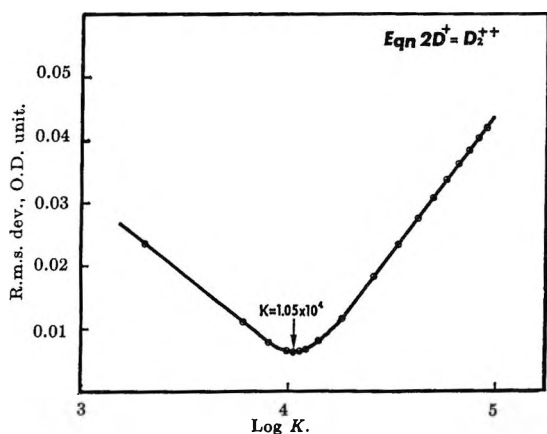


Figure 2. The average root-mean-square deviations in units of O.D. for plots of  $\epsilon$  vs.  $\alpha$  at 13 different wave lengths and eight concentrations are plotted against  $K$ .  $\epsilon$  is taken from the data of Figure 1.  $\alpha$  is computed from eq. 6 at each arbitrary value of  $K$ . The minimum deviation, 0.006, occurs at  $K = 1.05 \times 10^4 M^{-1}$ .

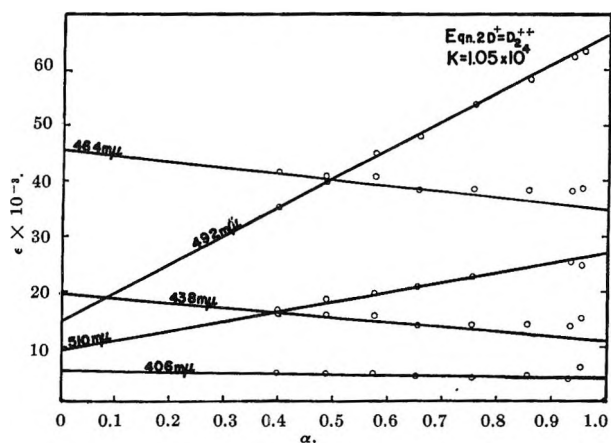


Figure 4. Molar extinction coefficients at the indicated wave lengths and at eight different concentrations are plotted vs.  $\alpha$ , the fraction of monomers. The value of  $\alpha$  is computed from eq. 6 using the value of  $K$  indicated in Figure 2 and the known dye concentration.

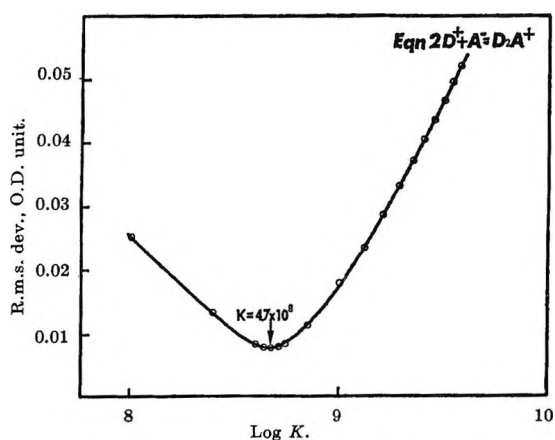


Figure 3. Same plot as in Figure 2 except that  $\alpha$  is computed from eq. 7. The minimum deviation, 0.007, occurs at  $K = 4.7 \times 10^8 M^{-2}$ .

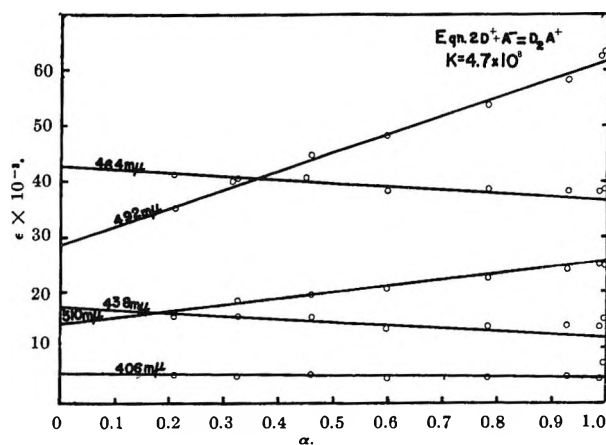


Figure 5. Same plot as in Figure 4 except the value of  $\alpha$  is computed from eq. 7 using the value of  $K$  indicated in Figure 3.

equally well. The agreement between the data and the two models can be better visualized in Figures 4 and 5, where  $\epsilon$  vs.  $\alpha$  is plotted at several wave lengths for both models using the best value of  $K$  for each case. The deviation of each point from the line represents the deviation of the data from the model. The derived dimer and monomer spectra shown in Figure 6 were obtained from the intercepts of the straight lines at  $\alpha = 0$  and  $\alpha = 1$  and include data obtained from additional solutions and wave lengths not used to determine the equilibrium constants.

**Discussion**

The surprising result of this study is the finding that both dimerization models fit the data. The difference

between the minimum root-mean-square deviations for each model, 0.001, is not significant. In general, both models fit the data equally well at all wave lengths except at the lowest concentrations where the points below 470 m $\mu$  show larger deviations.

Previous studies have reported dye dimer spectra derived on the basis of eq. 1. In each case a fit of the experimental data to the single model was taken as the major evidence in support of the model. It is obvious that the ability of a model to fit data is not sufficient cause for acceptance of the model, and, unless predictability is a major feature of a model, all other possible models must be eliminated by some means.

In the present study we have tested what we consider to be the two most likely dimerization models. Since

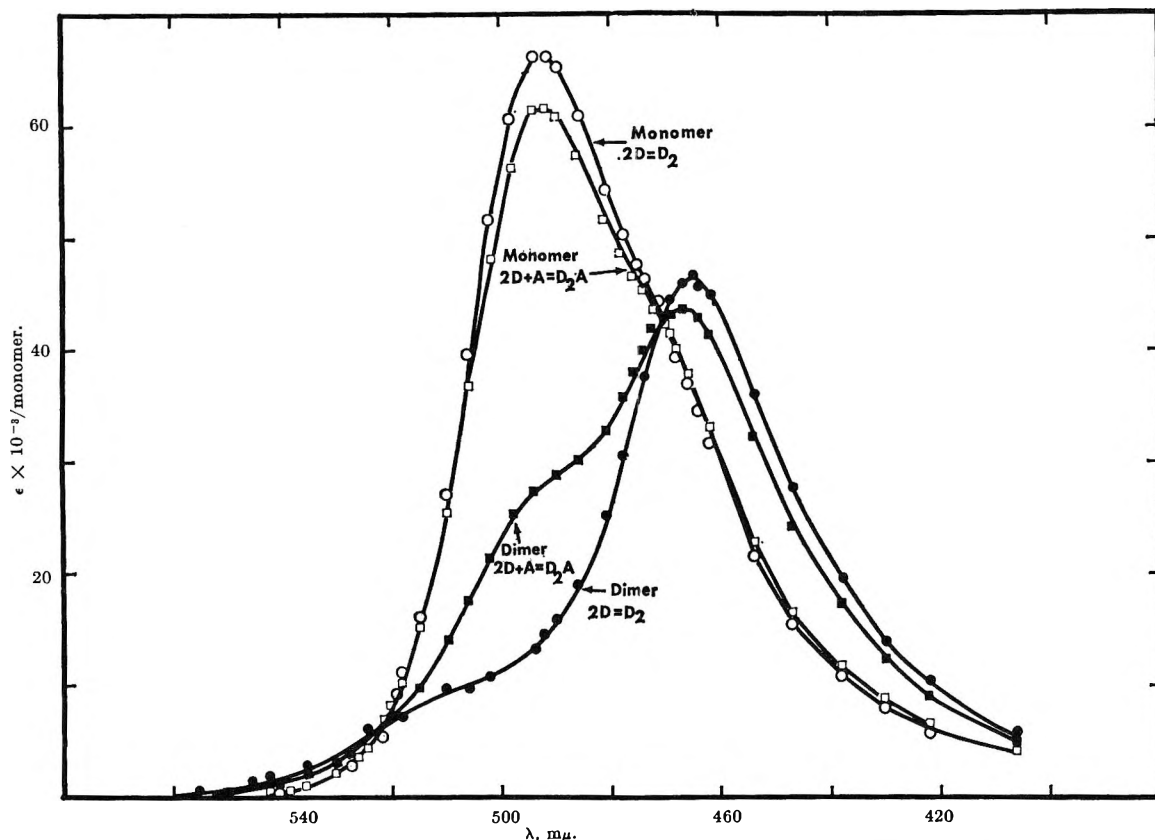


Figure 6. The extrapolated monomer and dimer spectra in units of molar extinction coefficient per monomer are shown for both equilibria.

the data presented here do not provide a basis for choosing between the models, and since the literature contains conflicting data on the question of anion participation in monomer-dimer equilibria,<sup>3,5,7</sup> we will discuss the significance of both sets of spectra, recognizing that at least one of them is incorrect.

The monomer spectra derived from the different dimerization equilibria are similar and closely resemble the spectrum of unassociated dye in organic solvents. Both spectra display a shoulder at shorter wave lengths ( $\sim 470$  m $\mu$ ) characteristic of monomeric cationic dyes. Sheppard<sup>8</sup> has proposed that the shoulder is derived from vibrational coupling with a single electronic transition. In support of this thesis, Zanker<sup>9</sup> has demonstrated a mirror image relationship between the monomer absorption and fluorescence spectra of acridine orange. From Zanker's data it appears that the 492-m $\mu$  peak and the 470-m $\mu$  shoulder represent the  $0 \rightarrow 0$  and  $0 \rightarrow 1$  transition of a major vibrational progression. The significance of the present study in relation to these data can be seen by examining the dimer spectrum derived on the basis of anion inclusion. The absorption maximum occurs at 470 m $\mu$ , coincident

with the  $0 \rightarrow 1$  transition while a prominent shoulder exists at  $\sim 495$  m $\mu$  coincident with the  $0 \rightarrow 0$  transition. If this represents the correct spectrum, it provides strong support for the idea of Sheppard and Zanker that dimerization induces a redistribution of the transition probabilities between the  $0 \rightarrow 0$  and  $0 \rightarrow 1$  states. In Zanker's scheme this is accomplished by a differential shift in the ground and excited state potential energy curves of each monomer, thus altering the Franck-Condon vibronic intensity factors. More recently, DeVoe<sup>10</sup> has shown that a similar redistribution of intensity within the band is predicted when the dyes are oriented parallel to one another in the dimer and the oscillators in the dyes are coupled by coulombic forces.

The dimer spectrum derived from eq. 6 fails to show a band in the region of the monomer  $0 \rightarrow 0$  transition. Instead, there are two bands roughly symmetrically

(8) S. E. Sheppard, *Rev. Mod. Phys.*, **14**, 303 (1942).

(9) V. Zanker, M. Held, and H. Rammensee, *Z. Naturforsch.*, **14b**, 789 (1959).

(10) H. DeVoe, *J. Chem. Phys.*, **41**, 393 (1964).

distributed above and below the  $0 \rightarrow 0$  band, a strong band at  $\sim 470 \text{ m}\mu$ , and a weak shoulder at  $\sim 515 \text{ m}\mu$ . This appears to be a property of dimer spectra derived from eq. 6 and has been noted for pyridocyanine,<sup>3</sup> rhodamine,<sup>4</sup> methylene blue,<sup>5</sup> and proflavine.<sup>6</sup> This type of spectral splitting is predicted for dyes which are oriented at a small angle to one another in the dimer, by the strong coupling exciton theory of Levinson, Simpson, and Curtis.<sup>3</sup> Their theory states that the degeneracy of the energy levels within the dimer results in a splitting of these levels and an unequal distribution of intensity between them.

We see then that depending on which equilibrium model is used we derive different dimer spectra, each of which tends to support different physical explanations of the spectral shifts. The conflicting evidence within the literature on the question of anion participation in dye dimerization equilibria points up the difficulty in designing experiments to test these models. Part of the problem is due to the narrow concentration range over which dye solutions are free from higher aggregates. The addition of electrolyte narrows this range even further, so that it becomes

difficult to distinguish between ionic strength effects and specific anion effects. To illustrate the complexity of the problem, we have noted that certain organic electrolytes such as guanidine hydrochloride can either promote association or dissociation depending on whether they are present in low or high concentrations.<sup>11</sup> This is undoubtedly due to the unique properties of the guanadinium ion, but it illustrates the hazards of drawing specific conclusions about ion participation in a given equilibrium when the ions in question may also alter the solvent structure.<sup>12</sup> Perhaps the least ambiguous experiments would be the determination of the association constants for a series of dye salts in the absence of added electrolyte. Anion participation should be reflected by variations in  $K$  among the various salts.

*Acknowledgment.* The authors are greatly indebted to Dr. H. DeVoe who made his computer program available for this study. The authors also wish to thank Dr. D. F. Bradley for many helpful discussions.

---

(11) D. M. Neville, Jr., unpublished data.

(12) W. P. Jencks, *Fed. Proc., Suppl.* 15, S-50 (1965).

# The Conductance of the Symmetrical Tetraalkylammonium Halides and Picrates in Acetonitrile at 25°<sup>1</sup>

by D. Fennell Evans, C. Zawoyski, and Robert L. Kay

Mellon Institute, Pittsburgh, Pennsylvania 15213 (Received June 1, 1965)

Conductance measurements are reported for Me<sub>4</sub>NBr, Me<sub>4</sub>NI, Me<sub>4</sub>NPi, Pr<sub>4</sub>NBr, Pr<sub>4</sub>NI, Bu<sub>4</sub>NBr, Bu<sub>4</sub>NI, and Bu<sub>4</sub>NPi at 25° in acetonitrile. The data, after analysis by the Fuoss-Onsager theory, produced a constant ion size parameter of  $(3.6 \pm 0.2)\text{\AA}$  for almost all of the salts. Only the tetramethylammonium halides were found to be associated to any appreciable extent in keeping with the behavior of these salts in nitromethane. The association behavior of electrolytes in acetonitrile, nitromethane, and nitrobenzene, solvents of almost identical dielectric constant, and acetone, a solvent of lower dielectric constant (20.5), are compared, after recalculation to bring the data into conformity with the Fuoss-Onsager theory. The association in nitrobenzene solutions is higher than expected, but for all of the solvents the association constants increase with decreasing crystallographic size in contrast to what is found in hydrogen-bonded solvents. KI in acetone is the one exception to this rule.

## Introduction

This work is part of a systematic study of the transport properties of the symmetrical tetraalkylammonium salts in dilute and concentrated solutions. We are particularly interested in the interaction of the hydrophobic side chains of these electrolytes with water. Before such interactions can be characterized, it is necessary to establish the behavior of these electrolytes under a variety of conditions. Here, we report the association behavior of these symmetrical electrolytes in a nonhydrogen-bonded solvent of lower dielectric constant. This work supplements investigations in methanol,<sup>2</sup> D<sub>2</sub>O,<sup>3</sup> and aqueous solutions,<sup>4</sup> which are to be reported in subsequent papers.

There has been no systematic investigation with the required precision for a detailed analysis of the concentration dependence for the symmetrical tetraalkylammonium halides in acetonitrile. Much of the early work<sup>5,6</sup> lacked the required precision, and other investigators measured only a limited number of salts.<sup>7,8</sup> Popov and co-workers have reported data for the tetramethylammonium halides and a number of polyhalides.<sup>9</sup> Other conductance investigations of this solvent have been concerned primarily with determining individual ion conductances from measurements

on salts composed of two large ions, such as tetrabutylammonium tetraphenylboride<sup>10</sup> or tetraisoamylammonium tetraisoamylboride.<sup>11</sup>

## Experimental Section

The Pyrex conductance cells were of the Erlenmeyer type as described by Daggett, Bair, and Kraus,<sup>12</sup> contained 500 ml. of solution, and had cell constants

(1) Presented in part at the 147th National Meeting of the American Chemical Society, Chicago, Ill., Sept. 1964.

(2) R. L. Kay, C. Zawoyski, and D. F. Evans, to be published.

(3) R. L. Kay and D. F. Evans, to be published.

(4) D. F. Evans and R. L. Kay, to be published.

(5) P. Walden and E. J. Birr, *Z. physik. Chem.* (Leipzig), **144A**, 269 (1929).

(6) J. C. Philip and H. R. Courtman, *J. Chem. Soc.*, **97**, 1261 (1910).

(7) C. M. French and D. F. Muggleton, *ibid.*, 2131 (1957).

(8) G. Kortum, S. D. Gokhale, and H. Wilski, *Z. physik. Chem.* (Frankfurt), **4**, 86 (1955).

(9) A. I. Popov and N. E. Skelly, *J. Am. Chem. Soc.*, **76**, 5309 (1954); A. I. Popov, R. H. Rygg, and N. E. Skelly, *ibid.*, **78**, 5740 (1956).

(10) D. S. Berns and R. M. Fuoss, *ibid.*, **82**, 5585 (1960).

(11) J. F. Coetzee and G. P. Cunningham, *ibid.*, **86**, 3403 (1964); **87**, 2529 (1965).

(12) H. M. Daggett, E. J. Bair, and C. A. Kraus, *ibid.*, **73**, 799 (1951).



of about  $1.3 \text{ cm.}^{-1}$ . The platinum electrodes were lightly platinized.<sup>13</sup> The cells were constructed by E. Sexton, University of Indiana, Bloomington, Ind. The conductance cell of Hawes and Kay<sup>14</sup> containing the guarded electrode was not suitable for these measurements, owing to its rather small cell constant, and construction of a second guarded electrode assembly was too formidable a task at this time. The cells were cleaned with boiling nitric acid, rinsed with conductivity water, and steamed before each run. Acetonitrile was delivered directly to the cell from the distillation receiver through an all-glass closed system under  $\text{N}_2$  pressure after the cell had been thoroughly rinsed with acetonitrile to remove the last traces of water. In the cell calibration runs, water was added to the cell directly from an ion-exchange column through polyethylene tubing and a Pyrex filling device fitted with appropriate stopcocks. The cell was fitted with the Hawes-Kay<sup>14</sup> salt cup dispensing device which permitted salt samples in 11-mm. Pyrex cups to be added to the solution successively without exposing the cell contents to the atmosphere. Both the cell and the dispensing device contained stopcocks which permitted the cells to be thoroughly swept with argon before addition of solvent, during the addition of solvent, and while the salt cup dispensing device containing the salt samples was placed on the cell. The use of the heavy inert argon and a completely closed system once filled resulted in solvents of specific conductance as low as  $1.4\text{--}3 \times 10^{-7} \text{ ohm}^{-1} \text{ cm.}^{-1}$  for water and  $3\text{--}9 \times 10^{-8} \text{ ohm}^{-1} \text{ cm.}^{-1}$  for acetonitrile that underwent almost no detectable conductance change once temperature equilibrium had been attained. Temperature equilibrium was hastened and maintained during a measurement by rapid magnetic stirring of the solution using a seamless Teflon-coated magnet. The room temperature was maintained above that of the bath to avoid condensation of the solvent in the cup dispensing device.

All resistance measurements were carried out using a calibrated Dikes-Jones bridge with an oscilloscope as detector. The constant-temperature oil bath was maintained within  $0.002^\circ$  by means of a mercury-in-glass thermoregulator. The absolute temperature was determined by a calibrated platinum resistance thermometer and a Mueller bridge. The cell constants were determined at  $25^\circ$  by measuring the conductance of aqueous KCl over the concentration range  $1\text{--}10 \times 10^{-3} M$  and using the averaged conductance equation of Lind, Zwolenik, and Fuoss<sup>15</sup> to obtain the absolute value. The maximum spread in the cell constants over the whole concentration range studied

was  $0.02\%$ . The measured resistances were corrected for the usual small frequency dependence.

All solutions were prepared by weight, vacuum corrected, and the concentration was calculated on a volume basis by means of solution densities determined from  $d = d_0 \pm A\bar{m}$  where  $\bar{m}$  is the concentration in moles of solute per kilogram of solution. A solvent density  $d_0 = 0.7767$  was measured, and  $A$  was determined from density measurements on the solution remaining after the conductance runs. Salt densities ranging from 1.6 for  $\text{Me}_4\text{NI}$  and 1.1 for  $\text{Bu}_4\text{NBr}$  were used in the vacuum correction.

*Conductivity water* was prepared by passing distilled water through a 1.53-m. column of mixed-bed ion-exchange resin. Conductivity water was collected from the column only after a thorough rinsing of the resin.

*Acetonitrile* (Fisher Scientific Co.) was purified by the procedure described by Coetzee<sup>16</sup> with the addition of a final fractional distillation under nitrogen from calcium hydride through a 1.22-m. Stedman column. The physical properties at  $25^\circ$  obtained for the purified solvent were  $0.7767 \text{ g. ml.}^{-1}$  for the density,  $0.003448$  poise (see below) for the viscosity,  $36.02$  for the dielectric constant, and  $3\text{--}9 \times 10^{-8} \text{ ohm}^{-1} \text{ cm.}^{-1}$  for the specific conductance. A single capillary pycnometer was used for the density measurements, and our value agrees well with literature values<sup>10,11,17</sup> with two exceptions.<sup>18,19</sup>

The viscosity was first determined in a Ubbelohde suspended-level-type viscometer (flow time 540 sec.) which was calibrated at  $25^\circ$  with water ( $0.008903$  poise).<sup>20,21</sup> The viscosity reported here for acetonitrile is in good agreement with the generally accepted values<sup>10,19,22</sup> that center around  $0.00344$  poise. However, a recent calibration with  $20\%$  aqueous sucrose,<sup>23</sup>  $n$ -decane,<sup>24</sup> and  $n$ -hexane<sup>24</sup> resulted in a value of  $0.00341$

(13) G. Jones and D. M. Bollinger, *J. Am. Chem. Soc.*, **57**, 280 (1935).

(14) J. L. Hawes and R. L. Kay, *J. Phys. Chem.*, **69**, 2420 (1965).

(15) J. E. Lind, Jr., J. J. Zwolenik, and R. M. Fuoss, *J. Am. Chem. Soc.*, **81**, 1557 (1959).

(16) J. F. Coetzee, G. P. Cunningham, D. K. McGuire, and G. R. Padmanabhan, *Anal. Chem.*, **34**, 1139 (1962).

(17) C. J. Janz, A. E. Marzinkowsky, and I. Ahmad, *Electrochim. Acta*, **9**, 1687 (1964).

(18) F. Accascina, S. Petrucci, and R. M. Fuoss, *J. Am. Chem. Soc.*, **81**, 1301 (1959).

(19) D. F.-T. Tuan and R. M. Fuoss, *J. Phys. Chem.*, **67**, 1343 (1963).

(20) J. F. Swindells, J. R. Coe, Jr., and T. B. Godfrey, *J. Res. Natl. Bur. Std.*, **48**, 1 (1952).

(21) J. R. Coe, Jr., and T. B. Godfrey, *J. Appl. Phys.*, **15**, 625 (1944).

(22) R. A. Robinson and R. H. Stokes, "Electrolyte Solutions," 2nd Ed., Butterworth and Co., Ltd., London, 1959.

poise. We have attributed the difference to a viscometer surface tension effect and suspect that this lower value is more nearly correct. We have used 0.003448 in all of our calculations since a change in the viscosity of as much as 3% was found to produce a negligible difference in the conductance parameters.

The dielectric constant was measured in a cell designed for absolute measurements<sup>26</sup> in which the cell constant was determined by direct capacitance measurements on the cell filled with dry nitrogen ( $\epsilon$  1.0005), using a General Radio Type 1615A capacitance-conductance bridge. The cell constant was approximately 2.2 pf. and reproducible to 0.05% after repeated cleanings with chromic acid solution. Our value of the dielectric constant of anhydrous acetonitrile agrees well with that reported by Fuoss and co-workers<sup>10,18</sup> but not with the previously accepted value of 36.7.<sup>26</sup>

All of the halide salts were commercial products (Eastman Kodak) whereas the picrates were prepared by neutralization of the appropriate tetraalkylammonium hydroxide with picric acid. All salts were dissolved in the appropriate solvents, filtered, and recrystallized three times. The solvents used for the recrystallizations were acetone-ether mixtures for Bu<sub>4</sub>NBr and Bu<sub>4</sub>NI and methanol-ether mixture for Pr<sub>4</sub>NBr and Pr<sub>4</sub>NI. Great care was taken to ensure that the ether was peroxide free. The salts were dissolved in a minimum amount of acetone or methanol, and ether was added until precipitation commenced, at which point the solution was cooled and the resulting crystals were filtered in a fritted-glass funnel. Me<sub>4</sub>NBr and Me<sub>4</sub>NPi were recrystallized from a 1:1 mixture of methanol-water, Me<sub>4</sub>NI from a 1:4 mixture of methanol-water, and Bu<sub>4</sub>NPi from a 1:1 acetone-methanol mixture, all on a volume basis.

After a preliminary drying, the salts were finely ground in an agate mortar and dried in a vacuum oven fitted with a liquid N<sub>2</sub> trap at the following temperatures: butyl salts and Me<sub>4</sub>NPi, 56°; Pr<sub>4</sub>NI, 70°; Pr<sub>4</sub>NBr, Me<sub>4</sub>NBr, and Me<sub>4</sub>NI, 90°. The salts were stored in glass bottles in darkened desiccators over CaSO<sub>4</sub>.

## Results

The measured equivalent conductances, the corresponding electrolyte concentration ( $M$ ), the solvent conductances,  $\kappa_0$ , and the density increments,  $A$ , are shown in Table I. The data were analyzed by the Fuoss-Onsager conductance theory<sup>27</sup> which can be expressed as

$$\Lambda = \Lambda_0 - SC^{1/2} + EC \log C + (J - F\Lambda_0)C \quad (1)$$

for unassociated electrolytes and as

$$\Lambda = \Lambda_0 - S(C\gamma)^{1/2} + EC\gamma \log C\gamma + (J - F\Lambda_0)C\gamma - K_A C\gamma \Lambda f^2 \quad (2)$$

for associated electrolytes. The symbols used here have the usual and accepted meaning.<sup>27</sup> The computer programs used for the analyses have been described in detail elsewhere.<sup>14,28</sup> The iterated  $\delta$  obtained from the  $J$  coefficient was used to estimate the mean ion activity coefficient  $f^2$ . The computation used unweighted values of  $\Lambda$  since the measurements were carried out at approximately equal increments in  $C$ .

It is necessary to make some kind of viscosity correction since these large electrolytes affect the solution viscosity to a significant extent. Although it is not altogether clear as to what form this viscosity correction should take,<sup>29</sup> we decided to set the coefficient  $F$  in eq. 1 and 2 equal to the viscosity  $B$  coefficient as first suggested by Fuoss.<sup>30</sup> In any case, the correction has no effect on  $\Lambda_0$  nor on the association constant and only results in small changes in  $J$  and  $\delta$ . In the most serious case (Bu<sub>4</sub>NPi),  $\delta$  is increased by 0.5, and in the case of Me<sub>4</sub>NI, by only 0.2.<sup>31</sup> The values of the viscosity  $B$  coefficients<sup>19</sup> used were: Me<sub>4</sub>NBr, 0.58; Pr<sub>4</sub>NBr, 0.77; Bu<sub>4</sub>NBr, 0.93; Me<sub>4</sub>NI, 0.52; Pr<sub>4</sub>NI, 0.71; Bu<sub>4</sub>NI, 0.87; Me<sub>4</sub>NPi, 0.78; Bu<sub>4</sub>NPi, 1.13.

The parameters obtained from an analysis of the conductance data are given in Table II. The results for more than one run are included for some salts, but in each run the first entry in Table II gives the parameters obtained from eq. 1 and the second entry, the parameters obtained from eq. 2. Included are the standard deviations in each parameter and the standard deviation of the individual points,  $\sigma_A$ . It should be noted that only the result from eq. 1 is listed for Bu<sub>4</sub>NPi owing to the fact that eq. 2 gave a very

(23) J. F. Swindells, C. F. Snyder, R. C. Hardy, and P. E. Golden, National Bureau of Standards Circular 440 Supplement, U. S. Government Printing Office, Washington, D. C., 1958.

(24) Cannon Instrument Co., State College, Pa.

(25) G. A. Vidulich and R. L. Kay, *J. Phys. Chem.*, **6**, 383 (1962).

(26) A. A. Maryott and E. R. Smith, National Bureau of Standards Circular 514, U. S. Government Printing Office, Washington, D. C., 1951.

(27) R. M. Fuoss and F. Accascina, "Electrolytic Conductance," Interscience Publishers, Inc., New York, N. Y., 1959.

(28) R. L. Kay, *J. Am. Chem. Soc.*, **82**, 2099 (1960).

(29) Possibly the correct form for this correction would result from measuring the conductance of these solutions with an inert substance present to give solutions of varying viscosity as suggested by E. R. Nightingale (private communication, 1964). Extrapolation to a viscosity equal to that of the solvent for each salt concentration would presumably give the corrected conductance.

(30) R. M. Fuoss, *J. Am. Chem. Soc.*, **79**, 3301 (1957).

(31) This calculation required a value of  $\partial J/\partial \delta$  which here depends primarily on  $\Lambda_0$  and varies between 340 for Bu<sub>4</sub>NPi and 470 for Me<sub>4</sub>NI.

Table I: Measured Equivalent Conductances in Acetonitrile at 25°

10°C	A	10°C	A	10°C	A
<b>Me<sub>4</sub>NBr</b>		<b>Bu<sub>4</sub>NBr</b>		<b>Bu<sub>4</sub>NI</b>	
10 <sup>8</sup> κ <sub>0</sub> = 8.7	A = 0.074	10 <sup>8</sup> κ <sub>0</sub> = 8.8	A = 0.096	10 <sup>8</sup> κ <sub>0</sub> = 5.9	A = 0.133
8.255	178.991	11.410	149.707	4.208	156.446
15.481	171.884	18.228	146.504	8.578	153.135
22.632	166.402	26.947	143.295	13.916	150.136
32.075	160.491	31.952	141.739	19.997	147.516
38.205	157.243	38.643	139.879	25.805	145.377
46.490	153.363	44.486	138.415	31.537	143.523
56.619	149.287	50.194	137.105	38.926	141.430
				45.488	139.803
<b>Pr<sub>4</sub>NBr</b>		10 <sup>8</sup> κ <sub>0</sub> = 6.2		10 <sup>8</sup> κ <sub>0</sub> = 5.1	
10 <sup>8</sup> κ <sub>0</sub> = 6.2	A = 0.086	4.422	154.394	4.058	156.620
3.725	163.728	9.847	150.526	10.345	152.114
9.715	158.978	17.061	146.968	14.937	149.743
15.575	155.750	22.953	144.666	19.395	147.813
22.243	152.859	29.779	142.422	25.521	145.549
29.839	150.104	35.344	140.775	34.077	142.875
37.652	147.695	43.194	138.743	42.878	140.531
44.949	145.699	47.610	137.700	48.591	139.173
52.267	143.913				
<b>Me<sub>4</sub>NI</b>		10 <sup>8</sup> κ <sub>0</sub> = 4.8	A = 0.109	<b>Me<sub>4</sub>NPi</b>	
10 <sup>8</sup> κ <sub>0</sub> = 7.4		6.042	185.330	10 <sup>8</sup> κ <sub>0</sub> = 4.7	A = 0.116
11.825	157.964	14.177	178.436	3.720	164.666
19.124	154.370	22.446	173.347	10.405	159.817
25.948	151.680	28.962	170.039	17.177	156.504
35.508	148.536	37.902	166.152	23.587	154.049
45.739	145.698	46.698	162.831	29.580	152.083
55.914	143.268	58.491	158.949	34.664	150.608
65.336	141.336	70.491	155.631	40.881	148.988
				48.335	147.231
<b>Pr<sub>4</sub>NI</b>		10 <sup>8</sup> κ <sub>0</sub> = 5.4	A = 0.121	<b>Bu<sub>4</sub>NPi</b>	
10 <sup>8</sup> κ <sub>0</sub> = 5.9		4.184	165.038	10 <sup>8</sup> κ <sub>0</sub> = 5.1	A = 0.124
4.449	162.972	9.869	160.734	2.594	133.860
9.901	158.889	17.383	156.734	8.073	129.971
17.271	154.994	23.832	154.121	13.688	127.132
25.399	151.681	30.825	151.713	19.758	124.866
33.685	148.901	38.904	149.308	25.835	122.933
41.946	146.536	47.283	147.123	34.631	120.712
47.199	145.166	53.297	145.701	41.806	119.110
56.450	142.984				
		10 <sup>8</sup> κ <sub>0</sub> = 9.2			
		5.019	164.319		
		10.809	160.099		
		16.661	157.065		
		24.081	153.984		
		31.219	151.526		
		39.025	149.199		
		50.087	146.359		
		60.068	144.184		

small and negative association constant, indicating a negligible amount of association.

The detailed results given in Table II are summarized in Table III where the results of multiple runs on the

**Table II:** Conductance Parameters for Acetonitrile Solutions at 25°

Salt	$\Lambda_0$	$\bar{a}$	$K_A$	$J$	$\sigma_A$		
Me <sub>4</sub> NBr	191.3 ± 0.7	0.21 ± 0.05	46 ± 1	2430	0.8		
	195.22 ± 0.07	4.4 ± 0.2			0.03		
Pr <sub>4</sub> NBr	170.84 ± 0.06	2.72 ± 0.04	5.4 ± 0.9	1880	0.09		
	171.09 ± 0.05	3.7 ± 0.2			0.03		
	170.87 ± 0.05	2.83 ± 0.03			0.05		
	171.19 ± 0.04	3.3 ± 0.1			3.3 ± 0.6	1725	0.02
	170.82 ± 0.04	2.75 ± 0.03			3.6 ± 0.5	1750	0.06
171.01 ± 0.03	3.4 ± 0.1						
Bu <sub>4</sub> NBr	162.01 ± 0.02	3.20 ± 0.02	1.8 ± 0.8	1730	0.03		
	162.09 ± 0.04	3.5 ± 0.2			0.02		
	162.01 ± 0.01	3.19 ± 0.01			0.01		
	162.10 ± 0.01	3.45 ± 0.04			1.4 ± 0.2	1700	0.004
Me <sub>4</sub> NI	195.03 ± 0.3	1.2 ± 0.1	19.3 ± 0.5	2050	0.5		
	196.73 ± 0.05	3.5 ± 0.1			0.03		
Pr <sub>4</sub> NI	172.63 ± 0.05	2.87 ± 0.04	4.5 ± 0.9	1895	0.08		
	172.86 ± 0.05	3.7 ± 0.2			0.03		
	172.60 ± 0.07	2.86 ± 0.04			0.1		
	172.90 ± 0.06	3.8 ± 0.2			5 ± 1	1920	0.04
Bu <sub>4</sub> NI	163.92 ± 0.03	3.09 ± 0.03	3.1 ± 0.9	1810	0.04		
	164.04 ± 0.04	3.7 ± 0.2			0.02		
	163.95 ± 0.02	3.14 ± 0.02			0.03		
	164.06 ± 0.02	3.6 ± 0.1			2.4 ± 0.5	1770	0.01
Me <sub>4</sub> NPi	171.78 ± 0.02	3.46 ± 0.01	1.2 ± 0.6	1890	0.02		
	171.84 ± 0.03	3.7 ± 0.1			0.02		
Bu <sub>4</sub> NPi	139.40 ± 0.04	4.05 ± 0.05		1890	0.07		

**Table III:** Averaged Conductance Parameters for Acetonitrile Solutions

Salt	$\Lambda_0$	$\bar{a}$	$K_A$
Me <sub>4</sub> NBr	195.2	4.4	46
Pr <sub>4</sub> NBr	171.1	3.4	4
Bu <sub>4</sub> NBr	162.1	3.5	2
Me <sub>4</sub> NI	196.7	3.5	19
Pr <sub>4</sub> NI	172.9	3.8	5
Bu <sub>4</sub> NI	164.0	3.6	3
Me <sub>4</sub> NPi	171.8	3.7	1
Bu <sub>4</sub> NPi	139.4	4.0	0

same salt have been averaged by weighting each parameter by its standard deviation.

The values of  $\alpha$ ,  $B$ ,  $E_1$ , and  $E_2$  for acetonitrile are 0.7374, 230.9, 5.474, and 251.0, respectively, where  $S$  and  $E$  in eq. 1 and 2 are given by  $S = \alpha\Lambda_0 + B$  and  $E = E_1\Lambda_0 - E_2$ .

## Discussion

A calculation of the conductance differences at infinite dilution between bromides and iodides and between tetramethyl- and tetrabutylammonium salts indicates an uncertainty in  $\Lambda_0$  of 0.2 conductance units

or 0.1%. In comparison to other results in nonaqueous solvents, this is quite satisfactory but somewhat greater than the experimental error expected. The cause cannot be attributed to salt impurities since the same halide salts were found to give excellent agreement in the ion conductances for aqueous<sup>4</sup> and methanol<sup>2</sup> solutions where transference data are available. We attribute this deviation in additivity of ionic conductance at infinite dilution to very slight amounts of impurities, possibly water, in the acetonitrile.

Our differences between the tetrapropyl and tetrabutyl salts of  $8.9 \pm 0.1$  and between the tetramethyl and tetrabutyl salts of  $32.8 \pm 0.2$  compare favorably with the values 9.0 and 32.8 obtained by Berns and Fuoss<sup>10</sup> from a series of tetraphenylboride salts. Also, our average difference of  $24.8 \pm 0.1$  between the iodides and the picrates with the same cation can be compared to the 25.0 reported by Coplan and Fuoss<sup>32</sup> obtained from triisobutylammonium salts.

A direct comparison of our  $\Lambda_0$  with those reported by other workers is not nearly so favorable. Before such a comparison can be made, it is necessary to recompute the data from the literature so as to bring them into conformity with the Fuoss-Onsager conductance equations. The results of such an analysis for all of the literature data for acetonitrile solutions that have the necessary precision are given in Table IV. A comparison of these results with those in Table II shows that our values of  $\Lambda_0$  for Me<sub>4</sub>NBr, Me<sub>4</sub>NI, Pr<sub>4</sub>NI, and Me<sub>4</sub>NPi are considerably higher (1–3 conductance units) than those measured by Popov and Skelly<sup>9</sup> and by Walden and Birr,<sup>5</sup> whereas our value for Bu<sub>4</sub>NPi is two conductance units lower than that calculated from the measurements of French and Muggleton.<sup>7</sup> The fact that our precision is considerably better and the fact that the ion conductances obtained from our salts in methanol and water are in agreement with transference data add considerable weight to the reliability of our data.

An inspection of Table III shows that, with the exception of Me<sub>4</sub>NBr,<sup>33</sup>  $\bar{a}$  values obtained for all of our salts are almost identical and equal to  $3.6 \pm 0.2$ . The same behavior was observed in the similar solvent, nitromethane,<sup>34</sup> where an  $\bar{a}$  of  $3.9 \pm 0.3$  was obtained for the tetramethyl- through tetrabutylammonium chlorides and bromides if the viscosity correction,  $F$ , is

(32) M. A. Coplan and R. M. Fuoss, *J. Phys. Chem.*, **68**, 1181 (1964).

(33) The high value of 4.4 for Me<sub>4</sub>NBr could be the result of a poor split between the term linear in  $C$  in eq. 2 and the association term. If  $K_A$  for this salt was reduced by only 3 units to 43, an  $\bar{a}$  of 3.6 would result. This illustrates the precision required for the accurate determination of  $\bar{a}$ .

(34) R. L. Kay, S. C. Blum, and H. I. Schiff, *J. Phys. Chem.*, **67**, 1223 (1963).

**Table IV:** Conductance Parameters for Acetonitrile Solutions at 25°

Salt	$\Lambda_0$	$\bar{a}$	$K_A$	Ref.
Me <sub>4</sub> NCl	192.9 ± 0.4	1.9 ± 0.8	56 ± 6	9
Me <sub>4</sub> NBr	193.2 ± 0.4	3 ± 1	36 ± 6	9
Me <sub>4</sub> NI	194.6 ± 0.3	1.3 ± 0.6	5 ± 4	9
Et <sub>4</sub> NI	187.29 ± 0.06	3.3 ± 0.3	5 ± 2	8
Pr <sub>4</sub> NI	169.9 ± 0.1 <sup>a</sup>	6.7 ± 0.5 <sup>a</sup>		5
	172.0 ± 0.3	3.3 ± 0.5	3 ± 3	9
Me <sub>4</sub> NPi	170.81 ± 0.09	5 ± 1	8 ± 4	5
Et <sub>4</sub> NPi	164.62 ± 0.07	5.0 ± 0.9	10 ± 4	7
Pr <sub>4</sub> NPi	147.2 ± 0.1 <sup>a</sup>	5.1 ± 0.2 <sup>a</sup>		5
Bu <sub>4</sub> NPi	141.28 ± 0.06	4 ± 2	13 ± 6	7
Am <sub>4</sub> NPi	135.1 ± 0.1	8 ± 2	39 ± 7	7
Me <sub>4</sub> NBPh <sub>4</sub>	152.28 ± 0.02 <sup>a</sup>	4.6 ± 0.1 <sup>a</sup>		10
Et <sub>4</sub> NBPh <sub>4</sub>	142.77 ± 0.03 <sup>a</sup>	4.9 ± 0.1 <sup>a</sup>		10
Pr <sub>4</sub> NBPh <sub>4</sub>	128.41 ± 0.006 <sup>a</sup>	5.3 ± 0.1 <sup>a</sup>		10
Bu <sub>4</sub> NBPh <sub>4</sub>	119.49 ± 0.04 <sup>a</sup>	5.3 ± 0.1 <sup>a</sup>		10
LiClO <sub>4</sub>	182.1 ± 0.4	3.1 ± 1.6	24 ± 8	36
NaClO <sub>4</sub>	191.2 ± 0.4	3.5 ± 2.0	23 ± 9	36
KClO <sub>4</sub>	205.7 ± 0.5	2.4 ± 1.6	33 ± 9	36
RbClO <sub>4</sub>	201.4 ± 0.8	8 ± 9	55 ± 31	36
CsClO <sub>4</sub>	204.5 ± 0.8	7 ± 5	63 ± 18	36
KI	186.6 ± 0.1 <sup>a</sup>	2.27 ± 0.08 <sup>a</sup>		17

<sup>a</sup> Parameters obtained from eq. 1; eq. 2 gives negative  $K_A$ .

assumed to be the same as that for acetonitrile solutions. There appears to be no relationship between  $\bar{a}$  and the contact distance between ions since the ion sizes in the salts involved here vary considerably. It should be noted in Table II that it is  $\bar{a}$  and not  $J$  that is constant for each salt. Thus, since  $J$  is a function of  $\Lambda_0$  and  $\bar{a}$ , it appears only necessary to remove  $\Lambda_0$  in order to obtain a relaxation effect that is independent of the particular salt under consideration. However, it should be noted that higher  $\bar{a}$  values are obtained from the data for the tetraalkylammonium tetraphenylborides. There is an indication of a decrease in  $\bar{a}$  with decreasing cation size, but this could be a reflection of a small amount of association as the cation size decreases.

It can be seen in Table II that, with the exception of the picrates,  $\sigma_A$  is lower for the results from eq. 2 than those obtained from eq. 1. This is the best criterion for association available at present. Only the tetramethylammonium salts show any appreciable amount of association, but all salts follow the same association pattern; namely, association decreases as the ion size increases. We do not consider the small increase in  $K_A$  for the tetrapropyl- and tetrabutylammonium iodides over that for the bromides to be

real but rather the result of experimental error. This association behavior has been confirmed in a number of other investigations. Salts involving very large ions, such as the tetraalkylammonium tetraphenylborides<sup>10</sup> and Bu<sub>4</sub>NPF<sub>6</sub>,<sup>35</sup> have been found to be unassociated, whereas Me<sub>4</sub>NPF<sub>6</sub><sup>35</sup> shows signs of very slight association in acetonitrile. The same behavior appears to be followed by all of the data found in the literature as recorded in Table IV with the exception of those of French and Muggleton<sup>7</sup> for the picrates, which are in direct contrast to our results. We found no association for Bu<sub>4</sub>NPi in acetonitrile. The data of Popov and co-workers<sup>9</sup> for the tetramethylammonium halides show appreciable association, but similar data for the trihalides show no signs of association. The association constants for the alkali perchlorates in acetonitrile, as reported by Minc and Werblan,<sup>36</sup> increase as the cation size increases, but a recalculation of their data on the basis of eq. 2, as given in Table IV, indicates that, although these salts appear to be associated to some extent, the precision of the measurements does not permit much to be said about the change in  $K_A$  with cation size. The  $K_A$  values for RbClO<sub>4</sub> and CsClO<sub>4</sub> appear to be somewhat higher than the others, but this is undoubtedly caused by a poor separation between the association term and the term linear in  $C$  in eq. 2. If  $\bar{a}$  is set equal to about 3.5 for these salts, association constants of about 40 ± 30 and 50 ± 20 result, making the  $K_A$  values for all the perchlorates identical within the precision of the measurements. Owing to the large uncertainty in these results for the alkali perchlorates, the question of the association behavior of the alkali metal salts in acetonitrile is still an open question.

The same association behavior is observed in nitromethane solutions<sup>34</sup> in that Me<sub>4</sub>NCl and Me<sub>4</sub>NBr have association constants of 45 ± 1 and 31 ± 1, respectively, Et<sub>4</sub>NCl and Et<sub>4</sub>NBr are only slightly associated,  $K_A \leq 2$ , and the halides of the larger quaternary cations show no signs of association.

The conductance data of Taylor and Kraus<sup>37</sup> and Witschonke and Kraus<sup>38</sup> for nitrobenzene solutions have been recalculated to conform to the Fuoss-Onsager theory and are given in Table V. It should be noted that for both the symmetrical tetraalkylammonium and the alkali picrates, the association constant increases with decreasing ion size in keeping

(35) J. Eliassaf, R. M. Fuoss, and J. E. Lind, Jr., *J. Phys. Chem.*, **67**, 1941 (1963).

(36) S. Minc and L. Werblan, *Electrochim. Acta*, **7**, 57 (1962).

(37) E. G. Taylor and C. A. Kraus, *J. Am. Chem. Soc.*, **69**, 1731 (1947).

(38) C. R. Witschonke and C. A. Kraus, *ibid.*, **69**, 2472 (1947).

with our results for acetonitrile. This is in contrast to what is found for the alkali metal salts in hydrogen-bonded solvents like the alcohols.<sup>28</sup>

The association pattern found for acetonitrile and nitrobenzene can be confirmed by comparison with the results for a similar solvent of lower dielectric constant such as acetone<sup>39,40</sup> as shown in Table V. Here, association is much more extensive, and the decrease in association as the ion size increases can be clearly seen. There is one notable exception: KI is less associated than potassium picrate by a considerable amount. This is confirmed by Walden's<sup>41</sup> result for NaI as compared to Kraus' value for NaPi. This inversion in association behavior has been noted by Kraus,<sup>39</sup> but he gave no explanation. It is difficult to attribute the result to an error in measurement since the precision of the measurements involved appears to be quite adequate. We attribute the small association of KI to small amounts of water in the acetone, a solvent that is extremely difficult to obtain in a completely anhydrous state.

**Table V:** Conductance Parameters for Nitrobenzene and Acetone Solutions at 25°

Salt	$\Delta_0$	$\bar{a}$	$K_A$	Ref.
Nitrobenzene				
Et <sub>4</sub> NCl	38.54 ± 0.03	7 ± 2	81 ± 6	38
Bu <sub>4</sub> NBr	33.46 ± 0.02	4.9 ± 0.7	56 ± 3	38
NH <sub>4</sub> Pi			6.9 × 10 <sup>20</sup>	38
Me <sub>4</sub> NPi	33.34 ± 0.01	3.6 ± 0.2	23.6 ± 0.9	37
Et <sub>4</sub> NPi	32.43 ± 0.003	3.89 ± 0.08	7.4 ± 0.4	37
Pr <sub>4</sub> NPi	29.48 ± 0.007	3.1 ± 0.2	3 ± 1	37
Bu <sub>4</sub> NPi	27.86 ± 0.004	3.3 ± 0.2	2.6 ± 0.9	37
LiPi			1.7 × 10 <sup>19</sup>	38
NaPi			3.6 × 10 <sup>19</sup>	38
KPi			1.46 × 10 <sup>20</sup>	38
Acetone				
Me <sub>4</sub> NF	182.7 ± 0.3	0.8 ± 0.5	1140 ± 40	39
Et <sub>4</sub> NCl	194.2 ± 0.2	16 ± 2	370 ± 20	41
Pr <sub>4</sub> NI	190.72 ± 0.03	5.2 ± 0.6	162 ± 7	40
Bu <sub>4</sub> NBr	183.2 ± 0.1	5.4 ± 0.2	264 ± 5	39
Bu <sub>4</sub> NI	180.3 ± 0.2	6.1 ± 0.3	143 ± 6	39
Am <sub>4</sub> NBr	174.7 ± 0.1	7 ± 1	220 ± 20	40
Me <sub>4</sub> NPi	183.4 ± 0.1	5.8 ± 0.1	67 ± 1	40
Et <sub>4</sub> NPi	176.65 ± 0.03	6.3 ± 0.1	45 ± 2	39
Pr <sub>4</sub> NPi	156.2 ± 0.1	5.2 ± 0.4	27 ± 8	41
Bu <sub>4</sub> NPi	152.34 ± 0.08	4.6 ± 0.2	17 ± 5	39
Bu <sub>4</sub> NClO <sub>4</sub>	182.8 ± 0.1	5.8 ± 0.2	80 ± 4	39
Bu <sub>4</sub> NNO <sub>3</sub>	187.11 ± 0.007	4.96 ± 0.02	143.1 ± 0.4	39
LiPi	157.7 ± 0.2	1.5 ± 0.1	819 ± 9	39
NaPi	163.5 ± 0.2	5.4 ± 0.3	680 ± 9	39
KPi	166.0 ± 0.1	5.0 ± 0.2	244 ± 5	39
KI	192.9 ± 0.2	5.2 ± 0.2	98 ± 5	39
	184.8 ± 0.1	7.1 ± 0.8	110 ± 10	41
NaI	183.6 ± 0.2	14 ± 1	177 ± 15	41

<sup>a</sup> From eq. 2 with  $E$ ,  $J$ , and  $B$  set equal to zero.

It is of interest to point out the higher association of salts in nitrobenzene as compared to those for the same salts in acetonitrile and nitromethane,<sup>34</sup> solvents with approximately the same dielectric constant. It is difficult to explain this result without resorting to some kind of specific solvation effects. For example, the high association constant for Bu<sub>4</sub>NBr<sup>42,43</sup> in nitrobenzene has been attributed to the formation of a nitrobenzene ion pair complex. However, it is difficult to attribute the extreme association of the alkali metal picrates to the formation of such complexes. We feel that a more likely explanation lies in assuming that an almost complete lack of solvation of the small alkali metal and halide ions in nitrobenzene accounts for the large association. Of course, the possibility exists that nitrobenzene was the only anhydrous solvent studied and that in acetonitrile and nitromethane the hydrated ions were being investigated. A 0.01 wt. % concentration of water would result in an equimolar mixture of salt and water at the highest concentrations studied.

It is appropriate at this point to bring up the question of small association constants, many of which were obtained in this investigation. It is possible to separate out the association term only with data of the highest precision if  $K_A$  is less than 5. It is possible that these so-called association constants are mere artifacts of the conductance theory. However, the consistency of the association pattern reported here for the more precise data and the fact that the association changes as predicted for a decrease in the dielectric constant add considerable weight to the reliability of these numbers as being at least proportional to association constants. It was hoped that by studying association in mixed solvents at lower dielectric constants it would be possible to extrapolate back and determine the association constants for solvents of higher dielectric constant like acetonitrile. However,  $\log K_A$  vs.  $1/\epsilon$  plots are generally not linear but instead are curved, owing possibly to specific solvent effects, with the result that the extrapolation of solvents of higher dielectric constant can be ambiguous.

Very recently Harkness and Daggett<sup>44</sup> have published their work on the conductance of the tetraalkylammonium halides in acetonitrile at 25°. Before

(39) M. B. Reynolds and C.A. Kraus, *J. Am. Chem. Soc.*, **70**, 1709 (1948).

(40) M. J. McDowell and C. A. Kraus, *ibid.*, **73**, 3293 (1951).

(41) P. Walden, H. Ulich, and G. Busch, *Z. physik. Chem.*, **123**, 429 (1926).

(42) J. B. Hyne, *J. Am. Chem. Soc.*, **85**, 304 (1963).

(43) R. L. Kay and D. F. Evans, *ibid.*, **86**, 2748 (1964).

(44) A. C. Harkness and H. M. Daggett, Jr., *Can. J. Chem.*, **43**, 1215 (1965).

these results could be compared to those reported here, it was necessary to recompute their data to bring the conductance parameters into conformity with the Fuoss-Onsager theory. Owing to the large proportion of data for extremely dilute solutions, a better fit was obtained by weighting the conductance values by  $C$ . The results are given in Table VI. Their  $\Lambda_0$  values are within 0.2 unit of our values except for  $\text{Bu}_4\text{NBr}$ ,  $\text{Me}_4\text{NI}$ , and  $\text{Bu}_4\text{NI}$ , in which case their values are considerably higher. Their differences in  $\Lambda_0$  between iodide and bromide average  $1.7 \pm 0.1$  if their very high result of 2.7 for the tetramethylammonium salts is ignored. This is in excellent agreement with the value  $1.7 \pm 0.2$  calculated from our results in Table III. This would indicate that our value of 196.7 is the more nearly correct  $\Lambda_0$  for  $\text{Me}_4\text{NI}$ . Also, the check with the data of Coplan and Fuoss as described above makes our  $\Lambda_0$  values for the tetrabutylammonium salts the preferred values. The  $\bar{a}$  and  $K_A$  values reported in Table VI show such large uncertainties, owing to lack of sufficient data for higher concentrations, that a rigorous interpretation is not possible. However, our conclusion that the larger the ions the less the degree of association in acetonitrile

**Table VI:** Conductance Parameters of Harkness and Daggett for Acetonitrile Solutions at 25°

Salt	$\Lambda_0$	$\bar{a}$	$K_A$
$\text{Me}_4\text{NBr}$	$195.0 \pm 0.5$	$4 \pm 1$	$40 \pm 5$
$\text{Et}_4\text{NBr}$	$185.3 \pm 0.1$	$4 \pm 0.5$	$10 \pm 4$
$\text{Pr}_4\text{NBr}$	$171.2 \pm 0.1$	$11 \pm 3$	$33 \pm 5$
$\text{Bu}_4\text{NBr}$	$162.9 \pm 0.04$	$4.4 \pm 0.02$	$6.6 \pm 0.1$
$\text{Am}_4\text{NBr}$	$156.8 \pm 0.2$	$11 \pm 2$	$23 \pm 5$
$\text{Me}_4\text{NI}$	$197.7 \pm 0.2$	$5.0 \pm 0.5$	$26 \pm 2$
$\text{Et}_4\text{NI}$	$186.9 \pm 0.2$	$3.6 \pm 0.6$	$5 \pm 3$
$\text{Pr}_4\text{NI}$	$173.1 \pm 0.2$	$4 \pm 2$	$6 \pm 8$
$\text{Bu}_4\text{NI}$	$164.6 \pm 0.1$	$5 \pm 1$	$8 \pm 5$
$\text{Am}_4\text{NI}$	$158.4 \pm 0.3$	$8 \pm 1$	$20 \pm 5$

solutions is verified by the tetramethylammonium halides. The abnormally high  $K_A$  value obtained for  $\text{Pr}_4\text{NBr}$ ,  $\text{Am}_4\text{NBr}$ , and  $\text{Am}_4\text{NI}$  can be attributed to a poor split between the last two terms of eq. 2 as indicated by the exceptionally large values of  $\bar{a}$ .

*Acknowledgment.* This work was supported by the Office of Saline Water, U. S. Department of the Interior, under Contract 14-01-0001-359.

## Raman Studies of Iodic Acid and Sodium Iodate

by James R. Durig, O. D. Bonner, and W. H. Breazeale<sup>1</sup>

Department of Chemistry, University of South Carolina, Columbia, South Carolina (Received June 2, 1965)

The Raman spectra of aqueous and crystalline sodium iodate, iodic acid, and deuterioiodic acid have been recorded. The vibrational assignment for the  $\text{IO}_3^-$  ion has been revised, and eight of the nine fundamental vibrations of iodic acid have been assigned. Osmotic and activity coefficients of aqueous solutions of iodic acid and sodium iodate have also been measured, and an ionization constant of  $0.18 \pm 0.01$  has been calculated from a combination of these data with the degree of ionization as determined from Raman measurements. This value is somewhat higher than those which have been reported from conductance measurements.

The Raman spectra of aqueous solutions of iodic acid and alkali metal iodates have been investigated by numerous workers.<sup>2</sup> The measurements of the depolarization values of the Raman lines of the chlorate, bromate, and iodate ions were made by Shen, Yao, and Wu.<sup>3</sup> In their study, they used the sodium salts for the chlorate and bromate ions while a 6.1 *N* solution of iodic acid was used to study the Raman spectrum of the iodate ion. The strong line at  $806 \text{ cm.}^{-1}$  in the  $\text{BrO}_3^-$  solution was quite symmetrical and assigned to  $\nu_1$  and the  $\nu_3$  fundamental was not observed. However, in the iodic acid solution the  $779\text{-cm.}^{-1}$  line was asymmetrical with a strong shoulder at  $826 \text{ cm.}^{-1}$ . The shoulder was assigned as the  $\nu_3$  fundamental of the pyramidal  $\text{IO}_3^-$  ion. Although this assignment for the  $\text{IO}_3^-$  ion has been accepted by recent research workers,<sup>4,5</sup> there is a strong indication that this shoulder arises from a vibration of the undissociated  $\text{HIO}_3$  molecule rather than from the  $\text{IO}_3^-$  ion.<sup>6</sup> Therefore, a reinvestigation of the Raman spectra of aqueous solutions of both sodium iodate and iodic acid was undertaken.

The Raman spectrum of crystalline  $\text{NaIO}_3$ <sup>2a</sup> has been studied and four frequencies of approximately the same intensities in the range 737 to  $808 \text{ cm.}^{-1}$  were reported. The Raman spectrum of crystalline iodic acid has also been studied<sup>2a,7,8</sup> but the earlier work is incomplete and no vibrational analysis has been carried out. A comparison of the strong Raman lines of the crystalline iodic acid in the I-O stretching region with those reported as fundamentals in a recent infrared study<sup>4</sup> shows a discrepancy between the frequencies chosen as

fundamentals in the infrared and the strong Raman lines we observed. Thus, the Raman spectra of crystalline  $\text{NaIO}_3$ ,  $\text{HO'IO}_2$  and  $\text{DO'IO}_2$  were investigated for the purpose of removing this discrepancy and giving a more complete vibrational assignment.

Many values have been reported for the ionization constant of iodic acid and these are summarized in Table I.<sup>9-15</sup> Most of them have resulted from meas-

(1) Tennessee Eastman Fellow, 1964-1965.

(2) For a review of the early spectrographic literature, see (a) J. H. Hiblen, "The Raman Effect and Its Chemical Applications," Reinhold Publishing Corp., New York, N. Y., 1939, pp. 378-381; and (b) J. W. Mellor, "Comprehensive Treatise on Inorganic and Theoretical Chemistry," Supplement 2, Part 1, Longmans, Green and Co., New York, N. Y., 1956, pp. 935-936.

(3) S. T. Shen, Y. T. Yao, and T.-Y. Wu, *Phys. Rev.*, **51**, 235 (1937).

(4) W. E. Dasent and T. C. Waddington, *J. Chem. Soc.*, 2429 (1960).

(5) K. Nakamoto, "Infrared Spectra of Inorganic and Coordination Compounds," John Wiley and Sons, Inc., New York, N. Y., 1963, p. 87.

(6) G. C. Hood, A. C. Jones, and C. A. Reilly, *J. Phys. Chem.*, **63**, 101 (1959).

(7) C. S. Venkateswaran, *Nature*, **140**, 151 (1937).

(8) L. Conture-Mathieu and J.-P. Mathieu, *Compt. rend.*, **231**, 839 (1922).

(9) A. O. McCougall and F. A. Long, *J. Phys. Chem.*, **66**, 429 (1962).

(10) R. M. Fuoss and C. A. Kraus, *J. Am. Chem. Soc.*, **55**, 476 (1933).

(11) L. Onsager, *Physik. Z.*, **28**, 277 (1927).

(12) H. Von Halban and J. Brull, *Helv. Chim. Acta*, **27**, 1719 (1944).

(13) C. A. Kraus and H. C. Parker, *J. Am. Chem. Soc.*, **44**, 2429 (1922).

(14) V. Rothmund and K. Drucker, *Z. physik. Chem.*, **46**, 827 (1903).

(15) E. Abal, O. Redlich, and P. Hersch, *ibid.*, **A170**, 112 (1939).



urements of the conductance of iodic acid solutions and have involved somewhat uncertain extrapolations. This is illustrated by the range of values which have been obtained. Only one value resulting from the measurement of a colligative property has been reported<sup>15</sup> and it is significantly higher.

**Table I:** Ionization Constant of Iodic Acid (Literature Values)

K	Method	Ref.
0.14	Conductance	9
0.1687	Conductance	10
0.17	Conductance	11
0.167	Indicator	12
0.0717	Conductance	13
0.175-0.201	Conductance and distribution measurements	14
0.26	Freezing point	15
0.19	Conductance	15
0.18	N.m.r.	6

Raman spectra have been useful in determining the degree of ionization of stronger acids such as nitric<sup>16</sup> and perchloric,<sup>17</sup> but spectra of iodic acid and iodate ion have not been used for the direct calculation of the ionization constant of iodic acid. Hood, *et al.*,<sup>6</sup> compared degrees of dissociation as calculated from Raman and n.m.r. measurements but used the n.m.r. data for the calculation of the ionization constant since the agreement was not entirely satisfactory. In these investigations, spectra of solutions of iodic acid and sodium iodate are directly compared. The data which were obtained have been corrected using activity coefficients reported in this paper.

### Experimental Section

All Raman spectra were recorded using a Cary Model-81 Raman spectrophotometer. The circulating filter solution used to isolate the 4358-Å. mercury exciting line was made of 125 ml. of *o*-nitrotoluene and 1.75 g. of ethyl violet in 3 l. of isopropyl alcohol. Depolarization values were measured using cylindrical polaroid sheets in the usual manner.<sup>18</sup> The frequencies reported for all sharp lines are expected to be accurate to  $\pm 2$  cm.<sup>-1</sup>. Raman spectra of the solid samples were recorded using a cell similar to the one described by Busey and Keller.<sup>19</sup> For the aqueous solutions, the standard Cary 7-mm. cell with a volume of 5 ml. was employed. Spectral slit widths of 10 and 5 cm.<sup>-1</sup> and a slit height of 10 cm. were used to record all spectra. Varying sensitivities and scanning times were used to give the best resolution and presentation (see Figures

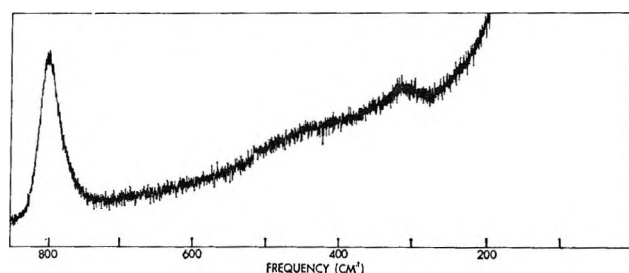
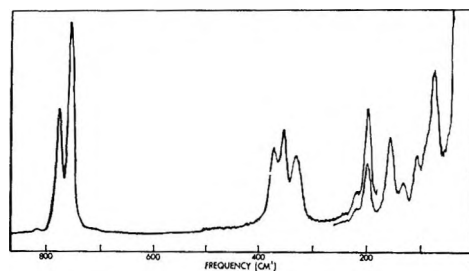


**Figure 1.** The upper curve is the Raman spectrum of crystalline  $\text{NaIO}_3$ : cell, solid, 1.75 g.; slit, single below 200 cm.<sup>-1</sup> and double above, 10 cm.  $\times$  10 cm.<sup>-1</sup>; sensitivity on single slits,  $1.6 \times 100$ ; double slit,  $1 \times 100$  and  $1 \times 10$ ; period, 1.0 sec.; scan, 2.5 cm.<sup>-1</sup>/sec.; zero suppression, none. The lower Raman spectrum is that of a 0.34 M solution of  $\text{NaIO}_3$ : cell, 5 ml., 7-mm. diameter; slits, double, 10 cm.  $\times$  10 cm.<sup>-1</sup>; sensitivity,  $1.4 \times 500$ ; period, 1.0 sec.; scan, 0.5 cm.<sup>-1</sup> sec.; zero suppression, none. Reference dynode was 5 and Raman dynode 3 for all spectra.

1-3). The temperature in the sample compartment was approximately 32° and it is believed that all of the samples reached this equilibrium temperature. Solutions of sodium iodate and iodic acid (Matheson Coleman and Bell, Rutherford, N. J., reagent grade and used without further purification) were filtered through a medium-porous Gooch crucible before use. The concentration of the sodium iodate solutions was determined by weight. Acid concentrations were determined by titration with standardized sodium hydroxide solutions. The deuterioiodic acid was prepared by the addition of iodine pentoxide (Fisher Scientific Co., Silver Spring, Md., C.P. grade) to heavy water (99.7 isotopic purity) and the solution was then filtered.

The Mechrolab Model 301A vapor pressure osmometer was used in the measurement of the osmotic and activity coefficients of iodic acid and sodium iodate.

(16) O. Redlich and J. Bigeleisen, *J. Am. Chem. Soc.*, **65**, 1883 (1943).

(17) O. Redlich, E. K. Holt, and J. Bigeleisen, *ibid.*, **66**, 13 (1944).

(18) B. L. Crawford, Jr., and W. Horwitz, *J. Chem. Phys.*, **15**, 268 (1947); J. T. Edsall and E. B. Wilson, *ibid.*, **6**, 124 (1938).

(19) R. H. Busey and O. L. Keller, Jr., *ibid.*, **41**, 215 (1964).

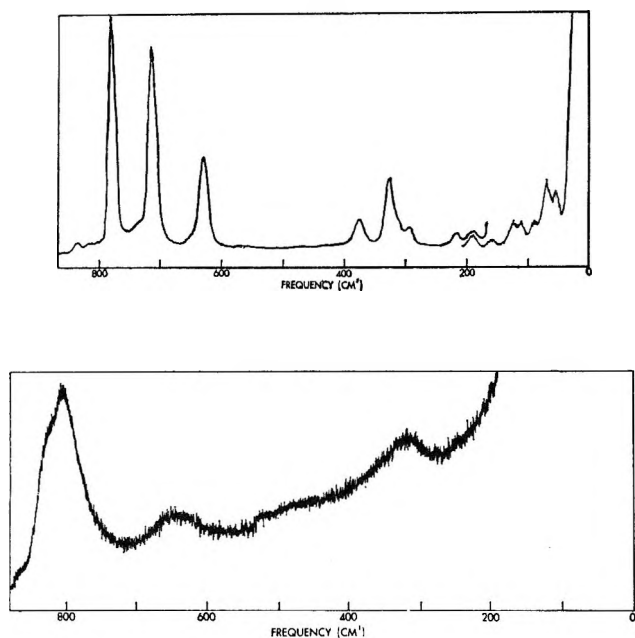


Figure 2. The upper curve is the Raman spectrum of solid  $\text{HIO}_3$ : cell, solid, 1.75 g.; slit, single below  $200 \text{ cm.}^{-1}$ ,  $10 \text{ cm.} \times 10 \text{ cm.}^{-1}$  and above  $200 \text{ cm.}^{-1}$ , double  $10 \text{ cm.} \times 10 \text{ cm.}^{-1}$ ; sensitivity on single slits,  $3 \times 100$ , double slits,  $1 \times 100$ ; period, 1.0 sec.; scan,  $2.5 \text{ cm.}^{-1}/\text{sec.}$ ; zero suppression, none. The lower Raman spectrum is that of a  $1.054 \text{ M}$  aqueous solution of  $\text{HIO}_3$ : cell, 5 ml., 7-mm. diameter; slits, double,  $10 \text{ cm.} \times 10 \text{ cm.}^{-1}$ ; sensitivity,  $2.8 \times 200$ ; period, 1.0 sec.; scan,  $0.5 \text{ cm.}^{-1}/\text{sec.}$ ; zero suppression, none.

Solutions of sodium chloride of known concentration were used to calibrate the instrument during each series of measurements on iodic acid or sodium iodate solutions.

### Discussion and Results

*Vibrational Assignment of Sodium Iodate.* Crystalline sodium iodate has been shown to contain discrete pyramidal  $\text{IO}_3^-$  ions<sup>20</sup> with the orthorhombic lattice having  $D_{2h}^{16}$ - $Pnma$  space group symmetry. There are four molecules in each primitive cell. Therefore, the  $\text{IO}_3^-$  ions have site symmetry  $C_s$ .<sup>21,22</sup> The individual  $\text{IO}_3^-$  ions must have molecular symmetry  $C_{3v}$  with four internal fundamental vibrational frequencies which are divided into symmetry species 2A and 2E. All four fundamentals are infrared and Raman active. The two vibrations of the E species may be split owing to the lower site symmetry. Thus, a maximum of six internal vibrations is expected, assuming there is no interaction of adjacent  $\text{IO}_3^-$  ions, which has usually proven to be true.<sup>19,21</sup>

An inspection of the Raman spectrum of crystalline sodium iodate (see Figure 1) shows two strong frequen-

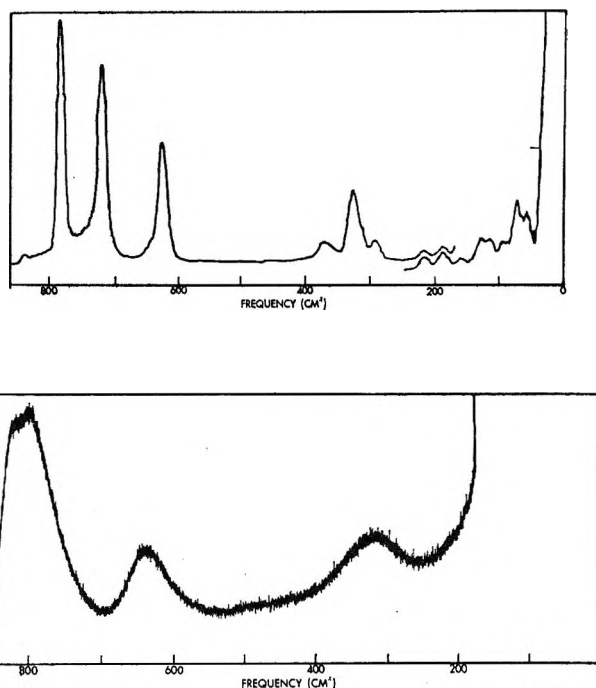


Figure 3. The upper curve is the Raman spectrum of solid  $\text{DIO}_3$  and the lower curve is that of an aqueous solution. Instrumental conditions approximately the same as described in Figure 2.

cies in the I-O stretching region. The lower one at  $754 \text{ cm.}^{-1}$  is assigned to the  $\text{IO}_3^-$  symmetric stretching vibration while the higher one at  $774 \text{ cm.}^{-1}$  is assigned to the doubly degenerate  $\text{IO}_3^-$  antisymmetric stretching frequency. This assignment is based on the assumption that the symmetric stretching will be the more intense Raman line and that the antisymmetric stretching will be the higher frequency vibration as it has been shown to be true for the  $\text{ClO}_3^-$  ion.<sup>3</sup> There are three frequencies of approximately the same intensity in the I-O bending region. Depolarization measurements<sup>3</sup> have shown the antisymmetric bending of the  $\text{ClO}_3^-$  and  $\text{BrO}_3^-$  ion to be at a lower frequency than the symmetric bending. Therefore, the  $373\text{-cm.}^{-1}$  line is assigned to  $\nu_2$ , the symmetric  $\text{IO}_3^-$  bending, and the degenerate bending,  $\nu_4$ , is assigned to the two frequencies  $355$  and  $332 \text{ cm.}^{-1}$ . The splitting of the degeneracy is expected from the lattice site symmetry as explained previously. Several lower frequencies were also observed in the Raman spectrum but these disappear in the solution spectrum and are assigned to lattice vibrations and are discussed later. In the aqueous solution

(20) I. Naray-Szabo and J. Neugebauer, *J. Am. Chem. Soc.*, **69**, 1280 (1947).

(21) R. S. Halford, *J. Chem. Phys.*, **14**, 8 (1946).

(22) D. F. Hornig, *ibid.*, **16**, 1063 (1948).

(lower curve, Figure 1), it is seen that the two vibrations in the higher spectral region merge into one symmetrical line at a much higher frequency of  $797\text{ cm.}^{-1}$ . The three lower frequencies also merge into only one discernable line centered at  $318\text{ cm.}^{-1}$ . The higher band of the aqueous solution is thus sharp and shifted to a higher frequency, while the lower band is broad and shifted to a lower frequency. The results of this study with the above vibrational assignment are summarized in Table III and should be compared to those given in ref. 3 and 4 and tabulated in Table II. The  $760\text{-cm.}^{-1}$  band observed in previous infrared studies is then  $\nu_1$ , the  $774\text{-cm.}^{-1}$  band is  $\nu_3$ , and there appears to be no Fermi resonance with  $2\nu_2$ . The  $796\text{-cm.}^{-1}$  infrared band is explained as a combination of a fundamental and a lattice mode of the crystal. The difference between the frequency  $\nu_1$  as observed in the Raman effect and by the infrared technique is readily explained as arising from the different symmetry species of the polarizability and the dipole moment of the primitive cell.<sup>19,22</sup> Thus, the small difference is a measure of the coupling of the iodate ions in the unit cell.

Table II: Previous Data on the Vibrational Frequencies of  $\text{NaIO}_3$

Raman <sup>a</sup>		Infrared	
Crystalline solid $\Delta\nu, \text{cm.}^{-1}$	Aqueous solution (0.25 M) $\Delta\nu, \text{cm.}^{-1}$	Ref. 4 $\nu, \text{cm.}^{-1}$	Miller <sup>b</sup> $\nu, \text{cm.}^{-1}$
	324(1)		
737(8)			
753(8)		760 s	767
789(5)		774 s	775
808(5)	803(6)	796 m $\nu_3$	800

<sup>a</sup> See ref. 2. <sup>b</sup> F. A. Miller and C. H. Wilkins, *Anal. Chem.*, **24**, 1253 (1952).

*Vibrational Assignment of Iodic Acid and Deuterioiodic Acid.* Dasent and Waddington<sup>4</sup> recorded the infrared spectra of iodic acid and deuterioiodic acid and gave a partial vibrational assignment (see Table IV). Each of the three I-O stretching fundamentals had three maxima which were essentially unchanged in the deuterioiodic acid spectrum. There was also a band at  $462\text{ cm.}^{-1}$  in the spectra of both molecules which was not assigned. As pointed out by these authors, iodic acid can have at most a plane of symmetry. Therefore, the spectra are interpreted in terms of  $C_s$  point group symmetry with the normal modes divided into symmetry species  $6A'$  and  $3A''$ . The crystal structure

Table III: Raman Spectrum and Vibrational Assignment of  $\text{NaIO}_3$ <sup>a</sup>

Crystalline solid frequency, $\text{cm.}^{-1}$	Intensity	Assignment	Description	Aqueous solution frequency, $\text{cm.}^{-1}$	Depolarization value
76	10		Lattice mode		
92 shoulder	4		Lattice mode		
108	4		Lattice mode		
132	v.w.		Lattice mode		
158	8		Lattice mode		
199	5		Lattice mode		
220 shoulder	v.w.		Lattice mode		
332 b	4	$\nu_4(E)$	Antisymmetric bending		
355	6	$\nu_4(E)$	Antisymmetric bending	318	
373	5	$\nu_2(A_1)$	Symmetric bending		
754	100	$\nu_1(A_1)$	Symmetric stretching	797	0.42
774	61	$\nu_3(E)$	Antisymmetric stretching		
817	v.w.	Combination			

<sup>a</sup> Abbreviations used: b, broad; w, weak; v, very.

has been determined<sup>23</sup> to belong to the space group  $D_2^4-P_{212121}$ , with four molecules per primitive cell. The site symmetry will be  $C_1$ ; since there are no degenerate vibrations and both symmetry species  $A'$  and  $A''$  are infrared and Raman active, the lower symmetry of the crystal will have no noticeable effect on the spectrum. In the Raman spectrum of crystalline iodic acid, there is found a rather weak but sharp line at  $3045\text{ cm.}^{-1}$  which is assigned to the O'-H stretching. A very broad line in the infrared spectrum with a center at approximately  $1110\text{ cm.}^{-1}$  is assigned to O'-H in-plane bending. The O'-H torsional vibration is expected to be weak in the Raman effect and could very well be obscured by the I-O stretching vibrations, or part of the intensity of the  $1110\text{-cm.}^{-1}$  infrared band could be due to this vibration.

Three strong, sharp Raman frequencies are observed in the spectrum of the crystalline material (see Figure 2). The lowest of these frequencies,  $631\text{ cm.}^{-1}$ , is polarized and assigned to  $\nu_4$ , the IO' stretching vibration. The line at  $713\text{ cm.}^{-1}$  is then assigned to the IO<sub>2</sub> symmetric stretching,  $\nu_3$ . The IO<sub>2</sub> antisymmetric stretching,  $\nu_8$ , is assigned to the  $780\text{-cm.}^{-1}$  Raman line.

(23) M. T. Rogers and L. Helmholtz, *J. Am. Chem. Soc.*, **63**, 278 (1941).

**Table IV:** Previous Data on the Vibrational Frequencies of HO'IO<sub>2</sub>

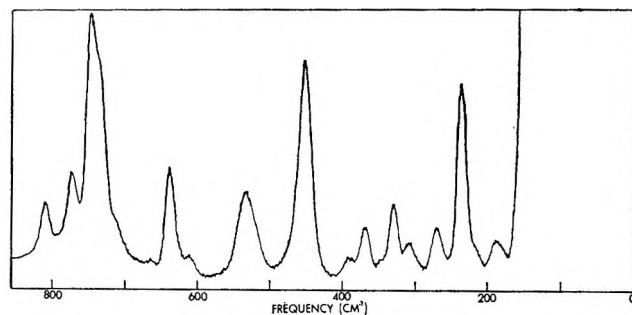
Raman <sup>a</sup>		Infrared Solid (see ref. 4)
Crystalline solid $\Delta\nu$ , cm. <sup>-1</sup>	Aqueous solution (6 M) $\Delta\nu$ , cm. <sup>-1</sup>	
64(1)		
80(1)		
97(0)		
115(0)		
128(1)		
163(0)		
198(0)		
220(1)		
295(1)		
314(0)		
328(6)	330(6)	
377(3)		
413(1)	463(0)	577
633(6)	644(5)	637 } $\nu_4$
652(0)		650
670(0)		
713(8)		718
739(1)		745
782(10)	796(6)	763 ( $\nu_8$ )
801(0)		804 ( $\nu_3$ )
823(0)	823(5)	820
842(2)		835
1249(0)		1101 ( $\nu_7$ )
1397(0)		1163 ( $\nu_2$ )
2979		2920 ( $\nu_1$ )

<sup>a</sup> See ref. 2 and 6.

The latter two assignments are considerably lower than those reported in the earlier infrared study.<sup>4</sup> The Raman line at 378 cm.<sup>-1</sup> is assigned to  $\nu_5$  because of the similarity of the motion of this vibration with  $\nu_2$  of the sodium salt. The other two frequencies at 328 and 296 cm.<sup>-1</sup> are arbitrarily assigned to  $\nu_6$ , the IO<sub>2</sub> deformation, and to  $\nu_9$ , the O'IO bending, respectively. The above vibrational assignment is summarized in Table V.

The infrared frequency reported<sup>4</sup> at 462 cm.<sup>-1</sup> is thought to be due to I<sub>2</sub>O<sub>5</sub> impurity. Figure 4 shows a Raman spectrum of partially dehydrated HOIO<sub>2</sub> and a strong, sharp frequency was observed at 462 cm.<sup>-1</sup>. This frequency rapidly disappeared when the sample was placed in a desiccator over H<sub>2</sub>O. The frequencies observed at 220 cm.<sup>-1</sup> and below are all believed to be due to vibrations involving the motions of the atoms of two or more molecules or lattice modes.

The low-frequency Raman lines have approximately the same value in all three molecules, NaIO<sub>3</sub>, HO'IO<sub>2</sub>, and DO'IO<sub>2</sub>. There is a large change in intensity and an additional line at 58 cm.<sup>-1</sup> is observed for the acid. The external vibrations of a rotatory origin are ex-

Figure 4 Raman spectrum of partially dehydrated solid HIO<sub>3</sub>.

pected to give the strongest Raman lines. The three rotatory vibrations can couple with adjacent molecules to give a total of six vibrations which will be even with respect to the center of symmetry and will be Raman active. Four of the remaining rotatory vibrations will be infrared active. There will also be six translatory vibrations which will be Raman active and can combine with the rotatory vibrations to give additional Raman shifts. Three rather strong Raman lines are observed at 76, 158, and 199 cm.<sup>-1</sup> in the spectrum of NaIO<sub>3</sub>. These frequencies are then assigned as the external rotatory vibrations with the assumption of a small amount of coupling between the molecules. The other frequencies are combinations with vibrations of a translatory origin. Interaction in the acid *via* hydrogen bonds is expected to split the rotatory vibrations, and the three pairs of frequencies with approximately the same intensity are assigned to these lattice modes in the acid. The assignment of these low-frequency vibrations is highly speculative and does not appear to merit further discussion at this time.

*Ionization Constant of Iodic Acid.* Four series of measurements on six iodic acid solutions were made in which the intensities of the Raman line at 797 cm.<sup>-1</sup> arising from the iodate ion in these solutions were compared with those intensities of sodium iodate solutions. In each instance the sodium iodate concentrations were chosen so that the intensities would be of the same magnitude as those of the acid solutions. It was possible to calculate from these measurements a degree of ionization,  $\alpha$ , for each solution and consequently an apparent ionization constant

$$k = \frac{\alpha^2 m}{1 - \alpha}$$

which was uncorrected for activity coefficients of both the ionized and un-ionized species. Osmotic and activity coefficients have not been reported for sodium iodate although data are available for sodium chlorate

Table V: Raman Spectra and Vibrational Assignment of HO'IO<sub>2</sub> and DO'IO<sub>2</sub><sup>a</sup>

Aqueous solution of HO'IO <sub>2</sub>						Crystalline solid HO'IO <sub>2</sub>			
Frequency, cm. <sup>-1</sup>					Depolarization values	Frequency, cm. <sup>-1</sup>	Intensity	Assignment	Approximate description
1.05 M	4 M	8 M	12 M	Intensity					
						58	8		Lattice mode
						72	12		Lattice mode
						91 shoulder	3		Lattice mode
						111	6		Lattice mode
						124	6		Lattice mode
						158	3		Lattice mode
						192	4		Lattice mode
						220	4		Lattice mode
						296	7	$\nu_9(A'')$	O'IO bending
319	324	324	324	18	6/7	328	28	$\nu_6(A')$	IO <sub>2</sub> deformation
						378	11	$\nu_6(A')$	O'IO <sub>2</sub> rocking
645	644	638	638	14	0.62	631	40	$\nu_4(A')$	IO' stretching
	760	737	737			713	87	$\nu_3(A')$	IO <sub>2</sub> symmetric stretching
						741 shoulder	...	$\nu_8 +$ lattice mode	
800	793	776	771	100	0.46	780	100	$\nu_8(A'')$	IO <sub>2</sub> antisymmetric stretching
824	831	821	814	75	...	839	4	$\nu_8 +$ lattice mode	
						1110 <sup>b</sup>	...	$\nu_2(A')$	O-H in-plane bending
						1346	v.w.	$\nu_3 + \nu_4 = 1344$	
						3045	v.w.	$\nu_1(A')$	O-H stretching

Aqueous solutions of DO'IO <sub>2</sub>			Crystalline solid DO'IO <sub>2</sub>		
Frequency, cm. <sup>-1</sup>	Intensity	Depolarization values	Frequency, cm. <sup>-1</sup>	Intensity	Assignment
			60	12	Lattice mode
			74	17	Lattice mode
			92 shoulder	3	Lattice mode
			113	5	Lattice mode
			126	7	Lattice mode
			157	2	Lattice mode
			187	55	Lattice mode
			216	5	Lattice mode
			292	10	$\nu_9(A'')$ bending
317	18	6/7	326	33	$\nu_6(A')$ IO <sub>2</sub> deformation
			370	10	$\nu_6(A')$ O'IO <sub>2</sub> rocking
637	28	0.62	623	52	$\nu_4(A')$ IO' stretching
			716	86	$\nu_3(A')$ IO <sub>2</sub> symmetric stretching
800	100	0.46	778	100	$\nu_8(A'')$ IO <sub>2</sub> antisymmetric stretching
817	97	0.48	836	5	$\nu_8 +$ lattice mode
			2235 v.b.	2	O-D stretching

<sup>a</sup> Abbreviations used: w, weak; v, very; b, broad. <sup>b</sup> This vibration was only observed in the infrared spectrum of the material using the Nujol mull technique.

and sodium bromate.<sup>24</sup> The measurements reported in Table VI were made using the Mechrolab vapor osmometer in the manner described previously. The temperature was maintained at 25° since activity coefficient data are normally reported at this temperature. The sodium iodate coefficients are qualitatively of the order which would be expected in the light of those reported

for the chlorate and bromate salt. The low values of the iodate coefficients are of course the result of incomplete dissociation.

The availability of stoichiometric activity coeffi-

(24) R. A. Robinson and R. H. Stokes, "Electrolyte Solutions," Butterworth and Co. Ltd., London, 1959, p. 492.

**Table VI:** Osmotic and Activity Coefficients of Iodic Acid and Sodium Iodate

<i>m</i>	HIO <sub>3</sub>		NaIO <sub>3</sub>	
	$\phi$	$\gamma$	$\phi$	$\gamma$
0.02	0.892	0.708	0.950	0.854
0.05	0.843	0.601	0.924	0.787
0.10	0.792	0.505	0.900	0.725
0.20	0.726	0.400	0.870	0.650
0.30	0.682	0.339	0.845	0.597
0.40	0.647	0.298	0.822	0.557
0.50	0.617	0.266		
0.60	0.594	0.242		
0.70	0.574	0.223		
0.80	0.554	0.206		
0.90	0.534	0.191		
1.00	0.515	0.179		

coefficients,  $\gamma_{\pm}$ , for iodic acid solutions still does not directly permit a correction to be made to the apparent ionization constant since the true ionization constant,  $K$ , is

$$K = k \frac{f_{\text{H}^+} f_{\text{IO}_3^-}}{f_{\text{HIO}_3}} = k \frac{f_{\pm}^2}{f_u}$$

where  $f_+$ ,  $f_-$ , and  $f_{\pm}$  represent the ionic activity coefficients and  $f_u$  represents the activity coefficient of the un-ionized acid. The latter coefficient may be assumed to be near unity in dilute solution. A quite accurate estimation may, however, be made of these ionic coefficients. If one notes the value of the function  $[\log \gamma_{\pm(\text{acid})} - \log \gamma_{\pm(\text{Na salt})}]$  for strong acids, it is found to be remarkably constant at any ionic strength up to perhaps 1.5 *m* regardless of the values of the individual coefficients. This is illustrated in Figure 5 by the behavior of perchlorates, nitrates, and iodides. With this knowledge and the values of the sodium iodate activity coefficients, one may estimate the ionic activity coefficients for iodic acid and thus calculate the ionization constant which is now in error only because of the neglect of the activity coefficient of the un-ionized species. An extrapolation of these data to infinite dilution should yield the true ionization constant. These calculations are presented in Table VII and the extrapolation, yielding a constant of  $0.18 \pm 0.01$ , is shown in Figure 6. This value is somewhat larger than most of these calculated from conductance data, but it is in perfect agreement with the recent value obtained from n.m.r. measurements.

The data of Figure 6 are of further interest in that they permit an estimation of the activity coefficients of the un-ionized iodic acid at any concentration. The slope of the curve indicates that the activity coefficient rises to a maximum value of about 1.2 at 0.6 *M* and then begins to decrease. Although this value is

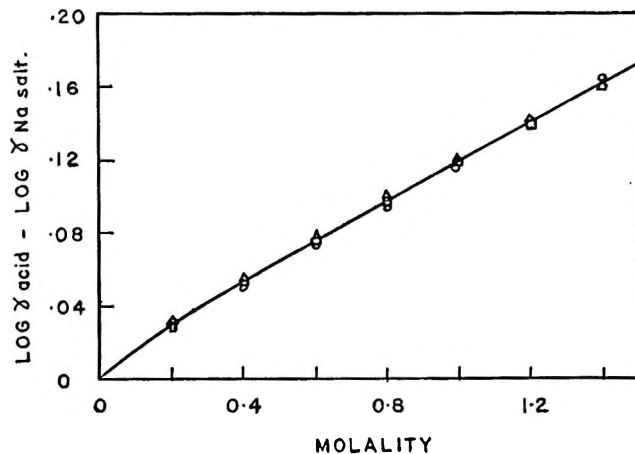


Figure 5. Differences of the logarithms of the coefficients of strong acids and their sodium salts: O, ClO<sub>4</sub>; Δ, NO<sub>3</sub>; □, I.

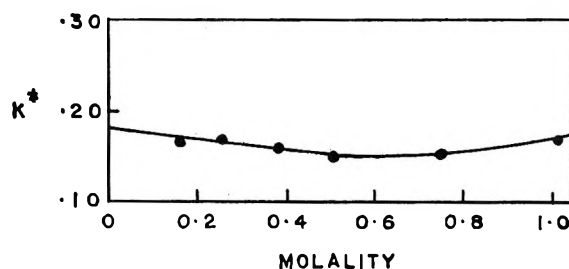


Figure 6. Ionization constant of iodic acid:  $K^* = \alpha^2 m / (1 - \alpha) \times f_+(\text{HIO}_3) = K f_u(\text{HIO}_3)$ .

**Table VII:** Ionization Constant of Iodic Acid from Raman Data at 32°

$M_{\text{HIO}_3}$	$\alpha$	$k = \frac{\alpha^2 m}{1 - \alpha}$	$\mu = \alpha m$	$-\text{Log } \gamma_{\text{NaIO}_3}$	$-\text{Log } f_{\text{HIO}_3}$	$K^* = \frac{k}{k f_{\text{HIO}_3}}$
0.160	0.723	0.303	0.116	0.152	0.133	0.164
0.251	0.665	0.331	0.158	0.170	0.147	0.168
0.382	0.598	0.341	0.228	0.198	0.166	0.159
0.513	0.546	0.337	0.280	0.216	0.177	0.149
0.750	0.500	0.376	0.375	0.247	0.197	0.152
1.054	0.481	0.468	0.507	0.287	0.222	0.168

somewhat higher than expected, it represents the behavior which is usual for solutes which hydrogen bond with the solvent, *e.g.*, sucrose, alcohols, etc. The occurrence of the maximum value at 0.6 *M* indicates that beyond this point the concentration of the HIO<sub>3</sub> dimer becomes appreciable. These data may be compared with those of Hood, *et al.*,<sup>15</sup> in which the extrapolation of  $K\beta$  indicates an activity coefficient of 3.3 for the un-ionized HIO<sub>3</sub> at 0.6 *M*.

*Acknowledgment.* Thanks are due to Dr. O. L. Keller for several helpful suggestions and discussions.

# Ionization and Dissociation of Ruthenium and Osmium Tetroxides<sup>1</sup>

by John G. Dillard<sup>2</sup> and Robert W. Kiser

Department of Chemistry, Kansas State University, Manhattan, Kansas 66504  
(Received June 3, 1965)

The principal ions resulting from ionization and dissociation produced by electron impact have been determined mass spectrometrically for ruthenium tetroxide and osmium tetroxide. The mass spectra and appearance potentials for the parent and fragment ions produced from the tetroxides have been measured. The heats of formation for the positive ions have been determined from the measured energetics. From a study of the negative ions it is concluded that  $\text{MO}_2^-$  is formed by dissociative electron attachment and that  $\text{MO}^-$  and  $\text{MO}_3^-$  are produced by ion-pair formation processes. It is found that  $I(\text{RuO}_4) = 12.33 \pm 0.23$  e.v.,  $I(\text{OsO}_4) = 12.97 \pm 0.12$  e.v.,  $D(\text{O-RuO}_3) = 104$  kcal./mole, and  $D(\text{O-OsO}_3) = 108$  kcal./mole.

## Introduction

The identification of gaseous ruthenium and osmium oxides at elevated temperatures has been the subject of several investigations.<sup>3-9</sup> Experiments involving vapor pressure measurements as a function of oxygen pressure for the ruthenium-oxygen system have shown<sup>5-7</sup> that the dominant species at  $T \geq 1200^\circ$  is  $\text{RuO}_3$ , whereas at  $800^\circ$  the primary molecular compound is  $\text{RuO}_4$ . A mass spectrometric investigation indicates that for the osmium-oxygen system in the  $827$ - $1477^\circ$  region, the predominant molecular components are  $\text{OsO}_3$  and  $\text{OsO}_4$ .<sup>8</sup> Some evidence exists that a stable  $\text{OsO}_2$  molecule is also present in small amounts at temperatures above  $1430^\circ$ .<sup>8</sup> At room temperature ruthenium and osmium tetroxides are stable molecules.

Aston<sup>10</sup> introduced ruthenium tetroxide and osmium tetroxide into the discharge tube of his mass spectrograph in order to determine the relative abundances of the ruthenium and osmium isotopes. Bell and Tagami<sup>7</sup> indicated that a mass spectrometric study of gaseous  $\text{RuO}_n$  species was in progress; recently, the ionization potentials and appearance potentials of  $\text{RuO}_n^+$ ,  $\text{RhO}_n^+$ ,  $\text{PdO}_n^+$ ,  $\text{PtO}_n^+$ , and  $\text{IrO}_n^+$  species have been determined.<sup>9</sup> In their mass spectrometric study of the osmium-oxygen system by the Knudsen effusion technique (in the temperature range  $800$ - $1450^\circ$ ) Grimley, *et al.*,<sup>8</sup> found that the most abundant ions were  $\text{OsO}_3^+$  and  $\text{OsO}_4^+$ , with approximate ionization potentials of  $12.3 \pm 1$  and  $12.6 \pm 1$  e.v., respectively. The forma-

tion of these ions was attributed to simple ionization of the  $\text{OsO}_3$  and  $\text{OsO}_4$  molecules. A mass spectrometric study of the  $\text{OsO}_4$  molecule would provide additional information about the formation of the  $\text{OsO}_3$  molecule at elevated temperatures.

The results of the present investigation of the ionization and dissociation of these tetroxides of ruthenium and osmium represent the first systematic investigation of the ions produced upon electron impact. It was the purpose of this study to determine the thermodynamic data for the gaseous ions and to ascertain the fragmentation pattern for these tetroxides.

## Experimental Section

Ruthenium tetroxide was obtained as a brown liquid

(1) This work was supported in part by the U. S. Atomic Energy Commission under Contract No. AT(11-1)-751 with Kansas State University. This study is a portion of a dissertation to be presented by J. G. Dillard to the Graduate School of Kansas State University in partial fulfillment for the degree of Doctor of Philosophy.

(2) National Aeronautics and Space Administration Fellow.

(3) C. B. Alcock and G. W. Hooper, *Proc. Roy. Soc. (London)*, **A254**, 551 (1960).

(4) H. Schäfer, W. Gerhardt and A. Tebben, *Angew. Chem.*, **73**, 27 (1961).

(5) H. Schäfer, G. Schneidreit, and W. Gerhardt, *Z. anorg. allgem. Chem.*, **319**, 327 (1963).

(6) H. Schäfer, A. Tebben, and W. Gerhardt, *ibid.*, **321**, 41 (1963).

(7) W. E. Bell and M. Tagami, *J. Phys. Chem.*, **67**, 2432 (1963).

(8) R. T. Grimley, R. P. Burns, and M. G. Inghram, *J. Chem. Phys.*, **33**, 308 (1960).

(9) J. H. Norman and H. G. Staley, private communications.

(10) F. W. Aston, *Proc. Roy. Soc. (London)*, **A132**, 487 (1931).

in a sealed vial and osmium tetroxide was received as a white crystalline solid. Both samples were purchased from commercial sources. The sealed samples were placed in Pyrex storage bulbs which were subsequently evacuated. The sample vials were broken under vacuum with a glass-enclosed metal hammer. The ruthenium tetroxide was stored in a blackened sample tube and preserved in a Dry Ice-methanol bath when not attached to the inlet system of the mass spectrometer. Even with these precautions some decomposition of the ruthenium compound to the nonvolatile dioxide was noted. No decomposition was noted for the osmium tetroxide.

The appearance potentials and mass spectra were determined with a Bendix Model 12-100 time-of-flight mass spectrometer which has been described in previous publications.<sup>11</sup> The ionization and appearance potentials were determined from the ionization efficiency curves by the linear extrapolation technique<sup>12</sup> and the semilogarithmic plotting method of Lossing, Tickner, and Bryce.<sup>13</sup> Appearance potentials were also determined by the extrapolated voltage difference method introduced by Warren<sup>14</sup> and were checked by the energy compensation procedure outlined by Kiser and Gallegos.<sup>15</sup> The calibrating gases for the positive ion energetic studies were nitrogen and mercury. The spectroscopic values for the ionization potentials of N<sub>2</sub> (15.58 e.v.<sup>16</sup>) and Hg (10.43 e.v.<sup>17</sup>) were employed. The appearance potential measurements were made using the most abundant ruthenium or osmium isotope (102 and 192 a.m.u., respectively). This technique permitted greater sensitivity in ion current measurements.

For negative ion studies the mass spectrometer was modified so that the polarity of the ion draw-out and accelerating potentials could be reversed from that in normal positive ion operation. Although with the present modification it was not possible to obtain a recorder representation of the negative ion spectra, the spectra were observed by displaying the amplified multiplier detector signal on an oscilloscope screen. A permanent record of the negative ion spectrum was obtained by successively photographing the positive ion spectrum and then the negative ion spectrum using a Polaroid-Land camera.

The reported "resonance" potentials for the negative ions represent the uncalibrated electron energy at which the maximum ion current was observed. The "appearance" potentials for the ions MO<sub>3</sub><sup>-</sup>, MO<sub>2</sub><sup>-</sup>, and MO<sup>-</sup> at about 15 e.v. correspond to the electron energy where the isotopic patterns for these ions became just discernible on the oscilloscope screen.

Immediately after introduction of the osmium tetrox-

ide into the mass spectrometer, a 30-50% decrease in the trap current was observed. Within a matter of a few minutes this decrease ceased and the value remained constant throughout a given appearance potential determination. Introduction of the ruthenium tetroxide into the instrument initially produced no deleterious effects. If the duration of a given experiment was prolonged, however, it was found that the sapphire spacers in the ion source lost their insulating ability and subsequent cleaning of the source components was required. The dynode and field strips in the magnetic electron multiplier detector were also cleaned when the ion source components were cleaned. It was found that the appearance potentials were reproducible within the error limits (one standard deviation) listed in Tables I and II.

## Results

The experimental results for this study of the tetroxides are presented in Tables I and II. In column two of these tables is given the relative abundance of the most abundant isotope in that group at a nominal ionizing energy of 70 e.v. The measured appearance potentials are listed in column three and the proposed process for the ionization and any dissociation are summarized in column four. In the last column the heats of formation of the ions are presented; these are consistent with the energetics and the proposed fragmentations. The following heats of formation, in kcal./mole, were employed in the thermochemical calculations: RuO<sub>4</sub>(g), -45.0 (the average of two reported values<sup>6,7</sup>); Ru(g), 154 (the average of two literature values<sup>18,19</sup>); OsO<sub>4</sub>(g), -79.9<sup>20</sup>; O(g), 59.2<sup>20</sup>; and Os(g), 187.<sup>18</sup>

The clastologs of RuO<sub>4</sub> and OsO<sub>4</sub> are shown in Figures 1 and 2. These figures, showing the variation of the

(11) E. J. Gallegos and R. W. Kiser, *J. Am. Chem. Soc.*, **83**, 733 (1961); *J. Phys. Chem.*, **65**, 1177 (1961).

(12) P. T. Smith, *Phys. Rev.*, **36**, 1293 (1930).

(13) F. P. Lossing, A. W. Tickner, and W. A. Bryce, *J. Chem. Phys.*, **19**, 1254 (1951).

(14) J. W. Warren, *Nature*, **165**, 810 (1950).

(15) R. W. Kiser and E. J. Gallegos, *J. Phys. Chem.*, **66**, 947 (1962).

(16) G. Herzberg, "Molecular Spectra and Molecular Structure. I. Spectra of Diatomic Molecules," D. Van Nostrand Co., Inc., New York, N. Y., 1950.

(17) C. E. Moore, National Bureau of Standards Circular 467, Volumes 1 and 3, U. S. Government Printing Office, Washington, D. C., 1949 and 1958.

(18) M. B. Panish and L. Reif, *J. Chem. Phys.*, **37**, 128 (1962).

(19) R. C. Paule and J. L. Margrave, *J. Phys. Chem.*, **67**, 1896 (1963).

(20) F. D. Rossini, D. D. Wagman, W. H. Evans, S. Levine, and I. Jaffe, "Selected Values of Chemical Thermodynamic Properties," National Bureau of Standards Circular 500, U. S. Government Printing Office, Washington, D. C., 1952.



**Table I:** Appearance Potentials and Heats of Formation for Ions Produced from Ruthenium Tetroxide

Ion	Relative abundance at 70 e.v.	Appearance potential, e.v.	Probable process	$\Delta H_f(\text{ion})$ , kcal./mole
$\text{Ru}^{2+}$	<0.1			
$\text{RuO}^{2+}$	<0.1			
$\text{Ru}^+$	30.4	$22.3 \pm 0.3$	$\text{RuO}_4 \rightarrow \text{Ru}^+ + \text{O}_2 + 2\text{O}$	351
$\text{RuO}^+$	22.7	$18.1 \pm 0.3$	$\rightarrow \text{RuO}^+ + \text{O}_2 + \text{O}$	313
$\text{RuO}_2^+$	38.0	$14.2 \pm 0.2$	$\rightarrow \text{RuO}_2^+ + \text{O}_2$	282
$\text{RuO}_3^+$	19.5	$15.7 \pm 0.3$	$\rightarrow \text{RuO}_3^+ + \text{O}$	258
$\text{RuO}_4^+$	100.0	$12.33 \pm 0.23$	$\rightarrow \text{RuO}_4^+$	239

**Table II:** Appearance Potentials and Heats of Formation for Ions Produced from Osmium Tetroxide

Ion	Relative abundance at 70 e.v.	Appearance potential, e.v.	Probable process	$\Delta H_f(\text{ion})$ , kcal./mole
$\text{Os}^+$	29.6	$26.8 \pm 0.5$	$\text{OsO}_4 \rightarrow \text{Os}^+ + \text{O}_2 + 2\text{O}$	420
$\text{OsO}^+$	32.0	$21.2 \pm 0.2$	$\rightarrow \text{OsO}^+ + \text{O}_2 + \text{O}$	350
$\text{OsO}_2^+$	48.0	$17.1 \pm 0.2$	$\rightarrow \text{OsO}_2^+ + \text{O}_2$	314
$\text{OsO}_3^+$	29.6	$17.00 \pm 0.10$	$\rightarrow \text{OsO}_3^+ + \text{O}$	253
$\text{OsO}_4^+$	100.0	$12.97 \pm 0.12$	$\rightarrow \text{OsO}_4^+$	219

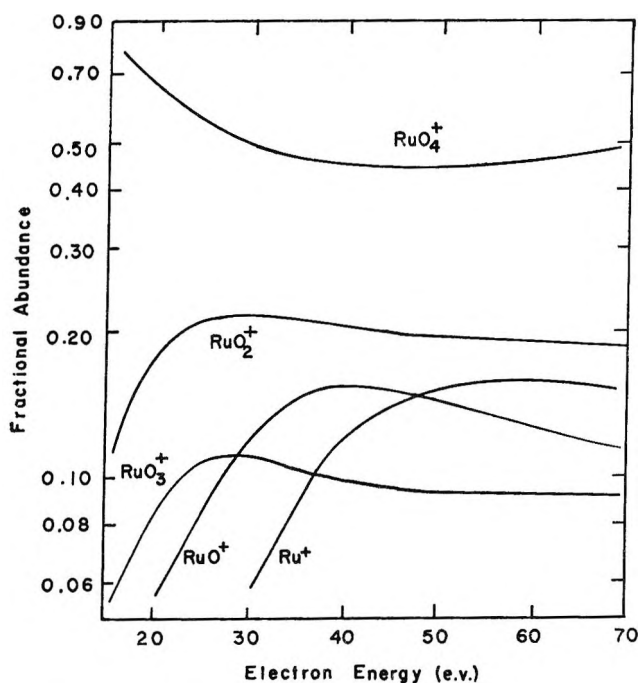


Figure 1. Clastolog for ruthenium tetroxide.

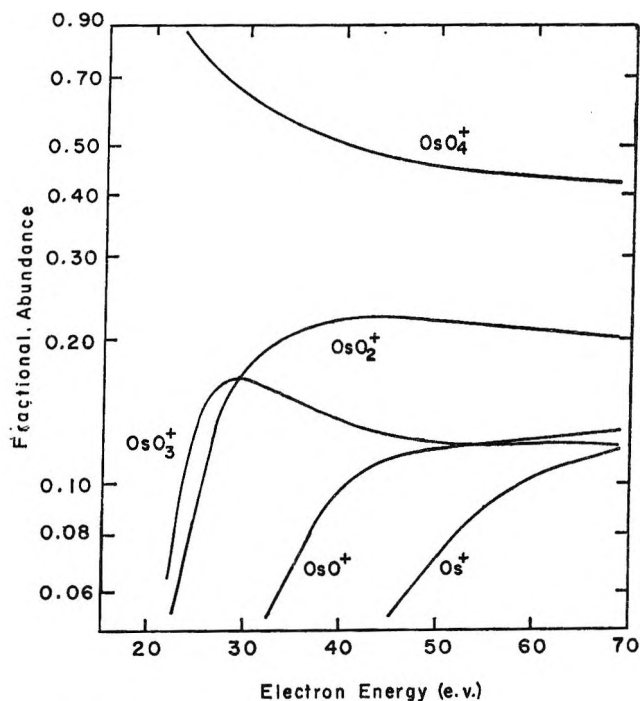


Figure 2. Clastolog for osmium tetroxide.

logarithm of the fractional abundance of the ions as a function of the electron energy, are very similar for the two tetroxides. The parent molecule ion decreases in abundance as the electron energy is increased until a nearly constant value is reached. The metal dioxide

ion, the metal monoxide ion, and the metal ion "grow in" and reach a plateau at higher electron energies, except for the ruthenium monoxide ion which shows a decrease in abundance at higher energies. The metal

trioxide ion appearance behavior is characterized by a distinct maximum in the formation curve.

The shapes of the ionization efficiency curves for the lower metal oxide positive ions indicate that these ions are formed by fragmentation rather than by decomposition followed by ionization. If the latter process were taking place, the appearance potentials for the ionic species  $M^+$ ,  $MO^+$ , and  $MO_2^+$  ( $M = Ru, Os$ ) would be expected to be in the range 7–11 e.v. by comparison with the measured<sup>8,9,21,22</sup> ionization potentials for other platinum metal oxide species.

In the study of the negative ions produced by electron impact,  $MO_3^-$ ,  $MO_2^-$ , and  $MO^-$  were detected.  $MO_4^-$  was never detected in any of the experiments. The  $MO_2^-$  species was found to exhibit a resonance capture peak at low energies (2–8 e.v.), when the ion current was followed as a function of the electron energy. The  $MO_2^-$  ion was also detected again at energies greater than about 15 e.v. Also, at energies above about 15 e.v. the  $MO_3^-$  and the  $MO^-$  ions were detected. From these experiments it is found that  $MO_2^-$  is formed by dissociative electron attachment at low voltages and by pair production at the higher energies.  $MO_3^-$  and  $MO^-$  apparently are formed in pair production processes only.

### Discussion

The relative abundances observed in the positive ion mass spectra of the ruthenium and osmium tetroxides are similar to those noted in the spectra of the transition metal oxyhalide derivatives  $VOCl_3$ ,<sup>23</sup>  $CrO_2Cl_2$ , and  $CrO_2ClF$ <sup>24</sup> in that the parent molecule ion is the most abundant ion in the spectrum. The fragment ions in the two tetroxides investigated are each less than half as abundant as the parent molecule ion. Of the fragment ions, the metal dioxide ion is the most abundant while the metal monoxide ion is always slightly more abundant than the metal trioxide ion. The lower abundance of the ruthenium trioxide and monoxide ions suggests a relative instability of these ions in the unimolecular decomposition process as compared to the corresponding ions of osmium.

From a consideration of the variation of the ion intensity as a function of electron energy and the measured appearance potentials, it is not unreasonable to postulate that the fragmentation processes involve competitive reactions producing  $MO_3^+$  and  $MO_2^+$  ions from  $MO_4^+$ .

The measured ionization potential for osmium tetroxide (12.97 e.v.) is in good agreement with the approximate value of  $12.6 \pm 1$  e.v. reported by Grimley, Burns, and Inghram.<sup>8</sup> The ionization potential determined for ruthenium tetroxide is compared with the

trend noted in the values of the ionization potentials determined for other platinum metal oxides, including the values determined by Norman and Staley<sup>9</sup> (see Table III) as well as with the specific value of  $I(RuO_4)$  found by Norman and Staley.<sup>9</sup> The electron removed from ruthenium tetroxide and osmium tetroxide upon ionization by electron impact most probably was localized on an oxygen atom. The ionization potentials for these tetroxides as well as for other platinum metal oxides are somewhat lower than that of oxygen (13.62 e.v.<sup>17</sup>) but much greater than the ionization potentials of the metal atoms [ $I(Ru) = 7.36$ ;  $I(Os) = 8.7$ ;  $I(Rh) = 7.46$ ;  $I(Ir) = 9$ ;  $I(Pd) = 8.33$ ; and  $I(Pt) = 9$  e.v.<sup>17</sup>]. A similar conclusion that the ionized electron was localized on an oxygen atom is derived from attempted Franklin calculations<sup>25</sup> for the ionization potentials of the  $RuO_n$  and  $OsO_n$  molecules.

Table III: Ionization Potentials (e.v.) of Gaseous Platinum Metal Oxides

Ru	7.364 <sup>a</sup>	Rh	7.46 <sup>a,b,f</sup>	Pd	8.33 <sup>a</sup>
RuO	8.7 <sup>b</sup>	RhO	9.3 <sup>f</sup>	PdO	9.1 <sup>f</sup>
RuO <sub>2</sub>	10.6 <sup>b</sup>	RhO <sub>2</sub>	10.0 <sup>b,f</sup>	PdO <sub>2</sub>	(10.0) <sup>d</sup>
RuO <sub>3</sub>	11.2 <sup>b</sup>	RhO <sub>3</sub>	(11.4) <sup>b</sup>		
RuO <sub>4</sub>	12.33 <sup>c</sup> ; 12.8 <sup>b</sup>				
Os	8.7 <sup>a</sup>	Ir	9.6 <sup>e</sup>	Pt	9.0 <sup>a</sup>
OsO	(9.7) <sup>d</sup>	IrO	10.1 <sup>e</sup>	PtO	10.1 <sup>b</sup>
OsO <sub>2</sub>	(11.2) <sup>d</sup>	IrO <sub>2</sub>	10.9 <sup>e</sup>	PtO <sub>2</sub>	11.2 <sup>b</sup>
OsO <sub>3</sub>	12.3 <sup>e</sup>	IrO <sub>3</sub>	11.9 <sup>e</sup>		
OsO <sub>4</sub>	12.97 <sup>c</sup> ; 12.6 <sup>e</sup>				

<sup>a</sup> See ref. 17. <sup>b</sup> See ref. 9. <sup>c</sup> This work. <sup>d</sup> Estimated; see text. <sup>e</sup> See ref. 8. <sup>f</sup> See ref. 21. <sup>g</sup> See ref. 22.

Combination of the ionization potential of the  $RuO_3$  molecule determined by Norman and Staley<sup>9</sup> with the appearance potential for  $RuO_3^+$  from  $RuO_4$  measured in this study permits a calculation of  $D(O-RuO_3)$ . Norman and Staley found  $I(RuO_3) = 11.2$  e.v.; the value reported for  $A(RuO_3^+)$  from  $RuO_4$  in Table II is 15.7 e.v. Therefore,  $D(O-RuO_3) = 15.7 - 11.2 = 4.5$  e.v. (104 kcal./mole).

In an analogous fashion a value for  $D(O-OsO_3)$  may

(21) J. H. Norman, H. G. Staley, and W. E. Bell, *J. Phys. Chem.*, **68**, 662 (1964).

(22) J. H. Norman, H. G. Staley, and W. E. Bell, *J. Chem. Phys.*, **42**, 1123 (1965).

(23) H. J. Svec and G. D. Flesch, paper presented at the 12th Annual Conference on Mass Spectrometry and Allied Topics, ASTM Committee E-14 on Mass Spectrometry, McGill University, Montreal, Canada, June 1964.

(24) G. D. Flesch and H. J. Svec, *J. Am. Chem. Soc.*, **81**, 1787 (1959).

(25) J. L. Franklin, *J. Chem. Phys.*, **22**, 1304 (1954).

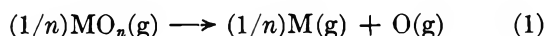
be calculated. Employing the ionization potential for  $\text{OsO}_3$  measured by Grimley, Burns, and Inghram<sup>8</sup> and the value for the appearance potential for  $\text{OsO}_3^+$  from  $\text{OsO}_4$  reported in this work, the magnitude of the bond dissociation energy,  $D(\text{O}-\text{OsO}_3)$ , is  $A(\text{OsO}_3^+) - I(\text{OsO}_3) = 17.00 - 12.3 = 4.7$  e.v. (108 kcal./mole).

These results require additional discussion. Schäfer, *et al.*,<sup>6</sup> found  $D(\text{O}-\text{RuO}_3) = 89.7$  kcal./mole while  $D(\text{O}-\text{RuO}_3)$  is calculated to be 87.9 kcal./mole from Bell and Tagami's data.<sup>7</sup> Schäfer, *et al.*,<sup>6</sup> have derived a value of  $\Delta H_f(\text{OsO}_3) = -66.2$  kcal./mole from Grimley, Burns, and Inghram's paper.<sup>8</sup> Using this value for  $\Delta H_f(\text{OsO}_3)$ ,  $D(\text{O}-\text{OsO}_3)$  is calculated to be 72.9 kcal./mole. It is noted that the magnitudes of  $D(\text{O}-\text{MO}_3)$  calculated using the appearance potential measurements in this study are consistently higher than the thermochemical values. However, considering the error in the precision of the energetic measurements, the agreement for  $D(\text{O}-\text{RuO}_3)$  calculated in this work with the high-temperature thermochemical investigation is acceptable. The corresponding agreement for  $D(\text{O}-\text{OsO}_3)$  is less favorable.

Since  $\bar{D}(\text{OsO})$  for  $\text{OsO}_4$  (126 kcal./mole) is greater than  $\bar{D}(\text{RuO})$  for  $\text{RuO}_4$  (109 kcal./mole), it is anticipated that  $D(\text{O}-\text{OsO}_3) \geq D(\text{O}-\text{RuO}_3)$ . Furthermore, the value of 73 kcal./mole for  $D(\text{O}-\text{OsO}_3)$  is very low compared to  $\bar{D}(\text{Os}-\text{O}) = 126$  kcal./mole for  $\text{OsO}_4$ . The remarkably short bond distance (1.66 Å.<sup>26</sup>) in  $\text{OsO}_4$  suggests a rather strong bond (double-bond character; not much triple-bond character<sup>27</sup>).

An examination of the electron impact data is also in order.  $I(\text{RuO}_4) = 12.33 \pm 0.23$  e.v. compares with  $I(\text{RuO}_4) = 12.8$  e.v. measured by Norman and Staley.<sup>9</sup> Furthermore,  $I(\text{OsO}_4) = 12.97 \pm 0.12$  e.v. reported here agrees with  $I(\text{OsO}_4) = 12.6 \pm 1$  e.v. determined by Grimley, Burns, and Inghram.<sup>8</sup> From Table III it is observed that a regular increase occurs in  $I(\text{MO}_n)$  as  $n$  increases. This same increase observed for the  $\text{OsO}_4$  studies indicates that the ionization potentials measured by Grimley, *et al.*,<sup>8</sup> are reasonably correct and therefore that  $D(\text{O}-\text{OsO}_3) = 108$  kcal./mole. This result is rather like  $\bar{D}(\text{Os}-\text{O}) = 126$  kcal./mole from  $\text{OsO}_4$ .

The above results permit the calculation of the dissociation energies for the reaction



The results are 126 kcal./mole for  $\text{OsO}_4$ , 131 kcal./mole for  $\text{OsO}_3$ , 109 kcal./mole for  $\text{RuO}_4$ , and 111 kcal./mole for  $\text{RuO}_3$ . If the value of  $D(\text{O}-\text{OsO}_3) = 73$  kcal./mole is used, the dissociation energies (eq. 1) for  $\text{OsO}_4$  and  $\text{OsO}_3$  are 126 and 144 kcal./mole, respectively; it can be seen that these values are much different from those for  $\text{RuO}_4$  and  $\text{RuO}_3$ . Therefore, it is believed that  $D(\text{O}-\text{OsO}_3) = 108$  kcal./mole is to be favored, although it is recognized that the bond energies derived from these electron-impact studies may be affected by uncertainties in the amounts of excess energy in the processes. A general observation is that  $D(\text{O}-\text{MO}_3) < D(\text{O}-\text{MO}_n)$ , where  $n = 0, 1$ , or 2 and  $\text{M} = \text{Ru}$  or  $\text{Os}$ .

The heats of formation of the metal oxide ions show a monotonic increase in magnitude as the number of oxygen atoms in the metal oxide ion decreases. It is noted that this increase is more pronounced for the osmium oxide ions than for the ruthenium oxide ions.

The calculated heats of formation of the metal ions, assuming the proposed processes, are in agreement with the presently accepted values [ $\Delta H_f(\text{Ru}^+)(\text{g}) = 324$  kcal./mole and  $\Delta H_f(\text{Os}^+)(\text{g}) = 388$  kcal./mole (calculated from the ionization potentials<sup>17</sup> and the heats of sublimation<sup>18,19</sup>] considering the large amount of fragmentation accompanying the formation of the metal ion. From the results of various workers, as given in Table III, it is possible to estimate that the ionization potentials of  $\text{OsO}$ ,  $\text{OsO}_2$ , and  $\text{PdO}_2$  are 9.7, 11.2, and 10.0 e.v., respectively.

It is anticipated that further work on the transition metal oxides will reveal characteristic processes in the fragmentation pattern of these compounds and will provide additional thermochemical data for the ions produced upon electron impact.

*Acknowledgments.* The authors wish to express their appreciation to Drs. John H. Norman and H. Gene Staley for communicating to us some of their experimental findings in advance of publication and for their permission to quote these results.

(26) L. O. Brockway, *Rev. Mod. Phys.*, **8**, 231 (1936).

(27) N. V. Sidgwick, "The Chemical Elements and Their Compounds," Vol. 2, Oxford at the Clarendon Press, London, 1950, p. 1504.

# The Elimination of HF from "Hot" Fluorinated Ethanes. An Estimation of the Activation Energies and Rate Parameters<sup>1</sup>

by Sidney W. Benson and Gilbert Haugen

*Department of Thermochemistry and Chemical Kinetics, Stanford Research Institute, Menlo Park, California  
(Received June 4, 1965)*

The classical Rice-Ramsperger-Kassel theory of unimolecular reactions is shown to give a quantitative description of the decomposition of a "hot" molecule of  $\text{CH}_2\text{FCH}_2\text{F}^*$ . The analysis also makes possible an estimate of the activation energy for the elimination of HF from this molecule within narrow limits:  $\text{CH}_2\text{FCH}_2\text{F} \rightarrow \text{CH}_2 = \text{CFH} + \text{HF}$ ;  $E_{\text{act}} = 62 \pm 3$  kcal./mole;  $\Delta E^\circ_{298^\circ\text{K.}} = 8$  kcal./mole. From the theory one predicts the observed reductions in the rate of the elimination reactions for the series of "hot" molecules  $\text{C}_2\text{H}_{6-x}\text{F}_x$  as  $x$  is increased. A similar analysis gives a theoretical explanation of the observed pressure dependence of the rates of stabilization of the "hot" molecules  $(\text{CH}_2\text{Cl}\cdot\text{CH}_2\text{Cl})^*$ ,  $(\text{CH}_2\text{Cl}\cdot\text{CHCl}_2)^*$ , and  $(\text{CHCl}_2\cdot\text{CHCl}_2)^*$ . A quantum modification of the classical Rice-Ramsperger-Kassel theory was found necessary when the magnitude of the unfixed internal energy approaches the size of a quantum of vibrational energy. This approximation of the classical theory predicted the correct rate of elimination of a Cl atom from the hot radical  $(\dot{\text{C}}\text{HCl}\cdot\text{CHCl}_2)^*$  which at the transition state had only 2 kcal./mole of unfixed energy. In these calculations the carbon-carbon bond energy in ethane was assumed to be invariant upon the replacement of hydrogen by halogen atoms.

## Introduction

Termination reactions such as radical recombination or disproportionations are strongly exothermic and give rise initially to very highly excited or "hot" molecules. Although it had been recognized for a long time that such hot molecules might subsequently decompose by unimolecular processes, very few quantitative data have been available for such systems.<sup>2</sup> In contrast to this, an extensive amount of work has been done by Rabinovitch and co-workers<sup>3-5</sup> on the decomposition of "hot" radicals generated mainly by H-atom addition to olefins.

A recent paper<sup>6</sup> on the photolysis of  $\text{CH}_2\text{FCOCH}_2\text{F}$  makes available for the first time a sufficient amount of quantitative data on the decomposition of a "hot" molecule,  $\text{CH}_2\text{F}\text{--}\text{CH}_2\text{F}^*$ , thereby making possible the kinetic analysis of its behavior. In a subsequent note,<sup>7</sup> it was observed that, whereas  $\text{CH}_2\text{F}\text{--}\text{CH}_2\text{F}^*$  was found to yield  $\text{CHF}=\text{CH}_2 + \text{HF}$ ,  $\text{CHF}_2\text{CHF}_2^*$  was completely stable under the same conditions. This appeared to the authors as an anomalous behavior of the latter species.

It is the purpose of the present paper to make a quantitative examination of the behavior of  $\text{CH}_2\text{F}\text{--}\text{CH}_2\text{F}^*$  from the point of view of the classical Rice-Ramsperger-Kassel theory (RRK) of unimolecular reactions and to show that the behavior of  $\text{CHF}_2\text{--}\text{CHF}_2^*$  agrees well with the expectations of the RRK theory. In addition, the data will be shown to yield the first reasonably precise value for the activation energy of the normal pyrolysis reaction,  $\text{CH}_2\text{F}\text{--}\text{CH}_2\text{F} \rightarrow$

(1) This work was supported in part by a Grant No. AP-00353-01 from the Air Pollution Division of the U. S. Public Health Service, and partly by Stanford Research Institute sponsored research project No. 184531-123.

(2) One recent exception is the pyrolysis of ethylene oxide which has been shown to follow a "hot" molecule rearrangement: S. W. Benson, *J. Chem. Phys.*, **40**, 105 (1964).

(3) B. S. Rabinovitch and M. C. Flowers, *Quart. Rev. (London)*, **18**, 122 (1964).

(4) G. H. Kohlmaier and B. S. Rabinovitch, *J. Chem. Phys.*, **38**, 1692 (1963).

(5) G. H. Kohlmaier and B. S. Rabinovitch, *ibid.*, **38**, 1709 (1963).

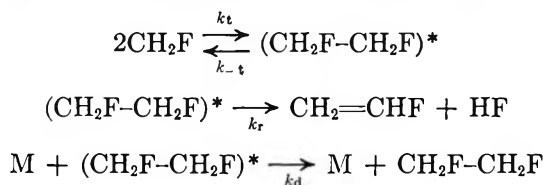
(6) G. O. Pritchard, M. Venugopalan, and T. F. Graham, *J. Phys. Chem.*, **68**, 1786 (1964).

(7) G. O. Pritchard and J. T. Bryant, *ibid.*, **69**, 1085 (1965).

$\text{CH}_2=\text{CFH} + \text{HF}$ . No quantitative kinetic data are available on the pyrolysis of alkyl fluorides.

### Mechanism

The recombination of two  $\text{CH}_2\text{F}$  radicals leads to formation of an excited ethane which can be collisionally deactivated or else decomposed to form vinyl fluoride



Applying stationary-state kinetics to this scheme we find for the rates of formation of products

$$R(\text{CH}_2\text{CHF}) = k_r(\text{CH}_2\text{FCH}_2\text{F})_{ss} \quad (1)$$

$$R(\text{CH}_2\text{FCH}_2\text{F}) = k_d(\text{CH}_2\text{FCH}_2\text{F})_{ss}(\text{M}) \quad (2)$$

For the ratio of quantum yields this gives

$$\frac{\Phi(\text{C}_2\text{H}_4\text{F}_2)}{\Phi(\text{C}_2\text{H}_3\text{F})} = \frac{R(\text{C}_2\text{H}_4\text{F}_2)}{R(\text{C}_2\text{H}_3\text{F})} = \frac{k_d(\text{M})}{k_r} \quad (3)$$

where (M) is the weighted sum of the concentration of quenching agents. In the present instance it will be simply the pressure of reacting ketone  $(\text{CH}_2\text{F})_2\text{CO}$ .

Figure 1 shows the data of PVG<sup>6</sup> plotted according to eq. 3 and, as can be seen, the data are in good accord at each temperature with the proposed mechanism. From the slopes of the different lines we can obtain the ratio of rate constants  $k_d/k_r$  as a function of temperature. In Figure 2 we note that this is, as expected, a slowly decreasing function of temperature.

### Kinetic Parameters

The RRK<sup>8</sup> theory of unimolecular decomposition relates the rate constant  $k_r$  to the internal energy content of the molecule. This is given by

$$k_r = A_r \left( 1 - \frac{E^*}{E} \right)^{n-1} \quad (4)$$

where  $E^*$  represents the critical energy necessary for decomposition,  $E$  represents the internal energy of the molecule, and  $n$  is the number of effective oscillators.  $A_r$  is the frequency factor for the unimolecular elimination. Rabinovitch and co-workers<sup>3-5</sup> have described the rate of collisional deactivation as a vibration cascade of the excess energy. This introduces too many parameters and is unnecessary for the present systems where the data can be satisfactorily reproduced by assuming deactivation to occur in a "single" collision. The rate of deactivation can be written as

$$k_d = \lambda Z \quad (5)$$

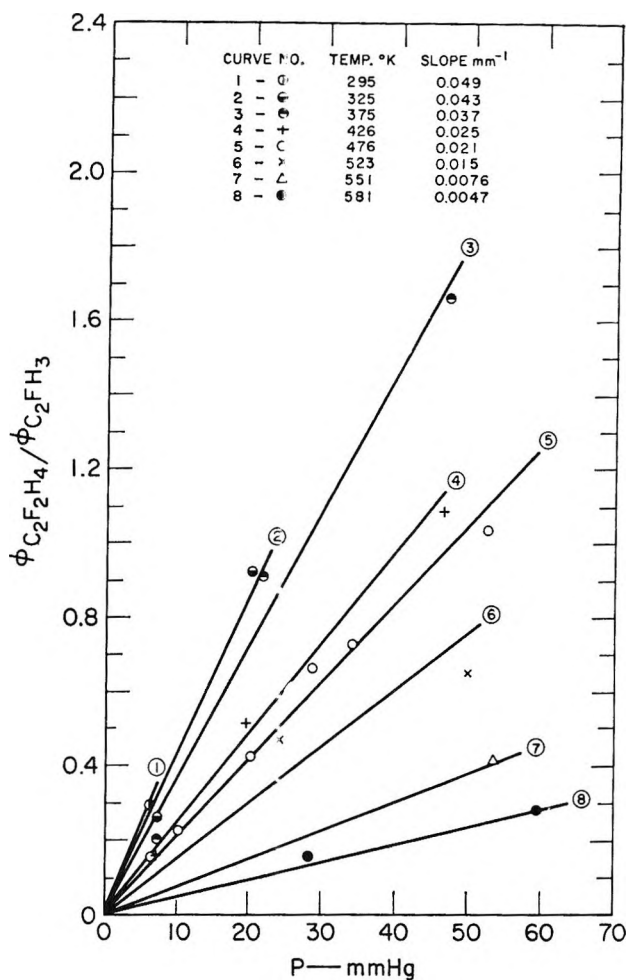


Figure 1. Pressure dependence of the quantum yield ratio  $\Phi_{\text{C}_2\text{F}_2\text{H}_4}/\Phi_{\text{C}_2\text{FH}_3}$ .  $P$  represents the initial pressure (mm.) of ketone. Runs with a total pressure of 7 mm. and temperature greater than 476°K. were omitted.

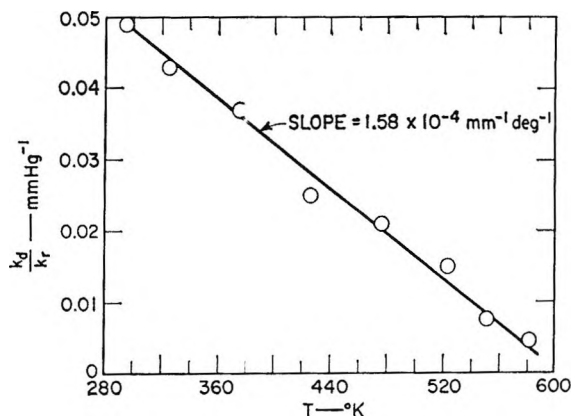


Figure 2. Temperature dependence of  $k_d/k_r$ .

(8) S. W. Benson, "The Foundations of Chemical Kinetics," McGraw-Hill Book Co., Inc., New York, N. Y., 1960, pp. 218-220.

where  $Z$  is the number of collisions per second per millimeter and  $\lambda$  represents the probability of "complete" deactivation on collision. From a cascade point of view  $1/\lambda$  measures the number of collisions required for deactivation.

Combining eq. 3, 4, and 5 we can write

$$\frac{1}{p} \frac{\Phi_{C_2H_4F_2}}{\Phi_{C_2H_3F}} = \frac{\lambda Z \left( \frac{E}{E - E^*} \right)^{n-1}}{A_r} \quad (6)$$

The temperature dependence of the ratio  $k_d/k_r$  is now contained in the separate terms  $\lambda$ ,  $Z$ , and  $E$ . There is a lack of data on the temperature coefficient of  $\lambda$  at high temperature and a disagreement between theory and experiment, at low temperature.<sup>3-5</sup> Accordingly, it is prudent to neglect the temperature dependence of the collision terms,  $\lambda Z$ . These are, in any case, expected to be very much smaller than the temperature dependence of  $E$ .

We have evaluated  $E$ , the total internal energy content of the  $(CH_2F-CH_2F)^*$  as follows. We estimate values for  $C_v^{vib}$ , the vibrational specific heat of the  $CH_2F$  radicals, over the temperature range of interest. This allows us to estimate  $E_{vib}$ , the total vibrational energy content of the two radicals, at each temperature. To this we add  $3/2RT$  for translational energy of one radical and another  $3/2RT$  of rotational energy of one radical which are converted into internal energy of the hot molecule. If we define  $\Delta C_v^{vib}$  as the difference in vibrational specific heat of the two radicals and the "hot" molecule, then we can write

$$E = E_0 + \Delta C_v^{vib}(T - 298) \quad (7)$$

where  $E_0$  is the energy change in the recombination.<sup>9</sup>

Table I gives values of  $E$  at different temperatures.

Table I: Value of  $E$  at Different Temperatures

$T$ , °K.	Thermal energy, <sup>a</sup> $\Delta C_v^{vib}(T - 298)$ , kcal./mole	$E$ , kcal./mole
298	0	85.4 <sup>b</sup>
325	0.5	85.9
375	1.4	86.8
426	2.6	88.0
476	3.9	89.3
523	5.4	90.8
551	6.9	92.3
581	8.1	93.5

<sup>a</sup> The change in the internal energy with temperature was calculated from the relation,  $\Delta C_v^{vib}(T - 298) = 3R(T - 298) + 2[C_v^{vib}(T)]T - 2[C_v^{vib}(298)]298$ . Vibrational contribution to heat capacity of  $CH_2F$  estimated from the measured heat capacity of  $CH_3F$ . <sup>b</sup> See ref. 9.

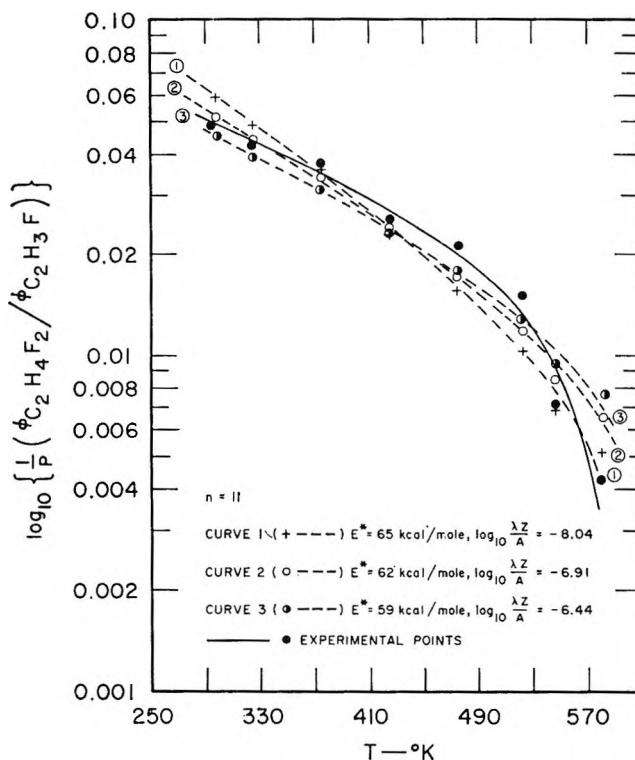


Figure 3a. Comparison of the theoretical and observed temperature dependence for  $n$  equal to 11.

In Figure 3 the theoretical curves computed from eq. 6 and 7 are compared with the experimental curve represented in Figure 2. The use of a logarithmic plot simplifies the curve fitting. The term,  $\log \lambda Z/A$ , shifts the curve vertically by a constant amount and the parameter  $n$  changes the slope of the curves. An inspection of Figure 3b demonstrates that the theoretical curve approaches the experimental curves at low temperature when  $E^*$  is equal to 59 kcal./mole and at high temperature when  $E^*$  is equal to 65 kcal./mole. Curve 2 ( $E^* = 62$  kcal./mole) in Figure 3 indicates that theoretical fit of the experimental data improves with low temperature and smaller value for  $n$  or high temperature and larger value for  $n$ . The fact that this analysis does not completely match the experimental data is anticipated since the influence of temperature on the number of effective oscillators and the efficiency of collisional deactivation has been ignored.

The variation of number of effective oscillators,  $n$ , with temperature is suggested by Figure 3. A collection of harmonic oscillators would be expected to behave in this manner. It would not be fair to include

(9)  $E_0 = DH^{\circ}(CH_3-CH_3) - \Delta nRT = 85.4$  kcal./mole. See S. W. Benson, *J. Chem. Educ.*, in press.

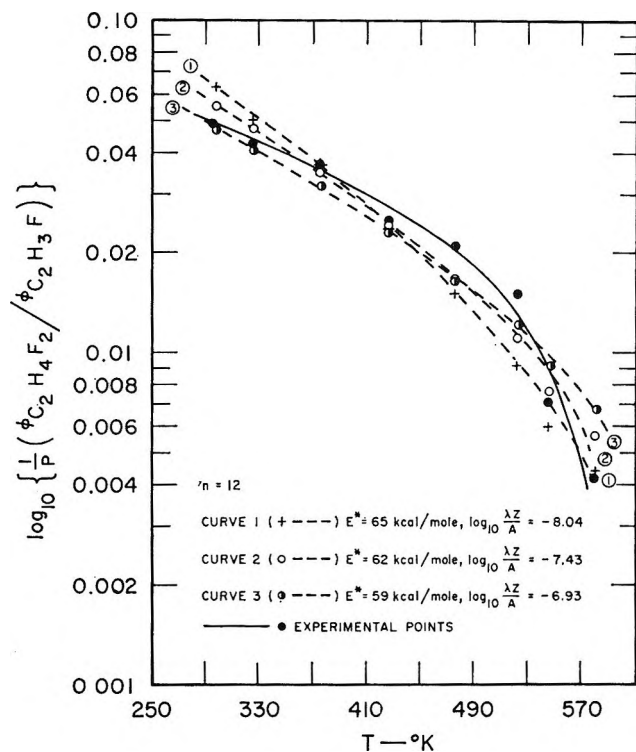


Figure 3b. Comparison of the theoretical and observed temperature dependence for  $n$  equal to 12.

this temperature effect without considering the temperature dependence of  $\lambda Z/A_r$ . However, the accuracy of this analysis does not seem to warrant the additional complications.

The most reasonable value for the number of effective oscillators,  $n$ , for analysis of this type is about two-thirds of the total number of oscillators; that is,  $n$  is equal to 12.<sup>10</sup> Once  $n$  has been chosen, it is possible to determine a probable value of  $E^*$  and  $\lambda Z/A_r$  by obtaining the best fit of eq. 7 to the experimental data. Figure 3b demonstrates an adequate fit with  $E^*$  equal to  $62 \pm 3$  kcal./mole and  $\log \lambda Z/A$  equal to  $-7.43 \pm 0.56$ . A reasonable value for the frequency factor,  $A_r$ , of the unimolecular elimination would be  $10^{13.5}$ . Combining this value with that for the collision frequency,  $Z = 10^6$ .<sup>96</sup>  $\text{mm.}^{-1}$ , allows the magnitude of the collision efficiency  $\lambda$  to be estimated. This is shown in Table II.

In this system the amount of energy that must be removed by collisional deactivation to stabilize the "hot" molecule is much larger than the corresponding quantity in the systems studied by Rabinovitch and Kohlmaier.<sup>3-5</sup> We would expect a much smaller collision efficiency than those suggested by Rabinovitch's investigations. Accordingly, a value of  $\lambda$  between 0.10 and 0.20 seems justifiable. Our original choice of

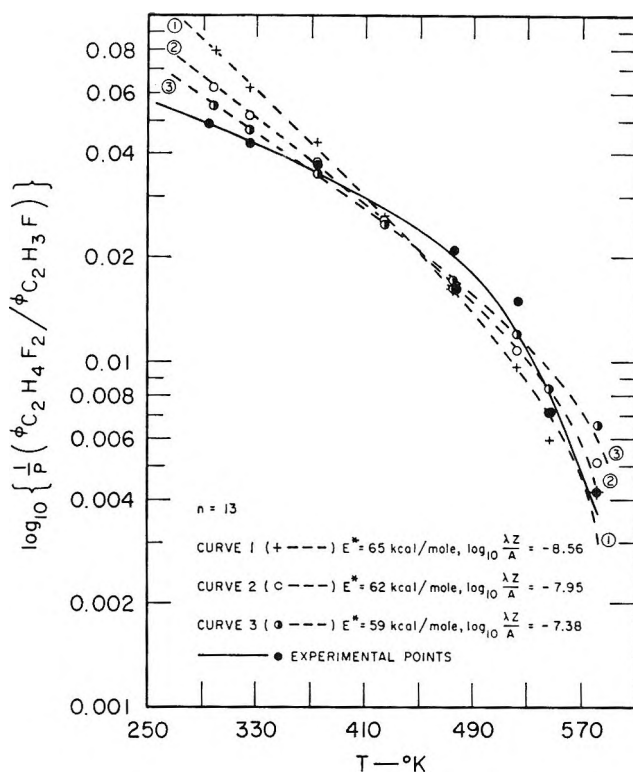


Figure 3c. Comparison of the theoretical and observed temperature dependence for  $n$  equal to 13.

Table II: Variation of  $\lambda$  with Different Choices of  $n$  and  $E^*$

$E^*$	$n$		
	11	12	13
65	0.12	0.032	0.0096
62	0.43	0.13	0.039
59	1.3	0.41	0.14

$E^* = 62$  kcal./mole and  $n = 12$  is consistent with this restriction on value of  $\lambda$ .

#### Calculation of $E^*$

An activation energy of  $54 \pm 3$  kcal./mole has been calculated<sup>11</sup> for the addition reaction,  $\text{HF} + \text{C}_2\text{H}_4 \rightarrow \text{C}_2\text{H}_5\text{F}$ . These theoretical calculations yield a similar value for the activation energy of the reaction  $\text{CHF}=\text{CH}_2 + \text{HF} \rightarrow \text{C}_2\text{F}_2\text{H}_4$ . The reactions  $\text{HCl} + \text{CHCl}=\text{CH}_2 \rightarrow \text{CH}_2\text{Cl}-\text{CH}_2\text{Cl}$  ( $\Delta H^\circ_{298^\circ\text{K.}} = -15.2$  kcal./mole) and  $\text{HCl} + \text{C}_2\text{H}_4 \rightarrow \text{C}_2\text{ClH}_5$  ( $\Delta H^\circ_{298^\circ\text{K.}} = -15.5$  kcal./

(10)  $n$  is a parameter which represents the number of "effective" oscillators. This ambiguity in the concept of  $n$  springs from the use of the classical viewpoint. It has been shown (G. M. Wieder and R. A. Marcus, *J. Chem. Phys.*, **37**, 1835 (1962)) that all vibrational modes participate in energy exchange in the active molecule when the quantum treatment is employed.

(11) S. W. Benson and G. R. Haugen, to be published.

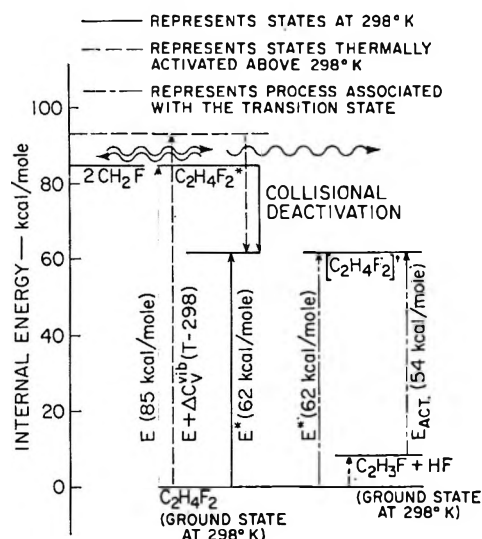


Figure 4. Relationship between  $E^*$ , activation energies, and internal energies.

mole) liberate nearly the same heat. Thus, it is expected that the heat liberated by the reactions  $\text{HF} + \text{C}_2\text{FH}_3 \rightarrow \text{C}_2\text{F}_2\text{H}_4$  and  $\text{HF} + \text{C}_2\text{H}_4 \rightarrow \text{C}_2\text{FH}_5$ , ( $\Delta E^\circ_{298^\circ\text{K}} = -8 \text{ kcal./mole}^8$ ) are the same.<sup>12</sup> This then gives for the activation energy of  $\text{C}_2\text{F}_2\text{H}_4 \rightarrow \text{C}_2\text{FH}_3 + \text{HF}$ ; the value of  $E = 62 \pm 3 \text{ kcal./mole}$ . This is in excellent agreement with the value suggested for  $E^*$  in this paper. The relationship between the two methods for estimating  $E^*$  is illustrated in Figure 4; consequently, the theoretical activation<sup>11</sup> energy for the process  $\text{C}_2\text{H}_5\text{F} \rightarrow \text{C}_2\text{H}_4 + \text{HF}$  is confirmed. This value is a reasonable extension of the observed halogen series, Table III.

Table III: Activation Energies for the Elimination of  $\text{HX}$  from  $\text{C}_2\text{H}_5\text{X}^a$

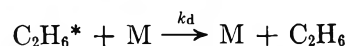
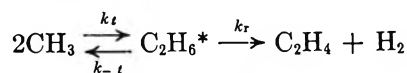
$\text{C}_2\text{H}_5\text{X}$	$E_{\text{act}}$ (kcal./mole) at 298°K.	Difference between consecutive activation energies
$\text{C}_2\text{H}_5\text{I}$	49.2	4.7
$\text{C}_2\text{H}_5\text{Br}$	53.9	3.2
$\text{C}_2\text{H}_5\text{Cl}$	57.1	4.9
$\text{C}_2\text{H}_5\text{F}$	62	

<sup>a</sup> S. W. Benson and A. N. Bose, *J. Chem. Phys.*, **39**, 3463 (1963).

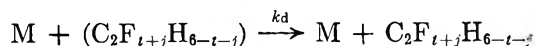
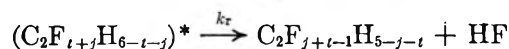
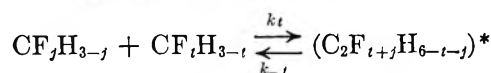
### Kinetic Parameters for the Series $(\text{CF}_j\text{H}_{3-j}\cdot\text{CF}_t\text{H}_{3-t})^*$

The mechanism for the kinetic behavior of the chemically activated species in the series  $(\text{CF}_j\text{H}_{3-j}\cdot\text{CF}_t\text{H}_{3-t})^*$  can be separated into two cases.<sup>13</sup>

Case I:  $j = 0$  and  $t = 0$



Case II:  $1 \leq j \leq 2$  and  $1 \leq t \leq 2$



The analysis presented in this article can be applied to the comparison of the rates of both elimination,  $k_r$ , and fragmentation,  $k_{-t}$ , to the rate of collisional deactivation,  $k_d$ . These comparisons are represented in the equations

$$\left(\frac{k_d}{k_r}\right)_{298^\circ\text{K.}} = 10^{-7.54} \left(\frac{85.4}{85.4 - E^*}\right)^{n-1} \quad (8)$$

$$\left(\frac{k_d}{k_{-t}}\right)_{298^\circ\text{K.}} = 10^{-11.0} \left(\frac{85.4}{nR/298}\right)^{n-1} \quad (9)$$

In the case of the fragmentation, the activation energy is zero and the frequency factor is generally about  $10^{17} \text{ sec.}^{-1}$ .<sup>14</sup> The ratios of the rates  $k_d/k_{-t}$  and  $k_d/k_r$  are dependent only on the number of effective oscillators,  $n$ , and the activation energies for the eliminations,  $E^*$ . We have calculated values of  $E^*$  for both cases I and II.<sup>11</sup>  $E^*$  is expected to be nearly the same for the similar molecules of case II;  $E^*$  for cases I and II are 73.4 and 61.8, respectively. The replacement of a hydrogen atom by a heavier fluorine atom increases the number of effective oscillators by 1 or 2. The probable value of  $n$  for the fluorinated ethane series increases as the number of fluorine atoms increases (see Table IV).

The trends in the ratio of rates  $k_d/k_{-t}$  and  $k_d/k_r$  for the series of fluorinated ethanes are depicted in Table V. The influence of the number of effective oscillators on the rates  $k_{-t}$  and  $k_r$  is apparent. The fragmentation rate is enormously reduced as the ineffective C-H oscillators are replaced by more effective C-F oscillators (*i.e.*, lower frequency). A similar reduction is observed for the rate of elimination of HF

(12) This is also the result anticipated from the law of additivity of group properties (S. W. Benson and J. H. Buss, *J. Chem. Phys.*, **29**, 546 (1958)).

(13) The case  $\text{CF}_3\cdot\text{CF}_3$  is not considered here because the elimination of  $\text{F}_2$  from  $\text{C}_2\text{F}_6$  is prohibited by the enormous activation energy for this process (239 kcal./mole). See ref. 9 and 11.

(14) S. W. Benson, "Advances in Photochemistry," Vol. 2, Interscience Publishers, Inc., New York, N. Y., 1964, Chapter 1.



**Table IV:** Mean Number of Effective Oscillators in Fluorinated Ethanes

Molecule	$\bar{n}$
C <sub>2</sub> H <sub>6</sub>	9.0
C <sub>2</sub> H <sub>5</sub> F	10.5
C <sub>2</sub> H <sub>4</sub> F <sub>2</sub>	12.0
C <sub>2</sub> H <sub>3</sub> F <sub>3</sub>	13.5
C <sub>2</sub> H <sub>2</sub> F <sub>4</sub>	15.0
C <sub>2</sub> HF <sub>5</sub>	16.5
C <sub>2</sub> F <sub>6</sub>	18.0

**Table V:** Ratios of  $k_d/k_{-t}$  and  $k_d/k_r$  Calculated from Eq. 8 and 9 at 298°K.

Molecule	$k_d/k_{-t}$ , mm. <sup>-1</sup>	$k_d/k_r$ , mm. <sup>-1</sup>	$k_r/k_{-t}$
C <sub>2</sub> H <sub>6</sub>	(1.00) <sup>a</sup>	$1.9 \times 10^{-1}$	5.3
C <sub>2</sub> H <sub>5</sub> F	$1.5 \times 10^1$	$5.9 \times 10^{-3}$	$2.5 \times 10^3$
C <sub>2</sub> H <sub>4</sub> F <sub>2</sub>	$1.8 \times 10^2$	$4.1 \times 10^{-2}$	$4.4 \times 10^3$
C <sub>2</sub> H <sub>3</sub> F <sub>3</sub>	$1.8 \times 10^3$	$2.9 \times 10^{-1}$	$6.2 \times 10^3$
C <sub>2</sub> H <sub>2</sub> F <sub>4</sub>	$1.4 \times 10^4$	1.8	$7.8 \times 10^3$
C <sub>2</sub> HF <sub>5</sub>	$8.9 \times 10^4$	13	$6.8 \times 10^3$
C <sub>2</sub> F <sub>6</sub>	$5.6 \times 10^5$		

<sup>a</sup> Equation 9 does not represent a satisfactory method for estimating the relative rates,  $k_d/k_{-t}$ . This inadequacy is a consequence of the discrete distributions of the unfixed energy among the quantum states. This manifests itself when the unfixed energy approaches the size of a quanta. An exact count of the number of configurations of the distribution of the quanta among the active states requires the complete description of the quantum states. To indicate the influence of the number of active oscillators on the ratio  $k_d/k_{-t}$ , without doing a detailed count, we have computed the ratio  $k_d/k_{-t}$  relative to the molecule C<sub>2</sub>H<sub>6</sub>.

from the fluorinated ethanes with an increase in the number of effective oscillators. The rate of elimination of H<sub>2</sub> from chemically activated ethane is much smaller than that expected from just a consideration of the number of active oscillators. This is attributed to the larger  $E^*$  for the elimination of H<sub>2</sub>. This elimination is also deterred by the fast fragmentation of the "hot" ethane molecules. The reported kinetic behavior<sup>6,7</sup> of the series CH<sub>2</sub>FCH<sub>2</sub>F, CF<sub>3</sub>CH<sub>3</sub>, CHF<sub>2</sub>CHF<sub>2</sub>, and CF<sub>3</sub>CHF<sub>2</sub> is simply explainable in terms of the change in the number of effective oscillators along this series. Table V demonstrates that the relative rate of elimination and fragmentation for this series is independent of the number of effective oscillators. In view of this, the appearance of elimination products depends on the relative rates of elimination and deactivation,  $k_d/k_r$ . This quantity is extremely sensitive to the number of fluorine atoms in the "hot" molecule. A comparison of the ratios  $k_d/k_r$  at 298°K. for C<sub>2</sub>H<sub>4</sub>F<sub>2</sub>

and C<sub>2</sub>H<sub>3</sub>F<sub>3</sub> indicates that the rate of elimination of HF from C<sub>2</sub>H<sub>3</sub>F<sub>3</sub> is approximately 0.14 of the rate of elimination from C<sub>2</sub>H<sub>4</sub>F<sub>2</sub>. This is seemingly not in accord with the findings of Alcock and Whittle.<sup>15</sup> Their studies indicated a ratio of  $R(\text{CF}_3\text{CH}_3)/R(\text{CF}_2=\text{CH}_2)$  equal to 1.0 for the "hot" molecule, CF<sub>3</sub>-CH<sub>3</sub><sup>\*</sup>, over the temperature range 353–488°K. This ratio is smaller than the comparable ratio for the "hot" molecule, CFH<sub>2</sub>CFH<sub>2</sub><sup>\*</sup>. The analysis of Alcock and Whittle's system is complicated by the presence of two quenching agents, and because of this a weighted sum of the quenching agents must be used in eq. 3

$$\frac{R(\text{CH}_3\text{CF}_3)}{R(\text{CH}_2=\text{CF}_2)} = \{k_d'(\text{CF}_3\text{COCF}_3) + k_d''(\text{CH}_3\text{I})\}/k_r$$

We would have expected a temperature dependence of the ratios  $k_d'/k_r$  and  $k_d''/k_r$  (see Figure 2); this was not observed. This lack of a temperature variation suggests that the ratio  $R(\text{CH}_3\text{CF}_3)/R(\text{CH}_3=\text{CF}_2)$  is not simply related to the intrinsic ratio,  $k_d/k_r$ . It would be appropriate at this point to emphasize caution in extrapolating the ratios  $k_d/k_r$  in Table V to other temperatures. In accordance with eq. 6 and 7 the ratio  $k_d/k_r$  will change with a variation in temperature. The extent of this change will depend on the quantities  $n$  and  $\Delta C_v^{\text{vib}}$ . On the basis of these considerations we can state that the "hot" molecules, CHF<sub>2</sub>CHF<sub>2</sub><sup>\*</sup> and CF<sub>3</sub>-CF<sub>2</sub>H<sup>\*</sup>, will be completely stable under the conditions that cause the HF elimination from the "hot" molecule, CH<sub>2</sub>FCH<sub>2</sub>F<sup>\*</sup>. This has been experimentally verified for the molecule CHF<sub>2</sub>CHF<sub>2</sub>.<sup>7</sup> The current investigation (see ref. 7) of the reactions of the "hot" molecule, CF<sub>3</sub>CF<sub>2</sub>H<sup>\*</sup>, have failed to detect C<sub>2</sub>F<sub>4</sub>. These experiments were not primarily designed to study the elimination reaction, and subsequently experimental justification of the stability of this "hot" molecule is lacking.

A comparison of the predicted values of the ratios  $k_d/k_r$  at 298°K. for the "hot" molecules, C<sub>2</sub>H<sub>5</sub>F<sup>\*</sup> and CH<sub>2</sub>FCH<sub>2</sub>F<sup>\*</sup>, indicates that the rate of elimination of HF from C<sub>2</sub>H<sub>4</sub>F<sub>2</sub><sup>\*</sup> is approximately 0.14 of the rate of elimination from C<sub>2</sub>H<sub>5</sub>F<sup>\*</sup>. The kinetic parameters for the series of chlorinated ethanes are listed in Tables III and VI. Introducing these values into eq. 4 allows the comparison of the rates of the chlorinated and fluorinated ethane series

$$\frac{k_r(\text{C}_2\text{H}_5\text{F})}{k_r(\text{C}_2\text{H}_5\text{Cl})} = \frac{10^{13.5} \left(1 - \frac{62}{85.4}\right)^{(0.15-1)}}{10^{12.7} \left(1 - \frac{57}{85.4}\right)^{(10.5-1)}} = 1.0$$

(15) W. G. Alcock and E. Whittle, *Trans. Faraday Soc.*, **61**, 244 (1965).

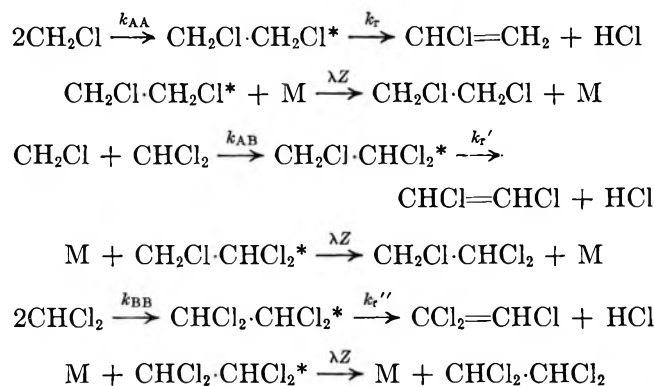
and

$$\frac{k_r(\text{CH}_2\text{FCH}_2\text{F})}{k_r(\text{CH}_2\text{ClCH}_2\text{Cl})} = \frac{10^{13.5} \left(1 - \frac{62}{85.4}\right)^{(12-1)}}{10^{12.7} \left(1 - \frac{59}{85.4}\right)^{(12-1)}} = 1.7$$

Thus, the rate of elimination of HCl from  $\text{CH}_2\text{ClCH}_2\text{Cl}^*$  is approximately 0.082 of the rate of elimination from  $\text{CH}_3\text{CH}_2\text{Cl}^*$ . This is in agreement with the estimates recently reported<sup>16</sup> for this ratio,  $k_r(\text{CH}_2\text{ClCH}_2\text{Cl}^*)/k_r(\text{C}_2\text{H}_5\text{Cl}^*) \approx 0.095$ .

### Kinetic Parameters of "Hot" Chlorinated Ethanes

Wijnen<sup>17</sup> has studied the rate of formation of chlorinated ethanes produced by the recombination of chlorinated methyl radicals. His investigation demonstrated a pressure dependence of the normally expected constant ratio of rates of formation of ethanes:  $R_{\text{CH}_2\text{ClCH}_2\text{Cl}}/[R_{\text{CH}_2\text{ClCH}_2\text{Cl}}]^{1/2} [R_{\text{CHCl}_2\text{CHCl}_2}]^{1/2}$ . The mechanism for the formation and deactivation of the "hot" molecules is



The steady-state ratio  $R_{\text{CH}_2\text{ClCH}_2\text{Cl}}/[R_{\text{CH}_2\text{ClCH}_2\text{Cl}}]^{1/2} [R_{\text{CHCl}_2\text{CHCl}_2}]^{1/2}$  can be represented as a function of the total pressure and these primary rate constants

$$\frac{R_{\text{CH}_2\text{ClCH}_2\text{Cl}}}{[R_{\text{CH}_2\text{ClCH}_2\text{Cl}}]^{1/2} [R_{\text{CHCl}_2\text{CHCl}_2}]^{1/2}} = \frac{k_{\text{AE}}}{k_{\text{AA}}^{1/2} k_{\text{BB}}^{1/2}} \frac{\left(\frac{k_r}{\lambda Z} + p\right)^{1/2} \left(\frac{k_r''}{\lambda Z} + p\right)^{1/2}}{\left(\frac{k_r'}{\lambda Z} + p\right)} \quad (10)$$

Substitution of eq. 4 into this expression reduces the equation to the form (see Table VI)

$$\frac{R_{\text{CH}_2\text{ClCH}_2\text{Cl}}}{[R_{\text{CH}_2\text{ClCH}_2\text{Cl}}]^{1/2} [R_{\text{CHCl}_2\text{CHCl}_2}]^{1/2}} = \frac{k_{\text{AB}}}{k_{\text{AA}}^{1/2} k_{\text{BB}}^{1/2}} \frac{(4.08 + p)^{1/2} (1.00 + p)^{1/2}}{(14.8 + p)} \quad (11)$$

Table VI: The Estimated Values or Kinetic Parameters in Eq. 10

Molecule	Log $A_r$	$\lambda$	Log $Z$	$E^*$ , kcal./ mole	$E$ , kcal./ mole	$n$
$\text{CH}_2\text{Cl}\cdot\text{CH}_2\text{Cl}$	12.7	0.3	7.0	59	85.4	12
$\text{CH}_2\text{Cl}\cdot\text{CHCl}_2$	12.7	0.3	7.0	53	85.4	13
$\text{CHCl}_2\cdot\text{CHCl}_2$	12.7	0.3	7.0	57	85.4	14

The examination of the rate constants for the elimination of HCl from a series of chlorinated ethanes allows a reasonably reliable evaluation of the parameters  $A_r$  and  $E^*$ .<sup>18</sup>

The restrictions on the range of values of  $\lambda$  and  $n$  are fully discussed in the preceding example. The reasonable values  $\lambda$  equal to 0.3 and  $n$  equal to 12, 13, and 14 for the molecules  $\text{C}_2\text{H}_4\text{Cl}_2$ ,  $\text{C}_2\text{H}_3\text{Cl}_3$ , and  $\text{C}_2\text{H}_2\text{Cl}_4$ , respectively, allow the demonstration of the pressure dependence of this system. Using reported results for total pressure of 20 and 4 mm., the rate ratio  $k_{\text{AB}}/(k_{\text{AA}})^{1/2}(k_{\text{BB}})^{1/2}$  can be calculated:  $p = 20$  mm.,  $k_{\text{AB}}/(k_{\text{AA}})^{1/2}(k_{\text{BB}})^{1/2} = 1.76$ ; and  $p = 4$  mm.,  $k_{\text{AB}}/(k_{\text{AA}})^{1/2}(k_{\text{BB}})^{1/2} = 1.77$ . This number is very near the statistical value of 2 expected for the ratio.

### Decomposition of "Hot" $\text{CHClCHCl}_2^*$

Knox<sup>19</sup> has determined the rate of decomposition of chemically activated  $\text{CHClCHCl}_2^*$  radicals formed in the Cl-catalyzed isomerization of *cis*-to *trans*-dichloroethylene,  $10^{9.4}$  sec.<sup>-1</sup>. To simplify the analysis, we have assumed that  $E^*$  is equal to the internal energy,  $E_0$  (zero activation energy for the decomposition), where the energy,  $E_0$ , represents the change in energy content for the reaction  $\text{CHClCHCl}_2 \rightarrow \text{CHCl}=\text{CHCl} + \text{Cl}$  at 0°K. ( $E_0$  is about 20 kcal./mole).<sup>20</sup>

The internal thermal energy in this radical under the experimental conditions reported by Knox was about 2.0 kcal./mole. This is the magnitude of the vibrational quanta in the radical. Consequently, the classical eq. 4 is not the appropriate formula to use for calculating the rate of this decomposition (see footnote in

(16) D. W. Setser, R. Littrell, and J. C. Hassler, *J. Am. Chem. Soc.*, **87**, 2062 (1965).

(17) Presented by M. H. J. Wijnen at Sixth Informal Photochemist Conference held at the Department of Chemistry, University of California at Davis, Davis, Calif.

(18) S. W. Benson, "The Foundations on Chemical Kinetics," McGraw-Hill Book Co., Inc., New York, N. Y., 1960, p. 258, ref. 9.

(19) J. Knox, Department of Chemistry, University of Edinburgh, private communication.

(20) Energy of this reaction was estimated from bond energies in the series  $\text{CH}_2=\text{CH}-\text{H}$ ,  $\text{CH}_2=\text{CH}-\text{Cl}$ ,  $\text{CH}_3\text{CH}_2-\text{H}$ ,  $\text{CH}_3\text{CH}_2-\text{Cl}$ , and  $\text{CH}_3\text{CH}_2-\text{H}$ ; see ref. 9.

Table V). A precise counting of the number of ways of distributing the energy among the quantum states will modify eq. 4 in the following manner<sup>8,21</sup>

$$k = A \left\{ \left( \frac{\prod_{i=1}^q \left( \frac{E - E_0}{h\nu_i} \right)}{q!} \right) \left( \frac{(s-1)! \prod_{i=1}^s h\nu_i}{E^{s-1}} \right) \right\} \quad (12)$$

where  $q$  is the number of vibrational states that can be excited by the energy  $E - E_0$  and likewise  $s$  is the number excited by energy  $E$ ;  $h\nu_i$  is the energy of the  $i$  vibrational state,  $E$  is the total internal energy, and  $E_0$  is the internal energy at 0°K. The quantity  $((E - E_0)/h\nu_i)$  depicts the maximum number of quanta in the vibrational state  $i$  that can be excited by energy  $E - E_0$ . The fundamental frequencies of vibrations of the molecule  $\text{CH}_2\text{ClCHCl}_2$ <sup>22</sup> were assumed to represent those of the radical,  $\dot{\text{C}}\text{HClCHCl}_2$ , with the exception that one C-H stretching and two C-H bending frequencies should be omitted in view of the differences in numbers of H atoms (see Table VII).

**Table VII:** Estimated Fundamental Frequencies of Vibrations of  $\text{CHClCHCl}_2$

Cm. <sup>-1</sup>	Cm. <sup>-1</sup>	Cm. <sup>-1</sup>
3014	1161	676.5
2998	1050	422
1437	936.5	390
1306	792.5	332
1260	742	255

Counting the number of these quantum states that can be excited by energies  $E$  (22 kcal./mole) and  $E - E_0$  (2 kcal./mole) establishes the number of effective oscillators as 15 and 6, respectively. Combining eq. 12 with these kinetic parameters ( $E = 22$  kcal./mole,  $E - E_0 = 2$  kcal./mole,  $q = 6$ ,  $s = 15$ , and  $A = 10^{13.5}$ ) gives a mean predicted rate of decomposition for this radical of  $10^{9.2}$  sec.<sup>-1</sup>. Using eq. 9 with an effective number of oscillators,  $n$ , of 10 predicts a rate of  $10^{7.8}$  sec.<sup>-1</sup>, an obvious example of the error that can

appear when the unfixed energy approaches the magnitude of the vibrational quanta. Equation 12 predicts a rate of  $1.6 \times 10^9$  sec.<sup>-1</sup>, in excellent agreement with Knox's experimental value  $2.5 \times 10^9$  sec.<sup>-1</sup>.

Giles and Whittle<sup>23</sup> have studied the photolysis of mixtures of acetone and hexafluoroacetone. Their investigation established that the behavior of the "hot" molecule  $\text{CH}_3\text{CF}_3^*$  is similar to that of the molecule  $\text{CH}_2\text{FCH}_2\text{F}^*$ . The ratio  $k_d/k_r$  at 423°K. was reported for the following quenchers: acetone, hexafluoroacetone, nitrogen, and perfluorocyclohexane. The observed temperature coefficient for this system allows the adjustment of these ratios to 298°K. These adjusted values are: perfluorocyclohexane,  $2.1 \times 10^{-1}$  (mm.<sup>-1</sup>); hexafluoroacetone,  $1.4 \times 10^{-1}$  (mm.<sup>-1</sup>); acetone,  $6.5 \times 10^{-2}$  (mm.<sup>-1</sup>); nitrogen,  $1.1 \times 10^{-2}$  (mm.<sup>-1</sup>). This demonstrates the variation of the quenching efficiency with molecular structure. In particular, the relative values of  $\lambda$  for this series of quenchers<sup>23</sup> are: perfluorocyclohexane, 1.0; hexafluoroacetone, 0.75; acetone, 0.39; nitrogen, 0.075. The value of  $k_d/k_r$  observed for "hot"  $\text{CH}_3\text{CF}_3^*$ , where the quencher is  $\text{CF}_3\text{COCF}_3$ , is a factor of 0.5 smaller than the predicted value (see Table V). The calculation of the ratio  $k_d/k_r$  is sensitive to the value of  $n$ ; if this parameter for the molecule  $\text{CH}_3\text{CF}_3$  is reduced to 13.0, then the calculated value of the ratio  $k_d/k_r$  decreases to  $1.5 \times 10^{-1}$  mm.<sup>-1</sup>. Consequently, upon consideration of the allowable margin of variation in the kinetics parameters  $n$  and  $\lambda$ , the concord between the theoretical model and the actual system is quite reasonable.

*Acknowledgment.* We are indebted to Dr. G. O. Pritchard for his constructive comments on the correlation of the material presented in this paper with the experimental observations.

(21) R. A. Marcus and O. K. Rice, *J. Phys. Colloid Chem.*, **55**, 894 (1951).

(22) R. H. Harrison and K. A. Kobe, *J. Chem. Phys.*, **26**, 1411 (1957).

(23) R. D. Giles and E. Whittle, *Trans. Faraday Soc.*, **61**, 1425 (1965)

## The Activity Coefficients of Solutes in Acid Solutions. II. The Relative

### Activity Coefficients of the Chloride and Silver Ions in Aqueous Sulfuric Acid

by Richard H. Boyd and Chin-hsien Wang

Department of Chemistry, Utah State University, Logan, Utah 84321 (Received June 4, 1965)

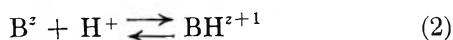
The solubility of silver chloride has been measured as a function of acid concentration in aqueous sulfuric acid solutions. A polarographic technique using a mercury-mercurous sulfate reference electrode was employed. The solubility of silver 1,1,2,3,3-pentacyanopropenide has also been measured spectroscopically as a function of acid concentration. From these data and previously determined data, the activity coefficients of the chloride and silver ions relative to the tetraethylammonium ion have been calculated. The abrupt increase in solubility of silver chloride at high sulfuric acid concentration has been used to obtain an estimate of the  $pK$  of  $HCl$  ( $\sim -8.4$ ).

#### Introduction

The effect of solvent acidity on acid dissociation equilibria has long been a subject of considerable interest. Concepts such as the acidity function have been developed<sup>1</sup> in order to systematize the behavior of these equilibria.

Knowledge of the acidity dependence of the activity coefficients appearing in the acidity function

$$H_2 = -\log a_{H^+} + \log \frac{f_{BH^{2+1}}}{f_{B^2}} \quad (1)$$



(where  $f$  is an activity coefficient and  $a_{H^+}$  the hydrogen ion activity) is essential to understanding the medium effect on such equilibria. Recently it has been possible to make activity coefficient measurements relative to a common standard ion on models of ions (and neutral species) appropriate to several acidity functions.<sup>2</sup> It is also important to determine the activity coefficient behavior of ions of more general types. The purpose of the present work is to investigate the activity coefficient behavior in aqueous sulfuric acid solutions of the chloride and silver ions. These are examples of a spherical anion and cation without specific structural features and should be illuminating in assessing the relation between solute structure and activity coefficient behavior.

The activity coefficients have been determined from

the solubilities in sulfuric acid solutions of silver chloride and silver 1,1,2,3,3-pentacyanopropenide.

#### Experimental Section

The solubility of silver chloride in sulfuric acid solutions was measured by polarographic determination of the silver ion. Cave and Hume<sup>3</sup> have described a polarographic method for silver, to which we have made certain modifications. The calomel electrode was found to result in diffusion of chloride ion into the cathode compartment. It was therefore replaced by a mercury-mercurous sulfate electrode and connected to the cathode compartment by means of a potassium nitrate agar bridge in the "H" cell. Measurements were made directly on acid solutions which had been equilibrated by mechanical shaking in stoppered flasks for at least overnight. Calibration runs with silver nitrate were made at each acid concentration. Plots of diffusion current *vs.* silver ion concentration were linear at all acid concentrations. The cathode compartment was kept free of oxygen by bubbling nitrogen through the solution for several minutes before (but not during) the measurement. The cell and equilibration flasks were wrapped in aluminum foil to protect

(1) See, for example, M. A. Paul and F. A. Long, *Chem. Rev.*, **57**, 1 (1957).

(2) R. H. Boyd, *J. Am. Chem. Soc.*, **85**, 1555 (1963), which constitutes paper I.

(3) G. C. B. Cave and D. N. Hume, *Anal. Chem.*, **24**, 588 (1952).

the solutions from light. Both were thermostated at  $25.00 \pm 0.05^\circ$  in a water bath. The polarograph was a Sargent Model XV recording polarograph.

No indication of change in the nature of the solid phase during equilibration was found when tested by the following procedure. Weighed amounts of silver chloride were equilibrated for 24 hr. in solutions of 0, 20, 40, and 60% sulfuric acid. The silver chloride was then recovered and washed with just sufficient water for transfer from the equilibration flasks. The silver chloride was then dried to constant weight (<5 hr.) under vacuum (0.1 mm.) at room temperature. Weight gains for samples from the above solutions of 0.0, 0.7, 0.7, and 0.0%, respectively, were found.

Results above 85% sulfuric acid became erratic, no doubt due to the formation of HCl which did not reach an equilibrium concentration owing to losses during the measurement under the conditions of our experiment. The results above 75% sulfuric acid could well be inaccurate for this reason. The solubility in pure water was found to be  $1.20 \times 10^{-5} M$  compared to a literature value<sup>4</sup> of  $1.32 \times 10^{-5} M$ .

Silver pentacyanopropenide was prepared by precipitation of sodium pentacyanopropenide with silver nitrate, followed by filtration and washing. The solubility was measured spectroscopically *via* the pentacyanopropenide ion by previously described techniques.<sup>2</sup> The solubility in pure water was also checked polarographically *via* the silver ion with good agreement ( $4.4 \times 10^{-4} M$  polarographically *vs.*  $4.3 \times 10^{-4} M$  spectroscopically). The solubility data and mean activity coefficients appear in Table I.

### Treatment of Data

The mean activity coefficients of silver chloride and pentacyanopropenide ( $\text{PCP}^-$ ) are related to solubility with a reference state of a dilute solution in pure water as

$$f_{\pm}(\text{Ag}^+, \text{Cl}^-) = \sqrt{f_{\text{Ag}^+} f_{\text{Cl}^-}} = \frac{C_0(\text{Ag}^+ \text{Cl}^-)}{C(\text{Ag}^+ \text{Cl}^-)} \quad (3)$$

$$f_{\pm}(\text{Ag}^+, \text{PCP}^-) = \sqrt{f_{\text{Ag}^+} f_{\text{PCP}^-}} = \frac{C_0(\text{Ag}^+ \text{PCP}^-)}{C(\text{Ag}^+ \text{PCP}^-)} \quad (4)$$

where the  $f$  terms are activity coefficients and  $C$  refers to the solubility in a given sulfuric acid solution and  $C_0$  to the solubility in pure water.<sup>5</sup>

As previously pointed out,<sup>2</sup> expressing activity coefficients relative to a standard ion greatly facilitates comparison among species. We have continued to use the tetraethylammonium ion ( $\text{TEA}^+$ ) as the standard and the following definitions

$$f_+^* \equiv f_+/f_{\text{TEA}^+} \quad (5)$$

$$f_-^* \equiv f_-/f_{\text{TEA}^-} \quad (6)$$

Under the assumption, expected to be valid for dilute solutes, that  $f_+$  and  $f_-$  in  $f_{\pm} = \sqrt{f_+ f_-}$  are independent, the relative activity coefficients were calculated from the present data and previous data<sup>2</sup> as

$$f_{\text{Ag}^+}^* \equiv f_{\text{Ag}^+}/f_{\text{TEA}^+} = \frac{f_{\pm}^2(\text{Ag}^+, \text{PCP}^-)}{f_{\pm}^2(\text{TEA}^+, \text{PCP}^-)} \quad (7)$$

and

$$f_{\text{Cl}^-}^* \equiv f_{\text{Cl}^-}/f_{\text{TEA}^-} = \frac{f_{\pm}^2(\text{Ag}^+, \text{Cl}^-) f_{\pm}^2(\text{TEA}^+, \text{PCP}^-)}{f_{\pm}^2(\text{Ag}^+, \text{PCP}^-)} \quad (8)$$

**Table I:** Solubilities<sup>a</sup> and Activity Coefficients<sup>b</sup> in Sulfuric Acid Solutions at 25°

Wt. % of $\text{H}_2\text{SO}_4$	Silver chloride		Silver pentacyano- propenide	
	Solubility	Log $f_{\pm}$	Solubility	Log $f_{\pm}$
0	$1.20 \times 10^{-5}$	0	10.0	0
2.00	$1.55 \times 10^{-5}$	-0.111	10.9	-0.042
4.00	$1.70 \times 10^{-5}$	-0.152	11.1	-0.056
6.00	$1.75 \times 10^{-5}$	-0.166	11.5	-0.060
10.00	$1.75 \times 10^{-5}$	-0.166	11.5	-0.064
15.00	$1.55 \times 10^{-5}$	-0.111	12.0	-0.077
25.0	$1.05 \times 10^{-5}$	0.058	14.0	-0.148
35.0	$0.80 \times 10^{-5}$	0.176	21.3	-0.328
45.0	$0.72 \times 10^{-5}$	0.222	32.2	-0.508
50.0	$0.70 \times 10^{-5}$	0.234	35.0	-0.552
55.0	$0.70 \times 10^{-5}$	0.234	37.8	-0.576
60.0	$0.72 \times 10^{-5}$	0.222	38.8	-0.586
65.0	$0.75 \times 10^{-5}$	0.204	39.8	-0.600
70.0	$0.80 \times 10^{-5}$	0.176	41.0	-0.610
75.0	$0.90 \times 10^{-5}$	0.125		
77.0	$1.10^c \times 10^{-5}$	0.038		
80.0	$2.15^c \times 10^{-5}$	-0.253		
85.0	$3.25^c \times 10^{-5}$	-0.453		

<sup>a</sup> Solubility of silver chloride is expressed as moles/liter; silver pentacyanopropenide, as optical density of 1 cm. of equilibrated solution without dilution at 410 m $\mu$ . Approximate molar concentrations can be calculated from  $\epsilon 2.3 \times 10^4$ . <sup>b</sup>  $f_{\pm}$  = mean ionic activity coefficient =  $\sqrt{f_+ f_-} = C_0/C$  where  $C_0$  is the concentration in pure water and  $C$  is that in acid solution. <sup>c</sup> These values could be somewhat inaccurate owing to possible loss of HCl during polarographic measurement although the true value at 80% sulfuric acid is probably not more than 20% greater than the reported value.

### Discussion

The relative activity coefficients of the silver and chloride ions are plotted in Figures 1 and 2 along with

(4) H. S. Harned and B. B. Owen, "The Physical Chemistry of Electrolytic Solutions," 3rd Ed., Reinhold Publishing Corp., New York, N. Y., 1958, p. 448.

(5) See ref. 4, p. 586.

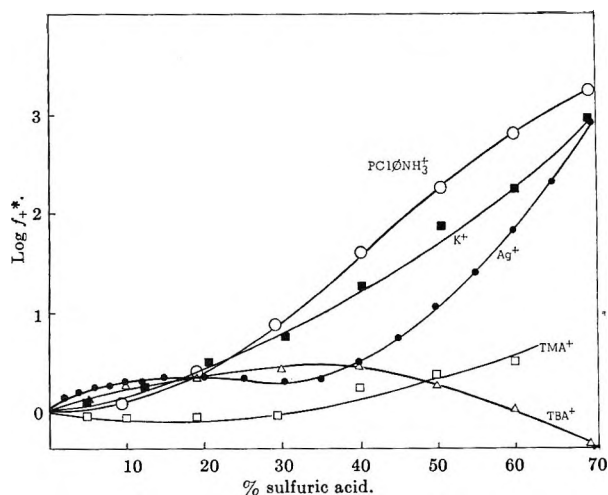


Figure 1. Relative activity coefficients of cations  $f_+^* = f_+/f_{\text{TEA}^+}$ , where  $\text{TEA}^+$  is tetraethylammonium ion, plotted against acid concentration.  $\text{TMA}^+$  and  $\text{TBA}^+$  are tetramethyl- and -butylammonium ions, respectively.

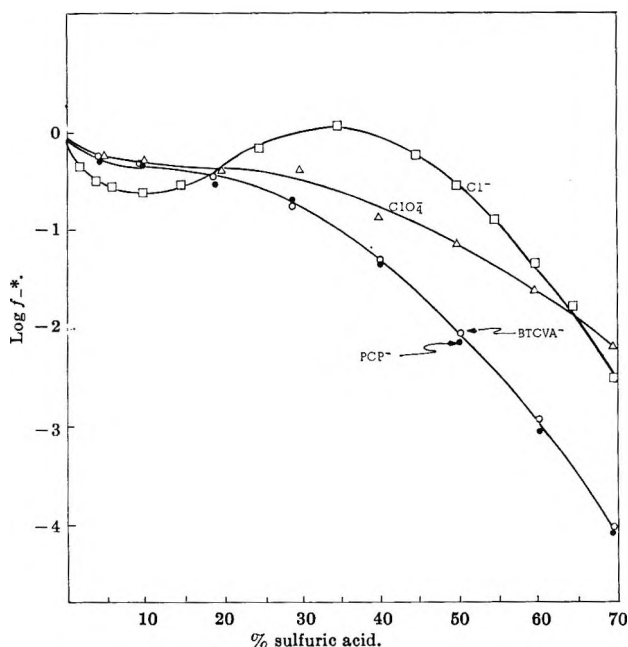


Figure 2. Relative activity coefficients of anions,  $f_-^* = f_-/f_{\text{TEA}^+}$ , plotted against sulfuric acid concentration.  $\text{PCP}^-$  is pentacyanopropenide and  $\text{BTCVA}^-$  is bis(tricyanovinyl)amine.

previously measured data for a number of other ions. The activity coefficients of the potassium and perchlorate ions were calculated from the data of Deno and Perrizzolo<sup>6</sup> on the solubility of potassium perchlorate and tetrabutylammonium perchlorate and our data on tetrabutylammonium pentacyanopropenide.<sup>2</sup> The large positive deviation shown by anilinium ions rela-

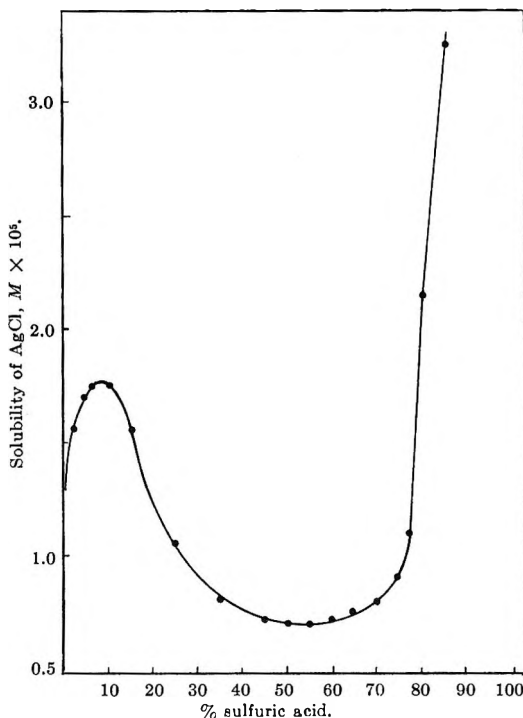


Figure 3. Solubility of silver chloride plotted against acid concentration.

tive to  $\text{TEA}^+$  has been attributed to a specific interaction of the  $\text{NH}_3^+$  group with the solvent.<sup>2</sup> The positive deviation shown by the potassium and silver ions is thus somewhat surprising. This perhaps points to a size effect since both silver and potassium ions have considerably smaller radii than  $\text{TEA}^+$ .<sup>7</sup> Several other supposedly "inert"<sup>8</sup> organic cations (tetramethyl-, tetrabutyl-, and phenyltrimethylammonium and tri(*p*-methoxyphenyl)carbonium) show rather small deviations compared to  $\text{TEA}^+$  but are all also considerably larger than silver or potassium ions. It is a matter of speculation whether the large positive deviation of the anilinium ions is due entirely to specific hydrogen-bonding interaction or is also influenced directly by the concentrated exposed charge. It will be interesting to determine the effect of increased charge by studying the activity coefficient behavior of divalent metal cations.

(6) N. C. Deno and C. Perrizzolo, *J. Am. Chem. Soc.*, **79**, 1345 (1957).

(7) The crystallographic radii of  $\text{Ag}^+$  and  $\text{K}^+$  are 1.26 and 1.33 Å, respectively: L. Pauling, "Nature of the Chemical Bond," 2nd Ed., Cornell University Press, Ithaca, N. Y. The crystallographic radii (in iodides) of  $\text{TEA}^+$  and tetramethylammonium are approximately 2.6 and 2.3 Å, respectively: R. W. G. Wyckoff, *Z. Krist.*, **67**, 91 (1928); E. Wait and H. M. Powell, *J. Chem. Soc.*, 1872 (1958).

(8) "Inert" is used in the sense there are no functional groups for obvious specific interaction with the solvent. Of course, any solute will undergo a general interaction, and it is one of the purposes of this type of measurement to attempt to delineate the relative importance of several types of interaction.

The chloride ion is similar to other anions in showing a negative deviation relative to  $\text{TEA}^+$  at high acid concentration (Figure 2). At lower acid concentration (5–30%) where the other anions show a relatively flat curve with an inflection, chloride shows a minimum followed by a maximum between 30 and 40% acid. The perchlorate ion is more similar to the large cyanocarbon anions but is not as negative. These results perhaps again point to a size effect. Unfortunately, this is difficult to explore further since there are few anions available that have very strong conjugate acids that remain undissociated in strong acid and also have salts of the requisite solubility.

The solubility of silver chloride has an abrupt increase at 75% sulfuric acid concentration (see Figure 3). Under the reasonable assumption that this increase is due to the formation of undissociated hydrochloric acid we can obtain an estimate of the  $pK$  of this acid. Use of the  $H_-$  acidity function<sup>9,10</sup> leads to

$$pK(\text{HCl}) = H_- - \log \frac{C_{\text{Cl}^-}}{C_{\text{HCl}}} - \log \frac{f_{\text{Cl}^-}}{f_{\text{A}^-}} - \log \frac{f_{\text{HA}}}{f_{\text{HCl}}} \quad (9)$$

where  $\text{HA}$  and  $\text{A}^-$  refer to the family of cyanocarbon indicators upon which  $H_-$  is based. If we assume that at ~75% sulfuric acid  $C_{\text{Cl}^-} = C_{\text{HCl}}$ , that  $f_{\text{HCl}} = f_{\text{HA}}$ , and extrapolate our measured data for  $f_{\text{Cl}^-}/f_{\text{PCP}}$  to 75% sulfuric acid to use as  $f_{\text{Cl}^-}/f_{\text{A}^-}$ , we can estimate  $pK(\text{HCl})$  from the  $H_-$  function. Combining our estimate of  $-\log f_{\text{Cl}^-}/f_{\text{A}^-}$  as  $-1.6$  with  $H_- = -6.8$  we arrive at  $pK(\text{HCl}) = -8.4$ . This value is to be compared with other estimates,<sup>11</sup> based on the vapor pressure of hydrochloric acid solutions, which lie between  $-6$  and  $-7$ .

*Acknowledgment.* The authors are greatly indebted to the National Science Foundation for support of this work. They are also grateful to Prof. J. T. Spence of this department for assistance with the polarographic technique.

(9) R. H. Boyd, *J. Am. Chem. Soc.*, **83**, 4288 (1961).

(10) R. H. Boyd, *J. Phys. Chem.*, **67**, 737 (1963).

(11) R. P. Bell, "The Proton in Chemistry," Cornell University Press, Ithaca, N. Y., 1959, p. 88.

# The Thermodynamics of Vaporization of Thallous Fluoride and Its Gaseous Dimerization<sup>1</sup>

by F. J. Keneshea and Daniel Cubicciotti

Stanford Research Institute, Menlo Park, California 94025 (Received June 4, 1965)

The vapor pressure of liquid thallous fluoride was measured by a quasi-static method. The results can be represented by the equation  $\log p$  (mm.) =  $[-5450/T + 7.841] \pm 0.016$  for the temperature range 420 to 820°. Mass spectrometric observation of the vapor showed that the dimer was the preponderant species and that trimer and tetramer existed in very small proportions. With the assumption that the heavier species had negligible importances, the partial pressures of the dimer and monomer were calculated by combining transpiration measurements with the absolute pressures. Extrapolation indicated that the dimer would constitute 63% of the vapor at the melting point (595.4°K.) and 59% at the normal boiling point (1099°K.). The enthalpies of evaporation at 1000°K. were 23.7 kcal./mole to monomer and 22.5 to dimer. The corresponding entropies were 19.5 and 19.1 e.u. Consideration of the absolute entropies of the gaseous monomer and dimer indicates that thallous fluoride dimer does not have the rhombic structure of the alkali halides. A linear structure appears to be more reasonable for thallous fluoride.

## Introduction

In our studies of the evaporation of thallous halides,<sup>2</sup> we have found for the chloride and bromide that the dimer constitutes an appreciable fraction of the equilibrium vapor. In this regard, they behave like the alkali halides<sup>3</sup>; in fact, similar to the halides of Rb and Cs, the importance of the dimer increases from the iodide to the bromide to the chloride. However, from considerations of the absolute entropy, it appeared that the structure of the thallium halide dimers was probably not the same as that of the alkali halide dimers. For the fluorides of the alkali halides the dimer is less important, relative to the monomer, than for the chloride. In this paper we report results on thallous fluoride in which we find that the dimer is more important than the monomer and so shows a marked difference in behavior from the alkali halides.

## Experimental Section

**Total Pressures.** The total pressure of species in equilibrium with liquid TlF was measured by the quasi-static method of Rodebush and Dixon that we have used in our previous work. Because molten TlF reacts rapidly with silica glasses, the cell used

was made of platinum-10% rhodium alloy. The two vapor jets, which primarily determine the characteristics of the Rodebush-Dixon cell, were 1 mm. i.d. and 2.5 cm. long. The inert gas used was pure, dry nitrogen. The operation of the cell was checked by determining the vapor pressure of water with helium as the inert gas. The thermocouples were Pt-10% Rh checked against an NBS standardized couple.

**Transpiration.** Measurements of the density of TlF in the vapor were made by the transpiration technique used previously. The cell and the collector system were constructed of Pt-10% Rh. They are shown schematically in Figure 1. The collectors had a small-bore end (0.6 mm. in diameter, 15 mm. long) to reduce the diffusional flow of gas from the cell into the collector. Pure, dry nitrogen was used as the flow gas and temperatures were measured with Pt-10% Rh thermocouples located outside the cell, near the liquid sample.

(1) This work was supported by the Research Division of the U. S. Atomic Energy Commission under Contract No. AT(04-3)-106.

(2) D. Cubicciotti, *J. Phys. Chem.*, **68**, 1528 (1964) (TlCl); 3835 (1964) (TlBr); **69**, 1410 (1965) (TlI).

(3) L. Brewer and E. Brackett, *Chem. Rev.*, **61**, 425 (1961).



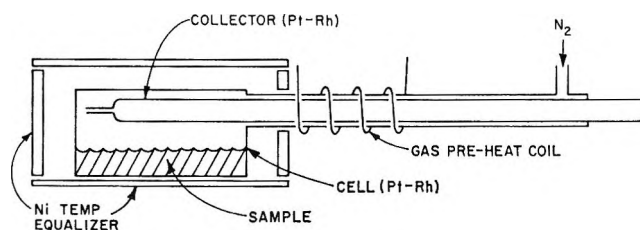


Figure 1. Diagram of transpiration apparatus.

**Mass Spectrometer Studies.** The gaseous species produced during the evaporation of TlF were identified in a mass spectrometer. The instrument used was a Bendix time-of-flight machine. A sample of TlF was heated in a graphite container that had a slit-orifice top. The beam of gaseous TlF so produced was directed into the ionization chamber of the mass spectrometer. The relative intensities of the ions produced were observed qualitatively only, because our instrument is not capable of quantitative measurements. The ion peaks observed occurred at masses corresponding to  $\text{TlF}^+$  (medium intensity),  $\text{Tl}_2^+$  (medium),  $\text{Tl}_2\text{F}^+$  (strong),  $\text{Tl}_2\text{F}_2^+$  (strong),  $\text{Tl}_3\text{F}_2^+$  (weak),  $\text{Tl}_3\text{F}_3^+$  (weak), and  $\text{Tl}_4\text{F}_3^+$  and  $\text{Tl}_4\text{F}_4^+$  (both very weak and questionable). These results were interpreted to indicate that the dimer ( $\text{Tl}_2\text{F}_2$ ) was the predominant species, the trimer constituted less than 1 or 2% of the total, and the tetramer was even less important. The importance of the monomer was not proportional to the  $\text{TlF}^+$  since the latter received an unknown contribution from fragmentation of dimer molecules.

**Preparation of Material.** Thallous fluoride was prepared from pure thallium (sticks of 99.95+% from American Smelting and Refining Co.) and hydrofluoric acid solution (48% analytical reagent from Mallinckrodt Chemical Co.). The metal was cleaned of its surface oxide in nitric acid and then dissolved in the hydrofluoric acid in a platinum dish, with warming. Apparently, the overvoltage for hydrogen on thallium is high because the hydrogen evolved from the platinum surface. Also, the thallium did not dissolve in a plastic dish. (As the metal was dissolving a few black specks—presumably oxide—were formed but they disappeared as the solution was fumed.) The solution was then evaporated in the platinum dish and gradually heated to heavy fuming—at which time the liquid was well above the melting point of pure TlF. This liquid was poured a little at a time onto a cold platinum dish where it froze and pulled away from the cold metal. The salt was ground to a powder and analyzed as described below. The salt is not hygroscopic and so all operations were performed in air.

**Analysis.** Several batches of TlF were prepared and analyzed by the chromate method,<sup>4</sup> with precipitation at 0°. The results indicated a thallium content several tenths of 1% higher than that expected for TlF. When the iodide method<sup>5</sup> was used, the results were somewhat low. It was suspected that the fluoride ion was interfering. A series of determinations by the chromate method was made on a solution of thallous sulfate to which known amounts of fluoride were added. The samples with added fluoride gave results that were high by a few tenths of 1%. Therefore, fluoride was removed from the samples to be analyzed by adding 0.1 g. of boric acid and 5 cc. of sulfuric acid and fuming. With this pretreatment, analyses of several batches of TlF by the chromate method gave results within one-tenth of 1% of theoretical; in particular, the batch of TlF used for the vaporization studies reported here was found to contain 91.46, 91.54, and 91.72% Tl in triplicate analyses compared to 91.49 theoretical.

## Results

The total pressure of all thallous fluoride vapor species was measured by the quasi-static method over the range from 1 to 700 mm. The results are shown in Figure 2. These data can be represented by the equation

$$\log p \text{ (mm.)} = \left[ -\frac{5450}{T} + 7.841 \right] \pm 0.016$$

for the temperature range of 420 to 820°. The error limits shown are the standard deviation of the experimental points from the equation. No other pressure measurements over liquid thallium fluoride have been reported in the literature except for a boiling point by Hayek.<sup>6</sup> His value of  $928 \pm 10^\circ\text{K}$ . differs by  $171^\circ$  from the value of  $1099 \pm 5^\circ\text{K}$ . obtained from our equation. Since Hayek gives no details of his method, it is not possible to reconcile the difference in the two boiling points. Barrow, Jeffries, and Swinstead<sup>7</sup> have reported absolute pressures over the solid and their results, which are also shown in Figure 2, when extrapolated to the melting point give a pressure of 0.05 mm. Our extrapolated value of 0.06 mm. at the melting point is in substantial agreement.

(4) O. L. Forchheimer and R. P. Epple, *Anal. Chem.*, **23**, 1445 (1951).

(5) W. F. Hillebrand, G. E. Lundell, H. A. Bright, and J. I. Hoffman, "Applied Inorganic Analysis," 2nd Ed. (rev.), John Wiley and Sons, Inc., New York, N. Y., 1953 p. 479.

(6) E. Hayek, *Z. anorg. allgem. Chem.*, **225**, 47 (1935).

(7) R. F. Barrow, E. A. Jeffries, and J. M. Swinstead, *Trans. Faraday Soc.*, **51**, 1650 (1955).

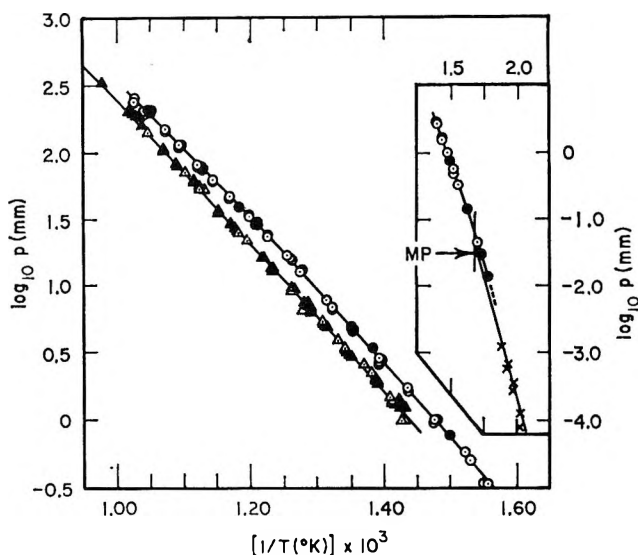


Figure 2. Vaporization data for thallium fluoride:  $\blacktriangle, \triangle$ , absolute vapor pressures by quasi-static method;  $\bullet, \circ$ , transpiration data calculated as monomer;  $\times$ , solid vapor pressures by Barrow, Jeffries, and Swinstead.<sup>7</sup> (Different symbols refer to different samples.)

The transpiration results were calculated as TIF pressures by using the monomer formula weight, 223.4, for the molecular weight of the gas. Pressures calculated in this way are greater than the total vapor pressures by approximately the partial pressure of the dimer, since the monomer and dimer were the only important species in the gas. The transpiration results are also shown in Figure 2. At certain temperatures, measurements were made over a tenfold range in flow rate and the pressures obtained were constant within a range of 4%, indicating that the carrier gas was saturated with the thallos fluoride and that diffusion effects were negligible. In addition to the measurements over the liquid, three experiments were made over the solid. These are shown in comparison with the data of Barrow, *et al.*,<sup>7</sup> in Figure 2, where it can be seen that the transpiration results were considerably higher than the (total pressure) measurements of Barrow, *et al.*, indicating the presence of a large fraction of dimer over the solid.

As described previously, the mass spectrometer results indicated that the gas consisted of monomer and dimer, with only 1 or 2% trimer and even less tetramer. Therefore, the vapor phase was assumed to consist of monomer and dimer only and their partial pressures were calculated from the combined absolute pressures and transpiration results. The method was the same as described for obtaining the partial pressures of thallos chloride monomer and dimer.<sup>2</sup> The partial pressures of monomer and dimer were calculated from

the smoothed data for several temperatures over the range in which the two sets of measurement overlap. The resulting partial pressure of each species was treated by the  $\Sigma$ -plot method.<sup>8</sup>

For the monomer, the heat capacity of the gas was calculated from molecular constant data.<sup>9</sup> It was found to be essentially constant in the temperature range of interest and equal to 8.78 cal./mole deg. The heat capacity of the liquid was recently measured in our laboratory<sup>10</sup> and was found to have a value of 16.08 cal./mole deg. The expression for  $\Sigma$  then may be written

$$\Sigma = \frac{\Delta H_0^\circ}{T} + I = -R \ln p_M(\text{mm.}) - 7.30 \ln T \quad (1)$$

A plot of  $\Sigma$  against  $1/T$  yielded a straight line from which the enthalpy of evaporation at 0°K.,  $\Delta H_0^\circ$ , and the constant  $I$  were evaluated. The equations thus derived for the monomer partial pressure,  $p_M$ , and the enthalpy of vaporization,  $\Delta H_M^\circ$ , are

$$\log p_M(\text{mm.}) = \left[ -\frac{6780}{T} - 3.67 \log T + 19.744 \right] \pm 0.023 \quad (2)$$

$$\Delta H_M^\circ = [31.0 - 7.3 \times 10^{-3}T] \pm 0.2 \text{ kcal./mole} \quad (3)$$

for the temperature range of 690 to 965°K.

The partial pressures of the dimer were also treated by the  $\Sigma$ -plot method. The heat capacity for the dimer was estimated to be 21 cal./mole deg. For this estimate the molecule was assumed to be linear and thus to have two rotational and five vibrational degrees of freedom. The resulting equations for the dimer pressure,  $p_D$ , and the heat of vaporization,  $\Delta H_D^\circ$ , are

$$\log p_D(\text{mm.}) = \left[ -\frac{7330}{T} - 5.55 \log T + 26.118 \right] \pm 0.023 \quad (4)$$

$$\Delta H_D^\circ = [33.5 - 11 \times 10^{-3}T] \pm 0.2 \text{ kcal./mole} \quad (5)$$

for 690 to 965°K.

The graphs of  $\log p$  vs.  $1/T$  for monomer and dimer, calculated from the above equations, are shown as solid lines in Figure 3. These were extrapolated to the melting point, as shown by the dashed lines. The

(8) G. N. Lewis and M. Randall, "Thermodynamics," revised by K. S. Pitzer and L. Brewer, McGraw-Hill Book Co., Inc., New York, N. Y., 1961, p. 175 ff.

(9) R. F. Barrow, H. F. Cheall, P. M. Thomas, and P. B. Zeeman, *Proc. Roy. Soc. (London)*, **A71**, 128 (1958).

(10) D. Cubicciotti and H. Eding, *J. Chem. Eng. Data*, to be published.

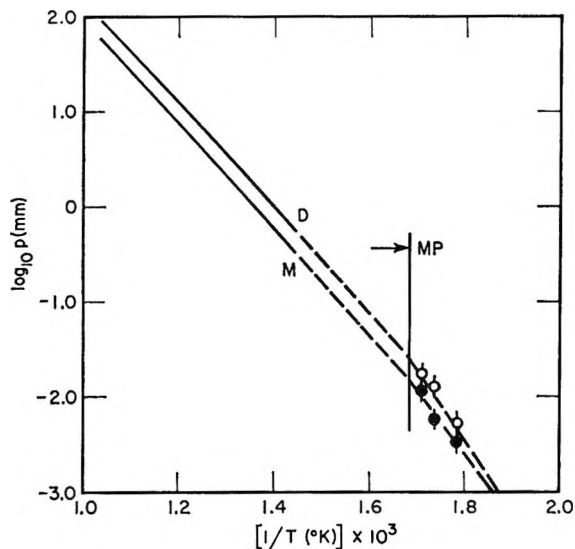


Figure 3. Partial pressures of thallium fluoride monomer (M) and dimer (D). The points over the solid (●, ○) were calculated from transpiration combined with the data of Barrow, *et al.*<sup>7</sup>

partial pressures of monomer and dimer over the solid were then estimated from the liquid pressures, the enthalpies of vaporization for the liquid at the melting point (595.4°K.<sup>10</sup>), and the enthalpy of fusion of 3315 cal./mole.<sup>10</sup> The enthalpies of vaporization of the liquid were calculated to be 26.7 kcal./mole to the monomer and 27.0 kcal./mole to the dimer at the melting point. Thus the enthalpies of sublimation used in deriving the curves over the solid shown in Figure 3 were 30.0 kcal./mole of monomer and 33.6 kcal./mole of dimer. The three sets of points shown in Figure 3 in the solid region were calculated from the three transpiration measurements made over the solid, combined with absolute pressures interpolated from the data of Barrow, *et al.*,<sup>7</sup> shown in Figure 2. The vertical lines through the points represent a range of  $\pm 10\%$  in the pressures. The agreement of the three sets of pressures with the extrapolated curves is reasonably good.

The second-law enthalpy of sublimation at 298°K. for the monomer,  $\Delta H^{\circ}_{298}$ , can be calculated from the enthalpy of evaporation at the temperatures investigated. At the midpoint of the temperature range, 850°K., eq. 3 above gives  $\Delta H^{\circ}_{850} = 24.8 \pm 0.2$  kcal./mole. From molecular constant data,<sup>9</sup> the quantity  $(H^{\circ}_{850} - H^{\circ}_{298})_{\text{gas}}$  is calculated to be 4.78 kcal./mole and from heat content measurements,<sup>10</sup>  $(H^{\circ}_{850} - H^{\circ}_{298})_{\text{cond}}$  is 11.55 kcal./mole. Thus  $\Delta H^{\circ}_{298}(\text{subl, TlF})$  is  $31.6 \pm 0.2$  kcal./mole. [The enthalpy of sublimation at 298° derived by Barrow, *et al.*, from their torsion-effusion data, namely 34.41, is not correct and

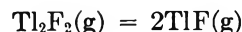
should not be compared with the present data. Their value is based on the incorrect assumption that the solid vaporizes only to monomer. We have shown in Figure 3 that it vaporizes to a mixture of dimer and monomer and over the solid the composition of the mixture changes with temperature.]

A third-law treatment of the data is not possible since the absolute entropy of solid thallos fluoride has not been measured. In fact, the present data together with molecular constant data for the gaseous monomer and enthalpy data for the condensed phases can be used to calculate the absolute entropy of the condensed phase. Thus, from the data at 850°K. the entropy of evaporation,  $\Delta S^{\circ}_{850}(\text{vap})$ , is found to be 20.7 e.u. From ref. 10 the absolute entropy of the gas,  $S^{\circ}_{850}(\text{gas})$ , is 67.52 e.u. and the entropy increment  $[S^{\circ}_{850}(\text{liq}) - S^{\circ}_{298}(\text{solid})]$  is 20.9 e.u. Thus the absolute entropy of the solid at 298°K.,  $S^{\circ}_{298}(\text{solid})$ , is  $25.9 \pm 0.4$  e.u. Free-energy functions for the condensed phases of TlF based on this value are given in ref. 10.

A second-law treatment for vaporization to the dimer can be made as follows. The enthalpy of vaporization to dimer at 850°K. is  $24.1 \pm 0.2$  kcal./mole from eq. 5. The enthalpy increment of the gas (from the estimated  $C_p$  of 21 e.u.) from 298 to 850°K. is  $11.6 \pm 1$  kcal./mole and that for 2 moles of condensed phase is 23.1; therefore, the enthalpy of sublimation to the dimer at 298°K. is  $35.6 \pm 1.5$  kcal./mole.

The enthalpies and entropies of evaporation at 1000°K. for thallos fluoride are shown in Table I, along with values for the other thallos halides. Also shown for comparison are the values for the potassium halides,<sup>11</sup> as a representative of the alkali halides. As far as the monomer thermodynamics are concerned, the main difference between the Tl and K halides is the much smaller enthalpies of evaporation of the Tl halides. For the dimer both the enthalpies and entropies of the Tl compounds are quite different from the potassium halides. These differences suggest, as noted before,<sup>2</sup> that the nature of the binding in the gas and/or liquid is different between Tl and K halides.

The enthalpy and entropy of dissociation of the dimer



at 1000°K. are  $\Delta H^{\circ}_{1000}(\text{dissociation}) = 24.9 \pm 0.4$  kcal./mole and  $\Delta S^{\circ}_{1000}(\text{dissociation}) = 19.9 \pm 0.5$  e.u. These values are larger than those for the chloride and bromide and give a much smaller equilibrium

(11) "JANAF Thermochemical Tables," The Dow Chemical Co., Midland, Mich., 1962.

**Table I:** Thermodynamic Data for Vaporization of Liquid Thallium and Potassium Halides at 1000°K.

Salt	$\Delta H^\circ$ (monomer), kcal./ mole	$\Delta H^\circ$ (dimer), kcal./ mole	$\Delta S^\circ$ (monomer), cal./mole deg.	$\Delta S^\circ$ (dimer), cal./mole deg.
TlF	23.7	22.5	19.5	19.1
TlCl	24.4	31.8	22.0	25.7
TlBr	24.3	50	22.0	42
TlI	25.2	...	23.8	...
KF	48.0	47.8	27.3	25.7
KCl	43.4	42.5	25.9	24.1
KBr	41.8	43.8	25.5	24.6
KI	38.1	38.4	23.7	22.0

constant for the dissociation reaction. The values for the three compounds are compared in Table II.

**Table II:** Thermodynamic Quantities for the Dissociation of Gaseous Thallium Halide Dimers at 1000°K.

Salt	$\Delta H^\circ_{1000}$ (dissociation)	$\Delta S^\circ_{1000}$ (dissociation)	Equilibrium const., $K_p$ , atm.
TlF	24.9 ± 0.4	19.9 ± 0.5	0.0775
TlCl	17.0 ± 0.8	18.3 ± 1.2	1.66
TlBr	-2 ± 5	2 ± 4	5

## Discussion

Perhaps the first point of interest is the fact that the dimer is more important than the monomer in the saturated vapor. Among the alkali halides, this situation occurs only with Li. In Table III the ratios of the partial pressures of dimer to monomer for the Tl halides are compared with those of the alkali halides.

**Table III:** Dimer: Monomer Ratio in the Saturated Vapor of Thallium and Alkali Halides at 1000°K.<sup>a</sup>

	Tl	Li	Na	K	Rb	Cs
F	1.53	0.74	0.15	0.14	0.14	0.12
Cl	0.15	3.0 <sup>b</sup>	1.0	0.35	0.3	0.22
Br	0.067	1.4	0.9	0.2	0.06	0.10
I	... <sup>c</sup>	(1.2)	1.0	0.2	0.04	0.02

<sup>a</sup> The alkali halide data are taken from Brewer and Brackett.<sup>3</sup>

<sup>b</sup> This value was misprinted in ref. 3. <sup>c</sup> This value is not established but is less than 0.05. See ref. 2.

halides by means of the dimensional theory of Blander<sup>12</sup> also shows a lack of correspondence between the two types of dimers. According to Blander, for geometrically similar configurations in different dimer molecules the law of corresponding states may be written as

$$\log K_2(T) + 3 \log g = \log K_{20}(T_0)$$

where  $K_{20}(T_0)$  is the dimerization constant for a "comparison" salt at temperature  $T_0$ ,  $K_2(T)$  is the dimerization constant for the salt to be compared at temperature  $T = gT_0$ , and  $g$  is a geometry factor which is the ratio of interatomic distances in the two monomer molecules. Following Blander, sodium iodide was taken as a comparison salt with  $T_0 = 1000^\circ\text{K}$ .,  $g = 2.7115/2.0844 = 1.30$ , and  $T = 1300^\circ\text{K}$ . From extrapolation of the data of Datz, *et al.*,<sup>13</sup>  $\log K_{20}(T_0)$  was calculated to be 4.48. From the present data  $K_2(T)$  for thallium fluoride is 80.6 l./mole and hence  $\log K_2(T) + 3 \log g = 2.25$ . The lack of agreement between this number and  $\log K_{20}$  further emphasizes the difference between thallium fluoride and the alkali halides.

In spite of the similarity in the values for the monomer:dimer ratios for the Cl, Br, and I compounds of Rb, Cs, and Tl, detailed consideration of the absolute entropies indicated that the structure of the Tl dimers is probably quite different from that of alkali halide dimers.<sup>2</sup> Some information about the possible structure of the gaseous thallos fluoride dimer molecule can be obtained from a consideration of its absolute entropy. The absolute entropy can be derived as follows.

At 1000°K. the absolute entropy of the gaseous monomer is 69.06 e.u. The absolute entropy of the dimer is twice this value minus the dissociation entropy or 118.2 e.u. It is interesting to compare this value with that estimated from different models of the dimer gas molecule. The translational entropy for the dimer is calculated to be 50.2 e.u. For a square-planar molecule, by analogy with  $\text{Li}_2\text{Cl}_2$ ,<sup>14</sup> taking the Tl-F distance equal to 2.3 Å. (10% larger than the monomer distance), the rotational entropy is calculated to be 31.0 e.u. Thus on a square-planar model the vibrational entropy should be 118.2 minus (50.2 + 31.0), or 37.0 e.u. Using the same approximations for the vibrational frequencies as were used for TlBr,<sup>2</sup> *i.e.*, four of the frequencies having values approximately two-thirds that of the monomer and two frequencies

(12) M. Blander, *J. Chem. Phys.*, **41**, 170 (1964).

(13) S. Datz, W. T. Smith, and E. H. Taylor, *ibid.*, **34**, 558 (1961).

(14) See S. H. Bauer and R. F. Porter in "Molten Salt Chemistry," M. Blander, Ed., Interscience Publishers, Inc., New York, N. Y., 1964, p. 652.

It is interesting to note that comparison of the thallium fluoride dimerization data with the alkali

having values approximately one-third that of the monomer, the vibrational entropy is calculated to be 24.0 e.u. Therefore, the value of the vibrational entropy calculated for this square-planar model is 13 e.u. smaller than the experimental value. The same situation was found for the  $\text{TlCl}$  and  $\text{TlBr}$  dimers and as in those cases suggests that the square-planar model is not correct for thallium fluoride.

As discussed earlier,<sup>2</sup> a linear molecule, such as  $\text{F-Tl-Tl-F}$ , might be expected to have a larger entropy than a square-planar molecule because it can have lower frequency vibrational modes. For such a molecule, with a  $\text{Tl-F}$  distance of 2.1 Å. and  $\text{Tl-Tl}$  distance of 2.4 Å., the vibrational entropy would have to be 45 e.u. to account for the experimental absolute entropy. This is possible if some of the bending vibrations have frequencies of the order of a few wave numbers.

The mass spectrometer studies provide additional experimental evidence to support the idea that the gaseous Tl halide dimers may have a linear structure with a  $\text{Tl-Tl}$  bond, in contrast to the rhombic structure of the alkali halides. As indicated in the Experimental Section, thallium fluoride showed a  $\text{Tl}_2^+$  ion as one of the mass peaks. This ion showed a medium strength intensity, comparable to  $\text{TlF}^+$ . Similar results have been observed with thallium chloride and bromide. For the alkali chlorides the  $\text{M}_2^+$  species is either too weak to detect or very weak in intensity.<sup>15</sup> Loss of the two bridging chlorine atoms in an alkali halide rhombic dimer molecule apparently results in two separate  $\text{M}^+$  ions rather than  $\text{M}_2^+$ ; hence the appearance of  $\text{Tl}_2^+$  in the thallos halides suggests a  $\text{Tl-Tl}$  bond in the parent molecule.

A reasonable electronic configuration can be assigned to the linear dimer molecule  $\text{XTlTlX}$ . The

s and three p orbitals of the Tl atom are hybridized into an sp pair and two p orbitals. One sp hybrid of each Tl is used for a  $\sigma$  molecular orbital between the halogen and Tl and the other for a  $\sigma$  molecular orbital between the two Tl atoms.<sup>16</sup> The two p orbitals remaining on each Tl center are combined into a degenerate pair of  $\pi$  molecular orbitals (m.o.). Of the six electrons of the two Tl's, two are used in the two  $\sigma$   $\text{Tl-X}$  bonds, two in the  $\sigma$   $\text{Tl-Tl}$  bond, and two in the two  $\pi$  m.o.'s. Since the two electrons only half-fill the two  $\pi$  m.o.'s, the electron spins should be parallel and the dimer, on this model, would be expected to be paramagnetic.

The above description is in accord with the fact that the dimer stability decreases in the order  $\text{F} > \text{Cl} > \text{Br} > \text{I}$ , corresponding to the order of decreasing electronegativity of the atom. Because of the shape of the sp hybrid bond the electrons in the  $\text{Tl-X}$  m.o. have a finite probability of being in the region between the Tl atoms. Thus the electrons in the  $\text{Tl-X}$  m.o. tend to weaken the  $\text{Tl-Tl}$  bond through electron repulsion. As the electronegativity of the halogen is increased, the electrons in the  $\text{Tl-X}$  bond are attracted more strongly by the halogen and have a smaller probability of being in the  $\text{Tl-Tl}$  region. Thus the  $\text{Tl-Tl}$  bond strength increases as the electronegativity of the halogen increases.

*Acknowledgment.* The authors are indebted to Mr. W. E. Robbins, who assisted in the experimental work.

(15) T. A. Milne, H. M. Kleir, and D. Cubicciotti, *J. Chem. Phys.*, **28**, 718 (1958).

(16) For a description of this type of m.o. see C. A. Coulson, "Valence," 2nd Ed., Oxford University Press, Oxford, 1961, pp. 202, 203.

# The Vapor Pressure and Enthalpy of Vaporization of Molten Bismuth Chloride to the Critical Point<sup>1</sup>

by J. W. Johnson, W. J. Silva, and Daniel Cubicciotti

Stanford Research Institute, Menlo Park, California 94025 (Received June 25, 1965)

The vapor pressure of molten bismuth chloride has been measured by an inverted capillary technique from 721°K. and 1.2 atm. to 1175°K. and 110.6 atm. The data are fitted by the equation  $\log P_{\text{atm}} = 5.2349 - 3725.7/T^{\circ}\text{K.}$ , with an average deviation of 0.7%. A critical pressure of  $118.1 \pm 4$  atm. is predicted from these data. The enthalpy of vaporization of molten bismuth chloride has been calculated from 900 to 1170°K. and near the normal boiling point; values at intermediate temperatures have been interpolated. The deviation of bismuth chloride vapor from the ideal gas relation has been found to begin just above the normal boiling point (714°K.).

## Introduction

The physical properties of electrically conducting molten salts have not been investigated to any great extent above their normal boiling points. The electrical conduction of molten bismuth chloride has been measured by Grantham and Yosim<sup>2</sup> to 625°. In a previous paper<sup>3</sup> we reported the critical temperature and coexistence curve for bismuth chloride liquid and vapor. This paper reports measurements on the vapor pressure of bismuth chloride from the normal boiling point to the critical temperature.

## Experimental Section

The vapor pressure measurements were made using an inverted capillary technique modified to use small-bore tubing that could withstand high pressures. The apparatus, described in detail elsewhere,<sup>4</sup> was made of quartz and consisted of a straight tube, 3-mm. bore  $\times$  6-mm. o.d.  $\times$  35-cm. length. The top end was flared for connection by a Bridgman seal to the pressurizing system; the bottom was sealed shut 2 cm. above the end to provide a thermocouple housing. An inverted capillary, 1-mm. bore  $\times$  2-mm. o.d.  $\times$  4-cm. length, had a length of platinum wire sealed in the top portion to increase the density and ensure that the open end of the capillary rested on the bottom of the tube. A schematic diagram of tube and furnace assembly is shown in Figure 1.

The furnace, 33 cm. long with a 15-cm. controlled-

heating zone, had two diametrically opposed slits 5 cm. long  $\times$  0.6 cm. wide so that the bottom of the tube containing the BiCl<sub>3</sub> and the inverted capillary tube, as well as the thermocouple bead, were viewed by transmitted light.

The BiCl<sub>3</sub> was distilled at 300° under a stream of oxygen into the tube containing the inverted capillary until a liquid height of 8 cm. was obtained. The salt was then cooled to room temperature under oxygen, removed from the distillation apparatus, and attached to the pressurizing system. The pressurizing system consisted of two Heise Bourdon tube gauges with ranges of 0–250 p.s.i. in 0.25-lb. graduations and 0–3000 p.s.i. in 2-lb. graduations, a compressed argon tank, and a connection to a vacuum line.

After attachment to the pressurizing system, the whole assembly was evacuated to remove air and oxygen and then repressurized with argon to approximately 150 p.s.i. The temperature was slowly raised until vigorous bubbling occurred at the base of the capillary; this served to purge the capillary of

(1) This work was made possible by the support of the Research Division of the U. S. Atomic Energy Commission under Contract No. AT(04-3)-106.

(2) L. F. Grantham and S. J. Yosim, *J. Phys. Chem.*, **67**, 2506 (1963).

(3) J. W. Johnson and D. Cubicciotti, *ibid.*, **68**, 2235 (1964).

(4) W. J. Silva, J. W. Johnson, and D. Cubicciotti, *Rev. Sci. Instr.*, in press.

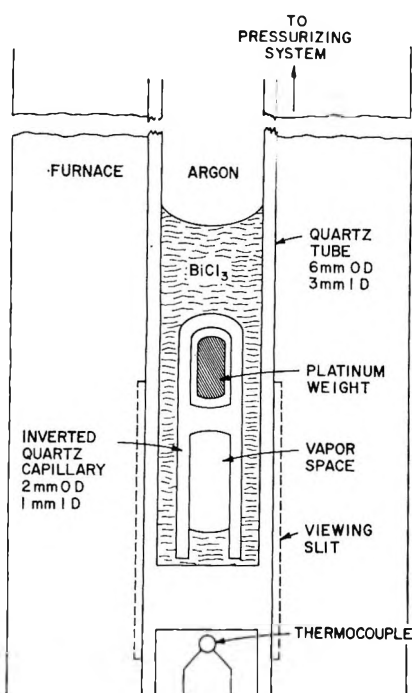


Figure 1. Boiling point apparatus.

entrapped oxygen. The pressure was then increased, and the rise of the liquid into the capillary was observed with a telescope.

In operation the pressure was set to a selected value, and the temperature was raised slowly to the point where the vapor pressure was slightly less than the applied pressure. The system pressure was slowly reduced until the liquid level in the capillary dropped to the bottom and occasional bubbling occurred. The applied pressure and the e.m.f. of the thermocouple were recorded. The pressure was then increased, and the same procedure was followed at another temperature.

There was a vertical temperature gradient in the tube because of the slits, and therefore the reading of the thermocouple had to be corrected. This was accomplished by inserting a platinum-platinum-10% rhodium thermocouple into the empty tube and comparing the reading of the two couples. This procedure established a calibration curve for the assembly. The system thermocouple and calibrating thermocouple had been compared with a standard platinum-platinum-10% rhodium thermocouple calibrated by the National Bureau of Standards.

The validity of this method was determined by measuring the vapor pressure of  $\text{CCl}_4$  from the boiling point to the critical point<sup>2</sup> with an average deviation of less than 1% from published values.

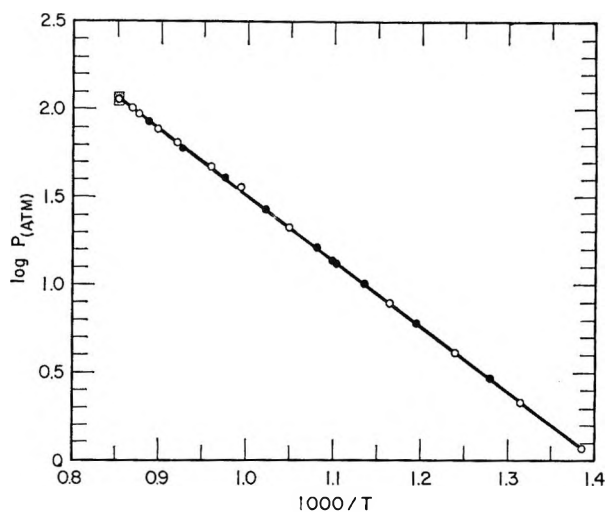


Figure 2. Vapor pressure of molten bismuth chloride.

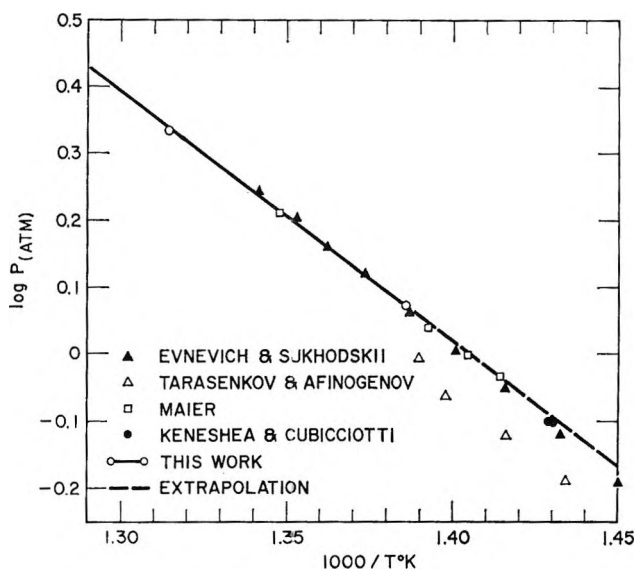


Figure 3. Comparison of bismuth chloride data.

## Results and Discussion

Measurements of the vapor pressure of molten bismuth chloride were made from 721 to 1175°K. over a pressure range of 1.18 to 110.6 atm. The experimental data are presented in Table I. The temperatures recorded are the corrected values obtained from the calibration curve run on the empty tube. These corrections ranged from 3 to 5°, the larger corrections being required at the higher temperatures. The observed pressures up to 17 atm. are corrected by the addition of 0.04 atm. for the static head of bismuth chloride in the tube. Above this pressure, where the 0-3000-p.s.i. gauge was used, the pressures are recorded to the nearest 0.1 atm., and the correction was not applied.



Table I: Vapor Pressures of Molten Bismuth Chloride

Run no.	Obsd.		Calcd.		% press. dev.	$T_{\text{calcd}} - T_{\text{obsd}}$
	$T, ^\circ\text{K.}$	$P, \text{atm.}$	$P, \text{atm.}$	$T, ^\circ\text{K.}$		
2	721.6	1.18	1.18	721.6	0	0
2	761.0	2.16	2.18	760.3	+1.0	-0.7
1	781.5	3.02	2.94	783.5	-2.6	+2.0
2	806.8	4.11	4.14	805.2	+0.7	-0.6
1	836.7	6.20	6.06	838.6	-2.2	+1.9
2	858.9	7.83	7.89	858.2	+0.8	-0.7
1	880.7	10.15	10.10	881.1	-0.5	+0.4
1	906.4	13.37	13.32	906.8	-0.4	+0.4
1	909.7	13.80	13.78	909.8	-0.1	+0.1
1	929.7	16.99	16.89	930.3	-0.1	+0.6
2	952.8	21.3	21.1	953.7	-0.1	+0.9
1	979.0	26.9	26.9	979.1	0	+0.1
2	1006.2	36.1	34.1	1013.1	-5.5 <sup>a</sup>	+5.9 <sup>a</sup>
1	1027.2	40.4	40.5	1026.8	+0.2	-0.4
2	1044.1	46.3	46.4	1043.8	+0.2	-0.3
1	1080.7	59.2	61.3	1076.0	+3.5 <sup>a</sup>	-4.7 <sup>a</sup>
2	1087.5	64.6	64.4	1087.9	-0.3	+0.4
2	1112.9	77.6	77.1	1113.8	-0.6	+0.9
1	1132.3	86.0	88.0	1128.9	+2.3	-3.4
2	1145.6	95.8	96.1	1145.1	+0.3	-0.5
2	1156.4	102.7	103.0	1155.9	+0.3	-0.5
2	1175.5	110.6	116.2	1167.5	+5.1 <sup>a</sup>	-8.0 <sup>a</sup>
	1178 ( $T_c$ )	...	118.1	...	...	...
				Av. dev.	0.7%	0.7%

<sup>a</sup> Values omitted in equation and deviation calculations.

Two runs were made using different samples of bismuth chloride. It was found that the data could be fitted by the relation

$$\log P_{\text{atm}} = 5.2349 - 3725.7/T \quad (1)$$

with an over-all average deviation in pressure of 1.2% for the 22 experimental points. If the three indicated values, obviously discordant, are ignored, the average deviation is 0.7%. The inverse calculation, *i.e.*, calculating the temperature by eq. 1 which corresponds to the observed pressure, is also listed in Table I. The average deviation is well within the error limits on the temperature which is estimated at  $\pm 2^\circ$  except at the highest temperatures where the limit is probably nearer  $\pm 4^\circ$ .

Figure 2 presents the data of Table I in graphical form. The solid circles represent the experimental values obtained in run 1; the open circles, values in run 2; and the line is calculated from eq. 1. The pressures observed in run 1 are slightly higher at low temperatures and lower at high temperatures than those calculated from eq. 1 but not significantly so.

The shaded area represents the uncertainty of temperature and pressure at the critical point. The critical temperature has been reported in a previous paper<sup>3</sup> as  $1178 \pm 5^\circ\text{K.}$  Using the critical temperature and the error limits set on the critical temperature, the critical pressure is calculated from eq. 1 to be  $118.1 \pm 4 \text{ atm.}$

As a check on the validity of applying the temperature correction curve obtained in air to the same tube filled with  $\text{BiCl}_3$ , the applied pressure was set at 135 atm., and the critical transition was observed to occur in the capillary tube at a corrected temperature of  $1178.3^\circ\text{K.}$  The agreement with the reported critical temperature is better than might be expected from our estimate of the accuracy of the temperature measurement.

Data available in the literature on the vapor pressure of  $\text{BiCl}_3$  overlap the present data only at the lower range of our measurements. Figure 3 presents the available data on a greatly expanded scale over that of Figure 2. The solid line is calculated from eq. 1, and the dashed portion represents an extrapolation of the present data from 720 to  $690^\circ\text{K.}$  Above  $720^\circ\text{K.}$  the data of Evnevich and Sukhodskii<sup>5</sup> and Maier<sup>6</sup> agree well with the present data. Below  $720^\circ\text{K.}$  the data of Maier fall on the linear extrapolation of the present data, while those of Evnevich and Sukhodskii and of Keneshea, Wilson, and Cubicciotti<sup>7</sup> fall below the linear extrapolation. The data of Tarasenkov and Afinogenov<sup>8</sup> are substantially lower than any of the other data available.

The normal boiling point of  $\text{BiCl}_3$  lies outside the range of the present data, but an extrapolated temperature of  $712^\circ\text{K.}$  is obtained; this compares with  $713.3^\circ$ ,<sup>5</sup>  $712.3^\circ$ ,<sup>6</sup> and  $714^\circ\text{K.}$ <sup>9</sup>

An examination of  $\text{BiCl}_3$  after completion of the run and cooling to room temperature gave no indication of darkening due to thermal dissociation of the salt at the high temperatures. The color of  $\text{BiCl}_3$  is very sensitive to the presence of excess bismuth metal both in the liquid and solid states. This was taken as evidence that  $\text{BiCl}_3$  is thermally stable at the critical temperature since the apparatus was such that any

(5) E. V. Evnevich and V. A. Sukhodskii, *J. Russ. Phys. Chem. Soc.*, **61**, 1503 (1929).

(6) C. G. Maier, U. S. Department of the Interior, Bureau of Mines, Technical Paper No. 360, 1925.

(7) F. J. Keneshea, W. Wilson, and D. Cubicciotti, *J. Phys. Chem.*, **64**, 827 (1960).

(8) D. H. Tarasenkov and B. P. Afinogenov, *Zh. Fiz. Khim.*, **9**, 889 (1937).

(9) K. K. Kelley, U. S. Department of the Interior, Bureau of Mines, Bulletin No. 383, U. S. Government Printing Office, Washington, D. C., 1935.



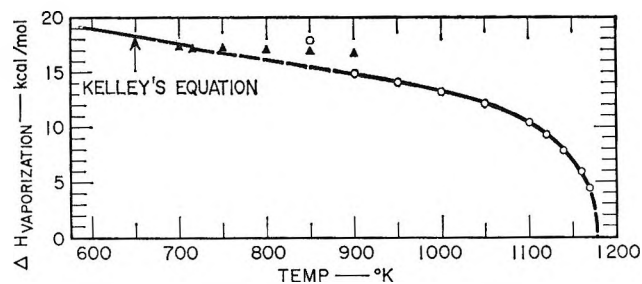


Figure 4. Heat of vaporization of bismuth chloride.

chlorine produced could escape from the heated zone. The bismuth would presumably have remained in solution and resulted in a darkened melt.

The enthalpy of vaporization of bismuth chloride may be calculated from the Clapeyron equation, which can be written

$$\Delta H_{\text{vap}} = \frac{T(V_g - V_l)(dp/dT)}{41,300} \quad (2)$$

where  $V_g$  and  $V_l$  are the orthobaric volumes of vapor and liquid, respectively,  $dp/dT$  is the rate of change of vapor pressure with respect to temperature; the numerical factor converts the value to kilocalories per mole. The orthobaric volumes were taken from the measurements of ref. 3 and  $dp/dT$  from eq. 1.

Figure 4 shows the variation of the enthalpy of vaporization as a function of temperature. The solid line below the normal boiling point (712–714°K.) is the enthalpy of vaporization calculated from Kelley's equation,<sup>9</sup> which was derived from the vapor pressure data of ref. 5 and 6. The triangles result from the use of the ideal gas relation for the vapor volume with  $dp/dT$  from eq. 1 and show the vapor begins to depart from ideality in the neighborhood of the normal boiling point. The circles represent the calculation of the volume change on vaporization from the Guggenheim relations for the orthobaric densities of bismuth chloride.<sup>3</sup> The vapor density of bismuth chloride has not

been determined between 714 and 900°K., and, as was pointed out earlier,<sup>3</sup> the Guggenheim relation predicts a vapor density of zero at 766°K., which would result in an infinite volume change on vaporization. The value for the enthalpy of vaporization calculated at 850°K. using the Guggenheim relation is much too high, owing to a high value for the volume change.

The enthalpy of vaporization cannot be calculated in the range of 714–900°K. owing to a lack of knowledge of the vapor density or a means of calculating it with any degree of reliability. The dashed line serves to bridge this temperature range and provides an estimate of the enthalpy of vaporization. There is no theoretical reason for making it a smooth curve, and, indeed, if association into polymers occurs in this range, the curvature may be greater than that shown. Table II presents the enthalpy of vaporization of bismuth chloride calculated and interpolated over the range from 700°K. to the critical temperature of 1178°K.

Table II: Enthalpy of Vaporization of Bismuth Chloride

$T$ , °K.	$P$ , atm.	$dP/dT$ , atm./°K.	$\Delta V_{\text{vap}}$ , cc./mole	$\Delta H_{\text{vap}}$ , kcal./mole
700	0.82	0.0143	73,000 <sup>a</sup>	17.7
714	1.03	0.0175	58,000 <sup>a</sup>	17.5
750	1.85	0.0282	...	(16.8) <sup>b</sup>
800	3.78	0.0507	...	(16.2) <sup>b</sup>
850	7.11	0.0844	...	(15.6) <sup>b</sup>
900	12.45	0.1319	5,200	14.9
950	20.6	0.1958	3,130	14.1
1000	32.3	0.2771	1,960	13.2
1050	48.6	0.3782	1,260	12.1
1100	70.4	0.4997	775	10.3
1120	81.0	0.5538	617	9.3
1140	92.6	0.6114	468	7.9
1160	105.5	0.6726	313	5.9
1170	112.3	0.7038	218	4.4
1178 ( $T_c$ )	(118.1)	...	(0)	(0)

<sup>a</sup>  $V_g$  calculated from ideal gas relationship. <sup>b</sup> Values interpolated from curve.

# Carbon-13 Magnetic Resonance Study of Alkyl Cyanides, Isocyanides, Isocyanates, and Isothiocyanates

by Gary E. Maciel and David A. Beatty

Department of Chemistry, University of California, Davis, California (Received June 7, 1965)

The  $C^{13}$  chemical shifts of the simple alkyl cyanides, isocyanates, and isothiocyanates as well as the cyanate and thiocyanate ions were found to cover the range of  $-5.7$  to  $10.8$  p.p.m. (with respect to benzene), while the  $C^{13}$  shifts of the simple alkyl isocyanides and cyanide ion range from  $-28$  to  $-40$  p.p.m. These shifts seem to reflect familiar similarities between the valence-bond descriptions of these compounds and those of carbon dioxide ( $3.7$  p.p.m.) or carbon monoxide ( $-53.4$  p.p.m.). In the methyl compounds the methyl  $C^{13}$  shifts vary monotonically but not linearly with the shifts of the other carbon in the molecule, covering the range from  $99$  to  $128$  p.p.m.

## Introduction

The molecular structures of simple alkyl cyanides, isocyanides, isocyanates, and isothiocyanates have served as interesting subjects of investigation by a variety of physical techniques. Infrared<sup>1-11</sup> investigations and microwave studies<sup>12-13</sup> have been carried out on the methyl compounds in these classes, and useful structural information has been derived. In addition, Raman<sup>1-3,9</sup> and/or electronic<sup>2</sup> spectra have been determined for some of these compounds.

Pauling, Wheland, and others<sup>3,8,9,16,19-22</sup> have interpreted the data from these and other physical measurements in terms of the valence-bond structures assigned to the compounds, and various relationships between their proposed structures and between these and the structures of carbon monoxide and carbon dioxide have been formulated. Recently, infrared evidence indicating hydrogen bonding of hydroxyl hydrogens to the carbon atoms of isocyanide groups has been presented,<sup>23,24</sup> and the application of organic cyanides and isocyanides as ligands in transition metal complexes has recently been established.<sup>25-27</sup>

In the light of the considerable qualitative success with which carbon-13 chemical shifts have been correlated to electronic structural properties in some classes of compounds such as substituted benzenes,<sup>28</sup> carbonyl compounds,<sup>29-32</sup> vinyl compounds,<sup>33</sup> and substituted ethanes and methanes,<sup>34</sup> we have determined the  $C^{13}$  magnetic resonance spectra of methyl, ethyl,

and cyclohexyl compounds of the alkyl cyanide, isocyanide, isocyanate, and isothiocyanate systems, as well as their related anions. Some interesting trends

- (1) F. A. Miller and W. B. White, *Z. Elektrochem.*, **64**, 7017 (1960).
- (2) C. N. Ramachandra Rao, J. Ramachandran, and S. Somasekhara, *Current Sci. (India)*, **27**, 474 (1958).
- (3) A. J. Castoulas and R. L. Werner, *Australian J. Chem.*, **12**, 601 (1959).
- (4) R. L. Williams, *J. Chem. Phys.*, **25**, 656 (1956).
- (5) D. J. David, *Anal. Chem.*, **35**, 37 (1963).
- (6) G. L. Caldow and H. W. Thompson, *Spectrochim. Acta*, **13**, 212 (1958).
- (7) J. P. Jesson, H. W. Thompson, *ibid.*, **13**, 217 (1958).
- (8) E. Lieber, C. N. R. Roa, and J. Ramachandran, *ibid.*, **13**, 296 (1959).
- (9) N. S. Ham and J. B. Willis, *ibid.*, **16**, 279 (1960).
- (10) H. W. Thompson and R. L. Williams, *Trans. Faraday Soc.*, **48**, 502 (1952).
- (11) M. G. Krishna Pillai and F. F. Cleveland, *J. Mol. Spectry.*, **5**, 212 (1960).
- (12) S. N. Ghosh, R. Tambarulo, and W. Gordy, *J. Chem. Phys.*, **21**, 308 (1953).
- (13) C. C. Costain, *ibid.*, **29**, 864 (1958).
- (14) R. F. Curl, Jr., V. M. Roa, K. V. N. Sastry, and J. A. Hodgson, *ibid.*, **39**, 3335 (1963).
- (15) H. H. Nielsen, *Phys. Rev.*, **77**, 130 (1950).
- (16) M. Kessler, H. Ring, R. Tambarulo, and W. Gordy, *ibid.*, **79**, 54 (1950).
- (17) C. I. Beard and B. P. Dailey, *J. Am. Chem. Soc.*, **71**, 929 (1949).
- (18) T. S. Jaseja, *Proc. Indian Acad. Sci.*, **50A**, 108 (1959).
- (19) L. Pauling, "The Nature of the Chemical Bond," Cornell University Press, Ithaca, N. Y., 3rd Ed., 1960, pp. 265-274, 331-338.

in chemical shift emerge which corroborate the ideas previously stated regarding analogies in electronic structures.<sup>19,20</sup>

### Experimental Section

**Materials.** Cyclohexyl cyanide was prepared from cyclohexanecarboxylic acid *via* the acid chloride and amide. The final step was accomplished by refluxing the amide in toluene with a twofold excess of phosphorus oxychloride for 1 hr. The organic mixture was decanted from solids and distilled, affording a colorless liquid, b.p. 80–81° (19 mm.),  $n_{D}^{24}$  1.4502 [lit.<sup>35,36</sup> b.p. 75–76 (16 mm.),  $n_{D}^{19}$  1.4515<sup>35</sup>; b.p. 69–70 (12 mm.),  $n_{D}^{25}$  1.4497<sup>36</sup>].

Methyl isocyanide was prepared by an adaptation of the method reported by Jackson and McKusick<sup>37</sup> for the preparation of ethyl isocyanide, involving the reaction of methyl iodide with silver cyanide, and the treatment of the resulting complex with aqueous potassium cyanide. Distillation afforded a nearly colorless material, b.p. 56–59° [lit.<sup>4</sup> 59–60°], which was found by gas chromatography to be contaminated by about 15% methyl iodide.

Ethyl isocyanide was prepared by the method of Jackson and McKusick,<sup>37</sup> affording a colorless liquid, b.p. 77–79° [lit.<sup>37</sup> b.p. 77–79°].

The following reagents were used as obtained from their suppliers: cyclohexyl isocyanide and cyclohexyl isothiocyanate were obtained from Aldrich Chemical Co., cyclohexyl isocyanate from K and K Laboratories; ethyl isocyanate was an Eastman Practical chemical (redistilled, b.p. 60–61°); ethyl isothiocyanate, methyl isothiocyanate, methyl isocyanate, and propionitrile were Eastman White Label samples; and the acetonitrile, potassium cyanide, potassium cyanate, and potassium thiocyanate were J. T. Baker reagents.

**N.m.r. Spectra.** The carbon-13 magnetic resonance spectra were obtained at a fixed frequency of 15.1 Mc./sec. by measuring natural abundance C<sup>13</sup> resonance, using dispersion mode and rapid passage conditions as described by Lauterbur.<sup>38</sup> Details of the procedure are reported elsewhere.<sup>39</sup> The results may be considered reliable to about ±0.8 p.p.m. All chemical shifts were determined on neat liquids except those of potassium cyanide, potassium cyanate, and potassium thiocyanate which were obtained as saturated aqueous solutions. In order to estimate the possible effect of the methyl iodide contaminant on the methyl isocyanide spectrum, we obtained the chemical shifts of acetonitrile both neat and in a 1:1 mixture with methyl iodide. Within the limits of experimental error no medium effect was detected.

### Results

The principal peaks of interest in the C<sup>13</sup> spectra of the compounds of this study were those due to the resonance of the carbon atom of the cyanide, isocyanide, isocyanate, or isothiocyanate groups. These peaks were found in approximately the same region of the spectrum as those due to the resonance of aromatic carbons, and covered a range from –39.9 p.p.m. with respect to benzene for the cyanide ion to 10.8 p.p.m. for acetonitrile. Peaks due to the alkyl groups were also observed and in the case of methyl compounds the simple multiplet structure and relatively favorable signal-to-noise ratios permitted reliable determinations of the corresponding shifts. These were found to range from 99.2 p.p.m. for methyl isocyanide to 128.2 p.p.m. for acetonitrile. These chemical shift data are collected in Table I and in Table II, which includes some relevant data from other sources.<sup>40–42</sup>

The only shifts in Table I which have appeared previously in the literature are those of acetonitrile, and there appear to be larger discrepancies than one would anticipate from expected experimental error of

(20) G. W. Wheland, "Resonance in Organic Chemistry," John Wiley and Sons, Inc., New York, N. Y., 1955, pp. 111–115, 156, 180–182.

(21) J. W. Linnett, *Nature*, **199**, 168 (1963).

(22) R. G. Gillis, *J. Org. Chem.*, **27**, 4103 (1962).

(23) L. L. Ferstandig, *J. Am. Chem. Soc.*, **84**, 1322 (1962).

(24) A. Allerhand and P. von R. Schleyer, *ibid.*, **85**, 866 (1963).

(25) L. Malatesta, *Progr. Inorg. Chem.*, **1**, 283 (1959).

(26) T. L. Brown and M. Kubota, *J. Am. Chem. Soc.*, **83**, 331 (1961).

(27) T. L. Brown and M. Kubota, *ibid.*, **83**, 4175 (1961).

(28) G. E. Maciel and J. J. Natterstad, *J. Chem. Phys.*, **42**, 2427 (1965), and reference therein.

(29) G. E. Maciel and J. J. Natterstad, *ibid.*, **42**, 2752 (1965), and references therein.

(30) D. H. Marr and J. B. Stothers, *Can. J. Chem.*, **43**, 596 (1965), and references therein.

(31) J. B. Stothers and P. C. Lauterbur, *ibid.*, **42**, 1563 (1964).

(32) G. B. Savitsky, K. Namikawa, and G. S. Zweifel, *J. Phys. Chem.*, **69**, 3105 (1965).

(33) G. E. Maciel, *ibid.*, **69**, 1947 (1965).

(34) H. Spiesscke and W. G. Schneider, *J. Chem. Phys.*, **35**, 722 (1961).

(35) R. Paul and S. Tchelitcheff, *Bull. soc. chim. France*, 470 (1949).

(36) S. M. McElvain and R. E. Starn, Jr., *J. Am. Chem. Soc.*, **77**, 4571 (1955).

(37) H. L. Jackson and B. C. McKusick, *Org. Syn.*, **35**, 62 (1955).

(38) P. C. Lauterbur, *J. Am. Chem. Soc.*, **83**, 1838 (1961).

(39) C. P. Nash and G. E. Maciel, *J. Phys. Chem.*, **68**, 832 (1964).

(40) R. Etinger, P. Blume, A. Patterson, Jr., and P. C. Lauterbur, *J. Chem. Phys.*, **33**, 1597 (1960).

(41) D. D. Traficante and G. Maciel, *J. Phys. Chem.*, **69**, 1348 (1965).

(42) R. A. Friedel and H. L. Retcofsky, *J. Am. Chem. Soc.*, **85**, 1300 (1963).

**Table I:**  $C^{13}$  Chemical Shifts of Alkyl Cyanides, Isocyanides, Isocyanates, and Isothiocyanates, P.p.m. with Respect to Benzene

Alkyl group	$\delta_{CN}$	$\delta_{NC}$	$\delta_{NCO}$	$\delta_{NCS}$
Cyclohexyl	7.1	-28.0	5.0	-3.7
Ethyl	7.7	-27.7	6.1	-2.1
Methyl ( $\delta_{CH_3}$ ) <sup>a</sup>	10.8 (128.2)	-30.0 (99.2)	7.2 (102.4)	0.0 (99.4)

<sup>a</sup> The numbers in parentheses represent  $\delta_{CH_3}$ .

**Table II:** Some Relevant  $C^{13}$  Chemical Shifts, P.p.m. with Respect to Benzene

$CO_2$	$CO$	$CS_2$	$(CN)^-$
3.7 <sup>a</sup>	-53.4 <sup>a</sup>	-65.0 <sup>b,c</sup>	-39.9 <sup>c,f</sup>
$(NCO)^-$	$(NCS)^-$	$n-C_4H_9-C \equiv C^{13}-CH_3$	$CH_3-C \equiv C-C^{13}H_3$
-1.1 <sup>c,f</sup>	-5.7 <sup>c,f</sup>	48.7 <sup>d</sup>	125 <sup>e</sup>

<sup>a</sup> Data from ref. 40. <sup>b</sup> Data from ref. 43. <sup>c</sup> Present work.

<sup>d</sup> Data from ref. 41, average shifts of  $\alpha$  and  $\beta$  carbons. <sup>e</sup> Data from ref. 42. <sup>f</sup> Data obtained on saturated aqueous solutions of the potassium salts.

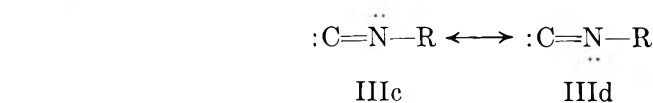
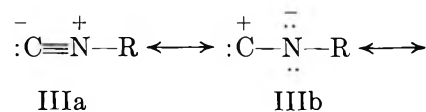
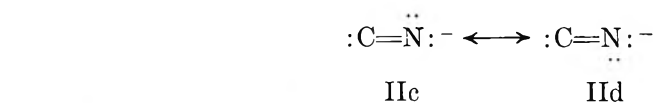
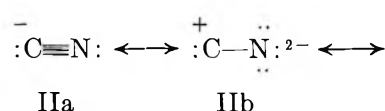
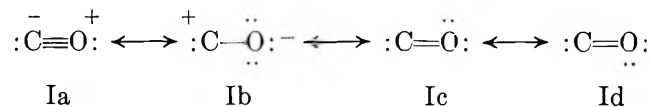
the dispersion mode, rapid passage method.<sup>34,43,44</sup> Frei and Bernstein<sup>44</sup> determined the chemical shifts for acetonitrile on a sample which was doubly labeled with carbon-13, using the more precise absorption mode technique. Their results, 10.4 and 127.8 p.p.m. with respect to benzene for the cyanide and methyl carbons, respectively, agree with our values reported in Table I within our experimental error.

## Discussion

Examination of the shifts in Tables I and II reveals that exclusive of carbon disulfide and acetylenic and methyl carbons which are considered in later sections, the carbon groups studied in this investigation can be separated into two classes, within which electronic similarities might be expected: (a) the group consisting of carbon monoxide, cyanide ion, and alkyl isocyanides with chemical shifts in the range -28 to -53 p.p.m., and (b) the group consisting of carbon dioxide, alkyl cyanides, isocyanates, and isothiocyanates, and the cyanate and thiocyanate ions with chemical shifts in the range -10 to 11 p.p.m. These groups are discussed separately below.

*Species of the CO Type.* Pauling,<sup>19</sup> Wheland,<sup>20</sup> and others<sup>25</sup> have pointed out the similarities in formulas and chemical properties among the "terminal carbon" species carbon monoxide, cyanide ion, and organic isocyanides. All three can be formally repre-

sented by the analogous resonance hybrids of I, II, and III, where R represents an alkyl group.



In each case, presumably the most important contributor is an a-structure, with a formal charge of -1 and a local electron density approaching 5 on the terminal carbon. The remaining species listed in Table I and II cannot be represented reasonably in this manner. From the available physical data, Pauling<sup>19</sup> has estimated that structure Ia contributes 50% to the electronic state of carbon monoxide, with the equivalent structures Ic and Id each contributing 20% and Ib contributing 10%. Similarly, he has estimated that the contribution of IIIa to methyl isocyanide is 74% with IIIc and IIId contributing 13% each. Since the formulas derived by Karplus<sup>45</sup> and Pople<sup>45,46</sup> for the dominant paramagnetic contribution to  $C^{13}$  chemical shifts show a general increase of shielding with increasing local electron density (assuming other factors such as average electronic excitation energies remain constant), one might expect the largest shielding among the series I, II, III, for the species with the highest contribution from the corresponding a-structure. If one is willing to place the relative importance of IIa intermediate between that of Ia and IIIa for their respective species, then the observed shifts appear consistent with Pauling's representations. That IIa and IIIa should be more important contributors than Ia to their corresponding species seems reasonable

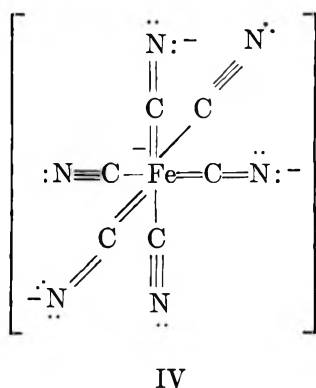
(43) P. C. Lauterbur, *J. Chem. Phys.*, **26**, 217 (1957).

(44) K. Frei and H. J. Bernstein, *ibid.*, **38**, 1216 (1963).

(45) M. Karplus and J. A. Pople, *ibid.*, **38**, 2803 (1963).

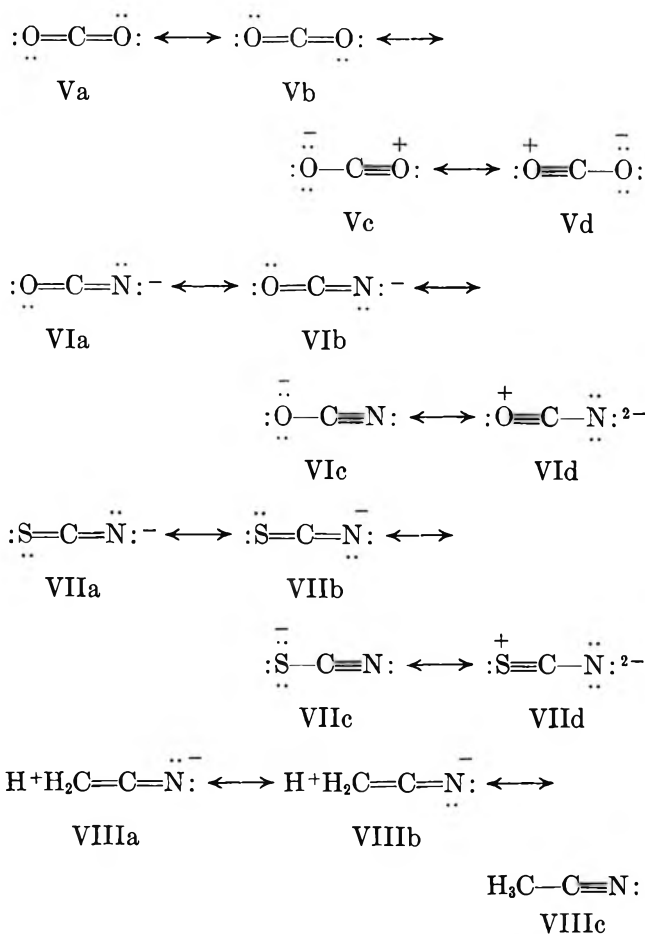
(46) J. A. Pople, *Mol. Phys.*, **7**, 301 (1964).

in terms of Pauling's estimates, and since the great electronegativity of a formally positive oxygen would seem to render Ib, Ic, and Id (none of which have formally doubly charged atoms) more important than their analogs in II and III. The relative importance of IIa to II compared to IIIa to III is more difficult to predict. The implication of the C<sup>13</sup> data, that IIIa may make a greater contribution to III than IIa does to II, is difficult to rationalize in terms of expected favorable charge distributions; however, a rather large contribution of IIc and IId to II seems consistent with the rather large contribution of analogous structures often attributed to transition metal complexes, as represented by the structure IV for the ferro-



cyanide ion.<sup>19</sup> Similarly, a CN double-bond character of about 50% has been proposed to account for the spectroscopically determined molecular geometry of the octahedral complex [Fe(CNCH<sub>3</sub>)<sub>6</sub>]<sup>2+</sup> between methyl isocyanide and Fe<sub>II</sub>.<sup>19</sup> In any case, the C<sup>13</sup> chemical shifts of species II and III differ only by about 11 p.p.m., and other factors such as average electronic excitation energies<sup>45,46</sup> would have to be taken into account in any complete explanation. Solvent effects may also play a role.

*Species of the CO<sub>2</sub> Type.* In this section we consider the C<sup>13</sup> chemical shifts of species of the type XCY, in which the central carbon atom bears zero formal charge in the most important contributor. Presumably, the central carbon atom is sp hybridized in all these species and the three central atoms are collinear in each case. Wheland<sup>20</sup> has expressed the opinion that organic isocyanates are structurally somewhat analogous to carbon dioxide. Also, the cyanate and thiocyanate ions are isoelectronic with carbon dioxide, and alkyl cyanides bear some resemblance in electronic structure. These similarities can be summarized in the corresponding resonance hybrid formulations V, VI, VII, and VIII.<sup>19,20</sup> The alkyl isocyanates or isothiocyanates



can be thought of in terms of the formula VI or VII if one considers replacing an appropriately situated electron pair on nitrogen by a covalent bond to an alkyl group, with the consequent increase of the formal charge on nitrogen by unity; of course, the resulting alkyl analog of VIc or VIIc would be especially unstable because of the nonlinearity of the OCNC or SCNC system.<sup>19,20</sup>

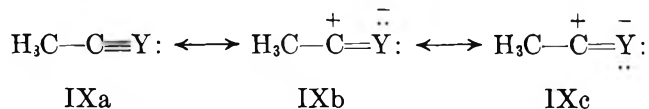
Pauling<sup>19</sup> has concluded from physical measurements on carbon dioxide that the normal state of the molecule can be described as arising from about a 25% contribution of each of the structures indicated for V, and that the experimentally determined dimensions of methyl isothiocyanate are compatible with what one would expect for resonance among the three most stable structures VIId, VIIfc, and VIIa or VIIb (depending on the orientation of the methyl group). For the latter compound, a controversy has existed concerning the interpretation of vibrational spectra with regard to the importance of the structure corresponding to VIIfc.<sup>3,8,9,47</sup> For isocyanic acid, Pauling concluded

(47) J. H. Hibben, "The Raman Effect and its Chemical Applications," Reinhold Publishing Corp., New York, N. Y., 1939, p. 283.

that the physical properties could be explained by assuming approximately equal contributions from the structures VIId and VIb or VIa, with VIc making a slightly smaller contribution because the H-N-C bond angles is only 128°. For methyl cyanide, he estimated that structures of the type VIIIa and VIIIb contribute a total of about 17%, the remaining contribution made by structures VIIIc. Thus all of these species can be represented as resonance hybrids between structures which have central carbons with a formal charge of zero and a formal electron density of four.

In view of the preceding discussion of the similarities in electronic structure between alkyl cyanides, isocyanates, isothiocyanates, carbon dioxide, and the cyanate and thiocyanate ions, it is not surprising to find the C<sup>13</sup> chemical shifts of these species covering a range of only about 16 p.p.m. Again, a satisfactory explanation of these small differences would require consideration of polar effects and electronic excitation energies,<sup>45,46</sup> as well as medium effects. One perplexing feature of the data of Tables I and II is the extremely low chemical shift of carbon disulfide compared to the shifts of the other species under discussion in this section. Thus, the shift of carbon disulfide is seen to be nearly 70 p.p.m. lower than that of carbon dioxide. In view of their similar electronic structures, this might not have been anticipated, especially since the expected difference in the bond polarities between these two compounds would seem to predict a chemical shift difference of the opposite sign. Most likely, the explanation of the observed shift difference is due to a much smaller average electronic excitation energy  $\Delta E$  for carbon disulfide. The factor  $(\Delta E)^{-1}$  occurs in each term of the expression derived by Karplus and Pople for  $\Delta\sigma_p$ , the local paramagnetic term for the electronic shielding of a carbon-13 nucleus.<sup>45,46</sup> Since this term is expected to dominate the shifts, a smaller value of  $\Delta E$  (which leads to a larger magnitude for  $\Delta\sigma_p$ ), gives rise to a lower shielding or chemical shift value. While it is usually difficult to estimate *a priori* a reasonable value for  $\Delta E$ , the evidence seems qualitatively satisfactory for a comparison of  $\Delta E$  for carbon disulfide and carbon dioxide. The latter compound is found to have electronic absorption only in the far-ultraviolet region<sup>48,49</sup> (1475, 1332, 1121 Å., etc.), whereas carbon disulfide is found to exhibit electronic absorptions in the near-ultraviolet region<sup>50-53</sup> (3500, 3300 Å.). Thus the much lower shift of carbon disulfide can be rationalized.

It is also worth noting that a considerable difference exists between the C<sup>13</sup> chemical shifts of similarly substituted nitrile and acetylenic carbons for which resonance structures formally analogous to VIII can be written. Perhaps this difference, about 38 p.p.m. for the methyl-substituted case, can be rationalized more satisfactorily by attributing it to the different polarities of the corresponding triple bonds, as represented in the structures IX. One would expect a



greater contribution of the energetically equivalent structures IXb and IXc and a correspondingly lower chemical shift (larger magnitude for  $\sigma_p$ ) when Y: is the more electronegative N: rather than the less electronegative C(CH<sub>2</sub>)<sub>3</sub>CH<sub>3</sub>.

*Alkyl Groups.* Table I displays a monotonic relationship between the methyl C<sup>13</sup> chemical shifts and the shifts of the corresponding carbon atoms in the groups to which they are attached. While the relationship is by no means linear, it may indicate a predominant influence of magnetic anisotropy in these linear or pseudo-linear systems. Thus, in a case of true axial electronic symmetry, as with isocyanide and cyanide substituents, the resulting increase in chemical shift due to the zero value of  $\sigma_{pz}$  would be manifested in the same sense all along the molecular axis.<sup>54</sup> While the electronic distributions in the isocyanate and isothiocyanate groups are not axially symmetrical, the still-present group magnetic anisotropy may give similar effects at both carbon nuclei, especially if the methyl groups do not lie too far from the NCO or NCS axis. Of course the inductive and resonance influences of these groups on the electron density of the methyl carbon may also be important.

(48) S. F. Mason, *Quart. Rev.* (London), 15, 287 (1961).

(49) E. C. Y. Inn, K. Watanabe, and M. Zelkoff, *J. Chem. Phys.*, 21, 1648 (1953).

(50) J. W. Sidman, *J. Phys. Chem.*, 61, 253 (1957).

(51) L. N. Liebermann, *Phys. Rev.*, 59, 106 (1941).

(52) L. N. Liebermann, *ibid.*, 60, 496 (1941).

(53) V. K. Wieldand, *Helv. Phys. Acta*, 31, 555 (1958).

(54) J. A. Pople, W. G. Schneider, and H. J. Bernstein, "High-Resolution Nuclear Magnetic Resonance," McGraw-Hill Book Co., Inc., New York, N. Y., 1959, pp. 178-180.

# Carbon-13 Magnetic Resonance Study of Some Saturated Heterocyclic Compounds<sup>1</sup>

by Gary E. Maciel and George B. Savitsky

Department of Chemistry, University of California, Davis, California (Received June 14, 1966)

Carbon-13 chemical shifts are reported for compounds of the type  $X(\text{CH}_2)_n$  with  $n = 2, 3, 4,$  and  $5$  for  $X = \text{O}$  and  $\text{S}$ , and for  $n = 2, 3, 4, 5,$  and  $6$  for  $X = \text{NCH}_3$ . In each series the largest shielding for the carbon atom adjacent to the heteroatom occurs for  $n = 2$  in agreement with the behavior of cycloalkanes, for which a large ring-current effect has been postulated to account for large positive C<sup>13</sup> and proton shifts in cyclopropane. This three-membered ring effect seems to be smallest for  $X = \text{S}$ , presumably because of a significant deviation from cyclopropane-type geometry. Aside from the high-field proton and carbon resonances for three-membered rings, the proton and carbon shifts of given methylene groups exhibit considerably different behaviors.

## Introduction

Small ring heterocyclic compounds have proved to be interesting subjects for a variety of physical and chemical investigations.<sup>2-6</sup> In particular, three-, four-, five-, and six-membered saturated heterocycles with nitrogen, oxygen, and sulfur as the heteroatoms have been studied by a variety of techniques including proton magnetic resonance spectroscopy.<sup>7-14</sup> In an early application of the concept of chemical shifts, Gutowsky and co-workers<sup>7</sup> used proton shifts to investigate the effects of ring size on the electron distribution of the simple three-, four-, and five-membered compounds in the saturated oxygen, sulfur, and nitrogen (NH) heterocycles. They concluded that observed trends in proton chemical shifts reflect the variations in local electron density and agree with observed orders of basicity.<sup>2-4</sup> More recently, Lippert and Prigge have reported a proton magnetic resonance investigation of these same heterocycles as well as their cycloalkane counterparts.<sup>14</sup> They have measured both chemical shifts and C<sup>13</sup>-proton spin-spin coupling constants, and have accounted for the results in terms of the influence of the heteroatom and ring size on hybridization parameters and local electron densities. Burke and Lauterbur<sup>10</sup> have reported the proton and carbon-13 chemical shifts and the C<sup>13</sup>-proton spin-spin coupling constants in cycloalkanes with ring size

varying from three to fifteen methylene groups. They interpreted the fact that the highest-field proton and carbon resonances occur with cyclopropane to a diamagnetic ring-current effect due to the specific electronic distribution in that system. This view is in agreement with similar previous rationalizations of high proton chemical shifts in cyclopropanes.<sup>8,9</sup>

We have measured the C<sup>13</sup> chemical shifts of some saturated heterocyclic compounds with sulfur, nitrogen,

- (1) Supported by a grant from the Research Corporation.
- (2) H. C. Brown and M. Gerstein, *J. Am. Chem. Soc.*, **72**, 2926 (1950).
- (3) S. Searles and M. Tamres, *ibid.*, **73**, 3704 (1951).
- (4) S. Searles, M. Tamres, and E. R. Lippincott, *ibid.*, **75**, 2775 (1953).
- (5) E. Lippert and H. Prigge, *Ber. Bunsenges. physik. Chem.*, **67**, 554 (1963).
- (6) C. A. Coulson and W. E. Moffitt, *Phil. Mag.*, **40**, 1 (1949).
- (7) H. S. Gutowsky, R. L. Rutledge, M. Tamres, and S. Searles, *J. Am. Chem. Soc.*, **76**, 4242 (1954).
- (8) D. J. Patel, M. E. H. Howden, and J. D. Roberts, *ibid.*, **85**, 3218 (1963).
- (9) K. B. Wiberg and B. J. Nist, *ibid.*, **83**, 1226 (1961).
- (10) J. J. Burke and P. C. Lauterbur, *ibid.*, **86**, 1870 (1964).
- (11) C. A. Reilly and J. D. Swalen, *J. Chem. Phys.*, **32**, 1378 (1960).
- (12) C. A. Reilly and J. D. Swalen, *ibid.*, **35**, 1522 (1961).
- (13) N. Sheppard and J. J. Turner, *Proc. Roy. Soc. (London)*, **A252**, 506 (1959).
- (14) E. Lippert and H. Prigge, *Ber. Bunsenges. physik. Chem.*, **67**, 415 (1963).



and oxygen as the heteroatoms with the aim of contributing to the understanding of the electronic distributions and magnetic resonance properties of these systems.

### Experimental Section

**Materials.** The acetonitrile and tetrahydrofuran were J. T. Baker reagents. Methyl iodide, trimethylene sulfide, ethylene oxide, and dimethyl carbonate were Eastman White Label samples. Trimethylene oxide, pentamethylene oxide, pentamethylene sulfide, tetramethylene sulfide, N-methylethylenimine, ethylene sulfide (redistilled, b.p. 55–56°), and 1,3-dioxane were from K and K Laboratories. N-methylpyrrolidine, N-methylpiperidine, cyclopropyl cyanide, and methyl cyclopropyl ketone were from Aldrich Chemical Co; and N-methyl trimethyleneimine and N-methyl hexamethyleneimine were kindly provided by Professor A. T. Bottini.

**Carbon-13 Magnetic Resonance Measurements.** The carbon-13 n.m.r. spectra were obtained at a frequency of 15.085 Mc./sec. by measuring  $C^{13}$  resonances in natural abundance on neat samples (except for ethylene oxide as noted below). Dispersion mode, rapid passage conditions as previously described by Lauterbur<sup>15</sup> were employed. The sample container was similar to that described by Spiesscke and Schneider<sup>16</sup> except for the absence of provision for spinning the sample, and consisted of two concentric thin-walled spherical bulbs, containing about 0.025 and 1.5 cc. in volume, a geometry which eliminates the need for bulk susceptibility corrections in these measurements. The small inner bulb (about 0.040-cc. outer volume) contained the reference, a saturated aqueous solution of sodium acetate enriched to 55% at the carbonyl carbon. The calibration of this reference was carried out by the previously reported procedure,<sup>17</sup> yielding a value of -54.2 p.p.m. with respect to benzene. Although side-band calibration of each spectrum was not possible due to the rather low intensity of the small reference sample, chart calibration was accomplished by frequent repetition of the spectrum of dimethyl carbonate for which the internal chemical shift is known to be 102.7 p.p.m.<sup>18</sup> During the entire period within which the data reported in this paper were obtained (about 3 days), only small, random statistical fluctuations in the chart calibration (p.p.m./cm.) were observed, and we believe that the shifts reported in Tables I and II constitute a self-consistent set of data with an internal reproducibility of about  $\pm 0.2$  p.p.m. (except for the shifts reported in parentheses).

The chemical shift for ethylene oxide, which has b.p. 11° (760 mm.), was obtained on a sample con-

sisting of a 1:1 (volume) solution of ethylene oxide and dimethyl carbonate which was sealed in a 15-mm. test tube at 0°. The use of dimethyl carbonate as a solvent and internal reference has been discussed previously.<sup>18</sup>

### Results

Carbon-13 magnetic resonance spectra were obtained of the three-, four-, five-, and six-membered ring compounds of the polymethylene oxide and sulfide series and of the three-, four-, five-, six-, and seven-membered ring compounds of the N-methylpolymethylenimine series. In addition, the  $C^{13}$  spectra of 1,3-dioxane and 1,4-dioxane were obtained for comparison. In most cases the peak assignments were straightforward because of clearly separated multiplets of the expected forms and intensities. However, in a few cases, where certain peaks overlapped, the assignments were made on the basis of assuming reasonable values for  $J_{C-H}$  and recognizing the multiplets in that manner. For example, the  $C^{13}$  spectra of tetramethylene sulfide and pentamethylene sulfide each consisted of only one intense triplet, indicating virtually complete overlap of the two triplets expected for the  $\alpha$  and  $\beta$  (and  $\gamma$  in the latter case) carbons. In the case of pentamethylene sulfide the peaks were quite broad, so that the derived shifts are uncertain by about 2.5 p.p.m. and are indicated in parentheses in Table I. In those cases where overlap was not complete, at least two components of each triplet and three components of each quartet were visible in the spectra, allowing meaningful assignments and permitting the derivation of all shifts. The resulting chemical shift data are collected in Tables I and II.

Of the shifts reported in this paper, only two had appeared previously in the literature, those of ethylene oxide (92 p.p.m.)<sup>19</sup> and 1,4-dioxane (61 p.p.m.).<sup>20</sup> For the latter compound the agreement with our value in Table I is excellent, and for the former compound it may be considered satisfactory, considering the difference in techniques for standardization with respect to a common reference. As might be anticipated, the shifts for N-methylethylenimine, N-methylpyrrolidine, and N-methylpiperidine reported in Table I are within a few p.p.m. of the corresponding

(15) P. C. Lauterbur, *J. Am. Chem. Soc.*, **83**, 1838 (1961).

(16) H. Spiesscke and W. G. Schneider, *J. Chem. Phys.*, **35**, 722 (1961).

(17) C. P. Nash and G. E. Maciel, *J. Phys. Chem.*, **68**, 832 (1964).

(18) G. E. Maciel and J. J. Natterstad, *J. Chem. Phys.*, **42**, 2752 (1965).

(19) C. H. Holm, *ibid.*, **26**, 707 (1957).

(20) P. C. Lauterbur, *ibid.*, **26**, 217 (1957).

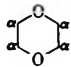
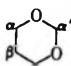
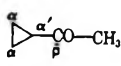
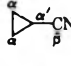
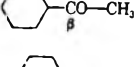
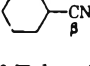


**Table I:** Carbon-13 Chemical Shifts in Compounds of the Type  $\text{X}(\text{CH}_2)_n$ , P.p.m. with Respect to Benzene

$n$	$\text{X} = \text{CH}_2$		$\text{X} = \text{O}$			$\text{X} = \text{S}$			$\text{X} = \text{NCH}_3$			
	$\delta_{\text{C}^\alpha}$	$\delta_{\text{C}^\beta}$	$\delta_{\text{C}^\alpha}$	$\delta_{\text{C}^\beta}$	$\delta_{\text{C}^\gamma}$	$\delta_{\text{C}^\alpha}$	$\delta_{\text{C}^\beta}$	$\delta_{\text{C}^\gamma}$	$\delta_{\text{C}^\alpha}$	$\delta_{\text{C}^\beta}$	$\delta_{\text{C}^\gamma}$	$\delta_{\text{CH}_3\text{N}}$
2	131.3	89.0				109.8			100.0			79.9
3	105.4	55.9	105.6			101.0	98.8		70.8	111.0		82.1
4	102.2	60.1	102.0			(96.0) <sup>c</sup>	(96.0) <sup>c</sup>		71.8	104.1		85.8
5	100.9	59.0	100.8	103.6		(99.1) <sup>d</sup>	(99.1) <sup>d</sup>	(99.1) <sup>d</sup>	71.3	102.1	102.1	80.8
6	99.7								69.6	100.0	100.0	80.5

<sup>a</sup> Shifts from ref. 10. <sup>b</sup> The subscripts  $\alpha$ ,  $\beta$ ,  $\gamma$  refer to positions relative to the heteroatom. <sup>c</sup> Reliable to only about  $\pm 1$  p.p.m. because of peak overlap. <sup>d</sup> Reliable to only about  $\pm 2.5$  p.p.m. because of peak overlap.

**Table II:** Chemical Shifts of Some Pertinent Compounds, P.p.m. with Respect to Benzene

	$\delta_{\text{C}^\alpha}$	$\delta_{\text{C}^{\alpha'}}$	$\delta_{\text{C}^\beta}$	$\delta_{\text{CH}_3}$
	60.9			
	61.0	33.7	101.0	
	118.3	106.8	-79.2	98.6
	121.3	131.8	5.0	
			-80.6 <sup>a</sup>	
			7.1 <sup>b</sup>	

<sup>a</sup> Taken from ref. 25. <sup>b</sup> Taken from ref. 26.

C<sup>13</sup> shifts previously reported for the analogous N-phenyl-substituted compounds.<sup>17</sup>

## Discussion

The main feature apparent from the data of Table I is the fact that in each series of compounds the three-membered ring substance gives the highest C<sup>13</sup> chemical shift. This is in agreement with case of C<sup>13</sup> shifts in cycloalkanes reported by Burke and Lauterbur.<sup>10</sup> It is also in line with the results reported by Lippert and Prigge<sup>14</sup> for the proton shifts in cycloalkanes and a series of saturated heterocyclic compounds similar to those employed in this investigation. In the cases of the nitrogen and oxygen heterocycles, the differences between the C<sup>13</sup> shifts for the three-membered ring compounds and the  $\alpha$ -C<sup>13</sup> shifts of the six-membered ring compounds are 28.7 and 30.0 p.p.m., respectively, nearly the same as the difference between the C<sup>13</sup>

shifts of cyclopropane and cyclohexane, 30.4 p.p.m. However, in the case of the sulfur heterocycles, the corresponding difference is only 10.7 p.p.m. This behavior is also reflected in the proton shifts, where it has been reported that the corresponding differences are 1.22, 0.98, 1.35, and 0.25 p.p.m. between the proton resonance positions of the three-membered ring compounds and the  $\alpha$ -CH<sub>2</sub> resonances of the six-membered ring compounds of the type  $\text{X}(\text{CH}_2)_n$

X = CH<sub>2</sub>, O, NH, and S, respectively.<sup>14</sup> The data of Burke and Lauterbur<sup>10</sup> show that the effect of ring size on C<sup>13</sup> shifts in cycloalkanes does not seem to change for rings larger than cyclohexane, so that the C<sup>13</sup> shift in a saturated six-membered heterocycle may be considered to reflect the properties of an approximately unstrained heterocycle with "normal" substituted alkane hybridization. Then if the differences in  $\alpha$  chemical shifts between corresponding three-membered and six-membered saturated heterocycles are taken as measures of the combined influences of strain effects and ring currents in three-membered rings as compared to the corresponding six-membered system,<sup>21</sup> one might conclude that these effects give a rather smaller resultant for X = S than for X = NH, NCH<sub>3</sub>, O, or CH<sub>2</sub>. The quite similar ring geometries of ethylenimine, N-methylethylenimine, ethylene oxide, and cyclopropane, and differences in bond lengths and angles of ethylene sulfide would seem to lend support to that view.<sup>14</sup> Of the heteroatoms nitrogen, oxygen, and sulfur, only sulfur introduces large alterations in the geometry of the three-membered ring relative to that in cyclopropane. Thus, the ring perimeter (sum of atom-to-atom distances in the ring) and the CCX bond angles in cyclopropane (X = CH<sub>2</sub>), ethylene oxide (X = O), ethylenimine (X = NH), and ethylene sulfide (X =

(21) This is based on the questionable assumption that the substituent effect of the heteroatom is independent of strain and changes in hybridization, but may be taken as a reasonable first attempt at separating influences.

S) have been given as 4.53 Å. and 60°; 4.35 Å. and 59.2°; 4.46 Å. and 60.2°; and 5.13 Å. and 65.2°, respectively.<sup>14</sup>

Burke and Lauterbur<sup>10</sup> noted that the hydrogen and carbon shieldings in cyclopropane, relative to those in central methylene groups in long-chain *n*-alkanes are 1.0 and 33 p.p.m., respectively. They accounted for this high shielding in cyclopropane by means of a ring-current calculation based on a flow of 3.5 to 4.5 electrons in a circle of radius 1.10 Å. compared to the radial distance to each carbon from the midpoint of the molecule of 0.88 Å. One might expect that a ring-current of magnitude sufficient to produce such an effect should influence appreciably the shifts of carbon nuclei attached to a cyclopropane ring. However, calculations based on the formulas of Johnson and Bovey<sup>22</sup> show that with expected molecular geometries these effects would be too small to distinguish from other complications. Thus, the facts that the C<sup>13</sup> shift of the carbonyl group in methyl cyclopropyl ketone (-79.2 p.p.m.) and that of the cyanide group in cyclopropyl cyanide (5.0 p.p.m.) are typical of ordinary methyl alkyl ketones and alkyl cyanides<sup>23-26</sup> (see Table II) and that the C<sup>13</sup> shifts of the NCH<sub>3</sub> groups given in Table I show no conclusive trend cannot add any new information relevant to the question of ring-current influences due to cyclopropane rings.

The result with proton shifts<sup>7,14</sup> that four-membered ring compounds exhibited by far the lowest  $\alpha$ -proton shielding within each series is clearly not general in the case of carbon-13 chemical shifts. Thus only the oxygen and possibly nitrogen heterocycles appear to exhibit this behavior, while in the sulfur heterocycles and cycloalkanes the four-membered ring compounds have the second highest  $\alpha$ -C<sup>13</sup> shieldings in their respective series. Thus it is clear that methylene groups cannot be considered validly as virtual basic units in discussing proton and carbon-13 shifts, both of which must be considered separately, and that some explanations of proton chemical shifts based on consideration of local electron densities<sup>7,14</sup> on CH<sub>2</sub> do not seem to be directly applicable to the corresponding carbon resonances. This distinction in the behavior of the proton and C<sup>13</sup> resonances may be consistent with explanations of proton shifts which attempt to include the influence of ring size by considering its relationship to carbon hybridization,<sup>14</sup> since changes in hybridization might be expected to influence electron densities on carbon and hydrogen atoms of the methylene group in somewhat different fashions. It is perhaps more difficult to rationalize this distinction in terms of the earlier discussions based on the relative basicities of the heterocycles<sup>7</sup>; however, recent results indicate

some inconsistencies and hence uncertainties in these basicities.<sup>27</sup> Furthermore, correlations of proton chemical shifts with electron densities generally have not been entirely successful, presumably because these shifts are not determined by a single dominating influence, and because the low electron densities in the region of a hydrogen nucleus render it particularly susceptible to the influences of electron currents flowing in other parts of the molecule.<sup>28</sup> Correlations between chemical shifts and electron density have also been reported for C<sup>13</sup> resonances.<sup>15,16,24,29-33</sup> Such correlations may be of considerable promise from a theoretical point of view, since the C<sup>13</sup> shifts are dominated by a single term, the paramagnetic term, in the shielding tensor.<sup>34,35</sup> Perhaps the present results provide an example where a correlation of electron density seems more apparent with C<sup>13</sup> chemical shifts than with proton shifts. Thus, in discussing the relative proton shifts for a given ring size for compounds of the type  $\text{X}(\text{CH}_2)_n$  with X = CH<sub>2</sub>, O, S, and NH, Lippert and

Prigge called upon the inductive effect of the electronegative heteroatoms oxygen and nitrogen to account for the invariably lower shifts of the  $\alpha$  protons in the corresponding heterocycles compared to the cycloalkane counterparts.<sup>14</sup> Then, in order to explain the similar downfield  $\alpha$ -proton shifts caused by introduction of the heteroatom sulfur, with an electronegativity the same as that of carbon,<sup>36</sup> a change in carbon hybridization was postulated.<sup>14</sup> The case of the  $\alpha$ -C<sup>13</sup> chemical shifts reported here seems more straightforward in this respect, as the downfield shifts due to introduction of the heteroatom sulfur are far less than those due to nitrogen and oxygen. In fact, in the series  $\text{S}(\text{CH}_2)_n$

(22) C. E. Johnson, Jr., and F. A. Bovey, *J. Chem. Phys.*, **29**, 1012 (1958).

(23) P. C. Lauterbur, *ibid.*, **26**, 217 (1957).

(24) G. E. Maciel, *ibid.*, **42**, 2746 (1965).

(25) J. B. Stothers and P. C. Lauterbur, *Can. J. Chem.*, **42**, 1563 (1964).

(26) G. E. Maciel and D. A. Beatty, *J. Phys. Chem.*, **69**, 3920 (1965).

(27) C. P. Nash, private communication.

(28) J. A. Pople, W. G. Schneider, and H. J. Bernstein, "High-Resolution Nuclear Magnetic Resonance," McGraw-Hill Book Co., Inc., New York, N. Y., 1959, p. 175.

(29) P. C. Lauterbur, *Tetrahedron Letters*, **8**, 274 (1964).

(30) H. Spiesecke and W. G. Schneider, *ibid.*, **14**, 468 (1961).

(31) G. E. Maciel and J. J. Natterstad, *J. Chem. Phys.*, **42**, 2427 (1965).

(32) H. Spiesecke and W. G. Schneider, *ibid.*, **35**, 731 (1961).

(33) P. C. Lauterbur, *J. Am. Chem. Soc.*, **83**, 1846 (1961).

(34) J. A. Pople, *Mol. Phys.*, **7**, 301 (1964).

(35) M. Karplus and J. A. Pople, *J. Chem. Phys.*, **38**, 2803 (1963).

(36) L. Pauling, "The Nature of the Chemical Bond," 3rd Ed., Cornell University Press, Ithaca, N. Y., 1960, p. 90.

the only appreciable downfield shifts of the  $\alpha$  carbon resonance with respect to the corresponding cycloalkanes occur for  $n = 4$  ( $\Delta\delta_{C\alpha} = -6.0$  p.p.m.) and  $n = 2$  ( $\Delta\delta_{C\alpha} = -21.5$  p.p.m.). The former apparent effect may have been exaggerated by experimental uncertainties (see Results) and, as discussed above, the latter may be due to a reduction in the ring-current effect resulting from alterations in the geometry of the three-membered ring caused by the sulfur heteroatom.

The C<sup>13</sup> shifts of the  $\beta$  carbons reported in Table I show the same trends to lower field with increasing ring size as found by Burke and Lauterbur for the cycloalkanes,<sup>10</sup> with the possible exception of the cyclic sulfides. However, in the latter case the uncertainties in shifts due to peak overlap render a definite judgment impossible at present. It is interesting to note that although the general trend of  $\beta$ -carbon shifts is to lower field with increasing ring size for the heterocycles and cycloalkanes of Table I, the corresponding  $\beta$ -CH<sub>2</sub> proton shifts show an upfield trend with increasing ring size.<sup>14</sup> This underscores the dangers of anticipating even roughly parallel effects on the proton and carbon shifts of methylene groups, and shows a need

for caution in correlations of either with changes in molecular structure.

The C<sup>13</sup> shifts of 1,3- and 1,4-dioxane reported in Table II exhibit some relatively precise additivity relationships and one marked deviation from additivity. If one takes the C<sup>13</sup> chemical shifts of the  $\alpha$ ,  $\beta$ , or  $\gamma$  carbons in pentamethylene oxide *with respect to that of cyclohexane* as a measure of the effect on the carbon shieldings in the former due to the presence of the oxygen heteroatom, then one computes the effects  $-41.9$ ,  $-0.1$ , and  $2.7$  p.p.m. at the  $\alpha$ ,  $\beta$ , and  $\gamma$  carbons, respectively. In that case, one would predict a C<sup>13</sup> shift in 1,4-dioxane of  $100.9 - 41.9 - 0.1 = 58.9$  p.p.m. with respect to benzene, only  $-2.0$  p.p.m. from the measured value. Similarly, for the  $\alpha$ ,  $\beta$ , and  $\alpha'$  carbons of 1,3-dioxane, C<sup>13</sup> shifts of  $61.7$ ,  $100.7$ , and  $17.1$  p.p.m. with respect to benzene, respectively, are predicted. Only the value predicted for the  $\alpha$  carbon deviates appreciably from the measured quantity. This deviation is not unexpected if one assumes that the decrease in electron density on the  $\alpha'$  carbon due to the presence of one adjacent oxygen atom reduces its polarizability for additional perturbations by the other oxygen atom.

## Adsorption of Polar Molecules on Metal Oxide Single Crystals

by Yung-Fang Yu Yao

*Scientific Laboratory, Ford Motor Company, Dearborn, Michigan (Received June 9, 1966)*

Micro single crystals of NiO,  $\alpha$ -Cr<sub>2</sub>O<sub>3</sub>, and  $\alpha$ -Al<sub>2</sub>O<sub>3</sub> exposing only or predominantly one of their crystalline faces are prepared. Isotherms and heats of absorption of H<sub>2</sub>O, CH<sub>3</sub>OH, CH<sub>3</sub>NH<sub>2</sub>, and CH<sub>3</sub>CN on these crystals were determined at 23°. All of these compounds chemisorb on the crystal surfaces to give a heat of adsorption of 20–30 kcal./mole. The stepwise heat curves obtained are attributed to adsorption on cationic and anionic surfaces with the initial higher heat plateau assigned to the cationic surface. Based on a simplified electrostatic interaction model, the adsorption bond energy of H<sub>2</sub>O to the cations of the (111) faces of NiO and the (0001) faces of Cr<sub>2</sub>O<sub>3</sub> and Al<sub>2</sub>O<sub>3</sub> were calculated as a function of bond distance. The maximum bond energies agree reasonably well with the experimental values for all three oxides. The equilibrium bond distances thus calculated are also of the expected order of magnitude. CH<sub>3</sub>OH and CH<sub>3</sub>CN behave like H<sub>2</sub>O and are held to the surface primarily by electrostatic force. Coordination bond formation by donations of electrons from the amino N to the d band of the cations also contributes to the adsorption bond energy of CH<sub>3</sub>NH<sub>2</sub> on NiO, Cr<sub>2</sub>O<sub>3</sub>, and Fe<sub>2</sub>O<sub>3</sub> but not on Al<sub>2</sub>O<sub>3</sub>. The heats of adsorption of the four adsorbates on the oxygen ions are approximately equal and are less than that on the cations. Results on the crushed NiO and the more heteroplanar Fe<sub>2</sub>O<sub>3</sub> are also included to show the effect of crystal face on chemisorption.

### Introduction

The interaction between organic molecules and surfaces of ionic solids such as metal oxides plays an important role in various surface phenomena. Very little is known about the nature and the energy of interaction or the stereochemistry of the adsorbed phase. Most experimental work in this field has been confined to either commercial catalysts or metal oxides prepared by thermal decomposition of their hydroxides or some unstable salts. The surfaces of these solids are not well defined. With the exception of some work on the physical adsorption of inert gases on halide crystals exposing a single crystalline face,<sup>1,2</sup> scarcely any work has been conducted on ionic single crystals with one or two crystalline faces predominantly exposed.

In this study, single crystals of NiO,  $\alpha$ -Al<sub>2</sub>O<sub>3</sub>,  $\alpha$ -Cr<sub>2</sub>O<sub>3</sub>, and  $\alpha$ -Fe<sub>2</sub>O<sub>3</sub> with a very limited number of their crystalline faces exposed have been prepared. These crystals exhibit no change in surface area after repeated evacuation at 900°. Calorimetric heats and adsorption isotherms of several polar organic compounds and

water on these surfaces have been determined in order to obtain some information on the nature of the chemisorption bond.

### Experimental Section

*The Preparation of the Crystals.* Since this is the first time such crystalline materials have been used as adsorbents, some detailed description of their preparation and properties will be given.

(1) *Nickel Oxide.* This crystal was prepared by mixing NiO powder (J. T. Baker, C.P. grade, 15 g.) with anhydrous Na<sub>4</sub>B<sub>2</sub>O<sub>7</sub> (Matheson Coleman and Bell, reagent grade, 28 g.) in a platinum crucible and firing in a muffle furnace at 1130° for 20 hr. It was then gradually cooled down to 750° in 8 hr. The Na<sub>4</sub>B<sub>2</sub>O<sub>7</sub> was leached out in hot dilute nitric acid, and the NiO crystals were recovered. The glittering green crystals were octahedrons as seen under the microscope (Figure 1a), and X-ray diffraction gave typical NiO patterns. The crystals were sieved; the ones passing 350 mesh

(1) D. M. Young, *Trans. Faraday Soc.*, **48**, 548 (1952).

(2) T. Hayakawa, *Bull. Chem. Soc. Japan*, **30**, 236, 343 (1957).

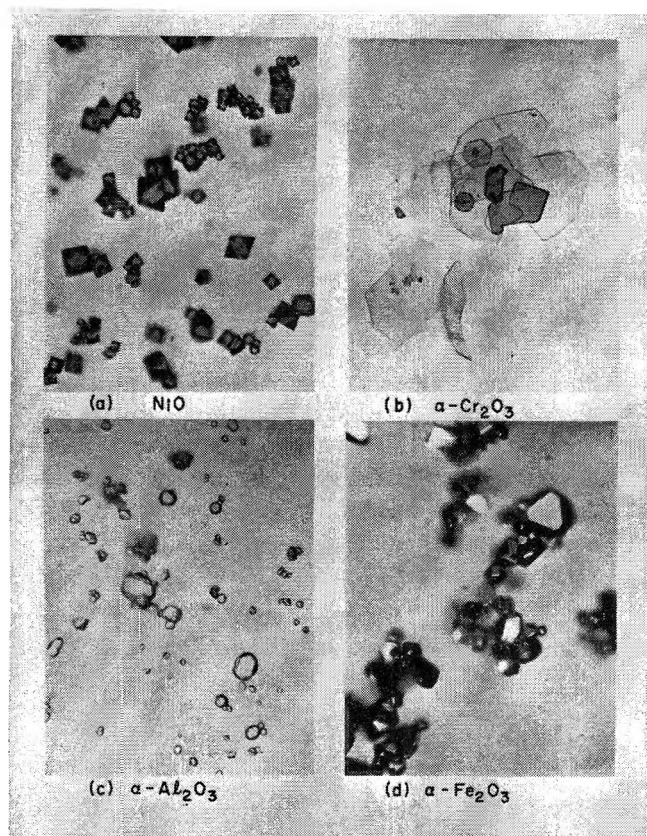


Figure 1.

sieve were used for adsorption studies, and the larger ones were crushed with a Wig-a-Bug and designated as sample NiO (C) for some supplementary adsorption studies. Emission spectral analysis of the final sample showed 0.01% B, 0.01% Na, and no Pt.

(2)  $\alpha\text{-Cr}_2\text{O}_3$ . These crystals were prepared by firing  $\text{K}_2\text{Cr}_2\text{O}_7$  (B and A reagent grade) in a gold crucible at  $900^\circ$  for 3 hr. followed by cooling to  $700^\circ$  in 2 hr. The crystalline platelets were recovered by hot dilute  $\text{HNO}_3$  treatment. The crystals, as seen under the microscope (Figure 1b), were green lustrous thin hexagonal platelets. The X-ray diffraction pattern of a crushed sample identified it as  $\alpha\text{-Cr}_2\text{O}_3$ , and that of the uncrushed platelets showed a single line indicating that the (0001) faces of the crystals were parallel with the plane of the platelets. Emission spectral analysis showed <0.02% K and no Au. The use of a platinum crucible in place of the gold crucible results in  $\text{Cr}_2\text{O}_3$  platelets contaminated with 2.5% Pt.

(3)  $\alpha\text{-Al}_2\text{O}_3$ . The  $\text{Al}_2\text{O}_3$  crystals were prepared by a method similar to that of Reimeica.<sup>3</sup> A mixture of  $\text{Al}_2\text{O}_3$  powder (B and A, purified, 7.4 g.),  $\text{B}_2\text{O}_3$  (B and A, purified, 4 g.), and  $\text{PbO}$  (B and A, reagent grade, 50 g.) was fired in a platinum crucible at  $1250^\circ$  for about 2 hr.; it was then slowly cooled to  $980^\circ$  in 16 hr. The

crucible was removed from the furnace and the molten flux poured off. The crystals thus obtained were washed repeatedly with dilute  $\text{HNO}_3$  and distilled water. Although thin hexagonal plates several millimeters across and  $10\text{--}50\ \mu$  thick were obtained at the top, the remainder were fine rhombohedral platelets  $5\text{--}10\ \mu$  in size (Figure 1c). X-Ray diffraction patterns identified it as  $\alpha\text{-Al}_2\text{O}_3$  with a strong preferred orientation of (0001) face parallel to the platelet surface. X-Ray spectroscopy showed no elements of mass number above 22 present as impurities. Emission spectral analysis showed less than 0.02% B and no Pb or Pt.

(4)  $\alpha\text{-Fe}_2\text{O}_3$ . Over a dozen combinations of various starting materials and firing conditions were used in attempts to prepare this material. None of the preparations gave crystals of both the desired purity and as strong a preferred orientation as that obtained in  $\text{Cr}_2\text{O}_3$ . The following method was chosen because it gave crystals of the desirable purity and a high percentage of tablets which exposed their basal planes (0001). Mixtures of 1:1 mole ratio of  $\text{Fe}_2\text{O}_3$  powder (B and A, reagent grade) and anhydrous  $\text{Na}_4\text{B}_2\text{O}_7$  (Matheson Coleman and Bell, reagent grade) were fired in a gold crucible at  $980^\circ$  for 3 hr. and cooled down to  $870^\circ$  slowly in 4–5 hr. Then it was removed from the furnace, cooled quickly, and the crystals were recovered by treatment with hot dilute nitric acid. The crystals are dark red hexagonal platelets to pseudo-cubic rhombohedrons (Figure 1d). The X-ray diffraction pattern of the crushed sample identified it as  $\alpha\text{-Fe}_2\text{O}_3$ , and that of the uncrushed crystals showed strong preferred orientation with the (0001) face parallel to the plane of the platelets; the presence of (11 $\bar{2}$ 0) and (10 $\bar{1}$ 0) faces was also indicated. Emission analysis of the sample gave 0.07% Na and 0.005% B as impurities.

*Sample Treatment.* As a general procedure, the washed and dried crystals obtained as described above were again placed in a platinum or gold crucible and heated at  $950\text{--}1000^\circ$  in air overnight. Washing with dilute  $\text{HNO}_3$  and triple-distilled water was repeated several times. This was designed to lessen the chance for any impurity to diffuse outward to the surface during subsequent heat treatments at  $900^\circ$  ( $750^\circ$  for  $\text{Fe}_2\text{O}_3$ ). Prior to each adsorption run on the bare surfaces, the sample was outgassed at  $25^\circ$  to less than  $10^{-6}$  mm. for at least 10 hr. and continued at  $900^\circ$  ( $750^\circ$  for  $\text{Fe}_2\text{O}_3$ ) for 4–5 hr. The closed sample was treated with dry oxygen at a pressure of  $\sim 10$  cm. at  $900^\circ$  ( $750^\circ$  for  $\text{Fe}_2\text{O}_3$ ) for 0.5 hr. to burn off any organic material present, and this was followed by outgassing

(3) J. P. Reimeica, U. S. Patent 3,075,831 (1963).

at 900° (750° for Fe<sub>2</sub>O<sub>3</sub>) for 1 hr. In the case of Al<sub>2</sub>O<sub>3</sub> and "evacuated" NiO, the sample was cooled down, and adsorption measurements were begun. For Fe<sub>2</sub>O<sub>3</sub>, Cr<sub>2</sub>O<sub>3</sub>, and "oxygenated" NiO the sample was treated with dry oxygen (900 or 750°, 10 cm.) for the second time and was kept closed in oxygen while it cooled down to 25°. The oxygen was pumped out at 25° for about 15 min. just before the adsorption measurements. During the second oxygen treatment, it was found that some oxygen was taken up by NiO. Samples of NiO with both kinds of pretreatment, evacuated and oxygen treated, were used for adsorption studies. No significant amount of oxygen uptake was observed for Cr<sub>2</sub>O<sub>3</sub>. Oxygen was also taken up by Fe<sub>2</sub>O<sub>3</sub>. This is rather expected owing to the ease with which Fe<sub>2</sub>O<sub>3</sub> loses oxygen to form lower oxides. To ensure the composition of Fe<sub>2</sub>O<sub>3</sub>, only the oxygen treated surface was used and only very brief pumping at 25° was applied to the sample after the oxygen treatment.

*The Adsorbates.* Matheson anhydrous methylamine was used. This gas contains a maximum of 0.8% H<sub>2</sub>O as reported by the manufacturer, and this water was kept from getting to the sample by maintaining the reservoir temperature at less than -50°. B and A reagent grade absolute CH<sub>3</sub>OH was used without further purification. A sample of the alcohol from the reservoir was analyzed by a mass spectrometer and found to be impurity free. Matheson Coleman and Bell spectroscopic grade CH<sub>3</sub>CN was dried with silica gel and used without further treatment. A new thoroughly dried reservoir was used for each adsorbate. Any trapped gas or volatile impurities present were removed by freezing-melting-pumping cycles; the last half of the liquid in the reservoir was never used.

*The Apparatus.* Both the organic and Kr adsorption were determined using a conventional volumetric adsorption apparatus consisting of mercury cutoffs, mercury-filled manometer, and a mercury-sealed Teflon-plug needle valve as the dosing valve. The manometer was read with the aid of a Gaertner cathetometer equipped with a 10-cm. microscope slide readable to 0.001 mm.

The calorimeter is essentially the same as that used previously.<sup>4</sup> The quartz sample container was modified to include a concentric heater well which was filled with a wound heater and a known amount of mercury to facilitate good thermal conduction during calibration. The heater and mercury were removed between runs so that the sample could be treated at high temperatures. The heat capacities obtained from electrical calibrations were checked against the calculated values based on the heat capacities of all the components. The agreement was within 5% for

all the samples used. All heat of adsorption measurements were made in the temperature range of 22-23°. About 0.5 mm. of He was present in the sample bulb throughout the heat of adsorption measurements to enhance the thermal conduction.

## Results and Discussion

*The State of the Surfaces.* The excellent octahedral appearance of the NiO crystals suggests that the surface is exclusively the (111) face. The faces are equilateral triangular arrays of all close-packed anions and all cations in alternate layers. Although  $\alpha$ -Cr<sub>2</sub>O<sub>3</sub>,  $\alpha$ -Fe<sub>2</sub>O<sub>3</sub>, and  $\alpha$ -Al<sub>2</sub>O<sub>3</sub> are all of the same crystalline structure, the external morphology of the crystals obtained differed considerably. The Cr<sub>2</sub>O<sub>3</sub> crystals were very thin hexagonal platelets in appearance, and X-ray diffraction patterns indicate that the surface is predominantly the basal plane (0001) face. These planes are composed of layers of close-packed O<sup>2-</sup> ions between which are layers of cations in which the cations can occupy two-thirds of the two different types of octahedral positions. The  $\alpha$ -Al<sub>2</sub>O<sub>3</sub> crystals were platelets exposing predominantly the basal plane, but, since the platelets were thicker than the Cr<sub>2</sub>O<sub>3</sub> platelets, it is estimated that up to 20% of the surface is the rhombohedral side faces exposed. The Fe<sub>2</sub>O<sub>3</sub> crystals ranged from thick platelets to pseudo-cubic rhombohedrons which exposed several crystal faces, chiefly (0001), (10 $\bar{1}$ 0), and (11 $\bar{2}$ 0).

Similar surfaces of (111) faces of f.c.c. alkali halides and (100) faces of b.c.c. alkali halides crystals have been assumed in the literature<sup>5,6</sup> to be composed of two types of surfaces, one side all cations and the opposite side all anions, with both sides fully populated. Kummer and Yao<sup>7</sup> have shown by energy calculations that the fully populated surface planes are much less stable as compared to the surface plane which is only half populated with counterions over a full layer. The entire surface of a crystal may be considered as being made up of patches of such half-populated planes, some of which are composed of all cations and others with all anions at the surface. The over-all crystal must, of course, remain electrically neutral. A sketch of the NiO surface is shown in Figure 2. At the top is the arrangement of the Ni<sup>2+</sup> and O<sup>2-</sup> ions viewed at a direction parallel to the (111) face. In the lower part is a schematic view at a direction perpendicular to the (111) face. The + and - signs indicate the

(4) Y.-F. Y. Yao, *J. Phys. Chem.*, **67**, 2055 (1963).

(5) W. J. C. Orr, *Trans. Faraday Soc.*, **35**, 1247 (1939).

(6) D. M. Young, *ibid.*, **47**, 1228 (1951).

(7) J. T. Kummer and Y.-F. Y. Yao, to be published.



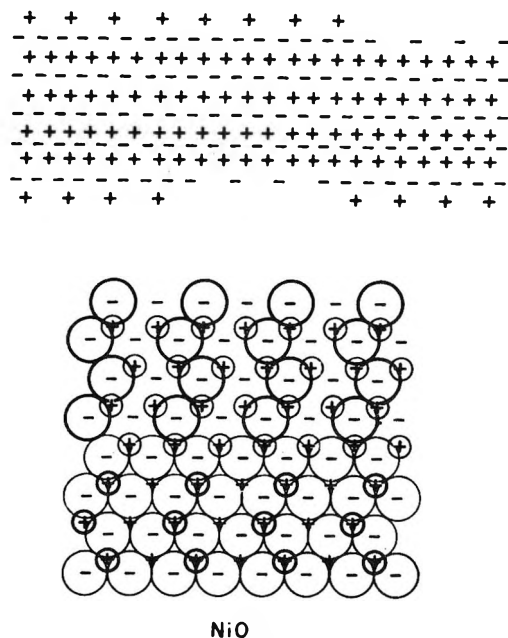


Figure 2. Schematic presentation of the surface.

locations of the underlying  $\text{Ni}^{2+}$  and  $\text{O}^{2-}$  ions. The large and small circles represent the  $\text{O}^{2-}$  and  $\text{Ni}^{2+}$  ions in the surface layer; the outermost ones are shown by heavy circles. As it is shown that the outermost layer can be either half populated with anions (top half) or cations (bottom half). Similar sketches can be drawn for the (0001) faces of the corundum-type crystals.

Based on the crystal lattice constants of these oxides, the concentration of the half-populated ions in the (111) face of NiO is  $11 \mu\text{moles of } (\text{Ni}^{2+} + \text{O}^{2-})/\text{m}^2$  and  $8.5x \mu\text{moles of } \text{Al}^{3+}$  and  $12.8(1 - x) \mu\text{moles of } \text{O}^{2-}/\text{m}^2$  in the (0001) face of  $\text{Al}_2\text{O}_3$ , where  $x$  is the fraction of the surface with cations at the surface. The surface concentrations of  $\text{Cr}^{3+}$  (or  $\text{Fe}^{3+}$ ) and the respective  $\text{O}^{2-}$  concentrations of the (0001) faces of  $\text{Cr}_2\text{O}_3$  (or  $\text{Fe}_2\text{O}_3$ ) are only slightly less than that for  $\text{Al}_2\text{O}_3$ . The other faces of the corundum-type crystals, particularly the  $(10\bar{1}0)$  and  $(11\bar{2}0)$  faces, are heteropolar (*i.e.*, cations and anions are located next to each other in the same plane); they are expected to have the same stoichiometric composition as the corresponding planes in the bulk, and on the average they are more densely packed than the half-populated (0001) faces.

**Adsorption Isotherms.** A typical set of adsorption isotherms on the evacuated NiO surfaces are shown in Figure 3. Similar isotherms are obtained on all the other surfaces. In general, if, after the adsorption measurement on a bare surface, the sample was evacuated overnight at  $22\text{--}23^\circ$  with a liquid nitrogen trap in the system and the adsorption was remeasured, the

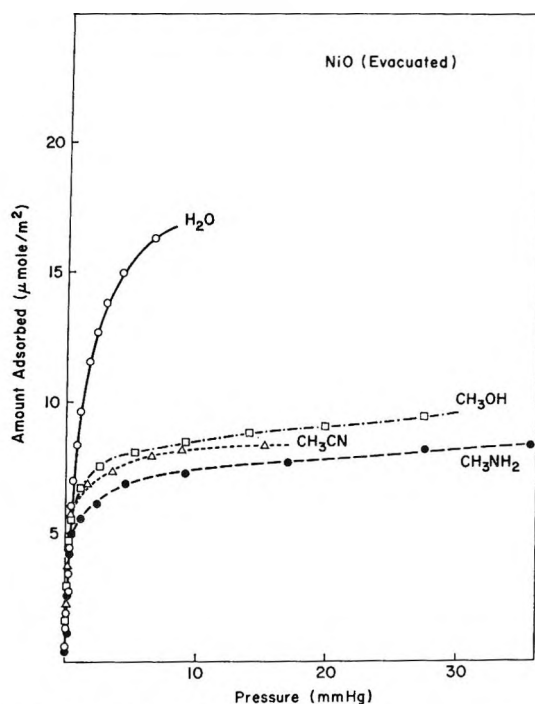


Figure 3. Adsorption isotherms.

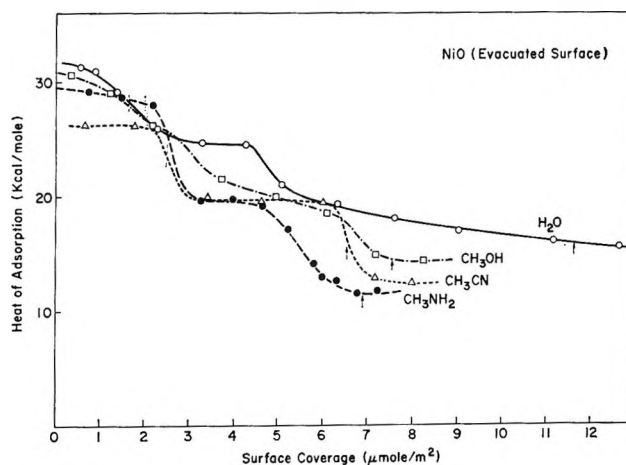


Figure 4. Heat of adsorption on evacuated NiO.

second isotherm obtained lies below and parallel to that of the first run. Both isotherms give good linear B.E.T. plots. The B.E.T.  $V_m$  values of the first runs and the difference between the two consecutive runs of the same system (*i.e.*, the amount not evacuated) are shown in the heat curves (Figures 4–11) by arrows and dotted lines, respectively, and Table I.

**Accuracy of Measurements.** The heat of adsorption measured calorimetrically consists of a series of integral heats each representing the average heat over a limited range of the surface coverage. In the results given here (Figures 4–11), the heats in kilocalories per mole

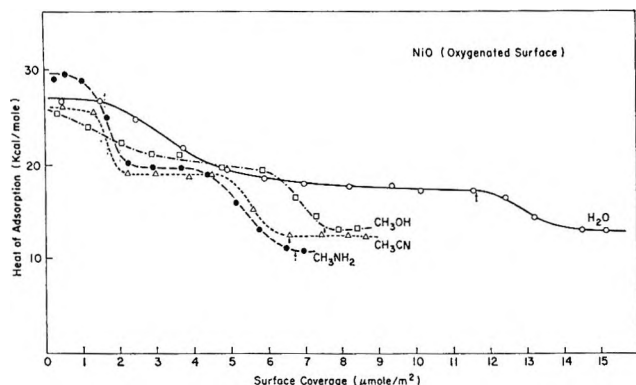


Figure 5. Heat of adsorption on oxygenated NiO.

Table I: B.E.T.  $V_m$  Values ( $\mu\text{mole}/\text{m}^2$ )

Substrate	Absorbate	$V_{m1}$	$V_{m11}$	$\Delta V_m$
NiO (evacuated)	H <sub>2</sub> O	11.60	9.95	1.65
	CH <sub>3</sub> OH	7.55	5.50	2.05
	CH <sub>3</sub> NH <sub>2</sub>	6.80	4.80	2.00
	CH <sub>3</sub> CN	6.55	4.15	2.40
NiO (oxygenated)	H <sub>2</sub> O	11.60	10.05	1.55
	CH <sub>3</sub> OH	7.50	6.00	1.50
	CH <sub>3</sub> NH <sub>2</sub>	6.60	4.60	2.00
	CH <sub>3</sub> CN	6.55	4.75	1.70
Cr <sub>2</sub> O <sub>3</sub>	H <sub>2</sub> O	7.95	6.40	1.55
	CH <sub>3</sub> OH	6.40	5.10	1.30
	CH <sub>3</sub> NH <sub>2</sub>	5.70	4.00	1.70
	CH <sub>3</sub> CN	4.45	3.95	0.50
Al <sub>2</sub> O <sub>3</sub>	H <sub>2</sub> O	9.00	5.30	3.70
	CH <sub>3</sub> OH	8.25	4.05	4.20
	CH <sub>3</sub> NH <sub>2</sub>	7.05	4.30	2.75
	CH <sub>3</sub> CN	6.20	4.50	1.70
Fe <sub>2</sub> O <sub>3</sub>	H <sub>2</sub> O	10.00	4.70	5.30
	CH <sub>3</sub> OH	7.80	1.40	6.40
	CH <sub>3</sub> NH <sub>2</sub>	7.20	2.55	4.65
	CH <sub>3</sub> CN	7.80	3.80	4.00

are plotted against the midpoints of the corresponding increments in surface coverage in micromoles per square meter of surface area. The surface areas of the crystals were determined by Kr adsorption at  $-183^\circ$  using the B.E.T. equation. With the exception of the crushed NiO(C), repeated outgassing and oxygen treatment at high temperature ( $750$ – $900^\circ$ ) did not change the surface area.

In the case of NiO, the adsorption and heat measurements of each adsorbate were repeated on three samples prepared by the same method but of slightly different particle sizes. For the other oxides, only one sample of each was used, but the measurements have been repeated in the majority of the cases to check the results.

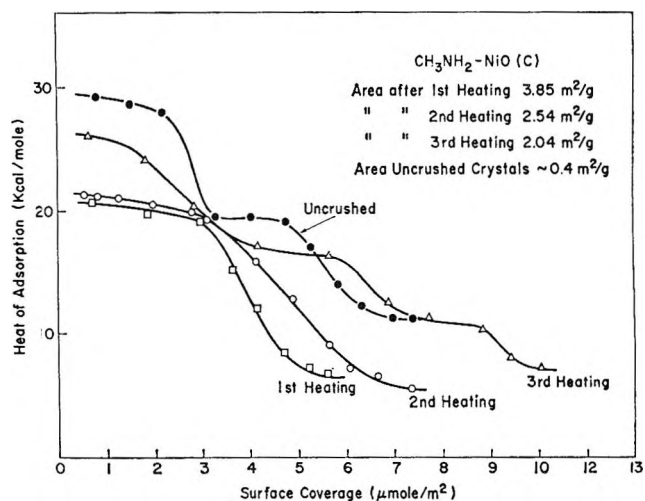
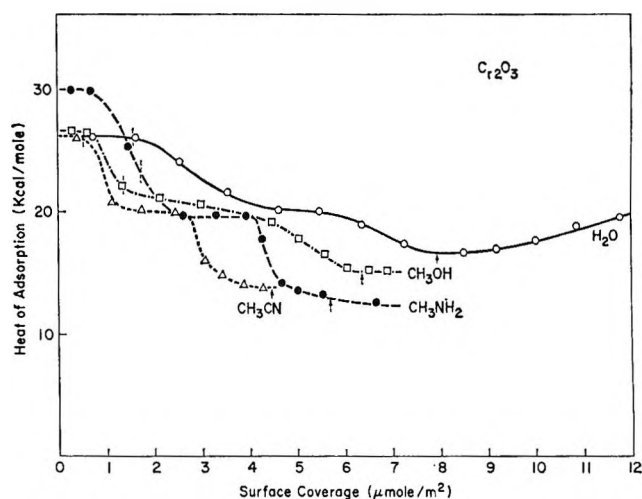
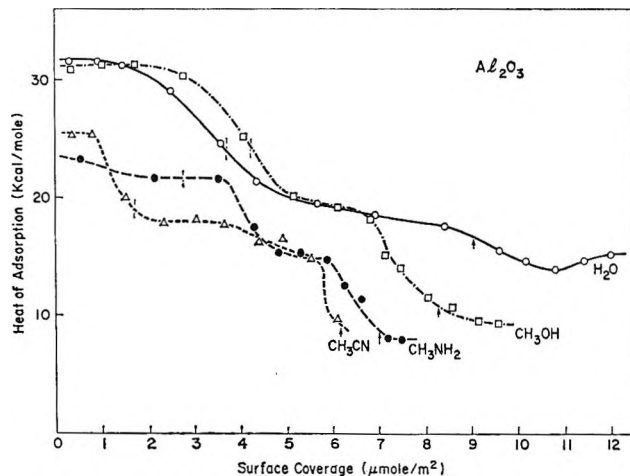


Figure 6. Heat of adsorption on crushed NiO.

Figure 7. Heat of adsorption on  $\alpha$ -Cr<sub>2</sub>O<sub>3</sub>.Figure 8. Heat of adsorption on  $\alpha$ -Al<sub>2</sub>O<sub>3</sub>.



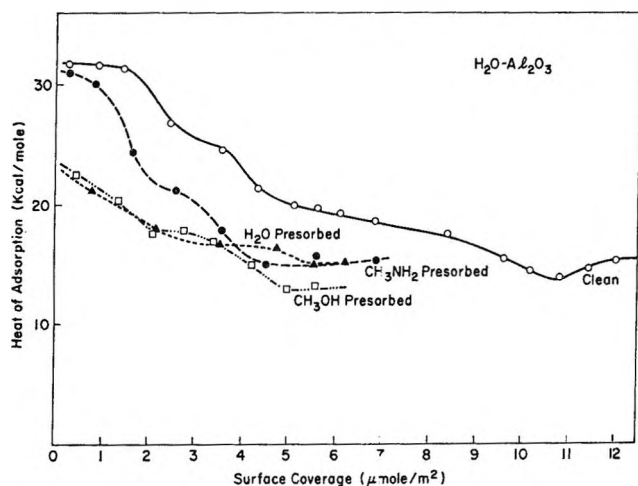


Figure 9. Heat of adsorption of  $\text{H}_2\text{O}$  on partially covered  $\alpha\text{-Al}_2\text{O}_3$ .

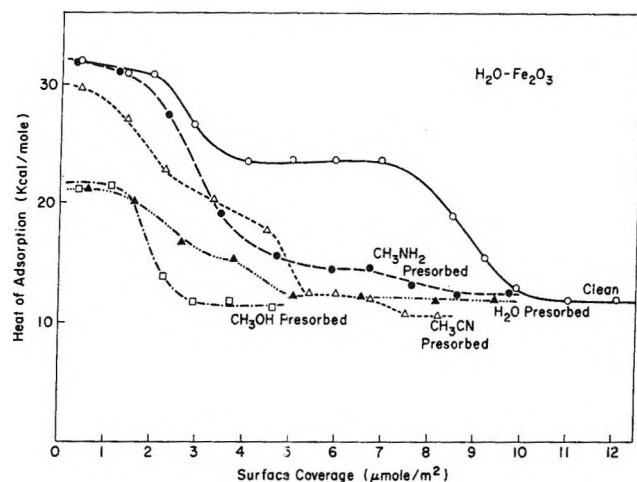


Figure 11. Heat of adsorption of  $\text{H}_2\text{O}$  on partially covered  $\alpha\text{-Fe}_2\text{O}_3$ .

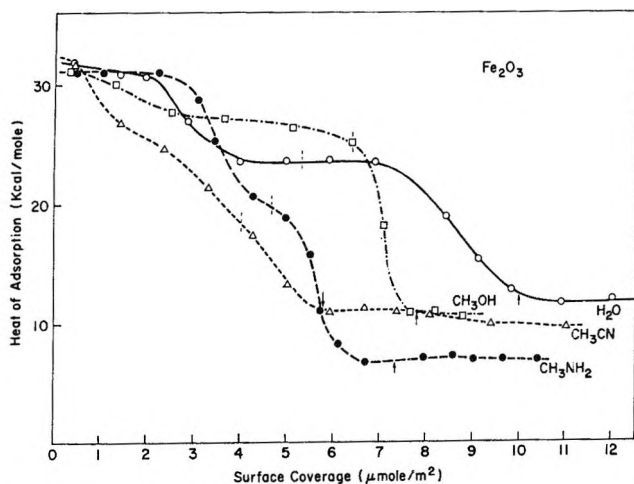


Figure 10. Heat of adsorption on  $\alpha\text{-Fe}_2\text{O}_3$ .

The reproducibility of the heat of adsorption is within  $\pm 1$  kcal./mole both for the initial heat and for the relatively constant heat regions. However, there is more scattering in the regions where the heat changes drastically with surface coverage. This probably results from the fact that only an average heat over a range of surface coverage was measured, and this value was given to the midpoint of the particular increment.

The heats up to near the B.E.T.  $V_m$  are all much greater than the heat of liquefaction of the adsorbates, so the term "chemisorption" is arbitrarily used for the entire range up to the B.E.T.  $V_m$  surface coverage.

At the end of the adsorption run, the gaseous phase was condensed in a cold finger immersed in liquid nitrogen; no noncondensable gas other than the He originally introduced was ever found in any of the experiments.

*The Heat of Adsorption on NiO.* The heat of adsorption of the four adsorbates on evacuated NiO surface are shown in Figure 4. For  $\text{CH}_3\text{NH}_2$  and  $\text{CH}_3\text{CN}$ , the heat curves show sharp steps; for  $\text{H}_2\text{O}$  and  $\text{CH}_3\text{OH}$  the steps are less well defined. The lowest heat region (third plateau) starts at near the B.E.T.  $V_m$  and, therefore, may be attributed to the second-layer adsorption. The adsorption before  $V_m$  can be considered as consisting of two steps of approximately equal surface coverage. This implies that there are two types of adsorption, or sites, and that the adsorption of the first type is almost complete before the second type starts. Based on the model of the surface states proposed above, one can relate the two steps in the heat curves with the two types of surface ions,  $\text{Ni}^{2+}$  and  $\text{O}^{2-}$ . At  $V_m$ , the number of water molecules (a small molecule) adsorbed is approximately equal to the number of the surface ions (both types, half populated). However, for the larger molecules,  $\text{CH}_3\text{OH}$ ,  $\text{CH}_3\text{NH}_2$ , and  $\text{CH}_3\text{CN}$ , a less dense arrangement must result since only about two-thirds of the surface ions are covered at  $V_m$ .

It is not evident which type of ions,  $\text{Ni}^{2+}$  or  $\text{O}^{2-}$ , gives the highest heat of interaction. Heats of chemisorption on the oxygenated NiO surface were made to gain some information that might be used to distinguish the two types of adsorption sites. The adsorption of oxygen on NiO has been discussed by several previous workers.<sup>8</sup> The oxygen molecules are adsorbed as oxygen anions  $\text{O}_2^-$  or  $\text{O}^-$  on the surface  $\text{Ni}^{2+}$  ions and are not absorbed into the interior.<sup>9</sup> Thus, the number of surface  $\text{Ni}^{2+}$  ions is reduced while that of  $\text{O}^{2-}$  is

(8) See, for example, H. B. Charman, R. M. Dell, and S. S. Teele, *Trans. Faraday Soc.*, 59, 453 (1963).

(9) H. Gossel, *Z. Elektrochem.*, 65, 98 (1961).

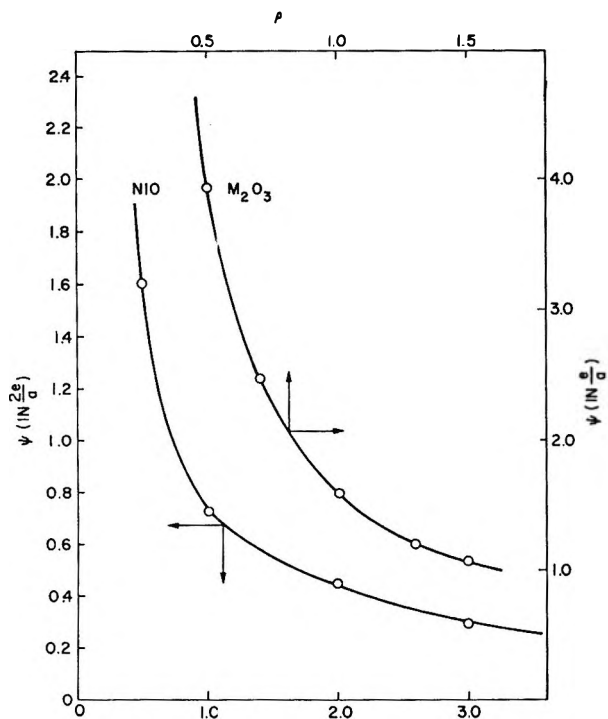


Figure 12. Electrostatic potential over a surface cation.

unchanged, and some new adsorbed oxygen anion species are added to the surface. The oxygen uptake by the sample during the second oxygen treatment at from 900 down to 25° was found to be of the order of  $3-4 \times 10^{13}$  oxygen atoms/cm.<sup>2</sup>. If it is assumed that none of the oxygen was desorbed during the 15-min. outgassing at 25°, then about one-tenth of the surface Ni<sup>2+</sup> ions (if about half the surface is cationic) are associated with the chemisorbed oxygen anion on the oxygenated NiO surface. This is of the same order of magnitude as that reported by the previous workers.<sup>8</sup>

The heats of adsorption on the oxygenated NiO surfaces are shown in Figure 5. The initial heat curve for all four adsorbates has been changed. The initial heats of adsorption of H<sub>2</sub>O and CH<sub>3</sub>OH are lower than those on the evacuated surface, and for CH<sub>3</sub>NH<sub>2</sub> and CH<sub>3</sub>CN the surface coverage corresponding to the first plateau is reduced by an amount approximately equal to the number of oxygen atoms taken up during the oxygenation process. The heat of adsorption in the second plateau is essentially unchanged for all four adsorbates. This implies that the initial high heat region for all four adsorbates corresponds to adsorption on the surface Ni<sup>2+</sup> ions since the number of these is reduced by O<sub>2</sub> adsorption. The adsorption on the chemisorbed oxygen anions will give heats probably the same as those for the second plateau, adsorption on the surface O<sup>2-</sup> ions. The  $V_m$  values are essentially unchanged by the oxygen treatment.

*Adsorption on Crushed NiO.* The surface area and heat of adsorption of CH<sub>3</sub>NH<sub>2</sub> on evacuated crushed NiO surface (large NiO octahedrons were crushed up) after successive heat treatments at 900° are shown in Figure 6. It was found that the crushed sample was severely sintered during the heat treatments. The amount of CH<sub>3</sub>NH<sub>2</sub> adsorbed per unit area up to  $V_m$  and the surface coverage of the initial high heat portion increased with increasing heat treatment. Although the evidence is by no means conclusive, it does indicate the following: (1) the crystalline faces exposed upon crushing are probably not the (111) face and they are less energetic toward amine; (2) during heating at 900° under vacuum, the surfaces are sintered and transformed gradually into the (111) face or some other face which interacts as strongly with CH<sub>3</sub>NH<sub>2</sub> as the (111) face.

*The Heat of Adsorption on  $\alpha$ -Cr<sub>2</sub>O<sub>3</sub>.* The heats of adsorption on Cr<sub>2</sub>O<sub>3</sub> are shown in Figure 7. They bear a resemblance to those on NiO in that they have two plateaus before they drop to a low heat at or near  $V_m$ . The second plateau has a heat value about 20 kcal./mole for all four adsorbates and is the same as that on NiO. Since the arrangements of O<sup>2-</sup> on the surface of the two oxides are not too different, it is not unreasonable to assume that their heat of adsorption on the O<sup>2-</sup> surface would be approximately the same. Therefore, one can again tentatively assign the high heat portion of the heat curves to the Cr<sup>3+</sup> ions. If the planes comprising both top and bottom of the Cr<sub>2</sub>O<sub>3</sub> platelets were half populated with Cr<sup>3+</sup> ions, then the Cr<sup>3+</sup> ion concentration in the surface would be 8.5  $\mu$ moles/m.<sup>2</sup>. Since the surface coverage of the first plateau is much less than one-third of the monolayer coverage, it is implied that less than half of the surface is the half-populated Cr<sup>3+</sup> surface. The rest of the surface is presumably then the half-populated anion surface. Since the Cr<sub>2</sub>O<sub>3</sub> surface was pretreated with oxygen in the same way as was the oxygenated NiO surface, some chemisorption of oxygen anion on the Cr<sup>3+</sup> is possible with a consequent reduction in Cr<sup>3+</sup> concentration although no oxygen uptake was actually observed during the second oxygen treatment. Voltz and Wheeler<sup>10</sup> reported that major portions of the oxygen taken up by Cr<sub>2</sub>O<sub>3</sub> at 500° could not be removed by outgassing at 500°, but no work at 900° was reported.

*The Heat of Adsorption on  $\alpha$ -Al<sub>2</sub>O<sub>3</sub>.* The crystals of Al<sub>2</sub>O<sub>3</sub> were not as monoplanar as the crystals of Cr<sub>2</sub>O<sub>3</sub>. The heats of adsorption on the Al<sub>2</sub>O<sub>3</sub> crystals are shown in Figure 8. The initial heats of water and CH<sub>3</sub>-

(10) S. W. Weeler and S. E. Voltz, *J. Am. Chem. Soc.*, 76, 4695 (1954).

OH are almost identical and are higher than on  $\text{Cr}_2\text{O}_3$ , possibly owing to the small size of the  $\text{Al}^{3+}$  ion. The initial heat of  $\text{CH}_3\text{NH}_2$  is much lower than that of  $\text{CH}_3\text{OH}$  and  $\text{H}_2\text{O}$  and lower than  $\text{CH}_3\text{NH}_2$  on  $\text{Cr}_2\text{O}_3$ . This probably reflects the lower tendency of the nitrogen to form coordinate bonds with  $\text{Al}^{3+}$  compared with  $\text{Cr}^{3+}$ . The heat curve for  $\text{CH}_3\text{CN}$  on  $\text{Al}_2\text{O}_3$  is similar in shape and initial heat value as on  $\text{Cr}_2\text{O}_3$ .

In order to gain more information about the adsorption sites responsible for the two heat plateaus, a series of experiments were conducted on this sample. After adsorption of the organic molecule on the bare surface, the sample was outgassed at  $22^\circ$  overnight in order to remove the weakly adsorbed molecules. Water adsorption was then redetermined on these partially covered surfaces. The amounts of organic materials left on the surface are shown as dotted lines in Figure 8, and the heat of adsorption on the presorbed surfaces is shown in Figure 9. The amount and heat of adsorption of water on an alcohol presorbed surface is very similar to that presorbed with  $\text{H}_2\text{O}$ . Therefore, the same sites are probably responsible for high heat adsorption of  $\text{H}_2\text{O}$  and  $\text{CH}_3\text{OH}$ . The high heat of adsorption of water on the amine presorbed surface was much less in extent but not completely blocked off. The general shape of the heat curve suggests that the high heat sites for water and  $\text{CH}_3\text{NH}_2$  are the same, but, owing to the size effect, some sites which cannot accept  $\text{CH}_3\text{NH}_2$  can still accommodate water molecules. As it is shown in Figure 8, the amount of amine presorbed on the surface is much less than that of  $\text{H}_2\text{O}$  and  $\text{CH}_3\text{OH}$ . As with  $\text{Cr}_2\text{O}_3$  and  $\text{NiO}$ , these high energy sites are thought to be the cation sites.

*The Heat of Adsorption on  $\text{Fe}_2\text{O}_3$ .* It was originally hoped that thin platelets of  $\text{Fe}_2\text{O}_3$  similar to those of  $\text{Cr}_2\text{O}_3$  could be prepared. The only crystals of high purity that could be obtained, however, were thick platelets or pseudo-cubic rhombohedrons (Figure 1d) in which X-ray diffraction showed other faces such as the  $(10\bar{1}0)$  and  $(11\bar{2}0)$  to be exposed in addition to the  $(0001)$  surface. These other faces are not composed of a single ion type but are heteroionic, and, as a result, the interpretation of the adsorption data on  $\text{Fe}_2\text{O}_3$  is very difficult. The data for  $\text{Fe}_2\text{O}_3$  are presented here as an additional illustration of how the presence of different crystal faces can greatly modify the adsorption behavior (the crushed  $\text{NiO}$  is the other example).

The heats of adsorption of the four adsorbates on the  $\text{Fe}_2\text{O}_3$  crystals are shown in Figure 10. These surfaces were all treated as oxygenated surfaces in order to avoid the loss of oxygen and the production of lower valent cations. The adsorption on  $\text{Fe}_2\text{O}_3$  differs from that on

$\text{Cr}_2\text{O}_3$  by the near absence of a second plateau for methylamine and methylnitrile, and by the higher initial heat of adsorption of water and methanol. This difference is associated with the presence of the heteroionic faces  $(10\bar{1}0, 11\bar{2}0)$ . The second heat plateau for water adsorption on  $\text{Fe}_2\text{O}_3$  has approximately the same heat value as the initial heat of water on  $\text{Cr}_2\text{O}_3$ . Since these two materials have the same crystal structure and very similar dimensions, we have assigned this second plateau heat for  $\text{Fe}_2\text{O}_3$  to the cations on the  $(0001)$  surface as in  $\text{Cr}_2\text{O}_3$ . The higher heat value of water and alcohol adsorption are thought to be due to adsorption on the other faces  $(10\bar{1}0, 11\bar{2}0)$ . It is possible that the stereochemistry of these heteroionic faces are such as to favor a stronger electrostatic interaction on adsorption as associated OH groups as that proposed by Blyholder and Richardson<sup>11</sup> for  $\text{H}_2\text{O}$  on  $\text{Fe}_2\text{O}_3$  powder.

The heat curves for water adsorption on surfaces partially covered with organic molecules were also determined on  $\text{Fe}_2\text{O}_3$ , as on  $\text{Al}_2\text{O}_3$ , and are shown in Figure 11. Again, it appears that the same sites are active for alcohol as for water adsorption. The heat curve for water adsorption on amine-presorbed surfaces suggests that the presorbed amine influences the high energy sites for water adsorption very little but does greatly influence the second heat plateau for water. Since the high heat for the amines is thought to be due to adsorption on the cations in the  $(0001)$  surface, this result would also suggest that the second plateau in the water heat curve is due to the adsorption on cations in the  $(0001)$  face.

*Theoretical Estimation of the Adsorption Bond Energy.* In order to understand the nature of the adsorption bond, it is desirable to compare the experimentally measured heat of adsorption with some theoretically derived value. The ionic contribution to the bond energy of a molecule with peripheral dipole on an ionic surface can be considered as the sum of the following interaction terms between the molecule and each ion of the substrate: (1) ion-permanent dipole interaction, (2) polarization effect or ion-induced dipole interaction, (3) van der Waals dispersion attractive energy, and (4) van der Waals repulsive energy. Owing to the complexity of the surface and the electronic structure of the polar molecule, the strong dependence of these energy terms on the distance between the molecule and the surface, the difficulty in determining the latter, and the lack of a unified expression for the repulsive force, an exact calculation of these energies is impossible at the present. Several attempts<sup>1,2,12</sup> using

(11) G. Blyholder and E. A. Richardson, *J. Phys. Chem.*, **66**, 2597 (1962).

(12) F. C. Tompkins, Report AF 61 (052)-190, (Ad 282141), 1961.

simplified models have been made to estimate the heat of adsorption for inert gases and very simple molecules on halides, but these systems are mostly concerned with physical adsorption only.

Based on a simple model, the adsorption bond energy of water over a cation on the (111) faces of NiO and (0001) faces of  $\text{Al}_2\text{O}_3$  and  $\text{Fe}_2\text{O}_3$  can be estimated as follows.

(1) *Ion-Dipole Interaction.* This energy has been generally calculated as

$$E_e = F_r \mu \quad (1)$$

where  $\mu$  is the permanent dipole moment of the adsorbed molecule and  $F_r$  is the electrostatic field over the surface at distance  $r$  from the surface. This is valid only when the length of the dipole,  $l$ , is much less than the distance between the molecule and the surface,  $r$ ; when  $r$  is comparable in magnitude to  $l$ , such as in the case of strong adsorption, a better approximation is

$$E_e = \epsilon(\varphi_{r_1} - \varphi_{r_2}) \quad (2)$$

In this case the adsorbed molecule is represented by a linear dipole with charge  $\epsilon$  and a charge separation of  $r_2 - r_1$ ;  $\varphi_r$  is the electrostatic potential at a distance  $r$  from the surface. For water, the values of  $1.567 \times 10^{-10}$  e.s.u. and  $1.2 \text{ \AA}$ . for  $\epsilon$  and  $r_2 - r_1$ , respectively, used by Tompkins,<sup>12</sup> are adopted. The electrostatic potential over the surface is  $\Sigma \pm z_i e / R_i$  where  $R_i$  is the distance from a point outside the surface to the  $i$ th ion of the substrate.  $z_i$  is the charge number of the  $i$ th ion, and  $e$  is the electronic charge. Based on the half-populated top-layer model described above, the electrostatic potential over a cation in the (111) faces of NiO and (0001) face of corundum-type crystal surfaces have been calculated. In the case of NiO, the summation was carried over a hexagonal sheet three NiO molecules thick containing 216 ions. The value was plotted against the number of ions included and extrapolated until a constant was obtained. In the case of the corundum-type crystals, the summation over a hemisphere containing 355 ions was carried out. The electrostatic potentials thus calculated are shown in Figure 12, where  $a$  is  $1/\sqrt{3}$  of the shortest O-O distance in the corundum-type crystals and  $1/\sqrt{6}$  of this distance in NiO,  $\rho = r/a$ .

(2) *Polarization Effect.* The energy of interaction between the surface cation and the dipole induced in the adsorbed molecule by the electrostatic field of the surface is

$$E_i = \frac{\alpha F^2}{2} \quad (3)$$

where  $\alpha$  is the polarizability of the molecule. In prin-

ciple, this term should be integrated over the whole volume of the molecule. As an approximation, the bond polarizability of the OH bond ( $0.73 \times 10^{-24} \text{ cc.}$ )<sup>13</sup> is taken since, as one moves away from the center of the cation toward the midpoint between neighboring ions, the field diminishes.  $F$  is calculated from the electrostatic potential as

$$F = \frac{\partial \varphi}{\partial r} \quad (4)$$

(3) *van der Waals Attractive Energy.* The Kirkwood-Müller<sup>14</sup> equation was used

$$E_v = 6mc^2 \Sigma \frac{\alpha_1 \alpha_2}{\chi_1 + \chi_2} \frac{1}{R^6} \quad (5)$$

where  $m$  is the mass of the electron,  $\alpha_1$ ,  $\alpha_2$ ,  $\chi_1$ , and  $\chi_2$  are the polarizability and the magnetic susceptibility of water and the metal (or oxygen) ions, respectively.<sup>13,15</sup>  $R$  is the distance between the center of water and the ion. Summations over the nearest 15 ions in NiO and 22 ions in  $\text{Al}_2\text{O}_3$  and  $\text{Cr}_2\text{O}_3$  were made.

(4) *Repulsive Energy.* Among the four energy terms, this is the most difficult to assess. There is no one preferred expression. In the general form,  $E_R = A/r^n$ , where  $n$  can vary from 9 to 12 and the constant  $A$  is approximated for only a very limited number of molecules. For a rough approximation, the method used by Tompkins<sup>12</sup> is adopted

$$E_R = \frac{A_{12}}{r^n} \quad n = 10.5 \quad (6)$$

and

$$A_{12}^{1/n} = 1/2(A_{11}^{1/n} + A_{22}^{1/n}) \quad (7)$$

where  $A_{11}$  is the repulsive constant for water and  $A_{22}$  is the repulsive constant of the ions; this is approximated by taking the repulsive constants of the nearest rare gas adjusted according to the size of the metal or oxygen ions.<sup>13,16</sup> The four energy terms and the net energy of adsorption  $E$  thus calculated are shown in

$$E = E_e + E_i + E_v + E_R \quad (8)$$

Table II. The distance corresponding to the maxima in the bond energy would then be the equilibrium distance  $r_e$ , and these are listed in the table also. There are no data available in the literature on the bond energy

(13) E. A. Moelwyn-Hughes, "Physical Chemistry," Pergamon Press Ltd., London, 1957.

(14) J. G. Kirkwood, *Z. Physik*, **33**, 57 (1932).

(15) L. Pauling, *Proc. Roy. Soc. (London)*, **A114**, 181 (1927).

(16) F. J. Garrick, *Phil. Mag.*, **7**, 76 (1930).

of such adsorbate-surface complex. However, a qualitative comparison with that of a gaseous complex may be illuminating. It was reported that<sup>17</sup> the average bond energy between water and  $\text{Fe}^{2+}$  and  $\text{Fe}^{3+}$  in their hexahydrates can be calculated using an electrostatic model to be 52 and 109 kcal./mole, respectively, and the corresponding experimental values are 58 and 116 kcal./mole. The bond distances used for the calculations are 2.21 Å. for  $\text{Fe}(\text{H}_2\text{O})_6^{2+}$  and 2.05 Å. for  $\text{Fe}(\text{H}_2\text{O})_6^{3+}$ . Since the electrostatic potential experienced by a water molecule over a surface cation is much less (one-fourth to one-third) than that exerted by a free ion at the same distance apart, the adsorption bond would be expected to be much weaker and longer than the hydration bond of the ions. Therefore, the  $r_e$  values obtained in this study appear to be quite reasonable.

**Table II:** Calculated Bond Energy between the Cation and  $\text{H}_2\text{O}$  (kcal./mole)

Oxide	$r_e$ , Å.	$E_e$	$E_i$	$E_v$	$E_R$	$E$
NiO	2.1	41.5	10.8	9.8	-47.2	14.9
(111) face	2.2	38.4	8.9	7.8	-29.0	26.1
$r_e = 2.5$	2.3	35.8	7.5	6.3	-18.2	31.4
$E_e = 34.5$	2.4	33.9	6.5	5.1	-11.6	33.9
	2.5	32.2	5.6	4.3	-7.6	34.5
	2.6	30.6	4.9	3.6	-5.0	34.1
	2.8	27.7	3.7	3.1	-2.30	32.2
$\text{Cr}_2\text{O}_3$	2.0	51.2	12.3	13.9	-58.8	18.6
( $\text{Fe}_2\text{O}_3$ )	2.1	42.0	7.8	10.7	-35.2	25.3
(0001) face	2.2	35.3	4.8	8.3	-21.6	26.8
$r_e = 2.2$	2.3	29.7	2.9	6.5	-13.6	25.5
$E_e = 26.8$	2.4	24.9	1.9	5.1	-8.7	23.2
$\text{Al}_2\text{O}_3$	2.0	49.0	12.5	2.7	-38.2	26.0
(0001) face	2.1	41.5	8.0	2.1	-22.9	28.7
$r_e = 2.1$	2.2	34.6	4.8	1.7	-14.1	27.0
$E_e = 28.7$	2.3	27.7	3.0	1.4	-8.8	23.3
	2.4	22.0	1.9	1.2	-5.6	19.5

*Type of Bond Formed between the Adsorbed Molecules and the Surface Cations.* Based on the conclusions drawn from the analysis of the experimental results given above, the experimental heats of adsorption on the surface cations without any lateral interactions are listed in Table III. In view of the assumptions involved in the calculations, the agreement between the experimental heat of adsorption and the calculated adsorption bond energy for water are extraordinarily good, perhaps even fortuitously so. Nevertheless, this suggests that the electrostatic model is probably a good one for the case of water.

**Table III:** Experimental Heat of Adsorption over Cations

Adsorbates	NiO, kcal./mole	$\text{Cr}_2\text{O}_3$ , kcal./mole	$\text{Al}_2\text{O}_3$ , kcal./mole
$\text{H}_2\text{O}$	32	26	32
$\text{CH}_3\text{OH}$	32	26	31
$\text{CH}_3\text{NH}_2$	29	30	23
$\text{CH}_3\text{CN}$	26	27	26

It is also of interest to note that, in contrast to that found in the bond energy in the gaseous complexes, the adsorption bond energy of water to  $\text{Ni}^{2+}$  is slightly higher than that to the trivalent cations. This probably reflects that the greater density of  $\text{Ni}^{2+}$  ions on the surface is more than enough to compensate for its lower valency.

Similar calculations for the bond energy have not been attempted for the other adsorbates because even less is known about these molecules than about water. A qualitative comparison among the adsorbates, however, is possible. The adsorption of  $\text{CH}_3\text{OH}$  has been found to follow the same pattern as water in all cases except that the amount adsorbed is less for  $\text{CH}_3\text{OH}$ , probably owing to its larger size. For all practical purposes the calculated values for water would also be fairly close to that expected for  $\text{CH}_3\text{OH}$ . Therefore, the same electrostatic model is probably valid for  $\text{CH}_3\text{OH}$  as well as water.

In the case of  $\text{CH}_3\text{NF}_2$ , the heat of adsorption is expected to be less than that for water if the electrostatic model also prevails for the following reasons. (1) The equilibrium distance for M-N should be larger than that for M-O since it was found by X-ray diffraction that the M-N bond is longer than the M-O bond in ammoniates and hydrates. For example,  $\text{Ni}^{2+}\text{-N}$  is 2.4 Å. while  $\text{Ni}^{2+}\text{-O}$  is 2.13 Å. and  $\text{Cr}^{3+}\text{-O}$  is 1.88 Å. where  $\text{Co}^{3+}\text{-N}$  is 2.07 Å. ( $r_{\text{Co}^{3+}} \approx r_{\text{Cr}^{3+}}$ ).<sup>18</sup> Therefore, lower  $\varphi$  and  $F$  result for  $\text{CH}_3\text{NH}_2$  than for  $\text{H}_2\text{O}$ . (2) The dipole moment of  $\text{CH}_3\text{NH}_2$  is only 1.29 D. against 1.84 D. for  $\text{H}_2\text{O}$ . (3) NH bond polarizability of  $\text{CH}_3\text{NH}_2$  is approximately equal to that of  $\text{H}_2\text{O}$ . However, it is found that only in the case of  $\text{Al}_2\text{O}_3$  is the heat of adsorption of  $\text{CH}_3\text{NH}_2$  less than that of  $\text{H}_2\text{O}$ . In all others it is either equal to or greater than that of  $\text{H}_2\text{O}$ . This difference can be attributed to the existence of some coordination bond character by the shifting of the lone pair of electrons of N to the d orbitals of  $\text{Ni}^{2+}$ ,  $\text{Fe}^{3+}$ ,  $\text{Cr}^{3+}$  ions, whereas this does not occur with  $\text{Al}^{3+}$  of which the d orbital is not available. The coordina-

(17) F. Basolo and R. G. Pearson, "Mechanism of Inorganic Reactions," John Wiley and Sons, Inc., New York, N. Y., pp. 46-50.

(18) R. N. G. Wyckoff, "Crystal Structure," Vol. III, Interscience Publishers, Inc., New York, N. Y., 1960.

tion bond formation is favored by  $\text{CH}_3\text{NH}_2$  rather than the other molecules because of its lower ionization potential ( $\text{CH}_3\text{NH}_2$ , 9.41;  $\text{H}_2\text{O}$ , 12.56;  $\text{CH}_3\text{OH}$ , 10.85; and  $\text{CH}_3\text{CN}$ , 12.42 v.).<sup>19</sup> The adsorption of  $\text{CH}_3\text{CN}$  is strongly favored by its large dipole moment (3.97 D.) and the polarizability of the CN bond ( $1.85 \times 10^{-24}$  cc. *vs.*  $0.73 \times 10^{-24}$  for OH),<sup>12</sup> but its distance from the cation would be at least as large as that of  $\text{CH}_3\text{NH}_2$  and thus bring the heat of adsorption close to that for  $\text{H}_2\text{O}$ . Its high ionization potential makes the formation of a coordination bond unlikely. This is supported by the fact that water and  $\text{CH}_3\text{CN}$  share the same active sites on  $\text{Fe}_2\text{O}_3$  although less  $\text{CH}_3\text{CN}$  can be accommodated per unit area and by the fact that the heats of adsorption of  $\text{CH}_3\text{CN}$  on  $\text{Al}_2\text{O}_3$  and  $\text{Cr}_2\text{O}_3$  are about the same.

*Adsorption on Surface  $\text{O}^{2-}$  Ions.* In principle, the adsorption bond energy between a polar molecule and the surface  $\text{O}^{2-}$  ion can be approximated in a similar fashion as that on the surface cations. The bond is formed by attaching the hydroxyl or amino hydrogen or the C atom of the CN group to the  $\text{O}^{2-}$  ions. The interaction again involves  $E_e$ ,  $E_i$ ,  $E_v$ , and  $E_R$  terms as defined above. Similar calculations have been performed by Coulson<sup>20</sup> for the hydrogen bond in ice. Owing to the complexity of the electronic structure of the water molecule,<sup>21</sup> the linear dipole model and the OH bond polarizability used above may introduce more error in this case than that over the cations. Therefore, no quantitative approximation was attempted. The assignment of the second plateau heat (with the exception of  $\text{Fe}_2\text{O}_3$ ) to the adsorption on the oxygen anions is based on the following points. (1) Chemisorption of oxygen on NiO does not affect the second-plateau heat. (2) The heat is generally in the range of 18–21 kcal./mole for all adsorbates on all surfaces. This would require that these sites be approximately equivalent both electrostatically and geometrically in all the surfaces.

Although it is conceivable that the electrostatic potential over the surface  $\text{O}^{2-}$  would be different for the different oxides, this difference is expected to be of smaller magnitude than that obtained for the cation surface owing to the following reasons. (1) The arrangement and density of the oxygen ions in the oxygen layer are approximately the same for all four oxides studied here. (2) The differences in number, size, and charge of the cations, which determine  $E_e$  over the cation surface, are less important in this case as they are located farther away from the adsorbate and are shielded by the large oxygen ions. The other energy terms  $E_v$  and  $E_R$  which are quite different over the cations of the different oxides are expected to be approximately the same over the oxygen ions for all four

oxides. Therefore, the heat of adsorption on the  $\text{O}^{2-}$  sites is expected to differ not more than 1–2 kcal./mole among the four surfaces.

The lower heat of adsorption on  $\text{O}^{2-}$  than on cations is consistent with the following consideration. The hydroxyl and amino groups have very small intrinsic polarity; their dipole moments are chiefly coming from the lone-pair electrons; *i.e.*, the electronic charge center of a water molecule is not at its volume center but closer ( $\sim 0.2 \text{ \AA}$ .) to the lone-pair electron end of the O atom.<sup>13</sup> Therefore, although the electrostatic potential over the surface  $\text{Ni}^{2+}$  and that over the surface  $\text{O}^{2-}$  are approximately the same, at same volume center of water to center of surface ion distance, the  $E_e$  and  $E_i$  energies will be greater when the molecule is oriented in the  $\text{M}^{2+}\text{-OH}_2$  position than that in the  $\text{O}^{2-}\text{-HOH}$  position.

One might suspect that the decrease in the heat of adsorption with increase in surface coverage is due to the deactivation or repulsive force exerted by an adsorbed molecule on its neighboring sites. If the surface contains all cations in the top half-populated layer, initial adsorption will take place at cation sites relatively far apart. Therefore, they behave as isolated sites with no lateral interaction and will display a constant heat of adsorption characteristic of an energetically uniform surface. When about one-third to one-half of these surface cations is taken up, adsorption on unoccupied sites between the occupied sites would experience a repulsion following the relation  $E_R' = \mu_A\mu_B/a^3$ , where  $a$  is the distance between sites and  $\mu_A$  and  $\mu_B$  are the dipole moments of the adjacently adsorbed molecules. A rough calculation shows that maximum  $E_R'$  for water would be of the order of 1–2 kcal./mole over the (0001) faces of the  $\text{M}_2\text{O}_3$  crystals and 4 kcal./mole over the (111) face of the NiO. This is much less than the difference in the heats of adsorption between the plateaus. Such repulsion is undoubtedly contributing in the transition region between two plateaus where each type of site is gradually filling up. The difference in the shape of heat of adsorption curves over NiO can also be explained on this basis.  $\text{H}_2\text{O}$  and  $\text{CH}_3\text{OH}$  adsorbed on the  $\text{Ni}^{2+}$  ions through pure electrostatic interaction in cooperation with their higher dipole moment and closer packing on the surface would experience more lateral repulsion than would  $\text{CH}_3\text{NH}_2$ ; therefore, the former show a greater dependence of the heat of ad-

(19) R. W. Kiser, "Tables of Ionization Potentials," U.S.A.E.C. Report TID 6142, 1960.

(20) C. A. Coulson, "Hydrogen Bonding," D. Hadzi, Ed., Pergamon Press Ltd., London, 1959, p. 339.

(21) See, for example, J. A. Pople, *Proc. Roy. Soc. (London)*, **A202**, 323 (1950); C. A. Coulson, *ibid.*, **A207**, 63 (1951); and F. O. Ellison and H. Schull, *J. Chem. Phys.*, **23**, 2348 (1955).

sorption on coverage. In the case of  $\text{Cr}_2\text{O}_3$ , the packing for all molecules is less dense, and a sharper distinction between the plateaus is observed.

*Acknowledgment.* The author is grateful to Dr. J. T. Kummer for many valuable discussions during the course of this work.

## Diffusion in the Three-Component Liquid System

### Acetone-Benzene-Carbon Tetrachloride

by H. T. Cullinan, Jr., and H. L. Toor

*Department of Chemical Engineering, Carnegie Institute of Technology, Pittsburgh, Pennsylvania*  
(Received June 9, 1965)

The diffusional behavior of the system acetone-benzene-carbon tetrachloride was studied at 25°. The diffusion coefficients for the binary systems which form the borders of the ternary system as well as those for the ternary system were measured using the diaphragm cell method. The binary data were found to be in agreement with previous measurements by other techniques. The four ternary diffusion coefficients were found to exhibit considerable nonlinear concentration dependence as do two of the three binary pairs. The concentration dependence of the ternary diffusion coefficients was qualitatively predicted by a modified form of the Stefan-Maxwell equations.

#### Introduction

A study of the diffusional behavior of completely miscible ternary liquid systems has been under way in these laboratories. The behavior of two relatively ideal systems of this type has already been reported.<sup>1,2</sup> As a continuation of this program, the diffusional behavior of the relatively nonideal system acetone-benzene-carbon tetrachloride has been investigated over the full concentration range.

#### Experimental Section

The diffusion coefficients for the system were measured using a modification of the diaphragm cell technique as described previously.<sup>1</sup> The reagents used were all Certified, spectranalyzed grade obtained from the Fisher Scientific Co. and were utilized without any further treatment. For the binary and concentrated ternary experiments, concentrations were measured by gas-liquid chromatography using a Beckman

GC-2A instrument with helium as a carrier gas. In the earlier stages of the work, the column used was a 3.6-m., 0.63-cm. diameter column packed with polyethylene glycol, standard concentration (Burrell Corp.). This column showed some deterioration in the later stages of the study and was replaced with a 3.0-m., 0.63-cm. diameter column packed with diethylene glycol succinate (supplied by Beckman Instrument Co.). Both columns gave reasonable resolution and short elution times. For experiments performed in regions of the ternary field in which one of the components was present in small quantity, concentrations were measured by mass spectrometry using a Consolidated Electroynamics 21-103C instrument maintained by the Department of Chemistry at Carnegie Institute of Technology.

- (1) J. K. Burchard and H. L. Toor, *J. Phys. Chem.*, **66**, 2015 (1962).
- (2) F. O. Shuck and H. L. Toor, *ibid.*, **67**, 540 (1963).



The four diaphragm cells used in this study were the same four cells employed by Shuck.<sup>2</sup> Recalibration of these cells (using 0.5 *N* HCl diffusing into pure water at 25.0°) was performed during the course of this work. The resulting cell factors,  $\beta$ , from several replicates and the 95% confidence ranges are

$$\beta_0 \text{ (cell 0)} = 0.1626 \pm 0.0021$$

$$\beta_1 \text{ (cell 1)} = 0.2028 \pm 0.0027$$

$$\beta_2 \text{ (cell 2)} = 0.1950 \pm 0.0032$$

$$\beta_3 \text{ (cell 3)} = 0.2537 \pm 0.0046$$

### Binary Systems

The mutual diffusion coefficients for the binary systems acetone–benzene, acetone–carbon tetrachloride, and benzene–carbon tetrachloride, which form the borders of the ternary system, were measured at 25° for several mean concentrations over the binary concentration ranges. Although these binary systems had been studied previously by other techniques,<sup>3,4</sup> a repetition using the diaphragm cell method seemed justified in order to test further the applicability of the diaphragm cell method to the present system as well as to afford an estimate of the accuracy of the experimental procedure.

In most cases two duplicate measurements were made at each average concentration. The standard cell equation<sup>5</sup> was used in the form

$$\frac{1}{\beta t} \ln \frac{\Delta C_i^0}{\Delta C_i^F} = \bar{D}_{ij} \quad (1)$$

where  $C_i$  is the molar concentration of component  $i$ ,  $t$  is the duration of the experiment in seconds, superscript 0 refers to initial conditions ( $t = 0$ ), superscript F to final conditions ( $t = t$ ), and  $\Delta C_i$  is the difference between the molar concentration in one cell chamber and that in the other.  $\bar{D}_{ij}$  is the integral binary diffusion coefficient, and since the two bulbs in each cell are of about equal volume and  $\bar{D}_{ij}$  is nearly linear with concentration over the concentration range used in an experiment,  $\bar{D}_{ij}$  may be taken to be the differential coefficient at the arithmetic average composition of the experiment. This average mole fraction of component  $i$  is denoted as  $X_i$ .

From these measurements it was confirmed that the concentration dependence of the diffusion coefficients for the acetone–benzene and acetone–carbon tetrachloride binary systems are nonlinear in nature, while the diffusion coefficient of the benzene–carbon tetrachloride system is a linear function of mole fraction. The results of this study are shown in Table I, while in Figures 1, 2, and 3 these results are compared with the

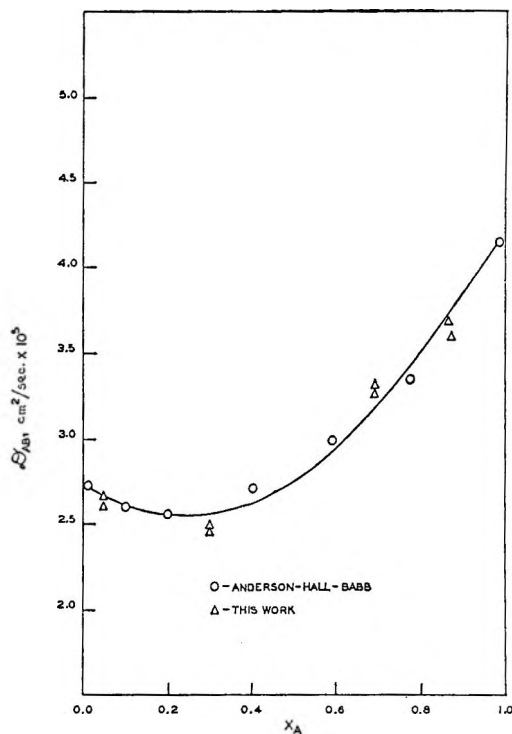


Figure 1. Binary mutual diffusion coefficient for the system acetone–benzene.

previous work.<sup>3,4</sup> Subscripts A, B, and C refer to acetone, benzene, and carbon tetrachloride, respectively.

Table I: Binary Diffusion Coefficients

$X_A$	$D_{AB}^a$	$X_A$	$D_{AC}$	$X_C$	$D_{BC}$
0.0655	2.655	0.0895	1.527	0.1457	1.841
0.0655	2.620	0.0919	1.432	0.1467	1.640
0.3052	2.506	0.6822	2.260	0.4865	1.591
0.3071	2.474	0.8896	2.881	0.4866	1.651
0.7132	3.298	0.8904	2.961	0.8062	1.545
0.7148	3.274			0.8076	1.543
0.9798	3.687			0.8078	1.520
0.8836	3.575				

<sup>a</sup> All values of  $D_{ij}$  are in  $\text{cm}^2/\text{sec.} \times 10^5$ .

Since the accuracy of the chromatographic analysis was determined to be approximately the same for all three binary systems, all of the measured binary diffusion coefficients were assumed to be from one

(3) S. C. Caldwell and A. L. Babb, *J. Phys. Chem.*, **60**, 51 (1956).

(4) D. K. Anderson, J. R. Hall, and A. L. Babb, *ibid.*, **62**, 404 (1958).

(5) A. R. Gordon, *Ann. N. Y. Acad. Sci.*, **46**, 285 (1945).



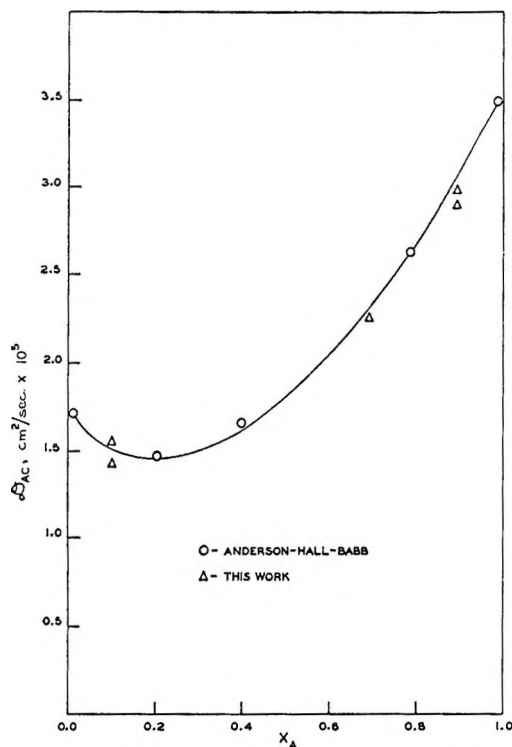


Figure 2. Binary mutual diffusion coefficient for the system acetone-carbon tetrachloride.

statistical population. Under this assumption the duplication of data at the various compositions afforded an estimation of the variance of this population, from which confidence intervals could be assigned to each individual measurement. The 95% confidence range for each measured binary diffusion coefficient reported in Table I, calculated in this manner, is  $\pm 0.042 \times 10^{-6} \text{ cm.}^2/\text{sec.}$

### Ternary System

The four diffusion coefficients to be measured are defined by the equations<sup>1</sup>

$$J_A = -D_{AA}\nabla C_A - D_{AB}\nabla C_B \quad (2)$$

$$J_B = -D_{BA}\nabla C_A - D_{BB}\nabla C_B \quad (3)$$

where  $J_i$  is the molar flux of species  $i$  with respect to the volume average velocity and  $C_i$  again is concentration of species  $i$  in moles per unit volume.

It was shown earlier<sup>1,2</sup> that in a diaphragm cell these expressions lead to the working equations<sup>6</sup>

$$\frac{1}{\beta t} \ln \frac{\Delta C_A^0}{\Delta C_A^F} = \bar{D}_{AA} + \bar{D}_{AB} \left( \frac{\Delta C_B}{\Delta C_A} \right)_{av} \quad (4)$$

$$\frac{1}{\beta t} \ln \frac{\Delta C_B^0}{\Delta C_B^F} = \bar{D}_{BA} \left( \frac{\Delta C_A}{\Delta C_B} \right)_{av} + \bar{D}_{BB} \quad (5)$$

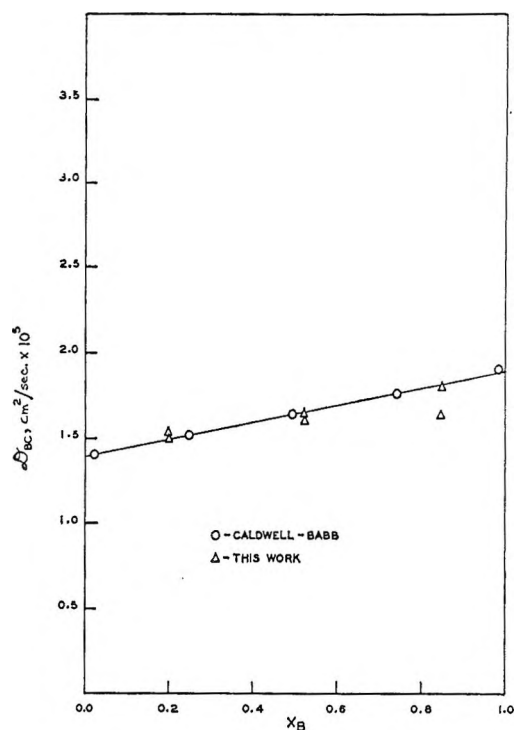


Figure 3. Binary mutual diffusion coefficient for the system benzene-carbon tetrachloride.

where the overbars refer to integral average values of the diffusion coefficients and the average of the ratio of concentration differences is the arithmetic average of the initial and final values.

As stated previously,<sup>1</sup> under the restriction that the cross coefficients ( $D_{ij}$ ,  $i \neq j$ ) and the differences between the main coefficients ( $D_{ii}$ ) are small compared to the main coefficients, eq. 4 and 5 approximate the exact solutions to the cell equations very closely if all the  $\Delta C_i^0$  are of the same magnitude or if  $\Delta C_C^0$  is small. Thus, both eq. 4 and 5 may be considered valid in regions of the ternary field where experiments may be performed with concentration differences of the same magnitude for all species. In regions where benzene is dilute,  $\Delta C_B^0$  will be restrictively small and eq. 5 is invalid. However, in this region eq. 4 remains valid, thus permitting evaluation of the coefficients,  $D_{AA}$  and  $D_{AB}$  in this region. Similarly, eq. 4 is invalid in regions of dilute acetone, while eq. 5 remains valid, thus permitting evaluation of  $D_{BA}$  and  $D_{BB}$  in this region. In regions of dilute carbon tetrachloride, eq. 4 and 5 both are valid, and all four diffusion coefficients may be evaluated in this region by use of these relations.<sup>1</sup>

(6) Reference 1 lists the assumptions necessary to obtain these relations. The errors caused by the use of eq. 4 and 5 in place of the more exact cell equations were found to be negligible in this study.

According to the above discussion, then, eq. 4 and/or eq. 5 may be utilized for the evaluation of the diffusion coefficients defined by eq. 2 and 3 in all regions of the ternary concentration field except for the following: (1) eq. 5 is not valid for the determination of  $D_{BA}$  and  $D_{BB}$  in dilute benzene solution; (2) eq. 4 is not valid for the determination of  $D_{AA}$  and  $D_{AB}$  in dilute acetone solutions. These restrictions on the applicability of the diaphragm cell technique may be essentially overcome by consideration of the following limiting relation for the cross coefficients<sup>2,7</sup>

$$\lim_{c_i \rightarrow 0} D_{ij} = 0, \quad \begin{matrix} i, j = A, B \\ i \neq j \end{matrix} \quad (6)$$

which indicates that, if component  $i$  is sufficiently dilute, the flux expression for component  $i$  will reduce to the uncoupled form,  $j_i = -D_{ii}\nabla C_i$ , so the cell equation for this species may be written, as  $C_i \rightarrow 0$

$$\frac{1}{\beta t} \ln \frac{\Delta C_i^0}{\Delta C_i^F} = \bar{D}_{ii} \quad (7)$$

In experiments designed to utilize eq. 7, the average value of the concentration of component  $i$  should be kept small enough to ensure the validity of the use of eq. 6, yet of sufficient magnitude to allow the use of measurable concentration differences.

Holmes, *et al.*,<sup>8</sup> assumed the validity of eq. 7 for the measurement of diffusion of dilute solutes in pairs of mixed solvents. The above analysis shows it to be valid subject to the above-mentioned restrictions.

According to the above scheme, the diaphragm cell is adaptable to the measurements of all four ternary diffusion coefficients at every point within the ternary concentration field, including all the (nontrivial) diffusion coefficients along the three borders of the ternary system.

Several investigations<sup>8,9</sup> have been carried out on a number of systems to characterize the behavior of the limiting value of the main diffusion coefficients indicated in eq. 7. However, these limiting coefficients are not the only experimentally accessible limiting values of the four ternary diffusion coefficients. In the present work, experimental values of all possible limiting values are reported.

The experiments performed in the concentrated regions of the ternary field were designed and analyzed according to the method set down by Shuck.<sup>2</sup> Several runs at each average concentration were made with varying initial values of the ratio of concentration differences. The diffusion coefficients were calculated from all of the data at a given average concentration by computing the quantities  $1/\beta t \ln \Delta C_i^0/\Delta C_i^F$  and  $(\Delta C_j/\Delta C_i)_{AV}$  and using the method of least squares

to determine the slope and intercept of the best straight line through the data (according to the form of eq. 4 and 5). An example is shown in Figure 4. Using this method the confidence ranges of the measured coefficients could also be easily calculated.

For the experiments in the dilute regions of the concentration field designed to utilize eq. 4 and/or eq. 5, data were not sufficient in number at any given average concentration to warrant a statistical regression analysis in the above manner. In these experiments the diffusion coefficients were simply calculated by averaging the slopes and intercepts of the several possible straight lines through the data at any given average concentration. An example is shown in Figure 5. The confidence ranges of the measured coefficients in these experiments were obtained by the method employed by Burchard<sup>1</sup> from an analysis of variances contributed by each experimental value used in the calculations.

It should be pointed out that in the dilute benzene and dilute acetone experiments designed to use eq. 4 and 5, respectively, the cross-diffusion coefficients were the primary objective since the following limiting relation is valid in these regions<sup>2,10</sup>

$$\lim_{c_i \rightarrow 0} D_{ii} = D_{iC} \quad \begin{matrix} i, j = A, B \\ i \neq j \end{matrix} \quad (8)$$

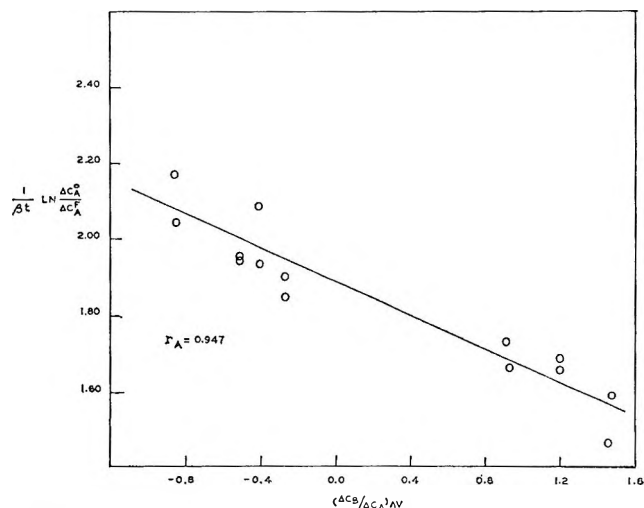


Figure 4. Determination of  $D_{AA}$  and  $D_{AB}$  at  $\bar{X}_A = 0.2989$ ,  $\bar{X}_B = 0.3490$ .

(7) I. J. O'Donnell and L. J. Gosting, "The Structure of Electrolytic Solutions," John Wiley and Sons, Inc., New York, N. Y., 1957.

(8) J. T. Holmes, C. R. Wilke, and D. R. Olander, *A.I.Ch.E. J.*, **8**, 646 (1962).

(9) Y. P. Tang and D. M. Himmelblau, *ibid.*, **11**, 54 (1965).

(10) In these dilute experiments, the measured value of the main diffusion coefficient did not differ significantly from the corresponding value of the binary coefficients thus indicating both the validity of eq. 8 and the use of eq. 4 or 5.

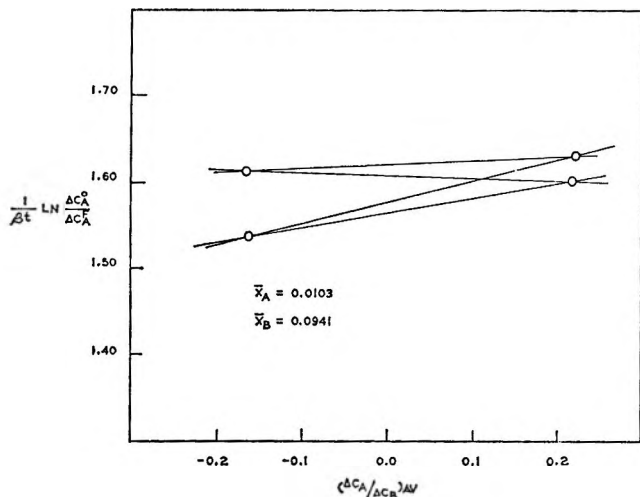


Figure 5. Sample determination of  $D_{BA}$  in dilute acetone solution.

Since the cross coefficients  $D_{ij}$  were the primary objectives of these experiments, the concentration difference ratio  $(\Delta C_j / \Delta C_i)_{AV}$  was varied from one run to the next at the same average concentration to permit a reasonable evaluation of the slope of  $1/\beta t \ln \Delta C_i^0 / \Delta C_i^F$  vs.  $(\Delta C_j / \Delta C_i)_{AV}$  to be made (see Figure 5). The fact that in these experiments performed in dilute acetone and dilute benzene solutions (approximately 1 mole % of the dilute species), the corresponding quantity  $1/\beta t \ln \Delta C_i^0 / \Delta C_i^F$  did not vary with changes in the gradient ratio, indicated that the dilute species was exhibiting uncoupled diffusional behavior at these levels of concentration. This serves to confirm the validity of eq. 6 in these regions, and hence, also eq. 7.

Equation 7 was utilized in the same manner as eq. 1 in the binary experiments with two duplicate measurements being made at each average concentration. The duplication of data at the various compositions afforded an estimate of variance from which confidence intervals could be assigned to each individual measurement.

The ternary diffusion coefficients obtained according to the above scheme are shown with their confidence ranges in Table II. The data presented in Table II together with the limiting information contained in eq. 6 and 8 and the additional limiting relations<sup>2</sup>

$$\lim_{C_i, C_c \rightarrow 0} D_{ii} = D_{ij}^0 \quad \begin{matrix} i, j = A, B \\ i \neq j \end{matrix} \quad (9)$$

$$\lim_{C_i, C_c \rightarrow 0} D_{ij} = (D_{Ci}^0 - D_{ij}^0) \frac{\bar{V}_j}{\bar{V}_i} \quad \begin{matrix} i, j = A, B \\ i \neq j \end{matrix} \quad (10)$$

thus permitted the behavior of each of the four diffusion coefficients defined by eq. 2 and 3 for the system ace-

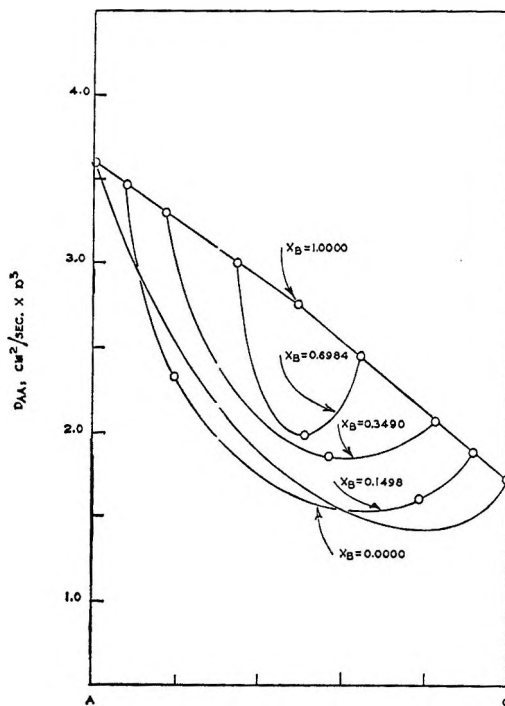


Figure 6. The ternary diffusion coefficient,  $D_{AA}$ .

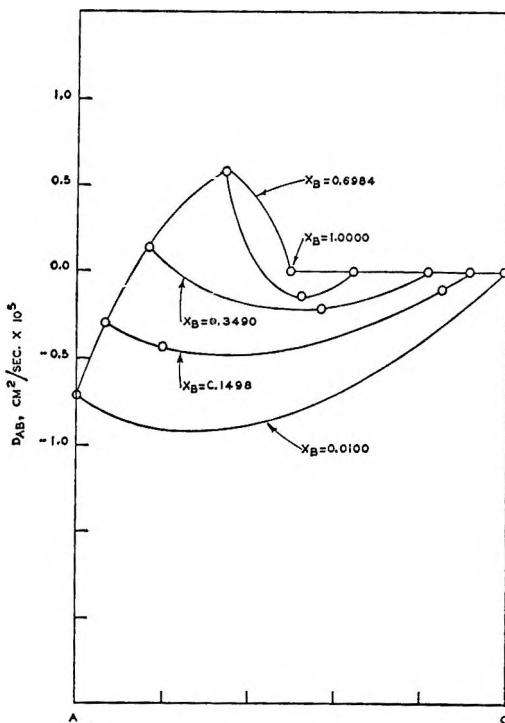


Figure 7. The ternary diffusion coefficient,  $D_{AB}$ .

tone-benzene-carbon tetrachloride to be mapped over the entire range of composition. To illustrate the interesting behavior of the four diffusion coefficient surfaces for this system, the following mode of represen-

Table II: Ternary Diffusion Coefficients

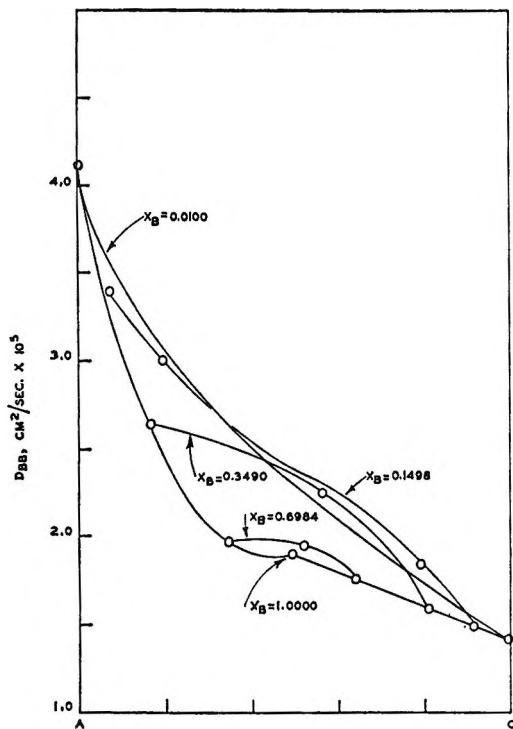
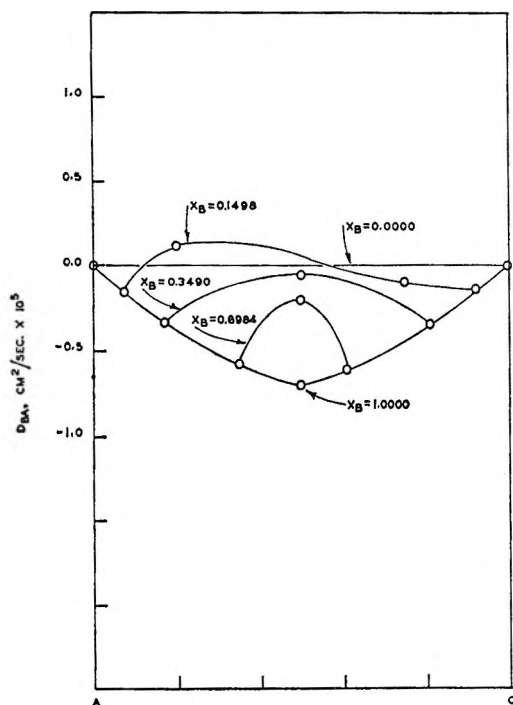
$X_A$	$X_B$	$D_{AA}^a$	$D_{AB}$	$D_{BB}$	$D_{BA}$
0.2989	0.3490	$1.887 \pm 0.041^b$	$-0.213 \pm 0.045$	$2.255 \pm 0.027$	$-0.037 \pm 0.014$
0.1496	0.1499	$1.598 \pm 0.047$	$-0.058 \pm 0.039$	$1.812 \pm 0.061$	$-0.083 \pm 0.040$
0.1497	0.6984	$1.961 \pm 0.063$	$0.013 \pm 0.051$	$1.929 \pm 0.102$	$-0.149 \pm 0.057$
0.6999	0.1497	$2.330 \pm 0.105$	$-0.432 \pm 0.094$	$2.971 \pm 0.101$	$0.132 \pm 0.052$
0.0964	0.0100			$1.555 \pm 0.068$	
0.0964	0.0100			$1.657 \pm 0.068$	
0.2416	0.0102			$1.513 \pm 0.068$	
0.2441	0.0100			$1.530 \pm 0.068$	
0.4921	0.0105			$2.401 \pm 0.068$	
0.4930	0.0100			$2.343 \pm 0.068$	
0.7456	0.0102			$2.863 \pm 0.068$	
0.7456	0.0104			$2.903 \pm 0.068$	
0.7419	0.0104			$2.719 \pm 0.068$	
0.7439	0.0103			$2.967 \pm 0.068$	
0.8951	0.0100			$3.351 \pm 0.068$	
0.8951	0.0100			$3.615 \pm 0.068$	
0.0952	0.0101		$-0.195 \pm 0.201$		
0.2436	0.0103		$-0.400 \pm 0.217$		
0.4947	0.0100		$-0.695 \pm 0.244$		
0.7461	0.0102		$-0.933 \pm 0.261$		
0.8956	0.0101		$-1.083 \pm 0.269$		
0.0100	0.0951	$1.813 \pm 0.068$			
0.0100	0.0974	$1.678 \pm 0.068$			
0.0101	0.2452	$1.903 \pm 0.068$			
0.0096	0.2452	$2.001 \pm 0.068$			
0.0094	0.4954	$2.357 \pm 0.068$			
0.0100	0.7452	$2.582 \pm 0.068$			
0.0095	0.7452	$2.525 \pm 0.068$			
0.0094	0.8950	$2.669 \pm 0.068$			
0.0093	0.8950	$2.510 \pm 0.068$			
0.0103	0.0941				$0.097 \pm 0.206$
0.0100	0.4930				$-0.620 \pm 0.217^c$
0.0102	0.7400				$-1.083 \pm 0.237$
0.0933	0.8967	$3.105 \pm 0.068$	$0.550 \pm 0.163$	$1.860 \pm 0.068$	$-0.780 \pm 0.113$
0.2415	0.7484	$3.069 \pm 0.068$	$0.603 \pm 0.191$	$1.799 \pm 0.068$	$-0.638 \pm 0.126$
0.4924	0.4972	$2.857 \pm 0.068$	$0.045 \pm 0.182$	$2.471 \pm 0.068$	$-0.289 \pm 0.124$
0.7432	0.2466	$3.251 \pm 0.068$	$-0.011 \pm 0.195$	$2.896 \pm 0.068$	$-0.301 \pm 0.132$
0.8954	0.0948	$3.475 \pm 0.068$	$-0.158 \pm 0.206$	$3.737 \pm 0.068$	$0.108 \pm 0.145$

<sup>a</sup> All values of  $D$  are in  $\text{cm.}^2/\text{sec.} \times 10^5$ . <sup>b</sup> 95% confidence range. <sup>c</sup> Measurement obtained by Mr. C. M. Yon.

tation was adopted. A triangular parallelepiped was constructed by erecting perpendiculars from the three apexes of the standard equilateral triangular composition diagram. On each of the three faces of this figure, the binary coefficients could be plotted, while the ternary coefficients could be plotted in the inner regions of the figure as the intersection of the perpendicular erected from the appropriate composition point on the base triangle with the plane parallel to the base corresponding to the value of the coefficient in question. Two-dimensional representations of the diffusion coefficient surfaces constructed in this manner were obtained by projecting the intersections of these surfaces with planes erected perpendicular to the base

triangle (so as to intersect the base triangle along lines of constant composition of a given component) onto a plane coinciding with one of the planes forming a face of the parallelepiped. The resulting two-dimensional diagram is a series of curves, at various levels of concentration of one component, depicting the variation of the diffusion coefficient with the relative composition of the remaining two components. The three-dimensional nature of the original representation is not completely lost in such projections since they are, in essence, side views of the parallelepiped taken parallel to the base triangle and perpendicular to a given face.

Four such diagrams constructed in this manner representing the complete behavior of each of the diffusion


 Figure 8. The ternary diffusion coefficient,  $D_{BB}$ .

 Figure 9. The ternary diffusion coefficient,  $D_{BA}$ .

carbon tetrachloride side of the three-dimensional figure. The surface of the main diffusion coefficient,  $D_{AA}$ , is convex in nature with the relative minimum in the limit of the binary coefficient,  $\mathcal{D}_{AC}$ , being reflected uniformly throughout the entire concentration field. The acetone to carbon tetrachloride ratios at which these relative minima occur within the field correspond closely to the ratio at which the binary diffusivity,  $\mathcal{D}_{AC}$ , exhibits a minimum value. The cross-diffusion coefficient,  $D_{BA}$ , also behaves in a fairly uniform manner with the concentration dependence close to the acetone-carbon tetrachloride border being reflected throughout the field but distorted by the limiting behavior along the acetone-benzene border. The behavior of the other main coefficient,  $D_{BB}$ , while still relatively smooth in nature, is more complicated with no easily recognizable trends. Unlike the coefficient,  $D_{AA}$ , the limiting behavior along the borders is not generally reflected within the field. The behavior of the remaining cross coefficient,  $D_{BA}$ , is complex, yet relatively well behaved.

The rather complicated behavior of the diffusion coefficient surfaces for the present system thus did not permit the statistical fitting of the experimental data with simple surfaces as was the case in previous work.<sup>1,2</sup> In the two thermodynamically relatively ideal systems which were studied previously, the binary diffusion coefficients were linear functions of concentration and this was reflected in a linear dependence of the ternary coefficients on concentration. The binary coefficients in the present relatively nonideal system are nonlinear functions of concentration and this is reflected in the nonlinear concentration dependence of the ternary coefficients. This correspondence between binary and ternary behavior is of course expected because the limiting values of the ternary coefficients are related to the binary coefficients through eq. 8, 9, and 10.

The fact that, in some cases at least, the ternary behavior seemed to some extent to be reflecting the behavior of the binary coefficients along the borders of the field did offer some hope for the explanation of the ternary complexities in terms of the binary interactions.

Burchard and Toor<sup>1</sup> used the Stefan-Maxwell equations for ideal gas mixtures in this manner with partial success. These equations give the ternary diffusion coefficients in terms of the binary coefficients as<sup>1</sup>

$$D_{ii} = \frac{\mathcal{D}_{iC}[(1 - X_i)\mathcal{D}_{ij} + X_i\mathcal{D}_{iC}]}{X_i\mathcal{D}_{iC} + X_j\mathcal{D}_{iC} + X_C\mathcal{D}_{ij}} \quad i, j = A, B \quad (11a)$$

$$D_{ij} = \frac{X_i\mathcal{D}_{iC}(\mathcal{D}_{iC} - \mathcal{D}_{ij})}{X_i\mathcal{D}_{iC} + X_j\mathcal{D}_{iC} + X_C\mathcal{D}_{ij}} \quad i, j = A, B \quad (11b)$$

The  $\mathcal{D}_{ij}$  in the above equations are, as before, the binary diffusion coefficients for a mixture of species  $i$  and  $j$ .

coefficients are presented in Figures 6, 7, 8, and 9. Each of these was obtained by projecting the intersections of the diffusion coefficient surfaces with planes of constant benzene composition onto the acetone-

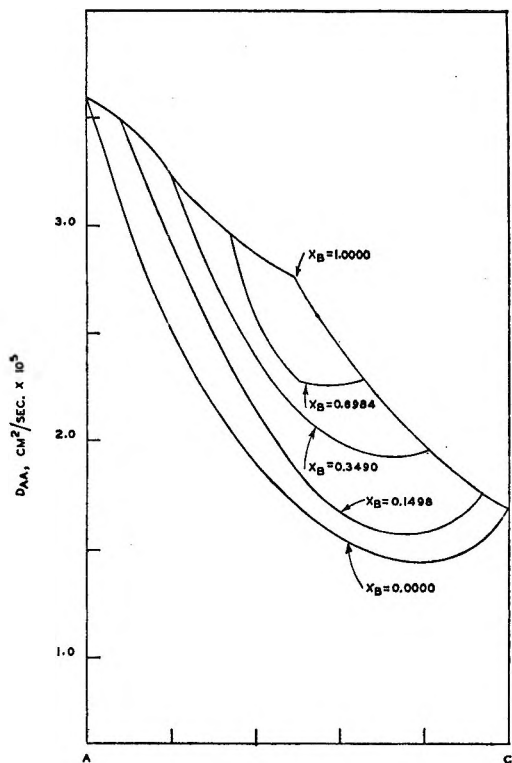


Figure 10. Prediction of  $D_{AA}$  from eq. 11a.

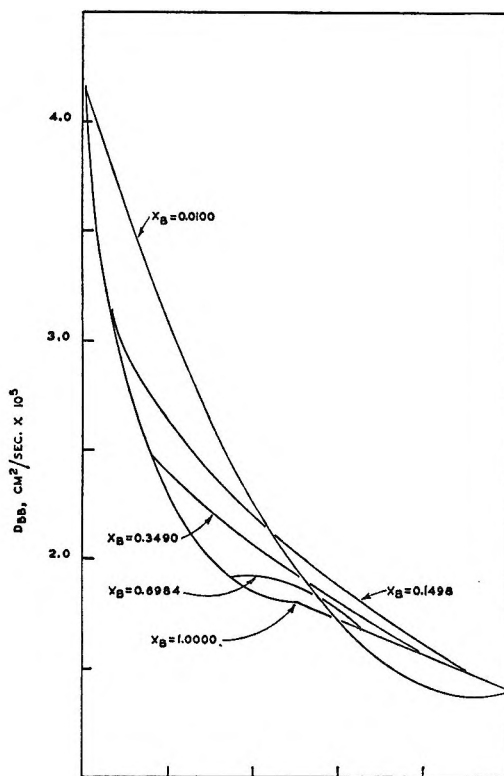


Figure 12. Prediction of  $D_{BB}$  from eq. 11a.

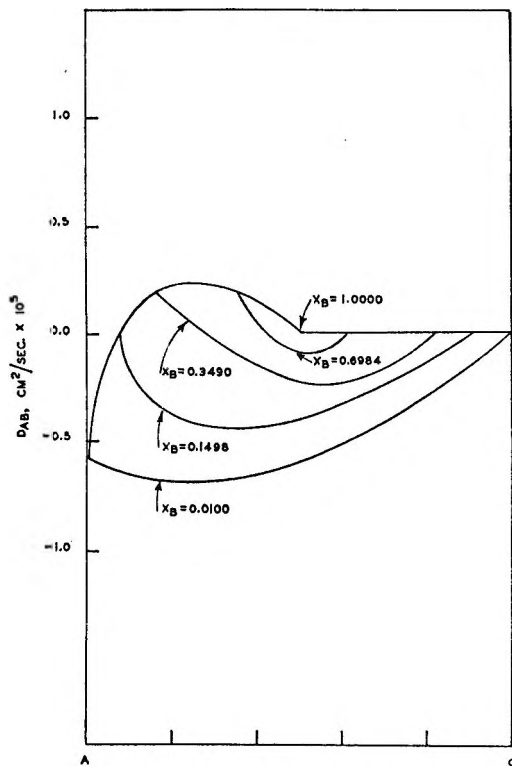


Figure 11. Prediction of  $D_{AB}$  from eq. 11b.

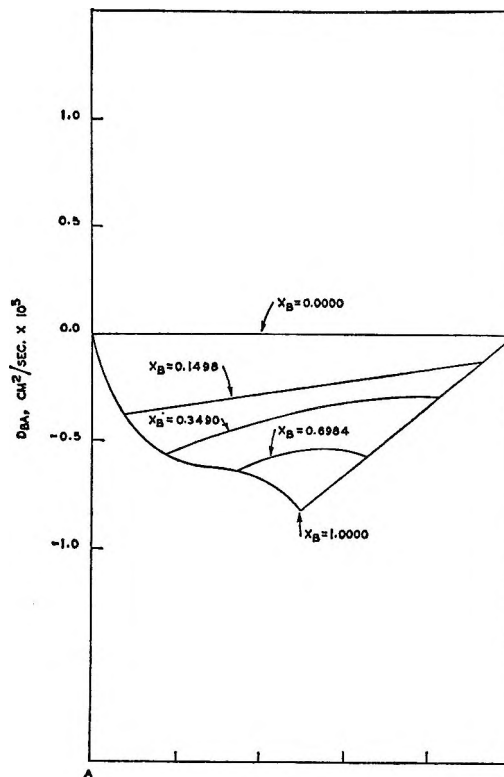


Figure 13. Prediction of  $D_{BA}$  from eq. 11b.

These equations were applied to liquids by evaluating the measured  $D_{ij}$  at the equivalent binary composition,  $\bar{X}_i = X_i/(X_i + X_j)$  of the ternary mixture in question.<sup>1</sup>

By applying eq. 11a and 11b to the present system in this manner using the binary data as presented in Figures 1, 2, and 3, diffusion coefficient surfaces analogous to Figures 6, 7, 8, and 9 could be generated. The four diffusion coefficient surfaces predicted by eq. 11 are presented in Figures 10, 11, 12, and 13. It is noted that the equations were used to predict the ternary coefficients at the borders as well as within the ternary field.

As can be seen from these representations, although the prediction of the ternary coefficients by means of eq. 11 are not quantitative, the general behavior of the four diffusion coefficient surfaces are fairly well reproduced in all four cases.

Although there is no *a priori* reason for applying the Stefan-Maxwell equations to liquid systems, these

equations represent essentially Bearman's<sup>11</sup> and Lightfoot, Cussler, and Rettig's<sup>12</sup> equations written for a thermodynamically ideal system. The binary activity data which are available<sup>13</sup> indicate that the present ternary system is far from ideal, but the lack of ternary activity data precludes any meaningful attempt to use the above equations to account for lack of ideality. For the same reason, it is not possible to carry out a meaningful check of the Onsager reciprocal relations.

*Acknowledgment.* The authors wish to thank the National Science Foundation for its financial support of this work, Mr. C. M. Yon for his assistance, and Professor G. J. Mains and Mr. S. Wrbican for the mass spectrometer analyses.

(11) R. J. Bearman, *J. Phys. Chem.*, **65**, 1961 (1961).

(12) E. N. Lightfoot, E. L. Cussler, Jr., and R. L. Rettig, *A.I.Ch.E. J.*, **8**, 708 (1962).

(13) J. Timmermans, "Physico-Chemical Constants of Binary Systems in Concentrated Solutions," Vol. I, Interscience Publishers, Inc., New York, N. Y., 1959.

## The Adsorption of Hexachloroacetone on Alumina-Containing Surfaces

by M. L. Hair and I. D. Chapman

*Exploratory Chemical Research Department, Research and Development Laboratory, Corning Glass Works, Corning, New York (Received June 10, 1965)*

The infrared spectra of hexachloroacetone adsorbed upon alumina-containing surfaces have been obtained. By analogy with the spectra of similar complexes with aluminum and boron halides, these spectra have allowed certain conclusions to be drawn concerning the strength and distribution of Lewis acid sites on such surfaces. The strengths of the sites on a silica-alumina gel were very similar to those on an alumina gel, and both of these surfaces contained at least three sites of differing strength.

The adsorption of nitrogenous bases on alumina-containing surfaces has been used by many workers as a method for the determination of surface acidity. The quantitative desorption of ammonia from such surfaces has been widely regarded as a measure of surface acidity, but the recent results obtained by Peri<sup>1</sup> on the infrared adsorption spectra of adsorbed ammonia species

show considerable decomposition of the ammonia and cast doubt on this technique as a method of determining surface acidity. It is generally accepted that the surfaces of catalytic aluminas and silica-aluminas contain sites which exhibit Lewis acidity, and many

(1) J. B. Peri, *J. Phys. Chem.*, **69**, 231 (1965).

workers believe that the silica-alumina surface contains acidic sites which are protonic in character.

Parry<sup>2</sup> has described the infrared spectrum of pyridine adsorbed on both alumina and silica-alumina surfaces, and from a comparison of the observed spectra with those of pyridine complexes with inorganic Lewis acid halides and hydrogen acids, concluded that both alumina and silica-alumina contained Lewis acid sites whereas only the silica-alumina-pyridine spectra were cognizant of a protonated molecule. Parry's work has been repeated and extended by Basila<sup>3</sup> and co-workers, who confirmed Parry's observations. No work, however, has yet been able to demonstrate the presence of protonic sites on alumina surfaces.

Whereas these studies of the infrared spectra of adsorbed molecules have provided valuable proof of the existence of Lewis and Brønsted acid sites on these acidic surfaces, they have suffered from the serious disadvantage in that the use of nitrogenous bases leads to spectra which show little perturbation attributable to differences in the strengths of the acid sites or the number of sites of differing acidity. Also, as the nitrogenous bases react with both Lewis and Brønsted sites, the spectra on some surfaces tend to be complicated and difficult to interpret. The purpose of the present work is to demonstrate that the use of a carbonyl-containing basic molecule can be used to give an indication of both the strength and distribution of the Lewis acid sites on the alumina-containing surfaces.

Lappert<sup>4</sup> has examined the infrared spectra of a number of complexes of ethyl acetate and inorganic Lewis acid halides and suggested that the shift in the carbonyl stretching frequency of the carbonyl group may be taken as a measure of the Lewis acidity of the coordinating halide. This work has been extended by Cook,<sup>5</sup> who examined the spectra of a series of metal halide complexes using xanthone as a ligand. In Figure 1 the shifts in the carbonyl stretching frequency for xanthone complexes of the boron halides are plotted as a function of the heat of formation of the pyridine complexes of these halides in nitrobenzene solution as determined by Brown and co-workers.<sup>6</sup> It is seen from this linear correlation that, at least in this series of similar complexes, the fundamental C=O stretching frequency can be taken as a measure of the Lewis acidity of the halides.

In these carbonyl compounds, the complex formation takes place *via* the oxygen atom of the carbonyl group. The donation of electrons from the oxygen atom into the vacant orbital of the boron halide leads to a delocalization of the electrons in the carbonyl double bond. This perturbation results in a shift of the carbonyl stretching frequency to lower wave numbers, the greater shifts

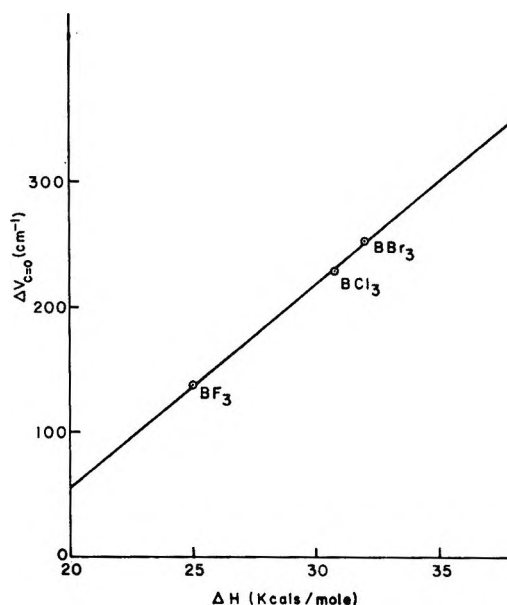


Figure 1. Shift in carbonyl stretching frequency of xanthone complexes of boron halides *vs.* heat of formation of analogous pyridine complexes in nitrobenzene solution.

being associated with increased Lewis acidity. This is clearly demonstrated in Figure 1 where the shift to lower wave numbers is in the order  $\text{BI}_3 > \text{BBr}_3 > \text{BCl}_3 > \text{BF}_3$ , in agreement with thermal data on the acidity of the halides.

Cook has specified five essential criteria which the ligand should fulfill before it can be used to estimate Lewis acidity.

(1) The ligand should not be easily protonated. This becomes even more important in dealing with surfaces on which strong protons may exist, as such sites would react with the donor molecule in the same manner as the Lewis acid sites.

(2) The complex formed should be stable and non-hygroscopic. This assumes importance if the technique is to be adapted to a routine estimation of surface acidity.

(3) Steric hindrance should be minimized. Again, this assumes greater importance in dealing with catalytically active solids where the pores may be small, rendering the sites inaccessible to large molecules.

(4) The carbonyl group should possess a large polar-

(2) E. P. Parry, *J. Catalysis*, **2**, 371 (1963).

(3) M. R. Basila, T. H. Kantner, and K. H. Rhee, *J. Phys. Chem.* **68**, 3197 (1964).

(4) M. F. Lappert, *J. Chem. Soc.*, 542 (1962).

(5) D. Cook, *Can. J. Chem.*, **41**, 522 (1963).

(6) H. C. Brown and R. R. Holmes, *J. Am. Chem. Soc.*, **78**, 2173 (1956).



izability—the larger the polarizability, the greater will be the shift for any given Lewis acid.

(5) There should be an absence of mechanical effects on the carbonyl group.

Cook suggested that the benzaldehyde molecule might fulfill all these criteria. However, the present authors<sup>7</sup> have shown that the benzaldehyde molecule is readily oxidized by alumina-containing surfaces, and application of this technique to such surfaces requires the further criterion that the donor molecule must not be easily oxidized. From experiments in this laboratory it has been shown that acetone, cyclohexanone, benzonitrile, and other more complicated ligands are oxidized by alumina surfaces. The oxidation apparently proceeds very rapidly if the molecule is able to undergo the keto-enol transformation and takes place at lower temperatures on silica-alumina surfaces than on alumina surfaces. This might suggest that the reaction is catalyzed by the protons which have been shown to exist on the silica-alumina surfaces. In order to negate this oxidative effect, hexachloroacetone was chosen as the donor molecule. This liquid (b.p. 203.6°) contains no hydrogen atoms and thus cannot undergo the tautomeric effect. Furthermore, it is oxidized only destructively.

### Experimental Section

The hexachloroacetone used in these experiments was supplied by K & K Laboratories. The silica-alumina cracking catalysts Aerocat 2000 and Aerocat Triple A were supplied by Cyanamid, and the sample of alumina used was prepared by the hydrolysis of aluminum isopropoxide and dried at 500°. X-Ray analysis showed it to be in the  $\gamma$  form. All the powdered solids were given a standard pretreatment which consisted of heating in oxygen at 500° for 12 hr. before being contacted with the hexachloroacetone. Initially, the solid sample was contacted with hexachloroacetone vapor at the required temperature before being cooled to room temperature, and the spectra were recorded. However, as there were no major differences in the spectra recorded using this method and those obtained by adsorption of the hexachloroacetone from benzene solution, evaporating and heating to the required temperature, this latter procedure was adopted for the spectra shown in Figures 2–5.

All spectra were recorded on a Perkin-Elmer double-beam 221G grating spectrophotometer. A mulling technique was employed, the mulling agent being a fluorolube oil supplied by Hooker Chemical Co. The reference sample was identical for any given series of experiments, and the quantity of samples used was adjusted *in situ* so that the absorptivities of all samples

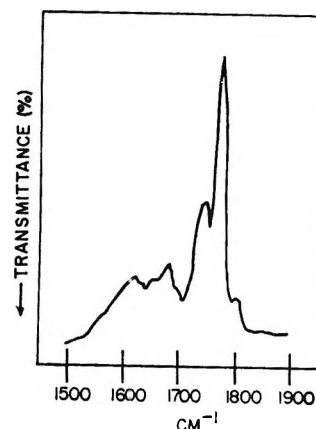


Figure 2. Infrared spectrum of hexachloroacetone adsorbed on Aerocat Triple A at room temperature.

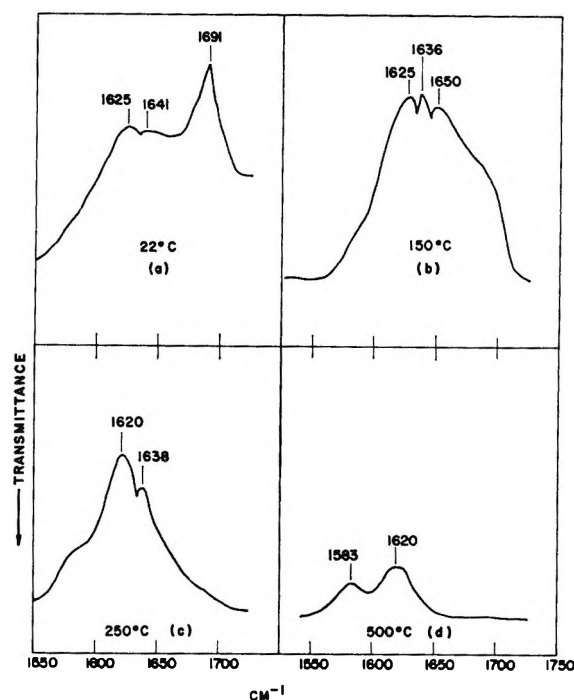


Figure 3. Spectrum of hexachloroacetone adsorbed on Aerocat Triple A (a) at room temperature, (b) after heating to 150°, (c) 250°, and (d) 500°.

were constant and equal to that of the reference sample at 1900  $\text{cm}^{-1}$ . Use of this procedure enables the intensities for any one series to be compared, and exceptionally straight backgrounds were obtained.

### Results

The spectrum of hexachloroacetone dissolved in carbon tetrachloride is shown in the region of interest

(7) I. D. Chapman and M. L. Hair, *Actes Congr. Intern. Catalyse*, 3°, Amsterdam, 2, 1091 (1964).

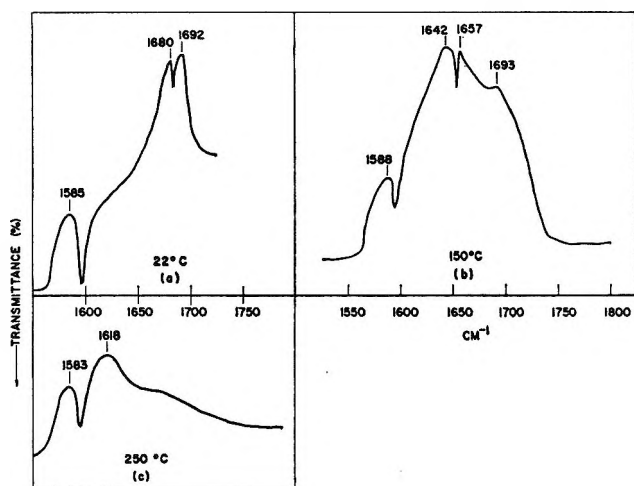


Figure 4. Hexachloroacetone adsorbed on  $\gamma$ -alumina at (a) room temperature, (b) 150°, and (c) 250°.

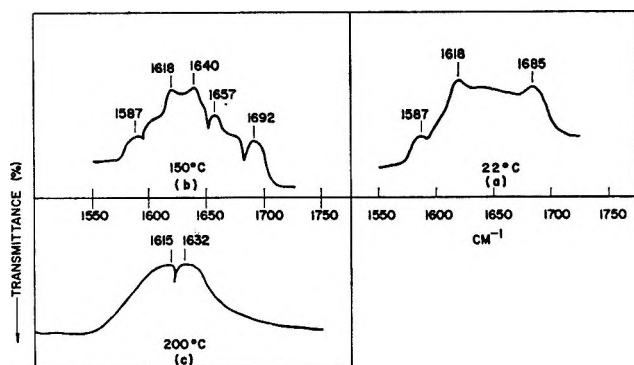


Figure 5. Hexachloroacetone adsorbed on Aerocat 2000 at (a) room temperature, (b) 150°, and (c) 200°.

(2000 to 1250  $\text{cm}^{-1}$ ) in Figure 6. The peak of interest occurs at 1780  $\text{cm}^{-1}$  and is identified as the fundamental stretching frequency of the carbonyl group. A second peak is observed at 1750  $\text{cm}^{-1}$ .

An examination of the literature reveals that the hexachloroacetone molecule has not been subjected to vibrational analysis, and it is difficult at this stage to explain the presence of the second band. This band disappears on complex formation and thus cannot be attributed to a C-Cl overtone. Moreover, the high wave number renders this unlikely. Since the intensity of the 1750- $\text{cm}^{-1}$  band relative to the 1780- $\text{cm}^{-1}$  band decreases on raising the temperature to 100°, it is clear that the 1750- $\text{cm}^{-1}$  absorption is not due to a hot band. The doublet formation is not observed in halogenated ketones which contain two or more fluorine atoms,<sup>8</sup> and it is possible that the second band arises from splitting due to the steric hindrance of the bulky chlorine atoms and consequent interaction with the  $\alpha$  carbonyl group.

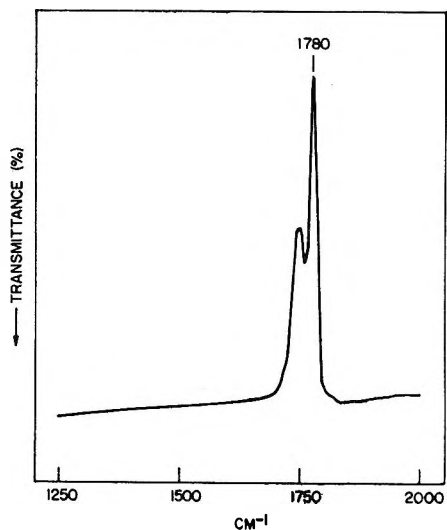


Figure 6. Infrared spectrum of hexachloroacetone in  $\text{CCl}_4$  solution.

The spectrum obtained with hexachloroacetone adsorbed on Aerocat Triple A at room temperature is shown in Figure 2. The large peak at 1780  $\text{cm}^{-1}$  shows that there is a considerable quantity of physically adsorbed hexachloroacetone. However, comparisons with the hexachloroacetone spectrum of Figure 6 shows that a broad band has appeared which extends from approximately 1720 to 1550  $\text{cm}^{-1}$ . This band is attributed to perturbation of the fundamental carbonyl stretching frequency due to complex formation with the surface Lewis acid sites. This portion of the spectrum is shown on an expanded scale in Figure 3a. It is seen that the broad distribution of sites contains at least three separate distributions which peak at 1691, 1641, and 1625  $\text{cm}^{-1}$ . On heating to 150° either in air or under vacuum, the spectrum shown in Figure 3b is obtained. This is identical with the spectra obtained by vapor deposition of the hexachloroacetone on the Aerocat Triple A surface at that temperature.

Two interesting effects are observed. First, that the large peak at 1691  $\text{cm}^{-1}$  is essentially removed: in other words, some of the weaker Lewis acid sites disappear. Second, new peaks are observed at 1625, 1636, and 1650  $\text{cm}^{-1}$ . On further heating to 250° the peak at 1650  $\text{cm}^{-1}$  disappears, and the distribution of sites appears to be much more symmetrical with peaks at 1638 and 1620  $\text{cm}^{-1}$  and a shoulder around 1580  $\text{cm}^{-1}$ . At 500° the peak at 1638  $\text{cm}^{-1}$  disappears, and the majority of the hexachloroacetone has been desorbed leaving only two small peaks at 1583 and 1620  $\text{cm}^{-1}$ .

(8) R. N. Haszeldine and F. Nyman, *J. Chem. Soc.*, 3015 (1961).

The spectra of hexachloroacetone adsorbed on alumina at various temperatures are shown in Figure 4a, again using expanded scale. These can be compared with the spectra for Aerocat Triple A. At room temperature there are again three distributions which are attributed to hexachloroacetone chemisorbed on three sites of differing energy on the alumina surface. The peaks of these distributions occur at 1692, 1680, and 1585  $\text{cm}^{-1}$ . On heating to 150° (Figure 4b), the peaks (1692 and 1680  $\text{cm}^{-1}$ ), due to the weaker acid sites, are lost and are replaced by a more symmetrical distribution centering around 1657  $\text{cm}^{-1}$ . However, it is seen that this in turn is split into three distributions, the peaks of which occur at 1642, 1657, and as a shoulder at 1693  $\text{cm}^{-1}$ . As with the Aerocat Triple A, the peak at 1588  $\text{cm}^{-1}$ , due to the strong acid sites, has been relatively unaffected by the heat treatment. At 250° (Figure 4c) the weaker Lewis acid complexes are again decomposed, and two peaks are observed at 1618 and 1583  $\text{cm}^{-1}$ . It is to be noted that the peak at 1583  $\text{cm}^{-1}$  changed little, if at all, in intensity during this series of heat treatments, whereas the other Lewis acid-carbonyl complexes are largely decomposed. Also, in comparing the spectra of alumina and Aerocat Triple A, it is to be noticed that there are two obvious differences, namely, the height of the peak at 1583  $\text{cm}^{-1}$  and the unsymmetrical distribution of sites which occurs on the alumina at 250° compared with the much more symmetrical distribution found on the silica-alumina surfaces.

The spectra of hexachloroacetone adsorbed on Aerocat 2000 cracking catalyst at various temperatures are shown in Figures 5a, b, and c. As might be expected from this mixture of synthetic and natural cracking catalysts, the spectra are very complicated, and at 150° it is seen that there are at least five separate site distributions, the peaks of which are observed at 1587, 1618, 1640, 1657, and 1692  $\text{cm}^{-1}$ . On heating to 200°, however, the distribution of sites is more symmetrical, and two peaks are observed at 1615 and 1632  $\text{cm}^{-1}$ .

## Discussion

An examination of the shifts of the fundamental carbonyl stretching frequency of the xanthone complexes obtained by Cook<sup>5</sup> shows that the order of Lewis acidity for the boron halides is  $\text{BI}_3 > \text{BBr}_3 > \text{BCl}_3 > \text{BF}_3$ . This series of Lewis acidities is the reverse of that which one would expect from application of normal electronegativity concepts.<sup>6</sup> This order, however, has been well documented by various authors.<sup>6,9</sup>

In Figure 7 the positions of the carbonyl stretching frequency of xanthone complexes of the boron halides

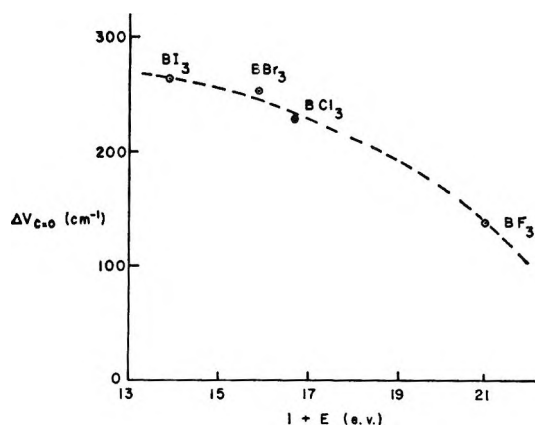


Figure 7. Shift in carbonyl stretching frequencies of xanthone complexes of boron halides vs. electronegativity of halogen atom.

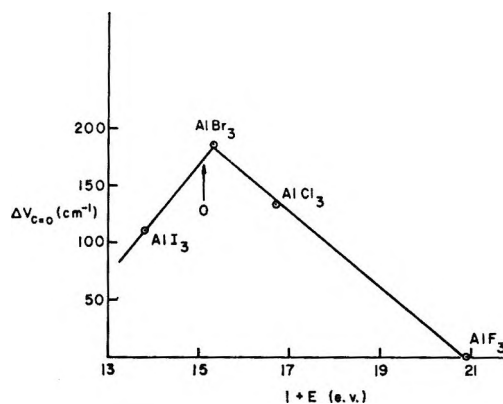


Figure 8. Shift in carbonyl stretching frequencies of hexachloroacetone complexes of aluminum halides vs. electronegativity of halogen atom.

are plotted as a function of the Mulliken electronegativity of the appropriate halogen atom. (The Mulliken definition of electronegativity is equal to half the sum of the ionization potential and the electron affinity of the atom concerned.<sup>10</sup> For convenience, the sum of the I.P. and E.A. has been taken as the ordinate in Figures 7 and 8.) From this plot it can be seen that the shift of the carbonyl stretching vibration is a function of the electronegativity of the substituent halogen atom, and, for the purposes of the ensuing arguments, this can be considered to be an approximately linear relationship.

In order to extend these considerations to the alumina surfaces, a series of complexes was prepared between hexachloroacetone and the aluminum halides. The spectra of these complexes were examined in car-

(9) J. M. Miller and M. Onyszchuck, *Can. J. Chem.*, **41**, 2898 (1963).

(10) R. S. Mulliken, *J. Chem. Phys.*, **3**, 573 (1935).

bon tetrachloride solution, and the shift in the carbonyl stretching frequency was plotted as a function of the electronegativity of the halogen atom. This is shown in Figure 8.

From this it can be seen that aluminum trifluoride does not undergo complex formation with hexachloroacetone, and there is, therefore, no change in the carbonyl stretching frequency. This is in character with the ionic structure of the compound and its general inability to form coordination complexes. Aluminum trichloride is a well-known Lewis acid and gives a complex with hexachloroacetone as do the tribromide and triiodide. As with the boron series, the tribromide is a stronger acid than the trichloride. In the case of the iodides, however, there is a difference in that aluminum triiodide is a weaker acid than the bromide. This can be traced to the increased ionic character of the aluminum iodide which is reflected in the different crystal structure.

If the electronegativity concept can be applied to atoms other than in the halogen series, then two interesting features emerge as far as the alumina-containing surfaces are concerned. Firstly, as the Lewis acid sites on both silica-alumina and alumina are expected to consist of aluminum atoms surrounded by three oxygen atoms and as the oxygen atoms might be expected to differ little in electronegativity in both cases, then the Lewis acid sites on both these surfaces should be similar, and the spectra of hexachloroacetone on such surfaces should show considerable similarities. Moreover, by inserting the value for the electronegativity of oxygen in Figure 8, it is seen that the observed shift should be about  $170 \text{ cm.}^{-1}$ .

Examination of the spectra shown in Figures 2-4 shows that these suppositions are essentially correct and that the peak of the distribution obtained for hexachloroacetone adsorbed on both silica-alumina and alumina at  $250^\circ$  is around  $1620 \text{ cm.}^{-1}$ —a shift of  $160 \text{ cm.}^{-1}$  from the free carbonyl vibration fre-

quency of hexachloroacetone in carbon tetrachloride solution. An examination of the spectra of hexachloroacetone adsorbed on Aerocat Triple A and alumina at  $150^\circ$  (Figures 3b and 4b) shows two distinct differences. First, the silica-alumina Lewis acid sites are apparently slightly stronger at this temperature than the alumina sites in that the peak of the distribution occurs around  $1636 \text{ cm.}^{-1}$  in the case of the Triple A and at around  $1657 \text{ cm.}^{-1}$  in the case of the alumina surface. However, on the alumina surface it is apparent that about 10% of the sites gives rise to a carbonyl peak at  $1588 \text{ cm.}^{-1}$ . This shift of  $200 \text{ cm.}^{-1}$  indicates that the Lewis acid sites are very strong in this case and more nearly comparable with the shift obtained for the boron halide complexes.

From these results it is readily apparent that the nature of the sites on alumina-containing surfaces is varied and that there is indeed a wide distribution range of sites of varying Lewis acidity. By using a more refined technique it should be possible to obtain a quantitative measure of the number of sites available for complex formation. The low vapor pressure of hexachloroacetone makes vacuum manipulation of this compound difficult. However, trifluorotrichloroacetone has been used successfully, and quantitative data obtained with this ligand will be published.

The results with hexachloroacetone indicate that the Lewis sites on the silica-alumina and alumina surfaces are in general very close in their acid strength. It has previously been proposed that protonic sites can be formed by reaction of a water molecule with a Lewis acid site to give an aluminol grouping and a proton. Such a mechanism should be wholly dependent on the strength of the Lewis acid and, in view of the present results, should take place as easily on an alumina surface as on a silica-alumina surface. Protons have not been observed on alumina surfaces, and thus this mechanism must be considered inadequate in accounting for the Brønsted acidity of silica-alumina surfaces.

## Conformation of Polystyrene Adsorbed at the $\Theta$ -Temperature<sup>1,2</sup>

by Robert R. Stromberg, Daniel J. Tutas, and Elio Passaglia

National Bureau of Standards, Washington, D. C. 20234 (Received June 10, 1965)

The conformation of polystyrene molecules adsorbed on metallic surfaces at the  $\Theta$ -temperature was investigated by measurements of the extension of the adsorbed molecule normal to the surface. This extension was studied *in situ* by means of ellipsometry. The study was carried out on a series of samples with molecular weights ranging from 76,000 to 3,300,000. The extension of the adsorbed polymer molecule increases with adsorption time, indicating an initial flat conformation for the early arrivals that changes to a more extended form as additional molecules adsorb. The equilibrium extension increases with increasing solution concentration until a plateau is reached, again indicating a conformation dependence on the number of molecules competing for adsorption sites. The extension at these plateau regions is approximately proportional to the square root of the molecular weight, except for the highest molecular weight sample studied. This relationship is interpreted to indicate that the polymer is adsorbed under these conditions as a random coil. Comparisons are made between the measured extensions and end-to-end distances at reflecting and absorbing boundaries. Only small differences in extension were observed among a number of different metallic surfaces, indicating the nonspecific nature of polymer adsorption on such high energy surfaces.

### Introduction

Much of the effort concerned with the adsorption of polymers has been directed toward a determination of the conformation of the adsorbed molecule at the surface-solution interface. It is generally accepted that a molecule is attached at a number of locations along the chain, the attached portions being separated by loops of unattached segments. The number and arrangement of the attached portions and the size and distribution of the unattached loops will, of course, define the conformation of the molecule. It is apparent, therefore, that measurement of the extension of the loops away from the surface is useful to determine the conformation of the adsorbed molecule.

The segments of polymer attached to the surface and loops extending into the solution may be considered to form a "film" over the surface. This adsorbed "film" consists of a mixture of polymer molecules and solvent. Removal of the solvent would result in collapse of polymer loops onto the surface. To prevent changes in the conformation, the adsorbed polymer layer must be measured *in situ*, *i.e.*, immersed in the polymer solution.

One technique for the measurement of thin films in liquid environments is ellipsometry. Changes in the state of polarization of light upon reflection from a film-covered surface are measured and used to calculate the thickness and refractive index of the film. It is possible, therefore, to measure simultaneously the extension of the polymer loops away from the surface, and from the refractive index, to determine the concentration of polymer in the adsorbed layer.

In an earlier paper,<sup>3</sup> we have reported the measurement of the thickness of the adsorbed film of polystyrene with a molecular weight of 76,000 on chrome surfaces at a temperature below the Flory  $\Theta$ -point.<sup>4</sup> In the present paper, we report the results of a study of the relation between molecular weight and extension for a number of metallic surfaces at the  $\Theta$ -temperature.

(1) Supported with funds provided by the Army Research Office (Durham).

(2) Presented in part at the 148th National Meeting of the American Chemical Society, Chicago, Ill., Sept. 1964.

(3) R. R. Stromberg, E. Passaglia, and D. J. Tutas, *J. Res. Natl. Bur. Std.*, **67A**, 431 (1963).

(4) P. J. Flory, "Principles of Polymer Chemistry," Cornell University Press, Ithaca, N. Y., 1953, p. 523.

Changes in conformation of the adsorbed molecule with solution concentration and time of adsorption are also reported, and the relation between the calculated thickness values and molecular dimensions is discussed.

### Treatment for Inhomogeneous Films

The technique of ellipsometry has been described in detail<sup>5-7</sup> and its application to the adsorption of polymers from solution has been discussed.<sup>3,8</sup> For a bare metallic surface two parameters,  $\tan \psi$ , the ratio of the magnitude of the reflection coefficient for light polarized with its electric vector in the plane of incidence to that polarized normal to the plane of incidence, and  $\Delta$ , the relative phase difference for these two polarizations, are obtained from the instrument readings. From these measured quantities it is possible to calculate directly the optical constants of the surface. All other parameters required for this calculation such as the wave length of light, refractive index of immersion medium, etc., are obtained by independent means. If this surface is now covered with a thin film, new values of  $\psi$  and  $\Delta$  will be measured. From these new values and the previously determined values of the optical constants of the surface, the thickness and refractive index of the film can be calculated by the equations of Drude.<sup>9</sup> Although these equations are exact, they cannot be solved in closed form and require trial-and-error iterative methods, necessitating the use of electronic computers for most applications.<sup>6</sup>

The model treated in the Drude equation is that of a homogeneous film of constant refractive index with discrete boundaries. However, the adsorbed polymer film, consisting of a mixture of polymer and solvent, would be expected to be an inhomogeneous film, with the polymer concentration and hence refractive index decreasing with the distance from the surface. The use of the Drude equations will result, therefore, in an "average" thickness value and it is necessary to relate this calculated average for a homogeneous film model to the inhomogeneous adsorbed polymer film, and if possible, to molecular parameters.

The effect of a film on the change in the values of  $\psi$  and  $\Delta$  will depend on the difference between the refractive index of the film and the index of the solution,  $(n_f - n_s)$ , as well as the thickness,  $t$ , of the film. (If the film has the same refractive index as the solution, the values of  $\psi$  and  $\Delta$  will remain, of course, those obtained for the bare surface itself.) For an inhomogeneous film,  $(n_f - n_s)$  is a function of the distance from the surface, and it may be shown<sup>10</sup> that the thickness,  $t_h$ , and refractive index,  $n_h$ , for the equivalent homogeneous

film are related to this refractive index difference by the equation

$$\int_0^\infty (n_f - n_s) dt = (n_h - n_s) t_h \quad (1)$$

It may also be shown<sup>10</sup> that the value of  $n_h$  can be determined separately by the equation

$$n_h = \frac{\int_0^\infty n_f (n_f - n_s) dt}{\int_0^\infty (n_f - n_s) dt} \quad (2)$$

which is just the definition of average refractive index with the quantity  $(n_f - n_s)$  acting as a "distribution function." From eq. 1 and 2, the equivalent homogeneous thickness is given as

$$t_h = \frac{\left[ \int_0^\infty (n_f - n_s) dt \right]^2}{\int_0^\infty (n_f - n_s)^2 dt} \quad (3)$$

Thus, if the distribution of refractive index,  $(n_f - n_s)$ , is known, the ellipsometrically equivalent homogeneous-film refractive index,  $n_h$ , and thickness,  $t_h$ , may be calculated. It is not possible, unfortunately, to obtain the distribution by ellipsometry.

It is possible, however, to relate the averages in eq. 3 to more common averages for certain reasonable distributions of refractive index. In particular, McCrackin and Colson<sup>10</sup> related  $t_h$  to  $t_{rms}$ , the root-mean-square average, which is defined by the equation

$$t_{rms}^2 = \frac{\int_0^\infty (n_f - n_s) t^2 dt}{\int_0^\infty (n_f - n_s) dt} \quad (4)$$

Since the quantity  $(n_f - n_s)$  is expected to be proportional to concentration, and hence segment density, eq. 4 is just the usual definition of mean-square average thickness. Working with linear, exponential, and

(5) A. B. Winterbottom, "Optical Studies of Metal Surfaces," The Royal Norwegian Scientific Society Report No. 1, 1955, published by F. Bruns, Trondheim, Norway.

(6) F. L. McCrackin, E. Passaglia, R. R. Stromberg, and H. L. Steinberg, *J. Res. Natl. Bur. Std.*, **67A**, 363 (1963).

(7) E. Passaglia, R. R. Stromberg, and J. Kruger, Ed., "Ellipsometry of the Measurement of Surfaces and Thin Films" (Symposium Proceedings), NBS Miscellaneous Publication 256, Superintendent of Documents, U. S. Government Printing Office, Washington, D.C., 1964.

(8) R. R. Stromberg, E. Passaglia, and D. J. Tutas, see ref. 7, p. 281.

(9) P. Drude, *Ann. Physik.*, **272**, 532 (1889); **272**, 865 (1889); **275**, 481 (1890).

(10) F. L. McCrackin and J. P. Colson, see ref. 7, p. 74.

gaussian distributions with  $n_t$  varying from 1.3 to 1.6, McCrackin and Colson showed that the ratio  $t_b/t_{rms}$  was 1.75 for the linear distribution, 1.47 for the exponential, and 1.73 for the gaussian.

The range of refractive indexes used for these calculations is somewhat greater than the maximum possible range for the polystyrene-cyclohexane films to be discussed here. The value of 1.3 is lower than that of the solvent and 1.6 is higher than that of the bulk polystyrene. The use of a narrower range of refractive indices, 1.4268 to 1.4768, that was closer to the indices actually measured, resulted in  $t_b/t_{rms}$  factors that were almost identical with the larger range for the linear and exponential distributions. For the gaussian distribution the value of  $t_b/t_{rms}$  was 1.58. Thus, if the distribution were known, one could compute  $t_{rms}$  from  $t_b$ .

Now, DiMarzio and McCrackin<sup>11</sup> have performed one-dimensional analytical and Monte Carlo calculations for the segment distribution away from the surface of an isolated adsorbed polymer molecule of segment length varying from 50 to 200. They find that at moderate to high attractive energies this distribution can be well represented by an exponential function. Hoeve<sup>12</sup> has carried out some theoretical studies of the distribution normal to the surface using a full three-dimensional model for isolated polymer molecules and for a highly populated surface at the  $\Theta$ -temperature. He finds that beyond a short distance away from the surface these distributions away from the surface also can be represented by an exponential function. We have, therefore, chosen to calculate values of  $t_{rms}$  from the measured values  $t_b$  by dividing the latter by 1.5, the factor for the exponential distributions. These are the  $t_{rms}$  values reported here.

### Experimental Procedure

The experimental procedure has been previously described.<sup>3,8</sup> The ellipsometer measurements were carried out with triple reflection techniques, one surface being held above the other with gage blocks. The advantages of multiple reflection over single reflection techniques and the resulting change in the measurement errors of  $\psi$  and  $\Delta$  for various metallic surfaces have been discussed in detail.<sup>8</sup> The optical constants of the freshly cleaned metal surfaces were measured under the solvent used in the adsorption studies. The solvent was exchanged for fresh solvent at least once to ensure that no changes in the ellipsometer readings occurred as a result of emptying and refilling the cell. The solvent was then exchanged for polymer solution by means of a hypodermic syringe, without moving the metallic surfaces. The changed values of  $\psi$  and  $\Delta$

were then obtained as a function of time for the polymer film adsorbing on the same locations on the metallic surfaces for which optical constants had been previously obtained under solvent alone. All adsorption measurements were made *in situ*, *i.e.*, under polymer solution. Only negligible changes in solution concentration occurred as a result of adsorption.

Chrome surfaces of slides cut from commercial ferrotype plate were used as the adsorption surface for much of the work reported here. They were cleaned with warm sulfuric acid-chromic acid cleaning solution and thoroughly rinsed. Immediately prior to use they were passed through an oxygen-gas flame to remove any hydrocarbon film that may have formed in air, and placed while still warm under solvent in the adsorption cell. Other metals were also used for adsorption surfaces. They were steel gage blocks, and chromium, silver, gold, and copper electrodeposited on the gage blocks. Copper and silver were also vacuum evaporated on gage blocks. These metal surfaces were not cleaned with the cleaning solution, but were passed through an oxygen-gas flame immediately prior to use. The solvent was cyclohexane and the measurements were carried out at 34°, which is approximately the  $\Theta$ -temperature for polystyrene in this solvent.

The polystyrene used, with the exception of one sample, was obtained from Dr. H. W. McCormick of the Dow Chemical Co. and had been prepared by an anionic polymerization technique. One sample with a molecular weight of  $1.9 \times 10^6$  was prepared by Mr. Warren H. Grant of NBS, also using an anionic polymerization method. All of the original samples had relatively narrow molecular weight distributions. All of the samples were further fractionated by ourselves using conventional precipitation methods, and the molecular weights were obtained by intrinsic viscosity measurements in benzene, using the relations given by Krigbaum and Flory.<sup>13</sup> Since the ratio of  $M_w/M_n$  for the fractionated material was probably lower than 1.05, except perhaps for the highest molecular weight sample, the reported molecular weights can be taken as either weight or number average. The molecular weights of the samples studied were 76,000, 207,000, 537,000, 1,370,000, 1,900,000, and 3,300,000.

### Results

The measurements were carried out on the ferrotype plate chrome surface for each of the molecular

(11) E. A. DiMarzio and F. L. McCrackin, *J. Chem. Phys.*, **43**, 539 (1965).

(12) C. A. J. Hoeve, *ibid.*, in press.

(13) W. R. Krigbaum and P. J. Flory, *J. Polymer Sci.*, **11**, 37 (1953).



weight samples given in the Experimental Procedure. A series of solution concentrations was studied for each sample, ranging from the lowest in which measurements could be obtained to those in which no further changes occurred with increasing solution concentration. This range varied with the molecular weight of the sample. For all of the molecular weights studied here, we observed an initial increase in adsorbed film thickness with increasing solution concentration and a plateau region at higher concentrations. There is a limitation in the minimum film thickness that can be measured for the small difference in refractive index between the adsorbed film and solution (approximately 0.02). The range of concentrations studied for a given molecular weight, therefore, was determined by the minimum thickness that could be measured and the concentration at which the plateau region was reached.

Typical results for the root-mean-square thickness of the adsorbing polymer film as a function of time are shown in Figure 1 for the  $5.37 \times 10^5$  and  $1.90 \times 10^6$  molecular weight samples. The thickness values did

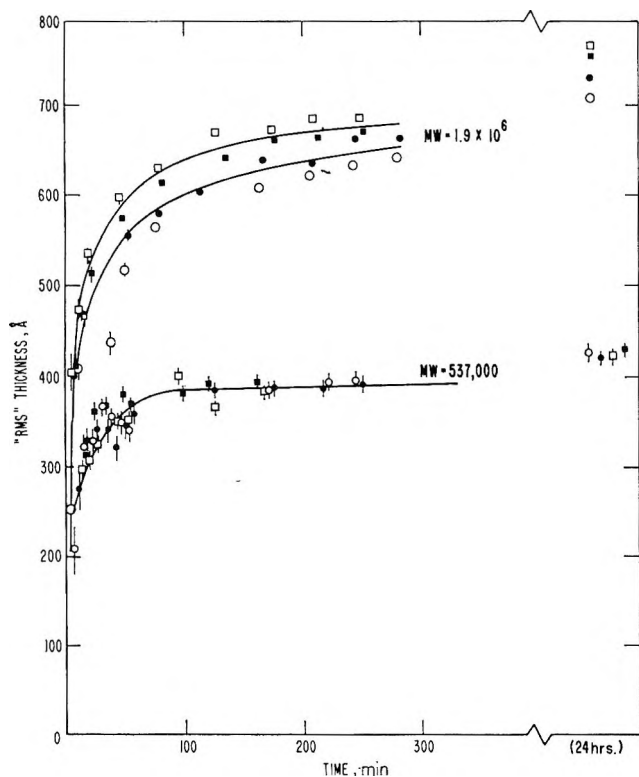


Figure 1. Extension of adsorbed polystyrene molecule, mol. wt. 537,000 and 1,900,000 from chrome ferrotype plate during the adsorption period. The solution concentration was 1.00 mg./ml. for the 537,000 mol. wt. and 1.15 mg./ml. for the 1,900,000 mol. wt. sample. The different symbols represent different runs and the open and closed points represent separate measurements made on the same set of slides.

not change from the overnight value when the surface was exposed to the polymer solution for an additional 2 days. The vertical line for each point represents the range of uncertainty in thickness for a single measurement that arises from the range of thicknesses which are consistent with the known precision of the ellipsometer measurements, the point itself representing the "best" value.<sup>3</sup> For the thicknesses shown in this figure, the range of uncertainty usually decreases as the film thickness increases.<sup>3,8</sup> The open and closed points represent different locations on the same set of slides and the different symbols represent separate runs. In addition to the uncertainties resulting from the precision of an individual ellipsometer measurement, there are also unavoidable variations in the surface from point to point on the slide and from run to run, small temperature changes, etc. These factors cause the scatter of points around the curve which they determine to be greater than the uncertainty calculated from the ellipsometer results alone.

The adsorbed film thickness increases with time until a final equilibrium plateau is reached. The time required to attain the plateau region is determined by both the molecular weight and the concentration of the solution. The lower the molecular weight and the more concentrated the solution, the sooner the final equilibrium value is attained. The results for both the individual locations on the same set of slides and the different runs are represented by one curve for the 537,000 molecular weight sample. A separate curve is used for each run for the 1,900,000 molecular weight sample, each curve representing the two locations on the same set of slides.

The adsorbance (amount adsorbed per unit area) was calculated from the thickness and refractive index of the film, using the Lorentz-Lorenz relation for the dependence of polymer concentration on film refractive index. Using the thickness and film concentration, it is not necessary to know the surface area of the substrate. Typical results are given in Figure 2. In a manner similar to the behavior of the thickness, the adsorbance increases with time until a final equilibrium value is attained. Again, the magnitude of this final adsorbance value and the rate of increase of adsorbance with time are dependent on the molecular weight of the polymer and the solution concentration.

A somewhat different behavior from that shown in Figure 1 was observed for the change in the thickness of the adsorbed film with time for the  $3.3 \times 10^6$  molecular weight sample. The lower concentrations studied behaved in the manner shown in Figure 1, exhibiting a continuing increase in film thickness, with an overnight value that appeared to be constant and which



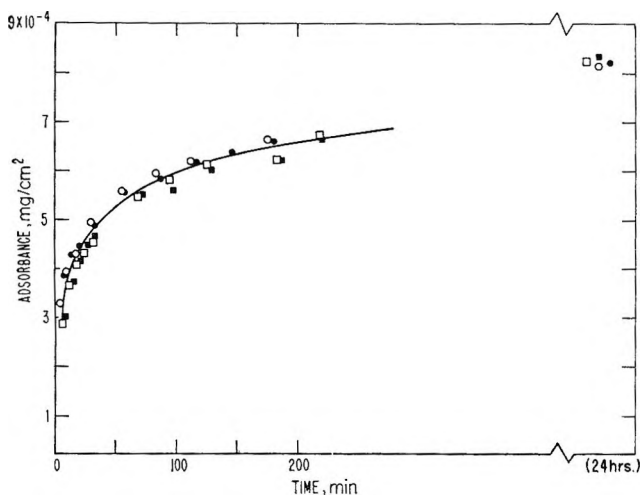


Figure 2. Adsorbance of polystyrene, mol. wt. 1,370,000, on chrome ferrotyp plate during the adsorption period. The solution concentration was 0.55 mg./ml. The different symbols represent different runs and the open and closed points represent separate measurements made on the same set of slides.

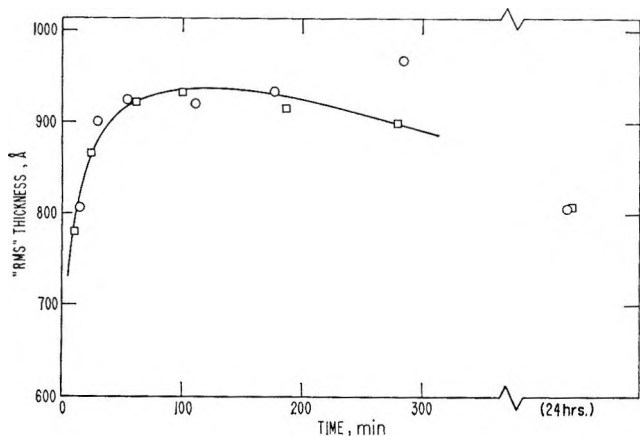


Figure 3. Extension of adsorbed polystyrene molecule, mol. wt. 3,300,000, from chrome ferrotyp plate during the adsorption period. The solution concentration was 0.55 mg./ml. The different symbols represent different runs.

was higher than any of the previous values. However, at solution concentrations of 0.5 mg./ml. or higher, the behavior was similar to that shown in Figure 3. The adsorbed film thickness initially increased, but after reaching a maximum value, decreased to a lower value. The adsorbance curves did not go through a maximum, nor reach a plateau at a time corresponding to the maximum in the thickness curve. Rather, the adsorbance curves were similar to the curve shown in Figure 2. The overnight values, both thickness and adsorbance, remained constant for a period of 3 days.

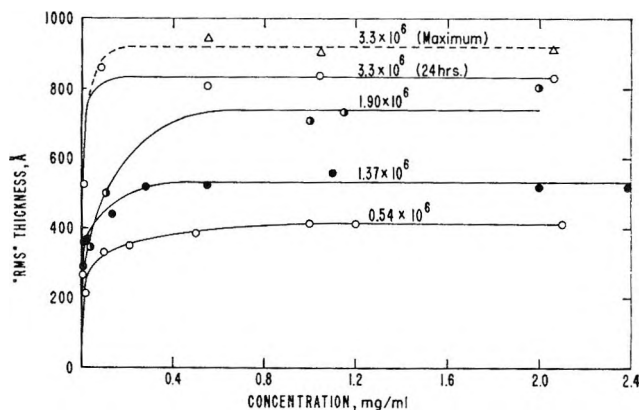


Figure 4. Extension of adsorbed polystyrene molecule on chrome ferrotyp surface as a function of solution concentration. Numbers on curves represent molecular weight. For the  $3.3 \times 10^6$  molecular weight sample, the dashed curve represents maximum value attained after approximately 100-min. adsorption time. Solid curve represents equilibrium value.

As described above, the measurement at a given concentration of the extension of the adsorbed polymer molecule from the ferrotyp chrome surface as a function of time, with the exception of the  $3.3 \times 10^6$  molecular weight sample, resulted in a continuing increase in thickness until a plateau region was reached. Average values from a number of runs for these final equilibrium extension values for a given concentration are plotted in Figure 4 as a function of solution concentration for four of the molecular weight samples studied. Two thickness curves are shown for the  $3.3 \times 10^6$  molecular weight sample. One curve represents the final value of the adsorbed film thickness and the other, the maximum film thickness which was attained approximately 100 min. after the start of the adsorption. The film thickness *vs.* time curves did not go through a maximum for the very low solution concentrations.

In all cases, as seen in Figure 4, the film thickness is observed to increase with increasing solution concentration from relatively low thickness values to a maximum film thickness which remains constant with increasing solution concentrations. The solution concentration at which this maximum film thickness is reached decreases with increasing molecular weight from approximately 1.0 mg./ml. for the 537,000 molecular weight sample to approximately 0.2 mg./ml. for the 3,300,000 molecular weight sample. Typical adsorbance curves are given in Figure 5. A similar behavior is exhibited with a maximum value attained at solution concentrations near that at which the film thickness curves attain their maximum values.

Adsorption measurements were also carried out on other metallic surfaces for two of the molecular weight samples. The metallic surfaces were prepared by electrodepositing or vacuum evaporating the metal on steel gage blocks. The behavior of the polymer film on these surfaces was very similar to that exhibited on the ferrottype surface. The dependence of adsorbed film thickness on time is shown in Figure 6 for an electrodeposited gold surface. The equilibrium root-mean-square film thicknesses, the adsorbances, and the concentrations of polymer in the film are given in Table I for the surfaces studied for two molecular weight samples. The steel surface is the surface of the gage block itself. The differences in film thicknesses among the surfaces studied are small. The adsorbance values are also relatively close together except for a small adsorbance value for copper.

**Table I:** Average Equilibrium Values for the Adsorption of Polystyrene on Various Metallic Surfaces

Surface	R.m.s. thickness, Å.	Adsorbance, mg./cm. <sup>2</sup> × 10 <sup>4</sup>	Concn. of polymer in film, g./100 ml.
Mol. wt. = 0.54 × 10 <sup>6</sup> ; c ~ 1.0 mg./ml.			
Chrome ferrottype	420	7.0	10.6
Chromium-electrodeposited	390	5.8	9.5
Steel	440	6.6	9.5
Gold-electrodeposited	410	6.9	10.7
Copper-evaporated and electrodeposited	460	2.5	3.4
Silver-evaporated and electrodeposited	510	7.7	9.6
Mol. wt. 3.3 × 10 <sup>6</sup> ; c ~ 2.0 mg./ml.			
Chrome ferrottype	830	5.4	4.1
Chromium-electrodeposited	930	4.0	2.7
Steel	790	4.6	3.7

## Discussion

In discussing these adsorption results the following experimental facts should be borne in mind. (1) The thickness monotonically increases with time from an initially very small value to a constant value, except for the highest molecular weight sample (Figures 1, 3, and 6). (2) The constant steady-state value of thickness increases with concentration, finally achieving a plateau value in which the thickness is independent of concentration (Figure 4). (3) Although the adsorbance increases with time at any concentration (Figure 2), within our experimental limitations the refractive index of the adsorbed film, and hence the average

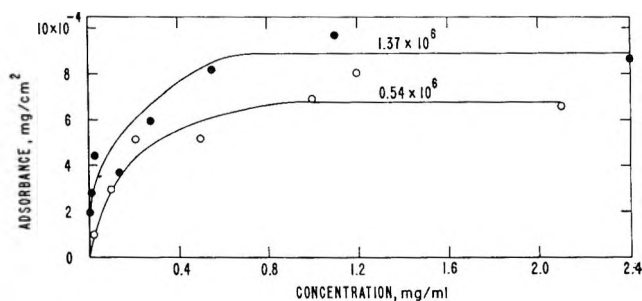


Figure 5. Adsorbance of polystyrene on chrome ferrottype plate as a function of solution concentration. Numbers on curves represent molecular weight.

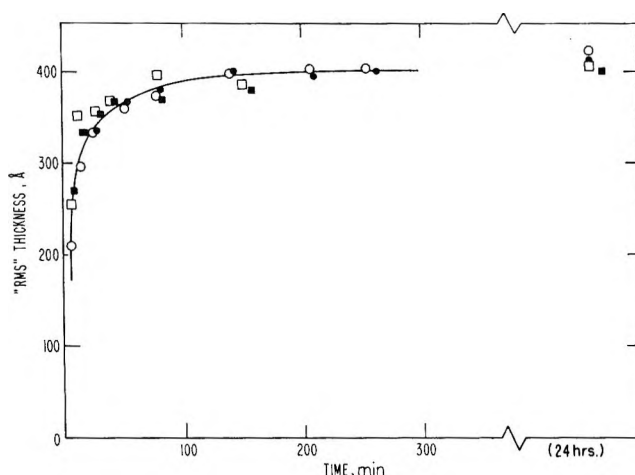


Figure 6. Extension of adsorbed polystyrene molecule, mol. wt. 537,000, from gold surface during the adsorption period. The solution concentration was 1.02 mg./ml. The different symbols represent different runs and the open and closed points represent separate measurements made on the same set of slides.

polymer concentration of this film, is essentially independent of time. (4) The value of thickness in the concentration range in which thickness is independent of concentration (and time) increases with molecular weight (Figure 4).

These experimental facts cannot be understood without considering the behavior of isolated molecules at a surface and their mutual interference when not isolated. A number of theoretical treatments of the adsorption of polymers on an infinite plane surface have been published. In particular, several recent such papers<sup>14-16</sup> have predicted that for an isolated flexible polymer molecule at an infinite substrate, the

(14) A. Silberberg, *J. Phys. Chem.*, **66**, 1872 (1962).

(15) C. A. J. Hoeve, E. A. DiMarzio, and P. Peyser, *J. Chem. Phys.*, **42**, 2558 (1965).

(16) R.-J. Roe, *Proc. Natl. Acad. Sci. U. S. A.*, **53**, 50 (1965).

fraction,  $p$ , of segments attached to the surface will be very high, even for small energies of attraction. Hence, in the absence of interference between molecules, one would expect the equilibrium conformation of an isolated polymer molecule to be one in which the molecule lies close to the surface, has many segments attached, and a small extension away from the surface. However, in the presence of other molecules competing for adsorption sites this situation may be drastically changed, and the equilibrium conformation will be expected to depend not only upon the fundamental energies of adsorption involved but also upon the number of molecules competing for adsorption sites.

Both these factors will influence the kinetics of the adsorption process. Fairly rigorous equations for the kinetics, and particularly the time dependence of thickness, may be formulated but they are intractable and difficult to solve<sup>17</sup> and hence only a qualitative discussion can be given. The kinetics will clearly depend upon two fundamental processes. (a) The arrival of molecules from solution and the attachment of at least one segment. The rate of this process will depend upon the solution concentration and the amount of free surface available. (b) The subsequent attachment of more segments once the molecule has been attached by at least one segment, *i.e.*, the "spreading out" of the molecule on the surface. This will be dependent on the amount of free surface available.

From the behavior of the experimental thickness curves, it appears that initially the rate of process (b) is, in all cases, much faster than the rate of process (a). The first arrivals at the surface attach and then very quickly spread out to attain the conformation predicted by the theories for isolated molecules. Subsequent arrivals will not be able to spread out as much or as quickly due to unavailability of sufficient sites.

Moreover, the adsorption of polystyrene on metallic surfaces has been shown to be reversible, although extremely long desorption times may be required for removal of the entire molecule.<sup>18</sup> Each attached segment can be considered to desorb and re-adsorb continually at a given site. As time increases and additional molecules arrive at the surface and are attached, competition for the vacant and the occupied sites continually increases. These later arrivals will have lower values of  $p$ , uncoil less, and be more extended from the surface. In addition, as the population of segments in the vicinity of the surface increases, the probability that a given polymer segment will be re-attached to the same site once it is desorbed decreases, and the probability that a different segment, either from the same chain or from a different molecule, will

be adsorbed at this site increases. There is a change, therefore, in the conformation of the attached polymer molecule with time, the initial molecules recoiling, occupying fewer surface sites, and becoming more extended away from the surface with increasing time. A final equilibrium conformation is established which is dependent upon the total rate of desorption, which in turn is dependent upon  $p$ ,<sup>19</sup> and upon the solution concentration. The value of  $p$ , however, cannot decrease continually, and reaches a limiting value determined by the energetics of the process.

For all molecular weights lower than  $3.3 \times 10^6$  and for times shorter than those necessary to achieve equilibrium, all molecules arriving after the first appear to have a lower extension away from the surface than the equilibrium extension for all concentrations. The behavior was similar for the highest molecular weight for low concentrations, but not for higher concentrations (Figure 3). This is explicable on the following basis. The higher the molecular weight, the larger the number of surface sites occupied per molecule.<sup>19</sup>

Now, the first arrivals clearly spread out much as the lower molecular weight samples. Subsequent arrivals, after attachment of their initial segments, however, must attach many more segments than the lower molecular weights before their conformation is appreciably changed. Thus, although the rate of the fundamental processes in (b) above are still faster than (a), the extent of process (b) must be greater to achieve an observable change in thickness, and under the conditions of sufficiently high solution (and hence surface) concentration a thickness higher than the equilibrium thickness could be observed. At low solution concentrations, and hence a slower rate of arrival at the surface, there is more time available for the necessary contacts to be made to lower the thickness because of less competition for surface sites. Under these conditions the extension of the molecule away from the surface would always be lower than the equilibrium extension for times lower than those necessary to achieve equilibrium.

While qualitative, this discussion seems to us to be a reasonable explanation of the facts. The behavior observed could also be considered on the basis of mole-

(17) J. I. Lauritzen, Jr., and E. Passaglia, unpublished results.

(18) R. R. Stromberg, W. H. Grant, and E. Passaglia, *J. Res. Natl. Bur. Std.*, **68A**, 391 (1964).

(19) The rate of desorption into cyclohexane of polystyrene adsorbed on chrome ferrotype surface was greater for a lower molecular weight polymer than for a higher molecular weight sample.<sup>18</sup> This was taken to indicate that the absolute number of attachments of the higher molecular weight molecule was larger and that longer times were required before all adsorbed segments were released, freeing the molecule from the surface.

cules adsorbed at different times having different but *static* conformations, and varying values of  $p$ . This leads to a nonequilibrium situation, for the state of the molecules on the surface at any concentration and at long times will clearly depend upon the history of the specimen. This could not be resolved with our previous desorption results.<sup>18</sup>

We have interpreted the results on the basis of a segment distribution away from the surface that remains approximately constant during the adsorption period. This appears to us to be a reasonable assumption inasmuch as recent theoretical treatments<sup>11,12</sup> predict exponential distributions both for the isolated molecule and for the highly populated surfaces at the  $\Theta$ -point. The constant value of refractive index and hence concentration of the adsorbed polymer layer with adsorbance also indicates that it is possible that the distribution remains constant as the adsorbance increases. In addition, different possible distributions<sup>10</sup> will result in changes in the root-mean-square thickness values that are too small to alter the general shape of the curves showing change of thickness with time.

For all molecular weights the final or equilibrium thickness of the adsorbed polymer film increases with increasing solution concentration until a plateau is reached, as shown in Figure 4. (Two thickness curves are given for the  $3.3 \times 10^6$  molecular weight polymer, one for the overnight value and one for the maximum thickness.) The increase in thickness with concentration is clearly an indication of a dependence of polymer conformation on solution concentration. At dilute solution concentrations each polymer molecule has a relatively flat conformation with larger values of  $p$  and smaller loops than at higher solution concentrations. As the solution concentration increases, the competition for available sites increases, resulting in a decreased number of attachments per molecule and an increase in the thickness of the adsorbed film, until a maximum extension from the surface is attained for that molecular weight material.

Our explanation of the differences in polymer conformation with adsorbance and solution concentration is consistent with results obtained from rates of desorption studies.<sup>18</sup> There it was found that the rate of desorption of polystyrene from metallic surfaces was a function of the adsorbance. The rate of desorption decreased with decreasing adsorbance, indicating an increase in the value of  $p$  and a more flattened conformation as the number of polymer molecules on the surface decreased. It is also consistent with results of Thies, Peyser, and Ullman,<sup>20</sup> who reported a decrease in the value of  $p$  with increasing adsorbance for polystyrene adsorbed on silica.

The conformation of the polymer molecule in the plateau region, *i.e.*, no increase in extension from the surface with increase in solution concentration, is shown in Figure 7 to be a linear function of the square root of the molecular weight up to  $1.9 \times 10^6$ . The equilibrium (24-hr.) thickness value of the  $3.3 \times 10^6$  polymer deviates from this linear behavior although the maximum thickness value falls relatively close to the straight line. An increase in the extension from the surface proportional to the square root of the molecular weight has been predicted for isolated molecules by DiMarzio and McCrackin<sup>11</sup> from their one-dimensional study of adsorption under conditions of few adsorption sites. This condition is met in our studies in the plateau regions where crowding of the molecules permits only relatively few contacts, and therefore, in effect only a few adsorption sites are available per molecule.

The conformation of a polymer molecule at an interface is often described by a random walk at a reflecting barrier. DiMarzio,<sup>21</sup> however, has shown that in general this does not give a proper counting of the conformations of a polymer molecule, and in order to do this correctly one should place an absorbing barrier one step behind the plane that represents the surface and exclude all walks that step onto this barrier. In Table II we have compared the measured root-mean-square thickness with  $(Z^2)^{1/2}$ , the root-mean-square end-to-end distance of a molecule with one end at-

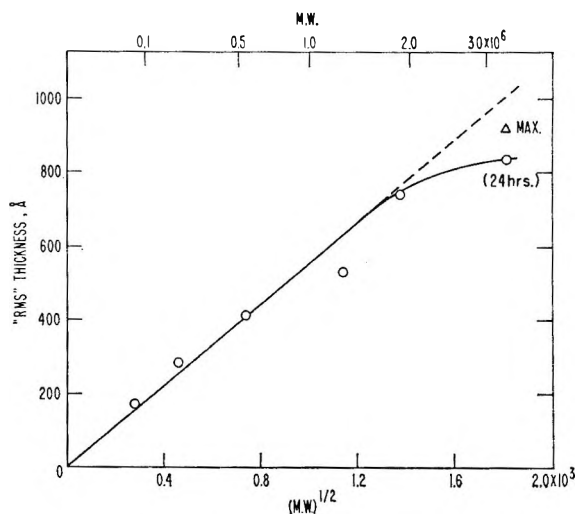


Figure 7. Root-mean-square thickness in the plateau region of polystyrene, adsorbed on chrome ferrotype plate as a function of the square root of the molecular weight.

(20) C. Thies, P. Peyser, and R. Ullman, *Proc. 4th Intern. Congr. Surface Activity, Brussels*, Sept. 1964.

(21) E. A. DiMarzio, *J. Chem. Phys.*, **42**, 2101 (1965).

tached to the surface, calculated both on the basis of a reflecting boundary and on the basis of this absorbing boundary. A better comparison would be between the measured values and the root-mean-square thickness calculated from the segmental distribution; unfortunately, this is not known. The experimental values fall between the two calculated quantities, although they are somewhat closer to the values obtained at the absorbing boundary. It appears that under the conditions of adsorption from a  $\Theta$ -solvent and in the plateau region, the molecule is adsorbed in a conformation very similar to that of a random coil.

The adsorbance was observed to increase initially with molecular weight and then decrease. We cannot

explain the decrease. The concentration of polymer in the film remains at about 10–12 g./100 ml. for most of the molecular weight range, decreasing as indicated in Table I to about 3–4 g./100 ml. for the highest molecular weight sample as a result of the decrease in adsorbance and increase in film thickness.

The only relatively direct comparison that can now be made between the results of our ellipsometric studies and the results of other techniques is with that of Rowland, *et al.*,<sup>22</sup> who used a viscosity technique to calculate the thickness of an adsorbed polymer layer on glass. The results that they obtained for the two polystyrene molecular weight fractions in cyclohexane were very close to our results. A dependence of the thickness on the square root of the molecular weight can also be inferred from this study.

The adsorption of polystyrene from cyclohexane at the  $\Theta$ -temperature appears to be approximately independent of the specific metallic surface, although low adsorbance values were obtained for copper. The most interesting comparison is between the inert gold surface and the highly oxidized chromium ferrotype surface. The film thickness and adsorbance values were approximately identical for both surfaces.

*Acknowledgment.* Some of the experimental data were taken by Mr. Leslie E. Smith to whom we are deeply indebted.

**Table II:** Comparison between Calculated Molecular Dimensions and Experimentally Determined Values of Molecular Extension of Adsorbed Molecule from Chrome Ferrotype Surface

Mol. wt.	R.m.s. thickness, Å.	$(\bar{Z}^2)^{1/2}_{\text{refl.}}$ , Å.	$(\bar{Z}^2)^{1/2}_{\text{abs.}}$ , Å.
76,000	170	110	170
207,000	290	190	270
537,000	420	300	440
1,370,000	530	440	630
1,900,000	740	580	810
3,300,000	830	760	1080

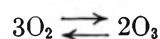
(22) F. W. Rowland, Ph.D. Dissertation, Polytechnic Institute of Brooklyn, 1963; F. Rowland, R. Bulas, E. Rothstein, and F. R. Eirich, *Ind. Eng. Chem.*, **57**, No. 9, 46 (1965).

# The Bromine Ultraviolet Lamp. Studies of the Oxygen-Ozone and Carbon Dioxide Equilibria<sup>1</sup>

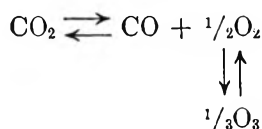
by B. A. Thompson, R. R. Reeves, Jr., and P. Harteck

Department of Chemistry, Rensselaer Polytechnic Institute, Troy, New York (Received June 11, 1965)

The persistent bromine line at 1633 Å. is obtained from a glow discharge of argon containing small amounts of bromine. A flow system has been used for the discharge incorporating Suprasil quartz which transmits the 1633-Å. line. Gases to be irradiated are contained in a concentric reaction chamber in which intensities up to  $10^{17}$  quanta/sec. can be readily obtained, permitting the attainment of steady-state equilibrium in 24 hr. or less. Incorporation of an outer cooling jacket allows irradiations to be carried out at any desired temperature. Two systems are under investigation: oxygen



and carbon dioxide



## Introduction

Recently, a new photochemical light source, the iodine lamp, has been developed which emits light at a wave length of 2062 Å.<sup>2</sup> This lamp has proved very useful for the study of reactions of excited  $\text{CO}(a^3\Pi)$  molecules. While considering other possible light sources, it was noted that the energy levels of bromine have a spacing similar to those of iodine with the corresponding emission lines having shorter wave lengths. Thus, lines are emitted at 1633, 1582 Å., and shorter wave lengths, but above 1633 Å. there is a gap in which no lines are emitted below  $\sim 3000$  Å. Figure 1 is an energy level diagram for bromine constructed from the detailed tabulation of Tech.<sup>3</sup> Only a few of the most intense transitions have been indicated, and the closely spaced d and f levels and some of the highest s and p levels have not been resolved. As Figure 1 shows, the 1633-Å. bromine line corresponds to the transition from the  $5s\ ^4P_{3/2}$  level to the  $4p^5\ ^2P_{1/2}$  level rather than the  $4p^5\ ^2P_{3/2}$  ground state and, thus, is not a resonance line. It would be very useful to have available for photochemical studies an intense light source in the 1600-Å. region where many

gases have high absorption coefficients. Other lamps which have been developed for such ultraviolet studies, such as the xenon lamp<sup>4</sup> and the krypton lamp,<sup>5</sup> normally have their outputs confined to a small window area. Thus, their total useful intensities are much lower than that of the iodine lamp whose emission occurs over the entire long inner tube. An effort therefore was made to develop a bromine lamp similar to the iodine lamp. This paper describes two types of lamps which have been built and some photochemical studies carried out with them.

## Apparatus

The wave length of the bromine emission is so short (1633 Å. and below) that most ordinary quartz will not transmit it. However, Suprasil quartz (distributed

(1) Presented in part at the 149th National Meeting of the American Chemical Society, Detroit, Mich., April 1965.

(2) P. Harteck, R. R. Reeves, Jr., and B. A. Thompson, *Z. Naturforsch.*, **19a**, 2 (1964).

(3) J. L. Tech, *J. Res. Natl. Bur. Std.*, **67A**, 505 (1963).

(4) P. Harteck and F. Oppenheimer, *Z. physik. Chem.*, **B16**, 77 (1932).

(5) W. Groth, *Z. Elektrochem.*, **58**, 752 (1954).

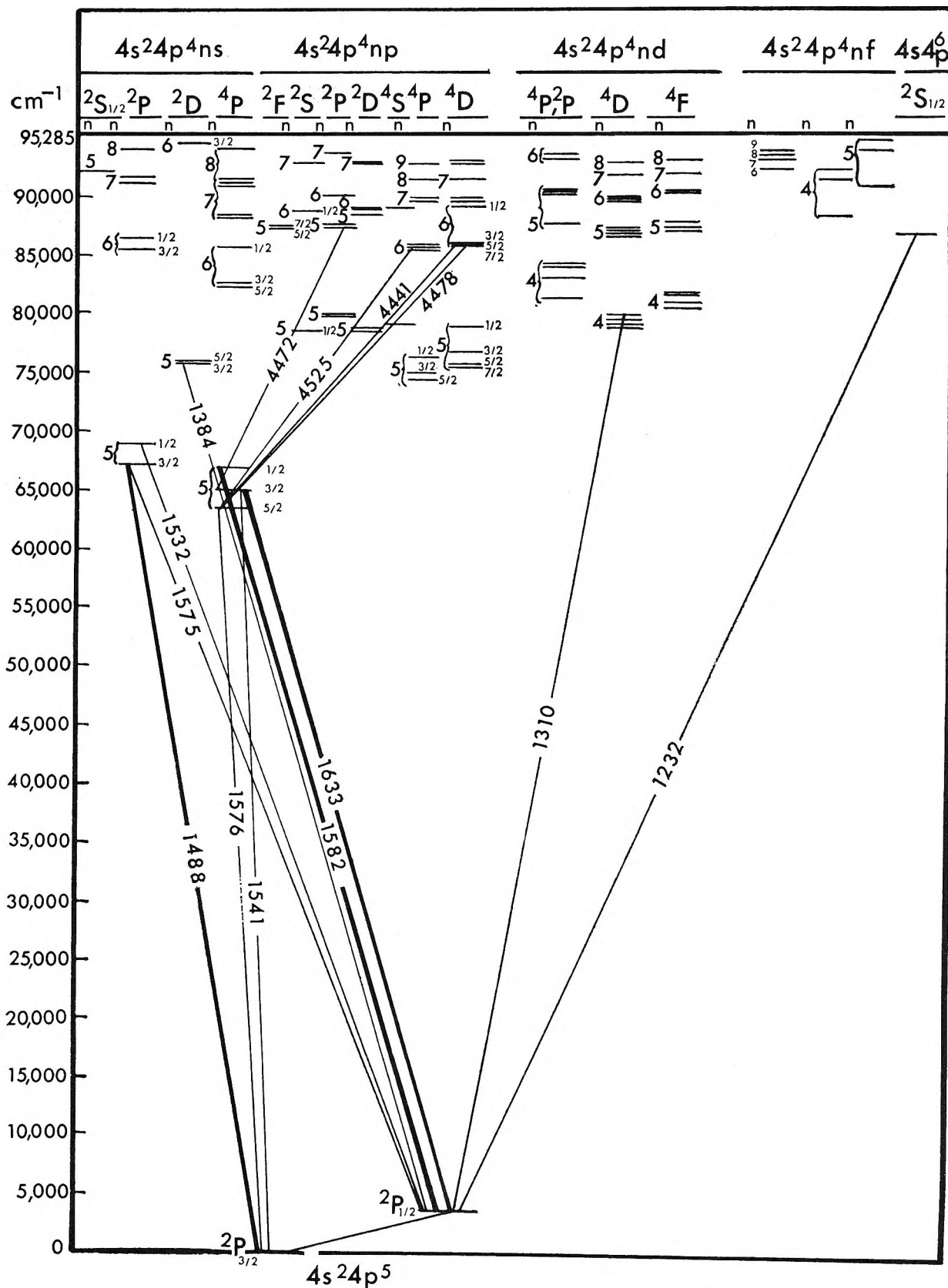


Figure 1. Energy level diagram for bromine.



by Amersil Quartz Division, Englehard Industries) has excellent transmission properties in this wave length region, and a 1-mm. thickness should transmit 50% of the 1633-Å. line and 10% of the 1582-Å. line. The first bromine lamp was therefore constructed exactly like the iodine lamp with an inner discharge tube made of Suprasil and an outer jacket of ordinary quartz to hold the gases to be irradiated. Bromine was admitted through a capillary leak from a reservoir. Argon was again used as a carrier gas to protect the electrodes and to stabilize the discharge. This lamp worked very well but, as expected, became excessively hot during operation. A water-cooled finger inserted lengthwise through the central discharge tube helped somewhat, but the temperature during operation was still high enough to introduce uncertainties into the results of some experiments.

A second, more complex lamp was then constructed which permitted gas samples to be irradiated at various temperatures. A schematic diagram of this lamp is shown in Figure 2. An insulating vacuum jacket was inserted between the discharge tube and the sample jacket, and an additional outer jacket was provided through which water or other coolant could be circulated. Irradiations could thus be carried out at any desired temperature. To allow transmission of the bromine line, both the innermost walls of the lamp were made of Suprasil. These modifications eliminated the heating problem although the output intensity was reduced substantially because of absorption by the second Suprasil wall. The output intensities were determined both by measuring the initial rate of decomposition of carbon dioxide and by measuring the rate of ozone formation in a flowing system. The methods gave nearly identical values of about  $3.0 \times 10^{17}$  quanta/sec. for the first lamp and about  $1.0 \times 10^{17}$  for the second lamp. These intensities refer to the entire reaction volume of 450 cc.

### Photochemical Experiments

The equilibrium between oxygen and ozone was studied, first by flowing oxygen or oxygen-ozone mixtures through the sample jacket. The ozone content of the irradiated gas was determined by bubbling it through potassium iodide solution and titrating the liberated iodine with standard sodium thiosulfate. The initial results on pure oxygen gave a steady-state ozone concentration of only about 1%. By flowing oxygen through the vacuum jacket to filter out the 1633-Å. line while transmitting wave lengths above  $\sim 2000$  Å., it was found that ozone was being destroyed by the bromine emission in the 2500- to 3000-Å. region. This emission was initially about  $10^{18}$  quanta/sec.

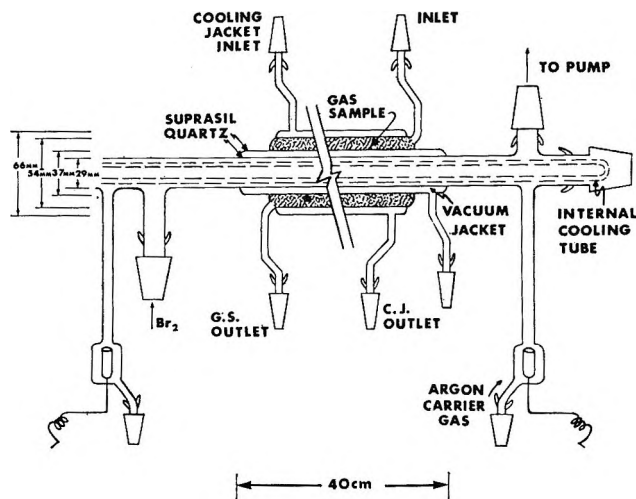


Figure 2. Schematic diagram of bromine lamp.

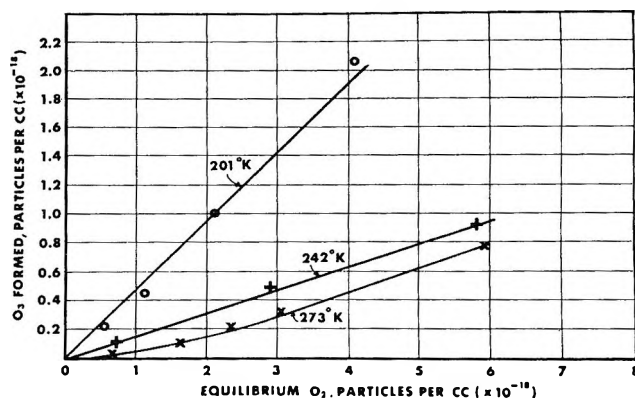


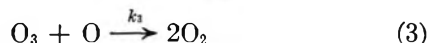
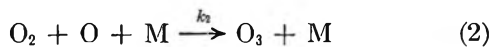
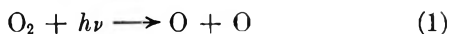
Figure 3. Equilibrium data obtained by irradiation of pure oxygen.

compared with about  $10^{17}$  for the 1633-Å. line. By using a smaller leak and by cooling the bromine reservoir with ice and salt, this ratio was reduced so that the intensities were about  $5.0 \times 10^{15}$  for the emission in the 2500- to 3000-Å. region and about  $3.2 \times 10^{16}$  for the 1633-Å. line. In all cases the argon pressure was of the order of 1 mm., and the bromine pressure was only a few tenths of a micron or less.

Under these conditions a series of irradiations was carried out on pure oxygen at several pressures and temperatures. In this series of experiments the irradiations were carried out with the oxygen under static rather than flowing conditions. In each case, irradiation was continued over several hours until equilibrium was complete. The results obtained at three different temperatures, 273, 242, and 201°K., are shown in Figure 3.

If it is assumed that ozone formation and destruction proceed according to the well-known mechanism





then the equilibrium ozone pressure should vary with total pressure as

$$[\text{O}_3] = \frac{k_2}{k_3} [\text{O}_2][\text{M}] \quad (I)$$

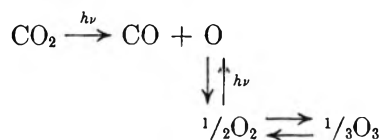
In pure oxygen  $[\text{M}]$  is equal to  $[\text{O}_2]$ , and the equilibrium ozone pressure should vary with the square of the oxygen pressure<sup>6</sup>

$$[\text{O}_3] = \frac{k_2}{k_3} [\text{O}_2]^2 \quad (II)$$

Instead, as Figure 3 shows, it was found that the equilibrium ozone pressure varied linearly with oxygen pressure at the two lower temperatures and exhibited only slight nonlinearity at 273°K. These results show that the equilibrium under these conditions is not controlled by the above mechanism, as had been thought, but by some alternate mechanism, at present unknown, possibly involving excited molecules and excited atoms. It may be noted that the results at the three temperatures gave an over-all activation energy of only about 2.5 kcal.

Preliminary experiments have also been made on  $\text{CO}_2$  at 201°K. and 150 mm. pressure. The irradiation was not carried to equilibrium, but about 9% of the

$\text{CO}_2$  was dissociated with a quantum yield of about 1. Ozone was present and the ratio of  $\text{O}_3$  to  $\text{O}_2$  was about 0.4, in agreement with that found for pure  $\text{O}_2$  at this temperature. Mass spectrometric analysis showed the ratio of  $\text{CO}$  formed to  $\text{O}_2$  formed (expressing both  $\text{O}_3$  and  $\text{O}_2$  as  $\text{O}_2$ ) was 2:1 as expected. To reach radiation equilibrium with  $\text{CO}_2$  requires a much longer time than with  $\text{O}_2$  alone because the absorption coefficient for the 1633-Å. line is much smaller ( $\alpha_{\text{CO}_2} = 2.5$ ;  $\alpha_{\text{O}_2} = 75$ ).<sup>7</sup> In addition, as dissociation of  $\text{CO}_2$  proceeds,  $\text{O}_2$  and  $\text{O}_3$  accumulate and compete for absorption of the 1633-Å. radiation. Therefore, any equilibrium study of the  $\text{CO}_2$  dissociation will be complicated by the oxygen-ozone equilibrium



*Acknowledgment.* The authors wish to thank Mr. R. W. Waldron for experimental assistance. The bromine lamps were fabricated by Wilt Laboratory Glass Blowing, Inc., Latham, N. Y. This work was carried out under Research Grant NsG-261-62 from the National Aeronautics and Space Administration.

(6) In cases where substantial amounts of ozone are formed the relative efficiency of ozone as a third body must also be considered.

(7) K. Watanabe, M. Zelikoff, and E. C. Y. Inn, "Absorption Coefficients of Several Atmospheric Gases," AFCRC Technical Report 53-23, 1953.

## Properties of Organic-Water Mixtures. V. Self-Diffusion Coefficients of $\text{Na}^+$ in Alcohol-Water Mixtures at 25<sup>o1,2</sup>

by Arthur E. Marcinkowsky, Harold O. Phillips, and Kurt A. Kraus

Chemistry Division, Oak Ridge National Laboratory, Oak Ridge, Tennessee (Received June 11, 1965)

Self-diffusion coefficients,  $\mathcal{D}_{\text{Na}}$ , of  $\text{Na}^+$  ( $\text{NaClO}_4$  or  $\text{NaCl}$ ,  $m = 0.1$ ) were measured for water mixtures of methanol, ethanol, and 1-propanol at 25° by the radiometric porous-frit method. In these systems the diffusion coefficient  $\mathcal{D}_{\text{Na}}$  is always less than its value in water ( $1.28 \times 10^{-5} \text{ cm.}^2 \text{ sec.}^{-1}$ ). The diffusion coefficients are lowest in the 1-propanol system and highest in the methanol system. In the methanol-water system  $\mathcal{D}_{\text{Na}}$  has a minimum value at about 60 vol. % methanol. A plot of the diffusion coefficient-viscosity products,  $\mathcal{D}\eta/\eta_0$ , vs. volume per cent alcohol shows that the data for the three systems can be described to a good approximation by a single curve; it has a slight maximum with  $\mathcal{D}\eta/\eta_0 \approx 1.45 \times 10^{-5} \text{ cm.}^2 \text{ sec.}^{-1}$  at about 40 vol. % alcohol and decreases to  $\mathcal{D}\eta/\eta_0 \approx 0.64 \times 10^{-5} \text{ cm.}^2 \text{ sec.}^{-1}$  in the pure solvents. For the methanol-water system the results are compared with available conductance data and with diffusion coefficient data of several nonelectrolytes.

While previous papers of this series have dealt with a variety of equilibrium aspects of water-organic-electrolyte systems, the present one addresses itself to one of the kinetic aspects, variation of the self-diffusion coefficient of an ion with the water content of such mixtures. The diffusion studies exploit the radiometric porous-frit method<sup>3</sup> by which completion of relatively ambitious comparative studies can be carried out rapidly though with still reasonable precision.

The present paper deals with a comparison (at 25°) of the self-diffusion coefficients of sodium ions for a simple series of organic components [methanol (MeOH), ethanol (EtOH), 1-propanol (PrOH)]. Salt concentration was constant at  $m = 0.1$  mole/kg. of solvent. Both  $\text{NaCl}$  and  $\text{NaClO}_4$  were used in the MeOH-H<sub>2</sub>O system. For the others, only  $\text{NaClO}_4$  was used because  $\text{NaCl}$  is too insoluble in the organic-rich regions of the systems. We have evaluated the effect of the viscosity of the solutions on the diffusion coefficients and compared the results with available conductance data and the diffusion coefficients of nonelectrolytes (urea, thiourea, and sucrose) which are available for the MeOH-H<sub>2</sub>O system.

### Experimental Section

1. *Method.* Self-diffusion coefficients were meas-

ured by the radiometric porous-frit method described earlier. Briefly, this involves soaking a thin slab of porous material in a solution containing a radioisotope of the element of interest. After mounting the slab in front of a detector, a solution of the same composition, but not containing tracer, is pumped rapidly past the frit. From the counting rate ( $C$ ) of the frit as a function of time, the (diffusional) "decay constant"  $\lambda$  is readily evaluated from the linear portion of a plot of  $\log C$  vs. time. The diffusion coefficient,  $\mathcal{D}$ , is obtained after calibrating the frit with a reference ion of known  $\mathcal{D}$ . The reference ion used in this study was  $\text{Na}^+$  in 1  $M$   $\text{NaCl}$  at 25°;  $\mathcal{D}_{\text{Na}} = 1.234 \times 10^{-5} \text{ cm.}^2 \text{ sec.}^{-1}$  as reported by Mills<sup>4</sup> was used. Measurements were carried out at several flow rates to assure that counting rate-time curves at the flow velocities selected were independent of flow rate. Temperature control for all measurements was maintained at  $25.0 \pm 0.1^\circ$ .

(1) Research sponsored by The Office of Saline Water, U. S. Department of the Interior, under Union Carbide Corporation's contract with the U. S. Atomic Energy Commission.

(2) Previous paper in series: R. J. Raridon and K. A. Kraus, *J. Colloid Sci.*, in press.

(3) A. E. Marcinkowsky, F. Nelson, and K. A. Kraus, *J. Phys. Chem.*, **69**, 303 (1965).

(4) R. Mills, *J. Am. Chem. Soc.*, **77**, 6116 (1955).

2. *Porous Frits.* Two porous gold frits with about 50% void volume and approximate dimensions of 1.2 × 0.7 × 0.07 cm. were used. The frits were prepared from finely divided gold powder (particle diameter 10–15 μ) by a cold-compression technique using a double-acting die.<sup>5</sup>

The frits were calibrated with sodium tracer in 1 M NaCl. The average diffusional decay constants, λ, from four measurements on each frit were 1.314 and 1.254 × 10<sup>-2</sup> sec.<sup>-1</sup> for the two frits, corresponding to diffusional half-lives of 52.75 and 55.25 sec., respectively. Distribution coefficient measurements showed that the gold frits did not adsorb sodium ions significantly from the mixtures.

3. *Tracers.* The radioactive tracer <sup>24</sup>Na (*t*<sub>1/2</sub> = 15.05 hr.) was obtained from the Radioisotopes Division of Oak Ridge National Laboratory; <sup>22</sup>Na (*t*<sub>1/2</sub> = 2.58 years) was obtained from the Nuclear Science and Engineering Corp. Examination of the γ-energy spectra showed no detectable impurities in either tracer, and no purifications were carried out. As expected, results obtained with either tracer were indistinguishable. The <sup>24</sup>Na tracer was always of high specific activity and had stated radiochemical purity greater than 99%. To avoid impurity buildup, use of <sup>24</sup>Na tracer was discontinued after approximately five half-lives had elapsed.

4. *Materials.* (a) *Salts.* Reagent grade NaCl was used without further purification. Fisher purified NaClO<sub>4</sub> was used in the hydrated form, and the water content was determined by Karl Fischer titration. The amount of water present was usually around 13.5%, just slightly more than that corresponding to the monohydrate (12.8%).

(b) *Solvents.* Analytical grade anhydrous methanol (0.15% H<sub>2</sub>O), U.S.P. grade 95% ethanol (7.5% H<sub>2</sub>O), 100% ethanol (0.4% H<sub>2</sub>O), and reagent grade 1-propanol (0.2% H<sub>2</sub>O) were used to prepare the various solutions. Water contents in weight per cent for the stock alcohols, given in parentheses, were determined by Karl Fischer titrations.

(c) *Solutions.* The alcohol-water mixtures were prepared on a weight basis. Volume per cent alcohol was calculated from the weights *w<sub>i</sub>* as volume per cent = 100/[*w<sub>1</sub>ρ<sub>3</sub>*/*w<sub>3</sub>ρ<sub>1</sub>*] + 1], where ρ<sub>1</sub> and ρ<sub>3</sub> are the densities of water and alcohol, respectively; this is equivalent to ignoring volume changes on mixing. (At 25°: ρ<sub>H<sub>2</sub>O</sub> = 0.99707, ρ<sub>MeOH</sub> = 0.7868, ρ<sub>EtOH</sub> = 0.7851, ρ<sub>PrOH</sub> = 0.7995.)<sup>6</sup>

The salt concentration *m* was maintained constant for all mixtures at 0.1 mole of salt/kg. of solvent. Each solution was separately analyzed for water content, and the results generally agreed within 0.5% with

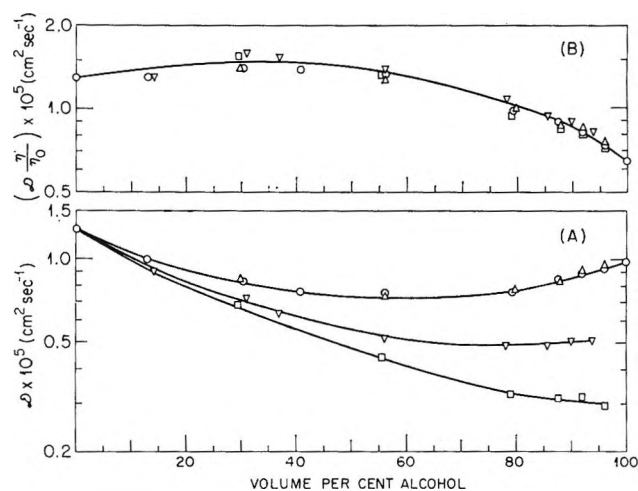


Figure 1. (A) Self-diffusion coefficient of Na<sup>+</sup> in alcohol-water mixtures (0.1 m NaCl, 25°). (B) Diffusion coefficient-viscosity product: O, NaCl-MeOH; Δ, NaClO<sub>4</sub>-MeOH; ▽, NaClO<sub>4</sub>-EtOH; □, NaClO<sub>4</sub>-PrOH.

the calculated compositions. The viscosity of the solutions was measured with a Cannon-Ubbelohde viscometer.<sup>7</sup>

## Results and Discussion

1. *Results.* The self-diffusion coefficients of Na<sup>+</sup> (*D*<sub>Na</sub>) at 25° in NaCl-MeOH-H<sub>2</sub>O, NaClO<sub>4</sub>-MeOH-H<sub>2</sub>O, NaClO<sub>4</sub>-EtOH-H<sub>2</sub>O, and NaClO<sub>4</sub>-PrOH-H<sub>2</sub>O mixtures at *m* = 0.1 are given in Tables I-IV. A plot of these results as a function of volume per cent alcohol is shown in Figure 1A.

The self-diffusion coefficient *D*<sub>Na</sub> in water (*m*<sub>NaCl</sub> = 0.1) was found to be 1.28 × 10<sup>-5</sup> cm.<sup>2</sup> sec.<sup>-1</sup>. This

Table I: Self-Diffusion Coefficients of Na<sup>+</sup> in NaCl-MeOH-H<sub>2</sub>O Mixtures at 25° (*m*<sub>NaCl</sub> = 0.1)

Wt. % MeOH	Vol. % MeOH	<i>η</i> / <i>η</i> <sub>0</sub>	<i>D</i> × 10 <sup>5</sup> , cm. <sup>2</sup> sec. <sup>-1</sup>	<i>D</i> * × 10 <sup>5</sup> , cm. <sup>2</sup> sec. <sup>-1</sup>
0.0	0.0	1.004	1.28	1.28
10.5	12.9	1.30	0.99	1.29
25.4	30.2	1.68	0.83	1.39
35.1	40.7	1.81	0.76	1.38
50.2	56.2	1.75	0.76	1.33
75.0	79.2	1.29	0.76	0.98
84.5	87.4	1.05	0.85	0.89
89.8	91.8	0.916	0.89	0.82
94.7	95.8	0.786	0.93	0.73
99.8	99.8	0.652	0.98	0.64

(5) We are indebted to Mr. D. Gray of the Oak Ridge Gaseous Diffusion Plant for preparation of the porous gold frits.

(6) R. A. Robinson and R. H. Stokes, "Electrolyte Solutions," Academic Press Inc., New York, N. Y., 1959.

(7) We are indebted to Dr. R. J. Raridon and Mr. C. G. Westmoreland for the viscosity measurements and the Karl Fischer titrations.

**Table II:** Self-Diffusion Coefficients of  $\text{Na}^+$  in  $\text{NaClO}_4\text{-MeOH-H}_2\text{O}$  Mixtures at  $25^\circ$  ( $m_{\text{NaClO}_4} = 0.1$ )

Wt. % MeOH	Vol. % MeOH	$\eta/\eta_0$	$\mathcal{D} \times 10^5$ , $\text{cm.}^2 \text{sec.}^{-1}$	$\mathcal{D}^* \times 10^5$ , $\text{cm.}^2 \text{sec.}^{-1}$
25.0	29.8	1.65	0.84	1.39
50.1	56.1	1.73	0.73	1.26
75.5	79.6	1.28	0.77	0.99
85.0	87.8	1.04	0.83	0.86
89.8	91.8	0.919	0.91	0.84
94.9	95.9	0.776	0.95	0.74

**Table III:** Self-Diffusion Coefficients of  $\text{Na}^+$  in  $\text{NaClO}_4\text{-EtOH-H}_2\text{O}$  Mixtures at  $25^\circ$  ( $m_{\text{NaClO}_4} = 0.1$ )

Wt. % EtOH	Vol. % EtOH	$\eta/\eta_0$	$\mathcal{D} \times 10^5$ , $\text{cm.}^2 \text{sec.}^{-1}$	$\mathcal{D}^* \times 10^5$ , $\text{cm.}^2 \text{sec.}^{-1}$
12.1	14.1	1.44	0.91	1.31
26.1	30.9	2.19	0.72	1.58
31.5	36.9	2.42	0.64	1.55
50.1	56.0	2.65	0.52	1.38
73.7	78.1	2.21	0.49	1.08
82.3	85.6	1.91	0.49	0.94
87.5	89.9	1.76	0.51	0.90
92.2	93.7	1.60	0.51	0.82

**Table IV:** Self-Diffusion Coefficients of  $\text{Na}^+$  in  $\text{NaClO}_4\text{-PrOH-H}_2\text{O}$  Mixtures at  $25^\circ$  ( $m_{\text{NaClO}_4} = 0.1$ )

Wt. % PrOH	Vol. % PrOH	$\eta/\eta_0$	$\mathcal{D} \times 10^5$ , $\text{cm.}^2 \text{sec.}^{-1}$	$\mathcal{D}^* \times 10^5$ , $\text{cm.}^2 \text{sec.}^{-1}$
25.0	29.3	2.27	0.68	1.54
50.0	55.5	2.99	0.441	1.32
75.0	78.9	2.88	0.325	0.94
85.0	87.6	2.67	0.314	0.84
90.0	91.8	2.55	0.317	0.81
95.0	96.0	2.44	0.294	0.72

agrees well with values of  $1.30 \times 10^{-5}$  and  $1.28 \times 10^{-5}$   $\text{cm.}^2 \text{sec.}^{-1}$  reported by Mills<sup>4</sup> and by Mills and Godbole.<sup>8</sup>

In the  $\text{MeOH-H}_2\text{O}$  system  $\mathcal{D}_{\text{Na}}$  first decreases as the alcohol content is increased; a shallow minimum occurs near 55 vol. % of MeOH with  $\mathcal{D}_{\text{Na}} = 0.73 \times 10^{-5}$   $\text{cm.}^2 \text{sec.}^{-1}$ . In pure MeOH,  $\mathcal{D}_{\text{Na}} = 0.98 \times 10^{-5}$   $\text{cm.}^2 \text{sec.}^{-1}$ . Values of  $\mathcal{D}_{\text{Na}}$  in chloride and perchlorate solutions ( $m_{\text{Na}} = 0.1$ ) are very nearly the same (compare Tables I and II).

Self-diffusion coefficients in the  $\text{EtOH-H}_2\text{O}$  system are lower than in the  $\text{MeOH-H}_2\text{O}$  system. In the  $\text{PrOH-H}_2\text{O}$  system they are still lower. For example, at 50 vol. % alcohol  $\mathcal{D}_{\text{Na}}$  is 0.73, 0.53, and  $0.45 \times 10^{-5}$   $\text{cm.}^2 \text{sec.}^{-1}$  for the MeOH, EtOH, and PrOH systems,

respectively. The  $\text{EtOH-H}_2\text{O}$  system seems to have a slight minimum near 80 vol. % alcohol.

The large differences in  $\mathcal{D}_{\text{Na}}$  for the three alcohol-water systems can be largely accounted for by differences in the viscosity of the solutions. A plot of the diffusion coefficient-viscosity product  $\mathcal{D}^* = \mathcal{D}\eta/\eta_0$ , where  $\eta$  is the viscosity of the solution and  $\eta_0$  is the viscosity of water, as a function of volume per cent alcohol shows (Figure 1B) that the data for the three systems can be described to a good approximation by a single curve; the maximum spread of points from the average curve seems less than 6%. The  $\mathcal{D}^*$  curve has a slight maximum ( $\mathcal{D}^* \approx 1.45 \times 10^{-5}$   $\text{cm.}^2 \text{sec.}^{-1}$ ) near 40 vol. % alcohol. The solvent composition at this maximum in  $\mathcal{D}^*$  corresponds closely to the solvent compositions at which the viscosities also have maxima. The value of  $\mathcal{D}^*$  decreases below its value in water near 60 vol. % alcohol and in the water-free solvents is ca. 50% of its value in water.

Very few self-diffusion data seem to exist with which current results may be compared. We have already mentioned the studies of Mills and Godbole<sup>4,8</sup> for aqueous solutions with which our results compare favorably. Ellard, Williams, and Dawson<sup>9</sup> studied self-diffusion of  $\text{Na}^+$  in pure MeOH for  $m_{\text{NaCl}} \leq 0.04$ . At their highest concentration, they found  $\mathcal{D}_{\text{Na}} = 1.15 \times 10^{-5}$   $\text{cm.}^2 \text{sec.}^{-1}$ , in reasonable agreement with our value  $\mathcal{D}_{\text{Na}} = 0.98 \times 10^{-5}$  at  $m_{\text{NaCl}} = 0.1$ .

In Figure 2 our self-diffusion measurements with  $\text{Na}^+$  in the MeOH system are compared with diffusion coefficients of various nonelectrolytes (urea, thiourea, sucrose) obtained by Longworth.<sup>10</sup> To normalize the plot, the ordinate gives the ratio  $R_{\mathcal{D}\eta}$  of the observed  $\mathcal{D}\eta$  product to its value in water,  $(\mathcal{D}\eta)_{\text{H}_2\text{O}}$ . Up to ca. 60 vol. % MeOH, the various sets of data define es-

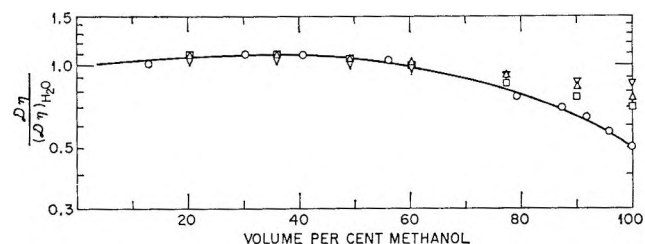


Figure 2. Relative diffusion coefficient-viscosity products in methanol-water mixtures: O,  $\text{Na}^+$  in 0.1 *m*  $\text{NaCl}$ . From Longworth, 1963: □, urea (infinite dilution); Δ, thiourea (infinite dilution); ▽, sucrose (ca. 0.01 *M*).

(8) R. Mills and E. W. Godbole, *J. Am. Chem. Soc.*, **82**, 2395 (1960).

(9) J. A. Ellard, W. D. Williams, and L. R. Dawson, *Trans. Kentucky Acad. Sci.*, **18**, 8 (1957).

(10) L. G. Longworth, *J. Phys. Chem.*, **67**, 689 (1963).

sentially a single curve; the slight maximum near 40% MeOH is shown by these various systems. At high methanol content  $R_{\mathcal{D}\eta}$  for the various nonelectrolytes is greater than for Na<sup>+</sup>, the divergence increasing with methanol concentration. Nevertheless the difference between the various systems is, on a normalized basis, remarkably small.

**2. Comparison of Self-Diffusion with Conductance Data.** The limiting self-diffusion coefficient  $\mathcal{D}_M^0$  of an ion M at infinite dilution is related to the limiting ionic conductance,  $\lambda_M^0$ , through the Nernst equation<sup>6</sup>

$$\mathcal{D}_M^0 = \frac{RT\lambda_M^0}{|z|F^2} = 2.663 \times 10^{-7} \frac{\lambda_M^0}{|z|} \text{ cm.}^2 \text{ sec.}^{-1} \quad (1)$$

where  $R$  is the gas constant (joules deg.<sup>-1</sup> mole<sup>-1</sup>),  $T$  is absolute temperature,  $F$  is the Faraday (international coulombs g.-equiv.<sup>-1</sup>),  $\lambda_M^0$  is limiting ionic conductance (cm.<sup>2</sup> ohm<sup>-1</sup> equiv.<sup>-1</sup>), and  $|z|$  the absolute value of the charge of the ion. The numerical coefficient applies at 25°; it is consistent with a recent tabulation of the constants.<sup>11</sup>

Table V lists the limiting ionic conductances for Na<sup>+</sup> and Cl<sup>-</sup> for various solvent mixtures; these were obtained from literature data of limiting equivalent conductances ( $\Lambda_{\text{NaCl}}^0$  in H<sub>2</sub>O,<sup>12</sup> in 50 mole % MeOH,<sup>13</sup> in MeOH,<sup>14</sup> and in EtOH<sup>15</sup>) and limiting transport numbers ( $t_{\text{Na}}^0$  in H<sub>2</sub>O,<sup>16</sup> in 50 mole % MeOH,<sup>17</sup> and in MeOH,<sup>18</sup> and  $t_{\text{Cl}}^0$  in EtOH<sup>19</sup>). The dielectric constants,  $\epsilon$ , for water,<sup>6</sup> 50 mole % MeOH,<sup>20</sup> MeOH,<sup>6</sup> and EtOH<sup>6</sup> are also included. The listed values of  $\mathcal{D}_{\text{Na}}^0$  were calculated according to eq. 1.

**Table V:** Solvent Dielectric Constants, Transport Numbers of Na<sup>+</sup>, and Conductivity Data of NaCl at Infinite Dilution in H<sub>2</sub>O, 50 Mole % MeOH-H<sub>2</sub>O, MeOH, and EtOH

System	$\epsilon$	$t_{\text{Na}}^0$	$\Lambda_{\text{NaCl}}^0$	$\lambda_{\text{Na}}^0$	$\lambda_{\text{Cl}}^0$	$\mathcal{D}_{\text{Na}}^0 \times 10^5$
H <sub>2</sub> O	78.3	0.3962	126.45	50.10	76.35	1.334
50 mole % MeOH-H <sub>2</sub> O	49.84	0.4437	66.62	29.56	37.06	0.787
MeOH	32.63	0.4633	97.61	45.22	52.39	1.204
EtOH	24.3	0.4813	42.16	20.31	21.85	0.541

A comparison for the MeOH-H<sub>2</sub>O system of the observed self-diffusion coefficients  $\mathcal{D}_{\text{Na}}$  and those computed from the conductance data ( $\mathcal{D}_{\text{Na}}^0$ ) are shown in Figure 3. The limiting values lie above the experimental ones qualitatively as expected from the Onsager theory.<sup>21,22</sup> Also, as expected from the Onsager theory, the divergence between the limiting self-diffusion coefficients and those observed at  $m_{\text{NaCl}} = 0.1$

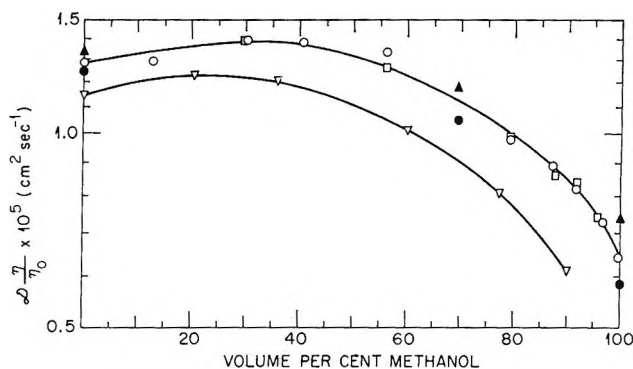


Figure 3. Comparison of self-diffusion coefficients with values obtained from conductance data: O, observed (0.1 m NaCl); □, observed (0.1 m NaClO<sub>4</sub>); ▽, from  $\lambda_{\text{Na}^+}$  at 0.05 M NaCl (Longworth and MacInnes); ▲, from  $\lambda_{\text{Na}^+}$  (Gordon, *et al.*); ●, calculated (0.1 m NaCl) from  $\lambda^0$  and the Onsager equation.

increases with methanol content, *i.e.*, with decreasing dielectric constant.

According to the Onsager theory the concentration dependence of the self-diffusion coefficient of an ion (1-1 electrolyte) is given by the equation

$$\mathcal{D}_M = 2.663 \times 10^{-7} \lambda_M^0 \left[ 1 - \frac{0.544 \times 10^3}{\epsilon^{3/2}} \zeta \sqrt{c} \right] \quad (2)$$

where  $\zeta = 1 - \sqrt{(3\lambda_k^0 + \lambda_M^0)/4(\lambda_k^0 + \lambda_M^0)}$ ;  $\lambda_k^0$  is the limiting ionic conductance of the counterion  $k$ , and  $c$  is concentration ( $M$ ). Equation 2 was obtained from an equation given by Gosting and Harned<sup>22</sup> through a suitable combination of terms.

Using the data of Table V, eq. 2 becomes, for water

$$\mathcal{D}_{\text{Na}} \times 10^5 = 1.334 [1 - 0.202\sqrt{c}] \quad (3a)$$

for 50 mole % MeOH-H<sub>2</sub>O

$$\mathcal{D}_{\text{Na}} \times 10^5 = 0.787 [1 - 0.422\sqrt{c}] \quad (3b)$$

- (11) *Natl. Bur. Std. (U. S.), Tech. News Bull.*, **47**, 175 (1963).
- (12) G. C. Benson and A. R. Gordon, *J. Chem. Phys.*, **13**, 473 (1945).
- (13) H. I. Schiff and A. R. Gordon, *ibid.*, **16**, 336 (1948).
- (14) J. P. Butler, H. I. Schiff, and A. R. Gordon, *ibid.*, **19**, 752 (1951).
- (15) J. R. Graham, G. S. Kell, and A. R. Gordon, *J. Am. Chem. Soc.*, **79**, 2352 (1957).
- (16) R. W. Allgood and A. R. Gordon, *J. Chem. Phys.*, **10**, 124 (1942).
- (17) L. W. Shemilt, J. A. Davis, and A. R. Gordon, *ibid.*, **16**, 340 (1948).
- (18) J. A. Davis, R. L. Kay, and A. R. Gordon, *ibid.*, **19**, 749 (1951).
- (19) J. R. Graham and A. R. Gordon, *J. Am. Chem. Soc.*, **79**, 2350 (1957).
- (20) P. J. Albright and L. J. Gosting, *ibid.*, **68**, 1061 (1946).
- (21) L. Onsager, *Ann. N. Y. Acad. Sci.*, **46**, 241 (1945).
- (22) L. J. Gosting and H. S. Harned, *J. Am. Chem. Soc.*, **73**, 159 (1951).

for MeOH

$$\mathcal{D}_{\text{Na}} \times 10^5 = 1.204[1 - 0.818\sqrt{c}] \quad (3c)$$

for EtOH

$$\mathcal{D}_{\text{Na}} \times 10^5 = 0.541[1 - 1.299\sqrt{c}] \quad (3d)$$

The self-diffusion coefficients in the MeOH-H<sub>2</sub>O system at  $m = 0.1$  computed with eq. 3a-c (after converting  $m$  to  $c$ ) are 1.249, 0.694, and  $0.912 \times 10^{-5}$  cm.<sup>2</sup> sec.<sup>-1</sup>, respectively. The corresponding values  $\mathcal{D}^* = \mathcal{D}\eta/\eta_0$  of 1.254, 1.054, and 0.589 are included in Figure 3. They are, as expected, below the observed values; the deviation increases, also as expected, with decreasing dielectric constant of the medium (increasing MeOH content).

Included in Figure 3 is also a curve of diffusion coefficients computed from conductance data of Longworth and MacInnes<sup>23</sup> by inserting their ionic conductances at  $M = 0.05$  ( $M$  is moles/liter of solution) in eq. 1. These computed "apparent" self-diffusion coefficients at  $M = 0.05$  are substantially smaller than the observed ones at  $m = 0.1$ , demonstrating the strong retarding influence of the electrophoretic effect in the conductance measurements.

For the EtOH-H<sub>2</sub>O system, transport numbers and conductance data at infinite dilution seem to be available only for the pure solvent system. The com-

puted value  $\mathcal{D}_{\text{Na}}^0 = 0.541 \times 10^{-5}$  is surprisingly close to the value  $\mathcal{D}_{\text{Na}} = ca. 0.52 \times 10^{-5}$  extrapolated from our self-diffusion coefficient measurements. In view of the strong concentration dependence of  $\mathcal{D}_{\text{Na}}$  implied by eq. 3d, a much larger ratio of  $\mathcal{D}_{\text{Na}}^0/\mathcal{D}_{\text{Na}}$  would have been expected.

For the PrOH-H<sub>2</sub>O system, transport numbers at infinite dilution are apparently not available. However, if we assume that  $t_{\text{Na}}^0 = 0.5$  (which is probably only slightly high), we compute from  $\Lambda_{\text{NaI}}^0 = 23.92$ ,<sup>24</sup>  $\mathcal{D}_{\text{Na}}^0 = 0.318 \times 10^{-5}$  cm.<sup>2</sup> sec.<sup>-1</sup>, which is essentially equal to the value ( $0.3 \times 10^{-5}$ ) which we extrapolate at  $m_{\text{NaClO}_4} = 0.1$  from the self-diffusion data. In view of the very low dielectric constant of PrOH, one would have expected on the basis of the Onsager theory that the observed self-diffusion coefficient is substantially less than  $\mathcal{D}_{\text{Na}}^0$ . The reasons for these discrepancies in the EtOH and PrOH systems are not clear.

*Acknowledgment.* It is a pleasure to thank Dr. G. Scatchard, Dr. R. M. Fuoss, and Mr. F. Nelson for a number of helpful discussions.

(23) L. G. Longworth and D. A. MacInnes, *J. Phys. Chem.*, **43**, 239 (1939).

(24) T. A. Grover and P. G. Sears, *ibid.*, **60**, 330 (1956).

# The Scandium-Yttrium-Hydrogen System<sup>1</sup>

by M. L. Lieberman and P. G. Wahlbeck

Department of Chemistry, Illinois Institute of Technology, Chicago, Illinois 60616 (Received June 14, 1965)

Equilibrium hydrogen pressures up to 1 atm. have been measured for the scandium-yttrium-hydrogen system at 700, 800, and 900°. These data indicate a large primary solid solution region of hydrogen in scandium-yttrium alloys and a three condensed phase region. The latter region indicates limited miscibility of the two metal dihydrides which was confirmed by X-ray diffraction analysis. The phase diagram at 700° has been constructed, and the relative partial molal and differential thermodynamic properties of hydrogen have been calculated. For scandium-yttrium alloys with at least 60 atomic % yttrium, evidence for a trihydride phase has been found at 242°. Hysteresis has been observed in the hydrogenation reaction to produce the trihydride phase.

## Introduction

Although numerous binary metal-hydrogen systems have been investigated, relatively few ternary metal-hydrogen systems have been studied. In 1948, Smith<sup>2</sup> listed only 15 ternary systems which had been studied. In 1962, Gibb<sup>3</sup> listed additional ternary systems which had been investigated. The only ternary system involving two rare earth metals that has been investigated has been the cerium-lanthanum-hydrogen system studied by Sieverts and Gotta.<sup>4</sup>

Reasons for the study of the scandium-yttrium-hydrogen system were the determination of (1) pressure-temperature-composition (*P-T-C*) data, (2) the phase diagram, (3) thermodynamic data, (4) possible existence of marked changes in the thermodynamic data as found for the binary metal-hydrogen systems, (5) ability to predict the thermodynamic data for the ternary system from the thermodynamic data of the binary systems, and (6) ability to predict the phase diagram from known data for the binary systems such as phase diagrams, thermodynamic properties, and structural parameters for metals and compounds. Scandium and yttrium hydrides are very stable toward the evolution of gaseous hydrogen and the possibility existed that hydrides of the alloys might be more stable than those of either of the metal-hydrogen systems.

Each of the two component systems had been investigated previously. Beaudry and Daane<sup>5</sup> found that the scandium-yttrium system shows complete solid solubility at all compositions. Yannopoulos, Edwards,

and Wahlbeck<sup>6</sup> obtained *P-T-C* data for the yttrium-hydrogen system; these data indicate formation of primary solid solution and apparently hydrogen-deficient dihydride and trihydride phases with intermediate two condensed phase regions. Lieberman and Wahlbeck<sup>7</sup> obtained *P-T-C* data for the scandium-hydrogen system which show formation of primary solid solution and apparently hydrogen-deficient dihydride phases with an intermediate two condensed phase region. No evidence for a scandium trihydride phase was observed.

## Experimental Section

**Apparatus.** A Sieverts' apparatus, modified so that equilibrium hydrogen pressures between 10<sup>-4</sup> mm. and 1 atm. could be measured, was used to obtain pressure-temperature-composition data. The apparatus has been described elsewhere.<sup>1,6,7</sup>

**Materials.** The scandium used in this research was

(1) Based on a thesis by M. L. Lieberman submitted to the Illinois Institute of Technology in partial fulfillment of the requirements for the Ph.D. degree, June 1965. Presented before the Physical Chemistry Division at the 149th National Meeting of the American Chemical Society, Detroit, Mich., April 1965.

(2) D. P. Smith, "Hydrogen in Metals," University of Chicago Press, Chicago, Ill., 1948.

(3) T. R. P. Gibb, Jr., *Progr. Inorg. Chem.*, **3**, 315 (1962).

(4) A. Sieverts and A. Gotta, *Z. Elektrochem.*, **32**, 105 (1926).

(5) B. J. Beaudry and A. H. Daane, *Trans. AIME*, **227**, 865 (1963).

(6) L. N. Yannopoulos, R. K. Edwards, and P. G. Wahlbeck, *J. Phys. Chem.*, **69**, 2510 (1965).

(7) M. L. Lieberman and P. G. Wahlbeck, *ibid.*, **69**, 3514 (1965).

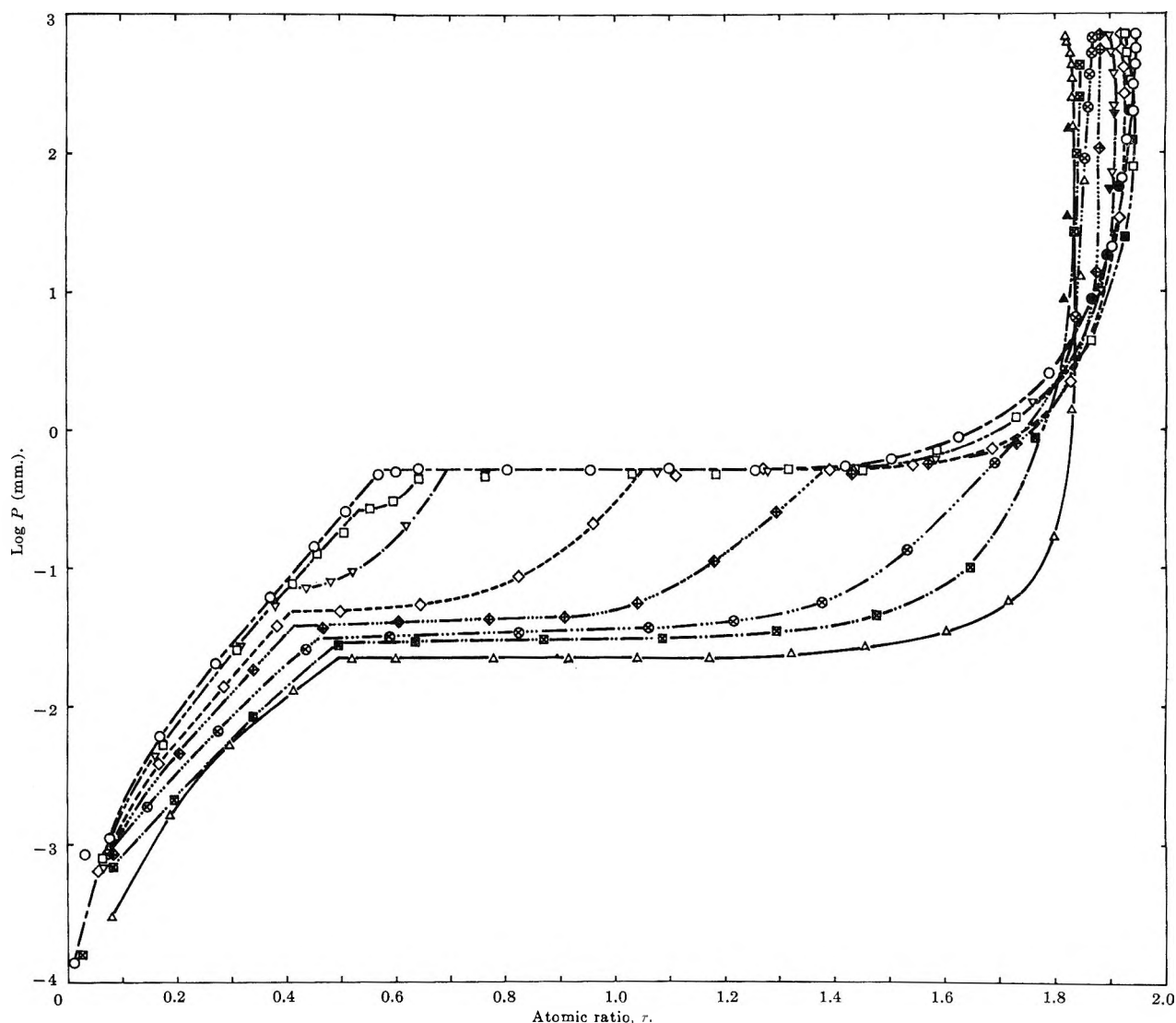


Figure 1. Isothermal data at  $700 \pm 0.7^\circ$ . Symbols indicate respective compositions:  $\circ$ , 0%;  $\square$ , 10.44%;  $\nabla$ , 20.20%;  $\diamond$ , 39.69%;  $\odot$ , 59.72%;  $\otimes$ , 79.99%;  $\boxtimes$ , 90.07%; and  $\triangle$ , 100%. Open symbols designate absorption points and solid symbols designate desorption points.

from the same supply as that used in the study of the Sc-H system.<sup>7</sup> It was prepared from  $\text{Sc}_2\text{O}_3$ , obtained from the American Scandium Corp., by reduction at the Ames Laboratory of Iowa State University. An analysis of the metal by the Ames Laboratory showed the following impurities: O, 1805 p.p.m.; N, 80 p.p.m.; H, 15 p.p.m.; Y, 0.03%; Er, <0.01%; Tm, <0.01%; Yb, <0.004%; Lu, <0.01%; Si, 80 p.p.m.; Ca, 320 p.p.m.; Fe, 180 p.p.m.; and Ta, 1000 p.p.m.

The yttrium metal used in this research was from the same supply as that used in the study of the Y-H system.<sup>6</sup> It was obtained from the Lindsay Chemical Division of American Potash and Chemical Corp. with a purity designation of 99.9%.

Scandium-yttrium alloys were prepared from weighed quantities of scandium and yttrium by arc melting four times. The multiple meltings of the alloys assured highly homogeneous "buttons." The compositions of the six alloys as determined by the initial masses of elements were 10.44, 20.20, 39.69, 59.72, 79.99, and 90.07 atomic % yttrium. Mass losses during transfers and arc meltings were no larger than 0.12% of the total sample masses. Turnings of the arc-melted "buttons" were prepared by means of a carefully cleaned lathe. The turnings were washed at least three times with reagent grade acetone and were dried under vacuum.

Gases were obtained from the Matheson Co. Ultra-



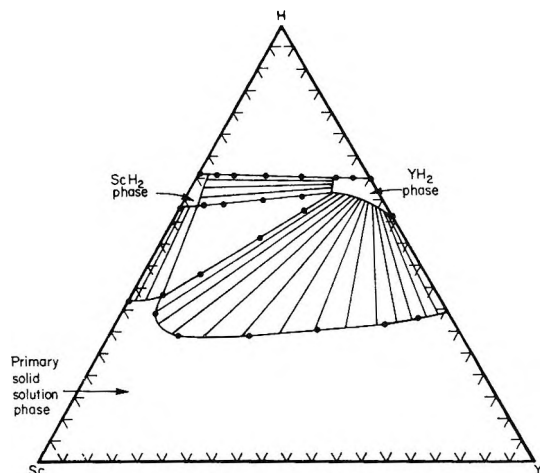


Figure 2. Sc-Y-H phase diagram at 700°. (Tie lines were not experimentally determined.)

pure grade hydrogen had a reported purity of 10 p.p.m. total impurities. Helium gas utilized in apparatus calibration had a designated purity of 99.99%. Both gases were further purified before use as described elsewhere.<sup>1,6</sup>

**Procedure.** The procedure for obtaining  $P$ - $T$ - $C$  data has been described elsewhere.<sup>1,7</sup>

**X-Ray Diffraction Analysis.** The sample of alloy containing 60 atomic % yttrium used to obtain  $P$ - $T$ - $C$  data was hydrided at 700° to a hydrogen pressure of ca. 330 mm. which corresponds approximately to the limiting hydrogen composition. The sample was cooled, ground in an agate mortar under argon, and placed in a 0.2-mm. glass capillary. The X-ray diffraction pattern was obtained with Cu  $K\alpha$  radiation using a General Electric Debye-Scherrer powder camera.

## Results

Equilibrium hydrogen pressures were measured as a function of temperature and composition variables. The composition variables are the atomic ratio of yttrium to total metal, which is constant for a given alloy, and the atomic ratio of hydrogen to total metal,  $r$ . Isothermal data at 700° are shown in Figure 1 for each alloy; *i.e.*, the former composition variable is constant for each curve. Data for the scandium-hydrogen and yttrium-hydrogen systems are also shown in Figure 1. Isothermal data were also obtained at 800 and 900° but are not presented.

The phase diagram, Figure 2, was constructed from the isothermal data shown in Figure 1. The compositions changed during each isothermal run along a line which could be drawn on the phase diagram from the

point on the Sc-Y axis representing the alloy composition to the H vertex.

The existence of a primary solid solution region extending to an  $r$  value of at least 0.4 is based on the initial rise in the isothermal curves of Figure 1. This representation is consistent with the observation of Beaudry and Daane,<sup>5</sup> who found that scandium and yttrium are completely miscible, and the observations of solid solution formation of hydrogen with yttrium<sup>6</sup> and scandium.<sup>7</sup>

From the isotherms of Figure 1, it is observed that there is a composition region for which the equilibrium hydrogen pressure is independent of the two composition variables. Gibbs' phase rule indicates that equilibrium hydrogen pressure is a function of temperature alone if four phases are present. Since one of the phases is gaseous hydrogen, one concludes that three condensed phases are in equilibrium.

For the composition region between the one and three condensed phase regions, the isotherms of Figure 1 show that the equilibrium hydrogen pressure is dependent on both composition variables. In the low composition portion of this region, the pressure is only slightly dependent on  $r$ ; in the high composition portion, the pressure is notably dependent on  $r$ . It is concluded that this composition region is a single two condensed phase region. Tie lines for this region have been sketched in Figure 2 and are consistent with the phase boundaries and the dependence of pressure on  $r$ .

The two condensed phase region between the primary solid solution region and the hydrogen-deficient scandium dihydride region was deduced on the basis of the lower boundary of the two condensed phase region of the Sc-H system.<sup>7</sup>

When sufficient hydrogen is added to hydrides whose compositions are in the three condensed phase region or the two condensed phase region of the 80 and 90 atomic % yttrium alloys, one observes that the isotherms are smooth curves. This indicates that the system passes from a three condensed phase region to a two condensed phase region or from a two condensed phase region to a single condensed phase region. The phase boundaries of the two condensed phase region between the dihydrides were drawn on this basis.

An X-ray diffraction pattern of a sample prepared in what was expected to be the two condensed phase region containing both dihydride phases was obtained. The sample was prepared from alloy containing 60 atomic % yttrium and hydrided to an  $r$  value of 1.78. Interplanar spacings were calculated and compared with spacings calculated from X-ray lattice parameters for ScH<sub>2</sub> obtained by McGuire and Kempter<sup>8</sup> and for YH<sub>2</sub> obtained by Lundin and Klodt.<sup>9</sup> It was found

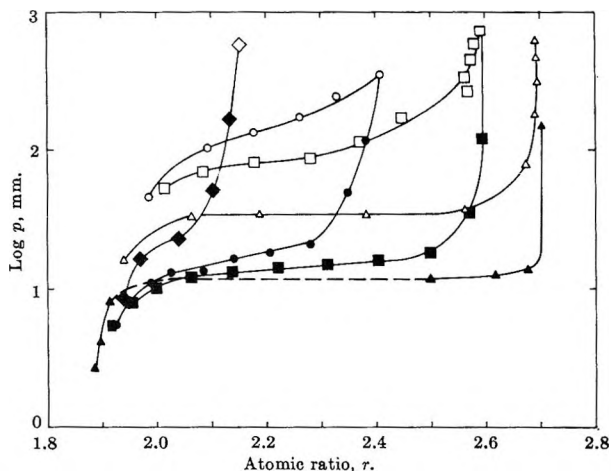


Figure 3. Isothermal data showing formation of an apparently hydrogen-deficient trihydride. Symbols are given with respective atomic per cent compositions of Y:  $\diamond$ , 59.72% at 241.0°;  $\circ$ , 79.99% at 241.6°;  $\square$ , 90.07% at 242.0°; and  $\triangle$ , 100% at 250.8°. Open symbols are absorption points; solid symbols are desorption points.

that both dihydride phases were present in the sample. The  $\text{ScH}_2$  lines yielded a face-centered-cubic lattice parameter of  $4.787 \pm 0.006 \text{ \AA}$ , compared with  $4.78315 \pm 0.00047 \text{ \AA}$ , of McGuire and Kempter.<sup>8</sup> The  $\text{YH}_2$  lines yielded a face-centered-cubic lattice parameter of  $5.110 \pm 0.006 \text{ \AA}$ , compared with the larger  $5.201\text{-\AA}$ , value of Lundin and Klodt,<sup>9</sup> which indicates that there is appreciable solution of scandium in the  $\text{YH}_2$  lattice.

An apparently hydrogen-deficient trihydride was observed in the study of the yttrium-hydrogen<sup>6</sup> system. The trihydride was found through isothermal hydrogen pressure-composition data which showed a hysteresis effect. Evidence of additional absorption of hydrogen beyond a dihydride composition was found at 242° for alloys with 90, 80, and 60 atomic % yttrium as shown in Figure 3. Hysteresis was also observed with these isothermal data.

Thermodynamic data were obtained from the hydrogen pressure data for fixed compositions in the ternary system at the three temperatures 700, 800, and 900° by a least-squares analysis applied to the equation

$$\ln p^{1/2} = \frac{\Delta \bar{H}_H}{RT} - \frac{\Delta \bar{S}_H}{R} + \frac{1}{2} \ln 760$$

The symbols  $\Delta \bar{H}_H$  and  $\Delta \bar{S}_H$  represent the relative partial molal and differential thermodynamic properties for the solid solution regions and the multi-condensed phase regions, respectively. To illustrate the fitting of the data, van't Hoff plots of the data for the 10.44 atomic % yttrium alloy are shown in Figure 4.

Thermodynamic data for the scandium-yttrium-hydrogen system are presented in Figures 5, 6, and 7.

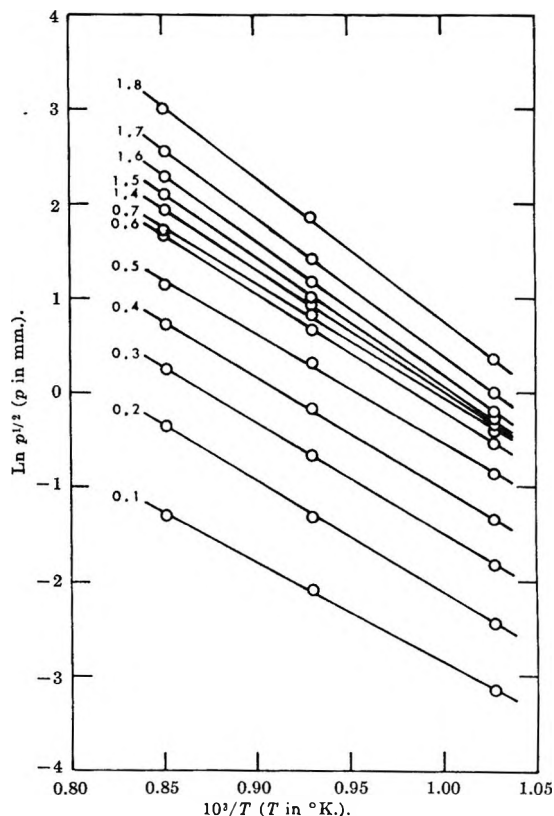


Figure 4. van't Hoff plots for 10.44 atomic % yttrium alloy. Numbers on the van't Hoff lines are  $r$  values.

In Figure 5,  $\Delta \bar{H}_H$  vs.  $r$  for 80, 90, and 100 atomic % yttrium alloys are plotted. From the phase diagram it may be seen that none of these alloys will have three condensed phases present at any hydrogen composition. In Figure 6,  $\Delta \bar{H}_H$  vs.  $r$  for 0, 10, 20, 40, and 60 atomic % yttrium alloys are plotted; all of these alloys give the three condensed phase region except the 0 atomic % yttrium alloy. In Figure 7,  $\Delta \bar{S}_H$  vs.  $r$  for scandium and yttrium are plotted; curves for the alloys are very nearly the same as those for the metals and have not been shown.

## Discussion

The first three reasons given in the Introduction for this investigation have been fulfilled in the presentation of the experimental results. The latter three reasons, namely: the possible existence of marked changes in the thermodynamic data, the ability to predict the thermodynamic data, and the ability to predict the phase diagram, will be discussed in this section.

(8) J. C. McGuire and C. P. Kempter, *J. Chem. Phys.*, **33**, 1584 (1960).

(9) C. E. Lundin and D. T. Klodt, APEX-349 (Nov. 1957); available from Office of Technical Services, Department of Commerce, Washington 25, D. C.

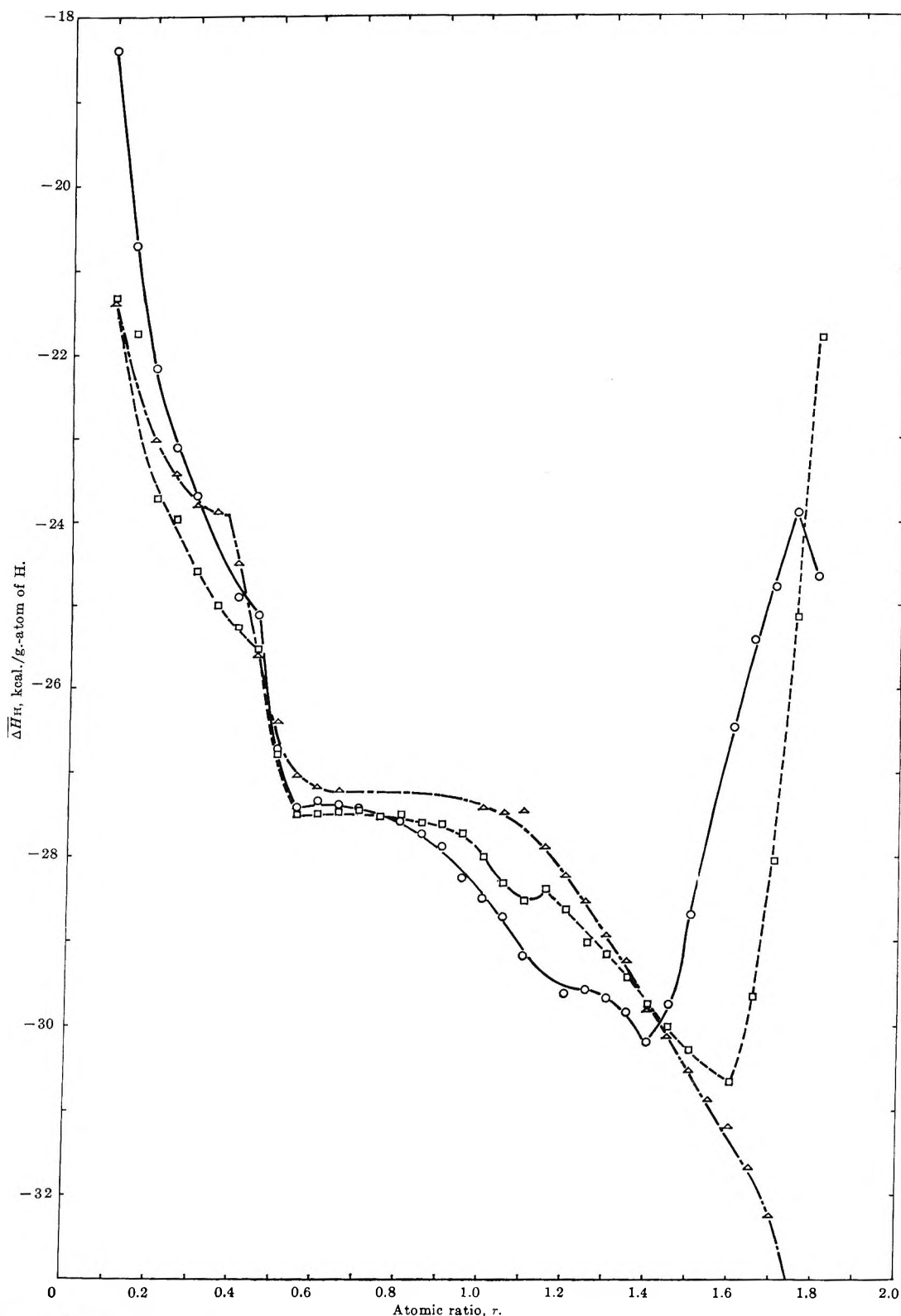


Figure 5. Plots of  $\Delta \bar{H}_H$  vs.  $r$ :  $\circ$ , 79.99 atomic % Y;  $\square$ , 90.07 atomic % Y;  $\triangle$ , 100 atomic % Y.

Marked changes in the relative partial molal enthalpy and entropy of hydrogen in the primary solid solution

region were observed in the case of the scandium-hydrogen<sup>7</sup> system and were hinted in the study of the

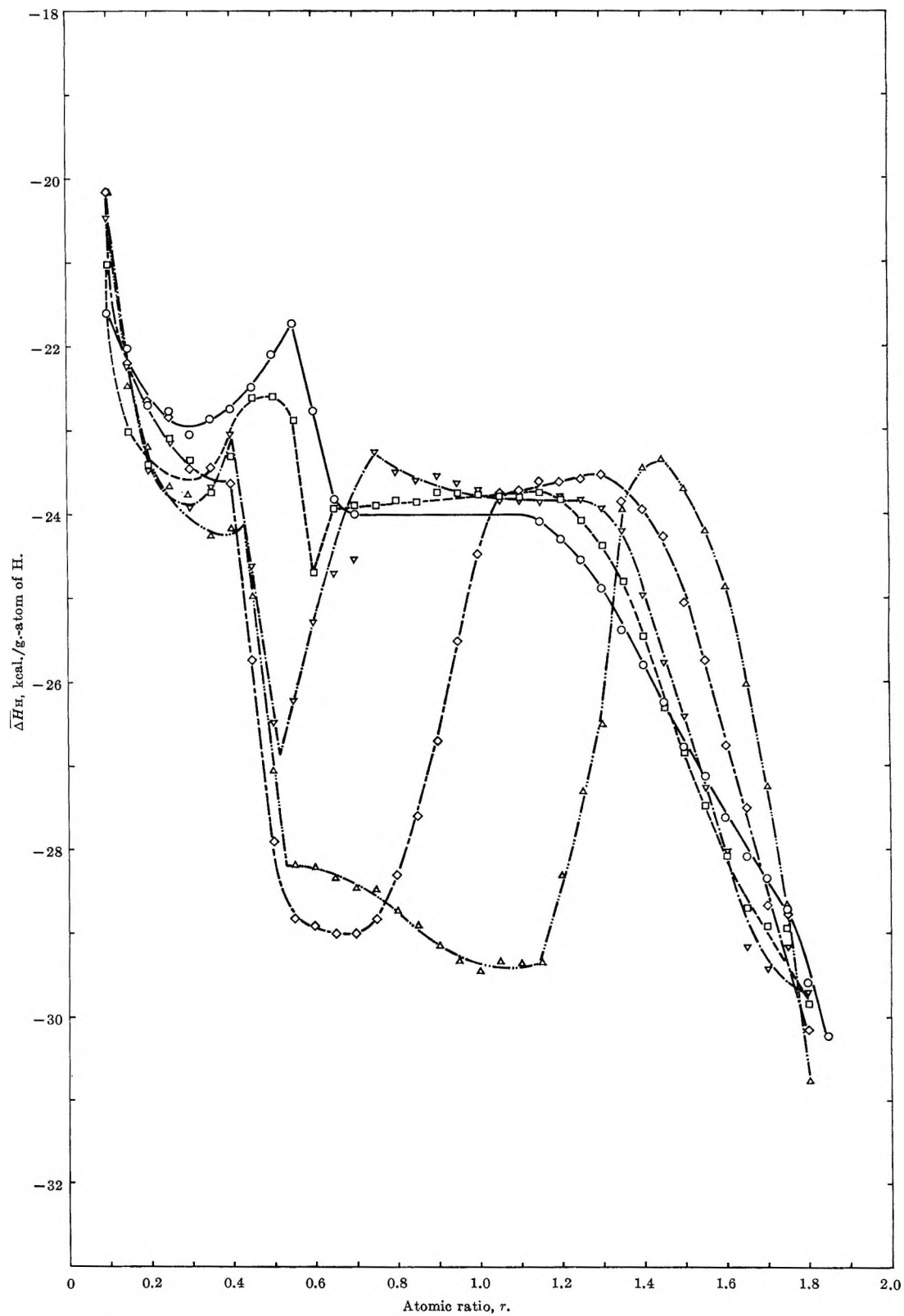


Figure 6. Plots of  $\overline{\Delta H}_H$  vs.  $r$ :  $\circ$ , 0 atomic % Y;  $\square$ , 10.44 atomic % Y;  $\nabla$ , 20.20 atomic % Y;  $\diamond$ , 39.69 atomic % Y;  $\triangle$ , 59.72 atomic % Y. For the three condensed phase region of each curve (except 0 atomic % Y), one would expect a constant value of  $\overline{\Delta H}_H$  of ca.  $-23.8$  kcal./g.-atom of H.

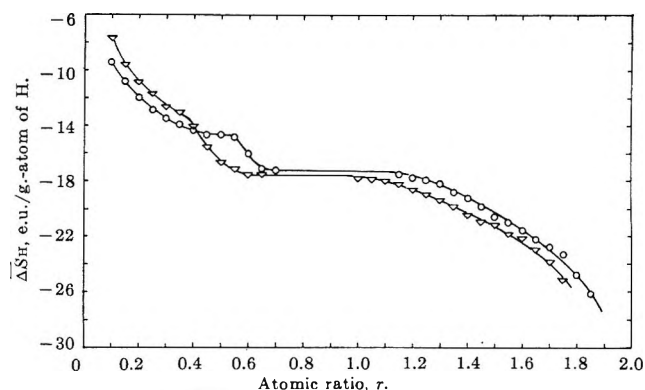


Figure 7. Plots of  $\Delta\bar{S}_H$  vs.  $\tau$  for the scandium-hydrogen system, O, and the yttrium-hydrogen system,  $\nabla$ .

yttrium-hydrogen<sup>6</sup> system. In the case of the primary solid solution region of hydrogen in scandium-yttrium alloys, one observes a trend from the actual minimum in the  $\Delta\bar{H}_H$  vs. composition plot for hydrogen in scandium-rich alloys (similar to the case of the scandium-hydrogen system) to the less noticeable change of curvature for hydrogen in yttrium-rich alloys (similar to the case of the yttrium-hydrogen system). The  $\Delta\bar{S}_H$  vs. composition plots for hydrogen in solution with scandium, yttrium, and scandium-yttrium alloys are all very similar since the hydrogen atoms enter similar sites in the metal lattice in all cases. An explanation for the marked changes in relative partial molal properties was made on the basis of Rees'<sup>10</sup> statistical mechanical model by Lieberman and Wahlbeck.<sup>7</sup> It was assumed that hydrogen atoms enter sites of the metal lattice which have the lowest energy or relative partial molal enthalpy associated with them. The successive filling of sites of differing energies produces the marked changes observed in relative partial molal enthalpies and entropies.

One is able to predict qualitatively the observed changes in relative partial molal thermodynamic properties.

For the scandium-hydrogen<sup>7</sup> and yttrium-hydrogen<sup>6</sup> systems, one finds nearly identical values for  $\Delta\bar{S}_H$  and rather small differences in  $\Delta\bar{H}_H$ . The similarity of  $\Delta\bar{S}_H$  values is a result of the hexagonal crystal structures of scandium and yttrium in the temperature range studied and indicates that the hydrogen atoms occupy similar positions in each metal. The small differences in  $\Delta\bar{H}_H$  values indicate that the hydrogen atoms are bonded more strongly for the case of yttrium than for scandium.

Only slight changes are seen in  $\Delta\bar{S}_H$  for the case of hydrogen in scandium-yttrium alloys from the case for scandium and yttrium. The differences between the  $\Delta\bar{S}_H$  values are in general less than the estimated

uncertainty of  $\pm 0.5$  e.u. This similarity in  $\Delta\bar{S}_H$  values is probably due to the structural similarities of the metals and alloys.

Observation of Figures 5 and 6 indicates that  $\Delta\bar{H}_H$  vs. composition curves for the primary solid solution region for scandium-yttrium alloys other than the 10 atomic % yttrium alloys are nearly identical with the yttrium curve within the estimated experimental error of  $\pm 500$  cal. On the basis of Rees'<sup>10</sup> statistical mechanical model, it is reasonable to assume that the hydrogen atoms prefer to occupy low energy sites near yttrium atoms rather than higher energy sites near scandium atoms. The values of  $\Delta\bar{H}_H$  in the multiphase regions are understood if one assumes that the yttrium dihydride phase is produced by addition of hydrogen to the primary solid solution since the hydrogen atoms preferentially occupy sites near yttrium atoms. After entering the multiphase regions, the values of  $\Delta\bar{H}_H$  initially correspond well with  $\Delta H$  for the two condensed phase region of the yttrium-hydrogen system. For scandium-yttrium alloy samples with 10, 20, 40, and 60 atomic % yttrium, when three condensed phases are present,  $\Delta\bar{H}_H$  corresponds closely with  $\Delta H$  for the two condensed phase region of the scandium-hydrogen system. One may explain these observations by assuming that the yttrium atoms are removed from the primary solid solution by formation of the yttrium dihydride phase; a solid solution of hydrogen in primarily scandium remains which gives results similar to those of the scandium-hydrogen system.

The phase relationships for the scandium-yttrium-hydrogen system are summarized with the phase diagram, Figure 2.

A solid solution of hydrogen dissolved in the metals and alloys at all alloy compositions is shown on the phase diagram. This is an expected consequence of the solid solution of hydrogen in both scandium and yttrium and the complete miscibility of the metals in each other.

The phase diagram leads one to conclude that there is limited miscibility of the metal dihydrides in each other. The limited miscibility was confirmed by X-ray diffraction analysis. One would expect the miscibility of the dihydrides to be dependent on their crystal structures. The structure of  $YH_2$  has been determined by Lundin and Klodt<sup>9</sup> as being face-centered cubic with a lattice parameter of 5.201 Å. The structure of  $ScH_2$  has been determined by McGuire and Kempter<sup>8</sup> to be face-centered cubic with a lattice parameter of  $4.78315 \pm 0.00047$  Å. The ratio of lattice parameters of  $YH_2$

(10) A. L. G. Rees, *Trans. Faraday Soc.*, **50**, 335 (1954).

to  $\text{ScH}_2$  is 1.087, which is very similar to the ratio of hexagonal lattice parameters of Y to Sc of 1.102 and 1.088 for  $a$  and  $c$ , respectively, based on the data of Spedding and Daane.<sup>11</sup> On the basis of complete miscibility of Sc and Y, one might suspect that  $\text{ScH}_2$  and  $\text{YH}_2$  would also be miscible. Beaudry and Daane<sup>5</sup> pointed out that yttrium and scandium atoms are sufficiently different in size that the modified Darken-Gurry plot of Gschneidner<sup>12</sup> showed that complete miscibility of scandium and yttrium would be questionable. Partial immiscibility of the dihydrides would be considered a possibility due to the difference in lattice parameters even though Sc and Y show complete miscibility. The yttrium dihydride phase exhibits a greater solubility for scandium atoms than the scandium dihydride phase does for yttrium atoms. This can be explained by recalling that yttrium atoms are larger than scandium atoms; fewer yttrium atoms are permitted in the scandium dihydride lattice than scandium atoms in the yttrium dihydride lattice before a new phase appears.

The greater stability of the yttrium dihydride phase over the scandium dihydride phase as revealed either through equilibrium hydrogen pressure measurements or through  $\Delta\bar{H}_H$  values enables one to predict that the yttrium dihydride phase would be in equilibrium with the primary solid solution region as the system initially enters the multiphase regions.

On the bases of the miscibility of the two metals, the partial immiscibility of the dihydrides, and the thermodynamic properties of the two metal-hydrogen sys-

tems, one would have been able to predict qualitatively the phase diagram for the scandium-yttrium-hydrogen system. An *a priori* prediction was not possible because data concerning the immiscibility of the dihydrides were not available.

The yttrium-hydrogen<sup>6</sup> system exhibits an apparently hydrogen-deficient trihydride phase, but no trihydride phase has yet been observed for the scandium-hydrogen system.<sup>7,8,13</sup> Pressure-temperature-composition data between the yttrium dihydride and trihydride phases exhibit a hysteresis effect. One also finds evidence for formation of a phase with hydrogen concentrations greater than the dihydride in the cases of alloys containing 90, 80, and 60 atomic % yttrium. As more scandium is added to the alloy, less hydrogen can be added to the alloy beyond the apparent dihydride. The hysteresis effect is observed also in the case of the alloys.

*Acknowledgments.* The authors gratefully acknowledge the financial support of this work by the U. S. Atomic Energy Commission under Contract No. AT (11-1)-1029. The authors wish to thank Mr. Larry Kane of the IIT Research Institute for preparation of the alloys by arc melting.

(11) F. H. Spedding and A. H. Daane, "The Rare Earths," John Wiley and Sons, Inc., New York, N. Y., 1961.

(12) K. A. Gschneidner, Jr., "Rare Earth Alloys," D. Van Nostrand Co., Inc., Princeton, N. J., 1961.

(13) J. C. Warf and K. Hardcastle, Office of Naval Research Reports 1 and 2, Contract No. 228 (15), Project No. NR-052-390.

## Studies of Membrane Phenomena. I. Membrane Potential

by Yonosuke Kobatake, Noriaki Takeguchi, Yoshinori Toyoshima, and Hiroshi Fujita

Department of Polymer Science, Osaka University, Osaka, Japan (Received June 14, 1965)

An equation is derived, on the basis of the thermodynamics of irreversible processes, for the electric potential,  $\Delta\varphi$ , which arises between two solutions of a uni-univalent electrolyte of different concentrations  $C_1$  and  $C_2$  that are separated by an (negatively) ionizable membrane. The most crucial in its derivation is to assume that the activities,  $a_+$  and  $a_-$ , of ions in the membrane are represented by  $a_+ = C_-$  and  $a_- = C_+$ , where  $C_-$  is the concentration of the negative ion species. An implication of this assumption is discussed at some length. The equation so obtained for  $\Delta\varphi$  is substantially the same as the previous one of Kobatake. It contains three parameters to be evaluated from experiment. Methods for this purpose are described which utilize limiting behaviors of observed  $\Delta\varphi$  at very high and low  $C_2$  for a fixed ratio of concentrations  $C_2/C_1$ . To check the theory, data are obtained with oxidized collodion membranes in aqueous NaCl, KCl, KI, KNO<sub>3</sub>, and HCl. It is demonstrated that these new data as well as typical ones of previous workers are fitted quite accurately by the equation derived. No such agreement with experiment is obtained in terms of the earlier theory of Teorell and of Meyer and Sievers, which corresponds to the case in which intramembrane ions behave ideally, *i.e.*,  $a_+ = C_+$  and  $a_- = C_-$ .

### Introduction

A steady electromotive force (e.m.f.) arises between solutions of an electrolyte of different concentrations at constant temperature and pressure when they are separated by a uniform membrane that contains fixed ionizable groups. This e.m.f., usually called the membrane potential, has been the subject of many theoretical and experimental studies,<sup>1-3</sup> but it appears that no satisfactory theory has as yet been established. Various membrane phenomena have been successfully correlated in a quantitative manner by the thermodynamics of irreversible processes.<sup>4-7</sup> This type of treatment, however, does not provide information about the actual mechanism which produces observed membrane potentials. The earlier theory of Teorell<sup>8</sup> and of Meyer and Sievers<sup>9</sup> (the T.M.S. theory) and its various refinements,<sup>4,5</sup> which all had been based on a fixed charge membrane model, were criticized recently by Hills,<sup>10</sup> who showed that these theories are inadequate to explain experimental results on membranes in which there is an incomplete ionic selectivity. Kobatake<sup>11</sup> integrated flow equations provided by the thermodynamics of irreversible processes to derive an equation for the membrane potential and found that the de-

rived equation agreed quite satisfactorily with typical experimental data available. However, in order to make the analytical integration possible he had to introduce an important assumption between the derivatives of the activities for the positive and negative ion species in the membrane. Furthermore, he used a capillary model for the membrane.

- (1) H. T. Clarke, Ed., "Ion Transport across Membranes," Academic Press, New York, N. Y., 1954.
- (2) "Membrane Phenomena," a General Discussion of the Faraday Society, University Press Ltd., Aberdeen, 1956.
- (3) R. Schlögl, "Stofftransport durch Membranen," D. Steinkopff Verlag, Darmstadt, 1964.
- (4) J. Staverman, *Trans. Faraday Soc.*, **48**, 176 (1952).
- (5) G. Scatchard, *J. Am. Chem. Soc.*, **75**, 2883 (1953); *Discussions Faraday Soc.*, **21**, 30 (1956).
- (6) K. S. Spiegler, *Trans. Faraday Soc.*, **54**, 1408 (1958).
- (7) J. G. Kirkwood in "Ion Transport across Membranes," Academic Press, New York, N. Y., 1954, p. 119.
- (8) T. Teorell, *Proc. Soc. Exptl. Biol.*, **33**, 282 (1935); *Prog. Biophys. Biophys. Chem.*, **3**, 305 (1953); *Z. Elektrochem.*, **55**, 460 (1951).
- (9) K. H. Meyer and J. F. Sievers, *Helv. Chim. Acta*, **19**, 649, 665, 987 (1936).
- (10) G. J. Hills, P. W. M. Jacobs, and N. Lakshminarayanaiah, *Proc. Roy. Soc. (London)*, **A262**, 246, 257 (1961); N. Lakshminarayanaiah, *J. Polymer Sci.*, **A2**, 4491 (1964).
- (11) Y. Kobatake, *J. Chem. Phys.*, **28**, 146, 442 (1958); *Progr. Theor. Phys., Suppl.*, **10**, 226 (1959).

In the present paper, we first describe a somewhat improved derivation of Kobatake's equation for the membrane potential. Here we have no recourse to the capillary model and discuss at some length the implication of the assumption that was basic to the treatment of Kobatake.<sup>11</sup> Second, we present membrane potential data which we have redetermined with oxidized collodion membranes in five uni-univalent electrolytes covering wide ranges of concentration and show that these new data as well as typical ones of previous investigators are fitted accurately by the equation derived.

### Theory

**Basic Equations.** The system considered is composed of an ionizable membrane of uniform thickness which separates two bulk solutions of a *uni-univalent* electrolyte of concentrations  $C_1$  and  $C_2$ . For convenience, we set  $C_1 < C_2$ . It is assumed that the system is isothermal and no pressure head is applied across the membrane. The ionizable groups are fixed on the polymer network which constitutes the given membrane and hence do not appear as the component in the flow equations.

The flows of ions and water molecules occur in the direction of membrane thickness. We take the space coordinate  $x$  in this direction, its origin being placed on the membrane surface which is in contact with the solution of concentration  $C_1$ . The value of  $x$  for the other membrane surface is denoted by  $L$ . Starting with the basic flow equations provided by the thermodynamics of irreversible processes,<sup>12</sup> we may derive the following equations for the flux of the electrolyte component  $(J_s)_e$  and the electric current density  $(I)_e$ , both relative to the frame of reference fixed to the membrane, when the system is in the steady state.

$$(J_s)_e = -(l_+C_+ - l_-C_-) \frac{d\varphi}{dx} - \frac{RT}{F} \left( l_+C_+ \frac{d \ln a_+}{dx} + l_-C_- \frac{d \ln a_-}{dx} \right) + (C_+ + C_-)U_m \quad (1)$$

$$(I)_e = -F(l_+C_+ + l_-C_-) \frac{d\varphi}{dx} - RT \left( l_+C_+ \frac{d \ln a_+}{dx} - l_-C_- \frac{d \ln a_-}{dx} \right) + F(C_+ - C_-)U_m \quad (2)$$

Here  $\varphi$  is the electric potential,  $C_+$  and  $C_-$  are concentrations of positive and negative ions in moles per cubic centimeter of solution,  $a_+$  and  $a_-$  are activities of positive and negative ions in moles per cubic centimeter of solution,  $l_+$  and  $l_-$  are molar mobilities of positive and negative ions defined in terms of the *mass-fixed* frame of

reference,  $U_m$  is the velocity of the local center of mass,  $R$  is the molar gas constant,  $T$  is the absolute temperature of the system, and  $F$  is the Faraday constant.

The evaluation of  $U_m$  is a formidably difficult problem. To solve this, the hydrodynamic equation which governs the viscous flow of an electrolyte solution through a complex polymer network must be derived and then integrated. Here we have recourse to a crude approximation, since the last term on the right-hand side of eq. 2 gives rise to only a small correction for the membrane potential, as will be seen below. We represent the viscous force acting on 1 cc. of solution in the membrane by  $-(1/k)U_m$ , where  $k$  is a constant which is considered to depend on the viscosity of the solution and the structural details of the polymer network of which the membrane is composed. The same volume of solution undergoes an electric force which is represented by  $-F(C_+ - C_-)(d\varphi/dx)$ . In the steady state, the sum of these two forces is zero, so that we have

$$U_m = -kF(C_+ - C_-)(d\varphi/dx) \quad (3)$$

For convenience, we consider a membrane which is ionized negatively with a charge density  $\theta$  (in moles/cc.). Then the requirement that the electric neutrality must be realized in any element of the membrane gives the relation

$$C_+ - C_- = \theta \quad (4)$$

Since in the system considered here no electric field is applied externally across the membrane, no net electric charge is transported from one side of the membrane to the other. This means that  $(I)_e$  must be zero at a cross section of the membrane. Substituting eq. 3 and 4 into eq. 2, putting  $(I)_e$  equal to zero, and solving for  $d\varphi/dx$ , we obtain

$$\frac{d\varphi}{dx} = -\left(\frac{RT}{F}\right) \times \frac{l_+(C_- + \theta)(d \ln a_+/dx) - l_-C_-(d \ln a_-/dx)}{(l_+ + l_-)C_- + l_+\theta + kF\theta^2} \quad (5)$$

To proceed further, the activities  $a_+$  and  $a_-$  must be known as functions of  $C_-$ .

**Assumptions for  $a_+$  and  $a_-$ .** It is one of the unsolved problems in the field of polyelectrolyte study to derive exact theoretical expressions for the activities of small ions in polyelectrolyte solutions. It is therefore understandable that Kobatake<sup>11</sup> had to assume

(12) H. J. V. Tyrrell, "Diffusion and Heat Flow in Liquids," Butterworth and Co. Ltd., London, 1961, p. 54; D. D. Fitts, "Nonequilibrium Thermodynamics," McGraw-Hill Book Co., Inc., New York, N. Y., 1962, p. 74.



rather intuitively an unjustified relation between  $a_+$  and  $a_-$ . His assumption is equivalent to setting such that

$$a_+ = C_-; a_- = C_+ \quad (6)$$

or

$$\gamma_+ = C_-/(C_- + \theta); \gamma_- = 1 \quad (7)$$

where  $\gamma_+$  and  $\gamma_-$  are the activity coefficients of positive and negative ions in the membrane. Although at present no theoretical justification exists for this arbitrary choice of the forms of  $a_+$  and  $a_-$ , an interesting result is obtained when it is applied to the membrane equilibrium problem.

Consider a negatively ionizable polyelectrolyte gel or membrane immersed in a solution of a uni-univalent simple electrolyte. At equilibrium the following relation must be obeyed

$$(C_0)^2 = (a_+)_i(a_-)_i \quad (8)$$

where  $(C_0)$  is the equilibrium concentration of the electrolyte (in moles/cc.) in the outer solution and  $(a_+)_i$  and  $(a_-)_i$  are the activities of positive and negative ions in the gel phase. It has been assumed that the outer electrolyte solution behaves ideally; this assumption is not unreasonable in the treatment of polyelectrolytes and may be taken out if desired. When the forms of  $a_+$  and  $a_-$  assumed above are valid, it follows from eq. 8 that

$$(C_-)_i = (C_0) \quad (9)$$

Thus the concentrations of the negative ion species in the two phases become identical. This result is not obtained when the ideal Donnan equilibrium is established between the phases. In this case, the concentration of negative ions in the gel phase,  $(C_-)_i$ , is always lower than that in the outer solution,  $(C_0)$ . In passing, we note that the ideal Donnan equilibrium corresponds to the case in which  $(\gamma_+)_i = (\gamma_-)_i = 1$ .

Applying eq. 7 to eq. 8 and using eq. 9, we obtain the relation

$$(C_0)^2/(C_+)_i(C_-)_i = (C_0)/[(C_0) + \theta] \quad (10)$$

We have found that this simple relation fits well typical data of previous workers, notably, Nagasawa, *et al.*,<sup>13</sup> Hills, *et al.*,<sup>10</sup> and Gregor, *et al.*,<sup>14</sup> who determined the concentrations  $(C_+)_i$  and  $(C_-)_i$  in ion-exchange resins or membranes equilibrated with simple electrolyte solutions of given concentrations  $(C_0)$ . Recently, Katchalsky, *et al.*,<sup>15</sup> have pointed out this similar fact. They also have demonstrated that equilibrium ion distributions between solutions of polyelectrolyte and simple salt separated by a semipermeable mem-

brane can be represented remarkably well by eq. 10, unless the polyelectrolyte concentration is too low. This interesting consequence from the assumptions  $a_+ = C_-$  and  $a_- = C_+$  suggests that the assumed forms for the activities of small ions in polyelectrolyte gels or membranes may have a broad applicability. Presumably, they may be a much better approximation to the actual state in polyelectrolyte solutions or gels than the assumption of thermodynamic ideality, *i.e.*,  $a_+ = C_+$  and  $a_- = C_-$ , which, as has been noted above, leads to the ideal Donnan distribution. However, it must be remembered that the agreement of eq. 10 with experiment does not always support the correctness of the underlying assumptions, eq. 6. The final justification is left for a theoretical study. For the time being, it would be most relevant to regard eq. 6 as a kind of working hypothesis and check with experiment the various consequences which would be obtained if this hypothesis were valid. In what follows we proceed along this line of thought.

*Equation for Membrane Potential.* With eq. 6 assumed for  $a_+$  and  $a_-$ , eq. 5 becomes

$$\frac{d\varphi}{dx} = -\left(\frac{RT}{F}\right) \frac{(l_+ - l_-)C_- + l_+\theta}{[(l_+ + l_-)C_- + l_+\theta + kF\theta^2]C_-} \frac{dC_-}{dx} \quad (11)$$

When the bulk solutions on both sides of the membrane are vigorously stirred, no potential gradient is set up in them, so that the desired membrane potential  $\Delta\varphi$  is obtained by integrating  $d\varphi/dx$  over the thickness of the membrane. Thus we have

$$\Delta\varphi = -\left(\frac{RT}{F}\right) \int_0^L \times \frac{(l_+ - l_-)C_- + l_+\theta}{[(l_+ + l_-)C_- + l_+\theta + kF\theta^2]C_-} \frac{dC_-}{dx} dx \quad (12)$$

The flows of ions and water molecules in the membrane are sufficiently slow so that it is not unreasonable to assume that at the boundaries between the membrane and the outer electrolyte solutions thermodynamic equilibria are established. Then eq. 9 holds at either membrane surface, and we have  $C_- = C_1$  at  $x = 0$  and  $C_- = C_2$  at  $x = L$  as the boundary conditions for  $C_-$  that are consistent with eq. 12. Performing the

(13) K. Kanamaru, M. Nagasawa, and K. Nakamura, *Kogyo Kagaku Zasshi*, **56**, 436 (1953); M. Nagasawa and I. Kagawa, *Discussions Faraday Soc.*, **21**, 52 (1956).

(14) H. P. Gregor, F. Gutoff, and J. I. Bregman, *J. Colloid Sci.*, **6**, 245 (1951); B. R. Sundheim, M. H. Waxman, and H. P. Gregor, *J. Phys. Chem.*, **57**, 974 (1953).

(15) A. Katchalsky, Z. Alexandrowicz, and O. Kedem, personal communication.

integration on the right-hand side of eq. 12 with these conditions into account, there results the final expression for the membrane potential

$$\Delta\varphi = -\left(\frac{RT}{F}\right)\left[\frac{1}{\beta}\ln\frac{C_2}{C_1} - \left(1 + \frac{1}{\beta} - 2\alpha\right)\ln\left(\frac{C_2 + \alpha\beta\theta}{C_1 + \alpha\beta\theta}\right)\right] \quad (13)$$

where

$$\alpha = l_+/l_+ + l_- \quad (14)$$

$$\beta = 1 + (kF\theta/l_+) \quad (15)$$

and these parameters have been assumed to be independent of salt concentration.

*Limiting Forms of Eq. 13.* As will be shown below, we have compared eq. 13 with the data from a series of measurements in which values of  $\Delta\varphi$  on a given membrane-electrolyte system were determined as a function of  $C_2$  with the concentration ratio  $\gamma = C_2/C_1$  ( $>1$ ) being fixed at a given value. We derive two limiting forms of eq. 13 useful for the analysis of this type of experimental data. (a) When  $C_2$  becomes sufficiently small with  $\gamma$  fixed, eq. 13 may be expanded to give

$$|\Delta\varphi_r| = \frac{1}{\beta}\ln\gamma - \frac{(\gamma - 1)}{\alpha\beta\gamma} \times \left(1 + \frac{1}{\beta} - 2\alpha\right)\left(\frac{C_2}{\theta}\right) + 0\left[\left(\frac{C_2}{\theta}\right)^2\right] \quad (16)$$

where  $|\Delta\varphi_r|$  is the absolute value of a reduced membrane potential defined by

$$\Delta\varphi_r = F\Delta\varphi/RT \quad (17)$$

Equation 16 indicates that the value of  $\beta$  and a relation between  $\alpha$  and  $\theta$  may be obtained by evaluating the intercept and the initial slope of a plot for  $|\Delta\varphi_r|$  against  $C_2$  obtained with  $\gamma$  fixed. (b) It is well known experimentally that at a fixed  $\gamma$  the inverse of an apparent transference number  $t_-$  for the co-ion species in a negatively charged membrane is proportional to the inverse of the concentration  $C_2$  in the region of high salt concentration. Here  $t_-$  is defined by the relation

$$|\Delta\varphi_r| = (1 - 2t_-)\ln\gamma \quad (18)$$

Substituting for  $\Delta\varphi$  from eq. 13 and expanding the resulting expression for  $1/t_-$  in powers of  $1/C_2$  gives

$$\frac{1}{t_-} = \frac{1}{(1 - \alpha)} + \frac{(1 + \beta - 2\alpha\beta)(\gamma - 1)\alpha\left(\frac{\theta}{C_2}\right) + 0\left[\left(\frac{\theta}{C_2}\right)^2\right]}{2(1 - \alpha)^2\ln\gamma} \quad (19)$$

which has the form expected from experimental information. Equation 19 indicates that the intercept for a plot of  $1/t_-$  against  $1/C_2$  at a fixed  $\gamma$  allows the value of  $\alpha$  to be determined. If this value of  $\alpha$  is inserted in the relation obtained from the initial slope for  $|\Delta\varphi_r|$  vs.  $C_2$ , the desired value for  $\theta$  can be determined. Once  $\alpha$  and  $\beta$  are known in the manner described above, the  $\theta$  may also be evaluated from the initial slope for  $1/t_-$  vs.  $1/C_2$ . Providing our membrane potential equation is correct, the two values of  $\theta$  obtained in this way from the opposite limits should agree with one another.

*Expression for  $(J_s)_c$ .* It is a simple matter to eliminate  $d\varphi/dx$  from eq. 1 and 2, using  $(I)_c = 0$  and eq. 3 for  $U_m$ . The resulting expression for  $(J_s)_c$  can be put in a form which contains only  $C_-$  as variable, by making use of the neutrality condition, eq. 4, and the assumptions for  $a_+$  and  $a_-$  made in eq. 6. By integration from  $x = 0$  to  $x = L$  of the equation so obtained for  $(J_s)_c$  we obtain the following expression for the steady-state flux of the electrolyte component

$$(J_s)_c = \left(\frac{D_0}{L}\right)\left[1 - \frac{(\beta - 1)(2\alpha - 1)}{2(1 - \alpha)}\right] \times \left[(C_2 - C_1) + (1 - \alpha\beta)\theta\ln\left(\frac{C_1 + \alpha\beta\theta}{C_2 + \alpha\beta\theta}\right)\right] \quad (20)$$

where  $D_0$  is the diffusion coefficient of the electrolyte component defined by

$$D_0 = \frac{2RT}{F}\left(\frac{l_+l_-}{l_+ + l_-}\right) \quad (21)$$

Experimental tests of eq. 20 will be reported in a forthcoming paper of this series.

### Experimental Section

Oxidized collodion membranes, which are negatively ionizable in aqueous media, were prepared according to the method reported by Sollner,<sup>16</sup> and those which had been found appropriate by preliminary experiments were chosen for the measurements. Except in the measurements with HCl, a given membrane was repeatedly used for different electrolytes, but no significant change occurred in measured e.m.f. when the experimental conditions were identical. Five uni-univalent electrolytes were examined, which were NaCl, KCl, KI, KNO<sub>3</sub>, and HCl. Before use, NaCl, KCl, and KNO<sub>3</sub> were purified by repeated recrystallization. Both KI and HCl of analytical grade were used as de-

(16) K. Sollner and H. P. Gregor, *J. Phys. Chem.*, **50**, 470 (1946); **51**, 299 (1947); *J. Phys. Colloid Chem.*, **54**, 325, 330 (1950); K. Sollner, *Ann. N. Y. Acad. Sci.*, **57**, 177 (1953); "Ion Transport across Membranes," Academic Press, New York, N. Y., 1954, p. 144.

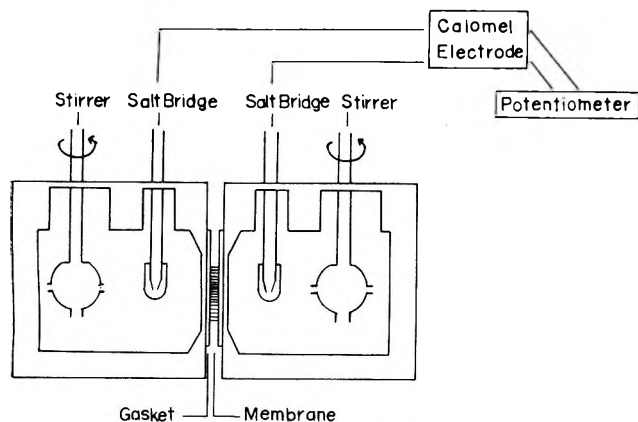


Figure 1. Schematic diagram of the cell used for the measurement of membrane potentials.

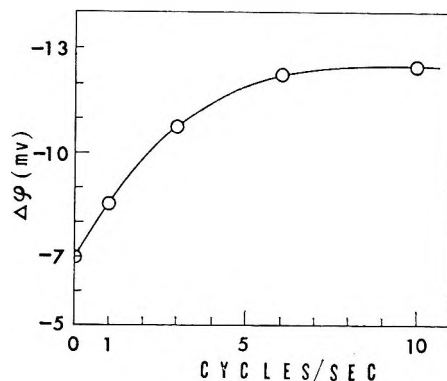


Figure 2. Effect of the rate of stirring on membrane potential.

livered. The water used as solvent was prepared by treating distilled water with both cation and anion exchangers. Carbon dioxide dissolved in it was not degassed.

Figure 1 shows a schematic diagram of the apparatus used for measuring membrane potentials. The e.m.f. which arose between the bulk solutions was conducted by saturated KCl bridges and calomel electrodes and measured by a vibrating reed electrometer (Takeda Riken Co. TR-84 B Type) or by an electronic potentiometer of a Du Bridge type. The caps of the salt bridges were carefully ground so that the test solutions might not be contaminated due to leakage of KCl. Since we have no definite information about the liquid junction potential between the salt bridge and the electrolyte solution, the measured e.m.f. were not corrected for this potential. The bulk solutions were stirred by a pair of plastic fans at a speed of 33 c.p.s. As illustrated in Figure 2, the measured potential became independent of stirrer speed when it was

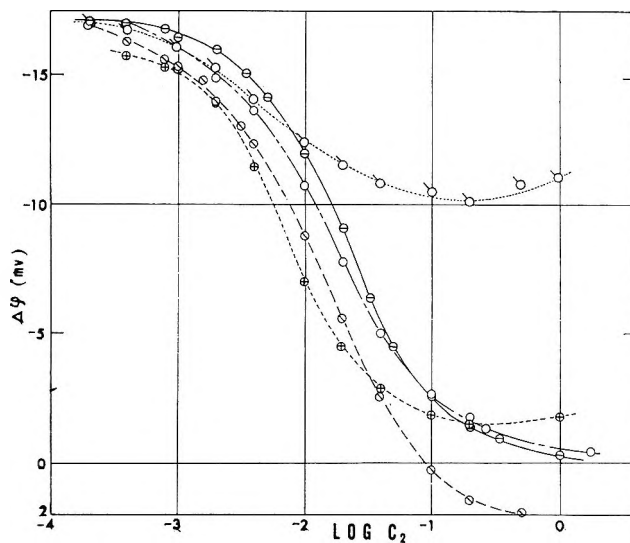


Figure 3. Typical data of the membrane potential as a function of  $\log C_2$  at constant  $\gamma (= C_2/C_1 = 2)$ :  $\ominus$ , KCl;  $\circ$ , KI with membrane 2;  $\odot$ , NaCl;  $\odot$ , HCl with membrane 3;  $\oplus$ ,  $\text{KNO}_3$  with membrane 4.

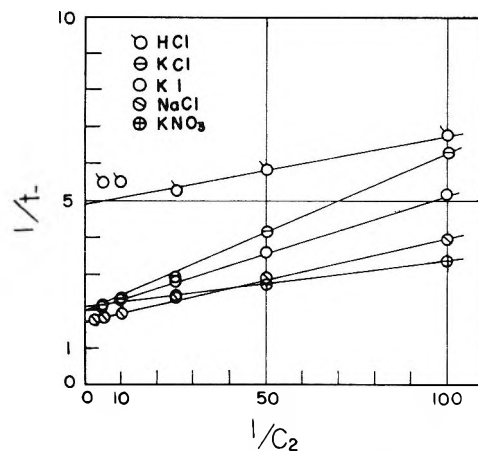


Figure 4.  $1/t$  vs.  $1/C_2$  plots for various electrolytes at  $\gamma = 2$ . Notations and membranes are the same as in Figure 3.

faster than about 10 c.p.s. On each system five determinations of e.m.f. were made. The results agreed within 0.2 mv. and their average was taken as the desired result. All measurements were made in an air oven at  $25^\circ$ .

For a given membrane-electrolyte system the data were taken as a function of  $C_2$  with the concentration ratio  $\gamma (= C_2/C_1)$  fixed to desired values. The values of  $\gamma$  studied were  $1 + \epsilon$  ( $\epsilon \ll 1$ ), 1.5, 2, 3, 5, 7, and 10.

## Results

By way of an example, the e.m.f. data obtained at  $\gamma = 2$  are plotted in Figure 3. The results at other values of  $\gamma$  were essentially similar to this graph.<sup>17</sup>

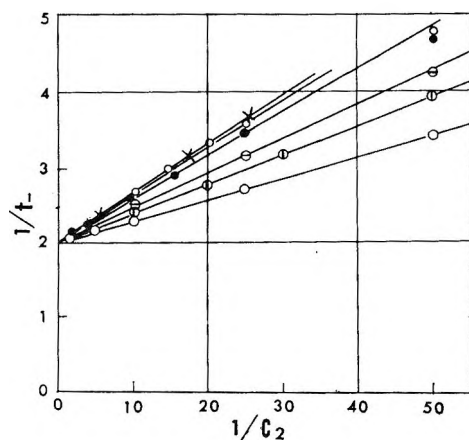


Figure 5.  $1/t_-$  vs.  $1/C_2$  plots at various  $\gamma$  on the system membrane 1-KCl: O,  $\gamma = 1.5$ ;  $\odot$ ,  $\gamma = 2$ ;  $\ominus$ ,  $\gamma = 3$ ;  $\bullet$ ,  $\gamma = 5$ ;  $\circ$ ,  $\gamma = 7$ ; and  $\times$ ,  $\gamma = 10$ .

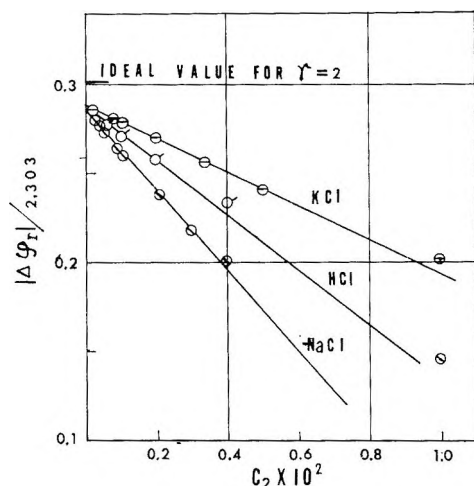


Figure 6.  $|\Delta\varphi_r|$  vs.  $C_2$  plots for KCl, NaCl, and HCl at  $\gamma = 2$ . Notations and membranes are the same as in Figure 3.

Figure 4 shows plots for  $1/t_-$  against  $1/C_2$  at  $\gamma = 2$  for five electrolytes, and Figure 5 the corresponding plots at various values of  $\gamma$  for KCl. The data of Figure 5 refer to an identical membrane. The intercepts and slopes of the straight lines indicated in these figures have been used to evaluate the parameters  $\alpha$ ,  $\beta$ , and  $\theta$ .

Figure 6 illustrates plots for  $|\Delta\varphi_r|$  against  $C_2$  in the region of very low concentration that were determined for three electrolytes at  $\gamma = 2$ . It can be seen that these plots converge, at the limit of zero concentration, to intercepts which are several per cent lower than the value (indicated by a short horizontal segment in the figure) corresponding to the ideal potential for this  $\gamma$ . Here by the ideal potential is meant a membrane potential which would be obtained if very

dilute solutions of an electrolyte of different concentrations were separated by a membrane perfectly impermeable to both positive and negative ions. It is given by  $(RT/F) \ln (C_2/C_1)$ , where  $C_1$  and  $C_2$  are the concentrations on both sides of the membrane. According to the membrane potential equation we derived, the result that the observed potentials do not tend to this limiting value at  $C_2 = 0$  can be ascribed to the fact that the parameter  $\beta$  is not equal to but slightly larger than unity, *i.e.*,  $kF\theta/l_+$  is slightly positive. This means that the mass flow does have a small but nonnegligible effect on the membrane potential.

The values of the parameters  $\alpha$ ,  $\beta$ , and  $\theta$  that have been determined, in the manner described above, from the intercepts and the initial slopes of plots for  $|\Delta\varphi_r|$  vs.  $C_2$  at low concentrations and of those for  $1/t_-$  vs.  $1/C_2$  at high concentrations are listed in Tables I and II. Substantially the same values have been obtained for  $\theta$  from the analyses at the limits of low and high concentrations. The values given in these tables refer to the high concentration limit. Table I shows that for a given membrane-electrolyte system the values of  $\alpha$ ,  $\beta$ , and  $\theta$  are essentially independent of  $\gamma$ , although there is observed such a trend that  $\theta$  decreases systematically in the region of  $\gamma$  larger than 5. The reason for this trend is not as yet clear to us. Table II summarizes the results obtained for various membrane-electrolyte pairs at  $\gamma = 2$ . The  $\alpha_{\text{bulk}}$  in the table refers to the ionic mobilities in free solutions (at infinite dilution).<sup>18</sup> The indicated agreements between  $\alpha$  and  $\alpha_{\text{bulk}}$  are rather surprising, since it can hardly be believed that the mobility of a given ion is the same in a charged membrane and in a bulk solution. However, this result is understandable if Walden's rule holds in these two media; note that  $\alpha$  depends on the ratio of  $l_+$  and  $l_-$  only. The data on KCl given in

Table I: Values of Parameters  $\alpha$ ,  $\beta$ , and  $\theta$  for a Membrane (No. 1)-KCl at Various  $\gamma$

$\gamma (= C_2/C_1)$	$\alpha$	$\beta$	$\theta$
1	0.5	1.04	0.019
1.5	0.5	1.05	0.019
2	0.5	1.04	0.020
3	0.5	1.04	0.019
5	0.5	1.05	0.018
7	0.5	1.05	0.016
10	0.5	1.05	0.012

(17) N. Takeguchi, M.S. Thesis, Osaka University, 1965.

(18) R. A. Robinson and R. H. Stokes, "Electrolyte Solutions," Butterworth and Co. Ltd., London, 1959, p. 465.

**Table II:** Values of Parameters  $\alpha$ ,  $\beta$ , and  $\theta$  for Various Membrane-Electrolyte Systems at  $\gamma = 2$ 

Electrolyte	Membrane no.	$\alpha$	$\alpha_{\text{bulk}}^a$	$\beta$	$\theta$
KCl	2	0.50	0.49	1.04	0.030
KI	2	0.50	0.49	1.05	0.022
NaCl	3	0.43	0.40	1.04	0.019
HCl	3	0.80	0.83	1.05	0.0035
KNO <sub>3</sub>	4	0.54	0.51	1.03	0.0071

<sup>a</sup> Calculated from limiting equivalent conductivities at 25°. <sup>18</sup>

Tables I and II indicate that  $\theta$  depends on the membrane sample used. This is the result that might be expected. However, it can be seen that even for a given membrane the value of  $\theta$  depends on the kind of electrolyte. At present we have no definite explanation of this effect. We rather conclude that  $\theta$  is the parameter characteristic of a given pair of membrane and electrolyte, not of a given membrane only. This point has been discussed in earlier work by Nagasawa and Kobatake. <sup>11,19</sup>

## Discussion

*Comparison of Theory and Experiment.* Once the values of the parameters  $\alpha$ ,  $\beta$ , and  $\theta$  for a given membrane-electrolyte system have been determined, one can calculate the theoretical  $\Delta\phi$  vs.  $C_2$  curve for any given  $\gamma$  and then compare it with the corresponding experimental data. For this comparison we first note that eq. 13 may be rewritten in the form

$$(\gamma - e^q)/(e^q - 1) = X \quad (22)$$

with  $q$  and  $X$  defined by

$$q = [|\Delta\phi_r| + (1 - 2\alpha) \ln \gamma] / [(1/\beta) + (1 - 2\alpha)] \quad (23)$$

$$X = C_2/(\alpha\beta\theta) \quad (24)$$

Thus if eq. 13 is valid, the values of  $(\gamma - e^q)/(e^q - 1)$  calculated from measured  $\Delta\phi$  with the predetermined  $\alpha$ ,  $\beta$ , and  $\theta$  and the given value of  $\gamma$  must fall on a straight line which has a unit slope and passes the coordinate origin, when plotted against  $X$ . This behavior must be valid irrespective of the value of  $\gamma$  and the kind of membrane-electrolyte (uni-univalent) system.

Figure 7 demonstrates that this theoretical prediction from our membrane potential equation is borne out quite satisfactorily by experimental results, except for the data with a sulfonated polystyrene collodion membrane. The plotted points include not

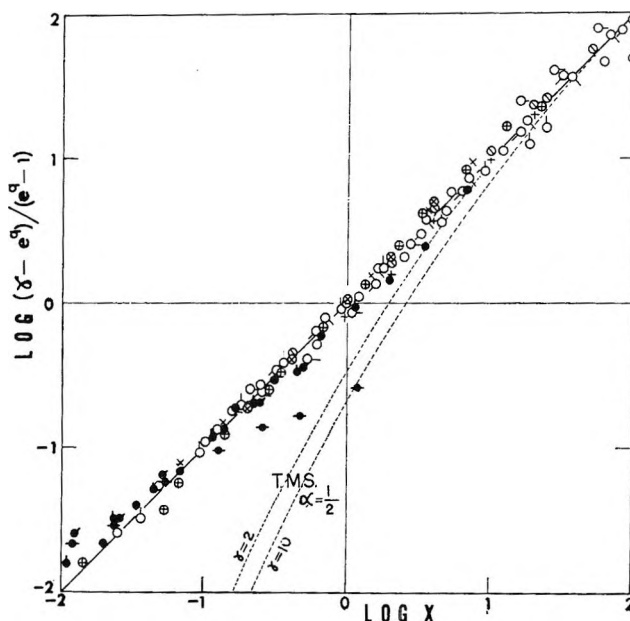


Figure 7. Linear relation between  $\log (\gamma - e^q)/(e^q - 1)$  and  $\log X$  for various membrane-electrolyte systems with various  $\gamma$ , where  $q = \frac{[|\Delta\phi_r| - (2\alpha - 1) \ln \gamma]}{[(1/\beta) - (2\alpha - 1)]}$  and  $X =$

$C_2/\alpha\beta\theta$ :  $\odot$ ,  $\gamma = 1.5$ ;  $+$ ,  $\gamma = 2$ ;  $\ominus$ ,  $\gamma = 3$ ;  $\square$ ,  $\gamma = 10$  for KCl with membrane 1;  $\oplus$ ,  $\gamma = 2$ ;  $\circ$ ,  $\gamma = 10$  for KCl with membrane 2;  $\diamond$ , KI at  $\gamma = 2$  with membrane 2;  $\times$ , HCl at  $\gamma = 2$ ;  $\circ$ , NaCl at  $\gamma = 2$  with membrane 2;  $\ominus$ , KNO<sub>3</sub> at  $\gamma = 2$  with membrane 4;  $\bullet$ , NaCl at  $\gamma = 2$  and 2.5 with phenolsulfonic acid membrane<sup>10</sup>;  $\bullet$ , KCl at  $\gamma = 2$  with protamine collodion membrane<sup>15</sup>;  $\bullet$ , KCl at  $\gamma = 2$  with oxidized collodion membrane<sup>16</sup>; and  $\bullet$ , KCl at  $\gamma = 2$  with sulfonated polystyrene collodion membrane.<sup>16</sup>

only all of our measurements but also some typical ones of previous authors. <sup>10,16</sup>

*The T.M.S. Theory.* If, instead of assuming eq. 6 for  $a_+$  and  $a_-$ , we consider that both positive and negative ions behave ideally in the membrane, i.e.,  $a_+ = C_+$  and  $a_- = C_-$ , and set  $k$  equal to zero (which implies neglecting the effect of mass flow), eq. 5 gives the following expression for  $\Delta\phi$

$$\Delta\phi = -\frac{RT}{F} \int_{C_1}^{C_2} \frac{(l_+ - l_-)}{(l_+ + l_-)C_- + l_+\theta} dC_- \quad (25)$$

where the condition of electric neutrality  $C_+ - C_- = \theta$  has been taken into account. As has been noted in foregoing lines, the concentration  $C_-$  just inside the membrane surface is lower than the concentration  $C$  in the outer solution when the activities  $a_+$  and  $a_-$  take the forms for ideal solutions. Thus a discontinuity occurs in the concentration  $C_-$  when we cross

(19) M. Nagasawa and Y. Kobatake, *J. Phys. Chem.*, **56**, 1017 (1952); M. Nagasawa, *Nippon Kagaku Zasshi*, **70**, 160 (1949).

the membrane surface. This discontinuity is calculated from the ideal Donnan condition that  $C^2 = C_+ (C_- + \theta)$  and has to be taken into account when the integral on the right-hand side of eq. 25 is evaluated. It can be shown that the resulting expression for  $\Delta\varphi$  agrees with that which had been derived by Teorell<sup>8</sup> and by Meyer and Sievers.<sup>9</sup> Thus we find that the T.M.S. theory refers to the case in which both positive and negative ions in the membrane behave thermodynamically ideally. It is not quite unlikely that such a situation is realized in charged membranes employed for a usual experimental study. By contrast, the present theory based on eq. 6 has introduced an ex-

treme asymmetry into the activities of positive and negative ions in the membrane. Thus in a charged membrane the co-ion species behaves ideally but the counterion species behaves extremely nonideally. The ion binding by the polyelectrolyte molecule may be primarily responsible for this latter effect. Whatever the mechanism may be, the success of our potential equation is associated primarily with the assumption of eq. 6 for the intramembrane activities of ions. The curves for  $\log [(\gamma - e^q)/(e^q - 1)]$  vs.  $\log X$  derived from the T.M.S. theory for  $\gamma = 2$  and  $10$  and  $\alpha = 1/2$  are shown for comparison in Figure 7. The insufficient nature of the T.M.S. theory is evident.

## The Activation Energy of Viscous Flow of Pure Water and Sea Water in the Temperature Region of Maximum Density

by R. A. Horne, R. A. Courant, D. S. Johnson, and F. F. Margosian

Arthur D. Little, Inc., Cambridge, Massachusetts (Received June 15, 1965)

The viscosities of pure water and sea water have been measured at 1 atm. over the temperature range  $-2$  to  $12^\circ$ . The temperature dependence of the activation energies of viscous flow of water and aqueous electrolytic solutions, unlike that of the activation energies of the electrical conductivities of aqueous solutions of salts, does not exhibit a maximum near the temperature of maximum density. This dissimilarity casts doubt upon the hypothesis that viscous flow and "normal" electrical conductivity both have the same slow step, namely, "hole" formation in the water.

### Introduction

Viscous flow and ionic conduction in water have long been believed to be closely related processes. Glasstone, Laidler, and Eyring<sup>1</sup> argue that "the fact that the activation energies, calculated from the ionic mobilities of most ions in a given solvent are the same, *e.g.*, 4.0 to 4.2 kcal. in water at  $25^\circ$ , and that the values are almost identical with that for viscous flow of the solvent, suggests that the rate of migration of an ion in an applied field is determined by the solvent molecules jumping from one equilibrium position to the next." However,

Wang, Robinson, and Edelman<sup>2</sup> concluded that self-diffusion, dipole-orientation, and viscous flow all have the same mechanism but that H-bond rupture and *not* vacancy formation is rate-determining.

Recent measurements of the electrical conduction of aqueous solutions in the region  $-2$  to  $10^\circ$  have

(1) S. Glasstone, K. J. Laidler, and H. Eyring, "The Theory of Rate Processes," McGraw-Hill Book Co., Inc., New York, N. Y., 1941, p. 557 ff.

(2) J. H. Wang, C. V. Robinson, and I. S. Edelman, *J. Am. Chem. Soc.*, **75**, 466 (1953).

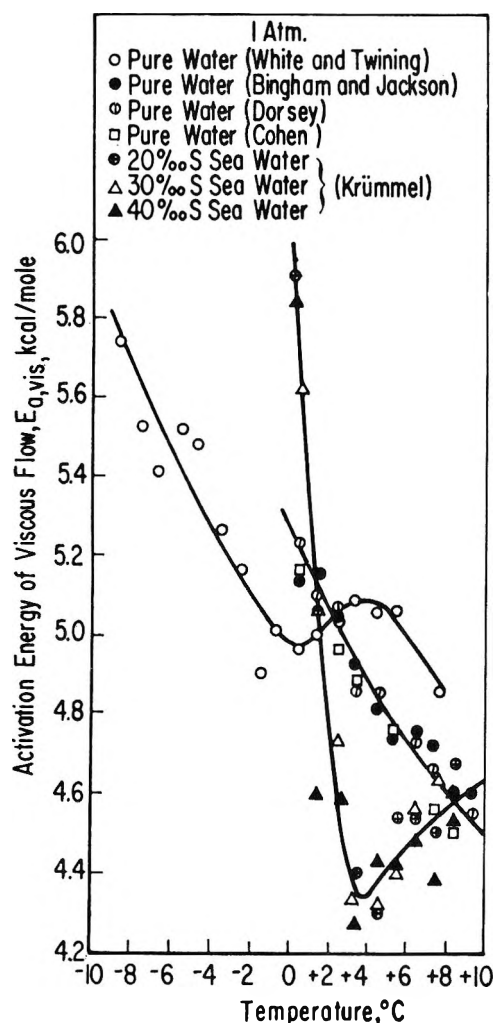


Figure 1. Activation energy of viscous flow of pure water and sea water calculated from literature data.

shown that, in the case of strong 1:1 electrolytes, the Arrhenius activation energy of conduction,  $E_{a,cond}$ , exhibits a pronounced maximum near the temperature of maximum density<sup>3,4</sup> and this maximum was attributed to the facilitation of "hole" formation in the relatively open water structures which are present below about 4°. A parallel maximum in the Arrhenius activation energy of viscous flow,  $E_{a,vis}$ , was expected near the temperature of maximum density. Miller<sup>5</sup> has made Arrhenius plots of the data summarized by Dorsey<sup>6</sup> and found that "there are no discontinuities at 0°, 4°, or 100° . . ." We found this result so surprising that we rechecked Miller's calculations and also calculated values of  $E_{a,vis}$  on the basis of a number of other different sources of data. These calculations revealed discrepancies so great (Figure 1) that we undertook to redetermine the viscosity of pure water and sea water in the temperature range -2 to 12°.

## Experimental Section

The viscosities were measured in a rolling-ball type viscometer<sup>7</sup> which had been previously calibrated at 25° with a series of water-glycerol solutions using the data of Sheely,<sup>8</sup> water-sucrose solutions using the data of Bingham and Jackson,<sup>9</sup> and aqueous NaCl solutions using "International Critical Tables" data. The more concentrated water-glycerol solutions gave viscosities differing by as much as 0.5% from the other standards presumably because of water absorption or because of too high a water content of the original "pure" glycerol.

Over the relatively small temperature range of the present experiments, the effects of temperature on the geometry of the viscometer are negligible (less than 0.07%). Deionized water and 19.375‰ chlorinity I.A.P.O. Standard Sea Water P<sub>32</sub> were used. At a given temperature the experiment was repeated from four to as many as ten times. The average deviation in roll time for a given set of experiments was only 0.10%. However, the fourth significant figure on the calibration curves could be estimated only to  $\pm 5$ ; thus the average deviation in the viscosity was somewhat larger being  $\pm 0.005$  cp. or about 0.3% for pure water and larger (for unknown reasons) or nearly  $\pm 0.01$  cp. for sea water. In the course of a given set of experiments, the average deviation in temperature ranged from  $\pm 0.005^\circ$  (for temperature near room temperature) to as much as  $\pm 0.02^\circ$  (for the lowest temperatures). Results from sets of experiments made with successively increasing temperatures agreed with results from sets made with successively decreasing temperatures. Values of  $E_{a,vis}$  were calculated by the integrated form of the Arrhenius equation

$$E_{a,vis} = [\log(1/\eta_2) - \log(1/\eta_1)]4.576T_2T_1/\Delta T \quad (1)$$

at 1° intervals from values of viscosity read from a computer-programmed second-order least-squares fit through the original viscosity-temperature data (such as Figure 2 but with expanded scales in order to be able to estimate the fourth significant figure) but with the presumably erratic value at  $-0.346^\circ$  for sea water

(3) R. A. Horne and R. A. Courant, *J. Phys. Chem.*, **68**, 1258 (1964).

(4) R. A. Horne and R. A. Courant, *J. Geophys. Res.*, **69**, 1152 (1964).

(5) A. A. Miller, *J. Chem. Phys.*, **38**, 1568 (1963).

(6) N. E. Dorsey, "Properties of Ordinary Water Substances," Reinhold Publishing Corp., New York, N. Y., 1940.

(7) The viscometer used is designed for studying the effect of high hydrostatic pressures on viscosity.

(8) M. L. Sheely, *Ind. Eng. Chem.*, **24**, 1060 (1932).

(9) E. C. Bingham and R. F. Jackson, *Bull. Natl. Bur. Std.*, **14**, 59 (1918).



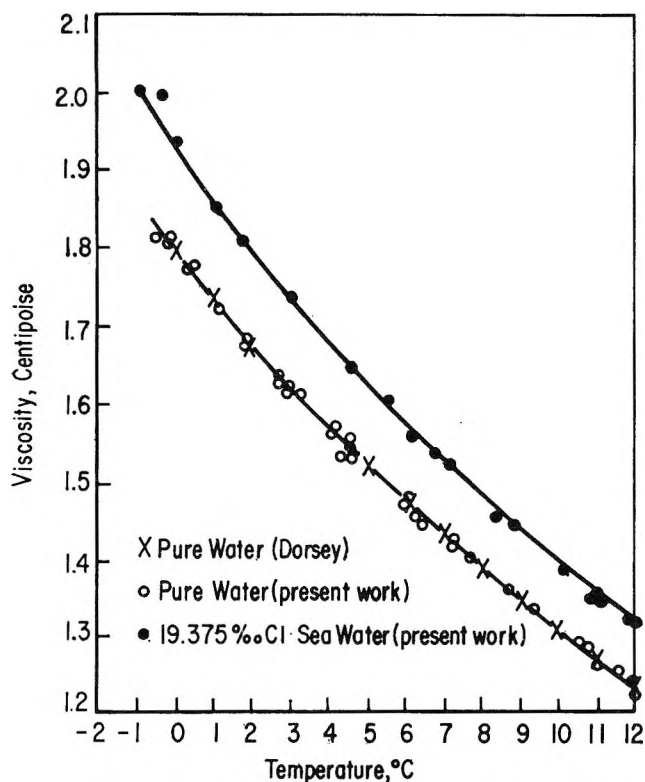


Figure 2. The temperature dependence of the viscosities of pure water and 19.375‰ Cl sea water.

deleted. The root-mean-square errors for pure water and sea water were 0.00764 and 0.00721, respectively. The standard deviation of  $E_{a,vis}$  in Figure 3 is  $\pm 0.1$  kcal./mole.

### Results and Discussion

Viscosities and activation energies of viscous flow for pure water and sea water are given in Figures 2 and 3. The present values for the viscosity of pure water are in agreement with the values reported earlier by Bingham and Jackson<sup>9</sup> and the "best" values of Dorsey.<sup>6</sup> Thus the values of  $E_{a,vis}$  for pure water are in agreement with values quoted by or calculated from Miller,<sup>5</sup> Bingham and Jackson,<sup>9</sup> Dorsey,<sup>6</sup> and Cohen,<sup>10</sup> but not White and Twining.<sup>11</sup>

The present values for the temperature dependence of the activation energy of viscous flow for sea water (Figure 3) are in poor agreement with the values calculated from the results of Krümmel (Figure 1) as quoted in "Landolt-Bornstein Physikalisch-Chemische Tabellen" (1923). We find, in agreement with Krümmel's data, that  $E_{a,vis}$  for sea water becomes much greater than the corresponding values for pure water as the temperature approaches 0°, but we find no evidence for a minimum around 4° (Figure 1).

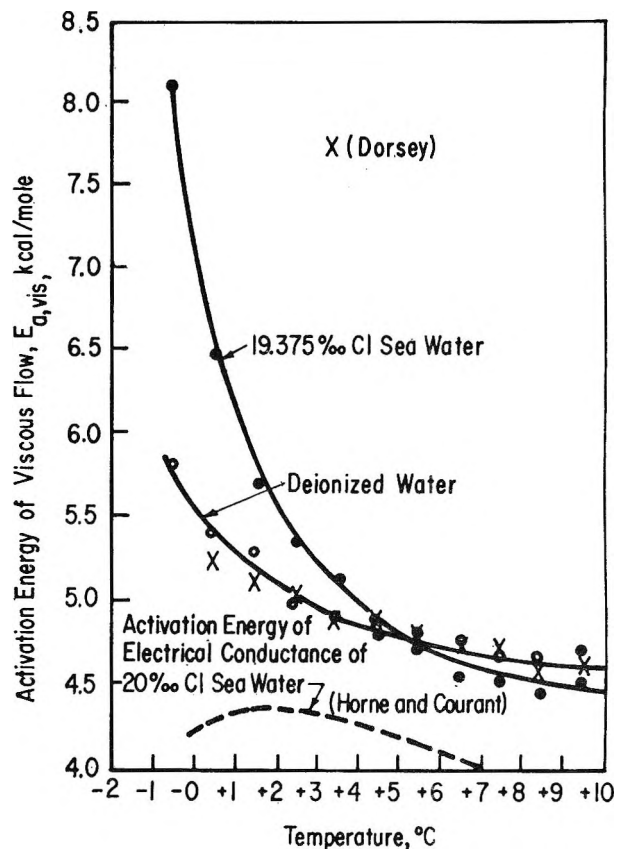


Figure 3. Activation energy of viscous flow of pure water and sea water.

Figure 3 shows that the presence of NaCl increases  $E_{a,vis}$  at low temperatures. This behavior is to be expected from the structure-making tendencies of this salt as evidenced by the positive viscosity  $B$ -coefficient.<sup>12</sup> In addition, sea water contains  $MgSO_4$ , a very effective structure maker.

Miller<sup>4</sup> suggests that "the molecular motion required for flow occurs only in the unbonded state." This is reminiscent of the Grotthuss component of protonic conduction in which the slow step is the rotation of water molecules and which is confined to the "free" rotatable water monomers between the structured clusters.<sup>13</sup>

The dissimilarity of the energetics of "normal" conduction and viscous flow of aqueous solutions as shown in Figure 3 renders suspect the hypothesis that

(10) R. Cohen, *Ann. Phys.*, **45**, 666 (1892).

(11) G. F. White and R. H. Twining, *J. Am. Chem. Soc.*, **35**, 380 (1913).

(12) R. W. Gurney, "Ionic Processes in Solution," McGraw-Hill Book Co., Inc., New York, N. Y., 1953, Chapter 9.

(13) R. A. Horne and R. A. Courant, *J. Phys. Chem.*, **69**, 2224 (1965).



these two processes have the same rate-determining step, at least in the region  $-2$  to  $12^\circ$ . Even in the temperature range  $10$  to  $60^\circ$ , the activation energies of "normal" conduction, protonic conduction, viscous flow, and self-diffusion appear to parallel one another rather than be numerically equal.<sup>14</sup> A recent examination of the temperature dependence of dielectric relaxation in water<sup>15</sup> has yielded results very similar to Miller's<sup>5</sup> viscosity studies. On the basis of the foregoing evidence we subscribed tentatively to the view that the slow step of "normal" ionic conduction in aqueous solution is "hole" formation, both in the free and the clustered water, while the slow step of the viscous flow of aqueous solutions is some sort of rotational tumbling of the "free" water or of the clusters through the "free" water. Alternatively, the differences in behavior of  $E_{a,\text{cond}}$  and  $E_{a,\text{vis}}$  could arise from a change in mechanism in the former process resulting from the structural changes that occur near  $4^\circ$ .

The possibility that water cluster break-up might

be the rate-determining step in either conductive or viscous processes is unlikely<sup>16</sup> in view of the relatively large concentration of unbound water available for transport processes. Némethy and Scheraga<sup>17</sup> estimate that the mole fraction of unbonded or "free" water varies from  $0.24$  to  $0.44$  over the range  $0$  to  $100^\circ$ .<sup>18</sup>

*Acknowledgment.* We are indebted to Dr. I. Simon for his assistance. This work was supported in part by the Office of Naval Research.

---

(14) See Figure 9 in R. A. Horne, *Water Resources Res.*, **1**, 263 (1965).

(15) R. C. Bhandari and M. L. Sisodia, *Indian J. Pure Appl. Phys.*, **2**, 132 (1964).

(16) Cf. ref. 2.

(17) G. Némethy and H. A. Scheraga, *J. Chem. Phys.*, **36**, 3382 (1962).

(18) Added note: D. P. Stevenson, *J. Phys. Chem.*, **69**, 2145 (1965), has recently argued that Némethy and Scheraga's estimate of the concentration of monomeric water is at least two orders of magnitude too high.

# Activity Coefficients of Sodium Chloride in Aqueous Three-Component Solutions by Cation-Sensitive Glass Electrodes<sup>1a</sup>

by R. D. Lanier<sup>1b</sup>

Chemistry Division, Oak Ridge National Laboratory, Oak Ridge, Tennessee (Received June 15, 1965)

Activity coefficients of NaCl in aqueous three-component solutions were measured at 25° at ionic strength 1–6 with cation-sensitive glass electrodes *vs.* silver–silver chloride electrodes. The second salts were MgCl<sub>2</sub>, CaCl<sub>2</sub>, SrCl<sub>2</sub>, BaCl<sub>2</sub>, NaC<sub>2</sub>H<sub>3</sub>O<sub>2</sub>, NaClO<sub>4</sub>, NaNO<sub>3</sub>, and Na<sub>2</sub>SO<sub>4</sub>. Agreement with available literature values is satisfactory. Except possibly at low NaCl contributions to total ionic strength, Harned's rule appears to apply. An approximate form of Brønsted's rule allowed in most cases good estimates of activity coefficients of NaCl at trace concentration in solution of a second electrolyte from the activity coefficients of two-component solutions of the two solutes at the ionic strength in question.

In recent experiments,<sup>2,3</sup> a cation-sensitive glass electrode silver–silver chloride cell was used to measure activity coefficients in water and water–organic mixtures. This paper reports measurements of NaCl activity coefficients in aqueous solutions containing a second electrolyte having one ion in common. Included were salt pairs with alkaline earth chlorides and pairs with Na<sup>+</sup> in common. Other alkali metal chlorides were not included because the response of the glass electrode to them is comparable to its response to Na<sup>+</sup>.

The ionic strength range of this study is 1–6 *m*. Recently,<sup>4</sup> similar measurements were reported for four of the present mixtures at an ionic strength of 0.7.

Measurements were carried out at constant ionic strength in order to test the applicability of Harned's rule<sup>5</sup>

$$\log \gamma_{i2} = \log \gamma_{i0} - \alpha_{i2} I_2 \quad (1)$$

which states that  $\alpha_{i2}$  is a constant at a given ionic strength. The symbols in eq. 1 and other symbols used in this paper are for the most part those used by Harned and are defined below.

$I$  is ionic strength,  $= \frac{1}{2} \sum m_i z_i^2$ ,  $m$  being concentration in moles/kg. of H<sub>2</sub>O, and the summation being over all ions. Subscript 1 refers to NaCl and 2 to the other solute.  $\gamma_{ij}$  is the mean ionic activity coefficient of solute  $i$  in a three-component solution also containing solute  $j$ .  $\gamma_{i0}$  is the activity coefficient of a two-

component solution of component  $i$  at the total ionic strength under discussion.  $\gamma_{0i}$  is the activity coefficient of component  $i$  in the presence of  $j$ , extrapolated to zero concentration of  $i$ .  $\phi_i$  is the osmotic coefficient of a two-component solution containing solute  $i$ .  $z_i$  is the charge on ion  $i$ .  $\beta_{ij}$  is the coefficient of a term quadratic in  $I_j$  added to eq. 1 for cases where a linear relationship is not adequate.  $\nu_i$  is the number of moles of ions/mole of component  $i$ .

## Experimental Section

1. *Potential Measurements.* A vibrating reed electrometer, in conjunction with a Rubicon or a Leeds and Northrup K-3 potentiometer, was used for measurements of e.m.f.<sup>6</sup>

2. *Electrodes.* The glass electrode (Cationic 39137) was obtained from Beckman Instruments, Inc., and its

(1) (a) Research sponsored by The Office of Saline Water, U. S. Department of the Interior under Union Carbide Corporation's contract with the U. S. Atomic Energy Commission; (b) Southwest Missouri State College, Springfield, Mo.

(2) R. D. Lanier, *J. Phys. Chem.*, **69**, 2697 (1965).

(3) M. M. Shul'tz and A. E. Parfenov, *Vestn. Leningr. Univ., Ser. Fiz. i. Khim.*, **13**, No. 3, 118 (1958).

(4) W. F. Fitzgerald, Abstracts, 148th National Meeting of the American Chemical Society, Chicago, Ill., Sept. 1964.

(5) H. S. Harned and B. B. Owen, "The Physical Chemistry of Electrolyte Solutions," ACS Monograph Series, 3rd Ed., Reinhold Publishing Corp., New York, N. Y., 1958, Chapter 14.

(6) K. A. Kraus, R. W. Holmberg, and C. J. Borkowski, *Anal. Chem.*, **22**, 341 (1950).

performance is described by their literature.<sup>7</sup> Reference 2 gives further data on the performance of this electrode in water-sodium chloride and water-organic-sodium chloride solutions.

The silver chloride electrodes were of the thermal type<sup>8</sup>; Ag<sub>2</sub>O and AgClO<sub>3</sub> paste were fired on Pt wires at 500–600°. These electrodes were shorted together and allowed to equilibrate in NaCl solution, which was initially at 80° and which cooled to room temperature overnight.<sup>9</sup>

The performance of the AgCl electrodes was satisfactory (rapid, accurate response to a change in Cl<sup>-</sup> concentration), if the solution being tested had been previously saturated with AgCl, except at very low chloride concentrations.

3. *Reagents.* Reagent grade salts were used without further purification. Laboratory distilled water, which had been run through a deionization column, was used to prepare solutions; from measurements of e.m.f. of dilute solutions (<0.01 M NaCl), errors from impurities in the water were estimated to be negligible. The pH of water fresh from the deionization column was ca. 7.8, and solutions were exposed to the atmosphere no more than necessary.

4. *Solutions.* Solutions were prepared by weight from saturated NaCl solutions (taken to be 6.144 *m*),<sup>10</sup> deionized water, and stock solutions of the second salt. The stock solution of the second salt was standardized by Mohr titration for Cl<sup>-</sup> in the case of MCl<sub>2</sub> salts. With NaX salts, stock concentrations were established by ion exchange of Na<sup>+</sup> on Dowex 50W-X12 cation-exchange resin in the H<sup>+</sup> form, followed by acid-base titration. Solutions were prepared initially for a total ionic strength of 6.0 (5.0 for sodium acetate and 3.0 and 5.0 for BaCl<sub>2</sub>) with several ionic strength fractions of NaCl. After potential readings were taken, these solutions were diluted by weight to a total ionic strength of 3.0 and finally to *I* = 1.0.

5. *Procedure.* Saturated NaCl solution was used as the reference point for the potential measurements because of the ease in preparation, although any other accurately known concentration of NaCl in water could have been used. The quantities of interest here are the differences of potential obtained for the mixed salt solutions from that of a two-component solution of NaCl of the same ionic strength. For a given series of test solutions containing NaCl and the second salt at a constant total ionic strength, the potential readings were made in the order of increasing NaCl concentration, and saturated NaCl solution (with no second salt present) was tested last. Activity coefficients of NaCl in the mixed salt solutions were then computed from the

difference of potential between test solution and saturated NaCl using the Nernst expression

$$(E - E_{\text{sat}}) = 0.05915 \log \frac{m_{\text{Na}} m_{\text{Cl}} \gamma_{12}^2}{a_{\pm \text{sat}}^2} \quad (2)$$

where  $a_{\pm}$  is the mean ionic activity of NaCl. Since the tables of Robinson and Stokes<sup>11</sup> were used to obtain log  $\gamma_{10}$  and osmotic coefficients for computing  $\alpha$ , a value extrapolated from their table for  $\gamma_{\pm \text{NaCl sat}} = 1.007$  was adopted. The potential measurement of each sample was usually repeated after agitating the e.m.f. cell and the electrode leads in order to reduce the possibility of gross error. Potentials were read when the drift of the potential of the cell, as indicated by a Brown recorder, became negligible. The vibrating reed system is capable of measuring potentials to 0.05 mv. or better,<sup>6</sup> but stray potential of the electrode leads and minor temperature fluctuations (less than 0.1°) limit the reproducibility to 0.1–0.2 mv. The ionic strengths of the solutions on which measurements were carried out varied from the round ionic strengths for which results are reported by as much as 0.3% in some cases, and the reported activity coefficients are adjusted to compensate; the corrections are almost negligible.

6. *Interferences.* In the results to be presented, positive deviations (usually less than 1 mv., but occasionally more) of e.m.f. values from those expected from Harned's rule were observed at low NaCl concentrations. Considerable effort was made to eliminate as a possible source of these discrepancies incomplete removal from the electrode of more concentrated solutions from previous measurements. The deviations appear to be real and of reproducible magnitude, if the chloride concentration is not too low. It does not seem likely, although it cannot be completely excluded, that the results indicate a failure of Harned's rule at low NaCl fractions. On the other hand, there appears to be no single explanation for all cases.

Monovalent impurities, to which the electrode is quite sensitive, are a possible source of error. Spectroscopic analysis of the reagents, however, coupled with measurement<sup>2</sup> of the electrode sensitivity to K<sup>+</sup>,

(7) Beckman Instructions 1154-A and 1155-A, Beckman Instruments, Inc., Scientific and Process Instrument Division, Fullerton, Calif., June 1962, 12TW392. 81154.

(8) C. K. Rule and V. K. La Mer, *J. Am. Chem. Soc.*, **58**, 2339 (1936).

(9) J. H. Ashby, F. M. Crooke, and S. P. Datta, *Biochem. J.*, **56**, 190 (1954).

(10) A. Seidell, "Solubilities of Inorganic and Metal Organic Compounds," Vol. I, 3rd Ed., D. Van Nostrand Co., New York, N. Y., 1953, p. 1217.

(11) R. A. Robinson and R. H. Stokes, "Electrolyte Solutions," 2nd Ed., Academic Press, New York, N. Y., 1959, Appendix 8.10.

make it unlikely that errors of this magnitude arise from potassium, the most likely contaminant. Possible interference of  $H^+$  was minimized by operation at pH 7. The solutions were saturated with  $AgCl$ , but its concentration should be too low for serious interference.

With mixtures containing alkaline earth ions, a sensitivity of the glass electrodes to  $M^{+2}$  ion could explain the deviations. Such sensitivity is said to be small,<sup>7</sup> and in fact must be at least in the case of  $Ba^{+2}$ , from the agreement of e.m.f. with isopiestic results (see below). A further test was possible with the highly soluble salt, calcium chloride, by addition of the salt to saturated  $NaCl$  solutions (in contact with solid  $NaCl$ ). No significant change of potential ( $\pm 0.2$  mv.) was noted, even though the molality of  $CaCl_2$  in some solutions was as high as 5 *m*. However, the test does not eliminate the possibility of effects at very low  $NaCl$  concentrations, and in the alkaline earth-sodium chloride solutions sensitivity to the divalent ion seems to us the most likely explanation of discrepancies.

Deviations at low  $NaCl$  in  $NaCl-NaX-H_2O$  systems were small at ionic strength 6 and seem more likely to stem from difficulties with the  $Ag-AgCl$  electrodes. At low chloride concentration, these electrodes tended to equilibrate slowly, to be unstable, and to deteriorate rapidly. They were replaced with each change of  $NaX$ . Deterioration in  $MCl_2$  solutions was not as rapid, though after 1-2 days speed and accuracy of response were noticeably less. If these electrodes were soaked in hot water and refred at  $600^\circ$ , their response was improved. This might mean that one cause of the deterioration is the occurrence of oxidation-reduction reactions involving  $Br^-$ ,  $BrO_3^-$ ,  $I^-$ ,  $IO_3^-$ , and similar trace impurities. Therefore, fresh electrodes were prepared in sufficient quantities to allow the  $AgCl$  electrodes to be replaced as often as was indicated by their performance.

7. *Temperature Control.* The temperature of the measurements was  $25^\circ$ . Saturated  $NaCl$  solutions, which were used as reference, have a temperature coefficient of about 2 mv./ $^\circ C$ .; *i.e.*, temperature must be controlled to  $0.05^\circ$  for 0.1-mv. precision. An error in the reference potential would not affect the linearity of  $\log \gamma_{12}$  vs.  $I_2$  but would affect the intercepts. The temperature coefficient of the more dilute solutions is smaller, and errors from temperature variation ( $\pm 0.1^\circ$ ) are small.

## Results and Discussion

1. *Activity Coefficients of NaCl.* The salts other than  $NaCl$  in the pairs having a divalent cation were magnesium, calcium, strontium, and barium chlorides. The second salts with sodium ion in common were the

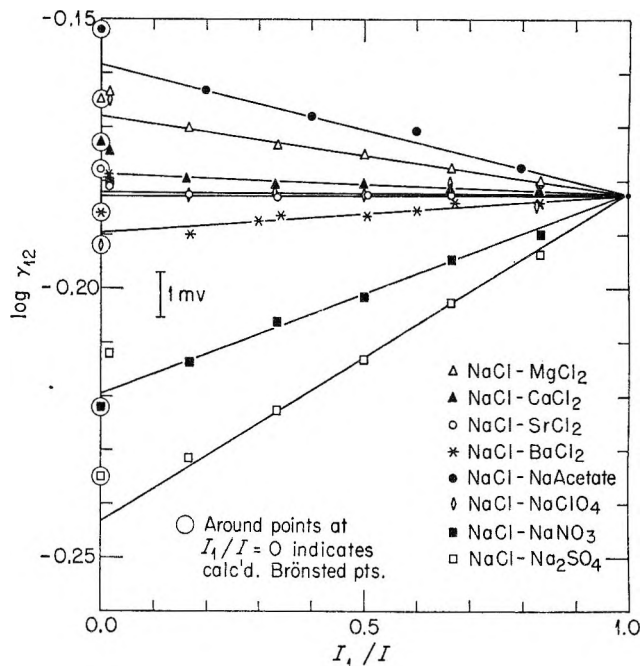


Figure 1. Activity coefficients of  $NaCl$  in  $NaCl$ -salt mixtures;  $I = 1.0$ .

acetate, nitrate, perchlorate, and sulfate. Results are presented in Table I as activity coefficients of  $NaCl$ , computed from the e.m.f. measurements by eq. 2.

2. *Applicability of Harned's Rule to NaCl. Comparison with Isopiestic Data.* Graphs of  $\log \gamma_{12}$  as a function of ionic strength are given in Figures 1-3. Except at low  $NaCl$  fractions, where results are suspect (see Experimental Section), most of the values fall within a fraction of a millivolt of a straight line (*i.e.*, Harned's rule is obeyed). If the low  $NaCl$  concentrations are ignored, the precision appears adequate for estimation of  $\alpha_{12}$  with uncertainties of from  $\pm 0.002$  at  $I = 1$  to  $\pm 0.001$  at  $I = 6$ .

With the alkaline earth chlorides, the values of  $\alpha_{12}$  increase from  $MgCl_2-NaCl$  to  $BaCl_2-NaCl$  mixtures (Table II). The values are a factor of five or more lower than those for  $HCl$  under similar conditions<sup>6</sup>; the activity coefficients of  $NaCl$  in these mixtures are thus much better approximated by their value in a two-component system of the same ionic strength than those of  $HCl$ .

The absolute magnitudes of  $\alpha_{12}$  are greater for mixtures of  $NaCl$  with  $NaNO_3$ ,  $Na_2SO_4$ , and sodium acetate than for the mixtures involving alkaline earth chlorides; for perchlorate, however, the value is very small.

Two of the systems studied here have recently been investigated by the isopiestic technique. With  $NaCl-$

Table I: Activity Coefficients of NaCl in NaCl-Salt Mixtures

A. NaCl-MgCl <sub>2</sub>				E. NaCl-NaC <sub>2</sub> H <sub>3</sub> O <sub>2</sub>			
<i>I</i> <sub>1</sub> / <i>I</i>	Log $\gamma_{\pm\text{NaCl}}$			<i>I</i> <sub>1</sub> / <i>I</i>	Log $\gamma_{\pm\text{NaCl}}$		
	<i>I</i> = 1.0	<i>I</i> = 3.0	<i>I</i> = 6.0		<i>I</i> = 1.0	<i>I</i> = 3.0	<i>I</i> = 5.0
0.01694	-0.163	-0.107	0.051	0.02098	-0.141	-0.094	-0.015
0.01681			0.054	0.02233			-0.013
0.1682	-0.170	-0.120	0.036	0.1998	-0.163	-0.119	-0.024
0.1681			0.035	0.2008			-0.024
0.3355	-0.173	-0.127	0.020	0.3994	-0.168	-0.126	-0.032
0.3352			0.020	0.2933			-0.031
0.5034	-0.175	-0.130	0.012	0.5999	-0.171	-0.133	-0.041
0.5022			0.012	0.5994			-0.040
0.6684	-0.178	-0.136	0.006	0.8000	-0.178	-0.139	-0.051
0.6696			0.006	0.8001			-0.049
0.8370	-0.180	-0.144	0.000	1.000	-0.183	-0.146	-0.059
0.8375			0.001	1.000			-0.058
				1.000	-0.182	-0.146	-0.058
B. NaCl-CaCl <sub>2</sub>				F. NaCl-Na <sub>2</sub> SO <sub>4</sub>			
<i>I</i> <sub>1</sub> / <i>I</i>	Log $\gamma_{\pm\text{NaCl}}$			<i>I</i> <sub>1</sub> / <i>I</i>	Log $\gamma_{\pm\text{NaCl}}$		
	<i>I</i> = 1.0	<i>I</i> = 3.0	<i>I</i> = 6.0		<i>I</i> = 1.0	<i>I</i> = 3.0	<i>I</i> = 5.0
0.01686	-0.174	-0.133	-0.001				
0.01652			0.001				
0.1620	-0.180	-0.140	-0.008	0.01705	-0.212	-0.289	-0.299
0.1652			-0.007	0.01702			-0.300
0.3317	-0.180	-0.142	-0.008	0.1658	-0.231	-0.282	-0.254
0.3307			-0.007	0.1662			-0.254
0.4990	-0.181	-0.144	-0.010	0.3326	-0.223	-0.254	-0.202
0.4986			-0.010	0.3334			-0.203
0.6644	-0.181	-0.146	-0.011	0.4993	-0.213	-0.224	-0.154
0.6614			-0.010	0.5003			-0.154
0.8335	-0.182	-0.145	-0.007	0.6670	-0.203	-0.201	-0.105
0.8290			-0.008	0.6669			-0.102
				0.8327	-0.193	-0.173	-0.055
				0.8328			-0.056
C. NaCl-SrCl <sub>2</sub>				G. NaCl-NaNO <sub>3</sub>			
<i>I</i> <sub>1</sub> / <i>I</i>	Log $\gamma_{\pm\text{NaCl}}$			<i>I</i> <sub>1</sub> / <i>I</i>	Log $\gamma_{\pm\text{NaCl}}$		
	<i>I</i> = 1.0	<i>I</i> = 3.0	<i>I</i> = 6.0		<i>I</i> = 1.0	<i>I</i> = 3.0	<i>I</i> = 5.0
0.01674	-0.181	-0.146	-0.035				
0.01673			-0.036				
0.1665	-0.182	-0.151	-0.034	0.01786	-0.180	-0.166	-0.209
0.1658			-0.033	0.01677			-0.209
0.3353	-0.183	-0.151	-0.030	0.1668	-0.214	-0.232	-0.181
0.3342			-0.030	0.1669			-0.181
0.5059	-0.182	-0.150	-0.022	0.3334	-0.206	-0.213	-0.146
0.5017			-0.026	0.3340			-0.145
0.6660	-0.182	-0.149	-0.019	0.5000	-0.202	-0.197	-0.114
0.6663			-0.018	0.5153			-0.109
0.8323	-0.180	-0.149	-0.011	0.6677	-0.194	-0.180	-0.077
0.8331			-0.012	0.6662			-0.076
				0.8343	-0.190	-0.163	-0.036
				0.8333			-0.037
D. NaCl-BaCl <sub>2</sub>				H. NaCl-NaClO <sub>4</sub>			
<i>I</i> <sub>1</sub> / <i>I</i>	Log $\gamma_{\pm\text{NaCl}}$			<i>I</i> <sub>1</sub> / <i>I</i>	Log $\gamma_{\pm\text{NaCl}}$		
	<i>I</i> = 1.0	<i>I</i> = 3.0	<i>I</i> = 6.0		<i>I</i> = 1.0	<i>I</i> = 3.0	<i>I</i> = 5.0
0.01706	-0.179	-0.182	0.02040	-0.140			
0.01711			0.02028	-0.140	0.01704	-0.165	-0.135
0.1701	-0.190	-0.179	0.1963	-0.130	0.01743		-0.057
0.1681			0.1966	-0.130	0.1675	-0.182	-0.152
0.3417	-0.186	-0.174	0.3863	-0.117	0.1630		-0.054
0.3400			0.3791	-0.118	0.3289	-0.182	-0.155
0.5064	-0.186	-0.166	0.5838	-0.100	0.3240		-0.046
0.5104			0.5860	-0.100	0.4979	-0.182	-0.149
0.6719	-0.184	-0.159	0.8004	-0.078	0.4986		-0.036
0.6757			0.7975	-0.078	0.6650	-0.180	-0.151
0.8346	-0.184	-0.154	1.000	-0.059	0.6656		-0.027
0.8223			1.000	-0.058	0.8330	-0.184	-0.148
0.3000	-0.187				0.8324		-0.018
0.6000	-0.185				1.0000	-0.182	-0.146

Table II: Results of Attempt to Calculate  $\alpha_{21}$  from  $\alpha_{12}$ 

System	I	Log $\gamma_{01}$ (exptl.)	Log $\gamma_{20}^a$	$\phi_2^a$	$\alpha_{12}$	$\alpha_{21}$	$S'$
NaCl-NaC <sub>2</sub> H <sub>3</sub> O <sub>2</sub>	1.0	-0.158	-0.121	1.002	-0.0242	0.0328	0.0172
	3.0	-0.112	-0.008	1.181	-0.0113	0.0289	0.0352
	5.0	-0.014	...	...	-0.0074	...	...
NaCl-Na <sub>2</sub> SO <sub>4</sub>	1.0	-0.243	-0.509	0.717	0.0605	-0.0141	0.3207
	3.0	-0.307	-0.690	0.642	0.0537	-0.0205	0.2607
	6.0	-0.306	-0.811	0.621	0.0500	-0.0333	0.1901
NaCl-NaNO <sub>3</sub>	1.0	-0.219	-0.261	0.851	0.0370	-0.0370	0.0000
	3.0	-0.247	-0.360	0.810	0.0336	-0.0336	0.0000
	6.0	-0.216	-0.431	0.788	0.0350	-0.0350	0.0000
NaCl-NaClO <sub>4</sub>	1.0	-0.182	-0.201	0.910	0.0000	-0.0228	-0.0456
	3.0	-0.155	-0.214	0.960	0.0030	-0.0208	-0.0356
	6.0	-0.066	-0.169	1.060	0.0100	-0.0205	-0.0210
NaCl-MgCl <sub>2</sub>	1.0	-0.168	-0.323	0.904	-0.0146	-0.0137	-0.1278
	3.0	-0.115	-0.245	1.108	-0.0104	-0.0159	-0.1101
	6.0	0.030	0.022	1.523	-0.0060	-0.0148	-0.0804
NaCl-CaCl <sub>2</sub>	1.0	-0.178	-0.344	0.882	-0.0040	+0.0002	-0.0234
	3.0	-0.140	-0.301	1.046	-0.0020	-0.0150	-0.0570
	6.0	-0.014	-0.101	1.376	0.0013	-0.0214	-0.0564
NaCl-SrCl <sub>2</sub>	1.0	-0.182	-0.357	0.868	0.0000	-0.0040	-0.0120
	3.0	-0.152	-0.333	1.009	0.0020	-0.0177	-0.0411
	6.0	-0.042	-0.171	1.292	0.0060	-0.0242	-0.0366
NaCl-BaCl <sub>2</sub>	1.0	-0.190	-0.379	0.848	0.0072	-0.0070	0.0222
	3.0	-0.187	-0.397	0.934	0.0135	-0.0164	0.0318
	5.0	-0.153	-0.352	1.044	0.0190	-0.0210	0.0510

<sup>a</sup> These values are taken from Robinson and Stokes.<sup>11</sup> Values for NaCl alone from Robinson are:  $I = 1.0$ ,  $\log \gamma_{10} = -0.182$ ,  $\phi_1 = 0.9363$ ;  $I = 3.0$ ,  $\log \gamma_{10} = -0.146$ ,  $\phi_1 = 1.042$ ;  $I = 5.0$ ,  $\log \gamma_{10} = -0.058$ ,  $\phi_1 = 1.192$ ;  $I = 6.0$ ,  $\log \gamma_{10} = -0.006$ ,  $\phi_1 = 1.271$ .

BaCl<sub>2</sub>, Robinson and Bower<sup>12</sup> found values of  $\alpha_{12}$  of 0.0141 at  $I = 3$  to be compared with  $\alpha_{12} = 0.0135$  obtained here. Scatchard and Yoest<sup>13</sup> found for NaCl-NaClO<sub>4</sub> for  $I = 1.0$ ,  $\alpha_{12} = -0.003$ , for  $I = 3.0$ ,  $\alpha_{12} = 0.003$ , and for  $I = 6.0$ ,  $\alpha_{12} = 0.011$ , to be compared with 0, 0.003, and 0.010 obtained by the e.m.f. method. The agreement inspires confidence in the reliability of the glass electrode for such measurements (see Figure 4).

3. *Activity Coefficients of the Second Salt.* If both electrolytes obey Harned's rule, one can readily obtain<sup>5</sup> the value of  $\alpha_{21}$  from values of  $\alpha_{12}$  and tables of the osmotic coefficients, of both solutes, with the equation

$$\frac{\alpha_{21}}{z_2 + |z_2^-|} = \alpha_{12} - \frac{2}{2.303I} \left[ \left( \phi_1 - \frac{\phi_2}{z_2 + |z_2^-|} \right) - \left( 1 - \frac{1}{z_2 + |z_2^-|} \right) \right] \quad (3)$$

Further, a criterion for observance of Harned's rule by solute 2 is constancy of the quantity  $S' = \nu_1 \alpha_{12}$ :

$(I_2/m_2) + \nu_2 \alpha_{21}(I_1/m_1)$ . If  $S'$  is not constant, a more complicated procedure is necessary.<sup>5</sup> Scatchard<sup>14</sup> has outlined an alternate approach.

Values of  $\alpha_{21}$  and  $S'$  are given in Table II, along with the literature<sup>11</sup> osmotic coefficients used in their evaluation. Only for NaNO<sub>3</sub>, where  $S' \approx 0$ , does constancy of  $S'$  indicate that the second solute obeys Harned's rule reasonably well. Evaluation of  $\beta_{21}$ , the coefficient of the quadratic term in the equation for  $\log \gamma_{21}$ , was not attempted.

4. *Estimation of Log  $\gamma_{01}$  from Two-Component Data.* There are of course many more activity coefficient data available for two-component than for three-component solutions, and it is of interest to see how well three-component activity coefficients can be estimated from

(12) R. A. Robinson and V. E. Bower, *J. Res. Natl. Bur. Std.*, **69A**, 19 (1965).

(13) G. Scatchard, private communication. Values of  $\alpha_{12}$  calculated from Ph.D. Thesis of R. L. Yoest, Department of Chemistry, Massachusetts Institute of Technology, 1964.

(14) G. Scatchard, *J. Am. Chem. Soc.*, **83**, 2636 (1961).

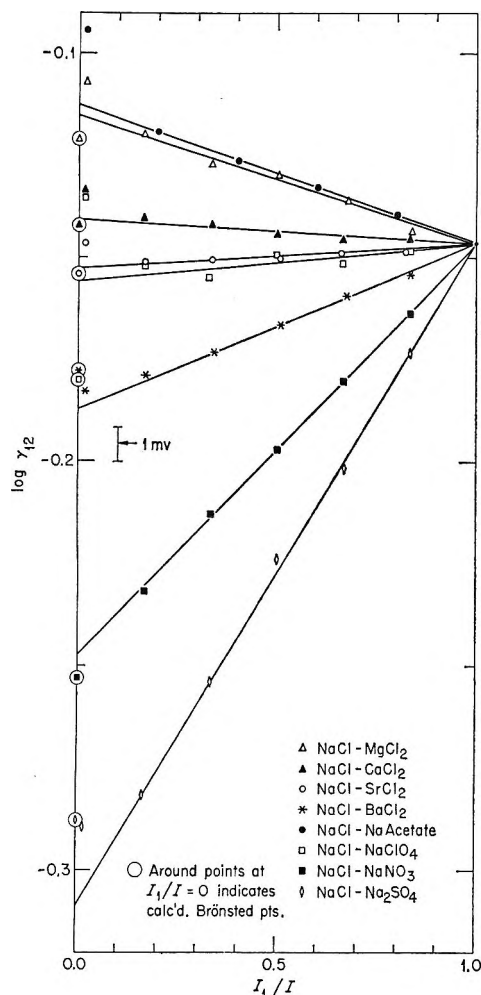


Figure 2. Activity coefficients of NaCl in NaCl-salt mixtures;  $I = 3.0$ .

values for the individual solutes. For an electrolyte obeying Harned's rule, a value of  $\log \gamma_{01}$  also implies a value of  $\alpha_{12}$ . If extrapolations to 0  $m$  NaCl of the linear portion of the  $\log \gamma_{12}$  graphs of Figures 1-3 are assumed to give the correct values of  $\log \gamma_{01}$ , the present data allow a test of the applicability of an approximate extension of Brønsted's rule, from which values of  $\log \gamma_{01}$  may be predicted from the two-component data at the same ionic strength. This rule may be stated<sup>15</sup>

$$\log \gamma_k = -\frac{0.509z_k^2\sqrt{I}}{1 + a'\sqrt{I}} + \sum_j f_{kj}(I)m_j = z_k^2 D_h + \sum_j f_{kj}(I)m_j \quad (4)$$

where  $\gamma_k$  is the activity coefficient of the  $k$ th ion;  $f_{jk}(I) = f_{kj}(I)$  is the interaction coefficient between ions of type  $k$  and ions of opposite charge sign  $j$  (by the Brønsted assumption,  $f_{jk} = 0$  for ions of the same charge sign);  $-0.509$  is the Debye-Hückel limiting slope;

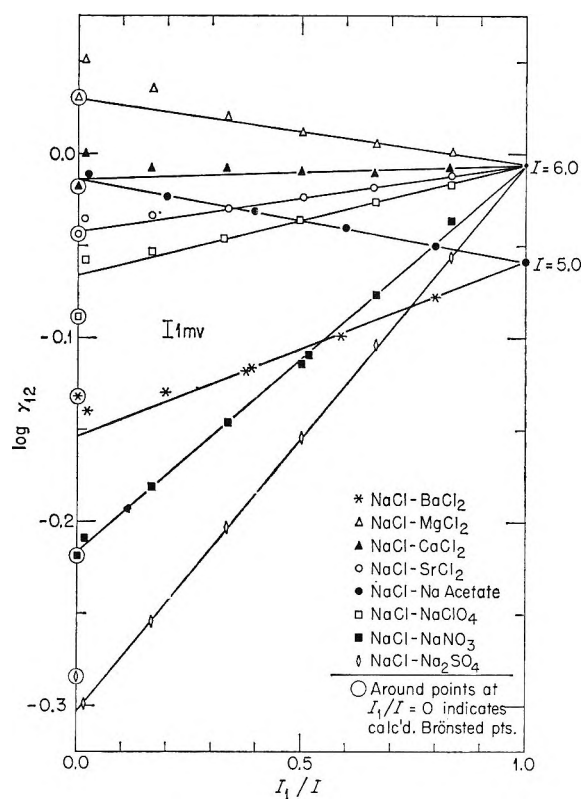


Figure 3. Activity coefficients of NaCl in NaCl-salt mixtures;  $I = 6.0$  except for NaCl-BaCl<sub>2</sub> and NaCl-acetate, where  $I = 5.0$ .

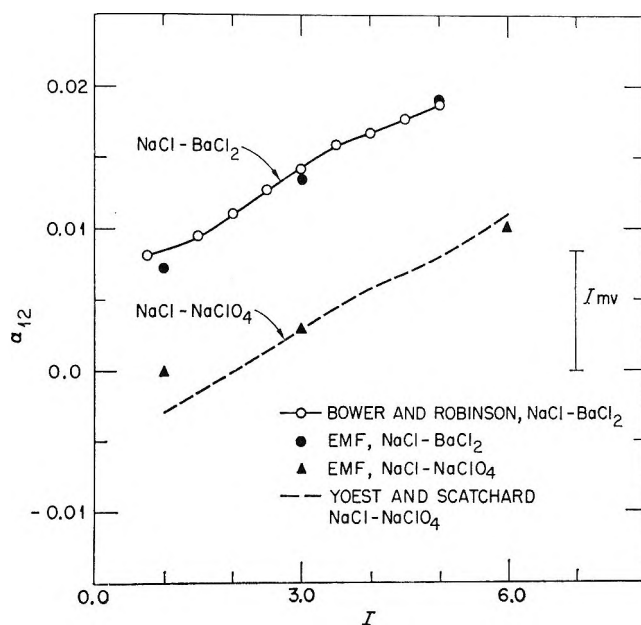


Figure 4. Comparison of  $\alpha_{12}$  values with literature.

(15) G. Scatchard, *Chem. Rev.*, 19, 309 (1936).

$a'$  is the "distance of closest approach" parameter (here taken to be 1.5 for all electrolytes); and  $D_h$  is the Debye-Hückel term for a 1-1 electrolyte ( $D_h = -0.509 \sqrt{I}/(1 + a' \sqrt{I})$ ).

By combining the equations for individual ions to give mean ionic activity coefficients, we obtain for a pair of 1-1 electrolytes

$$\log \gamma_{01} = (1/2)(\log \gamma_{10} + \log \gamma_{20}) \quad (5)$$

and for a 1-1 in the presence of a 2-1 electrolyte

$$\log \gamma_{01} = (1/3)(\log \gamma_{10}) + (3/8)(\log \gamma_{20}) - (1/12)(D_h) \quad (6)$$

Comparison of experimental and computed values are shown in Figures 1-3 (at  $I_1/I = 0$ ). Agreement is very good in most cases, especially in view of uncertainties in literature values of the two-component data, both

of primary isopiestic standards<sup>2</sup> and of extrapolations to infinite dilution (to which this computation is sensitive) of two-component data; two-thirds of the computed values lie within 1 mv. of the linear extrapolation and most values are much better than would be obtained by using the value of  $\log \gamma_{\pm \text{NaCl}}$  at the same ionic strength (*i.e.*, assuming  $\alpha_{12} = 0$ ). Agreement is worst with  $\text{NaClO}_4$  and not very good at some ionic strengths with sodium acetate,  $\text{Na}_2\text{SO}_4$ , and  $\text{BaCl}_2$ .

*Acknowledgments.* The author wishes to acknowledge the very sizable contribution of Dr. J. S. Johnson to this paper. His advice and assistance have greatly improved the final presentation. Thanks are also due to Prof. George Scatchard and to Dr. K. A. Kraus for many helpful discussions during the course of this work.

## Infrared Spectra and Bonding of Nitric Oxide Adsorbed on Nickel and Iron

by George Blyholder and Marvin C. Allen

Department of Chemistry, University of Arkansas, Fayetteville, Arkansas (Received June 21, 1965)

Infrared spectra of NO adsorbed on Ni and Fe have been obtained. The bands for the main NO on Ni structure are at 1840, 650, and 625  $\text{cm}^{-1}$ . These are assigned as the N-O stretch, Ni-N stretch, and Ni-N-O bend, respectively. This assignment gives force constants of 13.0, 5.7, and 0.56  $\text{mdynes}/\text{\AA}$  for these bonds, respectively. A weak band at 2205  $\text{cm}^{-1}$  is tentatively assigned to an adsorbed NO molecule on a site different from that producing the 1840- $\text{cm}^{-1}$  band. Variations in NO stretching frequencies as the NO is adsorbed on different sites are discussed in terms of a molecular orbital model of the Ni-N-O system. NO adsorbed on Fe produces two main bands at 1810 and 1720  $\text{cm}^{-1}$ . On both Ni and Fe some of the NO dissociates to produce a surface oxide which gives very broad infrared bands around 460 and 600  $\text{cm}^{-1}$ , respectively. On neither metal did the addition of  $\text{H}_2$  or  $\text{O}_2$  to the adsorbed NO interact to produce any new surface species.

### Introduction

In studying the structure of species adsorbed on metal surfaces, a large amount of attention has been focused on chemisorbed carbon monoxide with the result that considerable understanding of the nature of the carbon-metal bond formed upon chemisorption has been

gained, as well as information on the effect of chemisorption upon the carbon-oxygen bond. The NO molecule has an electronic structure which greatly resembles CO and yet differs significantly. Thus, NO is a good molecule to use in adsorption studies to see if ideas specifically developed for chemisorbed CO are valid



for other systems and to examine the effect of changing the electronic structure of the adsorbent upon the structure of the adsorbed species while still keeping a relatively similar structure. The molecular orbital view of NO differs from that for CO only in that NO has one electron in an antibonding  $\pi$  orbital that is empty for CO. Thus, for NO which has an excess of two bonding electrons in the  $\sigma$  system and four electrons in two  $\pi$ -bonding orbitals, together with the one electron in a  $\pi$ -antibonding orbital, the bond order is 2.5. For CO with the same electron count except for the antibonding  $\pi$  electron the bond order is 3. The view of chemisorbed CO that has been developed in this laboratory considers the  $\pi$  system for a linear M-C-O structure.<sup>1</sup> Variations in C-O stretching frequencies on a single sample are explained in terms of different electron densities in the  $\pi$  system as the adsorbent metal atom occupies different surface sites. We wish here to examine the ability of this model to account for data for the adsorption of NO on metals.

There has been very little work on the adsorption of NO on metals reported in the literature. Terenin and Roev<sup>2</sup> have investigated the infrared spectra in the 4000- to 1350-cm.<sup>-1</sup> region of NO adsorbed on several alumina-supported metals. They have assigned bands to structures described as ionic, covalent, or coordinative on the basis of comparison of the N-O stretching frequency observed to frequencies for nitrosyl-metal complexes. In a discussion of the paper by Terenin and Roev, Sachtler<sup>3</sup> has reported that NO partially dissociates on Ni and postulated the existence of both chemisorbed NO and oxygen on the basis of mass spectroscopic analysis of the gas phase. Also, Dunkel and Hobert<sup>4</sup> have reported infrared bands for NO adsorbed on silica-supported Pt and Pd.

Infrared spectral studies of gases adsorbed on silica- or alumina-supported metals have the disadvantage that the support limits the spectral range that can be studied to approximately from 4000 to 1350 cm.<sup>-1</sup>. Drawing structural conclusions from such a limited range has disadvantages and eliminates any possibility of observing bands for metal-nitrogen bonds. A technique which allows observation of the entire infrared spectral range for species adsorbed on metals has been developed in this laboratory and is used in this study.

### Experimental Section

The wide spectral range experimental technique, which has been described in detail elsewhere,<sup>5</sup> consists of evaporating Ni from an electrically heated tungsten filament in the presence of a small pressure of helium. The metal particles formed in the gas phase deposit in

an oil film on the salt windows of an infrared cell. The gas to be studied is then admitted to the cell, and the spectrum of the chemisorbed species is obtained. Spectra are recorded before and after admission of the gas to the cell. Five minutes of pumping has been found sufficient to remove all spectra due to gas phase molecules.

Some spectra were also run of species adsorbed on silica-supported metals. The experimental technique, cells, and sample preparation have previously been described in detail.<sup>6</sup> Essentially, a metal nitrate is dispersed on silica (Cab-O-Sil, donated by Godfrey L. Cabot, Inc., Boston, Mass.), pressed into a disk, and the disk is placed in a vacuum cell. The metal nitrate is reduced to metal in a stream of H<sub>2</sub> at temperatures up to 400°. This sample transmits infrared radiation over the range from 4000 to 1300 cm.<sup>-1</sup>.

H<sub>2</sub>, O<sub>2</sub>, and CO were obtained from the Matheson Co., Inc. NO was prepared by the reaction of KNO<sub>2</sub>, KNO<sub>3</sub>, and Cr<sub>2</sub>O<sub>3</sub> as given by Ray and Ogg.<sup>7</sup> All gases were dried by passage through a cold trap. H<sub>2</sub> was passed over hot copper turnings to remove O<sub>2</sub>; CO was passed through an activated-charcoal trap cooled with liquid air.

Spectra were obtained on a Perkin-Elmer Model 337 and a Perkin-Elmer Model 21 spectrophotometer. The latter is equipped with NaCl and CsBr prisms.

### Results

The spectrum of NO chemisorbed on Ni evaporated into hydrocarbon oil is shown in Figure 1. Bands are recorded at 2205 (w), 1840 (s), 650 (w), 625 (m), and about 460 cm.<sup>-1</sup> (svb). The intensity symbols are s, strong, m, medium, w, weak, v, very, and b, broad. In all cases the spectra shown are those recorded after the gas phase indicated in the figures has been pumped out.

The effect of exposure of chemisorbed NO to 10 mm. of O<sub>2</sub> pressure is to leave the band at 2205 cm.<sup>-1</sup> unchanged, reduce the intensity of the 1840-cm.<sup>-1</sup> band to about 10% of its original intensity, eliminate the bands at 650 and 625 cm.<sup>-1</sup>, produce absorption in the 1300-1600-cm.<sup>-1</sup> range, and increase the intensity of the broad band around 460 cm.<sup>-1</sup>.

- (1) G. Blyholder, *J. Phys. Chem.*, **68**, 2772 (1964).
- (2) A. Terenin and L. Roev, *Actes Congr. Intern. Catalyse, 2<sup>e</sup>, Paris, 1960*, 2183 (1961).
- (3) W. M. H. Sachtler, *ibid.*, 2197 (1961).
- (4) H. Dunkel and H. Hobert, *Z. Chem.*, **3**, 398 (1963).
- (5) G. Blyholder, *J. Chem. Phys.*, **36**, 2036 (1962).
- (6) G. Blyholder and L. D. Neff, *J. Phys. Chem.*, **66**, 1464 (1962).
- (7) J. D. Ray and R. A. Ogg, *J. Am. Chem. Soc.*, **78**, 5993 (1956).

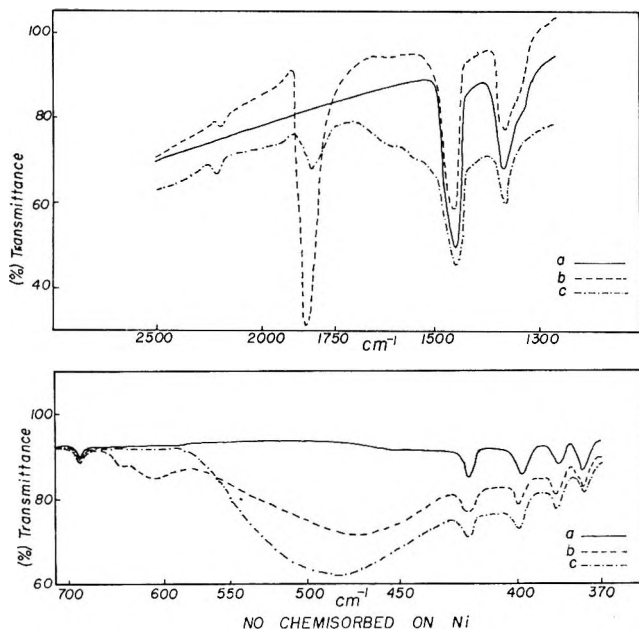


Figure 1. NO chemisorbed on Ni: (a) background, (b) after exposure to 10 mm. of NO for 1 hr., (c) after exposure to 10 mm. of  $O_2$  for 1 hr.

When chemisorbed NO on Ni evaporated into a fluorocarbon oil is exposed to 10 mm. of  $O_2$ , the results are the same as above except that the absorption in the 1300–1600- $cm^{-1}$  range is absent. The infrared region below 1300  $cm^{-1}$  is not observable because of fluorocarbon absorption so the bands in the far-infrared region cannot be checked.

Adsorption of NO on silica-supported Ni produced bands at 2220 (w) and 1840  $cm^{-1}$  (vs). The band at 2220 was removed by 3 hr. of pumping on the cell at  $10^{-5}$  mm.

The addition of 10 mm. of  $H_2$  to a sample of NO adsorbed on evaporated Ni results in the disappearance of the 2205- $cm^{-1}$  band. The intensity of the band originally at 1840  $cm^{-1}$  is reduced to about half of its original value, and the band maximum is shifted to 1800  $cm^{-1}$ . The intensities of the bands at 625 and 650  $cm^{-1}$  are cut about in half, and the broad 460- $cm^{-1}$  band is unchanged. While the band maximum of the 1800- $cm^{-1}$  band is shifted from 1840  $cm^{-1}$ , the envelope for the 1800- $cm^{-1}$  band is entirely within the envelope for the original 1840- $cm^{-1}$  band.

The spectrum of NO chemisorbed on nickel in hydrocarbon oil with CO chemisorbed immediately afterward on the same evaporated nickel sample can be seen in Figure 2. Peaks are recorded at 2180 (w), 2021 (s), 1905 (w), and 1840  $cm^{-1}$  (vs). Only the spectrum from 4000 to 1200  $cm^{-1}$  was recorded since this region was the only region of any real interest.

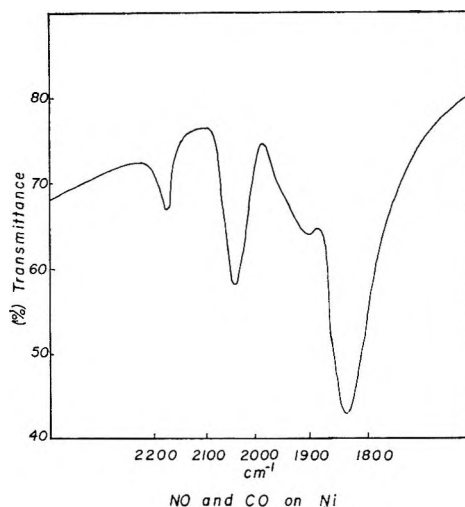


Figure 2. NO and CO chemisorbed on Ni.

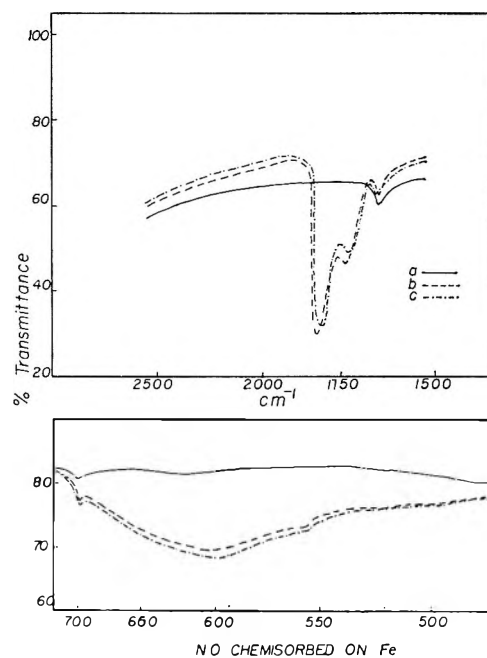


Figure 3. NO chemisorbed on Fe: (a) background, (b) after exposure to 10 mm. of NO for 1 hr., (c) after exposure to 15 mm. of  $H_2$  for 1 hr.

The spectrum of NO chemisorbed at 10 mm. pressure on evaporated Fe is shown in Figure 3. Bands are recorded at 1810 (s), 1720 (m), and 600  $cm^{-1}$  (vb). Addition of 10 mm. of  $H_2$  resulted in a small decrease in intensity and a shift of about 10  $cm^{-1}$  to lower frequencies by the two high-frequency bands. Addition of 10 mm. of  $O_2$  to NO adsorbed on a freshly evaporated Fe sample resulted in the intensities of the 1810- and 1720- $cm^{-1}$  bands dropping to about one-third

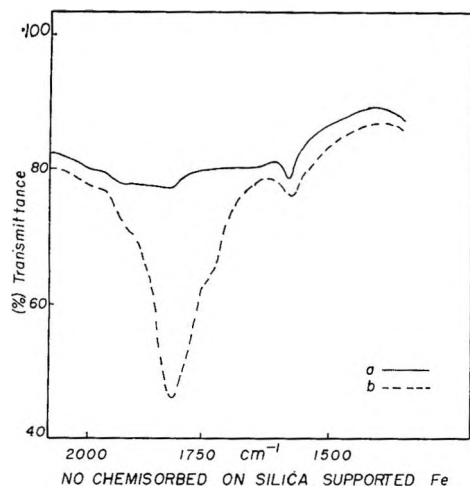


Figure 4. NO chemisorbed on silica-supported Fe: (a) background, (b) after exposure to 8 mm. of NO for 1 hr.

of their original value while the very broad 600-cm.<sup>-1</sup> band increased in intensity. No additional bands were detected after addition of CO to a sample with NO chemisorbed on Fe. The spectrum of NO chemisorbed on silica-supported Fe is shown in Figure 4 to have bands at 1820 and 1720 cm.<sup>-1</sup>, approximately the same as for evaporated Fe. However, the 1820-cm.<sup>-1</sup> band has broadened so that the 1720-cm.<sup>-1</sup> band appears only as a shoulder.

### Discussion

The results for NO adsorbed on Ni show five bands. The very broad band around 460 cm.<sup>-1</sup> has been found to be characteristic of chemisorbed oxygen.<sup>8</sup> This assignment is supported by the fact that the addition of H<sub>2</sub> to chemisorbed NO changes the intensity of the other bands while leaving the 460-cm.<sup>-1</sup> band unchanged, whereas addition of O<sub>2</sub> enhances the intensity of the 460-cm.<sup>-1</sup> band. Thus, one cannot obtain chemisorbed NO as the only adsorbate on a metal surface because NO partially oxidizes the surface so that adsorbed NO must coexist with adsorbed oxygen. This substantiates Sachtler's<sup>3</sup> assumption that there is oxygen on the surface since he detected N<sub>2</sub> in the gas phase after exposing a Ni surface to NO.

The results indicate that the weak 2205-cm.<sup>-1</sup> band, found at 2220 cm.<sup>-1</sup> on silica-supported Ni, behaves independently of the other bands and so should be assigned to an independent structure. This independence is shown by the facts that oxygen treatment greatly reduces the intensity of the 1840-cm.<sup>-1</sup> band while leaving the 2205-cm.<sup>-1</sup> band unchanged and that prolonged pumping on the silica-supported Ni sample removes the 2220-cm.<sup>-1</sup> band.

The three bands at 1840, 650, and 625 cm.<sup>-1</sup> behave as a unit and so are presumed to belong to a single structure. The hydrogen and oxygen treatments which vary the relative intensities of some bands greatly always make the same relative intensity changes in these three bands. Owing to the similarity in frequency of the 1840-cm.<sup>-1</sup> band to that of gas phase NO, this band is presumed to be due to an N-O stretching mode of a chemisorbed species of NO. We turn now to the problem of the structure of this species.

In view of the general unsuitability of molecules adsorbed on metal surfaces for X-ray and electron diffraction studies of structure, we shall have to rely on analogies to coordination complexes as a starting point in considering the structure of chemisorbed NO. It is generally assumed that nitrosyls have a linear M-N-O group, but few direct experimental investigations have been made. Microwave data indicate that the Ni-N-O linkage is linear in  $\pi$ -C<sub>5</sub>H<sub>5</sub>NiNO.<sup>9</sup> A preliminary report of preliminary X-ray work on [(CH<sub>3</sub>)<sub>2</sub>NCS<sub>2</sub>]<sub>2</sub>CoNO has suggested a nonlinear Co-N-O linkage, but this has not been substantiated.<sup>10</sup> In an electron diffraction study, a linear Co-N-O linkage was found to fit the experimental data quite well for Co(CO)<sub>3</sub>NO.<sup>11</sup> A normal coordinate vibrational analysis has also been made of this molecule.<sup>12</sup> The N-O stretch, Co-N stretch, and Co-N-O bend have been assigned to bands at 1822 (s), 594 (w), and 565 cm.<sup>-1</sup> (m), respectively. These assignments lead to a N-O stretching force constant of 14.0 mdynes/Å. and a Co-N stretching force constant of 3.87 mdynes/Å.

Comparison of the three observed bands for NO on Ni at 1840 (s), 650 (w), and 625 cm.<sup>-1</sup> (m) with the three NO-related bands in Co(CO)<sub>3</sub>NO shows a strong correlation. On the basis of this comparison and the general expectation from nitrosyl complexes of a linear system, the chemisorbed species is presumed to have a linear M-N-O linkage. Comparison of both the relative frequencies and intensities of the bending and stretching modes for the adsorbed species to Co(CO)<sub>3</sub>NO suggests the assignment of the bands at 1840, 650, and 625 cm.<sup>-1</sup> to N-O stretching, Ni-N stretching, and Ni-N-O bending modes, respectively.

The possibility of a bridging NO structure has been

(8) G. Blyholder, *Proc. Intern. Congr. Catalysis, 3rd, Amsterdam, 1964*, paper I-38.

(9) A. P. Cox, L. F. Thomas, and J. Sheridan, *Nature*, **181**, 1157 (1958).

(10) P. R. H. Olderman and P. G. Ourston, *ibid.*, **178**, 1071 (1956).

(11) L. D. Brockway and J. S. Anderson, *Trans. Faraday Soc.*, **33**, 1233 (1937).

(12) R. S. McDowell, W. D. Horrocks, Jr., and J. T. Yates, *J. Chem. Phys.*, **34**, 530 (1961).

considered. Bridging NO groups are relatively rare, but recently several compounds have been synthesized which are presumed to have bridging NO groups although no X-ray substantiation of the structures has been published.<sup>13</sup> In these compounds infrared bands for terminal NO groups have been assigned at 1672  $\text{cm}^{-1}$  and for bridging NO groups at 1505  $\text{cm}^{-1}$ . On the basis of these assignments, we have terminal and not bridging NO groups.

In their work Terenin and Roev<sup>2</sup> reported a strong band for NO adsorbed on Ni at 1850  $\text{cm}^{-1}$ , which corresponds well to our strong band at 1840  $\text{cm}^{-1}$ , and, in addition, four very weak bands in the 1750- to 1620- $\text{cm}^{-1}$  region. We observed no bands in this region and can only suggest that their alumina gel support for their Ni had a different influence on the Ni from our silica support and oil bath support.

The separation of the observed frequencies from the upper limit of metal lattice frequencies calculated from the Debye characteristic temperature indicates the adsorbed species may be treated approximately as a free three-atom system. This procedure has received formal mathematical justification.<sup>14</sup> For a linear three-atom system only three fundamental frequencies are predicted, and we have found three. If the linear structure is correct, we have then found all of the fundamentals. Using the free three-atom model, the force constants for the N-O bond stretching, Ni-N bond stretching, and Ni-N-O bending are found to be 13.0, 5.7, and 0.56  $\text{mdynes}/\text{\AA}$ , respectively.

A Hückel molecular orbital calculation, similar to that done<sup>1</sup> for CO adsorbed on metals, for the Ni-N-O  $\pi$ -electron system indicates three molecular orbitals in each of the two planes perpendicular to the bonding axis. An electron count shows that the lowest energy orbital,  $\psi_1$ , which is bonding for both the N-O and Ni-N bonds, would be filled. The highest energy orbital,  $\psi_3$ , would be empty. The second lowest orbital,  $\psi_2$ , which is antibonding for the N-O bond but bonding for the Ni-N bond, is a little lower in energy than an isolated metal d orbital.

The extent of filling of  $\psi_2$  depends on the interaction of metal d orbitals to produce molecular orbitals that can compete with  $\psi_2$  for the available valence-shell electrons and the electron which may be counted as originally in the NO antibonding orbital. This picture has been presented in somewhat more detail<sup>1</sup> for chemisorbed CO, to which the comparison of NO is obvious. The frequency of the C-O or N-O stretch for the adsorbed species decreases as the amount of charge in  $\psi_2$  increases. The amount of charge in  $\psi_2$  is expected to be least on high atom density plane surface sites where the number of metal atoms around the metal atom

to which the adsorbed molecule is bound is 8 or 9, thus providing much d orbital interaction to give metal molecular orbitals to compete for the electrons which could go into  $\psi_2$ . For adsorption on metal atoms at edges, corners, and dislocations where the number of surrounding metal atoms is 4 to 6, there is expected to be less competition and hence more electronic charge in  $\psi_2$ . This picture successfully explains a number of features of CO adsorption on metals.

For NO adsorption the band at 2205  $\text{cm}^{-1}$  is interpreted as adsorption on high atom density plane sites where  $\psi_2$  is relatively empty and an electron which may be counted as originally in the NO antibonding orbital is contributed to essentially metal orbitals. Thus, the N-O stretching frequency is quite similar to that of the  $\text{NO}^+$  ion near 2200  $\text{cm}^{-1}$ . Although other workers have emphasized the ionic nature of NO species giving a band near 2200  $\text{cm}^{-1}$ , we favor an essentially molecular orbital view of the bonding. The band at 2205  $\text{cm}^{-1}$  could be due to an adsorbed  $\text{NO}^+$  ion held to the surface purely by classical ionic attraction. However, the  $\text{NO}^+$  ion is isoelectronic with CO, which apparently does form a covalent bond with the surface. It seems reasonable to us, therefore, to treat the bonding of the species giving rise to the 2205- $\text{cm}^{-1}$  band, which has presumably from the position of the infrared band lost about one electron to become formally  $\text{NO}^+$ , within the same molecular orbital framework as is used for CO and "neutral" NO. If one makes the unsupported assumption that the extinction coefficients for the species producing the bands at 2205 and 1840  $\text{cm}^{-1}$  are not unequal, the amount of adsorption on the plane faces of the metal is relatively small.

The band at 1840  $\text{cm}^{-1}$  is interpreted as a linear Ni-N-O system in which the frequency at 1840  $\text{cm}^{-1}$ , being lower than the gas phase NO band at 1876  $\text{cm}^{-1}$ , indicates back donation of metal electrons into  $\psi_2$  in addition to the NO antibonding electron being retained in  $\psi_2$ . This interpretation is consistent with the adsorption site being edge, corner, and dislocation site atoms that have a low coordination number and hence compete less effectively for electrons.

In previous work<sup>1</sup> the infrared spectrum of CO chemisorbed on Ni has been interpreted in terms of a band around 2060  $\text{cm}^{-1}$  representing CO adsorbed on plane sites and a band around 1940 representing CO adsorbed on edges, corners, and dislocations. To examine the consistency of the NO and CO assignments, CO was adsorbed on a sample which had previously been ex-

(13) R. B. King and M. B. Bisnette, *Inorg. Chem.*, **3**, 791 (1964).

(14) T. B. Grimley, *Proc. Phys. Soc. (London)*, **79**, 1203 (1962).

posed to NO. The result, Figure 2, is bands at 2180 (w), 2020 (s), 1905 (w), and 1840  $\text{cm}^{-1}$  (vs). The bands at 2180 (slightly shifted from 2205) and 1840  $\text{cm}^{-1}$  for adsorbed NO were of about the same intensity as before, indicating that CO did not displace the adsorbed NO. For CO alone, adsorbed on evaporated Ni, the band in the 1900- $\text{cm}^{-1}$  region is more intense than the band above 2000  $\text{cm}^{-1}$ . The intensity of the CO bands, therefore, indicates that most of the edge, corner, and dislocation sites are covered with NO while most of the plane sites are not covered with NO. This is in accord with our previous interpretation of the adsorbed NO bands.

The analogy of adsorbed species to coordination complexes has most usually been made on the basis of stretching frequencies for bonds strictly within the adsorbate. Here, we see that comparison of the physical properties of the metal adsorbate, in this case Ni-N stretching and Ni-N-O bending frequencies and force constants, to complexes, in this case  $\text{Co}(\text{CO})_3\text{NO}$ , supports the similarity of the bonding. Using this comparison to look at the Ni-N bond order, it is noted that metal-nitrogen force constants for a number of ammine complexes are from 1 to 3  $\text{mdynes}/\text{\AA}$ .<sup>15</sup> Since this bond must be a single bond, the Ni-N bond for adsorbed NO is seen to have considerable double-bond character.

Admission of  $\text{H}_2$  at 10 mm. pressure to a cell at 20° with NO chemisorbed on Ni did not produce any infrared evidence of a new surface species formed by NO and  $\text{H}_2$  interaction. In fact, the  $\text{H}_2$  apparently caused the desorption of about half of the adsorbed NO responsible for the 1840- $\text{cm}^{-1}$  band and all of that responsible for the 2205- $\text{cm}^{-1}$  band. Hydrogen is generally believed to chemisorb with donation of electrons to the metal. This is expected to decrease the ability of the Ni atoms to accept charge from the NO when it chemisorbs. Apparently, this effect is strong enough that all of the NO on the relatively more saturated plane face sites that give rise to the 2205- $\text{cm}^{-1}$  band desorb and only the more strongly held NO on edge sites remain. The molecular orbital picture of the nature of  $\psi_2$  as an antibonding orbital for the NO bond and a bonding orbital for the metal-nitrogen bond indicates that the NO which is most tightly held to the surface will have the lowest frequency N-O stretch. The shift in the band maximum from 1840 to 1800  $\text{cm}^{-1}$  as NO desorbs as a consequence of the  $\text{H}_2$  treatment is then seen to be a result of the more weakly held NO being desorbed first.

Addition of 10 mm. of  $\text{O}_2$  at 20° to a cell with chemisorbed NO on Ni does not appear to produce any new species. The only effect of  $\text{O}_2$  observable in our spectra

is to cause desorption of much of the adsorbed NO and the production of more surface oxide. This is in marked contrast to the behavior of CO adsorbed on Ni, which upon exposure to  $\text{O}_2$  is oxidized to a bidentate carbonate complex.<sup>8</sup> The absorption in the 1300-1600- $\text{cm}^{-1}$  region produced by adding  $\text{O}_2$  to chemisorbed NO is assigned to  $\text{O}_2$  and hydrocarbon oil interaction on the Ni surface since absorption in this region is observed when only  $\text{O}_2$  is added to a freshly evaporated Ni sample.<sup>8</sup> This interpretation is further substantiated by the fact that, when NO adsorbed on Ni evaporated into a fluorocarbon oil is exposed to  $\text{O}_2$ , no absorption in the 1300-1600- $\text{cm}^{-1}$  range is observed.

In order to see if the oil was having an effect on the structure of adsorbed NO species, the spectrum of NO adsorbed on silica-supported Ni was obtained. The only change noted was a small shift of the weak band at 2205  $\text{cm}^{-1}$  to a slightly higher frequency. Since the intense 1840- $\text{cm}^{-1}$  band is unchanged, the oil is presumed not to have a substantial effect on the structure of the adsorbed NO on Ni.

The spectrum of NO chemisorbed on Fe shows two main bands at 1810 and 1720  $\text{cm}^{-1}$ , which by analogy to NO adsorbed on Ni are presumed to be due to linear M-N-O systems. The presence of two bands is interpreted, on the basis of the molecular orbital picture of adsorbed NO, to be the result of adsorption on edge, dislocation, and other low coordination number sites to give the 1720- $\text{cm}^{-1}$  band while the 1810- $\text{cm}^{-1}$  band is due to NO adsorbed on high coordination number plane face sites. The very broad band around 600  $\text{cm}^{-1}$  is taken as indicating dissociation of some of the NO to produce a surface oxide. Oxygen adsorbed on a freshly evaporated Fe sample produces a broad band around 600  $\text{cm}^{-1}$ .<sup>16</sup> Since  $\text{Fe}_2\text{O}_3$  solid has a broad band near 600  $\text{cm}^{-1}$ ,<sup>17</sup> this band for adsorbed oxygen is presumed due to the formation of a surface oxide. No bands were identified as being due to the Fe-N stretching or Fe-N-O bending modes. Presumably, these bands are obscured by the broad oxide band. Exposure of a chemisorbed NO on Fe sample to CO does not produce any bands attributable to adsorbed CO. This is consistent with the interpretation that both the high and low coordination number sites are covered by NO.

Neither the addition of  $\text{H}_2$  nor  $\text{O}_2$  to a cell with chemisorbed NO on Fe produced any new surface species

(15) K. Nakamoto, "Infrared Spectra of Inorganic and Coordination Compounds," John Wiley and Sons, Inc., New York, N. Y., 1963.

(16) G. Blyholder and M. Allen, *J. Phys. Chem.*, in press.

(17) E. A. Richardson, Ph.D. Dissertation, University of Arkansas, 1962.

detectable in our spectra.  $H_2$  results in a small shift in the NO stretching frequencies to lower wave numbers which is consistent with the previous interpretation of  $H_2$  donating electrons to the metal upon adsorption. The addition of  $O_2$  resulted in the desorption of much of the NO as indicated by the decrease in the 1810- and 1720-cm.<sup>-1</sup> bands.  $O_2$  also as expected increased the intensity of the 600-cm.<sup>-1</sup> band which has been interpreted as a surface oxide.

The similarity of the NO stretching bands at 1820 and 1720 cm.<sup>-1</sup> for NO adsorbed on silica-supported Fe to the bands for evaporated-into-oil Fe indicates that the oil does not substantially affect the nature of the adsorbed NO.

In view of the previously pointed out problems in obtaining structural information other than infrared, it would be difficult to obtain direct, firm experimental evidence for or against the bands at 2205 and 1840 cm.<sup>-1</sup> on Ni and at 1810 and 1720 cm.<sup>-1</sup> on Fe being, as suggested, due to NO adsorption on different types of sites. This suggestion is largely based on the lack of infrared bands in these regions for other known NO-containing molecules with different structures and the fact that a consistent picture of the electronic structure based on the suggested molecular structure could be built.

Over-all, the molecular orbital view seems to furnish a reasonable framework in which to consider the adsorption of NO on Ni and Fe. The finding of infrared frequencies for modes involving primarily the Ni-N bond allowed the nature of the metal-adsorbate bond to be discussed in some detail. Unfortunately, the data for Fe did not turn out to be nearly so complete. If the assumption is made that the  $\sigma$  bonds for the Ni-N and Ni-C bonds are equivalent, then the molecular orbital view of the bonding system should furnish a consistent interpretation of the relative values of the frequencies and force constants for the various bonds. Since the N-O frequency at 1840 cm.<sup>-1</sup> is less than the C-O frequency at 1940 cm.<sup>-1</sup>,<sup>8</sup> if the filling of  $\psi_2$  is the dominant factor in this difference, then the Ni-C stretching frequency should be lower than the Ni-N frequency. The Ni-C frequency<sup>8</sup> at 435 cm.<sup>-1</sup> and the Ni-N frequency at 650 cm.<sup>-1</sup> confirm this expectation. As expected, NO produces chemisorbed species quite similar to those of CO and, as hoped for both sets of species, can be set into a single framework.

*Acknowledgment.* Acknowledgment is made to the donors of the Petroleum Research Fund, administered by the American Chemical Society, for partial support of this research.

## Potentiometric Titration of Stereoregular Polyelectrolytes

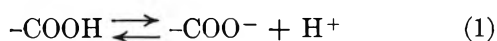
by Mitsuru Nagasawa, Takashi Murase, and Kotaro Kondo

Department of Synthetic Chemistry, Nagoya University, Chikusa-ku, Nagoya, Japan (Received June 21, 1965)

The potentiometric titration curves of conventional, isotactic and syndiotactic poly(methacrylic acid) were obtained in the presence of various concentrations of sodium chloride. The values of  $\text{pH} + \log [(1 - \alpha)/\alpha]$  for the isotactic form are always higher than those of the syndiotactic polymer; that is, it requires greater work to remove  $\text{H}^+$  from the former than from the latter. The corresponding values for the conventional poly(methacrylic acid) are intermediate. The difference between the two stereoregular polyacids may be accounted for by assuming that the isotactic poly(methacrylic acid) has a "locally" helical structure in solution. There are qualitative differences in the potentiometric titration behavior of poly(methacrylic acid) and poly(acrylic acid). It is observed that the electrostatic work required to remove  $\text{H}^+$  from the surface of a polymer rod calculated by Kotin and Nagasawa is in good agreement with the experimental results of syndiotactic or atactic poly(methacrylic acid) but disagrees with the results for poly(acrylic acid). If the comparison is confined only to experiments at a constant degree of neutralization, however, the data for poly(acrylic acid) are also in accord with the calculated results. This difference observed between poly(methacrylic acid) and poly(acrylic acid) seems to be due to a difference in over-all chain flexibility.

### Introduction

A carboxylic acid in aqueous solution dissociates as



Its thermodynamic dissociation constant,  $K_a$ , is expressed by

$$K_a = \frac{(-\text{COO}^-)(\text{H}^+)}{(-\text{COOH})} \quad (2)$$

where parentheses denote the activity of each species. Often, however, the conventional dissociation constant,  $K_0$ , defined by

$$K_0 = \frac{[-\text{COO}^-][\text{H}^+]}{[-\text{COOH}]} \quad (2')$$

is used instead of  $K_a$  since we do not know the activities (in parentheses) of  $-\text{COO}^-$  and  $-\text{COOH}$  but only their analytical concentrations (in brackets). Therefore,  $K_0$  is not always a true constant, while  $K_a$  must be.

Equation 2' can be written

$$\text{pH} = \text{p}K_0 - \log [(1 - \alpha)/\alpha] \quad (3)$$

where the degree of ionization  $\alpha$  is defined by

$$\alpha = \frac{[-\text{COO}^-]}{[-\text{COO}^-] + [-\text{COOH}]} \quad (4)$$

Ignoring the distinction between eq. 2 and 2',  $\text{p}K_0$  may be related to the standard free energy change of the dissociation process,  $\Delta G^\circ$ , as

$$\text{p}K_0 = -\log K_0 = 0.434\Delta G^\circ/RT \quad (5)$$

In the dissociation of polyelectrolytes, however, an additional amount of work,  $\Delta G_{e1}$ , is required; *i.e.*, it is necessary to remove  $\text{H}^+$  against the strong electrostatic forces of the charges already present in the molecule. Thus, eq. 3 must be modified to read

$$\text{pH} = \text{p}K_0 - \log [(1 - \alpha)/\alpha] + 0.434\Delta G_{e1}/RT \quad (6)$$

Here,  $\Delta G_{e1}$  can be expressed as

$$\Delta G_{e1} = e\psi_b \quad (7)$$

in terms of the electrostatic potential at the place where  $\text{H}^+$  originally exists,  $\psi_b$ .  $\Delta G_{e1}$  may also be expressed by

$$\Delta G_{e1} = \partial G_{e1}/\partial \nu \quad (8)$$



where  $G_{el}$  is the electrostatic free energy of the polyion having  $\nu$  ionized groups.

Equations 6–8 have been derived by several authors.<sup>1–5</sup> Among researchers, however, two different approaches are in common use for evaluating the potential  $\psi_b$  of eq. 7. In one approach, it is assumed that  $\psi_b$  is an average electrostatic potential within the polyion domain; this is sometimes evaluated as the electrostatic potential solved for a sphere model with uniformly distributed segments<sup>3</sup> or as the surface potential of a sphere determined from the observed electrophoretic velocity<sup>6,7</sup> of the polyion. In the other approach, it is assumed<sup>4,8–14</sup> that the polyion is a coiled thread or rodlike molecule and that the  $H^+$  is ionized from the surface of the rod. Thus,  $\psi_b$  can be assumed to be the electrostatic potential on the rod surface. Kotin and Nagasawa<sup>13</sup> reported that the latter model may be more appropriate for explaining dissociation phenomena in polyelectrolytes. They showed that good agreement between experiment and theory is obtained if  $\psi_b$  is calculated from the Poisson–Boltzmann equation

$$\begin{aligned}\nabla^2\Psi &= -\frac{4\pi}{D}\rho \\ &= -\frac{4\pi e N_{av}}{D 10^3}C_s[e^{-e\psi/kT} - e^{e\psi/kT}]\end{aligned}\quad (9)$$

where  $C_s$  is the molar concentration of added 1-1 electrolyte, using numerical integration performed on a high speed electronic computer. Later, Alexandrowicz and Katchalsky<sup>14</sup> presented an analytical calculation which leads to the same  $\Psi_b$  as is obtained by the numerical integration. It must be stressed that the use of the rod model in this context does not require that the polyion be fully elongated but only that its radius of curvature be large compared to the ionic atmosphere around the polyion skeleton.

Several important differences are found between potentiometric titration curves calculated from these two approaches. If the dissociation of the carboxyl group is governed by the average electrostatic potential inside the polymer domain, several characteristics should be observed: (1) the data should depend on the molecular weight of the polymer; (2) the potentiometric titration curves of maleic acid copolymers should not show the characteristic features of dibasic acids; (3) the stereoregularity of the polyelectrolyte should have little effect on potentiometric titration behavior since expansion of the polymer coil is little affected by stereoregularity.<sup>15</sup> On the other hand, if the rodlike model is employed, the opposite prediction would have to be made on all three points.

It is well known<sup>3,16</sup> that the potentiometric titration curve of a polyelectrolyte is independent of the molecular weight. It has also been reported many times that the potentiometric titration curves of maleic acid copolymers show the features characteristic of dibasic acids.<sup>12,17–19</sup> Thus, two of the listed experimental tests of the models have provided strong evidence in favor of the rod model.

However, the third possibility, the potentiometric titration of stereoregular polyelectrolytes, has not yet been fully studied although a few fragmentary results have appeared. Loebel and O'Neill<sup>20</sup> reported that the isotactic poly(methacrylic acid) is a weaker acid than the syndiotactic one and that their apparent dissociation constants differ by about 0.3 pK unit. Sakaguchi, Sakurada, *et al.*,<sup>21</sup> also reported a difference between the two forms of poly(methacrylic acid). On the other hand, Botty and Rauhut<sup>22</sup> detected no difference between the isotactic and atactic forms of poly(acrylic acid). Considering the differences in the conclusions of these authors and the accuracy of their experiments, it seemed desirable to perform similar experiments more carefully.

The purpose of the present paper is to report the

- (1) J. Th. G. Overbeek, *Bull. soc. chim. Belges*, **57**, 252 (1948).
- (2) A. Katchalsky and J. Gillis, *Rec. trav. chim.*, **68**, 879 (1949).
- (3) A. Arnold and J. Th. G. Overbeek, *ibid.*, **69**, 192 (1950).
- (4) F. E. Harris and S. A. Rice, *J. Phys. Chem.*, **58**, 725, 733 (1954).
- (5) G. S. Hartley and J. W. Roe, *Trans. Faraday Soc.*, **36**, 101 (1940).
- (6) A. Katchalsky, N. Shavit, and H. Eisenberg, *J. Polymer Sci.*, **13**, 69 (1954).
- (7) I. Sakurada, M. Hosono, and N. Ise, *Kobunshi Kagaku*, **15**, 175 (1958).
- (8) R. A. Marcus, *J. Phys. Chem.*, **58**, 621 (1954).
- (9) I. Kagawa and H. P. Gregor, *J. Polymer Sci.*, **23**, 477 (1957).
- (10) S. Lifson, *J. Chem. Phys.*, **26**, 727 (1957).
- (11) S. Lifson, B. Kaufman, and H. Lifson, *ibid.*, **27**, 1356 (1957).
- (12) M. Nagasawa and S. A. Rice, *J. Am. Chem. Soc.*, **82**, 5070 (1960).
- (13) L. Kotin and M. Nagasawa, *J. Chem. Phys.*, **36**, 873 (1962).
- (14) Z. Alexandrowicz and A. Katchalsky, *J. Polymer Sci.*, **A1**, 3231 (1963).
- (15) For example, G. V. Schulz, W. Wunderlich, and R. Kirste, *Makromol. Chem.*, **75**, 22 (1964).
- (16) W. Kern, *Z. physik. Chem. (Leipzig)*, **A181**, 249 (1938).
- (17) J. D. Ferry, D. C. Udy, F. C. Wu, G. E. Hockler, and D. B. Fordyce, *J. Colloid Sci.*, **6**, 429 (1951).
- (18) W. Dannhauser, W. H. Glaze, R. L. Dueltgen, and K. Ninomiya, *J. Phys. Chem.*, **64**, 954 (1960).
- (19) K. Monobe, *Rev. Phys. Chem. Japan*, **30**, 138 (1960); **31**, 50 (1961).
- (20) E. M. Loebel and J. J. O'Neill, *J. Polymer Sci.*, **45**, 538 (1960).
- (21) Y. Sakaguchi, *et al.*, *Kobunshi Kagaku*, **19**, 620 (1962); **20**, 81, 456, 657 (1963).
- (22) M. L. Miller, K. O'Donnell, and J. Skogman, *J. Colloid Sci.*, **17**, 649 (1962).



difference between the potentiometric titration curves of isotactic and syndiotactic poly(methacrylic acid). Our results confirm the conclusion drawn from other experiments that the rodlike model is more appropriate for explaining ionization phenomena in polyelectrolytes than the sphere model. We find, in particular, that the potentiometric titration curves of the syndiotactic form agree with the ones calculated for this model by the methods of Kotin and Nagasawa. Furthermore, the difference between the stereoregular poly(methacrylic acid)s can be well accounted for by assuming that the isotactic form has a locally helical conformation whereas the syndiotactic one has a planar zigzag conformation.

In addition, precise potentiometric titration data of a conventional (presumably atactic) sample of poly(acrylic acid) are shown for reference. The results show a qualitative difference in the shape of the titration curves of poly(methacrylic acid) and poly(acrylic acid), the difference probably being due to the differing flexibility of their backbone chains.

### Experimental Section

**Samples.** Isotactic poly(methyl methacrylate), P(MMA),<sup>23</sup> was kindly provided by Dr. M. Ishii of the Mitsubishi Rayon Co. The n.m.r. spectrum of the sample, which was run on a JNMC-60 spectrometer (Japan Electron Optics Lab., Tokyo, Japan), is shown in Figure 1(A). The degree of tacticity, calculated from the  $\alpha$ -methyl peak, is  $I = 0.78$ . It is well known<sup>24-28</sup> that complete hydrolysis of P(MMA) is difficult to effect but that isotactic P(MMA) can be hydrolyzed more easily than atactic P(MMA). Several methods were tried, and the following procedure<sup>28</sup> was found to be satisfactory. Isotactic P(MMA) was dissolved in 98% H<sub>2</sub>SO<sub>4</sub> and heated over a water bath for about 1 hr. Vigorous bubbling of N<sub>2</sub> was provided to prevent oxidation and to remove the methanol produced. The sulfuric acid digest was diluted with about five volumes of water and dialyzed against water. The aqueous polymer solution was then neutralized with NaOH. The resulting sodium salt of poly(methacrylic acid), P(NaMA), was purified by repeated precipitation from its aqueous solution with methanol. The degree of hydrolysis was 98% when calculated from the dry weight and the acid-group content of the sample. The n.m.r. spectrum of the isotactic P(NaMA) thus obtained was taken in D<sub>2</sub>O, as shown in Figure 1(B). It is observed that the peak of the methyl ester group disappeared completely.<sup>29,30</sup>

The molecular weight of the isotactic P(MAA) is  $4.8 \times 10^4$  as calculated from  $[\eta]$  in 0.002 N HCl at

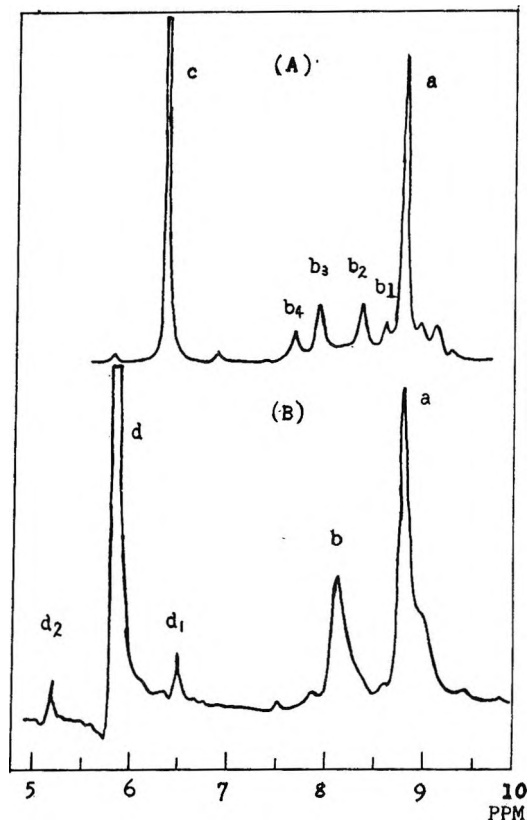


Figure 1. The n.m.r. spectra of the isotactic poly(methyl methacrylate) in CHCl<sub>3</sub> (A) and of poly(sodium methacrylate) in D<sub>2</sub>O (B). Temperature: A, 51°; B, 62°. Concentrations: A, ~10%; B, not determined. Peaks: a, CH<sub>3</sub>; b, CH<sub>2</sub>; c, COOCH<sub>3</sub>; d, DHO; d<sub>1</sub> and d<sub>2</sub>, side bands. The absolute positions of peaks were not well assigned.

30°, using the equation as obtained for conventional P(MAA).<sup>31</sup>

(23) According to a private communication from Dr. Ishii, this sample was polymerized with a phenylmagnesium bromide catalyst in toluene at 3°. The  $J$  value determined from the infrared spectrum is 27.6, and no absorption was observed at 1063 cm<sup>-1</sup>. The density of the sample film measured in cyclohexane-carbon tetrachloride is 1.22.

(24) H. Morawetz and P. E. Zimmerman, *J. Phys. Chem.*, **58**, 753 (1954).

(25) H. Morawetz and E. W. Westhead, *J. Polymer Sci.*, **16**, 273 (1955).

(26) H. Morawetz and J. Oreskes, *J. Am. Chem. Soc.*, **80**, 2591 (1958).

(27) F. J. Glavis, *J. Polymer Sci.*, **45**, 461 (1960).

(28) G. Smets and W. de Loecker, *ibid.*, **45**, 461 (1960).

(29) It is observed that the well-known feature of isotactic P(MAA), *i.e.*, the presence of four peaks for the CH<sub>2</sub> group, disappeared completely after hydrolysis. The reason is not clear at present, but a similar phenomenon was reported for isotactic poly(vinyl chloride).<sup>30</sup>

(30) S. Satoh, R. Chujo and E. Nagai, *Rept. Progr. Polymer Phys. Japan*, **7**, 299, 301 (1964).

(31) A. Katchalsky and H. Eisenberg, *J. Polymer Sci.*, **6**, 145 (1950).

$$[\eta] = 6.6 \times 10^{-4} M^{0.5} \text{ (100 ml./g.)} \quad (10)$$

Syndiotactic P(MAA), which was polymerized at a low temperature in methanol by initiation with  $\gamma$  rays of  $\text{Co}^{60}$ , was kindly provided by Dr. T. Matsuda of the Government Industrial Research Institute, Nagoya.<sup>32</sup> The purification process was the same as for the isotactic P(MAA). To determine the tacticity of the acid, it was converted to the methyl ester with dimethylamine in dioxane, and its n.m.r. spectrum was taken in chloroform. From the n.m.r. pattern, its tacticity was found to be  $S = 0.77$ , which is almost equal to the value obtained from the infrared spectrum.<sup>32</sup> The molecular weight of the sample was also determined from  $[\eta]$  using eq. 10 ( $M = 1.7 \times 10^4$ ).

The atactic P(MAA) used was a conventional one polymerized with ultraviolet initiation and purified by a similar method. The molecular weight is  $64 \times 10^4$ , and the tacticity determined by the same method is  $S = 0.58$ .

That  $\text{pH} + \log [(1 - \alpha)/\alpha]$  is independent of molecular weight was confirmed by using poly(acrylic acid), P(AA), of different molecular weights as used in a previous paper<sup>33</sup> though the lowest degree of polymerization used was 230, a little higher than that of the syndiotactic P(MAA), *i.e.*, 200. However, the sample of P(AA) mainly used was an unfractionated one, and its molecular weight is  $15 \times 10^4$ .

The sodium salts of all samples were converted to acid forms by passing them through a mixed-bed ion-exchange-resin column of Amberlite IR 120 and 400.

*pH Measurement.* A Horiba Model P pH meter was used with Beckman standard buffers. The sensitivity of the instrument is 0.002 pH unit. The titration was carried out in a nitrogen atmosphere at room temperature ( $23 \pm 2^\circ$  for P(MAA),  $15 \pm 2^\circ$  for P(AA)) using standard NaOH solutions delivered with a microburet. Fluctuations of the room temperature did not have any noticeable effect on the values of  $\text{pH} + \log [(1 - \alpha)/\alpha]$  obtained. The titration procedure was the same as described elsewhere.<sup>34,35</sup> Most of the standard NaOH solutions used contained NaCl of concentrations equal to that in the sample solutions. When NaCl is not contained in the titrating solutions, the ionic strength of the sample decreases during the course of the titration; however, the error is minor and was eliminated by extrapolating the data to infinite dilution of the polymer.

To calculate the degree of ionization,  $\alpha$ , at low degrees of neutralization, a correction for  $\text{H}^+$  concentration was made on the assumption that the activity coef-

ficient of  $\text{H}^+$  in the solution is equal to that of HCl at the same ionic strength.

*Calculation of  $\Psi_b$ .* The method has been reported by Kotin and Nagasawa in a previous paper.<sup>13</sup> The calculated values used here are the ones reported in that paper.<sup>36</sup> However, in comparing experimental and theoretical values, we must use the potential at the molecular surface, whereas the quantity calculated directly from the Poisson-Boltzmann equation is the potential at the distance of closest approach of the counterions,  $\Psi_a$ .<sup>34</sup> This correction is readily made using the relation

$$\frac{e\Psi_b}{kT} = \frac{e\Psi_a}{kT} + B\left(\frac{Z}{L}\right) \quad (11)$$

where  $Z$  is the total charge number of a polyion and  $L$  is the length of the fully stretched polymer.  $\Psi_a$  can be obtained from the computer solutions to eq. 9. Strictly, the constant  $B$  is defined by

$$B = \frac{2e^2}{DkT} \ln \frac{a}{b} \quad (12)$$

In practice, however,  $B$  is best treated as an adjustable parameter, chosen to fit the data best, so long as the value of  $a - b$  needed to produce agreement is roughly of the dimensions of a salt ion. A discussion of  $B$  has been given by Nagasawa and Holtzer.<sup>34</sup>

## Results

Data on the potentiometric titration of polyelectrolytes depend on the polymer concentration if the ionic strength from added salt is not high. This is because  $G_{ei}$  of eq. 6 or 8 is changed by dilution because of polymer-polymer interactions. Figure 2 shows two examples of the dependence of  $\text{pH} + \log [(1 - \alpha)/\alpha]$  on the polymer concentration in media of high and low ionic strengths. It is observed that, while  $\text{pH} + \log [(1 - \alpha)/\alpha]$  is practically independent of the polymer concentration at high ionic strength, it is markedly dependent on the polymer concentration at low ionic

(32) T. Matsuda, H. Yamakita, and Y. Sakai, *Kobunshi Kagaku*, **20**, 614 (1963).

(33) A. Takahashi and M. Nagasawa, *J. Am. Chem. Soc.*, **86**, 543 (1964).

(34) M. Nagasawa and A. Holtzer, *ibid.*, **86**, 531 (1964).

(35) M. Nagasawa and A. Holtzer, *ibid.*, **86**, 538 (1964).

(36) There was a mistake in reading the computer results in the paper of ref. 13. The calculated curves shown in Figure 3 of the paper should be slightly higher than the curves shown (about 0.15 pH unit at  $\alpha = 1$  for all NaCl concentrations). The corrected figure is almost the same as the figure shown if  $\text{p}K_0 = 4.72$  is used instead of  $\text{p}K_0 = 4.85$  used in the paper. The calculated curves shown in Figures 4 and 5 of the paper were also slightly lower than the correct curves. However, no change is required in the conclusions of the paper.

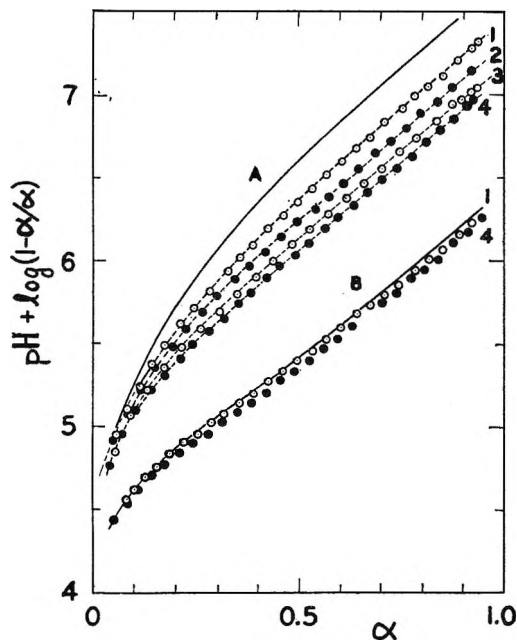


Figure 2. Examples of  $\text{pH} + \log [(1 - \alpha)/\alpha]$  vs.  $\alpha$  plots at various polymer concentrations for poly(acrylic acid). NaCl concentrations: A, 0.005; B, 0.100 *N*. Polymer concentrations: 1, 0.00829; 2, 0.0193; 3, 0.0335; 4, 0.0419 *N*. Temperature  $14 \pm 2^\circ$ ; solid lines show the values extrapolated to infinite dilution.

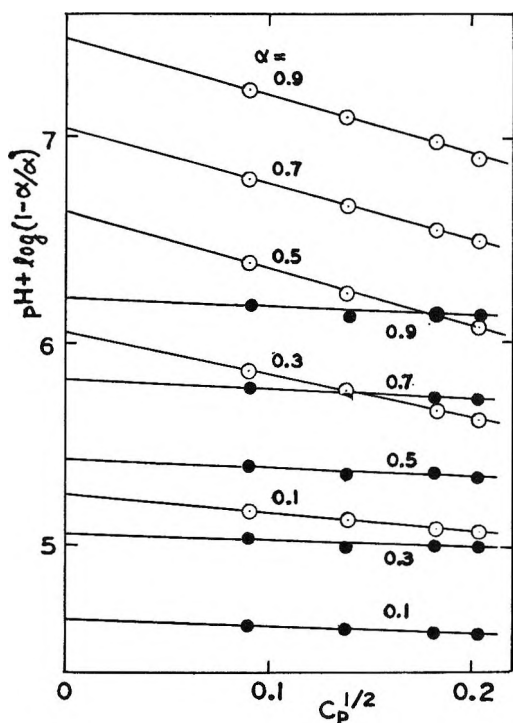


Figure 3. Examples of the linear relationship between  $\text{pH} + \log [(1 - \alpha)/\alpha]$  and the reciprocal root of polymer concentration (monomer moles per liter) at various degrees of neutralization for poly(acrylic acid). NaCl concentrations: A, black circles, 0.100 *N*; B, white circles, 0.00500 *N*. Temperature  $15 \pm 2^\circ$ .

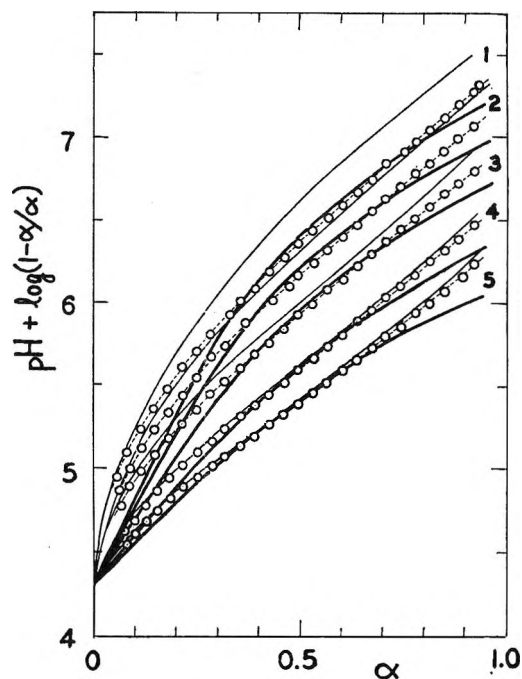


Figure 4. The potentiometric titration curves of poly(acrylic acid) at  $15 \pm 2^\circ$ . NaCl concentrations: 1, 0.00500; 2, 0.0100; 3, 0.0200; 4, 0.0500; 5, 0.100 *N*. The circles show the experimental values at the lowest polymer concentration (0.00829 *N*). The thin solid lines are the experimental values extrapolated to infinite dilution. The thick solid lines are the values calculated by Kotin and Nagasawa assuming  $a = 5.5 \times 10^{-8}$  cm.

strength. Therefore, an extrapolation to infinite dilution is required to obtain the "intrinsic" potentiometric titration curve. In the present paper, the extrapolation was carried out using a plot of  $\text{pH} + \log [(1 - \alpha)/\alpha]$  vs. the square root of the polymer concentration,  $C_p^{1/2}$ , since a good linear relationship was found between them. The linear relationships found for the data of Figure 2 are shown as examples in Figure 3. When the standard NaOH solutions did not contain NaCl, such linearity was not observed, and, hence, the extrapolation was done quite empirically.

The values of  $\text{pH} + \log [(1 - \alpha)/\alpha]$  thus extrapolated are shown in Figure 4 for P(AA) and in Figure 5 for P(MAA). In those figures, the experimental data obtained at the lowest polymer concentrations are shown in the same figures for reference.

There are several clear differences in behavior between P(AA) and P(MAA). First, there is the abnormal rise of  $\text{pH} + \log [(1 - \alpha)/\alpha]$  of P(MAA) at low degrees of neutralization. This abnormality is not observed for P(AA) which is more soluble than P(MAA). Leyte and Mandel<sup>37</sup> reported that this

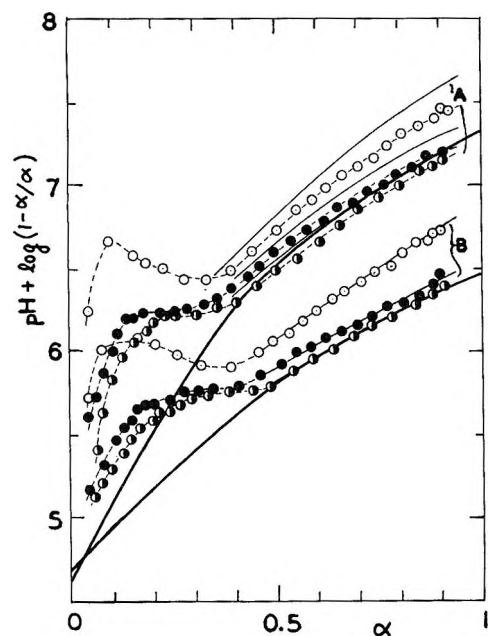


Figure 5. Examples of the potentiometric titration curves of poly(methacrylic acid) at  $23 \pm 2^\circ$ . NaCl concentrations: A, 0.0100; B, 0.100 *N*. The white, black, and half-black circles show experimental data at the lowest polymer concentrations of the isotactic, atactic, and syndiotactic forms, respectively. The thin solid lines are the values extrapolated to infinite dilution. The thick solid lines are the values calculated by Kotin and Nagasawa assuming  $a = 5.5 \times 10^{-8}$  cm. (The thin solid lines of the syndiotactic form are covered by the thick solid lines. All figures at 0.0500, 0.0200, and 0.00500 *N* NaCl are similar to the figures shown.)

feature is due to a molecular conformational transition of P(MAA). However, any discussion of this effect is beside the purpose of this paper. Second, the curves of  $\text{pH} + \log [(1 - \alpha)/\alpha]$  vs.  $\alpha$  of P(MAA) are concave downward, whereas those of P(AA) are clearly inflected. This difference is discussed in the following section.

In Figure 5, the potentiometric titration curves of isotactic, atactic, and syndiotactic P(MAA)'s are compared at two ionic strengths. Very similar curves were also obtained at three other ionic strengths. It is observed that the curve of the isotactic P(MAA) is always higher than that of the syndiotactic one. That is, the carboxylic acid groups of the isotactic P(MAA) are closer together than those of the syndiotactic one, so that more electrostatic work is required to remove  $\text{H}^+$  from the former than from the latter. The work necessary to remove a proton from the fully neutralized syndiotactic P(MAA) is approximately equal to that necessary to remove one from the isotactic P(MAA) of about 74% neutralization (75, 72, 73, 74, and 77% at 0.1, 0.05, 0.02, 0.01, and 0.005 *N*

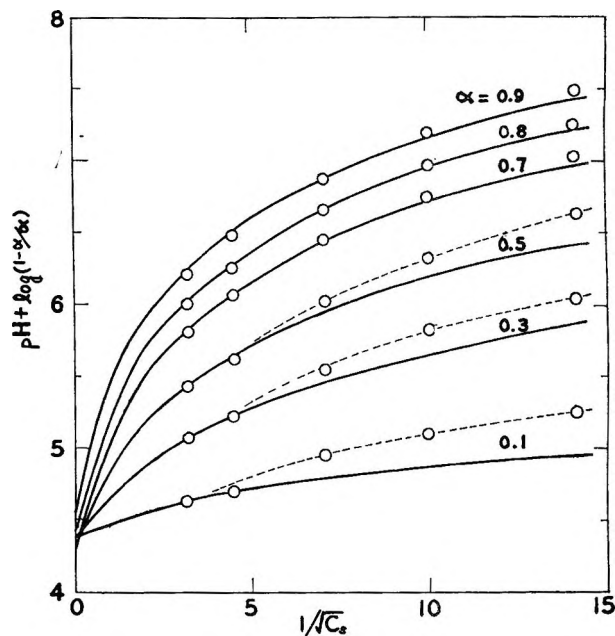


Figure 6. The relationship between  $\text{pH} + \log [(1 - \alpha)/\alpha]$  and the ionic strength of solvent at various degrees of neutralization of poly(acrylic acid). The thick solid lines are the values calculated by Kotin and Nagasawa assuming  $a = 5.5 \times 10^{-8}$  cm.; temperature  $15 \pm 2^\circ$ .

NaCl, respectively). The curve for atactic P(MAA) always falls between those of the two stereoregular P(MAA)'s.

## Discussion

*Comparison of P(AA) and P(MAA).* It has already been reported<sup>13</sup> that the experimental plots of  $\text{pH} + \log [(1 - \alpha)/\alpha]$  vs.  $\alpha$  for P(MAA) are in agreement with the calculated ones. Such agreement is also observed in the present work. The calculated curves of  $0.434 e\psi_b/kT$  vs.  $\alpha$  (assuming  $\text{p}K_0$  of P(MAA) = 4.67 and 4.60 at 0.1 and 0.01 *N* NaCl, respectively, and  $B = 0$ )<sup>38</sup> are shown by thick lines in Figures 4 and 5. The agreement between the calculated and experimental curves of syndiotactic P(MAA) in Figure 5 is very good at high degrees of neutralization. The agreement is also very good at other ionic strengths.

However, there is clear disagreement between the experimental curves and the calculated ones of P(AA) (Figure 4). The work required to remove  $\text{H}^+$  from a P(AA) molecule is greater than that calculated. However, this disagreement does not mean that the theory

(37) J. C. Leyte and M. Mandel, *J. Polymer Sci.*, **A2**, 1879 (1964).

(38) A constant value is expected for  $\text{p}K_a$  ( $= -\log K_a$ ) of eq. 2, but an absolutely constant value cannot be expected for  $\text{p}K_0$  because of the neglect of the activity coefficients of  $-\text{COO}^-$  and  $-\text{COOH}$ ; see ref. 34.

does not hold for P(AA) at all. If we compare the experimental results with the calculated ones as they depend on salt concentration at a constant degree of neutralization, we do find satisfactory agreement at high  $\alpha$ , as seen in Figure 6, though an additional amount of work,  $\Delta A(\alpha)$ , should be added as

$$\text{pH} + \log [(1 - \alpha)/\alpha] = \text{p}K_0 + \Delta A(\alpha) + 0.434e\psi_b/kT \quad (13)$$

As the degree of neutralization increases, the agreement becomes better. At infinite ionic strength,  $\psi_b$  must vanish, and hence  $\Delta A(\alpha)$  must be a free energy change due to a conformational change of backbone chain. Probably because the conformation of P(AA) is easily changed,  $\Delta A(\alpha)$  must be added to the electrostatic free energy change for P(AA), whereas the presence of the  $\alpha$ -methyl group gives negligible  $\Delta A(\alpha)$  for P(MAA). Therefore, it would be desirable to take into account the flexibility of the backbone chain in the theory of potentiometric titration. Such a development is difficult, however, so before the theory is completed, we should restrict our application of the rodlike model to relatively stiff polyelectrolytes or to data at a constant (and high) degree of neutralization. Lapanje<sup>39</sup> reported that the calculated results of Kotin and Nagasawa do not agree with his data for poly(ethylenimine). Though the hydrolysis of the sample is too great to allow precise comparison of his data with those calculated, it is likely that poly(ethylenimine) is also too flexible.

In studies of polymer solutions,<sup>40</sup> the flexibility of backbone chain is shown to appear in a  $\sigma$  value which is defined by  $\sigma = \langle r_0^2 \rangle / \langle r_\infty^2 \rangle$ , where  $\langle r_0^2 \rangle^{1/2}$  is the unperturbed dimension of the polymer and  $\langle r_\infty^2 \rangle^{1/2}$  is that of the corresponding ideal chain which is not restricted in rotation around the C-C bond of the backbone. The  $\sigma$  values of P(MAA) and P(MA) are almost equal; hence, there seems to be no great difference in the flexibilities of these two substances.<sup>41</sup> However, the flexibility of the polymer chain in organic solvents may differ from its flexibility in aqueous solution. It is possible that the methyl group has little effect on the flexibility of backbone chain in an organic  $\Theta$  solvent but has effect in aqueous solutions since H<sub>2</sub>O is an extremely poor solvent for polymers containing a methyl group. That is, the P(MAA) chain may be stiffer than the P(AA) chain in aqueous solutions.

*The Effect of Stereoregularity.* Since the electrostatic free energy ( $G_{e1}$  of eq. 6-8) is determined by the average distance between acidic groups, it is understandable that a difference in behavior is observed

between the two stereoregular P(MAA)'s if the molecular conformation differs with stereoregularity. Moreover, that good agreement between the calculated curves of  $0.434e\psi_b/kT$  and the data of the syndiotactic P(MAA) is found seems to imply that the syndiotactic P(MAA) has a (locally) planar zigzag conformation because the calculation was made on the assumption that the molecules are fully stretched and that the charges are distributed uniformly on the rod. Thus, it is clear that the isotactic P(MAA) has a conformation with a higher charge density than the stretched one.

Although the type of conformation possessed by the isotactic P(MAA) cannot be determined from the present experiments, we wish to point out here that the difference between the two stereoregular P(MAA)'s can be explained by assuming that the isotactic P(MAA) has a locally helical conformation. That is, if the molecule has a helical form with three monomers per turn,<sup>42</sup> the charge density of the molecule would be 1.39 times as high as that of the stretched molecule since the diameter of the molecule is not greatly changed. Therefore, the value of  $0.434e\psi_b/kT$  for the stretched molecule (*i.e.*, syndiotactic polymer) at  $\alpha = 1$  must correspond to that of the helical molecule at  $\alpha = 0.72$ . This speculation is in almost complete agreement with the experimental result (average 0.74) independently of the ionic strength. Even if the molecule has a helical form with four monomers per turn, the result is still almost the same because the charge density becomes larger, but the diameter is also increased.

There have been many discussions on whether or not isotactic polymers have helical forms in solution. As is pointed out in reviews by Krigbaum<sup>43</sup> and by Yang,<sup>44</sup> several workers (Salovey,<sup>45</sup> Takeda, *et al.*,<sup>46,47</sup> and Pino, *et al.*<sup>48</sup>) have provided evidence for the existence of helical forms of isotactic polymers in solution, but others (Kotera, *et al.*,<sup>49</sup> and Nozakura, *et al.*<sup>50</sup>)

(39) S. Lapanje, *Vestn. Sloven. Kem. Društva*, **9**, 5 (1962).

(40) P. J. Flory, "Principles of Polymer Chemistry," Cornell University Press, Ithaca, N. Y., 1953.

(41) M. Kurata and W. H. Stockmayer, *Fortschr. Hochpolymer Forsch.*, **3**, 196 (1963).

(42) G. Natta, *J. Polymer Sci.*, **16**, 143 (1955).

(43) W. R. Krigbaum in "Newer Methods of Polymer Characterization," B. Ke, Ed., Interscience Publishers, Inc., New York, N. Y., 1964, Chapter 1.

(44) J. T. Yang, ref. 43, Chapter 2.

(45) P. Salovey, *J. Polymer Sci.*, **50**, s7 (1961).

(46) M. Takeda, Y. Imamura, S. Okamura, and T. Higashiyama, *J. Chem. Phys.*, **33**, 631 (1960).

(47) M. Takeda, K. Imamura, A. Yamada, and Y. Imamura, *Bull. Chem. Soc. Japan*, **33**, 1219 (1960).

have questioned this conclusion. The reviewers mentioned above do not arrive at a firm conclusion on this question. Recently, Wunderlich and Kirste<sup>51</sup> reported the presence of a helical form of a syndiotactic poly(methyl methacrylate) in solution.

Considering these discussions of the conformation of stereoregular polymers in solution, we must be cautious in trying to explain the observed difference between the stereoregular polymers by postulating locally helical conformation of the isotactic P(MAA). However, the assumption of a helical conformation of the isotactic P(MAA) in solution does explain the results satisfactorily, and, to date, it is the only explanation that the authors have been able to find.

As mentioned above, a previous study of isotactic and atactic poly(acrylic acid) revealed no difference<sup>22</sup> between the forms. Although this is contrary to our findings with P(MAA), this should not necessarily be considered to be a contradiction since the conformation of a linear polymer depends greatly on its environ-

ment and, as pointed out above, may be influenced by the presence of side-chain methyl groups, particularly in aqueous solution.

*Acknowledgment.* We wish to thank Professor Alfred Holtzer and Mr. David Olander of Washington University, St. Louis, Mo., for critically reading our manuscript and Dr. Masao Ishii of the Mitsubishi Rayon Co. and Dr. Tatsuo Matsuda of the Government Industrial Research Institute, Nagoya, Japan, for generously supplying us with the samples.

(48) P. Pino, D. P. Lorenzi, L. Lardisci, and F. Ciardelli, *Vysokomolekul. Soedin.*, **3**, 1597 (1961); P. Pino and G. P. Lorenzi, *J. Am. Chem. Soc.*, **82**, 4745 (1960); *Makromol. Chem.*, **47**, 242 (1961); P. Pino, F. Ciardelli, G. P. Lorenzi, and G. Natta, *J. Am. Chem. Soc.*, **84**, 1487 (1962).

(49) A. Kotera, M. Shima, N. Fujisaki, T. Kitazawa, Y. Yasuhara, and S. Murahashi, *Bull. Chem. Soc. Japan*, **32**, 313 (1959).

(50) S. Nozakura, S. Takeuchi, H. Yuki, and S. Murahashi, *ibid.*, **34**, 1673 (1961).

(51) W. Wunderlich and R. G. Kirste, *Ber. Bunsenges. physik. Chem.*, 646 (1964).

## Tracer Diffusion in Binary Solutions Subject to a Dimerization Equilibrium

by R. H. Stokes<sup>1</sup>

*Institute for Enzyme Research, University of Wisconsin, Madison, Wisconsin (Received June 24, 1965)*

The dimerization of a solute leads to a tracer diffusion coefficient which falls more rapidly with increasing concentration than would otherwise be expected. The quantitative theory of this effect is developed and is shown to explain the experimental data of Albright and Mills for aqueous urea solutions.

### Introduction

When a solute diffusing through a solvent exists partly as a dimeric species, in equilibrium with the monomeric form, the mobility of the dimer will be lower than that of the monomer, though by no means as low as half that of the monomer. In mutual diffusion, the motion of a dimeric entity transports twice as much solute as that of a monomeric entity. In tracer diffusion, on the other hand, since the labeled

solute is at a low concentration relative to the unlabeled form, nearly all the labeled dimers contain one labeled molecule and one unlabeled one. Motion of a singly labeled dimeric entity therefore transports the same amount of labeled material as does that of a labeled monomeric entity. The consequences of these relationships will now be developed in detail and used

(1) University of New England, Armidale, N.S.W., Australia.

in the analysis of published data<sup>2</sup> on tracer diffusion in aqueous urea solutions.

### Definitions of Symbols Used

#### Subscripts

- s For stoichiometric quantity
- 0 For solvent
- 1 For monomer
- 2 For dimer
- N* For quantity measured on mole fraction scale

#### Superscript

- \* For singly labeled isotopic species
- m* Moles per kilogram of solvent
- W* Molecular weight
- $\alpha$  Fraction of solute in monomeric form
- $\mu$  Chemical potential
- $\mu^\circ_{(m)}$  Standard chemical potential on molality scale
- $\mu^\circ_{(N)}$  Standard chemical potential on mole fraction scale
- $\gamma$  Molal activity coefficient
- $K_{(N)}$  Mole fraction scale equilibrium constant
- $a_0$  Solvent activity
- c* Concentration in moles per unit volume (1 liter)
- J* Flux in moles per unit area per unit time
- D* Diffusion coefficient
- $D^0$  Limiting value of diffusion coefficient at infinite dilution
- $D_m$  Mutual diffusion coefficient
- $\eta_{rel}$  Relative viscosity
- p* Fluidity index
- $\bar{V}$  Molar volume

### Equilibrium Relationships for the Case Where the Various Species Mix to Form an Ideal Solution

We consider the case where the monomer (1), the dimer (2), and the solvent (0) form an ideal solution in the sense that the activity of each species is equal to its mole fraction. This does not, of course, mean that the stoichiometric activity of the solute component as a whole is equal to its stoichiometric mole fraction but means, rather, that we attribute the observed deviations from stoichiometric ideal behavior to the existence of the monomer-dimer equilibrium.

The stoichiometric molality is

$$m_s = m_1 + 2m_2 \quad (1)$$

The true mole fractions of monomer and dimer are

$$N_1 = \frac{m_1}{m_1 + m_2 + 1000/W_0} \quad (2)$$

$$N_2 = \frac{m_2}{m_1 + m_2 + 1000/W_0} \quad (3)$$

where  $W_0$  is the molecular weight of the solvent.

Let  $\alpha$  denote the fraction of the solute present as monomer, *i.e.*

$$\alpha = \frac{m_1}{m_s} = \frac{N_1}{N_1 + 2N_2} \quad (4)$$

Then

$$m_1 + m_2 = m_s(1 + \alpha)/2 \quad (5)$$

If the stoichiometric molal activity coefficient  $\gamma_s$  is known, we may calculate  $\alpha$  as

$$\mu_s = \mu^\circ_{(m)} + RT \ln m_s + RT \ln \gamma_s \quad (6)$$

Since the monomer and dimer are in equilibrium, we have  $\mu_2 = 2\mu_1$  and

$$\mu_s = \frac{N_1\mu_1 + N_2\mu_2}{N_1 + 2N_2} = \mu_1 \quad (7)$$

$$= \mu^\circ_{(N)} + RT \ln \frac{m_1}{m_1 + m_2 + 1000/W_0} \quad (7)$$

$$= \mu^\circ_{(N)} + RT \ln \frac{\alpha m_s}{(1000/W_0) + m_s(1 + \alpha)/2} \quad (8)$$

Equating (6) and (8) and determining the constant  $\mu^\circ_{(m)} - \mu^\circ_{(N)}$  by considering the limit when  $m_s \rightarrow 0$ ,  $\alpha \rightarrow 1$ , and  $\gamma_s \rightarrow 1$ , we obtain

$$\gamma_s = \frac{\alpha}{1 + 0.001W_0m_s(1 + \alpha)/2}$$

or

$$\alpha = \gamma_s \frac{1 + 0.0005W_0m_s}{1 - 0.0005W_0m_s\gamma_s} \quad (9)$$

For aqueous solutions (9) becomes

$$\alpha = \gamma_s \frac{1 + 0.009m_s}{1 - 0.009m_s\gamma_s} \quad (10)$$

The equilibrium constant for dimerization,  $K_{(N)}$ , may now be expressed as

$$\bar{K}_{(N)} = \frac{N_2}{N_1^2} = \frac{(1 - \alpha)[m_s(1 + \alpha) + 2000/W_0]}{4m_s\alpha^2} \quad (11)$$

If the measured activity coefficients  $\gamma_s$  lead by (9) and (11) to a constant and positive value of  $\bar{K}_{(N)}$ , the assumption of a dimerization equilibrium is reasonable. However, the existence of a dimerization equilibrium is not conclusively proved in this way, as other short-range interactions between solute molecules, short of recognizable dimer formation, will give an approximately constant  $\bar{K}_{(N)}$  in dilute solutions.

While expression 10 is the most convenient for obtaining values of  $\alpha$  from tables of molal activity coefficients, the data are, in fact, often obtained from

(2) J. G. Albright and R. Mills, *J. Phys. Chem.*, **69**, 3120 (1965).



isopiestic measurements which yield the stoichiometric molal osmotic coefficient

$$\phi_s = -\frac{1000}{W_0 m_s} \ln a_0 \quad (12)$$

from which the activity coefficients are subsequently calculated. In such cases relations 2, 6, and 7 are conveniently transformed as

$$N_1 = m_s \gamma_s W_0 / 1000 \quad (13)$$

Then, since

$$\alpha = N_1 / (N_1 + 2K_{(N)} N_1^2) = 1 / (1 + 2K_{(N)} N_1) \quad (14)$$

and

$$\frac{N_1 + 2K_{(N)} N_1^2}{N_0} = \frac{m_s W_0}{1000} \quad (15)$$

we obtain, equating the mole fraction of free water,  $N_0$ , to the water activity,  $a_0$

$$\alpha = \frac{1000 N_1}{m_s W_0 a_0} = \frac{\gamma_s}{a_0} \quad (16)$$

Hence

$$K_{(N)} = \frac{N_2}{N_1} \frac{1}{N_1} = \frac{1 - \alpha}{2\alpha} \frac{1}{N_1} = \frac{a_0 - \gamma_s}{m_s \gamma_s^2} \frac{1000}{W_0} \quad (17)$$

The neat result (16) can readily be shown to hold for any kind of solute-solute association, whether to dimers or any equilibrium mixture of polymers, subject, of course, to our assumed ideal mixing behavior of the various species. In the absence of association, we have  $\alpha = 1$ , and (16) reduces to

$$\gamma_s = a_0 = \frac{1}{1 + 0.001 W_0 m_s}$$

Since in this case the stoichiometric mole fraction scale activity coefficient is unity, this is simply the standard thermodynamic relation between the molal and mole fraction scale activity coefficients.

### Activities in Aqueous Urea Solutions

The dimerization of urea in aqueous solutions has been discussed by Schellman<sup>3</sup> and by Kresheck and Scheraga.<sup>4</sup> Both of these treatments contain a minor inconsistency, in that, while the water activity is correctly equated to the true mole fraction of water ( $a_0 = 1 - N_1 - N_2$  in our notation), the equilibrium constant is taken as  $K = m_2/m_1^2$ , which implies that the monomer and dimer have unit molality scale activity coefficients (or at least that the ratio  $\gamma_2/\gamma_1^2$  is independent of concentration). This has only a small effect on their main conclusions, which are based on

limiting slopes, but the present formulas in which the mole fraction scale activity coefficient of each solute species is taken as unity are thermodynamically exact for the model used by all parties. The 25° activity data<sup>5,6</sup> for urea solutions, revised to modern isopiestic standards for sodium chloride,<sup>7</sup> are consistent with simple dimerization with an association constant  $K_{(N)} = 1.8$  up to 4–5 *m*; thereafter, progressively smaller values of  $K_{(N)}$  are required. This is contrary to the conclusion of Schellman, who found that his formulas led to an extent of polymerization at high concentrations greater than could be explained by dimerization alone. The present results therefore suggest that the cyclic dimer proposed by Schellman, which would less readily undergo further polymerization, is the dominant species.

Since the tracer diffusion coefficient results extend only to 4 *M* solutions where the assumption of simple dimerization remains adequate, they will be analyzed on this model.

### Distribution of a Trace Isotopic Solute

Consider a trace amount of an isotopically labeled but otherwise identical solute present in the equilibrium mixture discussed above, at a stoichiometric concentration  $c_s^*$ . If we denote the single solute molecule by A, the label will be carried singly by each of the species A\* and AA\*, and doubly by the species A\*A\*. The species A\*A\*, however, will be at a negligible concentration relative to the other two, so that the effective distribution of the label will be given by

$$c_1^*/c_s^* = c_1/c_s = \alpha \quad (18)$$

where  $c$  denotes molar concentration. Hence

$$c_2^*/c_s^* = 1 - \alpha \quad (19)$$

in contrast to the result for the unlabeled species

$$c_2/c_s = (1 - \alpha)/2 \quad (20)$$

(It follows from these results that the equilibrium constant for the formation of AA\* is twice that for the formation of either AA or A\*A\*. This relationship is demonstrably necessary in order that the over-all equilibrium constant should be unaffected by information or lack of information about the isotopic composition.)

(3) J. A. Schellman, *Compt. rend. trav. lab. Carlsberg*, **29**, 223 (1955).

(4) G. C. Kresheck and H. A. Scheraga, *J. Phys. Chem.*, **69**, 1704 (1965).

(5) G. Scatchard, W. J. Hamer, and S. Wood, *J. Am. Chem. Soc.*, **60**, 3061 (1938).

(6) V. E. Bower and R. A. Robinson, *J. Phys. Chem.*, **67**, 1524 (1963).

(7) R. A. Robinson and R. H. Stokes, "Electrolyte Solutions," 2nd Ed., Butterworth and Co. Ltd., London, 1959, p. 476.



tion of the solute. The same conclusion may be reached from an elementary collision theory treatment of the equilibria in terms of balanced forward and backward reactions: the number of  $A + A$  collisions per unit volume is proportional to  $[A]^2/2!$ , while the number of  $A + A^*$  collisions is proportional to  $[A][A^*]$ .

### Tracer Diffusion

When a trace of a labeled species is allowed to diffuse in an otherwise uniform solution and the diffusion coefficient  $D_s^*$  is measured in terms of the stoichiometric flux and concentration of labels, as is normally done, the experimentally observed diffusion coefficient  $D_s^*$  is given by

$$-J_s^* = D_s^* \frac{\partial c_s^*}{\partial x} \quad (21)$$

We may also write the flux in terms of the gradients and diffusion coefficients of the monomer and dimer

$$-J_1^* = D_1^* \frac{\partial c_1^*}{\partial x} \quad (22)$$

$$-J_2^* = D_2^* \frac{\partial c_2^*}{\partial x} \quad (23)$$

and

$$J_s^* = J_1^* + J_2^* \quad (24)$$

whence

$$D_s^* = D_1^* \frac{\partial c_1^*}{\partial c_s^*} + D_2^* \frac{\partial c_2^*}{\partial c_s^*} \quad (25)$$

However, since the over-all concentration is effectively constant at  $c_s$  and  $\alpha$  depends only on  $c_s$ , we have from (18) and (19)

$$\frac{\partial c_1^*}{\partial c_s^*} = \alpha; \quad \frac{\partial c_2^*}{\partial c_s^*} = 1 - \alpha$$

and (25) becomes

$$D_s^* = \alpha D_1^* + (1 - \alpha) D_2^* \quad (26)$$

Though eq. 26 has been derived for the case where the labeled species is present only in a trace amount, the same result is reached for the "intradiffusion" case discussed by Albright and Mills,<sup>2</sup> where diffusion occurs between labeled and unlabeled solute at a constant total concentration. In this case, it is, of course, necessary to introduce the doubly labeled dimeric species  $A^*A^*$ , the mobility of which is the same as that of  $AA^*$  but which transports two labels. That the same result (26) is obtained is in accordance with the expectation that the diffusion mobility will be only

trivially altered by isotope effects. Exceptions might occur where deuterium is used as the tracer.

### Relation between Monomer and Dimer Mobilities

While eq. 26 gives the relation of the observed tracer diffusion coefficient to those of the monomer and dimer, its application requires further knowledge of the concentration dependence of  $D_1^*$  and  $D_2^*$ .

In the limit of low total solute concentration, since  $\alpha \rightarrow 1$ , we have

$$D_s^{*0} = D_1^{*0} = D_m^0 \quad (27)$$

where  $D_m^0$  is the limiting mutual diffusion coefficient.

For the somewhat unrealistic case where both monomer and dimer are spherical particles, large compared with the solvent molecules, the Einstein-Stokes relation

$$D^0 = kT/6\pi\eta r \quad (28)$$

leads to the further results

$$2^{1/2} D_2^* = D_1^* = D_1^{*0}/\eta_{rel} \quad (29)$$

since the volume of the dimer will be twice that of the monomer. When (29) holds, (26) becomes

$$D_s^* = D_m^0(0.7937 + 0.2063\alpha)/\eta_{rel} \quad (30)$$

In ordinary cases, where the solute and solvent molecules are not both spherical, we may expect the ratio  $D_2^*/D_1^*$  to remain more or less independent of concentration and certainly to be less than unity. If the monomer were a sphere and the dimer were regarded as two spheres in contact it would seem appropriate to take the hydrodynamic drag on the dimer as that in Figure 1 enclosed by the broken line. This would have a volume of  $2.5 \times 4\pi r^3/3$  and could be approximately treated as a prolate ellipsoid of axial ratio 2:1. Standard hydrodynamic results<sup>8</sup> would then give

$$D_2^*/D_1^* = 1/(2.5^{1/3} \times 1.044) = 0.706 \quad (31)$$

which is somewhat lower than the value  $2^{-1/3} = 0.794$  for the case of spheres with  $V_2 = 2V_1$ . Mills<sup>9</sup> found 0.687 for  $D_{diphenyl}^*/D_{benzene}^*$ , independent of composition, in solutions of diphenyl in benzene.

The approximation of putting the frictional drag on the moving particles proportional to the solution viscosity is however much less reasonable for small molecules. There is unquestionably a strong correlation between mobility and solution viscosity, but evidence from Mills' work on diphenyl-benzene solutions and from Van Geet and Adamson's<sup>10</sup> on octane-

(8) F. Perrin, *J. phys. radium*, **7**, 1 (1936).

(9) R. Mills, *J. Phys. Chem.*, **67**, 600 (1963).

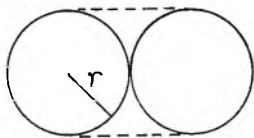


Figure 1.

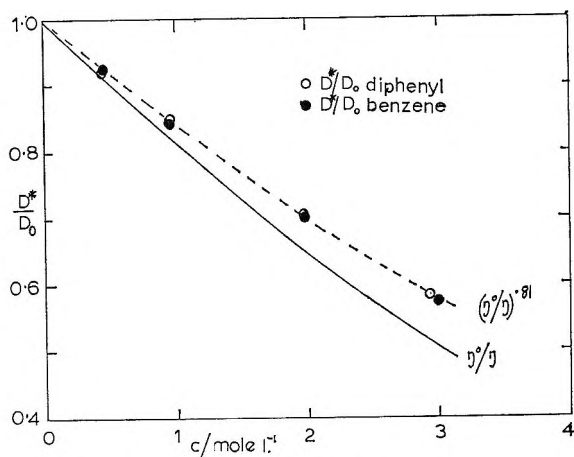


Figure 2. Tracer diffusion coefficients in benzene-diphenyl solutions compared with the first power and the 0.81 power of the relative fluidity.

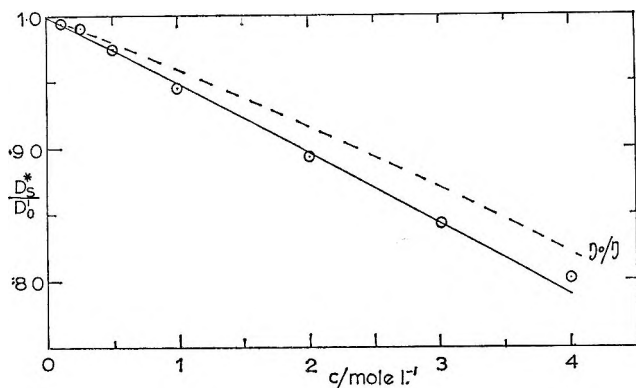


Figure 3. Tracer diffusion coefficients of urea in aqueous solution at 25° compared with eq. 34 (solid line) and relative fluidity (broken line).

dodecane solutions, as well as from extensive studies of ionic mobilities in aqueous solutions of sucrose and other nonelectrolytes, all shows that to write

$$D_1^* = D_1^0/\eta_{rel} \quad (32)$$

is an overcorrection and that at moderate concentrations a better expression is

$$D_1^* = D_1^0/(\eta_{rel})^p \quad (33)$$

where  $p$  has a value of about 0.8. Figure 1 shows that  $p = 0.81$  reproduces Mills' data for diphenyl-benzene solutions with satisfactory accuracy.

In the absence of dimerization, expression 32 should give a *lower* limit to the tracer diffusion coefficient, for particles much larger than the solvent molecules. When a case is found in which the tracer diffusion coefficient is *lower* than the prediction of eq. 32, it is reasonable to explain this behavior in terms of dimerization, according to eq. 26. Such behavior is shown by aqueous urea solutions<sup>2</sup> (Figure 2). Inserting (33) and its analog for  $D_2^*$  into (26) we find

$$\begin{aligned} D_2^* &= D_1^0[\alpha + (1 - \alpha)D_2^0/D_1^0]\eta_{rel}^{-p} \\ &= D_1^0[1 + (1 - \alpha)(D_2^0/D_1^0 - 1)]\eta_{rel}^{-p} \quad (34) \end{aligned}$$

and we can use this equation to interpret the urea data in two alternative ways. One is to estimate a value of the mobility ratio  $D_2^0/D_1^0$  and hence determine a value of the index  $p$ ; the other is to assume a reasonable  $p$  value and hence calculate  $D_2^0/D_1^0$ .

The relevant quantities are given in Table I; in case A we assume  $D_2^0/D_1^0 = 2^{-1/3}$  and conclude that  $p = 1$ ; in case B we assume  $p = 0.8$  and conclude that  $D_2^0/D_1^0 = 0.615$ . As Figure 2 shows, the predicted curves are almost indistinguishable and agree very satisfactorily with the results of Albright and Mills.<sup>2</sup> A series of intermediate values between these limits would also clearly be satisfactory. It is not possible to select any pair as giving a materially better fit than others.

Table I

$c$	$m$	$\alpha$	$1/\eta_{rel}$	$D_2^*/D_1^0$ (exptl.)	A	B
					$D_2^0/D_1^0$ (calcd.) <sup>a</sup>	$D_2^0/D_1^0$ (calcd.) <sup>b</sup>
0	0	1.000	1.000	1.000	1.000	1.000
0.1	0.1007	0.994	0.996	0.994	0.995	0.995
0.25	0.2535	0.984	0.990	0.991	0.987	0.986
0.5	0.5130	0.969	0.981	0.973	0.975	0.973
1.0	1.050	0.941	0.960	0.944	0.949	0.946
2.0	2.202	0.891	0.916	0.893	0.895	0.893
3.0	3.474	0.848	0.870	0.842	0.842	0.842
4.0	4.891	0.812	0.822	0.801	0.790	0.793

$$D_1^0 = 1.3817 \times 10^{-5} \text{ cm.}^2 \text{ sec.}^{-1}$$

<sup>a</sup> Calculated from eq. 34 with  $D_2^0/D_1^0 = 2^{-1/3} = 0.794$ ,  $p = 1$ .  
<sup>b</sup> Calculated from eq. 34 with  $D_2^0/D_1^0 = 0.615$ ,  $p = 0.8$ .

*Acknowledgments.* The author is grateful to Drs. J. G. Albright and R. Mills for access to their experimental work on tracer diffusion in urea solutions prior to publication. He also wishes to thank the University of Wisconsin for its hospitality and the U. S. National

(10) A. L. Van Geet and A. W. Adamson, *J. Phys. Chem.*, **68**, 238 (1964).

Science Foundation for the award of a Senior Foreign Scientist Fellowship during the tenure of which this work was done. This investigation was supported in

part by Public Health Service Research Grant AM-05177 from the National Institute of Arthritis and Metabolic Diseases.

## Electrokinetic Flow in a Narrow Cylindrical Capillary

by C. L. Rice and R. Whitehead

*Royal College of Advanced Technology, Salford 5, Lancashire, England (Received June 28, 1965)*

This paper is a theoretical study of electrokinetic flow in narrow cylindrical capillaries. It is concerned with the dependence of the usual electrokinetic phenomena on the electrokinetic radius. The results obtained for this dependence must, however, be treated with caution for the higher values of the interface potential due to the use of the Debye-Hückel approximation. Of interest is the prediction of a maximum in the electroviscous effect.

### Introduction

The results of applying pressure and potential gradients across a capillary are well known, the basic relationships involved having been formulated mainly by Smoluchowski.<sup>1</sup> However, all these relationships involve the assumption that the double-layer thickness is small compared with the capillary diameter.

In some investigations, this condition is no longer satisfied and the dependence of electroosmosis, the streaming potential, and the apparent viscosity of the capillary fluid on the electrokinetic radius must be taken into account. It has been shown<sup>2</sup> that a bed of fine particles or a porous diaphragm can be regarded in the same manner as a single capillary when the electrokinetic radius is large and probably also when it is not large, though greater care must be exercised here. Pertinent also is the fact that it is now possible to make a uniform capillary with a radius as small as  $10^{-5}$  cm.

In a recent paper, Burgreen and Nakache<sup>3</sup> studied the electrokinetic flow in a very fine capillary channel of rectangular cross section. In this paper we shall be concerned with a single long uniform circular capillary of radius  $a$ , containing an electrolyte, and no assump-

tions will be made as to the magnitude of the electrokinetic radius  $\kappa a$  where  $\kappa$  is the reciprocal of the Debye length.

### Double-Layer Potential and Net Charge Density

Consider a uni-univalent electrolyte of bulk ionic concentration  $n$  ions/unit volume, with the wall of the capillary at a potential  $\psi_0$  and a potential  $\psi$  at a point distance  $r$  from the axis. If the excess charge density at this point is  $\rho(r)$ , then the Poisson equation has the form

$$\frac{1}{r} \frac{d}{dr} \left( r \frac{d\psi}{dr} \right) = -\frac{4\pi}{\epsilon} \rho(r) \quad (1)$$

for, due to symmetry,  $\psi$  is a function of  $r$  only.  $\epsilon$  is the dielectric constant which is assumed to be uniform throughout the liquid.

From the Boltzmann equation

(1) M. von Smoluchowski in Graetz, "Handbuch der Elektrizität und des Magnetismus," Vol. II, Leipzig, 1914, p. 366.

(2) P. Mazur and J. T. G. Overbeek, *Rec. trav. chim.*, **70**, 83 (1951).

(3) D. Burgreen and F. R. Nakache, *J. Phys. Chem.*, **68**, 1084 (1964).

$$\rho(r) = -2ne \sinh \frac{e\psi}{kT} \quad (2)$$

If  $e\psi/kT$  is small,  $\sinh e\psi/kT \simeq e\psi/kT$ . When  $\psi \simeq 25$  mv.,  $e\psi/kT = 1$ , so that it would appear that the above approximation would only be applicable to very small values of  $\psi$ . Fortunately, however, this approximation results in an expression for the potential distribution at a single plane surface which is in good agreement with that obtained from the exact solution for values of  $\psi_0$  up to 50 mv. in the case of a uni-univalent electrolyte.

This approximation can be adopted in the case of a cylindrical capillary, with the proviso that any results derived must be viewed with caution when applied to higher values of  $\psi_0$ . This is particularly so when  $\kappa a$  is small, since it is for these values that the double layers begin to overlap in the center of the capillary.

The Poisson-Boltzmann distribution equation then becomes

$$\frac{1}{r} \frac{d}{dr} \left( r \frac{d\psi}{dr} \right) = \kappa^2 \psi \quad (3)$$

where  $\kappa = (8\pi ne^2/\epsilon kT)^{1/2}$  is the reciprocal of the double-layer thickness.

The solution of (3) which is finite at  $r = 0$  is

$$\psi = BI_0(\kappa r) \quad (4)$$

where  $I_0$  is the zero-order modified Bessel function of the first kind.

At  $r = a$  the condition is  $\psi = \psi_0$ ; therefore

$$\psi = \psi_0 \frac{I_0(\kappa r)}{I_0(\kappa a)} \quad (5)$$

From Poisson's equation, the net charge density is given by

$$\rho(r) = -\frac{\epsilon \kappa^2}{4\pi} \psi = -\frac{\epsilon \kappa^2}{4\pi} \psi_0 \frac{I_0(\kappa r)}{I_0(\kappa a)} \quad (6)$$

### The Equations of Motion

The basic equation of motion for the fluid is

$$\eta \nabla \Delta \nabla \Delta \mathbf{v} + (\mathbf{v} \cdot \nabla) \mathbf{v} + \nabla p = \mathbf{F} \quad (7)$$

with  $\nabla \cdot \mathbf{v} = 0$  as the fluid is incompressible.  $\eta$  is the coefficient of viscosity and  $\mathbf{F}$  is the body force per unit volume. In an infinite cylindrical tube under the influence of an axial applied electric field,  $\mathbf{v}_z = \mathbf{v}_z(r)$  and  $\mathbf{v}_r = \mathbf{v}_\phi = 0$ , in terms of cylindrical polar coordinates. Thus in this case the inertia terms  $(\mathbf{v} \cdot \nabla) \mathbf{v}$  vanish. Also,  $\nabla p = dp/dz \mathbf{e}_z$  and  $\mathbf{F} = F_z(r) \mathbf{e}_z$ . The equation of motion thus reduces to

$$\frac{1}{r} \frac{d}{dr} \left( r \frac{dv_z}{dr} \right) = \frac{1}{\eta} \frac{dp}{dz} - \frac{F_z}{\eta} \quad (8)$$

with the conditions that  $p$  and  $v_z$  must be finite everywhere, that  $p$  is a function of  $z$  only, and that

$$v_z(a) = \left. \frac{dv_z}{dr} \right|_{r=0} = 0 \quad (9)$$

In the following sections

$$-\frac{dp}{dz} = P_z$$

where  $P_z$  is the uniform applied pressure gradient, and the body force is caused by the action of the applied electric field,  $E_z$ , on the net charge density  $\rho(r)$  in the double layer.

### Electroosmosis

In the presence of an applied potential gradient and an applied pressure gradient, the equation of fluid motion is

$$\frac{d^2 v_z}{dr^2} + \frac{1}{r} \frac{dv_z}{dr} = -\frac{P_z}{\eta} - \frac{E_z}{\eta} \rho(r) \quad (10)$$

Substituting expression 6 for  $\rho(r)$  in this equation and using the boundary conditions (9), the solution of (10) is found as

$$v_z(r) = \frac{P_z}{4\eta} (a^2 - r^2) - \frac{\epsilon \psi_0}{4\pi \eta} \left[ 1 - \frac{I_0(\kappa r)}{I_0(\kappa a)} \right] \quad (11)$$

a sum of a Poiseuille flow term and an electrokinetic term.

Electroosmotic velocity and volume transport are observed under conditions of no applied pressure gradient; *i.e.*,  $P_z = 0$  and so

$$v_z(r) = -\Omega E_z \left[ 1 - \frac{I_0(\kappa r)}{I_0(\kappa a)} \right] \quad (12)$$

where  $\Omega = \epsilon \psi_0 / 4\pi \eta$ .

For  $\kappa a \gg 1$ , asymptotic expansions show that  $I_0(\kappa r)/I_0(\kappa a)$  is negligible, except in the double-layer region very close to the wall. Under these conditions (12) reduces to the classical formula

$$v_z(r) = -\Omega E_z \quad (13)$$

The function  $[1 - (I_0(\kappa r))/(I_0(\kappa a))]$  is plotted in Figure 1 to give velocity profiles for various values of  $\kappa a$ . This shows that eq. 13 holds for  $0 \leq r \leq 0.9a$  if  $\kappa a > 50$ . For  $\kappa a = 10$ , the divergence from (13) becomes marked as the double layers begin to overlap in the center of the capillary. For  $\kappa a \leq 2$ , the velocity profiles take on a noticeable Poiseuille form. Using

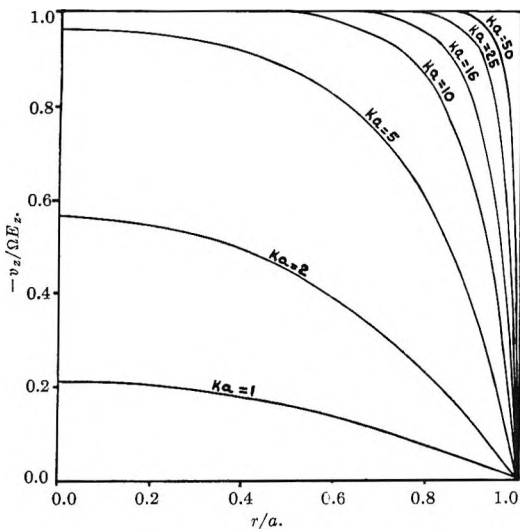


Figure 1. Velocity profiles at various values of  $\kappa a$ .

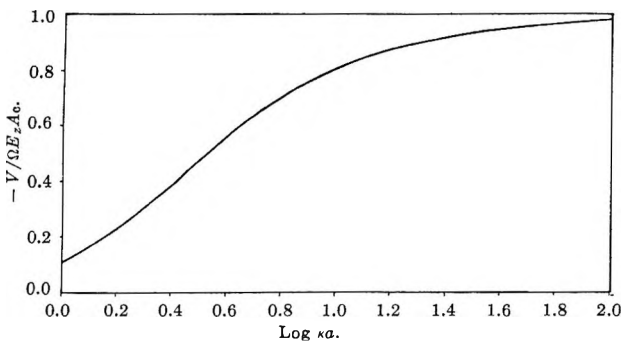


Figure 2. Volume transported per unit area and unit time for various values of  $\kappa a$ .

the series expansion for  $I_0$  and neglecting terms of  $O[(\kappa a)^4]$  and higher for  $\kappa a \ll 1$ , eq. 12 becomes

$$v_z(r) = -\Omega E_z \frac{\kappa^2}{4} (a^2 - r^2) \tag{14}$$

which is a Poiseuille flow with an effective pressure gradient equal to  $\Omega E_z \kappa^2 \eta$ .

Values of  $\kappa a < 1$  are not readily realizable in practice, but for  $\kappa a = 1$  the profile given by (12) agrees at worst to within 3% of the corresponding Poiseuille profile given by (14).

The Poiseuille characteristics at low values of  $\kappa a$  are due to the large overlap of the double layers with a virtually constant net charge density across the capillary, this giving rise to a fluid body force similar to that of a pressure gradient.

The volume transport,  $V$ , due to electroosmosis is obtained by integrating expression 12 for  $v_z(r)$  over a cross section of the capillary of area  $A_c$

$$V = 2\pi \int_0^a v_z(r) r dr = -\Omega E_z A_c \left[ 1 - \frac{2I_1(\kappa a)}{\kappa a I_0(\kappa a)} \right] \tag{15}$$

As  $\kappa a$  becomes large, the function in brackets tends to 1, giving

$$V = -\Omega E_z A_c \tag{16}$$

which is the usual classical result.

The function  $[1 - (2I_1(\kappa a))/(\kappa a I_0(\kappa a))]$  is plotted against  $\log \kappa a$  in Figure 2, which shows clearly that the greatest change of  $V$  with  $\kappa a$  is in the region  $1 < \kappa a \leq 10$  while  $V$  has 90% of its classical value for  $\kappa a = 20$ . The electroosmotic counter pressure can be obtained by first integrating eq. 11 for  $v_z(r)$  over a cross section, obtaining for the volume transport

$$V = \frac{P_z a^2}{8\eta} A_c - \frac{\epsilon \psi_0}{4\pi \eta} E_z A_c \left[ 1 - \frac{2I_1(\kappa a)}{\kappa a I_0(\kappa a)} \right] \tag{17}$$

The counter pressure is studied under conditions of no net volume transport; *i.e.*,  $V = 0$ . Using this in (17) gives the condition

$$\frac{P_z}{E_z} = \frac{2\epsilon \psi_0}{\pi a^2} \left[ 1 - \frac{2I_1(\kappa a)}{\kappa a I_0(\kappa a)} \right] \tag{18}$$

which for  $\kappa a \gg 1$  gives the usual form

$$\frac{P_z}{E_z} = \frac{2\epsilon \psi_0}{\pi a^2} \tag{19}$$

If condition 18 is substituted in eq. 11, the expression for the velocity distribution in the case of no total flow is obtained

$$\frac{v_z(r)}{E_z} = \Omega \left\{ 2 \left( 1 - \frac{r^2}{a^2} \right) \left[ 1 - \frac{2I_1(\kappa a)}{\kappa a I_0(\kappa a)} \right] - \left[ 1 - \frac{I_0(\kappa r)}{I_0(\kappa a)} \right] \right\} \tag{20}$$

When  $\kappa a \gg 1$  the above expression reduces to

$$\frac{v_z(r)}{E_z} = \Omega \left( 1 - \frac{2r^2}{a^2} \right) \tag{21}$$

except in the double-layer regions close to the wall.

The velocity profiles for a number of values of  $\kappa a$  are plotted in Figure 3. It can then be seen that near the walls the contribution of  $P_z$  to the flow is not as great as the contribution in the opposite direction caused by the migration of the ions under the applied field  $E_z$ . Thus if  $\psi_0$  is positive, there is in this region a preponderance of negative ions and the flow is in the negative direction. On the other hand, in regions nearer the center of the capillary the flow in the positive direction due to  $P_z$  is greater than the now much smaller

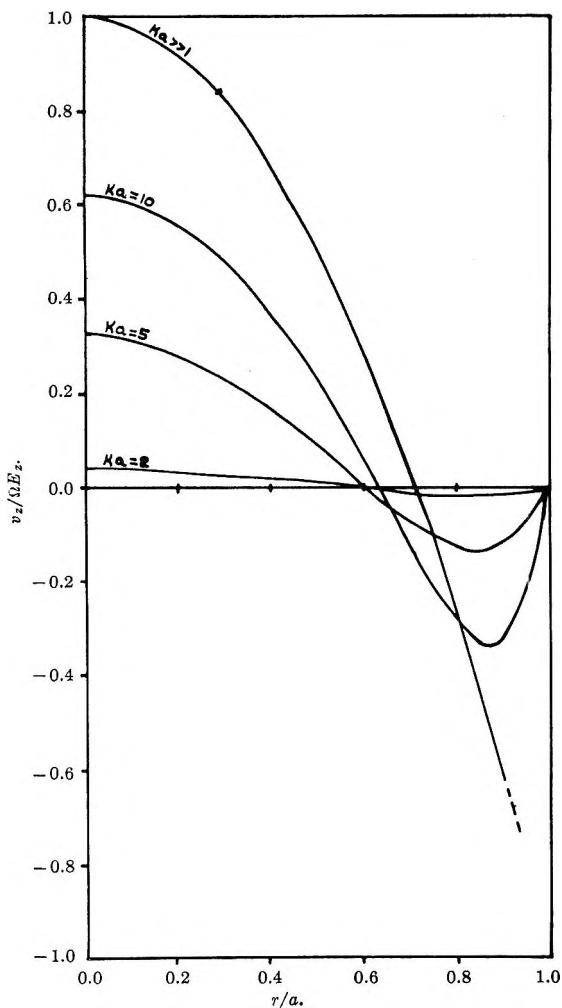


Figure 3. Velocity profiles for the electroosmotic counter pressure condition.

contribution in the negative direction to which  $E_z$  gives rise.

### The Current in Electroosmotic Flow

The current,  $i$ , flowing can be written as  $i = i_1 + i_2$ , where  $i_1$  is the current due to transport of charge by the fluid and  $i_2$  is the conduction current.

$$i_1 = 2\pi \int_0^a v_z(r) \rho(r) r dr \quad (22)$$

With both an applied electric field and a pressure gradient, expressions 11 and 6 for  $v_z(r)$  and  $\rho(r)$ , respectively, are used, giving

$$i_1 = -\frac{P_z A_c \Omega \kappa^2}{2} \left[ \frac{1}{I_0(\kappa a)} \int_0^a r I_0(\kappa r) dr - \frac{1}{a^2 I_0(\kappa a)} \int_0^a r^3 I_0(\kappa r) dr \right] + 2\pi \Omega^2 E_z \eta \kappa^2 \left[ \frac{1}{I_0(\kappa a)} \int_0^a r I_0(\kappa r) dr - \frac{1}{I_0^2(\kappa a)} \int_0^a r I_0^2(\kappa r) dr \right]$$

evaluating the integrals, noting that the last is of the Lommel type, we obtain

$$i_1 = -\Omega P_z A_c \left[ 1 - \frac{2I_1(\kappa a)}{\kappa a I_0(\kappa a)} \right] - \Omega^2 \eta \kappa^2 E_z A_c \left[ 1 - \frac{2I_1(\kappa a)}{\kappa a I_0(\kappa a)} - \frac{I_1^2(\kappa a)}{I_0^2(\kappa a)} \right] \quad (23)$$

If  $\lambda$  is the conductivity of the fluid and this is assumed to be uniform throughout the fluid up to the wall of the capillary, then

$$i_2 = \lambda E_z A_c \quad (24)$$

Hence

$$i = E_z A_c \lambda \left\{ 1 - \frac{\Omega^2 \eta \kappa^2}{\lambda} \left[ 1 - \frac{2I_1(\kappa a)}{\kappa a I_0(\kappa a)} - \frac{I_1^2(\kappa a)}{I_0^2(\kappa a)} \right] \right\} - \Omega P_z A_c \left[ 1 - \frac{2I_1(\kappa a)}{\kappa a I_0(\kappa a)} \right] \quad (25)$$

The first term in the above expression represents the current for electroosmotic flow, since in this case  $P_z = 0$ . The ratio of volume flow  $V$  to current  $i$  is then given by

$$\frac{V}{i} = -\frac{\Omega}{\lambda} f(\kappa a, \beta) \quad (26)$$

where  $\beta = \Omega^2 \eta \kappa^2 / \lambda$  and

$$f(\kappa a, \beta) = \frac{\left[ 1 - \frac{2I_1(\kappa a)}{\kappa a I_0(\kappa a)} \right]}{1 - \beta \left[ 1 - \frac{2I_1(\kappa a)}{\kappa a I_0(\kappa a)} - \frac{I_1^2(\kappa a)}{I_0^2(\kappa a)} \right]}$$

For water, where  $\epsilon = 81$ ,  $\eta = 10^{-2}$  c.g.s., the range of the parameter  $\beta$  is effectively covered by the values 0.1, 4.5, 27.0. The results for the higher values of  $\beta$  corresponding to high values of  $\psi_0$  will be less reliable, but they should nevertheless indicate the general trend and so are worth inclusion.

In Figure 4,  $f(\kappa a, \beta)$  is plotted against  $\log \kappa a$  for these three values of  $\beta$ . For large values of  $\kappa a$ , asymptotic expansions indicate that  $f(\kappa a, \beta)$  tends to 1 and we have the usual result that

$$\frac{V}{i} = -\frac{\Omega}{\lambda} \quad (27)$$

As the curves indicate, the deviations from this result become larger as  $\kappa a$  becomes progressively smaller and, when  $\beta = 4.5$ , they are important for values of  $\kappa a$  less than 5.0.

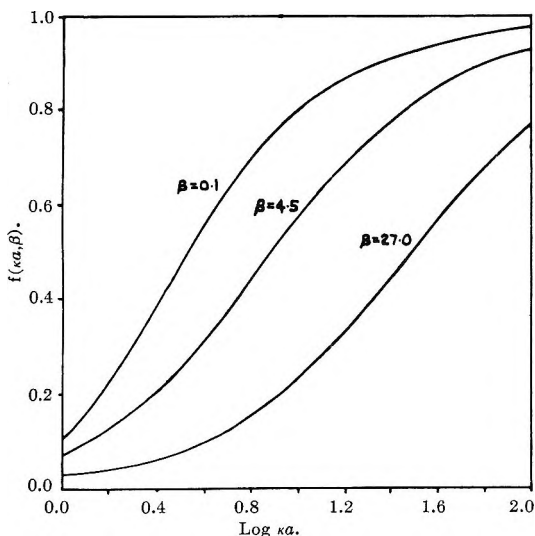


Figure 4. Variation of  $f(\kappa a, \beta)$  with  $\kappa a$ .

**Streaming Potential**

The streaming potential is the steady potential which builds up across a capillary in the presence of an applied pressure gradient and which is just sufficient to prevent any net current flow. Putting  $i = 0$  in eq. 25 and rearranging, the following condition is obtained

$$\frac{E_z}{P_z} = \frac{\Omega}{\lambda} f(\kappa a, \beta) \tag{28}$$

By comparison with (26) it is seen that

$$\frac{V}{i} = -\frac{E}{P} \tag{29}$$

as Mazur and Overbeek<sup>2</sup> have shown it must be, in accordance with the Onsager principle of reciprocity of irreversible phenomena.

The variation of the ratio  $E_z/P_z$  can therefore be inferred from Figure 4, and again for large values of  $\kappa a$  we have the well-known result that

$$\frac{E_z}{P_z} = \frac{\Omega}{\lambda} \tag{30}$$

If the  $\zeta$ -potential, where  $\zeta = \psi_0$ , is determined experimentally for narrow capillaries from measurements of the streaming potential on the basis of eq. 30, an apparent value  $\zeta_a$  would be found. This value is related to the electrokinetic potential  $\zeta$  by the relation

$$\frac{\zeta_a}{\zeta} = f(\kappa a, \beta) \tag{31}$$

Thus the apparent  $\zeta$ -potential would again be expected to vary with the electrokinetic radius after the manner shown in Figure 4.

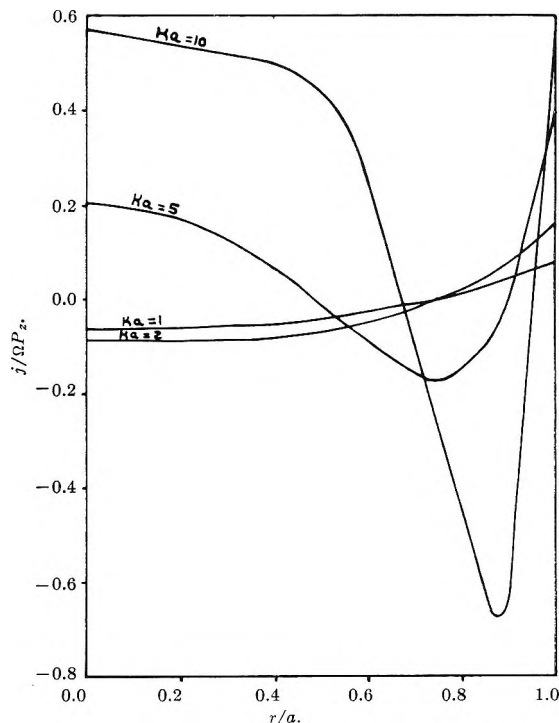


Figure 5. Variation of current density across the capillary with  $\beta = 4.5$ .

**Current Density Distribution**

The current density  $j(r)$  at a point in the fluid is given by

$$j(r) = v_z(r)\rho(r) + E_z\lambda \tag{32}$$

Substituting expressions 11 and 6 for  $v_z(r)$  and  $\rho(r)$ , respectively, we find that

$$\frac{j(r)}{P_z} = -\frac{(a^2 - r^2)}{16\pi\eta} \epsilon\kappa^2\psi_0 \frac{I_0(\kappa r)}{I_0(\kappa a)} + \frac{\epsilon^2\psi_0^2}{16\pi^2\eta} \kappa^2 \frac{E_z}{P_z} \left[ 1 - \frac{I_0(\kappa r)}{I_0(\kappa a)} \right] \frac{I_0(\kappa r)}{I_0(\kappa a)} + \frac{E_z}{P_z} \lambda \tag{33}$$

In the streaming potential case with no net flow of current, condition 28 for the ratio  $E_z/P_z$  is appropriate and eq. 33 becomes

$$\frac{j(r)}{P_z\Omega} = -\frac{(1 - r^2/a^2)}{4} (\kappa a)^2 \frac{I_0(\kappa r)}{I_0(\kappa a)} + \left\{ 1 + \beta \left[ 1 - \frac{I_0(\kappa r)}{I_0(\kappa a)} \right] \frac{I_0(\kappa r)}{I_0(\kappa a)} \right\} f(\kappa a, \beta) \tag{34}$$

With  $\beta = 4.5$ , the function on the right-hand side of expression 34 is plotted in Figures 5 and 6 for various values of  $\kappa a$ . In order to show the effect of the parameter  $\beta$ , the function is plotted in Figure 7 with  $\kappa a = 10$  for the three values of  $\beta$  which were used in Figure 4.

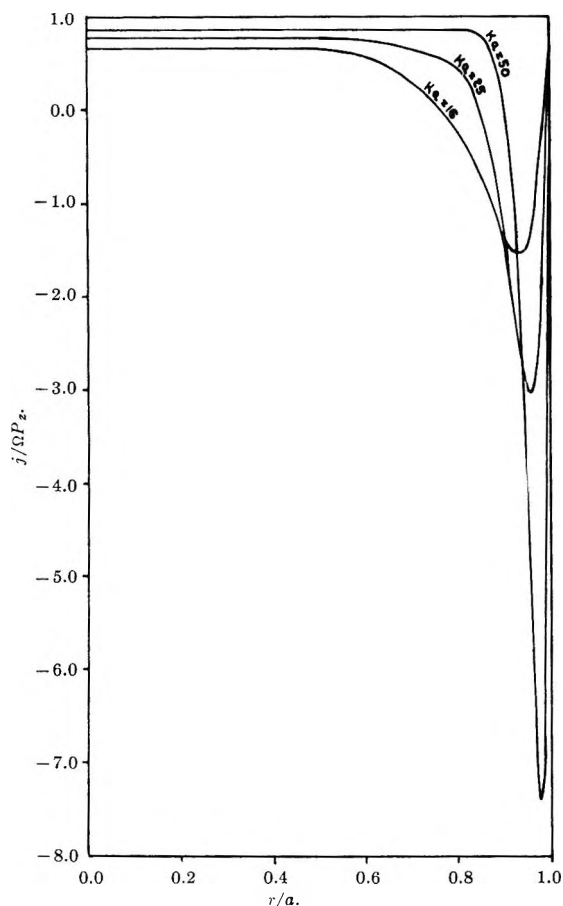


Figure 6. Variation of current density across the capillary with  $\beta = 4.5$ .

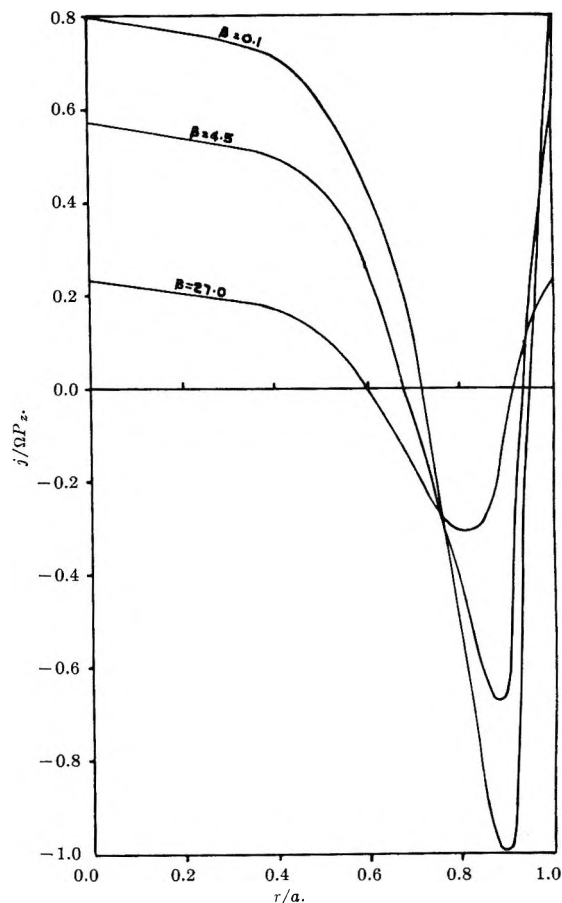


Figure 7. Variation of the current density across the capillary with  $\kappa a = 10$ .

The curves have been obtained by assuming that the conductivity  $\lambda$  is uniform throughout the fluid and by neglecting the effect of surface conductance. Due to this there must be some uncertainty as to the behavior of the curves at distances very close to the capillary wall.

For a capillary of radius  $a = 10^{-5}$  cm. containing a uni-univalent electrolyte of concentration  $10^{-1}$  M,  $\kappa a = 100$ , and the reversal point of the current nearest to the capillary wall occurs at a distance of  $10 \text{ \AA}$ . from it. For values of  $\kappa a$  less than 100 or for values of the radius greater than  $10^{-5}$  cm., the reversal point is at a larger distance than this from the wall. Despite the uncertainty in the behavior of the curves very close to the wall, it is felt that these reversal points are meaningful physically.

From Figures 5 and 6, it is seen that there is only one reversal point for each of the values  $\kappa a = 1, 2$ , but for the higher values of  $\kappa a$  there are two.

This can be explained if the situation pertaining for the higher values of  $\kappa a$  is considered first. Assuming

that  $\psi_0$  is positive, then  $\rho(r)$  is negative, and near the wall the negative ions move in the negative direction, as their mobility under the field  $E_z$ , which is set up, is in the negative direction and is greater than their transport in the positive direction due to  $P_z$ ,  $v_z(r)$  being very small. Thus  $j(r)$  is positive; *i.e.*,  $E_z\lambda > v_z(r)\rho(r)$ .

Near the center of the capillary  $\psi \simeq 0$  and so  $\rho(r) \simeq 0$ .  $j(r)$  then depends on the conductance and is virtually independent of  $P_z$ . Thus again  $j(r)$  is positive; *i.e.*,  $E_z\lambda > v_z(r)\rho(r)$ .

In part of the intervening region,  $\psi$  and  $\rho(r)$  are small but not negligible, and the transport of net negative charge in the positive direction outweighs the conductance effect in the opposite direction.  $j(r)$  is therefore negative, *i.e.*,  $E_z\lambda < v_z(r)\rho(r)$ , and there will be two reversal points.

For the lower values of  $\kappa a$ , *e.g.*,  $\kappa a = 1, 2$ , the situation near the center of the capillary is different from the above. Now as  $r \rightarrow 0$ ,  $\psi$  and  $\rho(r)$  are still appreciable and hence there is no region where the conduct-



ance contribution can again overcome the transport contribution, as it does near the wall. So  $E_z \lambda < v_z(r) \rho(r)$ ,  $j(r)$  remains negative, and there will be only one reversal point.

### The Electroviscous Effect

When a liquid is forced through a narrow cylindrical capillary under an applied pressure gradient, a streaming potential gradient is set up, and the volume flow is given by eq. 17. This reduced rate of flow results in the apparent viscosity  $\eta_a$  where

$$V = \frac{P_z a^2}{8\eta_a} A_c \quad (35)$$

Substituting this expression in eq. 17 gives

$$\frac{P_z a^2}{8\eta_a} A_c = \frac{P_z a^2}{8\eta} A_c - \frac{\epsilon \psi_0}{4\pi\eta} E_z A_c \left[ 1 - \frac{2I_1(\kappa a)}{\kappa a I_0(\kappa a)} \right] \quad (36)$$

In the streaming potential case we can substitute relationship 28 for  $E_z/P_z$  obtaining

$$\eta_a = \frac{\eta}{1 - \frac{8\beta \left[ 1 - \frac{2I_1(\kappa a)}{\kappa a I_0(\kappa a)} \right]}{(\kappa a)^2 \left\{ 1 - \beta \left[ 1 - \frac{2I_1(\kappa a)}{\kappa a I_0(\kappa a)} - \frac{I_1^2(\kappa a)}{I_0^2(\kappa a)} \right] \right\}}} \quad (37)$$

Using the asymptotic expansions, it is found that for very large values of  $\kappa a$

$$\eta_a = \frac{\eta}{1 - \frac{8\beta}{(\kappa a)^2}} = \frac{\eta}{1 - \frac{\epsilon^2 \psi_0^2}{2\pi^2 a^2 \lambda \eta}} \quad (38)$$

Under the conditions  $\epsilon = 81$ ,  $\eta = 10^{-2}$  c.g.s.,  $\psi_0 = 100$  mv.,  $\Lambda = 100$  ohm $^{-1}$  cm. $^2$  g.-equiv. $^{-1}$ , for a uni-univalent electrolyte of concentration  $10^{-3}$  M with a capillary radius  $a = 10^{-4}$  cm., then  $\kappa a = 100$  and  $\epsilon^2 \psi_0^2 / 2\pi^2 a^2 \lambda \eta \simeq 4 \times 10^{-3}$ . Expanding (38) by the binomial theorem, since  $\epsilon^2 \psi_0^2 / 2\pi^2 a^2 \lambda \eta \ll 1$ , we obtain

$$\eta_a = \eta + \frac{\epsilon^2 \psi_0^2}{2\pi^2 a^2 \lambda} \quad (39)$$

\* This was the result obtained by Elton and Hirschler<sup>4</sup> for the electroviscous effect. However, in deriving it, they assumed that  $E_z/P_z = \epsilon \psi_0 / 4\pi \eta a \lambda$ .

This assumption is not theoretically valid, although in practice it would be correct for values of  $\kappa a$  greater than 100, but not for values of  $\kappa a$  between 10 and 100 as implied in their treatment.

Equation 39 for the electroviscous effect holds then only for large values of the electrokinetic radius but under these conditions the effect is almost negligible, so that the equation has no real significance.

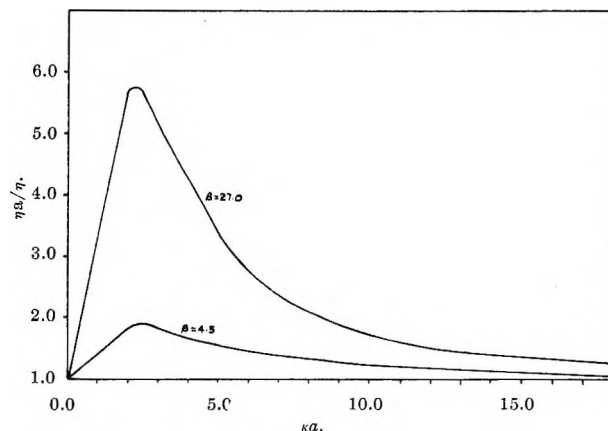


Figure 8. Variation of the apparent viscosity with  $\kappa a$ .

In Figure 8,  $\eta_a/\eta$  calculated from eq. 37 is plotted against  $\kappa a$  for two values of  $\beta$ . The curve for  $\beta = 0.1$  is not plotted since at its maximum value  $\eta_a$  is only about 2% greater than  $\eta$ . The curves show that the electroviscous effect has a maximum value when  $\kappa a = 2.2$ .

Burgreen and Nakache also predicted a maximum in the electroviscous effect for flow in capillary slits. This maximum occurred in the case of distilled water in equilibrium with the  $\text{CO}_2$  of the air, with the ionic concentration  $c = 2.1 \times 10^{-6}$  mole/l., when the half-width of the slit was  $1.7 \times 10^{-5}$  cm.

Under these same conditions, we find that the largest retardation in the flow occurs when the radius of the capillary is  $5.1 \times 10^{-5}$  cm. The fact that the maximum electroviscous effect occurs in a cylindrical capillary at a radius greater than the half-width of a capillary slit is to be expected on geometrical grounds.

When  $\beta = 27.0$ , the flow can be reduced by as much as 80%, making passage through the capillary difficult. If a bed of fine particles is considered as a network of more or less independent capillaries, then under the circumstances described above, it would not be very permeable.

In conclusion, it is worth repeating that the dependence of the various electrokinetic phenomena on the electrokinetic radius  $\kappa a$  has been calculated on the basis of the Debye-Hückel approximation for the net charge density in the double layer. This means that the above theory is satisfactory when used for low values of  $\psi_0$ , but that its results can only be used tentatively for higher values of  $\psi_0$ . In order to see whether the theory can be reasonably extended to these higher

(4) G. A. H. Elton and F. G. Hirschler, *Proc. Roy. Soc. (London)*, **A198**, 581 (1949).

values we propose to obtain a numerical solution of the Poisson-Boltzmann equation for a cylindrical

capillary and compare it with the approximate solution.

## Application of a High Intensity, Multislit Rayleigh Interferometer to Sedimentation Studies

by Irwin H. Billick and Robert J. Bowen

*Macromolecules Section, National Bureau of Standards, Washington, D. C. (Received March 8, 1965)*

In order to obtain a high light intensity interferometer for sedimentation studies, the multislit system of Svensson has been used with the Spinco Model E ultracentrifuge. Other advantages of the multislit system, in addition to greatly increased light intensity, are (1) the simultaneous recording of the schlieren pattern of the refractive index gradient as well as the integral interference curves and (2) the interference fringes, extending over about 150 fringes, which make it possible to follow one fringe across the entire cell, even for concentrated solutions. Examples are given of the application of this optical system to high speed velocity sedimentation and low speed equilibrium sedimentation of polystyrene in cyclohexane. In the case of the velocity sedimentation, studies were made over a concentration range below that normally used with schlieren optics. Accurate values of the concentration were obtained by suitable extrapolation to zero time of sedimentation, and values of the sedimentation coefficient and pressure dependence parameter could be calculated from the extrapolation data. For the particular systems studied, the existence of the plateau region was observed, within experimental error, contrary to the prediction of the theory of sedimentation of pressure-dependent solutions.

### Introduction

The use of interference optics for the measurement of concentration in a rotating ultracentrifuge cell has several advantages over the more commonly used optical systems. Foremost of these is its superiority over other optical methods for the accurate determination of concentrations.<sup>1</sup> In addition, since the sensitivity of the interferometer is greater than that of the more commonly used schlieren system, it is very important for studies of materials that exhibit large concentration dependence. While light absorption optics possesses even greater sensitivity, it is unfortunate that many macromolecules of interest do not have a chromophoric group in the molecule. In spite of its advan-

tages, the application of the interferometer for producing ultracentrifuge patterns has been slow<sup>2</sup>; what acceptance it has had, has been mainly for sedimentation equilibrium experiments or low speed velocity studies.

It has been observed that at the high speeds normally used for sedimentation velocity studies, the fringes produced by the Rayleigh interferometer become blurred and eventually disappear. Several possible steps which can be taken to improve the quality of the fringes have been suggested in the literature. For

(1) H. K. Schachman in "Ultracentrifugal Analysis in Theory and Experiment," J. W. Williams, Ed., Academic Press Inc., New York, N. Y., 1963.

(2) H. K. Schachman, *Biochemistry*, 2, 887 (1963).

example, replacement of the quartz cell windows with sapphire reduces some of the fringe distortion.<sup>3</sup>

A second procedure for improving the quality of the fringes is to reduce the width of the light source slit.<sup>4,5</sup> The dimension of the slit width depends upon the characteristics of the individual optical system; however, calculations which may be considered typical for the interference optical system in the Spinco Model E ultracentrifuge have been carried out by LaBar and Baldwin,<sup>4</sup> who found that the maximum permissible source slit width for their system was approximately 0.02 mm.

Decreasing the width of the source slit improves the quality of the fringes considerably and is independent of the experimental variables, such as material studied and centrifuge speed. However, it has been observed that the widths of the fixed apertures are not independent of these variables and that their modification also can improve fringe quality.<sup>1,3</sup> These apertures consist of two parallel slits and are usually fastened on the upper schlieren lens holder.<sup>3,6</sup> If the widths of these slits are too large, fringe distortion results which is a function of the speed of the centrifuge. In the first place, blurring results because too much of the rotating cell is "seen" at given times. Secondly, when large refractive index gradients are produced in the cell, the resulting interference patterns are blurred or annihilated.<sup>2</sup> Obviously, refractive index gradients, even with solvent alone, are produced by hydrostatic pressure, which is a function of speed, and are greater in the case of compressible organic solvents than in the case of relatively incompressible water. It was found<sup>2</sup> that decreasing the width of both the slits results in an improvement in fringe quality. A typical modification has been a reduction of width from 0.75 to 0.24–0.36 mm.<sup>2</sup>

Experiments were tried which applied all of the previous recommendations to the study of the velocity sedimentation of polystyrene in cyclohexane but met with little success. It was found that, in addition to the first two recommendations, it was necessary to reduce the upper lens slits to 0.20 mm. before good quality fringes were obtained.

When both the source and the upper aperture slits have been narrowed to the point where good quality fringes are observed, the intensity of the light that impinges upon the photographic film is so low that exposure times become too long for sedimentation velocity studies where a rapidly moving boundary is present. Some increase in light intensity can be obtained by redesigning the cell window holder,<sup>2</sup> but the increase is not as much as would be desirable.

The problem, therefore, is to increase the intensity

of light passing through the optical system. This, of course, can be accomplished by replacing the light source with one of greater intensity, but a simpler method exists. A design for a high intensity Rayleigh interferometer has been given by Svensson<sup>7</sup> and has been applied by him to diffusion studies.

In the present work, we have applied Svensson's method to the Spinco Model E ultracentrifuge. The only modification to the present commercial optical system is the replacement of the single light source slit by a multiple slit having specified dimensions.

In the single slit system, a series of fringes is produced within a central diffraction band. When multiple slits are used, an interferogram will be produced by each slit, and, if the spacings between the slits are sufficiently close together, the individual interferograms will overlap. If the separation is chosen correctly, the fringes from the individual patterns can be made to coincide, and the resulting multifringe pattern will now be much brighter than that resulting from a single slit. In addition, the resulting interferogram has the property that the fringes cover the entire photographic plate in the direction normal to the radial direction making it possible to follow a single fringe throughout the entire cell, even for a concentrated solution.

### Experimental Section

Svensson showed<sup>7</sup> that, for the type of Rayleigh interferometer presently used in the Spinco Model E, the requirement for fringe coincidence is given by

$$e = \frac{f\lambda}{d} \quad (1)$$

where  $e$  is the grating constant, *i.e.*, the slit separation,  $f$  is the focal length of the lower collimating lens,  $d$  is the separation of the slits in the Rayleigh mask, and  $\lambda$  is the wave length of light.

We have chosen values of the parameters, given in eq. 1, so that they are adaptable to available instruments. The fixed upper aperture was the symmetrical type<sup>3</sup> and also served as the Rayleigh mask. Several pairs of slits having variations in widths from 0.33 to 0.15 mm. were machined from brass. The separations of the centers of these slits were measured on a micro-comparator and were found to have an average value of

(3) E. G. Richards and H. K. Schachman, *J. Phys. Chem.*, **63**, 1578 (1959).

(4) F. E. LaBar and R. L. Baldwin, *ibid.*, **66**, 1952 (1962).

(5) F. A. Jenkins and H. E. White, "Fundamentals of Optics," McGraw-Hill Book Co., Inc., New York, N. Y., 1950, p. 314.

(6) Spinco Division, Beckman Instruments Inc., Technical Bulletin No. 6001-B, 1958.

(7) H. Svensson, *Acta Chem. Scand.*, **5**, 1301 (1951).

$d = 0.397 \pm 0.001$  mm. The various width slits were all tried in the optical system, and the pair having a width of 0.20 mm. was found to be the most suitable for general use. A Baird-Atomic interference filter having a peak wave length of  $\lambda$  5460 Å. and a half band width of 84 Å. was used although acceptable results were obtained using the Wratten 77 or 16 filters. The focal length of the lower collimating lens was measured by the Refractometry Section of the National Bureau of Standards and found to have an equivalent focal length of 587.75 mm., as contrasted to the nominal focal length of 590.55 mm. stated by the supplier. The value of the grating constant was therefore  $e = 0.0808$  mm.

The value of the maximum source slit width,  $PP'$ ,<sup>4</sup> for our system can be evaluated from the above data according to

$$PP' = \frac{f\lambda}{4d} = \frac{e}{4} \quad (2)$$

The value of  $PP'$  was found to be 0.0202 mm.; however, a value of 0.01 mm. was used in order to improve the image quality still further.

The light source in the Model E is a high-pressure mercury vapor lamp, Type AH-6. It has a usable length of 1.90 cm., and a grating of 201 slits with the above parameters was used so that the entire length of the source would be utilized. Rather than have only one grating made which would be used directly, a negative was manufactured to our specifications by the Bausch and Lomb Co. The master negative was constructed by ruling slits in a deposit of Inconel on glass. The dimensions of the negative were such that the positive slit dimensions were  $0.010 \pm 0.0025$  mm. by  $10.0 \pm 0.1$  mm. The spacing accuracy between any adjacent slits is  $\pm 0.0025$  mm. Working gratings were obtained by contact exposure of the master negative on  $2 \times 2$  in. Kodak High Resolution photographic plates.

At first, an attempt was made to place the grating directly over the light source.<sup>7</sup> However, even though water cooling was used, the grating was destroyed by heat in a matter of seconds. The final arrangement was to place the grating on top of the dust cover of the light source, separated from the source itself by a piece of heat-reflecting glass (Bausch and Lomb Type No. 90-12). The light filter, in turn, was mounted on top of the grating.

The alignment of the optical system was carried out following the procedure recommended by Gropper.<sup>8</sup> For initial positioning of the height of the light source, the multiple slit was replaced by a single slit, made by exposing a photographic plate over which a thin wire had been stretched. The slit was positioned emulsion

side up and the height of the source adjusted so that the slit image on the photographic plate was located in the focal plane of the lower collimating lens. The  $2/3$  plane was chosen for the plane of focus of the camera lens on the centrifuge cell<sup>9</sup> to eliminate Wiener skewness. As an aid in some steps of the alignment a Polaroid back was mounted over a hole in the back of the camera and was used where focusing on the plane of the photographic plate was not required.

For the current investigation, studies were made of the sedimentation of N.B.S. Standard Polystyrene Sample No. 705 in cyclohexane at 35°. A total of four concentrations, ranging from  $0.05 \times 10^{-2}$  to  $0.3 \times 10^{-2}$  g./cc., was investigated using a 12-mm. thick, aluminum-filled epoxy, double-sector centerpiece. Since it was desirable to have equal levels in both the solvent and solution compartments, the centerpiece was modified so that a connecting channel existed at the extreme top and bottom of the sectors. When the cell was filled, the amount of solution used was such that the solution was at a slightly higher level than the solvent. At a fairly low speed, the levels would equalize, and a synthetic boundary would be formed, which was always close enough to the cell bottom so that it would sediment to the bottom and no longer be visible in the pattern. The same cell was used, without disassembling, for all concentrations, and a blank was run using solvent in both sectors.

All runs reported here were made at 50,740 r.p.m.; however, runs made at speeds up to 60,000 r.p.m. exhibited satisfactory fringe patterns. Photographs were taken on Kodak II-G plates, with exposure times varying between 15 and 25 sec. In order to enhance the contrast, plates were underexposed and overdeveloped in D-19 developer. To increase contrast of the fringes further, contact prints were made on Kodak Metallographic plates, and the fringes were then read on a two-dimensional comparator. The comparator is accurate to  $\pm 1 \mu$ .

Figures 1 and 2 illustrate typical patterns obtained using this optical system. The pattern of Figure 1 was obtained from a  $0.3 \times 10^{-2}$ -g./cc. solution 80 min. after time zero at 50,740 r.p.m. Figure 2 is a photograph of the solvent pattern taken at the same speed.

One of the advantages of this multislit system is the extent of the pattern, which permits the same fringe to be followed throughout the entire cell.<sup>7</sup> This was, therefore, the procedure used when the fringes were measured. Measurements were taken beginning as close as possible to the meniscus and extending as near

(8) L. Gropper, *Anal. Biochem.*, **7**, 401 (1964).

(9) H. Svensson, *Opt. Acta*, **1**, 25 (1954).

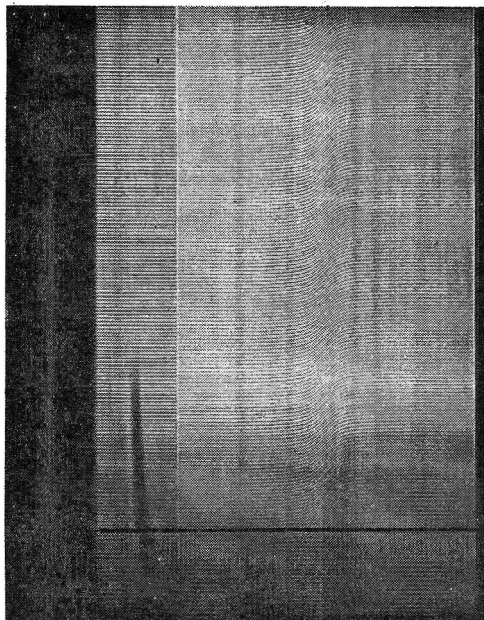


Figure 1. Photograph of interference pattern given by a  $0.3 \times 10^{-2}$ -g./cc. solution of polystyrene in cyclohexane using multislit optics. Pattern produced after 80 min. of centrifugation at 50,740 r.p.m.

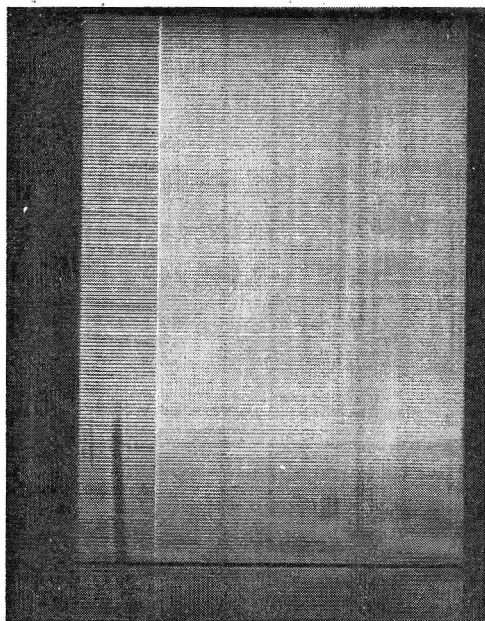


Figure 2. Photograph of solvent fringes obtained with multislit optics at 50,740 r.p.m.

to cell bottom as possible, recording both the displacement of the fringe and its position. The interval between measurements in the radial direction varied, with smaller intervals taken in the boundary region.

The particular system described produces a pattern containing about 150 fringes. Measurements of the

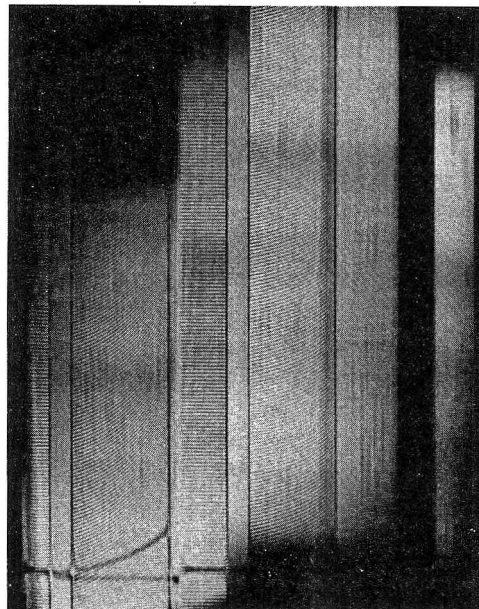


Figure 3. Patterns produced by two-cell operation at 5563 r.p.m. Solutions are polystyrene in cyclohexane: upper solution concentration  $0.398 \times 10^{-2}$  g./cc.; lower solution concentration  $0.208 \times 10^{-2}$  g./cc. Photograph shows both interference and schlieren patterns as described in text.

spacings between 20 successive fringes showed that the spacing on the photographic plate was 0.269 mm. with a standard deviation of 0.008 mm. Both the fringe spacing and the standard deviation are of the same magnitude as a comparable single-slit system.<sup>10</sup> Measurements of the blank showed that the fringes were not linear; however, the blank did not appear to be speed dependent and was reproducible, as has been reported by others.<sup>10</sup>

This particular optical system is also adaptable to multicell operation, by proper use of false bottoms and masking. Figure 3 illustrates a two-cell equilibrium run of polystyrene in cyclohexane. Results obtained from these experiments are not reported here, but the figure is included as an example of the utility of the optical system. It will be noticed that, here again, it is possible to follow one fringe throughout the entire pattern, so that fringe counting and calculation of fractional fringes<sup>4</sup> are not necessary. Figure 3 shows an additional advantage of this particular optical system, namely, its ability to produce the schlieren pattern of the refractive index gradient simultaneously with the integral interference curve.<sup>7</sup> To produce this particular pattern a slit 0.20 mm. wide was superimposed on the grating so that the slits on the grating were per-

(10) D. A. Yphantis, *Biochemistry*, 3, 297 (1964).

pendicular to the second slit, and an exposure was made. It was necessary, however, to increase the exposure time by a factor of 4. Figure 3 was taken at 5563 r.p.m. and a phase plate angle of  $75^\circ$ .

Preliminary processing of the data from the velocity experiments involved conversion of plate position to radial position followed by subtraction of the base-line reading at constant radius. The corrected data were then numerically differentiated twice with respect to radial distance and the results inspected. The boundary was chosen as the region over which the fringe displacement showed a monotonic increase with distance from the center of rotation.

In theory,<sup>11,12</sup> for a system in which the solvent and solute show a large pressure dependence, there is continuous increase in concentration from the solvent side, through the boundary region, and all the way to the cell bottom; *i.e.*, the "plateau" does not exist. At the velocity and concentrations used in this study, calculations according to the theory of Fujita<sup>12</sup> showed that this effect should be measurable within the experimental error of the multislit optical system. However, none of the data indicates this phenomenon, and, for all the systems reported, a "plateau" region was assumed to exist within experimental error. Therefore, the concentration change across the boundary was calculated from the difference in fringe height between an average of first and last points surrounding the boundary.

Three methods were used to locate the average boundary position, *viz.*, the second moment,<sup>13</sup> the radial position at which the concentration is equal to one-half the plateau concentration, and the radial position at which the second derivative of the concentration curve with respect to radial distance is equal to zero (*i.e.*, peak maximum). Analysis of the data did not show a significant difference for the values of the boundary position calculated by the above methods. Therefore, only the results based on the radial position at one-half the plateau concentration are given.

Sedimentation coefficients were calculated according to previously described methods<sup>14</sup> in which corrections were made for pressure effects and radial dilution. All calculations were carried out using an IBM 7094 electronic computer with programs written in FORTRAN.

## Results

If the assumption that a plateau region exists is valid, the concentration change across the boundary,  $c$ , is given by<sup>12,15,16</sup> eq. 3a and b, where  $y = (r/r_0)^2$ ,  $r$  being

$$\frac{c}{c_0} = \frac{1}{y(1 - m(y - 1))} \quad (3a)$$

$$\frac{c}{c_0} = \frac{1}{y^2} \exp(1 + m)\tau \quad (3b)$$

the radial position of the boundary and  $r_0$  the meniscus position,  $\tau = 2s_0\omega^2t$ ,  $\omega$  being the angular velocity,  $t$  the time,  $s_0$  the sedimentation coefficient at 1 atm. pressure,  $c_0$  the concentration at  $t = 0$ , and  $m$  the pressure dependence parameter as defined in ref. 12. These equations suggest plots from which values of  $c_0$ ,  $s_0$ , and  $m$  may be obtained from the measured values of  $c$  and  $y$ . Figure 4 shows data plotted as  $1/cy$  vs.  $y - 1$ , and Figure 5 shows plots of  $\ln cy^2$  vs.  $\omega^2t$ . A somewhat similar treatment of the data, obtained through the use of schlieren optics but at concentrations higher than those reported here, has been reported previously.<sup>17</sup>

The results for the concentrations at zero time and  $y = 1$  given in Table I were obtained by least-squares analysis of the data according to eq. 3a and b. Columns 1 and 2 give the calculated zero time concentrations using a value of  $dn/dc$  for polystyrene in cyclohexane of  $0.1707 \times 10^{-2}$  cc./g.<sup>18</sup> The concentrations

Table I: Concentration Determined Using Multislit Optics

$c_0 \times 10^2$ , g./cc.	$c_0$	$c_0$	$c_0$	$c_0$	$c_0$
	(calcd.), fringes	(measd.), <sup>a</sup> fringes	(measd.), <sup>b</sup> fringes	(measd.)/ $c_0$ (calcd.)	(calcd.) - $c_0$ (measd.), fringes
0.051	1.90	1.82	1.83	0.96	0.08
0.100	3.74	3.71	3.72	0.99	0.03
0.199	7.44	7.49	7.50	1.01	-0.06
0.297	11.10	10.88	10.88	0.98	0.22

<sup>a</sup> Determined from eq. 3a. <sup>b</sup> Determined from eq. 3b.

obtained by extrapolation of eq. 3a and b are given in columns 3 and 4, respectively. The ratios of  $c_0$  (measured) to  $c_0$  (calculated) are given in column 5 and, with the exception of the lowest concentration, show the good accuracy which is obtainable. The values of the differences between  $c_0$  (calculated) and  $c_0$  (measured) are given in column 6 and are, for the most part, of the order of magnitude which one would expect from the precision of measurement of the fringes. The agreement between  $c_0$  (calculated) and  $c_0$  (measured) indi-

- (11) A. F. V. Eriksson, *Acta Chem. Scand.*, **10**, 360 (1956).
- (12) H. Fujita, *J. Am. Chem. Soc.*, **78**, 3898 (1956).
- (13) R. J. Goldberg, *J. Phys. Chem.*, **57**, 194 (1953).
- (14) I. H. Billick, *ibid.*, **66**, 1941 (1962).
- (15) M. Wales, *J. Am. Chem. Soc.*, **81**, 4758 (1959).
- (16) I. H. Billick, *J. Polymer Sci.*, **62**, 167 (1962).
- (17) J. E. Blair and J. W. Williams, *J. Phys. Chem.*, **68**, 161 (1964).
- (18) J. H. O'Mara and D. McIntyre, *ibid.*, **63**, 1435 (1959).



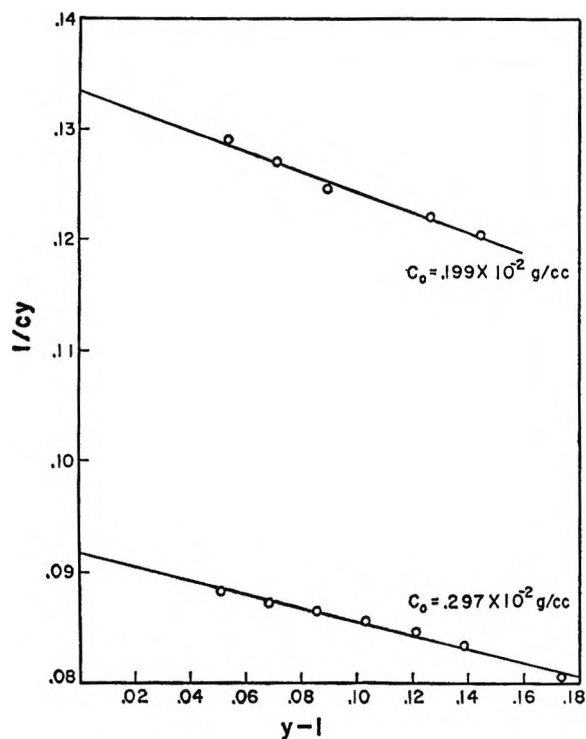


Figure 4. Plots of  $1/cy$  vs.  $y - 1$  for two concentrations of polystyrene in cyclohexane. Values of  $c$  are in centimeters.

icates that the assumption of a plateau region can be considered as valid.

The values of  $s_0$  and  $m$  obtained from the least-squares analysis of the data are given in Table II. Those given under I were obtained when eq. 3a and b were applied, and those under II were obtained from application of eq. 4<sup>14</sup>

$$\ln r = \ln r_0 + s_0 \omega^2 t - m(s_0 \omega^2 t)^2 \quad (4)$$

**Table II:** Sedimentation Coefficients and Pressure Dependence Parameter for Polystyrene 705 in Cyclohexane at 35°

$c_0 \times 10^2$ , g./cc.	I		II	
	$s_0$ , S.	$m$	$s_0$ , S.	$m$
0.051	6.93	0.91	6.71	0.68
0.100	6.63	0.63	6.74	0.79
0.199	6.56	0.68	6.39	0.46
0.297	6.32	0.71	6.32	0.71

Values of  $m$  and  $s_0$  obtained by the two methods are not in very good agreement with each other, with the exception of the highest concentration. However, the correct value for  $s_0$  probably lies intermediate between

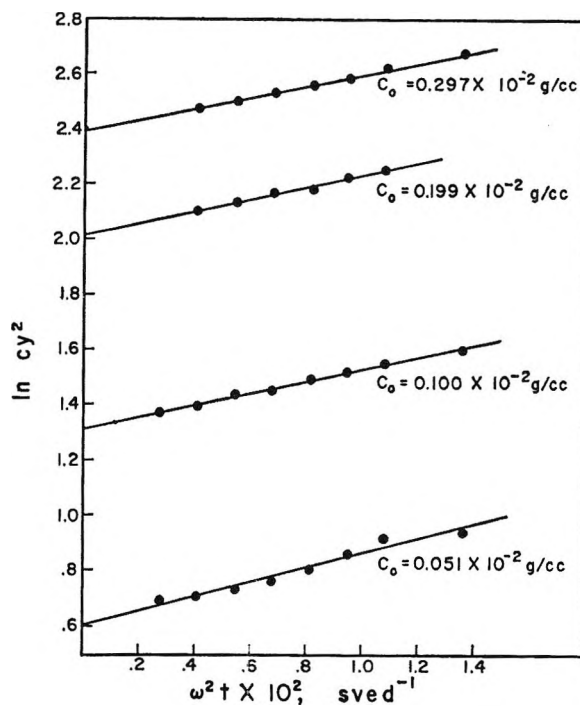


Figure 5. Plots of  $\ln cy^2$  vs.  $\omega^2 t$  for four concentrations of polystyrene in cyclohexane. Values of  $c$  are in centimeters.

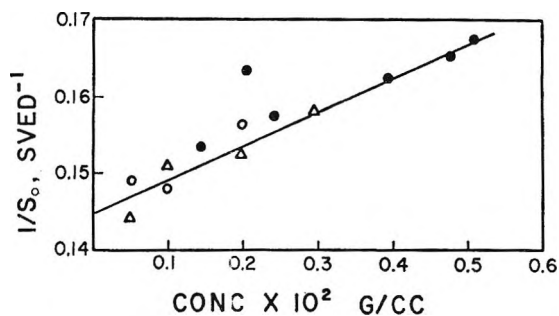


Figure 6. Variation of the sedimentation coefficients of polystyrene in cyclohexane at 35° with original concentration,  $c_0$ . The filled circles are from schlieren data; the open circles and the triangles are the data of Table II.

the two values as can be seen in Figure 6. This figure shows a plot of  $1/s_0$  vs.  $c_0$  obtained over a tenfold range of concentration. The data represented by the filled circles were obtained under the same experimental conditions used here but with schlieren optics and calculated according to eq. 4. The values of  $s_0$  obtained using the interferometer are in good agreement with those obtained using the schlieren optics. Methods of improving the precision of the measurement of  $s_0$  are being investigated.

The two major improvements that the multislit interferometer presents over the single-slit method are the increased light intensity and the ability to follow a

single fringe over the entire cell. An added feature is the simultaneous recording of both the differential and integral forms of the refractive index of the solution as a function of distance in the cell.

With regard to this latter point, the optical arrangement as described here does not produce a very high-quality schlieren pattern. Indeed, below a phase angle of  $75^\circ$  the resolution is not good. Preliminary investigations using a device which is composed of a horizontal slit and a series of vertical slits, side by side, as suggested by Svensson,<sup>7</sup> have shown very promising results. Other methods of improving the quality of both the interference and schlieren patterns are also being investigated.

The one major drawback of the system, as compared

with the single-slit system, is that the white light fringes are no longer obtainable. In all other respects the two systems are comparable, and any inherent limitations or advantages of one apply equally to the other.

The interferometric method described here permits accurate concentration measurements at concentrations that are about five times lower than those previously obtained with schlieren optics. This is of particular importance in boundary-spreading analysis where very dilute solution studies are required.<sup>19</sup> Indeed, if longer cells were used, the lower concentration range could be extended even further.

(19) R. L. Baldwin and K. E. van Holde, *Fortschr. Hochpolymer. Forsch.*, **1**, 451 (1960).

## NOTES

### The Enthalpy of Formation and the Dissociation Energy of Thallium Monofluoride<sup>1</sup>

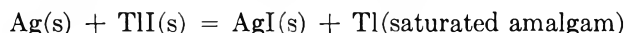
by Daniel Cubicciotti and Gettis L. Withers

Stanford Research Institute, Menlo Park, California  
(Received June 4, 1965)

Barrow and co-workers<sup>2</sup> have pointed out a discrepancy between the dissociation energy of TlF determined by them from spectroscopic data ( $109.5 \pm 0.6$  kcal./mole) and the thermochemically derived value (104.1, according to data available to them). The 5.4-kcal. difference was too large to be experimental error; this implied that some of the thermochemical data were in error. In a companion paper<sup>3</sup> we have shown that their enthalpy of sublimation of TlF was in error by 2.5 kcal./mole. (In their vaporization measurements, Barrow, *et al.*,<sup>4</sup> were unaware that the predominant vapor species was  $Tl_2F_2$ , not TlF.) In order to resolve the 3-kcal. difference that still remained, we have redetermined the enthalpy of formation of TlF. With this new value and recent values for the other quantities involved, the dissociation energy from thermochemical data is found to agree with the spectroscopic value within the uncertainties in the data.

### Experimental Section

The enthalpy of formation of solid TlF was determined relative to that of TlI by measuring the enthalpy of solution of TlF in water and subsequently measuring the enthalpy of precipitation of TlI from the same solution. The literature value for the enthalpy of formation of TlI was checked in two ways: (1) by measuring the enthalpy of solution of  $TlNO_3$  and its precipitation from solution as TlI and (2) from the e.m.f. of a galvanic cell in which the cell reaction was



and literature values for the absolute entropies of these substances.

*Enthalpy Measurements.* A very simple calorimeter was used. It consisted of a 500-ml. dewar with a hand-operated lift stirrer and a Beckmann thermometer. Two tubes closed at the bottom with rubber stoppers projected into the solution in the dewar. These contained the solids or solutions to be added, and at the

(1) This work was supported by the Research Division of the U. S. Atomic Energy Commission under Contract No. AT(04-3)-106.

(2) R. F. Barrow, H. F. K. Cheall, P. M. Thomas, and P. B. Zeeman, *Proc. Phys. Soc. (London)*, **71**, 128 (1958).

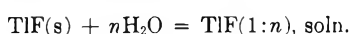
(3) F. J. Keneshea and D. Cubicciotti, *J. Phys. Chem.*, **69**, 3910 (1965).

(4) R. F. Barrow, E. A. N. S. Jeffries, and J. M. Swinstead, *Trans. Faraday Soc.*, **51**, 1650 (1955).



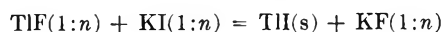
proper time the stoppers were pushed out so that the additive emptied into the dewar. About 400 g. of water was used in each determination together with the proper amounts of salts to produce the solution of specified concentration. The temperature changes ranged from 0° (for the formation of the most dilute TlF solution) to about 1.6° (for the precipitation of TlI from the most concentrated solution). The uncertainty in measuring the temperature change due to reaction was taken to be  $\pm 0.005^\circ$ . The calorimeter constant was determined by measuring the enthalpy of neutralization of 25.0 ml. of 1.00 *N* HCl (in 375 ml. of water) when 15.0 ml. of 2 *N* KOH was added from one of the side tubes. Values for the enthalpy of dilution of KOH and reaction of HCl and KOH solutions were taken from Circular 500.<sup>5</sup> The heat capacity of the calorimeter, exclusive of the water and chemicals, was found by these determinations to be  $40 \pm 3$  cal./deg. This value was combined with the heat capacities of water and chemicals in a determination to evaluate the calorimeter constant. The uncertainties associated with the individual enthalpy values (listed in Tables I and II) were calculated from that of the temperature measurement ( $\pm 0.005^\circ$ ) and of the calorimeter constant ( $\pm 3$  cal./deg.).

**Table I:** Enthalpy of Solution of TlF



Dilution, <i>n</i> , moles of TlF:mole of H <sub>2</sub> O	$\Delta H_{298}$ , kcal./mole of TlF
1:492	$0.41 \pm 0.05$
1:995	$0.2 \pm 0.1$
1:1010	$0.15 \pm 0.08$
1:2100	$0.0 \pm 0.2$

**Table II:** Enthalpy of Precipitation Reaction



Dilution, <i>n</i> , moles of salt:mole of H <sub>2</sub> O	$\Delta H_{298}$ , kcal./mole
1:492	$-17.4 \pm 0.1$
1:995	$-17.5 \pm 0.1$
1:1010	$-17.4 \pm 0.1$
1:2100	$-17.0 \pm 0.2$

*E.m.f. Measurements.* A galvanic cell that can be schematically represented as

Tl(saturated amalgam)-TlI(s) KI(0.1 *N*) AgI(s)-Ag was constructed. Three Ag-AgI electrodes were prepared by the "thermal-electrolytic" method described by Ives and Janz.<sup>6</sup> These were allowed to stand until the differences in their potentials in a 0.1 *N* KI solution dropped to less than 0.2 mv. They were then placed in one leg of an H-cell containing 0.1 *N* KI. About 25 g. of triple-distilled Hg was placed in the other, and N<sub>2</sub> was bubbled through the solution to expel dissolved air. A piece of about 30 g. of Tl (99.999% from the American Smelting and Refining Co.) was cleaned in HNO<sub>3</sub>, rinsed, and dropped into the Hg. About 1 g. of freshly precipitated TlI was added on top of the amalgam so formed. The cell was then immersed in a water bath, and N<sub>2</sub> was continually bubbled through each leg. The e.m.f. was read periodically with a Leeds and Northrup Type K potentiometer.

*Materials.* The TlF was a part of the material used in the vaporization studies.<sup>3</sup> Analysis for Tl showed 91.57% compared to 91.49% theoretical. TlNO<sub>3</sub> was made by dissolving Tl in nitric acid, recrystallizing twice from water, washing with alcohol, and drying. Triplicate analyses for Tl gave  $76.79 \pm 0.03\%$  compared to 76.73% theoretical.

## Results and Discussion

*Enthalpy of Formation of TlF.* The enthalpy of solution of TlF was obtained at four dilutions. The results are given in Table I. The present values are slightly endothermic, whereas the values obtained by Caunt and Barrow<sup>7</sup> were slightly exothermic. The reason for the difference may lie in the purity of the sample. We suspect that Caunt and Barrow may have had some TlHF<sub>2</sub> in their salt. We have found that it is necessary to heat TlF to temperatures of the order of 400° (presumably driving off the last traces of HF) to obtain a product with the theoretical Tl content.

The enthalpy of precipitation of TlI was measured with each of the solutions for which the enthalpy of solution of TlF had been determined. This was accomplished by adding a weighed amount of a 1:10 solution of KI (20% in excess of the TlF) to the solution in the calorimeter. The equation for the precipitation reaction and the enthalpies measured are given in Table II. Finally, the enthalpies of formation of TlI(s) and the solu-

(5) F. D. Rossini, D. D. Wagman, W. H. Evans, S. Levine, and I. Jaffe, National Bureau of Standards Circular 500, U. S. Government Printing Office, Washington, D. C., 1952.

(6) D. J. G. Ives and G. J. Janz, "Reference Electrodes," Academic Press Inc., New York, N. Y., 1961, Chapter 4.

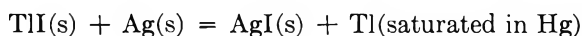
(7) A. D. Caunt and R. F. Barrow, *Trans. Faraday Soc.*, **46**, 154 (1951).

tions of KI and KNO<sub>3</sub> given in Circular 500<sup>5</sup> were used to calculate the enthalpy of formation of TlF(s). The resulting values were  $-77.9 \pm 0.15$ ,  $-77.7 \pm 0.2$ ,  $-77.6 \pm 0.2$ , and  $-77.9 \pm 0.4$  kcal./mole. The average for  $\Delta H_f^{\circ 298}(\text{TlF(s)})$  was  $-77.8$  kcal./mole. An uncertainty interval for this value, based on the over-all nature of the present experiments and those leading to the data for TlI, is about  $\pm 1$  kcal./mole.

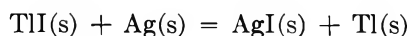
This value is about 1 kcal. more negative than that obtained by Caunt and Barrow. The difference is due to the fact that they found the enthalpy of solution to be about 1 kcal. more exothermic than we. Kubaschewski and Evans<sup>8</sup> report a value of  $-74$  kcal./mole for  $\Delta H_f^{\circ 298}(\text{TlF(s)})$  based on the data of Caunt and Barrow. It is not clear to the present authors why the value given by ref. 8 differs from that of ref. 7.

*Enthalpy of Formation of TlI.* A determination of the enthalpy of solution of TlNO<sub>3</sub> was made at a dilution of 1:489 and resulted in a value of  $9.58 \pm 0.05$  kcal./mole. The enthalpy for the precipitation of TlI from that solution was found to be  $-17.4 \pm 0.1$  kcal./mole. From the values of Circular 500 for the enthalpies of formation of TlNO<sub>3</sub>(s), KI, and KNO<sub>3</sub> solutions, the enthalpy of formation of TlI(s) at 298°K. is  $-29.7 \pm 0.15$  kcal./mole, in agreement with the value given in Circular 500. This measurement constitutes an independent determination of the value for TlI. The value for TlNO<sub>3</sub>(s) in Circular 500 is based on the enthalpy of solution, obtained by Latimer, *et al.*,<sup>9</sup> the enthalpy of formation of Tl<sup>+</sup>, from the cell measurements of Cowperthwaite, *et al.*,<sup>10</sup> and the enthalpy of formation of NO<sub>3</sub><sup>-</sup>, which presumably is well established.

Another scheme was used to establish the enthalpy of formation of TlI, relative to that of AgI. A galvanic cell was constructed, as described above, whose cell reaction was



The e.m.f. of this cell, after an initial aging period of about 8 hr., was  $0.6070 \pm 0.0005$  v. at 20.4° for 3 days and after that began to drop slowly. Richards and Smyth<sup>11</sup> have shown that at 20° the saturated Tl amalgam has a potential of 2.1 mv. compared to pure Tl. Thus, for the reaction



the e.m.f. is 0.6091 v. or  $\Delta F^{\circ 293} = -14.05$  kcal./mole. The absolute entropies at 298°K. for these solids are:  $S^{\circ}(\text{TlI})^{12} = 30.52 \pm 0.02$ ,  $S^{\circ}(\text{Tl})^{13} = 15.34 \pm 0.06$ ,  $S^{\circ}(\text{Ag})^{13} = 10.20 \pm 0.05$ , and  $S^{\circ}(\text{AgI})^{13} = 27.6 \pm$

0.4 e.u.; hence,  $\Delta S^{\circ 293} = 2.22 \pm 0.5$  e.u. Neglecting the small difference in the temperature of the measurements and 298°K., one obtains  $-14.70 \pm 0.2$  kcal./mole for the enthalpy change of the reaction. The enthalpy of formation of AgI is  $-14.91$  kcal./mole according to Circular 500; hence, the enthalpy of formation of TlI is  $-29.6 \pm 0.2$  kcal./mole from these measurements. Thus, this cell measurement gives a value in agreement with Circular 500 for TlI ( $-29.7$  kcal./mole).

*Dissociation Energy of TlF.* The enthalpies of the individual reactions that are combined to give the dissociation energy of TlF are given in Table III. The resulting dissociation energy ( $108 \pm 2.5$  kcal./mole) is in agreement with the spectroscopic value ( $109.5 \pm 0.6$  kcal./mole) within the uncertainties of the data.

**Table III:** Calculation of Dissociation Energy of TlF from Thermochemical Data

Reaction	$\Delta H^{\circ}$ , kcal./mole	Ref.
$\text{Tl(s)} + \frac{1}{2}\text{F}_2(\text{g}) = \text{TlF(s)} \text{ 298}^{\circ}\text{K.}$	$-77.8 \pm 1$	This work
$\text{TlF(s)} = \text{TlF(g)} \text{ 298}^{\circ}\text{K.}$	$31.6 \pm 0.2$	a
$\frac{1}{2}\text{F}_2(\text{g}) = \text{F(g)} \text{ 298}^{\circ}\text{K.}$	$18.9 \pm 0.3$	b
$\text{Tl(s)} = \text{Tl(g)} \text{ 298}^{\circ}\text{K.}$	$43.6 \pm 1$	c
$\text{TlF(g, 0}^{\circ}\text{K.)} = \text{TlF(g, 298}^{\circ}\text{K.)}$	2.2	d
$\text{Tl(g, 0}^{\circ}\text{K.)} = \text{Tl(g, 298}^{\circ}\text{K.)}$	1.5	e
$\text{F(g, 0}^{\circ}\text{K.)} = \text{F(g, 298}^{\circ}\text{K.)}$	1.6	e
<hr/>		
$\text{TlF(g, 0}^{\circ}\text{K.)} = \text{Tl(g, 0}^{\circ}\text{K.)} + \text{F(g, 0}^{\circ}\text{K.)}$	$108 \pm 2.5$	

<sup>a</sup> See ref. 3. <sup>b</sup> "JANAF Thermochemical Tables," The Dow Chemical Co., Midland, Mich., Dec. 31, 1964. <sup>c</sup> R. Hultgren, R. L. Orr, P. D. Anderson, and K. K. Kelley, "Thermodynamic Properties of Metals and Alloys," John Wiley and Sons, Inc., New York, N. Y., 1963. <sup>d</sup> D. Cubicciotti and H. Eding, *J. Chem. Eng. Data*, to be published. <sup>e</sup> K. S. Pitzer and L. Brewer, revision of "Thermodynamics," by G. N. Lewis and M. Randall, McGraw-Hill Book Co., Inc., New York, N. Y., 1961, Appendix 7.

(8) O. Kubaschewski and E. L. Evans, "Metallurgical Thermochemistry," Pergamon Press, Inc., New York, N. Y., 1958, p. 278.

(9) O. L. I. Brown, W. V. Smith, and W. M. Latimer, *J. Am. Chem. Soc.*, **59**, 921 (1937).

(10) I. A. Cowperthwaite, V. K. La Mer, and J. Barksdale, *ibid.*, **56**, 544 (1934).

(11) T. W. Richards and C. P. Smyth, *ibid.*, **44**, 524 (1922).

(12) Y. Takahasi and E. F. Westrum, Jr., *J. Chem. Eng. Data*, to be published.

(13) K. K. Kelley and E. G. King, U. S. Department of the Interior, Bureau of Mines, Bulletin 592, U. S. Government Printing Office, Washington, D. C., 1961.

## The Temperature Coefficient of Conductance of Aqueous Sodium Sulfate around 32.4°

by Robert L. Kay, George A. Vidulich, and Thomas Vituccio

Mellon Institute, Pittsburgh, Pennsylvania  
(Received June 22, 1965)

An abnormal temperature dependence of the conductivity of a 0.01 *M* aqueous sodium sulfate solution has been reported<sup>1</sup> for temperatures close to the decomposition temperature of the solid decahydrate. The temperature coefficient between 33 and 34° was claimed to be only one-third to one-fourth that found at higher and lower temperatures and the break in the conductivity curve between these temperatures was reported to amount to 2.5%. The same type of result has been reported<sup>2</sup> for 1% aqueous sodium carbonate solutions in that the change of viscosity with temperature showed two breaks at temperatures corresponding to solid hydrate transitions.

We have tried to reproduce the effect by measuring conductivities of 0.01 *M* Na<sub>2</sub>SO<sub>4</sub> and 15 wt. % Na<sub>2</sub>SO<sub>4</sub> in aqueous solution as a function of temperature.

The 0.01 *M* solution was measured in a Kraus-type Erlenmeyer conductance cell with a cell constant of 1.6. The solution was stirred continuously by a magnetic stirrer and Teflon-coated stirring bar. The more concentrated solution was measured in a Pyrex U-tube cell which had a cell constant of 205 and which was fitted with platinized platinum dip electrodes separated laterally by 22 cm. This cell exhibited no detectable frequency dependence within 0.1 ohm between 0.5 and 10 kHz. in the resistance range studied here. A description of the bridge, detector, and method of operation are reported in detail elsewhere.<sup>3</sup> The temperature was determined to 0.003° on a Beckmann thermometer calibrated by a platinum resistance thermometer and Mueller bridge. The constant temperature oil bath was regulated to ± 0.005°.

The resulting conductivities of the solutions are shown in Figure 1. Within 0.1% the conductivities of the 0.01 *M* solution are linear in the temperatures between 31 and 34° and the points for the 15 wt. % solution fall on a straight line between 31 and 37°. The magnitude of a 1% change in each case is shown on the plot. There is no indication of any abnormal temperature dependence of the conductivity for dilute or concentrated aqueous Na<sub>2</sub>SO<sub>4</sub> solutions at temperatures just above or below the decahydrate transition temperature.

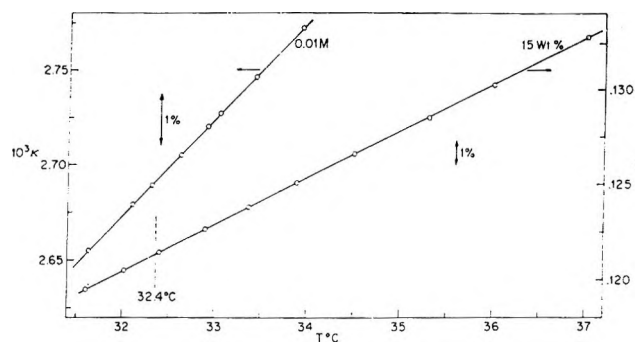


Figure 1. The specific conductance of a 0.01 *M* (left) and a 15 wt. % (right) solution of Na<sub>2</sub>SO<sub>4</sub> in aqueous solution as a function of temperature.

*Acknowledgment.* This work was supported by the Office of Saline Water, U. S. Department of the Interior.

- (1) K. Hirano, *Nippon Kagaku Zasshi*, **79**, 648 (1958).
- (2) K. Fuzita, *Bull. Chem. Soc., Japan*, **32**, 1004 (1959).
- (3) D. F. Evans, C. Zawoyski, and R. L. Kay, to be published.

## γ-Radiolysis of Ethylene Sensitized by "Inert" Gases

by A. Delle Site and A. Mele

Laboratorio di Chimica delle Radiazioni e Chimica Nucleare del C.N.E.N., Istituto di Chimica Generale ed Inorganica dell'Università di Roma, Italy (Received February 15, 1965)

A comparative study of the radiolysis of pure ethylene and argon-ethylene mixtures has been carried out by Lampe,<sup>1</sup> who found that addition of "inert" gas did not alter the yield of the more volatile products of reaction. The consideration that different "inert" gases could play different roles led us to study the radiolysis of ethylene in the presence of He, Ne, Ar, Kr, Xe, and N<sub>2</sub>.

### Experimental Section

Phillips research grade ethylene was distilled at -150° in an evacuated system and the middle fraction was collected in a receiver cooled in liquid nitrogen. The product, analyzed by gas chromatography, was better than 99.9% pure. The rare gases, obtained from Air Liquid Co., were used without further purification. Irradiation was carried out with a Co<sup>60</sup> source of 6000

(1) F. W. Lampe, *Radiation Res.*, **10**, 691 (1959).

curies at a fixed dose rate of  $4.17 \times 10^5$  r./hr. (Acetylene dosimeter  $G(-C_2H_2) = 72$ ).

The samples were irradiated at  $30^\circ$  in cylindrical Pyrex vessels (5 cm. long and 5 cm. in diameter) fitted with break-seals. The vessels were used only once. After irradiation, the samples were analyzed by gas chromatography on a silica gel column 3 m. long and 6 mm. in diameter at  $120^\circ$ , using helium as carrier gas and a gas conductivity cell with thermistors as detectors. Calibrations were made by means of mixtures of known composition.

The radiolysis of pure ethylene has been studied in the range of pressure from 123 to 593 mm. The  $G(-C_2H_4)$  values, measured at four different pressures, are reported in Table I. These values have been calculated from the initial slope of the curves (up to 3-4% of the ethylene consumed) obtained by plotting ethylene disappearance *vs.* total dose absorbed. As may be seen, the  $G$  values increase with pressure in agreement with previous findings for the low dose rate range.<sup>2,3</sup> The high  $G$  values between 33.1 and 42.0 follow the trend shown by Sauer and Dorfman,<sup>3</sup> who have found that by decreasing the dose rate, the 100-e.v. yields are larger.

**Table I:**  $\gamma$ -Ray Irradiation of Pure Ethylene (Dose Rate  $4.17 \times 10^5$  r./hr.)

Initial press. of $C_2H_4$ , mm.	$G(-C_2H_4)$
123	33.1
220	37.1
363	39.7
593	42.0

Mixtures of ethylene and "inert" gases of various compositions have been irradiated and the results are shown in Table II. The partial pressure of ethylene for all samples was 123 mm. and the added gases brought the maximum total pressure to about 600 mm. Generally, the compositions of the mixtures were such that the fraction of energy absorbed by the "inert" gas with respect to the total energy received by the mixture was between 10 and 90%, but for the helium mixtures this fraction was never greater than 33%.

These fractions, reported in column 3, naturally correspond to the electron fractions of "inert" gas. The  $G(-C_2H_4)$  values, reported in columns 4 and 5 of the same table, are referred to the energy absorbed by ethylene and to the total energy absorbed by the mixture, respectively. These  $G$  values have been calculated, analogously to those for pure ethylene,

**Table II:** Irradiation of Ethylene-"Inert" Gas Mixtures (Ethylene Partial Pressure: 123 mm. Dose Rate:  $4.17 \times 10^6$  r./hr.)

	Initial press. of mixture, mm.	% "inert" gas	Fraction of energy absorbed by "inert"	$G(-C_2H_4)$ , energy absorbed by $C_2H_4$	$G(-C_2H_4)$ , total energy absorbed by mixture
Helium	246	50.0	0.110	39.4	35.1
	410	70.0	0.226	44.8	34.7
	615	80.0	0.334	56.2	37.4
Neon	158	21.9	0.149	45.5	38.7
	208	40.9	0.302	55.2	38.5
	282	56.6	0.449	69.0	38.0
	420	70.7	0.601	98.3	39.2
	615	80.1	0.715	146.0	41.6
Argon	144	14.3	0.161	43.8	36.8
	189	34.9	0.378	53.2	33.1
	246	50.0	0.530	69.2	32.5
	352	65.0	0.676	95.5	30.9
	615	80.0	0.818	177.0	32.3
Krypton	136	9.3	0.186	42.3	34.4
	155	20.4	0.365	53.5	34.0
	189	35.0	0.548	76.4	34.5
	274	55.0	0.734	135.0	35.8
	610	79.9	0.899	380.0	38.4
Xenon	137	10.1	0.274	45.7	33.2
	141	12.6	0.327	50.5	34.0
	176	30.2	0.594	86.8	35.2
	233	47.3	0.752	149.0	37.0
	448	72.6	0.899	407.0	41.2
Nitrogen	152	19.3	0.174	42.1	34.8
	190	35.3	0.325	51.2	34.6
	251	51.1	0.477	62.3	32.6
	358	65.7	0.626	90.0	33.6
	615	80.0	0.777	160.0	35.6

from the initial slope of the curves obtained by plotting ethylene consumed (up to 3-4%) *vs.* total dose absorbed by ethylene.

### Discussion

The crude effect of the addition of "inert" gas to ethylene is to increase its rate of consumption. Helium gives only a slight increase and xenon gives an approximately fivefold increase for a 50:50 mixture. The effect of Ne,  $N_2$ , Ar, and Kr is intermediate between these two extremes and increases successively from Ne to Kr. The  $G(-C_2H_4)$  values reported in column 4 of Table II show this effect.

(2) J. C. Hayward, Jr., Ph.D. Thesis, Yale University, 1955.

(3) M. C. Sauer, Jr., and L. M. Dorfman, *J. Phys. Chem.*, **66**, 322 (1962).

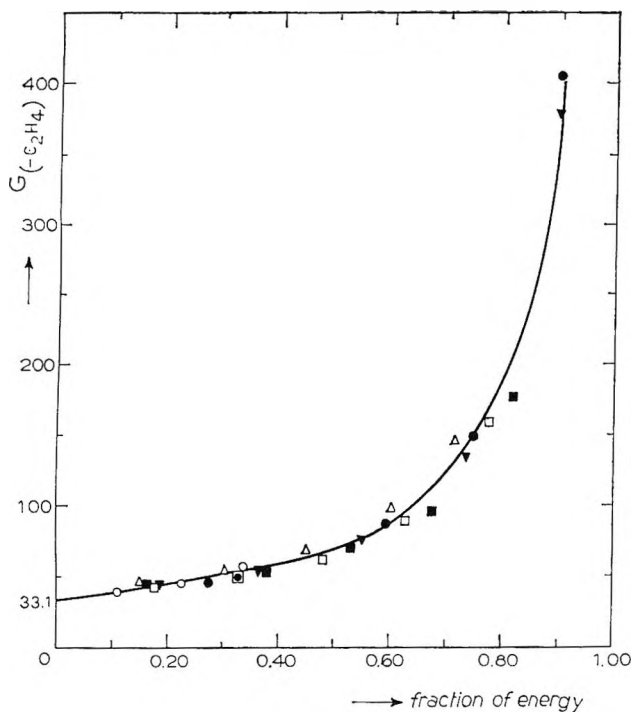


Figure 1.  $G(-C_2H_4)$  values referred to the energy absorbed by ethylene vs. the fraction of energy absorbed by the inert gas: O, helium;  $\Delta$ , neon;  $\blacksquare$ , argon;  $\blacktriangledown$ , krypton;  $\bullet$ , xenon;  $\square$ , nitrogen.

A plot of the  $G(-C_2H_4)$  values referred to the energy absorbed by ethylene molecules against the fraction of energy absorbed by the "inert" gas is shown in Figure 1. The experimental data seem to lie on the same curve and extrapolation at zero concentration of "inert" gas is the  $G(-C_2H_4)$  for pure ethylene at 123 mm. of pressure. This trend would indicate that  $G(-C_2H_4)$  does not depend on the nature of the "inert" gas, but on the fraction of energy absorbed by the "inert" gas itself and transferred to the ethylene molecules.

It is well known that energy transfer from a noble gas to ethylene is a highly efficient process.<sup>4-6</sup> Of course, the primary species generated in ethylene are different, depending on the nature of the "inert" gas.

The experimental results do not allow one to draw any conclusions on the mechanism of polymerization induced by energy transfer from the "inert" gas to ethylene molecules. The over-all effect on the  $G(-C_2H_4)$  values for ethylene consumption results is about the same whichever the sensitizer.

## The Thermodynamic and Physical Properties of Beryllium Compounds. VIII. Heat of Fusion and High-Temperature Heat Capacity of Beryllium Oxide

by Michael A. Greenbaum, Justine Weiher, and Milton Farber

Research Division, Marmont Corporation, Pasadena, California  
(Received March 11, 1965)

The lack of reliable values of the sensible enthalpy of  $BeO(c)$  in the vicinity of its melting point, 2825°K., and for the heat of fusion can, in large part, be attributed to the great reactivity of  $BeO$  with almost all container materials at elevated temperatures. The only previous experimental determination of the sensible enthalpy of  $BeO(c)$  above 2000°K. was reported by Kandyba, *et al.*, in 1960.<sup>1</sup> Based on an analysis of their data combined with several other experimental reports, a value of  $15.1 \pm 0.4$  kcal./mole has been derived for the heat of fusion of  $BeO(c)$  at the melting point.<sup>2</sup> No direct measurement of this quantity has been reported previously, however.

As a continuation of an extensive program in these laboratories aimed at the generation of reliable thermodynamic and physical data for compounds of beryllium,<sup>3-8</sup> a study of the high-temperature thermodynamic properties of  $BeO(c)$  was initiated. After extensive investigation it was determined that rhenium was completely unattacked by solid, liquid, or gaseous beryllium oxide at temperatures as high as 3000°K. and under vacuum ( $10^{-4}$  to  $10^{-6}$  mm.).

The experimental method employed to obtain the requisite thermodynamic data for  $BeO(c)$  involved the use of an electron bombardment furnace-drop calorimeter

(1) V. V. Kandyba, *et al.*, *Dokl. Akad. Nauk SSSR*, **131**, 566 (1960).

(2) "JANAF Thermochemical Tables," U.S.A.F. Contract No. AF 33(616)-6149, Advanced Research Projects Agency, Washington 25, D. C., March 1964.

(3) M. A. Greenbaum, J. N. Foster, M. L. Arin, and M. Farber, *J. Phys. Chem.*, **67**, 36 (1963).

(4) M. A. Greenbaum, R. E. Yates, M. L. Arin, M. R. Arshadi, J. Weiher, and M. Farber, *ibid.*, **67**, 703 (1963).

(5) M. A. Greenbaum, M. L. Arin, and M. Farber, *ibid.*, **67**, 1191 (1963).

(6) M. A. Greenbaum, R. E. Yates, and M. Farber, *ibid.*, **67**, 1802 (1963).

(7) M. A. Greenbaum, M. L. Arin, M. Wong, and M. Farber, *ibid.*, **68**, 791 (1964).

(8) R. E. Yates, M. A. Greenbaum, and M. Farber, *ibid.*, **68**, 2682 (1964).

(4) J. L. Franklin and F. H. Field, *J. Am. Chem. Soc.*, **83**, 3555 (1961).

(5) W. P. Jesse and J. Sadauskis, *Phys. Rev.*, **100**, 1755 (1955).

(6) R. L. Platzman, *J. Phys. Radium*, **21**, 853 (1960).

Table I: Experimental Results of BeO Enthalpy Measurements

Temp., °K.	Wt. of BeO, g.	Wt. of Re, g.	Mercury intake, g.	Mercury corrections, g.	Heat released, cal.	Re correction, cal.	$H - H_{298}$ , cal./mole
2273	1.1373	1.5636	91.700	75.347	1057.1	121.07	20,569
2283	1.0149	1.5586	119.001	103.627	993.7	121.73	21,488
2293	1.2237	1.5671	110.400	92.869	1133.1	123.23	20,640
2313	1.2248	1.5661	99.361	81.889	1129.3	123.99	20,528
2323	1.1147	1.5592	143.088	126.466	1074.4	124.70	21,307
2323	0.9228	3.1534	73.557	57.579	1032.8	247.23	21,291
2348	0.9827	1.6855	73.470	58.672	956.5	136.61	20,866
2348	1.2203	0.8170	104.970	89.048	1029.2	66.00	19,741
2373	1.2208	1.5675	91.750	73.109	1204.9	128.73	22,047
2378	1.2187	0.8198	96.766	79.716	1102.1	67.43	21,234
2383	0.9228	3.4999	109.409	92.999	1060.7	287.44	20,957
2383	0.9228	3.4859	59.238	42.753	1065.6	287.22	21,096
2393	0.9228	3.4973	59.870	43.215	1076.5	290.03	21,314
2433	1.1589	1.6855	69.977	50.978	1228.1	142.49	23,428
2433	1.1475	1.6855	79.188	60.629	1199.6	142.49	23,040
2433	1.2201	1.5840	69.502	51.142	1186.7	133.91	21,581
2443	1.2295	2.1544	69.039	50.535	1196.1	183.29	20,602
2473	1.2274	1.2835	58.471	38.833	1269.4	110.58	23,612
2473	1.0010	1.6855	64.084	48.070	1035.1	145.66	23,111
2513	1.2118	1.5817	77.313	57.446	1284.2	139.66	23,621
2523	1.2309	1.5823	57.305	36.627	1336.6	140.14	24,309
2523	1.2255	1.5836	64.781	44.455	1313.9	140.25	23,951

combination which was designed in these laboratories. The calorimeter section of the apparatus is based upon designs originally developed by the National Bureau of Standards<sup>9-12</sup> and subsequently modified by other investigators.<sup>13,14</sup> A detailed description of the apparatus together with its operation has been presented previously.<sup>15</sup>

Heating of the beryllium oxide sample was accomplished by the use of the electron bombardment furnace mentioned above. The sample encased in rhenium was suspended within the furnace by means of a rhenium wire which was attached to a 0.002-in. molybdenum wire. The molybdenum wire was connected to a 110-v. variable rheostat. When the sample temperature reached the desired point and equilibrium had been established, the molybdenum wire was broken by means of an electric current, thus allowing the sample to drop into the calorimeter. The beryllium oxide employed was 99.5+% pure in the form of 0.375 × 0.25-in. rods encapsulated in rhenium containers 0.012 in. thick. Temperature measurement was accomplished by a Leeds and Northrup optical pyrometer previously calibrated according to NBS standards. Temperature was controlled manually to within approximately ±5°. The absolute value of the temperature is considered to be accurate to ±20° at the present time.

Calibrations of the calorimeter were carried out using tantalum following the procedure of Hoch and John-

ston.<sup>13</sup> Agreement between our calibration data and that of Hoch and Johnston is quite good. Corrections for the enthalpy of the rhenium container for the BeO sample were carried out using the data of Hultgren, Orr, Anderson, and Kelley.<sup>16</sup>

The melting points of Al<sub>2</sub>O<sub>3</sub> and BeO were taken as the calibration points in the temperature range for the experiments. The melting points reported in the literature<sup>2</sup> for Al<sub>2</sub>O<sub>3</sub> and BeO are believed to have an uncertainty within ±20°K. The reproducibility of the temperature measurements of the experiments presented herein was within ±5%.

Since it was not feasible to take into account heat loss during the actual drop, this has been neglected. It should be pointed out that because of the special design

(9) D. C. Ginnings and R. J. Corruccini, *J. Res. Natl. Bur. Std.*, **38**, 583 (1947).

(10) D. C. Ginnings and R. J. Corruccini, *ibid.*, **38**, 593 (1947).

(11) D. C. Ginnings, T. B. Douglas, and A. F. Ball, *J. Am. Chem. Soc.*, **73**, 1236 (1951).

(12) J. C. Southard, *ibid.*, **53**, 3142 (1941).

(13) M. Hoch and H. L. Johnston, *J. Phys. Chem.*, **65**, 855 (1961).

(14) R. A. Oriani and W. K. Murphy, *J. Am. Chem. Soc.*, **76**, 343 (1954).

(15) M. A. Greenbaum, J. Weiher, and M. Farber, presented before the Symposium on Thermodynamics and Thermochemistry, Lund, Sweden, July 18-23, 1963.

(16) R. Hultgren, R. L. Crr, P. D. Anderson, and K. K. Kelley, "Selected Values of Thermodynamic Properties of Metals and Alloys," John Wiley and Sons, Inc., New York, N. Y., 1963.

**Table II:** Experimental Results of BeO Heat of Fusion Measurements

Temp., °K.	Wt. of BeO, g.	Wt. of Re, g.	Mercury intake, g.	Mercury corrections, g.	Heat released, cal.	Re correction, cal.	Total heat released from BeO, kcal.	Correction for BeO(c) enthalpy, kcal.	Heat of fusion, kcal./mole
2843	0.9232	6.0090	114.39	78.410	2325.4	620.90	46.2	28.1	18.1
2853	0.9232	5.3674	115.68	79.462	2313.0	554.60	47.6	28.2	19.4
2863	0.9232	6.0066	118.40	80.818	2429.3	625.49	48.8	28.3	20.5
2853 ± 10 <sup>a</sup>							47.5 ± 0.9 <sup>a</sup>	28.2 ± 0.2 <sup>a</sup>	19.3 ± 0.8 <sup>a</sup>

<sup>a</sup> Average.

of the experimental apparatus, it is considered that the heat loss would be very small. This is confirmed in large measure by the agreement of our calibration data for tantalum with the previously reported experimental data. The ±10% for the precision reported for the temperature at which the heat of fusion measurements were made is simply the average of the several actual runs.

The sensible enthalpy of BeO(c) was measured calorimetrically between 2270 and 2525°K. using the procedures and apparatus mentioned above. The results of this study are presented in Table I and graphically in Figure 1.

A least-squares analysis of the data fitted to an equation of the form  $y = mx + b$  yields the equation

$$H - H_{298} = 13.85T - 11,322 \pm 875 \text{ cal./mole}$$

Within the temperature range studied and within the admittedly large limits of error, the heat capacity of BeO(c) appears to be constant. Not included in the line analysis, and so indicated on the graph, are three measured points in the extrapolated region of the curve. These points were not included in the line equation because the rhenium-encased samples began to leak before confirming runs at these higher temperatures could be made.

Previous data<sup>2</sup> assume there is a phase change at 2323°K., in accordance with the results of other experiments,<sup>17,18</sup> although no phase change in this region was noted by Kandyba.<sup>1</sup> This phase transition observed by Austerman took place over a 30–60° temperature interval. The present experimental studies of the sensible enthalpy have been made beginning in the range in which phase change was reported. The accuracy of the present study would not permit a phase change observation here and it is presumed the experimental values include any enthalpy increases due to phase change.

Determinations of the heat of fusion of BeO were also carried out in the present study. These are summarized in Table II. It should be pointed out that the

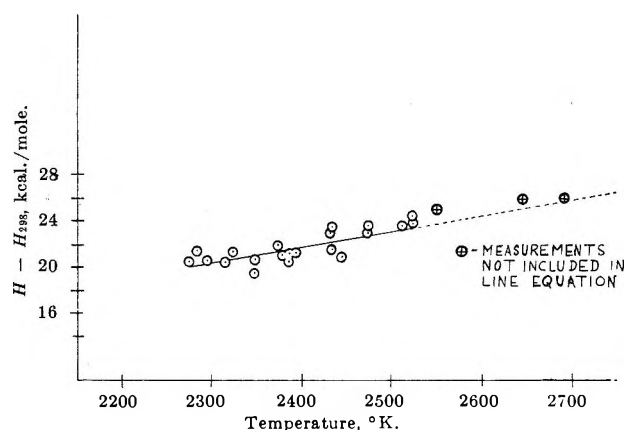


Figure 1. The sensible enthalpy of BeO(c) as a function of temperature between 2270 and 2525°K. with extrapolation.

three different temperatures reported in this table are essentially the same within the limits of temperature capability at present. Thus, based on an average temperature of 2853 ± 10°K., the net heat of fusion of BeO is found to be 19.3 ± 0.8 kcal./mole where the correction is an extrapolation of the determined enthalpy values reported in this study. The reported error of ±0.8 kcal./mole represents the statistical error of the several runs performed. The value 19.3 ± 0.8 kcal./mole may be compared with a value of 17 ± 1.4 kcal./mole reported by Long and Schofield<sup>19</sup> and with the value of 15.1 ± 0.4 kcal./mole previously reported.<sup>2</sup> However, if the gross value for the heat released is corrected using the previous data for the enthalpy of BeO(c) at those temperatures<sup>2</sup> instead of using these extrapolated data, the average heat of fusion is found to be 15.6 ± 0.8 kcal./mole. This is a difference of only 0.5 kcal./mole from the 15.1 kcal. value,<sup>2</sup> showing that variation in net heat of fusion may be attributable primarily to variation in enthalpy values of the crystal.

(17) S. B. Austerman, *Bull. Am. Phys. Soc.*, 7 (1), 28 (1962).

(18) T. W. Baker and P. J. Baldock, *Nature*, 193, 1172 (1962).

(19) R. E. Long and H. Z. Schofield, "Beryllia," AEC-TIS Reactor Handbook, Vol. 3, Section 1, 1955, Chapter 1.3.



## Salt Effects on Nonionic Association Colloids

by Pasupati Mukerjee<sup>1</sup>

Department of Physical Chemistry, Indian Association for the Cultivation of Science, Jadavpur, Calcutta-32, India  
(Received April 12, 1965)

The influence of added electrolytes on the critical micelle concentrations (c.m.c.) of nonionic association colloids in aqueous solution has been the subject of many recent studies.<sup>2-10</sup> The purpose of this note is to show that the effects can be fairly adequately understood in terms of some well-known salting-out and salting-in equilibria in aqueous solutions and that other suggested explanations, mentioned in the concluding remarks, are unnecessary or inaccurate.

The general problem of the salting out of nonelectrolytes by inorganic electrolytes has been extensively investigated and reviewed.<sup>11,12</sup> A fairly satisfactory theory has been offered by Long and McDevit<sup>12,13</sup> for the special case of nonpolar molecules. It is generally accepted that added electrolytes cause electrostriction of water and increase the internal pressure of the solution.<sup>11,12</sup> According to Long and McDevit, this extra pressure increases the activity of the nonpolar molecules, thus causing the salting out. The salt effects usually follow the empirical equation

$$\log f = k_s C_s \quad (1)$$

where  $f$  is the activity coefficient of the nonelectrolyte,  $k_s$  is the salt-effect constant, and  $C_s$  the molar concentration of the salt. Long and McDevit<sup>13</sup> derived an equation for  $k_s$

$$k_s = \bar{V}_i(V_s - \bar{V}_s)/2.3RT\beta_0 \quad (2)$$

in which  $\bar{V}_i$  is the partial molal volume of the nonelectrolyte,  $V_s$  the true molal volume,  $\bar{V}_s$  the partial molal volume of the electrolyte, and  $\beta_0$  is the compressibility of water at the absolute temperature  $T$ .  $V_s - \bar{V}_s$  can be considered to be the extent of the electrostriction of water.<sup>14</sup> Recently, Deno and Spink<sup>15</sup> have shown that some estimates made by the present author of the electrostriction from partial molal volume data<sup>14</sup> for a variety of inorganic electrolytes give a good correlation of the relative experimental  $k_s$  values for benzene although the absolute values are lower by a factor of 0.3.

The effect of salts on polar molecules is much more complicated and much less understood.<sup>12</sup> As association colloids contain both polar and nonpolar groups, they are expected to show a more complicated behavior

than purely nonpolar solutes. Considerable progress, however, can still be made for monomer-micelle equilibria.

If the number of monomers,  $L$ , in a micelle,  $M$ , is  $n$ , and the activity coefficients of the monomer and the micelle are  $f$  and  $f_m$ , the equilibrium constant for micelle formation,  $K$ , is given by

$$K = \frac{[M]f_m}{[L]^n f^n} \quad (3)$$

At the c.m.c.,  $[L]$  can be replaced by the c.m.c. Neglecting the term containing  $[M]$ , particularly for relative purposes,<sup>16</sup> the standard free energy per monomer,  $\Delta G$ , is derived to be

$$-\Delta G/2.303RT = -\log \text{c.m.c.} - \log f + \frac{1}{n} \log f_m \quad (4)$$

Equation 2 and the experimental results on many nonpolar organic solutes<sup>12,15</sup> indicate that salt effects, as represented by the  $k_s$  coefficients, are additive with respect to the parts of a nonpolar molecule to about the same extent as the volumes are additive. For the association colloids, we assume that the additivity of the  $k_s$  coefficients extends to both the nonpolar and the polar parts of a molecule. Using subscripts  $a$  and  $b$  for the hydrophobic part and the hydrophilic head group, respectively,  $\log f$  is thus expressed as  $\log f_a + \log f_b$ . For a micelle, the nonpolar surface exposed to the salt solution is small compared to the total surface of the monomers, particularly when the head groups are bulky. Neglecting this nonpolar contribution, we can write  $\log f_m = n \log f_{bm}$ , where  $\log$

- (1) Department of Chemistry, University of Southern California Los Angeles, Calif. 90007.
- (2) L. Hsiao, H. N. Dunning, and P. B. Lorenz, *J. Phys. Chem.*, **60**, 657 (1956).
- (3) K. Shinoda, T. Yamaguchi, and R. Hori, *Bull. Chem. Soc. Japan*, **34**, 237 (1961).
- (4) K. Kuriyama, *Kolloid-Z.*, **181**, 144 (1962).
- (5) P. Becher, *J. Colloid Sci.*, **17**, 325 (1962).
- (6) P. Becher, *ibid.*, **18**, 196 (1963).
- (7) K. Tori and T. Nakagawa, *Kolloid-Z.*, **189**, 50 (1963).
- (8) M. J. Schick, S. M. Atlas, and F. R. Eirich, *J. Phys. Chem.*, **66**, 1326 (1962).
- (9) M. J. Schick, *J. Colloid Sci.*, **17**, 801 (1962).
- (10) M. J. Schick, *J. Phys. Chem.*, **67**, 1796 (1963).
- (11) H. S. Harned and B. B. Owen, "The Physical Chemistry of Electrolytic Solutions," 3rd Ed., Reinhold Publishing Corp., New York, N. Y., 1958.
- (12) F. A. Long and W. F. McDevit, *Chem. Rev.*, **51**, 119 (1952).
- (13) W. F. McDevit and F. A. Long, *J. Am. Chem. Soc.*, **74**, 1773 (1952).
- (14) P. Mukerjee, *J. Phys. Chem.*, **65**, 740, 744 (1961).
- (15) N. C. Deno and C. H. Spink, *ibid.*, **67**, 1347 (1963).
- (16) P. Mukerjee, *ibid.*, **66**, 1375 (1962).



$f_{bm}$  corresponds to the salt effect on a single hydrophilic group on the micelle. Equation 4 can now be rewritten as

$$-\Delta G/2.303RT = -\log \text{c.m.c.} - \log f_a - (\log f_b - \log f_{bm}) \quad (5)$$

Several consequences of eq. 5 can be tested. First, if the salt effects are expressed by eq. 1, eq. 6 follows, the subscripts for the  $k$ 's having the same meaning as before.

$$\begin{aligned} \log \text{c.m.c.} &= \text{constant} - C_s(k_a + k_b - k_{bm}) \\ &= \text{constant} - k_s C_s \end{aligned} \quad (6)$$

The predicted linear dependence of  $\log \text{c.m.c.}$  on the salt concentration is followed by many systems.<sup>7,9</sup> Some polyoxyethylene derivatives show deviations from linearity,<sup>10</sup> which may be caused, in part, by the heterogeneity of the systems and variations in  $k_{bm}$  with changes in the size and composition of the micelles as salt is added.

In eq. 6, the terms  $k_b$  and  $k_{bm}$  are expected to cancel to a great extent but not exactly. On a micelle surface the hydrophilic head groups are highly concentrated. The effective concentration depends, in part, on the bulk of the head groups and may be several moles per liter. The  $k_s$  coefficients are known to depend on the concentration of the nonelectrolyte. The result of this "self-interaction" effect of the nonelectrolyte<sup>12</sup> is usually a reduction of the absolute magnitude of the  $k_s$  coefficient with the concentration of the nonelectrolyte. The cancellation of the  $k_b$  and  $k_{bm}$  terms may be expected to be less complete for larger absolute values of  $k_b$  and for larger bulk of the head group.

### Quantitative Calculations for NaCl Solutions

Several systems are analyzed in detail to emphasize the predictive value of the above theory and some of the important features of the salt effects. The calculations are restricted to the effect of NaCl at about 25°, the only conditions for which sufficient data are available, but the principles should apply generally.

The  $k_s$  values for long-chain hydrocarbons are not available experimentally. The data of Morrison and Billet<sup>17</sup> on short-chain compounds, methane to butane, in NaCl, when interpolated to 25°, can be expressed as

$$k_s = 0.132 + 0.032(N - 1) \quad (7)$$

where  $N$  is the number of carbon atoms in the aliphatic chain. This equation is used here, keeping in mind the uncertainty of long extrapolations.

The simplest association colloid to treat is octyl glucoside.<sup>3</sup> Kelly, Robinson, and Stokes<sup>18</sup> have re-

cently studied the effect of NaCl on the activity coefficient of mannitol, which is structurally similar to the glucoside group. In 1 *M* NaCl, mannitol has an activity coefficient of 0.986 at infinite dilution, indicating a slight salting in, and 1.002 at 1 *M* mannitol concentration, indicating a small effect of self-interaction of mannitol. It is thus expected that both  $k_b$  and  $k_{bm}$  for the glucoside group are small, and  $k_s$  for octyl glucoside should be due mainly to  $k_a$ . The experimental  $k_s$  value of 0.35, obtained from the data of ref. 3, is in good agreement with the value of 0.36 calculated for octane from eq. 7.

The low  $k_s$  value (0.134) for octylbetaine<sup>7</sup> must then be ascribed to a  $k_b - k_{bm}$  value of about 0.2. This appears to be quite reasonable. Zwitterionic molecules like betaine have high dipole moments and are salted in very substantially by ordinary electrolytes, as predicted by the theories of Debye, Scatchard, and Kirkwood and as experimentally observed.<sup>19</sup> Such dipolar molecules show strong self-interaction effects also, as exemplified by glycine, which, in its zwitterionic form, is structurally similar to betaine. In dilute NaCl, the  $k_s$  coefficient of glycine decreases from  $-0.28$  in dilute solutions of glycine to  $-0.02$  in 2 *M* glycine.<sup>19</sup> Thus, a considerable negative contribution of the  $k_b - k_{bm}$  term is expected for betaines although it cannot be estimated very well.

On the other hand, the change in  $k_s$  with increasing chain length should come mainly from the contribution of the additional CH<sub>2</sub> groups to  $k_a$ . The experimental  $k_s$  values of octyl-, decyl-, and dodecylbetaine are 0.134, 0.214, and 0.294.<sup>7</sup> The average increment per CH<sub>2</sub> group is 0.040, comparable to the value of 0.032 for short-chain alkanes (eq. 7).

The available  $k_s$  data for polyoxyethylene derivatives<sup>5,6,9,10</sup> are somewhat inconsistent. Nevertheless, here also the major contribution seems to be the  $k_a$  term. For example, the experimental  $k_s$  for some branched nonylphenol derivatives<sup>9</sup> is about 0.34 compared to the expected  $k_a$  of 0.39 for nonane. A dodecanol derivative with 30 ethylene oxide units<sup>10</sup> shows a nonlinear dependence of  $\log \text{c.m.c.}$  on  $C_s$ . The estimated mean  $k_s$  of about 0.8 is somewhat higher than the estimated  $k_a$  of about 0.5, indicating some contribution from the  $k_b - k_{bm}$  term.

### Other Salts

For approximate purposes, in the absence of suitable

(17) T. J. Morrison and F. Billet, *J. Chem. Soc.*, 3819 (1952).

(18) E. J. Kelly, R. A. Robinson, and R. H. Stokes, *J. Phys. Chem.*, 65, 1958 (1961).

(19) E. J. Cohn and J. T. Edsall, "Proteins, Amino Acids and Peptides," Reinhold Publishing Corp., New York, N. Y., 1943.

background information, eq. 2 may be employed to calculate relative  $k_a$  values in different salt solutions. It is interesting that for octyl glucoside, for which  $k_a \approx k_s$  in NaCl, the ratio of  $k_s$  values (calculated from ref. 7) in NaCl and  $\text{Na}_2\text{SO}_4$  is 1:2.7, in fair agreement with the ratio 1:3.2 predicted by eq. 2 and the ratio of 1:2.7 observed for benzene.<sup>15</sup>

### Salting Out of Ionic Association Colloids

Although the major effects of added electrolytes on the c.m.c. of ionic association colloids are due to inter-ionic interactions, the above analysis suggests that salting-out effects, generally neglected, can be quite substantial. The calculated  $k_s$  value for a dodecyl group is about 0.5. Therefore, the activity coefficient of an amphiphatic ion containing a dodecyl group should be increased by factors of 1.12, 1.78, and 3.2 in 0.1, 0.5, and 1 M NaCl because of the salting out of the chain.

### Concluding Remarks

The above analysis suggests that the problem of salt effects on nonionic association colloids can be profitably attacked in terms of some fairly well-established ideas developed for simple nonelectrolytes. Previous explanations, based on changes in water activity,<sup>5</sup> the presence of charged impurities,<sup>6</sup> or the unavailability of solute molecules,<sup>3</sup> need not be involved. Schick, Atlas, and Eirich<sup>8</sup> have suggested salting out of the ethylene oxide chains in some ethylene oxide condensates in terms of a dehydration mechanism. As indicated above, the salting out of the hydrophobic chains seems to be the most important factor to be considered for polyethylene oxide systems also.

*Acknowledgments.* The revision of this paper was done at the University of Southern California and was supported in part by P.H.S. Research Grant GM 10961-01 from the Division of General Medical Services, Public Health Service.

## Transitions in Gelatin and Vitrified Gelatin-Water Systems

by Joseph V. Koleske and Joseph A. Faucher

Research and Development Department, Union Carbide Corporation, Chemicals Division, South Charleston, West Virginia 25303 (Received April 13, 1955)

Yannas and Tobolsky<sup>1</sup> recently reported on the viscoelastic properties of plasticized and unplasticized

gelatin. We have studied the mechanical loss and shear properties of gelatin and vitreous gelatin-water systems at low temperatures and wish to present the results to provide more information on transitions that occur in this biopolymer.

### Experimental Section

Gelatin obtained from Atlantic Gelatin (a division of General Foods Corp.) was used without any further treatment. The properties of the gelatins studied are listed in Table I. The gelatin-water systems were prepared from Gelatin-I and distilled water by combining the two compounds and warming them in lightly stoppered test tubes in a water bath at about 90°. The desired concentrations were obtained by checking the solution weight and adding solvent to make up any weight loss occurring during the solution period. Concentrations are calculated on an oven-dry gelatin basis. Vitrification of the gelatin-water systems was accomplished by rapidly cooling in liquid nitrogen and mounting the specimens while they were in a glassy state. The unplasticized gelatin was molded into plaques at 110° and 3000 p.s.i. These plaques were desiccated until the experiment was performed. The moisture content of the Gelatin-I plaque was 9.6% and that of the Gelatin-II plaque was 8.3%.

Table I: Properties of Gelatin Used in Study

	Moisture content, <sup>a</sup> %	pH	Bloom <sup>b</sup>	Type <sup>c</sup>
Gelatin-I	10.8	6.5	200	B
Gelatin-II	9.0	4.35	200	A

<sup>a</sup> As-received basis. <sup>b</sup> Bloom is a standard measure of the gel strength of gelatin. It is defined as the number of grams required to force a 0.5-in. plummet of a Bloom gelometer 4 mm. into an aqueous 6.67% solids gelatin gel that has been chilled 17 hr. at 10° (J. F. Suter, U. S. Patent 3,164,560 (Jan. 5, 1965)). <sup>c</sup> Type B gelatin is obtained from lime-conditioned calfskin, beef hides, or ossein. Type A gelatin is obtained from acid-conditioned pigskin.

Mechanical loss measurements were made at about 1-5 c.p.s. with a recording torsion pendulum similar to that described by Nielsen.<sup>2</sup> These measurements were used to calculate the real,  $G'$ , and the loss,  $G''$ , components of the complex shear modulus.

(1) J. B. Yannas and A. V. Tobolsky, *J. Phys. Chem.*, **68**, 3880 (1964).

(2) L. E. Nielsen, *Rev. Sci. Instr.*, **22**, 690 (1951).

### Discussion

Figure 1 is a plot of the mechanical loss spectrum of Gelatin-I and an initially vitreous 54:46 gelatin-water gel. Examining the low-temperature data, we note that a peak occurs at about  $-85^\circ$  for both specimens. It seems this peak is associated only with the gelatin and it is affected by the water in an unusual manner. The position of maximum loss is unaltered, but the temperature range over which the transition occurs is markedly narrowed. Keeping in mind that a 65.5:34.5 gelatin-water solution cannot be frozen<sup>3</sup>—that is, only vitrification will take place regardless of the manner of cooling—most of the water in the 54:46 system must be bound to the gelatin in a very strong fashion. It is possible to argue that this bound water inhibits the onset of the energy-absorbing mechanism that produces the  $-85^\circ$  peak. Yet, if this were the case, one would expect the peak to be obscured, to occur at a higher temperature, or at least to be decreased in magnitude. If the water acted as a plasticizer for this mechanism, typical behavior would predict the transition to occur at a lower temperature and the breadth of the transition to be increased. Thus far we have found no way out of this dilemma and can only point out what seems to be a paradox—the peak is sharpened, increased in magnitude, and not shifted by the diluent. One wonders if the term plasticizer would be apt in this case.

The  $-10^\circ$  peak in the gelatin-water system can be ascribed to the devitrification which has been found by others to occur at this temperature.<sup>4</sup> We made no attempt to examine this sample above room temperature since in our apparatus the specimen would lose moisture at these temperatures. Table II summarizes the low-temperature transition data for the systems studied.

**Table II:** Low-Temperature Transitions in Gelatin and Gelatin-Water Systems

System	Transition temp., °C.	Frequency at transition, c.p.s.	Devitrification temp., °C.
Gelatin-I	-85	2.7	...
Gelatin-II	-85	3.4	...
Gelatin-I-water (54:46)	-88	4.3	-10
Gelatin-I-water (49:51)	-85	4.2	-10

Turning to the higher temperatures, we find from the data in Figure 1 that a large loss peak occurs at  $130^\circ$  and another at  $180^\circ$  for Gelatin-I. Gross melting seems to be occurring at  $220^\circ$  or perhaps somewhat higher. Okamoto and Saeki,<sup>5</sup> in their investigation of gelatin, found

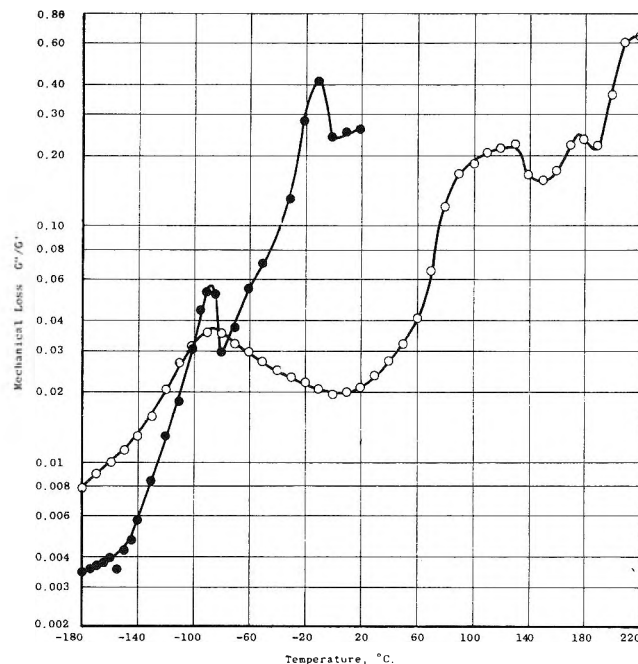


Figure 1. Mechanical loss characteristics of Gelatin-I (O) and 54:46 Gelatin-I/water (●) in an initially vitreous state. Measurements are independent of sample dimensions. See text.

that a second-order transition occurred in the amorphous regions at  $120^\circ$  and that small crystallites of widely distributed stability melt over a temperature range of  $80$ – $100^\circ$  and at  $180^\circ$ . The stable crystallites melted at about  $220^\circ$ . The previously cited work<sup>1</sup> ascribed the transition in the vicinity of  $190^\circ$  to the glass transition temperature. Above  $220^\circ$  these authors found that decomposition occurred and the possible melting of gelatin was thus obscured.

In the case of our gelatin specimens, we found that  $G'$  began to increase at moderately high temperatures as shown in Figure 2. Such behavior indicates that a change of sample dimensions is occurring or that the compound studied is crystallizing, cross linking, or possibly decomposing. Dimensional measurements made on the specimen after completion of the run (it is not practical for us to make these measurements during the run) indicate that the first reason is the most plausible, since the sample thickness increased by a factor of about 3. When the final data point is corrected by this factor, the solid point shown in Figure 2 at  $210^\circ$  is obtained and the data may actually be more accurately described by the dashed curve shown in this figure. However, the cross-linking and/or decomposition factors cannot

(3) T. Moran, *Proc. Roy. Soc. (London)*, A112, 30 (1926); cf. ref. 4.

(4) B. J. Luyet and P. M. Gehenio, "Life and Death at Low Temperatures," *Biodynamica*, Normandy, Mo., 1940, p. 214.

(5) Y. Okamoto and K. Saeki, *Kolloid-Z.*, 194, 124 (1964).

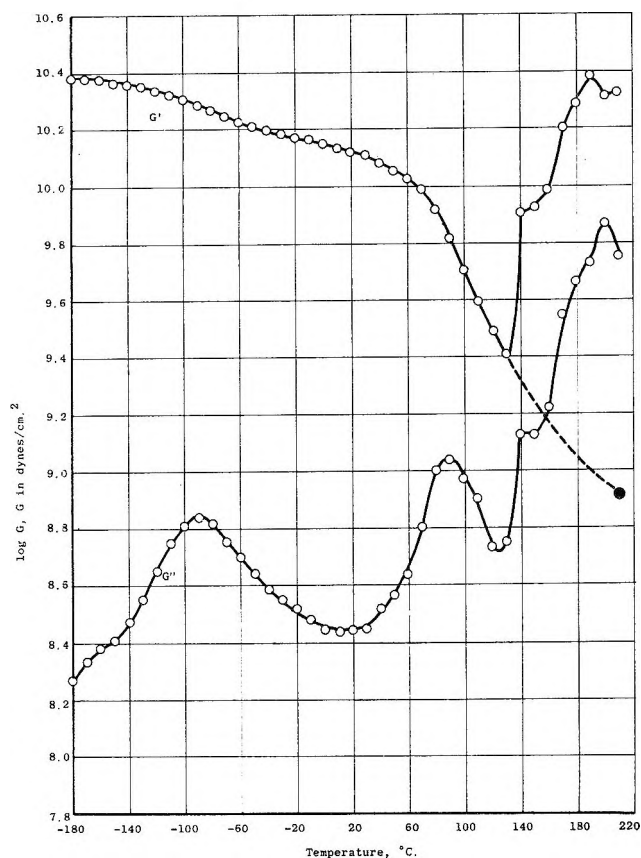


Figure 2. Real and loss components of the complex shear modulus for Gelatin-I. Note (see text) that there is considerable uncertainty about the sample dimensions at elevated temperatures and the open circle  $G'$  and  $G''$  data are apparent values. The solid point shows the true value of  $G'$  after correction for dimensional changes that have occurred.

be disregarded, for the specimen was very brittle after the run and seemed to have frothed during the latter stages of the experiment. It is well to note that although  $G'$  and  $G''$  are dependent on sample dimensions, which obviously are in doubt at the higher temperatures, the mechanical loss,  $G''/G'$ , is independent of dimensional changes.

Results similar to these were also obtained with Gelatin-II except that we found peaks at 90 and 115° with  $G'$  starting its increase at 120°. There were also indications of a melting or a large loss peak in the neighborhood of 180–190°.

To summarize, this torsion pendulum work indicates that gelatin has a mechanical loss peak, whose temperature position is unaffected by water, occurring at  $-85^\circ$ . For the gelatin-water systems studied, devitrification occurred at the expected temperature of  $-10^\circ$ . When the high-temperature data we obtained are compared with the current literature, there are indications that gelatin from different sources can have different proper-

ties (perhaps this is not too surprising when the complex structure of this copolymer is considered) and that the previous history of the sample can result in different mechanical properties at higher temperatures. Although differences in the high-temperature properties are found by different investigators, there seems to be a persistent loss peak at  $180^\circ$  and most sources agree that the major melting occurs near  $220^\circ$ .

### A Rotating-Disk Thermocell. I. Theory

by Benson R. Sundheim and Werner Sauerwein

Department of Chemistry, New York University, New York, New York 10003 (Received April 29, 1965)

Studies of thermoelectric properties entail the determination of electrode potentials across accurately known temperature and concentration distributions. A major experimental problem is the maintenance of these distributions free of convective perturbations.<sup>1</sup> A related problem, that of determining the concentration profile produced under certain circumstances by the passage of electricity through an electrochemical cell, has been satisfactorily treated by establishing a known forced convection pattern.<sup>2</sup> The rotating-disk electrode was used for this purpose since complete solutions to the hydrodynamic and diffusion problems are known in this case.<sup>2</sup> Here we explore the properties of the rotating-disk electrode system when the electrode and solution are held at different temperatures.

*One-Component System.* For a one-component electrolyte, e.g., fused  $\text{AgNO}_3$ , no composition gradients can occur. The thermopotential is readily expressed in terms of the temperature gradient<sup>3</sup> so that a knowledge of the temperature distribution is sufficient. A multicomponent system in which the convection is sufficient to prevent the establishment of the Sorët effect will behave in the same way. The meaning of the various symbols employed below is given in the Glossary.

(1) H. J. V. Tyrell, "Diffusion and Heat Flow in Liquids," Butterfield Scientific Publications, London, 1961. This work gives a critical review of experiment and theory as well as extensive references.

(2) (a) V. G. Levich, *Acta Physicochim. URSS*, **17**, 257 (1942); (b) V. G. Levich, *ibid.*, **19**, 117, 133 (1944); (c) V. G. Levich, "Physicochemical Hydrodynamics" (in English), Prentice-Hall, Inc., New York, N. Y., 1962.

(3) (a) H. Holtan, Thesis, University of Utrecht, 1953; (b) J. N. Agar in "The Structure of Electrolytic Solutions," W. Hamer, Ed., John Wiley and Sons, Inc., New York, N. Y., 1959, p. 200; (c) B. Sundheim, "Fused Salts," McGraw-Hill Book Co., Inc., New York, N. Y., 1964, p. 201.

For a uniform liquid the heat balance equation takes the form

$$q = -k\nabla T \quad (1)$$

Combining this with the equation of continuity for the heat flux in the absence of sources, sinks, or viscous dissipation<sup>4</sup>

$$\nabla \cdot q = \rho c_v \left( \frac{\partial T}{\partial t} + \vec{v} \cdot \vec{\nabla} T \right) \quad (2)$$

we obtain

$$\rho c_v \left( \frac{\partial T}{\partial t} + \vec{v} \cdot \vec{\nabla} T \right) = k \nabla^2 T \quad (3)$$

For the convective velocity,  $\vec{v}$ , we use the velocity found by solving the hydrodynamic equations for the rotating disk.<sup>2,5-7</sup> The velocity is given as a tabulated function or in asymptotic approximations expressed analytically. For the steady state, in cylindrical coordinates (3) becomes

$$v_r \frac{\partial T}{\partial r} + v_\phi \frac{\partial T}{\partial \phi} + v_y \frac{\partial T}{\partial y} = \frac{k}{\rho c_v} \left[ \frac{\partial^2 T}{\partial y^2} + \frac{\partial^2 T}{\partial r^2} + \frac{1}{r} \frac{\partial T}{\partial r} + \frac{1}{r^2} \frac{\partial^2 T}{\partial \phi^2} \right] \quad (4)$$

We seek a solution of the form  $T_y = T_y(Y)$ . Then

$$v_y(y) \frac{dT}{dy} = \frac{k}{\rho c_v} \frac{d^2 T}{dy^2} = \chi \frac{d^2 T}{dy^2} \quad (5)$$

$$T(0) = T_0; \quad T(\infty) = T_1$$

The solution to (5) meeting the appropriate boundary conditions is

$$T = T_0 + a_1 \int_0^y \exp \left[ \frac{1}{\chi} \int_0^t v_y(z) dz \right] dt \quad (6)$$

$$a_1 = (T_1 - T_0) / \int_0^\infty \exp \left[ \frac{1}{\chi} \int_0^t v_y(z) dz \right] dt$$

The required integrals have been computed<sup>8</sup> from the series expression for  $v$ . An approximate expression<sup>2</sup> for the integral leads to an equation for  $T$

$$T - T_0 = (T_1 - T_0) \int_0^Y e^{-u^3} du / \int_0^\infty e^{-u^3} du \quad (7)$$

$$Y = y/6^{1/3} \chi^{1/3} \nu^{1/6} / \omega^{1/2}$$

An estimate of the heat flux at the surface can be obtained from (7)

$$q = 0.62 \chi^{2/3} \nu^{-1/6} \omega^{1/2} (T_1 - T_0) \quad (8)$$

The major portion of the change in temperature takes

place within the region  $\delta$ , which is to be compared with the hydrodynamic boundary layer,  $\delta_0$ .

$$\delta = \chi(T_0 - T_1)/J \cong 0.5(\chi/\nu)^{1/3} \delta_0$$

$$\delta_0 = 3.6\nu/\omega$$

For usual values of  $\chi$ ,  $1.6 \times 10^{-3}$  for  $\text{H}_2\text{O}$ ,  $\nu = 10^{-2}$  cm.<sup>2</sup>/sec.

$$\delta \cong 0.15\delta_0$$

An important feature of the results is that the thickness of the effective boundary layer (and the detailed distribution) is independent of  $r$ . It is because of this property that the system has been characterized in diffusion as a "uniformly accessible surface."

A graphical representation of eq. 6 (ref. 2, p. 69) shows a nearly linear rise in  $(T - T_0)/T_0$  over approximately the first 80% of its range. The temperature change from surface to bulk naturally is unaffected by the rate of rotation of the disk although the distribution itself is proportional to  $\omega^{-1/2}$ .

Consider now a thermocell composed of two chemically identical electrodes in an electrolytic solution. Let one be a rotating disk held at temperature  $T$ , and the second stationary at  $T_0$  (the temperature of the bulk of the solution). It is the conclusion of this study that the temperature distribution between these electrodes is that given in eq. 6 without interference from casual convective mixing. In view of the generally observed<sup>1</sup> linear dependency of  $E$  on  $\Delta T$  over short temperature spans, it is expected that  $\Delta E/\Delta T$  observed by this method will be independent of the speed of rotation. It is not to be expected that a Sorët effect will be detected at moderate rotation speeds. An experimental test of this method will be published shortly.

### Glossary

$q$	Heat flux
$T$	Temperature
$E$	Internal (first-law) energy
$\rho$	Density (independent of $T$ )
$c_v$	Heat capacity at constant volume (independent of $T$ )
$\eta$	Viscosity
$\nu = \eta/\rho$	Kinematic viscosity
$k$	Thermal conductivity
$\vec{v}$	Convective velocity
$y, r, \phi$	Cylindrical coordinates

(4) E.g., R. Bird, W. Stewart, and E. Lightfoot, "Transport Phenomena," John Wiley and Sons, Inc., New York, N. Y., 1960, p. 315.

(5) T. Karman, *Z. angew. Math. Mech.*, **1**, 244 (1921).

(6) B. Cochran, *Proc. Cambridge Phil. Soc.*, **30**, 365 (1934).

(7) E. M. Sparrow and J. L. Gregg, *J. Heat Transfer*, **81**, 249 (1959).

(8) H. C. Riddiford and R. Gregory, *J. Chem. Soc.*, 3756 (1956).

- $\chi = k/\rho c_v$   
 $t$  Time  
 $Y$  Defined in eq. 7  
 $\omega$  Angular velocity  
 $\delta$  Boundary layer thickness for thermal diffusion  
 $\delta_0$  Boundary layer thickness for ordinary diffusion

*Acknowledgment.* It is a pleasure to acknowledge assistance to this work from the Office of Naval Research (Contract Nonr-285-37 with New York University).

## The Vapor Pressure and Heat of Sublimation of Chromium

by D. S. Dickson,<sup>1</sup> J. R. Myers, and R. K. Saxer

*Department of Mechanics, Air Force Institute of Technology, Wright-Patterson AFB, Ohio (Received June 11, 1965)*

A number of references describing the vapor pressure of solid chromium appear in the literature. These data were determined by a variety of techniques and are in fairly good agreement with the results of this investigation; however, the temperature ranges covered by previous investigators did not exceed 1675°K. The vapor pressures determined during this study by means of the Knudsen effusion technique included the temperature range 1560–1800°K. Because high-temperature vapor pressure data are lacking, it was considered that the results obtained during this study were significant.

### Experimental Section

*Equipment and Procedure.* The Knudsen method developed by means of statistical thermodynamics and kinetic theory postulates that the rate of effusion of a gas through an orifice into a high vacuum is related to the vapor pressure above the metal. The rate of effusion is related to the vapor pressure of the metal by the expression

$$P = \frac{W}{At} \sqrt{\frac{2\pi RT}{M}} = \dot{m} 2.258 \times 10^{-2} \sqrt{\frac{T}{M}} \quad (1)$$

In these expressions,  $P$  is the vapor pressure in atmospheres,  $W$  is weight loss in grams during the effusion time interval,  $A$  is orifice area in square centimeters,  $t$  is effusion time in seconds,  $R$  is the universal gas constant,  $T$  is absolute temperature in °K.,  $M$  is the molecular weight of the metal, and  $\dot{m}$  is the effusion rate in grams per second per square centimeter.

It is assumed in the above expressions that the orifice is ideal (*i.e.*, infinite thinness). In actual practice, the orifice does have measurable thickness and approximates a short tube or channel. Speiser<sup>2</sup> has given equations to correct for this condition. The need for correction factors was avoided in this work by reaming the orifice to a knife-edge of 30° included angle. Calculations based on Balson's<sup>3</sup> derivation showed the orifice to be nearly ideal.

The vacuum chamber used was fabricated from a 7-in. diameter brass cylinder which measured 13 in. high. Copper tubing was used to circulate coolant water around the chamber and through hollow electrode leads to the resistance furnace. A mechanical fore-pump and an oil diffusion pump were used to create an operating vacuum of at least  $10^{-6}$  mm. A liquid nitrogen trap prevented water and oil vapor in the diffusion pump from reaching the vacuum chamber. Operating temperatures were obtained with a wound, resistance-type, tungsten-wire furnace surrounded by three cylindrical tantalum heat shields. Power was supplied to the furnace by means of a constant-voltage transformer.

The Knudsen cells which contained the samples were fabricated from seamless tantalum tubing of 1-in. outside diameter and 0.020-in. wall thickness; cell bases and covers were formed from 0.010-in. thick tantalum sheet and welded in an argon atmosphere to the cells. A Leeds and Northrup disappearing-filament type optical pyrometer, calibrated against a National Bureau of Standards pyrometer by means of a standard tungsten ribbon filament lamp, was used to determine temperatures. The calibration was performed with the glass viewport in place to avoid corrections for window transmissibility. All temperature measurements were made at the orifice of the cell, which closely approximated blackbody conditions and eliminated the need for emissivity corrections.

Effective times at temperature were calculated to compensate for heating and cooling periods. The effective time was calculated from the equation

$$t_{\text{eff}} = \sum \Delta t_i [e^{-\Delta H_v/RT_A + \Delta H_v/RT_R}] \quad (2)$$

where  $\Delta t_i$  is the time interval between any two temperatures,  $T_A$  is the average temperature during that interval,  $T_R$  is the temperature of the test, and  $\Delta H_v$  is the heat of vaporization of chromium in calories per

(1) Submitted in partial fulfillment of the requirements for the degree of Master of Science.

(2) R. Speiser, "Vapor Pressure of Metals," Engineering Experiment Station, The Ohio State University, Columbus, Ohio, Vol. 19, No. 5, 1947, p. 12.

(3) E. W. Balson, *J. Phys. Chem.*, **65**, 1151 (1961).

gram-atom. An initial value for  $\Delta H_v$  of 91.0 kcal./g.-atom was obtained from Hultgren.<sup>4</sup> Measurements of experimental data were made to the following accuracy: weight loss to within  $\pm 0.05$  mg., time to within  $\pm 60$  sec., temperature to within  $\pm 4^\circ$ , and orifice area to within  $\pm 0.001$  cm.<sup>2</sup>. Orifice dimensions were corrected to account for the thermal expansion<sup>5</sup> of the tantalum cell cover. Specimen analysis is given in Table I.

Table I: Chromium Specimen Analysis

Element	Wt. %
Fe	0.008
S	0.007
C	0.005
Si	0.003
O	0.015
H	0.0003
N	0.010
Cr	Balance

## Results and Discussion

The vapor pressure of solid chromium in the temperature range 1560 to 1800°K., given in Table II and plotted in Figure 1, can be expressed by the equation

$$\log P(\text{atm.}) = -21,580/T + 8.01$$

The results agree very well with those obtained by Kubaschewski and Heymer<sup>6</sup> (1443–1673°K.) and McCabe, Hudson, and Paxton<sup>7</sup> (1381–1505°K.) using the Knudsen technique, Aldred and Myles<sup>8</sup> (1450–1650°K.) using the torsion-effusion technique, and Speiser, Johnston, and Blackburn<sup>9</sup> (1283–1561°K.), who used the Langmuir method. Excellent agreement also was reached with the lower temperature work of Gulbransen and Andrew<sup>10</sup> and Vintaikin.<sup>11</sup> Results of an earlier study by Baur and Brunner<sup>12</sup> appear to be too high. A literature survey revealed no solid chromium vapor pressure data exist above 1675°K.

A value of 98.7 kcal./g.-atom was obtained for the heat of vaporization as calculated from the slope of the log plot according to the Clausius-Clapeyron relation. This is 9% higher than the composite value of 91.0 kcal./g.-atom given by Hultgren<sup>4</sup> for 1700°K., the approximate average temperature of the present experiments. Hultgren's value was sufficiently accurate for effective time calculations. (See Table III for heat of vaporization results.)

The reliability of the vapor pressure data for pure chromium can best be established by the constancy and temperature dependence of  $\Delta H^\circ_0$ . The values of

Table II: Vapor Pressure of Pure Solid Chromium

Test	Temp., °K.	Time, sec.	Wt. loss, g.	Orifice area, cm. <sup>2</sup>	Pressure, atm.
1	1559	20420	0.0059	0.0256	$1.4 \times 10^{-6}$
2	1582	14100	0.0054	0.0256	$1.9 \times 10^{-6}$
3	1602	16010	0.0104	0.0219	$3.71 \times 10^{-6}$
4	1607	7390	0.0058	0.0257	$3.9 \times 10^{-6}$
5	1624	13900	0.0136	0.0219	$5.63 \times 10^{-6}$
6	1624	16500	0.0152	0.0257	$4.90 \times 10^{-6}$
7	1648	8810	0.0150	0.0257	$8.71 \times 10^{-6}$
8	1682	10740	0.0384	0.0257	$1.84 \times 10^{-5}$
9	1704	6950	0.0251	0.0210	$2.12 \times 10^{-5}$
10	1710	8690	0.0380	0.0263	$2.19 \times 10^{-5}$
11	1718	7910	0.0504	0.0257	$1.51 \times 10^{-5}$
12	1736	4530	0.0299	0.0210	$3.91 \times 10^{-5}$
13	1750	8480	0.0859	0.0257	$5.15 \times 10^{-5}$
14	1790	5190	0.0796	0.0262	$7.75 \times 10^{-5}$
15	1805	6190	0.1186	0.0257	$1.02 \times 10^{-4}$

Table III: Heat of Vaporization of Chromium at Absolute Zero

Temp., °K.	$-R \ln P$ , cal./mole deg.	$-(F^\circ - H^\circ_0)/T$ (vapor)	$-(F^\circ - H^\circ_0)/T$ (solid)	$\Delta H^\circ_0$ , kcal./mole
1559	26.73	44.894	10.60	95.1
1582	26.16	45.336	10.69	96.2
1602	24.85	45.026	10.79	94.7
1607	24.74	45.044	10.80	94.8
1624	24.30	45.096	10.86	95.2
1624	24.03	45.096	10.86	94.8
1648	23.15	45.171	10.97	94.5
1682	21.67	45.271	11.12	93.9
1704	21.39	45.337	11.20	94.6
1710	21.33	45.354	11.23	94.8
1718	22.06	45.381	11.26	95.5
1736	20.17	45.431	11.34	94.2
1750	19.62	45.471	11.39	94.0
1790	18.81	45.585	11.55	94.6
1805	18.26	45.627	11.62	94.3

Average value  $94.8 \pm 0.4$

(4) R. Hultgren, R. L. Orr, P. D. Anderson, and K. K. Kelley, "Selected Values of Thermodynamic Properties of Metals and Alloys," John Wiley and Sons, Inc., New York, N. Y., 1963, pp. 82, 83.

(5) G. L. Miller, "Tantalum and Niobium," Academic Press Inc., New York, N. Y., 1959, p. 28.

(6) O. Kubaschewski and G. Heymer, *Acta Met.*, **8**, 416 (1960).

(7) C. L. McCabe, R. G. Hudson, and H. W. Paxton, *Trans. A.I.M.E.*, **212**, 102 (1958).

(8) A. T. Aldred and K. M. Myles, *ibid.*, **230**, 736 (1964).

(9) R. Speiser, H. L. Johnston, and P. Blackburn, *J. Am. Chem. Soc.*, **72**, 4142 (1950).

(10) E. A. Gulbransen and K. F. Andrew, *Trans. A.I.M.E.*, **221**, 1247 (1961).

(11) E. Z. Vintaikin, *Dokl. Akad. Nauk SSSR*, **118**, 977 (1958).

(12) E. Baur and R. Brunner, *Helv. Chim. Acta*, **17**, 958 (1934).



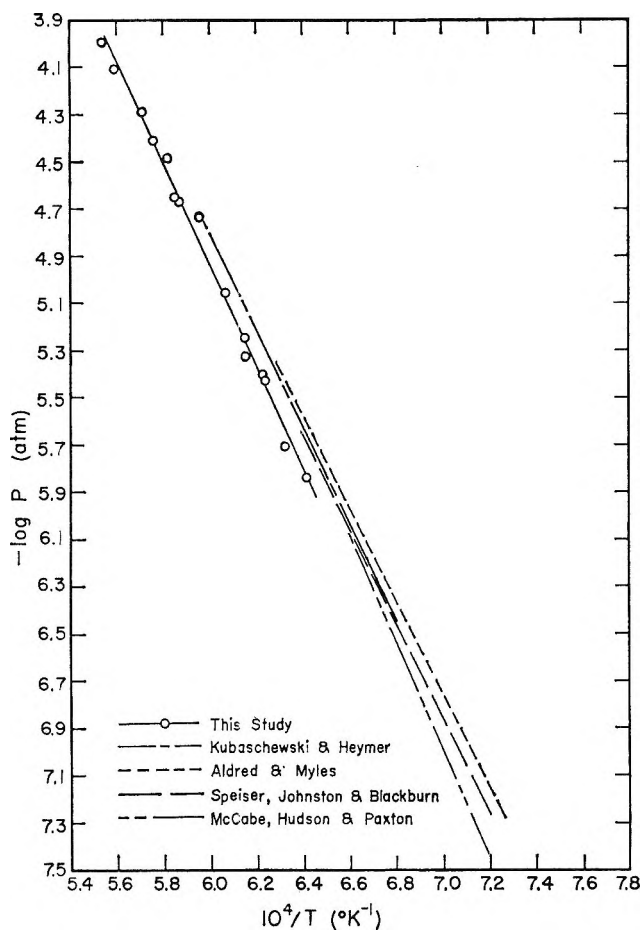


Figure 1. Vapor pressure of solid chromium.

$\Delta H^\circ_0$ , the heat of sublimation at absolute zero, were calculated by means of the third law from experimentally determined vapor pressures by using the expression

$$R \ln P = \left( \frac{F^\circ - H^\circ_0}{T} \right)_{\text{(solid)}} - \left( \frac{F^\circ - H^\circ_0}{T} \right)_{\text{(gas)}} - \frac{\Delta H^\circ_0}{T} \quad (3)$$

in which the parenthetical terms are the free energy functions of solid and gaseous chromium. The free energy values for the solid phase were calculated from the tabulated values of Stull and Sinke,<sup>13</sup> while the vapor phase free energy functions were computed from data compiled by Moore.<sup>14</sup> The heats of sublimation at absolute zero, by means of the third law, were calculated at each chromium test temperature to determine if any temperature-dependent trends were present. The  $\Delta H^\circ_0$  values between 1559 and 1648°K. yield an average value of 95.0 kcal./g.-atom while the

data between 1682 and 1805°K. yield an average value of 94.5 kcal./g.-atom. The over-all average value of  $\Delta H^\circ_0$  was determined to be  $94.8 \pm 0.4$  kcal./g.-atom. The higher values at the lower temperatures are in concordance with the difference between the third-law value of 94.8 kcal./g.-atom and the second-law value of 102.0 kcal./g.-atom (calculated from 1700°K.) corrected to 0°K. The vapor pressure data of Speiser, Johnston and Blackburn, McCabe, Hudson, and Paxton, and Gulbransen and Andrew were used to obtain third-law calculations of  $\Delta H^\circ_0$  by using the values of Stull and Sinke and Moore. These results are in good agreement with values obtained during this study (Table IV). Second-law calculations of reported vapor pressure data judged to be of reasonably good quality from 1280 to 1800°K. and (calculated from 1550°K.) corrected to 0°K. by using Hultgren's tables yield a value of  $\Delta H^\circ_0 = 96.9$  kcal./g.-atom.

Table IV: Heat of Sublimation at Absolute Zero

Investigator	$\Delta H^\circ_0$ , kcal./mole
Speiser, Johnston, and Blackburn <sup>9</sup>	$94.2 \pm 0.2$
McCabe, Hudson, and Paxton <sup>7</sup>	$94.5 \pm 0.4$
This investigation	$94.8 \pm 0.4$
Gulbransen and Andrew <sup>10</sup>	$95.4 \pm 0.2$

The compound  $\text{TaCr}_2$  is known to exist; however, no crucible reaction was noted.<sup>15</sup> Nevertheless, the vapor pressure data of other workers in the lower temperature range where comparison can be made tended to be higher. Calculated second-law  $\Delta H$  values obtained as a result of this work tended to be higher than the previously reported second-law values. If  $\text{TaCr}_2$  did form during these experiments, the exothermic reaction of this formation would tend to decrease the activity of Cr on the cell walls as the temperature was lowered, introducing the most error at these lower temperatures.

*Acknowledgments.* The authors gratefully acknowledge the assistance of Mr. S. G. Lee during the course of this investigation and the Union Carbide Metals Company for providing the high-purity chromium.

(13) D. R. Stull and G. C. Sinke, "Thermodynamic Properties of the Elements," American Chemical Society, Washington, D. C., 1956, p. 77.

(14) C. Moore, National Bureau of Standards Circular No. 467, U. S. Government Printing Office, Washington, D. C., 1952, p. 26.

(15) M. Hansen, "Constitution of Binary Alloys," McGraw-Hill Book Co., Inc., New York, N. Y., 1958, p. 563.



# COMMUNICATIONS TO THE EDITOR

## Photosensitization of Carbon Dioxide with Hg 6 <sup>1</sup>P<sub>1</sub> Atoms<sup>1</sup>

*Sir:* Due to experimental difficulties and the lack of developed techniques, there have been very few photosensitization studies with Hg 6 <sup>1</sup>P<sub>1</sub> atoms. We have developed suitable experimental conditions, including a new transmittance filter for the 1849-Å. mercury resonance radiation,<sup>2</sup> which enable such investigations with relative ease.

Hg 6 <sup>3</sup>P<sub>1</sub> (or Hg 6 <sup>3</sup>P<sub>0</sub>) atoms have been shown to decompose CO<sub>2</sub> slowly into CO and HgO as the final products.<sup>3</sup> This was assumed to occur through a two-step excitation resulting then in the C-O bond rupture. Hg 6 <sup>1</sup>P<sub>1</sub> atoms in the presence of Hg 6 <sup>3</sup>P<sub>1</sub> atoms have also been shown to produce CO and HgO,<sup>4</sup> the last product assumed either directly or through O atoms initially.

Experiments have been carried out under conditions where for practical purposes only the Hg 6 <sup>1</sup>P<sub>1</sub> atoms were produced in the reaction cell. The reaction between CO<sub>2</sub> and Hg 6 <sup>1</sup>P<sub>1</sub> was studied as a function of CO<sub>2</sub> and Hg vapor pressures under both static and flow conditions at room temperature. Various experimental arrangements were investigated, *e.g.*, different light sources, reaction, and filter cells.<sup>5</sup> Analyses were performed by gas chromatography and standard manometric methods. In this communication we wish to present evidence and discuss the unsuspected primary process of this reaction.

Carbon monoxide was produced as the gas phase product. An orange-yellow deposit was formed on the walls of the reaction cell. This solid deposit was partially decomposed at about 250° when the reaction cell walls were heated. This resulted in the production of CO<sub>2</sub> in the gas phase. The remaining orange-yellow deposit could be further decomposed when heated to about 500 to 600° and resulted only in O<sub>2</sub> in the gas phase. The composition of the solid deposit is limited to the elements C, O, and Hg. The only known compounds satisfying this would be: mercuric oxide, HgO; basic mercuric carbonate of varied composition, (HgO)<sub>2</sub>HgCO<sub>3</sub> or (HgO)<sub>3</sub>HgCO<sub>3</sub>; mercurous carbonate, Hg<sub>2</sub>CO<sub>3</sub>; mercuric oxalate, HgC<sub>2</sub>O<sub>4</sub>; mercurous oxalate, Hg<sub>2</sub>C<sub>2</sub>O<sub>4</sub>. The oxalates are colorless; the carbonates and the oxide are all yellow. The carbonates decompose thermally into CO<sub>2</sub> and HgO. Both the mercuric and mercurous oxalates on the other hand decompose into CO and CO<sub>2</sub> as gaseous products. Mercurous oxalate gave a CO:CO<sub>2</sub> ratio of  $18.4 \times 10^{-3}$

and for mercuric oxalate this ratio was  $6.82 \times 10^{-3}$ . Thus, under our reaction conditions the conversions would have been too small to be able to detect CO from the solid product decomposition. Aqueous solution of the solid deposit from our reaction cell was evaporated and fused with diphenylamine which resulted in a deep blue melt, the so-called aniline blue.<sup>6</sup> In addition, the solid deposit was shown to reduce KMnO<sub>4</sub> solutions. This could be followed spectrophotometrically. Thus it would seem that an oxalate and mercuric oxide are deposited as solid products on the walls of the reaction cell. The formation of carbonates does not seem to be indicated in the light of these observations and based on the photochemical reaction of the solid product as discussed later in this communication.

We observed that as the Hg vapor pressure in the reaction cell was decreased, resulting in a deeper penetration of the 1849-Å. resonance radiation in the cell, the gas phase CO yields decreased nearly linearly. The CO<sub>2</sub> yields from the solid product decomposition under the same conditions also decreased with decrease in Hg vapor pressure but the rate of decrease was less as compared to CO yields. In separate experiments our solid deposit was initially allowed to form on the cell walls, the excess CO<sub>2</sub> was pumped off, and then the cell was irradiated with 1849-Å. radiation. This resulted in the formation of CO in the gas phase and HgO on the walls if the decomposition reaction was allowed to go to completion. Furthermore, it was found that the use of the usual low-pressure resonance lamp produced a higher rate of decomposition as compared to a medium-pressure arc where the 1849-Å. resonance line is self-reversed. In separate solid phase decomposition experiments it was found that the rate of CO:CO<sub>2</sub> increased by a factor of about 10 for mercuric oxalate and by a factor of about 28 for mercurous oxalate when the irradiation was performed with the low-pressure resonance lamp rather than the medium-pressure arc under otherwise identical conditions. We can conclude from the above data that a collision complex was formed in the gas phase between excited singlet mercury

(1) This work was supported by a Contract with the U. S. Atomic Energy Commission [AT-(40-1)-2844].

(2) C. M. Wolff and R. Pertel, *J. Opt. Soc. Am.*, **54**, 1168 (1964).

(3) O. P. Strausz and H. E. Gunning, *Can. J. Chem.*, **39**, 2244 (1961).

(4) Y. Mori, *Bull. Chem. Soc. Japan*, **34**, 1128 (1961).

(5) A more detailed presentation of all the experimental techniques and data will be prepared and submitted from C. M. Wolff's Ph.D. thesis in the near future.

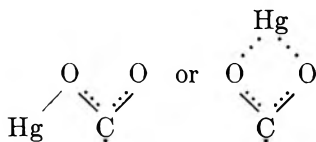
(6) F. Feigl, "Spot Tests in Organic Analysis," 5th Ed., Elsevier Publishing Co., New York, N. Y., 1956, p. 355.

atoms and CO<sub>2</sub> molecules. These complexes can stabilize on the walls, *e.g.*, by dimerizing into an oxalate. Once formed, the deposit can then photochemically decompose, especially easily with excited Hg atoms. Gas phase CO seems to be produced from such decomposition. This is also supported by measurements of gas phase CO yield as a function of CO<sub>2</sub> pressure. After an initial rise in the CO yield a nearly constant rate was observed.

Carbon dioxide is linear in its ground state (<sup>1</sup>Σ<sub>g</sub><sup>+</sup>). Both the lowest singlet excited states, <sup>1</sup>B<sub>2</sub> and <sup>1</sup>A<sub>2</sub>, are bent and probably have their vibrational zero levels near 7 e.v.<sup>7</sup> Similarly, the lowest triplet excited states, <sup>3</sup>B<sub>2</sub> and <sup>3</sup>A<sub>2</sub>, are also bent and probably have their vibrational zero levels near 5 to 5.5 e.v.<sup>7-9</sup> In the light of these spectroscopic estimates, the Hg 6 <sup>1</sup>P<sub>1</sub> atoms are capable of producing the <sup>1</sup>A<sub>2</sub> state of CO<sub>2</sub>. Thus one would be able to place an upper limit of 6.7 e.v. on the lowest vibrational energy level. An excited CO<sub>2</sub> molecule, on the other hand, is hardly expected to produce our observed solid phase products since it would lose its energy in collisions with other molecules and walls. Our postulated collision complex survives more readily near the walls as was shown by the data.

When the resonance lamp was used directly, without the filter, the ratio of the Hg 6 <sup>1</sup>P<sub>1</sub> atoms to the Hg 6 <sup>3</sup>P<sub>1</sub> atoms in the reaction cell was about 0.11. Carbon monoxide was found as the gas phase product. An orange-yellow deposit on the cell walls decomposed into oxygen and carbon dioxide when heated. The amount of CO<sub>2</sub> was considerably less than the comparable runs with filtered radiation. With a methanol filter, which allowed only the production of Hg 6 <sup>3</sup>P<sub>1</sub> atoms, no CO<sub>2</sub> decomposition would be detected under conditions of similar intensity and reaction time.

We conclude that a collision complex is formed only with singlet excited mercury atoms. The triplet excited mercury atoms seem to decompose a previously formed solid product into CO and HgO. From the spectroscopically assumed excited state configurations of CO<sub>2</sub> and our observed product—presumably an oxalate—the collision complex probably has one of the configurations



(7) R. S. Mulliken, *Can. J. Chem.*, **36**, 10 (1958).

(8) A. D. Walsh, *J. Chem. Soc.*, 2266 (1953).

(9) R. N. Dixon, *Proc. Roy. Soc. (London)*, **A275**, 431 (1963).

(10) To whom inquiries concerning this communication should be directed at the Department of Chemistry, University of Alberta, Edmonton, Alberta.

Dimerization of either of these complexes on the walls can now readily produce an oxalate.

DEPARTMENT OF CHEMISTRY  
UNIVERSITY OF HOUSTON  
HOUSTON, TEXAS 77004

C. M. WOLFF  
RICHARD PERTEL<sup>10</sup>

RECEIVED AUGUST 12, 1965

### Effects of Oxygen Absorbed in the Skin of a Platinum Electrode on the Determination of Carbon Monoxide Adsorption

*Sir:* Investigations<sup>1-10</sup> have shown that hydrogen and oxygen absorbed in the "skin" of a platinum electrode can significantly affect its electrochemical behavior. We<sup>9</sup> named this type of absorption "dermasorption." We demonstrated<sup>6,8,9</sup> that anodic and cathodic pretreatment to remove surface impurities can result in effectually changing the electrode material (by alloying metal atoms in the skin with H or O). Dermisorbed O or H also can lead to erroneous determinations of the identity and surface coverage of chemisorbed species by anodic stripping because some of the dermasorbed atoms may migrate to the surface.<sup>6</sup>

As an example of the effects of dermasorbed O, we shall discuss the differences in the degree of coverage of a platinum electrode with CO found by Brummer and Ford<sup>11</sup> and ourselves.<sup>5</sup> We shall also attempt to correct some of their misinterpretations of our work.<sup>5</sup>

The central difference between these two studies is the determined value of  $Q_{CO}$ , the charge required to remove adsorbed CO; Brummer and Ford<sup>11</sup> found  $365 \pm 36 \mu\text{coulombs/cm}^2$ , we<sup>5</sup> found  $453 \pm 20$ . These values depend critically on the shape and on the assumptions made about the significance of the various regions of the anodic charging curve. Since the voltage-time relation observed by them (Figure 1 in ref. 11) and by us (Figure 1 in ref. 5) differ greatly, it is not

(1) S. Schuldiner, *J. Electrochem. Soc.*, **107**, 452 (1960).

(2) C. H. Presbrey, Jr., and S. Schuldiner, *ibid.*, **108**, 985 (1961).

(3) S. Schuldiner and R. M. Roe, *ibid.*, **110**, 332 (1963).

(4) S. Schuldiner and T. B. Warner, *J. Phys. Chem.*, **68**, 1223 (1964).

(5) T. B. Warner and S. Schuldiner, *J. Electrochem. Soc.*, **111**, 992 (1964).

(6) S. Schuldiner and T. B. Warner, *Anal. Chem.*, **36**, 2510 (1964).

(7) V. I. Lukyanycheva and V. S. Bagotskii, *Dokl. Akad. Nauk SSSR*, **155**, 160 (1964).

(8) S. Schuldiner and T. B. Warner, *J. Electrochem. Soc.*, **112**, 212 (1965).

(9) T. B. Warner and S. Schuldiner, *ibid.*, **112**, 853 (1965).

(10) S. Schuldiner and T. B. Warner, *Electrochim. Acta*, in press.

(11) S. B. Brummer and J. I. Ford, *J. Phys. Chem.*, **69**, 1355 (1965).

surprising that determined values of  $Q_{CO}$  also differ. Temperature and electrolyte differences would not likely cause the discrepancy. The anodic cleaning pulse of 20–100 ma./cm.<sup>2</sup> applied for about 1 sec. by Brummer and Ford prior to CO adsorption may account both for their lower value of  $Q_{CO}$  and for the different appearance of the charging curves. Dermalisorbed O from the cleaning pulse (a) could affect CO oxidation kinetics and the shape of the anodic charging curve, and (b) O atoms could migrate to the surface and react with adsorbed CO reducing the charge necessary to strip CO.

Brummer and Ford's anodic charging curve shape is such that quantitative separation of  $Q_{CO}$  from  $Q_O$  is virtually impossible. Brummer and Ford indicate that our  $Q_{CO}$  region corresponds to their AB region (Figure 1 in ref. 11). Comparing our Figure 1<sup>5</sup> with theirs<sup>11</sup> shows that this is not accurate; we extrapolate two linear regions to find an intersection point and no point on their curve can be compared with ours due to the important differences in curve shapes. Also, they suggest that we found that the oxidation of the adsorbed CO and of the electrode occur completely separately. In fact, we<sup>5</sup> postulated that a small amount of O formed in the CO oxidation region oxidized adsorbed CO. The O concentration remained small because its reaction with adsorbed CO was much faster than the oxidation of water to O atoms.

Brummer and Makrides<sup>12</sup> show an anodic charging curve for CO oxidation similar in shape to ours.<sup>5</sup> Specific conditions were not given by Brummer and Makrides, but the same anodic pretreatment sequence used by Brummer and Ford<sup>11</sup> is unlikely; otherwise, the transients would have looked the same.

The presence of dermalisorbed O in Brummer and Ford's electrode is suggested also by the values of  $Q_O$  in Figure 6 of ref. 11. Oxygen determined following anodic pulses where less than a monolayer of CO was removed led them to suspect concomitant electrode oxidation and thus they subtracted these observed  $Q_O$  values when determining  $Q_{CC}$  from  $Q_a$ . However, they may have detected dermalisorbed O which migrated to the surface; this would invalidate their "correction." This is supported by the close correspondence of our<sup>5</sup>  $Q_O$  values in the presence and absence of CO in solution (Figure 3d in ref. 5) which showed that virtually as much O can be deposited after stripping CO as can be deposited on a clean electrode.

Brummer and Ford<sup>11</sup> agree with us<sup>5</sup> that physically adsorbed CO can exist on top of chemisorbed CO, but they feel that we used invalid evidence whereas their finding was based on solid facts. They state that physically adsorbed CO would be easier to oxidize

than chemisorbed CO. How these authors arrive at this unsupported statement is unknown. They may suspect that physically adsorbed CO oxidizes more easily than chemisorbed CO, but before generalizing, substantiating evidence is required. There is no reason, per se, why chemisorbed CO should not be oxidized more readily than physically adsorbed CO.

Brummer and Ford<sup>11</sup> conclude "... Warner and Schuldiner were incorrect in their assignment of charge to the various processes which occur during anodic transients with CO." They further state that they "... can see clearly the quantitative limit on the assumptions involved in deriving  $Q_{CC}$ , whereas in the previous work this was not possible." We feel that such conclusions are premature. Any decision as to the type of CO bonding with the surface must await a clear experimental answer to the question of how much CO is, in fact, adsorbed.

We suggest that dermalisorbed O formed during electrode "activation" may well account for many of the phenomena which are dependent on the time following such "activation" and for discrepant results obtained using different "activation" procedures. It appears that there is no easy way of avoiding expenditure of the time and effort required to make and maintain the clean electrochemical systems required for fundamental research.

(12) S. B. Brummer and A. C. Makrides, *J. Phys. Chem.*, **68**, 1448 (1964).

U. S. NAVAL RESEARCH LABORATORY THEODORE B. WARNER  
WASHINGTON, D. C. 20390 SIGMUND SCHULDINER

RECEIVED JULY 19, 1965

### The Correction for Electrode Oxidation in the Estimation of Adsorbed CO on Smooth Platinum by Anodic Stripping

*Sir:* Anodic galvanostatic stripping of CO adsorbed on Pt occurs at potentials where the electrode should normally be oxidized.<sup>1-4</sup> Consequently, some correction must be made for the oxidation which occurs when stripping CO. Three methods of doing this have been applied.<sup>2-4</sup> Warner and Schuldiner<sup>5</sup> suggest that

(1) S. B. Brummer and A. C. Makrides, *J. Phys. Chem.*, **68**, 1448 (1964).

(2) S. B. Brummer and J. I. Ford, *ibid.*, **69**, 1355 (1965).

(3) T. B. Warner and S. Schuldiner, *J. Electrochem. Soc.*, **111**, 992 (1964).

(4) S. Gilman, *J. Phys. Chem.*, **66**, 2657 (1962).

(5) T. B. Warner and S. Schuldiner, *ibid.*, **69**, 4048 (1965).

the procedure which we used,<sup>2</sup> where we reversed the current during the anodic stripping and determined surface oxide formed during the anodic removal of  $\text{CO}_{\text{ads}}$  by reduction, may be in error due to the effects of "dermasorbed" O. This, they believe, is oxygen dissolved in Pt<sup>6,7</sup> during the prior anodic cleaning pulse which we used.<sup>2</sup> It will be shown that the disagreement between the values of  $Q_{\text{CO}}$  cannot arise in this way and that the *results* of the two investigations agree remarkably well, the difference for  $Q_{\text{CO}}$  coming from a *difference in interpretation*. Thus, the central difference between the two studies lies in the computed values of  $Q_{\text{CO}}$  and these depend critically on the significance attached to the various regions of the stripping curves. It is suggested that these curves in ref. 2 and 3 "differ greatly" but in fact the charge in the region AB of our transients (tentatively identified<sup>2</sup> with their  $Q_{\text{CO}}$  value) agrees excellently with their data when their double-layer correction is eliminated. This indicates that the crucial difference is in the additional measurements which we made to interpret our chronopotentiograms correctly.

Warner and Schuldiner,<sup>3</sup> on the other hand, divided their transients (in the stripping region) into two parts. They considered that the first region ( $\sim$  a plateau) corresponds to oxidation of  $\text{CO}_{\text{ads}}$  ( $Q_{\text{CO}}$ ) and that the second (rising) part corresponds to electrode oxidation. Despite assertions to the contrary,<sup>5</sup> it is clear that, although they believed that the oxidation of  $\text{CO}_{\text{ads}}$  occurs *via* adsorbed O, they considered for *purposes of computing the charges* that the two processes occur separately.<sup>3</sup> The evidence presented to support such a separation is unconvincing. Thus in Figure 3(d) of ref. 3 there is considerable scatter and the charge in the so-called "oxygen region" is systematically less than expected, for rapid rates of charging. The most probable explanation for this discrepancy, directly supported by our measurements, is that the *two electrode processes overlap* and that the electrode is partially oxidized before all the  $\text{CO}_{\text{ads}}$  is removed.

It is suggested<sup>5</sup> that some of our  $\text{CO}_{\text{ads}}$  was oxidized by "dermasorbed" O released during the adsorption process. This would make our measured charges less than Warner and Schuldiner's.<sup>3</sup> We note above that this is not so. The quantity of any such "dermasorbed" O which could dissolve in the Pt during our cleaning pulse may be estimated from ref. 7 (Figure 2); thus, at a current density (1.77 ma./cm.<sup>2</sup>) such that the total anodic time is about 1 sec. (*cf.* our  $\sim$ 1-sec. cleaning pulse), it is  $\sim$ 1400  $\mu\text{coulombs/cm.}^2$ . Our stripping curves were taken 2 min. after cleaning, and in this time about 7200  $\mu\text{coulombs/cm.}^2$  of CO diffuses up to the electrode.<sup>2</sup> Thus, it is hardly likely that

"dermasorbed" O atoms could significantly reduce the subsequent CO stripping charge since diffusion can readily replace any  $\text{CO}_{\text{ads}}$  which might be lost to "dermasorbed" O. Also, our H-atom deposition experiments showed that the  $\text{CO}_{\text{ads}}$  concentration in our experiments was at least 0.98 of a monolayer. Thus, the possibility that the basis of the disagreement is due to reaction of  $\text{CO}_{\text{ads}}$  during the time since preanodization cannot be maintained.

It is also suggested<sup>5</sup> that the oxide which we found is from reduction of "dermasorbed" O migrating to the surface during the anodic transient. If this were so, the amount of this reducible oxygen would be greater for lower anodic current densities, when more time is available for such diffusion to occur. We found the opposite<sup>2</sup> which is expected for overlapping of  $\text{CO}_{\text{ads}}$  oxidation and electrode oxidation. A calculation of the rate of diffusion of O in the metal required to validate the suggested diffusion process also rules it out. Thus for the 147-ma./cm.<sup>2</sup> anodic pulse of ref. 2 (Figure 6), the average rate of diffusion would have to be  $\sim$ 20 ma./cm.<sup>2</sup>. Then, at least 2.4 coulombs/cm.<sup>2</sup> of "dermasorbed" O would have to diffuse out of the Pt during the 2 min. after cleaning. This is greater than the total charge passed in the anodic cleaning pulse ( $\sim$ 0.1 coulomb) and corresponds to about 6000 monolayers of O—too much by far.

Thus, while there may be effects of "dermasorbed" O on the properties of Pt electrodes, they are not responsible for the quantitative disagreement between the results for  $\text{CO}_{\text{ads}}$  stripping.

(6) S. Schuldiner and T. B. Warner, *Anal. Chem.*, **36**, 2510 (1964).

(7) S. Schuldiner and T. B. Warner, *J. Electrochem. Soc.*, **112**, 212 (1965).

TYCO LABORATORIES, INC.  
WALTHAM, MASSACHUSETTS 02154

S. B. BRUMMER

RECEIVED SEPTEMBER 29, 1965

### On the Number of Hydroxyl Groups at the Exterior Surfaces of Faujasite Crystals

*Sir:* In the Appendix to a recent paper, Uytterhoeven, Christner, and Hall<sup>1</sup> (UCH) propose a method for calculating the number of hydroxyl groups formed at the bounding surface of a faujasite crystal. Their crystal model was generated by stacking identical sheets of puckered hexagonal rings of cubeoctahedra (sodalite units) in a prescribed manner. An examination of this

(1) J. B. Uytterhoeven, L. G. Christner, and W. K. Hall, *J. Phys. Chem.*, **69**, 2117 (1965).

type of model reveals that there are two distinct ways of stacking the sheets of hexagonal rings—one of these leads to the model of UCH, the other to a model with a rhombohedral shape. Neither model, however, corresponds to the octahedral form observed in natural or synthetic crystals of faujasite.<sup>2</sup>

The model obtained by UCF suffers from the disadvantage that it carries both {111} and {100} faces, whereas in any real situation, one would expect the crystals to have one kind of face or the other, but not both. This disadvantage is not possessed by the rhombohedral and octahedral models which are defined solely by {111} faces.

From their model, UCH calculated the average number of surface hydroxyl groups per sodalite unit for a crystal having  $h$  hexagonal rings on the edge of a sheet, and  $h$  sheets, to be

$$f(\text{OH}) = \frac{12(2h + 1)}{h(h + 2)} \approx \frac{24}{h} \quad (1)$$

in the limit of large  $h$ . We have constructed an octahedral model for faujasite, and find that

$$f(\text{OH}) = \frac{72(h + 1)}{4(h + 1)^2 - 1} \approx \frac{18}{h} \quad (2)$$

Although either of the above equations is adequate for the purposes of UCH, we feel that proper appreciation of the crystal habit of faujasite dictates against the use of eq. 1.

Consideration of the structure of the diamond lattice and the arrangement of the hexagonal rings along the edge of a {111} face of length  $x$  gives the *precise* relation

$$\begin{aligned} x &= \frac{a_0}{\sqrt{2}} h \\ &= 1.749 \times 10^{-7} h \text{ cm.} \end{aligned} \quad (3)$$

using Baur's value<sup>3</sup> of the lattice parameter,  $a_0$ . This relation should be preferred to the estimate given in UCH's eq. VIII, which was also derived from Baur's data.

(2) R. M. Barrer, W. Buser, and W. F. Grütter, *Helv. Chim. Acta*, **39**, 518 (1956).

(3) W. H. Baur, *Am. Mineralogist*, **49**, 697 (1964).

SOCONY MOBIL OIL COMPANY, INC.  
RESEARCH DEPARTMENT  
CENTRAL RESEARCH DIVISION LABORATORY  
PRINCETON, NEW JERSEY

G. T. KERR  
E. DEMPSEY  
R. J. MIKOVSKY

RECEIVED SEPTEMBER 1, 1965

## A Direct Measurement of Surface Charge in the Presence of an Electrode Reaction

*Sir:* Properties of the electrical double layer on an ideally polarized electrode, such as mercury, are measured either with the capillary electrometer, which measures interfacial tension, or with an a.c. impedance bridge, which measures capacity. With a value for the zero-charge potential, the double-layer capacity may be integrated to find the surface charge on the electrode. Similarly, the interfacial tension may be differentiated with respect to potential to obtain surface charge.<sup>1</sup>

In the presence of an electrode reaction, however, interfacial tension measurements become dependent on the steady-state concentration of reacting species at the interface within the capillary electrometer, and capacity measurements become strongly frequency dependent. In order to separate faradaic impedance from the double-layer impedance, a complex analysis may be required.<sup>2</sup>

We propose here a very simple method for measuring directly the surface charge on a liquid metal electrode, such as mercury, gallium, or their amalgams, in the presence of electrode reactions. At constant potential, the surface charge per unit area,  $q$ , is constant, and the charging current at a spherical dropping electrode formed by a constant mass flow,  $m$ , is approximately

$$I_c = {}^{2/3} (36\pi)^{1/3} q \left( \frac{m}{\rho} \right)^{2/3} t^{-1/3} = At^{-1/3}$$

where  $t$  is the time from the birth of the drop, and  $\rho$  is the density of the electrode metal.

In contrast, the current due to an activation-controlled reaction at the electrode is directly proportional to the area of the drop, since the current density  $i_a$  is constant at constant potential

$$I_a = (36\pi)^{1/3} i_a \left( \frac{m}{\rho} \right)^{2/3} t^{2/3} = Ct^{2/3}$$

If the reaction is diffusion-controlled, the current due to the reaction varies approximately according to the Ilkovic equation

$$I_d = knD^{1/2} c \left( \frac{m}{\rho} \right)^{2/3} t^{1/6} = Bt^{1/6}$$

where  $n$  is the number of electrons transferred in the electrode reaction,  $D$  is the diffusion coefficient of the

(1) P. Delahay, "Double Layer and Electrode Kinetics," John Wiley and Sons, Inc., New York, N. Y., 1965.

(2) M. Sluyters-Rehbach and J. H. Sluyters, *Rec. trav. chim.*, **83**, 217 (1964).

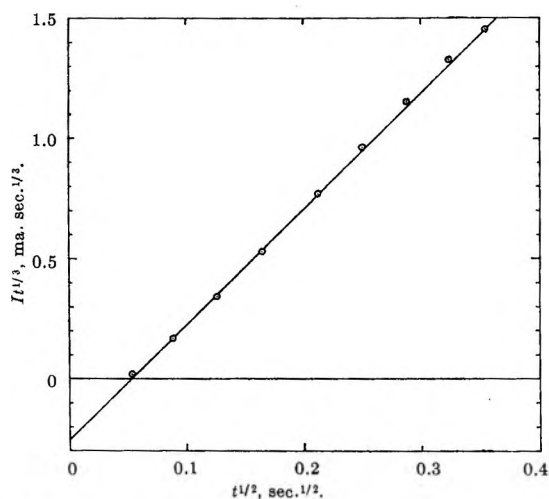


Figure 1.

reacting species at concentration  $c$ , and  $k$  is a geometrical constant.

Thus the total current  $I$  at a dropping amalgam electrode may be written as the sum of charging current ( $A$ ), faradaic current due to diffusion-controlled anodic dissolution ( $B$ ) and cathodic deposition ( $B'$ ) reactions, and faradaic current due to the activation-controlled hydrogen evolution reaction ( $C$ )

$$It^{1/3} = A + Bt^{1/2} - B't^{1/2} - Ct$$

We have measured current-time curves at a dropping gallium amalgam electrode (1.65 mole % Hg in Ga) at constant potential. Both anodic dissolution of Ga and cathodic hydrogen evolution occur in the region of the zero-charge potential, and a direct measure of surface charge was desired. These curves were obtained by polarizing the dropping amalgam electrode with a potentiometer and using an oscilloscope to measure the potential drop across a resistor in series with the cell. For larger currents, a Wenking potentiostat was used. A very fine capillary, approximately 1 mm. outside diameter, 0.1 mm. inside diameter, was

used, so that small, rapid (0.1 to 0.2 sec.), but well-formed spherical drops were obtained. In this way the charging current was increased relative to the dissolution current.

Figure 1 shows a plot of  $It^{1/3}$  vs.  $t^{1/2}$  for the curve obtained at  $-0.540$  v. vs. a reversible hydrogen electrode in  $0.1 M HClO_4$ . Note that the curve is almost exactly linear. The current throughout most of the drop lifetime is anodic, but the surface charge, as indicated by the extrapolation to zero time, is negative. The constant  $A$  is  $-0.25 \mu a. sec.^{1/3}$ , which corresponds to a surface charge density  $q = -1.30 \mu coulombs/cm.^2$ .

An important modification of this method is to fix the concentration of the soluble ion in solution (in this case  $Ga^{+3}$ ) and to measure current-time curves near the reversible potential for the dissolution reaction. In such a case, the coefficients  $B$  and  $B'$  are approximately equal, and  $It^{1/3}$  may be nearly independent of  $t$ , so that the extrapolation may be readily made. This is analogous to the "null solution" method of measuring zero-charge potentials.<sup>3</sup>

This method appears to be of high accuracy and wide applicability. Several problems where it may provide important information are: to determine the surface charge of cadmium, zinc, and thallium amalgams,<sup>3,4</sup> gallium,<sup>5</sup> and gallium alloys, all of which dissolve at potentials cathodic of the zero-charge potential; and to measure the surface charge of mercury at the limit of anodic dissolution<sup>2</sup> and from it to obtain the double-layer capacity. We are carrying out experiments on these systems and will report our results in detail in future communications.

(3) A. N. Frumkin and F. J. Cirves, *J. Phys. Chem.*, **34**, 74 (1930).

(4) J. N. Butler, *J. Electroanal. Chem.*, **9**, 149 (1965).

(5) A. N. Frumkin, N. B. Grigor'ev, and I. A. Bagotskaya, *Dokl. Akad. Nauk SSSR*, **157**, 557 (1964).

TYCO LABORATORIES, INC.  
WALTHAM, MASSACHUSETTS 02154

JAMES N. BUTLER  
MARY L. MEEHAN

RECEIVED SEPTEMBER 7, 1965